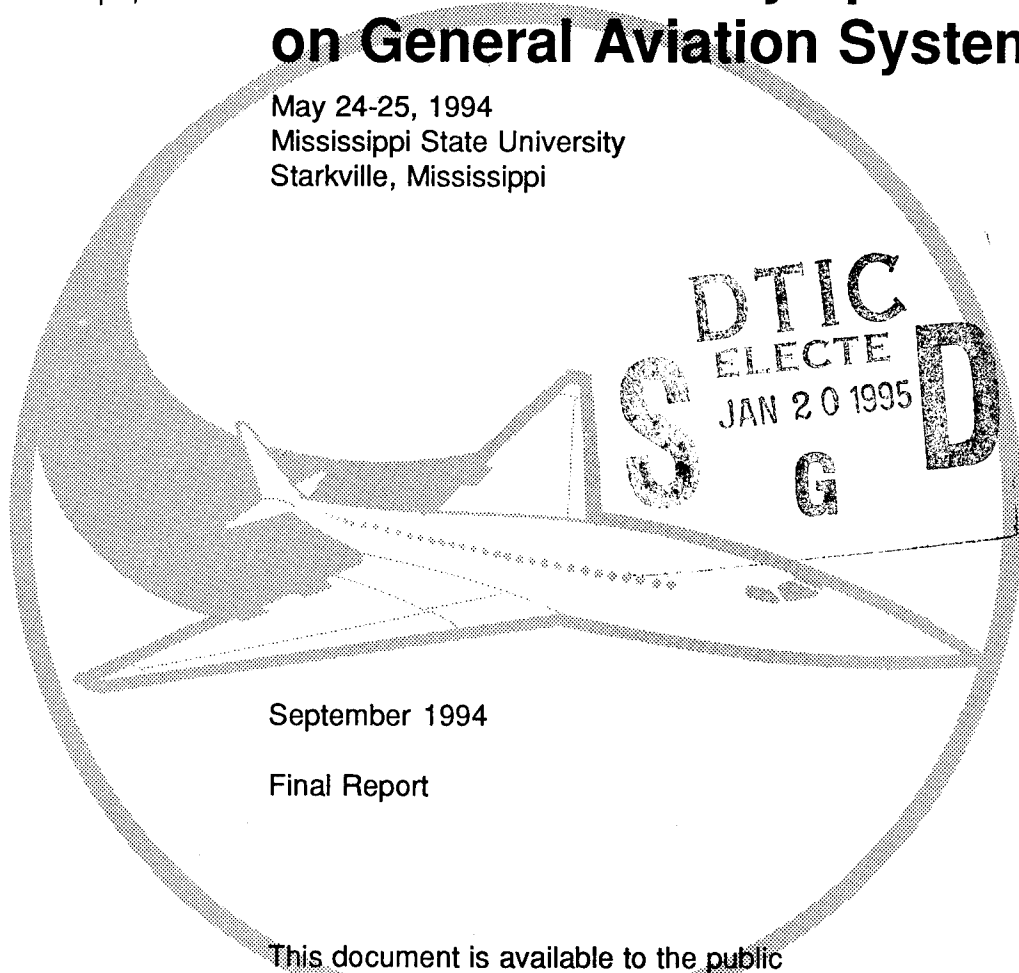


DOT/FAA/CT-94/63

FAA Technical Center
Atlantic City International Airport,
N.J. 08405

Proceedings of the 1994 AIAA/FAA Joint Symposium on General Aviation Systems

May 24-25, 1994
Mississippi State University
Starkville, Mississippi



September 1994

Final Report

This document is available to the public
through the National Technical Information
Service, Springfield, Virginia 22161.



U.S. Department of Transportation
Federal Aviation Administration

19950118 046

NOTICE

This document is disseminated under the sponsorship of the U. S. Department of Transportation in the interest of information exchange. The United States Government assumes no liability for the contents or use thereof.

The United States Government does not endorse products or manufacturers. Trade or manufacturers' names appear herein solely because they are considered essential to the objective of this report.

1. Report No. DOT/FAA/CT-94/63	2. Government Accession No.	3. Recipient's Catalog No.	
4. Title and Subtitle Proceedings of the 1994 AIAA/FAA Joint Symposium on General Aviation Systems, May 24-25, 1994		5. Report Date September 1994	
		6. Performing Organization Code	
7. Author(s) Compiled by Gus Ferrara and Roberto DiMichele		8. Performing Organization Report No.	
9. Performing Organization Name and Address American Institute of Aeronautics and Astronautics General Aviation Systems Technical Committee Federal Aviation Administration Technical Center		10. Work Unit No. (TRAIS)	
		11. Contract or Grant No.	
12. Sponsoring Agency Name and Address U.S. Department of Transportation Federal Aviation Administration Technical Center Atlantic City International Airport, NJ 08405		13. Type of Report and Period Covered Proceedings May 24-25, 1994	
		14. Sponsoring Agency Code ACD-210	
15. Supplementary Notes Mississippi State University, Starkville Mississippi			
16. Abstract The 1994 AIAA/FAA Joint Symposium on General Aviation Systems was the result of the combined efforts of the AIAA General Aviation Systems Technical Committee and the Federal Aviation Administration Technical Center. This symposium offered the opportunity to present and review the current state of the art in research that is being conducted in support of general aviation. All told, the papers presented covered the entire spectrum of research, and the participants had the opportunity to hear presentations on everything from alternate fuels to developments in air traffic control.			
17. Key Words Proceedings General Aviation Systems AIAA FAA		18. Distribution Statement Document is available to the public through the National Technical Information Service, Springfield, Virginia 22161	
19. Security Classif. (of this report) Unclassified	20. Security Classif. (of this page) Unclassified	21. No. of Pages 624	22. Price

Foreword

The 1994 AIAA/FAA Joint Symposium on General Aviation Systems was the result of the combined efforts of the AIAA General Aviation Systems Technical Committee and the Federal Aviation Administration Technical Center. This Symposium offered the opportunity to present and review the current state of the art in research that is being conducted in support of general aviation. All told, the papers presented covered a wide spectrum of research and the participants had the opportunity to hear presentations everything from aerodynamics to developments in the air traffic control system.

The FAA Technical Center and the AIAA General Aviation Systems Technical Committee would like to thank the authors for investing the resources needed to prepare the papers which were presented at the symposium and which are contained in this proceedings. We would also like to thank Mr. Bruce Holmes of NASA Langley for giving the keynote address and Mr. Emmett Krauss for the dinner presentation on tort reform. Mr. Mike Cavanaugh and the staff at Mississippi State University deserves credit for providing the administrative support required to host the symposium. Finally, we would like to thank the session chairmen, since their efforts were instrumental in getting the symposium underway. They are as follows:

Dr. George Bennett, Mississippi State University
Mrs. Gail Brinkman, Wichita State University
Dr. Randall Chambers, Wichita State University
Gus Ferrara, FAA Technical Center
Dr. T. David Kim, Embry-Riddle Aeronautical University
Doyle T. Peed, The MITRE Corporation
Dr. Michael Selig, University of Illinois at Urbana Champaign
Dr. Donald T. Ward, Texas A&M University

Accession For	
NTIS	CRA&I <input checked="checked" type="checkbox"/>
DTIC	TAB <input type="checkbox"/>
Unannounced <input type="checkbox"/>	
Justification _____	
By _____	
Distribution / _____	
Availability Codes	
Dist	Avail and/or Special
A-1	

Table of Contents

<u>Title</u>	<u>Page</u>
Author(s), Company/Organization; Co-author(s), Company/Organization	
 <u>Section I: Smart Cockpit/Human Factors I</u>	
<i>A Course Guidance Display and Algorithm Using the Aircraft's Velocity Vector</i>	1
C. R. Wanke, G.W. Flathers, II, E. C. Hahn and R. C. Strain, The MITRE Corp.	
 <i>Data Link Applications for General Aviation</i>	21
S. R. Bussolari, Ph.D., MIT Lincoln Laboratory	
 <i>FAA Certification of a Multi-Purpose Head Up Display (HUD) for General Aviation Aircraft</i>	37
M. W. Anderson, FAA Chicago Aircraft Certification Office	
 <i>Preliminary Conception of an Aircraft Lift Monitoring and Takeoff Advisory System</i>	65
G. A. Bécus and S. Kofman, University of Cincinnati	
 <u>Section II: Design Methodology</u>	
<i>Ducted Fan Propulsion for a General Aviation Replica Fighter Aircraft</i>	71
E. R. Jones, Ph.D., M. Stevens and A. Almeida, Embry-Riddle Aeronautical Univ.	
 <i>The World Class Glider-An International Experience</i>	95
O. W. Nicks, Texas A&M University	
 <i>Introduction of the MH-02 Experimental Aircraft, A Joint Research Program of MSU and Honda</i>	103
H. Nakayama, Honda R&D Company, LTD, Wako Research Center	
G. Bennett, Mississippi State University, Raspet Flight Research Laboratory	
 <i>The Effect of Occupant Crashworthiness Regulation Compliance on General Aviation Aircraft Size and Performance</i>	121
C. N. Eastlake, Ph.D. and J. G. Ladesic, Ph.D., Embry-Riddle Aeronautical Univ.	
 <u>Section III: Smart Cockpit/Human Factors II</u>	
<i>Advanced Flight Controls for General Aviation: An Overview</i>	137
J. Acree, University of Tennessee Space Institute	
 <i>Pilot Workload Assessment and Validity</i>	153
R. M. Chambers and K. J. Kilmer, Wichita State University NIAR	

Table of Contents (cont.)

<u>Title</u>	<u>Page</u>
Author(s), Company/Organization; Co-author(s), Company/Organization	
<i>A Robust Planning Technique for a General Aviation Smart Cockpit System</i> S. G. Pimentel, A. R. Gardner and L. M. Brem, Adriot Systems, Inc.	165
<u>Section IV: Propulsion/Alternative Fuels</u>	
<i>Overview of Automotive Gasoline Usage in Aircraft Engines</i> P. O. Pendleton, FAA Wichita Aircraft Certification Office	177
<i>Ongoing Studies in Unleaded Aviation Gasoline</i> D. H. Atwood, Galaxy Scientific Corporation; A. Ferrara and K. J. Knopp, Federal Aviation Administration Technical Center	203
<i>Comparative Materials Compatibility for Typical Aircraft Fuel System Materials and Components When Exposed to Auto Gas with Candidate Oxygenated Fuel Additives</i> J. J. Thomas, Ph.D., S. E. Adams and E. E. Gordon, Florida Institute of Tech.	219
<i>Alternative Fuels for General Aviation</i> R. Kimberlin and J. Acree, University of Tennessee Space Institute	241
<i>Certification of a Carbureted Aircraft Engine on Ethanol Fuel</i> M. E. Shauck, J. Tubbs, and M. G. Zanin, Baylor University	251
<i>Advanced Technology, Jet-A Fuel Stratified Charge Rotary Engines for General Aviation</i> R. E. Mount, Rotary Power International, Inc.	259
<u>Section V: Aging Aircraft</u>	
<i>A Numerical Study of Aircraft Aging Effects on Transonic Cruise Performance</i> L. C. Santos, Rolls-Royce, Inc.	279
<i>General Aviation Individual Airplane Load Monitoring Program</i> T. DeFiore, FAA Technical Center; D. Kim, Ph.D., Embry-Riddle Aeronautical University	293
<i>The Development of a Regional/Commuter Airline Flight Usage Database to Support a Structural Integrity Management Program</i> F. J. Giessler, A. P. Berens and J. P. Gallagher, U. of Dayton Research Institute	301

Table of Contents (cont.)

<u>Title</u>	<u>Page</u>
Author(s), Company/Organization; Co-author(s), Company/Organization	
<i>Life Cycle Design of Future General Aviation Airplanes</i> J. G. Ladesic, Embry-Riddle Aeronautical University	315
 <u>Section VI: Airspace/ATC</u>	
<i>The Airborne Positioning and Planning System: An Architecture for Future Avionics Systems Design</i> R. C. Strain and G. W. Flathers, II, The MITRE Corporation	331
 <i>Pilot and Controller Perspectives on TCAS II</i> R. F. Ripley, Ph.D. and M. F. Klemm, Ph.D., Auburn University	347
 <i>Integrating Helicopters into the National Airspace System</i> R. D. Kimberlin, Ph.D., University of Tennessee Space Institute	377
 <u>Section VII: Aerodynamics</u>	
<i>A Two Element Laminar Flow Airfoil Optimized for Cruise</i> G. G. Steen, K. D. Korkan, Ph.D. and O. W. Nicks, Texas A&M University	389
 <i>Winglet Performance for High Aspect Ratio Wing Planforms</i> D. Colling, Texas A&M University	415
 <i>Aerodynamic and Aeroelastic Design of the Experimental Aircraft, Honda MH-02</i> M. Fujino, Honda R&D Company, LTD, Wako Research Center	435
 <i>Flight and Full-Scale Wind Tunnel Investigations of Transition Physics on the Wing of a Propeller-Driven Aircraft</i> S. J. Miley, K. H. Horstmann and G. Redeker, German Aerospace Research Establishment, Braunschweig, Germany	461
 <i>Using LEWICE to Predict Deicing and Anti-Icing Requirements for General Aviation Aircraft</i> D. E. Smith, Ph.D., University of Oklahoma; B. R. Mullins, Ph.D., U. of Texas; K. D. Korkan, Ph.D., Texas A&M University	475

Table of Contents (cont.)

<u>Title</u>	<u>Page</u>
Author(s), Company/Organization; Co-author(s), Company/Organization	
<u>Section VIII: Advanced Materials/Manufacturing</u>	
<i>A General Overview of the Fabrication and Quality Control Activities for the Honda MH-02</i>	489
R. W. Sullivan and G. Bennett, Mississippi State University; K. Sato, Honda R&D Company, LTD, Wako Research Center	
<i>Evaluation of Tackifier Agents for Resin Transfer Molding</i>	509
G. Brinkman, C. Cadenas-Montes, R. Phillips and A. Arnold, Wichita State University NIAR	
<i>Crashworthiness Considerations in Aircraft Seat Cushion Design</i>	521
S. J. Hooper, Ph.D., T. Lim, M. Rahematpura, B. Goedken and E. Dakwar, Wichita State University NIAR	
<i>Assurance of the Safety of Flight for the Honda MH-02</i>	535
E. Misumi, Honda R&D Company, LTD, Wako Research Center	
<i>Lightning Protection Technology for Small General Aviation Composite Material Aircraft</i>	553
J. A. Plumer and E. Rupke, Lightning Technologies, Inc.; S. Siddiqi, Analytical Services & Materials, Inc.; T. Setzer, Stoddard-Hamilton Aircraft, Inc.	
<i>Box-And-Beam Carrythroughs of the RP-Series Composite Sailplanes</i>	563
B. E. Thompson, S. Doyle, V. Paedelt and O. Bauchau, Rensselaer Polytechnic Inst.	
<u>Section IX: Flight Test</u>	
<i>Determination of the Stability and Control Derivatives of a Turbo-Fan Research Aircraft Using a Maximum Likelihood Method</i>	579
C. Lewis, P. Bridges and M. Cavanaugh, Mississippi State University	
<i>Overview of Certification and Flight Testing of Primary Category Aircraft Using the Transport Canada TP101-41E Ultralight Design Standard</i>	587
M. W. Anderson, FAA Chicago Aircraft Certification Office	
<i>Procedures for Airspeed Calibration by Use of Global Positioning System</i>	597
H. C. Smith and R. P. Anderson, Penn State University	

Table of Contents (cont.)

<u>Title</u>	<u>Page</u>
Author(s), Company/Organization; Co-author(s), Company/Organization	
<i>Design of a Fully Automated PC Driven Data Acquisition System for an Experimental Aircraft</i>	603
V. G. Chaney, R. L. Lincoln and K. L. Ledlow, Mississippi State University; K. Motoyama, Ph.D. and Y. Otsuka, Honda R&D North America	
<u>Section X: Economics</u>	
<i>The Utilization Rate of General Aviation Aircraft: Recent Developments</i>	613
D. W. Cho, Wichita State University; G. S. McDougall, Southeast Missouri State University	
<u>General Interests/Dinner Presentation</u>	
<i>Revitalizing General Aviation - The Rest of the Story</i>	625
E. F. Kraus, Ph.D., The Cessna Aircraft Company	

A COURSE GUIDANCE DISPLAY AND ALGORITHM USING THE AIRCRAFT'S VELOCITY VECTOR

C. R. Wanke, G. W. Flathers, II, E. C. Hahn, and R. C. Strain
The MITRE Corporation
Center for Advanced Aviation System Development
7525 Colshire Drive, M.S. W273
McLean, VA USA 22102-3481

ABSTRACT

This paper presents a general algorithm for using the aircraft's velocity vector to assist the general aviation pilot in following a course. This velocity vector-based approach to course guidance greatly simplifies the pilot's task of maintaining a desired track, especially in the presence of wind. Until recently, such guidance has been solely available to transport-category aircraft using expensive inertial reference systems, and the accuracies of other available navigation systems have not been suitable to derive an aircraft's velocity vector for guidance applications. As a result, little has been done to provide the general aviation pilot with better course following guidance than lateral error, or displacement, from the desired course. Emerging technologies such as the Global Navigation Satellite System, however, offer the capability to derive an aircraft's velocity vector, along with several other useful navigation parameters, at a reasonable and justifiable cost. Two candidate course guidance displays based on this algorithm are presented, and a planned piloted experiment to evaluate the algorithm and displays is described.

INTRODUCTION

PROBLEM STATEMENT

For decades, pilots have relied on a course deviation indicator (CDI), driven by a VHF radio navigation aid, to navigate along a desired route. The CDI typically provides an angular indication of cross-track error, i.e. how far off-course the aircraft is, becoming more sensitive as the aircraft approaches the transmitting station. CDI displays for area navigation (RNAV) systems such as LORAN may provide a linear indication of course deviation. The CDI, however, does not give the pilot a good indication of how quickly he is closing on the route, or of the impact of winds on route tracking. In addition, ambiguities when using the CDI in a reverse sensing mode (as in a localizer backcourse approach) further complicate the navigation task. As a result, the pilot must apply significant mental computation and trial-and-error to visualize the situation, integrate information from the CDI and other indicators, and determine appropriate corrective actions.

Many of the difficulties with CDI-based guidance could be eliminated or reduced by using track-based guidance. Track-based guidance uses the aircraft's velocity vector (defined by track and groundspeed) in addition to cross-track error and route information to provide the pilot with a track-to-steer (TTS). The TTS tells the pilot explicitly the magnetic groundtrack he needs to fly to acquire and maintain the desired route.

To this point in time, such track-based guidance methods have been restricted to transport-category aircraft using expensive inertial reference systems, and the accuracy of other available navigation systems has not been suitable to derive an aircraft's velocity vector for guidance

applications. However, emerging technologies such as the Global Navigation Satellite System (GNSS) offer the capability to derive an aircraft's velocity vector, along with several other useful navigation parameters, at a reasonable and justifiable cost.

PURPOSE

With the availability of GNSS and affordable computer resources, the means now exists to provide improved route planning and guidance support to general aviation (GA) pilots at reasonable cost. This paper presents a preliminary design for a track-based guidance algorithm and displays for GA application. The algorithm produces lateral guidance, in the form of a track-to-steer (TTS), based on sensed aircraft position, velocity vector, and a preprogrammed lateral route. This TTS is presented on a computer-generated graphical display. The approach presented in this paper strives to achieve task compatibility with normal piloting activities and thereby reduce the pilot's mental workload. If successful, the utility and benefit to the pilot should outweigh any implementation costs. The intent here is not to provide the full range of capabilities associated with a flight director or an autopilot, but to provide supplemental guidance in the form of a TTS.

CONTEXT: THE AIRBORNE POSITIONING AND PLANNING SYSTEM

The guidance technique presented here is one element of a broader concept, the Airborne Positioning and Planning System (APAPS). APAPS is a concept and architecture for organizing cockpit navigation and communication capabilities, based on several newly available technologies including: high-precision navigational sensors, inexpensive computing power and electronic displays, and digital communications. APAPS is designed to simplify piloting activities, while providing a baseline set of capabilities to all classes of aircraft that will allow the aircraft to be more of a participant in the overall air traffic management (ATM) system.

These capabilities include automatic position fixing, basic mission definition and route planning, route guidance, and a digital data communications function that aids the pilot in constructing, sending, receiving, and interpreting routine data communications from ground systems or other aircraft. This includes exchange of position and intent information both between aircraft and ground elements, and possibly between equipped aircraft. An essential feature of APAPS is that it integrates navigation and communication functions, which simplifies the pilot's job. For example, ATC clearance amendments could be transmitted via digital datalink and automatically presented to the pilot in navigation-oriented terms related to his programmed route. Additionally, information known to APAPS can be conveniently packaged and transmitted to outside entities with little or no pilot effort.

A key element of the APAPS concept is that it "sell itself." As mentioned previously, the utility provided by any cockpit system should outweigh implementation costs and thus encourage voluntary equipage. If a large percentage of aircraft equip with the baseline set of APAPS navigation and communication capabilities, then it will be possible to implement some new, innovative techniques for doing air traffic management. For example, by having many more aircraft with an advanced positioning and route planning capability, direct routings could be routinely issued, and much more airspace could be effectively utilized. Further, the present airspace structure could be greatly simplified. Also, if air-to-air position reporting were available, then pilots could use traffic information to maintain situational awareness with respect to other aircraft. This would facilitate the flow of traffic, especially in dense areas.

The APAPS mission definition and route planning capabilities will allow the pilot to establish a mission objective and a waypoint-based route to meet that objective. Coupled with traffic flow and meteorological information from ground systems, the pilot will have the tools and the information he needs to effectively manage his flight. In turn, the pilot will be able to provide the ATM system with more accurate long- and short-term intent information that can be used for coordination and resource planning purposes.

The course guidance function described here is designed to support the pilot in navigating along the planned route. Interested readers are encouraged to see reference 1 for an in-depth description of APAPS and its potential benefits.

OVERVIEW

The following sections present the individual components of the track-based lateral course guidance algorithm (CGA). First design considerations are discussed. Then, two candidate course guidance displays (CGDs) will be presented, with an emphasis on how track-based guidance can simplify the navigation task. Next, the CGA specifically is discussed, in two parts. The CGA has a course acquisition mode, used when the aircraft is far from the desired route, and a course tracking mode, used for error corrections when the aircraft is on or near the route. Finally, a planned piloted flight simulator evaluation of the CGA and candidate CGDs is discussed.

Note that the course guidance function is currently limited to providing lateral guidance only. However, techniques for managing the velocity vector to provide vertical guidance (3D), as well as time (4D) will also be investigated and developed. As an initial step, lateral guidance provides the largest single benefit by giving the pilot cues to capture and track a route efficiently.

DESIGN CONSIDERATIONS

This section addresses the design considerations associated with the lateral course guidance function, both for algorithm and display design. These considerations reflect the operational requirements, constraints, and the simplifying assumptions made in order to execute a preliminary design.

TRACK-BASED GUIDANCE

The CGD should provide information to help the pilot manage his current track, as opposed to heading, and should provide cues which include the effects of wind. By presenting both current aircraft direction and desired aircraft direction as magnetic track (rather than heading), the effects of wind are effectively eliminated. When the aircraft is established on the desired course, the current and desired track will be identical even in the presence of crosswind, although the heading will be different. As a result, the pilot will not have to use trial and error to compensate for winds.

MEASUREMENTS

The guidance function provides the TTS information to the CGD. The TTS is derived using the aircraft position, aircraft velocity vector, and a set of course defining waypoints. For the purposes of design, perfect and continuous measurements of aircraft position, groundspeed, and track angle is assumed to be available. No particular measurement technology was assumed for

initial design purposes. Aircraft attitude information (i.e. pitch and roll angles) are assumed to be unavailable, since adding sensors to accurately measure these quantities would add significant cost and complexity to the guidance system.

The lack of bank angle information complicates the design of the guidance law, since the pilot's response to a commanded track angle change must be modeled. In executing a track (or heading) change, the pilot uses an internal feedback scheme in which he observes bank angle, heading, and heading change rate. In a full lateral flight director, on the other hand, the availability of roll angle information allows generation of more dynamic and immediate cues. The pilot reacts to these cues in a pure gain mode; when the flight director roll bar moves off-center, the pilot simply amplifies the deflection and translates it to a lateral stick/yoke input. So, for this design, a simple model of how the pilot/aircraft system executes a commanded track angle change was developed.

ROUTE INFORMATION

Additionally, it will be assumed that the capability exists for the pilot to construct a desired route and provide it to the guidance algorithm. The route is assumed to be constructed of discrete waypoints, connected by straight segments. At waypoints where a turn is required, circular arc segments (fillets) are inserted. Combinations of circular arc and straight segments may also be used to construct holding patterns, procedure turns, etc.

DISPLAY CONSISTENCY AND FACE VALIDITY

Upon initialization of the function, a TTS should be provided regardless of the orientation of the aircraft. Even for fairly large deviations, a TTS should be provided which aids the pilot in returning to the route in a direct and efficient way. In cases where the orientation and position of the aircraft with respect to the route make it impossible to determine what the active waypoint should be, a TTS should not be provided. In these cases, it is assumed that the pilot's intent does not coincide with his programmed route, and the failure to provide a valid TTS should be annunciated.

The TTS shown should not only enable the pilot to return to and track the route, but it should do so in a way consistent with the pilot's mental model of how that function should be performed. The maneuver generated by a pilot following the TTS should look like, for example, the maneuver performed by a very experienced pilot capturing a VOR radial. The path should be smooth, requiring only moderate bank angles, and should exhibit little or no "overshoot" of the desired route.

Finally, the guidance display should exhibit "face validity," meaning that the TTS should never "jump" or move unnaturally quickly. For example, transitioning between the course acquisition and course tracking modes should be seamless and transparent to the pilot. Similarly, when transitioning along the route from waypoint to waypoint, the TTS should not change abruptly, but should reflect a steady turn.

COURSE GUIDANCE DISPLAY

In this section, two candidate course guidance displays will be described. The first is a "map-compatible" display, that can be used with or without a moving map. The second is based on a more traditional Horizontal Situation Indicator (HSI) format.

MAP-COMPATIBLE GUIDANCE DISPLAY

DISPLAY ELEMENTS. This display is illustrated in Figure 1. Its primary components include an approximately 70-degree, expanded-scale segment of a compass rose from which the pilot can readily obtain track information. The compass rose "rotates" as the aircraft's track changes. The aircraft's instantaneous track is indicated by the "pointer-box" at the top center of the display. The pointer part of the box designates the instantaneous track on the compass rose, and the corresponding digital value (to the nearest degree) is provided within the box. Because air traffic procedures and control information is referenced to magnetic north, it is suggested that track information on the CGD be referenced to magnetic north. This would also be consistent with the coordinate convention used to describe such things as runway direction, instrument approach courses, departure courses, etc. The system translates to magnetic track simply by adding in the local magnetic variation, which can be stored in the navigation database.

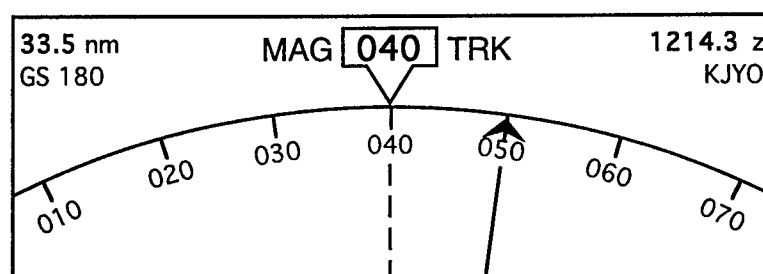


Figure 1. Map-Compatible Course Guidance Display. This display is primarily white-on-black, with the exception of the track-to-steer arrow, which is magenta to indicate a "command" value.

Because the pointer-box always stays at the top center of the display and graphically indicates the current track via the compass rose (which rotates as the actual track changes), this could be called a "track-up" display analogous to the track-up modes used in moving map displays. It should be noted that the CGD is not a moving map display, nor is a moving map display needed to provide the benefits of simplified and more accurate course tracking. However, the CGD could be incorporated into a moving map display if enough display space were available (Figure 2). The authors have implemented this CGD in a simulator both with and without a map display.

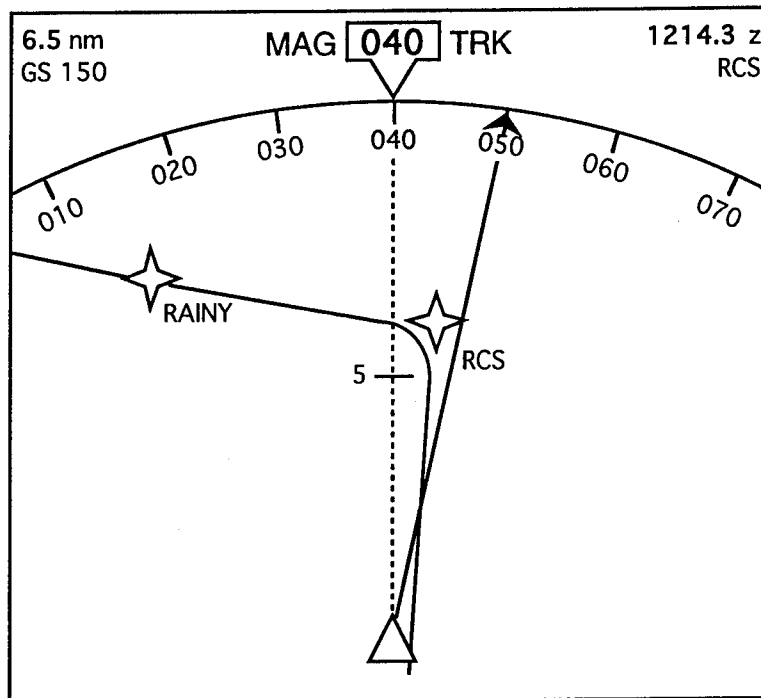


Figure 2. Map-Compatible Course Guidance Display Combined with a Moving Map. In this drawing, the aircraft is slightly to the left of a straight route leg. The route, colored magenta, is composed of straight segments, circular arcs, and star-shaped icons for waypoints.

The second primary component of the CGD is the TTS indication, provided by the arrow pointing to the compass rose from the inside of the compass rose's arc. The arrow simply points to the track on the compass rose to which the pilot should steer in order to achieve his defined navigation objective. The TTS value is produced by either the course acquisition or course tracking algorithms, depending on the aircraft's position with respect to the route. However, as stated in the design assumptions, the source of the TTS is not needed by or apparent to the pilot. Figure 1 illustrates a case where the aircraft is currently tracking 040 degrees, but the appropriate guidance loop is prompting the pilot to alter the track 10 degrees to the right so as to track 050 degrees magnetic. As the pilot makes the turn to the right, the compass rose rotates to the left (with the appropriate digital value updated in the box as the turn is made). In addition, the TTS arrow moves with the compass rose so that as the aircraft's instantaneous track reaches 050 degrees in the pointer-box, the TTS arrow is lined up beneath it (See Figure 3). Note that since the TTS depends on both lateral error and error rate, it will be dynamically changing during this maneuver.

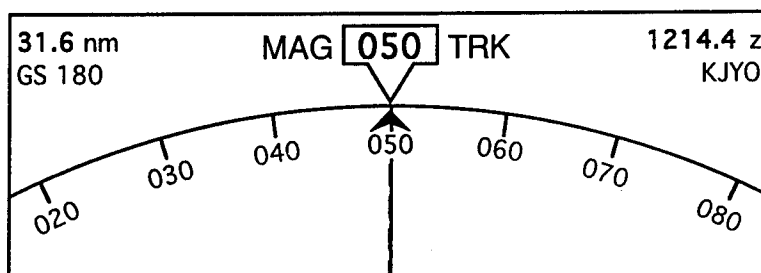


Figure 3. Map-Compatible Course Guidance Display: Aircraft Following the Track-To-Steer

The CGD includes other fields in which ancillary information might be displayed. The field in the upper left corner of the CGD shows the nautical mileage on the course to the next waypoint, and directly beneath it is the current groundspeed. The upper right corner gives the estimated time of arrival (zulu) at that waypoint based on current groundspeed, and below it is the waypoint name. There is room for other information which might be deemed appropriate during test and evaluation of this function, and as mentioned earlier, an investigation will be made on the suitability of providing vertical profile and time-based guidance information on the CGD as well.

STRAIGHT LEG GUIDANCE. From this point on, the pilot's tracking task to stay on defined straight-line courses is greatly simplified - just turn the aircraft left or right as necessary to keep the TTS arrow directly under the pointer-box index. In other words, the pilot maintains the current track consistent with the TTS. As the guidance algorithms determine that a track correction is necessary to stay established on the course, this track correction is portrayed by the TTS moving slightly left or right of top-dead-center, and the pilot simply executes a turn in the appropriate direction and rolls out when the TTS is top-dead-center. When intercepting a straight leg, the guidance algorithms use velocity-vector measurements to produce a TTS that leads the pilot to turn and roll out on the route without overshooting. This process is considerably easier for the pilot than trying to zero-out the angular or linear displacement error via a CDI.

It should be noted, though, that this display should be considered in concert with other displays the pilot may (or should) have to provide general orientation and situational awareness. When considered as a component of the total airborne navigation system, a better assessment can be made on what features should be incorporated into the CGD.

TURN GUIDANCE. In addition to providing enhanced guidance during straight-line course segments, it is also possible for the CGD to provide continuous closed-loop steering guidance to follow circular arcs. Arcs would be used in waypoint transitions from one leg to the next, and as part of procedures such as holding patterns, course reversal procedure turns, arc segments, etc. Figure 4 illustrates one technique for the CGD to provide such information to the pilot. The basic operation of the compass rose and pointer-box remain the same. However, when guidance is being provided to follow an arc, some new elements are added to the display.

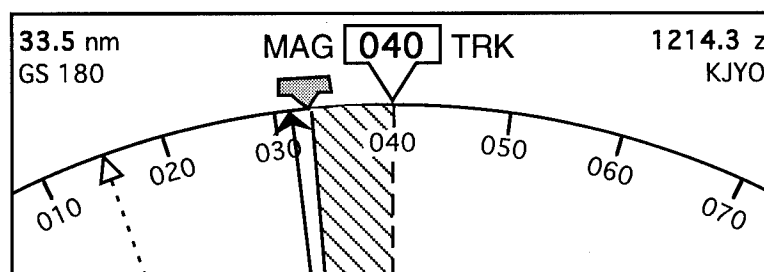


Figure 4. Course Guidance Display for Curved Segments. In this drawing, the pilot is following a left turn, indicated by a patterned magenta wedge extending counter-clockwise from center. The aircraft is slightly outside the turn track, indicated by the TTS displaced slightly to the left of the secondary pointer. This turn ends at a track of 015°, as indicated by a white end-of-turn arrow.

As the aircraft approaches a turn, a magenta wedge is created from the center towards the direction of the turn. It expands smoothly from zero to a value proportional to the required bank angle for the turn. The TTS fulfills the same function as for straight legs, but is now referenced

to a secondary pointer-box at the end of the wedge. In order to track the route in a steady turn, the pilot needs to match the TTS arrow to the secondary pointer-box, while maintaining a steady bank angle in the direction (and approximate relative magnitude) of the filled wedge. Figure 4 shows a situation where the guidance is commanding a left turn, and the aircraft is slightly outside of the arc segment that defines the turn.

As the aircraft nears the end of the turn, a secondary arrow comes into view, indicating the desired track to the next waypoint (the track of the next straight route segment). When the rollout point on the arc is reached, the wedge size decreases smoothly to zero, and the TTS transitions back to straight-leg following mode.

HSI-BASED GUIDANCE DISPLAY

DISPLAY ELEMENTS. Figure 5 illustrates an alternate Course Guidance Display which is based on a standard Horizontal Situation Indicator instrument. It provides information about the track of the current course leg, the lateral deviation of the aircraft from the course, and the track-to-steer required to intercept the course as computed by the guidance logic. This CGD was developed to create an intuitive context for those pilots already familiar with an HSI.

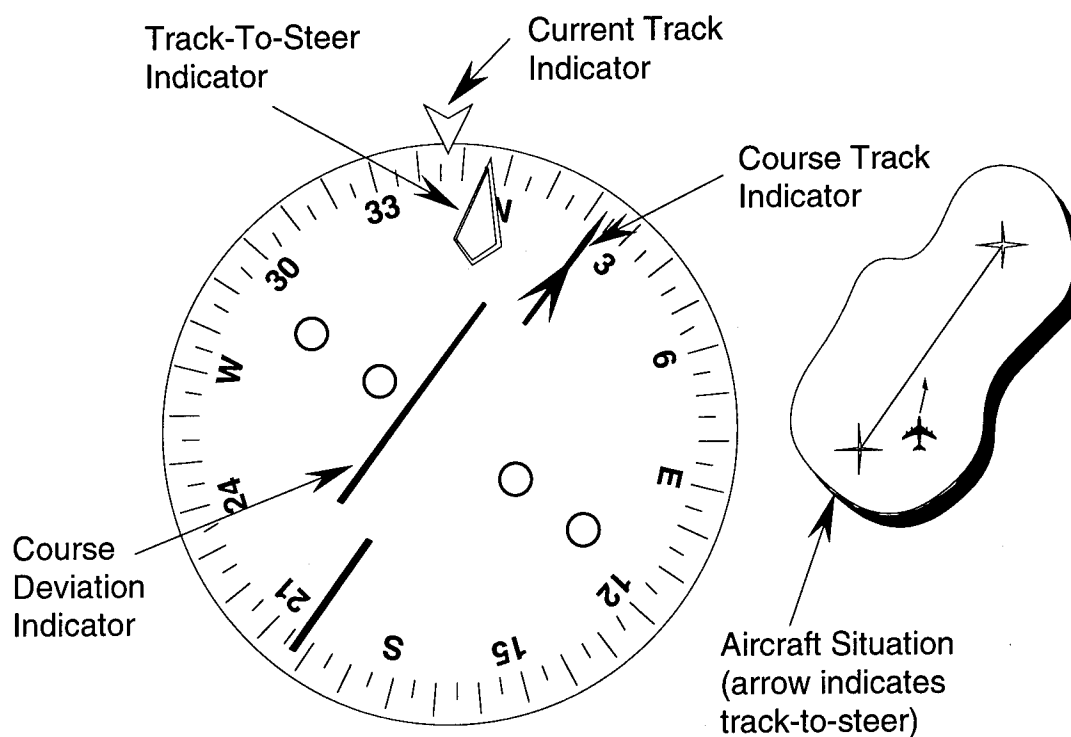


Figure 5: HSI-based course guidance display. In this display, a CDI is used to indicate lateral displacement from the route, while the TTS is used to guide the aircraft back to the route. As before, the display is white-on-black except for the magenta TTS arrow. The secondary data (ETA, distance, groundspeed) is also present on this display, but is absent from the drawing.

STRAIGHT LEG GUIDANCE. Figure 5 illustrates a situation where the aircraft is to the right of and is intercepting a straight route leg, and the guidance logic is commanding a slightly shallower intercept. Note that the CDI in this display would be used to show lateral cross-track error directly in distance units, rather than in angular units; in this way, the CDI sensitivity does not change as a function of range from a waypoint or transmitter. However, the CDI scale could

be changed to reflect the current navigation situation. For example, the maximum needle deflection on final approach would reflect a much smaller error than the maximum needle deflection when tracking an enroute leg. For example, if the display is based on GPS measurements, TSO C-129 specifies the appropriate full-scale values.

It should be noted that there is one major difference between this display and a standard HSI, in that the CGD is referenced to the aircraft track rather than the aircraft heading. This makes the CGD inappropriate as the primary heading indicator. However, it is believed that pilots are able to adapt to the track-up indication without difficulty. For example, users of existing Loran and GPS receivers must already take into account the difference between track and heading.

TURN GUIDANCE. During turns, the Course Track Indicator slews smoothly from the current leg course track to the new leg course track. This indicates to the pilot that a turn is in progress, and that a constant bank will be required to keep up with the TTS arrow. An optional display element (not shown) is a secondary arrow indicating the track which will be achieved at the end of the turn. Note that on a standard electromechanical HSI, slewing of the Course Track Indicator would be performed manually by turning a knob.

The display as initially defined does not provide any advance anticipation of turns; this may be added in the form of a turn arrow or other symbol.

COURSE GUIDANCE ALGORITHM

The course guidance function is partitioned into two modes, with commensurate yet different objectives. The two modes are referred to as the *course acquisition mode* and the *course tracking mode*. The objective of the course acquisition mode is to provide basic cues when the aircraft is far from the route, in order to bring the aircraft into the general area of the route. Once in the area, the course tracking mode provides cues for close-in capture and tracking. Together, these components provide seamless TTS information to the CGD. The modes will be discussed separately in the following sections.

COURSE ACQUISITION MODE

A hypothetical route illustrated in Figure 6 was used during development of the course acquisition mode. In addition to the route itself and a sample aircraft position, all of the parameters used to calculate the TTS are shown. The active leg is chosen based on the position of the aircraft relative to the bisector angle between two adjacent legs. In the case illustrated in the figure, the active leg lies between waypoints WPT01 and WPT02.

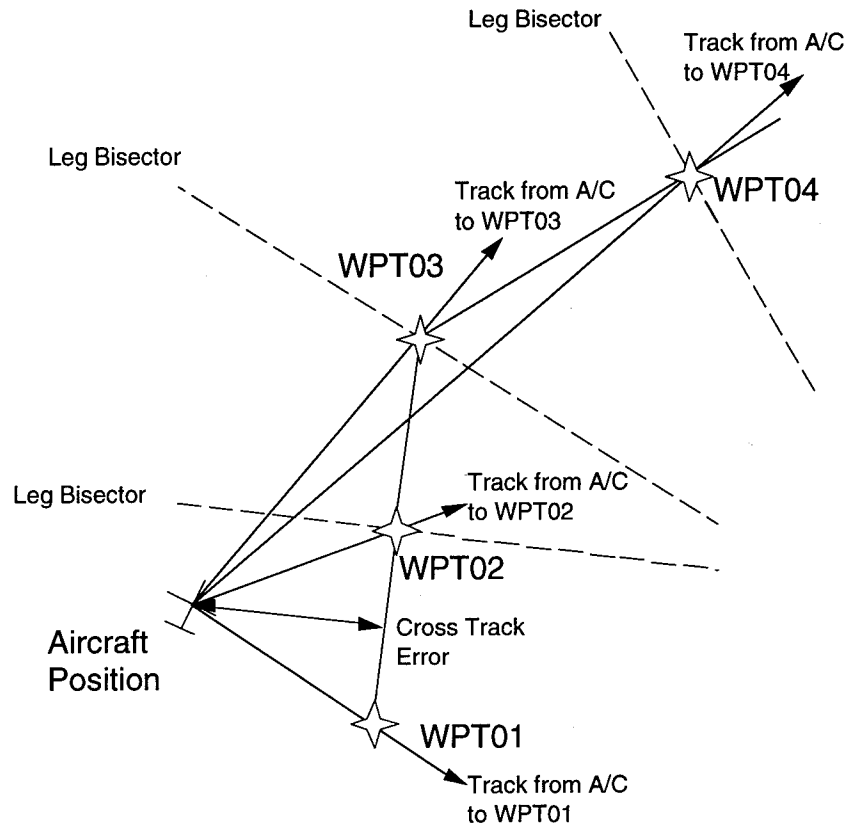


Figure 6. Hypothetical route with guidance parameters.

The guidance algorithm uses relative angles as opposed to explicitly using track or heading values. This generalization ensures that the algorithm can accommodate all possible course orientations. In the figure, for instance, it is determined that the aircraft is left of the active leg between waypoints WPT01 and WPT02 because the relative bearing to WPT02 is greater than the relative track between the waypoints (all angles referenced clockwise). Using relative angles also simplifies the task of deriving an appropriate TTS to comparing and adding several angular differences.

The decision tree used in the course acquisition mode is illustrated in Figure 7. In the simplest case, once the active route leg has been determined, the logic computes an intercept angle proportional to the lateral error. If this angle is less than the maximum intercept angle used by the course tracking mode (discussed in the next section), then the aircraft is assumed to be close enough to the route, and the course tracking mode is engaged. The remainder of the logic handles more specific cases, such as steering for the first waypoint and segment transitions.

The acquisition mode, since it is active only when the aircraft is far from the route, treats all route legs as straight lines. If the aircraft passes a waypoint when the course acquisition mode is active, the guidance will simply switch to the next leg without providing turn entry and exit cues on the display. These are only used in the course tracking mode. Also, because certain course properties do not exist for some waypoints, the acquisition mode must handle these as special cases. For example, there is no next leg after the second to last waypoint, and no leg bisector exists at the first or last waypoint.

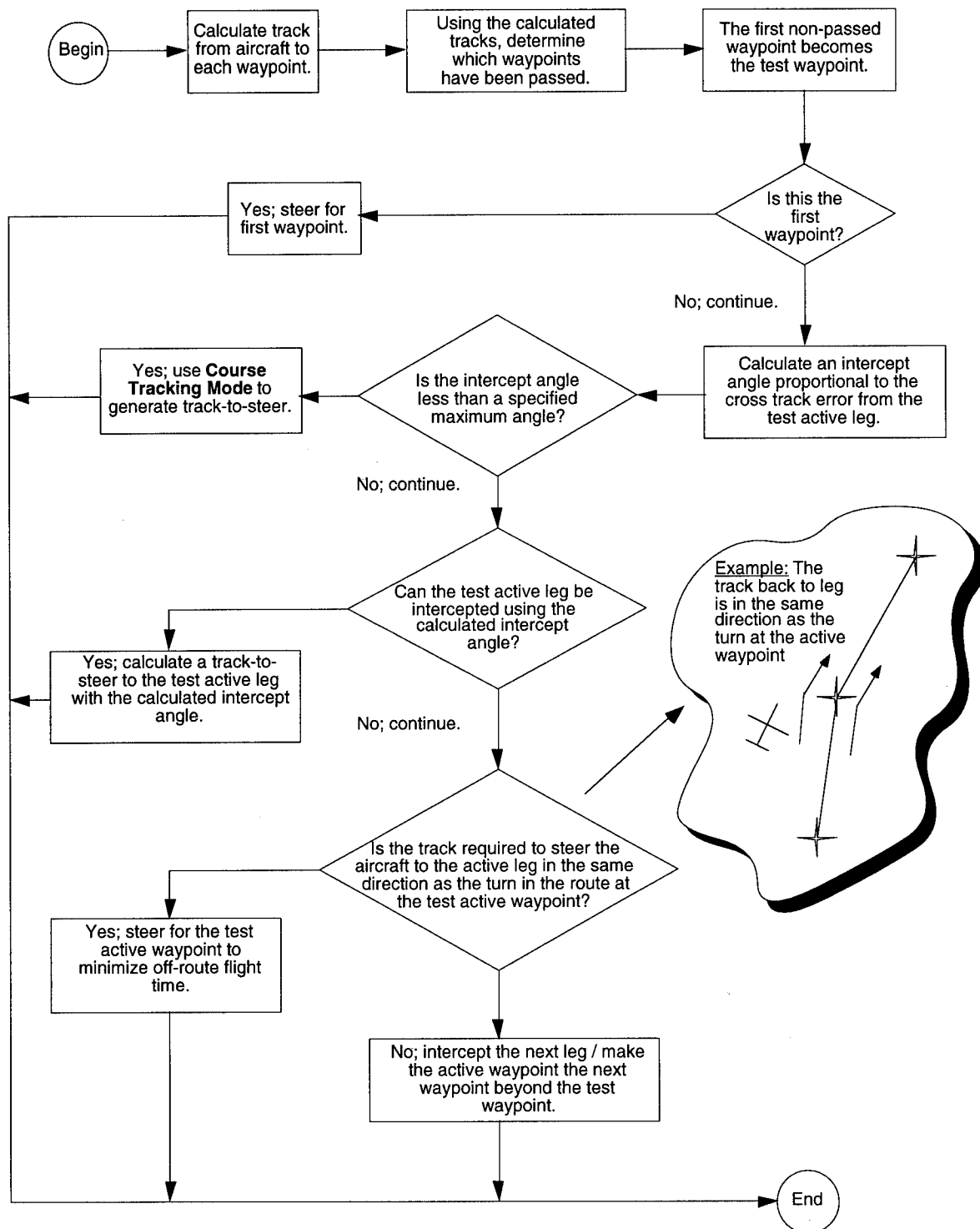


Figure 7. Logic diagram of course acquisition mode.

COURSE TRACKING MODE

The course tracking mode provides tactical guidance to the pilot to enable him to easily track a desired route once acquired. The following sections describe, in general terms, the design of the course tracking algorithm for a lateral course composed of straight and circular arc segments. Detailed description of the design techniques used can be obtained from the authors.

ROUTE CHARACTERISTICS. As mentioned previously, it is assumed that the programmed route can be approximated by straight lines and circular arc segments (Figure 8). This simplifies the guidance laws greatly. Two errors are introduced by this assumption. First, small lateral errors are introduced during turn entry and exit, as the aircraft rolls into or out of the bank required for the turn. Second, circular turns in the presence of wind require slight changes in bank angle during the turn; a constant-bank turn in the wind would not be quite circular. Neither of these errors should have a significant effect on navigation performance. The turn entry and exit errors are alleviated by a feed-forward bank command, which will be described below.

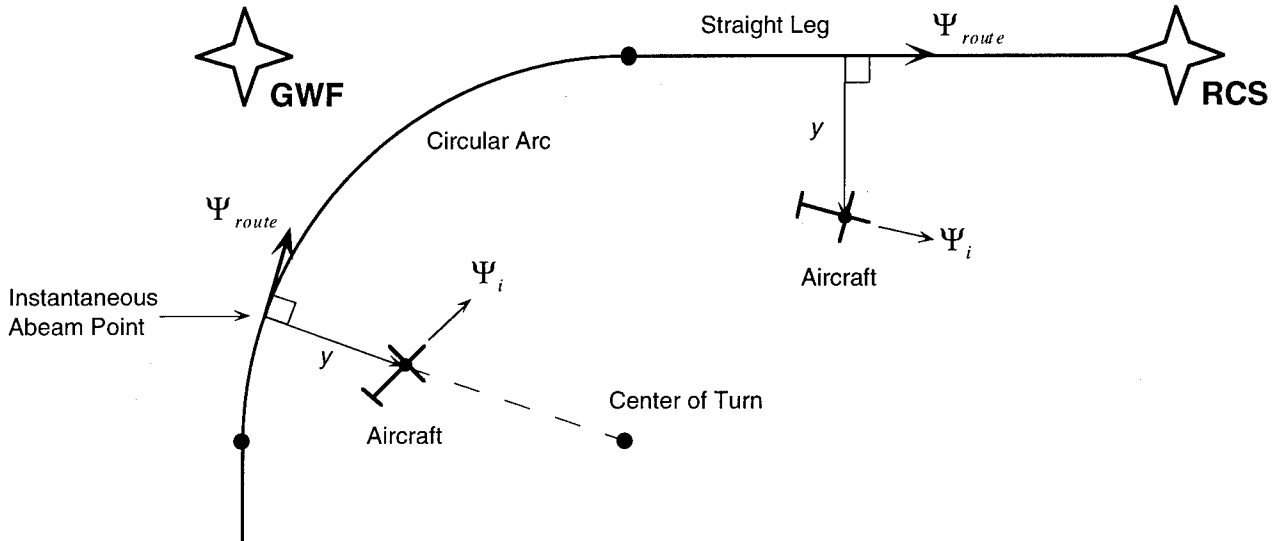


Figure 8: Generic route geometry. Shown is a 90° right turn and ensuing straight leg.

LATERAL ERROR AND ERROR RATE. Lateral route error, y , is computed directly from position measurements. For straight route legs, the error is computed by projecting the aircraft position perpendicularly to the leg. For arcs, a line is drawn from the turn center through the aircraft, and the computed distance between the aircraft and the arc segment is the error. Instantaneous lateral error rate, \dot{y} , is computed from:

$$\dot{y} = U_o \sin(\Psi_i - \Psi_{route}) \quad (1)$$

where groundspeed is U_o , the aircraft track is Ψ_i , and the route leg track at the instantaneous abeam point from the aircraft (see Fig. 8) is Ψ_{route} . Note that the aircraft's groundspeed and track angle come from the velocity vector measurement.

PILOT MODELING. In order to design a feedback law to give dynamic pilot cues, a simple model of pilot response to a TTS command was constructed. It is assumed that the pilot will always attempt to steer exactly to the presented TTS. Therefore, the pilot/aircraft system can be essentially modeled as a track angle servo-controller with a time delay. The parameters of the model are (1) a time lag between presentation of a new TTS and the initial pilot action, (2) a maximum roll angle to be used in turns, and (3) a time constant for the rolling motion of the aircraft. From these parameters, a pilot "servo gain" is computed which produces a well-damped track change response with a very small overshoot. For initial design, the model parameters were chosen from experience; refinement of these parameters through a simple piloted simulation is planned. Details of the pilot model are available from the authors.

GUIDANCE LAW FORM. Figure 9 illustrates schematically the dynamics of the course tracking task. The guidance law uses both lateral error and error rate, and can be expressed as a proportional-plus-derivative linear feedback rule:

$$\Psi_{TTS} = \Psi_{route} - \frac{K_{\dot{y}}}{U_o} \dot{y} - \frac{K_y}{U_o} y \quad (2)$$

where Ψ_{TTS} indicates the TTS, K_y is the lateral error feedback gain, and $K_{\dot{y}}$ is the lateral error rate gain. Note that the feedback gains are normalized by the groundspeed. This is due to the groundspeed multiplier in the lateral error equation (1). This normalization ensures that the guidance cues will be appropriate for the current groundspeed, and produce similar pilot/aircraft course tracking performance at any reasonable groundspeed.

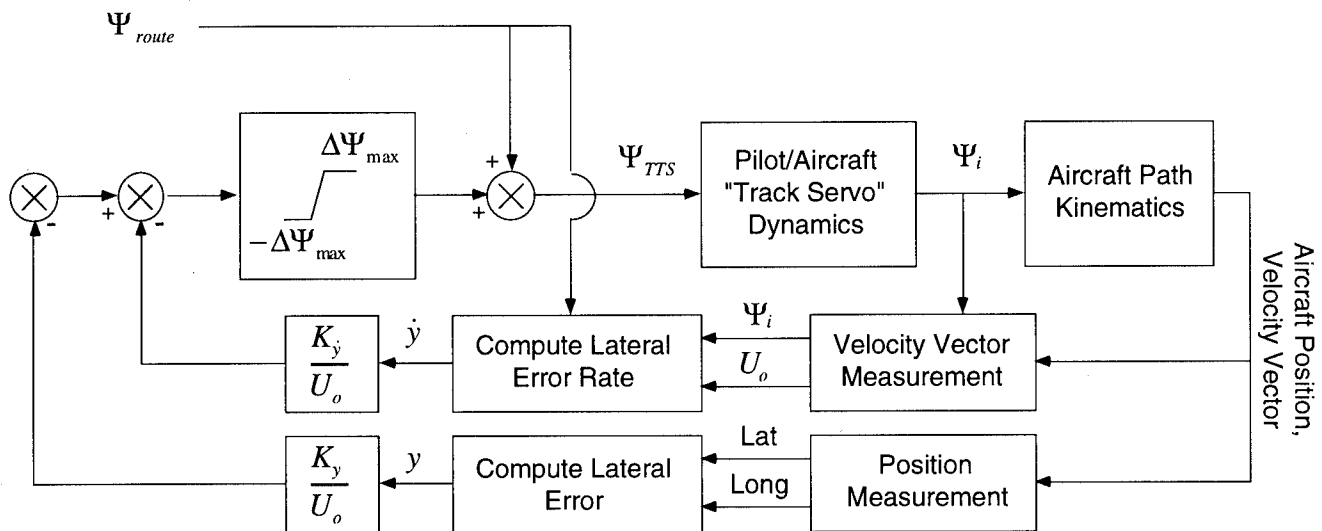


Figure 9: Capture and Maintain Guidance Structure.

Also, as shown in the diagram, the maximum commanded track change (due to the feedback terms) is limited to some maximum angle $\Delta\Psi_{max}$, typically about 30° . This corresponds to the maximum intercept angle that is commanded for large initial lateral errors. To ensure smooth transition between course acquisition and course tracking modes, this maximum angle should

correspond to the standard intercept angle used in the course acquisition logic. Otherwise, the TTS will "jump" as the aircraft approaches the route and transitions to the course tracking mode.

STRAIGHT SEGMENT TRACKING. The straight route segment tracking problem was used for initial selection of the feedback gains. Using linear models of the pilot/aircraft track response and the aircraft dynamics, standard frequency-domain control design techniques were used to determine feedback gains which satisfied the following desired characteristics and constraints:

- Gradual, continuous guidance cues
- Course capture with low overshoot (i.e. a well-damped response)
- No residual steady-state lateral error
- No excessive bank angles required to capture the course from the largest possible intercept angle

The resulting algorithm was simulated, using the same pilot model assumed for design purposes. Results for a sample case, in which the aircraft is given an initial lateral error of 1 nmi from a straight segment, are shown in Figure 10.

TURN SEGMENT TRACKING. Circular arc turn segments add some complexity and tradeoffs to the algorithm design. The straight segment feedback algorithm can be used essentially unchanged to provide TTS cues, except that y and Ψ_{route} must be computed differently for arc segments (this is shown in Figure 8). The TTS cues alone, however, are not sufficient to prevent "overshooting" the turn at the entry point and overturning at the exit point, since the pilot has no prior warning that he is about to enter or exit an arc segment. For this reason, some anticipatory guidance, or "feedforward" guidance, is required.

There are two initially apparent schemes for providing this information. One way is to use knowledge of upcoming changes in Ψ_{route} to modify the Ψ_{route} input to the guidance algorithm, shown in Figure 9. For example, the aircraft position could be projected ahead in time, and Ψ_{route} computed from this predicted position. The advantage of this technique is that it does not require any modification to the guidance display; the anticipation cue is built into the TTS value. However, this implementation would require a fairly complex algorithm, based heavily on an assumed model of how the pilot would react to advance changes in TTS. Also, it would be difficult for the pilot to differentiate a turn anticipation cue from a lateral error cue, which could lead to confusion.

An alternative method is to completely separate turn cues from error feedback, by using different elements of the guidance display. In this method, the TTS is always generated from the current lateral error and error rate, as in Figure 9. A separate bank angle feedforward cue alerts the pilot when to roll into and roll out of turns.

The map-type guidance display (Figure 4) will be used for illustration. When the aircraft approaches a turn segment, as measured by the projected "abeam" point on the current straight route segment, the bank angle required for the upcoming turn is computed based on the current groundspeed. When the aircraft comes within a preset time-to-roll of the turn point, a magenta arc appears on the guidance display and smoothly increases to the bank angle required for the turn. During the turn, this arc is recomputed periodically to reflect changing groundspeeds.

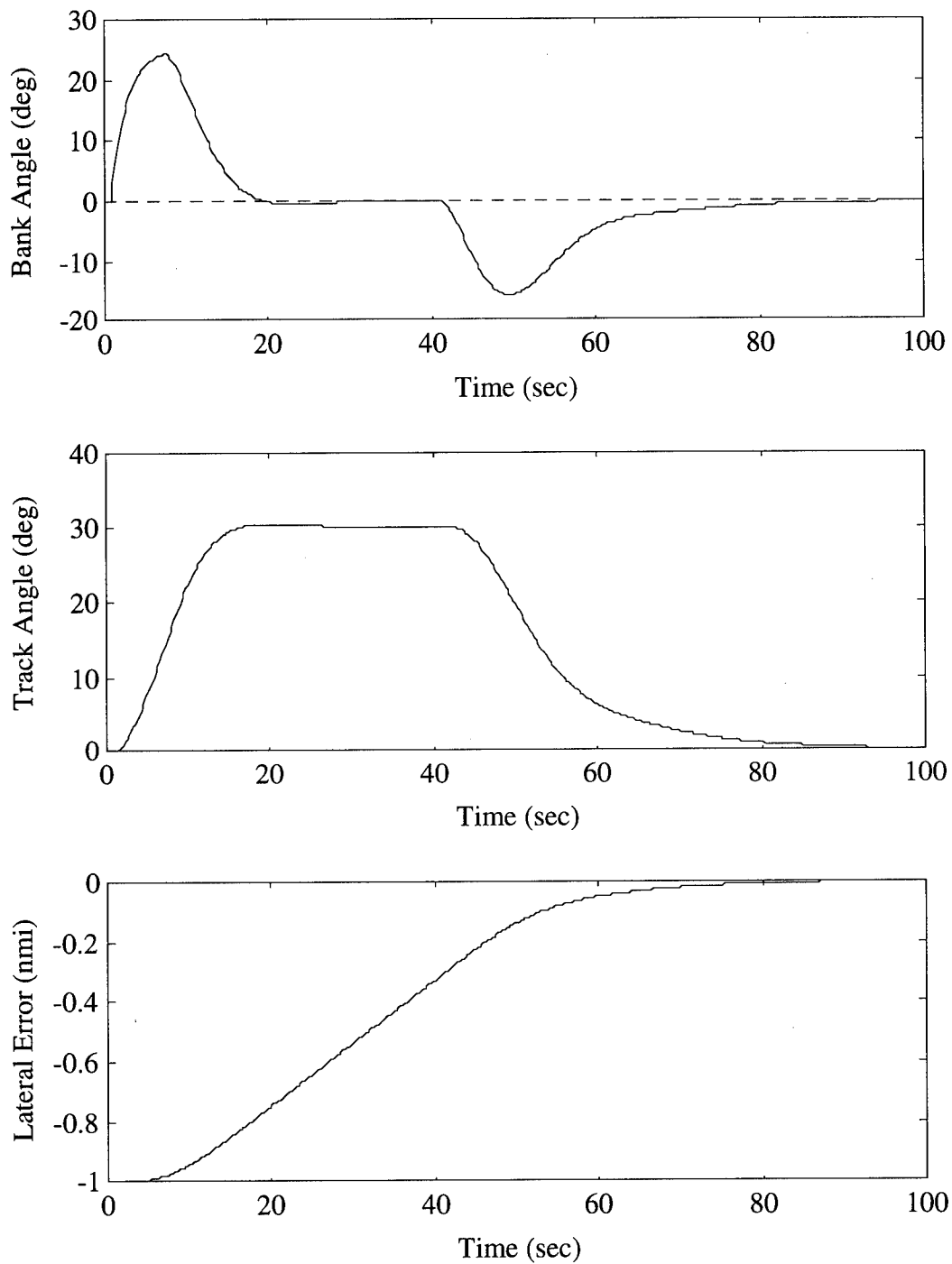


Figure 10: Simulated capture maneuver to a straight course leg. The aircraft was initially displaced 1 nmi from the course, flying parallel to the course, and with a groundspeed of 150 knots. Note the initial turn to a 30° intercept track, and the smooth return to the desired track when the course leg is acquired.

Finally, when the end of the turn segment approaches, the bank arc decreases to zero to indicate that the pilot should begin rolling out on the course to the next waypoint. An additional cue for turn end is provided by drawing a white final track arrow on the compass rose, to indicate the desired track at the end of the turn.

During the turn, the pilot uses the combination of the standard error-driven TTS indication and the bank cue for guidance. When the aircraft track pointer coincides with the TTS, and the aircraft bank angle corresponds to the bank angle cue, the aircraft is properly established in a steady-state turn. It is not expected that the pilot would read off the exact bank angle called for by the wedge, but that after some practice, the approximate size of the wedge would serve as a quick visual reference for the relative magnitude of the turn.

APPLYING A DEADBAND. Some preliminary evaluation of the algorithm was done by the authors using a fixed-base simulator. One major characteristic noted was that although the algorithm was effective at aiding the pilot in locating and intercepting the programmed route, it was perceived as being too sensitive to small route deviations. For this reason, a “deadband” was applied to the lateral error. When the aircraft is within some preset distance of the route (a distance of 0.1 nm appeared reasonable at groundspeeds of 140 knots) the lateral error is set to zero in the feedback equation (Eqn. 2), and the computed TTS stays close to the track of the current route leg. It is not exactly equivalent, since the lateral error rate may be non-zero. This deadband prevents the guidance from commanding corrective actions when the aircraft is “close enough” to the route such that no corrective action is really needed.

In order to prevent jumps in TTS when the aircraft crosses into and out of the deadband region, the constant deadband value must also be subtracted from the lateral error when the aircraft is outside the region.

FURTHER DESIGN AND EVALUATION ISSUES

The design discussed above was done for preliminary evaluation. A final version for field use would need to take into account some other constraints, and undergo piloted evaluation. These additional issues are discussed below.

SENSOR CHARACTERISTICS. Real-world sensor systems have limited accuracy and a finite update frequency, both of which impact the potential performance of the guidance algorithm. A typical, low-cost Global Positioning System (GPS) receiver for general aviation use advertises positioning errors of 15 meters SEP and velocity errors of 0.1 knots rms. Data is typically updated at 1 Hz. The 1 Hz update frequency adds a delay to the guidance loop, and the limited accuracy will introduce some noise into the guidance algorithm output. In addition, these error numbers assume that GPS Selective Availability is inactive; if Selective Availability is on, then the errors increase substantially (typically 100m 2 drms for lateral positioning).

These errors need to be simulated and accounted for in the design. Time delays of 1 second are already tolerated well by the specific design discussed above, but noisy measurements have not yet been considered. A filtering algorithm is probably necessary to alleviate noise effects, and to smooth the position and velocity signals between 1 Hz samples. A low-order, linear Kalman filter should be sufficient to handle both of these problems.

PILOT MODELING FOR DESIGN. The assumed pilot/aircraft track following model is useful for design purposes, but is not intended to accurately represent a human pilot for evaluation

purposes. Piloted evaluations are essential for both algorithm and display development. A piloted study is discussed in the following section.

Also, the pilot model used in the design of the course tracking mode has several parameters that were chosen arbitrarily. These parameters could be better selected if actual flight or simulation data were available. Another (simpler) piloted simulation experiment, in which the pilot/aircraft system is measured during a series of heading changes, may be done to obtain better parameters for the model.

PHASE OF FLIGHT SCHEDULING. It might be desirable to alter the characteristics of the algorithm to account for the phase of flight. For a simple example, the deadband value should be smaller during terminal maneuvering than for enroute legs. If this guidance algorithm were used to steer the aircraft onto an instrument approach, then the deadband should probably be reduced to zero in that phase of flight. The other guidance parameters (feedback gains, maximum intercept angle) might also be adjusted by flight condition to fine-tune the algorithm's performance.

PLANNED PILOTED EVALUATION STUDY

OBJECTIVES

There are two primary goals of this study. The first one is to determine the advantages, if any, of the track-based guidance strategy over a standard, CDI-based radio navigation system. In general terms, this will be evaluated in terms of pilot workload, route-tracking performance, and situational awareness. These quantities will be evaluated through a combination of subjective and objective measures.

The second goal is to obtain data for developing an improved course guidance display format, for use with further development of the guidance function and of the APAPS interface in general. These data will include subjective pilot comments as well as objective observations of which displays yield better route-tracking performance.

TEST PLAN

There will be four configurations tested:

- Two VHF NAV radios only (the "control" configuration). Both radios include VOR and DME, and one radio has an ILS receiver.
- The map-compatible CGD alone.
- The map-compatible CGD with moving map display of the route.
- The HSI-based CGD.

All other instrumentation will be the same, and the pilot will have the appropriate paper charts in all configurations. Each experimental subject will fly each configuration on two routes. The two routes are being constructed to include several turn segments of varying magnitude, a procedure turn, and winds of several different directions and magnitudes. These routes can be flown using standard VHF navigation procedures (i.e. an area navigation capability is not required). In addition, a practice scenario with three short route legs has been constructed.

The experimental procedure will begin by briefing the pilot on the APAPS architecture and on the role of the guidance algorithm within that architecture. A demographic questionnaire will be administered, and the features of each of the CGDs will be explained. The subject will then be asked to fly the simulator for practice, both without a route (to get a feel for the handling and performance qualities of the aircraft) and with the practice scenario, using all four display configurations. Next, the subject will fly both test routes with each of the displays, for a total of 8 flights. The order in which these occur will be counter-balanced between subjects to attenuate learning effects. Finally, the pilot will be given an exit interview consisting of informal discussion and a written questionnaire.

The subjects for this experiment will be general aviation pilots from a wide range of experience levels. An IFR rating will not be required of all subjects, although the experiment will be conducted in instrument meteorological conditions (IMC). This is to allow evaluation of differences in preference and performance between IFR-rated and VFR-only pilots. The number of subjects that will be required has not yet been determined.

EXPERIMENTAL SETUP

The evaluation will be done in a fixed-base part-task flight simulator at the MITRE Corporation's Center for Advanced Aviation System Development in McLean, VA. The simulator uses computer-generated instrumentation and a custom flight model to replicate a wide range of aircraft classes and types. For this experiment, the simulator flight instrumentation and performance characteristics are configured as a Cessna 182RG, a four-place, single piston-engine powered GA aircraft with retractable landing gear. A sidestick and throttle serve as primary controls. Although this is not a typical GA configuration, in a direct comparison evaluation such as this one, the results should not be measurably affected.

Secondary flight controls (flaps, gear) and buttons for the navigational radios are simulated on a color touchscreen display. An out-the-window visual system is available, but will not be used for this experiment since the aircraft is assumed to be in IMC for the duration of the flight. The standard instrument layout includes two VHF navigational radios and the associated CDI displays, in standard 3" square instrument slots. The candidate course guidance displays to be evaluated are presented in place of the second CDI display.

EVALUATION METRICS

A combination of objective and subjective data will be collected. Subjective data will be obtained from the exit interview and questionnaire, and from pilot comments during the experiment. These will be used to gain insight into such issues as how the pilot uses each feature of the displays, which features are desirable and which are undesirable, and which maneuvers give the greatest difficulty with each display. A subjective workload evaluation may also be administered.

The primary objective measure of display effectiveness will be recorded values of lateral route error along straight route legs, during intercept maneuvers, and during turns. Also, total effort used in lateral control of the aircraft (lateral stick motions) will be measured, and may yield some indication of the workload required to maintain route tracking.

VALIDATION

Once the simulator experiment is completed, and the course guidance displays and algorithms have been refined based on the experimental results, the next step will be flight testing. A prototype APAPS implementation is currently under development. The prototype runs on a laptop computer with a display mounted on the control yoke, and uses a GPS receiver for position and velocity measurement. Plans are to fly the same routes as used in the simulator experiment, and to evaluate the results using a similar set of metrics. The goals of the flight test are: (1) to provide supporting evidence for the simulator results, and (2) to identify real-world factors that may impact navigation performance or display design, and that were not discovered in the simulator-based experiments.

SUMMARY

A method has been presented for providing GA pilots with track-based lateral route guidance, based on measurements of the aircraft position and velocity vector by an advanced positioning system such as GNSS. Track-to-steer (TTS) cues are presented to the pilot on an electronic display, who simply steers his own ground track (also shown on the display) to match the TTS. This track-based guidance technique is simpler to use than CDI-based error displays (such as that used in VOR navigation) since it reduces the mental computation required to capture a route and to compensate for the effects of wind. Also, the method presented here can be used to provide guidance for curved paths such as waypoint leg transitions, procedure turns, and holding patterns. The guidance function is one part of an overall architecture, the Airborne Positioning and Planning System, which integrates a basic set of mission building, navigation, and communication functions to aid the pilot.

Two candidate graphical course guidance displays (CGDs) have been developed. One of these uses an expanded compass rose segment and can be used in conjunction with a moving map, and the other is based on a standard HSI. A two-mode lateral guidance algorithm has been developed to drive these displays, based on position and velocity vector information. An experiment has been planned to compare the track-based guidance technique with standard radio navigation using CDI-based displays, and to select an effective format for the CGD.

Work will continue in order to refine the course guidance algorithm and CGD. The effects of sensor errors for the specific case of GPS measurements will be addressed, and a filtering algorithm will be developed if required. In addition to lateral guidance, vertical guidance will be developed to assist the pilot with vertical speed targets.

REFERENCES

1. Strain, R. C., and G. W. Flathers, II, "The Airborne Positioning and Planning System: An Architecture for Future Avionics Systems Design." , *3rd Joint AIAA/FAA Symposium on General Aviation Systems*, Starkville, MS, May 24-25, 1994.

DATA LINK APPLICATIONS FOR GENERAL AVIATION

Steven R. Bussolari, Ph.D.
MIT Lincoln Laboratory
Lexington, Massachusetts

ABSTRACT

The Mode-S data link is a high capacity air / ground digital communications system that can deliver information to the cockpit in a form that will significantly improve pilot situational awareness and aircraft utility. The FAA is deploying Mode-S surveillance sensors with data link capability at 143 sites across the United States. Two Mode-S data link applications: Traffic Information Service and Graphical Weather Service have been developed to meet the specific needs of General Aviation (GA). Traffic Information Service uses the surveillance capability inherent in the Mode S sensor to provide the pilot with a display of nearby traffic. Graphical Weather Service provides a means to deliver real-time weather graphics to the cockpit. Additional Mode-S data link applications, including the broadcast of local area differential corrections for the Global Satellite Navigation System (GNSS) and the use of the Mode-S squitter for Automatic Dependent Surveillance Broadcast (ADS-B) also offer significant benefits to GA. Low-cost avionics have been developed to support these, and other Mode-S data link applications for General Aviation.

INTRODUCTION

Among the most important information that affects the situational awareness of pilots of both transport and general aviation aircraft is the relative location of nearby aircraft and the location and severity of hazardous weather. The flight crews of transport category aircraft have a variety of on-board systems to assist them with maintaining situational awareness of traffic and weather. The Traffic Alert and Collision Avoidance (TCAS)¹ system provides transport crews with a display of traffic and issues resolution advisories that suggest maneuvers to avoid an imminent collision. Airborne weather radar detects hazardous weather well ahead of the aircraft. Dedicated airline dispatchers and staff meteorologists on the ground are available on a company VHF voice radio frequency. The ACARS VHF data link provides the airline crew with text weather products, airline operations information, and pre-departure Air Traffic Control (ATC) clearances.

In contrast, the general aviation pilot faces the demanding task of flying the aircraft, operating the navigation radios, communicating with Air Traffic Control, and interpreting the verbal weather reports from a Flight Service Station, often without the benefit of a second crew member to share the load. While a transport pilot may spend a small fraction of a flight in the region below 10,000 feet (3000 m) where most of the adverse weather is found, a GA pilot typically spends the entire flight there.

Like their counterparts in the transport aircraft, the proficient GA pilot constantly searches for information to support decision making during the flight. ATC communications are monitored for valuable "party line" information pertaining to the current weather or traffic situation. When cockpit workload permits, the pilot may contact a Flight Service Station by voice radio for an update on the weather. An ATC controller may provide verbal reports of nearby traffic and may pass along valuable reports from pilots who have been through the weather ahead. Too often, even these limited sources of information are unavailable. Pilots not on an instrument flight plan are least likely to receive voluntary verbal traffic advisories when the traffic is heavy and the ATC controller is busy. When a line of storms passes through the area, the Flight Service Station VHF voice radio frequencies become saturated with requests for weather information, making it difficult for the pilot to obtain an update of the situation.

This research is sponsored by the Federal Aviation Administration

The technology currently available to the GA pilot is either limited in capability or costly. For instance, the cost of TCAS avionics exceeds the total value of a typical GA aircraft. Less expensive on-board weather detection alternatives (e.g., lightning detectors) can provide useful severe weather information, but have limited range and accuracy, and are subject to interference that produces missed detections and false alarms. Digital air / ground data link can provide a means by which the GA pilot can obtain routine and safety-critical information in flight.

In 1992, the FAA organized the Data Link Operational Requirements Team (DLORT) and gave it the responsibility to develop an operational concept for the introduction of digital data link in the National Airspace System. The DLORT identified a hierarchy of services that would be provided to pilots by data link: Air Traffic Management Services, Flight Information Services, Navigation Services, and Surveillance Services. Air Traffic Management Services (ATMS) are defined as the information currently exchanged by voice between Air Traffic Controllers and pilots (route clearances, altitude assignments, etc.) as well as data link communications that support future air traffic automaton (route negotiation, automatic sequencing, etc.). Flight Information Services (FIS) are defined to include weather text and graphics, Notices to Airmen (NOTAMS), and other information that is currently obtained by telephone or voice radio from a Flight Service Station. Navigation Services include the broadcast of differential corrections to the Global Navigation Satellite System (GNSS) to permit precision instrument approaches with satellite navigation to many GA airports. Surveillance Services include traffic information derived from ground-based radar systems and the automatic broadcast of position information by individual aircraft (Automatic Dependent Surveillance Broadcast or ADS-B). The DLORT selected the following services for nationwide implementation in the years 1996-2000: Basic Air Traffic Management Services, Basic Text Weather Products, Automatic Downlink of Pilot Weather Reports, Traffic Information, and Weather Graphics.

In order to be useful for GA, the services above require a digital air / ground data link of sufficient capacity to permit the participation of many thousands of aircraft. The required data link avionics must also be suitable for installation in typical GA aircraft, they must be affordable and easily used in single-pilot flight operations, and data link applications must be tailored to the flight regimes and specific needs of the GA pilot.

THE MODE-S DATA LINK

The Mode-Select (Mode-S) secondary radar surveillance system ² includes an integrated, high capacity, digital data link function. One Hundred Thirty-Seven Mode-S sensors are being deployed nationwide to replace the aging Air Traffic Control Radar Beacon System (ATCRBS) sensors. Figure 1 illustrates the basic components of the Mode-S data link. The Mode-S sensor, with its rotating surveillance antenna, is capable of transmitting approximately 1500 bits of data to an aircraft equipped with a Mode-S data link transponder—each time the antenna beam passes. A typical Mode-S terminal sensor, with a rotation period of approximately 5 sec., is capable of delivering an average net data rate of 300 bits/sec to each aircraft within its 100 nmi (185 km) range of coverage. In this context, and where elsewhere mentioned in this paper, net data rate is defined as the actual useful data delivered after all communications protocols and error protection overhead have been removed. For a realistic distribution of aircraft requesting data link service, a single Mode-S sensor is capable of transmitting at a net data rate of more than 60,000 bits/sec ³. By contrast, the ACARS VHF data link in use by the airlines, is capable of a net data rate of 600 – 1,000 bits/sec. An improved VHF data link, AVPAC, has been proposed with a net data rate of 5,000 - 8,000 bits/sec. Thus a single Mode-S sensor can deliver as much data as 60 ACARS or 8 AVPAC channels. The impact upon Mode-S data link capacity, of widespread use by General Aviation is addressed later in this article.

On the ground side of the data link, the Mode-S sensor provides a connection, through a data link processor, to network communications. The FAA is procuring a ground data link processor (DLP-II), scheduled for deployment in 1997, that will provide access to the Aeronautical Telecommunications Network (ATN) ⁴ for services such as Air Traffic Control Communications and text weather products (e.g., Surface Observations, Terminal Forecasts, etc.). In addition to the ATN data link services, the Mode-S data link can also provide services directly to the user without reliance on

the ATN communication network. These "local" services are called Mode-S Specific Services and have the advantages of a lower communications addressing overhead and do not require modification of the ATN data link processors and routers for implementation. Two data link services described below, Traffic Information Service, and Graphical Weather Service, are examples of data link applications that may be deployed initially as Mode-S specific services.

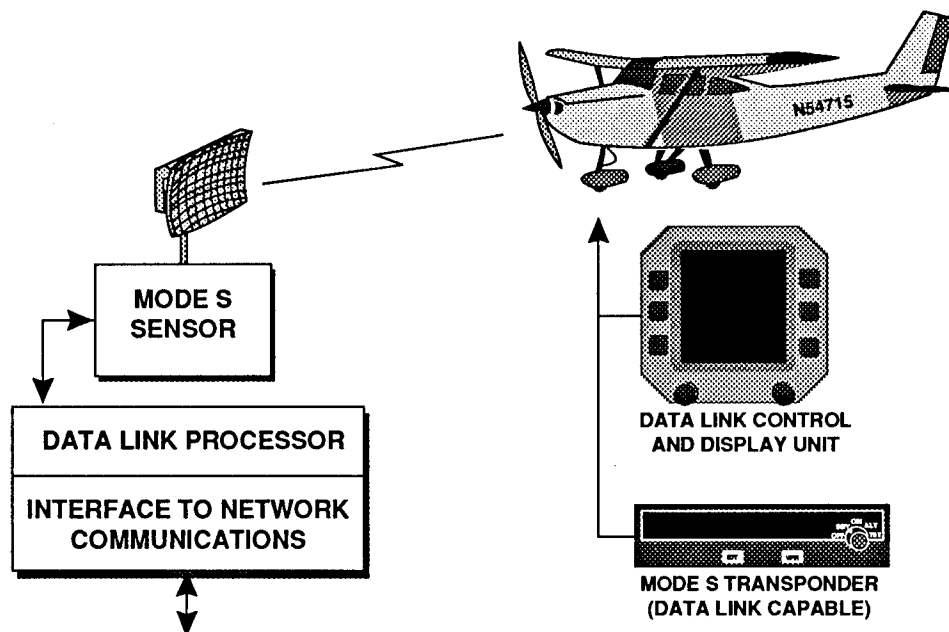


FIGURE 1. MODE-S DATA LINK COMPONENTS. The Mode-S surveillance sensor at left provides a connection to ground-based data link services. The aircraft is equipped with a data link Mode-S transponder and a Control / Display Unit (CDU).

THE OMNIDIRECTIONAL MODE-S DATA LINK GROUND STATION

The deployment of Mode-S secondary radar sensors will provide coverage over most of the contiguous United States airspace. However, there are a significant number of smaller airports that are located some distance from the nearest Mode-S sensor that will not have coverage below an altitude of approximately 2000 feet (620 m). The installation of a standard Mode-S surveillance sensor (see Figure 2) to provide low altitude coverage at smaller airports is prohibitively expensive. However, it is possible to construct a low-cost, omnidirectional, Mode S data link ground station. By taking advantage of data link features built into production TCAS avionics, MIT Lincoln Laboratory has developed a Ground Interrogator-Receiver Unit (GIRU)⁵ (see Figure 2), based on a modified TCAS unit. Connected to a simple omnidirectional antenna and located at a satellite airport, it is capable of providing two-way data link coverage from the surface to beyond the floor of coverage from conventional Mode-S surveillance sensors⁶.

MODE-S DATA LINK CAPACITY

Given the large number of GA aircraft operating in the United States, the potential demand for Mode-S data link services is significant. As described above, each terminal area Mode-S surveillance sensor, with its rotating antenna, is capable of delivering an average net data rate of 300 bits/sec to each aircraft within its 100 nmi (185 km) coverage radius up to a limit of approximately 200 aircraft,

given a net data rate per sensor of 60,000 bits/sec*. This aircraft density represents roughly that found in the Los Angeles basin, the region with the highest traffic density in the United States. Typically, aircraft in this congested airspace would be under the coverage of two or more Mode-S sensors, so that the actual data link load seen by any single sensor would be a fraction of its maximum capacity.

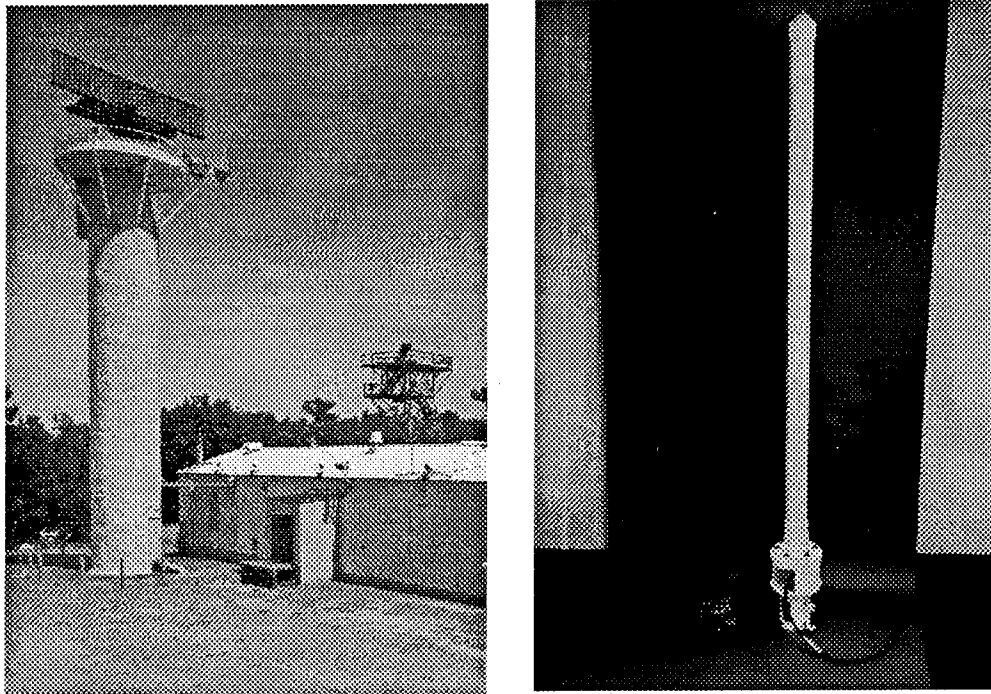


FIGURE 2. TWO TYPES OF MODE-S INSTALLATIONS. At left is the rotating antenna of a Mode-S terminal surveillance sensor. The antenna has an 8 m (26 foot) span and a rotation period of approximately 5 seconds. At right is the much smaller Ground Interrogator Receiver Unit (GIRU), suitable for data link coverage near smaller airports not within the coverage of a Mode-S surveillance sensor. The GIRU is shown connected to a standard Distance Measuring Equipment (DME) antenna with a height of approximately 2.2 m (7 feet).

In order to illustrate the average data link demand imposed on a Mode-S sensor by a GA aircraft, the values listed in Table 1 are used. It is assumed that, during a typical flight, a GA pilot might request a graphical weather image, a text weather message, and an ATIS message, on average, once every 2 minutes. In addition, ATC communication would take place in the form of a route clearance and a routine message every 2 minutes. It is assumed that the pilot would require the continuous display of data link provided traffic information, receiving an update every 5 seconds. Estimates of the data content of each message are based on the actual implementation of these services as they are described in the following sections. Because of the pilot attention required to attend to this significant amount of data link information, the services and update periods in Table 1 represent a rather conservative (high) estimate of the data link demand imposed by a GA aircraft. Nevertheless, the total average data rate utilized by the services in Table 1 is 60 bits/sec, approximately 20% of the total Mode-S data link available to the aircraft, even in the most congested airspace. All of the data link messages defined below, with the exception of the weather graphic, can be delivered by a Mode-

* The Mode-S sensor, as deployed, can provide data link service to a maximum of 400 aircraft. This limit will be upgraded within approximately one year to 700 aircraft.

S sensor within a single antenna scan (approximately 5 seconds). The weather graphic would require two antenna scans (approximately 10 seconds).

TABLE 1
ESTIMATE OF THE MODE-S DATA LINK LOADING
IMPOSED BY A TYPICAL GA AIRCRAFT

<u>Data Link Service</u>	<u>Data Content (bits)</u>	<u>Update Period</u>
Weather Graphic	2400	2 min
Weather Text	1200	2 min
ATC Route Clearance	600	2 min
Routine ATC msg	100	2 min
Traffic Information	112	5 seconds

Total Average Data Rate Required: 60 bits/sec.

GENERAL AVIATION DATA LINK AVIONICS

In order to receive data link services, an aircraft must be equipped with the proper avionics. In general, this includes a data link transceiver and a Control and Display Unit (CDU) (see Figure 1), which are analogous to the telephone modem and personal computer used for ground-based digital communications. In the case of the Mode-S data link, the function of the data link transceiver is served by a Mode-S transponder. The Mode-S transponder duplicates the function of the older Air Traffic Control Radar Beacon System (ATCRBS) transponder by replying to ATCRBS sensor interrogations with the standard four-digit identity code (Mode A) and altitude (Mode C) information². It also replies to the selective interrogations of the Mode-S sensor, including those that contain data link messages. Figure 3 illustrates a Mode-S transponder manufactured for General Aviation use.

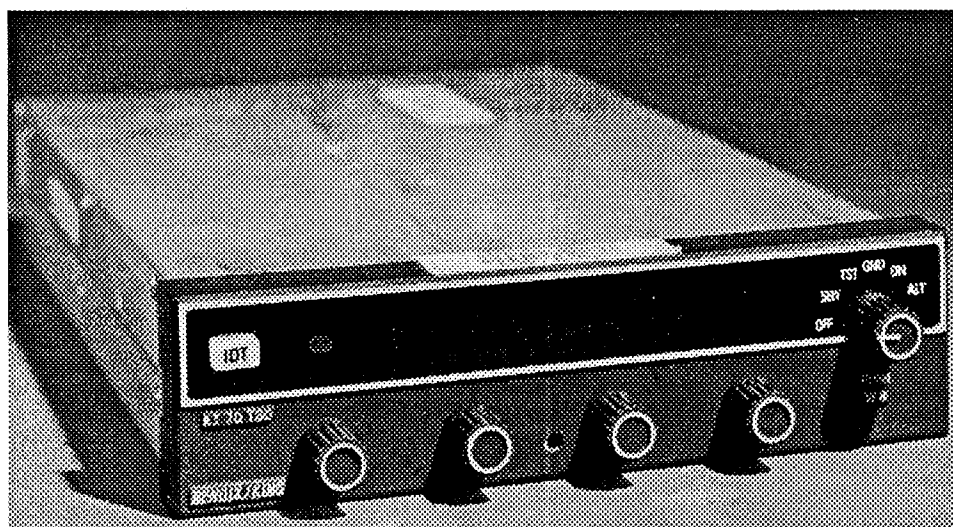


FIGURE 3. MODE-S TRANSPONDER. Mode-S transponders, similar to the panel-mount model pictured here, with a retail price of approximately \$3000, can provide data link capability to General Aviation aircraft.

The data link Control and Display Unit (CDU), serves as the display and input device for the pilot. Just as in the personal computer analogy, the data link communications and applications software resides in the CDU. Among the most challenging human factors issues associated with GA data link is the design of an appropriate pilot interface for single pilot operation. Instrument panel space in a typical GA aircraft limits display size. The challenging physical and mental workload environment places significant constraints on the design of input devices. Some of these issues have been addressed by the manufacturers of GPS and LORAN navigation equipment in the design of displays and input devices for navigation data bases. However, the multiple functions provided by data link will impose additional requirements on the design of pilot displays.

Recent developments in active matrix liquid crystal displays (LCDs) have made low cost color displays possible for GA aircraft. Figure 4 illustrates the installation of a color LCD suitable for data link applications in the instrument panel of a typical GA aircraft. Estimates of the cost of a production data link CDU range from \$2000 to \$5000, depending upon the complexity of the pilot interface, the size of the display, and the data link application software that it contains. When combined with the cost of a Mode-S data link transponder, the total estimated cost of data link avionics is \$5000 to \$8000.

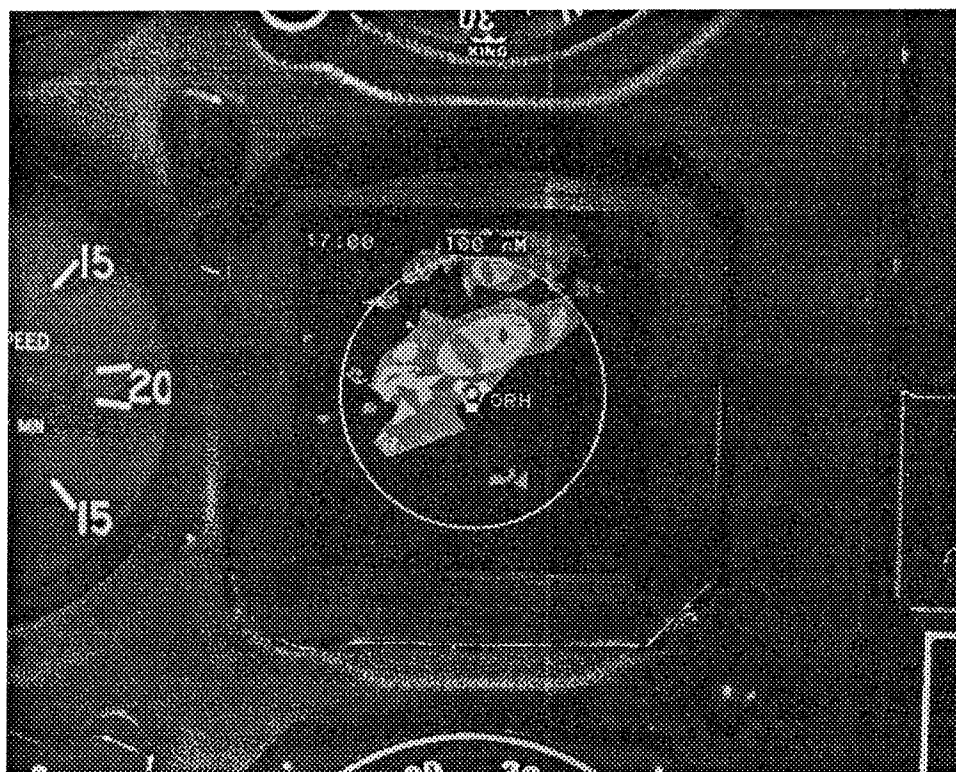


FIGURE 4. DATA LINK DISPLAY AS INSTALLED IN THE INSTRUMENT PANEL OF THE CESSNA 172 DATA LINK TEST BED AIRCRAFT. Shown is a color (green, yellow, red) radar precipitation image transmitted by Mode-S data link. Color LCD technology shows promise for low-cost data link Control / Display Units (CDUs) in the \$2000 - \$5000 price range.

MODE-S DATA LINK APPLICATIONS

TRAFFIC INFORMATION SERVICE

The primary method of collision avoidance employed by the pilots of GA aircraft is a constant visual search for traffic; the FAA term for this is "see and avoid". The goal of Traffic Information Service (TIS) is to assist the pilot with the task of "see and avoid" by providing an automatic display of nearby traffic, including visual and aural alerts of traffic that presents a potential collision hazard. The goal of assisting "see and avoid" is identical to that of TCAS-I which provides a display of nearby traffic and collision threats, but does not issue resolution advisory maneuvers to the pilot for collision avoidance. Figure 5 illustrates the operation of TIS.

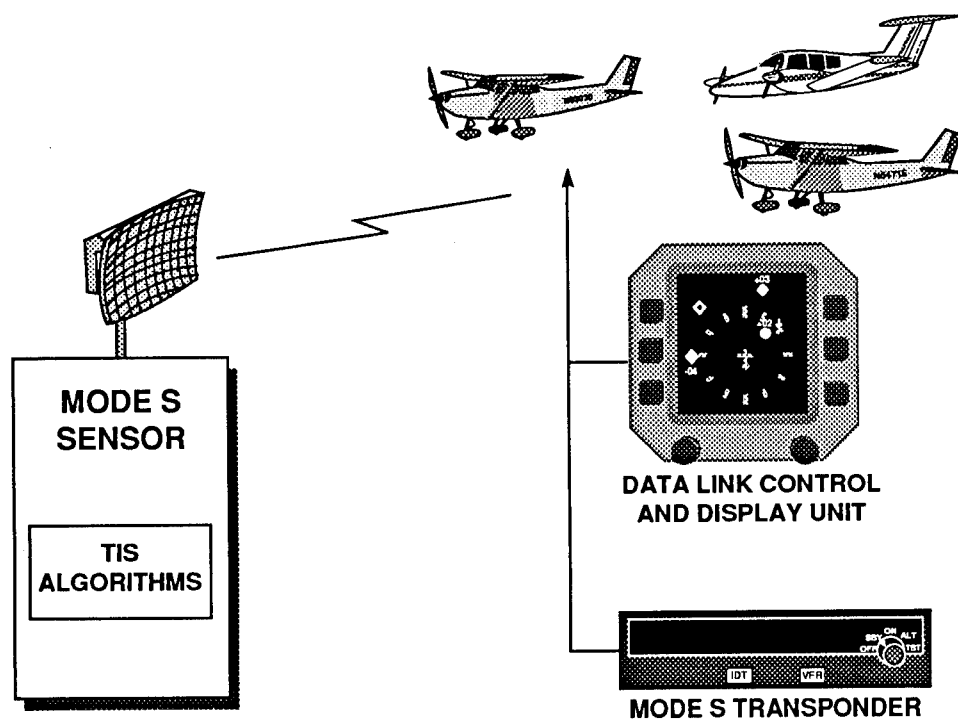


FIGURE 5. TRAFFIC INFORMATION SERVICE (TIS). The TIS algorithms operating in the Mode-S surveillance sensor at left determine the location of nearby traffic and transmit that information by data link to the requesting aircraft where it is displayed in TCAS-I format. The TIS display is updated each Mode-S antenna scan (approximately every 5 seconds).

When performing its function as a secondary radar surveillance system, the Mode-S sensor maintains a surveillance track file (identity, range, azimuth, and altitude) for each transponder-equipped aircraft within its coverage. TIS consists of a set of software algorithms that reside in one of the several redundant surveillance processors within the Mode-S sensor. Upon a data link request from a particular aircraft, the TIS algorithms use the Mode-S surveillance track files to determine the relative locations of all of the aircraft within 5 nautical miles (9.3 km) and ± 1200 feet (370 m) altitude of the requesting aircraft. In addition to the relative position of other aircraft, the TIS algorithms determine if the trajectories of those aircraft pose a collision threat to the requesting aircraft. The TIS logic that determines collision threat is similar to that used by TCAS-I. Using the relative range between the requesting aircraft and each of its neighbors, an alerting parameter, tau, ($\text{tau} = \text{range} / - \text{range rate}$) is computed for each nearby aircraft. Whenever tau is less than 30 seconds, the corresponding aircraft is declared a collision threat. The relative positions of each nearby aircraft and their threat status are sent to the aircraft as a Mode-S data link message. The data is displayed to the pilot using a standard

TCAS-I display format, including an audible alert that accompanies the declaration of a collision threat. The pilot, alerted of the intruding traffic, is able to determine its relative bearing, range, and altitude. With this information, the pilot can concentrate his visual search in the proper area, quickly see the traffic, and take appropriate action.

The effectiveness of TIS, or any similar collision avoidance system that relies on "see-and-avoid" can be measured by its effect on the pilot's ability to visually acquire nearby traffic. A mathematical model for pilot visual acquisition⁷ was developed and has been used to evaluate the performance of TCAS as well as other collision avoidance systems, including TIS. The TIS traffic display in the cockpit is updated each time the Mode-S sensor beam passes the aircraft, approximately once every 5 seconds. Flight tests with pilot subjects in general aviation aircraft have shown that this is sufficient to result in an approximately 8-fold improvement in visual acquisition efficiency - equivalent to that demonstrated with TCAS-I. A frequent observation made by pilots who have survived a mid-air collision is that they were not aware that there was another aircraft near them. Beyond simply making visual acquisition more efficient, TIS will significantly help the pilot maintain overall traffic situational awareness.

Because TIS relies on Mode-S surveillance information, it operates only in airspace for which there is Mode-S surveillance coverage. Though this is a significant fraction of the airspace used by general aviation aircraft, and includes all areas of high traffic density, TIS does not provide total airspace coverage. Despite this limitation, the significant advantage of TIS over other collision avoidance systems is its relatively low cost and the lack of requirement for all other aircraft to be equipped with collision avoidance equipment for TIS to be effective. A long-term solution to collision avoidance for general aviation aircraft is the use of Automatic Dependent Surveillance Broadcast (ADS-B) where each aircraft automatically broadcasts its own position. The GPS-Squitter⁵ system, discussed below, is an ADS-B concept that makes use of the Mode-S data link. TIS will provide immediate benefit to GA aircraft and a means to smoothly transition to a collision avoidance system based on ADS-B in the future.

GRAPHICAL WEATHER SERVICE

The goal of Graphical Weather Service (GWS) is to provide real-time weather information to pilots in a form that is relevant and easily interpreted. While some weather information, such as that found in a typical sequence report or terminal forecast, is adequately expressed in text form, much of the weather of significance to pilots is best presented as a weather graphic. Examples of this include regions of precipitation, lightning, icing, low ceiling and visibility, and turbulence. While it is possible for pilots to obtain weather graphics of some of these phenomena on the ground using land-line data communication, the dynamics of weather are such that the situation will have changed by the time the aircraft is in flight. Figure 6 illustrates a graphical depiction of the precipitation associated with a cold front in the northeastern United States. This image, a commercial product provided by WSI Corporation, is a composite mosaic of several ground-based weather radars. It is a real-time depiction of precipitation that is updated approximately every 15 minutes. Such an image is clearly valuable to pilots of GA aircraft, particularly those that have limited capability to fly in hazardous weather. It offers the pilot the ability to plan a route around the weather, divert to an alternate airport, or simply to land and wait until the weather improves.

The data link transmission of the precipitation image as depicted in Figure 6 would require a total message size of over 300,000 bits, exclusive of the geographical base map. This would require far more bandwidth than is available with any practical data link implementation. There is a need, therefore, for considerable data compression to permit routine transmission of weather graphics to the cockpit. A specialized image compression algorithm has been developed that maintains the overall morphology of weather images while maintaining reasonable image data size⁸. These algorithms exploit the inherent geometric shape of the weather phenomena by representing them as a series of polygons and ellipses rather than discrete pixels. Instead of transmitting the large amount of data required to describe the individual pixels, it is only necessary to transmit the location and shape of the geometric shapes that make up the image for reconstruction on the aircraft display. Using the Poly-Ellipse algorithm, an image that requires 131,000 bits to transmit can be reduced to 2413 bits (see

Figure 7), a message that can be transmitted to an aircraft from the rotating antenna of a Mode-S surveillance sensor in two scans (roughly 10 seconds). Although the Graphical Weather Service has been designed as a Mode-S data link application, its image compression algorithms can be equally applied to the transmission of weather graphics with any data link implementation.

As described above, the first generation of ATN ground data link processor (DLP-II) will have the capability to provide basic Air Traffic Control communications and text weather products through the Mode-S sensor. DLP-II, as it is currently planned for deployment, will have no provision for weather graphics. Figure 8 illustrates how the Graphical Weather Service could be implemented as a Mode-S specific service in advance of a permanent upgrade to DLP-II for weather graphics capability. An Image Compression Processor, a low-cost commercial computer workstation, is connected to one of the several Mode-S sensor data link ports in parallel to the DLP-II. The Image Compression Processor, which is connected by land-line or satellite link to a commercial or government weather provider, maintains a real-time data base of uncompressed weather graphics. Upon a data link request from an aircraft, the Image Compression Processor selects the area of interest from its weather data base, compresses it, and passes it to the Mode-S sensor for data link transmission. On board the aircraft, the weather image is decompressed and displayed to the pilot in either track-up (illustrated in Figure 8) or north-up format. The weather image may be integrated with navigation information to provide the pilot with a visualization of the weather relative to the proposed route of flight.

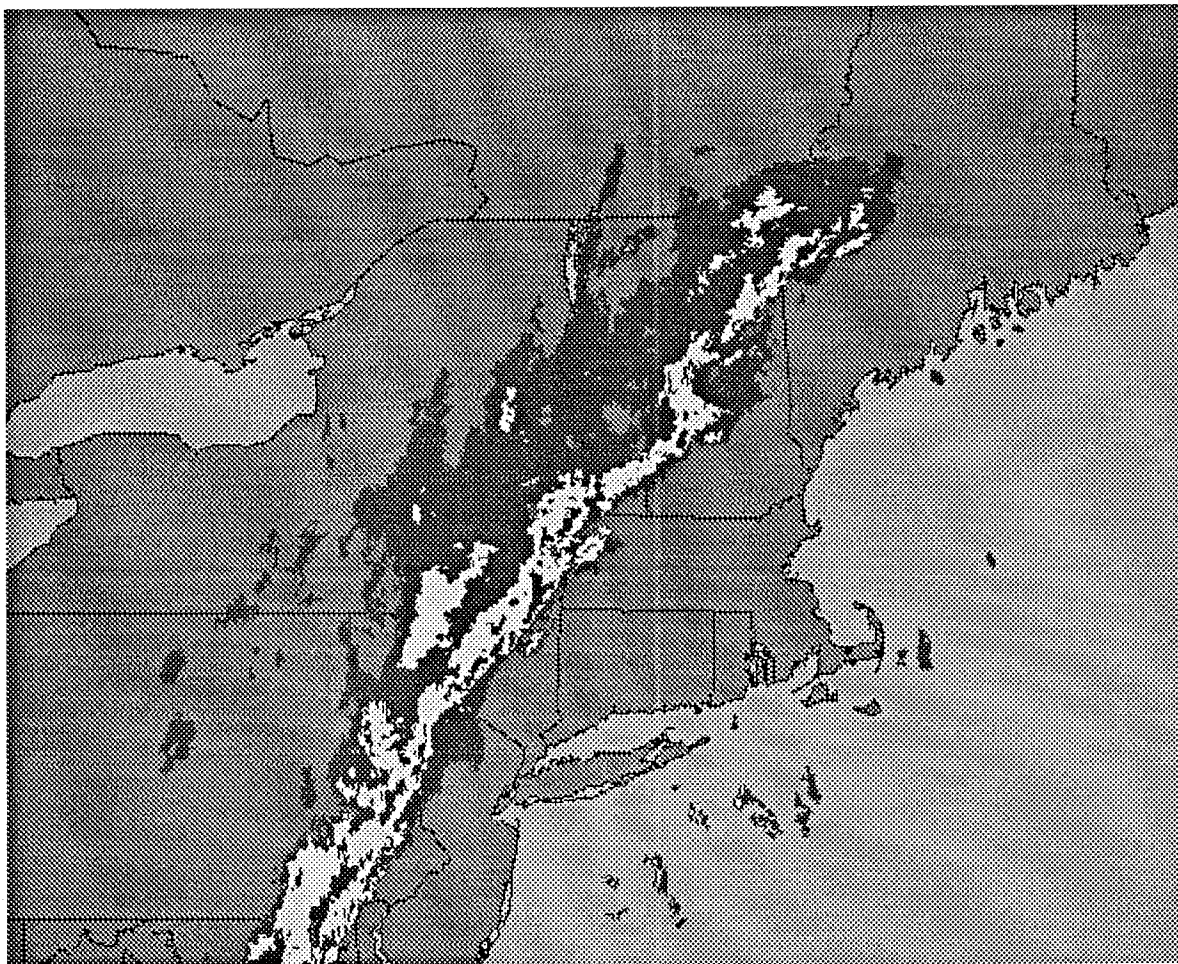


FIGURE 6. COMPOSITE RADAR PRECIPITATION IMAGE OF NORTHEAST U.S. This image, a commercial weather product provided by WSI Corporation, is a mosaic of ground-based WSR-57 and WSR-88 weather radars. In its color version, light precipitation is shown in green, moderate in yellow, and heavy in red.

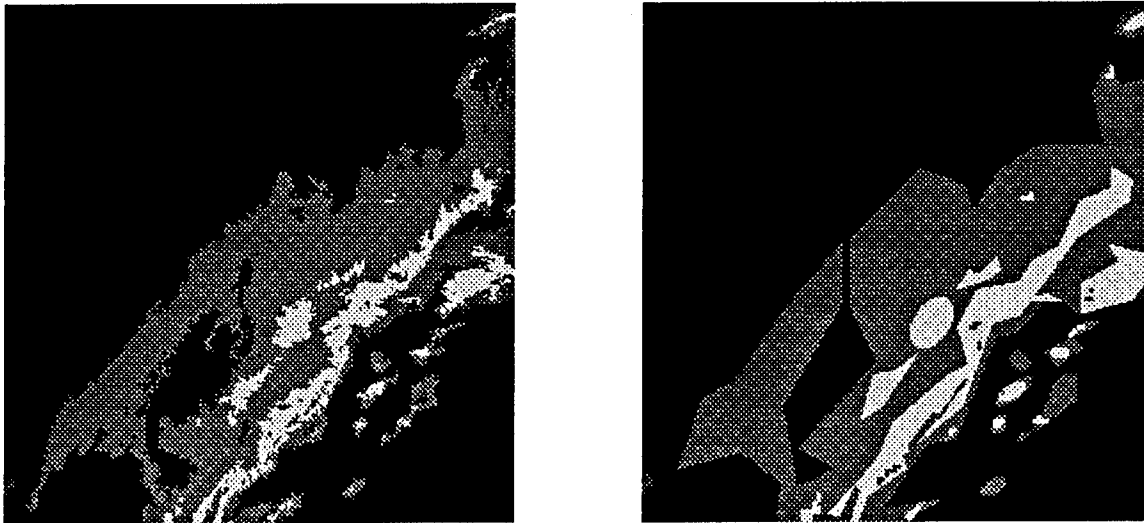


FIGURE 7. COMPRESSED AND UNCOMPRESSED WEATHER RADAR IMAGES Without data compression, the 512x512 km. image at left would require 131,000 bits to transmit. The image at right has been compressed to 2413 bits using the Polygon-Ellipse algorithms. The compressed image can be transmitted to the aircraft by Mode-S data link in 2 radar scans (approximately 10 seconds).

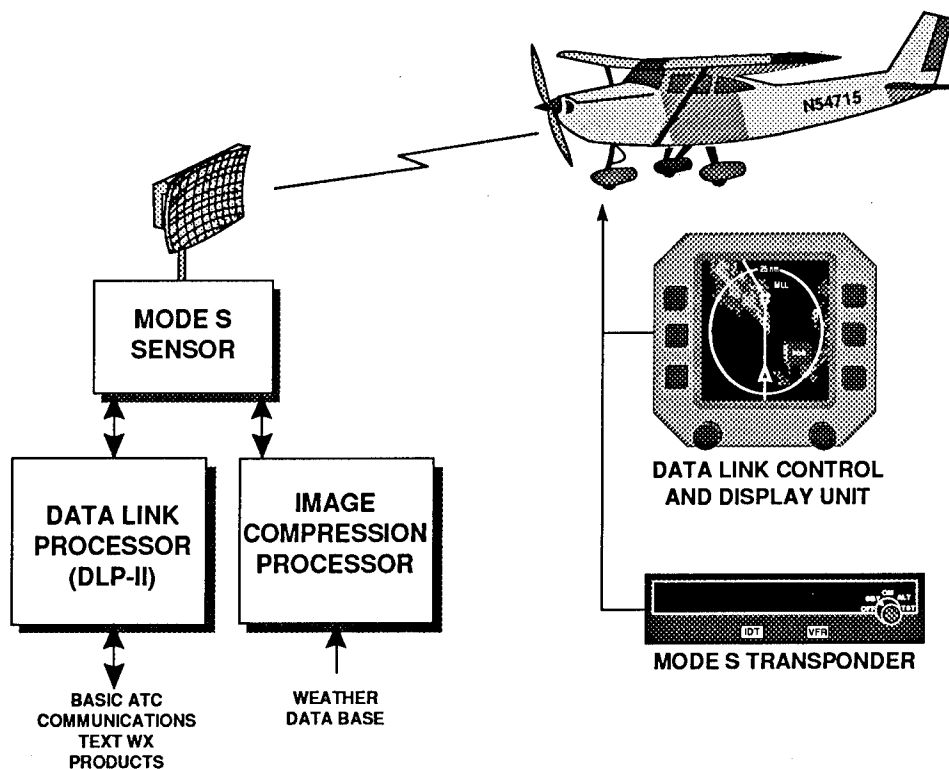


FIGURE 8. GRAPHICAL WEATHER SERVICE (GWS). A real-time weather data base is maintained in the image compression processor connected to the data link port of the Mode-S sensor. Upon a request from an aircraft, the appropriate image is selected, compressed, and transmitted by data link to the aircraft where it is displayed.

Results of a recent human factors study⁹ involving GA pilots, indicate that GWS had a substantial positive effect on their weather-related decision-making process. With the real-time graphical depiction of weather provided by GWS, pilots were able to make informed go / no-go decisions at the beginning of a simulated flight. During the simulated instrument flights, pilots were able to determine the need for course deviations without extensive use of verbal weather information provided by ATC controllers or Flight Service Station specialists. Both pilots of extensive flight experience as well as those with limited experience were found to benefit significantly from GWS.

LOCAL AREA DIFFERENTIAL GNSS

The accuracy of the Global Navigation Satellite System (GNSS) is limited by systematic bias errors, beyond those introduced by the Department of Defense through the Selective Availability feature. In order to achieve sufficient accuracy to conduct precision instrument approaches with satellite navigation, estimates of these biases must be formed and corrections applied to the navigation solution. One means to provide these corrections is the use of a fixed ground station that uses its known position to formulate bias estimates and transmits these estimates to aircraft via data link. When implemented in a small area (roughly 20 nmi, (37 km) radius), this technique is known as Local Area Differential GNSS (LADGNSS).

The choice of a data link to provide the LADGNSS corrections has been the subject of much study¹⁰. At issue is the availability of a data link that is available for use and protected from interference. The transmission of LADGNSS corrections has been demonstrated with the Mode-S

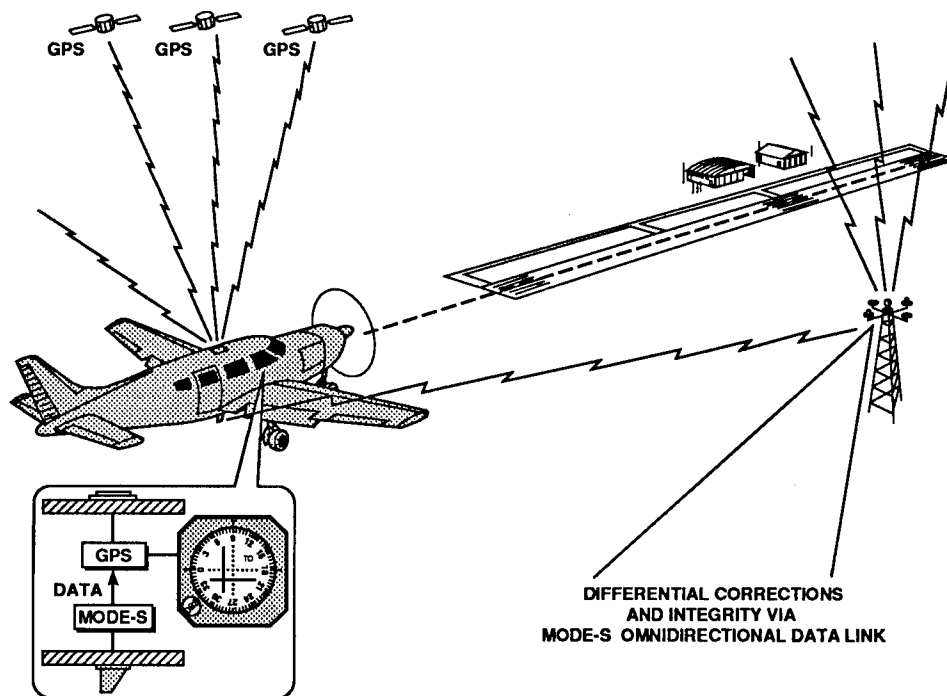


FIGURE 9. LOCAL AREA DIFFERENTIAL GNSS (LADGNSS) PRECISION INSTRUMENT APPROACH. An omnidirectional Mode-S ground station is used to broadcast differential GNSS corrections to the area surrounding an airport. An aircraft with a Mode-S transponder or a Mode-S receiver applies the corrections to the GNSS navigation solution to achieve sufficient accuracy to perform a precision instrument approach.

data link ¹¹. Using an omnidirectional Mode-S ground station as described above, the corrections are broadcast in the local area surrounding an airport (see Figure 9).

Aircraft with a data link capable Mode S transponder receive the corrections and pass them to the on-board GNSS navigation equipment where the corrections are applied to the navigation solution. Appropriate navigation displays (e.g., emulation of localizer and glide slope indicators) are then used to provide the pilot with guidance for the precision approach. Aircraft without Mode S transponders would be able to receive the corrections with a simple Mode-S receiver designed to capture the LADGNSS broadcast. Such a low-cost receiver could be incorporated within the GNSS receiver itself to provide precision approach capability.

GPS-SQUITTER

In addition to the replies generated by ATCRBS and Mode-S interrogations, the Mode-S transponder produces a spontaneous reply, called a "squitter", approximately once per second. This squitter, 56 bits in length, contains the unique Mode S address of the aircraft, and control and parity information. The squitter is designed to provide a TCAS-equipped aircraft with a means to acquire other Mode-S aircraft in its vicinity without the need for acquisition interrogations. With a minor modification to the software within the Mode S transponder, another standard Mode S message, 112 bits in length, can also be squittered. The additional 56 bits in this longer squitter format are used to provide GNSS-derived position information (see Figure 10). With this GPS-Squitter modification, an aircraft spontaneously broadcasts both its position and identification.

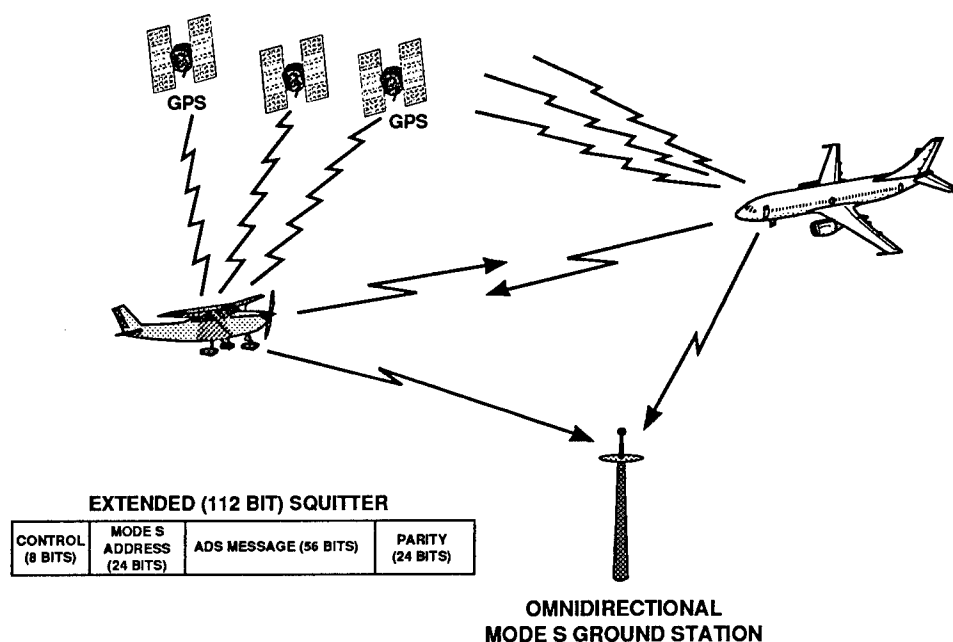


FIGURE 10. GPS-SQUITTER CONCEPT. Each aircraft derives its own position using satellite navigation and broadcasts an extended Mode-S squitter containing that information. GPS-Squitters can be received by ground stations for ATC surveillance and by other aircraft for collision avoidance.

With a simple Mode-S receiver, such as that provided by the omnidirectional Mode-S ground station described above, a ground station can monitor the GPS-Squitters broadcast by the aircraft in the vicinity. Such a ground station can then provide Air Traffic Control with surveillance information as well as data link. GPS-Squitter has been demonstrated for surface and airborne surveillance ⁵. When a significant fraction (greater than approximately 80%) of all aircraft are equipped with GPS-Squitter,

it becomes beneficial to use an airborne Mode-S receiver to perform traffic situational avoidance and collision avoidance.

A TYPICAL GA FLIGHT WITH MODE-S DATA LINK

In order to illustrate the operation of Mode-S data link services on a GA aircraft, a hypothetical flight scenario is described below. The flight originates at Hanscom Field (BED) in Bedford, Massachusetts, with a destination of Dulles International Airport (IAD) in Virginia. Such a flight might take place in the spring of 1998, after deployment of DLP-II, GWS image compression processors, and omnidirectional Mode-S ground stations at satellite airports (including Hanscom Field). The aircraft is equipped with a Mode-S data link transponder and CDU. The Mode-S transponder is also connected to an aircraft GPS receiver and has been modified to produce GPS-Squitters.

After obtaining a detailed weather briefing by voice from a Flight Service Station Briefer, or electronically with a personal computer and modem, the pilot files an Instrument Flight Rules (IFR) flight plan from Hanscom Field to Dulles International Airport. The route of flight will take the aircraft to the southwest across Long Island Sound, directly over Kennedy International Airport, then south along the New Jersey coast, west over the Chesapeake Bay to Baltimore, then directly to Dulles International Airport. The total flying time is estimated at 3 hours.

START-UP AND TAXI

Upon engine start up at Hanscom Field, the pilot activates the aircraft's Mode-S transponder and data link CDU. He makes a data link request for the Automatic Terminal Information System (ATIS) information and activation of his ATC clearance from a menu on the CDU. Because Hanscom Field is below the coverage of the Boston Mode-S sensor, the data link request sent by the Mode-S transponder is received by an omnidirectional Mode-S ground station located on top of the control tower at Hanscom Field. Within a second or two, the ATIS message appears on the CDU display. An additional menu item on the CDU display indicates that the route clearance has been received from ATC; the pilot selects it for display and reviews it. Noting that ATC has modified the route slightly, the pilot acknowledges receipt and acceptance of the ATC clearance via data link. Although full data link communication with the Hanscom Field control tower is technically possible through the omnidirectional Mode-S ground station, Hanscom Field does not support sufficient aircraft operations to justify the cost of the tower controller data link communications consoles necessary to permit this. However, when the Hanscom Field control tower is not in operation (e.g. late at night), the omnidirectional Mode-S ground station provides direct data link communication with the Boston Terminal Radar Approach Control (TRACON) facility. This would permit the pilot to request and receive ATC clearance for departure when the local tower controllers are not available by voice radio. Since the Hanscom tower is in operation, the pilot relies on VHF voice radio communication to obtain clearance to taxi to the active runway.

At the time that the pilot received the preflight briefing, ground-based weather radar showed no precipitation on the route of flight. However, the area forecasts include the possibility of afternoon thundershowers over a large portion of western Connecticut, eastern New York, and New Jersey. In order to obtain an update on the weather situation prior to departure, the pilot manipulates the menu-driven display on the CDU to request a current weather radar image of the subject area. The request is received by the omnidirectional Mode-S ground station, and a compressed weather image is transmitted to the aircraft. The image, less than 10 minutes old, shows some light to moderate shower activity over the Catskill mountains, but none along the route of flight. The pilot elects to depart and proceed on course, while monitoring the weather situation in flight. The pilot obtains clearance for departure from the control tower by VHF voice radio.

DEPARTURE AND ENROUTE

Once airborne, the pilot begins a climb to the ATC assigned initial altitude of 2000 feet (620 m). Although the aircraft is still below the radar coverage of the Boston Mode-S sensor, the GPS-Squitters that are spontaneously transmitted from the aircraft's Mode-S transponder are received at the Hanscom Field omnidirectional Mode-S ground station and the surveillance information that they contain is transmitted by land-line to the Boston TRACON where the symbol representing the aircraft appears on the ATC controllers display.

By selecting the appropriate menu on the data link CDU, it is possible for the pilot to perform all routine communications with ATC via Mode-S data link. However, the pilot wishes to devote the data link CDU display to traffic and weather information and therefore elects to use VHF voice for ATC communication. In the event of a VHF voice radio failure, the Mode-S data link will provide a back up means to communicate with ATC. From a menu on the CDU, the pilot requests activation of TIS and a traffic display appears as the aircraft enters the coverage of the Boston Mode-S sensor.

Once established at a cruising altitude of 8000 feet (2500 m), the pilot requests an updated surface observation at Dulles International Airport and the latest weather radar image within a 100 nmi (185 km) radius of Kennedy International Airport. As the aircraft proceeds southwest, it leaves the coverage of the Boston Mode-S sensor and enters the coverage of the Mode-S sensor located at Bradley International Airport in Windsor Locks, CT. The transfer of surveillance and data link coverage between Mode-S sensors is performed automatically without any action required on the part of the pilot. During the remainder of the flight, the aircraft will be constantly within the coverage of at least one Mode-S sensor. The Bradley sensor automatically receives notification from the transponder that the pilot has requested TIS and maintains this service. Should the aircraft leave coverage of a Mode-S surveillance sensor, and thus lose the ability to obtain TIS, the CDU display will alert the pilot that TIS is no longer available. Once across Long Island Sound, the transfer to the Mode-S sensor at Islip, NY takes place in a similar fashion.

ARRIVAL

The latest weather radar image received via data link indicates that the forecast thunderstorms are developing over the Catskill and Berkshire mountains and not in the New York City area, nor south along the route of flight. Therefore, the pilot elects to continue on the planned route. In order to monitor the situation closely, the pilot selects a function from a menu on the CDU that automatically requests a weather radar image update as soon as one becomes available (approximately every 10 minutes). Approaching Baltimore, under the coverage of the Baltimore Mode-S sensor, the pilot requests the Dulles ATIS via data link and begins planning for the instrument approach to runway 1R. Although Dulles is equipped for full data link communications with the Air Traffic Control Tower, the pilot elects to maintain VHF voice contact with ATC throughout the approach, landing, and taxi phases of the arrival.

CONCLUSION

The Mode-S data link has the capability to provide the GA pilot with significant benefits in the form of improved situational awareness. The avionics required to obtain Mode-S data link services can meet the cost and size constraints imposed by the typical GA aircraft. Data link applications such as Traffic Information Service and Graphical Weather Service can be provided with a relatively low investment in additional ground infrastructure. LADGNSS broadcast and GPS-Squitter can provide both Air Traffic Control and the GA community with significant benefits in terms of improved surveillance and increased aircraft utility.

REFERENCES

1. Harman, W.H., "TCAS: A System for Preventing Midair Collisions", Lincoln Laboratory Journal, 2:9, Fall 1989.

2. Orlando, V.A., "The Mode S Beacon Radar System", Lincoln Laboratory Journal, 2:9, Fall 1989.
3. M-J. Hirigaray and B. Conio, "Mode S Subnetwork Data Link Simulation Results," The International Civil Aviation Organization, SICASP, April, 1990.
4. The Aeronautical Telecommunications Manual, draft in process, the International Civil Aviation Organization, November 1993
5. Bayliss, E.T., Boisvert, R.E., and Knittel, G.H., "Demonstration of GPS Automatic Dependent Surveillance of Aircraft Using Spontaneous Mode-S Beacon Reports", Proceedings of the ION-GPS-93, Institute of Navigation, 1993.
6. Reiner, D., "Siting of GPS Squitter Ground Stations for Air Surveillance Coverage", ATC Project Memorandum, 42PM-SSS-0007, MIT Lincoln Laboratory, 1993.
7. Andrews, J.W., "Air-to-Air Visual Acquisition Handbook" ATC Report DOT/FAA PM-87-30, 1991.
8. Gertz, J.L., "The Polygon-Ellipse Method of Data Compression of Weather Maps", ATC Report DOT/FAA/RD-94/6, 1994.
9. Lind, A.T., Dershowitz, A., and Bussolari, S.R., "The Influence of Data Link-Provided Graphical Weather on Pilot Decision-Making", ATC Report DOT/FAA/RD-94/9, 1994.
10. RTCA Task Force Report, "The Transition to Digital Communications," RTCA, Inc., December 1993.
11. Bayliss, E.T., Incorporation of GNSS Technology in C/N/S - Demonstration of DGPS Precision Approach, Proceedings of the Symposium on Worldwide Communications, Navigation, and Surveillance, sponsored by US DOT, FAA, ARINC, Transport Canada, Reston, VA, 1993.

FAA CERTIFICATION OF A MULTI-PURPOSE HEAD UP DISPLAY (HUD) FOR GENERAL AVIATION AIRCRAFT

Mark W. Anderson
Federal Aviation Administration
Chicago Aircraft Certification Office
Des Plaines, Illinois

ABSTRACT

Advances in flight display technology have enabled manufacturers to provide a Head-Up Display (HUD) of aircraft control and performance parameters for use in general aviation aircraft without the use of inertial platforms or specialized data bus architecture. The Federal Aviation Administration (FAA) currently has no regulatory guidance regarding HUD or flight symbology certification. A specific HUD certification program is presented. The process of categorizing the HUD as a supplemental system is briefly discussed. Flight display symbology is discussed and the final symbology set presented. The certification flight test plan is discussed including the requirements for functional, usability and operational testing. Company and FAA flight test data are discussed. A HUD system was certified for single pilot use in instrument meteorological conditions in a general aviation aircraft.

INTRODUCTION

BACKGROUND

The head-up display (HUD) was developed in military aircraft from reflecting optical sights. The HUD places flight and navigation data in the pilot's forward field-of-view (FOV). This data symbology is presented as a collimated image which appears to be floating at infinity. A typical HUD displays flight information in the "basic T" convention: airspeed, altitude, pitch and roll attitude, and heading. In addition, appropriate navigation or mission data can usually be selected for display. Flight director modes, radar altitude and marker beacon passage can also be shown if available. Most HUDs can also display master warning and caution annunciators.

The subject HUD was built by Flight Visions, Inc. and designated the FV-2000. The FV-2000 HUD differs from most HUDs in that it uses conventional aircraft gyros and does not depend on an inertial navigation system platform for attitude information. Since conventional aircraft gyros are less precise than inertial platforms, the HUD symbology is not conformal in that the symbology does not align directly with real-world horizon cues. To minimize subjective discomfort, the HUD symbology is compressed relative to the real-world. This has the added benefit of enhancing pilot spatial orientation by reducing the rate at which pitch scale translates during maneuvering, and enables the horizon reference line to remain in view throughout more of the flight envelope.

The FV-2000 HUD is intended for use as a supplemental flight display designed to enhance flight safety by allowing the pilot to refer to flight data and clear the flight path for traffic, or acquire the runway environment during an approach simultaneously. The aircraft still must be equipped with a full complement of conventional panel instruments required by the appropriate certification and operating rules. In the event of HUD failure or a detected sensor failure, the HUD ceases displaying the appropriate information and the pilot reverts to the Head Down Display (HDD) instruments for missing flight information.

Prior to certification flights, an extensive symbology evaluation program was flown in a Grumman AA-5B aircraft equipped with a FV-2000 HUD. This program resulted in a symbology set that was found satisfactory for general aviation operations.

The symbology evaluation tests described here ensured that the results obtained in the AA-5B flights apply to multi-engine turboprop airplanes.

OBJECTIVES

GENERAL OBJECTIVE

The overall objective of the flight test program was to certify the Flight Visions Model FV-2000 Head-Up Display installation in a Beechcraft BE-A100 aircraft under a Supplemental Type Certificate. The FV-2000 HUD is intended to be a supplemental display providing flight and navigation information to the pilot and to be used during both visual and instrument meteorological conditions (VMC and IMC). Through flight test, the applicant was required to show that the pilot could fly the airplane to acceptable tolerances using the HUD in concert with HDD instruments and that any invalid data was clearly annunciated to the pilot.

SPECIFIC OBJECTIVES

The specific objectives of this test program were:

- (a) Demonstrate that the HUD provided an adequate VOR/ILS/ADF display to allow a pilot to fly an instrument approach,
- (b) Demonstrate that the pilot could safely execute the transition to visual conditions during an instrument approach and that he could safely land the aircraft or transition back to instrument flight and execute the published missed approach procedures using the HUD,
- (c) Demonstrate that the pilot could fly to acceptable enroute IFR accuracy using a VOR signal displayed on the HUD,
- (d) Demonstrate that the pilot could recognize and recover from unusual attitudes using the HUD and panel mounted instruments or using the panel instruments alone after detecting a HUD failure,
- (e) Demonstrate that the HUD had no adverse effect on aircraft systems with all systems operating,
- (f) Demonstrate that the HUD displayed accurate flight parameters (airspeed, altitude, magnetic heading, etc.) and annunciation's (master caution, altitude alert, etc.),
- (g) Demonstrate that the HUD provided adequate warning in the event sensor data is missing or is invalid,
- (h) Demonstrate that the HUD system performed satisfactorily during typical operations.

TEST EQUIPMENT

MODEL FV-2000 HUD

The Model FV-2000 HUD system consists of three line replaceable units. These are the pilot display unit (P/N 5210-101, S/N 001), the pilot control unit (P/N 6210-109, S/N 013), and computer unit (P/N 6210-100, S/N 002) unit. All units were inspected and conformed to the type design data prior to the start of certification flight test.

AIRCRAFT

The host aircraft for the certification program was a Beechcraft BE-A100, N-552GA, serial number B-215. Prior to the beginning of flight testing, the aircraft was thoroughly inspected and conformed to the

original type design data. Additionally, the FV-2000 installation was conformed on the aircraft to the installation design data.

VISION RESTRICTION SYSTEM

A complementary color vision restriction system was installed in the airplane in order to: simulate IMC, allow the evaluation pilot to view the HUD, and not restrict the view of the safety pilot. The system consists of a red film over the windshield and side windows. The view through the film is colored, but was found satisfactory for safe aircraft operation. During flights requiring vision restriction, the evaluation pilot wore green goggles. The view of the cockpit interior and HUD symbology was unaffected while external visual cues were blocked by the complementary color filters.

DATA RECORDING AND ANALYSIS

AIRCRAFT DATA

Aircraft position was determined using on-board navigation receivers, panel instruments and visual ground references as appropriate. Position data was hand recorded as required. The pitot-static system, airspeed indicators and altimeters were calibrated. All radio navigation equipment was also calibrated.

HUD DATA

Specific pilot observations were required to ensure that no adverse HUD induced effects were present. These observations were prompted by a general observations rating card used on all flights. In addition, specific tests were flown asking for specific problem areas, such as the presence or absence of light reflections during night evaluation.

During instrument approaches, the HUD output was recorded. A laptop computer was used to capture the HUD data stream for postflight analysis. Additionally, simulated faults and sensor failures could be injected into the HUD through the laptop computer. It was not possible to record data during those approaches with simulated sensor failures.

OTHER DATA

During instrument approaches, the weather conditions, specific approach flown and outcome of the approach were documented on an approach rating card. A display rating card based on the Cooper-Harper pilot rating was used to rate HUD usefulness during specific tasks.¹ Sample rating cards and decision trees are shown in Appendix 1. The use of this type of subjective rating scale requires the definition of specific flight tasks and performance criteria. Such tasks and criteria were derived from previous HUD programs and are described in Reference 2.

TEST PROCEDURE

Before testing could begin, the HUD system had to be categorized according to the intended use sought by the applicant. Properly categorizing a HUD as a primary or supplementary flight display is essential when building a certification test plan. The FV-2000 HUD was categorized as a supplemental flight display and the certification flight test program was built accordingly. Certification tests were grouped into three areas; system functional tests, pilot interface tests and operational tests. The Airplane Flight Manual Supplement (AFMS) was evaluated throughout the test program.

SUPPLEMENTAL FLIGHT DISPLAYS

The FV-2000 HUD was designed as a safety enhancement device to repeat HDD flight information into the HUD FOV. The intended use is to allow the pilot to perform climb, cruise and approach operations. Using the HUD in concert with HDD instruments is intended to facilitate head up tasks such as clearing for traffic and identifying airport and runway environments. The FV-2000 is not intended to be used as an independent guidance system or an enhanced approach tool. It is only a repeater of conventional panel instrument information into a HUD system. Using this approach, the HUD is merely a repeater device and no extra capability or operation unique to the HUD is provided or sought by the applicant. The fundamental differences between primary and supplemental displays lie in two areas: warning annunciation and display symbology. Although feasible, the FV-2000 is not designed to be used as a stand alone instrument system. Hence, head down cross-checking of navigation information, engine indications and flight director annunciators is still required. The HUD system is not considered as replacement for HDD instruments, but a tool to aid the transition to the Head-Up environment. Additionally not all of the information required to fly and monitor the aircraft in a totally head up environment is available. Head down cross-checking of engine instruments, system annunciation's, and verification of flight instrument setup is absolutely essential. The failure warning and annunciation scheme currently implemented is sufficient to alert the pilot to check HDD annunciation's to further analyze system anomalies. When preparing to fly instrument approaches, HDD instruments must be tuned, set and cross-checked with HUD indications to ensure proper approach setup. Although it is possible to control the aircraft by sole reference to the HUD, proper systems cross-check and engine monitoring is not possible. HUD use in this manner was not intended by the applicant.

Although Flight Visions intent was to install the HUD as a supplementary display, environmental qualification testing included complete RTCA DO-160C Environmental Tests such as susceptibility to high intensity radiated fields (HIRF) and the indirect effects of lightning. Flight Visions performed software qualifications per RTCA DO-178A, Level II (Essential). This level was deemed acceptable since the HUD is designed as a repeater of information from the primary flight instruments and not as a primary flight instrument.

The coordinated FAA position was to treat the FV-2000 as an aid to head up aircraft control that is not a primary flight instrument system. The system would be certified as a "non-essential installation accomplishing its intended function" with an equivalent level of safety to a conventionally designed cockpit.

SYSTEM FUNCTIONAL TESTS

System functional tests were designed to insure the HUD accurately transmitted and displayed data through the HUD. Accurate display of data from the HDD instruments was considered an essential requirement when evaluating system performance of intended function and determining equivalent levels of safety. The reception and accuracy flight test profiles described the FAA Flight Test Guide were used as a basis for evaluating the functional areas listed below.³

- Navaid accuracy (VOR and ADF)
- Navaid tracking (VOR, ILS, Flight Director)
- Navaid station passage (VOR, ADF, Marker Beacon)
- Localizer course intercepts
- ADF indicator response when switching between stations
- Proper DME indication
- Pitch and roll response of the attitude display during a variety of maneuvers
- Air data accuracy
- Systems compatibility to include electromagnetic compatibility and HUD interpretation of sensor failures

PILOT INTERFACE TESTS

Pilot interface tests were designed to evaluate the pilot/HUD interface in those areas listed below.

Display readability in various lighting conditions and optical deficiencies such as flicker or glare

Dynamic deficiencies such as jitter, noise and excessive lead or lag

Inflight initialization

Engine failure

Unusual attitude recognition and recovery

Sensor failure recognition

HUD modes of operation

Command carets

Traffic detection

Precision and non-precision instruments approaches

SUBJECTIVE PILOT RATINGS. Several tests required subjective pilot ratings or pilot observations. These tests centered on the usability of the HUD symbology.

Display Ratings. A display rating based on the Cooper-Harper pilot rating was used to rate the HUD during instrument approach tasks. As described earlier, a sample rating card and decision tree is shown in Appendix 1. The use of this scale required the definition of specific flight tasks and performance criteria. Such tasks and criteria were described earlier.

Pilot Observations. Specific pilot observations were required to ensure that no adverse effects were present. Observations were prompted by a rating card which was used on all flights. Data cards for these specific uses are shown in Appendix 1.

INSTRUMENT APPROACHES. During instrument approaches, the weather conditions, specific approach flown, and outcome of the approach were documented by the safety pilot on an approach rating card. These rating cards are shown in Appendix 1. During this phase evaluation pilots flew published instrument approaches such as; VOR, Localizer only, ILS, and ADF. All approaches were flown in simulated or actual IMC. Half were flown to touchdown and half to missed approach. Several different approaches were flown to minimums at different airports. Twenty such approaches of each type were flown for which approval was sought. Two approaches of each type were flown with a simulated engine failure during the approach. Half of all ILS approaches were flown using raw data and half using flight director guidance. Additionally, ten approaches were flown to circling minima, followed by a circling maneuver through at least 180 degrees to a landing. Half were flown at night. Two circling approaches were flown with a simulated engine out. Table 1 illustrates the instrument approach matrix.

TABLE 1. INSTRUMENT APPROACH TEST MATRIX

Type of Approach	Number	Land or Missed Approach		Engine Failure		Flight Director	
		L	MA	Yes	No	F/D	No
ILS	20	10	10	2	18	10	10
VOR	20	10	10	2	18	5	15
ADF	20	10	10	2	18		20
Localizer(FC)	10	5	5	1	9	3	7
Localizer(BC)	10	5	5	1	9	3	7
Circling (D)	5	3	2	1	4		5
Circling (N)	5	3	2	1	4		5
Total	90	46	44	10	80	21	69

The approach flown, weather conditions, landing or missed approach, and success or failure of the approach were recorded. To ensure uniformity in the data all approaches were flown with approach flaps and a reference airspeed of 120 knots. Approaches were flown using a combination of HUD and HDD instruments. Procedures and techniques for optimum use of the HUD in concert with HDD instruments were developed during flight test and incorporated in the Airplane Flight Manual Supplement (AFMS).

OPERATIONAL TESTS

An operational evaluation of twenty hours was flown in high traffic density areas to evaluate HUD performance in operationally representative environments. Fifteen of these hours were flown with representative operational pilots flying the aircraft. Data recording equipment was not required for these flights.

AIRPLANE FLIGHT MANUAL SUPPLEMENT EVALUATION

During all phases of certification flight tests, a concurrent evaluation of the adequacy of the AFMS was made. All evaluation pilots were asked to comment on the suitability of the material. Particular emphasis was placed on limitations, systems description and system operation.

SAFETY ISSUES

FLIGHT TEST SPECIFIC HAZARDS. The risks peculiar to these tests were the possibility of HUD induced instrument or radio failure during instrument flight and HUD induced loss of situational awareness. Before flight in actual IMC, sufficient VMC system testing was conducted to provide confidence in the HUD system and use of the HUD. Another risk was the possible loss of control during simulated engine-out flight. Project safety pilots were experienced instrument and multi-engine flight instructors and were responsible for the safety of flight during these tests. The safety pilots had a full complement of flight instrumentation available on their side of the cockpit to ensure that they were able to monitor the flight and take over if necessary without having to refer to flight instruments in a "cross cockpit" fashion.

PRECAUTIONS REQUIRED. Anti-collision lighting and landing lights were used at all times in the instrument pattern. During flight in clouds, these lights were turned off if desired by the evaluation pilot. Before flight into actual IMC, a safety review was conducted to ensure confidence in the HUD systems to be evaluated. For flights with the vision restriction system installed, an extra observer was used to supplement the safety pilot's view on the left side of the airplane.

TEST RESULTS

SYSTEM FUNCTIONAL TESTS

The HUD functional flight profiles followed the reception and accuracy profiles described in the FAA Flight Test Guide.³ These included:

- | | |
|-------------------------|-----------------------------|
| (a) Accuracy | (e) Indicator Response |
| (b) Tracking | (f) Proper Indication |
| (c) Station Passage | (g) Pitch and Roll Response |
| (d) Localizer Intercept | (h) Systems Compatibility |

ACCURACY (VOR, ADF). These flight profiles followed the reception and accuracy profiles described in the FAA Flight Test Guide.³

VOR Display. The VOR accuracy tests were flown overhead the Illinois Valley Airport and radials from Bradford (BDF), Polo (PLL), Joliet (JOT), and Pontiac (PNT) VORs used to confirm the calibration in four quadrants. In both clean and approach configurations, the indicated radials were within 2 degrees of the actual radial. The HUD indicators agreed with both head-down horizontal situation indicators for both numbers 1 and 2 VORS.

ADF Display. The ADF accuracy test was flown against the Valley (VYS) non directional beacon in the clean configuration and the Rockford (RF) outer locator in the approach configuration (gear down, flaps approach). The ADF bearing on the HUD agreed with both head-down indicators. All indicators were approximately 8 degrees off. The ADF was returned to the shop and calibrated. Following calibration, all indicators agreed within 1 degree.

TRACKING (ILS, VOR, Flight Director). These flight profiles followed the tracking profiles described in the FAA Flight Test Guide.

VOR Display. The VOR course width test was flown over the Illinois Valley Airport using radials from Bradford (BDF), Polo (PLL), Joliet (JOT), and Pontiac (PNT) VORs. The course width in all cases was 20 to 21 degrees. Both clean and approach configurations were evaluated. No flags were displayed. The HUD display agreed with the pilot's horizontal situation indicator (HSI).

ILS Localizer Display. The localizer courses flown were Rockford (I-RFD), Aurora (I-ARR), Illinois Valley (I-PYU), and Flying Cloud (I-FCM). The localizer behavior was examined throughout the final approach at 10 to 12 miles from the airport. In all cases, the localizer behaved normally with correct sensing. The evaluations were flown in clean and approach configurations. No flags were displayed. The HUD display agreed with the pilot's HSI.

ILS Glideslope Display. ILS courses were flown at Rockford (I-RFD), Aurora (I-ARR), and Flying Cloud (I-FCM). Glideslope behavior was examined from the final approach fix to category I decision height. In all cases, the glideslope behaved normally with correct sensing. The evaluations were flown in clean and approach configurations using normal pitch and roll attitudes. No flags were displayed. The HUD display agreed with the pilot's HSI.

Flight Director. ILS courses flown were Rockford (I-RFD), Aurora (I-ARR), Illinois Valley (I-PYU) and Flying Cloud (I-FCM). Flight director behavior was examined throughout the final approach beginning at 10 to 12 miles from the airport. The flight director behaved normally with correct sensing. The evaluations were flown in clean and approach configurations. VOR courses were flown using the Bradford (BDF) and Joliet (JOT) VORs. The flight director behavior was examined on a course from about 5 miles on either side of the VOR through to the opposite course. In all cases, the flight director behaved normally with correct sensing. The evaluations were flown in clean and approach configurations. The HUD display agreed with the pilot's attitude directional indicator (ADI).

STATION PASSAGE (VOR, ADF, MARKER BEACON). VOR Display. VOR courses were flown using radials from the Bradford (BDF) and Joliet (JOT) VORS. The deviation behavior was examined on a course from approximately 5 miles on either side of the VOR through to the opposite course. In all cases, the deviation behaved normally with correct sensing. The evaluations were flown in clean and approach configurations. The HUD display agreed with the pilot's HSI.

ADF Display. The ADF station passage was flown over the Chilicothe (COT) NDB in the clean configuration and the Valley (VYS) NDB in the approach configuration. The indicator made only one complete reversal during station passage.

Marker Beacon Display. The marker beacon annunciation in the HUD agrees with the head-down marker beacon lights. Tests were accomplished using the Aurora (I-ARR) and Rockford (I-RFD) ILS courses for both outer and middle marker signals.

LOCALIZER INTERCEPT. This evaluation was flown using the Aurora (I-ARR), Illinois Valley (I-PYU), and Flying Cloud (I-FCM) ILS courses in both clean and approach configurations. Course widths and behavior agreed between the HUD and the pilot's HSI. No flags were evident between the extreme course widths. The HUD display agreed with the pilot's HSI.

INDICATOR RESPONSE (ADF). This test was flown while tracking from Valley (VYS) NDB. The ADF receiver was switched between Valley (VYS) NDB and the WLUP radio broadcast station. The indicator correctly responded within 10 seconds while switching between stations.

PROPER INDICATION (DME). This test was piggybacked while conducting VOR/ILS tests described above at the Illinois Valley, Rockford, and Flying Cloud airports and during VOR tracking at the Bradford (BDF) and Joliet (JOT) VORs. The DME system tracked without dropouts during these tests and HUD data correlated with HDD indications.

PITCH AND ROLL RESPONSE. The HUD pitch and roll display was evaluated during the following maneuvers: full-flap instrument and visual approaches, go-arounds, steep turns, emergency descents and single-engine operation. Test results are shown in Table 2. The ratings are based on the tasks and criteria described in NASA TM-103947.² These tasks were flown solely by reference to the HUD when possible. During turning flight with simulated engine failure it was difficult to manage sideslip using only the HUD and required reference to the HDD sideslip indicator for accurate directional control. As a result, the AFMS was written to require the pilot to recover from an engine failure head-down, retrim, and then use the HUD. The emergency descent was difficult using the HUD alone. Precise airspeed control to maximize the descent rate without exceeding maximum airspeed limitations was difficult. The HUD can still be used during this phase of flight when used in concert with HDD instruments. All other maneuvers were satisfactorily flown by reference to the HUD.

SYSTEMS COMPATIBILITY. Electromagnetic Compatibility. All aircraft electrical and electro-mechanical systems were observed while power to the HUD was cycled. Test results are shown in Table 3. Several systems were activated and deactivated inflight with the HUD operating to evaluate aircraft systems compatibility with the HUD. Test results are shown in Table 4.

Sensor Failure. Sensor failure was simulated by pulling circuit breakers for navigation radios, radar altimeters etc. The effect on the HUD display was noted. With the exception of inverter power failure and air data computer failure, all simulated failures were performed in flight. The results are shown in Table 5.

HUD Warning Repeater. The master caution repeater on the HUD display was verified by switching off each engine driven generator in turn.

PILOT INTERFACE TESTS

The FV 2000 HUD display was evaluated under a variety of conditions to demonstrate that the controls and modes were usable and that the display was usable under normal flight conditions. In some cases, these evaluations were combined with instrument approaches.

- (a) Display Readability
- (b) Inflight Initialization
- (c) Engine Failure
- (d) Unusual Attitude Recognition
- (e) Sensor Failure Recognition
- (f) HUD Modes and Options
- (g) Command Carets and Indicators
- (h) Checklist Function
- (i) Traffic Detection

TABLE 2. HUD UTILITY DURING MANEUVERS

Maneuver	Config	Overall Ratings		Comments
		Read- ability	Control- ability	
Vis Approach	Approach	R3	C3	
Vis Approach	Landing	R3	C3	
ILS Approach	Landing	R3	C4½	
Balked Landing	Approach	R3	C3	
Balked Landing	Landing	R4	C5	Yaw Axis R5 Yaw Axis C6 Airspeed C5
Steep Turns	Clean	R3	C3	
Emerg. Descent	Clean	R4	C6	Pitch C6 Airspeed C6
Eng Fail-S/L	Clean	R3	C3	Yaw Axis R8
Eng Fail-S/L	Approach	R3	C3	Yaw Axis R8
Eng Fail-S/L	Landing	R4	C4	Yaw Axis R9
Eng Fail-turn'g	Clean	R6	C7	Yaw Axis R10
Eng Fail-turn'g	Approach	R5	C6	Yaw Axis R10
Eng Fail-turn'g	Landing	R8	C8	Yaw Axis R10

TABLE 3. HUD COMPATIBILITY WITH SYSTEMS

System	Effect on System	
	HUD off	HUD on
VOR-1	Normal Operation	No Effect Noted
VOR-2	Normal Operation	No Effect Noted
ADF	Normal Operation	No Effect Noted
DME	Normal Operation	No Effect Noted
Glideslope	Normal Operation	No Effect Noted
Air Data Computer	Normal Operation	No Effect Noted
Transponder	Normal Operation	No Effect Noted
Inverter	Normal Operation	No Effect Noted
Radar	Normal Operation	No Effect Noted
Attitude (ADI)	Normal Operation	No Effect Noted
Heading (HSI)	Normal Operation	No Effect Noted
Heading (RMI)	Normal Operation	No Effect Noted

TABLE 4. SYSTEMS COMPATIBILITY WITH HUD

System	Effect on HUD	
	System on	System off
VOR-1	Normal Nav Display	Nav Display Disappears
VOR-2	Normal Nav Display	Nav Display Disappears
ADF	Normal ADF Display	ADF Display Freezes
DME	Normal DME Display	DME Display Disappears
Glideslope	Normal G/S Display	G/S Display Disappears Cross Replaced By CDI NO GS Flag Appears
Radar Altimeter	Normal Display	Display Disappears
Air Data Computer	Normal airspeed, altitude, and VSI	Airspeed, altitude, and VSI Disappear
Transponder	Normal Display	No Change
Encoder	Normal Display	Normal Air Data Function
Inverter	Normal Display	Pitch Ladder Disappears Various Warnings Shown
Radar	On flight 1, HUD Display Failed. Unable to duplicate	Normal Display Normal Operation
Either Generator	Normal Display	Master Warning Appears

TABLE 5. FAILURE ANNUNCIATION

System	Effect on HUD	
	System on	System off
VOR-1	Normal Nav Display	Nav Display Disappears
VOR-2	Normal Nav Display	Nav Display Disappears
ADF	Normal ADF Display	ADF Display Freezes
DME	Normal DME Display	DME Display Disappears
Glideslope	Normal G/S Display	G/S Display Disappears Cross Replaced By CDI NO GS Flag Appears
Radar Altimeter	Normal Display	Display Disappears
Air Data Computer	Normal airspeed, altitude, and VSI	Airspeed, altitude, and VSI Disappear
Transponder	Normal Display	No Change
Encoder	Normal Display	Normal Air Data Function
Inverter	Normal Display	Pitch Ladder Disappears Various Warnings Shown
Radar	On flight 1, HUD Display Failed. Unable to duplicate	Normal Display Normal Operation
Either Generator	Normal Display	Master Warning Appears

The basic flight symbology shown in Figure 1 was the symbology set evaluated during certification flight tests. The compressed pitch scale, counter-pointer air data displays and heading tape have been used on other HUD development programs with success.⁴ Navigation and instrument approach data is available for display in the HUD field of view. Command caretters are also available for setting desired heading, airspeed and altitude. The figures shown in Appendix 2 illustrate HUD symbology with navigation and instrument approach fields activated. A decluttered display is also shown to illustrate the declutter mode used in unusual attitude recovery.

DISPLAY READABILITY

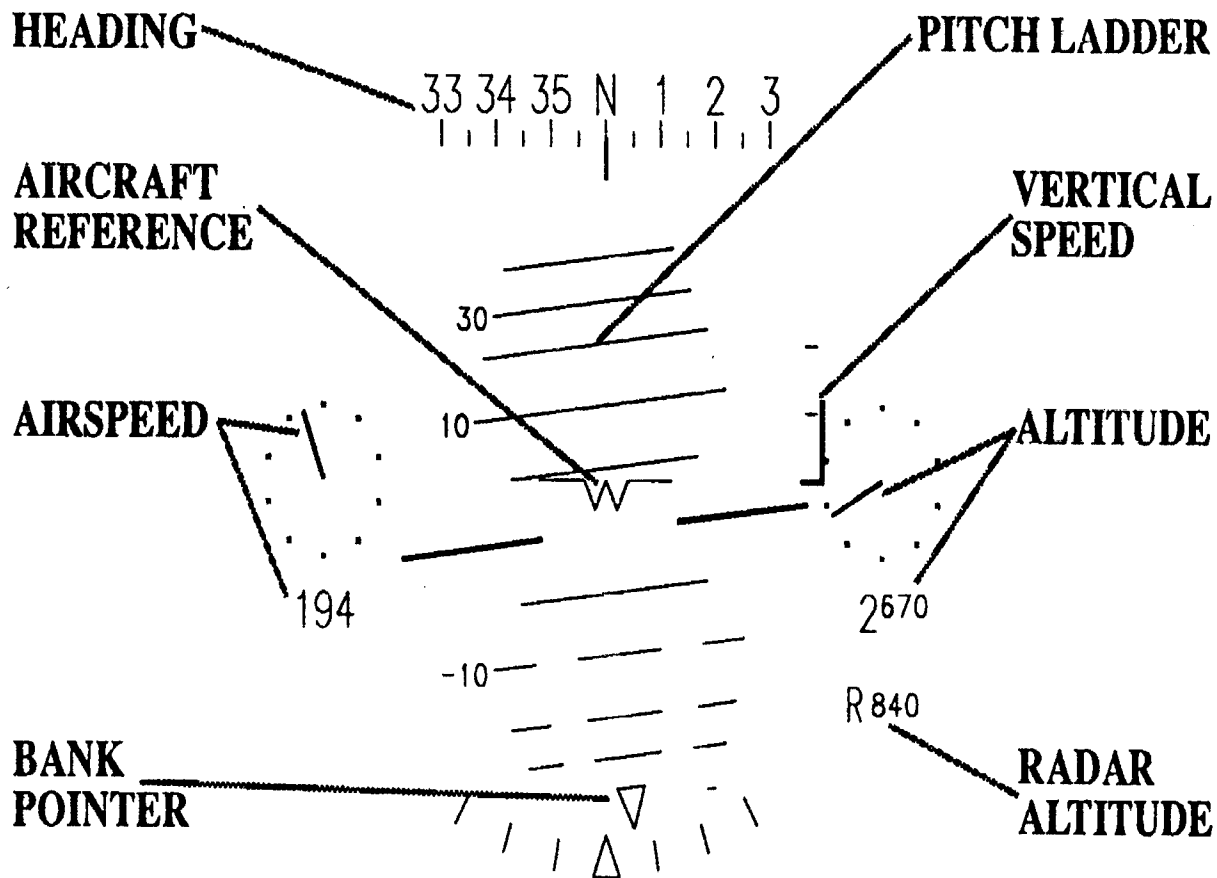


FIGURE 1. BASIC FLIGHT SYMBOLOGY

Brightness. The readability of the display was evaluated during day, dawn, dusk and night flights. The brightness range was adequate. The HUD symbology was bright enough to view when the sun was in the FOV through the combiner although the display was uncomfortable to use. The brightness range at night was adequate, although the symbology occasionally became lost in the city lights. It could be made visible, but no single brightness level worked for the airplane reference symbol and the side scales. If the side scales are adequately bright to see, the runway is obscured. If the brightness is low enough to view the runway, the side scales were not perceptible. During dusk, the ambient brightness changes, particularly with backlit clouds. This required frequent adjustments in brightness. Brightness control is a generic HUD problem and is managed by manually adjusting brightness during those occasions when atmospheric require.

Optical Deficiencies. The evaluation examined the HUD for optical deficiencies such as; flicker, excessive brightness variation across the FOV, symbol distortion, distortion of real world objects, legibility of symbols, secondary symbol images, reflections of real world images and lights, visual disparity and interference with view of real world cues. Optical characteristics were satisfactory. There was a secondary image of the symbology which could be seen if the pilot's head was lowered six to eight inches. Lowering of the head that distance while attempting to look through the HUD FOV and fly the airplane is not a natural movement that would occur during normal operation of the aircraft. The secondary image therefore was not considered a deficiency.

Display Dynamics. Tests evaluated the HUD for unsatisfactory display dynamics such as; jitter, excessive lead or lag, excessive noise, mutual interference of symbols. There was some minor jitter barely discernible during some night and IMC operations. It was not annoying and did not interfere with HUD operation or aircraft control.

INFLIGHT INITIALIZATION. Ease of in-flight initialization was verified. During flight, the system was switched off and on again to force an initialization. The workload was low as the HUD recovers to a smart condition and requires no pilot intervention.

ENGINE FAILURE. Simulated engine failures were accomplished by the safety pilot using throttle cuts. A zero thrust throttle setting was used in place of propeller feathering. Zero thrust was set by the safety pilot following identification of the failed engine by the evaluation pilot. The vision restriction system was used for all tests. Results indicated that following an engine failure, continued flight by reference solely to the HUD was difficult during turning flight. The absence of sideslip information increased pilot workload. Additionally, changes in power settings during missed approaches increased workload excessively, particularly during turning flight. The AFMS prohibits the use of the HUD during single-engine flight.

UNUSUAL ATTITUDE RECOGNITION AND RECOVERY. Unusual attitude recoveries were accomplished after the safety pilot maneuvered the airplane while the evaluation pilot looked away from the HUD and HDD instruments. The vision restriction system was in place during these evaluations. The results indicated that while recognizing an unusual attitude, flight by reference to the HUD could be accomplished if the upper and lower navigation areas of the HUD were deactivated so the entire pitch scale was visible. Recognition was hampered with the navigation areas active. A continually growing body of evidence in the HUD user community suggests that attempting to recover from an unusual attitude using the HUD alone can be an unsafe practice. The reasons are numerous and controversial, and include display dynamics, symbology design and human factors. For this reason, the AFMS requires cross-checking HDD instruments to confirm the unusual attitude and requires recovery from the unusual attitude using HDD instruments.

SENSOR FAILURE RECOGNITION. Sensor failures were simulated by pulling circuit breakers or by using flight test software designed to inject system failures through a laptop computer. Sensor failures were presented at unexpected times during the flights with emphasis on presentation during instrument approaches. The vision restriction system was in place during these evaluations. When the pilot recognized the failures, the system was restored and the approach or maneuver task continued. Table 6 summarizes the data. The results indicate that critical failures were detected immediately. Flight director failures took longer to develop but were detected before significant excursions from the flight path occurred. Secondary data such as DME and radar altitude were often missed for a long period since the pilot may not have been using the subject data at the time. The ADF failure was not obvious. The indicator simply froze. The frozen indicator took a significant time to detect. The head-down instrument has the same problem. A caution to this effect was placed in the AFMS.

HUD MODES AND OPTIONS. During all flights, the general utility of the HUD was evaluated. The HUD performed satisfactorily for the intended mission of a corporate aircraft. Two areas of deficiency were noted and corrected.

Radar Altitude. The radar altitude digits remained active at all times, even above the maximum display altitude of 2500 feet. This resulted in misleading data being presented and was corrected in the final software version. Additionally, below 2500 feet the terminal digit showing units was in constant motion and thereby distracting. Above 500 feet the display was changed to indicate to the nearest ten feet. That is, the units digit remains zero.

TABLE 6. SENSOR FAILURE DETECTION

Failure Type	Number	Mean Time to Detect (sec)	Number Missed
Primary Nav (ex ADF)	4	1.3	-
Glideslope	2	8.5	-
ADF	1	60.0	-
Air Data (exc VSI)	5	3.8	-
Vertical Speed	1	20.0	-
Gyros	8	1.5	-
Flight Director	5	10.2	-
Secondary Data (a)	4	9.5	2
Total	30	7.4	2
Note: (a) Radar altitude, DME, etc.			

Combiner Locking Mechanism. A placard indicating the action of the combiner locking lever was required.

COMMAND CARETS AND INDICATORS. The command carets and indicators used to set target airspeeds, altitudes and headings on the HUD functioned as intended.

TRAFFIC DETECTION. The HUD enhances the ability of the pilot to detect traffic during all phases of visual flight. No problems were indicated with detecting traffic. To the inexperienced HUD user, channelized attention in the HUD FOV is a common pitfall and can hinder traffic detection. The AFMS is explicit in describing the cautions pilots must be aware of when using a HUD system.

INSTRUMENT APPROACHES

A total of 88 approaches were flown with 6 pilots. Table 7 summarizes the approaches flown. The HUD was suitable for flying instrument approaches. In particular, pilots commented favorably that the HUD improved approach performance and enhanced situational awareness during night circling approaches.

OBJECTIVE RESULTS. Valid recorded data was obtained on 53 approaches. The results are summarized in Table 8. The errors listed in Table 8 are root mean square (rms) errors of airspeed from reference speed of 120 knots indicated airspeed. Lateral course errors (DevL), glideslope errors (DevG) and ADF bearing errors (DevA) were measured while on final approach inside the final approach fix. DevL and DevG are expressed in dots off course while DevA is expressed in degrees.

Approach airspeed error can usually be interpreted as a measure of pilot workload. Single-engine approaches had higher airspeed errors hence, higher workload than all engine approaches. Raw data localizer and backcourse approaches had slightly higher workload than VOR approaches, but that is generally true for those type approaches using HDD instruments.

SUBJECTIVE RESULTS. Valid data was obtained on 88 approaches. The results are summarized in Table 9. The ratings shown are the overall readability rating, the controllability rating using the HUD, and the orientation readability rating during interception. The single-engine approaches and ADF approaches were rated poorer than all others in terms of readability and controllability. interception at maintaining orientation.

ADF approaches were rated better during initial course and the safety pilots were asked if the airplane was within the safe landing window at minimums. Evaluation pilots were more critical of their performance than the

TABLE 7. INSTRUMENT APPROACH SUMMARY

Type of Approach	Number	Land or Missed Approach		Single Engine	Flt Dir or Raw Data	
		L	M/A		F/D	R/D
ILS	24	12	12	2	9	15
VOR	20	10	10	2	7	13
NDB	20	6	14	2	-	20
Localizer (FC)	13	6	7	1	6	7
Localizer (BC)	11	4	7	1	3	8
Total	88	38	50	8	25	66
Circling (a)						
Day	17	16	1	1	-	-
Night	6	3	3	1	-	-
Note: (a) Circling approaches included in above approaches						

TABLE 8. APPROACH OBJECTIVE DATA SUMMARY

Approach Description		Measured rms Errors			Mean IAS	
		IAS ^(a)	Dev _L	Dev _G	Dev _A	
Overall average		8.8	0.6	0.6	9.3	n = 53
Excl'dg ATC Problems		8.2	0.6	0.6	9.3	n = 51
Flight Director		7.4	0.5	0.5	---	n = 15
Raw Data		8.7	0.7	0.7	9.3	n = 36
Single-Engine		10.9	0.8	1.2	0.0	n = 7
All Engines Operatg		7.9	0.6	0.5	9.3	n = 44
F/D	ILS Approaches	7.3	0.4	0.5	---	n = 6
	LOC Approaches	8.3	0.1	---	---	n = 3
	B/C Approaches	7.1	0.2	---	---	n = 3
	VOR Approaches	6.8	0.9	---	---	n = 3
	ADF Approaches	---	---	---	---	n = 0
Raw Data	ILS Approaches	7.5	0.6	0.7	---	n = 7
	LOC Approaches	10.5	1.0	---	---	n = 6
	B/C Approaches	9.3	0.7	---	---	n = 9
	VOR Approaches	8.5	0.4	---	---	n = 10
	ADF Approaches	6.9	---	---	9.3	n = 4

Note: (a) Rms error from Vref = 120 KIAS.

safety pilots who were observing the approaches. Instrument approaches are generally considered high workload tasks and as such a workload issue surfaced during this portion of the evaluation. The FV-2000 HUD was not integrated with systems such as the flight director course and heading markers, altitude alerter and airspeed set markers. As a result, when flying an ILS approach with the flight director engaged, course and heading bugs had to be set on both the HUD and HDD instruments. The resulting workload was high and lead to confusion throughout

the approach. The final version software was changed to remove the HUD markers any time a flight director mode as engaged. The flight director steering references could still be monitored by crosschecking the HDD instruments. During raw data approaches, the HUD markers were available and enhanced approach performance. The AFMS was written to emphasize the advantages setting up approach and navigation aids early in the approach sequence.

TABLE 9. APPROACH SUBJECTIVE RATINGS

Approach Description	Ratings			
	Read	Cntrl	Read (a)	
All Approaches	2.8	2.8	2.9	n = 87
No ATC Problems	2.8	2.8	2.8	n = 86
Single-Engine	3.3	3.3	3.1	n = 7
All Engines Operating	2.7	2.7	2.8	n = 76
ILS Approaches	3.0	3.5	3.2	n = 13
N/P Approaches	2.6	2.8	2.9	n = 29
ADF Approaches	3.1	2.8	2.6	n = 21
ILS Approaches--F/D	2.6	2.5	2.7	n = 9
N/P Approaches--F/D	2.5	2.5	2.6	n = 11

OPERATIONAL TESTS

Following formal flight testing, a separate function and reliability test was conducted. The purpose of this test was to evaluate the HUD in operationally representative flight environments. Twenty hours in a representative environment were required. Twenty four flights totaling 28 hours yielded 20 hours of creditable operational testing. The representative conditions included high density airports and airspace, uncontrolled airports, and a broad spectrum of weather. Both single pilot and two pilot operations were conducted.

The following criteria were applied in order to meeting these goals:

- (a) No local flights.
- (b) At least two flights into primary airports with FAA Class B airspace (two arrivals and two departures).
- (c) At least two flights into uncontrolled airports (two arrivals and two departures).
- (d) Credit for up to fifteen minutes of cruise per flight in VMC was included in the twenty hours. Up to 1 hour in IMC per flight was included in the twenty hours. To be credited, the cruise flight time was handflown.
- (e) At least five flights using single pilot procedures. At least five flights using two pilot procedures.

PILOTS. The evaluation pilots were qualified in the aircraft. One FAA pilot and two Flight Visions pilots participated in the operational test program. A safety pilot familiar with the test program occupied the right seat and completed observation cards. For single-pilot flights, the safety pilot did not handle any cockpit or communications tasks.

RESULTS. In general, the evaluation pilots found the HUD presented them with useful cues which assisted in the conduct of the flights. Two items were noted. During one flight, a sloping cloud formation presented strongly

compelling false horizon cues. The pilot flew head-down for a brief period of time. The AFMS cautions the pilot about atmospheric phenomena that may be disorienting. During flights into a rising or setting sun, the visual discomfort of trying to view the HUD with the sun in the field-of-view also made use of the HUD uncomfortable.

AIRPLANE FLIGHT MANUAL EVALUATION

During all tests, a concurrent evaluation of the adequacy of the flight manual supplement was made. All evaluation pilots were asked to comment on the suitability of the material. As a result of the engine failure tests, a restriction on flying by reference to the HUD with an engine out was placed in the flight manual supplement. As a result of the unusual attitude recovery tests, a caution note regarding cross-checking with head-down instruments was added. As a result of the sensor failure tests, a caution note regarding ADF flight was included. The description of the ILS symbology was not clear to some pilots. This section was rewritten. The count-down timer created some difficulties. The text was re-written to make it clear that the timer must be cleared before the count-down value can be entered. On several occasions, the HUD symbology "locked up." This was caused by the system diagnostics detecting a failure which would normally cause a system reset. When the maintenance terminal was connected, this system reset was inhibited to allow a technician to diagnose the problem. Because of the likelihood of presenting invalid data, the flight manual supplement prohibits the use of the HUD in any conditions with the maintenance terminal connected.

CONCLUSION

A multiple Supplemental Type Certificate (STC) was issued on August 24, 1993. The Airplane Flight Manual Supplement approved with the STC requires that the FV-2000 be used in IMC conditions only when an appropriately rated pilot occupies the right seat. The findings detailed below required correction in order for the two pilot IMC operation restriction to be removed. The corrections were submitted for approval by the Chicago ACO. Specific findings and solutions are outlined below.

SYMBOLLOGY

- a. Provide improved discrimination of the VVI zero reference. The zero rate of climb index was easily obscured. The applicant provided a double stroke video line for the zero reference.
- b. Provide improved discrimination of the "on glide path" reference mark. The on glide path reference mark was double stroked to provide better discrimination.
- c. Eliminate the proximity of the digital altitude display and the radar altitude display. The current closeness of the two displays in the HUD field of view provided a potential for confusion. The radar altitude display was not moved, but the size of the digits was rescaled to provide better discrimination from the barometric altitude digital display.
- d. Eliminate the radar altitude display at altitudes above 1000 feet above ground level. The applicant removed the radar altitude display at radar altitudes above 1000 feet above ground level.

HUMAN FACTORS

- a. Implement an automated declutter function that removes the upper and lower navigation areas when an unusual attitude is encountered. Results of certification flight test indicated that unusual attitude recovery may be hampered when the NAV areas are displayed during recognition and recovery. The bank and pitch limits at which the display declutters should be related to the type and sensitivity of unusual attitudes likely to be encountered in the aircraft in which the system is installed. The decluttered display is presented in Appendix 2, Figure 4. The HUD symbology is set to automatically declutter at 20 degrees positive pitch, 15 degrees negative pitch or 45 degrees of bank. Additionally, a manual declutter switch is provided on the pilot yoke to provide the declutter function whenever desired. The normal display returns when normal flight parameters are regained for a predetermined period.

FOLLOW ON TESTS

The proposed changes addressing these findings, after engineering review, were evaluated by the Flight Test Branch using appropriate portions of the Type Inspection Authorization used to originally certify the system. All changes were found satisfactory and the Supplemental Type Certificate was amended to delete the multiple pilot requirement for flight in IMC.

REFERENCES

1. G. E. Cooper and R. P. Harper, The Use of Pilot Rating in the Evaluation of Aircraft Handling Qualities, NASA TN-D-5153, April 1969
2. L. A. Haworth and R. L. Newman, Flight Test Techniques for Display Evaluation, NASA TM-103947, February 1993
3. Flight Test Guide for Certification of Normal, Utility, and Acrobatic Category Airplanes, FAA AC-23-8A, February 9, 1989
4. R. L. Newman, Head-Up Display Design Guide, AFWAL TR-87-3055, Vol I, September 1987

ACKNOWLEDGMENTS

The author expresses his sincere thanks to Mr. Richard L. Newman of Crew Systems, Inc. Mr. Newman's insights and experience in display design and evaluation were extremely helpful in completing this work .

All tables and figures in this paper were reprinted from test plans and reports provided by Flight Visions, Inc. They were reproduced here with the expressed written permission of Flight Visions, Inc.

APPENDIX 1
FLIGHT TEST DATA CARDS

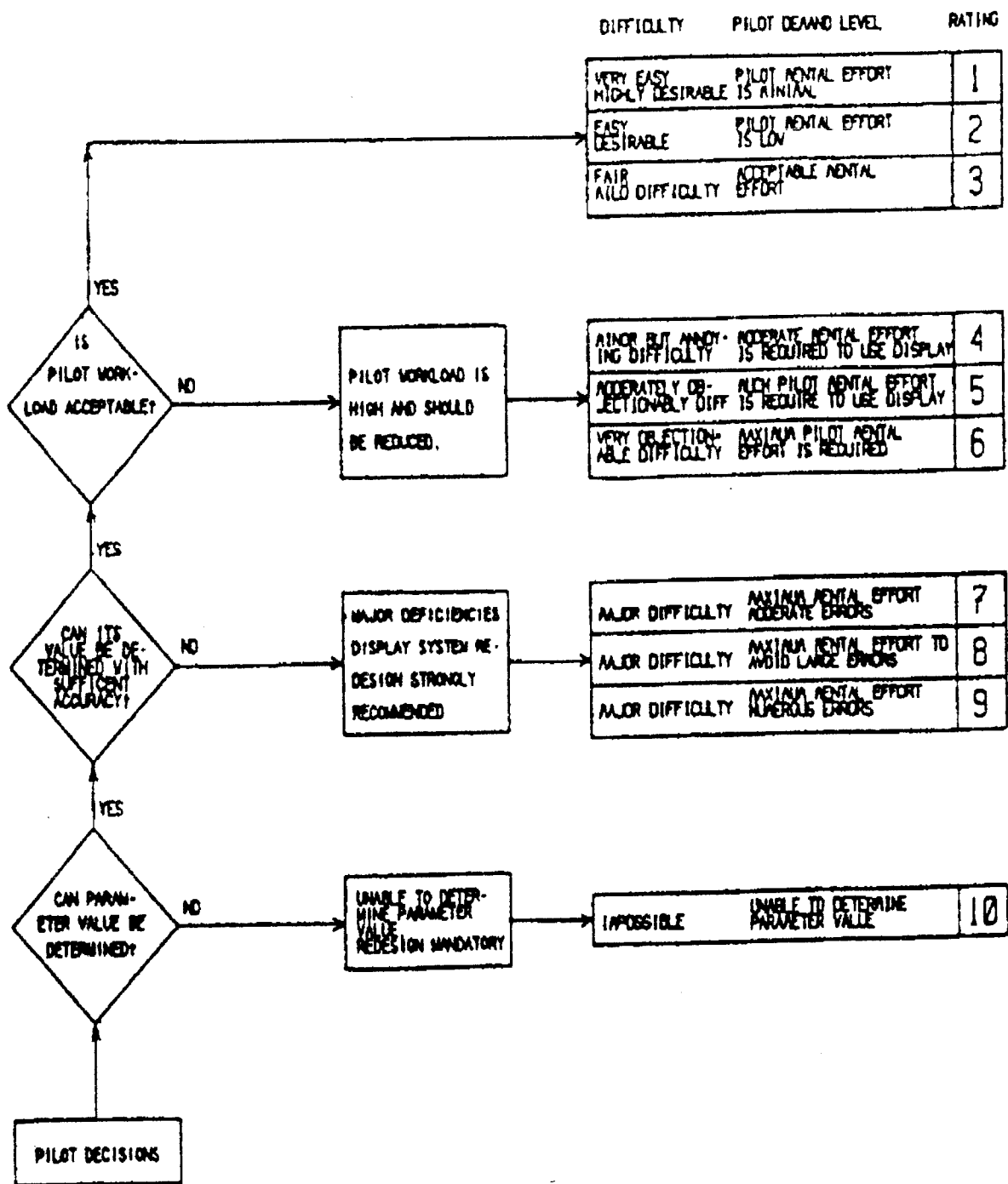


**Figure 1: Display Rating Decision Tree,
Ease of Reading Data**

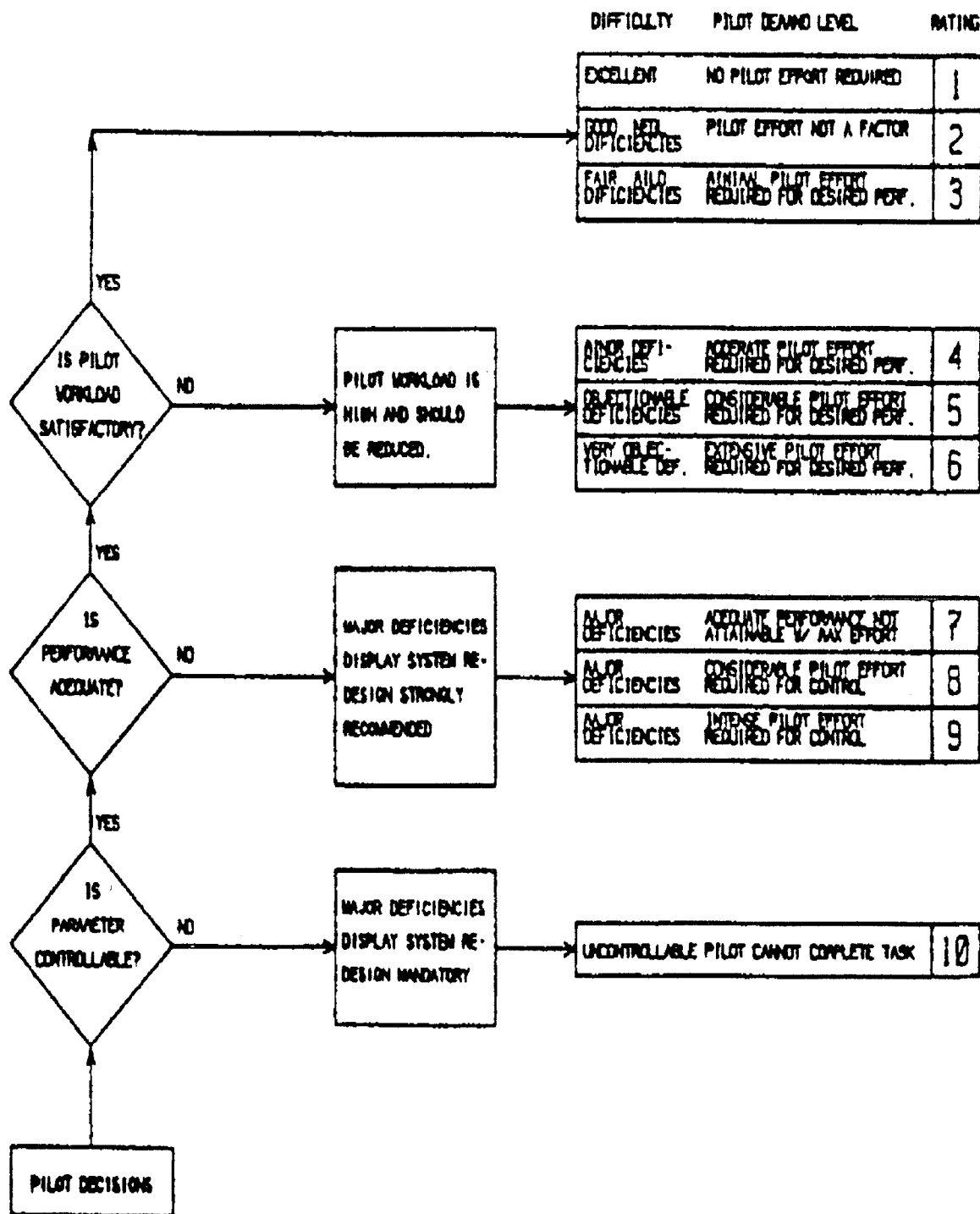


**Figure 2: Display Rating Decision Tree,
Ease of Control**

PITCH/ROLL RESPONSE DATA CARD

Pilot: _____

Maneuver: _____

Configuration: _____

Sortie: _____ Date: _____

PARAMETER	READ- ABILITY RATING	CONTROL- LABILITY RATING	REMARKS (include estimate of precision, need for parameter, reason for rating, etc.
Pitch Axis			
Lateral Axis			
Yaw Axis			
Airspeed Control			
OVERALL ORIENTAT'N			
OVERALL CONTROL			

Comments:

APPROACH: PILOT RATING CARD

Pilot: _____

Approach No: _____

Airport: _____

Approach: _____

Landing Runway: _____

Vref: _____

PARAMETER	READ- ABILITY RATING	CONTROL- LABILITY RATING	REMARKS (include estimate of precision, need for parameter, reason for rating, etc.
Pitch Axis			
Lateral Axis			
Airspeed Control			
Distance to go			
Interceptn Orientat'n			
OVERALL ORIENTAT'N			
OVERALL CONTROL			

Maximum deviation between FAF and minimums: Lateral: _____
 Vertical: _____
 Airspeed: _____

Within Safe Landing Window at straight-in minimums? () Yes
 () No
 () N/A

Landing or Missed Approach? () Straight-in
 () Circle-to-Land
 () Intentional Missed Approach
 () Traffic Induced Missed Approach
 () Missed Approach (Pilot Decision)

APPROACH: SAFETY PILOT RATING CARD

Pilot: _____ Approach No: _____
 Airport: _____ Sortie: _____ Date: _____
 Approach: _____ Time: _____ D() N()
 Weather: _____ Landing Runway: _____
 Flap Setting: _____ Vref: _____

DEVIATION	VERTICAL	LATERAL	AIRSPPEED	REMARKS
Interceptn				
Final Ap- roach Fix				
400 ft				
300 ft				
200 ft				
Minimums				
Initial Climb				
Circle to Land				

Maximum deviation between FAF and minimums: Lateral: _____
 Vertical: _____
 Airspeed: _____

Within Safe Landing Window at straight-in minimums? () Yes
 () No
 () N/A

Landing or Missed Approach? () Straight-in
 () Circle-to-Land
 () Intentional Missed Approach
 () Traffic Induced Missed Approach
 () Missed Approach (Pilot Decision)

POST FLIGHT DATA CARD

Pilot: _____

Sortie: _____ Date: _____

Was the HUD suitable for the flight tasks flown?

Comments:

Were the following functions used?

Used	Function	Comments
------	----------	----------

<input type="checkbox"/>	Airspeed	
--------------------------	----------	--

<input type="checkbox"/>	Altitude	
--------------------------	----------	--

<input type="checkbox"/>	Course	
--------------------------	--------	--

<input type="checkbox"/>	Heading	
--------------------------	---------	--

<input type="checkbox"/>	Stopwatch	
--------------------------	-----------	--

<input type="checkbox"/>	Checklist	
--------------------------	-----------	--

Were there any problems with detecting other traffic caused by the HUD?

Were the flight manual procedures clear and appropriate?

Any other problems, comments, or observations?

APPENDIX 2
HUD DISPLAY SYMBOLOGY

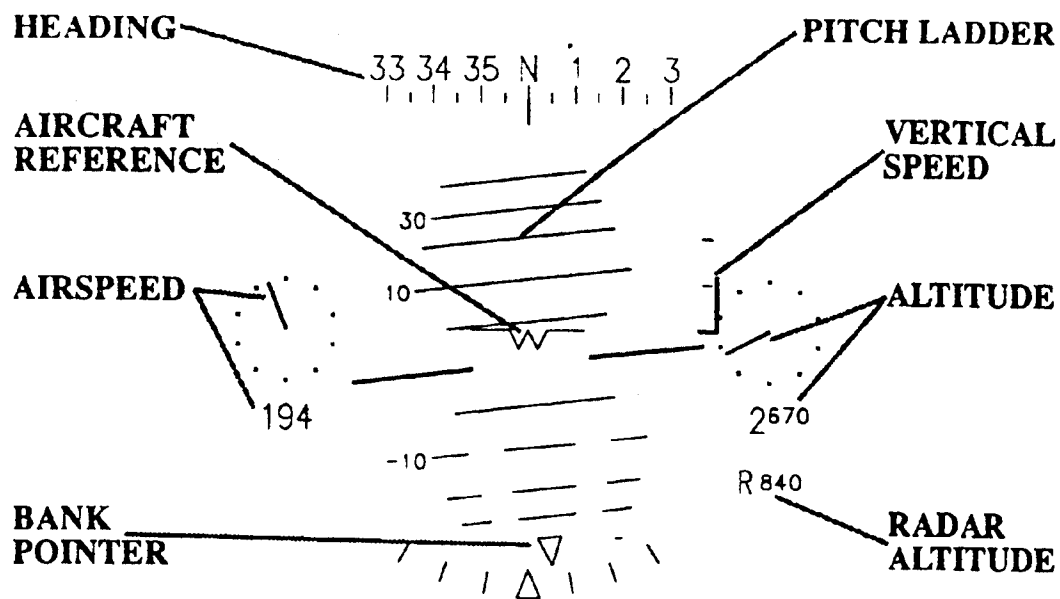


FIGURE 1. BASIC FLIGHT SYMBOLOGY

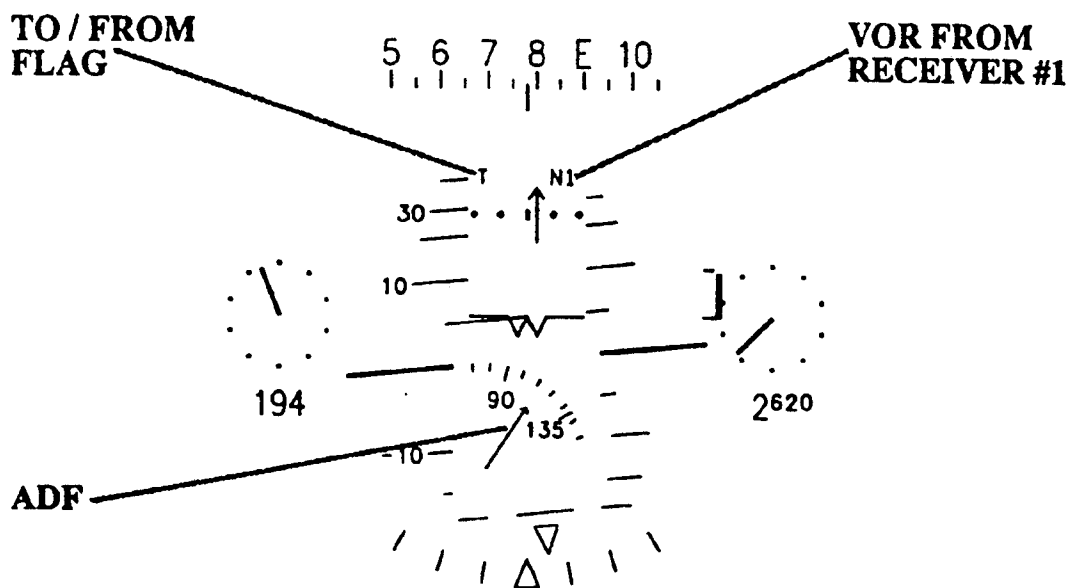


FIGURE 2. BASIC NAVIGATION SYMBOLOGY

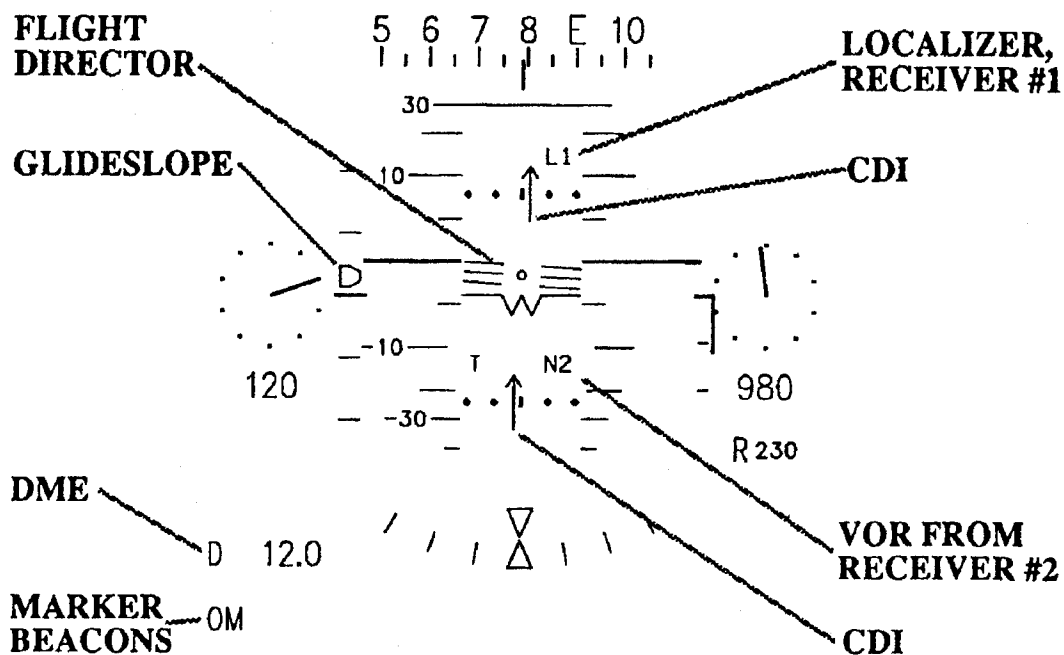


FIGURE 3. ILS WITH FLIGHT DIRECTOR SYMBOLOGY

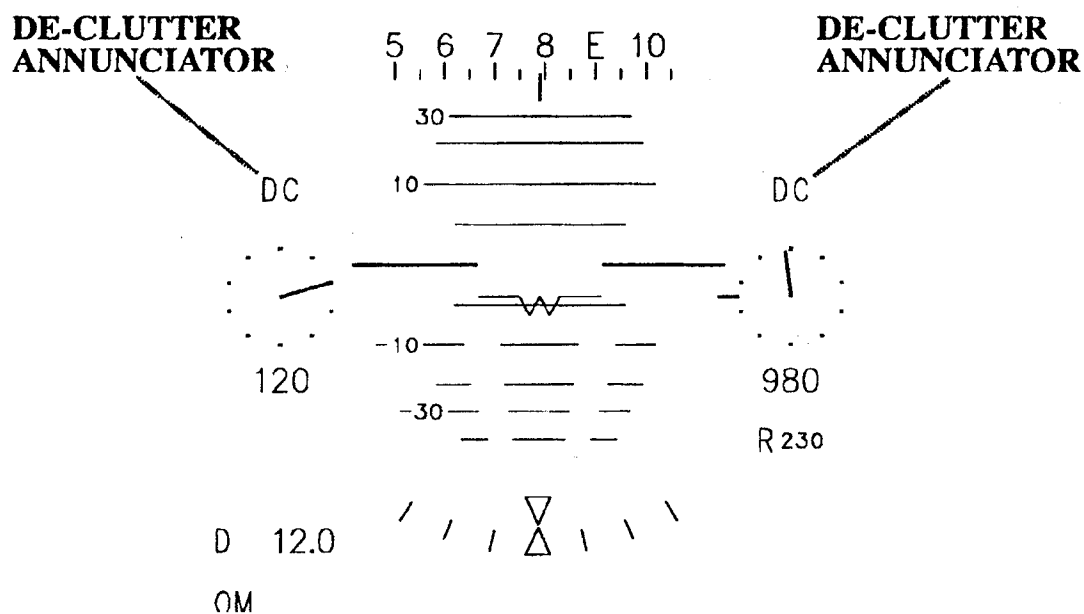


FIGURE 4. DECLUTTER MODE

PRELIMINARY CONCEPTION OF AN AIRCRAFT LIFT MONITORING AND TAKEOFF ADVISORY SYSTEM

Georges A. Bécus* and Sergey Kofman†
University of Cincinnati, Cincinnati, Ohio 45221-0070

ABSTRACT

A preliminary conception of an aircraft lift monitoring and takeoff advisory system is proposed. The system is based on a comparative analysis of the takeoff characteristics of the actual aircraft and those of an aircraft model. The integration of aircraft mathematical model is carried out during the aircraft takeoff in real time. Differences between real and nominal characteristics are used in graphical visualization program to display the information to the pilot and in an advisory module which analyzes this information and provides suggestions for probable causes and remedies. To improve the accuracy and reliability of the system it is proposed to introduce learning capabilities in the model, using artificial neural networks, for adaptation to unmodeled dynamics, changes in dynamics and various takeoff procedures.

INTRODUCTION

One important aspect of aviation safety is to provide the aircraft pilot with all the necessary information about the aircraft characteristics and flight conditions, especially during such critical flight regimes as takeoff and landing. About 12% of all aircraft accidents are classified by NTSB and NASA researchers as takeoff-related accidents and the accident rate during takeoffs has remained constant (about 2 per million flights), while the rate for other types of accidents has decreased. This flight regime demands from the pilot special attention and quick reaction to any unforeseen incidents, such as system failure (engine, control system, avionics, etc.) or abrupt change in weather conditions (e.g. wind shear), etc. [1]. During takeoff, the high speed, close proximity to the ground and especially lack of adequate information do not leave much time for the pilot to evaluate decisions and take the appropriate action; this can lead to fatal consequences [2].

Existing takeoff monitoring systems, which have been developed since 1983 by NASA, provide the pilot with information about the aircraft speed during takeoff and predict the approximate takeoff point [3]. At present time, there is no capability to determine the actual lift force and/or actual stall parameters for the aircraft (which can be significantly affected by wing contamination), although this information is very important, especially during takeoff. The long term goal of the research is the development of a monitoring and advisory system which can analyze aircraft aerodynamics during takeoff, determine variations in lift and stall characteristics, display this information to the

* Associate Professor, Aerospace Engineering and Engineering Mechanics, Senior Member AIAA

† Graduate Student, Aerospace Engineering and Engineering Mechanics, Student Member AIAA

pilot in a form which can be readily interpreted and provide the pilot with advice regarding probable causes for differences and suggestions for appropriate action.

GENERAL APPROACH

The lift and stall monitoring system is based on the real time analysis and comparison of the outputs of an (adjustable) model of the aircraft and those of the actual aircraft. The overall architecture of the proposed system is shown in the functional diagram of Figure 1 below.

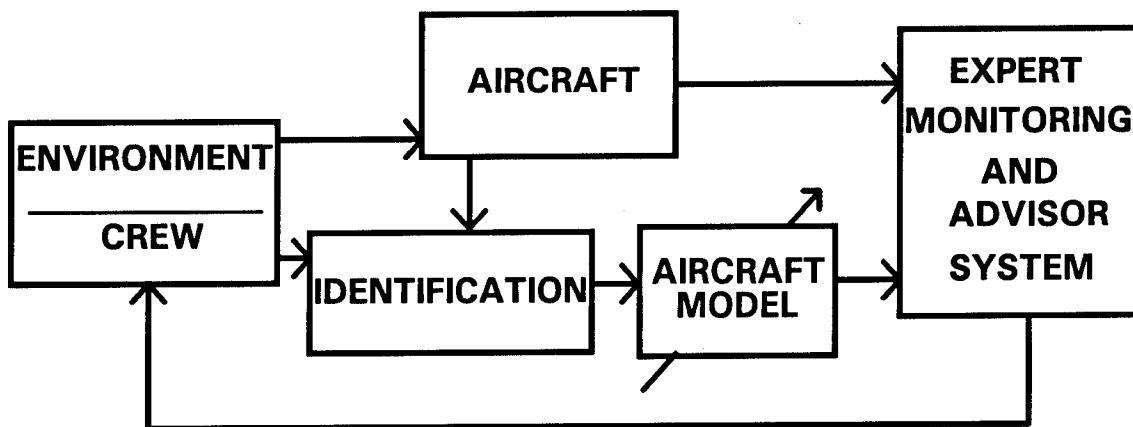


Fig. 1 Architecture of Proposed System

We now provide some details on the overall operation as well as on the various functions of the system.

Assume that all information, such as aircraft data before takeoff (aerodynamic, thrust and weight characteristics), initial takeoff data (conditions and length of runway, weather conditions, atmospheric pressure at airport level, wind speed and direction, etc.), airspeed sensor and lift sensor readings, etc. required for accurate simulation of the takeoff is available. (All of this information, except for lift, is currently available on modern aircraft.) In the above functional diagram, this information is relayed to the AIRCRAFT MODEL module via the IDENTIFICATION module by the ENVIRONMENT/CREW and AIRCRAFT modules. Using a model of the aircraft and the knowledge of its nominal aerodynamic characteristics, the expected value of lift on the aircraft at any airspeed can be calculated. We call this "nominal lift". We can determine not only the numerical values of nominal lift, but also its behavior as a function of airspeed so that it is possible to predict future values of lift based on predicted values of airspeed. These computations are carried out by the AIRCRAFT module.

In the EXPERT MONITORING AND ADVISOR SYSTEM module a COMPARATOR system compares this nominal lift (current or predicted) with the "actual lift", obtained from lift sensors measurements provided by the AIRCRAFT module to determine differences, if any, between nominal and actual lift. This information is relayed to a MONITOR system (part of the EXPERT MONITORING AND ADVISOR SYSTEM module) which, through graphical display of aircraft lift and airspeed (provided by a DISPLAY system also part of the EXPERT MONITORING AND

ADVISOR SYSTEM module), allows the pilot to visualize differences, if any, in the development of nominal and actual lift. When there is a difference in behavior, an EXPERT SYSTEM (also part of the EXPERT MONITORING AND ADVISOR SYSTEM module), uses its DATABASE, RULE BASE and INFERENCE ENGINE to determine the probable cause, which is most likely is aerodynamic in nature, and may, for example, be connected with wing contamination (ice, snow, etc.) or inadequate takeoff configuration [4,5]. The EXPERT SYSTEM relays this information to an ADVISOR system (also part of the EXPERT MONITORING AND ADVISOR SYSTEM module), which provides the pilot with advice regarding probable causes for differences and suggestions for appropriate action. A functional diagram of the EXPERT MONITORING AND ADVISOR SYSTEM module appears in Figure 2 below.

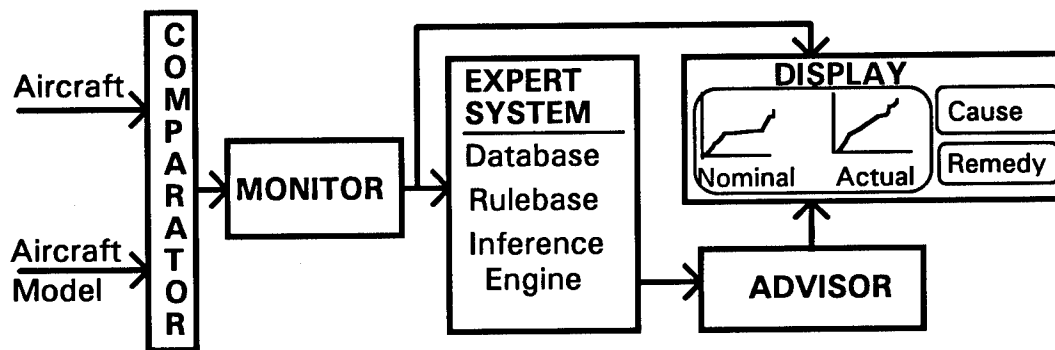


Fig. 2 Expert Monitoring and Advisor System

Thus the monitoring and advisory system proposed gives the pilot a picture of the actual lift, how it differs from nominal, determines whether this difference is dangerous, calculates the new stall angle of attack and stall airspeed, and, based on this information, predicts the new takeoff point and takeoff speed. All this information will help the pilot in getting a more complete picture of the aircraft during takeoff than he presently has, in avoiding reaching the stall angle of attack and stall airspeed, as well as in making an informed decision to abort takeoff when, for example, the aircraft has adequate airspeed but inadequate lift.

Lift sensors which are used to determine actual lift play a key role in this monitoring system. These are part of the AIRCRAFT module of Fig. 1 as we adopt the standard control theory convention that actuators and sensors are part of the plant. Conceptual details about their implementation are now provided. First of all, these can be pressure sensors on the upper and lower surfaces of the wings and stabilizer and left and right surfaces of the vertical tail. The pressure differences can be used to estimate actual lift and side force (which can develop on the tail due to ice). Lift estimates can also be obtained by independent measurements of the loads the on landing gears (while the aircraft is in contact with the runway). These loads equal the weight of the aircraft at zero airspeed, then decrease as airspeed increases (due to lift development) and equal zero at the takeoff point. These two independently obtained estimates can be compared and combined (also in the AIRCRAFT module) to obtain the actual lift which is then relayed to the EXPERT MONITORING AND ADVISOR SYSTEM module. This partial redundancy in lift measurements provide the proposed monitoring and advisory system with a degree of fault tolerance.

The lift monitoring system described above would be effective primarily at detecting and warning the pilot of changes in aircraft performance due to improper take-off configurations. (Malfunctioning of control system can leave control surfaces like flaps, or leading edge in an inadequate position.) The effect of inadequate takeoff configuration on stall margin was recently studied by the authors [6,7]. The major effects of wing contamination (on lift and stall margin, see [6,7]) do not appear however until after rotation (when take-off cannot be aborted anymore). For this reason, the proposed system will also include "contamination sensors" (based on capacitance measurements for example, and also part of the AIRCRAFT module of Fig. 1) to accurately determine contamination and predict its effects on take-off.

In order for such a monitoring and advisory system to become a useful and reliable tool, several issues need to be addressed. The primary issue concerns tradeoffs between the accuracy and the computational complexity of the aircraft model. To achieve the degree of accuracy required for reliable monitoring and advisory functions, it is proposed to use adaption of the model. This adaption should be carried out at a slower rate than the monitoring. In addition, it is envisioned to use different levels of adaption: First, ordinary parameter estimation techniques can be used to update the model parameters using the (stored) outputs of aircraft sensors. Second, as this type of adaption does not account for unmodeled dynamics, and since a mathematical model which would simulate to a high degree of accuracy the behavior of the aircraft would be too complex to carry out real time simulations, it is proposed to introduce learning capabilities into the system, using a connectionist system approach based on artificial neural networks, for adaption to unmodeled dynamics, changes in dynamics and various takeoff procedures. In this scheme, run in parallel with ordinary parameter estimation techniques, but at a different rate (slower), a feedback controller, based on artificial neural networks techniques, adapts the simple mathematical model of the forward loop and uses each takeoff for system training. Note that one advantage of this adaption is that it can also be used for aircraft health monitoring.

A secondary issue, in addition to model adaption, concerns the needs of the expert system for learning capabilities in order to fine tune the advisory system. Here again, this learning could be carried out by an connectionist system (artificial neural network) which could, after the fact, utilize each takeoff for training purposes. The performance evaluation required for such a system could be provided in part by the pilot who would act as a critic for the monitoring and advisory system.

The need for adaption raises another important issue: the timing of the various adaption mechanisms. While it is clear that these should be carried out at different rates, the proper timing for accurate and reliable operation needs to be investigated. An ADAPTION SCHEDULER module may have to be added to the architecture of Fig. 1 to resolve these timing issues.

Feasibility studies for such a monitoring and advisory system are currently carried out. They are based on computer simulations both for the actual aircraft and its model. Details of these simulations are provided in the following section.

SIMULATION PROCEDURES

The motion of the aircraft is obtained by integration of the system of differential equations modeling the aircraft dynamics using simulated measurement inputs. In this simulation, the following assumptions were made:

- the aircraft is a rigid body

- only longitudinal motion was considered
- all control surface deflections occur instantaneously
- the drag force due to control surface deflections is neglected
- during take off the aircraft rotates around the center of gravity
- the position of engine control levers is not changed during takeoff

The following equations of aircraft longitudinal motion were used [8],[9]:

$$\begin{aligned}\dot{V} &= \frac{1}{m} [T \cos(\alpha + \varphi_{\text{eng}}) - W \sin \gamma - D - f R_{\text{gear}}] \\ \dot{\alpha} &= \dot{\theta} - \dot{\gamma} \\ \dot{\theta} &= Q \\ \dot{Q} &= \frac{M}{I_{yy}} \\ \dot{H} &= V \sin \gamma\end{aligned}$$

where:

T is the thrust force,

L is the lift force: $L = C_L \bar{q} S$,

D is the drag force: $D = C_D \bar{q} S$,

W is the weight of the aircraft: $W = mg$, with m = mass of the aircraft,

R_{gear} is the normal reaction on the landing gears: $R_{\text{gear}} = W - L - T \sin(\alpha + \varphi_{\text{eng}})$,

f is the friction coefficient,

α is the angle of attack,

φ_{eng} is the angle between thrust vector and longitudinal body axis X ,

γ is the flight path angle: $\dot{\gamma} = \frac{1}{mV} [T \sin(\alpha + \varphi_{\text{eng}}) + C_L \bar{q} S - W \cos \gamma]$,

θ is the pitch angle,

Q is the pitch rate,

M is the aircraft moment: $M = M_{\text{aero}} - M_{\text{gear}}$ with

$M_{\text{aero}} = C_m \bar{q} S \bar{c} + (C_{mq} Q + C_{m\dot{\alpha}} \dot{\alpha}) \frac{\bar{q} S \bar{c}^2}{V}$ = aerodynamic moment of aircraft, where

$C_m = C_{m0} + C_{m\alpha} \alpha + C_L (x_{cg} - x_{ac}) + C_{m\delta_a} \delta_{el} + C_{m\delta_e} \delta_{le}$, and

$M_{\text{gear}} = R_{\text{gear}} (x_{\text{gear}} - x_{cg})$ = moment of landing gears on the aircraft,

and H is the altitude.

Two simulation procedures, one for the real aircraft and the other for mathematical model provide the necessary information to a graphic visualization program which displays on the computer screen differences in nominal and actual lift, physical locations of these differences (wing, tailplane, etc.) and probable cause (wing contamination, non takeoff configuration, etc.). During this simulation stage, simple computer models of the various phenomena or malfunctions which can affect lift: engine failure, non nonstandard aircraft configuration (e.g. flaps are not in takeoff position), modeling of ice on the wing (due to the absence of analytical models of wing contamination effects), disturbances in lift coefficient, etc. are used.

CONCLUSIONS

A preliminary conception of aircraft takeoff monitoring system has been introduced. A preliminary version of the system is currently being developed and tested, using aircraft mathematical models and computer simulations. A simple graphical visualization program has been developed; it uses the information, provided by two simulation processes (real aircraft and mathematical model), running simultaneously. The next step will be an attempt to introduce adaption capabilities in the system, using ordinary parameter estimation first, then artificial neural networks.

REFERENCES

1. **"Flight Standards/Aviation Accidents Prevention Program,"** Federal Aviation Administration, Washington DC, 1987.
2. **Aircraft Accident Report PB91-910410,** National Transportation Safety Board publication NTSB/AAR-91/09, Washington DC, 1991.
3. **Takeoff Performance Edition, Up Front,** Flight Safety Publication of Delta Airlines, Special Edition February, 1990.
4. J.W. Steenbilk, **"Turboprop Tailplane Icing,"** *Airline Pilot Magazine*, pp. 30-33, January, 1992.
5. M. Ingelman-Sundberg, **"Why Icing Causes Tailplane Stalls,"** *Airline Pilot Magazine*, pp. 34-36, January, 1992.
6. S. Kofman and G.A. Bécus, **"Determination of Aircraft Stall Margins during Take-Off,"** Final Report, NTSB Grant RA-3-013, October 1993.
7. S. Kofman and G.A. Bécus, **"Determination of Aircraft Stall Margins during Take-Off,"** to be submitted, 1994.
8. B. Etkin, **"Dynamics of Atmospheric Flight,"** Wiley, New York, 1972.
9. B.L. Stevens and F.L. Lewis, **"Aircraft Control and Simulation,"** Wiley, New York, 1992.

DUCTED FAN PROPULSION FOR A GENERAL AVIATION REPLICA FIGHTER AIRCRAFT

Dr. Ernest R. Jones, Associate Professor
Mr. Mike Stevens, Graduate Student
Mr. Adriano Almeida, Graduate Student
Embry-Riddle Aeronautical University
Daytona Beach, FL

ABSTRACT

Scale fighter plane replicas are becoming increasingly popular in Sport Aviation, which is one important aspect of revitalizing general aviation. However, no suitable propulsion systems exist for jet sport aircraft. The technology for ducted fan propulsion of larger aircraft has been established, but applications to light aircraft have been few.

The feasibility of using ducted fan propulsion for a 2/3 scale replica of the Douglas A-4 "Skyhawk" fighter plane was determined by performing a complete conceptual design of the aircraft. Results of the study show that such a design is feasible, and that the performance in all flight regimes is acceptable if a readily attainable power loading is used.

Compared to conventional aircraft, the advantages of such a design are; ownership of a unique and exciting aircraft, quiet operation, enhanced ramp safety due to enclosed propeller, and performance exceeding most general aviation aircraft. Disadvantages include; slightly increased weight and cost (both initial and operating), limited fuselage volume and center of gravity travel, and more difficult engine accessibility.

A complete ducted fan propulsion system concept has been developed, including design of the fan, inlet ducts, and outlet ducting. A structural design concept is also shown accounting for all of the required systems, and which would permit fabrication of a prototype at low cost.

INTRODUCTION

Sport Aviation has grown steadily since the mid 50's and has now reached a level of maturity such that a greater number of homebuilt aircraft are taking to the air each year than production aircraft by the major manufacturers. Some high performance homebuilts are also exceeding functionality and performance of production aircraft, and they are gradually shedding their former slightly disreputable status.

The FAA is even encouraging the development of new light aircraft by simplification of the certification process, and a number of homebuilt aircraft are being certificated for production under these new regulations. The future of sport and light aviation looks brighter than it has for years, and many new aircraft are under development to try to catch the resurgent wave of popularity for sport flying whether it be fixed wing, rotary wing, sailplanes, aerobatics, warbirds, or restoration of classic and antique aircraft.

Replica fighter aircraft are a popular alternative for the average pilot without the means and training to own and operate one of the increasingly rare "Warbirds". These are almost entirely propeller driven

aircraft however, since jet powered sport aircraft are, and will continue to be, very rare due primarily the high cost of purchasing and operating gas turbine engines.

However, the thought of flying around in a jet fighter aircraft is an intriguing one. A possible method for achieving much of the "look and feel" of a jet without the associated high cost is to use a ducted fan propulsion system powered by a conventional reciprocating engine. The purposes of this design study were to (1) investigate whether a ducted fan propulsion system is a feasible means of powering a replica jet fighter, and (2) to determine if adequate performance levels are attainable.

The results of that design study are summarized in the following report. Interested readers may contact the authors for more detailed information.

DESIGN REQUIREMENTS

The proposed aircraft is a single seat sport plane which will be flown only for pleasure and display purposes. It should be a subscale replica of a jet fighter aircraft having wide recognition and appeal, and maintain the scale appearance in so far as possible. The aircraft would be designed using FAR 23¹ regulations as a guideline, but would be certified in the experimental category. The structure would be designed for the aerobatics, although there is no intent to make the aircraft competitive in aerobatics.

A reasonable high level of performance would be required to make the airplane attractive, and the following performance goals were specified:

- Stall speed = 61 kts maximum
- Cruise speed = 175 kts minimum
- Range = 450 nm plus reserves minimum
- Payload = 170 lb pilot plus 35 lb baggage
- Take off and landing from typical GA airports = 3000 ft over 50 ft obstacle.

REPLICA AIRCRAFT SELECTION

The selection of a suitable aircraft for scaling is partially governed by the size of the cockpit relative to the overall external dimensions. When a large aircraft is selected as a candidate, the size must be reduced sufficiently to accommodate a reasonable sized, low cost powerplant. However, the cockpit must remain large enough to fit the pilot. A subtle change in the geometry should not offend the replica enthusiast, but as seen in the case of the BD-10, the required cockpit size tends to be larger than is aesthetically pleasing. Other complications arise with mid-mounted wing configurations, especially if the landing gear retracts into the fuselage. The internal fuselage volume is important in ducted fan design, since the thrust and efficiency are dependent on the fan diameter.

The F-15, F-16, F-4, F-18, and the A-4⁵ were among the many aircraft considered. The A-4 Skyhawk was found to present the minimum number of problems in terms of powerplant installation and pilot integration. Moreover, the A-4's low wing allows for easy engine access, wing mounted landing gear, and ease of fuselage to wing integration.

All of the low aspect ratio fighters have similar problems in the lower speed and high angle of attack regime, since the induced drag is high for this type of configuration. In addition, as the vortex flow begins

to dominate at the higher angles of attack, the maximum lift is typically delayed to the angles beyond 20 degrees for symmetrical airfoils. Although low aspect ratio invokes a large penalty in terms of induced drag and minimum lift, the affects can be minimized by having a light span loading. If the wind loading is sufficiently low, the penalties imposed by the low aspect ratio are bearable. Examples of successful low aspect ratio sport aircraft are the Dyke Delta and the Rutan Variwidge, which have reportedly pleasant flight characteristics and attractive performance levels.

CONFIGURATION LAYOUT

As shown in the 3-view drawing in Appendix 1, the 2/3 scale replica A-4, dubbed the "Minihawk" has a wing span of 18.3 ft, a total length of 27 ft, and a height of 5 ft at the nose. With the exception of a thicker wing section, a slightly larger canopy, and modified ailerons, the replica has dimensions scaled precisely from the original aircraft.

AERODYNAMIC SURFACES

The wing section is a NACA 0012 symmetrical airfoil and tail surfaces are NACA 0009 sections. Longitudinal control is provided by a stabilator while roll and yaw are provided by a conventional aileron and rudder.

LANDING GEAR

The landing gear system for the Minihawk is similar to the original configuration. The replica's landing gear features some key changes which make the system more affordable. The primary changes are the incorporation of a castoring nose wheel and a simplified retraction geometry. The increased wing thickness and slightly larger retractions pods allow the main gear to be retracted forward without having to undergo a 90 rotation as the A-4 does. The retraction system operates on manually actuated hydraulic pumps and the up and down locks are cable actuated for overall simplicity and ease of design.

The landing gear legs consist of telescoping steel tubes that use a system of rubber donuts between each tube for proper shock absorption. The gear doors will be sequenced with the retraction through mechanical linkages. The nose gear retracts forward into the cockpit such that the gear leg is positioned beneath the seat and the wheel fits between the rudder pedals. Emergency gear extension will rely on g-loading and flow induced forces such as on the original A-4.

During low to intermediate taxi velocities, directional control is provided through the use of differential braking, while during takeoff and landing the rudder provides sufficient authority for ground control due to the higher velocities. The primary drawback of a castoring nose wheel is that during pushback operations, there is a tendency for the wheel to cock sideways.

The fact that the Minihawk sits fairly high on its gear and has a relatively large fuselage area could create some difficulties during cross wind operations. The operator will have to ensure that the established cross wind limitations are not exceeded for safe flight.

WEIGHT AND BALANCE

The gross and empty weights, as well as the center of gravity position and range, were calculated using the methods given by Raymer⁴ and available in Raymers Design Software (RDS). The initial weight estimates

were somewhat low at approximately 1500 lb whereas the revised weights of 1829 lb gross and 1407 lb. empty seem more reasonable for this size aircraft. Due to the internal ducting requirements associated with this type of aircraft, the conservative weight estimates were used as given by the general aviation category in the RDS software. At \$100 per pound saved, an additional 70 lb. can be save by substituting an aluminum block engine for the conventional cast iron block.

The static margin changes from 11% to 16% of the mean aerodynamic chord depending on the fuel load and pilot weight. The baggage allowance of 35 lb. has little effect on the aircraft CG because of the proximity of the load to the aircraft CG.

The replica configuration is very susceptible to pilot weight however, since a relatively long moment are exists between the cockpit and the aircraft center of gravity, and since the pilot weight makes up a higher percentage of the gross weight than in the original A4. If the pilot weight is increased by 30 lb., the CG is shifted forward by one inch, corresponding to a 2% change in the static margin. The shift in CG resulting from changes in the cockpit weight is not a major problem for a single seat version, but would probably create the need for ballasting in a two seat variant. Table 1 summarizes the resulting weight estimates.

TABLE 1. WEIGHT AND BALANCE SUMMARY

<u>Structures Group</u>	<u>Weight (lb)</u>	<u>Equipment group</u>	<u>Weight (lb)</u>
wing	150	flight controls	28
horizontal tail	26	hydraulics	2
vertical tail	55	electrical	54
fuselage	225	avionics	25
main landing gear	97	total	109
nose landing gear	39		
total	592		
<u>Propulsion Group</u>	<u>Weight (lb)</u>	<u>Useful Load Group</u>	<u>Weight (lb)</u>
installed engine	683	pilot	170
fuel system	23	fuel	210
total	706	oil	7
		cargo	35
		total	422
			<u>Distance from nose</u>
Empty Weight	1407 lb.	CG (no fuel)	162.5 in
Gross Weight	1794 lb.	CG (gross weight)	158.5 in

COCKPIT

The cockpit was one of the important criteria considered during the aircraft selection process. The published minimum acceptable dimensions for the 90th percentile pilot were used as the guide lines in selecting the aircraft scale factor. The cockpit dimensions arrived at should be comfortable for the average pilot. The proposed mission of the aircraft is mainly for sport flying, therefore the required instrumentation is minimal. Basic VFR instrument, navcom, transponder, and handheld GPS would be more than adequate for the mission requirements. The minimal instrumentation helps keep weight and cost down, but if

desired, one could capture the jet image by making use of one of the recently developed heads up display units that provide performance and navigation data all in one location. Available heads up displays sell for as low as \$5000 depending on the navigation capability.

The use of a sidestick controller is employed in order to establish more precise control during slow flight, when the stick forces are lower. Moreover, it helps to reduce the required cockpit depth. The flight control system is simpler than in many general aviation production aircraft, such as that found in the TB-9.

The entire nose and cockpit of the aircraft is seen as being a cohesive structural unit that maintains its integrity in the event of an incident, with the canopy frame and forward bulkhead providing the required roll over protection.. Recent data published by Cirrus Aircraft Corporation indicates that seat energy absorption requirements can be achieved through the use of TemperfoamTM, which greatly simplifies the design of the seat and associated structure. The canopy design replicates that of the original but the requirements for impact and battle damage are less severe.

STRUCTURAL CONCEPT

The basis for the prototype Minihawk structure is foam and fiberglass composite sandwich construction using a wet lay up technique. The wing has three spars which were designed to handle the flight loads as well as loads imposed by the retractable landing gear during ground operation. In order to accommodate the complex spanwise taper geometries, the wing spars are constructed from foam stabilized graphite composite. Instead of using a solid foam core, ribs are cut from foam and spaced at approximately 1 foot intervals. A solid foam core was found to produce a large weight penalty which could be overcome by using the more conventional built-up approach. The entire wing structure is covered with 1/16 inch plywood and 2 layers of very light weight glass cloth. The plywood is equal in strength to fiberglass in terms of capability to transmit shear loads, but it also reduces the amount of filling and sanding required for a suitable finish when compared to a strictly glass over foam construction. The two layers of 3/4 oz. glass serve to seal the surface and to protect it from the environment. Another advantage of the plywood is that the structure can be painted any color with no risk of losing strength at elevated temperatures, such as with a typical wet lay-up. The control surfaces are cut from a single piece of foam, a spar is installed, and the assembly is skinned with plywood and fiberglass.

Detailed design of the fuselage structure is a challenging task. The prototype will utilize two frames to support the fan-engine integration, as well as to transmit the wing shear loads. The forward fuselage bulkhead is a focal point for the loads imposed by the nose gear and the pilot, and it also acts as the firewall. The ducting is a thin walled fiberglass construction inside the tail which is designed to withstand the hoop stresses resulting from elevated pressures. The fiberglass inlet ducting needs to be reinforced, since there will be negative gage pressures in that region during takeoff and acceleration. The inlet ducting will follow similar paths to that of the original A4, except for the addition of a large *cheater hole* in the bottom of the fuselage. The *cheater hole* is necessary for providing the fan with sufficient mass flow during takeoff.

The horizontal stabilizer consists of a plywood skinned foam core, with a spar and torque tube along with several ribs made of light plywood. The rudder is virtually identical to the aileron in construction and hinging.

PROPULSION SYSTEM

The propulsion system is the key technology of the proposed concept, and consists of an engine, ducted fan, drive shaft, fuel tank and system components, intake and exit ducts, and cooling system (radiator). Each of these propulsion system components is discussed in what follows.

ENGINE SELECTION

A number of engines were considered for the Minihawk, including small gas turbojet engines, however it was quickly obvious that no suitable jet engine exists that can be purchased for any reasonable price. Thus, the ducted fan propulsion system, powered by a reciprocating engine was selected.

Both aircraft and automotive engines were considered for the powerplant. Aircraft engines in the required power range (300 to 400 hp) were very expensive as shown in the table below. Also shown in the table are two of the many automotive engines considered. The usual drawbacks of automotive engines for propeller driven aircraft are actually advantages in a ducted fan design. The operating range of the fan is in the vicinity of 4,000 to 6,000 rpm, which is about the same as the average V-8 automobile engine. It is probable that a direct drive system could be utilized without problems, making the propulsion system simple and light weight.

TABLE 2. COMPARISON OF A TYPICAL AIRCRAFT ENGINE TO AUTOMOTIVE ENGINES

Engine	Cost	Weight (lb.)	BHP	Fuel Consumption	Overhaul Cost
Lyc IO-720	\$70,000	568	400	18 gph	\$8000
Ward V-8	\$20,000	535	475	15 gph	\$800
ZR-1 V-8	\$3,000	605	350	13 gph	\$800

From Table 2 it is seen that a ZR-1 V-8 engine (Chevrolet small block) is slightly heavier than a Lycoming IO-720, but it has a lower fuel consumption and is much cheaper. The Aluminum block Ward V-8 save 70 lb. in weight but adds approximately \$7000 to the acquisition cost. Since the ZR-1 is relatively inexpensive and comes ready to run from the factory with an output of 350 hp at 5600 rpm, it was used as the baseline for the replica propulsion system.

The Chevrolet small block is one of the most popular engines in the hotrod market, so there are numerous after market options available at reasonable prices. For example, a Paxton supercharger is available for \$4000 complete. Using a supercharger would allow the replica jet to maintain rated power to 10,000 ft., where the increase in true airspeed would be a significant factor in the overall aircraft performance. There are also available automatic mixture control carburetors and fuel injection systems. Figure 1 shows the performance of a slightly modified ZR-1 engine.

Other engines considered, but not reported here, were the Mazda rotary, Ford SVO group, and the Cadillac Northstar engine. The Northstar⁶ is of particular interest due to its ladder style construction, low weight, and numerous safety features to prevent engine failure, e.g., the *limp home* mode which provides alternate cylinder firing in order to maintain acceptable cylinder head temperatures in the event of coolant loss.

The use of the liquid cooled engine adds complexity to the aircraft since it requires a radiator, but the technology to cool engines in aircraft is well proven and should not present major difficulties. Of greater concern is the dependence of the automotive engine on battery power for the production of spark. The

majority of the converted auto engines flying today utilize a backup system which is used to provide an alternative source of power in the event of alternator or other electrical failure.

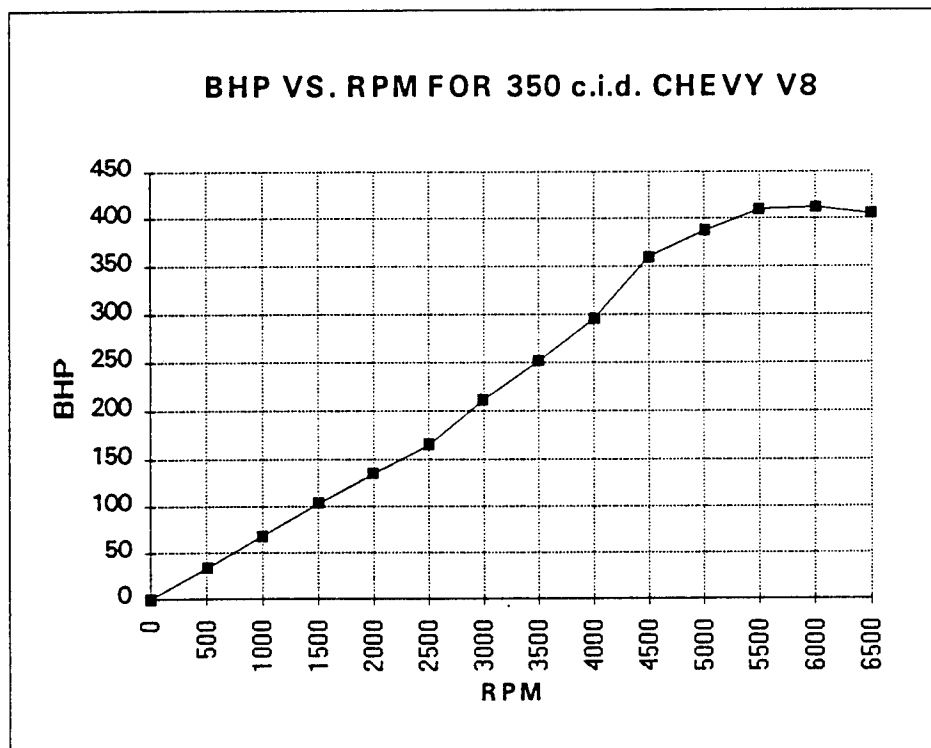


FIGURE 1. PERFORMANCE DATA FOR THE CHEVROLET V-8 ENGINE

ENGINE LOCATION

The location of the engine is governed to a great extent by the need to maintain a scale vehicle appearance and acceptable CG range. Its center of gravity needs to be located approximately 168 inches aft of the aircraft nose in order to attain the correct aircraft cg location. The pusher configuration is the best design from an internal aerodynamics point of view and for ease of engine to airframe interface. Since a direct drive shaft is used to rotate the fan, the engine crankshaft must be aligned with the thrust line. The crankshaft on most V-8's is approximately 18 in below the top surface of the engine, which leads to conflicting requirements in engine placement. Since the fan needs to be as large as possible without interfering with the wing carry through structure, the engine clearance from the tip of the fuselage must be minimized, but susceptibility of the room temperature cured composite materials to high temperatures places a limit on this clearance. A drawing which shows engine placement with structural details is given in Appendix 1.

ENGINE COOLING

The ZR-1 engine is cooled by the usual 50/50 mixture of ethylene glycol and water. The cylinder head temperatures and specific fuel consumption of the liquid cooled engine are typically much lower than for an equivalent air cooled engine. The primary advantages in the operational characteristics of the liquid cooled

engine are the reduced sensitivity to shock cooling as well as the increased resistance to overspeeding. The heat rejection rate of the internal combustion engine can approach 30% of the total energy of the fuel consumed. For the Minihawk, the heat rejection rate will approach 4000 BTU/min for the engine coolant and 1000 BTU/min for the engine oil.

An accepted cooling configuration is to use an aluminum core custom made radiator with a built in heat exchanger for the engine oil. Preliminary calculations show that an inlet capture area of 45 square inches for engine cooling should be sufficient. An 18 x 31 inch radiator is incorporated such that the required capture area is in the duct inlets. After passing through the radiator, air passes over the engine and is then bled back into the internal slipstream just forward of the fan guide vanes. The requirements for a clean, cool source of induction air is met by designing the Minihawk with a pair of 12 square inch flush NASA inlets, as shown in the inboard profile drawing.

FAN DRIVE SHAFT

The drive shaft from the engine to the fan is of critical importance since poor shaft design has been the downfall of several promising designs. The V-8 engine coupled with the short shaft promises to be free from the effects of torsional resonance. The detail design of the stator and rotor shows that the thrust and gyroscopic loads will be handled entirely by the stator, which consists of four streamline steel tubes. The engine is isolated from the rotor and stator by the use of a splined sliding shaft and universal joints. The drive shaft material used is mild steel with a thin walled tube making up the bulk of the shaft.

FUEL SYSTEM

The prototype Minihawk design utilizes a single fuel bladder installed in the area just behind the pilot. The race-car style fuel cell is adequate for 35 gallons on internal volume. The system will need an electrical fuel pump as backup to the usual engine driven pump. The fuel compartment will also be isolated from the engine and cockpit by firewall bulkheads. Since engine fire would be catastrophic for the Minihawk, precautions have to be taken to ensure safety. The fuel cell, emergency fuel shut off, and Halon fire extinguishers should provide sufficient protection for the prototype. Kit produced versions of the Minihawk would employ the familiar wet wing concept. In addition to being safer, a wet wing configuration would ease the CG travel due to fuel burn, improving the operational characteristics of the Minihawk.

FAN DESIGN

An extensive literature search was required to find the information required to design and analyze the fan. Very little information was found when searching using the DUCTED FAN keyword. Most of the useful information was found by using reports written for the design of wind tunnels¹⁰ or for the aerodynamic design of axial flow compressors⁸. Two older reports⁷ were found which provided a complete design methodology using cascade theory. A very useful and extensive source of current information was provided by Dr. Terry Wright, et al, at the Georgia Institute of Technology in Atlanta, GA. After some study, all of these reports were found to contain the information necessary for the design and analysis of ducted fans.

However, the method finally selected was based on a 1973 report⁹ entitled "Q-Fans For General Aviation Aircraft" by Rose Worobel and Millard Mayo of Hamilton Standard in Windsor Locks, Connecticut. This report examined the use of ducted fans powered by either piston or gas turbine engines where the primary emphasis was on reduced noise, hence the term Q-FanTM.

The Q-fan is a low noise propulsor concept which was developed in the early seventies to meet the expected noise restrictions of the future. Although Q-fans require more engine power in order to match current propeller performance at low speeds, this penalty is compensated by the fact that it provides cleaner airframe design alternatives.

The report is an extensive design study for ducted fan propulsion for several classes of general aviation aircraft aimed at improving safety, utility, performance, and cost. Complete analytic methods are given, as well as a tabulated step by step procedures for designing a ducted fan, including numerous design charts. Although not reported here, several checks were made using the methods of the previous reports in order to validate the Q-fan method and insure that the results were realistic.

A comparison of a Q-fan design and a conventional propeller system is provided in Table 3. From this table it is seen that in order to match the thrust of a propeller driven by a 285 hp engine at seal level and 66 kts, a 387 hp engine is required for the fan. The penalty associated with using a Q-fan design is not as severe at higher flight speeds, where the 387 hp engine can be used to produce higher thrust levels than the propeller system driven by a 285 hp engine.

TABLE 3. COMPARISON OF PROPELLER AND Q-fan

	<u>Current Propeller</u>	<u>Q-FAN</u>
Diameter (ft)	6.5	3.0
Number of blades	3	9
RPM	2700	4060
Sea Level Thrust @ 66 kts (lb)	880	880
Sea Level Thrust @ 218 kts (lb)	316	329
Weight (lb)	77	175
Noise Level (dB)	99.5	79
1980 Cost without engine	\$803	\$1650
Required Engine Horsepower	286	387

The design charts developed by Hamilton Standard combine propeller analysis theory with experimental data obtained from tested Q-fans of various configurations. Factors such as fan diameter, blade total activity factor, blade structure, tip speed, geometric pitch at 3/4 radius, inlet to exit area, duct length, advance ratio, and engine power were all considered in order to arrive at a working design. An iterative approach was taken such that the power required by the fan at each condition was equal to power supplied by the engine. A summary of the fan design process and a sample calculation are given in Appendix 2. The values used for calculating the fan performance are also given in Appendix 2. The numbers extracted from each chart were entered into a spreadsheet template which was programmed to solve for the thrust, power required, and efficiency.

The engine output at the design point was fixed at 330 HP at 4330 rpm and a tradeoff study was conducted by determining the performance for different pitch angles at 3/4 radius. Once the rpm and blade pitch were established at the design point, the total blade solidity was varied until the power required by the fan was equal to the power available by the engine.

To calculate the fan performance for off design conditions, an iterative approach was taken which involved selecting a fan rpm and calculating the power required for the given flight speed and blade activity factor.

If the power required did not match the power available by the engine, as given by the manufacturer, the rpm was adjusted until the condition was met. As shown in Figure 2, higher pitch angles, such as 57 degrees, produce minor benefits at higher velocities and result in significantly lower thrust levels at low velocities as a result of blade stall.

Propulsive efficiencies were calculated for different pitch angles by dividing the product of thrust and velocity by the engine power input. As can be seen in Figure 3 the propulsive efficiency of the fan peaks at a pitch angle of 55 degrees for all flight velocities studied. For structural purposes, the pitch angle selected for the preliminary fan design was 54 degrees, which requires four blades with an average chord of 4.0 inches each.

Although 55 degrees pitch produces slightly higher efficiencies, it requires a lower blade activity factor, which would result in a smaller blade width if four blades are used. Of course the activity factor could be reduced without reducing blade width if three blades are used instead of four, but a lower number of blades increases the noise level due to flow pulsation.

Having established the blade pitch angle at $3/4$ radius, the actual blade design is governed by the condition of obtaining constant lift coefficients of 0.7 throughout the blade at the design point. As recommended in Hamilton Standard's report, the proposed Q-fan uses NACA 65 series airfoils of varying thicknesses.

The thrust produced by the fan at different flight velocities is given in Figure 4 for a standard sea level condition and for an 8000 ft altitude. At higher altitudes, the output of normally aspirated engines is reduced, but the power required by the fan also falls. As mentioned previously, the use of a readily available turbochargers or superchargers would result in very attractive performance figures at high altitudes.

Fabrication of a fan with ground adjustable pitch angles would be highly desirable, since the performance is, like a propeller system, sensitive to blade pitch. Slight disturbances in the internal flow caused by the engine or inlet ducting could result in a fan which is not optimum and a means of adjustment may be better than making new fans until the correct pitch is obtained by trial and error.

PERFORMANCE

Performance estimates were obtained by entering the Minihawk's design parameters, such as weight, thrust, and geometry into Raymer's Design Software.

The internal ducting concept used in the Minihawk design represents a large increase in wetted area as compared to a conventional propeller driven aircraft. It is estimated that 30% of the total parasite drag is due to the ducting. In order to minimize friction drag, the wetted surfaces must be made as smooth as possible and number of protruding members and gaps must be kept to a minimum. The drag polar shown in Figure 5 assumes a friction drag coefficient of 0.005 for the internal ducting. The resulting minimum parasite drag coefficient for the aircraft is 0.0195 and the maximum lift to drag ratio for level flight is 8.5 at a C_L of 0.3 and a velocity of 122 kts.

The Minihawk's flight envelope includes a maximum level flight velocity of 207 kts and a 56 kt stall speed. With 80% cruise power setting, the Minihawk's airspeed is 185 kts. Assuming 15 gallons per hour fuel consumption, a range of 450 nautical miles and an endurance of at least 2.3 hours can be attained.

THRUST VERSUS VELOCITY FOR DIFFERENT PITCH ANGLES AT 3/4 RADIUS

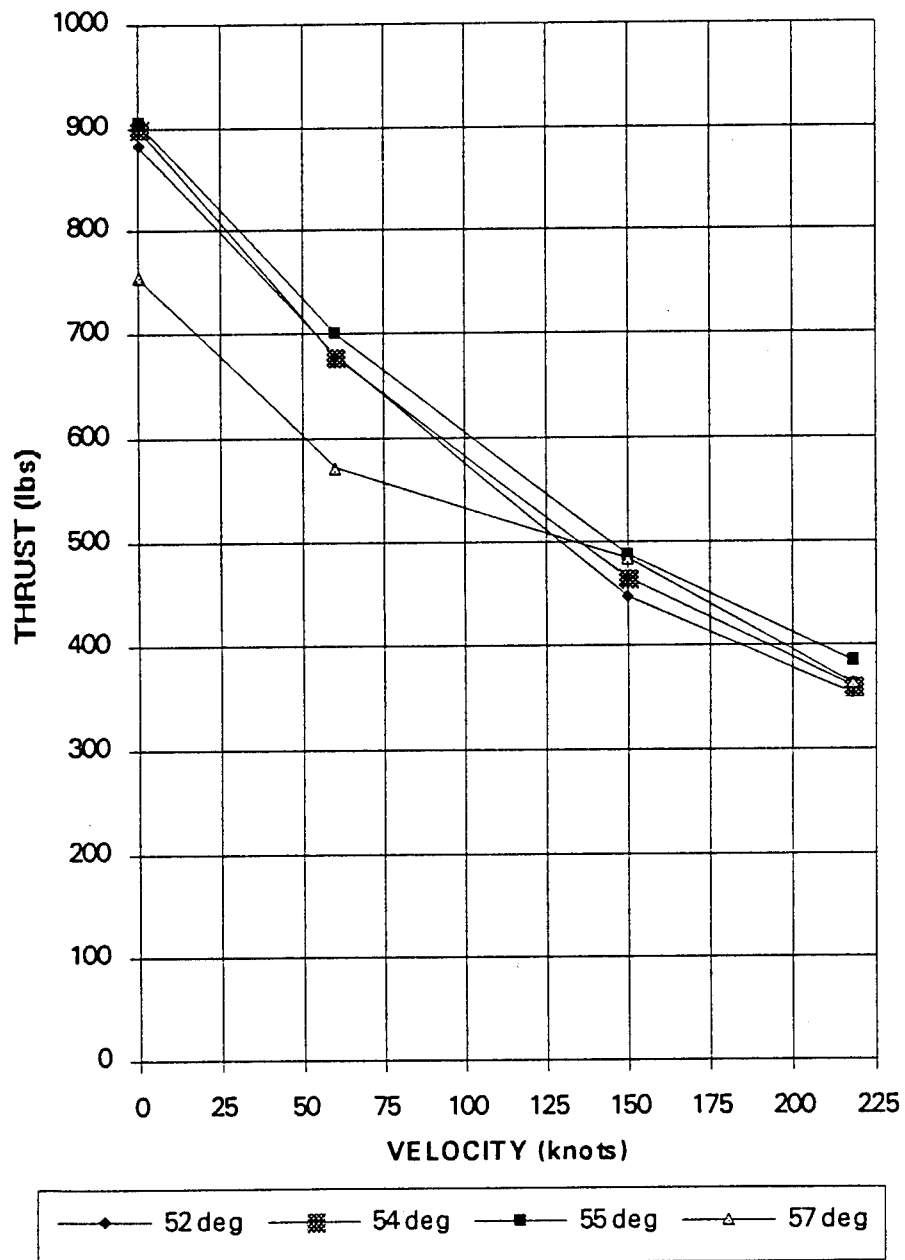
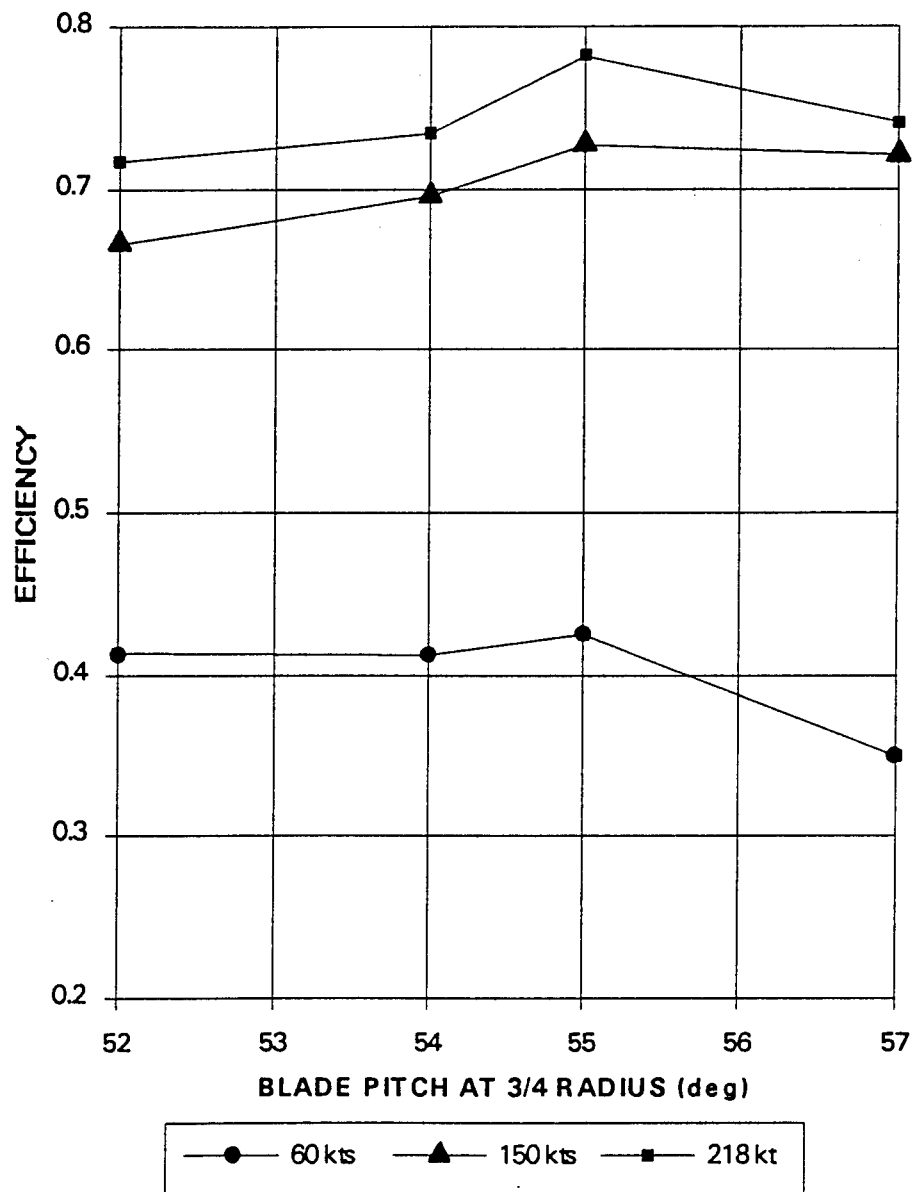


FIGURE 2. FAN PERFORMANCE FOR DIFFERENT PITCH ANGLES AT 3/4 RADIUS

**PROPULSIVE EFFICIENCY VERSUS BLADE
PITCH AT 3/4 RADIUS FOR DIFFERENT
VELOCITIES**



**FIGURE 3. PROPULSIVE EFFICIENCY FOR DIFFERENT PITCH ANGLES
AND FLIGHT VELOCITIES**

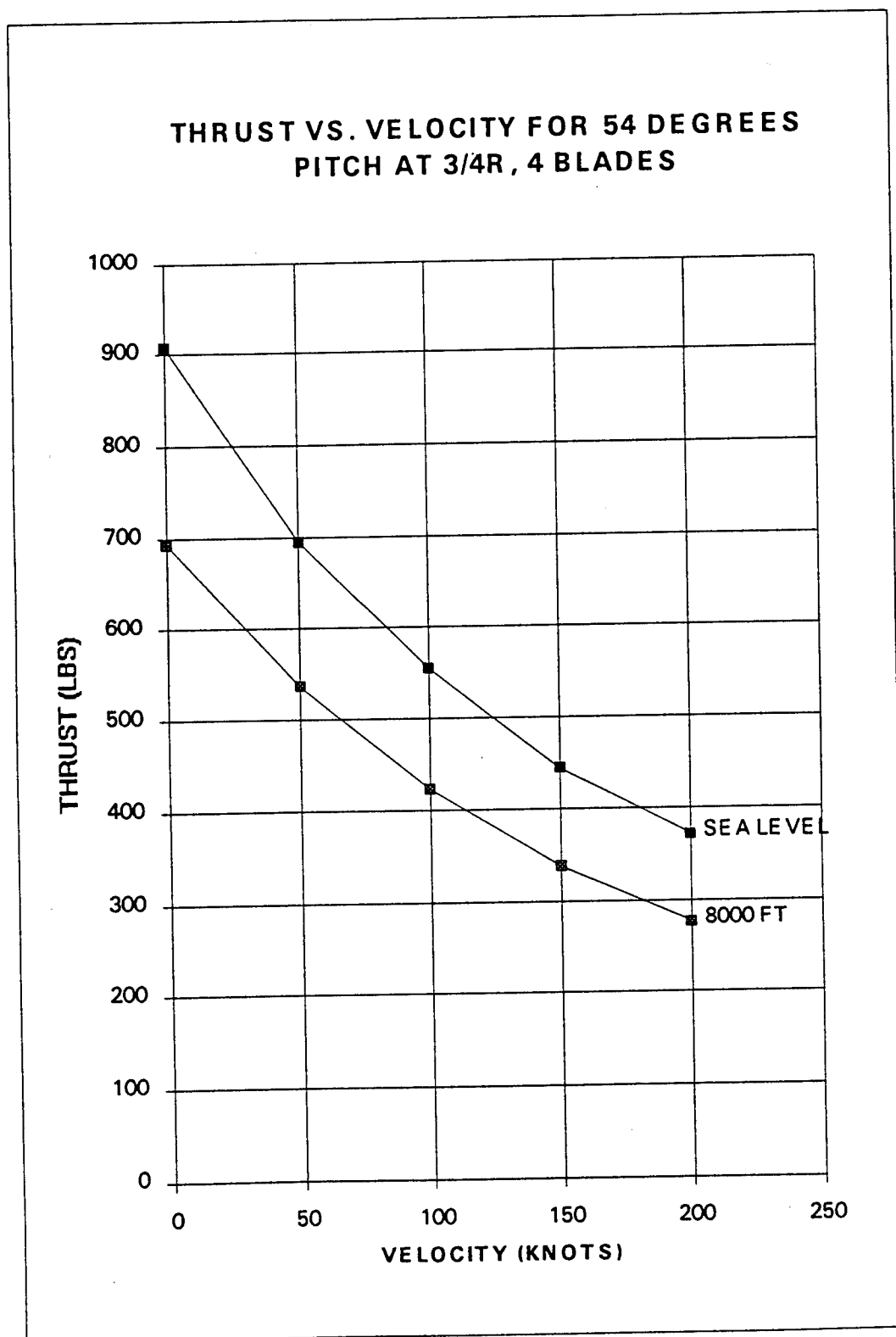


FIGURE 4. PERFORMANCE OF SELECTED QFAN CONFIGURATION

The large power to weight ratio enables the Minihawk to break ground in less than 600 ft at standard sea level conditions. Total takeoff distance over a 50 ft obstacle can be accomplished in less than 1200 feet. Total landing distance, including a 600 foot flare, is less than 1320 ft, which is adequate for most airfields.

The maximum rate of climb at sea level is 2300 feet per minute at 125 kts. This rate decreases to 1250 feet per minute at 8000 ft altitude (Figure 6). The specific excess power plot shows that the maximum continuous load factor for sustained level flight is 2.1 g's at 150 kts. (Figure 7). As indicated in Figure 8, the maximum turn rate is 43 degrees per second at a corner speed of 150 kts.

STABILITY

Radio controlled models of the A-4 are stable and easy to fly for intermediate to advanced R/C pilots, thus no problems are expected with the 2/3 scale Minihawk. Static stability of the Minihawk was calculated using the methods of Torenbeek¹², Perkins and Hage¹³, and Etkin¹¹, resulting in a neutral point at approximately 37% of the mean aerodynamic chord. The as-drawn center of gravity is 158.5 inches aft of the datum (aircraft nose), yielding a static margin of 15% with a 170 lb pilot.

The Minihawk was found to be sensitive to pilot weight due to a long moment arm from the crew station to the center of gravity. The proposed CG envelope for the Minihawk gives static margins of 5 to 15 percent of the mean aerodynamic chord. This static margin results in an allowable CG travel of 8.7 inches. If the nominal CG location is positioned in the mid range of the static margin, the acceptable range in pilot weights covers the 25th to 75th percentile.

A check of lateral stability characteristics was also made. The directional stability derivative with respect to sideslip (C_{nb}) was found to be .0005 per degree, which is acceptable.

COST

The estimated cost for building the prototype is approximately \$80,000. This includes minimum required avionics, engine and fan, and assumes labor costs corresponding to 3000 man hours.

CONCLUSIONS

The design study summarized in this report has shown that it is feasible to make a 2/3 scale replica of the A-4 fighter aircraft which is powered by a ducted fan propulsion system. There is sufficient information on ducted fan design in the literature to approach the project with a high degree of confidence in the resulting performance.

The resulting aircraft would have a very realistic appearance, and would provide the owner with a unique and enjoyable sport aircraft. The resulting aircraft could be expected to have excellent performance and normal flight characteristics. However, more power is required compared to conventional aircraft due to the increased wetted area and limited fan diameter; this is somewhat offset by the ability to use a direct drive automotive engine. Other disadvantages include a sensitivity to pilot weight range, more complex structure, and more difficult engine access. Major advantages of the ducted fan propulsion system include ramp safety from the enclosed propeller and significantly reduced noise.

DRAG POLAR AT SEA LEVEL

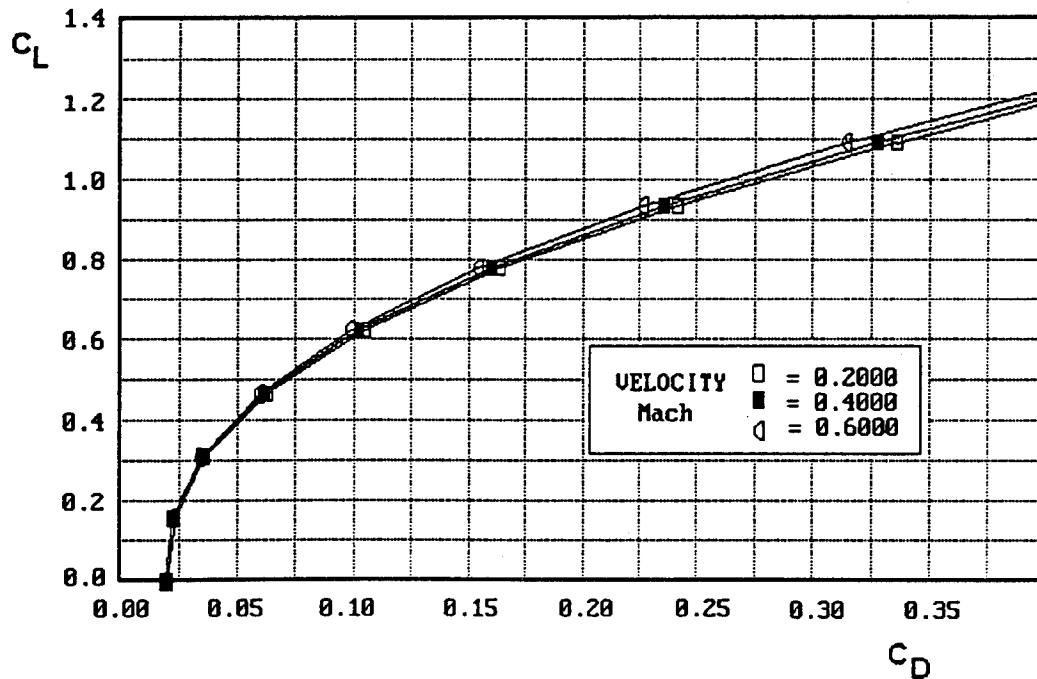


FIGURE 5. DRAG POLAR FOR DIFFERENT FLIGHT SPEEDS

RATE OF CLIMB VERSUS VELOCITY

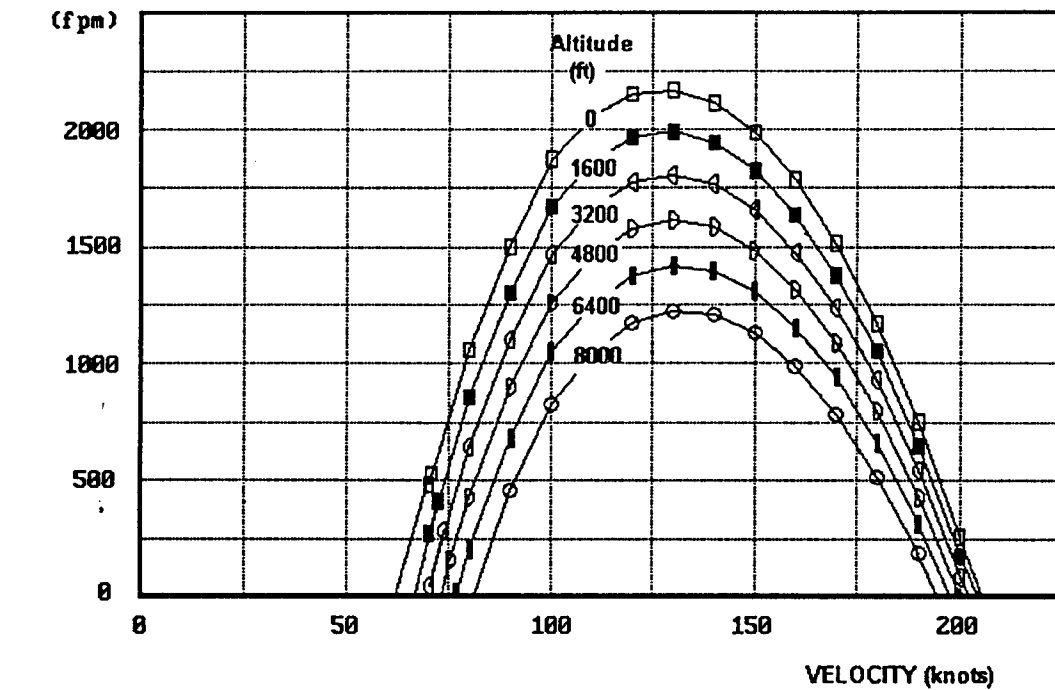


FIGURE 6. RATE OF CLIMB VERSUS SPEED FROM SEA LEVEL TO 8000 FT.

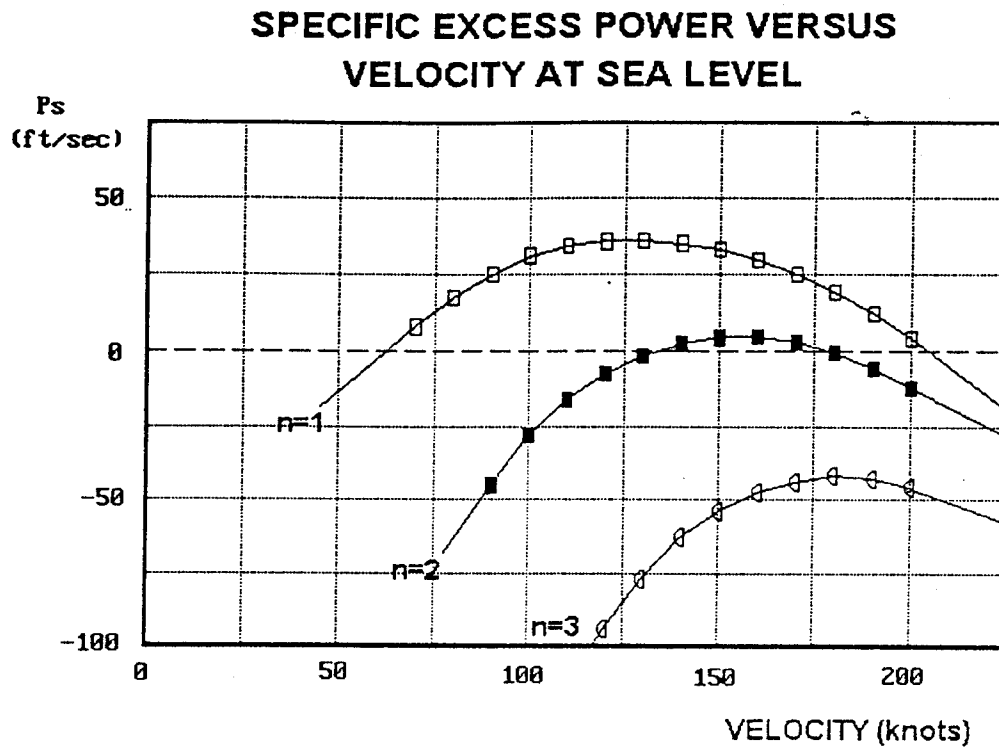


FIGURE 7. SPECIFIC EXCESS POWER FOR DIFFERENT LOAD FACTORS

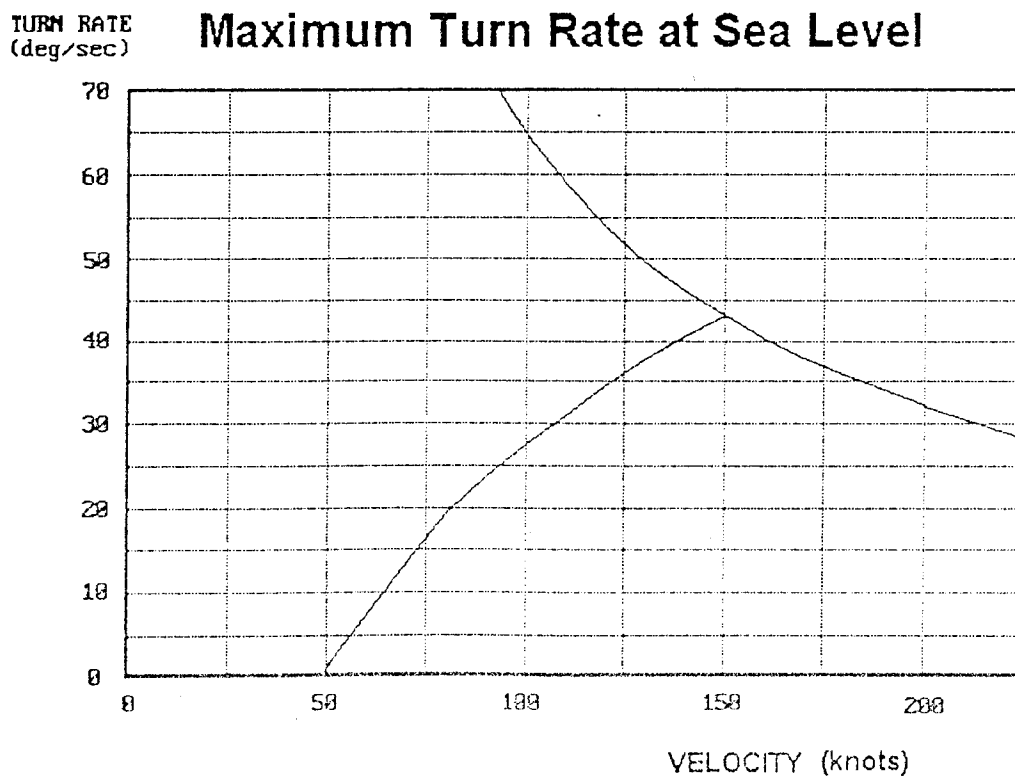
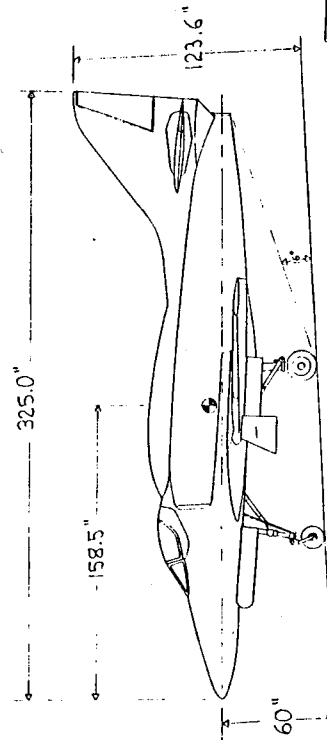
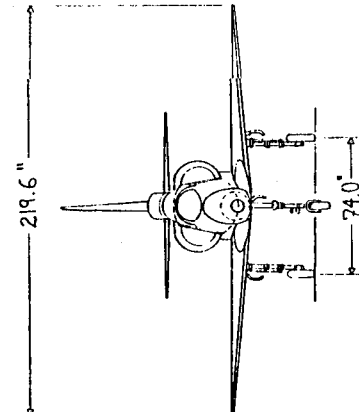
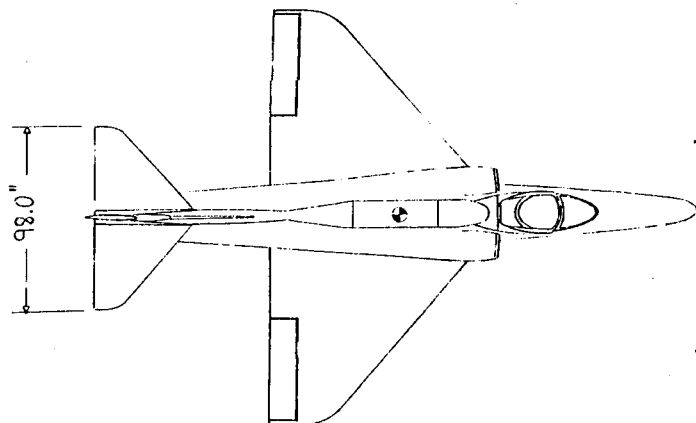


FIGURE 8. CORNER SPEED DIAGRAM

References

1. FAR Part 23 "Airworthiness Standards: Normal, Utility, Acrobatic, and Commuter", 1991 Sections 23.301-23.344, Appendix A.
2. Niu, Michael C., "Airframe Structural Design", Technical Book Co., New York, 1988.
3. Roskam, Jan, "Airplane Design, Part 1", Roskam Aviation and Engineering Corp., Ottawa, KS., 1990.
4. Raymer, Daniel P., "Aircraft Design: A Conceptual Approach", AIAA Press, Washington D.C., 1989.
5. Bell, Danna, "A-4 in Detail and Scale", Aero Press, Blue Ridge Summit, PA, 1986.
6. Stevens, Mike; Personal conversation with local GM Dealer, Daytona Beach, FL, 15 OCT 93.
7. Collar, A.R., "The Design of Wind Tunnel Fans", NASA Report No. 1889, 10 AUG 40.
8. NASA SP-36, "Aerodynamic Design of Axial Flow Compressors", NASA Lewis Research Center, 1965.
9. Worobel, Rose, "QFANS for General Aviation Aircraft", Hamilton Standard, NASA CR 114665, 1973.
10. Pope, Alan and Rae, H. William, "Low Speed Wind Tunnel Testing", John Wiley and Sons, New York, 1959.
11. Etkin, Bernard, "Dynamics of Flight", John Wiley and Sons, New York, 1959.
12. Torenbeek, Egbert, "Synthesis of Subsonic Airplane Design", Delft University Press, Delft, The Netherlands, 1986.
13. Perkins and Hage, "Airplane Performance, Stability, and Control", John Wiley and Sons, New York, 1946.

APPENDIX 1. DRAWINGS OF 2/3 SCALE DOUGLAS A-4 SKYHAWK "THE MINIHAWK"

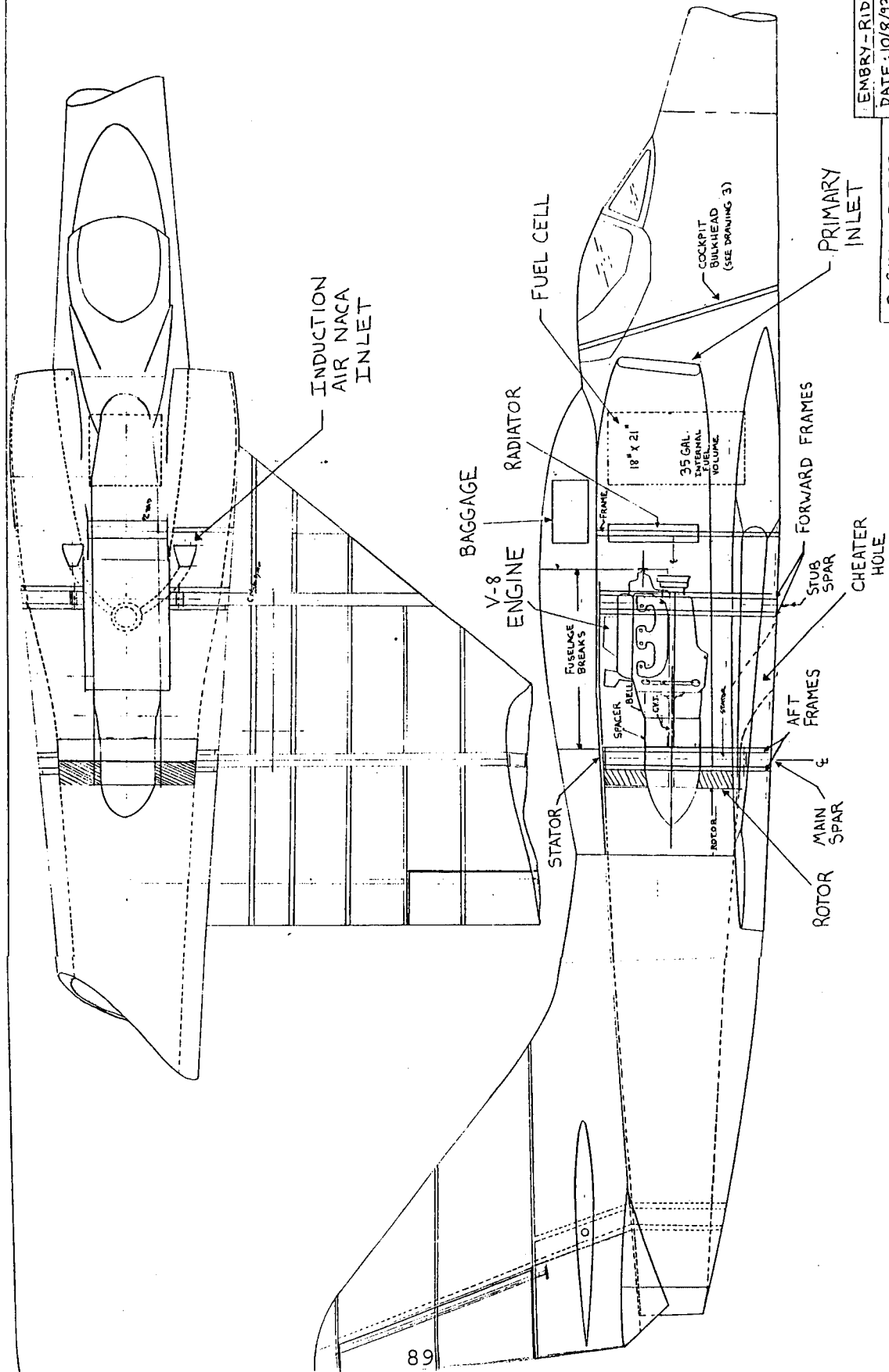


WING	
Airfoil	NACA 0012
Reference Area	118.0 sq. ft
Tip Chord	31.5 in
Root Chord	128 in
Taper Ratio	0.25
Aspect Ratio	2.8
L.E. Sweep	38 deg
C/4 Sweep	30 deg
M.A.C.	87 in
Aleron Area	3.12 sq. ft (each)

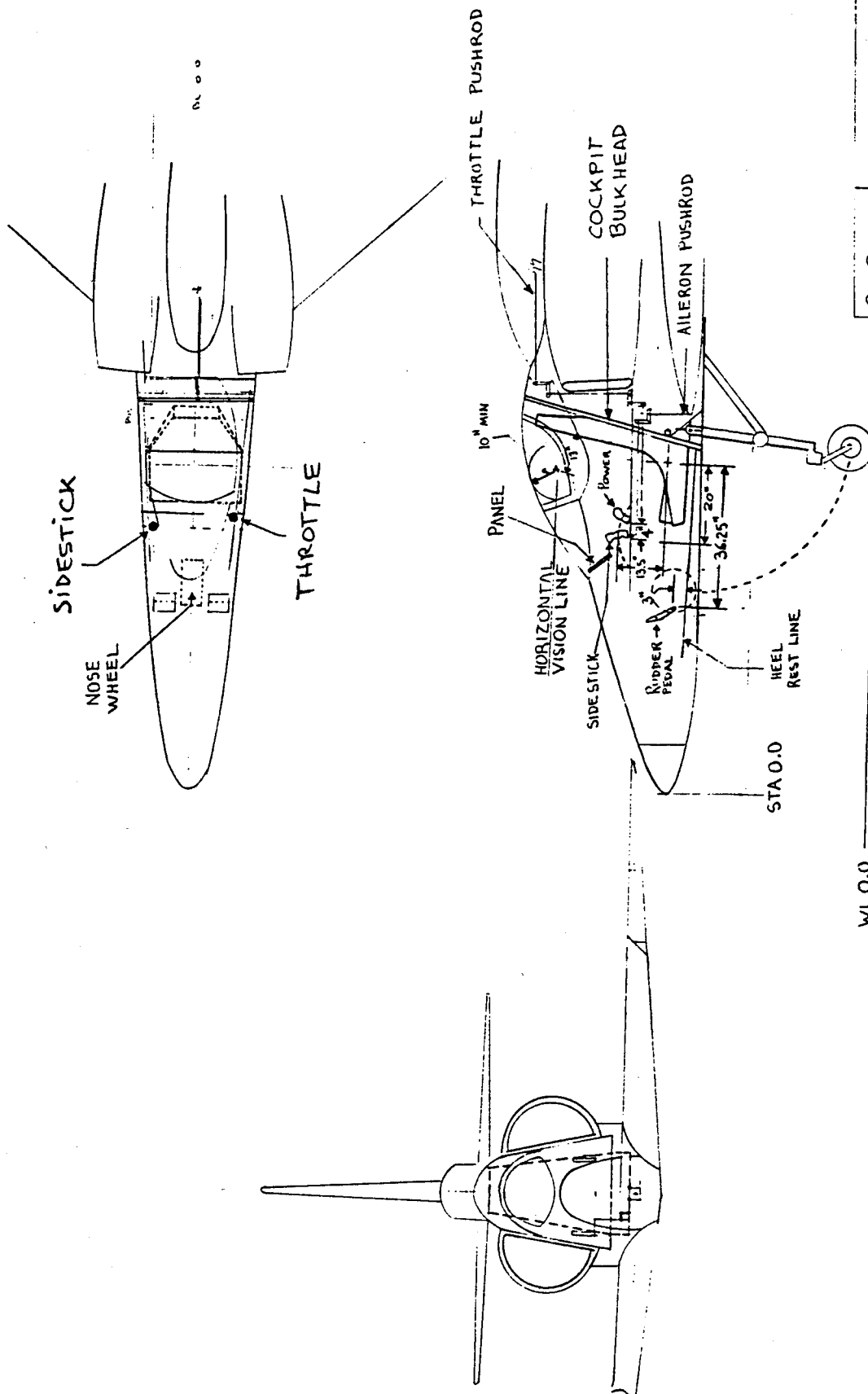
VERTICAL TAIL	
Airfoil	NACA 0009
Area	15.0 sq. ft
L.E. Sweep	38 deg
Rudder Area	3.6 sq. ft

HORIZONTAL TAIL	
Airfoil	NACA 0009
Area	22.9 sq. ft
L.E. Sweep	40 deg

EMBA-RIDDLE NEW NAUTICAL UNIVERSITY
 DATE 10/11/93
 D-SIZE PAPER
 SCALE 1:30
 A-4 MINIHAWK 3-VIEW
 DRAWING 1



EMBRY-RIDDLE AERO.	
DATE: 10/8/93 <small>DATE OF</small> MIKE STEVENS	
D-SIZE PAPER	A-4 MINIHAWK
SCALE 1:10	DRAWING 2



WLO:0

C-SIZE

SCALE
1:20

DATE 11/11/93

EMBRY RIDDLE AERONAUTICAL UNIVERSITY
DATE 11/11/93
NAME: MIKE STEVENS

COCKPIT LAYOUT

DRAWING 3

Sheet 1 of 1

APPENDIX 2: DESIGN PROCESS FOR FIXED PITCH PROP-FAN

Reference: "QFANS For General Aviation Aircraft", NASA-CR 114665, Hamilton Standard, 1973

A blade angle, $\beta_{3/4}$ can be selected from computed $\beta_{3/4}$ for a specific operating condition (or conditions) for a constant speed Q-Fan. Then, for the selected $\beta_{3/4}$ and a range of engine rpm's, the corresponding power and thrust are computed for a given velocity and altitude by the following procedure. Then, the rpm most suitable for the aircraft operation can be selected.

STEP 1: IDENTIFY THE FOLLOWING

Attitude	Identify flight condition
Engine rpm	N_e - select a range of rpm's
Altitude	ft (m)
Velocity	V - airplane forward speed knots true airspeed (m/s)
$\beta_{3/4}$	Select

STEP 2: CALCULATE THE FOLLOWING

ρ_o/ρ	Density ratio
f_c	Ratio of speed of sound at standard day sea level to speed of sound at operating conditions.
N	Rotor speed = $N_e \times G.R.$
J_o	Rotor advance ratio - $K1/\overset{V}{(ND)}$

where $K1 = 101.4 (60.)$

STEP 3: READ FROM FIGURES OR CALCULATE THE FOLLOWING

C_{PE}	Read from fig. A-14, A-15, A-16, A-17 for J_0 and $\beta^{3/4}$. Interpolate, if necessary.
TAF	$AF \times B$
\dot{P}_{TAF}	TAF adjustment to power (fig. A-4)
T.S./ f_c	Rotor tip speed = $\frac{(Kr) ND}{60 f_c}$
	where $K4 = \pi (10.31)$
P_{MN}	Tip speed/Mach no. adjustment to power (fig. A-6)
C_P	$C_P = \frac{C_{PE}}{P_{TAF} \times P_{MN}}$
Power	$\text{Power} = \frac{(K6) N^3 D^5 C_P}{\rho_o / \rho}$
	where $K6 = 2 \times 10^{-11} (1.112 \times 10^{-11})$
C_{TE}	Read for proper AR, C_{PE} and J_0 from fig. A-10, A-11, A-12, A-13. Interpolate, if necessary.
T_{TAF}	TAF adjustment to C_T (fig. A-5)
T_{MN}	Tip speed/Mach no. adjustment to C_T (fig. A-7)
$\Delta C_{Tnet} (L/D)$	Duct length/rotor diameter adjustment (fig. A-8)
$\Delta C_{Tnet} (acc.)$	Performance penalty for acoustical treatment to reduce noise 4.5 PNdB (fig. A-9)
C_T	$C_T = \frac{C_{TE} + \Delta C_{T(L/D)} - \Delta C_{T(acc.)}}{T_{TAF} \times T_{MN}}$
Thrust	$\text{Thrust} = \frac{(K5) C_T N^2 D^4}{\rho_o / \rho}$

where $K5 = 0.661 \times 10^{-6} (2.94 \times 10^{-6})$

DESIGN PROCESS SAMPLE CALCULATION

DIAMETER = 2.5 ft.
SEA LEVEL STANDARD CONDITIONS
 $\beta = 55^\circ$
AREA RATIO = $\frac{\text{INLET AREA}}{\text{EXIT AREA}} = 1.1$

ENGLISH UNITS

VELOCITY	0	60 kts 101.16ft/s M=.09	150 kts 252.9ft/s M=.23	218.3 kts 368.5ft/s M=.33
ENGINE RPM	3900	3910	4000	4150
DENSITY RATIO (ρ_o/ρ)	1	1	1	1
SPEED OF SOUND RATIO (f_c)	1	1	1	1
RPM ROTOR SPEED (N)	3900	3910	4000	4150
ADVANCE RATIO: $J_o = \frac{101.4V}{ND}$	0	.608A	1.521	2.214
C_{P_e} (A14-A17)	3	3	2.8	2.5
$AF = 6250 \int \frac{b}{D} X^2 dX$	228	228	228	228
TAF = AF x B	2052	2052	2052	2052
P_{TAF} (A4)	.98	.98	.98	.98
$\frac{\text{Tip Speed}}{f_c} = \frac{N 2\pi (\text{Tip Radius})}{60 f_c}$	510	512	523	543
P_{MN} (A-6)	1.015	1.016	1.018	1.022
$C_p = \frac{C_{P_e}}{P_{TAF} \times P_{MN}}$	3.016	3.01	2.81	2.5
Power = $\frac{(2E-11) N^3 D^5 C_p}{(\rho_o/\rho)}$	349.4	351.4	351.2	350
C_{TE} (A11-A13)	2.5	1.9	1.25	.80
T_{TAF} (A5)	≈ 1	1	1	1
T_{MN} (A7)	1.01	1.015	1.02	1.03
$\Delta C_{T_{NET}}$ (L/D) (A8)	0	.01	.02	.03
$\Delta C_{T_{NET}}$ (ACC.) (A9)	0	0	.005	.007
$C_T = \frac{C_{TE} - \Delta C_T (L/D) + \Delta C_T (ACC)}{(T_{TAF}) (T_{MN})}$	2.48	1.86	1.21	.754
THRUST = $\frac{(.661E-6) C_T N^2 D^4}{\rho_o/\rho}$	974	734	500	335.3

THE WORLD CLASS GLIDER-AN INTERNATIONAL EXPERIENCE

A REVIEW AND STATUS REPORT FOR THE AIAA 1994

Oran W. Nicks
Texas A&M University
College Station, TX

ABSTRACT

In March 1994, a new 1-Design glider received tentative approval from the Federation Aeronautique Internationale-International Gliding Commission (FAI-IGC) as a so called "World Class" glider to be produced and used around the world for at least fifteen years. The winning design was chosen after a rigorous design and prototype fly-off competition sponsored by the IGC, involving experts, judging panels and juries from over 27 nations. The winning design was developed by a team from the Warsaw University of Technology and the prototype was produced with help from the PZL Swidnik factory in Poland. Meeting specific technical specifications and requirements developed by an international group, the design for a single seat glider is a compromise that is substantially lower in cost than existing FAI glider classes, incorporating safety, good flight and ground handling qualities.

Under the FAI-IGC rules, the glider may be built anywhere in the world under license to the Swidnik factory. It may also be built by manufacturers or homebuilders using different materials and processes. This provision will hopefully encourage competition and evolution in manufacturing technologies to help reduce costs, while maintaining basic safety and handling quality features. This paper will review the process and results of the competition.

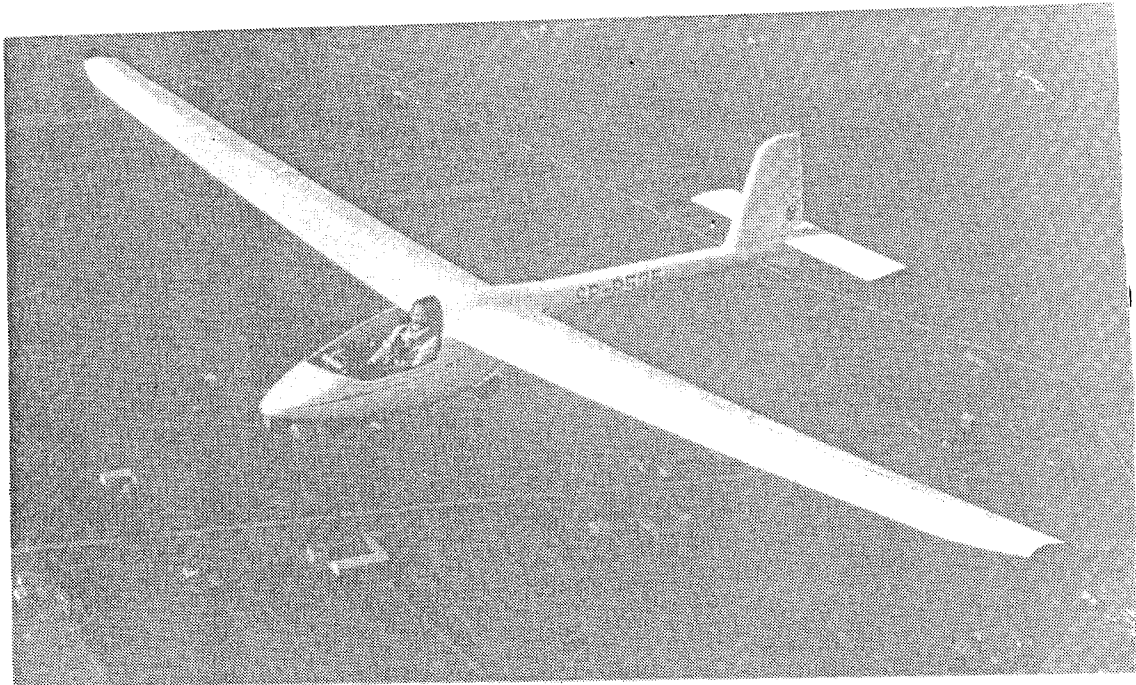


Figure 1: PW-5 World Class Glider In Flight Over Poland

BACKGROUND

About seven years ago, an organized effort began to define a single place, 1-Design glider that would satisfy a need perceived by many in the soaring community. There was general agreement that the gliders available for first-owner candidates who had just completed their training were not really suitable. Choices ranged from 30-year old Schweizer 1-26's made of steel tube, fabric and aluminum to 20-year old ex-competition fiberglass sailplanes made in Germany. The 1-26 had been a good 1-design type with an advertised glide ratio of 23:1 that had become somewhat obsolete, and the higher performance gliders were a bit tricky for new pilots to fly. Furthermore, most first-owners wanted a new glider and the cost of these second-hand gliders was more than many buyers were willing to pay.

The SSA Technical Board began discussing ways to offer technical help for addressing this problem, and after deciding that a current technology 1-Design glider with better qualities was feasible, began to develop a set of General Criteria and Technical Specifications for such a glider. It took awhile to exchange views and develop drafts, but with a fair consensus they were circulated for review. With the help of a few qualified designers, an attempt was made to define the characteristics of a sample sailplane that might be appropriate for meeting the established objectives (Ref. 1).

In January 1987, Paul Schweizer, retired Vice-President of Schweizer Aircraft, presented a paper at the Organisation Scientifique et Technique International du Vol' a Voile (OSTIV) Congress in Benalla recommending a new class of sailplane suitable for Olympic type competitions that would be a low-cost, safe, perhaps kit-built glider available to all nations around the world (Ref. 2). This was not a new idea for Paul. Always an avid supporter of and participant in 1-26 Nationals, he properly represented the views of many who believed this type of glider to be a mainstay of grass-roots soaring. Furthermore, he had been preaching this concept since he first formally proposed it to OSTIV officials in Frankfurt in 1984. His proposal at Benalla rang the bell again, and this time the International Gliding Commission heard it.

In March 1988, the OSTIV Sailplane Development Panel met in Rochester England and one of the last items on the agenda was a brief discussion about the possibilities of a 1-design glider. The Chairman, Professor Piero Morelli of Italy, had heard about the Soaring Society of America (SSA) Technical Board efforts and had asked in advance for permission to use the draft Criteria and Specifications to stimulate debate. Needless to say there were critics, but there were also a number of positive supporters for the concept. A very skilled and diplomatic Chairman, Morelli turned a debate into the beginning of a new international effort to develop a 1-Design glider. The concept was to be adopted shortly by the International Gliding Commission and they suggested a new FAI racing class planned to use what they termed the World Class Glider.

The first challenge was to succinctly define the objectives of the World Class effort. Combining the worldwide need for a new low cost, safe, easy to fly glider with the goal of having a single design, suitable for Olympic or world championship competitions, stimulated international discussions of an unprecedented nature. In the past, advances in performance had driven the evolution of new designs, and compromises to reduce cost and accommodate pilots from all nations had not been emphasized. It was necessary to coalesce subjective judgments such as, what was meant by low cost, how much performance was enough, what factors were most relevant to safety and what range of pilot size was reasonable in order to develop technical specifications and requirements. Some remarkable results from this activity not only led to the development of technical specifications for the World Class glider, but actually benefited the evolution of all gliders. A principal factor was the stimulus

to review the state of the art, with special emphasis on low cost, safety, general utility and performance in that order. A summary of the key requirements is presented below.

- COMPLIANCE WITH JAR-22, CAT. U
- STALL SPEED LIMIT-GW-65 Km/H (38.5 KTS)
- AUTOMATIC ELEVATOR HOOK-UP
- CRASHWORTHY COCKPIT - 15 — 20 g's
- L/D MIN 30:1 ROLL RATE ~ 25°/SEC.
- SINKRATE MIN 0.75 M/S (1.5 KTS)
- PILOT SIZE - HT. 5' — 6'5", WT. 120 — 242 LB.
- STANDARD INSTRUMENTS - EQUIPMENT
- LIFETIME - 20 YEARS; 9000 HOURS
- PROVISION FOR FIXED BALLAST TO GROSS WEIGHT
- EASY TO RIG; MOVE ON GROUND

Figure 2: Key Requirements

MARKET SURVEY

Before developing any new product, a market survey is vital. For the World Class glider, this meant determining what was really needed to satisfy the user community, including students, clubs, first-owners and racing pilots. Such a broad spectrum is highly unusual, and made the subjective judgments more difficult to address. The polling and discussion process started by the SSA Technical Board was continued on an international basis, led by participants associated with the Sailplane Development Panel. It is especially important to note the influence of the emerging nations, which, because of new freedoms, had new opportunities to participate in international sport activities, but were severely constrained financially. The low cost aspect was especially significant to them, if they were to be able to compete with more affluent nations. Furthermore, the small size being encouraged for the design would be easier to store and lighter, smaller trailers would be easier to tow with low powered autos on unimproved roads. Along with these qualities, the idea that such a glider might be produced anywhere in the world gave them a chance to compete with Germany and other developed nations in the manufacture of such gliders.

SAFETY AND UTILITY

The clubs and first owners needed a safe, easy to fly glider that could be used by pilots of various skill levels, sizes and weights without difficulty. This influenced landing speeds, stall characteristics, complexities of rigging and controls, spoilers, flaps and retractable landing gear. Stall speed set the limit on safe approach and landing speed and specifically, the energy involved in a hard landing. The sizes and weights of pilots dictated the need for large cockpits, adjustable seating/control linkages, and most importantly, insensitivities to pilot

weight on center of gravity position. Stability and control provisions set tail volumes and C.G. ranges needed to insure that if a large student got out of the glider and a small student followed that balance problems would be avoided. Another factor which became a major topic of debate was crashworthiness. The concept of engineering cockpit structures to help survive hard landings had not been generally applied to composite gliders, but the Schweizer 1-26 had been designed with high-g impacts in mind and had an amazing record of low fatalities from crash landings including stall-spin accidents. Using this as a model, along with experience provided by NASA research, our first SSA draft called for unusually high impact requirements for the pilot and equipment. These were lowered somewhat before the final specifications were evolved, but the World Class requirements for crashworthiness set new norms being considered for incorporation into Joint Airworthiness Regulations (JAR-22), currently in use by most nations for certifying gliders.

TECHNICAL DATA

wing span	13.44 m
wing area	10.16 m.sq.
aspect ratio	17.8
wing profile	NN 18 -17
weight of a single wing	36 kgs
overall length	6.20 m
overall height	1.95 m
tail plane span	2.4 m
tail plane area	1.2 m.sq.
vertical tail unit area	0.94 m.sq.
glider empty weight	166 kgs
max. allowable weight during flight	280 kgs

Results of measurements taken during flight
(take-off weight 250 kgs):

min. airspeed	62 km/h
best glide ratio at V = 80 km/h	1:32.5
min. sinking at V = 73 km/h	0.64 m/sec
sinking at V = 100 km/h	1.0 m/sec
sinking at V = 140 km/h	2.2 m/sec
max. speed	220 km/h
g limits	+5.3/-2.65

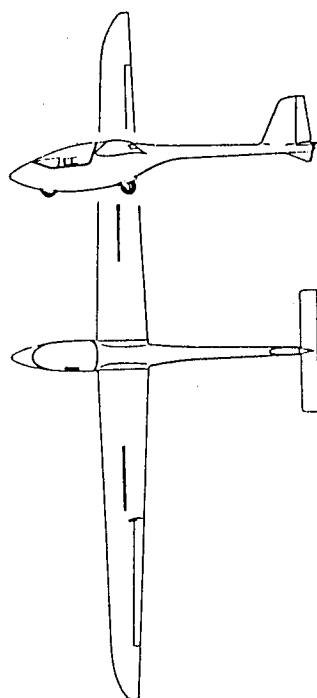


Figure 3: Technical Data and Layout of the PW-5

PERFORMANCE

The decisions on performance requirements demanded the assimilation of many viewpoints. All pilots had ideas about how much glide ratio is enough, but the majority finally settled on an L/D=30 as suitable for allowing fun soaring, for meeting FAI badge requirements, and for having meaningful racing contests. This glide performance would allow for some design compromises to reduce costs. A minimum L/D=30 was also believed important to enhance safety, as it was deemed enough to allow getting to the next thermal and not result in as many off-field landings as were usual in 1-26 or training sailplanes having about 10 points less L/D. As to handling qualities, roll rates somewhat higher than those of typical racing gliders were specified, and it was believed that the glider should be safe to spin and easy to recover so that spin training could be safely done. Minimum sink rate is an important factor for soaring

in weak conditions, which exist at many soaring sites and during certain seasons everywhere. For this glider to be effective everywhere, there were strong advocates for this "soarability" factor associated with wing loading, although it is somewhat at odds with good penetration capability required for cross-country soaring. Juggling all these tradeoffs of a subjective nature was challenging, but after much iteration, parameters were set that have been generally accepted by the soaring community

MANUFACTURING AND PRODUCTION

The design and prototype competition encouraged consideration of various materials. Many thought that new construction technologies might favor the integration of steel tube, metal, wood, glass, aramid or carbon composites. The IGC rules will allow the final World Class design to be constructed of any materials, as long as external geometry and mass limitations can be met and certification obtained. The prototypes that were evaluated included a design to be made largely from aluminum extrusions, one with metal sandwich, one of conventional aluminum construction and four using GRP composites. The winning prototype was made of composites, but other builders may choose other materials. One of the unique aspects of the World Class program is that the manufacturing and production competition may continue for at least fifteen years, as that is the period stated by the IGC for planned use of the configuration in International competitions. We are just entering that exciting manufacturing and production phase. Another offshoot of the program is the development of kits that can be built by homebuilders. Kits should help to further lower the cost of soaring and also increase the chances for innovation in manufacturing techniques. Gliders that can be transported in a trailer and be assembled in minutes have always had kit-like attributes, and the lack of power plants, propellers, fuel and oil systems make gliders readily adaptable to kit construction. Kitbuilding has evolved to a high degree in the U. S., and the World Class groundrules should offer an opportunity for U. S. production and marketing of the glider.



Figure 4: Prototypes at Oerlinghausen, Germany Undergoing Evaluation

DESIGN AND PROTOTYPE EVALUATION

After it had been decided that a one design sailplane was needed and that current technology could be applied to achieve several goals, the general objectives were framed as indicated and a design competition announced. Forty-two design entries were received from 22 nations, and a panel of five judges from five nations selected 12 candidate designs to enter the prototype phase of the competition. These designs were judged to be suitable for meeting the general objectives, technical specifications and requirements established by the experts who had assimilated inputs from throughout the World.

The 12 winners of the design competition were invited to prepare prototypes for evaluation and testing within approximately one year. Arrangements were made to hold the prototype evaluations at the World's largest glider training school in Oerlinghausen Germany during September and October of 1992. Seven of the 12 designs that had been selected as suitable for the prototype phase were delivered to Oerlinghausen for evaluation by an International jury, supported by four respected test pilots and with operational assistance by the Deutsch Forschungsanstalt fur Luft- und Raumfahrt (DLR). The airfield, tow and winch launch capabilities, plus lodging and meals for the Jury and other officials were kindly provided by the German Aero Club and the DLR. Documentation of each design, along with test information, discussions with the design and prototype teams, and detailed ground inspections provided an assessment of each configuration.

The Jury decided that two of the prototypes were not ready for flight evaluation, however, five were tested thoroughly during a three week period by test pilots, jury members, IGC officials and invited pilots from several countries. Ground handling, measurements, weights and balances, assemblies and disassembles and operational demonstrations were performed for the jury in accord with predetermined guidelines. Participants in these evaluations lived and worked together continuously through three and a half weeks of intense activities, compiling data and weighing findings against the general criteria, technical specifications and requirements.

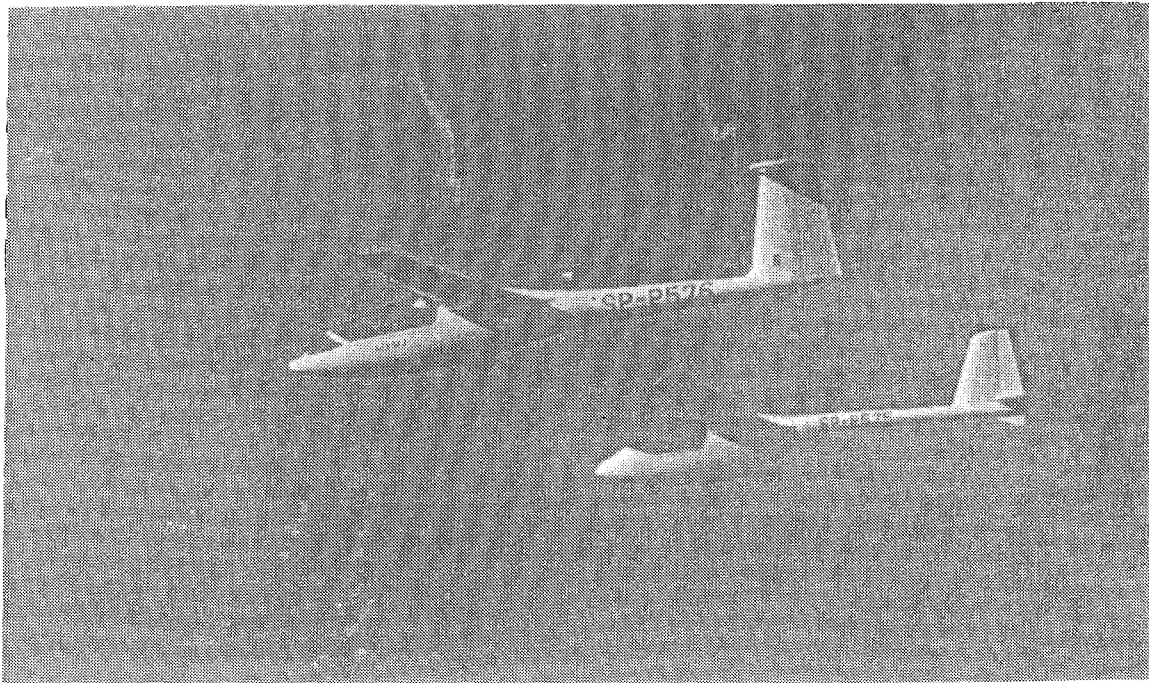


Figure 5: PW-5 and PZL 51-2 Gliders During Flight Tests

Flight tests were conducted using one of the gliders, a slightly modified production version of a club class glider, as a standard for comparison flying. This PZL 51-2 glider had been thoroughly tested by German authorities and documentation existed for its performance, however, these data were confirmed by local flight tests. The DLR provided all the flight test instrumentation needed to equip each prototype and helped the evaluation test pilots and crews apply proven methods for measuring the performance of each prototype. The performance of all of the five prototypes was documented and officially analyzed by the DLR support group and the Jury. Data relevant to the manner and cost of production, fatigue life, flutter testing and other factors were available in limited quantity during the prototype evaluation; however, all entrants were required to address these topics with documentation and discussions so that judgments could be made by the jury.

The winner of the prototype competition was the PW-5, designed by a team from the Warsaw Technical University, led by Professor Roman Switkiewicz and built by students with help from the PZL Swidnik factory. The winner was officially announced by the IGC in March 1993, after a thorough review and discussion of an evaluation report of the jury findings. The winner was then notified and according to pre-established conditions, was given one year to incorporate several changes recommended by the jury, to achieve certification in accord with JAR-22, to develop plans for production and for preparing technical design information that could be made available to others who wished to build PW-5 gliders.

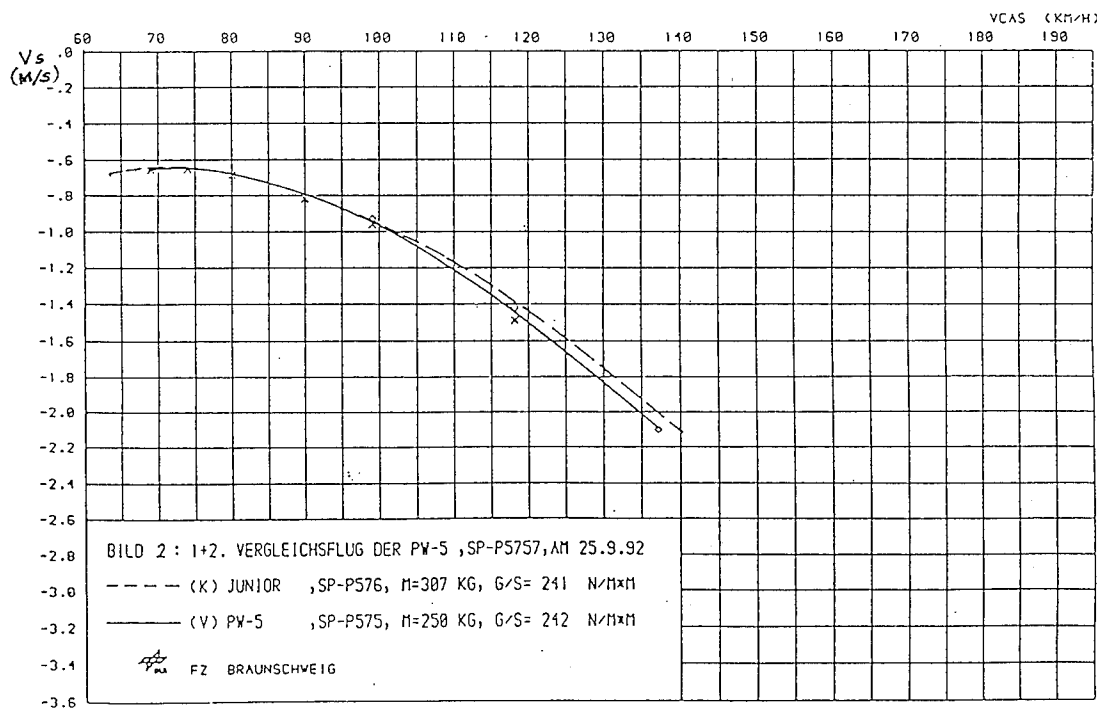


Figure 6: Example Data Showing Glide Performance Comparison of Two Gliders

WORLD CLASS EXPERIENCE-UNIQUE ASPECTS AND STATUS

Although there was broad agreement that a new I-Design glider was needed, there was no corporation willing to risk the capital required for defining and producing such a design for the marketplace. In creating plans for using such a glider in World competitions for at least

fifteen years, and by establishing a method of getting an International team of experts to develop a set of Technical Specifications and Requirements, the FAI-IGC essentially conducted a market survey and obtained inputs from a group of experts concerning the readiness and suitability of existing technologies for this glider. The design and prototype competition then solicited from designers all over the World, including corporations and individuals, methods of implementing these requirements. With this overall IGC leadership and support from concept through prototype evaluation, current technologies were applied for the benefit of the entire gliding community.

The certification of the PW-5 by Polish authorities in accord with Joint Airworthiness Regulations (JAR- 22) has just been completed. A formal agreement on the terms and conditions for the production and licensing is undergoing final review by Polish and IGC officials and is expected to be signed soon. Production of the PW-5 is underway in Poland, and many orders have been received. Several requests for licensing arrangements are under consideration, and the gliding community is anxiously awaiting delivery of the first production units. Formal arrangements are being made with Olympic officials to include gliding among the Olympic Air Sports, and an IGC representative from Australia has proposed that the PW-5 be used during the Olympics to be held in Australia in 2000.

If the production and use phases of the World Class program continue as successfully as the earlier phases described herein, the gliding community of the entire world will be served by having a glider based on inputs from a unique team of international experts. Manufacturers and builders will have the opportunity to produce one or more copies of the design, or to improve on the manner in which it is built and distributed, as long as the external lines and mass constraints are maintained. The winning design and prototype team will have the rights to continue production and will receive royalties for each glider made anywhere in the world. Persons wishing to have a well-designed 1-Design glider will have the benefit of knowing that their glider will not become obsolete in the short term, because of the specified use over a long period of time. This international experience may offer a precedent of unusual merit.

REFERENCES AIAA PAPER 1994

1. Nicks, Oran. "The World Class Sailplane." Soaring, Vol. 54, No. 5, May 1990.
2. Schweizer, Paul A. "An International One Design Class and the Olympic." Technical Soaring, Vol. 13, No. 2, April 1989.
3. Nicks, Oran. "The World Class Competition." Soaring, Vol. 56, No. 12, December 1992.
4. Morelli, Piero. "World Class' Present Status and Expected Future Developments." Soaring, Vol. 57, No. 12, December 1993.

INTRODUCTION OF THE MH-02 EXPERIMENTAL AIRCRAFT
A JOINT RESEARCH PROGRAM OF MSU AND HONDA

Haruo Nakayama †, George Bennett ‡

† Honda R & D Co.,LTD
Wako Research Center,Japan

‡ Miss.State University
Raspet Flight Research Lab.
Miss.State MS 39762

1.0 ABSTRACT

A proof of concept aircraft has been developed and flown in a joint research program by Mississippi State University's Raspet Flight Research Laboratory and Honda R&D. This aircraft has several innovative features including an all graphite composite airframe, forward swept wing, wing-top mounted turbofan engines, slats and triple slotted flaps, etc. A broad overview of this aircraft is presented which describes the design concept, performance objectives, structural architecture, systems, materials, and fabrication.

2.0 INTRODUCTION

Reduced vehicle weight is a continuing goal for all land, sea and air transportation modes. Recently, composite materials have shown the most promise ,and the aerospace industry has the most advanced technology for weight reduction. Honda R&D and Mississippi State University have made a study of the composite materials as a weight reduction technology which is needed for future transportation vehicles. In this long term study, two proof-of-concept experimental aircraft have been developed.

In 1986, a joint research contract was made between Mississippi State University (MSU) and Honda R&D. In the initial study, a Soloy turbine engine conversion Beech A-36 was modified in a step by step sequence to replace major structural elements with a composite structure.This process helped us to learn the basics of composite material technology and the basics of aircraft design, fabrication, and testing. First, a composite empennage was built and flight tested, then a composite wing was fabricated and flight tested. Details of this study have been given by Bennett, et al (Ref.1).

The MH-02 research aircraft project was started in 1989. Honda was in charge of the configuration design, aerodynamic design, structural design, and fabrication excluding the empennage. Mississippi State University was in charge of design verification, safety verification, and empennage fabrication. In all stages of the project, very close cooperation was required and actually performed.

At the initial stage, the research environment of this project was not desirable at either Honda or MSU since a twin turbo fan class aircraft and a graphite autoclave-cure prepreg material structure were new to both MSU and Honda. Within the joint MSU-HONDA team, the number of persons with experience in complex aircraft development was limited, and the processing and facilities for aerospace quality fabrication and assembly were sufficient. Initial tasks for the team were to locate experienced consultants and facilities. Several design areas critical to safety, such as flutter, and the fuel system were conducted by or reviewed by an outside consultant. Fabrication of critical parts was made by a contractor and the RFRL Annex was constructed to have sufficient space to assemble and test the MH-02 aircraft. The MH-02 aircraft was completed in December 1992, and after exhaustive ground tests, the first flight was successfully accomplished on March 5, 1993. Several test flights have been conducted since the initial flight.

MH-02 picture in flight test is shown in Fig. 1.

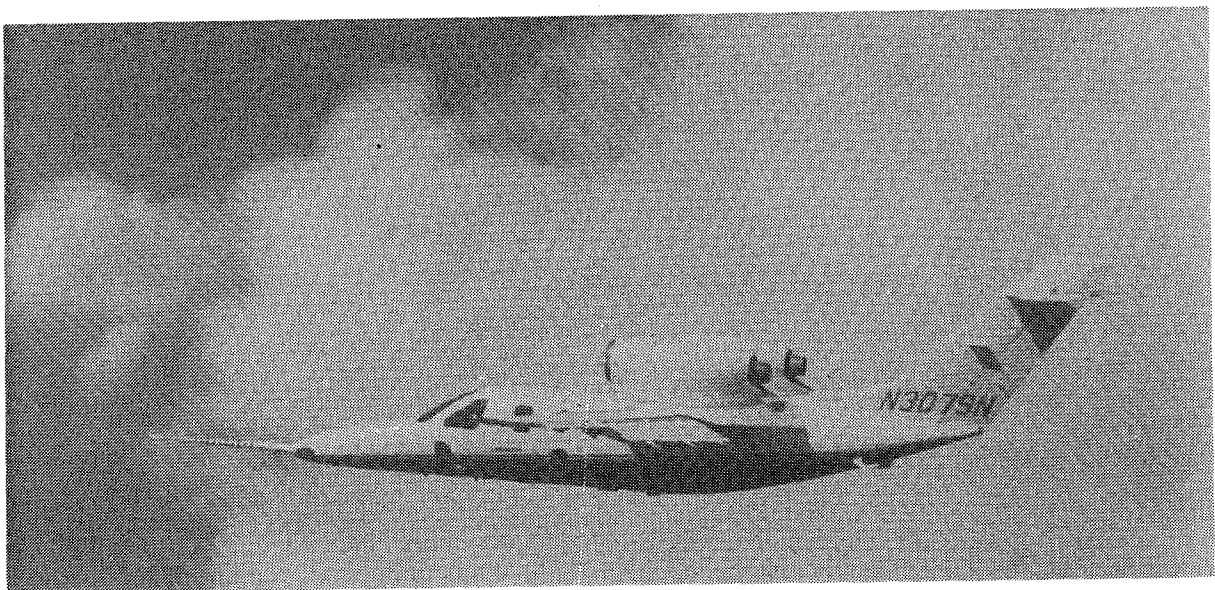


Fig.1 Flight Test Picture Of MH-02

3.0 MH-02 CONFIGURATION OBJECTIVES

The MH-02 research aircraft is a light weight, small turbo jet developed to operate primarily on short runways and with relatively short range. The MH-02 configuration is characterized by

- (1) Short landing gear and low cabin floor
- (2) Swept forward wing
- (3) Triple slotted flap with leading edge slat
- (4) Over-the-wing mounted engine

The general arrangement and dimensions of the MH-02 are presented in Fig.2.

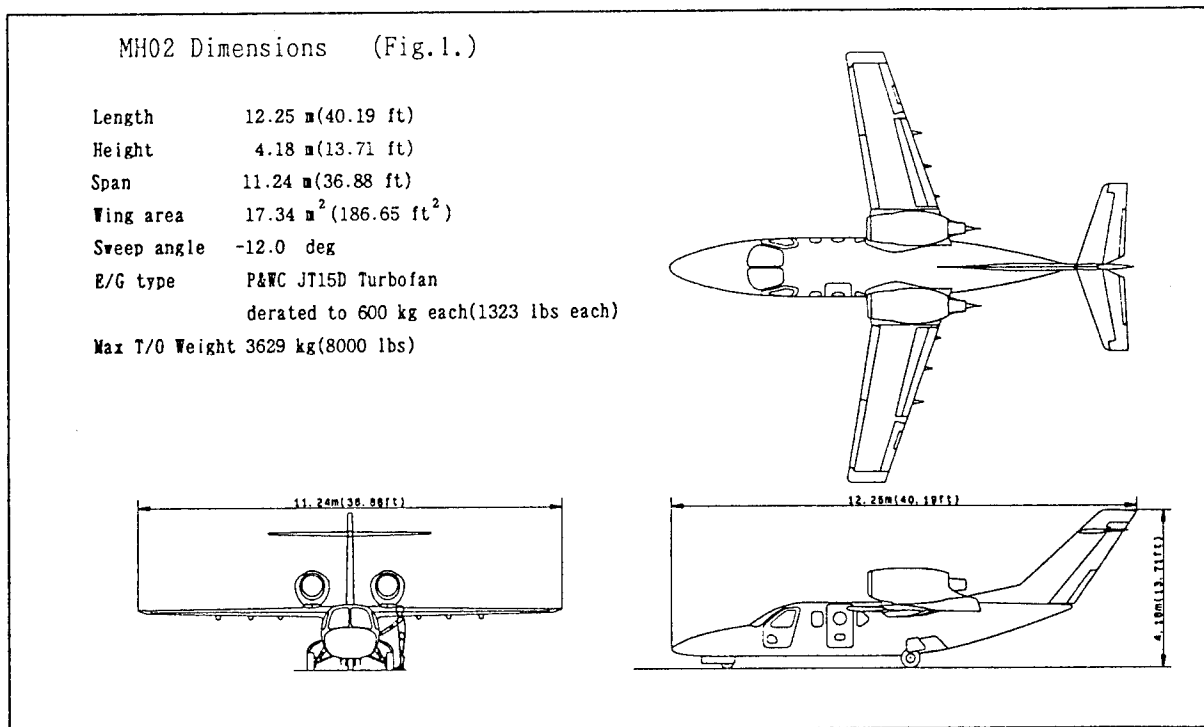


Fig2. MH-02 Dimensions

3.1 Short Landing Gear and Low Cabin Floor

It is important for the passengers to have easy access to the aircraft. The short landing gear and low cabin floor configuration allow passengers to enter the airplane like an automobile. The short landing gear is also advantageous to save weight and minimize the landing gear storage space.

3.2 Forward Swept Wing

The forward swept wing configuration employed for the MH-02 is to satisfy the requirement of the maximum cabin volume and stall characteristics. By employing the forward swept wing, the carry-through structure can be located behind the cabin and maintain the correct center of gravity range. The forward sweep also ensures wing stall would begin from the inboard of the wing and the roll control effectiveness could be maintained up to the stall. Aeroelastic analysis showed there is no weight penalty from a divergence point of view, as long as the forward sweep angle is small.

3.3 Triple slotted flap and leading Edge Slat

To achieve the short runway performance objective, complex high lift devices--triple slotted flaps with leading edge slats were chosen. High lift device selection for an aircraft should be determined based on the trade studies of aerodynamic efficiency, structural weight penalty, mechanical complexity, and costs. To investigate the feasibility of using complex high lift devices on small airplanes, triple slotted flaps and slats would need to be installed on the MH-02 as a major research theme.

3.4 Over-the-Wing Mount Engine

Because of the other design objectives favoring a configuration of a high wing with forward sweep, the location of the engine and inlet location was a major design decision. For a small jet, the aft fuselage engine position is the usual choice. For the high wing aircraft, the engine is mounted below the wing in a nacelle. However, these positions were not suitable for the MH-02 aircraft. For the forward swept wing, the C.G. of the aircraft tends to be aft because the heavy structures, such as the carry-through, are located in the rear part of the fuselage. The aft fuselage mounted engines move the aircraft C.G. more aft and, as a result, a large tail is required. If the engines were installed under the wing, the flaps would need to be cut out or the deflection of the flaps limited to prevent the jet exhaust impingement. Because of low aircraft height, there was concern about injection of foreign objects(FOD).

After considering the possibilities, an unusual over-the-wing engine position was chosen. For the over-the-wing engine configuration, the engines are located near the C.G. of the aircraft so that the tail moment arm is not reduced. A wide range of engines could be installed regardless of their weight and diameter. FOD problems are minimized and single engine(OEI) considerations are minimized. Negative aspects of the over-the-wing configuration such as the inlet distortion, power-pitch coupling, and tail aerodynamic interference were carefully investigated during the development process with analysis and wind tunnel testing.

3.5 Engine Selection

The MH-02 aircraft was designed to be suitable for around a 600kg-(1320lb) thrust class high-bypass-ratio turbofan engine installation. However, since those engines were not available, a Pratt and Whitney JT15D engine was selected. The thrust of JT15D is much higher, 1000kg(2200lb), so the thrust was derated to 600kg. Because of the over-the-wing mount configuration, it was possible to install these engines even though the weight is heavier and the diameter is larger than anticipated.

Many details of the development of the MH-02 proof-of-concept aircraft are given in Fujino(Ref.2), Misumi(Ref.3), Sato et al(Ref.4), Chaney et al(Ref.5), Lewis(Ref.6).

4.0 MH-02 AIRCRAFT STRUCTURE AND MATERIAL

4.1 Design Philosophy

The MH-02 development group was relatively inexperienced, yet they were interested in understanding both conventional and composite aircraft structural technologies. The following structural design philosophy was followed.

1. Select an advanced composite material for the structure. We considered that the application of an advanced material was a driving force in the study of modern aircraft materials and structure technology.
2. Use simple structures to reduce the part count. Simple structures were preferable because time and cost of fabrication could be reduced. Sandwich panels were used to reduce the part count. Since the corresponding reduction of the number of joints made structural analysis easier, which might compensate for our lack of experience, this philosophy had an advantage in the design stage of the structural development, also.
3. Safety First. Select a conservative design approach that assured safety. An additional safety factor was applied to many components so we could assure the structural integrity without a strength test. For example, a special factor of 1.33 in addition to the usual safety factor of 1.5 was applied to the composite primary structures. Although the MH-02 was an experimental aircraft which could easily be inspected and maintained in normal use, an ultimate design strain of 4000 micro strain was selected. Strength reduction due to impact damage was taken into consideration. Buckling was not allowed up to ultimate loading for all the composite parts to minimize the possibility of premature failures due to out-of-plane forces.

4.2 Material Selection

Advanced composite materials such as CFRP and KFRP have the most attractive characteristic of possible weight reduction of a structure as well as advantages in processing and corrosion resistance. Graphite-epoxy prepreg composite materials, cured in an autoclave, were reported by others to be the most reliable path to reduce weight of many aircraft structural parts. Material selection has a great effect on not only development of each technology, but the success of a project. The choice of cure temperature, 250° F or 350° F, was the first decision in selecting materials. The experiments prior to this decision had shown that either was applicable. Since the MH-02 was an experimental aircraft, the selection of 250° F cure epoxy prepreg was a short cut to airframe completion. However, since the control of heat and pressure was the most important, the material system with 350° F, autoclave cure epoxy was elected to explore current aerospace technology.

CF/EPOXY fabric HMF322/34 (FIBERITE) and uni-directional HYE-1034 were selected for the prepreg material. The 3-M 350 F-cure epoxy film adhesive AF191 was used for the sandwich panel fabrication, and 250° F-cure epoxy paste adhesive EC3448 for airframe assembly. Nitrile phenolic film adhesive AF30 was used on the outer surface of the skin sandwich panels for abrasion protection and surface finish. Hexcel nomex honeycomb of 3 PCF and 8 PCF was selected as core material.

Material tests were carried out not only to develop a data base for structural design but to study the characteristics of composite materials and test methods. The mechanical properties of a composite, modulus and strength of a lamina are indispensable for laminate design. Bearing strength and compression strength after impact (CAI) and impact strength of a laminate, and bending strength of a sandwich panel, etc., were obtained.

4.3 Structural Configuration

4.3.1 Wing

As shown in Fig.3 a two-piece construction has been selected for the wing which considers the capacity of available facilities and reduce the risks in fabrication. The wing is a two spar configuration with a sub-spar at the root to support the engine. The spars are bolted together at the center of the wing and joined to the fuselage frames with six pins.

The spars have a simple "C" cross-section laid-up in a female mold, which reduced cost and risk in fabrication. To further reduce risk in the fabrication of the main spars, the spars were made in two parts spanwise, then joined permanently before being assembled. Unidirectional plies dominate the flanges to carry bending loads, and fabric prepregs form the shear web and are interlaced in the flanges. The skin and rib are made of sandwich panels using fabric prepregs. Unidirectional prepreg was used in the wing skins to introduce bending-torsion coupling effects. The skins are directly bonded to the spar and rib flanges.

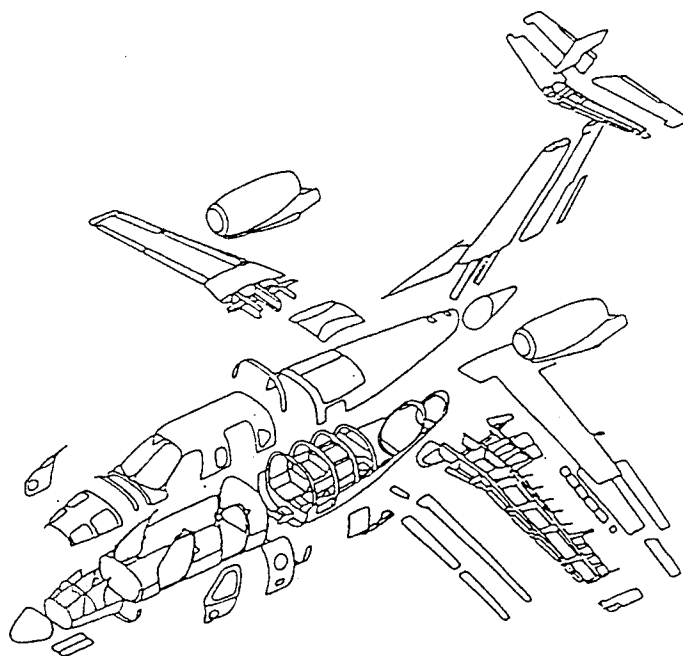


Fig.3 Sectioned View Of MH-02

4.3.2 Horizontal and Vertical Stabilizers

The construction of the stabilizers is similar to the wing. The parts are composed of similar materials. Both stabilizers are joined with metal fittings. The spars of the vertical fin are joined to the fuselage frames with four pins. The tail surfaces were constructed first, and the many lessons learned were used to improve the wing fabrication process.

4.3.3 Lifting And Controlling Surfaces

The flap, aileron, rudder and elevator structures are similar to the wing, using spars, skins and ribs with sandwich panels. Composite application to these components showed no weight reduction because of minimum gauge limitation of prepregs and adhesive weight for sandwich panels. As the study of new fabrication method, the flap vane, rudder tab, and elevator tab are of cocured construction.

4.3.4 Fuselage

The fuselage consists of three subassemblies nose, cabin, and aft fuselage individually assembled and bonded together.

The nose, a bonded sandwich panel structure, has keels that support the nose landing gear. Except for the frame around the door cutouts for reinforcement, the cabin section and the door are of monocoque

sandwich panel construction. The aft fuselage has six frames, with "C" cross sections, through which the concentrated loads from the wing, the vertical stabilizer and the landing gear are introduced. The landing gear storage area, located below the wing-to-fuselage joints in the aft fuselage, requires large cutouts in the skin. The keel, which is supported by the frames, compensates lack of longitudinal fuselage strength due to the cutouts.

All the fuselage parts, except the keel, are made of fabric prepregs to simplify the lay-up task. The keel is reinforced with unidirectional plies in addition to fabric prepreg.

4.4 Structural Analysis

The initial structural sizing was carried out by means of conventional analysis, using beam theory and classical laminate theory. After the sizing was completed, detailed stress analysis was conducted, using finite element analysis. The FEA was applied to major components such as the wing, a support structure introducing a concentrated load, and cutouts causing stress concentration.

In determining lay-up sequence of the wing skin, after satisfying the requirement for torsional rigidity with $\pm 45\text{deg}$, additional plies, $\pm 22.5\text{ deg}$. plies were employed to restrain torsion due to bending. The restraint effect by means of torsion-bending coupling was confirmed by FEA. FEA was also required for the fuselage analysis to account for cutout effect. Member stresses and joint forces were calculated using the model shown in Fig.4.

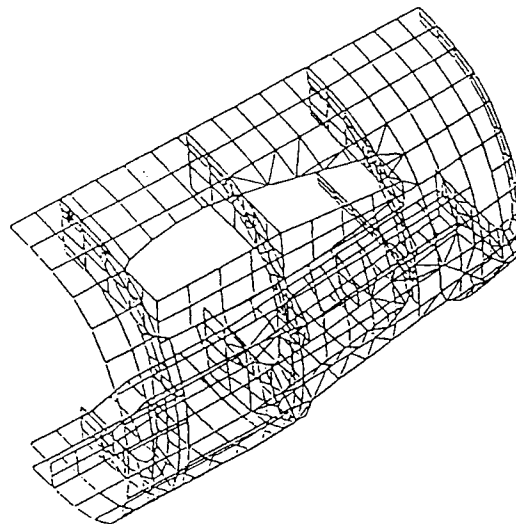


Fig.4 Finite Element Model Of
Aft Fuselage

5.0 SYSTEM

5.1 Flight Control System

The flight control system in the MH-02 aircraft was designed and fabricated following FAR Part 23 guidelines. A brief overview of the systems is described in the following paragraphs.

1. The MH-02 aircraft has a conventional three control surface system (ailerons, elevator, rudder) as the primary controls. All of these systems are reversible with no redundancy. Proven standard aircraft parts are used for systems reliability.
2. As secondary control system (tabs), each primary control surface has its own trim tab surface. The trim tab systems are driven irreversibly. In case of a system failure, the tab actuator irreversibility secures the tab surface and prevents flutter.
3. Dual control wheels and rudder pedal systems are installed for a two crew operation.

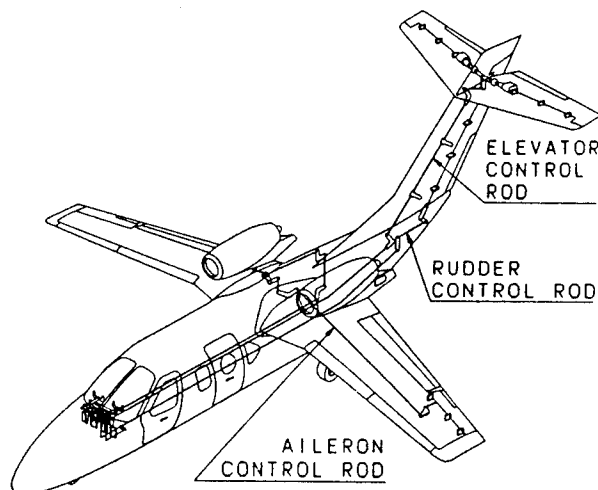


Fig.5 Flight Control System Outline

A special feature of the MH-02's flight control system was the use of push-pull rod linkage for the primary control system.

The objectives of this system are: (a) to achieve low maintenance, (b) to keep the external aircraft surfaces as smooth as possible, reducing access panels and cutouts, (c) to keep the cabin space as large as that of automobile, reducing the space below the cabin floorboards for rigging push rods, and keeping the fuselage cross section area relatively small.

Flight test measurement data of the control systems (operating forces, operating speed, strokes) will be studied and lessons learned will be used in future design activities.

5.2 Flap System

The MH-02 aircraft has a triple slotted flap on the wing trailing edge that is commonly used on large transport aircraft. The maximum deflection angle is 24 degrees for the main(#2) flap, and 28 degrees for the #3 flap. The #1 flaps (vanes) are fixed to the main flap.

Three track rails attached to the wing rear spar support each main flap. An electric DC motor and reduction gear box at the center of the main wing provides mechanical motion when commanded by the flap controller. The rotary motion is interconnected by torque tubes to the four flap actuators in main

wing.

In an ordinary triple slotted flap system, the #3 flap is mechanically linked to the main flap and extended during the main flap deployment. The MH-02, as a research airplane, has an electric DC motor and actuator (reduction gear box and jack screw) inside each main flap so that the flap controller can move the main and both #3 flaps independently. The purpose of this complex system is to obtain aerodynamic data with the flaps extended in arbitrary position during flight test. All of the #3 flap driving mechanisms are contained inside the main flap contour and require no fairings.

To prevent asymmetric flap deployment during the flight test, flap position sensors installed on each flap actuator provides position output signals to the controller and the co-pilot. Logic circuits will halt flap deployment if significant flap asymmetry is detected.

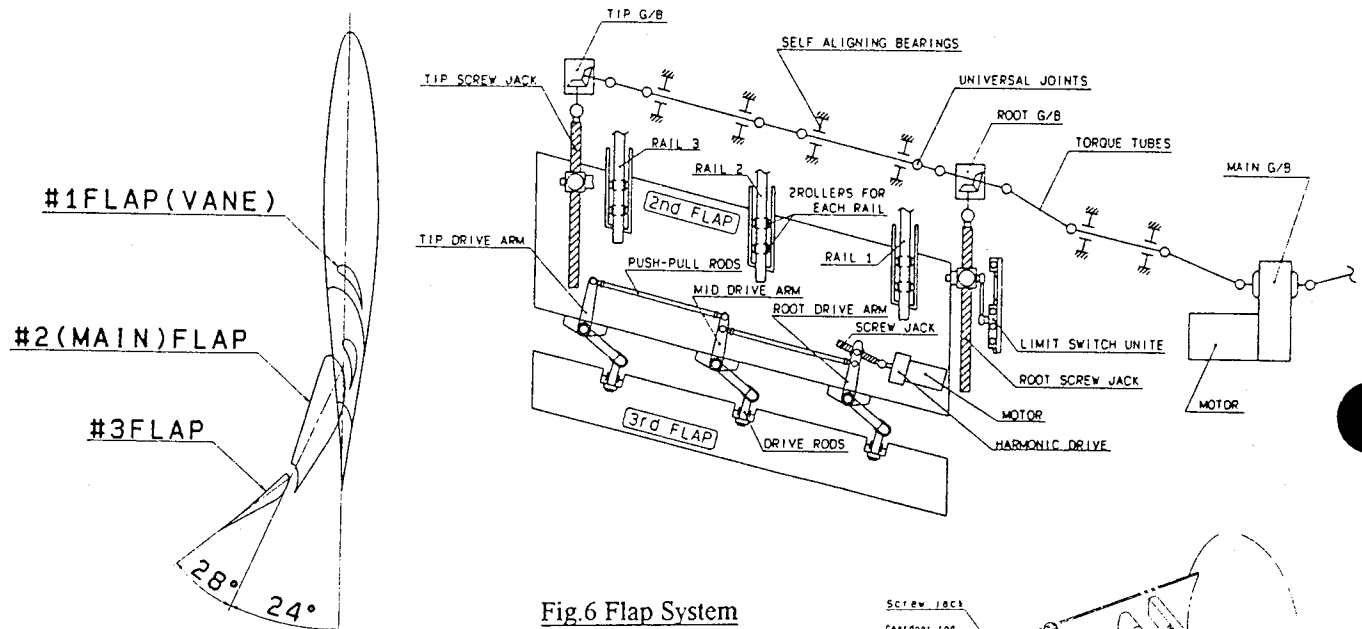


Fig.6 Flap System

5.3 Landing Gear

The landing gear system is designed to be able to support the ground reaction load factor 3.0. In an operation time of about 25 seconds. The nose gear is retracted forward by a motor driven jack screw actuator. The nose gear doors are driven by a mechanical linkage to the nose gear motion.

The main gear is retracted backward into the fuselage by an electric motor driven ball screw actuator. The forward main gear doors are mechanically linked to the main gear. The aft main gear doors are operated by an electrically driven

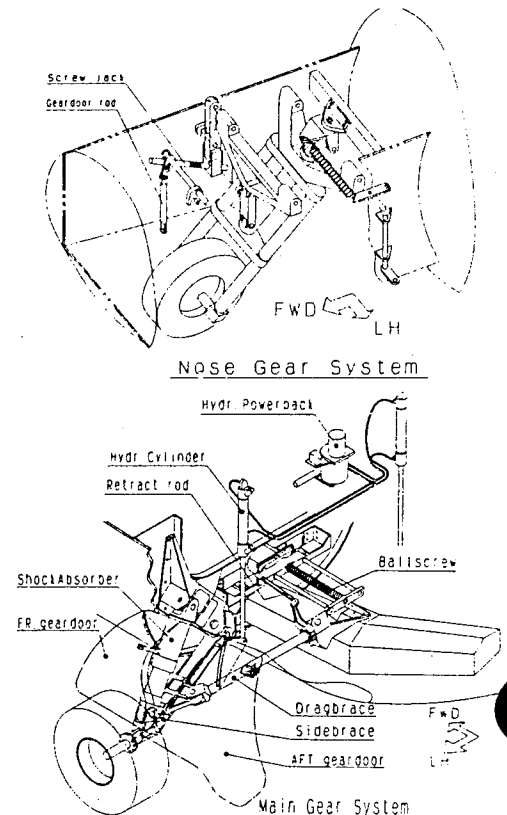


Fig.7 Landing Gear System

hydraulic system which open when the main gear is operating. After the main gear is extended, the doors close again. Both nose and main gear systems have their own lock release actuating systems driven by electric motors. The brake system does not have power assist system nor an anti-skid control system.

In case of a landing gear system failure, the hydraulic system pressure on the aft main gear doors is released and both nose and main gear can be extended by manual extension system which uses flexible shafts to connect the extension crank to the nose and main landing gear actuators.

5.4 Fuel System

The airplane has 11 bladder tanks in the main wing and an aluminum collector tank in fuselage. Fuel in the wing tanks flow into the collector tank by gravity, while the pumps in collector tank supply fuel to both engines. Two electric fuel boost pumps and two ejector type fuel pumps are installed in the bottom of the collector tank. Ejector pumps are operated by high-pressure fuel from the engine driven fuel pump and supply fuel to its respective JT15-D engine during normal operation.

Six ram air scoops on the lower surface of the main wing provide dynamic pressure in the tank cavity and maintain positive pressures within the structural limitations.

Since the main wing of MH-02 has no dihedral, a fuel transfer system was installed in each wing tip to prevent fuel from remaining in the wing outboard tank. If the fuel level is high, the float switch provides a signal to the controller and the electric transfer pump moves fuel from the wing outboard to the center collector tank.

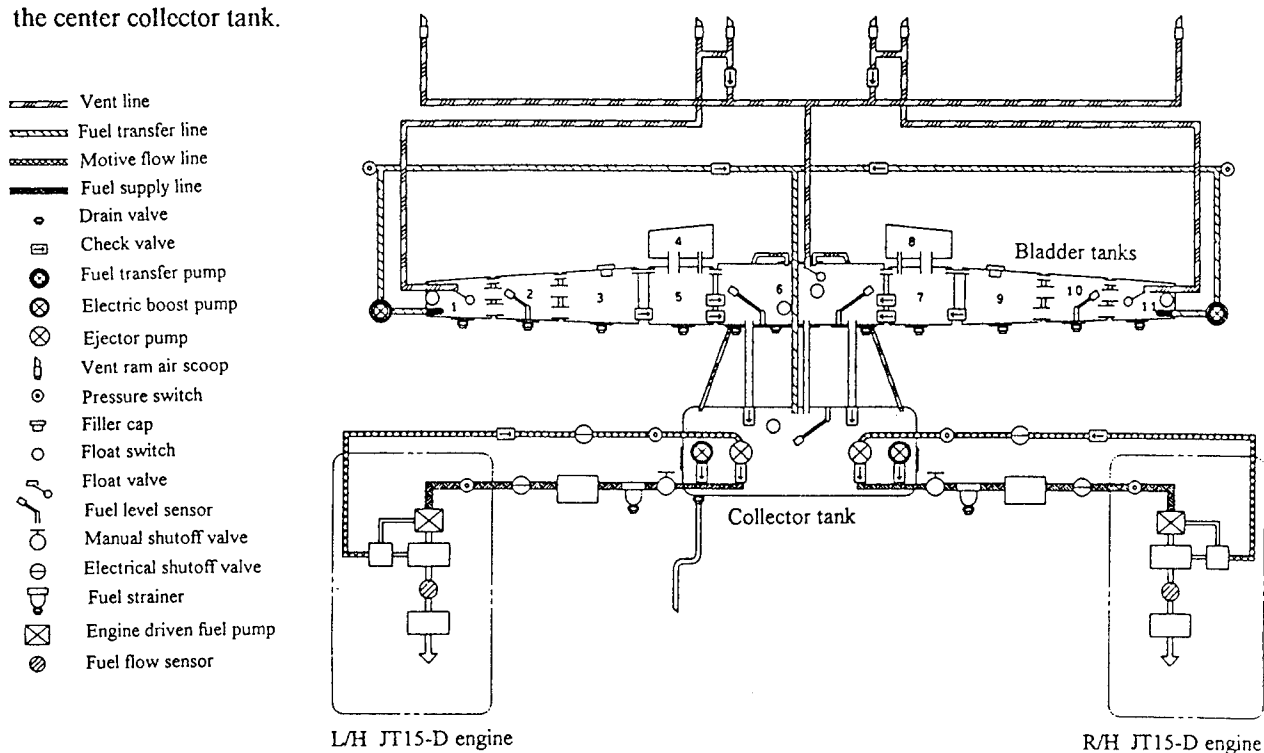


Fig. 8 Fuel System Schematic

6.0 COMPOSITE FABRICATION

6.1 Mold Fabrication Process

6.1.1 FRP Mold

The plastic faced plaster forming process generally used for making FRP mold takes much time and is costly because of intermediate molds. A one step method was used for this project which formed the female lay-up mold directly on a master male model.

Since the HONDA Company had obtained much experience in resin mold fabrication through automobile modeling, it was possible to make the master model with a numerically controlled machine. For accuracy, carbon fiber was used for the mold material because the thermal expansion coefficient of the mold is the same as the part being cured. Carbon fiber tooling prepreg was preferable for the mold fabrication because of the working environment and long mold endurance. Although processing tests using tooling prepreg showed good results, a fiberglass wet lay-up system was selected because of the acceptable properties and significantly lower costs. Glass fabrics were laid up using CIBA-GEIGY EPOCAST 88432 high temperature resin. They were then vacuum bagged and cured. Heat resistance was achieved through post cure schedule. Although the mold endurance test was not defined, the glass molds were suitable for autoclave processing.

6.1.2 Metal Mold

Simple metal molds were used for the spars of the flaps and the control surfaces. A pair of aluminum angles were precisely aligned and fastened onto a flat aluminum plate. Since the taper ratio in the spanwise direction was small, they were very accurate in spite of the large thermal expansion of aluminum.

6.1.3 Plaster Mandrel

The skin of the elevator tab and the rudder tab was cured over a plaster mandrel to study a new fabrication method. Prepregs were wound onto the mandrel made from resolvable plaster. After cure in a autoclave the mandrel was resolved away with water.

6.2 Sandwich Panel Fabrication

Prepregs, honeycombs, and adhesives were cocured into a sandwich panel. Slipping and core crush were troublesome. As for the honeycomb with a thickness of up to 12.7 mm (1/2 inches), the edge with an angle from twenty to thirty degrees was able to endure the crush. Cores more than 12.7 mm thick were fabricated by bonding layers of thinner honeycomb.

6.2.1 Door Panel

The door panel required a core with a thickness of 28.575 mm (9/8 inches) for the sufficient stiffness. Because the 28.575 mm thick honeycomb did not fit the mold and suffered from core crushes, three 9.525 mm (3/8 inches) honeycomb pieces were laid up on the mold with 0.127 mm (0.005 inches) thick prepregs for core stabilization as shown in Fig 9 and cured with a vacuum bag. The steep edge was filled with epoxy resin with filler to prevent crushing. The core material was cocured with prepregs and adhesives.

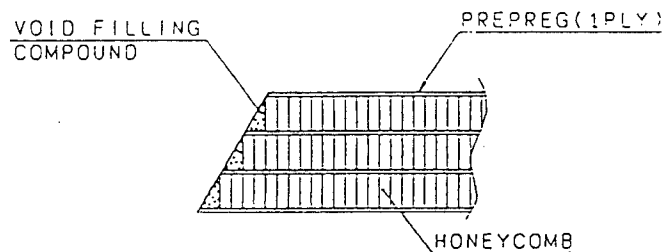


Fig.9 Core Stabilization For Door Panel

6.2.2 Flap Vane

A structural architecture different from the conventional aluminum model one, is sometimes applied to a composite structure when using composite fabrication features. Full depth honeycomb construction and an integrally cocured structure are examples. A full depth honeycomb construction was developed for the flap vanes. Since a thick low density (3PCF) honeycomb was difficult to shape with a numerical mil, the solution was to stack thinner sections using a prepreg cloth to bond each layer together for stabilization. After the block was machined into the flap vane profile, film adhesives and prepregs were wrapped around the surface and cured in an autoclave. The schematic drawing is shown in Fig. 10.

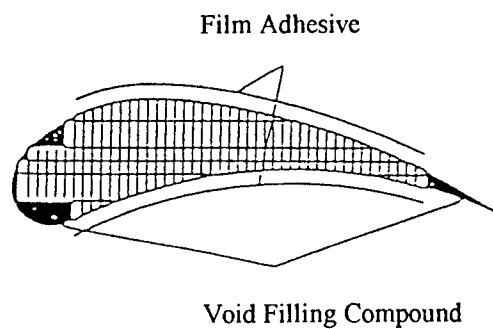


Fig. 10 Core Of Flap Vane

6.3 Part Inspection

Process control and non-destructive evaluation (NDE) have an important role in quality assurance of composite products. To verify material properties, all the primary structures were cured with a test panel from which coupons were cut to be tested. The primary structure that was not of sandwich panel construction, such as the wing spar and the fuselage frame, was inspected with the ultrasonic "C" scan technique. For the sandwich panels, the quality of adhesion between the core and the face sheets was checked with a tap scan. The adhesive fillets between the face sheet and the honeycomb core were checked with test panels cured along with the panel.

6.4 Airframe Assembly

All the structural parts were joined using only adhesives with exception of a few parts bonded with fasteners for redundancy. The 3M EC3448 250 ° F cure paste adhesive was used in the airframe assembly. Control of the adhesive bond line thickness was the most important aspect of assuring bond quality. All joint bond line thicknesses were checked by covering both joint surfaces with a release film and temporarily assembling the structure with a room temperature cure adhesive and apply process pressure during the cure. The bond line thickness was measured and shims were added to keep the thickness within the allowable limits. Cleco fasteners and lead shot bags were used for clamping pressure on the parts during the oven cure.

The wing was assembled in the skin mold with its surface used as a datum plane. The accuracy of the part location was confirmed with an optical transit. In the fuselage assembly, the skins were mounted on a dolly, and the internal parts were positioned with steel jigs frames.

The wing assembly process, which had several cure stages, exposed the parts to 250 ° F temperatures for a maximum of three times. The fuselage assembly, which had three subassemblies, had more cure stages than the wing. Although the exposures to the temperature were supposed to degrade composite parts and adhesive joints quality, coupon tests showed no degradation.

7.0 TEST

Since it was impractical in this research program to prepare a dedicated structures test airframe in addition to the flight airframe, a concept described in MIL-A-87221 (Ref.7) was used, which was to utilize in the case of identical article for both ground test and flight test. The method was to apply 115% of proof load on the ground test, then 100% load was used as the limit load in the air. The flight test envelope of the MH-02 proof-of-concept research aircraft was conservatively limited to +2 to -1 "g" and a 250 knot maximum speed even though the structure was designed to a FAR 23 envelope (3.6g limit load). This concept was used for the wing, horizontal tail, vertical fin. For the wing, planning limit load in the air was used as 100% for the empennage maximum estimated aerodynamic load among all conditions was used as 100%. Ground vibration tests were conducted to verify the computed flutter speed.

Many ground tests were needed to prove structural and mechanical integrity, coupon, element, sub-component. Complete aircraft level tests were conducted. The number of total test subjects was sixty, and the total number of test reached approximately one hundred. Test subjects are shown on Table-1.

Table-1 Test Subject

<u>WING</u> <ul style="list-style-type: none"> • STRENGTH TEST OF FRONT SPAR • STRENGTH TEST OF INBOARD TORQUE BOX • STRENGTH TEST OF FLAP RAIL SUPPORT STRUCTURE • STRENGTH TEST OF SLAT RAIL SUPPORT STRUCTURE • STRENGTH TEST OF REAR SPAR FLAP RAIL HOLL • WING PROOF TEST • WING STIFFNESS TEST • FLAP PROOF TEST • SLAT PROOF TEST • AILERON PROOF TEST • ENGINE NACEL INSTALLATION STRENGTH TEST 	<u>FUSELAGE</u> <ul style="list-style-type: none"> • PANEL INSERT STRENGTH TEST • STRENGTH TEST OF SEAT BELT ATTACHMENT STRUCTURE • STRENGTH TEST OF VERTICAL STABILIZER AND FUSELAGE JOINT STRENGTH • PROOF TEST OF LANDING GEAR ATTACHMENT STRUCTURE • EMERGENCY EGRESS DOOR FUNCTIONAL TEST
<u>ENGINE MOUNT</u> <ul style="list-style-type: none"> • STRENGTH TEST OF ENGINE MOUNT • ENGINE MOUNT STIFFNESS TEST • ENGINE MOUNT VIBRATION TEST • ENGINE MOUNT AND ENGINE NACEL STIFFNESS TEST ON THE AIRCRAFT 	<u>ENPENNAGE</u> <ul style="list-style-type: none"> • HORIZONTAL TAIL PROOF TEST • HORIZONTAL TAIL STIFFNESS TEST • VERTICAL STABILIZER PROOF TEST • VERTICAL STABILIZER STIFFNESS TEST • VERTICAL STABILIZER TORSIONAL PROOF TEST • ELEVATOR STIFFNESS TEST • VT - HT JOINT TORSIONAL STIFFNESS TEST
<u>FLAP SYSTEM</u> <ul style="list-style-type: none"> • MOTOR DRIVE TORQUE MEASUREMENT • MOTOR CHARACTERISTIC MEASUREMENT • SCREW JACK ENDURANCE TEST • UNIVERSAL JOINT ENDURANCE TEST • PRELIMINARY FUNCTIONAL TEST • COMPLETE SYSTEM FUNCTIONAL TEST 	<u>FLIGHT CONTROL SYSTEM</u> <ul style="list-style-type: none"> • CONTROL LINKAGE M/U TEST • STIFFNESS AND FUNCTIONAL TEST OF CONTROL WHEEL AND RUDDER PEDAL • IRON - BIRD OF ELEVATOR AND RUDDER CONTROL LINKAGE • PROOF TEST(PILOT LIMIT FORCE)
<u>LANDING GEAR</u> <ul style="list-style-type: none"> • SHOCK ABSORBER DROP TEST • PRELIMINARY FUNCTIONAL TEST • GEAR DOORS OPERATIONAL TEST • ACTUATOR ENDURANCE TEST • LANDING GEAR PROOF TEST 	<u>FUEL SYSTEM</u> <ul style="list-style-type: none"> • FUSELAGE TANK LEAKAGE AND VIBRATION TEST • MOCK - UP FUNCTIONAL TEST • COMPLETE SYSTEM FUEL FLOW TEST (COMPLETE AIRCRAFT)
<u>ELECTRIC SYSTEM</u> <ul style="list-style-type: none"> • STARTER GENERATOR FUNCTIONAL TEST • WIRING MOCK - UP TEST • COMPLETE SYSTEM FUNCTIONAL TEST 	<u>VENTILATION SYSTEM, INSTRUMENT</u> <ul style="list-style-type: none"> • PLUMBING LEAKAGE TEST AND PRESSURE - RESISTANCE TEST • PRESSURE REGULATOR FUNCTIONAL TEST • SENSOR CALIBRATION TEST
<u>COMPLETE AIRCRAFT FUNCTION</u> <ul style="list-style-type: none"> • ENGINE RUN UP • RADIO FUNCTIONAL TEST • LOW SPEED TAXI TEST • HIGH SPEED TAXI TEST 	<u>GVT</u>

8.0 PROJECT MANAGEMENT

Almost all the design work for the MH-02 was done in Japan, and most of the fabrication and tests were conducted in the United States. During the major fabrication and testing phase of the project, good communications, careful planning, and willing and eager participants were required. Later in the project, a significant number of Honda team members were sent to the Raspet Flight Research Laboratory in the United States to participate in the fabrication, assembly, and testing. It was essential to establish smooth and rapid communication between two project centers, Wako, Japan and Starkville, Mississippi, USA which had 14 hours time differences and 12,400Km (7,750 miles) distance. After some experience, it was found that, in addition to the usual international telephone and facsimile communication, a CAD file transfer system and static image transfer system were necessary to further develop the communication pathways to support the project. The CAD file transfer system was used almost daily for completed design drawing transfer from Japan to US. The static image transfer system was utilized to conduct interactive design reviews and problem resolution sessions between the RFRL and Wako teams when unexpected problems were encountered such as parts mismatch, interference, premature failure or crack, etc.

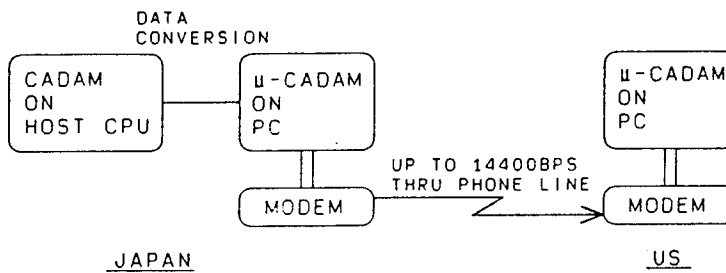


Fig. 11-A Drawing Data Transfer

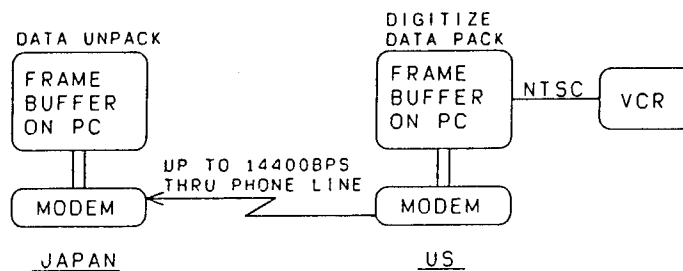


Fig. 11-B Image Data Transfer

In the busiest period of the fabrication, the parts fabrication, was conducted in three work centers, Wako Japan, Starkville, Ms, and Clearwater, FL. Since the parts fabricated by each group in each center had to be laid up, cured, inspected, evaluated using the same process, several standards and manuals were established and applied to all fabricated parts. Details for these were discussed by Sullivan and Sato (Ref.4) .

Even though the design team had the experience of the modification of the A-36 (Ref.1), this was the first experience to design an entirely new complex aircraft. "Safety First" was the guiding principle in the development of the MH-02 aircraft. As the aircraft approached first flight, a safety assurance review was conducted to ensure the safety objectives were satisfied. The safety review program proved to be very essential and quite workable. Several potential problems were discovered in the review and corrected before the flight test operations began. A detailed discussion of this program is described in a study by Misumi (Ref.3).

9.0 CONCLUSIONS

The objective of this project was to explore the feasibility of composite materials and aerospace structures for light weight structures. At this time, the following conclusions can be drawn relative to this objective:

1. The capability to fabricate aerospace quality composite structures was established, but it is necessary to improve the analytical methods, design techniques, and test methods to achieve the potential weight reduction promised by modern composite material.
2. Light weight structures concepts for an aircraft was learned, but it was realized that the design requirements for an aircraft are quite different from the design requirements of ground vehicles such as automobiles. Thus, it is difficult to apply lessons learned about aircraft to the weight reduction of the ground vehicle in the near future.
3. However, in the future, if the requirement to the weight reduction for ground vehicles is greatly increased, then the structural weight requirements gap between aircraft and automobiles will become smaller.
4. Generally speaking, much experience is necessary to design and develop an aircraft, but it has been proved that a team with limited experience can design, fabricate, test, and fly a fairly complex airplane safely by following a conservative development plan, a prudent schedule, and a "Safety First" decision policy.

10.0 ACKNOWLEDGMENTS

The author would like to express his appreciation to Dr. Albert G. Bennett, Director of Raspet Flight Research Laboratory of Mississippi State University, Dr. John C. McWhorter, Head of Aerospace Engineering Department of Mississippi State University, and Mr. Grady W. Wilson, Chief Test Pilot of Raspet Flight Research Laboratory of Mississippi State University for their overall cooperation to the project. The author also would like to express his appreciation to Mr. Leon Tolve for his flutter analysis, Mr. Rieherd for his fuel system evaluation, Mr. William R. Higgins, President and Mr. Joe Rayhill, Vice President, of Advanced Technology Inc. for their fabrication support, and finally to Mr. Jim Reeves, Manager Aviation Safety Inspector, and Mr. Richard Arnett, Aviation Safety Inspector, FAA Atlanta MIDO, for their guidance in the issuance of the experimental flight certificate.

11.0 REFERENCES

- 1) G. Bennett, J. McWhorter, G. Bryant, H. Koelling, G. Bull, Composite Prototype Aircraft Development, A Method For Design, Fabrication, and Test Training SAE 911015.
- 2) M. Fujino, Aerodynamic and Aeroelastic Design of Experimental Aircraft Honda MH-02.
- 3) E. Misumi, Assurance of the Flight for the Honda MH-02.
- 4) R. Sullivan, K. Sato, A General Overview of the Fabrication and Quality Control Activities for the Honda MH-02.
- 5) V.G. Chaney, R. Lincoln, K. Motoyama, Design of a Fully Automated PC Driven Data Acquisition System for the MH-02 Experimental Aircraft.
- 6) C. Lewis, Determination of the Stability and Control Derivatives of a Turbo-fan Research Aircraft Using a Maximum Likelihood Method.
- 7) MLL-A-87221, General Specification For Aircraft Structures.

THE EFFECT OF OCCUPANT CRASHWORTHINESS REGULATION COMPLIANCE ON GENERAL AVIATION AIRCRAFT SIZE AND PERFORMANCE

Prof. Charles. N. Eastlake and Dr. James G. Ladesic
Embry-Riddle Aeronautical University
Aerospace Engineering Department
600 S. Clyde Morris Blvd.
Daytona Beach, FL 32114-3900

ABSTRACT

The U.S. needs a new primary flight trainer for use in general aviation. As part of this general need, such aircraft must be designed for attributes like forgiving flying qualities, controllability, easy maintenance, low operating cost, reasonable performance, and safe operating life. But occupant safety is possibly the single most important aspect of this design and should not be compromised in favor of any other attributes. In this study occupant safety considerations were investigated for a number of primary flight trainer designs. Configurations were established using traditional airplane design methods. Typical training mission requirements dictated the performance criteria for each, leading to designs embodying several configurations that offered a reasonable, although minimal, amount of occupant space. A detail design activity was then focused on occupant safety for each configuration accounting for various structural load paths needed around the occupants to assure them reasonable protection in an emergency situation. Multiple load paths, energy absorbing structure and break-away structure are all considered in these designs. As a result cabin volumes often increased, thereby changing the performance. The unfavorable impact that these changes had on fuselage weight and aerodynamic drag were subsequently investigated and the results are presented in this paper.

INTRODUCTION

PURPOSE

There is an urgent need for a modern General Aviation (GA) Primary Flight Trainer (PFT) vehicle ¹. Demand for pilots in the near future is predicted to tax the U.S. capability to train new pilots due in part to the limited availability of single engine, low operating cost training airplanes. At present the average age of the single engine general aviation airplane is 28 years, a working life their designers are unlikely to have anticipated during the design activity. Production of this class of airplane, extensively used in the past for training, business and recreational flying, has all but ceased in the U.S. The need is being met by the aging fleet of existing airplanes or by imports. Some observers blame management failures and the reluctance of the industry to modernize, while others cite crippling legal encumbrances and limitless product liability as the explanations for the situation. Others target governmental regulations at home and foreign government subsidization of national industries which compete against us in the world market.

In truth, all of these have played a part in the demise of the U.S. GA industries. But no matter what the cause, aviation transportation in this nation must look to the future. We must look toward new trainers for future pilots as well as new transport category aircraft. New trainer designs must include consideration of the current Federal regulations, the training environment and the existing legal situation. Placing occupant safety first and foremost on the design priority lists appears to be one of the best means for providing needed improvements in product liability risk while satisfying regulatory mandates. The U.S. automotive

and motor sports industries have made significant advances in reducing fatalities by the implementation of occupant safety features within their vehicles ^{2,3}. Motor racing teams design for occupant safety dealing with speeds and situations very similar to the emergency landing conditions for GA airplanes. Technological advances in these areas have been significant. Motor sports design evolution has some interesting lessons learned that may be applied to GA vehicle design. By contrast the stagnant GA industry has made little progress toward improved safety over the years. The last Cessna 152 to roll off the line in 1986 was, for the most part, the same airplane as the original model 150 designed in the mid 50's. Placing such designs back into production would surely place more airplanes on the market but would do little to improve the accident rate or the fatalities associated with emergency situations. The decision to change the design priorities and make use of these lessons learned lies within the control of current as well as aspiring aircraft manufactures. The investigation presented here is offered as a catalyst for such decisions.

A SPECIAL ERAU FOCUS

While any airplane that could meet existing FAR23 airworthiness requirements as a Normal Category airplane would satisfy a great deal of the requirements for training in primary flight, the need for spin training and other more advanced maneuvers requires that the airplane meet Utility Category standards, at least in some load configuration. Of particular interest might be vehicle designs that permit two occupants in a Utility Category spin training configuration and three occupants during fundamental Normal Category training missions. This conforms to Embry-Riddle's Gemini Flight Training concept - a student pilot, an instructor pilot and a second student as an in-flight observer.

BACKGROUND

In 1980 the National Transportation Safety Board (NTSB) began a five year study of general aviation airplane occupant restraint and seat systems under the title of the "General Aviation Crash Worthiness Program". The results of this study were published in three separate Phase Reports. The Phase One ⁴ report defined the rationale for the program and gave the proposed program plan. It also described the analytical methodology to be used in developing the material addressed in the program. The Phase One Report was released June 27, 1983.

Phase Two ⁵ involved evaluating data gathered from over 500 accident involving more than 1,200 occupants of general aviation type aircraft. It was in this phase that the NTSB defined accident survivability as "...an accident in which the forces transmitted to the occupant through the seat and restraint system do not exceed the limits of human tolerance to abrupt acceleration and in which the structure and the occupants' immediate environment remains substantially intact to the extent that a livable volume is provided throughout the crash sequence". It was also in the Phase Two report that the potential benefits of using shoulder harnesses and energy absorbing seats as a means of significantly reducing occupant injuries were demonstrated. The NTSB in this report concluded that if shoulder harnesses had been worn in all of the accidents investigated in the program a 20 percent reduction in fatalities could have been realized. Similarly, 88 percent of the serious injuries that were encountered would have been substantially reduced in severity. The NTSB also concluded in Phase Two that energy absorbing seats could have reduced the potential for injuries in 34 percent of the cases involved. Phase Two results were released March 15, 1985.

Phase Three ⁶ of this program was completed September 4, 1985. It detailed on-scene investigations of 39 selected "survivable" accidents that were subsequently evaluated and ranked. It was in this report that the NTSB also declared its support of the General Aviation Safety Panel (GASP) recommendation for comprehensive dynamic testing of seat/restraint systems to 26g's. (The GASP had been formed February 1983 as an industry task force at the invitation of the Federal Aviation Administration (FAA) and was

composed of representatives from airplane manufacturers, government and pilots in the GA field.) Peak longitudinal and vertical accelerations determined in Phase Three effort were developed and justified by calculations. Then they were compared against the injuries incurred by the occupants. It was concluded by the NTSB that the GASP recommendations were valid and applicable to general aviation. As a result, the NTSB issued a Class II Priority Action to the FAA to amend 14CFR23 to include the GASP recommendations. The NTSB also called for multi-axis dynamic seat/restraint testing "...as necessary to demonstrate energy management in the vertical direction and structural adequacy in the longitudinal and lateral directions" in this same recommendation.

As a result of these NTSB/GASP actions and recommendations, Amendment 23-36 was implemented in the form of Change 24 to 14 CFR 23, effective September 15, 1988 ⁷. This change to the airworthiness regulations has far reaching implications for general aviation regarding occupant safety and restraint. In this amendment significant changes to the emergency landing condition, to include Paragraph 23.562 requiring dynamic seat tests, have been introduced for the qualification of occupant/restraint systems as well as the seat and its support hardware. In addition, cargo and concentrated mass item restraint, both in and outside of the cabin, have been significantly changed.

Future aircraft will need to be substantially different from that of the classic single engine PFT in the design of their cabin volumes and systems in order to meet airworthiness certification requirements from December 15, 1988 and onward. The study presented here represents a year and a half investigation into some of the effects these regulations will have on airplane configurations and their resulting operational performance. This work was conducted as part of the Embry-Riddle Aeronautical University (ERAU) Advanced Design Program (ADP) sponsored by NASA Langley Research Center and administered through the Universities Space Research Association.

FOCUS ON OCCUPANT SAFETY WITHIN THE ADP

ERAU is to spend three years (92-95) investigating and exercising the design aspects of the GA primary flight trainer. In addition to the traditional airplane design activities which focus on mission performance, operational costs and minimum weight, a special emphasis is being placed on occupant safety and crash survivability in these designs. This is currently being accomplished within the two semester airplane design sequence which serves as the capstone for our undergraduate Aerospace Engineering curriculum.

Because there are no PFT airplanes currently in existence which fully comply with the present FAR Part 23, the first year of the program (the 1992-93 school year) was directed toward developing two modern FAR 23 certifiable baseline designs to be used as a standard against which all future designs would be compared. Constraints were imposed such as using certified, in-production engines, selecting only proven aircraft aerodynamic configurations, and employing only proven fabrication methods. In short, the design goal was to create what could be termed a "Now Airplane" as the baseline design.

In the first semester, preliminary designs for eight PFTs were completed. The results were fairly predictable, showing configurations much like many existing trainers. Two seats, side-by-side predominate, with three seats an infrequent selection. Four seats were permitted but never chosen. Aspects of FAR 23 regarding occupant safety, crashworthiness and the Head Injury Criterion (HIC), regulatory details which current trainers do not meet, were included in the design requirements though were not checked for compliance in a very strict manner. The HIC did not previously apply to aircraft at all. It is an integral equation which places a specific upper limit on the integral of acceleration of the CG of the head, integrated over the time duration of an impact. All during the initial year design process, great

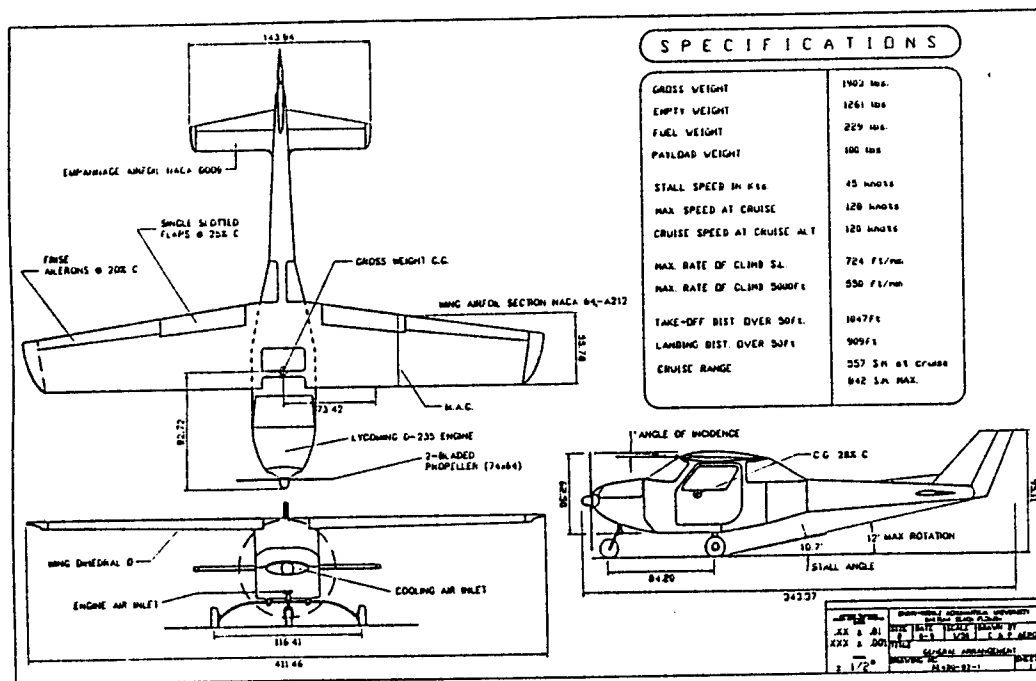
emphasis was placed on documentation of the designs for future use and on team decision making, integrating information from non-engineering sources like ERAU flight operations and maintenance technology personnel. From the original eight airplane designs two were selected for continued study in detail design; one high wing resembling a Cessna 152 called Triton and a low wing design named Viper which resembled a two-seat Mooney. These are shown in Figure 1. Fourteen detail design teams directed their attention toward the structural design of the wings, aft fuselage, tail surfaces and control systems for each of these airplanes during the Spring 1993 school term. This yielded reasonably believable final weight estimates and cost estimates for these aircraft.

As part of the continued evaluation of these two designs during the second year of the ADP, the Fall 1993 preliminary design students were encouraged to consider new versions of the designs incorporating staggered seating to allow narrower fuselages, and to consider three seats instead of two-versus-four, both things the industry has not looked at very seriously. Several of the design groups developed a new twin-boom pusher design while most considered the redesign of the two baseline airplanes. These new and re-designed airplanes still had to meet the original mission requirements for a Primary Flight Trainer airplane, comply with the current FARs, and were required to use state of the art technology and manufacturing capabilities in the form of Natural Laminar Flow (NLF) airfoils and recently developed engines which are commercially available but not FAA certified.

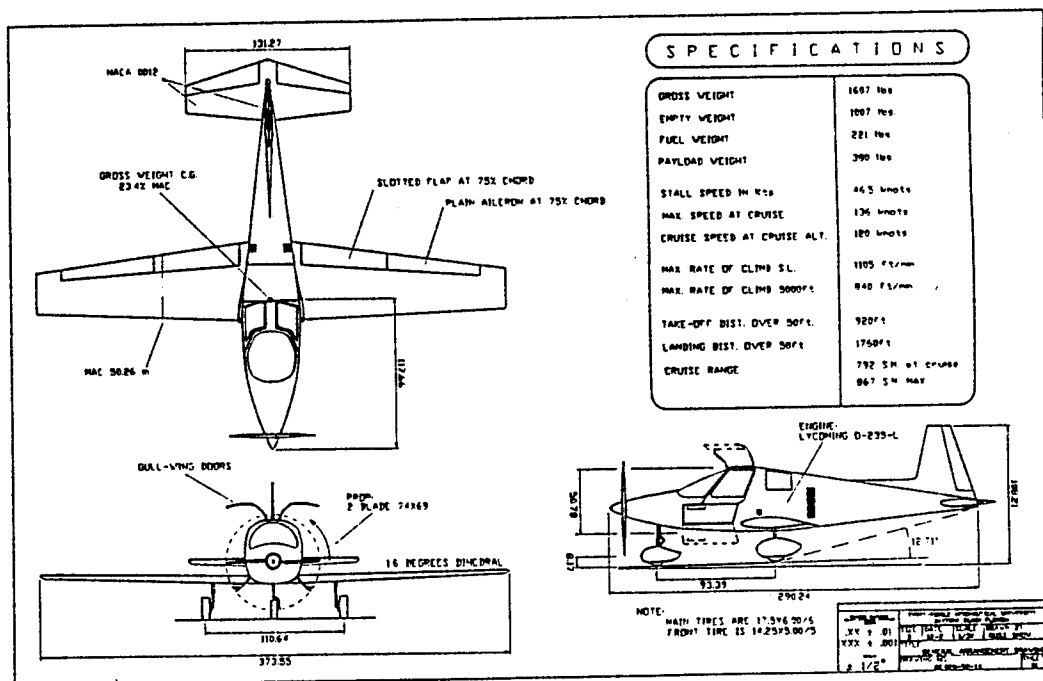
Meanwhile, Fall '93 detail design groups investigated in more detail the previous teams' cabin-fuselage designs. A variety of occupant seating configurations were proposed for seven of the second generation baseline designs. Teams developed, from a structural detail design perspective, a set of "Spatial Requirements Specification Documents" (SRSDs) that demonstrated compliance with governing regulations through analytical substantiation. These SRSDs were intended to determine the size, shape, weight and c.g. position of the cabin volumes needed to safely house the occupants in emergency conditions, based on the 95th percentile standard man⁸. In addition, they considered the space needed for the control systems previously designed and adequate routing space for other systems like hydraulic, electrical, heating and ventilation. The human factors and ergonomics of the cockpit were taken into consideration for ingress/egress as well as instrument panel and engine control layout. Formal specifications were produced defining minimum external dimensions needed to accommodate the internal needs and the intermediate structure required for meeting all of the design conditions of the particular airplane configuration and chosen occupant seating arrangement. These were submitted in the form of the SRSD's to be used by future preliminary design teams in developing new airplane concepts. Table 1 lists the configurations investigated in this detail design activity.

Table 1 Cabin Volume Configurations Investigated

Config.	Occupant Seating		Airplane Configuration		
	Places	Arrangement	Engine/Propeller	Wing	Tail
1	2	Side-by-side(SBS)	Front/Tractor	Low	Conventional
2	3	2SBS + 1 Rear	Front/Tractor	High	Conventional
3	2	Side-by-side	Mid/Tractor	Low	Conventional
4	2	Staggered	Front/Tractor	Low	Conventional
5	2	Staggered	Aft/Pusher	Mid	Twin-boom/Conv
6	3	Staggered	Aft/Pusher	Mid	Twin-boom/Conv
7	2	Tandem	Front/Tractor	Low	Conventional



Triton



Viper

Figure 1. Baseline Configurations

FAR23 LOADS AND CONDITIONS

The current version of FAR23 has a number of different normal flight and emergency landing condition loading requirements that may be substantiated by static test under limit load and ultimate load scenarios. An additional emergency landing dynamic condition defines dynamic tests for seats and occupant restraint systems to be conducted using anthropomorphic test dummies.

In accordance with paragraph 23.562(b) "each seat/restraint system, for crew or passenger occupancy in a normal, utility and acrobatic category airplane, must successfully complete dynamic tests or "be demonstrated by rational analysis supported by dynamic tests..." for the dynamic conditions defined in terms of rise time, velocity change and peak acceleration. As a starting point for this design investigation, demonstration by rational analysis supported by test was satisfied by the student teams by selecting a seat/restraint configuration developed by the Jungle Aviation and Radio Service⁹, often referred to as the "JAARS seat", affixing a head rest to the seat back and designing the seat/cabin interface to the loads cited in their test report using accepted structural analysis methods. At present there appears to be no alternate seat available that meets the requirements of 23.562 and that is applicable to the GA-PFT need. Therefore, the initial internal size requirement is established using the JAARS seat. As the next step the 95th percentile standard man (6'2" tall and approximately 220 lb) was selected as the upper limit of the volume requirement. Figure 2 illustrates the combined results of these selections. The HIC requirement of 23.562(c)(5)(i) is best handled in preliminary design, as suggested by Smith¹⁰ and demonstrated by Metz and Irwin¹¹. This involves assuring that the internal volume of the cabin is sufficiently large so that under anticipated emergency conditions, with the associated seat/torso/head excursions, head contact with any portion of the cabin structure will not occur. Zones to be avoided during the cabin configuration and shaping activity are shown in Figure 2.

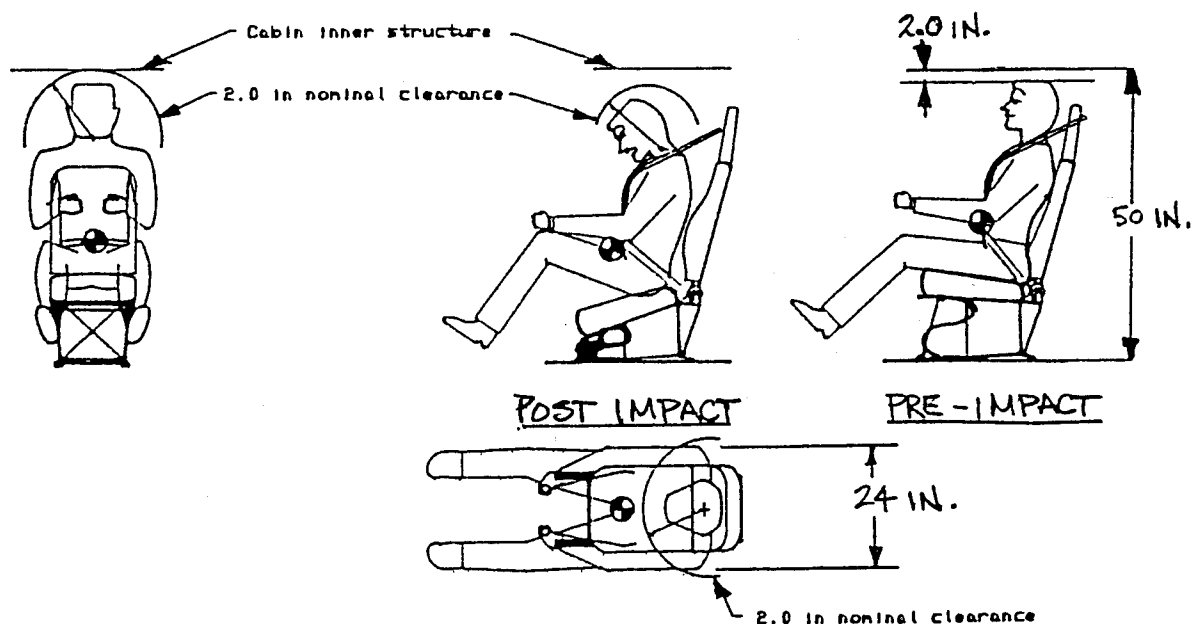


Figure 2 Standard 95th Percentile Man and JAARS Seat Configuration.

With the internal volume thus defined the structural load paths needed to safely transmit all the loads can now be assessed as a function of the airplane configuration. The structural needs of the cabin shell in normal flight are controlled by the aerodynamic loads produced by various flight conditions and by the location of concentrated loads created by attachment of the seats, engine, wing, tails and landing gear. All of these conditions must be substantiated in preliminary structural design to the extent that no permanent structural deformations occurs under limit load conditions nor any failure of primary structure occurs at ultimate load conditions. For conventional single engine airplanes of 6,000 lb or less maximum weight the maneuvering and gust load factors can be fixed values and are given in FAR 23.

Emergency landing conditions, defined in Table 2, require that the cabin shell offer the occupants protection against ground impacts of varying orientation. In this scenario, structure may permanently deform, break away, crush or collapse in any safe sequence (i.e., maintaining a livable cabin volume) to absorb energy and reduce the impacts transmitted to the cabin occupants. For these conditions the structural cabin shell requirements are controlled by the inertia loads produced as a result of vehicle mass distributions, the relative position of the engine, wing, tail and landing gear with respect to the cabin shell and by the direction of the impact load factors with respect to all of these.

Table 2 Emergency Landing Condition Static Load Factors
{Ref: FAR23.561 General [Ch 24(amdt. 23-36, Eff. 9/14/88)]}

Condition	Upward	Forward	Lateral
Aircraft static inertial loads	3.0g	9.0g	1.5g
Cabin mass items	3.0g	18.0g	4.5g
Turnover at max weight.	1.0g	9.0g	---

The product of these detail design considerations for four representative configurations selected from Table 1 are shown in the following four figures. Figure 3 is a two seat, side by side cabin applicable to either the Triton or the Viper baseline aircraft. It shows underfloor space for a Viper low wing spar, but a similar extra height (8.66 inches) overhead would approximate the space for the high wing Triton. The student teams felt obliged to be pretty generous about allocating interior width in the interest of minimizing impact injuries. They provided 48 inches, which is quite a bit wider than typical production trainers. The interior height of 49.2 inches is not larger than typical production trainers but appears to compensate well for the HIC given the assumption of a functioning shoulder belt. It is, however, probably worthy of note here that many of the older training aircraft still in widespread operational use do not have shoulder belts. They were not required before the mid-1970's. Figure 4 shows a third seat added in back to create a seating arrangement compatible with the Gemini training concept to which ERAU's flight department is committed. The cabin envelope is about 37 inches longer than the two seat arrangement, but the shape of the envelope is such that little or no overall lengthening of the fuselage exterior would be required.

Figures 5 and 6 show the benefits of staggered seating, still possibly a bit too generous in allocating interior width. Figure 5 is a two seat cabin envelope seven inches narrower than the side by side envelope in Figure 3. The width increment seems reasonable, whether or not one agrees with the individual measurements. Figure 6 shows a three seat staggered arrangement, again seven inches narrower than the comparable Figure 4. It is roughly 24 inches longer than the two seat arrangement (the front seats are staggered by different amounts). In this configuration some lengthening of the fuselage exterior is more likely to be required to provide head clearance for the occupant in back because the rear seat is not centered and cannot be. The interior heights of all configurations are similar, as one would expect, at about 50 inches.

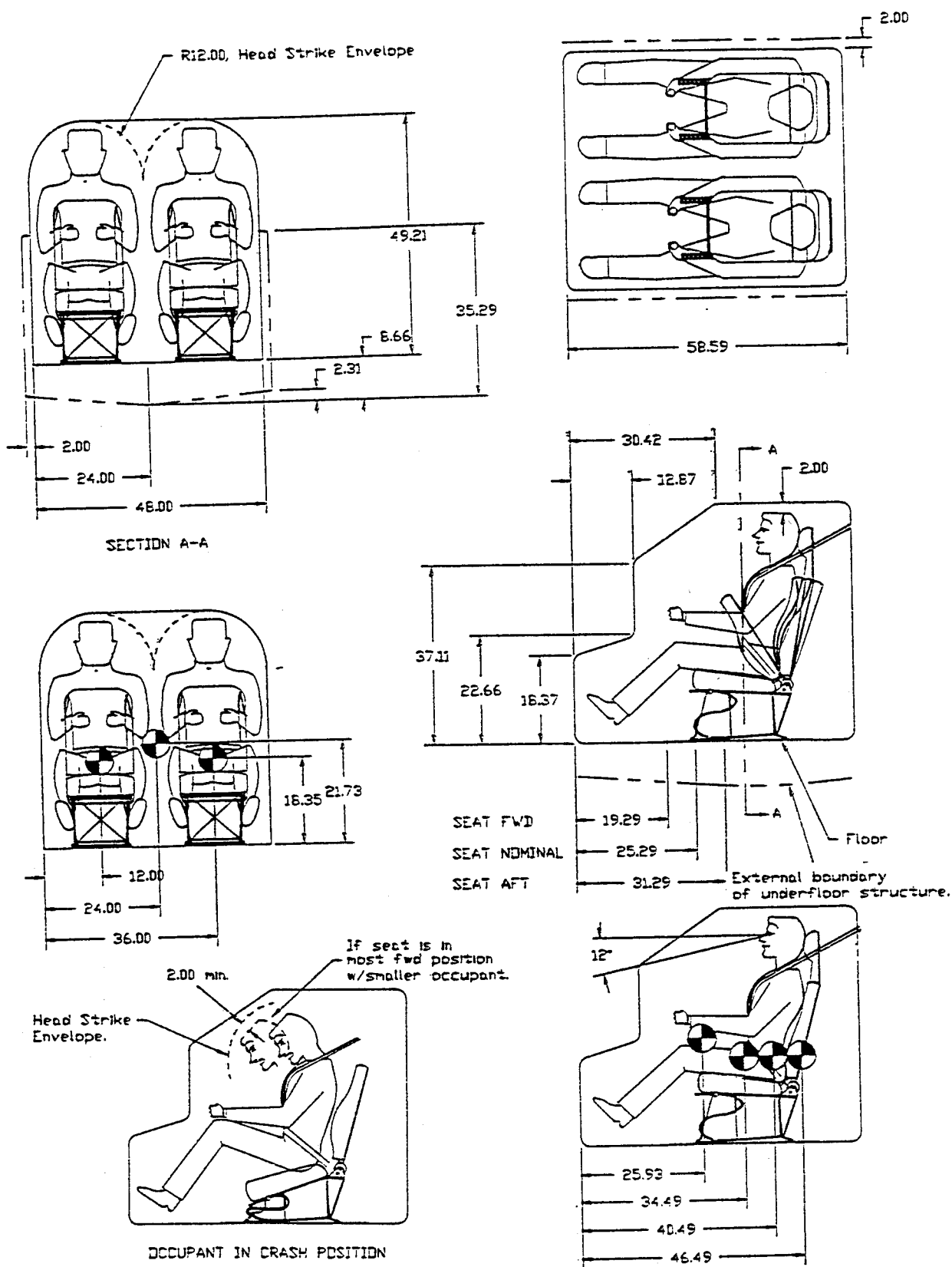


Figure 3. Configuration #1, 2-Place, Front Engine/Tractor, Low Wing, Conventional Tail

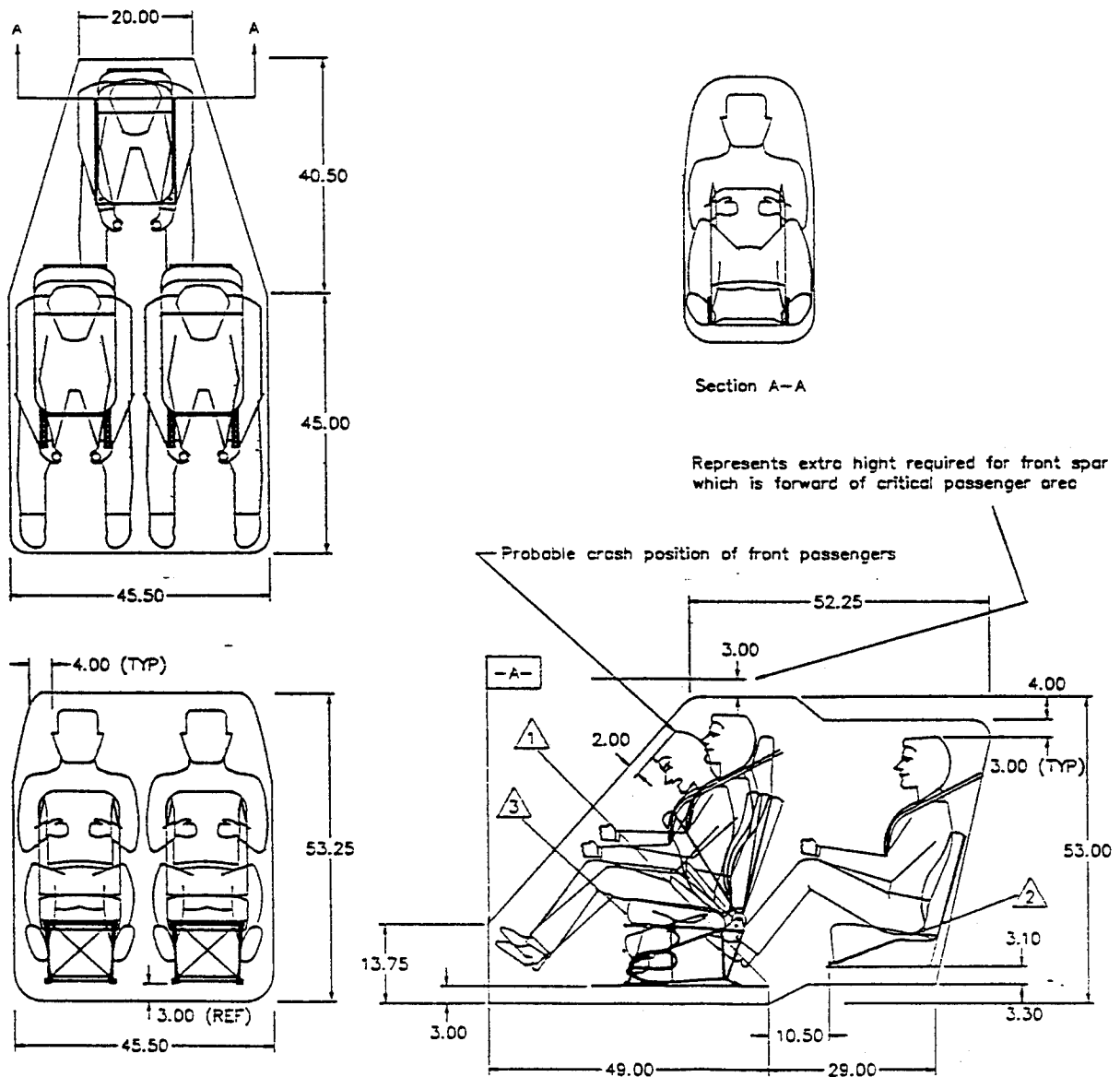


Figure 4. Configuration #2, 3-Place, Front Engine/Tractor, High Wing, Conventional Tail

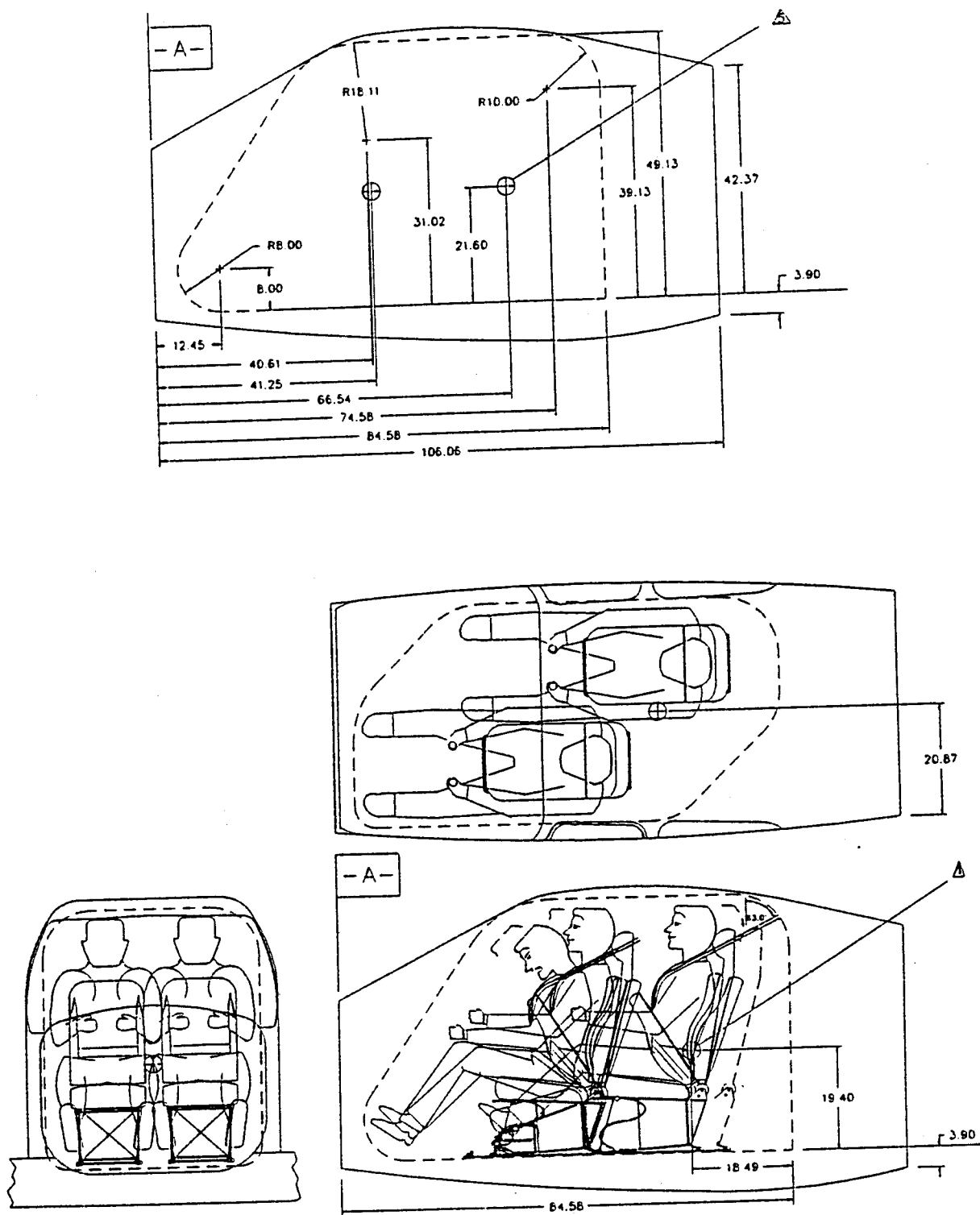


Figure 5. Configuration #4, 2- Staggered, Front Engine/Tractor, Low Wing, Conv. Tail

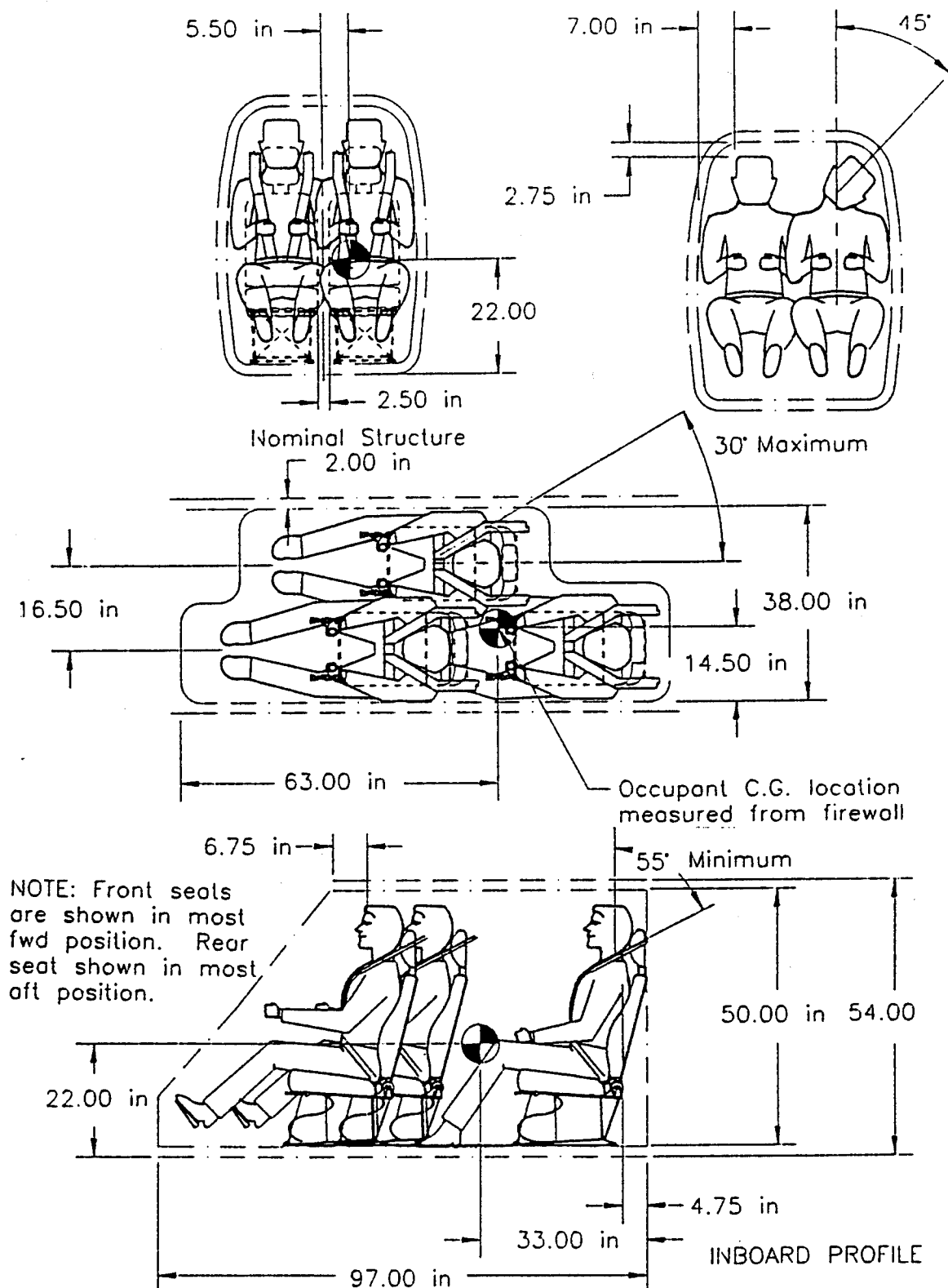


Figure 6. Configuration #6, 3-Staggered, Aft Engine/Pusher, Mid Wing, Twin-boom/Conv. Tail

RESULTS

What ultimate effect did all of this design activity have on the fuselages? Table 3 shows a comparison of cabin envelope dimensions. The table summarizes the cabin volume envelopes (SRSDs), the baseline Viper and three evolutions of it, the baseline Triton and one evolution of it, and the new twin-boom pusher called Vision. It also lists, for comparison with current real world vehicles, the Cessna 152, the Piper Cherokee, and two small automobiles, the Mazda RX-7 and the Honda Civic.

The interior dimensions of the cabin volume show relatively strong consistency in interior height, which is the predominant factor in avoiding head injury assuming that the shoulder belt holds. Most are near 50 inches, and ± 3 inches covers the whole set of data. Interior width, however, is a totally different situation. All layouts which incorporate the 95th percentile standard man are five to seven inches wider than current production light aircraft and show greater data scatter than the height. The exception is the baseline Viper, which is the same as the Piper Cherokee at 41 inches wide and only two inches wider than the common but cramped Cessna 152. However, the Viper design team later admitted to having scaled down the standard man to the size of a team member who is a flight instructor and is about the 50th percentile size. The ubiquitous Cessna 152 is sized for comfortable accommodation of only about the 5th percentile standard man, according to Reference 8 dimensions. It seems clear if that there is any veracity to these student teams' opinion of width required to minimize impact injury due to head movement or intertangling of flailing arms, there is a need for a significant fuselage width increase. It is very interesting to note that even the widest of these cabin layouts is still narrower than the Honda Civic and Mazda RX-7, both small cars by anyone's definition. Both of the cars are also much lower, yet presumably have passed crash tests using the anthropomorphic dummies required by the HIC, which has been applied to cars for some time before being adopted by the FAA.

What was the fuselage weight penalty? Certainly, a wider fuselage will be heavier, all other things being equal. But there is no consistent trend to the teams' data, which is listed in Table 4. This is a result of the large number of variables in the weight estimating equations of Raymer's textbook ¹² used by the student teams. The teams were not required to hold all of these absolutely fixed---they were only required to maintain the same general configuration. To more specifically define the trend, the fuselage weight equation from the text was exercised by holding all dimensions constant except fuselage width. The result was that the fuselage weight increases by only about 2 pounds per inch of increased width, a modest penalty indeed.

The performance penalty is similarly modest. This was something of a surprise to the authors. It seems obvious that a wider fuselage will have more drag. The key question is will the difference be significant. Tabulated cruise speeds in Table 5 have been calculated at 82.6 HP req'd. This is 70% of the rated power of the Textron Lycoming O-235, which is the overwhelmingly predominant engine in current training aircraft. This comparison data had to be calculated from the drag polar equations provided for each design, since they did not all actually employ this engine. The cruise speed penalty was expected to be in the neighborhood of 5-10 knots. In fact it was barely visible, definitely not of significance to training operations. Since the student team designs have other minor configuration variations besides fuselage width, the drag estimating equations from the text were again exercised with a set of averaged "typical" values for all parameters held constant except fuselage width. The result was a troubling surprise, as mentioned above. A ten inch range of fuselage widths produced only a 2 knot range in cruise speeds, plotted in Figure 7. This was far smaller than was expected and was thus checked carefully and then verified by another set of calculations from a different source ¹³. What this means is that there is no performance-based excuse for resisting the use of crashworthy cabin sizes and seats. An oft discussed historical anecdote which is consistent with this unexpected phenomenon involves the famous classic

TABLE 3. CABIN DIMENSIONS COMPARED

CONFIGURATION	SEATING	WIDTH (IN.)		HEIGHT (IN.)	
		INT.	EXT.	INT.	EXT.
BASLINE VIPER	SBS	41	45	47	51
MOD 1 VIPER	SBS	44	47	50	58
MOD 2 VIPER	SBS	42	45	53	60
MOD 3 VIPER	SBS	47	50	53	59
BASLINE TRITON	SBS	46	50	52	63
MOD 1 TRITON	STAGGER	38	42	52	61
VISION	STAGGER	36	38	49	55
PIPER CHEROKEE	SBS	41	44.5	49.5	51.5
CESSNA 152	SBS	39	42	50	58
HONDA CIVIC	SBS	53	—	43.5	—
MAZDA RX-7	SBS	55	—	41	—
SRSD 1 (FIG. 3)	SBS	48	52	49.2	57.9
SRSD 2 (FIG. 4)	SBS + 1	45.5	49.5	50.3	53.3
SRSD 4 (FIG. 5)	STAGGER	41	45	47	58
SRSD 6 (FIG. 6)	STAGGER+1	38	42	50	54

TABLE 4. FUSELAGE WEIGHT COMPARISON

CONFIGURATION	FUS. WT. (LBS.)
BASLINE VIPER	159
MOD 1 VIPER	127.5
MOD 2 VIPER	151.1
MOD 3 VIPER	110
BASLINE TRITON	188.8
MOD 1 TRITON	182.2
VISION	80

TABLE 5. DRAG AND CRUISE SPEED COMPARISON

CONFIGURATION	FUSELAGE C_{D_0}	AIRCRAFT C_{D_0}	V_{CRUISE} (KTS)
BASLINE VIPER	.00679	.0267	126.5
MOD 1 VIPER	.01207	.0340	128.0
MOD 2 VIPER	.0083	.0357	125.1
MOD 3 VIPER	.0111	.02862	128.3
BASLINE TRITON	.00574	.0260	119.6
MOD 1 TRITON	.01099	.0269	133.6
VISION	.01138	.0289	129.2

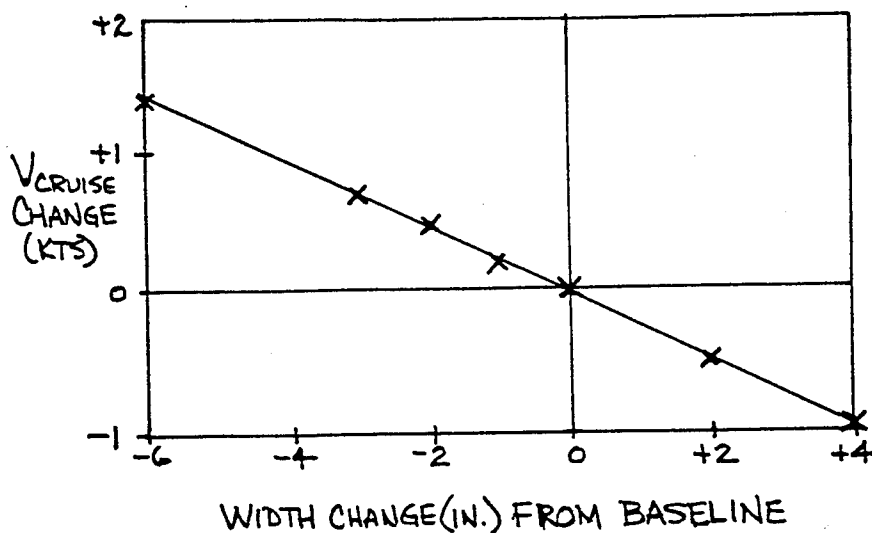


FIGURE 7. EFFECT OF EXTERIOR WIDTH ON CRUISE SPEED

aircraft built by in large numbers by Aeronca Aircraft Corporation, the tandem seating Champion (best known simply as the Champ) and the side-by-side seating Chief. The late 40's models of these two aircraft had the same 85 HP engine and prop and were almost the same in weight and physical dimensions. The wider Chief, defying standard wisdom, is listed ¹⁴ as 3 MPH faster than the narrower Champ at cruise conditions.

Did NLF airfoils compensate for fat fuselages? The drag coefficient data in Table 5 indicates consistently that fuselage drag coefficients for modified designs (all of which used NLF airfoils) went up by a large percentage, yet total drag coefficients went up in some instances only slightly relative to the two baselines (which used NACA 6-series airfoils). Bearing in mind that these are student calculations which may still have undetected errors, the conclusion seems to be that NLF airfoils probably could compensate for the increased drag of wide fuselages. That is both good news and bad news. The NLF airfoils have high maximum lift coefficients, and the designs were constrained to keep the same stall speed as the baselines, typically around 50 knots. The result of this constraint is that wing areas in the modified designs are smaller than those of the baselines. This helps the drag situation. However, as our NASA sponsor warned us to be careful about, the drag coefficients of the NLF airfoils are unusually high at high angle of attack. This results in operation at high power settings to fly at or near stall speed, way up on the back side of the power curve. This is a tricky area for neophyte pilots to handle safely, and might be viewed by flight school operators as unacceptable.

CONCLUSION

An up-to-date primary flight trainer, probably two or three seats, can and must be built in the U.S as part of the reestablishment of a healthy general aviation industry. Recent economic and regulatory changes make such a rebirth more feasible, but they must be supplemented by technological improvements in the actual vehicles. Compliance with recently established crashworthiness regulations will significantly decrease the risk of occupant injury and will have surprisingly little detrimental effect on performance. The effect can be minimized by incorporating improved technology elsewhere in the design, such as NLF airfoils, improved engines, and staggered seating. Some traditional configurations may disappear, particularly the low wing with the spar carrythrough passing under the seats and cabins sized for the only 50th percentile standard man. New configurations like the mid wing pusher look better than ever due to the availability of an out-of-the-way spar location. And race car design has proven that a rear engine does not constitute an insurmountable safety problem. It also appears that the application of various aspects of crashworthiness technology can significantly reduce the litigation threat to the financial well being of manufacturers of new airplanes. This could include such items as airbags and crash-resistant fuel cells in addition to compliance with the basic seat restraint and HIC criteria. The designs developed during the 1993-94 school year will be carried forward into the 1994-95 ADP activity for further consideration and improvement along these lines.

REFERENCES

1. Eastlake, C.N. and Ladesic, J.G., "The Next Generation General Aviation Primary Flight Trainer", AIAA Aircraft Design, Systems and Operations Meeting, Monterey, California, August 11-13, 1993.
2. Jennings, R.T., Mohler, S.R., "Potential Crashworthiness Benefits to General Aviation from Indianapolis Motor Speedway Technology", Aviation, Space, and Environmental Medicine, January, 1988.
3. Hackney, Kahane, and Quarles, "The New Car Assessment Program - Historical Review and Effect", National Highway Traffic Safety Administration, SAE SP- 1045, Paper #941052, 1994.

4. "General Aviation Crashworthiness Project: Phase One", National Transportation Safety Board, Washington D.C. 20594 , June 27, 1983 (NTSB/SR- 83/01).
5. "General Aviation Crashworthiness Project: Phase Two - Impact Severity and Potential Injury Prevention in General Aviation Accidents", National Transportation Safety Board, Washington D.C. 20594 , March 15, 1985 (NTSB/SR-85/01).
6. "General Aviation Crashworthiness Project: Phase Three - Acceleration Loads and Velocity Changes of Survivable General Accidents", National Transportation Safety Board, Washington D.C. 20594 , September 4, 1985 (NTSB/SR-85/02).
7. Federal Aviation Regulations, Part 23, "Airworthiness Standards: Normal, Utility, and Acrobatic Category Airplanes". Code of Federal Regulation 14, U.S. Government Printing Office, Washington, D.C., September, 1988.
8. "Military Standard: Human Engineering Design Criteria for Military Systems, Equipment and Facilities", MIL-STD-1472, U.S. Department of Defense, U.S. Government Printing Office, Washington, D.C., 1983.
9. Siahaya and Jarrett, " A Retrofit Crash Protection Installation in Two Models of General Aviation Airplanes", Jungle Aviation and Radio Service, SAE General Aviation Aircraft Meeting and Exposition, SP-716, Paper #871008, Wichita, Kansas, 1987.
10. Smith, H.W., "Airplane Designer's Checklist for Occupant Injury Prevention", AIAA/AHS/ASEE Aircraft Design Systems and Operations Meeting, San Diego, California, 1984.
11. Metz, H.J., Irwin, A.L., "Brain Injury Risk Assessment of Frontal Crash Test Results", General Motors Corporation, SAE SP-1045, Paper #941056, 1994
12. Raymer, D.P., "Airplane Design: A Conceptual Approach", AIAA Education Series, 1989.
13. Torenbeek, E., "Synthesis of Subsonic Airplane Design", Delft University Press, Delft, The Netherlands, 1982.
14. "The Aircraft Yearbook for 1949", Official Publication of the Aircraft Industries Association of America, Lincoln Press, Washington, D.C., 1949.

ADVANCED FLIGHT CONTROLS FOR GENERAL AVIATION: AN OVERVIEW

Jim Acree
University of Tennessee Space Institute
Tullahoma, TN 37388

ABSTRACT

Highly-augmented aircraft control systems are becoming the standard for commercial and military applications. Recent technology and experience has shown these systems to be highly-reliable and robust in nature, especially as currently utilized by commercial transport-category airframes and by the modern military forces of the world. As reliable state-of-the-art components have continued to drop in price, these systems will soon be applied to the General Aviation (GA) sector in a large scale; this is beginning to happen, and largely without regulatory guidance in place. The flexible nature of these systems, an important attribute, allows the control response of the aircraft to be tailored as desired. "Classic" aircraft responses can be altered according to a point-design. The opportunity to reduce pilot workload and recommended minimum training/currency levels exists. Likewise, aviation safety is improved tremendously. However, the flexibility of these systems brings new perils for the tester and the user.

The capabilities of today's control-dominant (vice stability-dominant) aircraft have allowed integrated flight and propulsion controls, direct force controllers, the independent or coupled control of any one or all of the six degrees of freedom, expanded flight envelopes, reduced drag, increased maneuverability, made practical gust alleviation, active flutter suppression, and provided for damage-tolerant flight controls. Expanding flight envelopes with maneuverability and more powerful engines has led to large non-linearities which are difficult to compensate for by the machine or pilot. This resulted in highly complex flight controls with multiple dynamic modes.

This paper offers an overview of highly-augmented flight control systems being used, in development, and offers options to the general aviation designer and operator. Critical technologies involved with the development of advanced flight control systems are numerous. Reference will be made herein to Fly-By-Wire (FBW) systems, and Command Augmentation Systems (CAS); in the context of this paper they are one and the same type of system.

INTRODUCTION

BACKGROUND

Until the second world war, aircraft flight controls were easy to define. Ailerons, rudders, and elevators were the method to control inherently stable platforms; the exceptions were the very early models, such as the Wright Flyer, which utilized moveable canards on a marginally-stable platform. Often control forces were very high, causing physical exhaustion in pilots of fighter aircraft, who had to frequently make large control movements. Trims for the relief of forces during cruise, or transit portions of the flight, were just coming into being in the 1930's. With these came trim tabs and mass or aerodynamic balancing of control surfaces to reduce the required control forces (in addition to reducing hinge moments for structural relief). Aircraft designers used the brute force method where stability and control was concerned. Yet, autopilots were developed during the war, especially as a weapons-placement tool for bombers. Before the end of the war, an autonomous guidance and control system had been introduced by the German V-2 bomb.

Post-war efforts led to transonic aircraft flight, and the effort to improve deficient flying qualities with new technologies. Transonics, with its inherent instabilities in pitch, introduced problems for the designers. Additionally, high-speed flight usually required that some kind of force augmentation was available to help the pilots overcome the dynamic pressure feedback from deflected control surfaces. Hydraulically-boosted flight controls came into being, and with it, partially or completely irreversible flight controls systems. Technologies to cope with transonic difficulties focused on aerodynamic solutions, but transonic instability could not be made transparent without complex flight control compensations. Digital guidance and control was first implemented operationally in the intercontinental ballistic missiles developed in the late 1960's and the Concorde airliner.

Truly augmented flight control systems were incorporated into nearly all military tactical aircraft during the 1960's. Examples were the A-7 Corsair, F-4 Phantom, and F-8 Crusader; all utilized some form of a Stability Augmentation System (SAS) in at least one axis. Also, hydraulic flight controls were assumed; none of these three aircraft could expect to return for landing without the use of their hydraulics. By the 1970's, the military aircraft depended upon SAS integration for nearly all axes of control. These systems were implemented to give the pilot the ability to accurately track a target and to better maneuver his aircraft without undue fatigue, which could otherwise give the enemy an advantage. On some aircraft they were necessary to reduce transonic stability deficiencies. Now most military tactical aircraft acquisitions are of fly-by-wire aircraft. Examples are the analog-processed F-16 Falcon in the mid-1970's, the digitally-processed F-18 Hornet in 1980, the F-117, the YF-22 and YF-23 advanced tactical fighters, B-2 bomber, V-22 Tiltrotor, and the C-17 transport. Foreign equivalents include the Tornado, Gripen, Rafale, Mirage 2000, European Fighter Aircraft, Russian SU-27, IL-96, AN-225, and TU-204. Military forces are sold on the advantages of these systems in order to optimize mission performance.

The air transport community did not have the precise tracking requirements of the military, but began to use simple rate dampers for passenger comfort and a few SAS operations for designs of relaxed stability. In the early 1960's the Boeing 727 was fitted with a yaw damper; flight without proper operation of this damper remains undesirable to the 727 operator through today's scheduling. Control augmentation through autopilot control became increasingly popular as a passenger comfort device. Now, air carriers have hands-off autopilots capable of flaring, landing, and stopping a vehicle with the integration of brakes and ground spoilers into the autopilot control system.

In 1985, Airbus Industries introduced the A320. This was the first truly FBW transport internationally certified for commercial use (the Concorde had a mechanical backup system). Airbus Industries applied the same control architecture to follow-on airframes, in the A330, A340, and A320 derivatives (A321 and A319). The Boeing Company is building their first FBW aircraft in the B777 transport which will fly in the very near future. There exist plans for more commercial fly-by-wire control systems in countries such as India, Japan, Taiwan, and Indonesia, some of which will fly in commuter and business-class aircraft. The air transport community is becoming sold on the advantages of these flight control systems, but will require time for complete confidence in this technology.

General aviation aircraft have not yet implemented these advanced systems into their community. Cost, liability, and complexity concerns have kept many new developments away from this aspect of aviation. With the exception of innovative home-built designs, GA aircraft have not advanced at the same pace as the other aviation communities for some twenty years. The GA community has been stifled during this time, with the only real developments being simple avionics, such as GPS navigation sets, and LORANs with extensive databases. Engines, controls, and aerodynamic improvements have been sparse.

FLY-BY-WIRE FOR WIDESPREAD USAGE

Analog flight systems have been in use in the air transport sector for decades. Digital implementation is almost as old. Yet, most advances in computing technology have been in the last decade and a half. The hand-held calculator made its debut in the mid-1970's, but who would have expected PCs and laptops to be second nature to the public a decade later? Today's portables have many times the power, a fraction of the weight, size and cost, of the mainframes of the 1970's. Processing and sensor technology is, and has been advancing in great strides. Aircraft avionics have similarly advanced through multiple generations of radios, navigation sets, and displays. Are we ready for computer-controlled flight, configuration, and engine control?

Many flight-critical items have been electronically-dependent for some time now. Airbrakes, leading and trailing edge flaps, and landing gear motion have been electronically-controlled, and/or electronically-actuated for decades. Full Authority Digital Engine Controls (FADECs) and electronic Direct Lift Control (DLC) systems are now commonplace. In some cases, conventional methods to control such items have been incorporated as redundancies, should the electronics fail.

Work on the subject of un-coupled flight controls for general aviation users has been conducted by researchers at the NASA-Langley Research Center during ground-based simulation. This effort has led to significant findings, and a recommendation to further this pursuit. Researchers at North Carolina State University worked hard to develop a operator-friendly aircraft, and finished with a complex design which could have been made much less complex if modern electronic augmentation had been available for consideration.

Kawasaki Industries in Japan anticipates adding FBW flight control systems to small- and medium-sized helicopters as retrofits (reference 1). In particular, the company is leading the way with an experimental FBW system in a BK-117 helicopter. The application is fitting, as helicopter control is usually more demanding than fixed-wing counterparts, resulting in a potential very marked improvement in handling qualities; many inherently non-linear responses can be linearized through FBW applications in order to improve handling qualities. In the military helicopter community, the effort is to make the flight controls secondary to the pilot.

Through in-flight simulation in variable-stability and response airplanes, the results of these efforts can be continued to a practical end: true application. Follow-up opportunities exist to implement a "production" version of the flight control laws into a general aviation aircraft for proof-of-concept testing and evaluation.

FLY-BY-WIRE SYSTEMS

ADVANTAGES OF FLY-BY-WIRE DESIGN

The reasons to pursue development of advanced flight controls are many. Benefits can be seen in performance, safety, maneuverability, and training requirements. All have a beneficial influence on system and lifecycle cost.

The ways by which FBW designs can enhance aircraft stability must first be considered, before discussing performance benefits. A CAS consists of the inner feedback loop of a FBW system. It can produce an apparently stable aircraft, where airframe instabilities truly exist, and in any or all of the stability axes. Therefore, aircraft that are marginally stable, or even statically unstable, can be operated without undue pilot effort. Longitudinal and directional instability will not be apparent to the pilot of such a vehicle; the vehicle is made to handle as a conventionally-stable airframe. No to-date FBW airliner has been designed to be unstable, however several FBW military aircraft are unstable in pitch or yaw. The F-16 and F-117 are unstable in pitch; the F-117 is unstable in pitch and yaw.

Performance enhancements can be realized in many different ways. Decreased aerodynamic drag is achieved by lowering trim drag, decreasing aerodynamic and control surface sizes, decreasing aircraft weight, and allowing automatic control of lift-enhancing devices for best aerodynamic efficiency. Aircraft trim drag is produced by the tail producing downwards lift, in opposition to the lift produced by the wing; this is necessary to balance an inherently stable aircraft in pitch. Thus, the horizontal tail produces an element of drag directly attributable to the airframe's positive longitudinal stability. Utilizing FBW technology, an neutrally-stable aircraft (or one with a much reduced static stability margin) can be flown that will not have significant trim drag; the design would be such that the aircraft would be neutrally-stable in the cruise condition.

Airframe drag can be reduced by the minimization of surface areas. Neutrally-stable platforms do not require the large stabilizing tails of conventionally-stable aircraft. Also, FBW systems can respond to disturbances more quickly than a human, and smaller control surfaces are therefore required. For instance, vertical tail size on conventional multi-engine aircraft is usually predicated by the asymmetric moment capable of being generated by an engine-out condition; minimum standards are required by the Federal Aviation Regulations (FARs). A FBW-controlled rudder can respond more rapidly to an engine failure than a pilot, making more efficient use of the rudder, and thus offering the designer a reduction in required tail area. The same logic applies to the horizontal tail for other flight considerations. Also, performance-enhancing non-standard designs can be implemented, if inherent static stability is not required of the designers. Well-placed canards for pitch control provide one notable example.

Weight savings manifest themselves in performance improvements. The reduction of control and other surfaces (mentioned in preceeding paragraph) is a savings in itself. The structural requirements in order to support these surfaces are also decreased. This allows designers to focus on performance first, and implement control as a secondary consideration. Otherwise, conventionally-controlled aircraft require cabling, push-rods, bell-cranks, and other gimmicks. FBW technology involves only a few electrical components in addition to the power-boost and actuator systems (commonly hydraulic systems). Given the existence of the hydraulic boost systems on transport-category aircraft already, the weight savings of the electrical components over the steel cabling and support structure is considerable; this is especially true when the existence of auto-pilot flight control computers already existed in conjunction with the conventional controls.

Automatic scheduling of lift-enhancements devices can improve cruise condition efficiency. Leading and trailing edge flaps can be manipulated to optimize wing camber for a given condition. Trailing edge flaps on highly-augmented aircraft are often deflected upwards in high-speed cruise by about two to three degrees for this reason. The F-18 does this to improve range characteristics. While it is conceivable that such a function could be manually controlled by the pilot, continuous and small adjustments would be time-consuming; not only would this be an annoyance, but it could prove to be a safety hazard.

Enhanced safety is easily accomplished with the use of FBW technology. Programmed flight control outputs can be tailored to resist unsafe maneuvers. Angle-of-attack limiters, airspeed limiters, normal acceleration limiters, rate limiters, attitude limiters, and automatic flap control can help a pilot stay within the published flight envelope. Also, automatic recovery systems have been developed for the military in order to save an aircraft in the event of pilot disorientation (G-lock) or loss of control (spins). For example, reference 2 details some of the improvements and proposed improvements for the F-16 fighter. Specifically, spin resistance and recovery characteristics were deemed necessary for the aircraft, including a possible future incorporation of an automatic (hands-off) deep stall recovery mode which can offer much faster recoveries to controlled flight. These systems can be automatically engaged or be manually selected, with pushbutton simplicity. Lastly, backup control characteristics for degraded systems can be implemented; automatic compensation for engine-out conditions and structural damage is readily incorporated into FBW systems.

Maneuverability has been enhanced by the incorporation of FBW flight control systems. This has been realized mostly by the military tactical aircraft, whose mission success may depend upon maximizing agility. The use of inherently less stable aircraft allows greater instantaneous maneuvering, and the automatic scheduling of lift-enhancement devices allows wing camber to be optimized for a specific maneuvering condition. The use of automatic flap extension at high angles of attack is an example of this. Also, the expansion of the flight envelope to otherwise "unstable" regimes (high-AOA) is afforded.

A large potential cost savings occurs with reduced training requirements. FBW technology allows designers to tailor the aircraft's handling qualities as desired. If the resulting flying qualities do not have the difficulties of their conventional counterparts, flying is made easier, and the requirements (including cost) for initial training, recurrent training, and high skill levels will be alleviated. In concept, an airplane could be made to handle like an automobile. Methods to compensate for cross-axis coupling tendencies can be implemented (de-coupling). Pitching moments and yawing moments due to power (or thrust changes) and control over dihedral effects are some such examples. Automatic turn coordination is a simple example which is already used amongst many transport-category aircraft and military aircraft. Control characteristics can be tailored for each flight condition (landing, enroute, etc.), and can automatically change with changing conditions. Perhaps this is the single most important application to the civil aircraft community of the future. Other examples of handling quality improvements include safety items such as flight envelope limiting and the improvement of annoying handling qualities generated by engine-out conditions, crosswind landings, and flight through turbulence or significant weather.

A notable training example has been proposed by Airbus Industries. They contend that since the cockpits of all of their FBW aircraft are similar, and that the handling qualities have been tailored to be similar, that training in any one of the models would qualify a pilot to fly any of the series (A320, A330, A340). If certified as such by the authorities, this concept could realize tremendous savings in direct training costs for the airlines and flexibility in aircrew scheduling.

A last item to be offered by FBW technology, is particular to military use only. As already mentioned under aerodynamic considerations, the aircraft can be designed without first priority to the consideration for inherent stability and control. This allows designers to focus on other subject areas first, notably stealth characteristics. Control surfaces can be designed for low observable technology first, and control margins second.

CHALLENGES OF FLY-BY-WIRE DESIGN

Processing technology has moved forward at such a pace, that the architecture of these systems has several configurations. Digital seems to be the choice, however, analog can be made to meet just about any requirement as well. Microprocessing technology need to develop further to keep weight and size manageable as the requirements imposed on these systems increases. High-speed processing is a requirement in order to remove lags in control. Reliabilities may depend upon dedicated avionics cooling equipment; if so, this adds considerable weight and space requirements to the design. Also, flight control laws need to be tailored towards the aircraft type (even so-called "robust laws" must be altered to fit the host aircraft).

Currently, no dedicated guidance from the FAA exists to certify FBW flight control systems (the 10^{-9} probability of failure remains the rule). These control systems are dealt with strictly on an individual basis, as each design is produced; the Airbus 320-340 series, the Boeing 777, and civil tilt-rotor all have different approaches towards regulatory compliance. This cumbersome method will not work as the flight control applications become more widespread. Failure modes and their operational requirements need to be better defined as well.

As a relatively new development, expertise with advanced flight control systems remain with a privileged few. The benefits can only be realized if this expertise can be distributed to more of the aviation industry. Industry experience is necessary for this technology to mature. This is a domain of flight control algorithms, commonly referred to as "control laws" by users. The complexity of these systems to the novice designer needs to be dealt with. There are several areas to be concerned with if these advanced systems are developed for widespread usage. Handling qualities have to be modelled extremely well, as control augmentation can actually degrade stall character and rolling dynamics, slow down control response, and even cause severe Pilot-Induced Oscillations (PIO). Control system saturation must also be cautiously avoided.

The public image of the FBW design remains skeptical. Perceptions are of a futuristic system that puts human life in the hands of electronic devices. Most electronics remain a mystery to the user, and are referred to as "black boxes", whose reliability and operability are unknowns.

Electro-Magnetic Pulse (EMP) susceptibility remains a serious concern, where electrical interference with a full-authority FBW system can mean disaster. This means electrical system shielding, elimination of control transients when the system is disturbed for a fraction of a second or so, and easily-reset primary control modes.

TYPES OF FBW SYSTEMS

The applications of full-authority FBW control systems have been diverse in mission and design. The flexible nature of this technology offers the designer many options. Decisions must be made regarding control configuration, types of central processing, sensors, redundancies, failure modes, and control laws.

CONTROL CONFIGURATION. Control configuration refers to the control architecture. It is first governed by the method of control implementation, such as the decision to use canards for pitch control and ailerons for roll control. Where two controls are used in one axis (such as differential stabilators and ailerons), priority must be given to one, and the design such that these controls will not fight each other during dynamic situations.

PROCESSING METHODS. Processing can be either digital or analog. Digital processing offers faster modification and updating through programmable control algorithms. With recent advances in digital hardware, it also offers space and weight savings, and allows sufficient processing speed for complex designs. Analog systems have been favored in the past, due to high processing speeds and independence from development of computer programs which can often cause unseen problems. Reference 3 offers some insight, crediting Kalman filtering with making digital systems a reality. Where analog systems tend to drift with time, requiring re-calibrations, digital systems often introduce time delays.

SENSORS. Sensors must be specified with careful consideration. Flight control system sensors might include those for angle of attack, attitude, rates, accelerations, altitude and airspeed (but not necessarily all of these). Instrumentation calibration becomes a critical and expensive flight item. Where current small aircraft AOA sensors are generally used for stall warning only (in an on-off mode), FBW alpha sensors must be calibrated over the entire permissible envelope. This may require calibrations to plus and minus 90 degrees for maneuverable aircraft. Likewise, beta vanes, rate inputs, and accelerations (possibly in three axes) may have to be calibrated through the possible ranges of travel.

As one of the primary sensors, the pilot controls can be either of a control motion type (displacement controllers) or of a force-type (force controllers). Correspondingly, the decision whether to implement control loaders must be made. Control loaders offer artificial control feedback to the pilot, which is absolutely necessary for satisfactory flying qualities. At a basic

level this might only be spring cartridges as used in unaugmented, irreversible flight controls. At a more advanced level this might include programmed control stiffening as an airframe limit is reached (to resist overstress). Additionally, smaller and lighter controls can be easily implemented in FBW applications. Sidearm controllers, used in few conventional systems due to the complications in proper gearing for control force and authority compatibility, have become popular in FBW systems. The Airbus transports, the F-16, the F-22 prototype, and the RAH-66 helicopter all make use of the sidearm controller. While not in itself anything special, it does clear space for additional cockpit displays.

REDUNDANCIES. Redundancies must be provided, given the current level of component reliability, including processors as well as sensors. For instance, a control system that primarily uses angle-of-attack for pitch motion commands might dictate that two AOA sensors be provided.

Backup modes of operation may be considered, depending upon the level of redundancies provided in the primary system. In its simplest form, a backup mode of a FBW system may be a conventional flight control system, complete with cables and actuator overrides. The F-18 uses this type of system. However the F-16, due to its inherently unstable pitch configuration, was not designed to provide this option to the pilot as he would not be capable of manually controlling the vehicle in this axis. Instead, alternate control modes are available which do not require the same complexity. Commonly used is the Direct Electrical Link (DEL), which may not incorporate any safety features such as envelope protection or provide turn coordination. However, it may provide the pilot a means to safely land the aircraft. Hardware considerations may include a backup power supply. These include batteries, Ram Air Turbines (RATs) and Emergency Power Units (EPUs) for continued electrical power to the FBW system.

CONTROL LAWS. The types of flight control logic vary widely, depending upon their intended application. These control algorithms, or control laws, can be extremely complex or very simple; processing power (speed) drives these capabilities as the computer must sort out the commands without inputting delays into the control path.

Roll. Generally, rate-commands are used in roll. This is similar to the conventional aircraft, in that roll-rate is proportional to controller displacement (actually conventional aircraft are proportional deflection-command, but reflect rate-command in this axis). Auxiliary control laws for wing-levelling, rate-limiting, and even bank angle limiting can be implemented.

Yaw. Directional control inputs traditionally offer a given sideslip (beta) angle; sideslip is proportional to pedal displacement. In contrast, a conventional hovering helicopter offers rate-command in that pedal displacement offers a proportional yaw rate. Auxiliary control laws might include sideslip limiters, rate limiters, and even anti-spin logic.

Pitch. Pitch control algorithms typically demand the most rigorous scrutiny in the design process. Command logic may be oriented towards pitch rate, acceleration, attitude, angle of attack, flight path vector, or commonly some combination of these.

Pitch rate-command systems, referred to as Rate-Command Attitude-Hold (RCAH), are favored by aircraft that require agility and predictability. Characteristics are similar to acceleration-command (g-command) systems. Rate-command systems usually incorporate an airspeed-dependent gain to reduce sensitivity with increasing airspeed; this often makes it nearly identical to g-command. These rate-command systems are generally simple, and do not require as many inputs or as much processing power as other modes. User aircraft include F-16, F-18 (in the cruise condition only), the developmental RAH-66 Commanche helicopter (in the cruise condition only), and the space shuttle. Advantages include freedom from trim requirements, and a deliberate absence of motion when control inputs are removed (no phugoid). Apparent longitudinal static stability is neutral. Unfortunately, simple rate-command systems do not lend themselves to good handling qualities

during the landing task; it has been determined that pilots prefer some control feedback during high-gain tasks such as flaring to land.

Pitch attitude-command systems, also referred to as Attitude-Command Attitude-Hold (ACAH), are superior for landing tasks. Characteristics are similar to angle of attack-command (alpha-command) system, which is what a conventional (inherently stable) aircraft exhibits naturally (an aircraft with no control augmentation). Unfortunately, these types of systems require pilot-trimming. The ACAH system does not exhibit long-term residual motion (phugoid) in that the loop is not open, but generally requires non-linear programming for optimization. These types of systems are somewhat simple in processor and sensor requirements. The A320 uses this control law in the final portion of the landing approach. FBW helicopters will likely make use of this control law during similar flight phases.

Flight Path vector-command, also referred to as gamma-command, requires a more complex design. It is a flight path angle rate-command system, which holds a constant flight path vector when pitch control is released. Direct advantages are the windshear protection, and the absence of the long term residual motion. Yet, in order to achieve these advantages, automatic throttle control is a co-requirement of the system. This type of system has more complex design requirements, and will necessitate an accurate navigational reference such as an INS. Reference 4 displays results of simulations to determine favored pitch control laws in the approach and landing task; the flight path vector system was the much favored design by the pilots.

A combination of the above concepts is also an option. Airbus uses a C* command, which is a blend of load factor and pitch rate-command; this concept is used by Airbus at low speeds only. It requires substantial gain scheduling to offer consistency in handling qualities and is of a complex design. Reference 5 reviews the use of these laws in the airbus series.

Other Considerations. A merging of the axes is desirable; this can be referred to as de-coupling of the axes (inner-loops), or in some applications, coupling of the axes (outer loops). For instances, helicopters traditionally have too much coupling between axes, making pilot inputs in one axis result in considerable motions in all three axes. Reference 6 studies the development considerations of the RAH-66 Commanche military helicopter. As the second FBW operational rotorcraft in the U.S. (after the V-22 tilt-rotor), it will incorporate a sidearm controller instead of a cyclic (center-stick), incorporate both RCAH and ACAH pitch control laws, and will have a new control law implemented when in or near hover. This is the Translational Rate-Command with Position-Hold (TRCPH) mode as also described in reference 7. The flexibility of the full-authority FBW concept becomes apparent.

A final consideration must be given to the design of breakpoints between different control law utilizations. An transport-category airplane might use a control law for takeoff and landing, another for enroute flight, and another for ground handling. In addition to these, a helicopter should use a control law designed only for hovering flight. Ground handling demands careful considerations not yet mentioned. For instance, roll control inputs during runway operations (takeoff and landing) should certainly not command a roll rate, but perhaps be of a displacement-command type for utilization against crosswind effects. Similarly, pedal commands in fixed-wing aircraft should not seek sideslip conditions at slow taxi speeds. The placement of breakpoints between the control laws must be handling qualities driven. Furthermore, the breaks must be blended, so that sudden motion transients don't occur with the changes of control laws.

FBW DEVELOPMENT FOR GENERAL AVIATION

ADVANTAGES OF FBW FOR GENERAL AVIATION

Enhanced safety, decreased training requirements, and better integration into the airspace system of the future are potential reasons to incorporate advanced flight control systems into general aviation aircraft. With envelope limiters and/or protection devices, safety and training are directly affected. The improvement of handling qualities will decrease cockpit workload, having the same benefit.

CHALLENGES OF FBW FOR GENERAL AVIATION

GA aircraft typically include a structure of comparatively light weight, and with limited space for complex systems. The weight and space requirements of the FBW system itself will not be the problem. From a design standpoint only, the weight and space required of a system to power the flight control surfaces will be the biggest challenge. Current hydraulic systems will be impractical for most aircraft smaller than business jets. Alternatives may include pneumatic power or Power-By-Wire (PBW) systems. Pneumatically-operated actuators have been used in auto-pilots for some time, but not generally in full-authority systems in three axes; the critical response capabilities of these pneumatic controls are somewhat limited. PBW systems may alleviate the need for a central system, allowing independent actuations. Also, cooling system requirements may be a concern, where weight, space, and cost are impacted.

The nature of the FBW system itself poses several challenges. Flight instrumentation will become much more critical in terms of reliability than before. For instance, the loss of an airspeed indicator usually means some level of compensation by the pilot; depending upon pilot experience, it may not be a worry at all. But loss of airspeed data to an improperly designed FBW computer can be catastrophic. This typically necessitates redundant inputs for critical flight inputs as well as flight control reversion modes which may not require certain inputs, such as airspeed.

The single biggest challenge to implementation of FBW in a GA aircraft remains the cost-effectiveness of such a system in a comparatively inexpensive airframe. The advantages in safety and savings in reduced training requirements must be weighed against the cost of installing and maintaining a FBW system. This should be feasible, given the sponsorship, or reduction of development costs. Perhaps the solution will be in the development of common systems by some manufacturers, whereby one type of system can be applied to several types of airframes; this will disperse development costs between more users.

TYPE OF GA FBW SYSTEM

Consider the most basic FBW system: one that would simply provide electrical signals to the control actuators that were directly proportional to the angular displacement of the pilot's controls, without any form of enhancement. This type of aircraft would have the handling qualities expected of a conventionally-controlled aircraft, and would offer no handling quality or safety benefits (neglecting system reliabilities). Add to that: stability augmentation, envelope limiting or protection, and control shaping for better handling qualities. Add other considerations such as turn compensation, wings levellers, automatic engine-out compensation, spin resistance or automatic spin recovery modes, and engine control for flight path optimizations. Gust alleviation can be an option. Now many of the benefits of this technology have been realized.

Control methodology can be expanded in consideration of cockpit controllers and control surfaces. Not many improvements have been realized in this area by most GA aircraft for many years. Where required training is to be kept to a minimum, the use of displacement controllers with motion feedback will be preferred (vice force controllers, and controllers with no motion). This includes the throttle(s), as pilots prefer to observe control inputs; one pilot-criticism of the Airbus

design is the absence of throttle motion with certain flight control computer-commanded power changes.

Design of cockpit displays has to be revolutionized for GA aircraft. Whereas FBW systems act in parallel to pilot commands, the pilot has to be kept informed of system intentions. Control limiting, and control degradations must be made apparent to the pilot.

Control laws need to be defined. In this regard, different systems for different airframes may be apparent, leaving the choice to the customer. In roll, most will find rate-command to be most easily adaptable and predictable. Yaw response in fixed-wing GA aircraft and helicopters in forward flight will generally be of sideslip-command, or similarly proportional-command systems. Helicopters near hover will want rate-command systems in yaw, perhaps blended with sideslip as forward airspeed increases. In pitch, many options present themselves. Rate-command in cruise flight provides the most comfortable handling qualities. However, this type of system will not be practical in the slow flight and landing phase without significant increases in training requirements. One of the most promising, where handling qualities are a priority, may be flight path-command systems. Implementation of FBW systems in only one or two axes have been utilized. Reference 8 outlines the SAAB 2000 commuter aircraft which utilizes true FBW in the directional (yaw) sense only.

Reference 9 reports the work of NASA on a simulated light aircraft FBW control system with a head-up display with non-pilots. The subjects were able to complete tasking for a full flight on the first try. The so-called "Easy-to-Fly" controls offered gamma-command in pitch, heading-rate command in roll, sideslip-command in yaw, and airspeed-command with the throttle. The controls were designed to create a response in one axis each, utilizing de-coupling as a priority. The project points to the continuing nature of FBW system development, with flying qualities as a priority.

Aircraft design implications will be many. Designed instability in any axis will continue to be a function of control system architecture (especially reliability). Mechanical control backup devices will also be a function of control reliability, and inherent aircraft stability. Reference 5 reveals many of the thoughts in designing the Airbus FBW system. Limiters on commanded bank angle (65 degrees), pitch angle (plus 35 and negative 15 degrees), angle of attack (below stall), and load factor (2.5G) were implemented; many of these were programmed to vary in order to become more confined at extremes of the flight envelope. In most applications, this type of system has proved itself to be "carefree" in handling. Limiters are more than just stops, they begin to act as the limit is dynamically-approached in order to avoid overshoots; this is used by Airbus in angle of attack. In contrast, the Boeing 777 will be designed to incorporate envelope protection, vice limiters. This is a philosophy of making it difficult for the pilot to push the edges of the established flight envelope, not impossible. Where a GA aircraft is not aerobatic, many of these features should be considered.

DEVELOPMENT AND TESTING

FBW system testing continues to be a problem area, even to the most experienced designers and testers. Unexpected mishaps early in the life-cycle of the Airbus 320, F-16, F-22, and Swedish Gripen were due to flight control problems. Consider the conventional method of test and development where simulations are confined to those absolutely necessary, and flight simulations are, at best, in a 3-degree of freedom device with simplistic models. These will simply not suffice, regarding the successful development of electric full-authority flight controls. Simulation becomes a focus early in the program, and flight control development costs are driven by this simulation. Flight testing will focus more immediately upon handling qualities in order to reduce risks; this will happen much earlier than for conventionally-controlled aircraft. However, the purpose is to make flight control changes in the simulator, not in the aircraft; in this way developmental costs are kept to a minimum.

Usually problems in FBW systems are first detected by one member of the flight test team, and through performance of a task, vice an established flight test procedure. The emphasis will be on task-intensive evaluations under high-gain conditions (turbulence, bad weather, etc.). These problems can be detected early if all involved in test remain skeptics (reference 10). Handling qualities "cliffs" are usually well-hidden in a well-designed system, but may remain to be seen at some time by the unexpected user (sometimes catastrophically).

The evaluation of software-intensive systems typically requires about two-thirds of flight testing based upon compiled data from military programs such as the F-14, F-15, F-16, F-18, B-1, and B-2 (reference 11). Correspondingly, the estimation of the time to evaluate these systems has been less than optimal, and often one-fourth of the actual time required. In theory, we should be able to evaluate most of these problems during ground-simulation (avoid fly-fix-fly philosophy).

CERTIFICATION

Airworthiness Standards define required handling characteristics, set control system requirements, and set equipment & powerplant requirements (including those for failures). Specifically, the FARs Parts 23, 25, 27, and 29 (references 12, 13, 14, and 15) apply directly to the aircraft category. The transport-category FARs require a 10^{-9} probability of total loss of function (reference 16); beyond this the designer has some freedom. This level of confidence can be shown through analysis, simulation, flight test, and/or operational flight experience. There are no dedicated regulations that have been tailored to meet the designs of full authority fly-by-wire; reference 17 is a FAA advisory circular that places some general requirements on active flight controls regarding load alleviation systems, stability augmentation systems, and flutter suppression systems. The Airbus A320 design, inherent in the A330 and A340 transports as well, is the only civil transport model that has achieved FBW certification through the FARs and JARs. Specific and dedicated guidelines for certification were agreed to by the FAA, JAA, and Airbus Industries. This was necessary, in part, due to the non-conventional handling qualities that were intentionally-designed (and such that they would not abide by current certification requirements).

According to the FAA in reference 18, the realized flying qualities benefits of FBW technology have not kept pace with the technology. Furthermore, advances in electronics has out-paced advances in human-factors engineering, to a point where workload has often increased when dealing with "automatic systems". Worse yet, it can require the pilot to spend more time heads-down in the cockpit under VFR conditions/flight. Certification issues are flight test & digital system validation, human factors/workload, displays, integrated controls, digital "bugs" & errors, side-stick controller issues, envelope-limiting functions, novel aircraft configurations, and task-oriented functions such as windshear control.

The regulatory challenges will be enormous, considering the diverse concepts that are possible with emerging technologies. The regulatory agencies will need to come to terms with new guidelines for highly-augmented flight control system designs. Amongst the items that will need attention are:

- (1) *Allowable relaxation of static longitudinal stability.* Most designs prefer neutral apparent stability for normal operations, but at least some level of airspeed feedback during slow-flight operations; RCAH is the popular example.
- (2) *Basis for a stall reference speed.* For aircraft which are stall-protected, by a limiting feature for instance, what should be the stall speed reference? Should it be the minimum allowable by design, a demonstration of true stall speed, a theoretical or windtunnel-based stall speed (or should it matter at all)?
- (3) *Dive Speed Demonstrations.* For aircraft with limit speed protection, through limiters for instance, should the requirement to demonstrate any capability above that limit be required?

- (4) *Stall and Spin Demonstrations.* For aircraft with stall-protection, should stalls be demonstrated in any way ? If so, to what degree ? What about spins ?
- (5) *Controller Forces.* What control forces are applicable to non-standard devices such as side-sticks ? Current standards do not apply well to such mini-sticks.
- (6) *Task Demands.* Should new requirements that are task-oriented be subjected to the certification process ? The military specifications are favoring this method.
- (7) *Frequency Testing.* This method has also been adopted by the military test community for the testing of highly-augmented flight control systems. This method is designed to discover any inherent PIO-causing tendencies of the system.
- (8) *Desired or Required Limiters.* With the introduction of these systems, should the regulator demand more from them as well ? Envelope limiters and other safety features can and should be taken advantage of if they can be easily implemented.
- (9) *Backup Modes.* What sort of reversion modes should be available in the event of partial or complete system failures, if any ? Should reconfigurable controls be required to compensate for damaged or failed components ?
- (10) *Added Protections.* Should automatic windshear or engine failure compensation be required ?

The proposed rules for the Boeing 777 (reference 19) add standards to the existing FAR Part 25 (reference 13). Some issues are:

- (1) Operation without normal electrical power for safe flight and landing.
- (2) Integrity of the FBW system to a safety level equivalent to that of conventional counterparts; secondary modes must be called upon less than 10^{-5} /ft hr.
- (3) Protection of the FBW system from lightning and other EMP hazards (there is nothing addressing this in Part 25); function must be restoreable in a timely manner.
- (4) Structural implications of load alleviation or limiting functions of the FBW system.
- (5) Additional design maneuver requirements are imposed, due to the unknown nature of the FBW system.
- (6) The use of handling quality ratings methods for flight characteristics compliance.
- (7) Display of control surface position in order to make the aircrew cognizant of surface movements, especially as they might indicate rate limiting or malfunctions otherwise unknown to the crew until failure.

Recent FAA concerns over advancing flight control systems (reference 20) have proposed a dedicated method of evaluation, based upon the traditional handling qualities rating scales. It is the Handling Qualities Rating Method (HQRМ) and has its root in the current FAR requirement for continued safe flight and landing. Three levels are specified much like the three levels specified by military handling qualities specifications (reference 21); in descending order they are satisfactory, adequate, and controllable. Reference 21 is the latest military standard concerning flying qualities and is a radical change from its predecessor in that FBW considerations are extremely subjective; over 750 pages of information concerning highly-augmented flight control systems is provided such that the user may subjectively determine conformance.

FUTURE DEVELOPMENTS

Fly-By-Wire is not the future, it is already in common use amongst some aviation communities. There are many new technologies that might be incorporated in these flight control systems. Among these are learned systems, fuzzy logic processing, and continued systems integration with displays, other avionics, and datalinks.

Learned systems are those that might incorporate neural networks and are characterized by systems that adapt independent of human interface and programming. The military has had a program called the "Pilot's Associate", whereby a computer makes certain decisions independently of the

pilot and can learn from past experiences as a human would. Discrete gain-scheduling for control laws can be replaced by variable gains, that are optimized by the processor to provide the pilot with his desired flight path commands. Reference 22 details some of the work done in this area to improve system robustness. Similarly, reference 23 discusses research into neural networks to improve target tracking for the military. These systems can be used to re-configure control laws in the event of aircraft damage or other unusual situations. To-date, this has been focused upon battle-damage applications for the military, but can in the future be applied to civil transports as well. This technology could easily apply to light aircraft that have been structurally-compromised or otherwise damaged. In this regard, failure detection is the challenge (via appropriate sensors and system logic).

Fuzzy-logic is the use of "grey" considerations to a problem. Instead of being programmed to consider and act on "on" or "off" conditions (black and white), intermediate steps may be taken by a computer. In this regard, a computer is programmed to consider several pertinent inputs, merge these into a specific action by way of "weighting" each input.

Systems integration allows ease of control, especially by way of automation. If the flight control computer is aware of the navigation problem, it is in a position to help optimize the flight path. At basic levels, one would call this type of system an autopilot. In advanced applications, the computer might be merging navigational inputs by considering all available, and even receiving information directly from ground controllers through data links.

Some research and testing initiatives with PBW systems are discussed in reference 24. PBW is a control surface actuator system that is not only electrically-controlled, but also is electrically-actuated (replaces the hydraulic system). Together with FBW, this offers all-electronic flight controls, in that any hydraulic-dependency can be eliminated. This offers performance improvements by way of weight savings, improved reliability by way of reduction of mechanical devices, and reductions in ground support equipment.

Other future hardware developments include Fly-By-Light (FBL) technology. In FBL, fibre-optic paths replace electronic wiring; this has the potential of weight savings and higher resistance to electromagnetic disturbances. Also, new control methods, such as direct sideforce control and direct lift control are amongst concepts that have come to life in recent designs. Both will likely be applied in near-future civil transport-category aircraft as landing aids and gust alleviation devices.

CONCLUSIONS

Fly-By-Wire control technology is being considered for use at every level of aviation. Starting with the experimental systems of the 1950's and 1960's, true fly-by-wire has been extensively utilized operationally by the modern military forces of the world and is being introduced steadily into the air transport community. Such systems are being developed for use for business and commuter aviation, and especially for rotary wing aviation. Systems for small fixed-wing aircraft are already on the drawing board. The challenge remains to market these systems at an affordable price, and without detriment to safety. A bigger challenge, perhaps, exists with the regulators, who must be in a position to keep pace with this technology. Without regulatory guidance, the certification process will fast become a tremendous obstacle.

Innovation in aircraft development has been stifled by the liability concerns of the GA industry. If this roadblock can be surmounted, perhaps GA aircraft design can again advance with emerging technologies, including the modernization of flight control systems.

REFERENCES

1. *Aerospace America*, AIAA, November, 1993.
2. *F-16 Digital Flight Control System Improvements*, W. Flynn, D. Janzen, J. Fergione, SETP, 1993.
3. *Overview of Aerospace Vehicle Computer Applications*, R.K. Smyth & G.H. Smith, AGARD Proceedings, 1970.
4. *A Simulator Evaluation of Various Manual Control Concepts for Fly-By-Wire Transport Aircraft*, P.J. Van der Geest, A.M.H. Nieuwpoort, J. Borger, AIAA, 1992.
5. *Airbus A320 side Stick and Fly By Wire - An Update*, S.G. Corps, AIAA, 1986.
6. *Development Status of the RAH-66 Comanche*, L. Stiles, SETP, 1993.
7. *Design of Flight Control Systems to Meet Rotorcraft Handling Qualities Specifications*, E. Low and W.L. Garrard, AIAA, 1991.
8. *The SAAB 2000: Initial Flight Test Status Report*, G. Singer, SETP, 1992.
9. *A Piloted Simulation Study of Advanced Controls and Displays for Novice General Aviation Pilots*, E.C. Stewart, AIAA, January 1994.
10. *Fly-By-Wire Design Considerations*, C.J. Berthe, L.H. Knotts, J.H. Peer, & N.C. Weingarten, SETP, 1988.
11. *Test & Evaluation Challenges in the Nineties*, C.E. Adolph, AGARD, 1992.
12. *Part 23 - Airworthiness Standards: Normal, Utility, Acrobatic, and Commuter Category Airplanes*, Federal Aviation Administration, 1993.
13. *Part 25 - Airworthiness Standards: Transport Category Airplanes*, Federal Aviation Administration, 1993.
14. *Part 27 - Airworthiness Standards: Normal Category Rotorcraft*, Federal Aviation Administration, 1993.
15. *Part 29 - Airworthiness Standards: Transport Category Rotorcraft*, Federal Aviation Administration, 1993.
16. *System Design and Analysis*, Advisory Circular 25.1309-1A, Federal Aviation Administration, 1988.
17. *Active Flight Controls*, Advisory Circular, Federal Aviation Administration, 1983.
18. *Flying Qualities and Operations*, J. Traybar, AIAA, 1993.
19. *Proposed Rules, Boeing Model 777 Series Airplane*, Federal Register, FAA, 1993.
20. *FAA Handling Qualities Assessment - Methodology in Transition*, C.E. McElroy, SETP, 1988.
21. *Flying Qualities of Piloted Airplanes*, MIL-STD 1797A, U.S. Department of Defense, 1990.
22. *Learning Augmented Flight Control for High Performance Aircraft*, W.L. Baker and J.A. Farrell, AIAA, 1991.
23. *Flight Control Law Synthesis Using Neural Network Theory*, R. DiGirolamo, AIAA, 1992.
24. *C-141 and C-130 Power-By-Wire Flight Control Systems*, R. Alden, IEEE, 1991.

TERMINOLOGY

ACAH	Attitude-Command Attitude-Hold
CAS	Command Augmentation System
DEL	Direct Electrical Link
DLC	Direct Lift Control
EMP	Electro-Magnetic Pulse
EPU	Emergency Power Unit
FAR	Federal Aviation Regulation
FADEC	Full Authority Digital Engine Control
FBW	Fly-By-Wire
FBL	Fly-By-Light
GA	General Aviation
HQRM	Handling Qualities Rating Method
PBW	Power-By-Wire
PIO	Pilot-Induced-Oscillations
RAT	Ram Air Turbine
RCAH	Rate-Command Attitude-Hold
SAS	Stability Augmentation System
TRCPH	Translational Rate-Command Position-Hold

PILOT WORKLOAD ASSESSMENT AND VALIDITY

Randall M. Chambers and Kevin J. Kilmer
Department of Industrial Engineering
National Institute for Aviation Research
The Wichita State University
Wichita, Kansas

ABSTRACT

The design, development, operation, and test of smart cockpits for the 21st Century will require the pilots to make valid and reliable assessments of pilot workload during various phases of development, flight test, and evaluation. This study examined the psychometric issue of predictive validity for pilot workload assessments in the cockpit, with emphasis on the need for valid and reliable assessments of pilot workload in future smart cockpits. This research was conducted to evaluate the predictive validity of subjective workload assessments judged by pilots performing flight maneuvers, and to evaluate the similarities and differences among subjective ratings and workload indices. Each of seven IFR pilots flew ILS (instrument landing system) approaches under three levels of wind gust disturbance in a flight workload validation simulator. Their NASA TLX Task Load Index pilot workload ratings for each flight were compared with their subjective judgments of difficulty level. The results of statistical tests for mean differences and standard deviations demonstrated that the workload scores were not significantly different from the difficulty level scores, and that the subjective ratings of workload were nearly equivalent to difficulty level judgments. Linear regression analysis yielded high correlation. These results provided initial support for the validity of subjective assessments of workload by pilots, and provided favorable comparisons in similarity for judgments based on two different subjective scales.

INTRODUCTION

In assessing workload, it is generally assumed that there is a given (measurable) quantity of work capability and capacity, and that a certain proportion of this work capability and capacity is needed to perform the task. Workload, whether physiological,

physical, psychological, or psychophysical, is a resource construct, in that a portion of the total capacity to perform a task is being expended as the resource reserve which is resupplied and maintained at levels which help the pilot maintain maximal performance capacity, even as the task requirements change. Multiple-resource capacities are assumed, and the pilot controls and utilizes his capacities to meet his judged task requirements. The pilot is prepared for overload, in which the demand may be excessive; and the pilot is prepared for underload, in which the pilot may maintain a residual capacity for the unexpected or difficult future requirements.

The use of subjective assessment methodologies has almost become second nature in the evaluation of mental workload. A scan of the literature from the previous decade provided demonstrative evidence for this conclusion (Nygren, 1991; Hart and Staveland, 1988; Kilmer, 1988; Chambers and Cihangirli, 1990; Reid and Nygren, 1988; Wierwille and Eggemeier, 1993; Wierwille and Casali, 1983). However, in the zeal to find a methodology that provides useable information regarding mental demands and their effects on human performance, some fundamental issues regarding the psychometrics of subjective assessment, notably, validity, may have been overlooked. Remembering fundamentals, validity is defined as, "The property of a measuring device that it measures in fact what it is intended to measure. Validity is established by correlating the results of the test with an outside criterion or independent measure" (Chaplin, 1985, p. 484). The process necessary in establishing validity should be presented along with consideration of the fundamental psychometric properties of at the most widely used subjective assessment scales, such as the Subjective Workload Assessment Technique (SWAT, Reid and Nygren, 1988), the NASA Task Load Index (TLX, Hart and Staveland, 1988), the Modified Cooper Harper Scale (MCH, Wierwille and Casali, 1983). According to Nygren (1991), it is possible to establish predictive validity using a simple independent ranking methodology wherein the subject after performing several tasks provides subjective ratings for each experience, and then is asked after some time has elapsed to rank order each task in terms of its difficulty level. If the ratings are a true reflection of difficulty, the subject will rank each task according to the subjective rating given at the end of each trial. For example, if the subject rated three levels of difficulty for a task as 90, 80, and 70, the subject would then rank order each task as 3, 2, and 1, reflecting the level of difficulty. High

correlations with NASA TLX ratings made by the same pilots flying the same tasks, would indicate high similarity among the rank orders for TLX ratings and the difficulty level ratings, for example. They would offer some suggestions regarding workload and validity issues for assessing pilot workload.

PURPOSE

The purpose of the present experiment was to examine the issue of validity assessment, using the method as described in Nygren (1991). The specific hypothesis for this experiment was: the subjective task load ratings provided by the pilot on the TLX Task Load Index will be an indication (predictor) of how the pilot will rank order the difficulty of each task in the post flight difficulty level rating, resulting in a "no difference" condition existing between the subjective workload ratings and the post-flight difficulty level ratings. Validity assessment was studied as a psychometric issue of predictive validity for pilot workload assessments in the cockpit, with emphasis on the need for valid and reliable assessments of pilot workload in future smart cockpits. The validity of subjective assessments of workload by pilots was hypothesized, and similarities among judgments of pilot workload based on two different subjective scales were predicted.

METHOD

PILOT SAMPLE

Seven instrument rated pilots from the Wichita, Kansas, area were selected for the pilot sample for pilot workload testing. The pilots were required to meet the minimum level of instrument flight rules (IFR) proficiency which are under Federal Aviation Regulation (FAR) 61.57 paragraph e. Each pilot was given an explanation of the rationale behind the experiments program, and presented with a subject consent form. After reading and signing the consent form, each pilot was given refresher documentation and a briefing for instrument approach procedure, along with the appropriate flight departure instructions, and each pilot was given a briefing regarding the NASA TLX Task Load Index and the subjective task difficulty scale.

TEST APPARATUS

The apparatus used in this experiment was the ATC-810 Twin Engine CPT/IFR Flight Simulator, maintained as the Workload Validation Simulator, produced by Analog Training Computers. Figure 1 presents a photograph of the instrument panel and controls in the

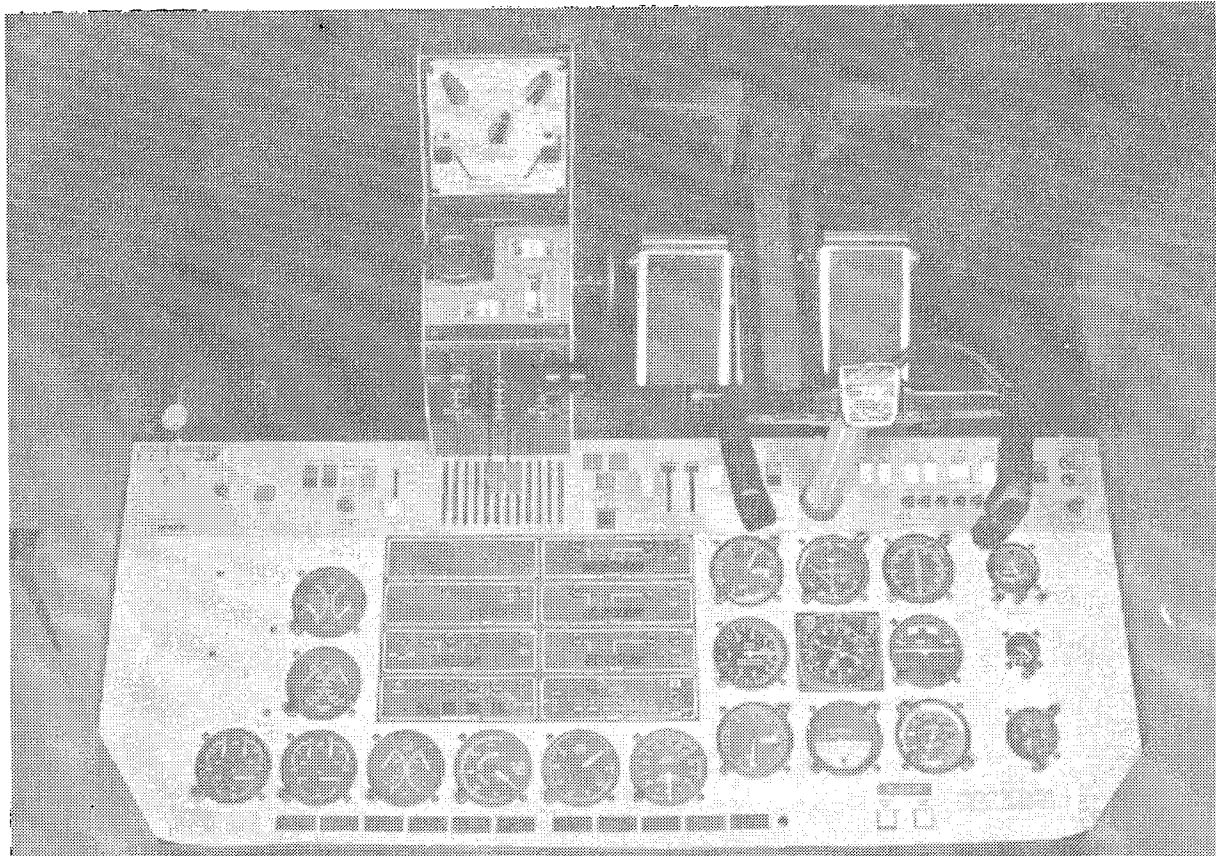


Figure 1. The ATC-810 Twin Engine CPT/IFR Flight Simulator

cockpit of the ATC-810. This unit is fully equipped and instrumented to represent the cockpit of a light or medium weight (< 12,500 pds) twin-engine aircraft, and serves as a flight and instrument procedures trainer. It provides the FAA required regulations procedures and IFR simulation. The instrument approach used in this experiment was an ILS approach to runway 1R at Wichita's Mid-Centimeter Airport (ICT) using NOS Instrument Approach Procedures North Central Region (U.S. Department of Commerce, and National Oceanic and Atmospheric Administration, 1985). This

instrument approach, which is presented in Figure 2, was programmed into the ATC-810 Twin Engine CPT/IFR Flight Simulator.

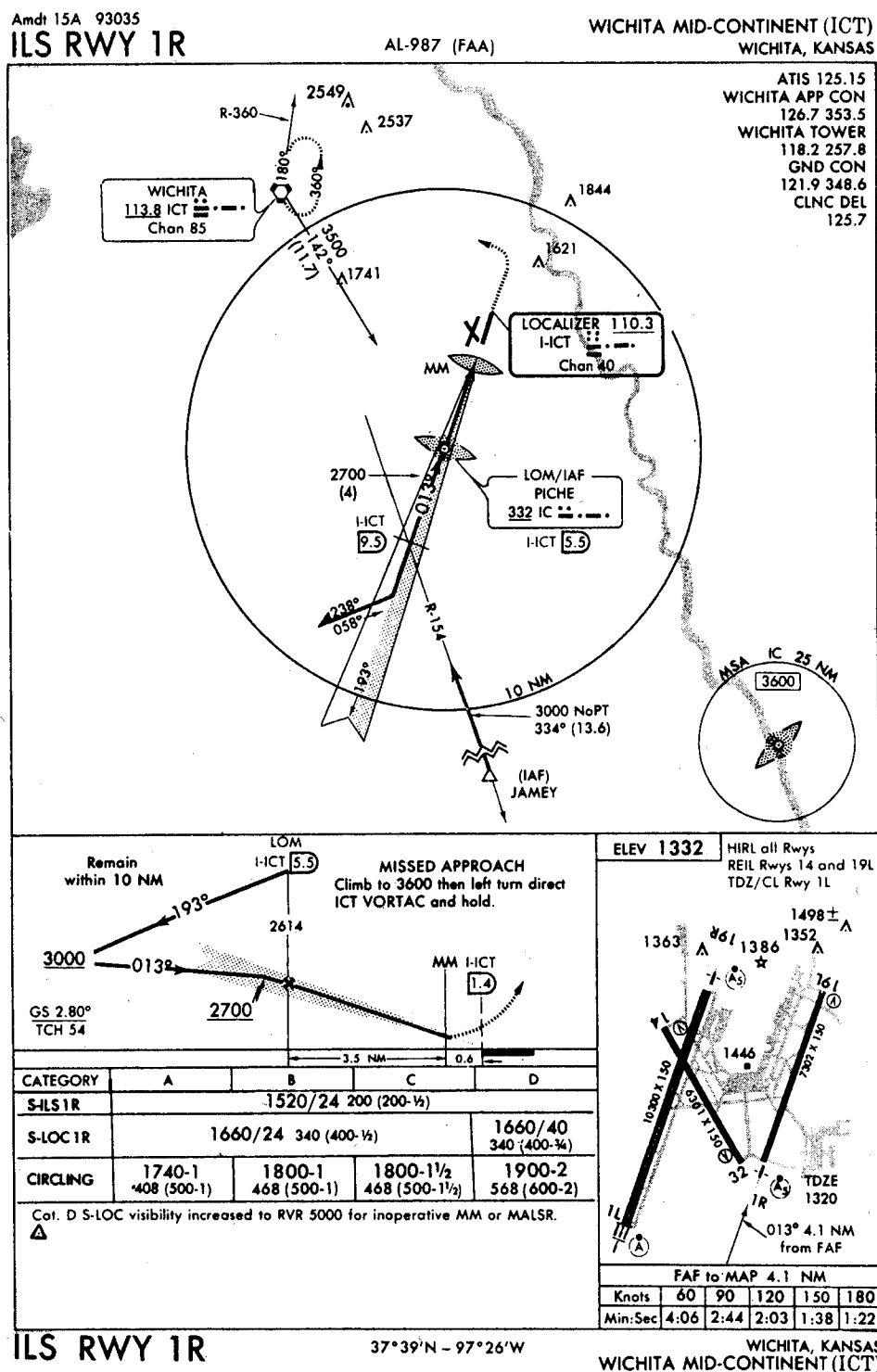


Figure 2. NOS Approach Plate for Wichita, Kansas Mid-Continent Airport Runway 1r

TEST PROCEDURE

Each pilot was given an explanation of the rationale behind the experiment, and was presented with a test subject consent form. After reading and signing the consent form, each subject was given refresher documentation and a briefing for the instrument approach procedure for this experiment, along with the appropriate flight departure instructions. The subjective workload assessment data was collected using the NASA TLX Task Load Index (1989). This multi-dimensional rating scale included judgments about the magnitude and sources of six workload-related factors which are combined to derive a sensitive and reliable estimate of workload. Administration of the NASA TLX Task Load Index occurred during each flight simulation as he approached landing. At the outer marker, the pilot would intercept the glideslope and begin preparations for landing, maintaining localizer and glideslope until reaching the middle marker; at this point, the pilot was presented with the NASA TLX scales and asked to make workload ratings. Using a scale from 0 to 100, the pilot rated each of six task load dimensions: mental demand, physical demand, temporal demand, performance, effort, and frustration. These are shown in Table 1.

TABLE 1. WORKLOAD RATINGS BY PILOTS USING THE
NASA TLX TASK LOAD INDEX

DIMENSION	SUBJECTIVE SCALE
Mental Demand	Low-High (0-100)
Physical Demand	Low-High (0-100)
Temporal Demand	Low-High (0-100)
Performance	Low-High (0-100)
Effort	Low-High (0-100)
Frustration	Low-High (0-100)

After the completion of each flight simulation, the pilot ranked each of the three approach scenarios by using a simple one, two, three ranking methodology. This ranking methodology is shown in Table 2. This experiment was a four-step process: (1), A pretest briefing outlining the instrument approach, and a brief explanation

of the rationale behind the experiment; (2) the three ILS approaches to ICT IR with random turbulence with steady winds at 10, 35, and 50 knots from 30 to 90 degrees counterclockwise from the runway heading (winds 340 degrees at 35 knots); (3) NASA TLX Task Load Index after each ILS Approach; and (4) after each simulation test flight, a post-flight rank ordering of the difficulty level of each approach.

TABLE 2. THE POST EXPERIMENT RANK ORDERING PROCEDURE

APPROACH	RANKING
1st Approach	1 = Least Difficult 2 = Moderately Difficult 3 = Most Difficult
2nd Approach	1 = Least Difficult 2 = Moderately Difficult 3 = Most Difficult
3rd Approach	1 = Least Difficult 2 = Moderately Difficult 3 = Most Difficult

After reading and signing the test pilot consent form, the pilot was given the documentation and briefing for the instrument approach procedure, along with the appropriate departure instructions, and was told to disregard the holding pattern. While flying in the second phase of the experiment, the pilot flew three instrument approaches with randomly presented turbulence and steady winds. The pilot departed ICT IR and climbed to 4000 msl (mean sea level) and tracked inbound to the ICT VOR (Very High Omnidirectional Range). Once the subject had reached the VOR a left standard rate turn was initiated to intercept the 142 radial outbound, once established on the 142 radial the subject tracked outbound until intercepting the initial approach fix (IAF) at the localizer outer marker (LOM). Upon interception of the LOM the pilot initiated a right standard rate turn to a heading of 193 and flew this heading for one minute. After one minute the pilot would begin the procedure turn by entering a right standard rate turn to a heading of 238 and flew this for one minute, after one minute the pilot then began a left standard rate turn to a heading of 058 and flew this until intercepting the localizer. Upon intercepting the

localizer the pilot would then make a left standard rate turn to a heading of 010, or as necessary to maintain the localizer. The pilot would fly this heading until reintercepting the outer marker. At the outer marker the pilot would intercept the glideslope begin preparations for landing. The pilot would maintain localizer and glideslope until reaching the middle marker at which point the pilot was presented with the TLX scales and asked to make the task load ratings. These were accomplished during the third phase. After the completion and termination of the flight simulations, during the fourth phase of the experiment, pilot was asked to make judgments for the difficulty level of the flight simulations.

RESULTS AND DISCUSSION

For each pilot during each approach simulation, the NASA TLX TLX Index scores were calculated from the six task dimensions. These composite Index Scores were compared with difficulty ratings provided by each pilot. A *t*-test for correlated samples was used to determine if a significant difference existed between the TLX and the difficulty level scores. The calculation of the *t*-test showed that *t* = .571. This *t* value indicated that no difference existed between the predicted scores (difficulty level scale) and the actual scores (TLX workload scores). A *t* value of at least 2.086 would have been required in order to reach the 5% confidence level. The results of this analysis are shown in Figure 3, in which the

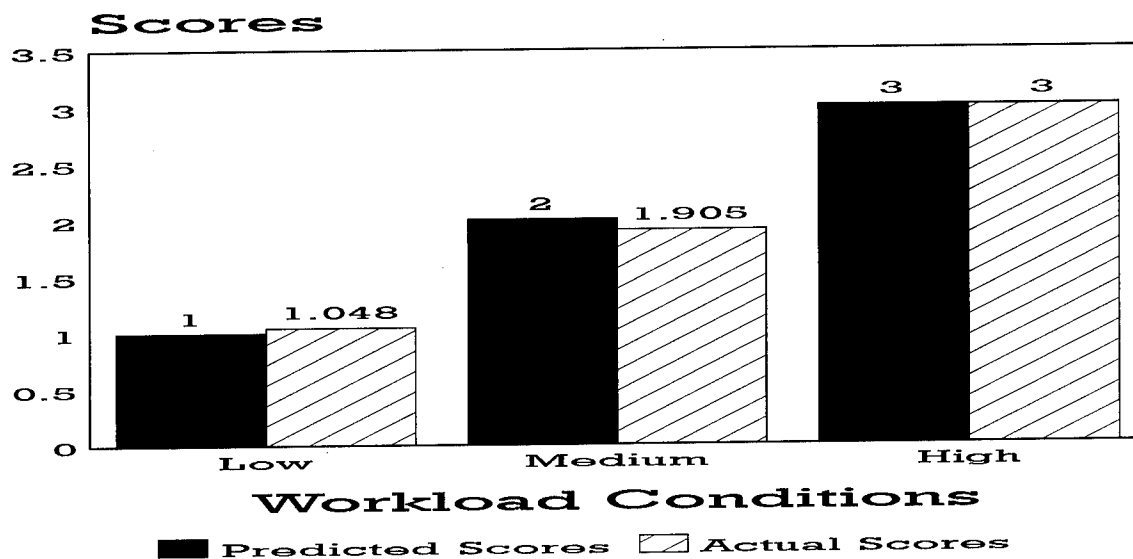


Figure 3. Means for Actual vs Predicted Scores.

means for these arrays of scores are shown for the actual versus the predicted scores. Figure 3 indicates that no differences existed between the predicted scores and the actual scores.

In addition to the t-test, a simple linear regression was performed to establish the strength of the correlation between the groups and provide a prediction equation. This is shown in Figure 4. The results of the regression analysis show that a high

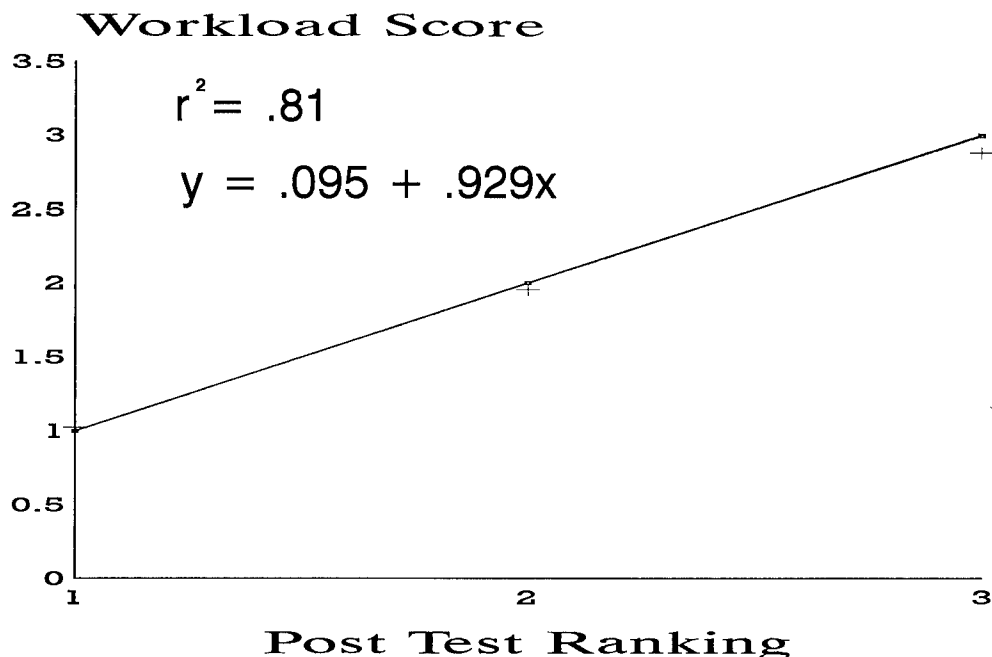


Figure 4. Regression Analysis with Prediction Equation and Correlation

correlation ($r^2 = 0.81$) was found between the NASA TLX Task Load Index Scores and the difficulty level ratings. The regression analysis with prediction equation and correlation are also shown in Figure 4.

DISCUSSION

Taken together the results of the t-test and the regression analysis provide initial evidence supporting the predictive validity argument of subjective workload assessment. This research was part of a long term effort to evaluate the predictive validity of subjective workload assessments judged by pilots performing flight maneuvers, such as landing approach. The research flight workload was used to compare two different sets of pilot opinions regarding subjective workload assessments by the pilots who

performed these instrument landing approaches. There are many additional aspects of subjective workload validity which need to be established (Wierwille and Eggemier, 1993). The NASA TLX ratings were found to be very similar to the judgments of level of difficulty made by the same pilots, as indicated by the the high correlation found in the regression analysis, and the similarities among the means for the difficulty ratings and the TLX ratings, as indicated by the t-test and variance analysis. The NASA TLX Task Load Index is a multi-dimensional rating scale which includes information about the magnitude and sources of six workload-related factors which are combined to derive a sensitive and reliable estimate of workload: mental demand, physical demand, temporal demand, performance, effort, and frustration level. As is pointed out by Hart and Staveland (1988), workload may be caused by different factors from one task to the next, regardless of how individuals might personally define workload. Evaluation of pilot's responses to a task may provide additional information as well as highly correlated information.

Using possible a priori biases of pilots and experimenters about the workload to weigh or organize subscale ratings into a single workload value may not provide sufficiently sensitive subjective rating predictions regarding special attributes of newly designed flight tasks for future smart systems. Research is needed on the pilot workload and assessment and validity for new special attributes of flying tasks which are being designed for future flight systems. These will require the pilots to make valid assessments of pilot workload for future phases of development, flight test, and operations. This study demonstrated some predictive validity for pilot workload assessments using the NASA TLX Task Load Index. It is believed that these findings have some applications to the issues of predictive validity for smart cockpits for the 21st century. The psychometric issues of predictive validity of the opinions of pilots will be applicable to the new cockpit designs and developments. However, establishing all of the aspects of subjective workload assessment and validity for the dimensional components of pilot workload needs to be accomplished.

REFERENCES

Chaplin, J. P. Dictionary of Psychology. New York, NY: Laurel, 1985.

Chambers, R. M. and Cihangirli, M. Human Performance in Cockpit-Related Systems, pp. 66-80, in Proceedings of the 1990 AIAA/FAA Joint Symposium on General Aviation Systems, FAA Technical Center, Atlantic City International Airport, N.J., DOT/FAA/CT-90 11, May, 1990.

Hart, S. G., and Staveland, L. E. Development of the NASA Task Load Index (TLX): Results of Empirical and Theoretical Research. In P. A. Hancock and M. Meshkati (Eds.) Human Mental Workload. (pp. 139-183). Elsevier Science Publishers B.V. Amsterdam: North Holland, 1988.

Kilmer, K. J. Toward a Standardized Subjective Workload Assessment Methodology: a Comparison of the Subjective Workload Assessment Technique and Modified Cooper-Harper Scales. Unpublished M. S. Thesis, Wichita State University, Wichita, Kansas, 1988.

Nygren, T. W. Psychometric Properties of Subjective Workload Assessment Techniques: Implications for their Use in the Assessment of Perceived Mental Workload. Human Factors, 1991, 33, 17-34.

Reid, G. B. and Nygren, T. E. The Subjective Workload Assessment Technique: A scaling procedure for measuring mental workload. In P. A. Hancock and N. Meshkati (Eds.) Human Mental Workload. (pp. 185-218). Elsevier Science Publishers B.V. Amsterdam: North-Holland, 1988.

Wierwille, W. W. and Eggemeier, F. T. Recommendations for Mental Workload Measurement in a Test and Evaluation Environment. Human Factors, 1993, 35(2), 263-281.

Wierwille, W. W. and Casali, J. G. A valid Rating Scale for Global mental Workload Measurement Applications. In Proceedings of the Human Factors Society 27th Annual Meeting. Santa Monica, CA: Human Factors and Ergonomics Society, 1983.

United States Government, U.S. Department of Commerce, National Oceanic and Atmospheric Administration, National Ocean Service. Instrument Approach Procedures, U.S. North Central, U.S. Government Printing Office, Washington, D. C., 4 July 1985, Vol. 2, p. 461.

A ROBUST PLANNING TECHNIQUE FOR A GENERAL AVIATION SMART COCKPIT SYSTEM

Stephen G. Pimentel

Amy R. Gardner

Lawrence M. Brem

Adroit Systems, Inc.

209 Madison Street

Alexandria, VA 22314

ABSTRACT

Smart cockpit systems are being developed for general aviation to improve the process of cockpit information management. Automated planners employing artificial intelligence technology can serve within such systems to assist the pilot with decision-making during flight. We present a novel, decision-theoretic approach to increase the robustness of planning in smart cockpit systems. The concept improves upon conventional, goal-oriented planning by using utility functions to guide the planner through the space of alternatives. The results of actions, including the possibility of execution failure, are modeled using probability functions. The planner is, therefore, able to manage uncertainty by seeking to maximize the expected utility of a plan, rather than the value of a plan assuming successful execution. Using a robustness factor to parameterize the utility function, the system designer will have control over the degree of risk-reduction. Via a look-ahead search, the planner seeks to find an optimal plan, using the robustness-parameterized expected utility as its optimization criterion. This paper demonstrates the advantages and use of a robust planner in a smart cockpit system. This system will aid cockpit decision-making, thus reducing pilot workload and increasing safety.

INTRODUCTION

Cockpit information management systems are being developed that will incorporate multiple types of sensor data and use it to aid the pilot with decision-making, particularly during single pilot operations. Various systems have been developed by the U.S. Air Force to assist pilots during missions. These systems can improve a pilot's situational awareness through the use of advanced computerized systems that employ artificial intelligence (AI) technology. They employ short and long-term planning mechanisms which incorporate data from system and environmental sensors and recommend the best course of action, based on preset criteria. We have developed a planning technique that will analyze future events and incorporate the possibility of alternate outcomes to improve the safety and reliability of these systems.

These types of systems have also been examined for use in the general aviation (GA) industry, particularly to assist pilots flying under Instrument Flight Rules (IFR) conditions. Such a system could integrate weather, navigation, communication, and systems information and present this information to the pilot, along with recommended courses of action. By combining several different types of data and presenting the processed information and recommendations in a prioritized, more efficient manner, the pilot's situational awareness is increased and workload is decreased, thus improving safety.

In the late 1980's, researchers began to examine ways of incorporating probabilistic information into planners [Kanazawa], and using decision theory to control the way searches are conducted [Russell]. While building on these previous approaches, we have designed a planner that uses a robustness factor to modulate the degree of risk-aversion sought by the planner. The design improves upon conventional, goal-oriented planning by using utility functions to guide the planner through the space of alternatives. The results of actions, including the possibility of execution failure, are modeled using probability functions. The planner is, therefore, able to manage uncertainty by seeking to maximize the expected utility of a plan, rather than the value of a plan assuming successful execution. Using a robustness factor to parameterize the utility function, the system designer will have control over the degree of risk-reduction. Via a look-ahead search, the planner seeks to find an optimal plan, using the robustness-parameterized expected utility as its optimization criterion.

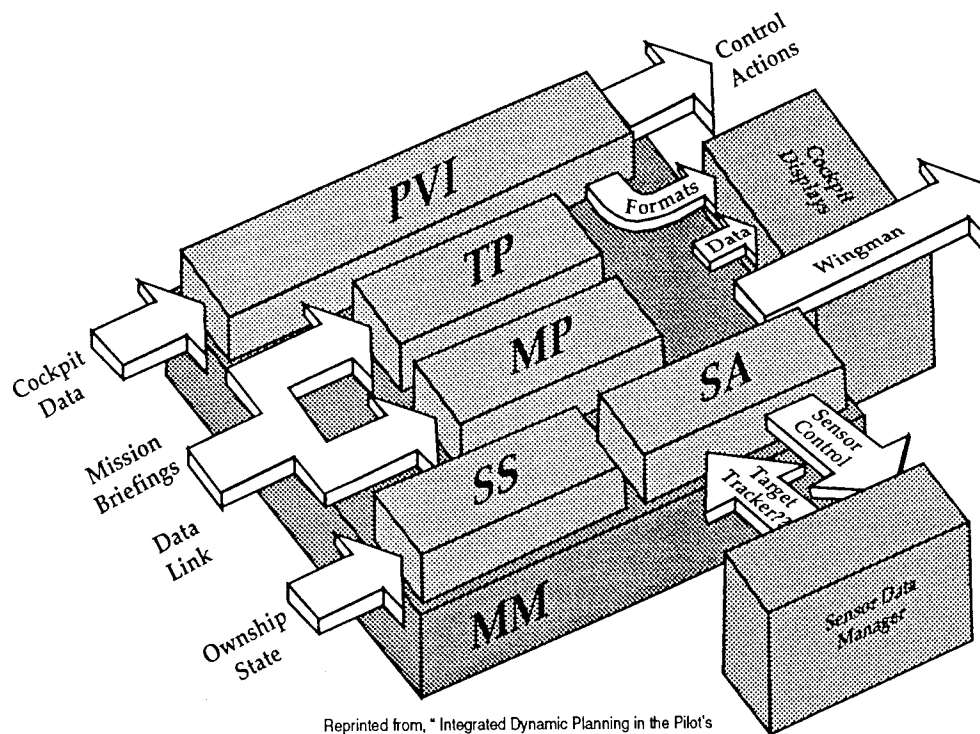
In this paper, we present examples of existing smart cockpit systems and discuss the need for robustness in general aviation planning. We present an example that demonstrates the difference between a robust planner and a standard planner in reacting to unforeseen conditions such as bad weather. We then explain our robust planning methodology and its implementation using the Generic Optimization System, GENOS.

EXISTING SYSTEMS FOR SMART COCKPITS

The U.S. Air Force and the Advanced Research Projects Agency (ARPA) are developing a Pilot's Associate (PA) system that will aid cockpit decision-making during military missions and improve pilot situational awareness and cockpit information management. These systems will utilize advanced computerized systems that employ artificial intelligence (AI) technology to perform planning and decision aiding tasks. The PA represents one of the most sophisticated and complex systems for automated information management and pilot aiding developed to date. [Miller]

As shown in Figure 1, the PA is divided into five modules: mission management, systems status, situational assessment, mission planning, and tactics planning. All of these modules communicate with the pilot through an intelligent pilot-vehicle interface. The mission management module facilitates the transfer of information between all the modules. The systems status and situational assessment modules monitor the state of aircraft systems and the aircraft's environment, respectively. Information received from these modules is conveyed to the pilot through an intelligent pilot-vehicle interface. In addition, this information is provided to the planning modules for assessment.

The mission planning module monitors events relative to the established mission plan and assists the pilot in responding to contingencies that threaten mission success. The tactics planning module is responsible for short-term planning and resolution of threats or emergency situations. It also monitors information from the systems status and situational assessment modules. A course deviation due to a tactics planner recommendation may result in necessary changes by the mission planning module to the overall mission plan. In-flight generation of a mission plan is performed by a set of path planning and resource planning modules that are controlled by a planning framework. Other similar scripts are used to generate more immediate, tactical level responses to threats, to respond to mission redirects or new information on target location and to respond to situations where resources have been depleted. [Corrigan]



Reprinted from, "Integrated Dynamic Planning in the Pilot's Associate," by C.A. Leavitt and D.M. Smith, Lockheed Aeronautical Systems Company, Marietta, GA

Figure 1. PA System Design

Cockpit resource management is a critical safety factor in general aviation as well, particularly when flying under Instrument Flight Rules (IFR) conditions. Research has shown that the majority of general aviation accidents are caused by human error. [Wittig] The pilot must assess information he receives about his environment from Air Traffic Controllers, weather advisories, and maps, in addition to systems and navigation information from many cockpit sensors. General aviation aircraft are not as sophisticated as advanced military fighters; as a result, most general aviation pilots often fly without benefit of advanced cockpit systems or ground control. A system similar to the military's PA that improves cockpit information management and assists pilots with decision making, particularly during single pilot IFR, emergency situations, or other high workload operations, would be useful to general aviation pilots and make significant contributions to safety.

Researchers at the University of the German Armed Forces in Munich are developing a Cockpit Assistant System (CASSY) for general and civil aviation use. CASSY is divided into four modules: dialogue manager, automatic flight planner (AFP), piloting expert, and pilot intent and error recognition. The dialogue manager facilitates communication between the system modules; in addition, it is responsible for managing the flow of information to the pilot. CASSY also incorporates a speech recognition and synthetic speech capability, which is contained in the dialogue manager. The pilot intent and error recognition module monitors the actions of the pilot to detect deviations from the original flight plan. These deviations are either recognized as purposeful, in which case the AFP re-calculates a new flight plan; or as pilot error, in which case the pilot is warned. The AFP performs both short-term and long-term (tactical and strategic) planning tasks. It is activated when events such as adverse weather conditions, system failures, or traffic avoidance warnings occur such that changes to the original flight plan must be made. The

piloting expert executes the flight plan that the AFP recommends. The piloting expert module determines which actions it expects the pilot to carry out during the various flight segments. It determines these expected actions through a rule-based modeling procedure based on rules derived from piloting regulations. [Wittig]

A planner for a smart cockpit system must assimilate information about nearby obstacles, weather, other traffic, and surrounding airspace and choose a safe course of action. A standard planner, of the sort used in the PA and CASSY systems, evaluates these options and recommends a course of action, based upon the assumption that the pilot's actions will be successful. Planning is envisioned as the generation of a complete set of actions that, when executed, will allow the pilot to maneuver the aircraft from its current state to a desired state in its surrounding environment. This model of planning assumes that the effects of actions can be fully determined beforehand.

THE NEED FOR ROBUSTNESS IN GENERAL AVIATION PLANNING

Unfortunately, due to the dynamic environment in which aircraft operate, the aviation domain has an element of unpredictability which forces the planner to estimate some of the possible results of actions and events that may occur. Uncertainty can occur for several reasons. First, planned actions, when executed by the pilot, may fail. Second, the environment may permit exogenous events, i.e., events which are not caused by the pilot. If the frequency with which exogenous events occur is sufficiently high, as in weather disturbances, then standard planning techniques will have decreased effectiveness. Third, the planner may have incomplete information about its environment. A planning system that could incorporate probabilistic information and identify the level of risk that the pilot is willing to take will provide safer performance.

Shown in Figure 2 is a simple example where a planner within a smart cockpit system would recommend an action to the pilot. In this figure, a thunderstorm cell has been detected crossing the original intended flight path of the aircraft. At the decision point, the pilot must choose which direction the aircraft should go. In this example, there are two possible choices if the pilot wishes to avoid the storm: go left in front of the oncoming storm or go right behind the storm.

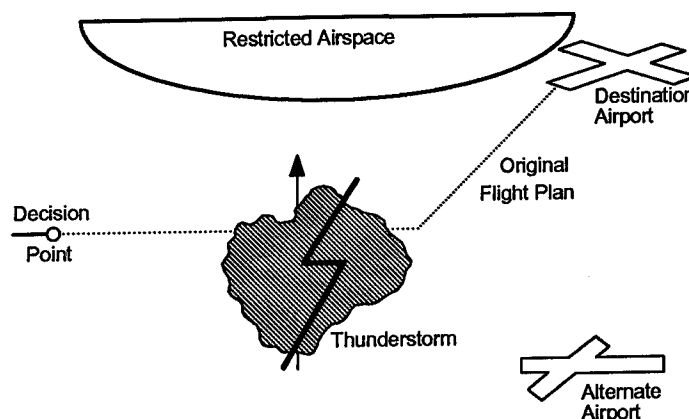


Figure 2. An example situation where a Reactive Planner would be used.

A standard reactive planner would assume that the pilot's action will be successful, dealing with the possibility of other problems as they arise. In this example, the standard planner might choose

the shorter flight path shown in Figure 3a. In this plan, the aircraft will pass in front of the storm in a corridor between the storm and the restricted airspace. If the storm remains far enough away from the restricted airspace, then the pilot can fly successfully to the destination airport. If, on the other hand, the storm moves faster than anticipated towards the restricted airspace, then the pilot will be forced to either turn back, circle and wait for the storm to pass, or violate the restricted airspace. If he circles or has to turn back, the additional fuel consumption may force him to land at the alternate airport. Figure 3b shows the search tree that the standard planner would use at the initial decision point to evaluate possible actions.

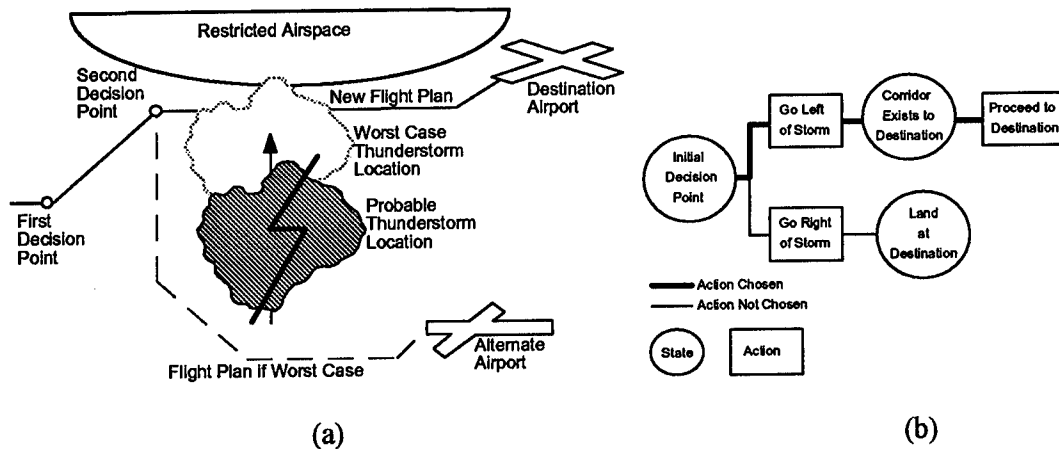


Figure 3. A Flight Plan created using a Standard Reactive Planning System

The robust reactive planner might choose the longer flight path shown in Figure 4a. In this plan, the pilot would fly the plane to the right of the storm, pass behind it, and proceed to the destination airport. The plane taking the route in Figure 4a would be able to avoid the storm without risk of violating the restricted airspace. Though the plane would take longer to get to the airport, it would be less likely to encounter further difficulties due to the unpredictable storm movement. Figure 4b shows the search tree that a robust reactive planner would use to evaluate possible courses of action at the initial decision point. It demonstrates how a robust planner takes into account the possibility that an action may fail.

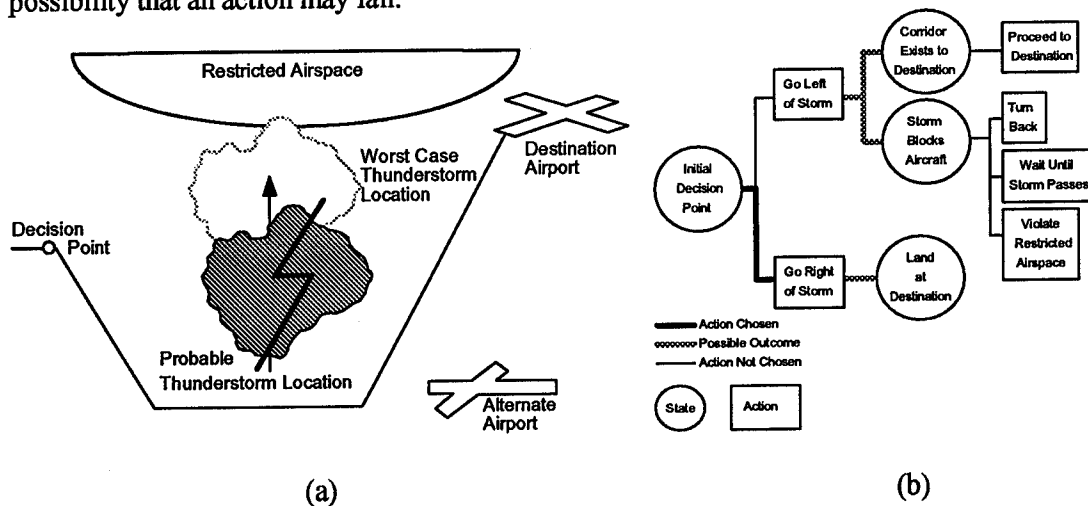


Figure 4. A Flight Plan created using a Robust Reactive Planning System

APPROACH TO ROBUSTNESS

In the above example the robust planner evaluated the available actions and the possible outcomes of those actions. From that information it determined that diverting to the right of the storm would still allow the pilot to reach the destination airport regardless of the progression of the storm. A major advantage of our decision-theoretic framework is that it allows the robustness of plans to be defined in terms which are independent of specific planning algorithms and aviation domains, but which can be readily applied to both. In our approach, robustness is a measure of a plan's capacity for "graceful degradation." It measures how well a plan performs when one or more actions within the plan fail, as illustrated in the previous example.

Risk aversion in the aviation domain is high, but not absolute. The risks must be weighed against the value of completing a mission. Our approach facilitates the adjustment of robustness by a numeric *robustness factor*, R . A robustness factor of $R = 0$ indicates complete risk-indifference, while a robustness factor of $R = 1$ indicates complete risk-aversion. The planner employs a utility function to incorporate R into its evaluation of states and actions. The utility function is a function $U_R(V)$ which is continuous on $0 \leq V \leq 1$ and undefined outside that range. An appropriate value for R is determined during the requirements analysis and design of the smart cockpit system by the avionics engineer.

A decision-theoretic planner selects actions which will lead to the best possible solution, as measured by expected utility. The expected utility of states and actions are described by the following mutually recursive pair of equations. A state will be called *terminal* if it is a possible final state for a planning scenario, and *non-terminal* otherwise. The expected utility of a state s will be given by

$$EU_R(s) = \begin{cases} U_R(V(s)) & \text{if } s \text{ is terminal,} \\ \max_a \{EU_R(a|s)\} & \text{if } s \text{ is non-terminal.} \end{cases}$$

The expected utility of an action a executed in a state s will be given by

$$EU_R(a|s) = \begin{cases} \sum_{i=1}^k P_a(i|s) EU_R(\text{result}_i(a,s)) & \text{if the preconditions of } a \text{ are satisfied in } s, \\ 0 & \text{otherwise} \end{cases}$$

In the example of the previous section, the plan shown in Figure 4 will have higher expected utility than the plan shown in Figure 3 due to the increased likelihood of arriving at the destination airport.

IMPLEMENTATION

In principle, the above equations can be directly implemented as a recursive algorithm starting with an initial state $S1$ as shown in Figure 5. The search proceeds from $S1$, to action $A2$, $S3$, $A4$ and then $S5$. $S5$ is a terminal state (e.g. plane arrives at destination, plane is diverted to alternate airport). The system evaluates the utility of this state. $S6$, the other terminal state off of $A4$, is

evaluated next. The utilities from S5 and S6 are used to compute the expected utility of A4. The expected utility of A7 is computed in the same manner. The expected utility of S3 is equal to the maximum expected utility of A4 and A7. The planner computes the expected utility of all the states to determine the best possible choices of actions that the pilot could make.

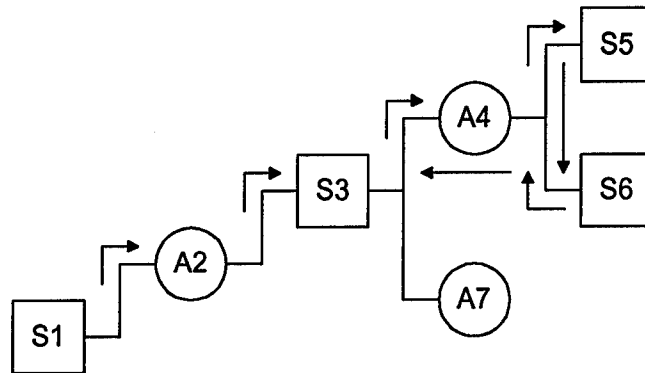


Figure 5. An example showing a traversal of a robust search tree

In practice, however, a direct implementation of the equations for expected utility would be very inefficient, because the size of the resulting search trees will grow exponentially. Such an implementation would not be suitable for a reactive planner, which needs to interact within tight time bounds with other modules of the system. Nevertheless, this algorithm provides a baseline for more efficient algorithms which support reactive planning. The direct implementation assumes that search can proceed to the end of a planning scenario, so that an exact value for expected utility can be computed. By sacrificing exact computation of expected utility and imposing a limited search horizon, an efficient reactive planning algorithm can be derived.

The technique of depth-limited search can be applied very simply in this setting. Rather than defining a terminal state as one that is at the end of the planning scenario, we define it as one that is at some fixed depth from the initial state in the search tree (e.g., plane goes around storm). The equations for maximum expected utility can then be used to retrace expected utilities to the initial state. The depth limitation, used in this fashion, will have two impacts. First, the evaluated search tree will correspond only to a prefix of a complete plan, extending out only as far as the depth limit. Second, the expected utilities computed will be approximate, and therefore the actions chosen may not be perfectly optimal.

A more sophisticated use of depth-limitation is the technique of *iterative deepening*. Iterative deepening involves the repeated execution of a depth-limited search, beginning with a small depth limit and incrementing it each time the search is performed. The iteration is continued until an externally defined limit on computation time is reached. This procedure results in a so-called *any-time* algorithm, which produces viable results within a limited period of time and continually improves them thereafter, until either the time limit is elapsed or an optimal solution is found. An any-time algorithm based on iterative deepening is a suitable implementation technique for a reactive planner.

PLANNER DESIGN

Typical search algorithms work by conducting an intelligent exploration through a state space. The algorithm in Figure 6 describes the process of heuristic search.

1. Initialize the state set with the start state.
2. Select a state from the state set.
3. Generate a new state from the selected state.
4. Evaluate the newly generated state.
5. Insert the newly generated state into the state set.
6. If termination criteria are not met, go to step 2.

Figure 6. Abstract of Heuristic Search Approach

The approach in Figure 5 shows the heuristic search process for any domain. The exact technique used to generate a new state, evaluate an existing state, and identify termination criteria can be extracted from this process and developed separately. We have designed a system, GENOS (GENeric Optimization System), to support the development of combinatorial optimization problems in a more efficient manner by using the above concept.

The GENOS architecture illustrated in Figure 7 shows the basic modules of the system. GENOS provides the developer with standardized interfaces between the heuristic search algorithms and the different domain models.

The GENOS design is motivated by the fact that some search algorithms will be more efficient and produce better solutions for a given application. Hence, the framework allows alternate search algorithms to be inserted for evaluation against the application. Likewise, a particular search algorithm may be effective in a variety of domains. By inserting a different domain model into the framework, the same search algorithm may be used in different applications without reimplementing.

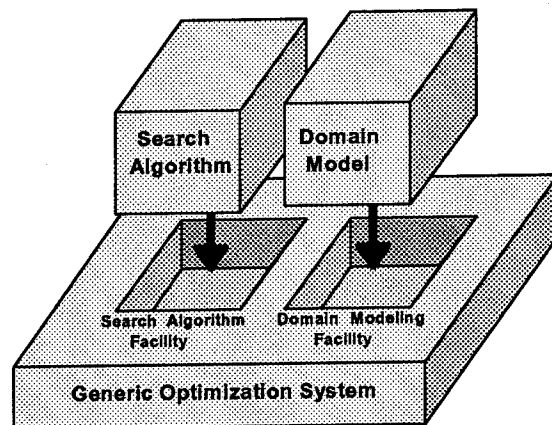


Figure 7. The GENOS Architecture

GENOS provides a carefully controlled system of communication between the search algorithm and the domain model. As shown in Figure 8, there are six basic functions required for a GENOS-based tool to function.

The *successor generator* is responsible for generating adjacent states from any given state. For the robust planner, the successor generator will employ the decision operators to generate successor states. The *evaluator* computes the objective function, which implements the optimization criteria. For the robust planner, the evaluator will

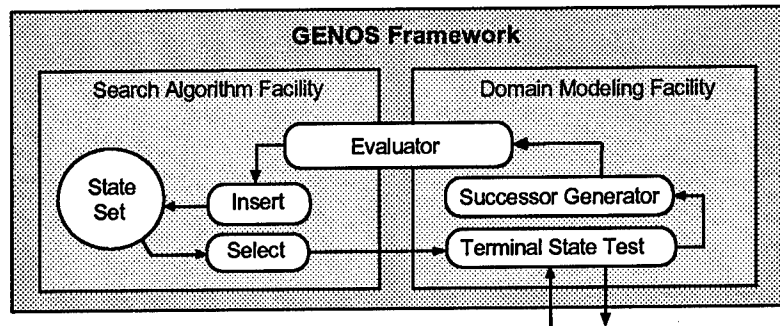


Figure 8. The GENOS Protocol Diagram

use expected utility as its objective function. The evaluator then passes the resulting value along with the state to the *insert* function in the search algorithm facility. This function places the state in the proper position within the state set. The *select* function then chooses the next state, which is tested to determine if it is a *terminal state*. If so, it is output to the user. If not, it is passed to the successor generator, and the process is repeated. In the simplest approach, the test for a terminal state would be based on having reached the end of a planning scenario. In more sophisticated approaches, it may be based on computation time expended, depth in the search tree, or other performance-related factors.

A preliminary version of GENOS has been implemented by the authors within ASI's Airborne Reconnaissance Evaluation and Analysis System (AREAS). It has been successfully used to develop a tasking model which assigns reconnaissance aircraft to different target sets over a period of operations.

ADVANCED APPLICATIONS

We have presented a simple example of how a robust planning system could function in a general aviation problem. However, the usefulness of a robust planner is best demonstrated in a more complicated scenario, such as a single engine, single pilot aircraft under actual Instrument Meteorological Conditions. When the Global Positioning System is certified for use with IFR navigation and a datalink provides information about local traffic and weather, pilots will have more flexibility in determining their flight path, thus allowing them to choose a more efficient route and make enroute changes. Single pilot IFR operations place a high workload on the pilot because navigation and communication tasks are increased. A robust planner could monitor the current position of the airplane and condition of its systems, and provide the pilot with options that will reduce the possibility of problems further along in the flight. In this way, the planner aids with decision making and information prioritization by assisting cockpit resource management and increasing the pilot's situational awareness.

Currently, there are many displays available that integrate traditional cockpit information (e.g., altitude, airspeed, attitude, and system status) with navigation information, such as position inputs from LORAN-C or GPS. These devices often include extensive airport and navaid databases, moving map displays, and standard cockpit information. A robust planning algorithm could be incorporated into such a system. It would process the information, anticipate future problems, evaluate several possible courses of action, and make recommendations to the pilot. A robust

planner could also aid with preflight planning as well as enroute replanning as various conditions change or emergencies arise.

CONCLUSIONS

There are significant applications to general and commercial aviation for a robust planning system. This paper demonstrates the advantages and use of a robust planner in a smart cockpit system. This system would not only improve information management in the cockpit during normal operations, it could also be used for inflight replanning during IFR operations or providing emergency procedures during emergency situations. We have presented a technique for increasing the robustness of planning in such a system by the use of utility functions. In addition, we have proposed a reactive implementation of the planner based on the GENOS framework for optimization.

Planning systems are also utilized in other areas of aviation. Air traffic control systems could benefit from the use of a more robust planning device, one that has the capability to "look ahead" and evaluate the effects of current actions on future events with more certainty. Maintenance and flight scheduling for commercial operations could also benefit from this technology.

One of the least expensive ways of increasing the productivity of a resource is to create a plan that better utilizes that resource. A robust planner is better able to account for unknowns, and consequently will increase the productivity of resources that operate in uncertain environments.

REFERENCES

- Corrigan, J., and Keller, K., "Pilot's Associate: An Inflight Planning Application," *AIAA Guidance, Navigation, and Control Conference*, Aug. 1989.
- Kanazawa, K., and Dean, T. "A Model for Projection and Action," *Proc. IJCAI-89*, Detroit, Michigan, pp. 985-99.
- Miller, C., Shalin, V., Geddes, N., and Hoshstrasser, B., "Plan-Based Information Requirements: Automated Knowledge Acquisition to Support Information Management in an Intelligent Pilot-Vehicle Interface," *Proc. of the 11th IEEE Digital Avionics Systems Conference*, Seattle, Washington, 1992, pp. 428-433.
- Russell, S., and Wefald, E., "Principles of Metareasoning," *Proc. of the First Int. Conf. on Principles of Knowledge and Reasoning*, Morgan-Kaufman Los Altos, California, 1989, pp. 400-411.
- Wellman, M., and Doyle, J., "Modular Utility Representation for Decision-Theoretic Planning," *Proc. First Int. Conf. on Artificial Intelligence Planning Systems*, 1992, pp. 236-242.
- Wellman, M., and Doyle, J., "Preferential Semantics for Goals," *AAAI-91*, pp. 698-703.

Wittig, T., and Onken, R., "Pilot Intent and Error Recognition as Part of a Knowledge Based Cockpit Assistant," *AGARD Combat Automation for Airborne Weapon Systems Man/Machine Interface Trends and Technologies*, Edinburgh, Scotland, 1993.

**PRESENT & FUTURE FUELS FOR RECIPROCATING
ENGINE POWERED AIRCRAFT
(OVERVIEW OF AUTOMOTIVE GASOLINE USAGE IN AIRCRAFT ENGINES)
PAUL O. PENDLETON
FEDERAL AVIATION ADMINISTRATION
1801 AIRPORT ROAD ROOM 100
WICHITA KANSAS 67209**

ABSTRACT

The purpose of this paper is to describe the current progress and problems associated with the use of automotive gasoline in aircraft and work on a new aviation fuel grade derived from automotive gasoline. Certain other countries' automotive gasoline will be reviewed. Anticipated performance of various automotive gasolines blended for international use are evaluated for their potential use, in aircraft and reciprocating aircraft engines. The potential of current and future gasoline blends consisting of high percentages of oxygenates [alcohol and Methyl Terterchary, Bunyl Ether (MTBE)] are assessed for their applicability to aircraft and aircraft engines.

INTRODUCTION

Aviation fuel refiners introduced 100 low lead (100LL) as an all purpose aviation gasoline to replace 80/87 and 100/130 grades during the earlier 1970's. Since that time, 100LL has been the primary gasoline available for certificated reciprocating engine/powered aircraft in the United States. Low compression engines power approximately 65% of the general aviation fleet. Low compression reciprocating engines were suspected to have an increase in maintenance and reduced time between overhaul (TBO) when subjected to continuous usage of 100LL aviation gasoline. Engine manufacturers subsequently made upper cylinder components available which improved the degraded TBO interval and reduced unscheduled maintenance costs. However, many owners and operators of low compression engine powered aircraft were not satisfied with the cost and performance of 100LL aviation gasoline when compared with their previous experiences with leaded 80/87 aviation gasoline.

Other than octane, the most significant difference between 100LL and 80/87 aviation gasoline is the tetraethyl lead (TEL) content. The maximum TEL content, as defined by the American Society for Testing and Materials (ASTM) Specification D910 for Standard Specification 100LL Aviation Gasoline, is 2 milliliter per gallon as compared to 0.5 milliliter per gallon for 80/87 aviation gasoline. Grade 100/130 aviation gasoline has a maximum of 4 milliliters of

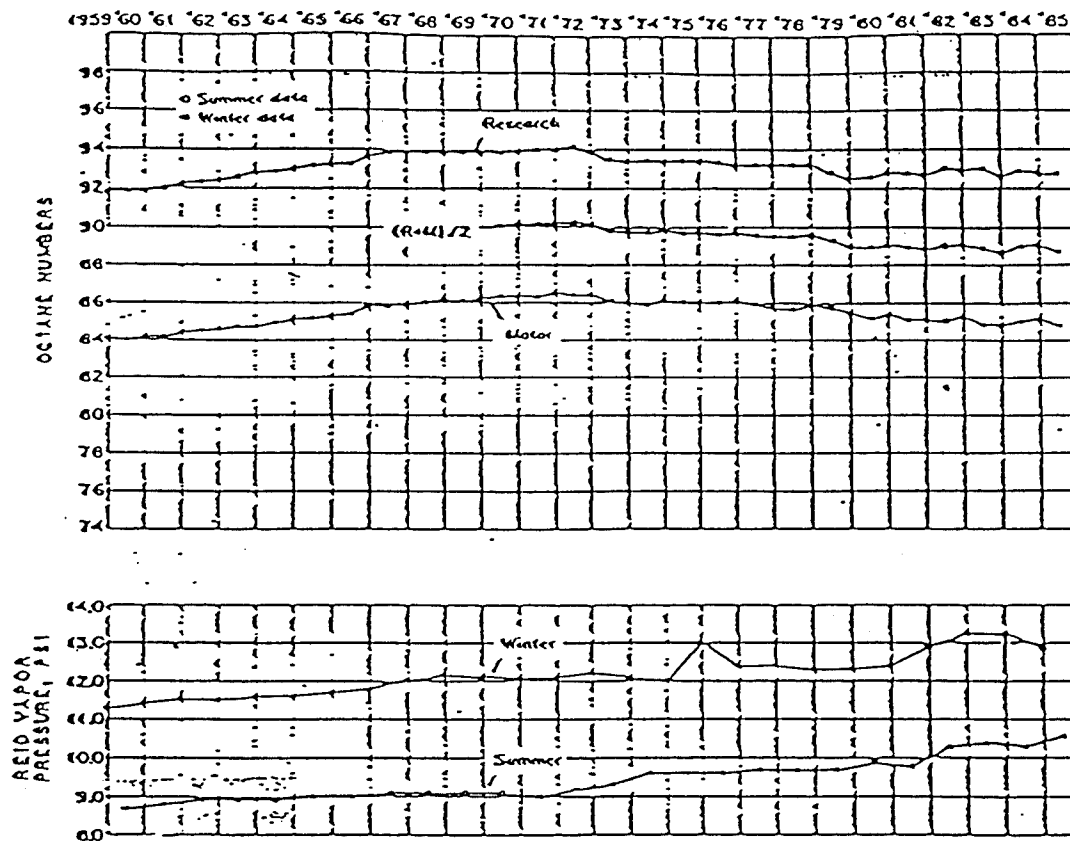
TEL per gallon. Therefore, there is approximately 4 times as much TEL per gallon in 100LL aviation gasoline as the maximum allowed for 80/87 aviation gasoline. Also, aromatics are used in unleaded 80/87 aviation gasoline and 100LL aviation gasoline as well as automotive gasoline to obtain higher fuel octane with no, or low amount of TEL.

A significant difference between aviation and automotive gasoline is the vapor pressure which is approximately twice as high on automotive gasoline as the maximum permitted on aviation gasoline. The two primary differences (TEL & Vapor Pressure) will be addressed in detail. A survey of service difficulty problems comparing the effects of 100LL and unleaded 80/87 aviation gasoline with automotive gasoline will also be presented. Environmental Protection Agency (EPA) involvement in gasoline will be reviewed.

BACKGROUND

Approximately 65% (125,000) of the general aviation fleet consist of aircraft powered by low compression engines. As of December 1993, approximately 48,000 type certificated civil aircraft were legally operating on automotive (motor) gasoline. Approximately 10,000 additional aircraft are suspected to be operating on automotive gasoline without obtaining approval from a certificate holder. These aircraft are mostly unmodified as far as the airframe and engine fuel system are concerned. They include low and high compression engines. Some aircraft have had extensive airframe & engine modification for suppression of detonation and vapor lock problems. Use of automotive gasoline in aircraft has risen from approximately 1 million gallons in 1983 to over 50 million gallons in 1993.

The topics presented in the abstract of this paper are considered significant to aircraft operating with any amount of motor gasoline. The author previously prepared a paper for publication by the Society of Automotive Engineers (SAE) No. 871012 and American Society for Testing & Materials (ASTM) No. STP1048, which reviewed the concerns of certificating and operating civil aircraft on automotive (motor) gasoline. The Federal Aviation Administration (FAA) aircraft certification regulatory body has reviewed this and the previous papers on aircraft operating on automotive (motor) gasoline and concur with its content. Future work by the FAA on alternate gasoline for piston engine powered aircraft involves determination of acceptable single grades octane for rating the fuel and establishment of acceptable single grade specifications.



OCTANE AND VAPOR PRESSURE COMPARISON 1959 THRU 1985

FIGURE 1

The data supplied by Figure 1 was provided by the National Institute for Petroleum and Energy Research (NIPER) and reproduced with their permission.

The data supplied by Figure 2 was derived from FAA Malfunction and Defect Reports.

The data supplied by Appendix A was provided by the Associated Octel Company Limited (OCTEL) and presented with their concurrence.

DISCUSSION

Octane (antiknock) Values & Detonation

The most significant concern of the majority of those associated with gasoline usage in civil aircraft has been that any alternate fuel octane (antiknock) value be sufficient to insure rated engine power is developed with adequate fuel flow margins to prevent detonation and that the alternate fuel vapor pressure is adequate for prevention of fuel flow interruption. Other less significant concerns address the potential of fuel extender and additives (hydrocarbon/and oxygenates) to adversely influence the airframe fuel system, engine combustion chamber and valve operation.

FUEL OCTANE

Most all low compression aircraft engines have been certificated for operation on automotive (motor) gasoline. There have not been any reports of engine detonation problems with any FAA type certificated aircraft engines approved for operation on 80/87 octane aviation grade gasoline and motor gasoline. Also, there have been no reports to the FAA, or the people involved in obtaining approval for use of motor gasoline in high compression aircraft engines, that these type certificated aircraft engines have had any operational problems when operated on motor gasoline with FAA approval. FAA witnessed test results reviewed to date indicate that engine detonation will very likely result in serious damage to those high compression aircraft engines operated on low octane (antiknock) motor gasoline. Some of the aircraft engines with compression ratios above 7.5 to 1 presently approved for operation on motor gasoline have been extensively modified, while others require no alterations to maintain adequate fuel flow margins against engine detonation. All aircraft engines with compression ratios above 7.5 to 1 that are approved for operation on motor gasoline require a fuel with an antiknock index (similar to octane rating) above 90 to insure there will be adequate margins to prevent detonation during normal engine operations. The limited number of approved high compression aircraft engines currently operating on motor gasoline have not reported any fuel related problems. There are several hundred aircraft equipped with mechanically supercharged engines rated above 1000 horsepower that are approved for operation on motor gasoline. These airplanes are equipped with engines that are considered to have low compression ratios, but use mechanical supercharger to increase takeoff and maximum continuous power. These engines have been reported to provide satisfactory service on motor gasoline when they are

operated in accordance with the approved airplane and engine type design.

FUEL VAPOR LOCK

The airframe and engine fuel systems have been reported to be free from vapor lock on all but a very few airplanes certificated for and operating on motor gasoline. Aircraft reported to have takeoff and/or inflight fuel vapor locking problems have been isolated to low wing models equipped with auxiliary fuel pumps mounted in a parallel arrangement. Some of the airplanes reporting a fuel vapor problem on motor gasoline were previously suspected to have similar problems on aviation gasoline. Certification test procedures for aircraft to be operated on automotive gasoline have been amended to include cold winter blend fuel subjected to a high (hot) temperature environment. The current procedures for hot weather evaluation of aircraft with pump fed fuel systems considered susceptible to vapor locking is as follows:

1. Use winter grade fuel with a Reid Vapor Pressure of 12.5 minimum.
2. Keep fuel cooled at a temperature of 11°C (52°F) or cooler in non-vented container.
3. Heat the aircraft with a minimum safe amount of automotive gasoline to a temperature of 43°C (110°F+0-5°F). (Reference FAA Advisory AC 23.961-1).
4. Prepare the airplane for takeoff in a manner that will insure the fuel temperatures do not fall below the values listed in 3 above.
5. Climb at maximum continuous power at best angle of climb to maximum altitude or at least 10,000 feet.
6. Perform normal cruise and descent operations.

The FAA Advisory AC 23.961-1 also states that service experience indicates the following test should be conducted on airplanes proposed for certification on motor gasoline. Use the fuel identified in 1 and 2 above and heat the airplane with a minimum safe amount of fuel to 29°C (85°F±2°F). Prepare the airplane for take off in a manner that will insure the fuel temperature does not fall below 28°C (83°F).

Perform 5 and 6 above.

The fuel temperatures for hot weather tests are based on the initial boiling point of motor gasoline. This is true for motor and aviation gasoline test method. Aviation grade gasoline has a higher initial boiling temperature and correspondingly lower Reid Vapor Pressure. Other than evaluation of any previous airframe or engine alterations, the fuel vapor locking tendencies of the airframe and engine fuel system is the only test currently being performed on those airplanes being considered for approved operation on motor gasoline. Some type certificated aircraft that previously were approved for operation on aviation gasoline did not demonstrate satisfactory performance when subjected to the automotive gasoline test procedure previously described.

Consequently, some civil type certificated aircraft will require modifications to the airframe and/or engine fuel system in order to safely operate on single grade high vapor pressure gasoline. Evaluation of gravity feed fuel systems has indicated that inflight testing for hot weather sensitivity to vapor lock is seldom necessary. There have been some informal reports of high wing gravity feed fuel system equipped airplanes operating on motor gasoline experiencing fuel vapor problems. However, these reports are not wide spread. The gravity fuel feed airplanes, informally reported to have had fuel vapor problems previously, reported similar problems on aviation gasoline.

Figure Number 1 depicts the octane and fuel vapor pressures of automotive gasoline for a 25 year period. They have been maintained recently, primarily due to environmental considerations. These fuels are shown to have been consistent in values on a nationwide basis. The consistency is expected to be maintained; but the increasing use of higher cut hydrocarbons, aromatics or (unsaturated cyclic hydrocarbons) or oxygenates may possibly adversely affect the weathering (prolonged storage and/or elevated temperature) effects of motor gasoline. Weathering effects of Non oxygenated motor gasoline octane ratings have had no adverse influence on fuels tested in laboratories. Field experience obtained during the twelve years of aircraft operating on motor gasoline supports the results of the weathering tests.

Altitude influenced pressure changes have not been thought to create problems for the aircraft engines presently approved for operation on motor gasoline. This is true for the normally aspirated and mechanically supercharged engines which are rated from 65 to 1250 horsepower. The 12 years of operating civil aircraft at low and high altitudes up to 20,000 feet during winter and summer weather have only required occasional use of the fuel boost pump to maintain normal engine power. However, as previously stated, some

gravity feed fuel system equipped airplanes have reported fuel flow interruption problems similar to problems previously reported on these same airplanes when they were operated on aviation gasoline.

FUEL EXTENDERS

Alcohol blended gasoline is considered likely to reduce the range of intermittent combustion aircraft engines as the heating value of this is less than hydrocarbon based gasoline. The range of aircraft operating on non oxygenated motor gasoline today is as good as when these same airplanes were operated exclusively on aviation gasoline. This is because the heating value of non oxygenated motor gasoline is slightly higher than aviation gasoline.

Oxygenated motor gasolines containing Methyl Tertiary Butyl Ether (MTBE) are presently approved for operation of type certificated civil aircraft and/or aircraft engines. Oxygenated fuels containing Alcohol are considered to rapidly age some natural rubber aircraft fuel system components. Also, oxygenated fuels containing alcohol have been determined to be corrosive and unstable and they tend to encourage the alcohol to separate from the gasoline. MTBE is considered an acceptable oxygenate blended gasoline. The aging problem of alcohol is thought to be resolvable by using synthetic materials such as the Dupont trademark Teflon, which are considered compatible with alcohol. The water suspension problem may require the use of special filters that might not presently be cost effective. Alcohol blended oxygenated gasoline has demonstrated more vapor locking tendencies than any hydrocarbon based gasoline. The approval of MTBE has not resulted in an increase in any adverse service reports on aircraft operated on automotive gasoline.

DETERGENTS AND AROMATICS

Most aircraft presently approved for operation on motor gasoline were originally required to have aviation gasoline with an octane rating of 80/87 or lower. Grade 80/87 aviation gasoline has never had detergents. Aviation grade 80/87 available in the US today has no lead content. Aromatics are used for octane enhancement of 80/87 aviation gasoline that has been refined for that last 10 years. Detergents and aromatics are both currently used in motor gasoline. Aromatics are used in 100LL aviation gasoline. The levels of such components are acceptable at the present time, but their future concentrations should be kept under review. The potential for an increase in detergents may be initiated by continued fouling problems with automotive fuel injection systems. The potential for an increase in

aviation or motor gasoline aromatics may be brought about by a demand for high octane no lead fuel.

Present levels of detergents and aromatics in motor gasoline are considered acceptable for usage in fuels used for intermittent combustion engine (spark ignition) piston powered aircraft. Varnish removal could result in sticking carburetor needle valves and other fuel metering controls. This has not been reported as a service problem to date (see Figure 2).

LEAD

Lead corrosion is not likely to be a problem on reciprocating aircraft engines operated with the reduced amount of lead presently available and anticipated to be used in countries with rigid air pollution programs. All gasoline currently available contain less lead than previous aviation gasoline of the same approximate grade.

FACTORS INFLUENCING FIELD EXPERIENCE

Suspected factors that might adversely affect aircraft operated on motor gasoline are most often related to fuel additives that are capable of deteriorating, softening or drying out certain nonmetallic airframe and engine fuel system components. Some of the components perceived as being adversely affected by exposure to motor gasoline are fuel quantity transmitter floats, carburetor floats, flexible fuel lines, fuel metering seals, valves, diaphragms, fuel bladders, fuel system seals and pump components. Analysis of adverse service reports submitted on motor gasoline indicate that most of the problems are similar when operating on aviation fuel (see Figure 2). The motor gasoline additives that are used to maintain an acceptable antiknock index (octane rating) are those same additives used in aviation gasoline. These additives (most likely high cut hydrocarbons) best known as aromatics, are thought to accelerate the aging process of certain nonmetallic airplane fuel system components.

As the availability of tetra/ethyl lead (TEL) in motor (automotive) gasoline is eliminated, the practicality of using TEL to increase octane or performance values in aviation gasoline will be severely curtailed. Grade 80/87 aviation gasoline available in the US for the past 10 years has had no lead. Due to the comparatively low volume of leaded aviation gasoline being refined (less than 0.5% of automotive gasoline), this product may soon become more expensive to provide nationwide. This assessment is based on the geographic locations of those refineries currently capable of providing leaded gasoline in accordance with aviation specifications.

Aircraft and intermittent combustion aircraft piston engines that can be economically modified for operation on motor gasoline should be able to use the fuels anticipated to be available for the next twenty years. Aircraft that have been operated on 100LL aviation gasoline that were originally designed for operation on 80/87 aviation gasoline have reported more problems associated with flexible fuel hoses and fuel bleeders. These same problems have been reported to a lesser degree when similar aircraft are operated on motor gasoline. It is thought that the availability of 100LL, in advance of widespread motor gasoline usage in aircraft, encouraged more timely replacement of components susceptible to the aromatics currently used in all domestic gasoline. Aromatics are expected to continue to be a problem for aircraft engine and airframe non-metallic fuel system components.

Reports of deterioration of nonmetallic fuel floats (carburetor and fuel quantity gauging) fuel injector seals and gaskets continue to be received. This is true despite the obvious decline in the usage of general aviation aircraft.

The reports received indicated that the number of safety related occurrences have not exceeded previous levels. Most automotive gasoline related reports are still fewer in number than those same type of reports on aircraft operated on 100LL aviation gasoline (see Figure 2).

Aircraft engine overhaul facilities and operators are reporting overhaul intervals for engines operated on motor gasoline are equivalent to those intervals for engines designed for and operated on 80/87 aviation gasoline. This statement applies to those engines that are occasionally subjected to a leaded fuel. Aircraft engines operated with a wide variety of lubricating oils and exclusively on unleaded motor or aviation gasoline have been reported to be unable to maintain overhaul intervals established for operation on leaded aviation gasoline. All aviation gasoline ratings above 100 performance ratings which are currently maintained by including a fixed amount of TEL.

Many aircraft operators are mixing unleaded motor gasoline with aviation gasoline in order to maintain an acceptable amount of TEL, which is reported to act as a lubricant and heat dissipater on the engine valve face and stem as well as the valve seat and guide. This procedure is preferred by some operators rather than limiting their engine oil lubricants to specific brands and grades. The original problems associated with 100LL aviation gasoline were related to a lead content significantly above that used in 80/87 grade fuel. Therefore, the maximum and minimum amount

of TEL in an engine over its service life has been determined to be a significant factor in relation to its anticipated hours between minor and major overhaul when a variety of approved engine oils are used.

It is thought that there will be an increase in the usage of portable fuel storage facilities of airfields dispensing gasoline. This perception is based on an anticipated increased aircraft usage of motor gasoline. If this concept materializes, it is thought there will be a decrease in aircraft accident and/or incidents related to low or contaminated fuel.

Motor gasoline purchased for aircraft consumption is most often provided by the same wholesaler providing this product to retail automobile gasoline dealers. Motor gasoline is though to be closely monitored by the Environmental Protection Agency (EPA) for its chemical composition. As a result of the EPA monitoring it is believed that motor gasoline quality is as consistent as the quality established for aviation gasoline.

AVIATION GRADE GASOLINE DERIVED FROM AUTOMOTIVE GASOLINE

A proposal is being made to the American Society of Materials and Testing (ASTM) for a new aviation gasoline specification based on the ASTM automotive gasoline specification D4814. The proposal is intended to enable facilities such as gasoline refiners and distributors to select certain stocks of gasolines refined to D4814 and reidentify these gasoline stocks as aviation graded gasoline. The proposal is intended to enable D4814 refined gasolines that meet the motor test method for octane ratings that contain no lead and no alcohol with a certain maximum Reid vapor pressure to be reidentified to the as yet unidentified proposed aviation gasoline. This work is being accomplished by ASTM Committee D2 on Petroleum Products and Lubricants. It is anticipated the proposed ASTM aviation gasoline specification will be available for low octane fuels by December 1995. In Sweden, unleaded aviation gasoline has been used between the years 1980 through 1992 (last reporting period) without any adverse service problems. However, the producers of the Swedish Avgas (91/96UL) recommend that aircraft be operated with full or semi-synthetic engine oils that are multi grade and only specific single grade oils.

CONCLUSION

Usage of automobile (motor) gasoline in civil aircraft has been known to exist for many years. The FAA approved usage of this product has met with widespread acceptance by the owners and operators of civil aircraft. Gasoline should be capable of being refined that will be marketed as

satisfactory for ground and airborne intermittent combustion reciprocating engine powered vehicles. Oxygenated gasoline's containing alcohol are considered the only motor gasoline not presently compatible with aircraft and aircraft engine fuel systems. High compression and turbocharged aircraft engines may require extensive modifications in order to maintain rated engine power with adequate margins to prevent engine detonation. If Reid vapor pressure can be maintained at a maximum of 7 as identified by the current aviation gasoline specification ASTM D910, airframe fuel systems should not require major modifications for fuel vapor lock control. Otherwise, as reported when testing winter blend autogas with Reid vapor limits of 15, airframe fuel system alterations will be necessary.

**FAA SUMMARY OF FUEL RELATED INCIDENTS
JANUARY 1988 THRU DECEMBER 1992**

**A. FUEL CONTAMINATION - 209 REPORTS BROKEN DOWN
AS FOLLOWS:**

- 10 TURBINE FUEL AIRCRAFT
- 85 PISTON AIRCRAFT - TYPE OF FUEL NOT REPORTED
- 82 PISTON AIRCRAFT - AVGAS FUELED
- 32 PISTON AIRCRAFT - AUTOGAS FUELED

B. MATERIAL COMPATIBILITY PROBLEMS

- 2 REPORTS ON AUTOGAS FUELED AIRCRAFT
- 1 REPORTS ON AVGAS FUELED AIRCRAFT

C. FUEL VAPOR LOCK

- 2 REPORTS ON AUTOGAS FUELED AIRCRAFT
- 1 REPORT ON AVGAS FUELED AIRCRAFT

D. VALVE TRAIN PROBLEMS (GUIDE & STEM EROSION)

- 1 REPORT ON AUTOGAS FUELED AIRCRAFT

E. CARBURETOR ICING

- 1 REPORT ON AUTOGAS FUELED AIRCRAFT

FIGURE 2

REFERENCES: (SEE PAGE 3)

APPENDIX-A: (SEE PAGE 12 thru 25)

(APPENDIX -A)

AFRICA	Grade	Range of Octane Number		Range of Lead Content Grams Metallic Lead=gPb United States Gallon=USG	
		Research Method	Motor Method	gPb/litre	gPb/USG
Algeria	Premium	98	---	0.65	2.46max
		96	---	0.65	2.46max
	Regular	90min	---	0.65	2.46max
Angola	Regular	90	---	0.77max	2.91max
Benin	Premium	95	---	0.84max	3.18max
	Regular	83	---	0.84max	3.18max
Botswana	Premium	93	84	0.44	1.67
Burkina Faso (Upper Volta)	Regular	83	---	0.84max	3.18max
Burundi	Premium	95	---	0.84max	3.18max
		93	---	0.84max	3.18max
	Regular	90	---	0.84max	3.18max
		87	---	0.84max	3.18max
Cameroon	Premium	96	---	0.84max	3.18max
		95	---	0.84max	3.18max
	Regular	91	---	0.84max	3.18max
		85	---	0.84max	3.18max
Canary Islands (Spain)	Premium	97min	85min	0.46max	1.51max
	Regular	92min	80min	0.40max	1.51max
Cape Verde Islands	Regular	85	80	0.63	2.38
		84	79	0.11	0.42
Central African Republic	Premium	95	---	0.84max	3.18max
	Regular	83	---	0.84max	3.18max
Chad	Premium	95	---	0.84max	3.18max
		93	---	0.84max	3.18max
	Regular	85	---	0.84max	3.18max
		83	---	0.84max	3.18max
Comoros	Regular	87	---	0.35	1.32
Congo	Premium	96	---	0.60	2.27
		95	---	0.34	1.29
Djibouti	Premium	93	---	0.55	2.08
	Regular	79	---	0.55	2.08

AFRICA	Grade	Range of Octane Number		Range of Lead Content	
		Research Method	Motor Method	gPb/litre	gPb/USG
Egypt	Super 90	90min	--	0.02	0.08
	Super 80	80min	--	0.30	1.14
Equatorial Guinea	Regular	87		0.84max	3.18max
Ethiopia	Regular	79		0.42max	1.60max
Gabon	Premium	95	83	0.84max	3.18max
		93	81	0.84max	3.18max
	Regular	85	74	0.84max	3.18max
		84	73	0.84max	3.18max
Gambia	Premium	95	--	0.80max	3.03max
	Regular	93	--	0.84	3.18
Ghana	Premium	94	--	0.63max	2.38max
		93	--	0.63max	2.38max
	Regular	85	--	0.53max	2.01max
Guinea	Regular	93	--	0.84max	3.18max
Guinea, Bissau	Premium	96	--	0.84max	3.18max
	Regular	86	--	0.84max	3.18max
Ivory Coast	Premium	95	--	0.46	1.74
	Regular	87	--	0.51	1.93
Kenya	Premium	95	--	0.84max	3.18max
		93	--		
	Regular	83	--	0.84max	3.18max
	Gasohol	93	--		
		83	--	--	--
Lesotho	Regular	93	--	0.60	2.27
		87	--	0.60	2.27
Liberia	Regular	93	85min	0.77max	2.91max
		83			
Libya	Premium	98max	89	0.80max	3.03max
Madagascar	Premium	95	--	0.84	3.18
	Regular	87	--	0.84	3.18
Madeira (Portugal)	Premium	98min	--	0.40max	1.51max
	Regular	90min		0.40max	1.51max

AFRICA	Grade	Range of Octane Number		Range of Lead Content	
		Research Method	Motor Method	gPb/litre	gPb/USG
Malawi	Gasohol	93	--	0.53	2.01
Mali	Premium	97	--	0.80	3.03
		95	--	0.46	1.74
	Regular	88	--	0.44	1.67
		87	--	0.31	1.17
Mauritania	Premium	97	--	0.80	3.03
		95	--	0.40	1.51
	Regular	90	--	0.80	3.03
		87	--	0.40	1.51
Mauritius	Premium	97	85	0.84	3.18
		95	--	0.84	3.18
Morocco	Premium	97	--	0.55	2.08
		95	--	0.01	0.04
	Regular	88	--	0.20	0.76
		87	--	0.01	0.04
Mozambique	Premium	93	83min	0.65	2.46
	Regular	83	--	0.40	1.51
Namibia	Regular	93	83	0.60	2.27
Niger	Premium	96min	--	0.65max	2.46max
	Regular	90min	--	0.65max	2.46max
Nigeria	Premium	90	--	0.66	2.50
Reunion	Premium	95	85	0.84	3.18
	Regular	79	--	0.84	3.18
Rwanda	Premium	95	--	0.84max	3.18max
	Regular	83	--	0.84max	3.18max
Sahara West (Morocco)	Regular	83	--	0.84max	3.18max
Saint Helena	Super	98	84	0.46	1.74
	Premium	93	--	0.46	1.74
Senegal	Premium	97	--	0.80	3.03
		95	--	0.46	1.74
	Regular	88	--	0.44	1.67
		87	--	0.31	1.17

AFRICA	Grade	Range of Octane Number		Range of Lead Content	
		Research Method	Motor Method	gPb/litre	gPb/USG
Seychelles	Premium	95	—	0.84max	3.18max
Sierra Leone	Premium	91	—	0.85max	3.22max
	Regular	86	—	0.85max	3.22max
		83	—	0.45max	1.70max
Somalia	Regular	79	—	0.84max	3.18max
South Africa	Super	98	88	0.60	2.27
	Premium	93	85	0.60	2.27
	Regular	87	—	0.60	2.27
				0.40	1.51
Sudan	Premium	98	—	0.53	2.01
		90	—	0.49	1.85
	Regular	84	—	0.34	1.29
		78	—	0.20	0.76
Swaziland	Premium	98	89	0.84max	3.18max
	Regular	93	85	0.84	3.18max
Tanzania	Premium	94	—	0.70	2.65
		93	—	0.50	1.89
	Regular	84	—	0.40	1.57
		83	—	0.20	0.76
Togo	Premium	93	—	0.84max	3.18max
	Regular	83	—	0.84max	3.18max
Tunisia	Premium	99	—	0.63max	2.38max
		97	—	0.63max	2.38max
	Regular	91	—	0.63max	2.38max
		89	—	0.63max	2.38max
Uganda	Premium	93	83	0.84max	3.18max
	Regular	83	—	0.84max	3.18max
Zaire	Regular	93	—	0.63max	2.38max
Zambia	Premium	95	—	0.71max	2.69max
	Regular	87	—	0.71max	2.69max
Zimbabwe	Regular	93	—	0.84max	3.18max

Australia, New Zealand and Pacific Islands	Grade	Range of Octane Number		Range of Lead Content	
		Research Method	Motor Method	gPb/litre	gPb/USG
Australia	Premium	97	88	0.84max 0.40	3.18max 1.51
	Unleaded Reg.	93	82	<0.013	<0.05
		91	82	<0.013	<0.05
Fiji, Niue, Western Samoa, Tonga, Kiribati and Cook Is.	Premium	97	88	0.84max	3.18max
	Regular	90	--	0.63max	2.38max
Guam	Premium	97	--	0.84max	3.18max
	Regular	92	--	0.84max	3.18max
	Unleaded Reg.	91	--	<0.01	<0.05
Hawaii (U.S.A.)	Premium	98	89	0.29	1.10
		95	84	0.15	0.57
	Regular	94	86	0.29	1.10
		91	84	0.03	0.11
	Unleaded Prem.	97	87	<0.01	<0.05
	Unleaded Reg.	89	80	<0.01	<0.05
Marshall Islands	Premium	95	--	0.84max	3.18max
Nauru and Ocean Islands	Premium	97	88	0.84max	3.18max
New Caledonia, Vanuatu	Premium	97	88	0.84max	3.18max
New Zealand	Premium	96	89	0.45max	1.70max
	Regular	91	85min	0.84max	3.18max
	Unleaded Reg.	93	82min	<0.01	<0.05
		91	82min		
Norfolk Islands	Premium	97	88	0.84max	3.18max
Papua, New Guinea and Solomon Islands	Premium	97	88	0.84max	3.18max
Tahiti, Society Islands	Premium	97	--	0.84max	3.18max
	Regular	95	--	0.84max	3.18max

Caribbean Area	Grade	Range of Octane Number		Range of Lead Content	
		Research Method	Motor Method	gPb/litre	gPb/USG
Antigua	Premium	93	--	0.84max	3.18max
Aruba	Premium	95	--	0.84max	3.18max
	Regular	92	--	0.84max	3.18max
Bahamas	Super	97	--	0.84max	3.18max
	Premium	93min	--	0.67max	2.54max
Barbados	Premium	95min	--	0.84max	3.18max
Cuba	Premium	96	--	0.84max	3.18max
	Intermediate	84	--	0.84max	3.18max
Curacao	Premium	97	85	0.84max	3.18max
	Intermediate	92	--	0.84max	3.18max
Dominican Republic	Premium	95min	85	0.84max	3.18max
Guadeloupe	Premium	98	--	0.64max	2.42max
		97	--	0.64max	2.42max
	Regular	90	--	0.64max	2.42max
Haiti	Premium	95min	--	0.84max	3.18max
Jamaica	Premium	95	85	0.84max	3.18max
	Regular	87	80	0.84max	3.18max
Martinique	Premium	98	--	0.64max	2.42max
		97	--	0.64max	2.42max
	Regular	90	--	0.64max	2.42max
Puerto Rico	Premium	95min	83min	<0.13	<0.49
	Unleaded Reg.	91min	83min	<0.005	<0.02
Saint Martin	Regular	93min	--	0.84max	3.18max
Trinidad and Tobago	Premium	97	--	0.77	2.91
		95	--	0.77	2.91
	Regular	88	--	0.77	2.91
Virgin Islands	Premium	94	84	1.12max	4.24max
	Unleaded Reg.	91min	83min	<0.005	<0.02

Central America	Grade	Range of Octane Number		Range of Lead Content	
		Research Method	Motor Method	gPb/litre	gPb/USG
Belize	Premium	94	89	0.84	3.18
	Regular	90	86	0.75	2.84
Costa Rica	Regular	88min	79min	0.84max	3.18max
El Salvador	Premium	95	85min	0.70max	2.65max
	Regular	87	77min	0.50max	1.89max
Guatemala	Premium	95	--	0.63max	2.38max
	Regular	87	--	0.22max	0.83max
Honduras	Premium	95	--	0.84max	3.18max
	Regular	87	--	0.84max	3.18max
Nicaragua	Premium	95	--	0.84max	3.18max
	Regular	87	--	0.63max	2.38max
Panama	Premium	95	87	0.84max	3.18max
	Regular	87	81	0.84max	3.18max
Europe					
Austria	Premium	98	87	0.15max	0.57max
	*Regular	88	79	0.15max	0.57max
	Unleaded Prem.	95	85	Nil	Nil
	Unleaded Reg.	91	82.5	Nil	Nil
Azores (Portugal)	Premium	98min	--	0.40max	1.51max
	Regular	90min	--	0.40max	1.51max
Belgium	Premium	98	86	*0.40max	1.51max
	Regular	91	82	*0.40max	1.51max
		90	81	0.40max	1.51max
		95	85	Nil	Nil
	Unleaded Reg.	91	82.5	Nil	Nil
Bulgaria	Premium	96min	--	0.35max	1.32max
	Intermediate	93min	--	0.35max	1.32max
	Regular	86min	--	*0.20max	0.76max
Cyprus	Premium	98	--	0.84	3.18
			--	0.45	1.70
	Regular	89	--	0.40	1.51
		87	--	0.10	0.38

Europe	Grade	Range of Octane Number		Range of Lead Content	
		Research Method	Motor Method	gPb/litre	gPb/USG
Czechoslovakia	Premium	96min	88min	0.25max	0.94max
	Regular	90min	82min	0.25max	0.94max
	Unleaded Reg.	91	82min	<0.01	<0.05
Denmark	Premium	98min	88min	0.15max	0.57max
	*Intermediate	96	85	0.15max	0.57max
	Regular	92	83	0.15max	0.57max
	Unleaded Prem.	95	85	Nil	Nil
	Unleaded Reg.	91	82.5	Nil	Nil
Eire	Premium	97.4	86.5	0.15max	0.57max
	Intermediate	93	--	0.15max	0.57max
	Regular	90	82	0.15max	0.57max
Faroe Islands (Denmark)	Premium	97	86	0.15max	0.57max
Finland	Premium	99	87	0.40max	1.51max
	Regular	92	83	0.15max	0.57max
	Unleaded Prem.	95	85	Nil	Nil
France	Premium	98	88	0.40max	1.51max
		97	86	0.40max	1.51max
	Regular	91	84	0.40max	1.51max
		89	82	0.40max	1.51max
Germany, East	Extra	92min	84min	0.31max	1.17max
	Regular	88min	84min	0.31max	1.17max
Germany, West	Premium	100	90	0.15max	0.57max
		98	88	0.15max	0.57max
	Regular	95	85	0.15max	0.57max
		92	82	0.15max	0.57max
	Unleaded Prem	95min	85min	0.013max	0.05max
	Unleaded Reg	91	82.5	0.013max	0.05max
Gibraltar	Premium	98	87	0.84max	3.18max
	Regular	88	--	0.84max	3.18max
Greece	Premium	98	--	*0.40max	1.51max
		96	--	*0.40max	1.51max
	Regular	90	--	*0.40max	1.51max
Hungary	Super	98min	88	0.40max	1.51max
	Premium	92min	83	0.40max	1.51max
	Regular	86min	77	0.40max	1.51max

Europe	Grade	Range of Octane Number		Range of Lead Content	
		Research Method	Motor Method	gPb/litre	gPb/USG
Iceland	Premium	98	—	*0.40max	1.51max
	Regular	93	85	*0.40max	1.51max
Italy	Premium	98	91	0.40max	1.51max
		97	87	0.40max	1.51max
	Regular	86	83	0.40max	1.51max
		85	82	0.40max	1.51max
	Agricultural	86	83	0.40max	1.51max
Luxembourg	Premium	99	92	0.15	0.57
		98	88	0.15	0.57
	Regular	93	87	0.15	0.57
		91	82	0.15	0.57
	Unleaded Prem.	95	85	Nil	Nil
Malta	Premium	98	87	0.84max	3.18max
Monaco	Premium	98	91	0.40max	1.51max
		97	86	0.40max	1.51max
	Regular	91	85	0.40max	1.51max
		89	82	0.40max	1.51max
Netherlands	Premium	98	88	*0.40max	1.51max
			87	*0.40max	1.51max
	Regular	91	82.5	*0.40max	1.51max
	Unleaded Reg.	91	82.5	0.013max	0.05max
Norway	Premium	98min	89	0.15max	0.57max
		98min	87	0.15max	0.57max
	*Regular	94	88	0.15max	0.57max
		93	85	0.15max	0.57max
	Unleaded Prem.	95min	87	0.013max	0.05max
		95min	85	0.013max	0.05max
Poland	Premium	94	86	0.33	1.25
	Regular	78	76	0.55	2.08
Portugal	Premium	98min	—	0.40max	1.51max
	Regular	90min	—	0.40max	1.51max
Romania	Premium	97	88	0.60max	2.27max
		95	86	0.60max	2.27max
	Regular	89	81	0.60max	2.27max
		87	79	0.60max	2.27max

Europe	Grade	Range of Octane Number		Range of Lead Content	
		Research Method	Motor Method	gPb/litre	gPb/USG
Spain	Premium	97min	85min	0.40max	1.51max
	Regular	92min	80min	0.40max	1.51max
Sweden	Premium	98min	87min	0.15max	0.57max
	Blend	96min	86min	0.15max	0.57max
	*Regular	93min	—	0.15max	0.57max
	Unleaded Prem.	95min	85min	0.013max	0.05max
Switzerland	Premium	98.5	88.5	0.15max	0.57max
	Regular	91.5	84.5	0.15max	0.57max
	Unleaded Prem.	95	85	Nil	Nil
	Unleaded Reg.	91	82.5	Nil	Nil
Turkey	Premium	95min	84	0.84max	3.18max
	Regular	91min	81	0.42max	1.59max
Union of Republics	Premium	98	89	0.38max	1.44max
	Regular	93	85	0.38max	1.44max
		80	76	0.18max	0.68max
	Unleaded Prem.	95	86	Nil	Nil
	Unleaded Reg.	93	85	Nil	Nil
		80	76	Nil	Nil
United Kingdom	Premium	97min	86min	0.15max	0.57max
	Intermediate	93min	82min	0.15max	0.57max
	Regular	90min	80min	0.15max	0.57max
Yugoslavia	Premium	98min	91	0.60	2.27
		—	81	0.40	1.51
	Regular	87	82	0.60	2.27
		86	76	0.10	0.38
	Unleaded Prem.	95	85min	Nil	Nil
North America					
Alaska	Premium	98	89	0.29	1.10
		95	84	0.15	0.57
	Regular	94	86	0.29	1.10
		91	84	0.03	0.11
	Unleaded Prem.	97	87	<0.01	<0.05
	Unleaded Reg.	89	80	<0.01	<0.05
Burmuda	Premium	97	87	0.84max	3.18max

North America	Grade	Range of Octane Number		Range of Lead Content	
		Research Method	Motor Method	gPb/litre	gPb/USG
Canada	Regular	94	86	*0.65	2.46
		93	85	*0.30	1.14
	Unleaded Prem.	97	87	<0.01	<0.05
		96	86	<0.01	<0.05
	Unleaded Reg.	94	84	<0.01	<0.05
		93	83	<0.01	<0.05
Greenland	Premium	97	87	0.15max	0.57max
Mexico	Unleaded Reg.	91	84	0.014max	0.05max
	Regular	81	78	0.28max	1.06max
United States of America	Unleaded Prem.	100	89	<0.01	<0.05
		93	84	<0.01	<0.05
	Unleaded Reg.	96	87	<0.01	<0.05
		88	80	<0.01	<0.05
	Regular	97	87	<0.03	<0.10
		87	82	<0.03	<0.10
Orient					
Brunei	Premium	95	—	*0.84max	3.18max
	Regular	85min	—	*0.50max	1.89max
Burma	Regular	79	—	0.56max	2.12max
China	Premium	97	89	0.78	2.95
		95	85	0.27	1.02
	Regular	93	81	0.48	1.82
		81	71	0.01	0.04
	Unleaded Reg.	93	85	Nil	Nil
		76	71	Nil	Nil
Hong Kong	Premium	97	85	0.25max	0.95max
Indonesia	Premium	98	—	0.84max	3.18max
	Regular	87	—	0.70max	2.65max
Japan	Unleaded Prem.	99	87	Nil	Nil
	Unleaded Reg.	91	83	Nil	Nil
	Premium	98	89	0.21	0.80
Korea South	Premium	95	87	0.32max	1.21max
	Regular	88	78	0.32max	1.21max
Laos	Super	95	—	0.40	1.51
	Regular	85	—	0.40	1.51

Orient	Grade	Range of Octane Number		Range of Lead Content	
		Research Method	Motor Method	gPb/litre	gPb/USG
Macau(China)	Premium	98	88	0.84max	3.18max
	Regular	85	80	0.84max	3.18max
Malaysia West	Premium	97min	88min	0.40max	1.51max
	Premium	85min	—	0.40max	1.51max
	Premium	95min	86min	0.40max	1.51max
	Regular	85min	—	0.40max	1.51max
Phillippines	Premium	93	86	1.05max	3.97max
	Regular	81	—	1.05max	3.97max
Singapore	Premium	97	88	0.40max	1.51max
	Premium	95	—	0.40max	1.51max
	Special	92	—	0.40max	1.51max
Taiwan(China)	Premium	95	86	0.15max	0.57max
	Unleaded Reg.	92	—	Nil	Nil
Thailand	Premium	95	86	0.45	1.70
	Regular	83	—	0.45	1.70
South America					
Argentina	Gasohol Prem.	97	—	0.48	1.82
	Gasohol Regular	86	—	0.48	1.82
	Premium	93.5min	—	0.63	2.38
	Regular	84	—	0.74	2.80
		83	—	0.74	2.80
Bolivia	Premium	90min	—	0.24	0.91
				0.29	1.10
	Special	80min	—	0.08	0.30
				0.16	0.61
Brazil	Fuel Alcohol	109	90	Nil	Nil
	Gasohol	97	80min	0.84	3.18max
Chile	Premium	93	84	0.80max	3.03max
	*Intermediate	91	80	0.80max	3.03max
	Intermediate	86	78	0.80max	3.03max
	Regular	81	76	0.80max	3.03max
Columbia	Premium	92	—	0.84max	3.18max
	Regular	80min	—	0.40max	1.51max

South America	Grade	Range of Octane Number		Range of Lead Content	
		Research Method	Motor Method	gPb/litre	gPb/USG
Ecuador	Super	92	---	0.40max	1.51max
	Extra	80	---	0.84max	3.18max
	Unleaded Reg.	60	---	Nil	Nil
Guiana, French	Premium	98	---	0.64max	2.42max
	Regular	90	---	0.64max	2.42max
Guyana	Premium	93min	--	0.54	2.04
	Regular	83min	---	0.54	2.04
Paraguay	Methanol	109	89	Nil	Nil
	Premium	93min	--	0.84max	3.18max
	Regular	85min	--	0.84max	3.18max
Peru	Premium	95	---	0.84max	3.18max
	Regular	84	---	0.84max	3.18max
		80	---	0.84max	3.18max
Surinam	Premium	95	---	0.66	2.50
				0.50	1.89
				0.55	2.08
	Regular	83	---	0.12	0.45
Uruguay	Premium	95	--	*0.30	1.14
	Regular	80	---	*0.30	1.14
Venezuela	Premium	95	87min	0.84max	3.18max
		91	87min	0.84max	3.18max
	Regular	89	80min	0.84max	3.18max
		83	80min	0.84max	3.18max
South-West Asia					
Afghanistan	Regular	83	---	0.56max	2.12max
Bahrain	Super	98	---	0.84max	3.18max
	Premium	90	---	0.84max	3.18max
Bangladesh	Premium	98	---	1.11	4.22
	Regular	80	---	0.44	1.67
India	Premium	93min	---	0.80max	3.03max
	Regular	87min	--	0.56max	2.12max

South-West
Asia

	Grade	Range of Octane Number		Range of Lead Content	
		Research Method	Motor Method	gPb/litre	gPb/USG
Iran	Premium	95	—	0.56max	2.12max
	Regular	88	—	0.56max	2.12max
Iraq	Premium	93	86	0.79max	2.99max
	Regular	88	82	0.79max	2.99max
Israel	Premium	96	86	0.40max	1.51max
	Regular	91min	82	0.40max	1.51max
Jordan	Premium	96	—	*0.59	2.23
	Regular	88	—	*0.24	0.91
Kuwait	Premium	98	89	0.84	3.18
	Regular	90	83	0.53	2.01
				0.84	3.18
				0.53	2.01
Lebanon	Premium	93	86	0.84max	3.18max
		92	85		
Oman	Premium	97min	—	0.62max	2.35max
	Regular	90	—	0.62max	2.35max
Pakistan	HOBC	97min	—	0.84	3.18
	Regular	80min	78min	0.42	1.59
Qatar	Premium	97	91	1.06	4.00
	Regular	90	85	0.85	3.22
Saudi Arabia	Premium	95min	86min	0.84max	3.18max
	Regular	83min	80min	0.84max	3.18max
Sri Lanka	Regular	90min	—	0.84max	3.18max
Syria	Regular	90min	—	0.40max	1.51max
United Arab Emirates	Premium	97	—	0.84max	3.18max
	Regular	90	—	0.84max	1.51max
Yemen AR(North)	Super	93	—	0.84max	3.18max
	Regular	83	79	0.84max	3.18max
Yemen PDR(South)	Premium	93	87	0.55	2.08
	Regular	83	80	0.55	2.08

ONGOING STUDIES IN UNLEADED AVIATION GASOLINE

David H. Atwood
Galaxy Scientific Corporation
Pleasantville, N.J.

Augusto Ferrara, Kenneth J. Knopp
Federal Aviation Administration Technical Center
Pomona, N.J.

ABSTRACT

The FAA Technical Center is working on the development of an unleaded aviation gasoline for use in the existing fleet of general aviation aircraft. This program is primarily concerned with safety (certification) issues, but data is being generated on environmental and maintenance issues as well. This report summarizes the results generated by the program over the period of the past nine months. The principal topics addressed include octane requirement studies, emissions tests, and endurance tests. The emission tests compared a base fuel to the base fuel containing various percentages of MTBE with fuel flows adjusted to obtain equivalent energy densities. Exhaust gas components such as: carbon monoxide (CO), carbon dioxide (CO₂), oxygen (O₂), total hydrocarbons (THC), and nitrogen oxides (NO_x) were measured. Points of engine operation included the following modes: taxi out, takeoff, climb, cruise, approach, and taxi in. The octane ratings were performed at the three most critical power points. A survey identifying the properties of autogas which is currently used in light aircraft is included. This survey is concerned with the effects of detergents on fuel quality. Also presented is an aircraft registry summary showing the number of single engine piston aircraft certified on each fuel grade, and a fuel consumption survey.

INTRODUCTION

The 1990 Clean Air Act Amendments call for the removal of lead from all motor gasolines by the end of 1995. This law also required engine manufacturers to certify their engine for operations on unleaded gasolines by 1992. At the request of the General Aviation Manufacturers Association (GAMA), the US EPA has ruled that aircraft engine manufacturers were not required to certify production engines on unleaded fuels by 1992. This ruling does not affect the 1995 deadline for removing lead from all fuels, and to date, there is no indication as to how the EPA will rule on this issue. Even if the EPA exempts aviation gasolines, the anticipation is that the economics of providing special handling and facilities for aviation fuels will render leaded aviation fuels uneconomical. As an example, burning waste oil from engines that operate on leaded fuels may soon be impossible. In light of this and in response to a request from the Congress, the FAA has begun research toward developing an unleaded aviation gasoline.

The research conducted by the FAA is primarily intended to address certification issues, but data is being generated on environmental and maintenance issues as well. The research plan also calls for developing a data base to be used by the concerned organizations in addressing their particular needs. The FAA is cooperating with the engine manufacturers, the airframe manufacturers, user groups, the oil industry, and the American Society of Testing and Materials (ASTM) in performing this research.

This report summarizes results generated by the program over the period of the past nine months from the FAA Technical Center's studies on emissions, engine wear, and octane requirement. A summary list showing the number of single engine piston aircraft certified for each fuel grade along with a fuel survey are presented. Also described are future plans for emissions testing, flight testing, endurance testing, and engine octane rating to be performed at the Technical Center. Previous testing and results were presented in the FAA Interim Report DOT/FAA/CT-93/65.

BACKGROUND

Due to the use of high octane additives, the unleaded test fuel has less energy than existing aviation gasoline (i.e., a lower energy density). In theory, certain operating conditions allow for the recovery of the lost energy by operating

at a more efficient configuration (hence the term recovery). For example, the use of oxygenates should allow for operations lean of stoichiometric fuel to air ratios, and in theory these operations should be more efficient than operations rich of stoichiometric fuel to air ratios.

The American Society of Testing and Materials specifies several different octane ratings, which measure the fuel's resistance to knock for different duty cycles. The motor octane number (MON) indicates performance under a heavy duty cycle, and the Technical Center uses the MON for reporting purposes. The Aviation Lean Rating can be calculated from the MON. The Aviation Rich Rating depends on the energy density of the fuel, and it is not considered repeatable for oxygenated fuels. The Technical Center used oxygenated fuels throughout this program, so the Aviation Rich Rating is not reported.

The Technical Center uses SI (metric) units in accordance with federal law. English units are presented in parentheses.

TESTING PROCEDURES / RESULTS

ENDURANCE

Endurance tests were performed on two Lycoming IO320 engines. For these tests the cylinder head temperatures were kept as close to 260 °C (500 °F) as possible.

First the Lycoming IO320 engine which was used in vapor lock tests, power baseline tests, and detonation tests was used for endurance tests. Due to a limited amount of fuel containing MMT the engine could not be put through a typical 150 hour endurance test. The first test fuel blend was prepared by the Pittsburgh Applied Research Center (PARC) which contained unleaded autogas, 30 percent MTBE by weight, and 0.1 g/gal MMT. This fuel supply ran out after the first thirteen hours of operation. Chevron supplied enough fuel for fifty more hours of operation which contained 85 percent C4 alkylate, 15 percent MTBE, and 0.5 g/gal MMT.

Initial inspection of the cylinders using a boroscope did not expose any unusual wear. Valve degradation measurements were taken initially and at the end of the test. The results of the wear tests can be seen in table 1.

When reviewing the data, delta 20 is the wear over the past twenty hours of operation. Similarly, delta 33, delta 43, delta 53, etc. are the changes in the wear measurements compared to the initial measurement. All valve wear measurements in the table are in inches.

The discrepancy in the leak down in cylinder 1 between the 0-hour and the 13-hour measurements was probably due to the valves being staked at the 13-hour mark but not at the 0-hour mark. The compression loss in cylinder 3 at the 13-hour mark was due to carbon buildup on the exhaust valve, which resulted in a poor seat. Cylinder 3 was pulled at the 13-hour mark and the exhaust valve was lapped to remove the carbon buildup. Cylinder 3 also showed large amounts of exhaust valve seat wear after the 53-hour mark.

After thirteen hours of operation on the 0.1 g/gal MMT blend and twenty hours of operation on the 0.5 g/gal MMT blend the spark plugs were pulled because of a poor magneto check. The plugs were found to be coated with an orange deposit, which was later analyzed to be mostly manganese and oxygen. In all of the plugs the buildup was significant and in one of the plugs the buildup was enough to bridge the gap and foul the plug.

After the endurance runs the engine was shipped to Lycoming to be torn down and inspected. The insides of the cylinders were found to be coated with the manganese based deposit.

The inspection also showed that the number 3 cylinder exhaust valve seat was badly worn and the valve stem had an unusual deposit on one side. Lab analysis had determined that the deposit was sodium oxide. Apparently, the sodium in the valve had leaked out and had burned as it leaked. Since the valve was pulled and lapped at the 13-hour mark it appears that the probable cause of failure was chattering as the valve worked in the deep recess of the valve seat. The data supports this conclusion since the greatest wear is shown to occur after the 13-hour mark.

Table 1. Wear Measurements for the Lycoming IO320 Engine Run on Blends Containing MTBE and MMT.

Hours	Cyl 1	Intake Cyl 2	Valve Cyl 3	Cyl 4	Cyl 1	Exhaust Cyl 2	Valve Cyl 3	Cyl 4
0	0.572	0.572	0.602	0.581	0.564	0.565	0.573	0.572
Leak down	66/80	78/80	60/80	78/80	66/80	78/80	60/80	78/80
13	0.571	0.572	0.602	0.581	0.562	0.565	0.573	0.571
delta 13	0.001	0	0	0	0.002	0	0	0.001
Leak down	74/80	78/80	22/80	74/80	74/80	78/80	22/80	74/80
33	0.57	0.571	0.602	0.58	0.56	0.564	0.542	0.571
delta 20	0.001	0.001	0	0.001	0.002	0.001	0.031	0
delta 33	0.002	0.001	0	0.001	0.004	0.001	0.031	0.001
Leak down	68/80	76/80	66/80	70/80	68/80	76/80	66/80	70/80
53	0.571	0.571	0.602	0.58	0.556	0.564	0.512	0.571
delta 20	-0.001	0	0	0	0.004	0	0.03	0
delta 53	0.001	0.001	0	0.001	0.008	0.001	0.061	0.001
Leak down	62/80	68/80	66/80	68/80	62/80	68/80	66/80	68/80
63	0.571	0.571	0.6	0.58	0.555	0.564	0.502	0.571
delta 10	0	0	0.002	0	0.001	0	0.01	0
delta 63	0.001	0.001	0.002	0.001	0.009	0.001	0.071	0.001
Leak down	68/80	68/80	67/80	66/80	68/80	68/80	67/80	66/80

The exhaust valve seats in cylinders 1 and 4 looked like they were getting ready to leak. The contact area was minimal and there was a considerable amount of manganese dioxide deposited on the valve seat area. The inserts (in cylinders 1, 2, and 4) in the heads had orange pits on them, and they looked like there was some wear occurring. This is confirmed by the data in the table which shows the cylinders losing compression. The number 2 cylinder intake valve was starting to tulip. This could be from the knock work and the high temperatures. The rings were also found to have some deposits on them. The oil sump had black varnish on all surfaces. This could also be a consequence of running the engine at maximum operating temperatures. Also, the #1 and #4 cam followers showed signs of pitting and the #1 cam lobe was worn. This could be from the knock work or from old age. This particular engine had an indeterminate number of hours on it.

Table 2 shows the schedule for the 150 hour endurance test performed on an overhauled Lycoming IO320 engine.

Table 2. Typical Schedule for the Endurance Tests with a Lycoming IO320 Engine.

Hours	Point	MAP mmHg (inHg)	Rpm	Torque Nm (Ft·Lbf)	Mixture Setting
90	takeoff	FT	2700	365 (270)	F/R
15	75% power	620 (24.5)	2460	290 (215)	Lean to Best Power
10	70% power	600 (23.5)	2425	280 (205)	Lean to Peak EGT
10	climb	635 (25)	2500	300 (220)	F/R
5	75% power	620 (24.5)	2460	285 (210)	F/R
5	70% power	600 (23.5)	2425	270 (200)	F/R
5	65% power	580 (23)	2350	260 (190)	F/R
5	60% power	570 (22.5)	2280	250 (185)	F/R
5	50% power	530 (21)	2150	215 (160)	F/R

Table 3 shows the results from the wear tests on the overhauled IO320 engine. The fuels used for this wear test were an unleaded avgas containing 30 percent MTBE by weight and an unleaded autogas containing 30 percent MTBE by weight.

Table 3. Wear Analysis for the Overhauled Lycoming IO320 Engine. All Values are in Inches.

Hours	Cyl 1	Intake Cyl 2	Valve Cyl 3	Cyl 4	Cyl 1	Exhaust Cyl 2	Valve Cyl 3	Cyl 4
0	0.566	0.553	0.570	0.592	0.600	0.556	0.661	0.586
leak down	71/80	74/80	77/80	72/80	71/80	74/80	77/80	72/80
20	0.569	0.554	0.556	0.592	0.5615	0.555	0.598	0.584
delta 20	-0.003	-0.001	0.014	0	0.0385	0.001	0.063	0.002
leak down	70/80	78/80	76/80	78/80	70/80	78/80	76/80	78/80
40	0.569	0.554	0.556	0.592	0.559	0.553	0.597	0.580
delta 20	0	0	0	0	0.0025	0.002	0.001	0.004
delta 40	-0.003	-0.001	0.014	0	0.041	0.003	0.064	0.006
leak down	78/80	78/80	76/80	76/80	78/80	78/80	76/80	76/80
60	0.569	0.554	0.556	0.592	0.556	0.553	0.599	0.580
delta 20	0	0	0	0	0.003	0	-0.002	0
delta 60	-0.003	-0.001	0.014	0	0.044	0.003	0.062	0.006
leak down	75/80	78/80	78/80	75/80	75/80	78/80	78/80	75/80
80	0.568	0.554	0.556	0.590	0.556	0.552	0.599	0.579
delta 20	0.001	0	0	0.002	0	0.001	0	0.001
delta 80	-0.002	-0.001	0.014	0.002	0.044	0.004	0.062	0.007
leak down	76/80	79/80	77/80	78/80	76/80	79/80	77/80	78/80
100	0.568	0.554	0.556	0.591	0.558	0.552	0.597	0.579
delta 20	0	0	0	-0.001	-0.002	0	0.002	0
delta 100	-0.002	-0.001	0.014	0.001	0.042	0.004	0.064	0.007
leak down	77/80	77/80	75/80	79/80	77/80	77/80	75/80	79/80
120	0.569	0.554	0.556	0.592	0.559	0.552	0.597	0.579
delta 20	-0.001	0	0	-0.001	-0.001	0	0	0
delta 120	-0.003	-0.001	0.014	0	0.041	0.004	0.064	0.007
leak down	74/80	79/80	76/80	78/80	74/80	79/80	76/80	78/80
140	0.568	0.554	0.556	0.592	0.558	0.552	0.597	0.579
delta 20	0.001	0	0	0	0.001	0	0	0
delta 140	-0.002	-0.001	0.014	0	0.042	0.004	0.064	0.007
leak down	77/80	79/80	76/80	79/80	77/80	79/80	76/80	79/80
160	0.569	0.554	0.556	0.592	0.558	0.552	0.597	0.579
delta 20	-0.001	0	0	0	0	0	0	0
delta 160	-0.003	-0.001	0.014	0	0.042	0.004	0.064	0.007
leak down	74/80	78/80	76/80	78/80	74/80	78/80	76/80	78/80
166	0.569	0.554	0.556	0.592	0.559	0.552	0.596	0.579
delta 20	0	0	0	0	-0.001	0	0.001	0
delta 166	-0.003	-0.001	0.014	0	0.041	0.004	0.065	0.007
leak down	74/80	76/80	76/80	79/80	74/80	76/80	76/80	79/80

The IO320 engine was operated for approximately 160 hours with 150 hours of that time at specific power settings. The remaining time was either spent at idle or used for operations checks.

No unusual wear or compression loss was discovered in these tests. The initial high rates of wear in cylinders 1 and 3 occurred during the first twenty hours of operation and was probably due to normal engine break-in.

Future testing will include an overhauled Continental GTSIO520H engine operated on aviation alkylate containing various percentages by weight of ethyl tertiary butyl ether (ETBE).

OCTANE REQUIREMENT

After 160 hours of endurance testing the Lycoming IO320 engine was octane rated. The results from this octane rating were compared to the results from the rating performed after the break-in period to determine the octane requirement change due to normal wear. John Fowlks and Roger Gaughan, trained representatives from the Exxon Research and Development Company, supplied the fuel and were on hand for these tests. Knock was determined by the use of piezoelectric pressure transducers mounted in each cylinder and was coordinated with a trained ear. The cylinder head temperature boss was drilled out in each cylinder and rethreaded so that the pressure transducers could be flush mounted with each cylinder head.

Only the three most critical points were tested to save fuel. Previous knock studies at the Technical Center determined that for the IO320 engine the three worst points were: 640 mmHg (25 inHg) manifold pressure, 2500 rpm and the mixture set at 12 percent lean of full rich; full throttle, 2500 rpm, and full rich mixture setting; and full throttle, 2700 rpm, and full rich mixture setting. A 12 percent lean mixture setting satisfies the certification requirement that the engine be knock free up to 12 percent lean of full rich.

After each point was set the engine was allowed to stabilize and the cooling pressure differential was set so that the cylinder head temperatures were kept as close to 260 °C (500 °F) as possible. The induction air and cooling air temperatures were regulated at 38 °C (100 °F).

The minimum motor octane requirement was found to be 91 MON before and after the endurance testing. The octane ratings were also performed with and without a muffler. The minimum motor octane requirement was found to be 91 MON with and without the muffler. Previous testing with a Lycoming IO320 engine at the FAA Technical Center suggested that the addition of a muffler resulted in a MON requirement increase of 2 to 3 numbers.

A Continental GTSIO520H engine was also octane rated. The knock free motor octane requirement was found to be 97 with the intercooler and 98 without the use of the intercooler. The intercooler was blocked off to simulate high altitude effects.

Knock number calculations were performed on the pressure data by the use of a technique which was conceived at the FAA Technical Center (Atwood, D., Ferrara, A., Ringenbach, P., Unleaded Avgas Program Interim Report, DOT/FAA/CT-93/65). Fast Fourier Transforms were also performed on the pressure data. The largest amplitudes were found near the 4500 Hz, 7200 Hz, and 10200 Hz frequencies for the GTSIO520H engine. These frequencies correspond to the first three knock modes. Correlations between the knock modes, knock numbers, and maximum pressures are presented in Table 4.

The knock numbers correlated very well with the higher knock modes. This was expected since the knock number is directly proportional to the amplitude of the "ringing" on the pressure trace. The knock number also correlated fairly well with the maximum pressures. Typically, knock cycles have higher peak pressures than normal combustion cycles, with the peak pressure proportional to the level of knock. Also, the knock numbers correlated better with the FFT amplitudes than did the maximum pressures. Calculation of the FFT was very time consuming and therefore this method was simply used as an accuracy measurement for the Technical Center's method, and was not pursued further. The technique developed at the FAA Technical Center appears to be a fairly accurate method of determining the level of knock for a given engine cycle.

Table 4. Correlations Between the Fast Fourier Transform Amplitudes, Knock Numbers, and Maximum Pressures.

	Pmax	Knk #	FFT @ 4500 Hz	FFT @ 7200 Hz	FFT @ 10200 Hz
Pmax	1	0.78	0.55	0.70	0.75
Knk #	0.78	1	0.67	0.89	0.90
FFT @ 4500 Hz	0.55	0.67	1	0.51	0.56
FFT @ 7200 Hz	0.70	0.89	0.51	1	0.77
FFT @ 10200 Hz	0.75	0.90	0.56	0.77	1

key: FFT @ 4500 Hz = amplitude generated by the Fast Fourier Transform method at 4500 Hz frequency, Pmax = the maximum pressure for each cycle, Knk # = the knock number calculated from the previously described method.

EMISSIONS

The emissions tests compared the exhaust components of a blend fuel to that of the base fuel on the basis of equivalent fuel flow and equivalent energy densities. The base fuel used for this test was an unleaded motor gasoline and the additive was MTBE. Percentages of 5, 10, 15, 20, 25 and 30 percent MTBE by weight were added to the autogas. Exhaust components measured were carbon monoxide (CO), carbon dioxide (CO₂), nitrogen oxides (NO_x), total hydrocarbons (THC), and oxygen (O₂). For the equivalent energy density comparisons the fuel flow of the base fuel was multiplied by the energy density ratio of the blend to the base.

The Technical Center monitored the test engine to ensure it did not knock during these tests.

The procedure included setting the engine point and then allowing ample time to purge the fuel system between tank switching and allowing time for the engine to stabilize. Table 5 shows the emissions profile for the Lycoming IO320 engine.

Table 6 contains the results from the emissions testing with the Lycoming IO320 engine. For each blend the values for the different points for all of the runs were averaged together. The base fuel values were averages of all the base values from all of the runs at both full rich and lean to peak exhaust gas temperature. In the table MO989 is an abbreviation for a neat motor gasoline with an RVP of 9 psi and a MON of 89, likewise MO98905 is the MO989 base fuel with 5% MTBE added per weight.

When comparing normal operation on the neat fuel to normal operation on the 30 percent blend the results in table 5 show that for a two percent lower average fuel flow rate there was a 3 percent increase in power, and a 11 percent decrease in BSFC. This suggests that there is some recovery taking place. When comparing the emissions between the base fuel and the 30 percent blend there is a 28 percent decrease in THC, 25 percent decrease in CO, 14 percent increase in CO₂, 40 percent increase in NO_x, and a 3 percent decrease in O₂. In general, the trends described above show a gradual transition with concentration from the values obtained with the base fuel, to the values obtained with the 30 percent blends. These trends were as expected since operation on oxygenated fuels results in a leaner configuration that should result in lower levels of O₂, CO, and THC and higher levels of NO_x, and CO₂ in the exhaust. The differences noted when looking at the emissions for the base fuel, when the engine was operated at equivalent energy densities, and for the various blends suggest that the oxygenate in the fuel is having an effect on the emissions.

At the cruise point the equivalent fuel flows were obtained with the mixture set at lean to peak exhaust gas temperature on the blend fuel. The high level of NO_x and the fact that the BSFC for the base fuel was the same for the blend fuel, even though the blend has a lower energy density, suggests that the blends seem to operate just lean of stoichiometric. Calculations of the air-to-fuel ratio also suggested that operation with the blend fuels at this setting was lean of stoichiometric.

When leaning to peak it is found that slight changes in the mixture setting make large differences in the NO_x and THC levels. This helps to explain any scatter in the data.

Table 7 contains the average values for the lean to equivalent energy density points. In this table, the values presented for the base fuel are the average of the data, which were collected on the base fuel, when the data for the particular blend was collected. This reduces the influence of run to run variations.

Table 5. Emissions Profile for the Lycoming IO320 Engine.

Point	Tank	MAP mmHg (inHg)	Rpm	Mixture
Taxi out	Base	380 (15)	1200	F/R
Taxi out	Blend	380 (15)	1200	F/R
Taxi out	Base	380 (15)	1200	Lean to Energy Density Equivalent
Take off	Base	FT	2700	F/R
Take off	Blend	FT	2700	F/R
Take off	Base	FT	2700	Lean to Energy Density Equivalent
Climb	Base	635 (25)	2500	F/R
Climb	Blend	635 (25)	2500	F/R
Climb	Base	635 (25)	2500	Lean to Energy Density Equivalent
Cruise	Blend	580 (23)	2300	Lean to Peak EGT
Cruise	Base	580 (23)	2300	Equivalent Fuel Flow
Cruise	Base	580 (23)	2300	Lean to Energy Density Equivalent
Approach	Base	480 (19)	2000	F/R
Approach	Blend	480 (19)	2000	F/R
Approach	Base	480 (19)	2000	Lean to Energy Density Equivalent
Taxi in	Base	380 (15)	1200	F/R
Taxi in	Blend	380 (15)	1200	F/R
Taxi in	Base	380 (15)	1200	Lean to Energy Density Equivalent

Table 6. Results from Emissions Testing with the Lycoming IO320 Engine.

Fuel	Corrected Power kW (Hp)	Fuel Flow L/Hr (Lbm/Hr)	BSFC L/kW·Hr (Lbm/Hp·Hr)	THC ppm	CO %	CO2 %	NOx ppm	O2 %
MO989 F/R & Equivalent Fuel Flow	53.4 (71.6)	28.5 (45.2)	0.53 (0.63)	692	8.99	8.36	259	0.36
MO98905	54.2 (72.7)	28.4 (45.0)	0.52 (0.62)	622	8.80	8.51	235	0.35
MO98910	53.6 (71.9)	28.7 (45.5)	0.54 (0.63)	689	8.50	8.59	284	0.42
MO98915	54.4 (73.0)	28.8 (45.6)	0.53 (0.62)	612	8.71	8.62	236	0.33
MO98920	54.1 (72.5)	28.3 (44.9)	0.52 (0.62)	557	7.29	9.29	465	0.35
MO98925	54.6 (73.2)	28.3 (44.9)	0.52 (0.62)	588	7.72	9.11	374	0.35
MO98930	54.9 (73.6)	27.8 (44.1)	0.51 (0.60)	499	6.71	9.57	363	0.35

If operations are compared at equivalent energy densities then the findings show something different (see table 7). The neat fuel shows slightly higher levels of THC and CO, slightly lower levels of CO₂, no change in O₂, and a significantly higher level of NO_x. Setting equivalent energy densities at the cruise point results in leaning an already lean configuration and hence results in a drop in THC, and CO, and an increase in O₂ and CO₂ and a sharp

increase in NO_x. This implies that an engine operated on a blend of MTBE and the base fuel will emit fewer emissions overall than operations on the base fuel. This is true regardless of the operating mode, when using the base fuel.

The BSFC values in table 7 suggest that operation with the 30 percent blend, containing five percent less energy than the base fuel, results in significant recovery.

Table 7. Results from Emissions Testing with the IO320 Engine at Equivalent Energy Densities.

Fuel	Corrected Power kW (Hp)	Fuel Flow L/Hr (Lbm/Hr)	BSFC L/kW·Hr (Lbm/Hp·Hr)	THC ppm	CO %	CO ₂ %	NO _x ppm	O ₂ %
MO989	54.2 (72.7)	28.2 (44.7)	0.52 (0.61)	611	8.71	8.65	321	0.36
MO98905	54.2 (72.7)	28.4 (45.0)	0.52 (0.62)	622	8.80	8.51	235	0.35
MO989	53.1 (71.2)	28.5 (45.2)	0.54 (0.63)	719	8.78	8.44	286	0.41
MO98910	53.6 (71.9)	28.7 (45.5)	0.54 (0.63)	689	8.50	8.59	284	0.42
MO989	53.99 (72.4)	28.4 (44.9)	0.53 (0.62)	654	9.40	8.32	227	0.33
MO98915	54.4 (73.0)	28.8 (45.6)	0.53 (0.62)	612	8.71	8.62	236	0.33
MO989	53.7 (72.0)	27.8 (44.1)	0.52 (0.61)	622	7.96	8.96	430	0.35
MO98920	54.1 (72.5)	28.3 (44.9)	0.52 (0.62)	557	7.29	9.29	464	0.35
MO989	53.9 (72.3)	27.8 (44.1)	0.52 (0.61)	651	8.62	8.66	368	0.36
MO98925	54.6 (73.2)	28.3 (44.9)	0.52 (0.61)	588	7.72	9.11	374	0.35
MO989	53.9 (72.3)	27.2 (43.1)	0.50 (0.60)	595	7.88	9.00	374	0.35
MO98930	55.0 (73.8)	27.8 (44.1)	0.51 (0.61)	499	6.71	9.57	363	0.35

FUEL BLENDS

Fuel blends were prepared by the Pittsburgh Applied Research Center (PARC) to measure the effectiveness of methyl tertiary amyl ether (TAME) as a blending agent. The results from the octane tests for blends containing only TAME, both TAME and MTBE, and TAME, MTBE and MMT can be seen in table 8.

Table 8. Lab Results on Various Blends.

Alkylate (% by weight)	TAME (% by weight)	MTBE (% by weight)	MMT g/gal	Motor Octane Number
100	0	0	0	92.3
90	10	0	0	92.8
80	20	0	0	93.3
80	10	10	0	92.8
70	30	0	0	93.2
70	15	15	0	94.0
70	15	15	0.1	94.2
60	40	0	0	94.4
60	20	20	0	94.0
0	100	0	0	96.9 (TAME blending value)
0	50	50	0	96.9 (TAME + MTBE blending value)
100	0	0	0.1	92.5

The table shows that the blending value for TAME is 96.9, the blending value for a 50/50 mix of TAME and MTBE is 96.9, and that the average MON increase per 0.1 g/gal of MMT added is 0.25.

The blending values for MTBE and ETBE were previously reported to be 102.4 and 102.2, respectively (Atwood D., Ferrara A., Unleaded Avgas Program, DOT/FAA/CT-93/65, 3/94).

FUEL SURVEY

The Southwest Research Institute conducted a survey of the summer fuels that are available throughout the United States for the Cessna Aircraft Company and the Federal Aviation Administration. During the course of this survey, samples were collected from throughout the United States. Samples were taken of all grades of gasoline and they included leaded as well as unleaded fuels. The following parameters were measured for each sample taken:

- Oxygen Content (weight %)
- Methanol Concentration (volume %)
- Ethanol Concentration (volume %)
- TBA Concentration (volume %)
- MTBE Concentration (volume %)
- ETBE Concentration (volume %)
- DiPE Concentration (volume %)
- TAME Concentration (volume %)
- Unwashed Gum Content (ASTM D381, mg/100 ml)
- Washed Gum Content (ASTM D381, mg/100 ml)
- Interface Rating (ASTM D1094)
- Separation Index (ASTM D1094)
- Aqueous Volume Change (ASTM D1094, ml)

The grade and posted antiknock index were recorded for each sample as well.

The oxygen concentration was performed by a Petrospec GA150 analyzer with the higher concentrations of oxygen confirmed by test D4815-9x.

The Technical Center reviewed the data with the intent of identifying the effects of the gum and alcohol content on the quality of the fuel, as indicated by the interface rating, the separation index and the aqueous volume change. For the purposes of this analysis the interface rating of 1B is listed as 1.5. This facilitated the data sort routines.

Initially, the Technical Center compared the fuels that contained either no ethanol or no methanol against those that contained either ethanol or methanol. This analysis did not reveal any clear trends. Likewise, when the data were sorted by the unwashed gum content, there were no clear trends evident. The Technical Center then looked at the data with the intention of separating the fuels with alcohols from the fuels without alcohols. The alcohols identified in the survey include methanol (MeOH), ethanol (EtOH) and tertiary butyl alcohol (TBA) and the ethers identified were methyl tertiary butyl ether (MTBE), ethyl tertiary butyl ether (ETBE), methyl tertiary amyl ether (TAME), and di-isopropyl ether (DiPE). Only 22 of the 497 samples did not contain alcohol and all but one of the samples contained an oxygenate. The survey has also determined that 29.4 percent of the fuels contained MeOH, 29.6 percent contained EtOH, 80.3 percent contained TBA, 48.9 percent contained MTBE, 28.6 percent contained DiPE, 61.0 percent contained ETBE, and 31.6 percent contained TAME. In addition, the Technical Center calculated the net gum content (unwashed gums - washed gums) for use in its sorting routines.

In figure 1, the Technical Center looked at fuels without alcohols. These data were sorted by the net gum content.

Figure 1a shows the interface rating as a function of the net gum content. If net gum content is above 45, the probability of failing the interface rating increases, but there is no definitive pattern. This was true for any of the other correlations that the Technical Center tried with the interface rating data. In figure 1b, the separation index is plotted as a function of net gum content. In this case, the fuel was likely to fail the separation index test if the gum

content was higher than 45. The one point that failed below 45 was a fuel from Alaska. Both fuels from this particular source failed even though there was no obvious reason for them to do so. In figure 1c, the aqueous volume change is plotted as a function of net gum content. In this case, a net gum content of 45 or higher was likely to result in a high volume change.

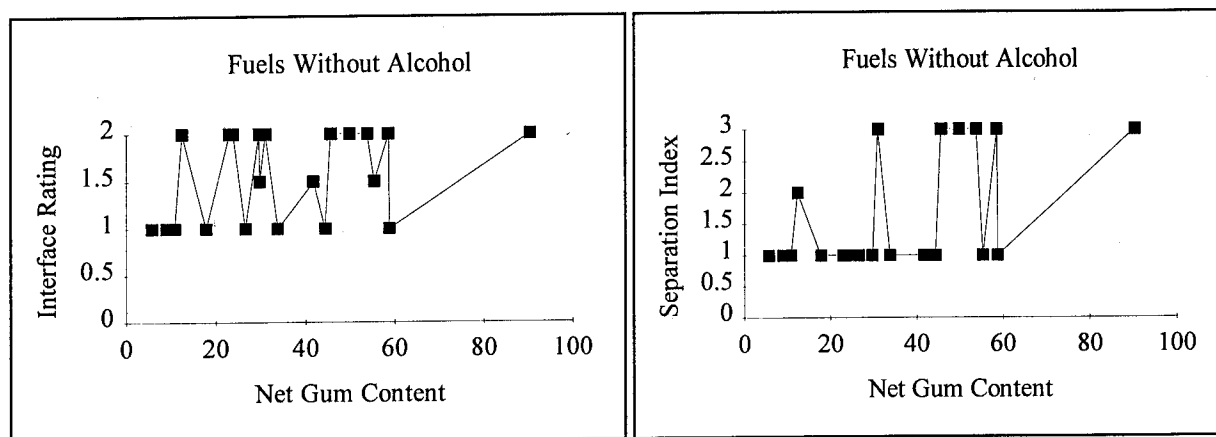


Figure 1a. Interface Rating vs. Net Gum Content

Figure 1b. Separation Index vs. Net Gum Content

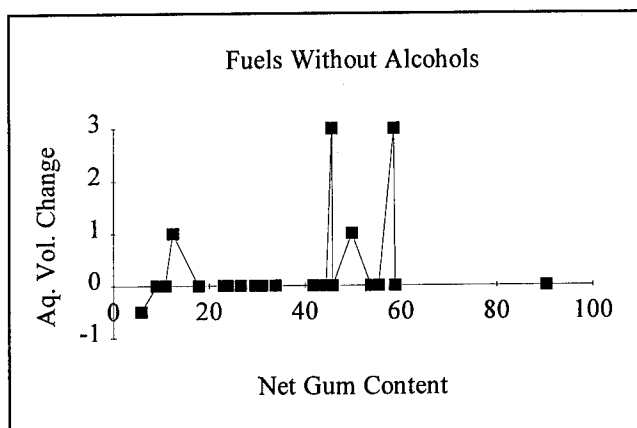


Figure 1c. Aqueous Volume Change vs. Net Gum Content

Figure 1. The Interface Rating, the Separation Index, and the Aqueous Volume Change as a Function of the Net Gum Content for Fuels Without Alcohols.

The Technical Center looked at the effect of the alcohol concentration on how well the net gum content correlated with the indicators of fuel quality. Figure 2 shows the data for fuels with an alcohol concentration of less than 0.25 percent.

In figure 2a, the probability of the aqueous volume change being greater than 1 increases when the net gum content increases above 45. The one point below a net gum content of 45 that shows a high change is the second fuel sample from Alaska that was discussed earlier. In figure 2b the separation index is shown as a function of the net gum content. In this case the separation index has roughly a 50/50 probability for failing if the gum levels are below 45. If the Gum levels are above 45 the fuel will fail the separation index test. The addition of even low levels of alcohol affects the separation index. The interface rating had no apparent correlation with the gum content for the fuels with alcohol concentrations less than 0.25 percent.

Figure 3 shows the aqueous volume change as a function of net gum content for all fuels with an alcohol

concentration of less than 0.5 percent. In this case the clear cutoff at a gum content of 45 is no longer apparent. Clearly the alcohol concentration as low as 0.5 percent affect all three quality control tests used to screen aviation fuels for water or phase separation problems. At these levels of alcohol concentration the separation index and the interface rating are likely to exceed the limits allowable for aviation fuels.

The Technical Center looked at the water volume change as a function of MTBE content (figure 4). In this case there is an inverse relationship that indicates the probability of a failure will decrease with increasing MTBE concentration. This relationship is tenuous at best and cannot be relied upon. Attempts to look at fuels with lower alcohol contents, and at concentration of the different ethers also failed to identify a relationship between concentration and the aqueous volume change.

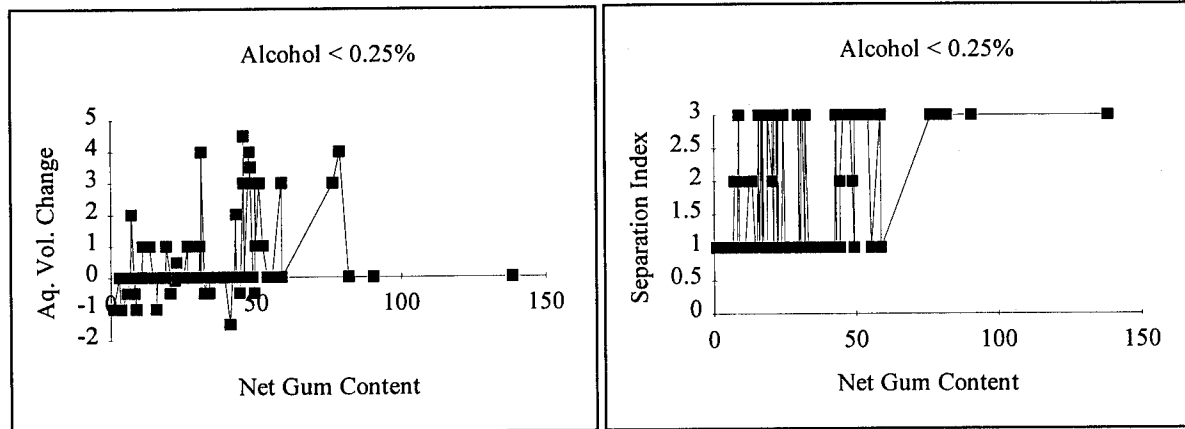


Figure 2a. Aqueous Volume Change vs. Net Gum Content

Figure 2b. Separation Index vs. Net Gum Content

Figure 2. The Aqueous Volume Change and the Separation Index as a Function of Net Gum Content for All Fuels With Less Than 0.25% Alcohol.

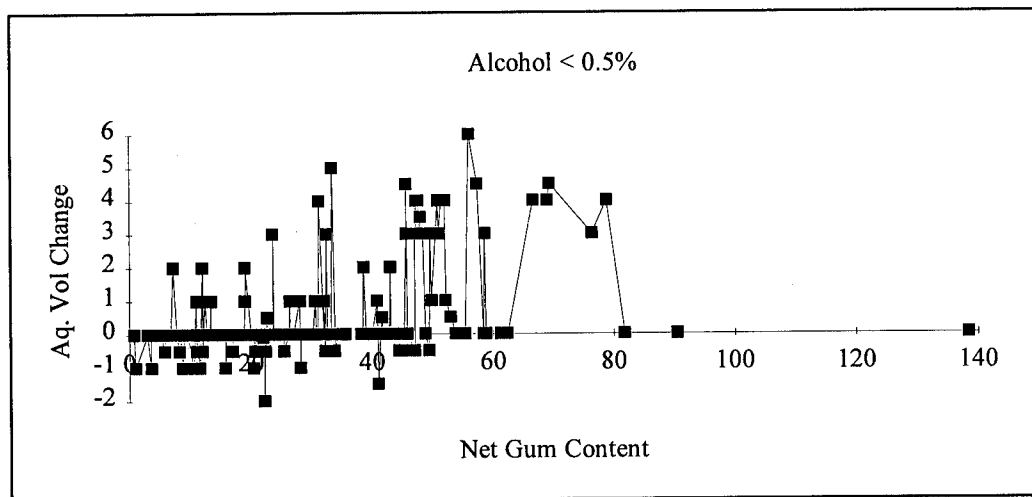


Figure 3. The Aqueous Volume Change as a Function of the Net Gum Content for All Fuels With an Alcohol Concentration of Less Than 0.5%

The Technical Center was unable to develop a correlation between the oxygen content and the gum content. Likewise, the Technical Center was unable to develop a relationship between the aqueous volume change and the oxygen content.

The data will be supplemented with a survey of winter grade fuels and until that data are available, the results presented are preliminary. To date, the data indicate that the alcohol concentration will affect the quality of the results obtained. For the aqueous volume change test, the alcohol concentration may go as high as 0.5 percent before it affects the results. Alcohol concentrations as low as 0.25 percent affect the separation index and the interface rating. Overall, the interface rating did not correlate well with any of the other parameters measured during this study. The data indicate that a net gum content greater than 45 affects the results of both the separation index and the aqueous volume change tests.

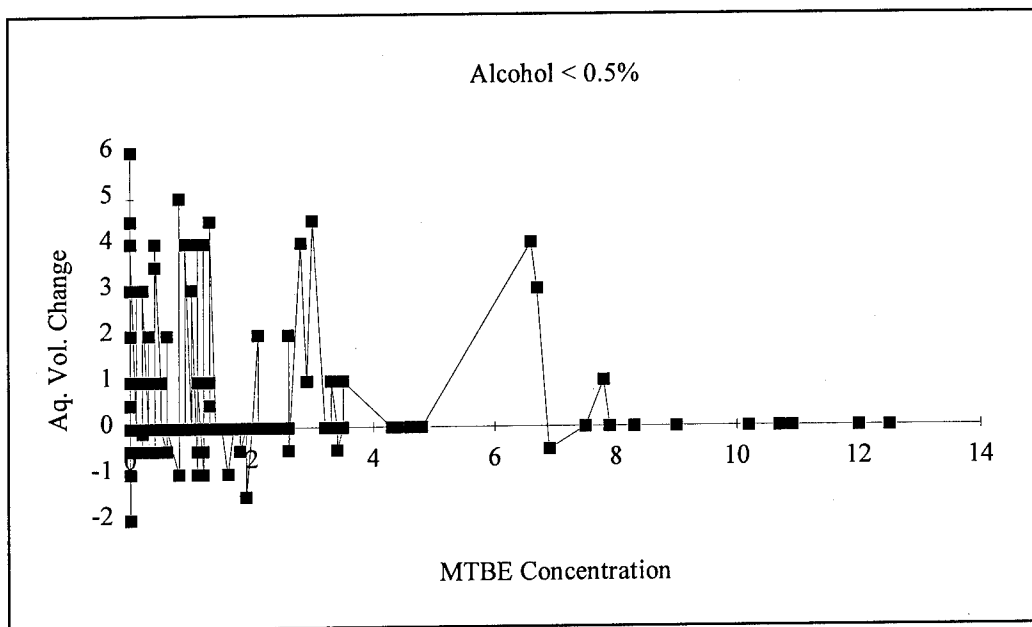


Figure 4. The Effect of MTBE Concentration on the Aqueous Volume Change for Fuels With Less Than 0.5% Alcohol.

FUEL CONSUMPTION SURVEY

The FAA has compiled the total annual fuel usage of piston engine powered aircraft. Results of the survey are contained in Table 9. The fuel consumption of the general aviation fleet was studied to gain an understanding of the current octane requirements of the general aviation fleet. The survey is based on the FAA aircraft registry summary from 1992.

When observing the fuel usage the Technical Center is quick to note that the figures in Table 9 are only an indication of the actual grades of fuel used and not indicative of the actual fuel requirements of the general aviation fleet. Several reasons exist for this, which include primarily fuel distribution and availability. This resulted in the need to conduct further studies of the general aviation fleet.

Table 9. 1992 General Aviation Fuel Consumption

GRADE OF FUEL	FUEL CONSUMPTION (MILLIONS OF GALLONS)	PERCENT OF TOTAL
80/87 OCTANE	10	3
AUTO GASOLINE	13	4
100 OCTANE LOW LEAD	236	77
100/130 OCTANE	47	16
TOTAL	306	

The table shows that 93 percent of the fuel used was of a high octane number while only 7 percent was of a low octane number. The 93 percent represents a total of 283 million gallons of fuel that currently uses tetraethyl lead as an octane enhancer to obtain the high octane values. This displays the magnitude of the current avgas problem which will require the removal of tetraethyl lead.

REGISTRATION LIST

The FAA has reviewed the registration list of piston engine powered aircraft and the fuels that they are certified on. Table 10 contains the results of the survey. The survey is based on the FAA aircraft registry summary from 1991. This survey was conducted to obtain an understanding of what grade fuel would be required to satisfy the bulk of the fleet.

When reviewing the registration list the Technical Center made every attempt to refer back to the original type certificate for the particular model designation. The reason for this is that some of the engines that were originally certified on 91/96 octane avgas are listed as being certified on 100LL in more recent documentation.

The table shows that 58 percent of the registered aircraft are certified to operate on 80/87 fuel, and 42 percent are certified to operate on 100 low lead avgas.

When comparing the fleet requirements with the actual fuel consumption from the FAA source, it is interesting to note that 80 octane fuel and avgas comprise only 6 percent of the total fuel consumed.

As a follow up activity of the registration list, table 11 was compiled, which compares total fuel consumption and activity by aircraft type. The table displays a summary of the activity and fuel used by piston engine aircraft. The table was compiled using the FAA aircraft registry summary from 1992.

An important comparison between single and twin engine aircraft is that single engine aircraft have almost 10 times as many flight cycles as twin engine aircraft, while using only twice the amount of fuel. One additional item to note is that almost 90 percent of the general aviation fleet is composed of single engine aircraft.

Table 10. Aircraft Registry Summary.

Fuel ID	Number*	Notes		
Antiques	694			
50...74	23,841	50,54,58,59,65,67,68,70,71,72,73,74		
73/80	1,293			
80	16,959			
80/87	69,003		Total 80/87	111790
87...91	1,153	87,90,91		
91/96	13,324			
100	359			
100LL	23,612			
100/130	40,769	Contains Some Derated Engines		
115/145	13			
Unknown	317	Most Are Probably Antiques	Total 100LL	79547
			Total Aircraft	191337

*End of calendar year 1991.

Table 11. 1992 General Aviation Activity by Aircraft Type.

Fixed Wing Piston	Total Number of Aircraft	Flight Cycles (millions)	Flight Hours (millions)	Average Fuel Consumption (gallons/hour)	Total Fuel Consumption (millions of gallons)
1 Engine, 1-3 Seats	52,500	11.63	5.68	9.4	53.392
1 Engine, 4+ Seats	91000	17.42	12.39	11.4	141.246
2 Engines, 1-6 Seats	11800	1.92	1.86	26.6	49.476
2 Engines, 7+ Seats	6600	1.17	1.31	35.1	45.981
Other	900	0.01	0.004	238.7	0.9548

FLIGHT TESTING

The FAA has plans to utilize a twin engine aircraft to perform actual flight testing on a fuel that will be representative of the probable high octane unleaded aviation fuel. The FAA plans to conduct these tests during the summer of 1994.

CONCLUSIONS

- a. Previous testing suggested that the use of unleaded gasoline affects valve seat wear. The testing completed under this phase of the program did not show excessive valve seat wear. There are a number of factors that could affect these results such as material specification, seat design, and whether or not the engine is turbocharged. Valve seat wear will be further studied under the Unleaded Avgas Program.
- b. The test engine described in this report did not experience an increase in octane requirement as a consequence of normal wear or as a consequence of adding a muffler. As with the valve seat wear, previous data indicates that both items could affect the octane requirement increase.
- c. TAME did not prove effective as a blending agent for improving the octane of a typical aviation alkylate. In these studies, the blending octane was 96.9.
- d. The use of MMT proved ineffective as an octane blending agent. In this study, the addition of 0.1 g/gal of MMT increased the octane of the test blends an average of 0.25 MON.
- e. Leaning to peak exhaust gas temperature on a blend fuel containing MTBE appears to result in operation at just lean of stoichiometric.
- f. Operations on the blend fuels appeared to result in recovery. The BSFC's for the neat and 30 percent blends were 0.50 and 0.51 L/kW-Hr, respectively, despite the 30 percent blend containing 5 percent less energy.
- g. Using standard operating procedures, the use of fuels that contain MTBE results in an increase in NO_x, CO₂, and O₂, and a decrease in CO, and THC due to operation at a leaner configuration. The amount of change is proportional to the amount of MTBE in the blend.
- h. Alcohol concentration as low as 0.5% affects the aqueous volume change test, and as low as 0.25% affects the separation index and the interface rating.
- i. The interface rating did not correlate well with any of the control variables such as gum or ether content.
- j. A net gum content greater than 45 affects the results of both the separation index and aqueous volume change tests.
- k. While 58 percent of the registered aircraft are certified to operate on 80/87 avgas, only 11 percent of the gasoline consumed by general aviation aircraft is either 80/87 avgas or autogas.

Endurance testing and emissions testing will be performed with the GTSIO520H engine using autogas containing ETBE. An octane rating will also be performed on the GTSIO520H engine. Flight tests will be conducted during fiscal year 1994.

**COMPARATIVE MATERIALS COMPATIBILITY FOR TYPICAL
AIRCRAFT FUEL SYSTEM MATERIALS AND COMPONENTS
WHEN EXPOSED TO AUTO GAS WITH CANDIDATE
OXYGENATED FUEL ADDITIVES**

Dr. John J. Thomas
Steven E. Adams
Erik E. Gordon
Florida Institute of Technology
150 W. University Blvd.
Melbourne, FL 32901

ABSTRACT

This experiment was designed by the EAA for preliminary testing of materials compatibility on typical aircraft fuel system materials. The fuels to be used are 87 and 93 octane auto gas, oxygenated auto gas, and 100 LL aviation gasoline as the standard to compare the dimensional changes. The oxygenated fuel additives will include Methyltetrahydrofuran (MTHF), Methyltertiarybutyl-ether (MTBE), Ethyltertiarybutyl-ether (ETBE), Tertiaryamylmethyl-ether (TAME), Ethanol (ETOH) and mixtures of MTBE and ETOH. The fuel mixtures will increment from 0% oxygenate, 2.7% Oxygen by weight, 5.4% Oxygen by weight, and 40% by volume of oxygenated additives mixed with 87 and 93 octane auto gas. The test procedure requires that the components be soaked in the fuel mixtures at -54°C (-65°F) for 24 hours and then at 79°C (175°F) for 24 hours, and finishing the 90 day trial at random ambient temperatures. Dimensional changes will be measured every 24 hours then first ten day and then incrementally there after for the remainder of the 90 days. The first phase of testing has started with sample parts including: O-ring Seals (MS 29512 & NAS 1593), Gaskets (AN 902-6 & AN 6290-6), Fuel Tank Material Sample-Composite, Fuel Tank Material Sample-Bladder, Aluminum Test pieces treated with fuel tank sealing compound, Hose-Stratoflex 124, Hose-MIL-H-6000B, Automotive fuel line hose from an after-market supplier.

INTRODUCTION

PURPOSE

A need exists for alternative fuels for aircraft because of regulatory requirements to remove all lead from aviation gasolines and to reduce ozone forming pollution in those metro areas served by major airports which are considered "non-attainment" areas. "Non-attainment" means those areas which do not meet ozone level standards. Also, domestic supply of alternate fuel is in almost continuous financial difficulty and any disruption, real or imagined, in fuel supply from the Mid-East causes fuel price increases which affects profit / loss margins substantially. Therefore, a substantial contribution of economical domestically supplied oxygenated fuel could be a significant aid to the financial health of the airline industry. Oxygenated fuels generally reduce hydrocarbon and carbon monoxide emissions, while increasing NOx and aldehyde emissions from internal combustion (IC)

engines. Several of these, such as methanol, ethanol and methyl tertiary butyl ether (MTBE) have been already tested in aircraft or aircraft engines. All have some advantages and disadvantages, and it should be stressed that materials compatibility issues must be really understood before intensive flight activity with these fuels can continue. The highest priority for further work involves materials compatibility testing of various oxygenate fuel blends effects on key metal, rubber and composite materials.

1. Evaluation of oxygenated fuels for key parts materials compatibility.
2. Evaluation of oxygenated fuels for performance / emissions characteristics in all common types of aviation engines.

Fuel Mixtures.

1. Reference fuel, 100 LL aviation gasoline
2. Unleaded regular gasoline
3. Unleaded regular gasoline with 5% ETOH / 4.22% MTBE-2.7% oxygen by weight
4. Unleaded regular gasoline, with 2.17% ETOH / 10% MTBE-2.7% oxygen by weight
5. Unleaded regular gasoline, with 29% MTBE-5.4% oxygen by weight
6. Unleaded regular gasoline, with 14.4% MTBE-2.7% oxygen by weight
7. Unleaded regular gasoline with 16.7% ETBE-2.7% oxygen by weight
8. Unleaded regular gasoline with 16.1% TAME-2.7% oxygen by weight
9. Unleaded regular gasoline with 7.06% ETOH-2.7% oxygen by weight
10. Unleaded premium gasoline with 14.6% MTBE-2.7% oxygen by weight
11. Unleaded premium gasoline, with 16.8% ETBE-2.7% oxygen by weight
12. Unleaded premium gasoline, with 16.2% TAME-2.7% oxygen by weight
13. Unleaded premium gasoline, with 7.15% ETOH-2.7% oxygen by weight
14. Unleaded premium gasoline with 30% MTBE-5.5% oxygen by weight
15. Unleaded regular gasoline with 12.4% MTHF-2.7% oxygen by weight

Sample Parts.

1. O-ring seals — MS 29512-06
2. O-ring seals — NAS 1593-012
3. Gaskets — AN 902-6
4. Gaskets — AN 6290-6
5. Fuel tank specimens
6. Aluminum test pieces treated with fuel tank sealing compound
7. Hose — Stratoflex 124
8. Hose — MIL-H-6000B
9. Automotive fuel line hose

This project is being conducted with the support of the Federal Aviation Administration and the Experimental Aircraft Association.

TEST PROCEDURE

PHASE I.

The fuel mixtures increment from 0% oxygenate, 2.7% oxygen by weight, 5.4% oxygen by weight, and 40% by volume of oxygenated additives mixed with 87 and 93 octane auto

gas. The test procedure requires that the components be soaked in the fuel mixtures at -54°C (-65°F) for 24 hours and then at 79°C (175°F) for 24 hours, and finishing the 90 day trial at random ambient temperatures. Dimensional changes are measured every 24 hours for the first ten days and then incrementally thereafter for the remainder of the 90 days.

PHASE II.

Worst case ether content will be determined and a blend prepared of 50% aviation gasoline and balance of D 4814 with ether to achieve this content. Phase I low-temperature protocol and high-temperature protocol will then be repeated.

MEASUREMENT PROTOCOL

1. Safely vented closed containers will be used.
2. Baths will be maintained at temperatures noted.
3. Parts from bath, dried, measured and data recorded.
4. For first ten days, above step 3 will be conducted approximately every 24 hours.
5. The following will be recorded:
 - a. Date, hours of exposure
 - b. Significant dimensions
 - c. Other items — appearance, changes noted other than dimensional

Materials.

1. Synthetic rubber seals.
2. Fuel line cut sections containing metallic and non-metallic components.
3. Fuel tank material samples, bladder and composite.
4. Carburetor components, floats, needles and gaskets.

Examples of representative parts in use in the general aviation piston aircraft are as follows:

1. Hose — Stratoflex 156
2. Hose — MIL-H-6000 B
3. O-Ring Seals MS 29513; NAS 1593
4. Gaskets AN 902-6; AN 6290-6
5. Primer Piper — P / N 451-103 (PA-28)
6. Fuel Selector Valve Cessna — P / N 0311070-1 (C180)
7. Fuel Level Transmitter & Float Cessna — P / N 0726110-1
8. Fuel Strainer Assembly. Cessna — P / N 0422130 (C 150)
9. Carburetor Float Facet — P / N 30-766
10. Needle Valve Bendix — P / N 2523047
11. Fuel Tank Material Sample — Composite (several vendors)
12. Fuel Tank Material Sample — Bladder (several vendors)
13. Aluminum Test Piece (coated with sloshing compound)

LOW-TEMPERATURE PROTOCOL.

Phase I requires that the aircraft components be soaked in the various fuels at -54°C (-65°F) for 24 hours. Several systems were suggested to accomplish this task. Low temperature testing is being accomplished using a digitally controlled Baxter Scientific Cryo-Fridge

capable of maintaining -121°F . This cryogenic freezer allows for low temperature testing without the constant attention necessary of the suggested dry ice—solvent bath. All testing is being done in glass containers with teflon lids. This system will also be used to accomplish the low temperature phase of the EAA composite testing.

HIGH-TEMPERATURE PROTOCOL.

Phase I also requires that the aircraft components be soaked in the various fuels at 79°C (175°F) for 24 hours. Again, there are several systems which may be used to accomplish this task. High temperature testing is accomplished using a Precision Scientific Co. hot bath. The bath is filled with ethylene glycol instead of water to reduce the rate of evaporation from the bath. The glass containers, fuels, and test specimens are then placed within the bath set at 79°C (175°F). The entire test set-up is then placed under a fume hood in order to safely vent vapors from the laboratory. This system will also be used to accomplish the high temperature phase of the EAA composite testing.

RESULTS

Although Phase I testing is not complete, preliminary data for all of the o-rings, gaskets, and aluminum / sloshing compound samples are available. The graphs show the average percent change along with a 95% confidence interval for the entire 90 day testing cycle, Figures 1-12. Also, reference lines are drawn to denote the 95% confidence interval for Fuel 1 (100 LL AVGAS) for comparison with the other fuel blends. The data is presented without showing the means and standard deviations at each of the 15 separate measurement time increments that they were measured at because of the physical space limitations of this paper. Such an effort would require hundreds of graphs. The average percent change was determined by first finding the percent change of each measurement as compared to the pre-exposure measurements and taking the average over all of the measurements in the 90 day testing cycle. The standard deviation was likewise found over the entire 90 day testing cycle. The general trend for all fuel blends, o-rings, and gaskets was to increase the respective measurement.

Graphs for the aluminum / sloshing compound samples show their average percent change as well as their respective 95% confidence intervals, as shown in Figures 13-14. The average percent change and standard deviations were determined as the o-rings and gaskets were. Lines are also drawn at the 95% confidence interval of Fuel 1 for comparison with other fuel blends. The general trend with respect to the cross section of the aluminum / sloshing compound samples is that of increasing except for fuel blends 1,3,4, and 13, Figure 13. The trend with respect to the weight of these samples is that of increasing for all blends except for Fuel 1, 100 LL AVGAS, Figure 14.

During the 90 day testing cycle, the o-rings and gaskets did not appear to change in color or texture. The aluminum / sloshing compound samples, however, did change in color. The original color of the sloshing compound samples were of a light gray tone. Exposure to the fuel blends during the 24 hours at -54°C did not change their appearance. However, after the 24 hour exposure to the 79°C hot bath all samples took on a different color than the original. The samples exposed to Fuel blend 1, AVGAS, took on the light blue color of the fuel. Samples exposed to Fuel blends 2-9 and 15 took on a light brown color. These blends all contained a light yellow 87 octane component. Samples exposed to fuel blends 10-14 took on a darker shade of gray than the light gray before exposure. Each of these

blends contained a clear 93 octane component. Texture for all the samples and fuel blends were not noticeably different.

Overall, preliminary Phase I data shows that swelling occurs with most fuel blends and samples. However, there is no significant statistical difference between the means at the 95% confidence level in almost all cases when compared with Fuel 1, Tables 1-3. However, the safety significance of swelling depends largely on where the affected materials are located in the aircraft. Depending upon the application, some swelling may actually improve functions. However, in some cases, swelling may actually cause a malfunction.

Table 1. Significant difference at the 95% confidence level for the average percent change of the diameter of the various o-rings and gaskets.

	<u>NAS 1593</u>	<u>AN 902</u>	<u>MS 29512</u>	<u>AN 6290</u>
Fuel 2	N	N	N	N
Fuel 3	N	N	Y	N
Fuel 4	N	N	Y	N
Fuel 5	N	N	N	N
Fuel 6	N	N	N	N
Fuel 7	N	N	N	N
Fuel 8	N	N	N	N
Fuel 9	N	N	N	N
Fuel 10	N	N	N	N
Fuel 11	N	N	N	N
Fuel 12	N	N	N	N
Fuel 13	N	N	N	N
Fuel 14	N	N	N	N
Fuel 15	N	N	N	N

Table 2. Significant difference at the 95% confidence level for the average percent change of the cross section of the various o-rings, gaskets, and metal.

	<u>NAS 1593</u>	<u>AN 902</u>	<u>MS 29512</u>	<u>AN 6290</u>	<u>METAL</u>
Fuel 2	N	N	N	N	N
Fuel 3	N	Y	N	Y	N
Fuel 4	N	Y	N	Y	N
Fuel 5	N	Y	N	Y	N
Fuel 6	N	N	N	N	N
Fuel 7	N	Y	N	N	N
Fuel 8	N	Y	N	N	N
Fuel 9	N	Y	Y	Y	N
Fuel 10	N	Y	N	N	N
Fuel 11	N	N	N	N	N
Fuel 12	N	Y	N	Y	N
Fuel 13	N	Y	N	Y	N
Fuel 14	N	Y	N	Y	N
Fuel 15	N	Y	Y	Y	Y

Table 3. Significant difference at the 95% confidence level for the average percent change of the weight of the various o-rings, gaskets, and metal.

	<u>NAS 1593</u>	<u>AN 902</u>	<u>MS 29512</u>	<u>AN 6290</u>	<u>METAL</u>
Fuel 2	N	N	N	N	N
Fuel 3	N	N	N	N	N
Fuel 4	N	N	N	N	N
Fuel 5	N	N	N	N	N
Fuel 6	N	N	N	N	N
Fuel 7	N	N	N	N	N
Fuel 8	N	N	N	N	N
Fuel 9	N	N	N	N	N
Fuel 10	N	N	N	N	N
Fuel 11	N	N	N	N	N
Fuel 12	N	N	N	N	N
Fuel 13	N	N	N	N	N
Fuel 14	N	N	N	N	N
Fuel 15	N	N	N	N	N

CONCLUSION

The main objective of this experiment was to compare the dimensional changes of several different typical aircraft component materials using several candidate oxygenated fuel additives. Although only part of Phase I testing is complete, the general trend of all of the fuel mixtures was to increase the dimensions of the elastomeric samples. In general, these increases were not statistically significant at the 95% confidence level.

REFERENCES

Draft Final Report. Determination of the Feasibility of Ethyl Tertiary Butyl Ether (ETBE) as a Fuel for Light Piston Engine Aircraft, by the National Institute of Petroleum and Energy Research, Bartlesville, Oklahoma, 74005, for the FAA, Atlantic City, New Jersey. Project No. B06825.

Final Report. The Performance of Alternative Fuels in General Aviation Aircraft, by Augusto M. Ferrara and Richard Wares of the FAA Technical Center and the National Institute of Petroleum and Energy Research, Bartlesville, Oklahoma, 74005, July 1988, DOT / FAA / CT-88 / 13.

Final Report. Autogas in General Aviation Aircraft by H. Steward Byrnes, William C. Cavage and Augusto M. Ferrara, March 1985, DOT / FAA / CT-87 / 05.

Technical Note. Comparison Between Unleaded Automobile Gasoline and Aviation Gasoline on Valve Seat Recession in Light Aircraft Engines, by Jerry R. Allsup, National Institute for Petroleum and Energy Research, Bartlesville, Oklahoma, 74005, May 1989, DOT / FAA / CT-TN89 / 33.

Technical Note. Analysis of the T63-A-700 Engine Used in Alcohol Turbine Fuel Extender Test, by John S. Glaeser, Depot Engineering and RCM Support Office, U.S. Army Aviation System Command, Naval Air Station, Corpus Christi, Texas, August 1990, DOT / FAA / CT-TN90 / 18.

APPENDIX

AVERAGE PERCENT CHANGE OF AN 6290-06 DIAMETER

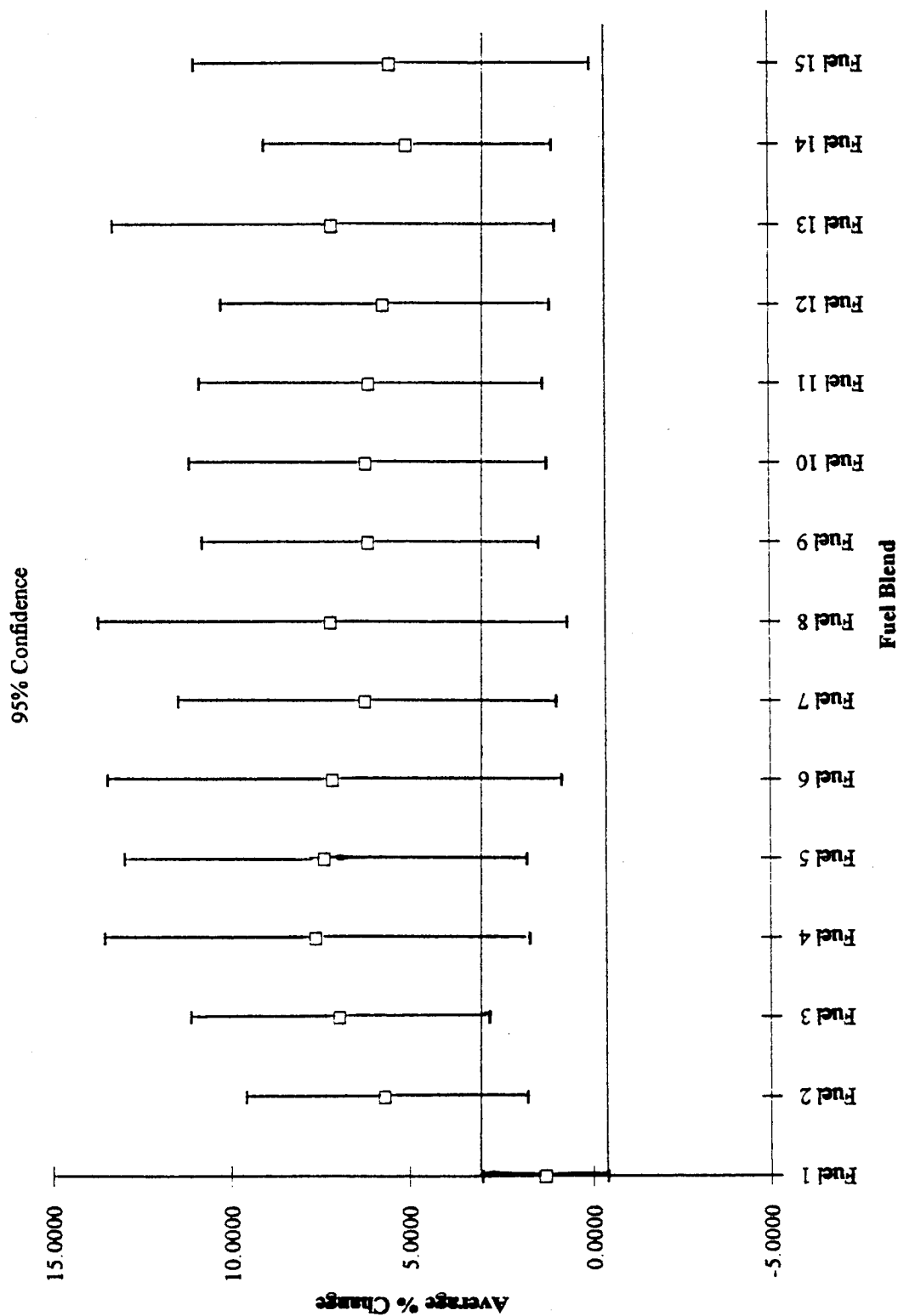


Figure 1. Average percent change of AN 6290-06 diameter.

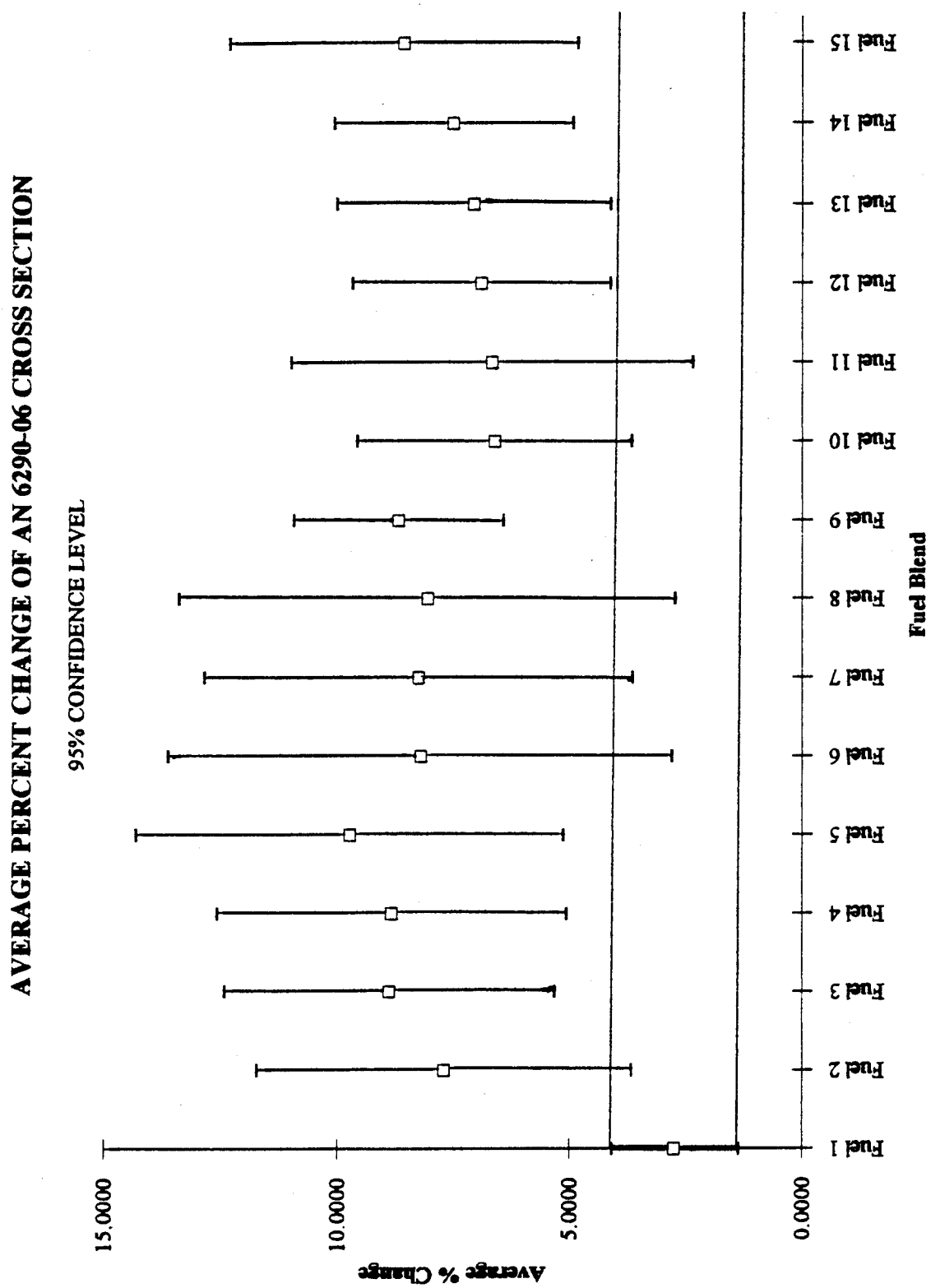


Figure 2. Average percent change of AN 6290-06 cross section.

AVERAGE PERCENT CHANGE OF AN 6290-06 WEIGHT

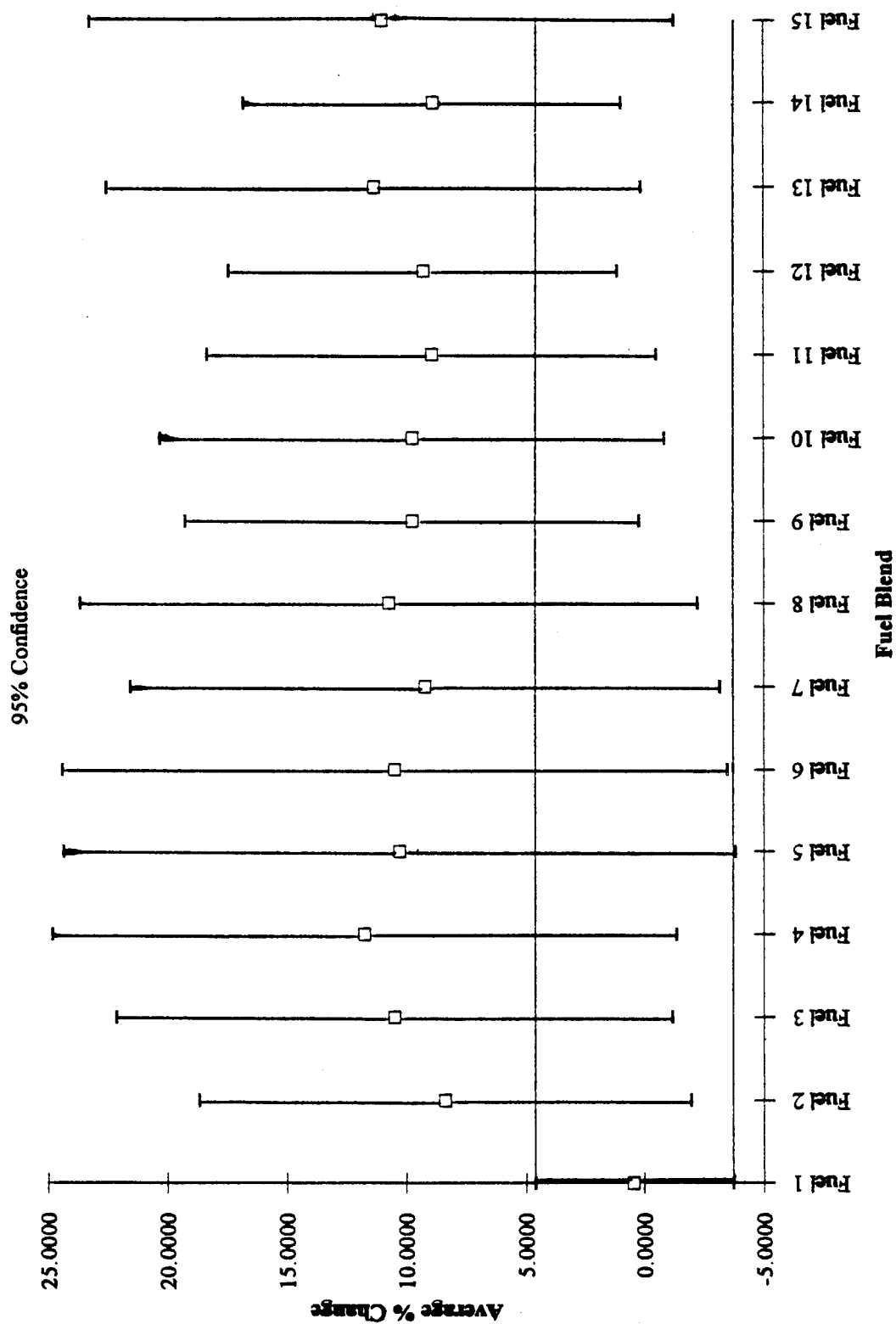


Figure 3. Average percent change of AN 6290-06 weight.

AVERAGE PERCENT CHANGE OF MS 29512-06 DIAMETER

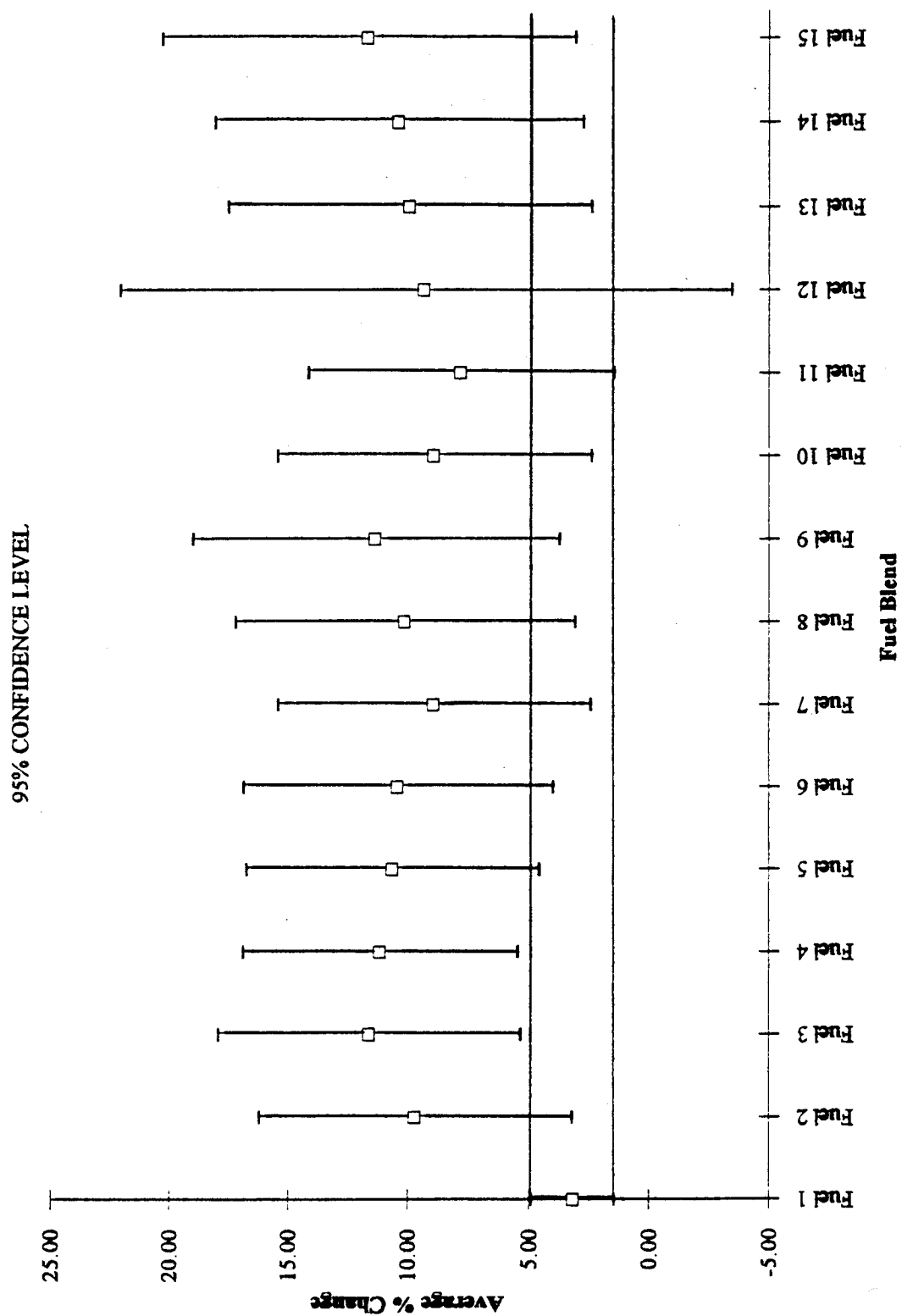


Figure 4. Average percent change of MS 29512-06 diameter.

AVERAGE PERCENT CHANGE OF MS 29512-06 CROSS SECTION

95% CONFIDENCE LEVEL

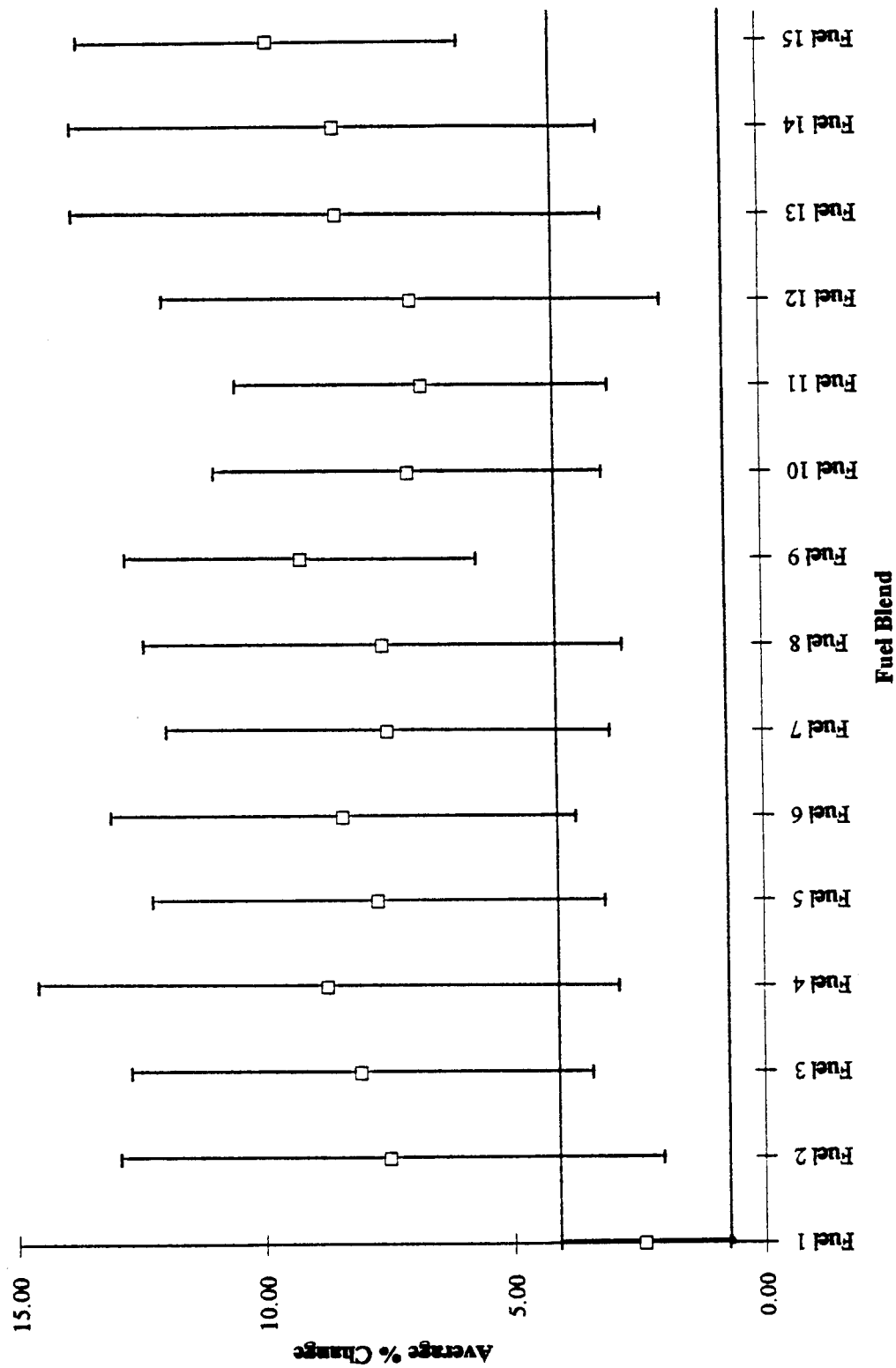


Figure 5. Average percent change of MS 29512-06 cross section.

AVERAGE PERCENT CHANGE OF MS 29512-06 WEIGHT

95% CONFIDENCE LEVEL

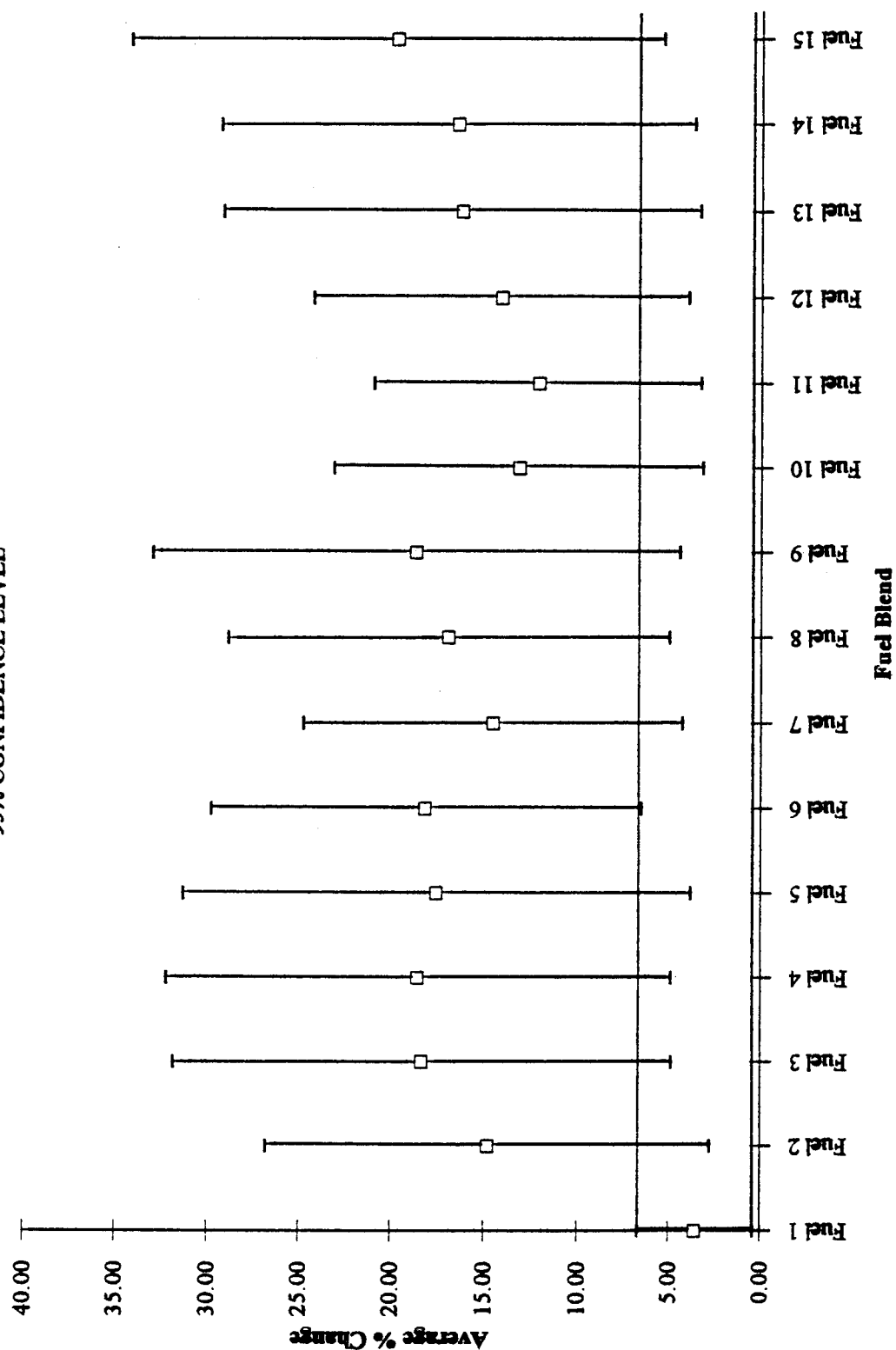


Figure 6. Average percent change of MS 29512-06 weight.

AVERAGE PERCENT CHANGE OF NAS 1593-12 DIAMETER

95% CONFIDENCE LEVEL

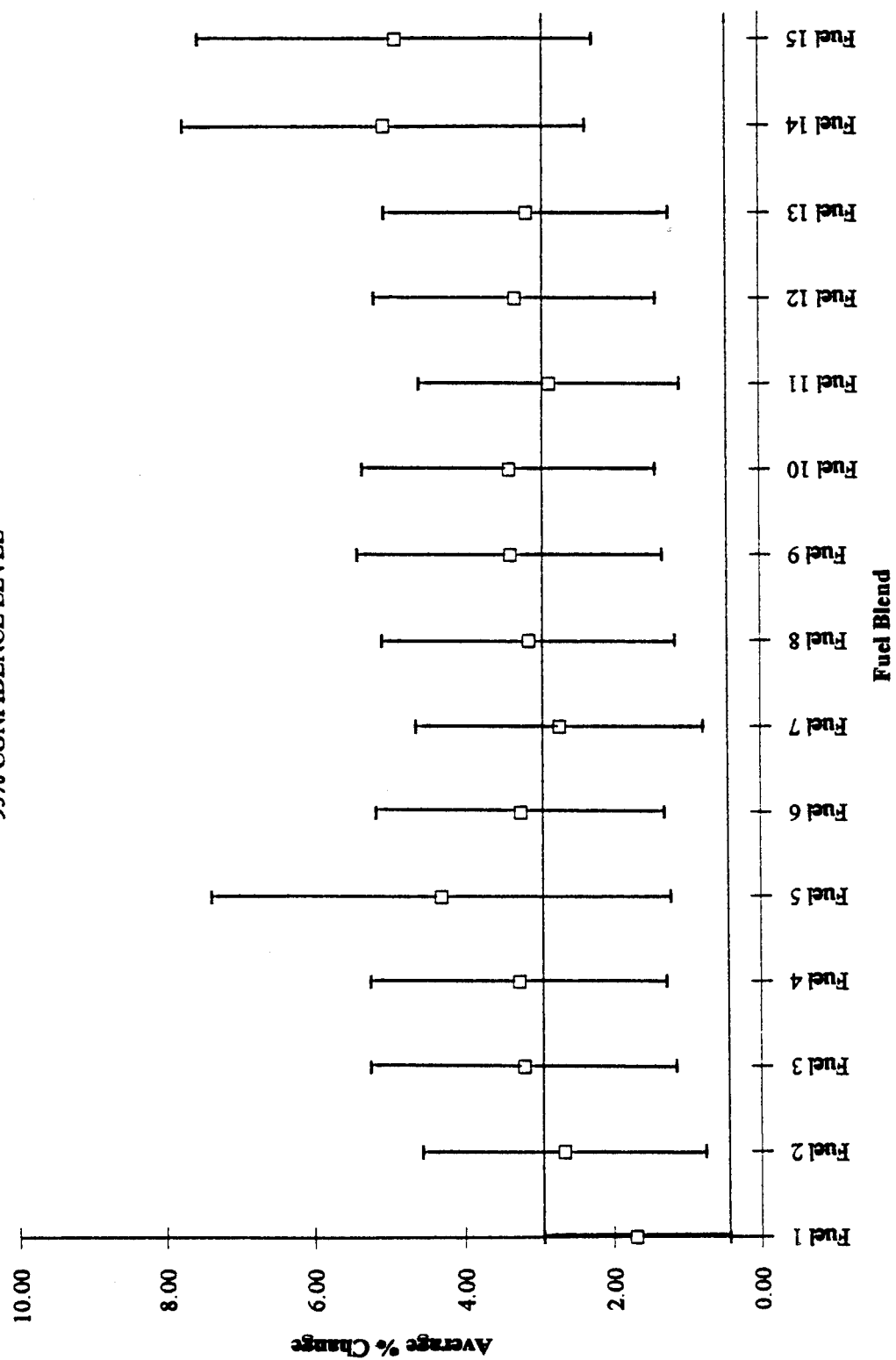


Figure 7. Average percent change of NAS 1593-12 diameter.

AVERAGE PERCENT CHANGE OF NAS 1593-12 CROSS SECTION

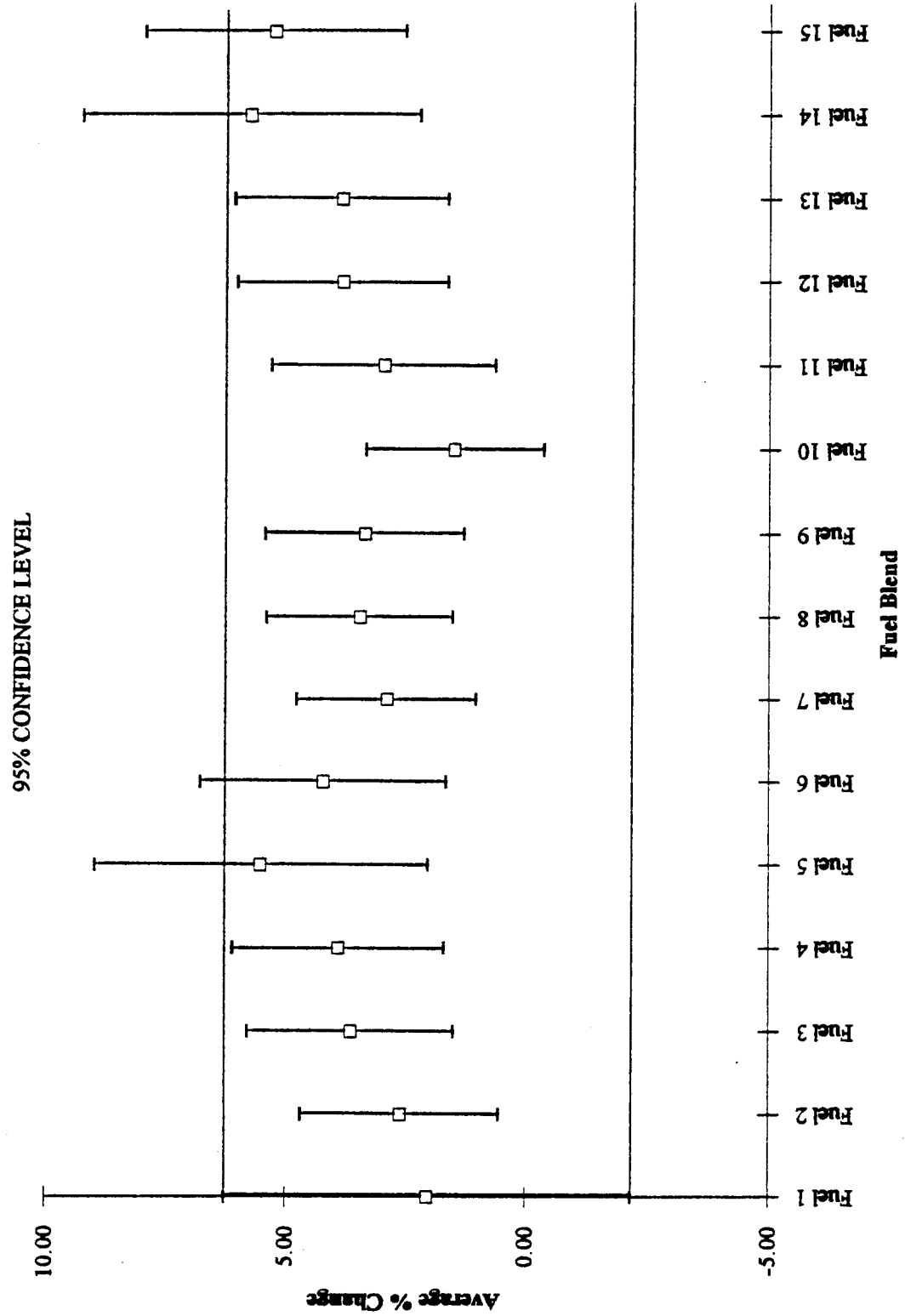


Figure 8. Average percent change of NAS 1593-12 cross section.

AVERAGE PERCENT CHANGE OF NAS 1593-12 WEIGHT

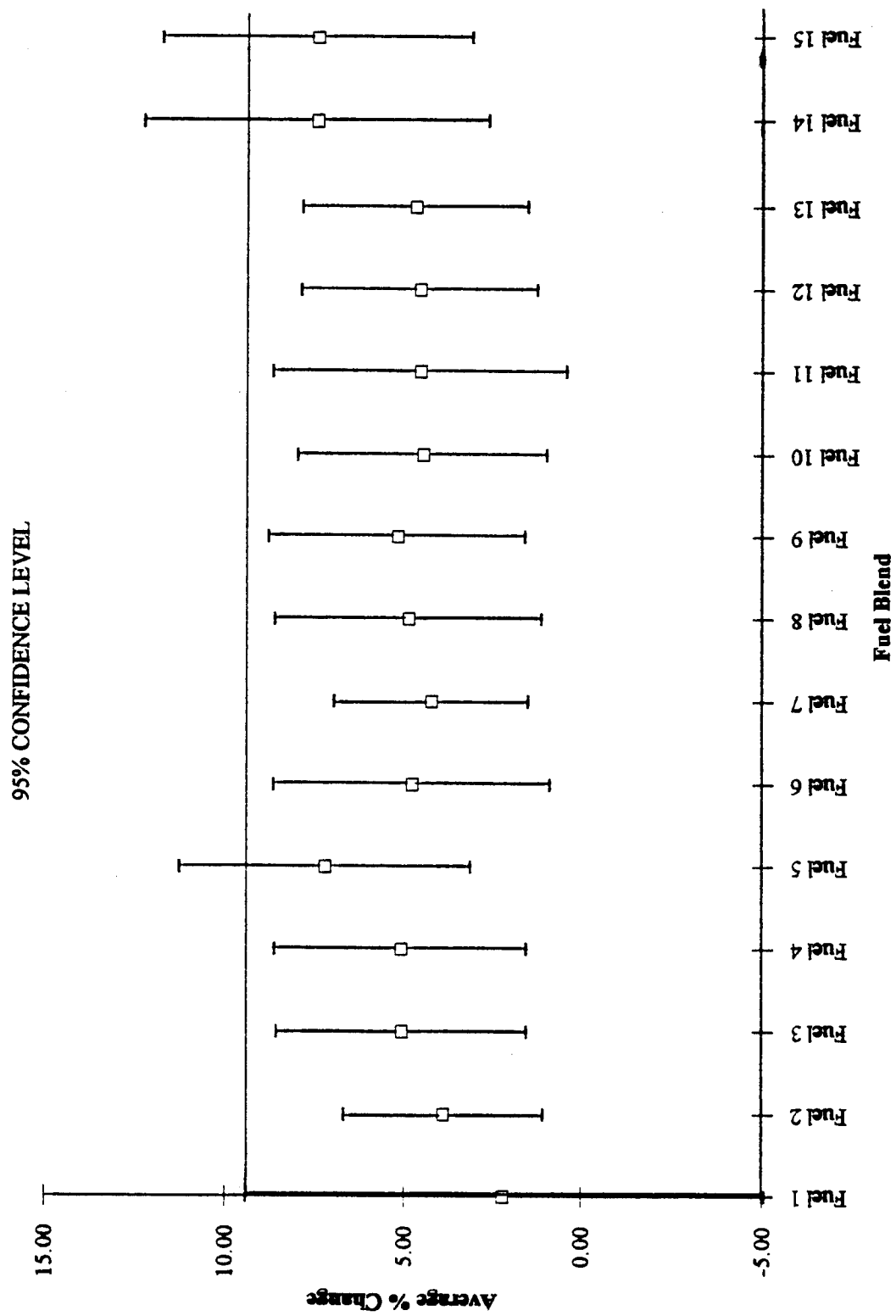


Figure 9. Average percent change of NAS 1593-12 weight.

AVERAGE PERCENT CHANGE OF AN 902-06 DIAMETER

95% CONFIDENCE LEVEL

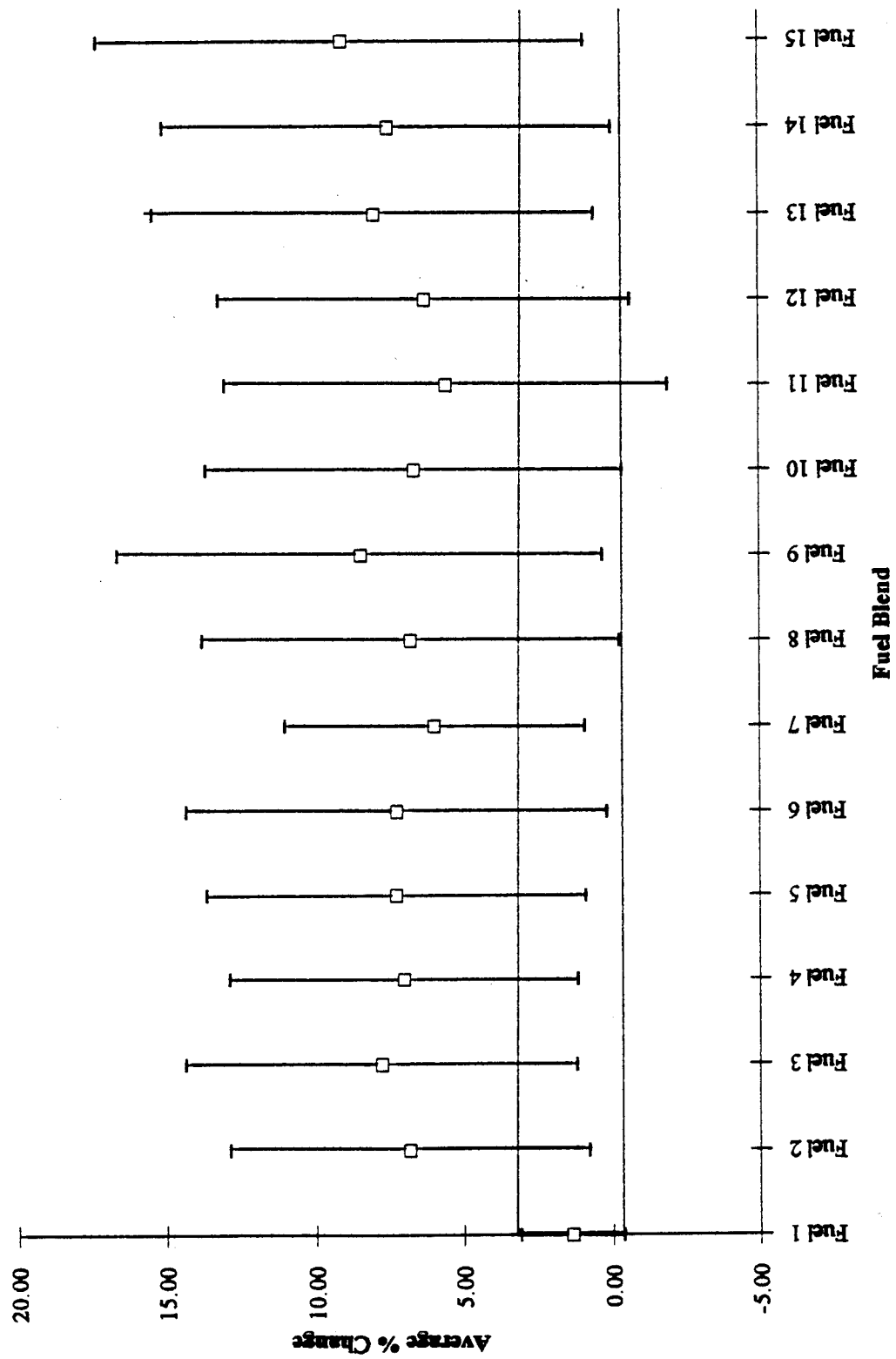


Figure 10. Average percent change of AN 902-06 diameter.

AVERAGE PERCENT CHANGE OF AN 902-06 CROSS SECTION

95% CONFIDENCE LEVEL

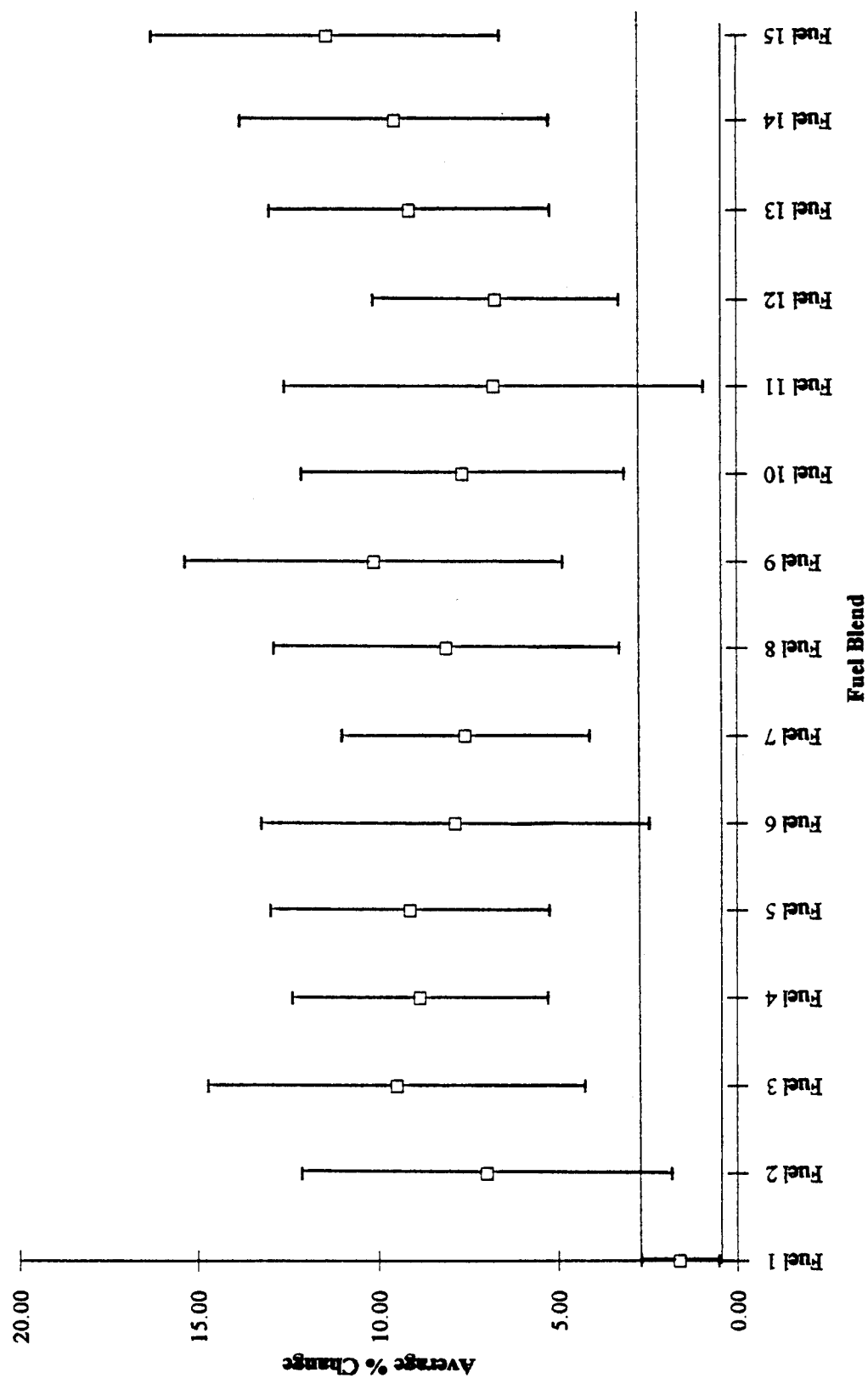


Figure 11. Average percent change of AN 902-06 cross section.

AVERAGE PERCENT CHANGE OF AN 902-06 WEIGHT

95% CONFIDENCE LEVEL

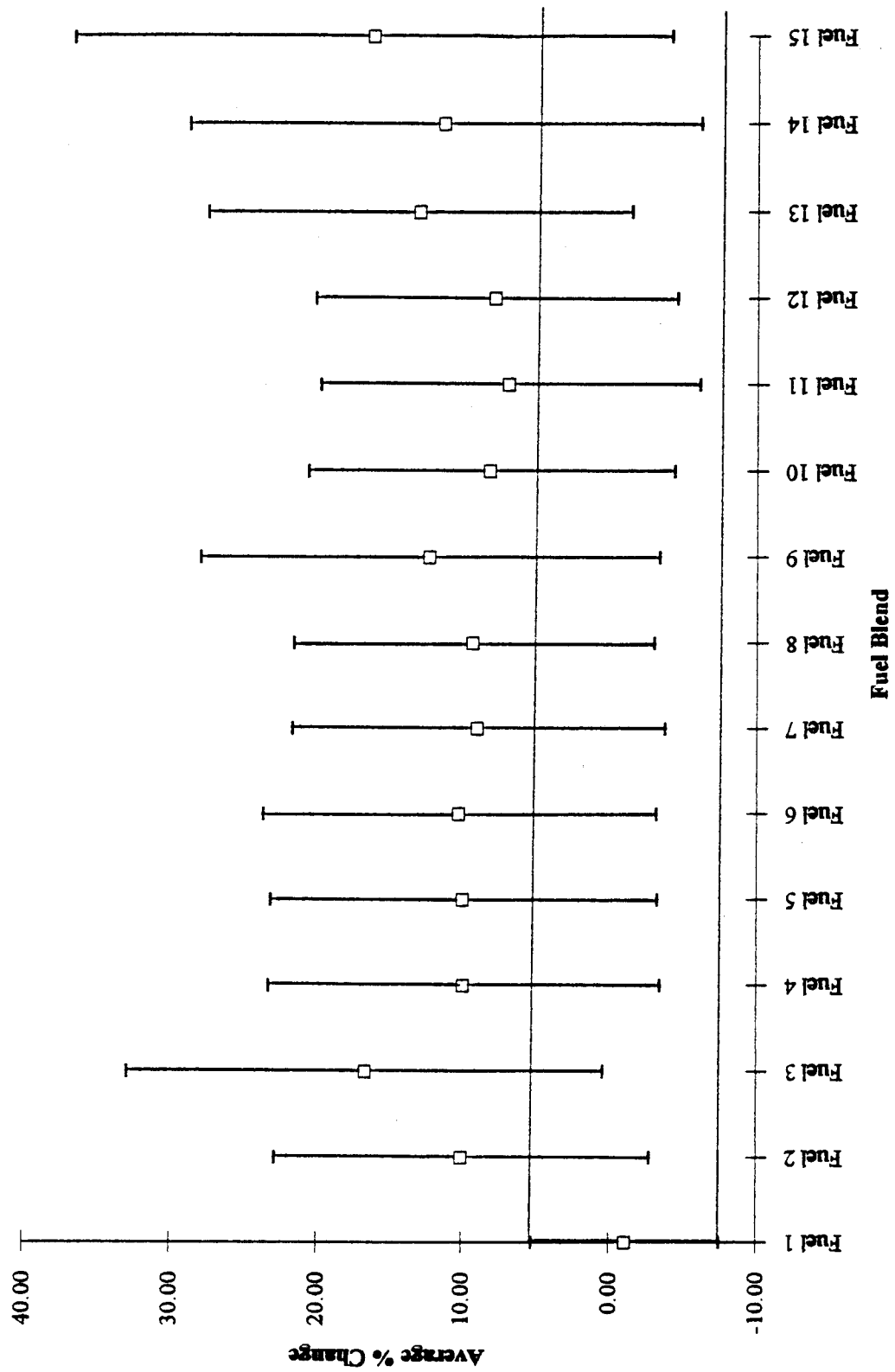


Figure 12. Average percent change of AN 902-06 weight.

AVERAGE PERCENT CHANGE OF ALUMINUM/SLOSHING COMPOUND CROSS SECTION

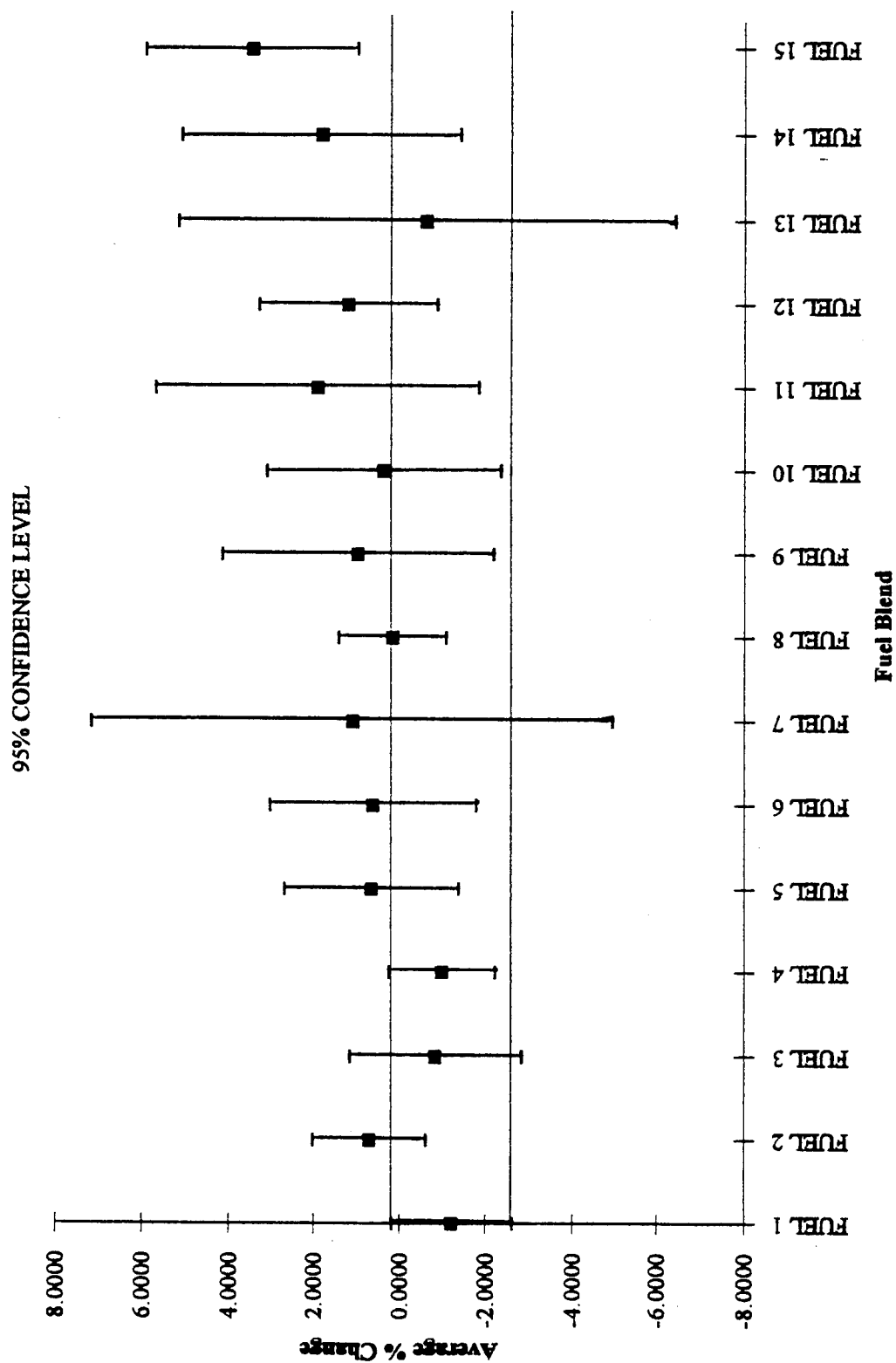


Figure 13. Average percent change of Aluminum/Sloshing compound cross section.

AVERAGE PERCENT CHANGE OF ALUMINUM/SLOSHING COMPOUND WEIGHT

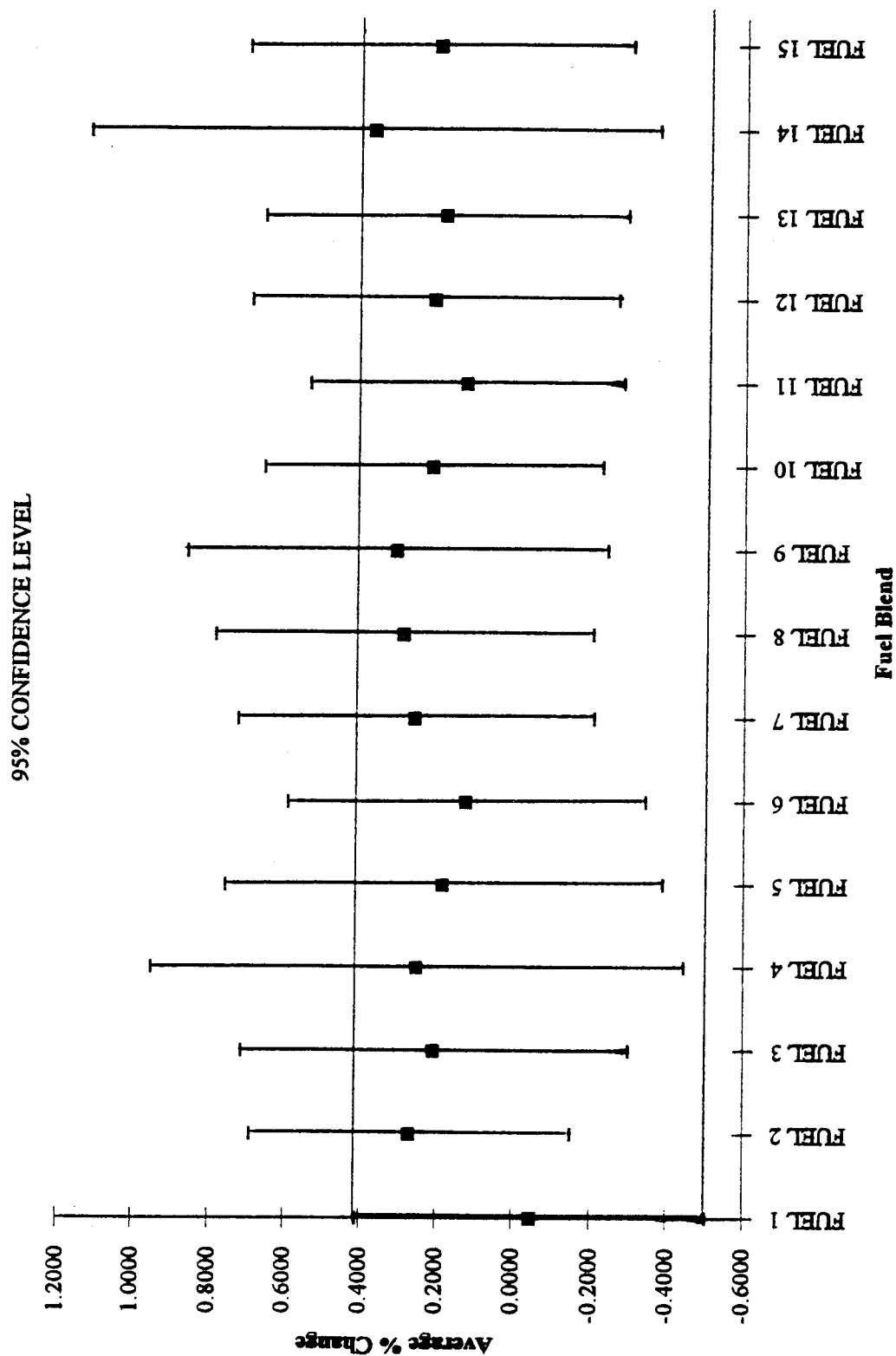


Figure 14. Average percent change of Aluminum/Sloshing compound weight.

ALTERNATE FUELS FOR GENERAL AVIATION

Ralph Kimberlin & Jim Acree
University of Tennessee Space Institute
Tullahoma, TN 37388

ABSTRACT

There is a critical need to improve the affordability and performance of General Aviation (GA) aircraft. Concepts and technologies need to be developed which can reduce propulsion system certification, acquisition, and life-cycle costs, and improve environmental compatibility and air vehicle performance.

The GA community has suffered through a diminished availability of aviation gasoline options through the past 20 years. Low-compression engines have already been approved for the use of automotive fuel, but high-compression engines have no approved substitute to date. A solution needs to be readily available, compatible with current designs, and cost-effective. Alcohol-based fuels appear to have potential. Ethanol, in particular, can boost the performance of automotive gasoline to a level compatible with most aircraft engines.

INTRODUCTION

BACKGROUND

The rapidly rising cost of 100-octane, low-lead (100 LL) aviation gasoline has been a setback for the GA community, both owners and manufacturers. This fuel is double what it was during the GA community's prosperous period of the 1970's. Accordingly, the availability and use of aviation fuel has diminished over the past two decades to a fraction of what it was. In many instances, 80-octane fuel for lower-compression engines has been replaced by automobile gasoline, which is sold at over 100 U.S. airports and used by a much larger number of individual activities. However, fuel for the more common high-compression engines, is still without a substitute. Due to these circumstances, the GA community may be forced to find an alternative fuel in the near future. For example, one viable fuel is a blend of 200-proof anhydrous ethanol and automotive gasoline as a replacement for aviation gasoline. Unfortunately, there have persisted significant misconceptions regarding ethanol use in engines, and confusion between ethanol and inferior methanol blends.

Aviation gasoline constitutes only 0.4% of the total gasoline produced domestically (reference 1), and so does not receive the brunt of research attentions. It has been argued that some of the major refiners favor doing away with this production, as it constitutes such a small market. The fuel transport problem is further complicated by denial of access to the nation's pipelines due to new regulations against the pipeline transport of these leaded fuels.

In 1985, the FAA issued an advisory circular that addressed the process with which to get approval to operate aircraft with new fuels (reference 2). This document, in conjunction with Federal Aviation Regulations (FARs) Chapter 33 (reference 3), clearly delineate the areas of concern when dealing with new fuels. The FAA Technical Center conducted a limited series of tests involving alcohol fuels in 1988 (references 4, 5, and 6). These tests served mainly to substantiate the methods to be used to qualify new fuels, anticipating the eventual introduction of alcohol-blended

fuels. Unfortunately, the Federal Aviation Regulations (FARs) do not define a specification for existing Aviation gasolines (reference 7, ASTM D-910 deals with it, but companies are not tied to it). The true make-up of aviation gasolines is ambiguous.

The benefits that can be realized with a new fuel include:

- (1) A reduction in harmful emissions;
- (2) A revitalization of GA industry, providing jobs, etc.;
- (3) An end to fuel contaminations in GA aircraft;
- (4) The use of a renewable resource, less reliance on foreign oil; and
- (5) An increase in aviation activity.

Problem areas to be worked out with new fuels for aviation include:

- (1) Establishing a practical distribution network;
- (2) Dealing with misconceptions (i.e. methanol vs. ethanol);
- (3) Verifying materials compatibility;
- (4) Encountering resistance from GA manufactureres (re. product liability); and
- (5) Integration of new fuels into the system.

Cost is an important consideration in the practical determination of an alternate fuel. Petroleum products change price frequently, however at this writing, current aviation gasoline (100 LL) costs to the consumer are roughly \$2.⁰⁰ per gallon. Proposed federal taxation of aviation and automotive gasoline will further increase the price to the consumer. However, high-octane automotive gasoline prices are currently less than \$1.³⁰ per gallon. Anhydrous ethanol, at 200-proof, is priced much less, at \$0.⁸⁰ per gallon. As an example, a mixture of 65% automotive fuel and 35% ethanol would be priced at approximately \$1.¹⁰ per gallon (using simple math and neglecting unforeseen production costs). Both automotive gasoline and ethanol are readily available.

PURPOSE

The purpose of this program is to provide an affordable, environmentally-conscious, and readily-available aircraft fuel which can offer performance better or virtually equal to current aviation gasolines. These is little benefit to the consumer when provided with a fuel which cannot be incorporated into the GA community without substantial and costly modifications in materials, production, transfer, and operating procedures. A co-requirement is the determination of a practical and common method to re-certify individual aircraft models for the use of the new fuel. Finally, the ultimate purpose is to enhance and revitalize the GA industry.

FUELS

Automotive Gasoline

Automotive gasoline currently available domestically is unleaded, in that Tetra-Ethyl Lead (TEL) has been phased out; TEL was previously used as an octane enhancer. As unblended automotive gasoline has a low octane value, MTBE is added as an octane enhancer in varying amounts in order to produce the desired octane rating (87, 89, and 90 are commonly advertised at the pumps). Autogas is mixed so as to have summer or winter blends; this offers lower Reid Vapor Pressures (RVP) in the summer in order to minimize vapor lock tendencies, and higher RVPs in the winter to augment cold start performance.

Aviation Gasoline

Aircraft gasoline (Avgas) has been offered in two grades in the past, 80/87 and 100LL. As discussed above, 80/87 is being phased out as it is less available. Both grades are leaded (contain TEL) and use Ethyl-Di-Bromide (EDB) to help neutralize the undesirable combustion byproducts. Avgas is produced in one blend, in that it is not sensitive to season as is autogas. Aircraft frequently must fly between hot and cold extremes during the course of a single flight and tank of fuel; the threat of vapor lock drives the blend to favor a low RVP. In cold weather, primers are used to augment poor starting performance.

Methanol

Methyl alcohol, commonly referred to as wood alcohol, is odorless and colorless and soluble in gasoline under benign conditions. Methanol has favorable octane ratings (112 RON and 91 MON), and can be mixed with gasoline to increase its octane number. Broad flammability limits allow methanol to burn in even leaner fuel-air ratios than straight gasolines; this has the potential of increasing aircraft specific range. On the negative side, methanol has been shown to be incompatible with many materials. This can manifest itself as a corrosive to fuel system components, such as filters and seals. Worse yet, the effects on aluminum are also negative, and this has a significant effect on aircraft engines and tanks. Methanol can also damage fiberglass storage tanks commonly found at refueling facilities, it can shrink cork gaskets found on aircraft, and destroys painted surfaces when spilled. Also, methanol is toxic, and it is very difficult to determine the water content in a given sample.

Higher Order Alcohols

Tertiary-Butyl Alcohol (TBA), Isopropyl (rubbing) alcohol, and higher order alcohols can be used as fuel blending agents as well. Higher order indicates more carbon composition of the product, and an associated better blending with water (less phase separation). However, the higher the order, the lower the associated octane value. The very requirement for TEL or alcohols in fuels is to create a blend that will increase the octane number.

MTBE

Methyl-Tertiary-Butyl Ether is a high octane (116 RON and 98 MON) agent which has replaced TEL in automobile gasolines during the 1980's. It is derived of alcohols and butanes, is similar in relevant properties to gasoline, and does not separate from water as easily as the alcohols. MTBE is compatible with the materials used in automobile engines and fuel systems.

ETBE

Ethyl-Tertiary-Butyl Ether is a high octane (117 RON and 99 MON) agent which has been studied for possible replacement of MTBE in automotive fuels (reference 8). It is derived of isobutylene and ethanol. While not as commonplace as MTBE, it has a higher octane blending value than MTBE and a lower RVP. It is also fairly compatible with the materials used in automotive engines and fuel systems.

Ethanol

Ethyl alcohol, commonly referred to as grain alcohol, is also odorless and colorless, but is less sensitive to water contamination than methanol. Ethanol is more expensive than methanol. Ethanol has high octane ratings (106 RON and 89 MON), though not quite as high as methanol. Like methanol, ethanol can be burned under very lean conditions, extending specific ranges.

Ethanol is compatible with most engine materials and will not contribute to engine wear; however, ethanol is not compatible with some rubbers that are utilized as fuel tank bladders.

"Gasohol" is a registered trademark of the University of Nebraska Agricultural Products Industrial Utilization Committee. It consists of a blend of 10 percent anhydrous ethanol in unleaded gasoline, and has been commercially available at the pumps for automobiles since the late 1970's.

Research on ethanol-based fuels to date has been limited, and of limited benefit community-wide. Vapor-lock tendencies of this type of fuel blend have been a concern, but any degradation beyond standard fuels has not been proven or defined. For example, studies investigating vapor lock have been conducted since 1948 when a Cessna 140 reported vapor lock with an alternate fuel, but then experienced vapor lock again when using standard 100 LL aviation fuel (reference 9). Documented flight tests under representative conditions have been limited.

The incompatibility of some materials used in engine fuel systems with ethanol blends has also been cause for concern (references 10 and 11); ethanol will dissolve a few types of non-metallic constituents of fuel systems such as polyurethane. However, these components are easily and economically replaced. Many other plastics and alternative materials are fully compatible with ethanol.

Another cause for testing is phase separation tendencies of ethanol-blends; yet studies on this issue have also been inconclusive, and very contradictory. While one source is pessimistic (reference 12), another claims smooth engine operation using such mixtures (reference 13). In 1985 the University completed a limited in-house effort towards flight testing ethanol-gasoline mixtures with tremendous success.

Concerns over the degree of benefit of ethanol as an octane booster have not been substantiated. Alcohol-based fuels are used in high-performance racing fuels. Ethanol's octane performance value of 89 is not truly representative of its ability to boost the overall performance value of the fuel blend. It has been suggested that it might be satisfactory for engines which operate on up to 91/96 avgas, but no more. This also has not been demonstrated conclusively.

AIRCRAFT ENGINES & OPERATIONS

AIRCRAFT ENGINES

General aviation aircraft that use spark-ignition engines have generally used either a low-compression fuel or a high-compression fuel. These fuels are commonly referred to as 80/87 or 100LL. Low compression engines are found on many older models, especially those requiring less horsepower. With exceptions, these engines typically develop up to 150 horsepower. The high-compression engines will develop horsepower above that amount.

Octane numbers have been developed that express a fuel's performance value and its ability to ultimately provide power. A good explanation of the octane rating scale development is presented in reference 14. There are several definitions involved with octane ratings. The most commonly used commercially are the Research Octane Number (RON), and Motor Octane Number (MON) which are averaged to be advertised at the automotive gasoline pumps. The RON is a figure that refers to the performance of the fuel under light demand conditions (slow driving), and the MON measures performance under heavy demand conditions (high power settings). It is the MON that is most closely associated with the demands of aircraft flight. However, two other scales have been created to deal with the aircraft fuels. The Aviation Lean Octane Number (ALON) is a measure of the performance of aircraft fuels at lean fuel-air mixture settings. The Aviation Supercharge Octane Number (ASON) is a measure of the performance of fuels at rich fuel-air

mixture settings. These are displayed on the aviation product label as two numbers; the first is the ALON, and the second is the ASON. The most common, as mentioned above, are the 80/87 and the 100/130 aviation fuels. Others that have been used are an intermediate blend (91/96) and higher performance blends (115/145, 137/190, 157/252).

GA aircraft engine components are designed to handle aviation gasolines as are currently available at the pumps. Carburetors, compression ratios, spark plugs, and spark advance figures are optimized for these petroleum-based fuels. In order to be optimized about alcohol-based fuels, engines would need to be designed and tuned according to different criteria. If designed about alcohol-based fuels, engine performance can be increased significantly (reference 4). If major modifications are avoided, such as changing compression ratios or carburetion, alcohol-based fuels can still match petroleum-based fuels in performance. This can be done through simple adjustments to spark advance, and carburetor jet size. Generally, alcohol-based fuels tend to operate at a slightly higher Brake Specific Fuel Consumption (BSFC) with current engine tunings; this decreases either aircraft range or power available to a small degree. However, alcohol-based fuels have the capability to operate an engine at a leaner fuel-to-air ratio, ultimately allowing better range performance on a given tank of fuel. This is due to the lean misfire limit being lower for the alcohol-based fuels. But they also require that a spark advance of 35 to 40 degrees be utilized, vice an advance of 20 to 25 degrees as is used for gasolines (reference 15). This is to optimize the burn around the slower flame front of the alcohol, as compared to gasolines. Additionally, the potential of alcohol-based fuels to increase the octane performance rating can actually allow an increase in available power when engines are tuned according to alcohol-based fuel considerations.

GA engines can efficiently handle both alcohol-based fuels, and current petroleum-based fuels. The object of a program to demonstrate this would consider the optimum parameters for petroleum fuels (current engine settings), discover the optimum setting for the selected alcohol-based fuel, and make a recommendation to the best intermediate settings that could accommodate both fuels. Optimally, no adjustments would be necessary, until the operators were sure of the future available of the alcohol-based fuel. At this point, the criteria for engine tuning could be based solely upon the alcohol-based fuels. Petroleum-based fuels could still be utilized in such an engine, however not at peak efficiency; a petroleum-based fuel would be an alternate fuel.

Another concern of engine operations with alcohol-based fuels is that of cold starts. This problem is predominant within the agricultural community who is trying to develop methods to start engines utilizing neat methanol as the primary fuel. Similar problems occur with alcohol-blends that have sat for awhile. This is due to the phase separation that can sometimes occur, which leaves the alcohol-based portion at the bottom of the tank and which is seen first by the engine. However, much still needs to be quantified when blends are concerned.

The phase separation phenomenon continues to plague alcohol-based fuels initiatives. It is claimed by some researchers that this is the ultimate undoing of the alcohol fuels concept. Innovative solutions such as continuous mixing of the fuels via submerged fuel tank pumps, or the development of a stabilizing agent have been proposed. Phase separation was observed by a University of Tennessee Space Institute (UTSI) study (references 16 and 17), but not observed to be a problem as far as engine operation was concerned. Quantifying the detrimental effects of phase separation has yet to be completed. An advantage of alcohol-based fuel is its ability to dissolve in water, vice completely separate from it. The FAA addresses the problem of water in aviation fuels in reference 18.

Vapor lock is a concern that must be addressed early in the fuel development cycle. This is the tendency of a fuel to vaporize prior to carburetion at higher operating temperatures, prevent the engine from receiving an adequate fuel-to-air mixture, and causing loss of combustion and operation. RVP has been used by operators to measure vapor-locking tendencies. However, the RVP does not appear to define the vapor-locking tendency of a fuel with any accuracy (reference

19). New methods have been proposed , using a modified reid procedure that increses the test vapor-to-liquid ratio of the apparatus used. In any case, practical demonstrations will need to be completed with respect to aircraft engines and their operating environment. The FAA has an advisory circular (reference 2) that defines the test procedure for alternate aircraft fuels that includes a requirement to demonstrate this.

Alcohols tend to dissolve gums that have been deposited inside the engine. During initial usage, these materials will form sediment on filters and other components. However, the burning of alcohol fuels will ultimately lead to cleaner engines in the long run. Similarly, alcohol-based fuels tend to run substantially cooler than gasolines. Cooler temperatures and cleaner engines, in themselves, ultimately lead to less engine wear and so prolong the life of the engine. This will substantially reduce operating costs through repairs and overhauls.

Pure alcohols do not run well on currently designed and tuned engines. Without adjustments, aircraft engines run roughly on pure ethanol and may not run at all on pure methanol. The addition of at least some gasoline is an essential compromise (reference 4). This is especially so, considering the self-imposed requirement to find a fuel that will run well on either gasoline or alcohol-based fuels.

Specific engine designs react differently to the addition of alcohol fuels. Heated intake air is preferred by ethanol-based fuels (reference 4). Equivalent inlet air temperature to a supercharged engine can be 100° F. higher than for non-supercharged models (reference 15). This can lead to better operating characteristics. Reference 4 reports worse operation of some alcohol-blends on fuel-injected engines, as compared to carbureted engines. In this respect, even the type of carburetion will affect fuel-air mixing qualities.

ENVIRONMENTAL CONCERNS

Engine emissions, in terms of both content and total amount of unwanted products are a real concern in the development of new technologies. The removal of TEL from automotive gasolines to minimize leaded emissions is an example. A large part of the nation's pipeline network is prohibited from transferring leaded fuels now; this encompasses current aviation fuels and adds to the general aviation fuel distribution problem.

The reduced lead content of the unleaded automotive gasoline and ethanol mixture offers several advantages. A significant reduction in lead-fouling of the engine spark plugs and valves enhances the engine component life, in itself, saving significant maintenance costs to the user (references 9 and 20). Also, the reduced lead content causes the exhaust emissions to be less toxic. This offers a safety advantage, as well as an environmental advantage. Ethanol, as an ingredient, reduces emissions of oxides of nitrogen and sulfur, carbon monoxide, smoke, unburned hydrocarbons, and polynuclear aromatics (reference 21).

RESULTS OF TESTS TO DATE

Fuels research is active amongst industry and universities. Generally, the target of ongoing fuels research has been automotive or agricultural in nature. However, the Experimental Aircraft Association (EAA) has been active for many years in the pursuit of Supplemental Type Certificates (STCs) for various aircraft such that they may use automotive gasoline as a substitute for 80/87 (reference 22). Unfortunately, higher compression aircraft engines cannot also benefit from this pursuit; these aircraft continue to use the 100 LL aviation gasoline, still the general aviation standard. Gasohol has been used on a number of EAA aircraft and functionally performed satisfactorily; yet material compatibility and vapor lock characteristics were not fully investigated

(reference 23). The EAA continues to work with the use of automotive gasolines and Gasohol on a limited scope (reference 24). The EAA effort has benefitted a significant segment of the general aviation community already, with thousands of STCs approved for aircraft that range from Cessna 150s and Piper Cherokees to the Douglas DC-3.

The Illinois Department of Transportation conducted flight tests using 190-proof ethanol, experienced no major difficulties, and found that the ethanol burned cooler and cleaner with less wear (reference 25). A 1941 study concluded that the addition of 10% or 25% ethanol additive to automotive gasoline increased full-throttle power and part-throttle specific fuel consumption (reference 26).

In 1985, UTSI performed research on four ethanol/automotive gasoline blends (15%, 25%, 35%, and 45% ethanol by volume). Results showed tremendous potential, but the program was limited in scope (references 16 and 17).

PLANS

NASA's Advanced General Aviation Transport Experiments (AGATE) program has the primary objective of reducing direct operating costs of engines by more than 10%. Fuels research alone can hope to beat this goal.

The University of Tennessee Space Institute is planning a fuels research program to be sponsored in part by an industry team and in part by the federal government. The program will include a laboratory phase, a ground test phase, and a flight test phase. Research fuels will include automotive gasoline with an ethanol content of between 15 and 45 percent, and with additives deemed practical; methanol blends are known to be too corrosive. Aviation gasoline will have to be tested as a baseline from which to compare tests. The challenge is to identify a fuel that is cheap, available, and would require minimal (if any) modifications to typical aircraft fuel and propulsion systems. This fuel needs to be compatible with current systems and 100LL avgas as it would realistically be phased in over several years before becoming the standard (hopefully). Additionally, the program will test and recommend a common, repeatable method to certify individual aircraft models for the new fuel. This will speed up the STC process, of benefit to the regulators as well as the operators.

The primary goal of the first phase is to identify fuel blends with which to commence aircraft engine tests. The following fuel static properties will be determined in the laboratory:

- (1) Absolute vapor pressure versus temperature using the Reid method;
- (2) Distillation profile; initial boiling point and end point; residue;
- (3) Motor octane number;
- (4) Lead content;
- (5) Gum;
- (6) Sulfur;
- (7) Copper corrosion; and
- (8) Fuel separation (water formation).

Testing in a Cooperative Fuels Research (CFR) engine will help to define favorable blends and the engine adjustments necessary for smooth operation. Specific objectives of testing with the CFR engine include:

- (1) Determine whether the test fuels will support efficient combustion;
- (2) Determination of anti-knock characteristics;
- (3) Determination of exhaust emissions;
- (4) Determination of comparative fuel consumption rates;

- (5) Comparison of brake horsepower produced; and
- (6) Comparison of engine operating temperatures and profiles.

The primary goal of the second phase is to define which blend(s) with which to commence flight tests. Aircraft engines will be operated on deck with the test fuels to pinpoint problems and further optimize engine adjustments. Objectives are similar to those for the CFR engine, with the addition of an aircraft fuel system compatibility study, and determination of vapor lock characteristics. This phase will afford an opportunity to inspect engines for unusual wear before continuing with flight profiles.

The goal of the third phase is to specify the best fuel for operational use and recommend a simple, repeatable procedure from which to certify individual aircraft models for use of this fuel. This will be accomplished by flight testing of the selected test blends. Specific goals of the flight tests include:

- (1) Determination of engine operating temperatures and temperature profiles;
- (2) Determination of vapor lock tendencies;
- (3) A further determination of aircraft fuel system compatibility with test fuels; and
- (4) Determine any change in engine/aircraft performance.

Flight tests will need to be conducted with takeoff fuel temperatures as high as 120° F. in order to demonstrate a practical resistance to vapor lock, and flights to the service ceiling of the aircraft will be required. Proper engine cooling and engine response to rapid throttle changes are other valid concerns. Upon completion of flight testing the test aircraft will receive complete test engine teardown and inspection in order to determine unusual wear or corrosion due to the use of the test fuels. A recommended procedure by which to test other aircraft types, regarding use of the fuel blend will consider critical tests required, tests not required, minor engine adjustments (if necessary), and minor fuel system components to replace. The intent of this program remains to find a fuel blend that will operate in production engines as presently configured (or at negligible cost of modification to the user) and such that 100LL aviation gasoline may also continue to be utilized.

Test aircraft selection is based upon the assumption that there are four popular types of engine fuel systems installed on reciprocating-engined general aviation aircraft. These include:

- (1) Float-type carburetion;
- (2) Pressure carburetion;
- (3) Fuel-injection; and
- (4) Turbo-charged systems.

Other factors in determining suitable test aircraft include:

- (1) Sensitivity of the particular design to vapor lock problems. Low wing aircraft are more susceptible to vapor lock and usually provide the limiting case.
- (2) Popularity of selected test engine and fuel systems among other aircraft. Lycoming and Continental engines should be represented. Both metal and bladder-type fuel cells should be used.
- (3) Aircraft to be used should have more than one fuel tank. This will allow regular aviation fuel to be selected as desired.
- (4) Multi-engine aircraft should be used to further safety of test. However, credibility suffers if at least one test aircraft is not single-engine.

CONCLUSIONS

Alternate fuels testing for general aviation aircraft has not had the attention that is truly deserved. It potentially offers the GA community a more cost-efficient method of operations, which in turn, enhances the community in terms of production, usage, and attractiveness to future participants. Testing on fuel blends has been inconclusive to date, and a comprehensive program to define a near-term alternative fuel needs to be accomplished. Fuels programs that conclude only with a recommendation for further testing are not called for in this current aerospace climate.

REFERENCES

1. *Alternate Fuels for General Aviation*, Sport Aviation, D.H. Scott, October 1983.
2. *Qualification of Fuels, Lubricants, and Additives for Aircraft Engines*, Advisory Circular, Federal Aviation Administration, 20 December 1985.
3. *Airworthiness Standards: Aircraft Engines*, Federal Aviation Regulations, Ch. 33, 1993.
4. *Alternate Fuels for General Aviation Aircraft with Spark Ignition Engines*, DOT/FAA/CT88/05, A.M. Ferrara, FAA Technical Center, June 1988.
5. *The Performance of Alternate Fuels in General Aviation Aircraft*, DOT/FAA/CT88/13, A.M. Ferrara, FAA Technical Center, July 1988.
6. *Comparison Between Unleaded Automobile Gasoline and Aviation Gasoline on Valve Seat Recession in Light Aircraft Engines*, DOT/FAA/CT-TN89/33, J.R. Allsup, National Institute for Petroleum and Energy Research, May 1989.
7. *ASTM Manual of Engine Test Methods for Rating Fuels*, ASTM, 1952.
8. *Use of Ethyl-t-Butyl Ether as a Gasoline Blending Component*, Shiblom, Schoonveld, Riley, and Pahl, 1990.
9. *Autogas Versus Avgas: Myths and Realities*, Cessna 150-152 Newsletter, D. Meinhardt, December 1984.
10. *Ethanol Fuels: Use, Production, and Economics*, S. J. Winston, 1981.
11. *Alcohol-Gasoline Blends as Vehicular Fleet Fuels*, C. L. Knapp, Solar Energy Research Institute, September 1981.
12. *Ethyl Alcohol Production and Use as a Motor Fuel*, J. K. Paul, 1979.
13. *Small-Scale Fuel Alcohol Production*, U.S. Department of Agriculture, 1980.
14. *Military Fuel Characteristics: 1917-1945*, R. Kerley, SAE, October 1993.
15. *Aviation Fuel Economy and Quality - Brothers Under the Aircraft Skin*, SAE, H.E. Alquist, E.A. Droegemueller, and H.N. Taylor, April 1953.
16. *A Feasibility Study on the Use of Ethanol/Automotive Gasoline Blends in General Aviation Aircraft*, Society of Automotive Engineers (SAE) paper #852105, L. J. Hughes and R. D. Kimberlin, 1985.
17. *An Analysis of Ethanol/automotive Gasoline Blends for use in General Aviation Aircraft*, Master's Thesis, UTSI, L.J. Hughes, March 1985.
18. *Water in Aviation Fuels*, Advisory Circular, Federal Aviation Administration, Dec. 1985.
19. *Vapor-Locking Tendencies of Fuels - A Practical Approach*, General Motors Corp., J.D. Caplan and C.J. Brady, June 1957.
20. *Should You Switch to Auto Fuel?*, Cessna 150-152 Newsletter, K. Thomas, Dec. 1983.

21. *Alternative Fuels for Spark-Ignition Engines*, R. H. Thring, Paper #831685 presented at Fuels and Lubricants Meeting, San Francisco, California, November 1983.
22. *Auto Fuel STC Approved*, Sport Aviation, October 1982.
23. *Autogas for Your Airplane*, Sport Aviation, H. Zeisloft, June 1983.
24. *Auto Gas Update: Ten Years of Experience*, Sport Aviation, H. Zeisloft, April 1993.
25. Private Communication, C. Wells & D. Lewis, Illinois Department of Transportation, Division of Aeronautics, January 1985.
26. *Comparative Performance of Alcohol-Gasoline Blends in a Gasoline Engine*, Journal of the Aeronautical Sciences, A. R. Rogowski & C. F. Taylor, August 1941.

TERMINOLOGY

AGATE	Advanced General Aviation Transport Experiment.
ALON	Aviation Lean Octane Number; a measure of the performance of fuels at lean fuel-air mixture settings; commonly seen as the first number in the aviation product label (100/130).
Anhydrous	Without water; anhydrous alcohol has no (or very little) water content.
ASON	Aviation Supercharge Octane Number; a measure of the performance of fuels at rich fuel-air mixture settings; commonly seen as the second number in the aviation product label (100/130).
ASTM	American Society for Testing and Materials; publications offer procedures and equipment requirements for various products, including fuels.
BSFC	Brake Specific Fuel Consumption.
CFR	Cooperative Fuels Research; the term commonly applied to fuels research engines.
Denatured	Modification such that the product is unfit for drinking. Denatured alcohol is that which usually contains some quantity of methanol.
EAA	Experimental Aircraft Association.
EDB	Ethyl-Di-Bromide; added to leaded gasoline to minimize the unwanted lead deposits that occur due to combustion of TEL. EDB is corrosive.
ETBE	Ethyl-Tertiary-Butyl Ether; a proposed octane booster.
FAR	Federal Aviation Regulation.
GA	General Aviation.
MEB	An additive used with TEL in gasolines to reduce leaded emissions.
MTBE	Methyl-Tertiary-Butyl Ether; an octane booster use in premium unleaded gasolines.
MON	Motor Octane Number; a measure of the performance of fuels under conditions of heavy demand, or high power settings (aircraft operations). Related closely with ALON with respect to aircraft operations.
Neat	Not diluted; a neat alcohol is the same as anhydrous alcohol for purposes of this study.
RON	Research Octane Number; a measure of the performance of fuels under conditions of light demand, or reduced power settings (automobile city driving).
RVP	Reid Vapor Pressure; used to measure the volatility of fuels; high RVPs mean good ignition and starting behavior, but can indicate increased vapor-locking behaviors.
STC	Supplemental Type Certificate; issued by the FAA for modifications to the original type certificate; in this context it applies to certification of alternate fuels for operation of a specific aircraft or aircraft model.
TEL	Tetra-Ethyl Lead; an octane enhancer used until late 1980's in automotive gasoline (leaded gas), but phased out in favor of environmental concerns.
UTSI	University of Tennessee Space Institute.

CERTIFICATION OF A CARBURETED AIRCRAFT ENGINE ON ETHANOL FUEL

M. E. Shauck, J. Tubbs, M. G. Zanin
Renewable Aviation Fuel Development Center
Department of Aviation Sciences
Baylor University
Waco, TX. 76798-7413

ABSTRACT

Aircraft used in commercial operations must be licensed by the Federal Aviation Administration (FAA) in a certified category. In order to certify a new fuel, the engine and the airframe must both satisfy FAA requirements. The technical feasibility of ethanol as an aviation fuel was established over a 13 year period of research, development, flight test and demonstrations. A previous program obtained FAA certification for a fuel injected aircraft engine to use denatured 200 proof ethanol. It was determined that the use of ethanol in flight training operations would best establish the economic viability of ethanol while avoiding distribution problems. The most common flight trainer, the Cessna 152, was chosen to be certified. This aircraft is powered by a carbureted Lycoming engine, the O-235. This engine was modified to use ethanol and a test plan for certification was submitted to the FAA. The plan was accepted and the test conditions successfully met. After airframe certification, this aircraft will be placed in the flight training program at Baylor University and Texas State Technical College.

INTRODUCTION

The development of ethanol as an aviation fuel was initiated because of a threat to the supply of aviation gasoline as a result of the Arab oil embargo in 1973. While supply was never curtailed as a result of the embargo, US dependence on imported oil has increased over the years and the development of a domestic fuel supply has become critically important. In the course of a 13 year program of research, development, flight testing and certification at Baylor University, ethanol has proven to be a high performance, reliable and economically competitive replacement for 100 octane aviation gasoline. The passage of the Clean Air Act and the mandate to remove all lead from fuel has provided an additional reason to seriously consider the replacement of aviation gasoline by this renewable, clean burning, domestically produced fuel.

The use of ethanol in flight training operations offered the best arena to demonstrate that ethanol is an economically competitive, reliable and high performance fuel. Accordingly, the Cessna 152, the most common flight trainer was chosen to be certified.

The first step in the certification of a new fuel is to certify the engine. The engine in the Cessna 152, is the Lycoming O-235.

CERTIFICATION PROCEDURE

Reciprocating engine test procedures are established by the FAA. The certification of the IO-540 Lycoming series engine on ethanol was completed by the Baylor project and described in a previous publication. After a test plan submitted by the applicant was

approved by the FAA, the engine was disassembled and all components subject to wear induced by use of the fuel were measured. The engine was then placed on a test stand calibrated and approved by the FAA. A dynamometer run established the development of power. Detonation testing was performed at this time. The engine was then run according to a schedule of power settings, cylinder head and oil temperatures prescribed by the FAA. The total time established by the FAA for the endurance test is 150 hours. At the end of the endurance test, the engine was again tested to determine if it developed rated power and then disassembled. The components measured at the beginning of the test were measured again to determine the amount of wear induced during the run.

LYCOMING O-235 ETHANOL CERTIFICATION TEST

The test engine was installed on the torque measuring test cell and operated on gasoline prior to conversion to ethanol. The accuracy of the torque measuring cell was verified during this testing and general operating parameters were reviewed for comparison to the ethanol testing. This test showed that the engine produced 125 HP at 2800 RPM, which is the rated power for this engine with the high compression pistons (9.7:1).

The carburetion was modified to permit the engine to operate on ethanol. The adjustments were made to permit what was considered to be adequate fuel flow for the testing. Initial tests revealed the engine produced more power on ethanol than had been anticipated. The engine produced very close to 150 HP at 2800 RPM and 28.3" HG. Additionally, the engine would overspeed using the same propeller that was used with gasoline.

During this test period the propeller was repitched numerous times in an attempt to lower the horsepower output of the engine. Finally, another propeller was obtained and was pitched to limit the engine speed to approximately 2700 RPM. However the power output remained at approximately 143 HP. It was decided to conduct the endurance test using 2700 RPM as the takeoff power and 2600 (126 HP) as the maximum continuous value, which is almost the same as the O-235F series engines use as both takeoff and maximum continuous power.

The official power and detonation test for the certification run was conducted on November 24, 1992. The test showed the engine produced 143 HP at 2725 RPM and 126 HP at 2600 RPM. The detonation test phase demonstrated that, as in the case of the IO-540 test, ethanol expands the limits of detonation over avgas. It was not possible to produce detonation within the operating envelope of the engine.

A problem was encountered during this phase of the test which has also been experienced using avgas. Rapid leaning of the fuel mixture to stoichiometric increases the amount of heat in the combustion chamber so fast that the piston cannot reject the heat fast enough to prevent loss of side clearance with the cylinder bore. The interference between the piston and cylinder wall produces a condition that has been noted for some time. The problem results in scuffed, glazed and sometimes rippled cylinder walls. The piston shows evidence of high heat and scuff marks that extend completely around the piston rather than just on the thrust surfaces. This phenomenon will be discussed in the operating manual. The damage that was produced in this incident required the rework of the cylinder barrels.

The endurance test was started on December 11, 1992, according to the test plan. Toward the end of the first block of testing, there was a noticeable loss in exhaust valve seating, and investigation revealed severe recession of the exhaust valve seat on the hottest running cylinder. The valve seat was replaced, but additional valve seat problems were experienced in short order. An evaluation of the problem resulted in finding that the mixture was extremely lean at full power. The decision was made to modify the carburetor further to

increase fuel flow at the maximum power condition. The altered carburetor permitted the fuel flow to be increased from slightly more than 13 gallons per hour to more than 15 gallons per hour at 2700 RPM (140+ HP). Seven hours of additional maximum temperature operation were extended in the later blocks of operation, and the engine was subsequently operated until all blocks were completed without incident.

The engine was performance tested in the same manner as the pre-endurance performance test. The engine power recorded was approximately 5 HP more at the end of the test at the same engine speed as at the start of the test. This phenomenon was noted at the end of the IO-540 certification tests as well. Environmental conditions at the test cell will create some differences, but all indications are that the engine was producing slightly more power at the completion of the test.

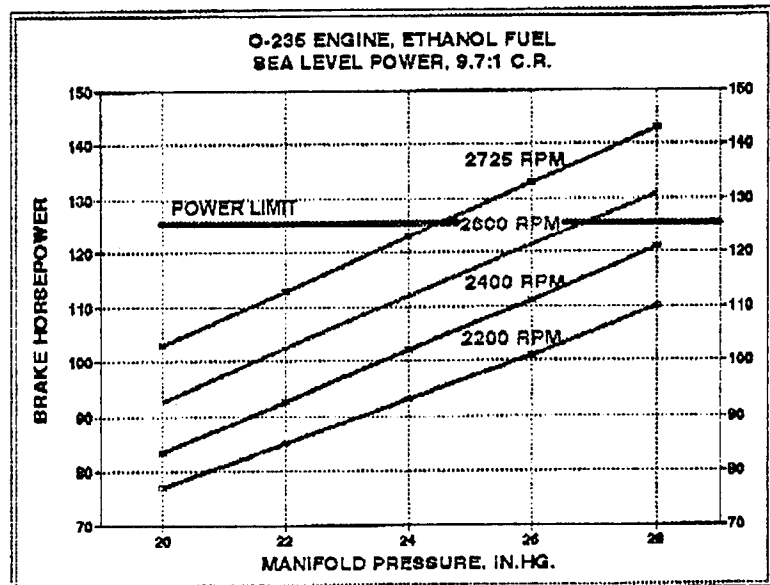
TEST DATA SUMMARY:							
BLOCK NO	1	2	3	4	5	6	7
START DATE	12/29/92	01/5/92	01/13/93	01/28/93	2/08/93	2/11/93	2/15/93
FINISH DATE	02/11/93	01/7/93	01/28/93	02/07/93	2/11/93	2/13/93	2/17/93
TOTAL HOURS							
TEST TIME	30HRS	20HRS	20HRS	20HRS	20HRS	20HRS	20HRS
HOT TIME	15HRS	15HRS	12HRS	15HRS	15HRS	0	0
HIGH RPM	2700	2600	2600	2600	2600	2600	2600
HIGH MP	28.6	27.8	27.5	26.5	26.5	25.5	26.1
LOW RPM	2425	2480	2425	2370	2303	2166	2200
LOW MP	23.4	24.8	23.5	23.8	22.0	19.8	19.9
TOTAL TIME							
ENDURANCE							
TEST	177.3 HRS						
TOTAL HOT							
TIME							
ENDURANCE							
TEST	57.0 HRS						

NOTE: As the engine operated throughout the test program, the friction horsepower was apparently reduced. Accordingly, the engine was able to hold the target speeds (RPM) at lower and lower manifold pressures. The environmental conditions also created some differences in engine operation, and probably influenced the increase in power obtained at the completion of the test. Instrumentation calibration at the completion of the engine test verified the accuracy of the measuring system, so the slight increase in power indicated is probably correct.

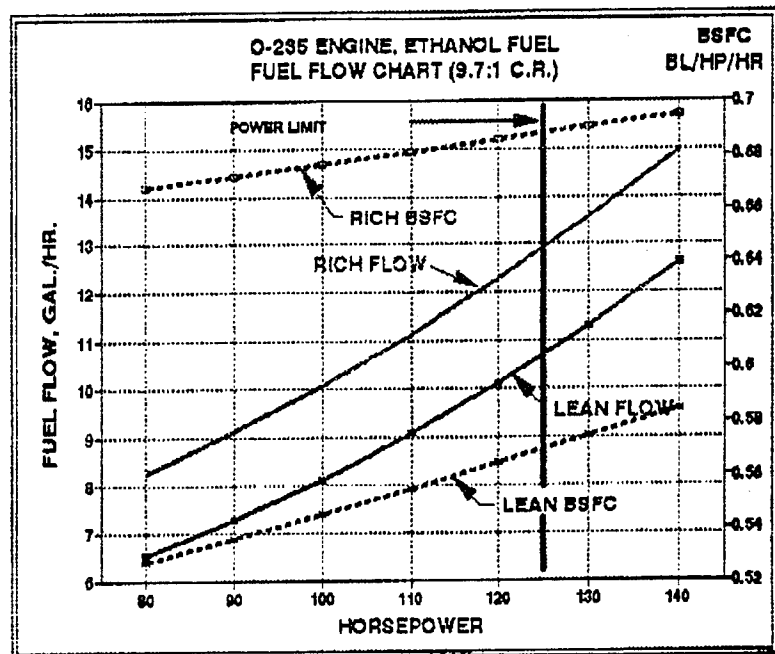
ENGINE OPERATING PARAMETERS

The test engine operating parameters have been validated through the performance, detonation and endurance certification testing. The nature of the test program included some research elements that have been investigated and resolved. These findings are to be included as part of the operating instructions. The performance data has been reduced to standard day conditions and is provided in the charts below.

Engine Operating Parameters



Fuel Flow Characteristics



ETHANOL OPERATING EVALUATION

The operation of the engine was evaluated during exploratory and FAA testing. The anomalies found during the test were primarily due to the limited experience with carburetor equipped engine on ethanol. However, these anomalies identified areas of concern that will be addressed in the engine operating manual and in flight testing of the engine installation.

1. Cold Starting.

The Reid Vapor Pressure (RVP) of denatured ethanol is 3.0 psi, compared with 5.5-7.5 for avgas. Low RVP is desirable from a safety standpoint as it means vapor lock is less likely, but it also means there is a cold start problem. This problem is easily resolved by a normal engine priming system drawing a small amount of gasoline from an auxiliary canister.

2. Detonation While Changing Fuels.

In the course of the testing, detonation was induced when ethanol was introduced into the fuel system when the engine was running under a high power setting on gasoline. Apparently, a momentary lean condition in the engine was created and serious detonation occurred in a matter of seconds. Although the engine can function on any percentage mixture of ethanol and gasoline, the change from straight avgas to straight ethanol cannot safely be accomplished while under power.

3. Valve seat Recession and Fuel/air Mixture.

Incidents of exhaust valve seat recession occurred during the endurance test that required repair. Evaluation of test conditions showed that the engine was operating at a very lean condition during maximum power conditions. A larger float needle and seat were installed in the carburetor and additional hot penalty time was accomplished without incident.

4. Power Increases.

The use of ethanol fuel resulted in significant increases in power. The maximum power obtained during the program was in excess of 150 HP at 2800 RPM. The endurance testing was conducted at 143 HP Take Off and 126 HP Maximum Continuous. Ethanol appears to produce greater average pressures without the severe peak pressures obtained using gasoline. Preliminary testing revealed some movement between crankcase halves resulting from operation at the high power setting. However, the torque of the thru-bolt and cylinder studs was slightly low, and after reassembling the engine using proper torque values, the endurance test was completed without further evidence of fretting. The possibility of fretting when using the entire power capability of the engine makes it incumbent to warn operators to recheck cylinder torque values after a period of operation.

5. Detonation.

The use of ethanol fuel precludes the possibility of detonation throughout the operation range of the engine. During the testing, a case where temperatures increased rapidly was encountered as a result of leaning the mixture too rapidly. This caused the loss of piston to barrel clearance resulting in damage to the cylinder.

TEAR DOWN INSPECTION

The test engine was visually inspected and compression tested at the completion of the endurance test and then disassembled for evaluation. The results of the evaluation are shown in the following table.

ITEM	NEW	SERVICE	CYL#1	CYL#2	CYL#3	CYL#4
TOP RING GAP	.045/.055	.067	.054	.035	.050	.061
2ND RING GAP	.015/.030	.047	.035	.035	NOTE 1	.040
OIL RING GAP	.015/.030	.047	.037	.036	NOTE 2	.034
CYL. BORE	4.3745/ 4.3765	4.380	4.375- 4.375	4.376- 4.375	4.3735- 4.377	4.370- 4.370
CYL. HEAD	N/A	N/A	GOOD	NOTE 3	GOOD	GOOD
INTAKE VALVE STEM	.4022/ .4030	.4010	.4023	.4025	.4026	.4020
INTAKE GUIDE ID.	.4040- .4050	NOT LISTED	.4047- .4088	.4047- .4056	.4047- .4050	.4046- .4062
INTAKE VALVE& GUIDE CLEAR.	.0010/ .0028	.006 NOTE 4	.0022/ .0065	.0022/ .0031	.0021/ .0024	.0026/ .0042
EX. VALVE STEM	.0010/ .0028	NOT LISTED	.4329	.4322	.4322	.4321
EX. GUIDE I.D.	.4370/ .4380	NOT LISTED	.4382- .4403	.4378- .4464	.4378- .4450	.4378- .4432
EX. VALVE& GUIDE CLEAR.	.004/.006	NOTE 5	.0053/ .0074	.0056/ .0142	.0056/ .0128	.0057/ .0111
PRESS. TEST LEAK.	20 LB. IN 5 SEC.		2 LB. IN 5 SEC.	13 LB IN 5 SEC.	0 LB	0 LB
COM. TEST	60/80		75/80	64/80	75/80	75/80
PISTON PIN DIA.	1.1241/ 1.1246	NOTE 6	1.124	1.125	1.124	1.124
PISTON DIA.	4.329/ 4.3605	NOTE 7	4.365	4.363	4.3645	4.362

NOTE 1: The Number 3 cylinder 2nd compression ring was .001 over service limits on end gap. However, review of the build up data showed the ring was within service limits at installation so the actual wear was insignificant.

NOTE 2: The Number 3 cylinder oil ring was broken when the cylinder was removed at the completion of the test. This happens occasionally, and since the ring had an otherwise normal appearance, this was considered incidental.

NOTE 3: The Number 2 cylinder was found to have a small crack in one spark plug boss. Additionally, this cylinder had a crack between the fins under the exhaust port and another small crack across a fin around the exhaust port. The cracks between and across the fins did not extend through to the inside of the cylinder and could have existed in smaller form at the time of engine build-up.

NOTE 4: The Number 1 cylinder intake guide and valve clearance was slightly above the listed service limits. However, the build up clearance was close to the maximum new limits, and the average clearance was well within the service limits. The value of the clearance was therefore considered incidental and inconsequential.

NOTE 5: Lycoming Service Bulletin 338B establishes a procedure for checking and continuing operation with up to .030 valve movement in the exhaust guide. Lycoming has experienced exhaust valve and guide wear, and the clearances found at the completion of the test were considered normal.

NOTE 6: There is no listed service limit for the piston pin, but there is a service limit for the fit between the pin and piston. The difficulty in measuring .0001 tolerance and the uncertainty regarding the original diameter resulted in the belief the wear was nil.

NOTE 7: There is no current listing for the skirt diameter for the new Lycoming piston used in the test. This is a new type that has a different mass than the original piston, and Lycoming may have to increase the skirt diameter to help alleviate cylinder barrel cracking problems. The piston wear is judged to be minimal, and the new part tolerances are probably not correct for this piston.

CONCLUSION

This certification test demonstrated that the Lycoming O-235 series of engines operate on ethanol fuel within the provisions of the Federal Air Regulations when the engine is modified, installed and operated in accordance with the information supplied to the FAA in the application packet for the Supplemental Type Certificate.

Despite the high compression (9.7:1) of the test engine, detonation could not be induced during the testing while using just the ethanol fuel. Wear of components during the test was generally found to be minor. The somewhat high valve, valve guide and valve seat wear is attributed to the excessively lean mixture coupled with the extreme cylinder temperatures. Additionally, there is a general high exhaust valve and guide wear in the Lycoming engine series, and high guide wear exacerbates valve seat wear.

The relatively low wear and general engine cleanliness indicates that the engine can operate on ethanol fuel for longer time periods than on 100LL avgas. An additional test is planned in which the engine will run according to the schedule met in this test, except for 300 hours rather than 150 hours, to justify an increase in recommended TBO for the engine operating

on ethanol fuel. The wear should be considerably lower when operated at normal temperatures and limited to the original power of the C, F, L and N series engines.

BIBLIOGRAPHY

1. FERRARA, A. M. , WARES, R., "The Performance of Alternate Fuels in General Aviation Aircraft", Federal Aviation Administration Technical Center, Report No. DOT/FAA/CT-88/13
2. FERRARA, A.M., "Alternate Fuels for General Aviation Aircraft with Spark Ignition Engines", Federal Aviation Administration Technical Center, Report No. DOT/FAA/CT-88/5.
3. RUSSELL, J.A., "Characterizations of Certain Key Properties of Enhanced Ethanol Fuel", Southwest Research Institute Report, July 1988.
4. SHAUCK, M.E., TURNER, D.W., "Ethanol as an Aviation Fuel" Proceedings of the VI International Symposium on Alcohol Fuels Technology, pp. 352-356, Ottawa, Canada, May, 1984.
5. SHAUCK, M.E., TURNER, D.W., and RUSSELL, J.A., "Flight Test Comparisons of Avgas versus Ethanol/Methanol Blends" Proceedings of VII International Symposium on Alcohol Fuels Technology, pp. 402-405. 1986, Paris, France, October, 1986.
6. SHAUCK, M.E., "Performance Report on an Alcohol Powered SIAI Marchetti SF-260 C Aircraft", Proceedings of the VIII International Symposium on Alcohol Fuels Technology, pp. 669-670, Tokyo, Japan, November, 1988.
7. SHAUCK, M.E., ZANIN, M.G., "The First Transatlantic Crossing in an Aircraft Powered by Ethanol Fuel", Proceedings of the VIII International Symposium on Alcohol Fuels Technology, Florence, Italy, November, 1991.
8. SHAUCK, M.E., ZANIN, M.G., "Certification of an Aircraft Engine on Ethanol Fuel", Proceedings of the VIII International Symposium on Alcohol Fuels Technology, Florence, Italy, November, 1991.
9. SHAUCK, M.E., ZANIN, M.G., "Ethanol in Reciprocating Aircraft Engines" Proceedings of the 1992 AIAA/FAA Joint Symposium on General Aviation Systems, Wichita, Kansas, March 1992.
10. SHAUCK, M.E., ZANIN, M.G., "Ethanol as an Aviation Fuel: An Overview of the Program at Baylor University", Proceedings of the IX International Symposium on Alcohol Fuels Technology, Colorado Springs, USA, November 1993.

**ADVANCED TECHNOLOGY, JET-A FUEL
STRATIFIED CHARGE ROTARY ENGINES
FOR GENERAL AVIATION**

By

Robert E. Mount
Rotary Power International, Inc.
P.O. Box 128
Wood-Ridge, New Jersey

For Presentation at the AIAA/FAA 3rd Joint
Symposium on General Aviation Systems
Mississippi State University
Starksville, Mississippi
May 24 & 25, 1994

ABSTRACT

Technology advancements with the Stratified Charge Rotary Engine for General Aviation applications will be discussed. During 1994, technology enablement progress in power and fuel consumption will be demonstrated on the Model 2013R two rotor, 1.3 liter total displacement engine. This effort is being conducted under NASA Contract No. NAS3-26920. The demonstration will consist of operation on Jet-A fuel at 340 BHP/254 Kw Take-off power and 255 BHP/190 Kw maximum cruise power conditions, 0.435 lbs/BHP-Hr (264 G/KwH) Brake Specific Fuel Consumption (BSFC). Higher specific power output of 5 HP/cu.in (230 Kw/L) and lower cruise power specific fuel consumption of 0.375 lbs/BHP-Hr (230 G/KwH) levels have been demonstrated at Rotary Power International in supportive research work with the NASA single rotor component research engine. The power and BSFC levels targeted for demonstration in the two rotor engine reflect a level appropriate to a full-up aircraft engine configuration with full range operational capability over start, idle, taxi, take-off, climb and cruise regimes. Planned industry programs toward final product development and FAA certification, necessary to transition the technology to the General Aviation field, will be discussed.

INTRODUCTION

A new technology, low cost engine offering Jet fuel capability and high efficiency is needed in General Aviation. An alternative to current reciprocating engines (generally restricted to aviation gasolines) and to small turbines (high in cost) is desired. A new technology powerplant could perhaps revitalize a currently depressed and historically a U.S. dominated industry. NASA has sponsored competitions between reciprocating, rotary and small turbine advanced technology powerplants toward this end.

Substantial progress has been made sequentially by Curtiss-Wright, John Deere Technologies International and presently Rotary Power International in the advancement of the basic technology associated with Stratified Charge Rotary Aircraft Engines. This work, originating in 1982 and receiving long standing support from NASA-Lewis Research Center and NASA Headquarters, has identified and advanced the critical technologies involved to a degree whereupon an industry development and FAA certification program can be initiated. Initiation of that program is of course dependent upon numerous factors other than the technology including market conditions, potential investment return and investment risk. Transition of this technology from the research and technology enablement phases (as supported by NASA) to the General Aviation community can provide an efficient, Jet-A fueled, low cost propulsion system for light aircraft of fixed-wing and rotary-wing configurations. A multi-fuel capability engine not dependent upon high octane, leaded gasoline fuels and insensitive to Octane and Cetane ratings is provided. Low drag, high performance twin engine aircraft configurations are possible with the small diameter rotary engine packaging. Military and commercial light aircraft will benefit from the size, weight, Jet fuel capability, high power output and efficient operational features of the Stratified Charge Rotary Engine.

PURPOSE

During the early 1980's NASA-Lewis Research Center sponsored a competition between aircraft engine companies to define an advanced technology General Aviation engine for the mid-1990's timeframe. The need for an engine non-dependent upon high octane, leaded aviation gasoline was identified based upon the growing problem of limited distribution of Avgas in various parts of the world. This competition involved reciprocating spark ignition, reciprocating diesel, turbine and Stratified Charge Rotary Engine configurations (Reference 1). Two major airframers were contracted by NASA to conduct studies of airplane design possibilities and performance achievable with the various engine designs (References 2 and 3). The Stratified Charge Rotary Engine defined by Curtiss-Wright Corporation was ranked as the leading candidate. NASA then sponsored a series of contractual efforts (sequentially with Curtiss-Wright, John Deere Technologies International and then Rotary Power International, successive owners in that order of the rotary engine assets and technology) to build a research engine and to evaluate component and critical technologies. These efforts have advanced the technology to a point where final development and FAA certification requirements can be defined. The present NASA contractual effort with Rotary Power International is for demonstration of the two rotor engine system technology as noted in the Abstract.

BASIC STRATIFIED CHARGE ROTARY ENGINE TECHNOLOGY. An inherent compatibility exists between the rotary engine and unthrottled, direct chamber injection stratified charge combustion. With rotation of the triangular shaped rotor, all of the air for a given lobe on the rotor passes by the top dead center zone when traversing from compression to the expansion portions of the cycle (Figure 1).

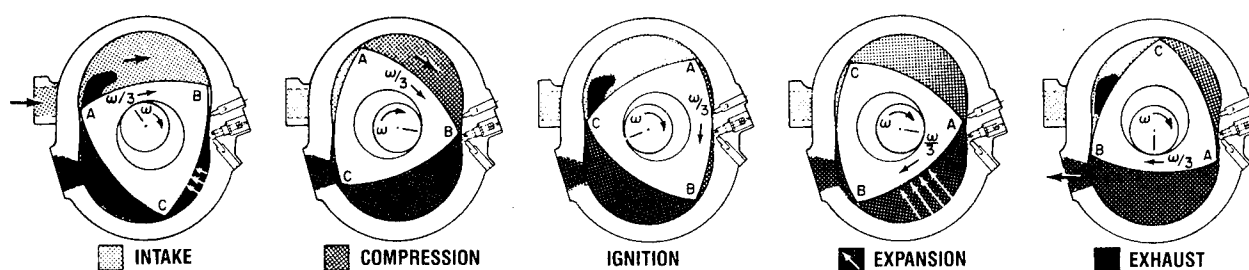


**FIGURE 1 - BASIC GEOMETRY AND OPERATING CYCLE
STRATIFIED CHARGE ROTARY ENGINE**

By placement of a high pressure pilot injection nozzle in the top dead center zone, in close proximity to an ignition source, a locally rich fuel-air mixture region can be generated and ignited. Overall fuel-air mixtures that would be too lean for normal spark ignition can be ignited by the initiation of combustion in the locally rich zone. Octane and cetane sensitivities are not present and therefore, operation on a variety of fuels (i.e., Jet-A, Diesel, JP-5, JP-8, gasoline) can be accommodated and has been demonstrated.

Early versions of the Stratified Charge Rotary Engine utilized a single fuel injector. This resulted in limitations over the full speed and load range with the large variation in fuel flow through the light-off zone necessary in responding to variations in load demand. Operation at selected conditions could be optimized, however, at the compromise of other conditions. A significant breakthrough in achieving full load and speed range operation, including starting, idling, efficient part load and full load operation and cold starting occurred during the late 1970's period with introduction of a dual injector configuration (Figure 2). This configuration permitted consistent light-off over the full operational range by maintaining the volume of fuel per stroke through the pilot nozzle at a constant level, optimized for consistent ignition. Since the $\text{mm}^3/\text{stroke}$ were held constant, conditions in the light-off zone were essentially constant regardless of speed and power changes. Large variations of fuel flow through the main injector, separated from the pilot injector/light-off zone, could vary widely as a function of load demand with no effect upon the light-off action.

- COMPETITIVE FUEL CONSUMPTION
- COLD STARTING CAPABILITY
- BROAD OPERATING RANGE
- INDEPENDENT FROM CETANE NUMBER

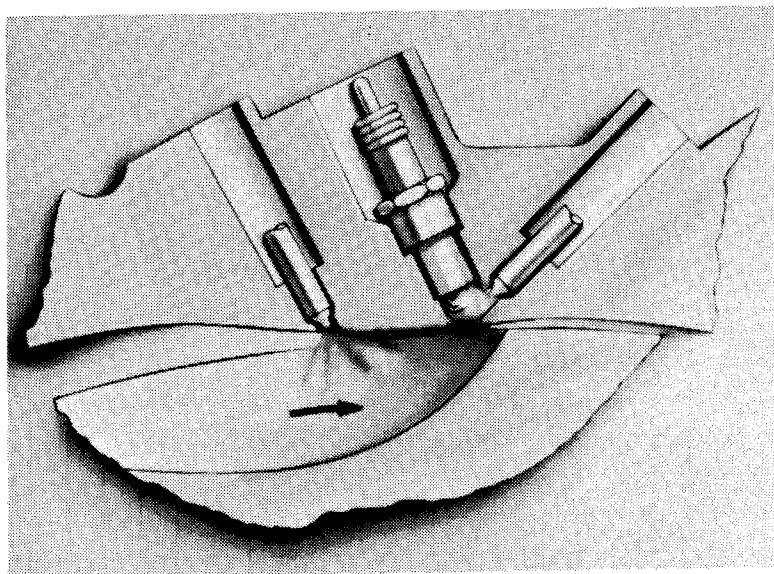


FIGURE 2 - STRATIFIED CHARGE ROTARY ENGINE COMBUSTION SYSTEM

Injection and Ignition Sequence. The sequence of ignition, pilot injection and main injection is presented in Figure 3. As can be noted the ignition is initiated prior to start of pilot injection and main injection and is overlapped by a portion of the pilot injection, which in turn is overlapped by the main injection. Timing and variation in durations can easily be accommodated in conventional control systems.

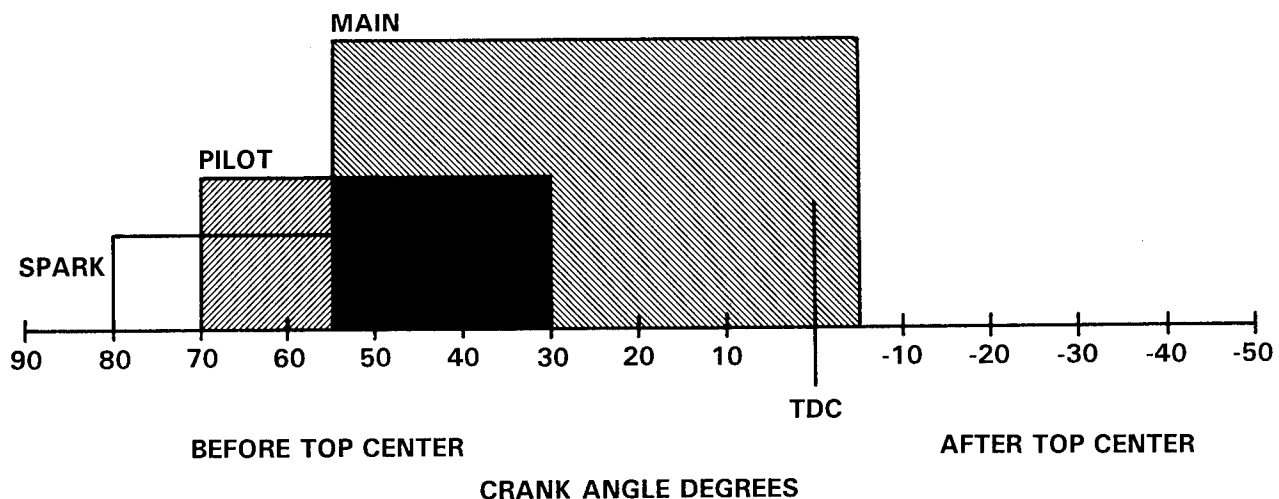


FIGURE 3 - TYPICAL IGNITION AND INJECTION TIMING

NASA TECHNOLOGY ENABLEMENT/RESEARCH. Early work with the rotary aircraft engine under NASA contract investigated exhaust emissions for the RC2-75 gasoline rotary engine. The engine demonstrated the capability of meeting anticipated emissions standards at that time (Circa 1980) at all mission conditions without any after treatment. However, interest in Jet fuel capability became a predominant factor in consideration of advanced engine technologies. Initial work defining the characteristics of an advanced Stratified Charge Rotary Aircraft Engine design was conducted under contract to NASA Lewis Research Center, Cleveland, OH during 1982 (Reference 1, previously noted). Detailed studies by general aviation airframe manufacturers compared overall effects on airplane design, performance, operational and life cycle costs for four engine candidates in advanced and highly advanced categories.

- Stratified Charge Rotary
- Small Turbine
- Spark Ignited Reciprocating Engine
- High speed Lightweight Air-Cooled Diesel

These studies (References 2 and 3, also previously noted) ranked the Stratified Charge Rotary Engine as the number one candidate.

The Research Rig Engine. A research rig engine (Figure 4) was designed and built for explorations of power, BMEP and speed levels above and beyond those required for the highly advanced aircraft engine projections. The intent was to provide a working unit capable of exploring performance trends up to and above actual engine maximum design point conditions. This permitted the evaluation of component technologies throughout the advanced and highly advanced regimes without mechanical or thermal restrictions in the base rig engine. The research rig engine has been the primary research tool used in the initial and follow-on phases of NASA Technology Enablement.

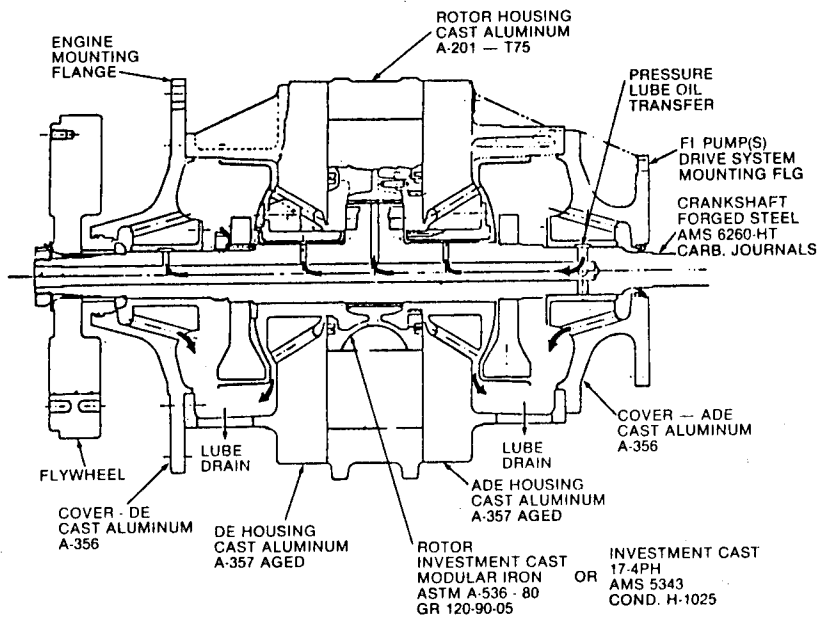


FIGURE 4 - NASA RESEARCH RIG ENGINE - 0.66 LITERS, (40 CU.IN.) DISPLACEMENT, LIQUID COOLED

Figures 5 and 6 show the basic research rig engine. In Figure 6, a technician is installing a tool for crankshaft positioning purposes during the assembly/measurement process. General construction, cooling passages and basic size can be noted in this photograph. Conventional Stratified Charge Rotary Engine materials are used including cast aluminum housings, investment cast steel (or nodular iron) rotor and a carburized steel crankshaft. Detailed design features for the 1007R research rig have been published in Reference 4.

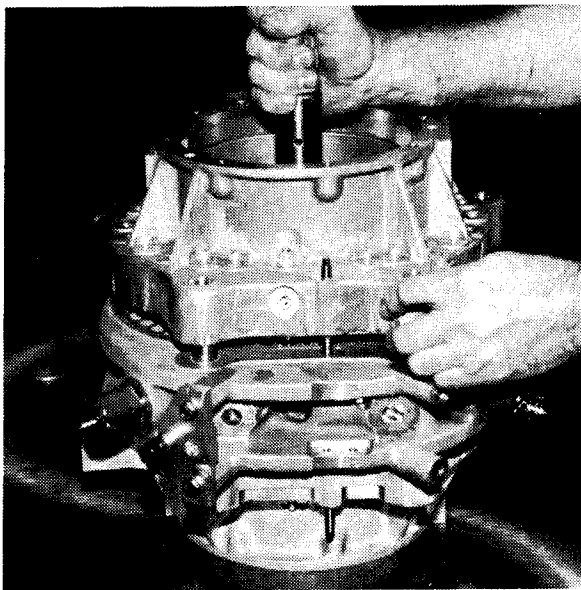
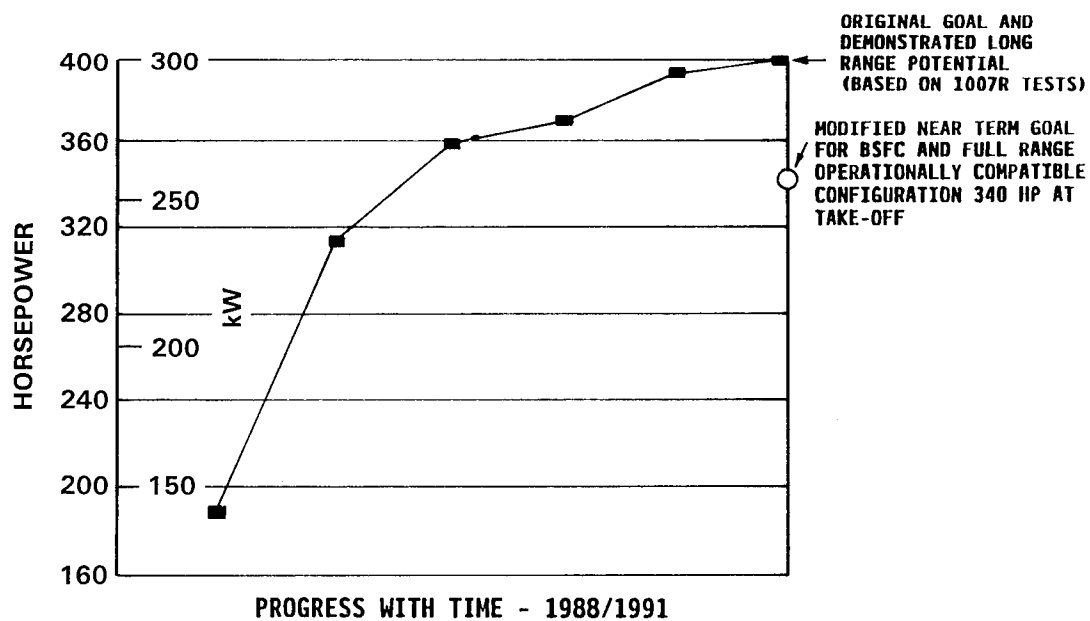


FIGURE 5 - 1007R SINGLE ROTOR RESEARCH RIG ENGINE



FIGURE 6 - 1007R RESEARCH RIG ENGINE COMPONENTS



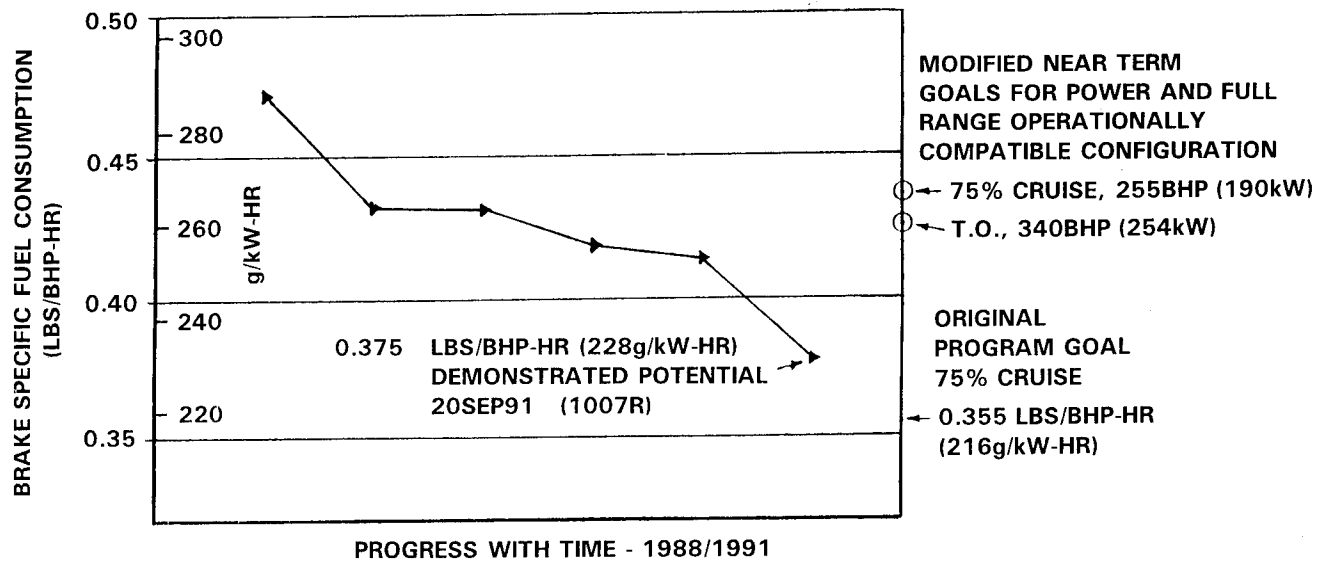
**FIGURE 7 - NASA SCRE CRITICAL TECHNOLOGY ENABLEMENT
MAXIMUM POWER
MODEL 2013R ENGINE**

Figure 7 presents the power output progress with time as demonstrated with the 1007R single rotor research rig engine and referred to the two rotor, Model 2013R engine configuration. As can be noted, the goal in the NASA work of 200HP (150kW) per rotor, or 400HP (300kW) on a two rotor engine basis was achieved. To permit some margin for achieving reasonable and competitive fuel consumption levels while not compromising full range operational capability (start, idle, taxi, take-off, climb, cruise, descent) a modified near term goal of 340HP (254kW) at take-off was selected.

Figure 8 presents the fuel efficiency progress with time as demonstrated with the 1007R single rotor research rig engine and referred to the two rotor, Model 2013R engine configuration. As was noted in the preceding discussion on power output, near term, full range operational compatible levels of 0.425 Lbs/BHP-Hr (258 g/kW-Hr) at take-off and 0.430 Lbs/HP-Hr (262g/kW-Hr) at 75% cruise were selected.

Reference 5 summarizes "NASA's Rotary Engine Technology Enablement Program - 1983 Through 1991."

Present Activity. The present activity in the overall NASA Technology Enablement effort consists of a Two Rotor Stratified Charge Rotary Engine (SCRE) System Technology Evaluation. The master schedule for that effort, starting January 21, 1993 is presented in Figure 9. The effort essentially combines the best component technology items deriving from approximately ten years of technology enablement activities into a two rotor system.



**FIGURE 8 - NASA SCRE CRITICAL TECHNOLOGY ENABLEMENT
BRAKE SPECIFIC FUEL CONSUMPTION
MODEL 2013R ENGINE**

YEAR	1993												1994											
MONTH	01	02	03	04	05	06	07	08	09	10	11	12	13	14	15	16	17	18	19	20	21	22	23	24
<u>SCHEDULE</u>																								
CONTRACT START (JAN 21, 1993)	△																							
TWO ROTOR SCRE BASELINE ENGINE EVALUATION	<div></div>																							
ADVANCED TWO ROTOR SCRE ENGINE DEFINITION	<div></div>																							
ADVANCED TWO ROTOR SCRE ENGINE SYSTEM/ACCESSORIES DEFINITION	<div></div>																							
FABRICATION/INSTALLATION	<div></div>																							
TEST	<div></div>																							
FINAL REPORT	<div></div>																							
<u>MILESTONES</u>																								
1. ADVANCED CORE ENGINE DEFINITION	△																							
2. ADVANCED ENGINE SYSTEM AND ACCESSORIES CONFIGURATION	△																							
3. ADVANCED ENGINE FABRICATION AND INSTALLATION	△																							
4. ADVANCED ENGINE TESTING COMPLETED	△																							

**FIGURE 9 - NASA CONTRACT NAS3-26920
TWO ROTOR STRATIFIED CHARGE ROTARY ENGINE
(SCRE) SYSTEM TECHNOLOGY EVALUATION**

Demonstration of 340HP (254kW)/8000RPM take-off power and 0.435 Lbs/BHP-Hr (265g/kW-Hr) at max. cruise will be achieved by the eighteenth month (July 1994, Milestone No. 4).

Figure 10 denotes key technologies deriving from the NASA program supportive of establishing a technology baseline with which the industry development and certification program can be achieved.

<u>TECHNOLOGY NEED/GENERAL AVIATION</u>	<u>DERIVES FROM NASA?</u>
<u>ROTARY ENGINE</u>	
POWER 340 HP	YES
BSFC 0.435 LBS/HP-HR @ MAX CRUISE 255HP	YES
PORTING AND BASIC HOUSING GEOMETRY (FOR ABOVE PERFORMANCE)	YES
FUEL INJECTION SYSTEM	YES
IGNITION SYSTEM (DUAL SPARK PLUG AT PILOT)	NO (SINGLE SPARK PLUG AT PILOT)
TWO ROTOR SYSTEM FULL RANGE OPERATION	YES
TURBOCHARGER FOR 27,000' ALTITUDE	NO (TURBOCHARGER WILL BE SEA LEVEL ONLY)
MANIFOLDING FOR TWO ROTOR SYSTEM: INTERACTION, INFLUENCES FOR TWO ROTOR SYSTEM	YES
REDUCED WEIGHT (11%)	NO (BUT CONSIDER WHERE WEIGHT REDUCTION CAN BE ACHIEVED)
DURABILITY	NO

FIGURE 10 - TECHNOLOGY SUPPORT TO GENERAL AVIATION AIRCRAFT ENGINE PROGRAM

Figure 11 presents the overall schedule for the NASA effort (early 1993 to late 1994) and parallel but lagging industry development and certification effort (mid 1994 through FAA certification in early 1997).

YEARS	1993	1994	1995	1996	1997
NASA NAS3-26920 TWO ROTOR STRATI- FIED CHARGE ROTARY ENGINE (SCRE) ENGINE SYSTEM TECH- NOLOGY EVALUATION (21JAN93-21OCT94)	██████████	██████████			
DEVELOPMENT/FAA CERTIFICATION		██████████	██████████	██████████	██████████
FAA 150 HR MODEL TEST/CERTIFICATION					██████████
PRODUCTION PLANNING AND PREPARATION				██████████	██████████
PRODUCTION					██████████

FIGURE 11 - NASA STRATIFIED CHARGE ROTARY ENGINE CRITICAL TECHNOLOGY ENABLEMENT RESEARCH LEADING TO INDUSTRY DEVELOPMENT, FAA CERTIFICATION AND PRODUCTION

70 SERIES AIRCRAFT ENGINES

One engine configuration currently under consideration for General Aviation application is the Model 2013R, Figure 12. The preliminary engine specification is defined in Figure 13. Engine performance characteristics are presented in Figure 14. Basic dimensional data are presented in Figure 15. A 26 in. (660mm) nacelle diameter requirement is projected. The engine at 340 HP (254kW) at Take-off is believed to offer a desirable alternative engine, with Jet -A fuel capability, for many retrofit and/or new aircraft application.

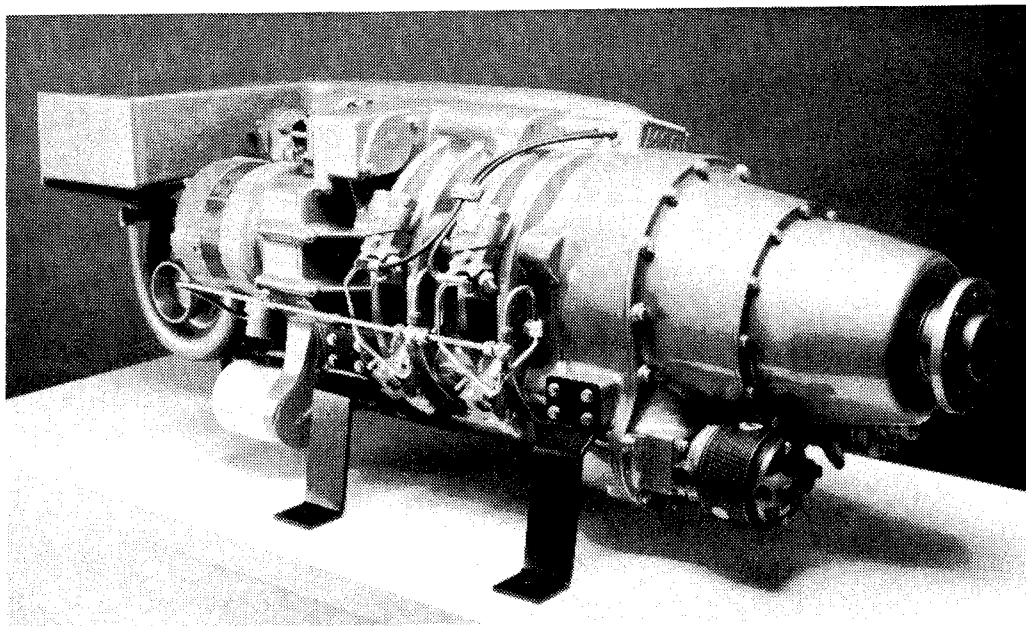


FIGURE 12 - THE STRATIFIED CHARGE ROTARY AVIATION ENGINE

FUEL INJECTED, TURBOCHARGED, LIQUID COOLED, GEARED,
INTERCOOLED, WITH CABIN AIR BLEED PROVISIONS

TAKE-OFF POWER	254kW (340HP)
TAKE-OFF CRANKSHAFT SPEED	8000RPM
TAKE-OFF ALTITUDE CAPABILITY	SEA LEVEL TO 6100m (20,000 ft)
CRUISE POWER (75% CRUISE)	190kW (255HP)
CRUISE CRANKSHAFT SPEED	7250RPM
CRUISE ALTITUDE CAPABILITY	TO 7620m (25,000 ft)
ENGINE WEIGHT GOAL, DRY	193Kg (425 Lbs)
BSFC AT TAKE-OFF	258g/kW-Hr (.425 Lbs/BHP-Hr)
BSFC AT 75% CRUISE	262g/kW-Hr (.430 Lbs/BHP-Hr)
TBO	2000 HOURS
FUEL, AVIATION GRADE	JET-A

FIGURE 13 - PRELIMINARY ENGINE SPECIFICATION MODEL 2013R

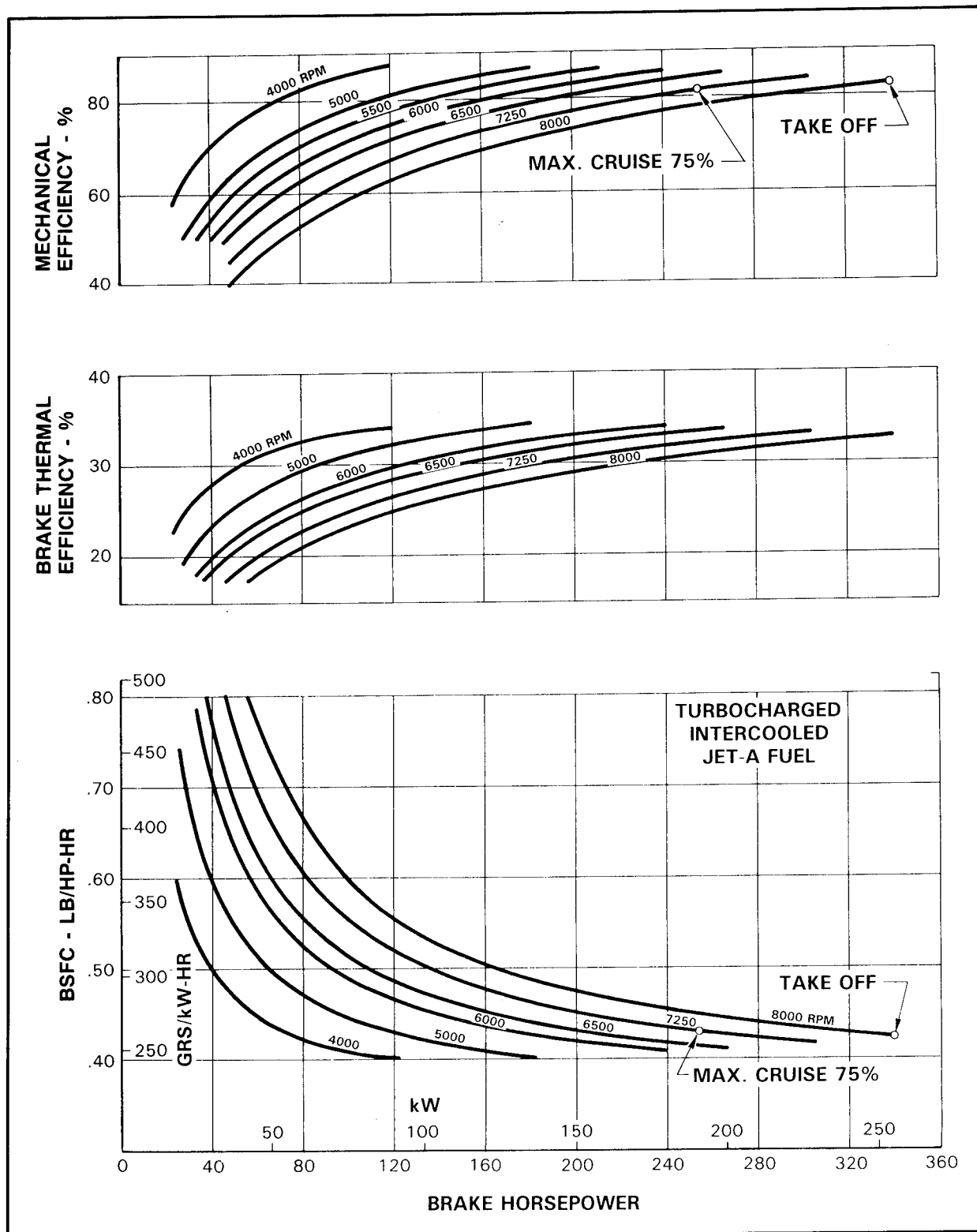
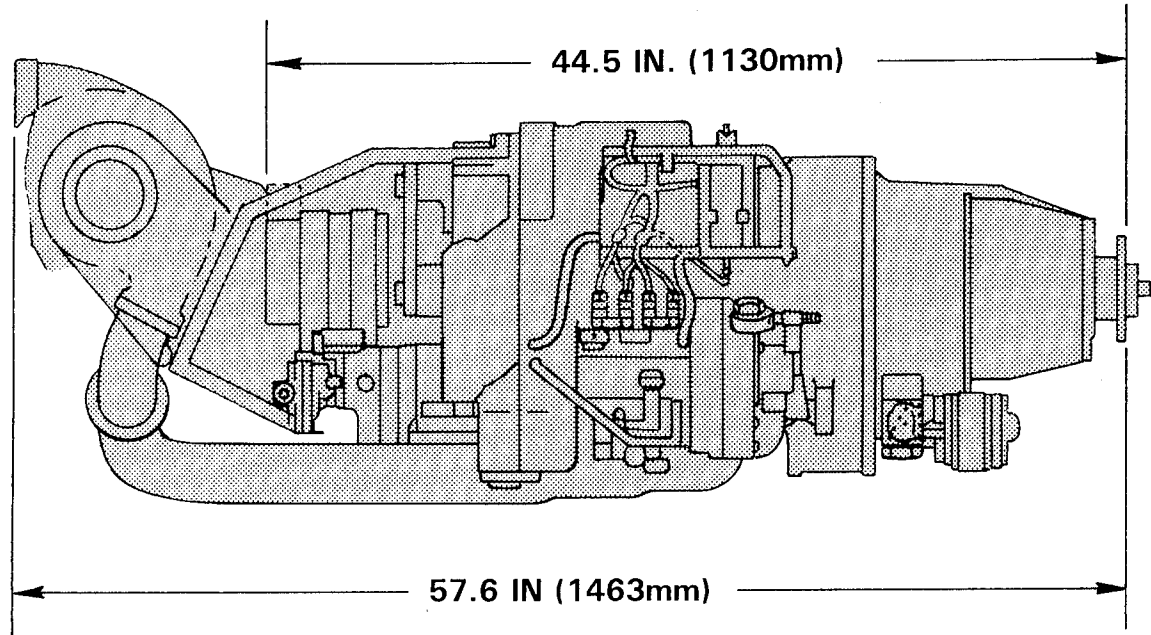


FIGURE 14 - ESTIMATED PERFORMANCE MODEL 2013R

RIGHT SIDE VIEW



ACCESSORY END VIEW

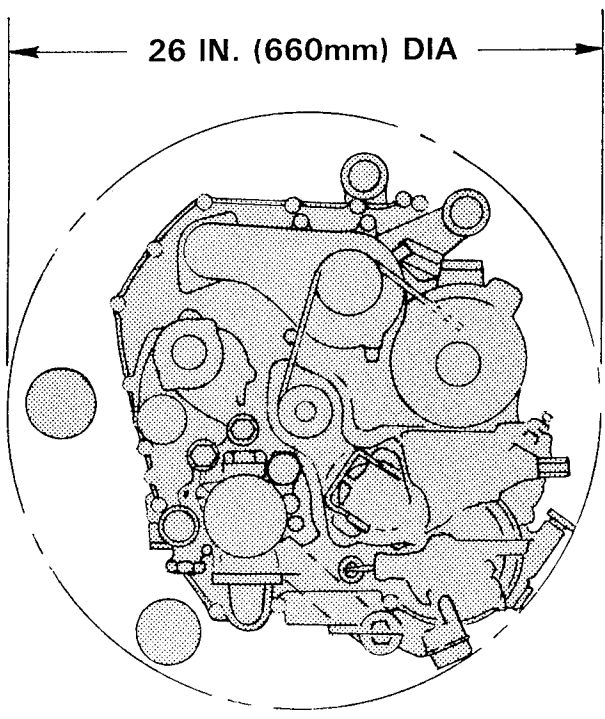


FIGURE 15 - PRELIMINARY INSTALLATION DRAWINGS MODEL 2013R

Figure 16 presents a longitudinal cross-section of the Model 2013R engine. The core two rotor, stratified charge rotary engine power section, deriving from the NASA Technology Enablement efforts, is packaged into a complete aircraft engine powerplant. The aircraft accessories complement consists of alternator, vacuum pump, air conditioning compressor and propeller control. The engine required to run accessories consist of fuel injection pump, oil pump, oil scavenge pump, starter, coolant pump, turbocharger and intercooler. A planetary reduction gear is considered in providing a propeller speed in the 2000RPM range vs. the crankshaft speed of 8000RPM at Take-off power.

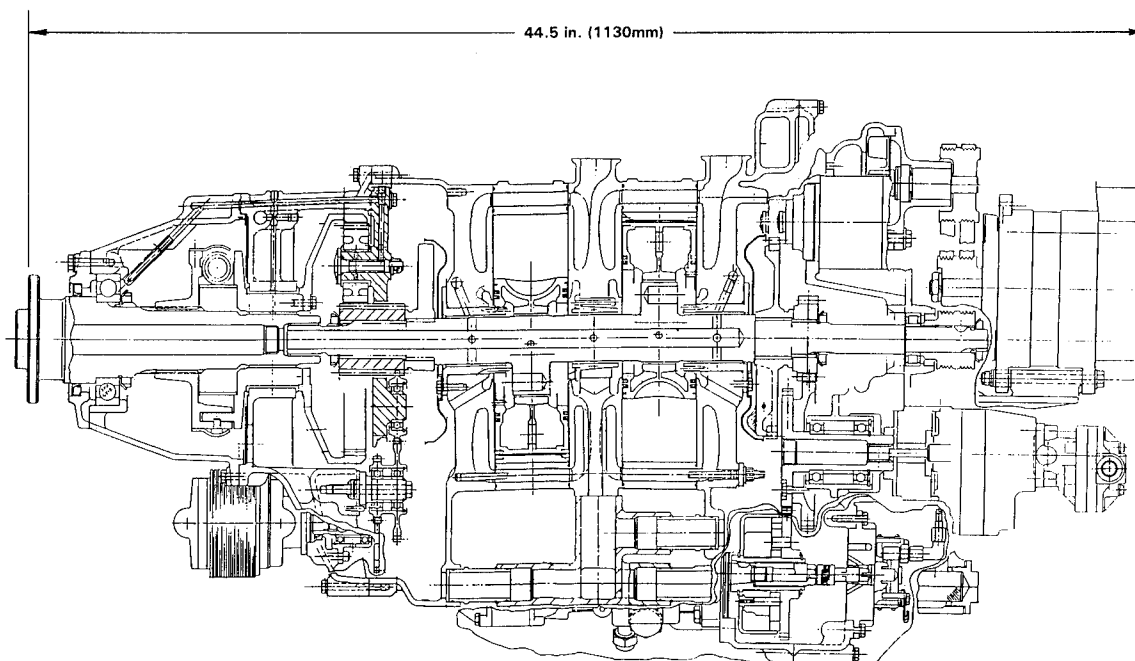


FIGURE 16 - LONGITUDINAL CROSS SECTION MODEL 2013R

170 SERIES AIRCRAFT ENGINES

A second configuration currently under consideration for General Aviation application is the Model 2034R. An early version of this configuration, rated at 400HP (298kW) at take-off was designed and tested at RPI's predecessor, John Deere Technologies International, Inc. (JDTI), in conjunction with AVCO-Lycoming, Williamsport Division during the 1985-1989 time period (Figure 17). This engine (Reference 6) operated at a take-off BMEP of 130 psi (896kPa) and at 5800RPM. It is a two rotor, 1.72 Liter (105 cu.In.) per rotor engine and represented a nearer term technology level than that being pursued in the longer range, more aggressive NASA effort. Following completion of the joint design and procurement in 1987 AVCO-Lycoming was forced to withdraw from the joint program after experiencing an extraordinary increase in their product liability insurance premiums and concern for the market as affected by product liability problems. The engine was assembled and tested at JDTI in conjunction with McDonnell Douglas and USAF Wright Field, Reference 7.

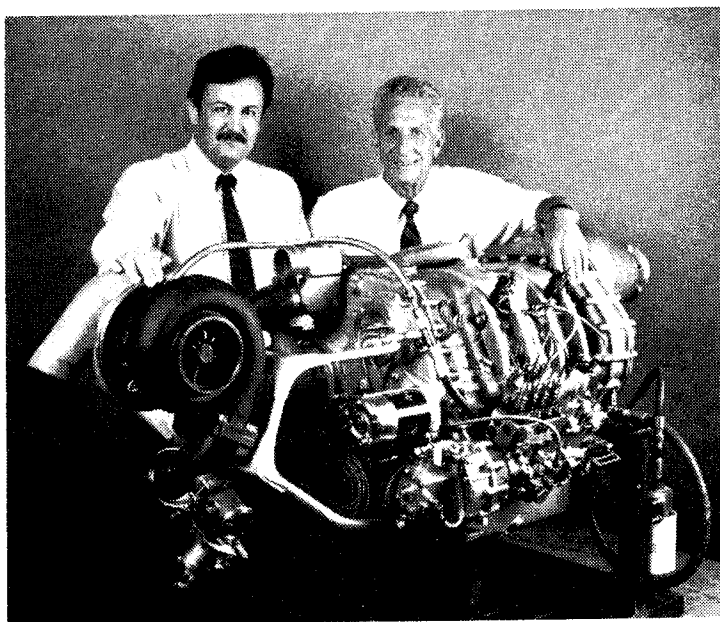


FIGURE 17 - 170 SERIES MODEL 2034R

The preliminary specification for that engine is presented in Figure 18. The designation 2034R refers to two rotor, 3.4 liters total displacement and R for rotary.

FUEL INJECTED, TURBOCHARGED, LIQUID COOLED, GEARED,
INTERCOOLED, WITH CABIN BLEED AIR PROVISIONS

Take-off Power	300kW (400hp)
Take-off Crankshaft Speed	5800 RPM
Take-off Altitude Capability	Sea level to 6000m (20,000 Ft.)
Cruise Power (75% Cruise)	225kW (300HP)
Cruise Crankshaft Speed	4350 RPM
Cruise Altitude Capability	To 7500m (25,000 Ft.)
Engine Weight Goal	228kg (506 Lbs.)
BSFC at Take-off	243-255 g/kW-Hr. (.40-.42 Lbs./BHP-Hr.)
BSFC at 75% Cruise	231-249 g/kW-Hr. (.38-.41 Lbs./BHP-Hr.)
TBO	2,000 Hours
Fuel, Aviation Grade	Jet-A

FIGURE 18 - PRELIMINARY ENGINE SPECIFICATION 170 SERIES MODEL 2034R

The engine was rated at 400 HP (300kW) at 5800RPM in take-off conditions (Figures 19 and 20) and will maintain that power to 20,000 ft. (6096 meters) altitude. Cruise conditions for the engine were 300 HP (225kW) at 4350RPM and that power could be maintained to 25,000 ft. (7620 meters) altitude. The engine was liquid cooled with a 50/50 mixture of ethylene glycol and water. Liquid cooling in an aircraft engine offers some advantages over air cooled engines permitting more rapid descents and possible use of the warm coolant for de-icing and safe cabin heat. An generally, liquid cooling offers an advantage of better control of engine operating temperatures while maintaining even temperature distributions. An air-cooled oil cooler is incorporated with the radiator.

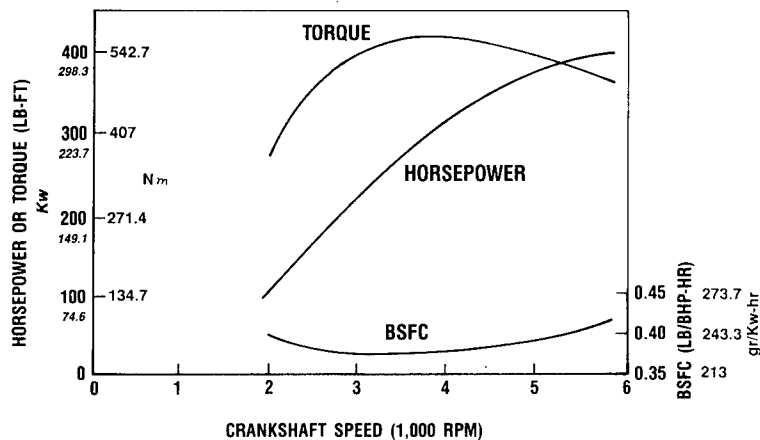


FIGURE 19
ESTIMATED
FULL LOAD PERFORMANCE
ENGINE MODEL 2034R

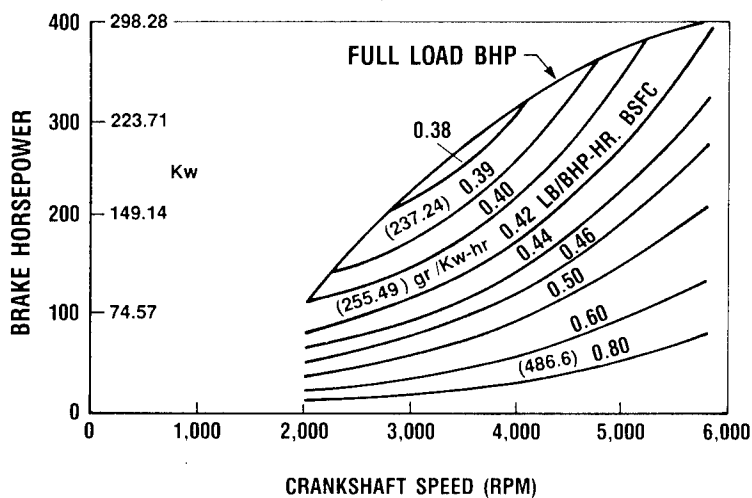


FIGURE 20
ESTIMATED
PART LOAD PERFORMANCE
ENGINE MODEL 2034R

TESTING. Testing of the 2034R engine was initiated in late 1987 with the initial test consisting of operation of a highly instrumented engine for the acquisition of housing strain gage data over a wide range of internal pressures. The objective was to validate the finite element models used to design the core engine. Once validated, the finite element models are then available for use in weight control.

Initial testing was accomplished to 200 HP (149 Kw) using Jet-A fuel. This included investigations necessary to obtain uniform ignition, combustion and stable operation and a degree of trial and error in establishing the dual spark plug configuration at the pilot nozzle, necessary for FAA Certification.

The second phase of testing was initiated in 1988 with operation through full take-off power. This testing was accomplished in conjunction with a Douglas Aircraft Company/USAF contract to investigate the Stratified Charge Rotary Engine as a potential candidate prime-mover for an energy efficient APU. The testing involved operation to the take-off condition of 400 HP(298 Kw)/5800 RPM and operation on three different fuels; Jet-A, 100 Octane low lead AVGAS and No. 2 diesel. Cold starting was demonstrated on the three fuels in unaided cold starts at -25°F (-32°C).

Take-off Power and Fuel Consumption. Full load performance through the 5800 RPM take-off speed with Jet-A fuel is shown in Figure 21. A maximum power of 430 BHP(320 kW) was demonstrated at 5800 RPM. The specific fuel consumption of approximately 0.44 lbs/BHP-hr (268 gr/kW-Hr) at the maximum power in this initial testing was slightly above the 0.42 lbs/BHP-hr (255.5 gr/kW-Hr) projected for the engine take-off condition at the end of the overall development program.

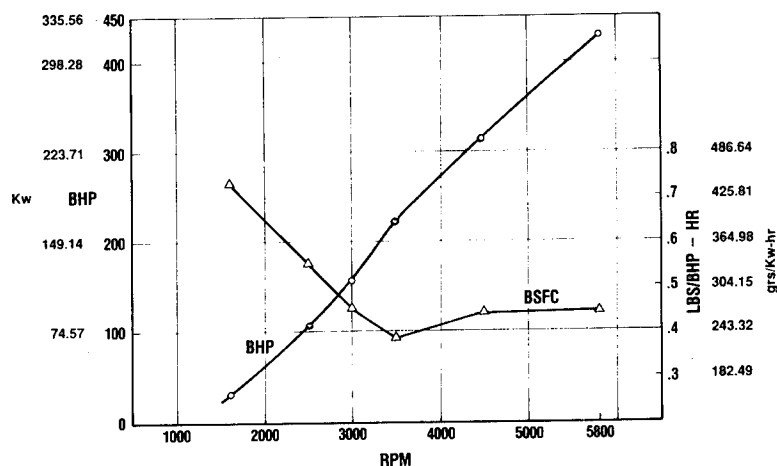


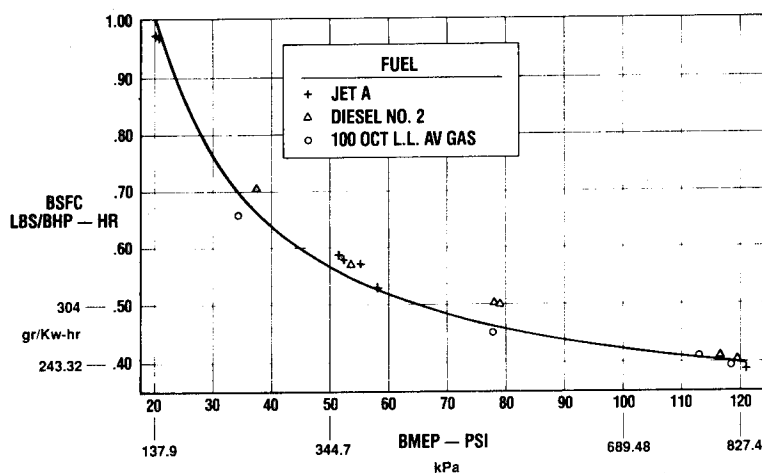
FIGURE 21

**STRATIFIED CHARGE
ROTARY AIRCRAFT ENGINE
MODEL 2034R
BASIC PERFORMANCE**

Multifuel Testing and Cruise Power Fuel Consumption. In the multifuel testing, Jet-A, 100 Octane low lead AVGAS and No. 2 diesel fuels were used. Starting and general operation through take-off power was essentially equal for the three fuels. Figure 22 shows the resulting specific fuel consumption for the mid-cruise range speed of 3500RPM over the 20 to 120 psi (138 to 827 kPa) BMEP range. The best BSFC noted was 0.387 lbs/BHP-hr (235.4g/kW-Hr) on JET-A, 0.390 Lbs/BHP-Hr (237.3 g/kW-Hr) on AvGAS and 0.405 Lbs/BHP-Hr (246.4g/kW-Hr) on No. 2 Diesel, all at the 225 HP (168kW)/3500RPM condition.

FIGURE 22

**STRATIFIED CHARGE
ROTARY AIRCRAFT ENGINE
MODEL 2034R
FUEL CONSUMPTION AT 3500 RPM**



Cold Starting. Cold start demonstrations were conducted consisting of unaided starts after a 24 hour cold soak period at -25°F (-32°C). Batteries were not at the low temperature for these tests. Successful starts were achieved on the three fuels (Jet-A, 100 octane low lead AvGAS and No. 2 Diesel) at -25°F (-32°C).

These tests confirmed operation of the Stratified Charge Rotary Engine in a complete aircraft configuration and demonstrated power and fuel consumption on Jet-A and other fuels.

40 SERIES AIRCRAFT ENGINES

During 1993 Rotary Power International (RPI) acquired the assets and technology rights from Defense Group Industries, Inc. (DGII) for a small displacement rotary engine, 407 cc (26.05 cu.in.) per rotor. These engines are also capable of operation on a wide variety of fuels including gasoline, Jet fuel and diesel. Figure 23 presents a summary performance chart for advanced 40 Series rotary engines having 1, 2, 3 or 4 rotors.

			1 ROTOR	2 ROTOR	3 ROTOR	4 ROTOR
G A S O L I N E	NATURAL ASPIRATED	HP @ 6000 RPM	50	100	150	200
		APPROX. WEIGHT (LBS)	50	80	110	140
	TURBO CHARGED	HP @ 6000 RPM	75	150	225	300
		APPROX. WEIGHT (LBS)	70	90	120	140
DIESEL & JP FUELS	TURBO CHARGED	HP @ 6000 RPM	55	110	160	220
		APPROX. WEIGHT (LBS)	75	95	130	150

NOTE: The above performances have been demonstrated on gasoline and diesel fuel on a single rotor engine.

**FIGURE 23 - PERFORMANCE CHART OF ADVANCED 40 SERIES
ROTARY ENGINES**

PRODUCTION MACHINES

During 1989 systems were selected and installed for initial low volume production of the rotary engine housings. Initial capacity is for 6 engines per day. The machinery is capable of producing parts for Series 40, 70, 170 and 580 engines. Capacity can be expanded to 30 engines/day. Figures 24-27 present the machinery items in operation at Rotary Power International.

FIGURE 24 - KEARNEY & TRECKER ORION 2300 4-AXIS MACHINING CENTER

FIGURE 25 - CUSTOM-BUILT WELDON CNC GRINDER

FIGURE 26 - GRIND EQUIPMENT MACHINERY TROCHOID LAPPER

FIGURE 27 - CONE BLANCHARD SURFACE GRINDER (MODEL 22 AD 42)

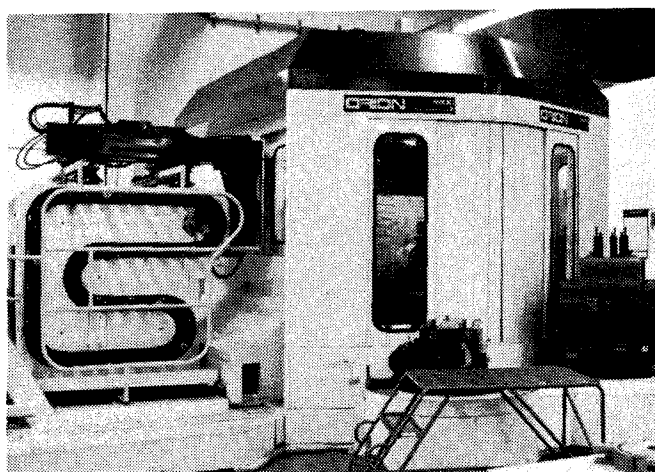


FIGURE 24

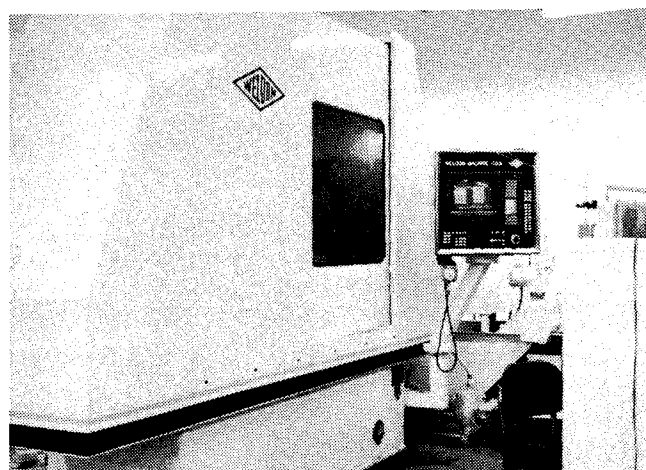


FIGURE 25

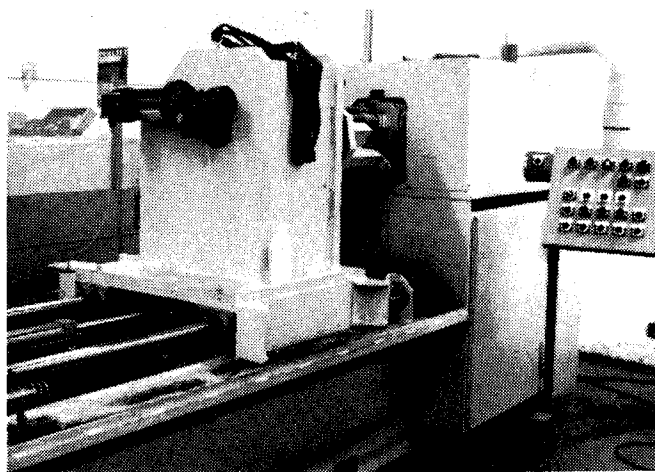


FIGURE 26

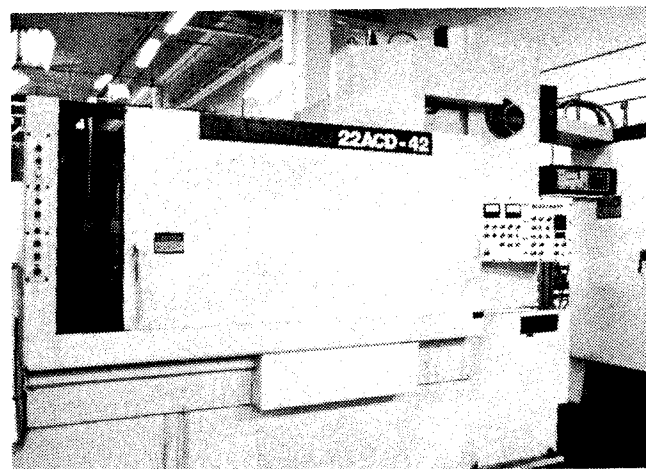


FIGURE 27

RESULTS

1. Advanced Technology Jet-A fuel Stratified Charge Rotary Aircraft Engine configurations have been defined covering a wide power range (50 to 1000HP).

<u>Series</u>	<u>Number of Rotors</u>	<u>Power Class</u>
40	One	50 HP (37kW)
40	Two	100 HP (75kW)
70	Two	340 HP (254kW)
70	Four	680 HP (507kW)
170	Two	350-500 HP (261-373kW)
170	Three	750 HP (559kW)
170	Four	1000 HP (746kW)

2. Testing has been conducted with the 40 Series single rotor engine, 70 Series single rotor research rig (NASA), 70 Series two rotor engine (RPI, NASA) and the 170 Series two rotor engine (RPI).
3. Plans have been defined for final development and FAA certification for all series providing the basis for developer, user and investor discussion.

CONCLUSIONS

1. NASA's long term support to Technology Enablement with the Stratified Charge Rotary Engine and industry's continued technology development work has defined an advanced technology powerplant for General Aviation engines of the mid-1990's and beyond with the following listed features:
 - o Jet-A fuel capability
 - o Non-dependency upon leaded AvGas
 - o Environmentally Acceptable
 - o High power to weight ratio
 - o Small size
 - o Light weight
 - o Low vibration
 - o High reliability/simplicity
2. Transition of this advanced General Aviation Systems technology to the aviation field through industry supported development and FAA Certification is in the formative stages at Rotary Power International. Discussions with airframers, retrofitters, engine manufacturers and other potential partners are in progress.
3. The Stratified Charge Rotary Aircraft Engine addresses advanced propulsion system needs and short term development and certification timing as noted in NASA's technology objectives for revitalization of U.S. General Aviation, Reference 11.
4. The Stratified Charge Rotary Engine propulsion system technology is applicable to a wide variety of applications including aviation (commercial and military), marine, vehicular and utility systems.

REFERENCES

1. P. Badgley, M. Berkowitz, et al "Advanced Stratified Charge Rotary Aircraft Engine Design Study", Curtiss Wright Corp., Wood-Ridge, N.J, CW-WR-81.021, Jan. 1982. (NASA CR-15-65398).
2. G. L. Huggins and D. R. Ellis, "Advanced General Aviation Comparative Engine/Airframe Integration Study", Cessna Aircraft Co., Wichita, KS, Cessna-AD 217, 1981. (NASA CR-165564).
3. Beech Aircraft Corporation Report No. 165565, "Advanced General Aviation Comparative Engine/Airframe Integration Study", prepared under Contract NASA-22220, March 1982.
4. C. Jones and R. E. Mount: "Design of a High Performance Rotary Stratified Charge Aircraft Engine", AIAA Paper 84-1395. June 1984
5. E.A. Willis and J.J. McFadden, "NASA's Rotary Engine Technology Enablement Program - 1983 through 1991," 920311, Society of Automotive Engineers, International Congress & Exposition, Detroit, MI, February 24-28, 1992.
6. Robert E. Mount and Edward S. Wright, "Advanced Stratified Charge Rotary Engine Technology for General Aviation Systems," AIAA/FAA Joint Symposium on General Aviation Systems, Ocean City, NJ, April 11, 1990.
7. James P. Mitchell et al, "Energy-Efficient Multifuel Auxiliary Power Unit (APU), WRDC-TR-89-2132, Aero Propulsion Laboratory, Wright Patterson Air Force Base, OH, December 1989.
8. Advanced System Propulsion Studies, Naval Air Development Center, Warminster, PA, Contract No. N62269-90-C-003, Final Report.
9. Dankwart Eiermann, Roland Nuber, Joachim Breuer, Michael Soimar and Mihai Gheorghiu, "An Experimental Approach for the Development of a Small Spark Assisted Diesel Fueled Rotary Engine," 930683, Society of Automotive Engineers, International Congress and Exposition, Detroit, MI, March 1-5, 1993.
10. William T. Figart and Robert E. Mount, "Advanced Stratified Charge Rotary Aircraft Engines - The Transition from Research to General Aviation Application," SAE, 1993 General, Corporate & Regional Aviation Meeting and Exposition, Century 11 Convention Center, Wichita, Kansas, May 18-20, 1993.
11. Bruce J. Holmes, "U.S. General Aviation: The Ingredients for a Renaissance," SAE, 1993 General, Corporate & Regional Aviation Meeting and Exposition, Century II Convention Center, Wichita, Kansas, May 18-20, 1993.

A NUMERICAL STUDY OF AIRCRAFT AGING EFFECTS ON TRANSONIC CRUISE PERFORMANCE

Luis C. Santos

Rolls-Royce, Inc., Atlanta, GA USA 30339-3769

ABSTRACT

This paper describes a Computational Fluid Dynamics tool developed to theoretically analyze the effects of aging on a given wing design. Random disturbances are introduced in the wing geometrical parameters and also some sections are deformed to simulate local damage. A full-potential flow solver is used to compute the pressure distribution and the aerodynamic coefficients. Several analysis are performed for Mach numbers to produce a $\frac{ML}{D_w}$ curve for both original and "aged" wings. The results indicate that the optimum cruise point is shifted to a lower cruise Mach number as the geometry differs from the original. Also the appearance of strong shocks, in some portions of the wing, provide additional structural stresses that must be accounted for, during the inspection cycle. This technique allows aircraft designers to anticipate the degradation of the wing performance as the aircraft ages.

INTRODUCTION

A new type of successful air transportation business has appeared due to the world economic recession. A larger number of small companies have entered the market offering very low fares. Those companies take advantage of the large fleet of aircraft out of operation due to bankruptcy of bigger corporations, like for example Eastern Airlines. This fleet consists of used aircraft, therefore cheaper to lease. The only feasible way to operate those aircraft is to keep the costs low. Discarding maintenance costs, which are a primary function of the mechanical design, the main part of the operational cost comes from fuel consumption. The aerodynamic characteristics of the aircraft as the airframe ages do not correspond anymore to the original design point. Therefore the age of the aircraft can substantially affect the performance, and the original flight envelope would not be cost efficient anymore.

Economical issues have been increasingly addressed as the aerospace industry faces today's challenges. Therefore the effects of aging, due to structural fatigue, should start to be evaluated still in the design phase, to anticipate the degradation of performance as geometry is deformed. The wing deformation is directly associated to structural stresses. The successive landings, vibration in flight and several other situations associated to daily operations, cause some wing panels to buckle in a random pattern.

The present work describes the use of a Computational Fluid Dynamics tool, a full-potential flow solver to evaluate the sensibility of the wave drag with respect to changes in the original geometry. Although inviscid, the full-potential code can accurately predict the drag rise due to the formation of strong shock waves. Although important a viscous analysis would require much more computational time and consequently cost, and therefore such analysis is discarded at this time.

A typical transport wing is analyzed for several degrees of deformations and the performance degradation compared. The whole procedure is extremely cost efficient due to the low CPU time required by the full-potential solver. The results presented, in the form of pressure distribution and cruise performance plots indicate a relationship between aircraft age and cruise Mach number.

THE FULL-POTENTIAL FLOW SOLVER

To conduct wing design it is necessary to have a reliable flow solver, able to handle the non-linear phenomena that occur in transonic flow. The Navier-Stokes equations are the most comprehensive set available, but its extremely costly solution, specially in three-dimensional cases, limits its applications to the research level, still today.

The nature of flow for typical cruise conditions, favors the use of a subset of the Navier-Stokes equations, which is the so called full-potential equation. The three-dimensional steady transonic potential flow is governed by:

$$(\rho\Phi_x)_x + (\rho\Phi_y)_y + (\rho\Phi_z)_z = 0 \quad (1)$$

The conservation of energy is given by:

$$a_\infty^2 + \frac{\gamma-1}{2}V_\infty^2 = a^2 + \frac{\gamma-1}{2}(\Phi_x^2 + \Phi_y^2 + \Phi_z^2) \quad (2)$$

and the gas follows an isentropic relation:

$$\rho = \rho_\infty \left(\frac{a^2}{a_\infty^2} \right)^{\frac{1}{\gamma-1}} \quad (3)$$

The velocity potential is denoted by Φ , the density by ρ , the undisturbed flow velocity by V_∞ . The quantities a and a_∞ are respectively the local and freestream speeds of sound, and γ is the ratio of specific heats.

To avoid inaccuracies due to the numerical discretization scheme, the preceding equations can be written in strong conservation form in a body-fitted system of coordinates. The conservation of mass becomes:

$$\left(\frac{\rho U}{J} \right)_\xi + \left(\frac{\rho V}{J} \right)_\eta + \left(\frac{\rho W}{J} \right)_\zeta = 0 \quad (4)$$

The conservation of energy and the isentropic relation can be combined:

$$\rho = \left[1 + \frac{\gamma-1}{2} M_\infty^2 (1 - U\Phi_\xi - V\Phi_\eta - W\Phi_\zeta) \right]^{\frac{1}{\gamma-1}} \quad (5)$$

where the contravariant velocities are defined applying the appropriate metrics:

$$\begin{aligned} U &= A_1\Phi_\xi + A_2\Phi_\eta + A_3\Phi_\zeta \\ V &= A_2\Phi_\xi + A_4\Phi_\eta + A_5\Phi_\zeta \\ W &= A_3\Phi_\xi + A_5\Phi_\eta + A_6\Phi_\zeta \end{aligned} \quad (6)$$

The metrics terms A_1, \dots, A_6 are given by:

$$\begin{aligned} A_1 &= \xi_x^2 + \xi_y^2 + \xi_z^2 \\ A_2 &= \xi_x\eta_x + \xi_y\eta_y + \xi_z\eta_z \\ A_3 &= \xi_x\zeta_x + \xi_y\zeta_y + \xi_z\eta_z \\ A_4 &= \eta_x^2 + \eta_y^2 + \eta_z^2 \\ A_5 &= \eta_x\zeta_x + \eta_y\zeta_y + \eta_z\eta_z \\ A_6 &= \zeta_x^2 + \zeta_y^2 + \zeta_z^2 \end{aligned} \quad (7)$$

The Jacobian of the transformation:

$$J = \xi_x(\eta_y\zeta_z - \eta_z\zeta_y) + \xi_y(\eta_z\zeta_x - \eta_x\zeta_z) + \xi_z(\eta_x\zeta_y - \eta_y\zeta_x) \quad (8)$$

There several solution approaches to the transonic full-potential equation. Holst [3, 4, 5] and Sankar Malone and Tassa [6, 7] describe the use of implicit conservative solution schemes. The present work

follows an approach similar to Hazarika [10], where all time dependent terms are dropped and the steady solution obtained.

The finite volume method uses a volumetric discretization of the flow field, which results in cubic cells in the computational plane. Denoting the cell center as i, j, k and representing the cell faces by half indexes, the full-potential equation can be approximated by:

$$\left(\frac{\rho U}{J}\right)_{i+\frac{1}{2},j,k} - \left(\frac{\rho U}{J}\right)_{i-\frac{1}{2},j,k} + \left(\frac{\rho V}{J}\right)_{i,j+\frac{1}{2},k} - \left(\frac{\rho V}{J}\right)_{i,j-\frac{1}{2},k} + \left(\frac{\rho W}{J}\right)_{i,j,k+\frac{1}{2}} - \left(\frac{\rho W}{J}\right)_{i,j,k-\frac{1}{2}} = 0 \quad (9)$$

The above discretization is second order accurate for smoothly stretched grids.

Defining a correction vector: $\Delta\varphi_{i,j,k}^{n+1} = \varphi_{i,j,k}^{n+1} - \varphi_{i,j,k}^n$, where $\varphi = \Phi - V_\infty(x\cos\alpha + y\sin\alpha)$, the full-potential equation can be rewritten:

$$(\bar{\rho}A_1\Delta\varphi_\xi)_\xi + (\hat{\rho}A_4\Delta\varphi_\eta)_\eta + (\bar{\rho}A_6\Delta\varphi_\zeta)_\zeta = R_{i,j,k}^n \quad (10)$$

where A_1, A_4, A_6 are metrics terms, a more detailed description can be found in [9]. The residual $R_{i,j,k}$ is given by equation(6).

In transonic flow, subsonic and supersonic regions coexist. To take into account the distinct domains of dependence of those regions, the full-potential equation must change accordingly. The use of artificial compressibility [11] provides the change from elliptic (subsonic) to hyperbolic (supersonic) behaviour by the adequate bias of density. For example in the ξ -direction the density at $i + \frac{1}{2}, j, k$ is computed by:

$$\bar{\rho}_{i+\frac{1}{2},j,k} = \rho_{i+\frac{1}{2},j,k} + \nu_{i,j,k} \left(\rho_{i+\frac{1}{2},j,k} - \rho_{i-\frac{1}{2},j,k} \right) \quad (11)$$

where the local mach based switching operator $\nu_{i,j,k} = \max \left[0, 1 - \frac{1}{M^2} \right]$. A similar bias can be applied to the other directions.

The numerical approximation of the derivatives in equation (7) results in a non-linear matrix system. Introducing the shift operators $\delta_\xi, \delta_\eta, \delta_\zeta$ of the form:

$$\delta_\xi^\pm \Delta\varphi_{i,j,k}^{n+1} = \Delta\varphi_{i\pm 1,j,k}^{n+1} \quad (12)$$

Similarly the operators $\delta_\eta, \delta_\zeta$ work in their respective directions. So being eq.(10) can be rewritten as:

$$\left(E_1 + Z_1\delta_\zeta^- + B_1\delta_\eta^- + D_1\delta_\xi^- + F_1\delta_\xi^+ + H_1\delta_\eta^+ + S_1\delta_\zeta^+ \right) \Delta\varphi^{n+1} = -R(\varphi^n) \quad (13)$$

where

$$\begin{aligned} Z_1 &= (\bar{\rho}A_6)_{i,j,k-\frac{1}{2}} & B_1 &= (\hat{\rho}A_4)_{i,j-\frac{1}{2},k} \\ D_1 &= (\bar{\rho}A_1)_{i-\frac{1}{2},j,k} & F_1 &= (\bar{\rho}A_1)_{i+\frac{1}{2},j,k} \\ H_1 &= (\hat{\rho}A_4)_{i,j+\frac{1}{2},k} & S_1 &= (\bar{\rho}A_6)_{i,j,k+\frac{1}{2}} \\ E_1 &= -(Z_1 + B_1 + D_1 + F_1 + H_1 + S_1) \end{aligned} \quad (14)$$

Since a large number of grid points is necessary to accurately describe the flowfield, direct inversion is discouraged. Stone [8] proposed an LU-type algorithm, named Strongly Implicit Procedure (SIP), which performance is expected to be superior than approximate factorization schemes. After the LU decomposition eq.(14) becomes:

$$[L][U]\Delta\varphi^{n+1} = -R(\varphi^n) \quad (15)$$

The matrices $[L]$ and $[U]$ are iteratively found using the values of $Z_1, B_1, D_1, F_1, H_1, S_1$ and E_1 . For a more detailed description references [8, 6, 7, 9] should be consulted. The SIP method applies an

automatic filtering of both high and low frequency errors accelerating convergence. This algorithm is implemented in the present work.

To demonstrate the accuracy of the full-potential code, the numerical solution and the experimental results for the ONERA M6 wing [12], at several flow conditions, were compared. The figures 1,2 and 3 present the corresponding experimental and numerical values for each wing station for several transonic Mach numbers.

Considering that the ONERA M-6 wing has a low aspect ratio ($\Lambda = 1.7$) and close to tip the viscous and rotational effects, due to vortex roll-up, the results presented confirm the accuracy of the scheme, since the only discrepancies are limited to regions of high viscous interactions. This fact leads to the conclusion that the accuracy of the analysis satisfies the requirements for transport wing cruise optimization.

Another important point to stress is the low computational cost of the analysis. The code requires 1.5 Mb of memory for 44,000 grid points and takes 20 minutes of CPU time to converge, in a HP-Apollo workstation, which clearly encourages its use not only as analysis but also as design tool.

NUMERICAL RESULTS

To simulate the effects of aging, the geometry will be randomly modified by a series of sinusoidal functions:

$$z^{aged} = z^{new} + a \left(\frac{t}{c} \right) \sin \left(n\pi \left(\frac{x}{c} \right) \right) \quad (16)$$

The parameters a and n control respectively the amplitude and frequency of the geometric perturbations. By a structural analogy high frequency oscillations show lower amplitude, while lower frequency produce a higher amplitude of deformation therefore, the parameters a and n will be chosen accordingly. The maximum amplitude of the oscillations will be limited to 10 % of the section maximum thickness and the frequency number n will lie between 1 and 20.

The analysis is performed on a typical transport wing planform, as shown in Fig.4. The wing has aspect ratio 4 and the profiles for the root, kink (where the engine will be placed) and tip sections are shown in figures 5,6 and 7, respectively. The wing has a typical downwash with the root at 3° , the kink at 1° and the tip at 0° . The wing angle of attack is zero, for all Mach numbers tested.

Three wings are compared, wing 0 which has no geometrical disturbances, wing A with a 0.25% maximum amplitude of the disturbances only on the upper surface and wing B with also 0.25%, on both surfaces. The number of modes n is set to 20.

The full-potential solver was used to analyze the three wings and the $M \frac{CL}{CDw}$ for Mach numbers in the 0.7 to 0.8 range computed as shown in Figure 8. The analysis of the curve indicates the degradation of cruise performance. If the original design operates at $M = 0.8$ the "aged" or "damaged" wing would be limited to $M = 0.71$ to maintain the range, or the payload unaltered. To keep flying at $M = 0.8$ the reduction of $M \frac{CL}{CDw}$ would force a significant reduction of range and/or payload.

The lift distribution along the wing span, presented in Figures 9, shows no alteration which indicates a reduction root bending moment. The analysis of pressure distribution reveals the increase of the shear moment on the wing skin, which can stimulate more buckling and fracture growth. Figures 10 to 15 show the original and "aged" pressure distributions for $M = 0.8$.

CONCLUSIONS

The analysis of the results reinforces the importance of maintaining a smooth wing surface, specially for the transonic flight regime. The use of a full-potential tool allows a preliminary analysis of the impact on performance due to wing superficial fatigue. Since no viscous effects were included, the degradation of performance and even control qualities can be even worse.

Acknowledgments

The author wishes to acknowledge the support from EMBRAER and ROLLS-ROYCE, Inc. The support from Dr. Carlos Cesnik, during the computational phase, is also appreciated.

References

- [1] Miranda,L., "Applications of Computational Aerodynamics to Airplane Design", Vol. 21, No. 6, 1984.
- [2] Chandrasekaran,R., Murphy,W., Taverna,F. and Boppe,C., "Computational Aerodynamic Design on the Gulfstream IV Wing", Journal of the Aircraft, Vol. 22, No. 9, 1985.
- [3] Holst,T.L. and Balhaus,W.F., "Fast, Conservative Schemes for the Full-Potential Equation Applied to Transonic Flows" , AIAA Journal, Vol.17, No.2, 1979.
- [4] Holst,T.L., "Implicit Algorithm for the Conservative Transonic Full-Potential Equation using an Arbitrary Mesh", AIAA Journal, Vol.17, No.10, 1979.
- [5] Holst,T.L., "Fast, Conservative Algorithm for Solving the Transonic Full-Potential Equation" , AIAA Journal, Vol.18, No.12, 1980.
- [6] Sankar,L.N.,Malone,J.B. and Tassa,Y., "An Implicit Conservative Algorithm for Steady and Unsteady Three-Dimensional Transonic Potential Flows", AIAA paper 81-1016, AIAA 5th Computational Fluid Dynamics Conference, 1981.
- [7] Sankar,L.N.,Malone,J.B. and Tassa,Y., "A Strongly Implicit Procedure for Steady Three-Dimensional Transonic Potential Flows", AIAA Journal, Vol.20, No.5, 1982.
- [8] Stone,H.L., "Iterative Solution of Implicit Approximations of Multidimensional Partial Differential Equations", SIAM Journal of Numerical Analysis, Vol. 5, No. 3, 1968.
- [9] Santos,L.C., "A Hybrid Inverse Optimization Method for the Aerodynamic Design of Lifting Surfaces," Ph.D. Thesis, Georgia Institute of Technology, Atlanta, GA, 1993.
- [10] Hazarika,N., "An Efficient Inverse Method for the Design of Blended Wing-Body Configurations," Ph.D. Thesis, Georgia Institute of Technology, Atlanta, GA, 1988.
- [11] Hafez,M.,South,J. and Murman,E., "Artificial Compressibility Methods for Numerical Solutions to the Transonic Full Potential Equation", AIAA Journal, Vol.17, No.8, 1979.
- [12] AGARD-AR138, "Experimental Database for Computer Program Assessment", 1979.

Pressure Coefficient - ONERA M6 wing
 $M = 0.839$ $\alpha = 3.06^\circ$ $y/b = 0.20$

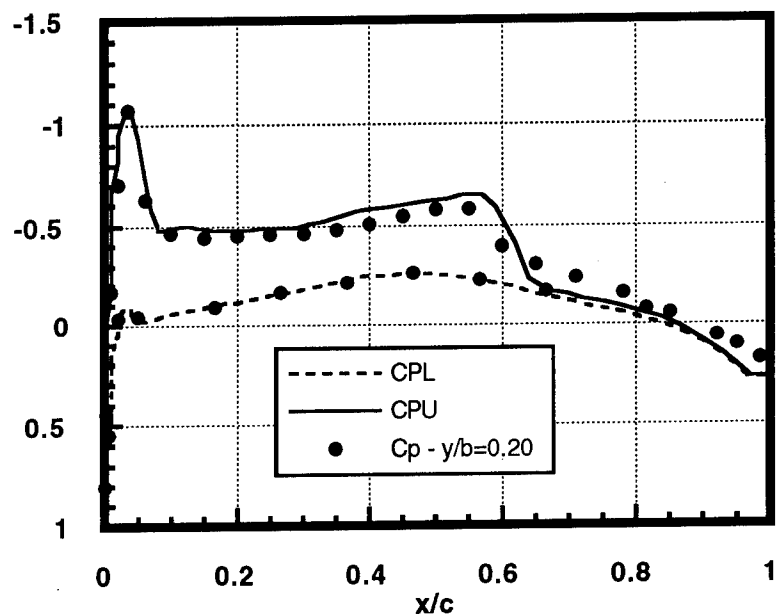


Fig. 1 - ONERA M6 wing station $y/b = 0.20$

Pressure Coefficient - ONERA M6 wing
 $M = 0.839$ $\alpha = 3.06^\circ$ $y/b = 0.80$

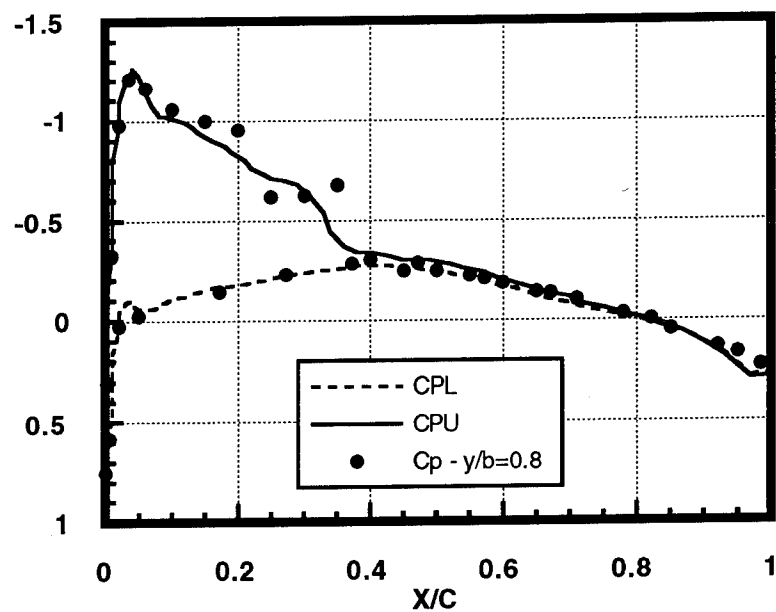


Fig. 2 - ONERA M6 wing station $y/b = 0.80$

Pressure Coefficient - ONERA M6 wing
 $M = 0.839$ $\alpha = 3.06^\circ$ $y/b = 0.99$

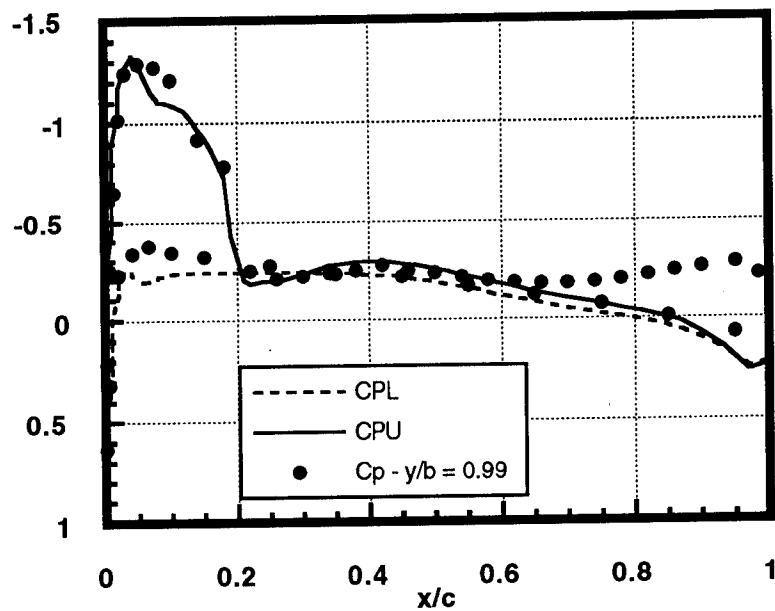


Fig. 3 - ONERA M6 wing station $y/b = 0.99$

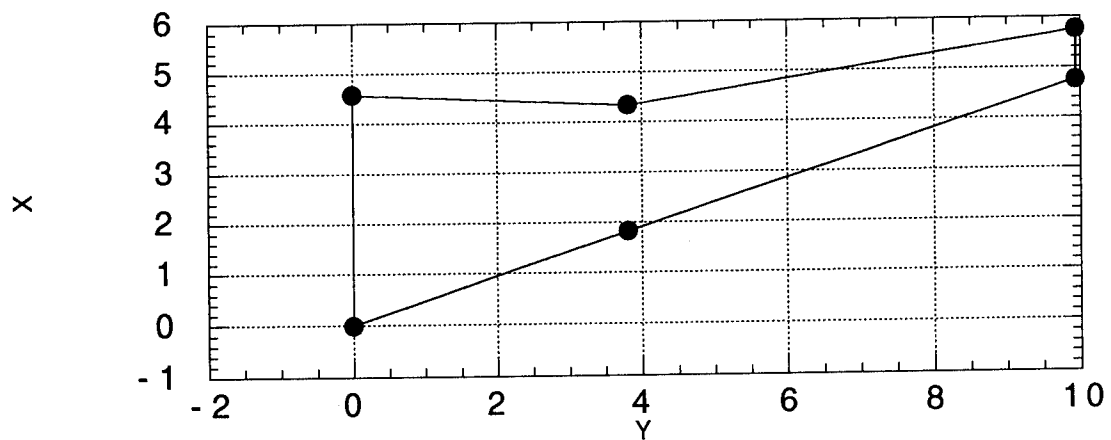


Fig. 4 - Transport wing planform

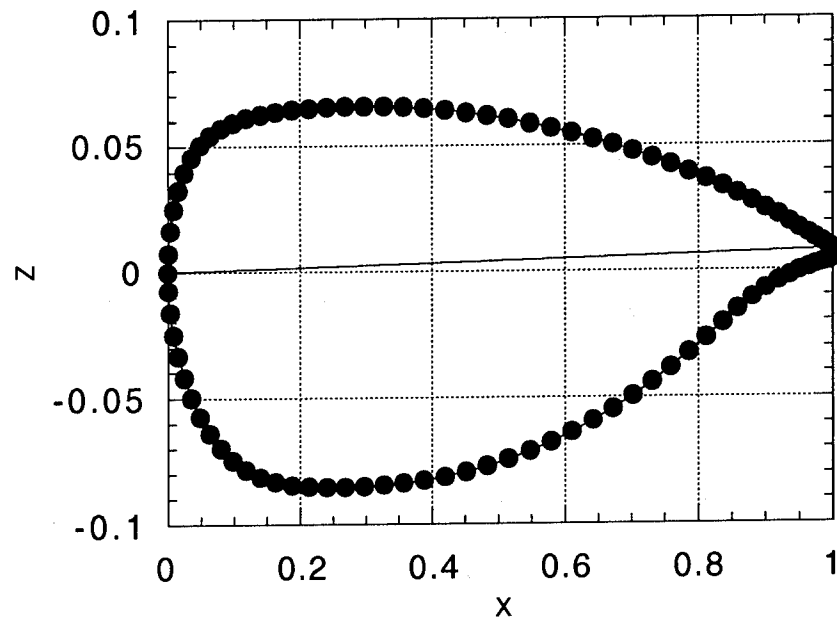


Fig. 5 - Transport wing root section

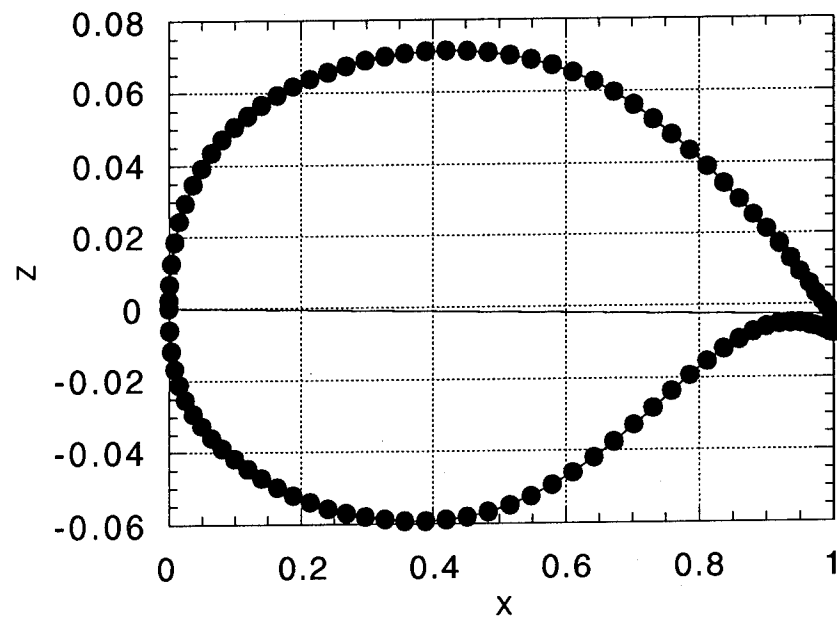


Fig. 6 - Transport wing kink section

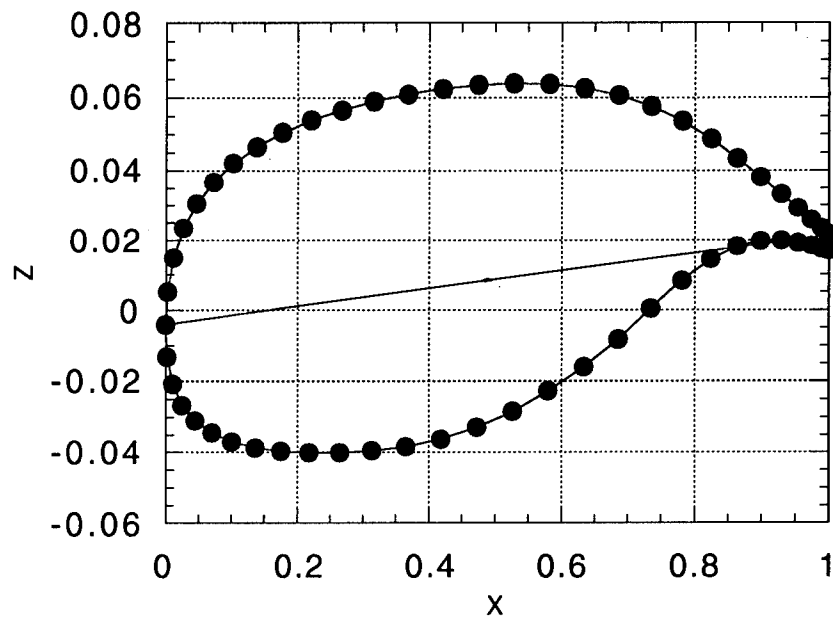


Fig. 7 - Transport wing tip section

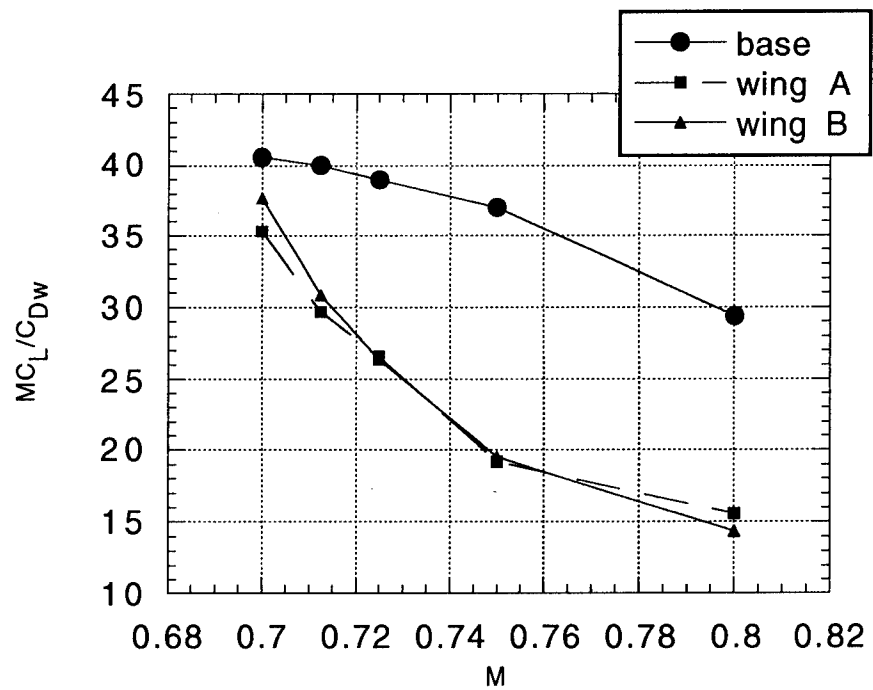


Fig. 8 - Aerodynamic Range Parameter

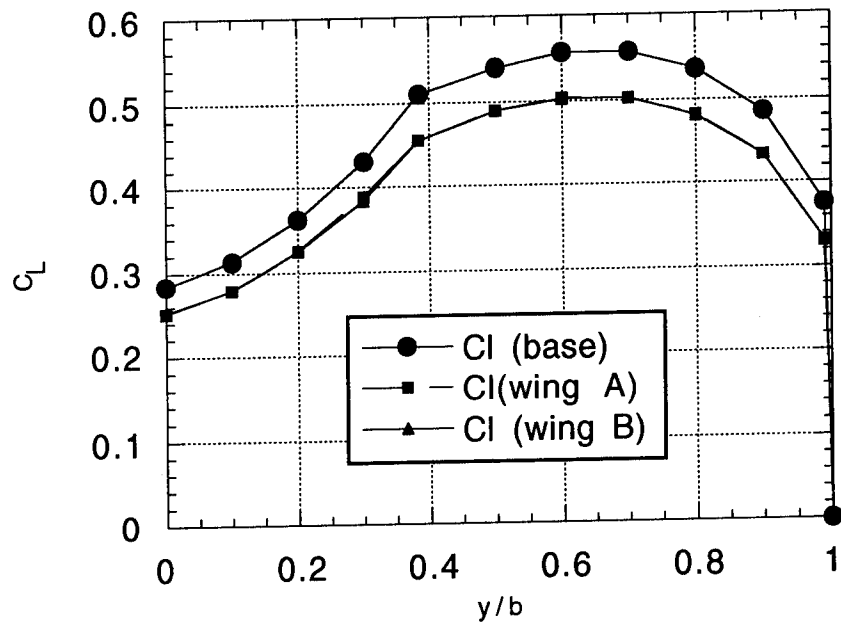


Fig. 9 - Lift Distribution along the span $M = 0.8$

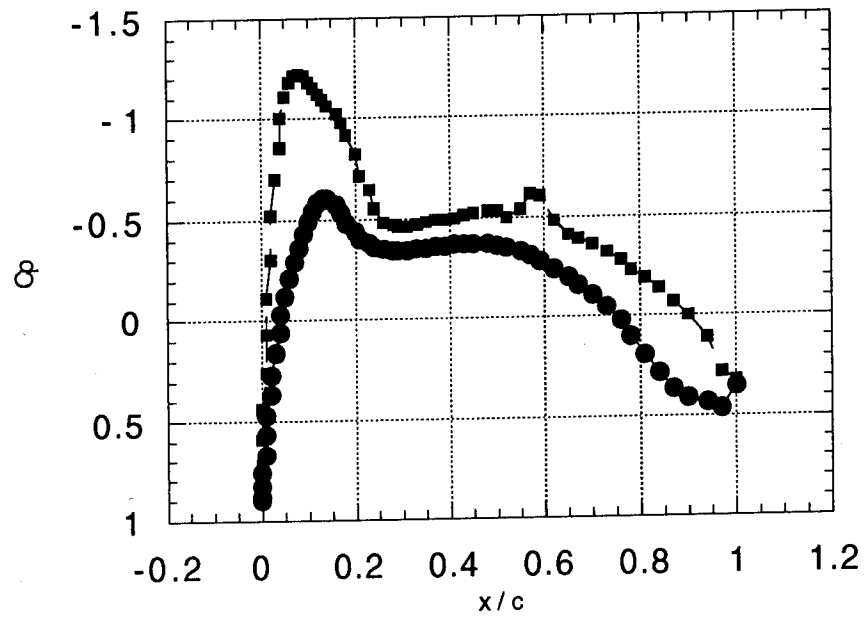


Fig. 10 - Base wing root pressure distribution

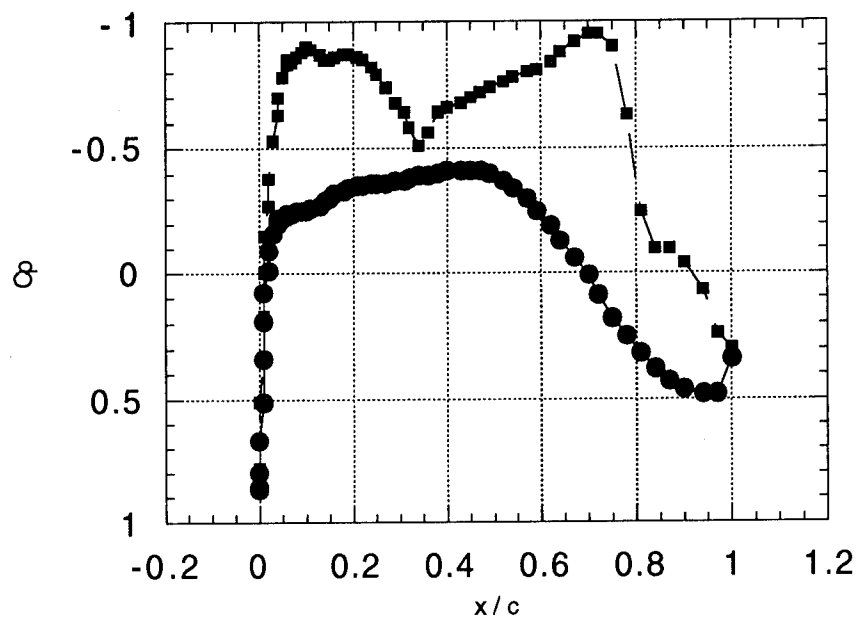


Fig. 11 - Base wing kink pressure distribution

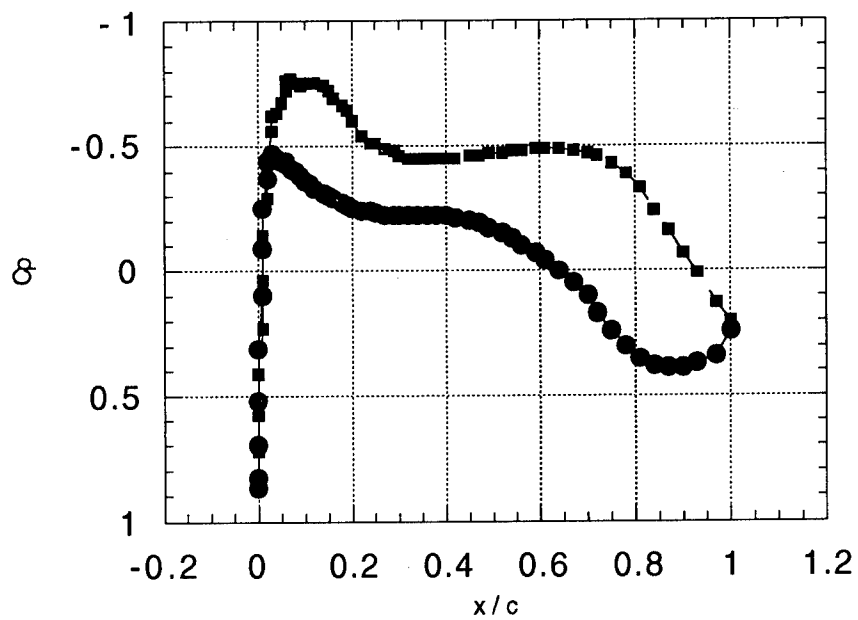


Fig. 12 - Base wing tip pressure distribution

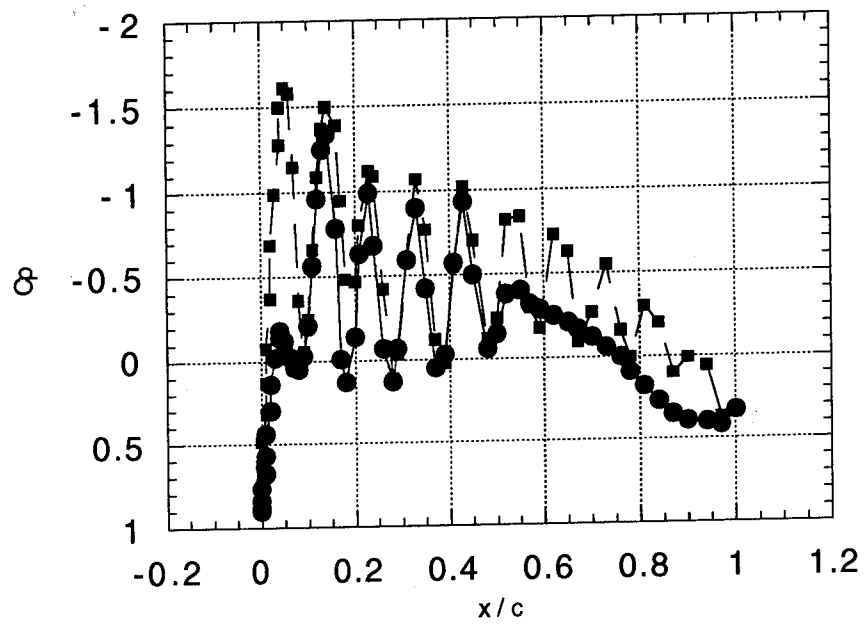


Fig. 13 - Base wing root pressure distribution

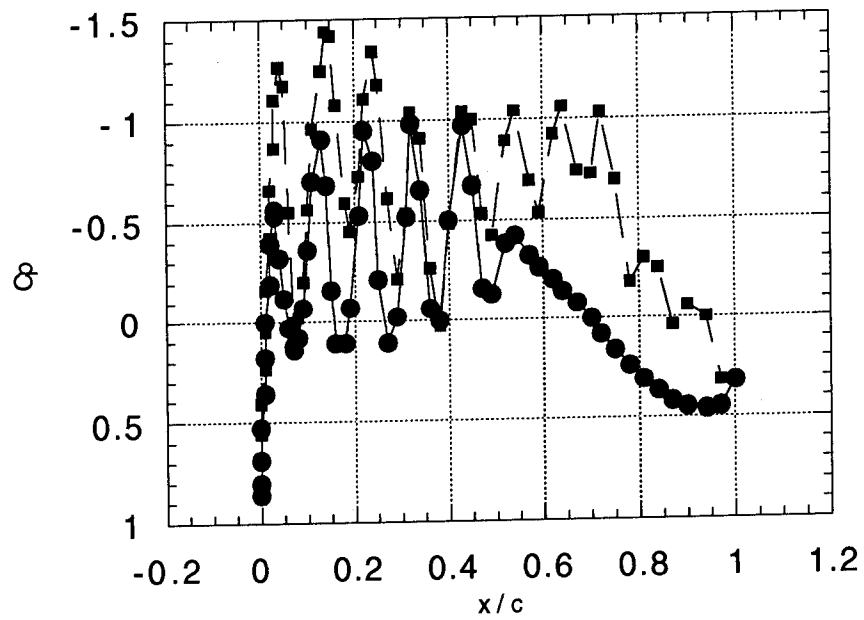


Fig. 14 - Base wing kink pressure distribution

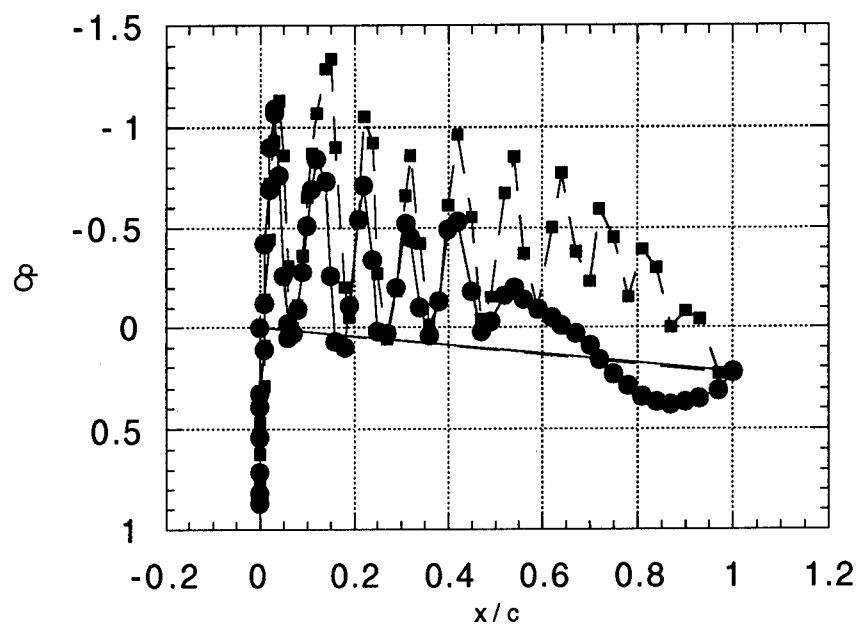


Fig. 15 - Base wing tip pressure distribution

GENERAL AVIATION INDIVIDUAL AIRPLANE LOAD MONITORING PROGRAM

Thomas DeFiore^a

FAA Technical Center, Atlantic City Int'l Airport, NJ 08405

and

David Kim^b

Embry-Riddle Aeronautical University, Daytona Beach, FL 32114

ABSTRACT

In General Aviation (GA) industry, there is a wider range of aircraft age, type, and fleet service usage than exists among the major carriers. Thus, standards for the frequency of structural safety inspections are correspondingly more difficult to determine. A major consideration in establishing this frequency is aircraft usage, i.e., accumulated flight hours and ground operation hours, combined with the severity of cumulative load history experienced during those service hours. In spite of this, operators are continuously required to meet an inspection schedule that has been developed for relatively severe usage. This current practice results in a possibly unwarranted financial burden to many of the operators, while it does not necessarily add to the safety of those aircraft typically operated in a lesser severe environment. The purpose of this Federal Aviation Administration (FAA) research task is to develop a practical means to monitor and assess the structural loads utilization of GA aircraft. This paper describes the initial phase of the FAA research and development effort to make available to GA operators a flight load data recording system appropriate for small aircraft--a small, compact, inexpensive, stand-alone unit that requires minimal modification or addition to existing equipment and is easily certified.

INTRODUCTION

Engineering materials subjected to cyclic loadings are susceptible to fatigue failures. In aviation, catastrophic failures due to structural fatigue have received much public exposure and consequently, prediction of time-to-failure is of the utmost concern. Flight and ground operations produce alternating stresses in loaded structural members that result in fractional damages to the crystal structure of the material. Estimating fatigue damage is possible using methods such as Palmgren-Miner's Rule, where material fatigue data and the number of cycles experienced at applied stress levels must be known. Fatigue data can be obtained from fatigue testing of notched and unnotched material samples and are readily available to the designer. The number of stress cycles is obtained from statistical databases and, if available, from actual, measured, in-service load spectrum. Recently,

^aProgram Manager, Flight Loads.

^bAssociate Professor, Aerospace Engineering Department, Member AIAA.

the Federal Aviation Administration (FAA) published a report, "Statistical Analysis of Fatigue Load Spectra Determined from the NASA VGH General Aviation Data Base" [1]. It contains VGH summaries of 95 airplanes flying 42,155 flight hours including: 1) Statistical estimates of vertical load factors separated into gusts and maneuvers; 2) Airplane characteristics; and 3) Basic exceedance spectra for wing structural fatigue analysis. These data are being used to update FAA Report No. AFS-120-73-2, "Fatigue Evaluation of Wing and Associated Structure on Small Airplanes" [2], and as load spectrum input to Advisory Circular AC 23-13, "Fatigue and Fail-Safe Evaluation of Flight Structure and Pressurized Cabin for Part 23 Airplanes" [3]. Monitoring stresses/strains and their cycles in a load bearing member furnishes a measure of the amount of fatigue damage that has been accumulated and therefore a yardstick for time-to-failure estimation. In damage tolerance structural life analysis, stress/strain histories are used as input to any of the commonly used crack growth formulations. The purpose of this FAA research is to develop a practical means to monitor and assess actual in-service (structural) usage of light general aviation aircraft and to quantify individual airplane usage differences.

BACKGROUND

Many of today's aircraft (both large and small) are being flown beyond their original intended service lifetimes. For large aircraft, the only feedback that the FAA and the manufacturers receive is the number of flight hours and landings. Load information on aircraft, i.e., wing, tail, flaps, controls, landing gear, etc., which is dependent on flight and ground operations, is assumed from aircraft usage information, but is largely unconfirmed. Because the practice of flying both large and small aircraft beyond their original intended service lifetimes is expected to continue into the foreseeable future, a need exists to acquire accurate usage information to assure that the design criteria for future generation of aircraft are based on operationally relevant and verified data.

As a part of the International Aging Aircraft Research Program, the Federal Aviation Administration has established a flight load (profile) data collection program for small aircraft. Data collected in this program will provide the necessary mission profiles and load spectra to accurately characterize small aircraft usage. These data are applicable for both safe-life fatigue analysis and damage tolerance fracture mechanics analysis. This paper describes the FAA Flight Load Program to instrument a fleet of aircraft in service and to collect data. Included primarily is the FAA's effort to support the development of a light-weight low-cost flight data recorder for small aircraft that can be used to provide individual airplane usage information from which more reliable inspection programs can be formulated. Manufacturers and operators of both regional/commuter and general aviation (GA) aircraft have indicated a strong interest in collecting large amounts of in-service usage data to obtain actual, accurate, aircraft fleet service histories. In response to this, the FAA has established a comprehensive program to conduct research in the following specific areas:

- Characterization of typical service usage data by developing a fleet tracking system to provide fleet usage information, trend data, and design criteria for future aircraft.

- Development of a reliable lateral load usage spectra for empennage service life determination.
- Assessment and verification of FAR 23.337-limit maneuvering load criteria.
- Characterization of differences in aircraft usage by geographical locations.

Successful completion of this effort will provide the FAA with: 1) Documented characterization of typical commercial/GA aircraft operations; 2) Substantiated data to ascertain if the loading spectra and aircraft operating envelope being used under current FAR 23 are representative of actual operational usage data. Reports of detailed service usage data and/or technical advisory materials will be the principal products of this research.

DISCUSSION

Relatively little is known about the actual service load experience of GA aircraft, but there are indications that, in particular, small GA trainer aircraft may be frequently subjected to high percentages of their design limit load. Taking into account that many of these aircraft are kept in service for very long periods of time, particularly so now that new primary trainers are scarce, the possibility of fatigue problems is far from hypothetical. From an air safety point of view, the development of a method to monitor and assess the in-service load experience of this category of aircraft is urgently needed.

In commuter airline and GA industry, there is a wider range of aircraft age, type, and operation as compared to major air carriers. Correspondingly, standards for determining the required frequency of structural safety inspections are more difficult to establish, and criteria for developing service life assessment and extension programs remain to be defined. However, it has been proposed that this frequency be based on individual aircraft usage, i.e., accumulated flight and ground operation hours and the severity of cumulative load history experienced during those service hours. Currently, aircraft operators are required to meet inspection schedules that have been developed for "severe" service conditions irrespective of their actual usage. This practice results in unwarranted financial burdens to many operators who operate in less severe environment, while not necessarily adding to the overall safety of aircraft flight operations. On the other hand, if an aircraft is operated under an unusually severe service condition, this inspection schedule may not be adequate. The successful development, implementation, and certification of a cost effective individual aircraft flight loads monitoring system can optimize inspection schedules and prevent in-flight structural failures of airplanes and their resulting product liability lawsuits.

This research program is being conducted as a response to a General Aviation Manufacturers Association (GAMA) recommendation, where GAMA provided numerous proposals regarding research and development programs that should be undertaken (or sponsored) by the FAA. Two of the recommendations are:

- Development of a certified light-weight, low-cost, airframe strain or flight load recorder for low-end GA aircraft; and
- Development of inspection schedules that realistically reflect typical usage of individual airplanes.

The following statement from an August 8, 1990, GAMA letter to the FAA was the trigger for the initiation of this research and describes the thrust of this research and development effort:

With today's technology in electronics, computers, data recording, etc., it appears feasible to develop a light-weight, low-cost and reliable airframe strain recording instrument. When this unit is available, it would be offered as an equipment item for each aircraft. The unit would have sufficient storage capacity so that data interrogation would (only) be required annually or every 400 to 500 hours (of flight and ground operations). With the growing use of fracture mechanics, the strain data could be used to predict realistic inspection intervals for each operator, and with the computer/software tools available today, this procedure could be implemented and be more cost effective than today's inspection programs. It would also improve the level of safety.

APPROACH

Through the Small Business Innovation Research Program (SBIR), the FAA Technical Center Aging Aircraft Research Program requested and received numerous proposals for the design and development of an airframe fatigue/strain monitoring system. When successfully developed, tested, and certified, the device could be installed on aircraft in order to measure actual in-service usage and determine more appropriate and realistic inspection intervals for the operator. It is envisioned that the implementation of such a program would be more cost effective than today's inspection programs, while still maintaining the same or higher levels of safety.

To be viable, the system would have to have sufficient storage capacity so that data interrogation would be required during regularly scheduled maintenance. Many of the systems proposed were judged to be excessively sophisticated, complex, and hence most likely too expensive. Thus, the approach adopted herein was that much could be learned using readily available accelerometers and strain gauges strategically located throughout the airframe. In addition, whatever instrumentation is finally adopted for general use, it: 1) must be a small, compact, 'stand alone' unit, requiring little in the way of modifications to existing airplane, and 2) must not in any way interfere with existing on-board systems, or produce any condition that could lead to difficulties with certification. Reference 4 describes the results of the Phase I SBIR prototype recording system.

It is clearly impractical to cover any fleet airplane with numerous strain gauges or any other kind of residual strength monitoring sensors. Consequently, stress levels will be determined analytically using results from accelerometer data and a limited number of strain gauges installed on one test airplane. Specific steps to be undertaken in this research include the following:

- Develop a number of relatively simple in-service loads monitoring systems using strain sensors, accelerometers, or a combination of both.
- Install, calibrate, and evaluate the relative merits of each system on a small test aircraft.
- Certify the most effective and reliable system for installation in selected fleet of aircraft.
- Install these systems in 6-8 regular fleet aircraft from a volunteer operator.
- Collect data from these aircraft for a period of twelve months, removing the data from each aircraft approximately every three months.
- Compute and report individual aircraft loads usage summaries quarterly.
- Publish a report describing instrumentation, data collection, and data reduction procedures.
- Develop technical data that could form the basis for a possible future FAA advisory circular describing an approved procedure for individual aircraft loads usage monitoring system based on the research results from this program.

A flight test program currently underway at the FAA Technical Center (FAATC) uses: 1) Systems & Electronics, Inc. (SEI) Airframe Cumulative Flight Loads Monitoring System; 2) ESPIRIT Technology (ESPIRIT) Flight Loads Recorder; and 3) NOVATECH Corporation (NOVATECH) 16-Channel recorder.

INSTRUMENTATION

The testbed airplane, a Cessna 172P, has three separate flight loads recorder systems installed. One is the baseline system, and it records both the applied loads (strains) and their induced aircraft motions (accelerations). It is the analysis of these data that will provide the necessary information, i.e., correlation between loads and measured accelerations, to test and certify any "non-intrusive" flight loads/aircraft usage monitoring systems. The other installed systems records only aircraft accelerations, and one of them will be installed on 6-8 fleet airplanes.

System 1. The baseline system is a NOVATECH TSR-16 Airborne Data Recorder (Figure 1). This unit is a 16-channel recorder system that has a built-in clock to provide time-tag of data. Data storage is provided by Storage and Transport Module (STM) available in standard 16 Kbytes (Model M-2M) memory module or optional 32 Kbytes (Model M-4M) memory module. Dimensions of the TSR-16 are 12.62" x 4.88" x 7.62" and weighs 9.5 lbs. STM is 4.17" x 1.31" x 3.69" and weighs 6.5 oz. While the complete unit requires an external power source to operate, internal batteries maintain

data in the STM and system setup information in the TSR-16. This recorder is configured to measure:

- 1) a_y , y-axis acceleration near aircraft CG
- 2) a_z , z-axis acceleration near aircraft CG
- 3) a_y , y-axis acceleration in aircraft tailcone
- 4) a_z , z-axis acceleration in aircraft tailcone
- 5) axial strain in right wing forward upper spar cap near wing strut attachment point
- 6) axial strain in right wing forward lower spar cap near wing strut attachment point
- 7) axial strain in left horizontal stabilizer forward upper spar cap near stabilizer root section
- 8) axial strain in left horizontal stabilizer forward lower spar cap near stabilizer root section
- 9) tangential strain around left-half of the centerline lightening hole in horizontal stabilizer forward spar web
- 10) tangential strain around right-half of the centerline lightening hole in horizontal stabilizer forward spar web
- 11) axial strain in vertical fin forward left spar cap near fin root section
- 12) axial strain in vertical fin forward right spar cap near fin root section
- 13) dynamic pressure (airspeed)
- 14) static pressure (pressure altitude)
- 15) angle-of-attack
- 16) sideslip

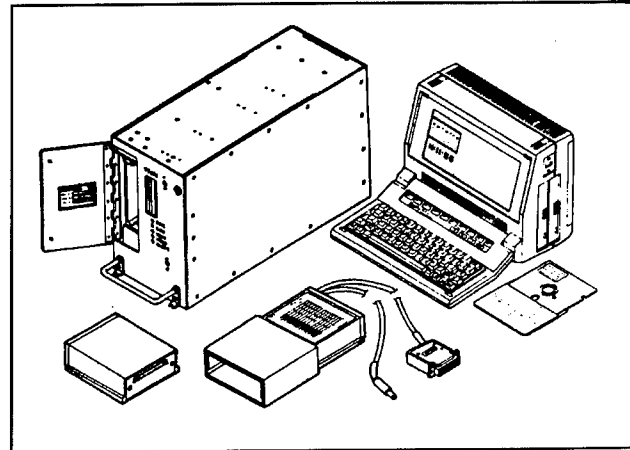


Figure 1

System 2. The SEI Flight Loads Recorder (Figure 2) is an inexpensive lightweight system developed under the FAATC SBIR (Small Business Innovative Research) Program and is designed to record up to 8 parameters for 400-500 flight hours. It contains an internal accelerometer and up to 7 input channels that can be connected to accelerometers, strain gauges, pressures transducers, etc. Its dimensions are 6" x 4" x 3.25" and weighs approximately 4.5 lbs. The data sampling rate is 32 Hz with 32 Kbytes of memory. This recorder is configured to measure:

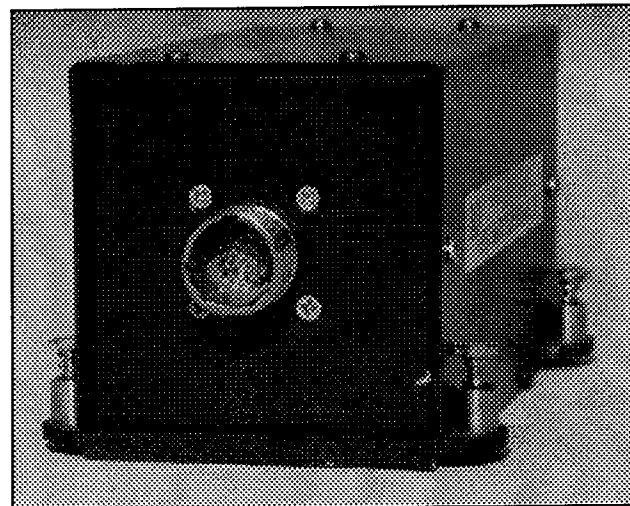


Figure 2

- 1) a_z , z-axis acceleration near aircraft CG
- 2) a_y , y-axis acceleration in aircraft tailcone
- 3) a_z , z-axis acceleration in aircraft tailcone
- 4) dynamic pressure (airspeed)
- 5) static pressure (pressure altitude)

System 3. The ESPIRIT Flight Loads Data Recorder (FLDR) (Figure 3) was developed under the Naval Air Warfare Center SBIR Program and is designed for Load/Environment Spectrum Surveys (LESS) and Individual Aircraft Tracking (IAT) based on MIL-STD-1530A. The miniature battery-operated 8-bit recorder uses Load Assessment and Profile System (ELAPS) I microprocessor FLDR and accepts up to four external signals such as strain gauges, pressure transducers, and accelerometers. It also contains an internal accelerometer that can be used as input to the first channel. The dimensions of a functional unit are 5" x 2.25" x 1.5" and weighs approximately 14 oz. The battery life is estimated at 100 hours of data recording or 1 month of idle-time. In two channel mode, each channel has a bandwidth of 2.5 to 20 Hz with a data memory of 2K x 8 static Random Access Memory (RAM). This recorder is instrumented to measure:

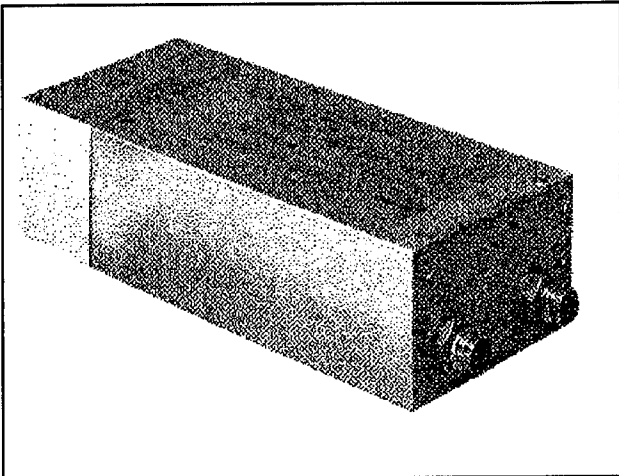


Figure 3

- 1) a_z , z-axis acceleration near aircraft CG
- 2) a_y , y-axis acceleration in aircraft tailcone
- 3) dynamic pressure (airspeed)
- 4) static pressure (pressure altitude)

CERTIFICATION

In order to consider deviations from FAA approved structural inspection intervals, the flight loads recorder system must meet certification requirements such as accuracy of measured data and system reliability. In addition, in order for this program to be successful, the system certified must be flexible enough to be adaptable to different aircraft models with ease. Finally, the system must be self-powered, operate independently, and not interfere with any existing on-board avionic systems.

SCHEDULE.

ID	Name	1993	1994	1995	1996	1997
1	Develop alternative strain and (or) accelerometer load monitoring system					
2	Install/evaluate systems on a testbed airplane					
3	Certify systems for fleet service use					
4	Install systems in 6-8 Embry-Riddle airplanes					
5	Collect usage data for 12 Months					
6	Process usage data					
7	Report on individual airplane loads usage monitoring					

REFERENCES

(1) DOT-FAA-92/20, "Statistical Analysis of Fatigue Load Spectra Determined from the NASA VGH General Aviation Data Base," December, 1992.

(2) FAA Report No. AFS-120-73-2, "Fatigue Evaluation of Wing and Associated Structure on Small Airplanes," May, 1973.

(3) Advisory Circular AC 23-13, "Fatigue and Fail-Safe Evaluation of Flight Structure and Pressurized Cabin for Part 23 Airplanes," April, 1993.

(4) DOT/FAA/CT-TN93/23, "Design, Manufacture, and Test of a Flight Load Recorder for Small Aircraft," February, 1994.

THE DEVELOPMENT OF A REGIONAL/COMMUTER AIRLINE FLIGHT USAGE DATABASE TO SUPPORT A STRUCTURAL INTEGRITY MANAGEMENT PROGRAM

F. Joseph Giessler*, Alan P. Berens, and Joseph P. Gallagher
The University of Dayton Research Institute
Dayton, Ohio 45469-0120

The University of Dayton is conducting research on the structural integrity requirements for the commercial regional/commuter airline fleet. The ultimate objective of this research is to provide information which will enable the Federal Aviation Administration (FAA) to better understand and control those factors that influence the structural integrity of commercial commuter aircraft. The information being gathered covers the design, development, certification, and life management of the aircraft structure. The interdisciplinary relationships between technical areas such as design, testing, analysis, manufacturing, quality assurance, inspection, and maintenance for structural integrity are being considered.

The University of Dayton is accomplishing this research effort in three one-year phases. The first year effort, reported in this paper, has been devoted to the collection and analysis of data which will better define the service-related factors that affect the expected operational life of commercial aircraft fleets. It has included visits to the various manufacturing and operating organizations which currently comprise the small transport and commuter aircraft community. It will also include an evaluation of the methods currently being used by industry to comply with the aircraft structural integrity requirements established by the Department of Defense and the FAA. During the second phase (the second year), the University of Dayton will study usage data processing methods for various types of structural integrity programs that meet the FAA and industry's needs for evaluating the structural integrity of operational airframes. Current data collection programs being initiated by the FAA will be reviewed. Here we will focus on determining how the data must be processed to make it applicable for structural integrity monitoring, and propose to develop a prototype system to demonstrate feasibility. In the third phase (the third year), the University of Dayton's engineers will concentrate on evaluating the applicability of a comprehensive structural integrity methodology for monitoring the structural health of a fleet of commercial commuter aircraft. The third phase will also include the transfer of the technical database activities from the University of Dayton to the FAA Technical Center.

THE AIRCRAFT STRUCTURAL INTEGRITY PROBLEM

This section presents an overview of the problem of guaranteeing aircraft structural integrity. The problem is defined and the key elements during the life cycle of an aircraft system are identified. The objectives of an aircraft structural integrity program are identified and a general approach to developing such a program for commuter aircraft is outlined.

STATEMENT OF THE PROBLEM

Structural integrity of an airframe is achieved when no critical component of the airframe fails during its operational life. Critical components can be structurally significant or maintenance critical items. A structurally significant item (SSI) is a detail, element, or assembly whose failure would result in a direct adverse effect on operating safety. A maintenance critical item is a detail, element, or assembly whose

*AIAA Member

failure could have significant operational, maintenance, or cost impact. These definitions focus attention on the identification of the critical components and all factors which can lead to their failure.

The critical components of an airframe are determined by considering the failure consequences of each component. This process is largely guided by experience and is dependent on the specific design. Since the design process is iterative and experience is not available for innovative design concepts, the critical components list must be evaluated throughout the design period.

Next consider the avoidance of failure. The strength of a detail is a quantity that can only be defined in a statistical sense and which reduces under the application of stress cycles greater than a fatigue threshold. For example, let $f(x, \mu_T, \sigma_T)$ represent the probability density of strength in a population of structural details, where μ_T and σ_T are measures of the central tendency and scatter of the strength of the population at T flight hours. Since stresses greater than the fatigue threshold cause damage to initiate and grow, μ_T is a decreasing function of flight hours. Further, σ_T may well increase due to differences in detail response to applied stress or to the usage experienced by different aircraft. Failure occurs when an applied stress exceeds the strength of a detail. Let $g(y)$ represent the probability density of applied stresses that the population of structural details will experience in a flight. It is reasonable to assume the statistical independence of the strength and stress distributions. Then, at T flight hours, the probability of failure, $P(F)$, is given by

$$P(F) = \int_{-\infty}^{\infty} \left[\int_x^{\infty} g(y) dy \right] f(x, \mu_T, \sigma_T) dx \quad (1)$$

The degradation of strength due to fatigue and increasing chances of failure are illustrated in Figure 1 in which the failure probability is a function of the area of the overlapping probability distributions. Figure 1 illustrates that fatigue damage is not a static situation with regard to the residual strength. As the damage grows in the structure, the strength curve moves to the left which increases the probability of failure. By taking appropriate actions of inspection and restoration (repair), the strength curve is moved back to its initial position. To avoid failures, conservative design practices are adopted or structural details are maintained (inspected, repaired or replaced) at conservative estimates of failure times.

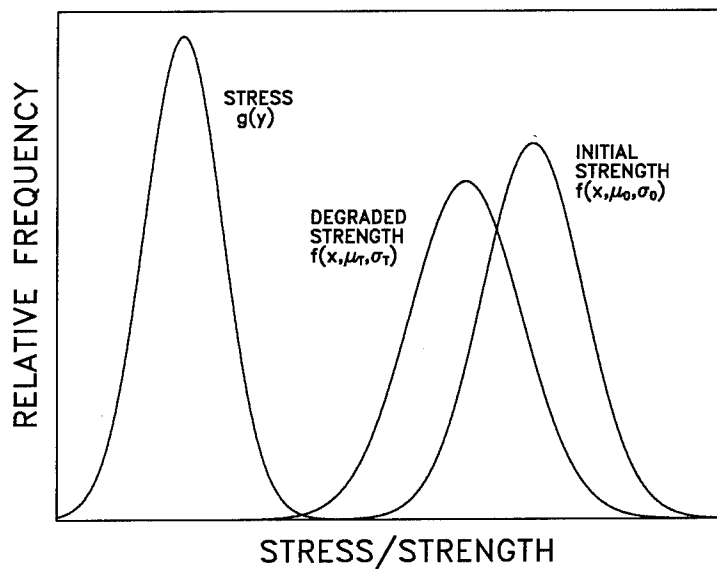


FIGURE 1. PROBABILITY OF FAILURE CALCULATION.

Conceptually, an airframe could be designed such that all expected stresses would be below the fatigue damage limit. This degree of conservativeness would, however, have an inordinately adverse affect on performance. Therefore in aircraft applications, trade-offs are necessary between the degree of conservativeness (stress levels) in structural design and the performance required by the intended mission of the aircraft system. This trade-off forces the designer to accommodate stresses in the fatigue life limiting range, that will limit the service life of the structure which in turn focuses attention on anticipated external loads (predicted usage), predicted internal loads and stresses, and the material selection and detail design of all critical components.

Given perfect knowledge of the critical components and the internal loads and stresses to be encountered, it is theoretically possible to design an airframe such that there would be a rational trade-off between performance and the probability of a failure in the fleet of aircraft. If each such airframe was fabricated exactly according to design specifications and if the actual operational usage matched the design usage, no structural integrity problems would occur during the life of the structure. However, as far as is known, at least some of these assumptions have been violated for every aircraft system designed to date.

In a survey of structural problems associated with military service operations (Reference 1), it was discovered that most common structural problems are due to corrosion and cracking at fastener holes. The primary causes of corrosion were due to improper protection procedures and stress corrosion. The primary cause of cracking at fastener holes was identified as operating stresses higher than anticipated as a result of improper loads estimates, improper design, and aircraft usage more severe than anticipated. However, poor selection of material as well as manufacturing and maintenance errors were also isolated as sources of problems. Eighty (80) percent of the structural failures that occurred during ground tests were caused by deficiencies in stress analysis and detail design.

Structural integrity problems occur despite our best efforts during design and manufacture. Therefore, a cohesive plan is needed to economically maximize the chances for avoiding or eliminating structural failures. Frequently, the plan incorporates the need to periodically inspect the structure to ensure that any cracks present in critical locations are identified and repaired. This approach is illustrated in Figure 2, where an inspection returns the structure to a safe level of residual strength.

OBJECTIVES OF AN INTEGRITY PROGRAM

An aircraft structural integrity program is a unique set of specifications and actions whose objective is the economical avoidance of structural problems during the life of a fleet of aircraft. There are two major aspects of this objective. From the viewpoint of safety, the plan must prevent failures by ensuring that the residual strength of each structurally significant item (SSI) is sufficiently great throughout the life of the structure. From the viewpoint of economics, the plan must (a) minimize maintenance costs either through avoidance or optimal scheduling and (b) maximize the life of each individual airframe (or major component). The objectives of these viewpoints are distinct but complimentary.

Structural failure results when damage is initiated and grows to a size that reduces the strength to the applied stress. Failures can be avoided by preventing damage from initiating or by detecting and repairing it before the damage grows to a potentially critical size. Every attempt is made during design and manufacturing to ensure that damage will not initiate due to fatigue.

However, this process fails on occasion and damage can be initiated due to accidental causes or inappropriate controls. Therefore, there is a possibility of damage being present in SSIs and the structural integrity program must account for this possibility. The current approach is through the choice of damage tolerant materials and the use of inspections at intervals based on projected damage growth.

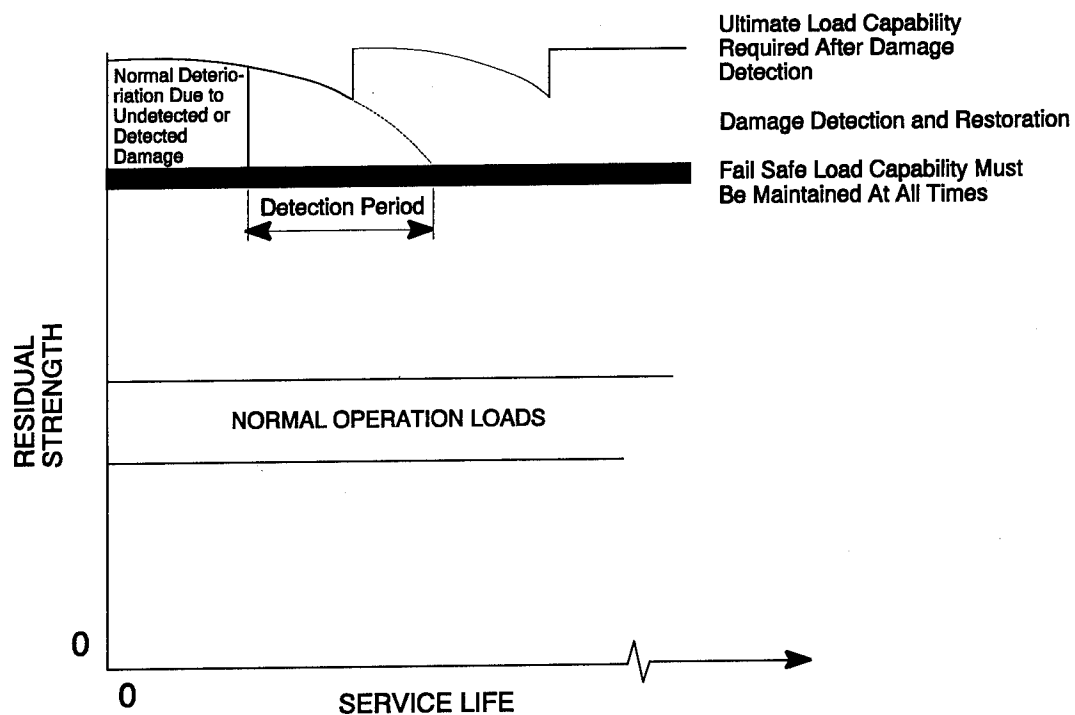


FIGURE 2. STRENGTH CRITERIA FOR PERIODICALLY INSPECTED DAMAGE TOLERANT STRUCTURE.

The economic aspect is dominated by the concept of proper design and manufacturing to avoid the potential for any fatigue crack initiation. When cracks do initiate in service, the maintenance actions must be scheduled to minimize both costs of repair and the risk of failure. The economic aspect of structural integrity also requires monitoring individual aircraft usage so that maintenance and structural retirement can be based on a measure of severity of usage rather than based on a fleet wide average.

GENERAL APPROACH

As noted earlier, structural integrity is best achieved through proper design and manufacturing. It was also noted, however, that structural integrity considerations also are present throughout the operational life of the fleet. Figure 3 (Reference 2) presents a schematic of the relationship between major elements of an aircraft structural integrity program as separated by the major functions of design, manufacturing, and operational use.

The design criteria are derived from the planned missions of an aircraft system and summarize the intended use in terms of parameters which can be used to evaluate the strength, rigidity, and fatigue resistance in the usage environment. In general, the criteria are based on mission analyses, historical data, or load spectra from operations with analogous performance characteristics and missions. A current key problem is the anticipation of the loads which result from control system innovations or from new structural concepts.

Given the design criteria, the design process consists of the joint, iterative considerations of material selection, prediction of external loads, detail design and prediction of internal loads and stresses for all critical locations. Structural integrity is evaluated on the basis of available material properties data or new test data obtained for specific materials, environments, or configurations of interest. Since damage toler-

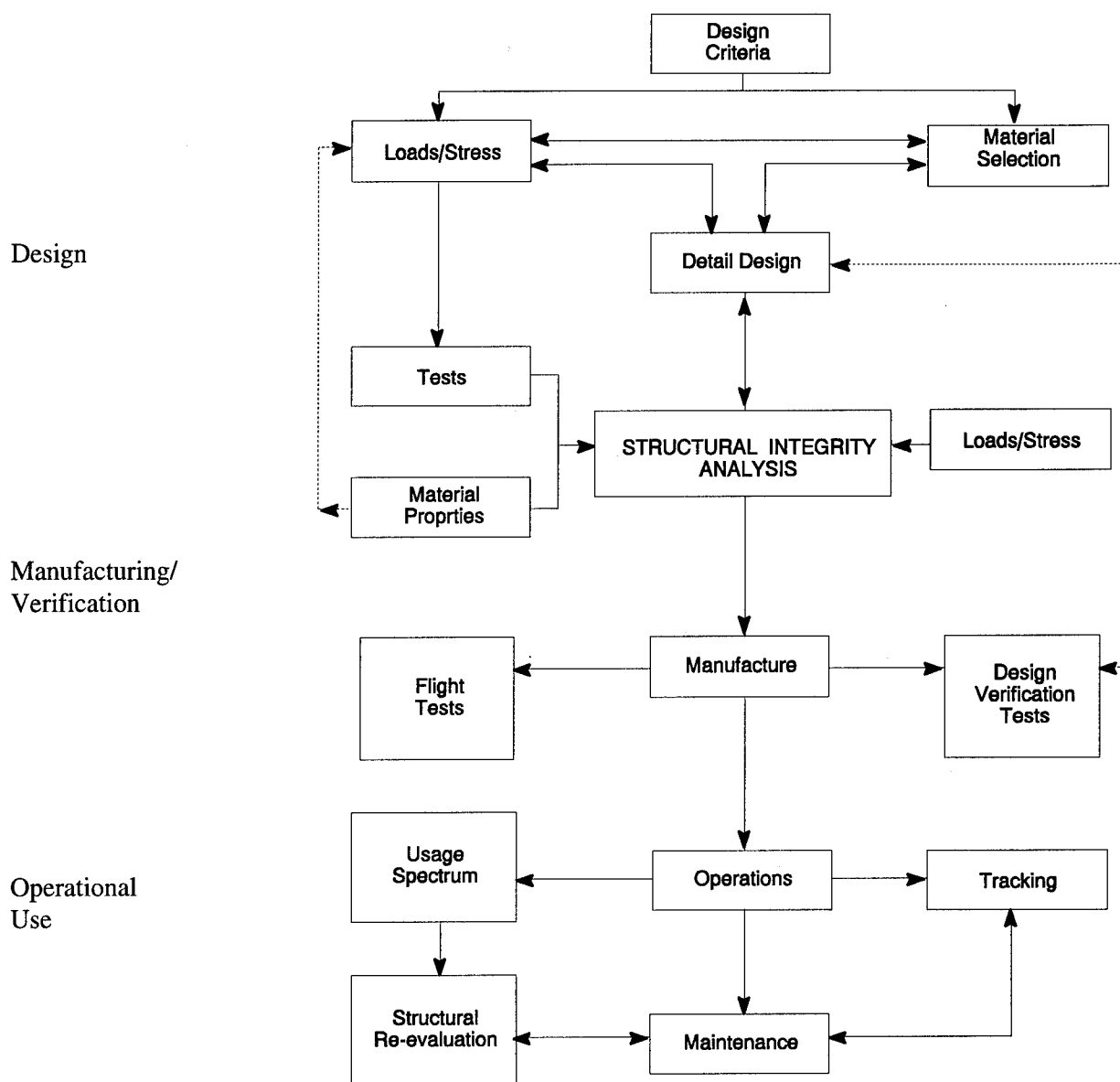


FIGURE 3. MAJOR TASKS SUPPORTING A COMMERCIAL AIRCRAFT STRUCTURAL INTEGRITY PROGRAM, TIME-PHASED ACCORDING TO THE THREE PHASES OF AIRCRAFT DESIGN, MANUFACTURE, AND OPERATION.

ance analyses are based on the growth of the potential damage that exists in a structure at the start of a usage period, the quality control capability of the manufacture and maintenance processes must be quantified as input for this analysis. For example, if the integrity is based on a damage tolerance analysis, the quality control capability of the manufacture and maintenance process must be quantified as input to this analysis.

The manufacturing process includes the procurement of raw materials and the fabrication and assembly of the structural items. The manufacturing process also includes the quality control systems which ensure that the raw materials meet procurement specifications and that fabrication and assembly meet design specifications.

Two extremely important steps in the structural integrity process are (a) the flight tests which verify the loads and stress analyses and (b) the design verification tests which verify the structural integrity based on the design spectra. These sets of tests are performed as early as possible in the life cycle to permit design changes, if necessary. This possibility is indicated by the dotted lines in Figure 3.

During the operational usage phase, the structural integrity program requires the verification of design usage and provides a database for scheduling maintenance actions. The operational load spectra are compared with the design spectra to see if significant differences are present. Such differences could impact maintenance schedules or necessitate redesign. If usage spectra vary significantly between aircraft, a tracking program provides the data for scheduling maintenance actions based on usage severity. In continuing operations, feedback is required from the maintenance actions to update the tracking database. Structural re-evaluations can be initiated as a result of unexpected failures or cracking problems detected during service or as a result of mission changes/life extension requirements. Structural re-evaluations may result in redesign and a development of a new structural integrity plan for that structurally significant item (SSI). Reference 3 contains a description of methods which are available to be applied to, this operational usage phase of the structural integrity plan.

STRUCTURAL INTEGRITY PROGRAM FRAMEWORK

The structural integrity process comprises a series of actions that are taken to ensure against premature failure and uneconomical maintenance during the life of a structural detail. The major areas of a structural integrity program as outlined in Figure 3 have been codified into six generic tasks which are given in Table 1 (Reference 4).

TABLE 1. THE GENERIC TASKS OF A STRUCTURAL INTEGRITY PROGRAM

NO.	GENERIC INTEGRITY TASK
I	DESIGN INFORMATION
II	DESIGN ANALYSIS AND DEVELOPMENT TESTS
III	COMPONENT TESTS
IV	FULL SCALE TESTS
V	INTEGRITY MANAGEMENT DATA PACKAGE
VI	INTEGRITY MANAGEMENT

These six generic tasks provide a time phasing to the integrity process and can be achieved through the performance of following seven process steps:

- (1) Identify the critical details and failure modes.
- (2) Define the design environment in terms of the stressing parameters.
- (3) Demonstrate that the detail meets the life and durability requirements through analysis (redesign, if necessary).
- (4) Demonstrate or verify that the detail meets the life and durability requirements through tests (redesign, if necessary).
- (5) Verify that actual usage environment is equivalent to the design environment (reevaluate life and durability if necessary).

- (6) Establish a maintenance plan for the detail based on a selected measure of use (i.e., hours, flights, a tracking parameter).
- (7) Establish and maintain an information system for tracking and maintenance feedback.

Table 2 (Reference 4) defines the generic tasks during which the process steps are implemented.

TABLE 2. GENERIC INTEGRITY PROCESS TASKS IN WHICH INTEGRITY PROCESS STEPS ARE IMPLEMENTED

INTEGRITY PROCESS STEPS	GENERIC INTEGRITY PROCESS TASKS					
	I	II	III	IV	V	VI
Criticals Details/Failures Modes	●					
Design Environment	●					
Life Analysis		●			●	
Life Verification			●	●		
Usage Environment					●	●
Maintenance Plan					●	●
Information System					●	●

Engineering input and tools must be available to perform these steps for any particular application of the integrity process. The input and tools required are specific to the application and can include data, analysis methods, test methods, information systems, and correlating parameters as well as the hardware necessary for taking diagnostic measurements, recording data and making inspections. While not all such tools can be listed for all applications of the integrity process, a general set was defined to aid the identification of potential gaps in the process for specific applications and the objectives of recommended programs. The twelve categories of input and tools and their descriptions are as follows:

- (1) Design Usage - A description of the expected usage environment in terms of factors which influence the integrity of the structure during its life.
- (2) Design Criteria - A description of the integrity requirements which must be met by the structure throughout its life.
- (3) Critical Details/Failure Modes - The isolation of the structural details which drive integrity and the modes or failures of these details.
- (4) Damage/Life Analysis - A model for predicting life or damage accumulation during operational usage.
- (5) Damage/Life Verification - Tests based on the environmental descriptions which are designed to verify life or damage accumulation requirements and predictions.
- (6) Environmental Parameters - The definition of the environmental parameters which must be monitored to define operational usage for comparison with design usage or damage/life evaluations.
- (7) Environmental Monitoring System - The establishment of the data collection and processing system for monitoring the operational usage environment.
- (8) Tracking Parameters - The definition of the parameters which must be monitored to track usage severity of individual aircraft.
- (9) Tracking System - The establishment of the data collection, processing, and analysis system for tracking usage severity of individual aircraft.

- (10) Maintenance Diagnostics - The correlation of indirect parameter measurements with damage accumulation in individual details.
- (11) Non-Destructive Evaluation (NDE) - Methods for inspection for damage in the critical details.
- (12) Design Feedback - The development of a system for ensuring field failure experience is maintained and used as input to the design of future systems.

The correlation of the generalized set of structural integrity inputs and tools with the integrity process steps is presented in Table 3 (Reference 4).

REVIEW OF CURRENT METHODS AND DATA

The University of Dayton is conducting an assessment of existing approaches to integrity management which are being used by industry to ensure the safe operational life of commuter aircraft. Integrity management covers those activities controlled by Tasks V and VI of the structural integrity program (See Table 1).

This review activity is being conducted in two tasks, Task 1 constitutes a review of the structural integrity process and procedures that are directed at integrity management, and Task 2 explores the feasibility for using a broader collection of methods and procedures that could improve operator confidence in the manner with which commuter aircraft are safely used, maintained, and retired.

TASK I - REVIEW OF THE CURRENT STATE-OF-THE-ART

Ideally, the structural integrity for each aircraft in a fleet would be achieved through proper design and manufacturing. The objective is to design a structure which can withstand the peak design loads as well as to resist strength degradation resulting from cyclic loading and the operational environment. This objective has never been totally met for a variety of reasons which include the use of non-conservative design stress spectra, inadequate detail design, manufacturing errors, accidental damage, mission modification, and extensions of the time that the aircraft will spend in service. Since structural integrity cannot be ensured only on the basis of care in design and manufacture, a long-term plan for continued surveillance and maintenance of each airframe is established to ensure safety and economic repair if needed. The maintenance actions include inspections and replacement of structurally significant details and repairs of environmentally and accidentally induced damage.

To obtain information on current methods visits have been made to Fairchild, Beech, Cessna, and Learjet.

TASK 2 - ANALYSIS OF EXISTING METHODS AND INPUT DATA

During this task, which is currently underway, the University of Dayton is determining the feasibility of using the information currently available as input to an integrity management database and is evaluating the methods and tools available for ensuring the continuing structural integrity of commuter aircraft during the operational phase. The methods and tools will also

TABLE 3. APPLICATIONS OF INPUT AND TOOLS TO INTEGRITY PROCESS STEPS

INPUT AND TOOLS	INTEGRITY PROCESS STEPS						
	Critical Details/Failure Modes	Design Environment	Life Analysis	Life Verification	Usage Environment	Maintenance Plan	Information System
Design Usage		•	•	•	•	•	
Design Criteria		•					
Critical Details/Failure Modes	•						
Damage/Life Analysis			•		•	•	
Damage/Life Tests				•			
Environmental Parameters					•		•
Environmental Monitoring System					•		•
Tracking Parameters						•	•
Tracking System						•	•
Maintenance Diagnostics						•	
NDE						•	
Design Feedback	•	•					•

include those used by various Department of Defense agencies to manage the structural integrity of their operational fleets.

The concept of determining feasibility rests upon the development of requirements against which feasibility can be determined. In this case, these are the steps in the integrity process as listed in Table 2, and have been outlined in Figure 3. Secondary requirements or constraints which must also be considered take the form of current availability of personnel, technical resources, and economic resources.

Determining feasibility must also be a function of the ability of the data and the tools to establish and maintain an acceptable level of structural integrity. As was discussed in the early problem statement, the relation between strength and stress must be maintained at the desired level. Thus, a requirement for feasibility is that those inputs and tools for stress determination do not allow stress to be underestimated, and that the input and tools for the determination of strength do not allow strength to be overestimated.

The evaluation of the various approaches requires sample computations to be made with representative data. These data, both in regard to stress histories and structural details, are being derived from prior experience of both the FAA and the University. These preliminary data will be selected to be appropriate to the small transport type of aircraft. Flight loads data for commercial aircraft will also be available from other FAA programs. These data will provide us with an opportunity to evaluate alternate schemes for processing and presenting usage information in a form useful to commercial aircraft integrity managers.

While the commuter aircraft manufacturers are familiar with damage tolerance philosophies, their design methodologies have traditionally focused on the application of fail safe concepts and on safe (crack initiation) life analyses. Combining these traditional methodologies with elements of the safe crack growth life methodology could provide integrity managers with additional capability for evaluating the effects of operational usage on both the individual aircraft and the fleet. This combination is suggested in Figure 4 which presents the crack initiation and crack growth life behavior associated with a given structural detail.

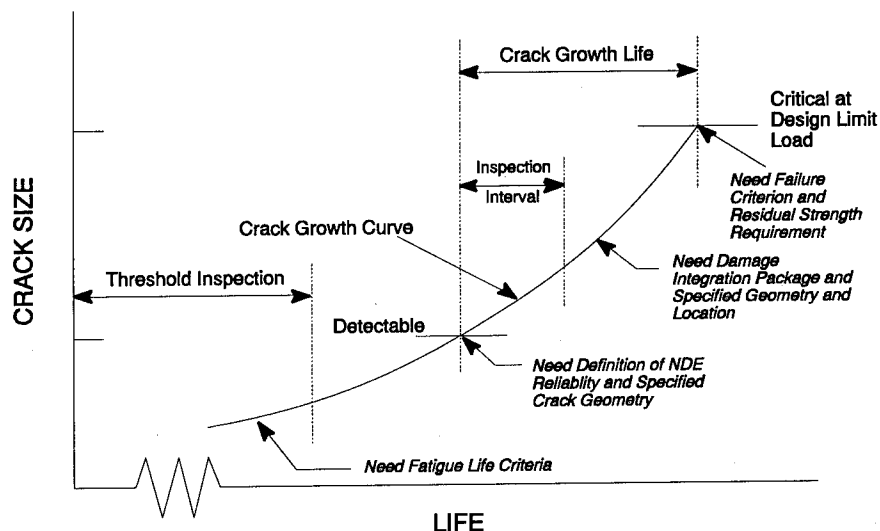


FIGURE 4. RELATIONSHIP BETWEEN CRACK LENGTH AND LIFE EXPENDED SHOWING A MONOTONIC INCREASE IN CRACK LENGTH UP UNTIL FAILURE. (Shown are the various technology and specification requirements needed to define the crack growth curve which, in turn, establishes the life limit.)

Also included in the assessment is a summary of the input and tool descriptions when a combination initiation/growth model is used as the basis for a structural integrity evaluation, and subsequent inspection requirements. Note that the behavior in Figure 4 presumes a specific type of operational usage. If one changes the operational usage, then the life curve will shift.

EVALUATION OF USAGE INFORMATION FOR INTEGRITY MANAGEMENT

The development and maintenance of technical databases are necessary to conduct a structural integrity program. These databases include such information as recorded flight data, pertinent aircraft information, descriptions of the structural integrity process being used by each aircraft, and any feedback information obtained as the result of inspections and maintenance actions. The form of the data storage must be such as to provide for quick and efficient retrieval and presentation.

Task 3 will continue the evaluation and assessment of the methodologies that could be used to improve the process for managing the structural integrity for a fleet of commuter aircraft. Specifically, it will focus on developing an appropriate set of methods for processing usage data. Task 4 will include the identification of the contents and the organizational structure for, a technical database which could provide the basis for integrity monitoring.

TASK 3 - USAGE DATA PROCESSING METHODS

The purpose of this task is to focus on the processing of usage information so that a technical database can be constructed to meet the needs of the user community. The FAA has an on-going program of flight data records development and data recording and processing of data from large transports (Reference 5). Presentation and storage formats are being developed to fit the end use of these data. The parallel efforts to develop similar capabilities for the regional/commuter aircraft will include many of the characteristics of the large aircraft. However, the methods, inputs, and tools which are identified in the earlier efforts for commuter/regional aircraft, may indicate that some differences in the details of recording and data processing will be necessary.

The necessity of developing a method of accounting for the empennage loading history will influence the data to be recorded. Although the normal acceleration is a good indicator of wing and forward fuselage loading, it does not correlate well with empennage loads and the resulting aft fuselage loads. It is usually necessary to add lateral acceleration and roll and yaw rates and accelerations in order to adequately characterize the empennage and aft fuselage (Reference 6).

The ultimate purpose of an operational usage database is to provide usage data to users and manufacturers so they can evaluate current life expended (or damage accrued) and can apply the data as representative usage for the design of new aircraft. This implies the conversion of these data into stress histories. These histories typically consist of stress cycle endpoints or peaks and valleys. Sufficient data must be saved to allow this computation. These data must also be maintained in a form to allow the creation of a statistically valid representation of the stresses. That means identifying those parameters whose individual peak and valley variation is representative of the peak and valley variation of the desired stress. However, since stress is not the result of a single parameter, the other related parameters must be kept in a fashion that allows their correct combination statistically (Reference 7). Thus, joint-probability tables must be retained. It will be the purpose and goal of this task to identify these storage requirements for the various parameters.

While the computation of stress histories is important, the ability to review the various parameter variations with respect to specified operating conditions is also important. Thus, the database will also contain a set of presentation programs to provide for tabular and graphical presentations. Tabular presentations are typically bi-variate and tri-variate which show how a selected parameter varies as one or two other related parameters vary. There is usually a distribution of values of the primary parameter in each cell of the secondary parameters. Graphical presentations are usually in the form of histograms and exceedance plots. The histograms show percentages of time in ranges of the time dependent parameters, such as airspeed and altitude, and the exceedance plots show the cumulative occurrences of the peaking parameters such as accelerations. The form of these outputs for review will be selected to best convey the information. While tables and plots of the data are important aspects of the presentation, the conversations with the manufacturers in Task 1 emphasized that the data formats should also allow the formation of flight profiles. Such profiles should consist of the representative histories of airspeed, altitude, gross weight, and the corresponding occurrences of the normal acceleration peaks and valleys. The data storage formats will be developed to allow the construction of such profiles. It is important that time be retained in the storage records to allow the profile formations. It is noted that these presentation formats are not usually the storage formats. The storage formats must be such that additional data can be incorporated easily and take a multi-dimensional matrix form.

TASK 4 - STRUCTURAL USAGE MONITORING DATABASE

Using the results of Task 3 evaluation and analysis, a usage database which has the flexibility to store the types of usage data collected on both large and small commercial/commuter aircraft will be developed. Experience has shown that such a database can be handled with many types of shell structures, but that a relational type is usually the best, since it allows for more efficient input and output, and for the easy modification of presentation data and formats. A detailed plan will be prepared to outline the data requirements and the processing methods that are proposed for the storage and presentation of usage data. Also presented will be the types of reports that a user could obtain from the database. Upon approval of the plan, the feasibility and utility for such a database will be demonstrated by storing existing commuter aircraft type data and using the database to create reports which could be used to support structural integrity monitoring of operational aircraft fleets.

INTEGRITY MANAGEMENT METHODOLOGY

Task 5 comprises the preparation of a plan which can be used to implement an operational integrity management database which would contain all the information that would be needed to safely use, maintain, and retire commuter aircraft. Task 6 is concerned with the transfer of the usage monitoring technical database to the FAA.

TASK 5 - PLAN FOR AN INTEGRITY MANAGEMENT DATABASE

Using the results of Tasks I through 4, a plan will be prepared that can be used to create an operational Integrity Management Database for monitoring the structural integrity status of operational aircraft fleets. This document will outline the activities which are to be accomplished during the life of any aircraft coming under this plan. The database will be described with an explanation of how the data are to be used. The tools selected for use in verifying and maintaining the aircraft structural integrity will be described.

TASK 6 - UPDATE AND TRANSFER DATABASE TO FAA

By the time the program reaches this task, several years of data will have been collected using both the large aircraft system and the prototype small aircraft system. These data will have been inserted into the structural usage database and this initial collection of data will be ready for transfer to the FAA Technical Center.

LIST OF REFERENCES

1. Whitman, B., Jr., "Development of an Updated Design Philosophy for U.S. Navy Metallic Structure, Contract N00019-81-C-0191, Phase II: Review of Data," Report Nav-DP-02, Naval Air Systems Command, Washington, D.C., January 1982.
2. Berens, A. P., et al., "Development of a Structural and Safety and Life Management System for Naval Aircraft," UDR-TR-85-23, University of Dayton Research Institute, Dayton, Ohio, February 1985.
3. Berens, A. P., et al., "Handbook of Force Management Methods," AFWAL-TR-81-3079, Air Force Wright Aeronautical Laboratories, Wright-Patterson Air Force Base, Ohio, April 19, 1981.
4. Berens, A.P., et al., "A Proposed Roadmap for Improving Component Reliability," WL-TR-91-3053, Flight Dynamic Directorate, Wright Laboratory, Wright Patterson Air Force Base, Ohio, May 1991.
5. Barnes, T., and T. DeFiore, "The New FAA Flight Loads Monitoring Program," AIAA 91-0258, 29th Aerospace Sciences Meeting, January 7-10, 1991.
6. "Fatigue Evaluation of Empennage, Forward Wing and Winglets/Tip Fins on Part 23 Airplanes," FAA Report No. ANM-105N-88-63D,
7. Mayer, John P. et al., "Notes on a Large Scale Statistical Program for the Establishment of Maneuver Loads Design Criteria for Military Aircraft," NACA RM L57E30, July 1957.

LIFE CYCLE DESIGN OF FUTURE GENERAL AVIATION AIRPLANES

J. G. Ladesic

Embry-Riddle Aeronautical University

600 S. Clyde Morris Bl.

Daytona Beach, Florida

ABSTRACT

Single engine piston-powered airplanes have been the main stay of the General Aviation flight training fleet for the past ninety years. The average age of these airplanes in the U.S. has now reached 28 years and the production of new replacement aircraft has nearly ceased. Significant changes in Federal Airworthiness Regulations have occurred since the majority of these designs flying were certified. In order for future airplanes to be successful a substantially greater engineering expertise and manufacturing base, along with a considerable amount of test data that do not presently exist, will be required. Design methods and tools must be developed for application to future General Aviation designs in order to yield safe, cost effective airplanes and to reduce the business risk presently associated with aircraft product liability. A review of present airworthiness regulations and their impact on future is made and applied to developing such a tool. A review of the available safe-life design literature is given and a simple method for first-pass safe life design sizing is offered. Recommendations for future fatigue life-related product development testing are made. It is suggested that improved vehicle safety through the application of modern technology could substantially reduce liability risks.

INTRODUCTION

The recent changes in airworthiness regulations which require the fatigue assessment of critical structures will challenge future GA aircraft designers in producing cost effective airplanes. Very few in-service or laboratory test data are available for use in the design of new General Aviation (GA) vehicles and practically no information exists regarding design methodology that applies to typical light GA aircraft structures. Little is known about the accumulation of cyclic stress related damage or about the determination of multiple site damage areas for these airplanes. In order for the next generation designs of GA-Primary Flight Trainers (PFTs) to be successful a much greater expertise and a considerable amount of test data will be needed. Similarly, very little guidance is presently available regarding methods required for applying the limited amount of spectral data that does exist to the design of new airplane configurations, especially as it would apply in the early stages of the design activity. Likewise there is

no methodology for integrating such dynamic environmental data into the conceptual detail design activities. Most of what does exist is in a form best suited for analysis applications to fully developed airplane structures (1, 2, 3) that are fully documented and tested vehicles. An attempt to use these at the conceptual design point presently requires somehow establishing a baseline design then employing a trial and error approach to obtain a solution that would comply with the desired mission requirements. The number of iterations needed could be substantially reduced if the "first guess" made for the principal structural elements, like the wing structure, represented a closer estimate of what would actually be needed. A good "first guess" could possibly be made by design engineers who have had extensive experience in cyclic life design of such elements but, in the case of the light GA-PFT aircraft design, such engineering expertise is nearly non-existent.

The view points and recommendations presented in this paper are directed toward creating a logical approach to conceptual detail design that would lead to a reasonable safe life estimate of airplane principal structural elements for new, FAR23-type, aircraft designs used in commercial applications. Small, light, single engine GA airplanes, often used commercially as flight trainers, are of significant interest. Such aircraft, certified under CAR3 (4) have also served as part of this nation's fleet of commuters and air taxis as well as thousands of privately owned and operated sport aircraft. Many of these aircraft are still actively used as part of the national transportation system commuter fleet (5). The airplanes flown by many commuters and air taxis were designed and type certified as long as thirty ago, well before many of the fatigue and safety requirements were installed in the current revision of FAR Part 23. Such designs developed by consideration of static strength at limit load and at ultimate load include structural redundancies and have yielded aircraft which display safe life as well as fail safe potential even though they were not developed with such considerations in mind. At the "Third International Conference on Aging Aircraft and Structural Airworthiness", held Washington D.C. November 19-21 1991, Mr. William Keil of the Regional Airlines Association addressed the role that the commuter fleet plays in the U.S. air transportation system. He made an appeal for support regarding research and development into fleet safety with respect to the aging problem. Mr. Keil pointed out that the small commuters often bear the same logos, very often fly a similar number of missions and carry nearly the same number of passengers annually as their big brothers but, their profit margins being smaller, they do not receive the attention given their larger counterparts regarding meaningful technological developments, risk evaluations, and company R&D dollars spent.

As a nation we face the problem of determining how we will train the future pilots this country needs for the continued growth and maintenance of the air transportation system. Demands for pilots in the near future are expected to tax the U.S. capability of providing them with adequate training. The main reason will be the lack of available single engined, low operating cost airplanes in good working order in which to conduct such training. For decades we have relied on single engine, two or four place, conventional configuration aircraft as the vehicle for this mission. As the numbers of these aircraft have dwindled, the extension of their use through the repair and replacement of principal structural elements and other critical components has become necessary. Designed to static strength limitations, they have manifested a safe life potential as the result of marginal over building that aided

manufacturing needs, or resulted from needed redundancy to account for multiple loading conditions as well as the application of conservative engineering substantiation methods. However, precise safe life cycle of any one design is essentially unknown.

PURPOSE

Production of U.S.-built single engine airplanes, extensively used in the past for training, business and recreational flying, has all but ceased, with the flight industry needs being met by the existing fleet of aging airplanes or by foreign designed and manufactured imports, a group that is rapidly acquiring the available U.S. market share. Some blame our GA-industry for management failures and the reluctance of that industry to modernize, others cite crippling legal encumbrances and limitless product liability, while many target governmental airworthiness regulations and the certification processes as culprits. Still others point to foreign government subsidization of their national industries, which compete in the common world market, as the explanation for the current situation.

In truth, all of these have played a part in the demise of the U.S. GA industry, but, no matter what the cause, the future of aviation transportation in this nation depends on training of future pilots and a supply of new aircraft for use as flight trainers and commuters. Future trainers need to be designed to meet the current and future market. These designs must include considerations of the current Federal regulations, the training environments, new technologies and the existing legal situations. Placing occupant safety first and foremost on the design priority list is believed to be one of the best ways for realizing needed reductions in product liability risk and in meeting FAA regulatory mandates. Introducing new technologies that are closer to those incorporated in modern transport category airplanes also makes great sense and appears to be more and more achievable from a cost point of view. All of these objectives require a fresh approach to design.

The stagnant GA industry in the United States has made little progress toward improved single engine trainer airplane design in recent years. The last Cessna 172 that rolled off the production line in 1986 was, for the most part, the same airplane as the original model designed in the mid 50's. One solution sometimes offered to increase the supply of usable trainers has been to re-start manufacturing airplanes like the 172. Placing such old designs back into production would surely put more airplanes on the market but would do little to improve their inherently unknown, designed-in, resistances to aging, fatigue and deterioration. There appears to be an urgent need for a modern, newly designed, GA-Primary Flight Trainer (PFT) vehicles (6). The discussion presented here is offered as an encouragement for the creation of conceptual design tools to be used in the development of new airplane designs that will truly be an advance on the state-of-the-art in single engine GA-PFT's. This paper is focused on developing an algorithm for use in assessing the safe life potential of GA airplane concepts as an integral part of the preliminary structural design process.

BACKGROUND. Single engine piston-powered airplanes in the U.S. have now reached an average age of 28 years - an age certainly none of their designers ever expected or anticipated during the design activity. Time has clearly shown that a number of these are good airplane designs that employ many cost effective manufacturing concepts which could easily be adapted and applied to new designs. They also have included some undesirable features which should be avoided wherever possible in new designs. For the most part these aging airplanes are thin-skinned, reinforced, light-weight, riveted, 2000-series aluminum structures which have a multitude of potential stress concentration points, regions where damage and corrosion are difficult to detect and have many potential zones where multiple site damage can and does occur. The safe life monitoring of these airplanes has currently attracted keen interest (7). The measurement of in flight loads experienced during normal operation and the nature of the operational mission of these airplanes has also been a topic of interest for over twenty years (8, 9). Significant changes in federal airworthiness regulations, which include structural airworthiness requirements for fatigue assessment of critical structures, occupant safety related dynamic seat tests, material flammability tests, and substantial increases in the emergency landing requirements (10, 11), have occurred since the majority of the airplanes currently flying were certified.

Knowledge is limited about the nature of accumulated cyclic stresses and the effects they have on damage to principal structural elements of these light airplanes. There is not much in the way of proven methods for determining or predicting the locations of site damage areas in such light structured aircraft. Plans for both in-service and laboratory tests that will significantly expand our understanding of the dynamic air loads and their effects on principal structural elements are under way (12) and data should be available for use in the design of future vehicles. Easily applied methods for conceptual design are needed not only to support the GA industry but as pedagogical tools useful in the instruction of neophyte engineers. If the GA industry is to survive in the United States totally new designs must be developed. In order for the next generation designs of GA-PFTs to be successful improved engineering expertise in applying new test data during the early design stages will be needed. Many of these data do not exist but are being developed by current studies. In designing new GA-PFT airplanes, engineers will make use of modern computer software not imagined when the current fleet of GA trainers were developed. However, these engineers will still need simple design estimating tools and procedures to "ball park" solutions and to use as gages in assessing the credibility of computer-derived results as part of the substantiation process.

SAFE-LIFE ASSESSMENT OF EXISTING AIRPLANES.

The Federal Aviation Administration has developed procedures and examples of methods that can be used in the safe-life assessment of existing GA-PFT type airplanes (13). Gust, maneuvering and taxi load spectra are offered for various airplanes. In-flight measured data for velocity, altitude and accelerations near the vehicle center of gravity (c.g.) have been accumulated (14) for over 42,000 hours of operation time in 105 different kinds of aircraft. This unfortunately represents only a very small fraction, about 0.02 percent by conservative estimate, of all of the flight

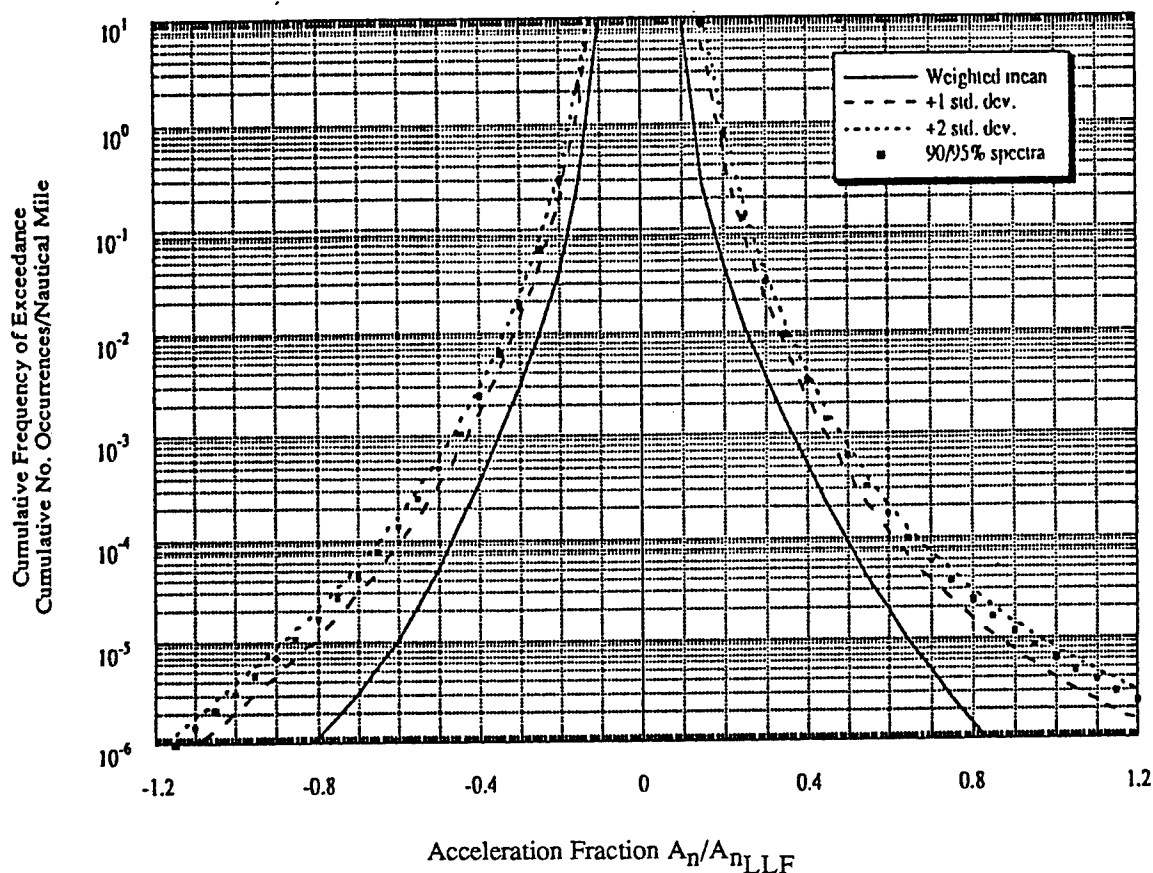


Figure 1 Gust Load Spectra: Single Engine General Usage
(Basic flight Instruction and Business/Personal Combined)

hours that have been accumulated in all such aircraft over the past ninety years, but it is the only information presently available and serves as the best source of actual in-flight loads data. It should be noted that, historically, these data appear in customary units that have been accepted for decades in aviation. No attempt to convert these historical data to SI units is made here in order to preserve the applicability of the archives. For this study, the single engine general usage data are selected for use. Figure 1, developed by Gabriel et al.(8), is a typical form in which such data normally appears in the literature. Here A_n is the incremental load factor experienced under a given flight condition and A_{nLLF} is the incremental limit load factor for a design condition (like the gust limit load factor -1). As can be seen from Figure 1, the variation of the cumulative exceedances per nautical mile is definitely nonlinear but somewhat symmetric with respect the the acceleration fractions.

At the onset it must be realized that in-flight acceleration data measured at the airplane c.g. may not accurately represent the actual structural loading experienced by the wing and becomes even more questionable for application to the tail and empennage structure. Furthermore, theories for fatigue failure of structural elements subjected to

combined stresses produced by bending, torsion and shear loads are incomplete. Be that as it may, for the safe life evaluation of the wing structure for an existing airplane, detailed and definitive information is normally available in the form of production drawings, engineering design and analysis reports, structural test data and even in-flight test data. Therefore the methods that have been developed for assessing the safe-life potential of such existing airframe structures given in AFS-120-73-2 (13) are applicable and an estimate of life, in hours, may be calculated. An outline of this procedure is developed here to help clarify some of the vagueness in AFS-120-73-2 and to illustrate the information needed to better understand the application.

At the start, in all cases to be evaluated, whether for an existing airplane or for a new design concept only vaguely defined on paper, there are assumptions about the wing lift loading distribution under various conditions of flight that must be made. These may or may not have been validated by wind tunnel test or flight tests. Consider Figure 2 as a representation of the worst case combinations of a 1.0-g normal span loading distributions (this would include flaps, ailerons, clean wing and so on) for an example airplane. In all cases, the appropriate shear and moment diagrams are simple to develop and should be available from this loading information. In the case of an existing airplane, the same span loading information would have also been used to develop ground tests to substantiate the wing structure to limit load and ultimate load conditions. Accurate estimates of the wing cross-section properties (area, moment of inertia and section modulus) would normally be available from analysis reports. These may also be rationalized with test data where wing displacements were measured along the span (However, the same would not be true for a new design since one of the objectives of the design activity is to determine such information and design the structure accordingly). From all of these the 1.0-g stress condition of the wing can be determined. This stress information, along with the normal airplane performance information that would also be available, serves as the starting point for a safe-life assessment.

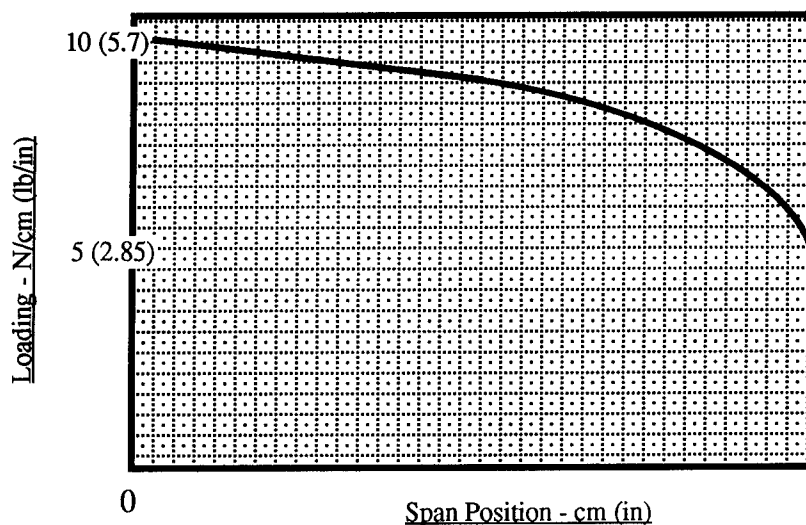


Figure 2 Wing Load Distribution - Typical

This procedure has been computerized by S. K. Kaul (15) of the FAA Small Airplane Directorate to reduce the many calculations needed when evaluating an existing airplane structure. It could also assumably be used as a design iteration tool if an initial guess as to the nature of the structure and the value of the worst case 1-g stress could be made. Even though such a computerized version of the method is available the prudent engineer would be well served to fully understand the procedure involved to best realize its limitations and assumptions, either directly stated or implied. Therefore an assessment of the factors involved in this method is needed and is developed here in algebraic terms to support this discussion.

The case of a nearly symmetric exceedance distribution is selected for this illustration and is shown in Figure 1. "The Gust Load Spectra" is decomposed into "k" Acceleration Fraction ($A_n/A_{nLLF} = a_{n_i}$) increments, Δa_{n_i} , not larger than 0.2 g per increment, beginning with an acceleration fraction at $i = 0$ for a_{n_0} that represents the endurance limit stress for the alloy being used divided by the 1-g stress or -

$$a_{n_0} = A_n/A_{nLLF} = [S_a(\text{endur.})]/[S_m(LLF-1)]$$

where $S_a(\text{endur.})$ = The alternating endurance strength component of the material selected for design,
 S_m = The mean stress of the material selected for design - related to the worst case 1-g stress,
 and LLF = The appropriate "Limit Load Factor", Positive Gust or Maneuver, Negative Gust, etc.

The accurate determination of a_{n_0} is a very critical because the largest values of the Cumulative Frequency of Exceedance per Nautical Mile occur for the smallest a_{n_i} values. From the starting a_{n_0} value, the average value of each increment ($a_{n_{avg_i}}$) is determined as:

$$a_{n_{avg_i}} = (a_{n_{i+1}} + a_{n_i})/2$$

The Cumulative Frequency of Exceedance per Nautical Mile (C_{f_i}) at the end points of each increment are noted and their difference calculated (ΔC_{f_i}). The frequency of exceedance per hour, or cycles, (n_i) is obtained by multiplying ΔC_{f_i} by the cruise velocity (V_c) (cruise is used here for the gust condition but the appropriate velocity should be chosen for the appropriate case like maneuvering or landing) to give:

$$n_i = \Delta C_{f_i} \times V_c \quad [1]$$

The limit load factor acceleration increment is: $A_{nLLF} = LLF - 1$

The incremental load factor A_{n_i} for each C_{f_i} can be obtained by multiplying A_{nLLF} by each average acceleration fraction increment:

$$A_{n_i} = A_{n_{LLF}} \times a_{navg_i} \quad [2]$$

The worst case 1.0-g stress (S_0) is chosen as the mean or average stress (S_m) and the alternating stress component (S_a) can then be estimated as

$$S_{a_i} = A_{n_i} \times S_0 \quad [3]$$

Stress versus cycles to failure curves (S-N curves) that map S_m against S_a and cycles to material failure are provided in AFS-120-73-2, labeled as "Endurance of Complete Wings and Tailplanes (Aluminum Alloy Materials)", Figure 3 (These data are left in their original customary units for historical purposes). These can be used to determine the cycles to failure (N_i). The S-N curves in AFS-120-73-2 appear to be nearly the same data that can be found in MIL-HDBK-5 (13) for 2000-series aluminum (2024 is most common and S_m v S_{max} plots are given) like the one shown in Figure 4. Using either data set, a reasonable estimate of the cycles to failure (N_i) can be determined for each acceleration fraction incremental from the S_a and S_m values. The weighted inverse life contribution (n_{N_i}) for each Δa_{n_i} increment can be calculated using Equation [1] and N_i as:

$$n_{N_i} = n_i / N_i$$

and the total weighted inverse life contribution is the sum of all the "i" values assessed ($\sum_{i=0}^k [n_{N_i}]$).

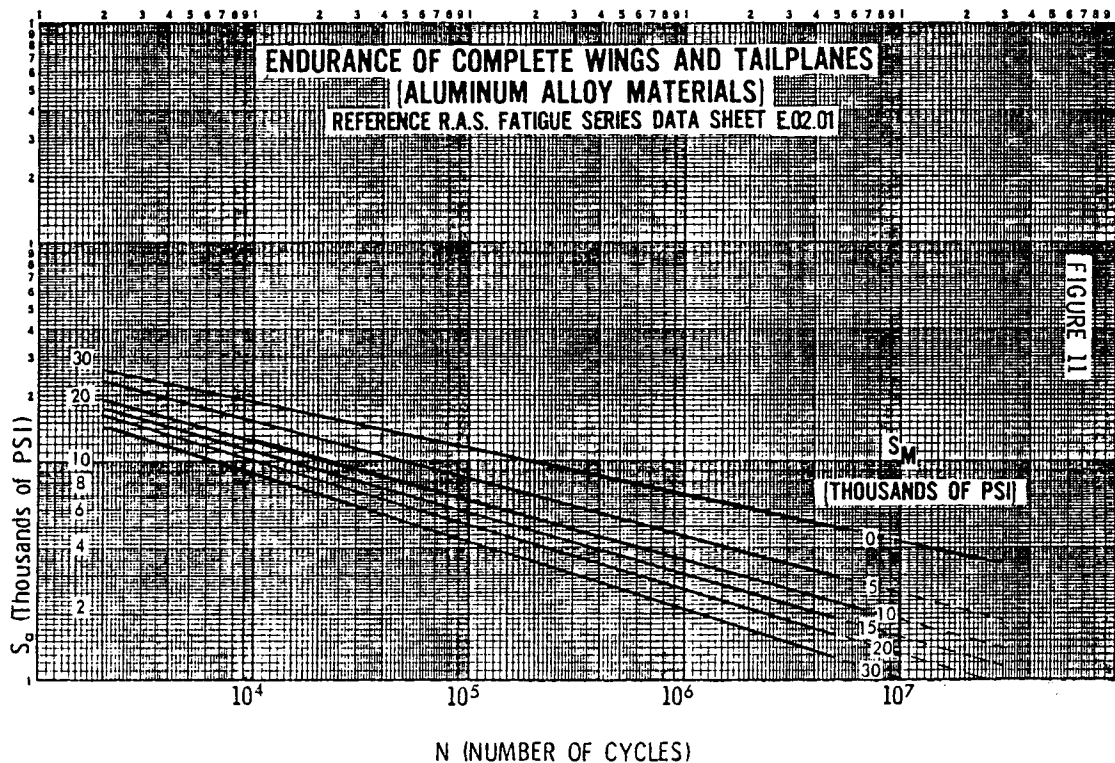


Figure 3 S-N Curves for Aluminum Alloy Materials (Ref 13)

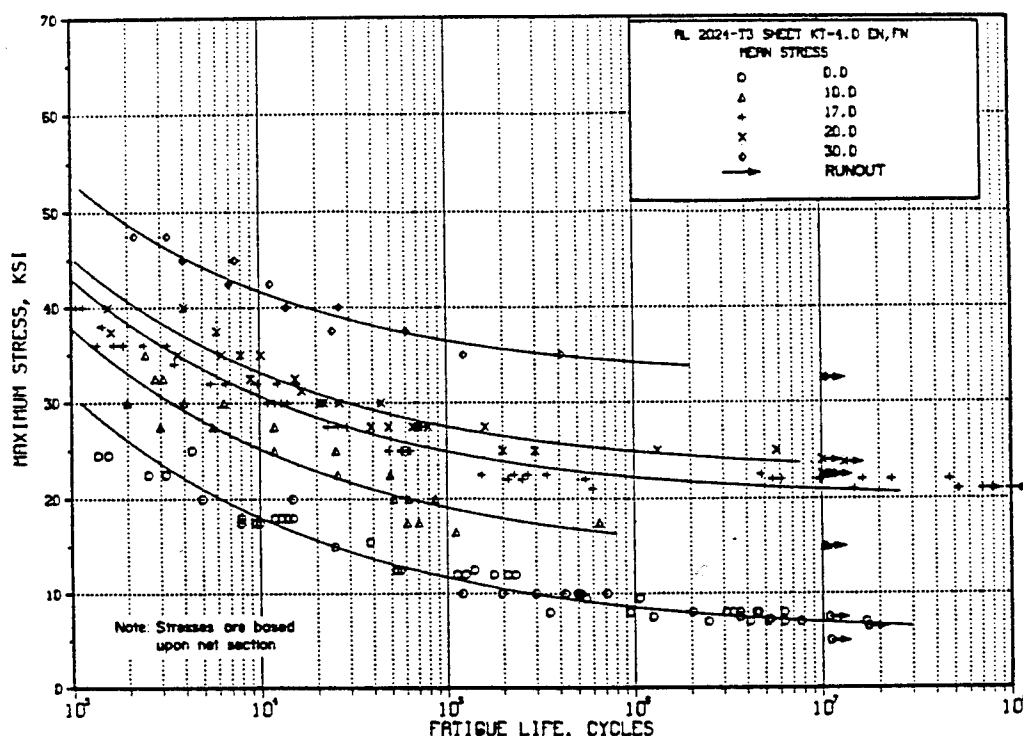


Figure 4 S-N for 2024-T3 Aluminum, $K_t = 4$ (Ref 16)

This procedure is applied to each of "j" load spectra for gust, maneuvering, taxi and landing with the appropriate S_m determined for each of the limit load and ultimate load conditions that comply with the airworthiness requirements for the category of airplane under investigation [It should be noted that, for an existing airplane, all of these loading conditions and resulting stresses would normally have been determined as part of the structural substantiation (analysis and test results) and should readily be available - this is not the case for an airplane concept in the early design mode.]. The ground-air-ground (GAG) cycle is developed by identifying the weighted average minimum and maximum stress exceedance values for each spectrum and determining an average mean stress that represents the aggregate; an involved process that requires reducing the stress exceedances to a common base, cross plotting the results, and then calculating the GAG cycle contribution. A final tally of the total weighted inverse lives can then be made, the inverse of which gives the unfactored estimated vehicle life in hours. If, as suggested here, this has been accomplished without any specific component testing or full scale vibration testing, a scatter factor of "8" is to be used and thus the safe life is found as the unfactored life divided by the scatter factor.

$$\text{Safe Life} = \{ [\sum_j \{ \sum_{i=0}^k [n_{N_i}] \}] \times 8 \}^{-1} \quad [4]$$

Evaluation of Equation 4 reveals that the safe life achievable, in its simplest form where $S_m = S_o$, is a complicated non-linear function of the 1-g stress. In the conceptual design environment it is often desirable to attempt to "size"

principal structural elements by inverting a typical stress relation and solving for the section properties, like area or section modulus, required to achieve a given performance. As an example, consider maximum wing bending stress or:

$$S_{bnd} = Mc/I$$

For the Limit Load condition where no permanent deformation is permissible, let $S_{bnd} = C_0 F_{ty}$ where C_0 is a reduction factor used to guarantee that the allowable stress for the material intended to be used in the design will be less than the yield strength of the material.

$$C_0 F_{ty} = Mc/I$$

Solving for the section modulus required gives

$$\{I/c\}_{Req'd} = M/[C_0 F_{ty}]$$

Similarly, the Ultimate Load condition (taken as equal to or greater than 1.5 x Limit Load per FAR23) needs to be evaluated to guarantee no failure will occur by demonstrating that the ultimate stress is less than the ultimate strength of the candidate material or

$$\{I/c\}_{Req'd} = 1.5M/[C_0 F_{tu}]$$

The resulting two calculated $\{I/c\}_{Req'd}$ values are a function of how the material yield and ultimate strengths compare. Based on the larger of these two values and the intended structural configuration, a decision must be made, tempered with manufacturing, assembly and maintenance considerations, to guarantee the larger required value is either met or exceeded. Thus the principal structural element, in this case the spar, would be "sized".

To comply with the fatigue requirements of FAR 23, future designs will need to include fatigue assessment as part of this "sizing" activity. In attempting to size for a desired life, Equation [4] would need to be inverted to express S_0 as a function of N_f . However the complexity of Equation [4] does not readily permit such an inversion. As part of this investigation, a study was performed to develop possible design process simplifications based on AFS-120-73-2 as modified by Gabriel et al. (8) which could be used for first pass detail design to give a "feel" for the relative merit structural safe life sizing would have on an intended configuration. This first pass estimate is based on a selected Desired Design Life (DDL) defined in hours of operation for the vehicle.

A METHOD FOR THE SAFE-LIFE DESIGN OF NEW GA-PFT AIRPLANES.

Assumptions about the wing lift loading distribution under various conditions of flight must be made at the start and would be similar to that available for an existing design. From these shear and moment diagrams can be developed. Mission definition, loading distributions as a function of configuration choices, and performance predictions are

typically calculated in the early phases of design and that is just about all. Information about structural elements within a configuration are, in fact, the desired outcome of the conceptual detail design activity. Thus, nearly every part of the information needed to assess safe-life by the procedure described above is nonexistent at this phase of the vehicle development. Material selection and manufacturing methods are also parts of the desired information to be defined during these activities. Both will have an important influence on the life cycle of the design.

In order to to reduce the complexity of the problem at hand the following assumptions are made

- 1) The weighed mean values of exceedances per nautical mile versus acceleration fraction for single engine piston airplanes from Gabriel et al. (8) are an improved statistical representation over AFS-120-73-2 and are used in modified form in this assessment
- 2) GAG represents approximately 31% of the DDL (8)
- 3) Since a_{n0} is undefined because S_0 is undefined, the entire ΔC_f range is used (conservative)
- 4) Landing and taxi contributions to design life for GA-PFT's are negligible (8, 13)
- 5) Both the Gust and Maneuver exceedance distributions are assumed to be symmetric about $a_n = 0$ and the mean stress for both (S_m) is assumed to equal the 1-g stress, (S_0) (conservative).
- 6) 2024-T3 aluminium ($K_t = 4$) is the material of choice and material data from MIL-HDBK-5E is selected for use over that offered in ASF-120-73-2.
- 7) The region of the 1-g stress in the principal structural element of interest is away from major fittings or interfaces and represents a well-established stress distribution according to appropriate theory.
- 8) A scatter factor of 8 is appropriate (13)

Using the MIL-HDBK-5E data from Figure 4, constant life diagrams are prepared and then linearized in a conservative fashion so that a simple representation of the variation in alternating stress allowables can be defined in terms of the mean stress and some intercept value S_{a0} for selected constant value of N (See Figure 5) according to the form

$$S_a = mS_0 + S_{a0}$$

The slopes (m) of the family of constant life lines produced were noted to be very similar and are assumed to be constant for this simplification. As can be seen in the plots illustrated in Figure 5 for Allowable Alternating Stress versus Mean Stress for the alloy selected, 2024-T3 with $K_t = 4$, $m = -1/6$. For other aluminum alloys a similar behavior has been observed, but the slope value as well as the vertical axis intercepts will be different. An acceptable curve fit is achieved for the variation of S_{a0} as a function of N for the 2024 alloy in the form of an exponential model or

$$S_{a0} = \alpha N^b$$

where $\alpha = 98,240$ psi (A theoretical extrapolation liken to the ultimate strength of the material)
and $b = -0.178$

As a result, the allowable alternating stress can be expressed as

$$S_a = mS_o + \alpha N^b \quad [5]$$

Equating [5] to Equation [3], where $A_{n_i} = A_n = a_{navg}(LLF-1)$, and solving for N gives

$$N = [(a_{navg}(LLF-1) - m) \times S_o / \alpha]^{1/b} \quad [6]$$

$$\text{Or} \quad N = \beta_K (S_o)^{1/b} \quad [6a]$$

$$\text{Where} \quad \beta_K = [(a_{navg}(LLF-1) - m) / \alpha]^{1/b}$$

Thus, for gust conditions,

$$N_g = [(a_{navg_g}(GLLF-1) - m) / \alpha]^{1/b} [S_o]^{1/b}$$

or

$$N_g = \beta_G (S_o)^{1/b}$$

For maneuvering conditions,

$$N_m = [(a_{navg_m}(MLLF-1) - m) / \alpha]^{1/b} [S_o]^{1/b}$$

so

$$N_m = \beta_M (S_o)^{1/b}$$

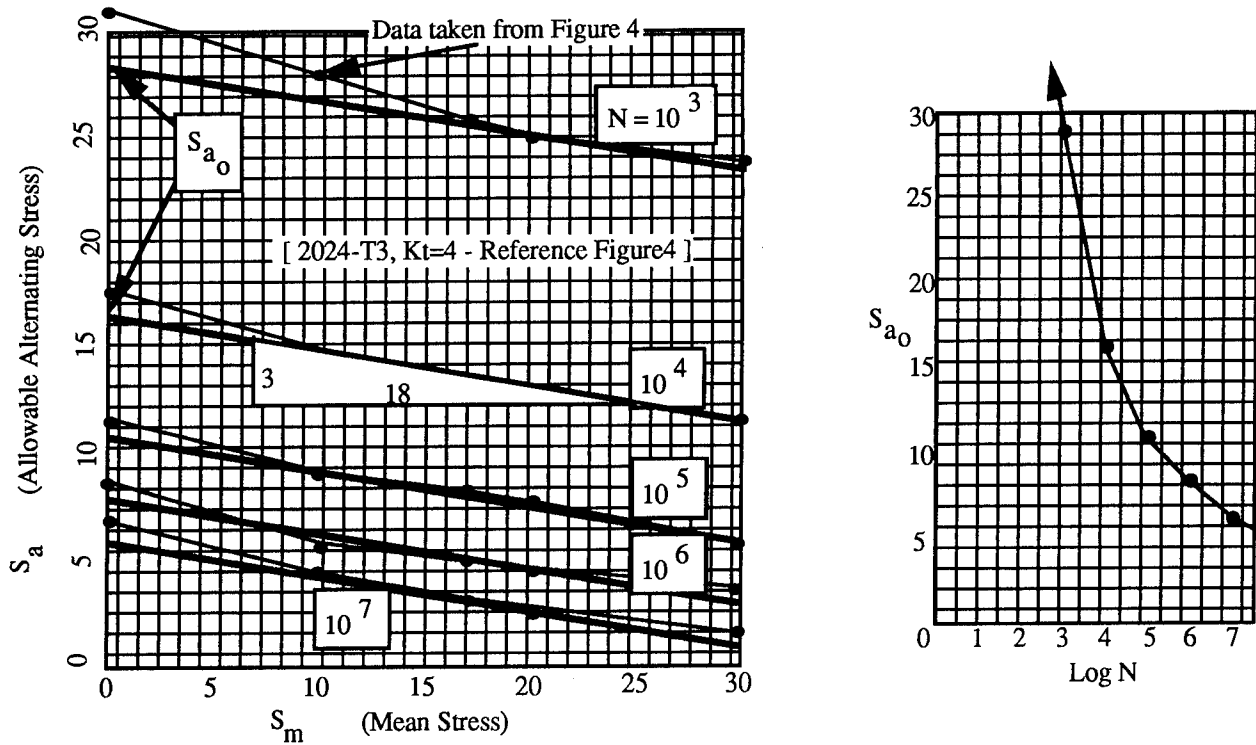


Figure 5 Constant Life Linear Models and Intercept Curve Fit Data

Re-plotting the Acceleration Fractions versus Cumulative Exceedances per Nautical Mile curves of Gabriel et al. in cartesian coordinates suggests that the preponderance of the cycle accumulations occur at acceleration fractions of less than 0.30 as shown in Figure 6. Applying assumptions 1), 3), and 5) leads to the conclusion that the appropriate values of ΔC_f for the entire spectrum of both the gust and the maneuver conditions are 10.0 exceedances per nautical mile. Also from Figure 6 the average values of a_n ($a_{n\text{avg}} = A_n/A_{n\text{LLF}}$) that correspond to these ΔC_f range values are calculated for the entire range of exceedances as:

$$\begin{aligned} \text{Gust Condition:} & \quad a_{n\text{avg}} = 0.128 \\ \text{Maneuver Condition:} & \quad a_{n\text{avg}} = 0.092 \end{aligned}$$

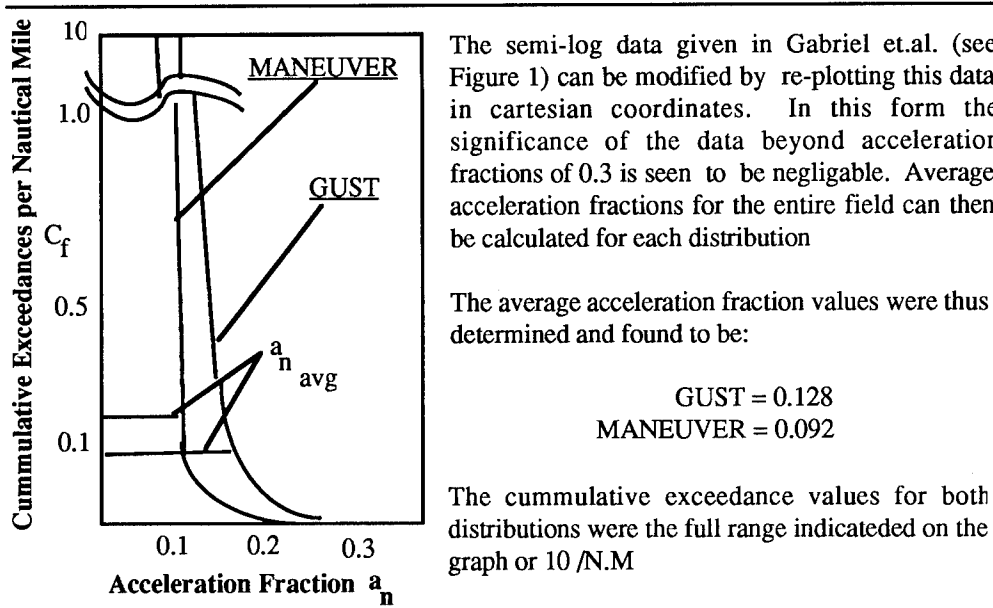


Figure 6 Modified Cartesian Plot of Acceleration Fractions vs Cumulative Exceedances per Nautical Mile

The corresponding total accumulation of cycles for both conditions can be calculated using Equation [1]

$$\begin{aligned} \text{Gust} & \quad n_g = 10 \times V_c \\ \text{Maneuver} & \quad n_m = 10 \times V_a, \text{ (Where } V_a \text{ is the maneuver speed)} \end{aligned}$$

$$\begin{aligned} \text{Then} & \quad n_{N_g} = n_g / N_g = 10 \times V_c / N_g \\ \text{and} & \quad n_{N_m} = n_m / N_m = 10 \times V_a / N_m \end{aligned}$$

$$\text{From Equation 6a,} \quad N_g = \beta_G (S_o)^{1/b} \text{ and } N_m = \beta_M (S_o)^{1/b}$$

Applying Assumptions 2) and 4) Equation [4] simplifies to

$$\text{Safe Life} = \text{DDL} = (0.69) \{ [n_{N_g} + n_{N_m}] \times 8 \}^{-1} \quad [7]$$

Substituting from the definitions given above for the SE-PFT and for 2024 aluminum alloy, the desired design life can be derived as:

$$\text{DDL} = (0.69)(S_0)^{1/b} \{ 10 (V_c / \beta_G + V_a / \beta_M) \}^{-1} \quad [7a]$$

Solving for the 1-g stress, S_0 , gives the desired relation.

$$S_0 = \{ 116 \text{ DDL } [V_c / \beta_G + V_a / \beta_M] \}^b \quad [8]$$

Using gust and maneuvering limit load factor values (GLLF and MLLF respectively) of 3.8 g's and estimating the maneuvering speed as 15/17 of the cruise speed (ref. FAR23A), examples are developed as test cases using data extracted from references 8 and 13 where the 1-g stresses were known *a priori* and the airplane design lives were previously calculated. The calculated design life, along with the appropriate cruise speed for each, were treated as the desired design life (DDL) conditions for each airplane configuration. Equation [8] was used to predict the allowable 1-g stress thereby allowing a comparison to be made with the known stress for each case. As can be seen from the values listed in Table 1, Equation 8, as a simple estimating tool, yields very acceptable results. The predicted values of 1-g stress are all of the correct magnitude and are within 7% of the actual stress values.

Table 1 Comparison of Estimated and Calculated Results

<u>Source</u>	<u>Vc(kts)</u>	<u>DDL (hrs)</u>	<u>Reported 1-g Stress (psi)</u> (Used in AFS120)	<u>Allowable, 1-g Stress (psi)</u> (Predicted using Eqn [8])
AFS-120	139.5	12,484	5,500	5,930
Gabriel	133.0	9,745	6,150	6,285
Gabriel	113.0	178,810	3,930	3,876

To complete the sizing activity the assessment of the limit and ultimate load conditions would also be evaluated at this point and compared with the the fatigue-based 1-g stress in order to find the limiting condition. First pass design decisions can thus reflect not only the traditional static stress estimates needed for airworthiness substantiation but also include the affects of fatigue sizing by employing the methods discussed here.

CONCLUSIONS

In order for the next generation designs of GA-PFTs to be successful a much greater expertise and a considerable amount of test data will be needed. The simplified design estimating procedure developed here represents a start. The

possibility of selecting a desired design life and quickly determining the allowable 1-g stress is possible. The accuracy of the predictions made for the limited test cases evaluated is quite good and should be sufficient to give the designer a feel for the success of a potential structural concept without expending an inordinate amount of time. In future GA airplane designs the application of static and dynamic tests plus the use of sophisticated computer-aided analysis capabilities, well beyond those used for the design of the current fleet of GA trainers must be employed in order to yield safe, cost effective airplanes and to reduce the business risk presently associated with aircraft product liability.

RECOMMENDATIONS

Research is needed to develop technologies to assess the risk and prevention of defects, failures and malfunctions of airplanes planned for future operations as FAR23 certified aircraft. The level of risk associated with their operational profiles needs to be defined in order to provide insight as to their operational safety throughout their life cycle. A portion of this analytical effort could be validated through statistical samples of in-flight data at locations other than the airplane c.g. In so doing, it is believed that a potential benefit to the long-term growth of general aviation can be achieved by increasing the awareness of the level of risk and defining how this risk changes as such aircraft age. Retired airframes could be used to conduct structural investigations into the effects of crack damage and corrosion on critical portions of the major load carrying structural members. The application of Impedance and Mobility (IM) testing techniques, using strategically placed sensors, structural characterization research in addition to in-flight real time PC-based/CD-recorded monitoring may together provide valuable insights to the resolution of fatigue life determination. A research program is needed to develop the methodology for dynamic testing, both on the ground and in the air, using strategically located sensors to characterize structural attributes and to define stress cycle accumulations along with changes in these structural attributes as a function of time and age and correlating the results with respect to load factors and accumulated cycles. Actual in-flight stress levels need to be determined through instrumentation. Damage site zone locating capability is also needed. The sum of all such data could result in improved capabilities for predicting service life, reducing maintenance costs, reducing liability risk, increasing awareness of flight handling techniques and improving flight training environments by having additional data available for debriefing.

REFERENCES

- 1) Bruhn, E. F., "Analysis and Design of Flight Vehicle Structures", S. R. Jacobs Co., Indianapolis Indiana, 1973.
- 2) Niu, Michael C., "Airframe Structural Design", Technical Book Co., 2056 Westwood Bl, Los Angeles, Ca, 1988.
- 3) Shigley, J.E., Mitchell L.D., "Mechanical Engineering Design", Fourth Edition, McGraw-Hill Series in Mechanical Engineering, New York, 1983.

- 4) "Airplane Airworthiness; Normal, Utility, and Acrobatic Categories", Civil Air Regulations, Part 3, Civil Aeronautics Board, U.S. Government Printing Office, Washington, D. C., 1956.
- 5) Sexton, Bobby. W., "FAA's Aging Commuter Airplane Program", Paper No. 931248, 1993 SAE General Corporate, & Regional Aviation Meeting & Exposition, Wichita, Kansas, May 18-20, 1993.
- 6) Eastlake, C.N. and Ladesic, J.G., "The Next Generation General Aviation Primary Flight Trainer", AIAA Aircraft Design, Systems and Operations Meeting, Monterey, California, August 11-13, 1993.
- 7) DeFiore, T. and Barnes, T., "The FAA Regional/Commuter Aircraft Flight Loads Data Collection Program", Paper No. 931258, 1993 SAE General Corporate, & Regional Aviation Meeting & Exposition, Wichita, Kansas, May 18-20, 1993.
- 8) Gabriel, Locke, DeFiore and Smith, "General Aviation Aircraft-Normal Acceleration Data Analysis and Collection Project", Report No. DOT/FAA/CT-91/20, U.S. Department of Transportation, Federal Aviation Administration, Technical Center, Atlantic City, NJ, February, 1993.
- 9) Jewel, J. W., "Flight Duration, Airspeed Practices, and Altitude Management of Airplanes in the NASA VGH General Aviation Program", NASA Technical Memorandum 89074, Langley Research Center, Hampton Virginia, 1987.
- 10) "Airworthiness Standards: Normal, Utility, Acrobatic and Commuter Category Airplanes", U.S. Department of Transportation, Federal Aviation Administration, Federal Aviation Regulations - Part 23, Washington, DC, Eff. October 26, 1989.
- 11) "Fatigue and Fail-Safe Evaluation of Flight Structure and Pressurized Cabin for Part 23 Airplanes", Advisory Circular 23-13, U.S. Department of Transportation, Federal Aviation Administration, Washington, D. C., April 15, 1993.
- 12) DeFiore, T., "The FAA Regional/Commuter Aircraft Flight Loads Data Collection Program Presentation", SAE Aerotech'93 Conference and Exposition, Orange County Airport, Costa Mesa, CA, September 27-30, 1993.
- 13) "Fatigue Evaluation of Wing and Associated Structure on Small Airplanes", Report No. AFS-120-73-2, U.S. Department of Transportation, Federal Aviation Administration, Federal Aviation Regulations, Washington, D. C., May, 1973.
- 14) Jewel, J. W., "Tabulations of Recorded Gust and Maneuver Accelerations and Derived Gust Velocities for Airplanes in the NASA VGH General Aviation Program", NASA Technical Memorandum 84660, Langley Research Center, Hampton Virginia, September, 1983.
- 15) Kaul, S. K., "Fatigue Life Estimation Program for Part 23 Airplanes, AFS.FOR", Paper No. 931249, 1993 SAE General Corporate, & Regional Aviation Meeting & Exposition, Wichita, Kansas, May 18-20, 1993.
- 16) Military Handbook 5D, "Metallic Materials and Elements for Aerospace Vehicle Structures." U.S. Government Printing Office, Washington, D. C. 1986.

THE AIRBORNE POSITIONING AND PLANNING SYSTEM: AN ARCHITECTURE FOR FUTURE AVIONICS SYSTEMS DESIGN

R. C. Strain and G. W. Flathers, II
The MITRE Corporation
Center for Advanced Aviation System Development*
7525 Colshire Drive, M.S. W273
McLean, VA USA 22102-3481

ABSTRACT

In this paper, a high-level functional architecture of the Airborne Positioning and Planning System (APAPS) is presented. This system is comprised of a set of basic navigation and communication functions which are organized in such a way as to (1) assist the pilot in positioning and moving his aircraft through the airspace in pursuit of the goals that he has established for the flight, and (2) provide the basis to coordinate such movement with other aircraft in the context of a revised philosophy of air traffic control. The functional architecture presented here is the result of a holistic design approach which jointly considers the needs of the pilot and the air traffic system, and makes possible a whole new array of innovative, cost-effective, and convenient methods for coordinating aircraft movement. It was also designed with the full spectrum of airspace users in mind to ensure that benefits from improved safety, flexibility, and airspace access and utilization are realized by all segments of the user community.

INTRODUCTION

With the advent of several new technologies, the flight decks of modern commercial, business, and general aviation aircraft are providing the pilot with greater support in controlling the aircraft, navigating precisely through the airspace, and exchanging information with entities outside the cockpit. Improved sensors, computer automation, electronic displays, and digital data communications are key technology areas that have enhanced cockpit capabilities. They are also areas that have benefited from advances in related fields which make cockpit applications more feasible in terms of weight, space, power, and especially cost. Indeed, flight deck features which were once in the realm of only the most advanced transport-category aircraft are becoming more commonplace in basic general aviation aircraft. Moving map displays and precise area navigation features, for example, are now packaged in several battery-powered, hand-held Global Positioning System (GPS) receivers, thus making some very advanced features available even in aircraft which do not have electrical generating systems. As a result, the full spectrum of the user-community is becoming increasingly sophisticated in terms of the types of missions they fly and the capabilities of the avionics they carry to support those missions.

While most users choose to equip their aircraft with these advanced features in hopes of gaining direct economic benefit or utility, there is growing interest in also using these capabilities to

* This work was produced by the Center for Advanced Aviation System Development of The MITRE Corporation. The work is preliminary in nature and has not been formally reviewed, endorsed, or approved by any other organization, including the Federal Aviation Administration or any of its representatives.

modify and enhance the process of air traffic control (ATC). In our current approach to ATC, an air traffic controller on the ground (with his supporting infrastructure) maintains primary responsibility for keeping aircraft under his control from running into one another, and for organizing the use of such resources as airways and runways. This "ground-centered" philosophy has dominated the evolution of ATC since its inception almost 50 years ago, mainly because there have been inadequate resources in the cockpit to permit the aircraft to provide more assistance in this process. Now, however, aircraft cockpits are becoming increasingly capable of contributing resources and information to enhance the ATC process. The challenge before the aviation industry today is not the discovery of new key technologies, but rather the effective application of technologies that are readily available, and in some cases even commonplace.

With that in mind, this paper presents a high-level description of the functional elements of the Airborne Positioning and Planning System (APAPS): a concept for organizing and using those new airborne tools and capabilities to reduce the pilot's workload while enhancing the ability of the pilot to aviate, navigate, and communicate. This is achieved primarily by coupling the navigation and communication elements more closely, enabling the pilot to manage air traffic control issues in a manner which is non-intrusive and compatible with his other flying responsibilities. From a systems perspective, fresh thinking about the way air traffic control is performed can be done when it is assumed that aircraft navigation data can be conveniently exchanged with other air traffic system components. Therefore, the functional elements of APAPS are being developed using a holistic design approach in which the requirements of the pilot are considered in concert with the needs of the other components in the air traffic system, namely controllers and their supporting automation, other pilots, operations centers, etc. This is a marked departure from other development efforts which require the pilot and the cockpit systems to conform to the constructs of the current ground-based philosophy of ATC.

The term APAPS will be used throughout this paper as though it were a stand-alone unit. However, this is not completely accurate and the term is used this way merely as a matter of convenience in discussion. In reality, the functional elements of APAPS may presently exist to one degree or another in many different systems, such as a flight management system (FMS) or a GPS receiver. A more appropriate interpretation of the term APAPS is that it is an aircraft-generic architecture, to which manufactured units may conform, that defines the necessary elements to achieve a desired minimum operational capability. Furthermore, the organization of the functional elements are such that the pilot's interaction is minimal and task-compatible, and that information exchanged with external entities is convenient and necessary to the overall flight mission.

SCOPE

This paper is limited to a description of the APAPS functionality from the pilot-user's perspective. There are numerous potential benefits to that can be attained given that most, if not all, aircraft have a minimum operational capability, such as that defined by the APAPS architecture. Benefits to the controller and the pilot are associated with situational awareness, mission effectiveness, and workload. Benefits to the air traffic system are associated with cost, efficiency, capacity, and safety. However, the discussion of these benefits is beyond the scope of this paper. Concepts associated with the role that APAPS-equipped aircraft will play in a future air traffic management (ATM) system to achieve these benefits requires special attention and will be discussed in other papers currently in production.

THE AIRBORNE POSITIONING AND PLANNING SYSTEM

DESIGN GOALS

In a world of tight budgets and narrow profit-margins, the success of a new idea depends significantly on its ability to illustrate operational benefit to the aircraft operator, whether that is a commercial airline, the military, a corporation, or a private owner. From this perspective, three goals were established to guide the functional design process. First, APAPS should "sell itself" - there should be no need to mandate equipage using the regulatory process. Historically, mandatory equipment requirements have served primarily to regulate access to the ATC system, but have done little to increase system capacity, improve traffic efficiency, or benefit the user. Rather, the approach taken in developing a functional architecture for APAPS was to provide tangible, operational utility such that the pilot would consider an APAPS unit to be essential to his flight even if his aircraft was the only aircraft in the sky. This was pursued through the provision of enhanced, integrated navigation and communication features which are helpful to the pilot, regardless of the density of air traffic.

A second design goal was to enhance the pilot's ability to maintain a safe distance from other air traffic. By far, most of the volumes of airspace in the world today are fairly benign, "low density" environments in which aircraft should be capable of performing separation on their own. In fact, this principle is the rule in visual flight conditions in most airspaces as pilots are expected to "see-and-avoid" other aircraft. However, concepts such as Cockpit Display of Traffic Information (CDTI - using such techniques, for example, as automatic dependent surveillance broadcasts) offer the opportunity for not only improving the see-and-avoid concept, but essentially allowing very efficient station keeping techniques to be applied in instrument meteorological conditions as well.

The third design goal was to greatly simplify the process by which an aircraft participates as part of the air traffic system in those "high density" cases where an ATC function is desirable to organize the use of a scarce resource (such as a runway). This involved, among other things, rethinking the traditional flight plan for ATC purposes, and revising the information and techniques by which the pilot expresses his intentions to the ATC system. It also involved a new approach to conveying constraints and instructions to the pilot. These were accomplished using digital communication techniques and integrating such information in task-compatible, navigation-related terms. It is envisioned that the basic APAPS features will be available to virtually every aircraft, such that equipment level (or functional capability) will no longer be a means to restrict access to busy airspace.

THE AIRBORNE SYSTEM

Prior to describing each of the primary functions of APAPS, it is helpful to envision where this system will fit into the context of the overall airborne system. Figure 1 provides such an organizational overview of the significant airborne system elements. The pilot interacts with APAPS and a digital communication systems using a single, integrated interface. This interface will be a graphics-based display, and could employ any of several techniques for the pilot to manage input and output. The digital communication system is used for exchanging data with both ground-based systems and other aircraft. The system assumes a digital datalink capability exists but, as noted in the first design goal, a datalink capability is not required for the pilot to realize many of the benefits of APAPS. If a suitable datalink capability does not exist, APAPS would still provide useful positioning, course guidance, and mission planning services to the

pilot. Voice communications capabilities in some form are assumed to be available for those communications that are better suited for voice format.

On the right side of the radio frequency (RF) segment are ground-based systems and other aircraft. The ground-based systems include those ATC functions that would be used to organize the flow of traffic in higher density situations, such as on and around busy airports. Also, with respect to the "other aircraft" on the right side of the RF segment, it is envisioned that at a minimum, positioning and pertinent intent information will be exchanged between APAPS-equipped aircraft providing a positional awareness capability. This is in response to the second design goal to supplement visual acquisition of other aircraft and enhance pilot situational awareness, and also to enable greater pilot contribution to the ATC process in high-density situations, such as assisting with in-trail spacing. The results of several on-going research efforts in this area would fit nicely into this architecture.

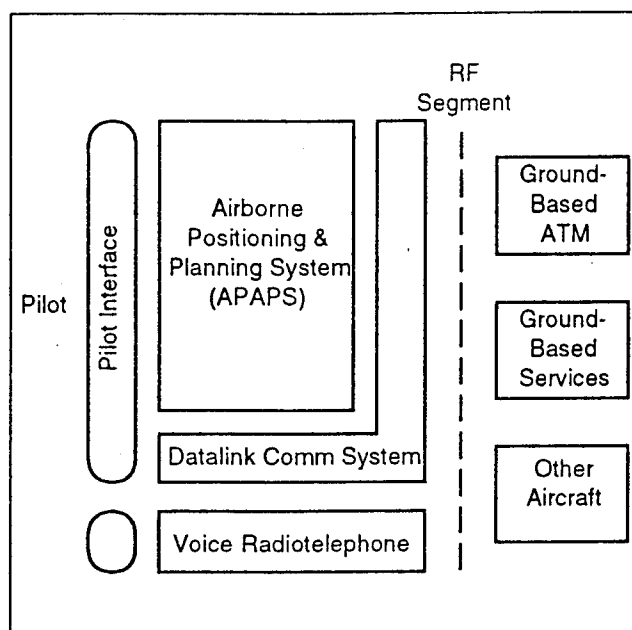


Figure 1. Airborne Nav/Com System Architecture.

The APAPS architecture design emphasizes compatibility with normal piloting tasks and "pilot-friendliness". The functionality is organized efficiently to minimize pilot interaction and ensure the presentation of information is intuitive and timely. The pilot interacts with APAPS to the degree that is appropriate for his mission and APAPS manages information for the purpose of providing decision support. APAPS performs some activities autonomously, but the pilot maintains a supervisory role and makes all mission critical decisions.

Several features of APAPS may appear similar to flight management systems (FMS) found in many commercial and high-end business aircraft. An example FMS for a Boeing 737-300 is shown in Figure 2. Compatibility between the two systems at some level is beneficial since it provides a baseline of capabilities that can be counted on when experimenting with air traffic system concepts. However the two systems do have significant differences.

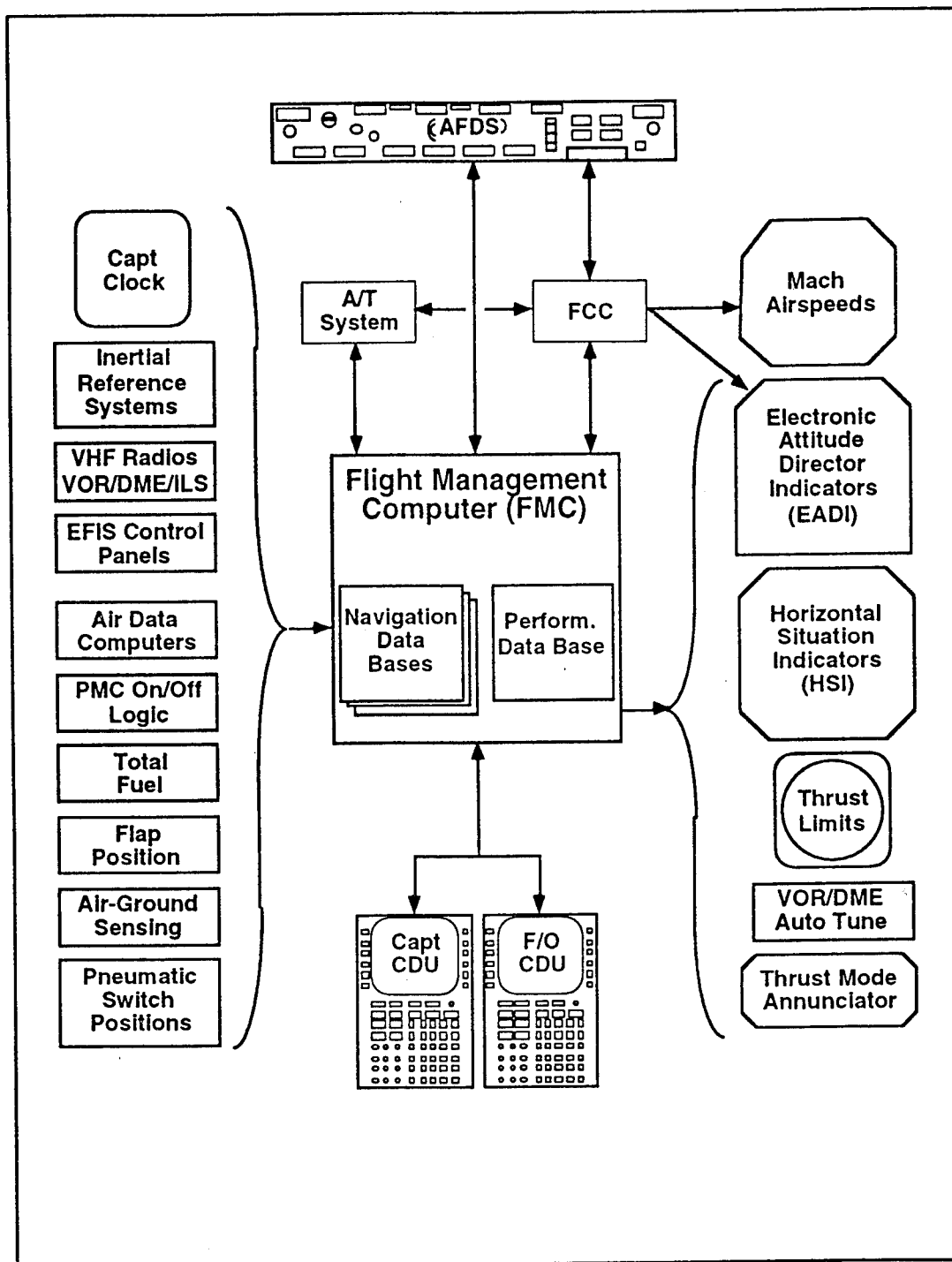


Figure 2. Flight Management System schematic for a Boeing 737-300 aircraft. Reproduced from [1]

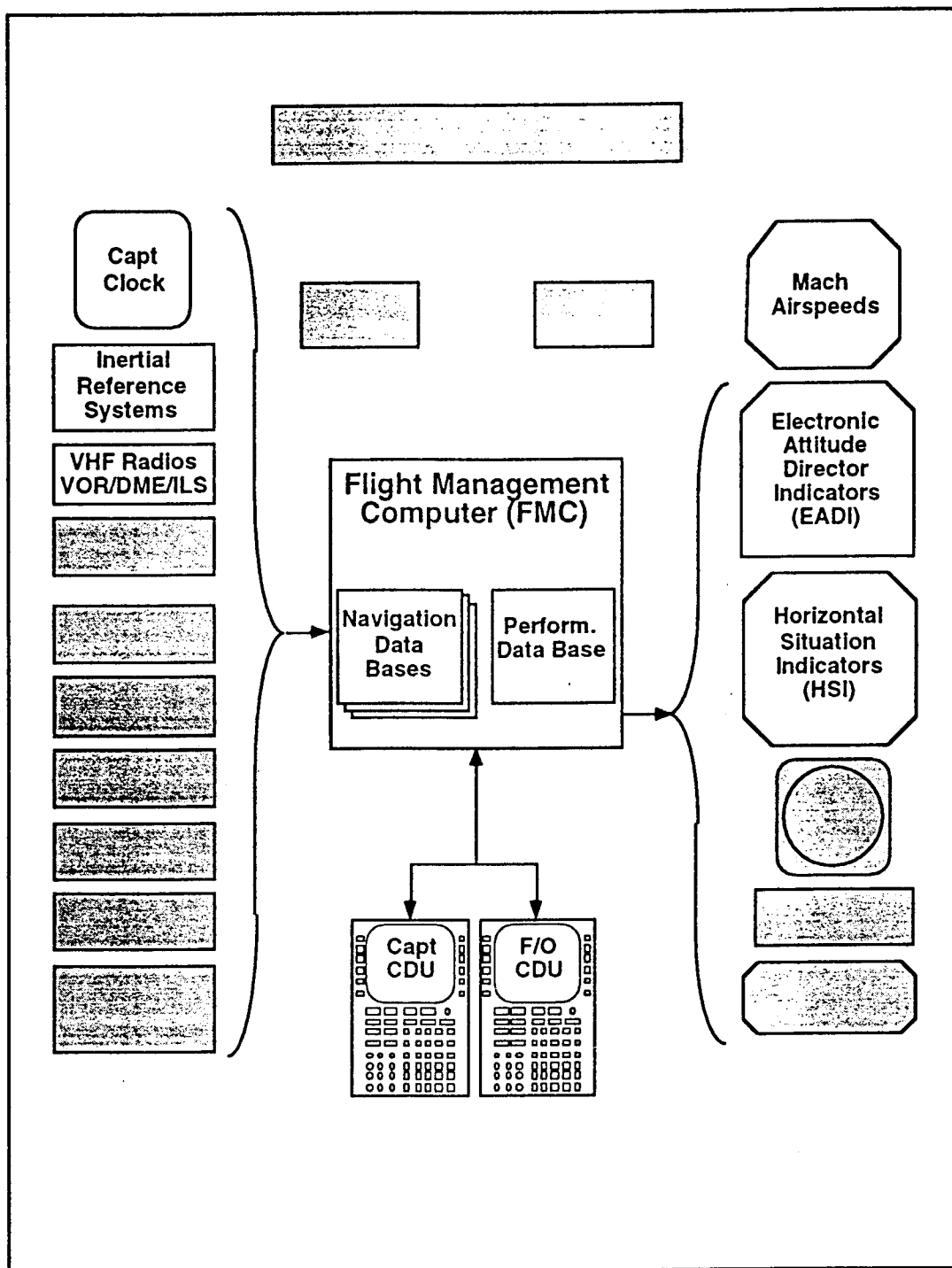


Figure 3. Flight Management System schematic for a Boeing 737-300 with only the elements necessary for basic navigation shown. Reproduced and modified from [1].

The primary difference between APAPS and FMS is complexity. This is illustrated in Figure 3, which shades the elements of the FMS that are not necessary for basic navigation. The FMS relies on data from numerous sensors to manage complex air data and flight control systems that help to optimize the operation of the aircraft according to the weighting scheme selected by the user. APAPS simply capitalizes on its ability to support area navigation (RNAV), making no attempts to perform flight control or optimization. Therefore, the data requirements for APAPS, and correspondingly the interfaces, are few and simple. The only sensors APAPS requires are antennas for positioning and communication and possibly a blind-encoding altimeter. The reduction in complexity translates into lower cost for both initial installation and maintenance.

As previously mentioned, primary design considerations were to keep the cost low and the utility to the pilot and the air traffic system high. In part, this can be accomplished by using GPS and minimizing the technical interfaces with other cockpit systems. Ideally, pilots should be able to place APAPS into a rack, connect the power and antenna, and be ready to fly. There are certainly certification issues that must be addressed, especially concerning transport category aircraft, but this reflects the level of simplicity the design that is trying to achieve.

ORGANIZATION OF COMPONENTS

The APAPS is comprised of five functions and a navigation database as depicted in Figure 4. The five functions are the following:

- position fixing
- mission definition
- course building
- course guidance
- external data integration

The position fixing function determines the present position of the aircraft and the aircraft's velocity vector. It works autonomously when the system is on and requires little or no pilot action. There are several methods that could be used perform this function, including:

- GPS
- inertial reference system
- long range navigation (LORAN) system
- distance measuring equipment (DME)/DME RNAV
- blended multisensor RNAV
- barometric altimeter

Looking at the above list, there are various levels of sophistication and associated cost for each option. The source, or sources, will depend on the operators' mission needs or present equipment. It is believe, however, that over time the source of choice will be GPS. Therefore,

for this discussion GPS will be assumed to be the source used for positioning and velocity vector determination.

The mission definition function allows the pilot to specify his overall goal and general information about how he would like to accomplish it. If the goal of the flight is to fly from airport A to airport B, the pilot would supply the destination and the estimated time of arrival (ETA). Otherwise, the pilot may provide an interim location that may serve as a point of reference for training, sight-seeing, skydiving or any number of other activities that a defined route would be inappropriate for. Any information the pilot provides is stored and may be used by other APAPS functions or packaged in outbound messages. The purpose for defining a mission is characterize the pilot's general intent. The mission definition provides APAPS with a point of reference for filtering mission-pertinent information. This information may include: weather, notices to airmen, airspace activity, or airport specifics, to name a few.

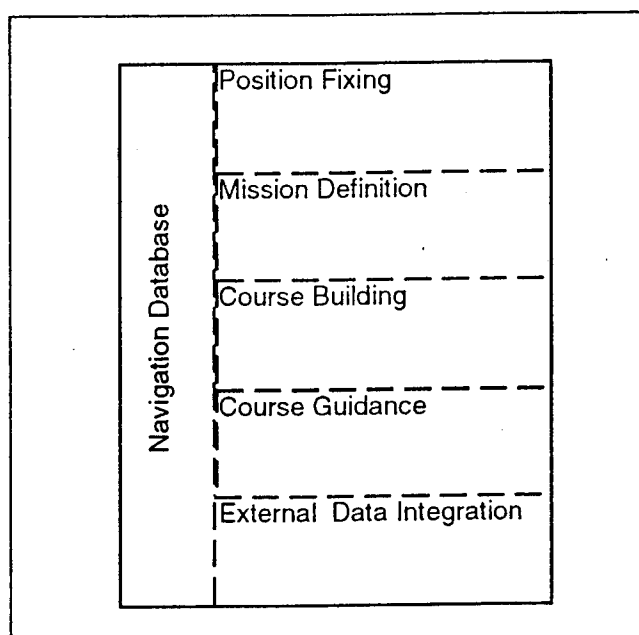


Figure 4. Logical Organization of APAPS Functions

The controller and ground automation also benefit from having this information. In the spirit of a revised concept for flight plan submission and processing, ATM system components could query for this information for strategic planning purposes, thereby obviating the need for the pilot to engage in the current cumbersome process of flight plan submission. Additionally, the controllers may query the aircraft at will for this type of information if there is no flight plan on file. This would solve a problem that exists today of the controller not knowing the intent of an aircraft that is not monitoring the same frequency. This structure opens the door for thinking about dynamic flight planning to enhance flight flexibility. Some consideration needs to be given to the impact on the controllers and the fate of flight progress strips given these options.

The course building function allows the pilot to specify or modify a course that accomplishes the mission. Ideally, direct course will be the norm, which APAPS can generate accurately given the

mission definition. Other course building options will exist to support the present air route structure. Once again, the course definition can be exchanged with other system components for the purpose of conveying intent.

The APAPS-generated course consists of waypoints connecting straight segments. Smoothed transitions from one leg to the next can be figured out automatically by APAPS using industry-adopted standards. Using this approach, the dependency on three-to-five letter identifiers for waypoints per present standards can be virtually eliminated since the computer representation of a waypoint can be different from the representation used by the pilot and controller. The pilot and controller can use graphical interfaces to display and manipulate the course as necessary. Any names that are assigned to points along the course can be local to the individual making the assignment. This permits the use of meaningful names.

As with the mission definition, the course definition can only be modified with pilot acknowledgment. Modifications to address self-determined conditions or in response to ATM instructions are accommodated in a simple navigation-based and situation-related manner.

The course guidance function uses information from the position fixing function, the course building function, and the navigation database to provide the pilot with information to accurately and easily follow a course. Considering a course as the pilot's stated near-term intent, the guidance function provides information from which the pilot takes action to follow the course. This information could take the form of a traditional course deviation indicator which provides a measure of error from the course. Alternatively, if the positioning function is supported by a system capable of supplying velocity vector data, the course guidance function could return a track-to-steer (TTS) to help the pilot acquire and track the course. The TTS by its nature accounts for wind effects and eliminates ambiguities. For vertical guidance, a target vertical speed (TVS) is provided. The TVS is useful in situations when guidance to a three-dimensional point in space is desired. The guidance information is supplemental since there is no interface with a flight director or autopilot systems (not to say these interfaces are not feasible). The course guidance function is discussed in detail by Flathers, et al [2].

The external data integration function collects and integrates inbound information to be displayed for the pilot, stored in the database, or used by the APAPS functions. Possible outside sources include: other aircraft, ATM facilities, flight service stations, airline operations centers, fixed-base operators, etc.

The navigation database is a resource for the pilot and the APAPS functions and contains the customary navigation data. The following list, though not complete, is representative of the kind of information that may be stored in the database:

- airports
- airspace
- navaids/fixes/waypoints
- routes
- facility information

There is available memory to hold pilot-supplied-data and received communication messages. The pilot may want to store relatively static data such as SAR data or user-defined waypoints. The database also holds mission specific data provided by the pilot such as the destination, route of flight, estimated time of arrival, etc. Pertinent navigation and flight-related data received from outside sources are stored in the database for reference by APAPS functions. The communication system will probably store other data temporarily. The database is accessed by APAPS functions while performing their respective activities. The pilot's access to the database is principally through the APAPS functions.

PROCESS AND INFORMATION FLOW

The functional architecture for APAPS exemplifies how components associated with navigation and communication may be organized to satisfy the information needs of the pilot and other ATM system entities. This section describes the APAPS functional architecture from a process and information flow perspective as opposed to a logical-organization perspective presented in the last section. The process and information flow perspective provides operational insights by illustrating the interaction between the activities in each function.

A brief note on the nomenclature used in this section. The APAPS process is described using the IDEF₀ methodology [2][3][4][5]. IDEF₀ is a graphical language that produces a structured model of the activities and the information and objects which interrelate the activities. The IDEF₀ process description uses activities to represent the components of a process. Activities transform inputs into outputs using controls to define how the transformation will occur. The directional lines represent the flow of events, data, or objects between activities. Information enters an activity from the left; the main product of an activity exits to the right; and controls that effect how the activity is performed enter the top. The arrangement of the activities in a diagram is done for presentation simplicity and does not imply timing or prioritization. Each activity is decomposed hierarchically into more fundamental activities. A new diagram is used for each level of decomposition to maintain readability

The APAPS process description defines the activities required to perform aircraft-based positioning and mission planning independent of aircraft platform and operational location. The viewpoint used for the description is from within the APAPS automation. Therefore, the interfaces outside the construct of APAPS are not represented here. These external interfaces would include the pilot interface and the digital communication system interface.

The most general activity APAPS performs is assisting the pilot in navigation. This is accomplished by providing him with aircraft positioning information and supporting the planning tasks. As shown in Figure 5, the pilot controls the process by specifying operational and system configuration preferences and by making selective choices while interacting with APAPS. Positioning data, course and mission data, data characterizing other aircraft, routing instructions, and flight information services (FIS) data are all viable inputs. These aggregated categories of input data, which will be more specifically defined as the process is decomposed, may come from several different sources. In other words, each category is not tied to a particular source. The inputs are transformed to produce analogous output data, supplying both the pilot and external consumers.

Decomposing the top level activity reveals three principle activities, shown in Figure 6, that correspond loosely to the organization presented in the previous section. The activities are the following:

- Determine Aircraft Position and Velocity
- Manage Mission and Course
- Provide Course Guidance
- Integrate and Process External Data

The core activity APAPS performs is to determine the aircraft position and velocity vector. This activity is performed continuously and, for the most part, autonomously. The position is represented in altitude, latitude, and longitude. The velocity vector is comprised of the aircraft track and ground speed. This information is readily available using GPS.

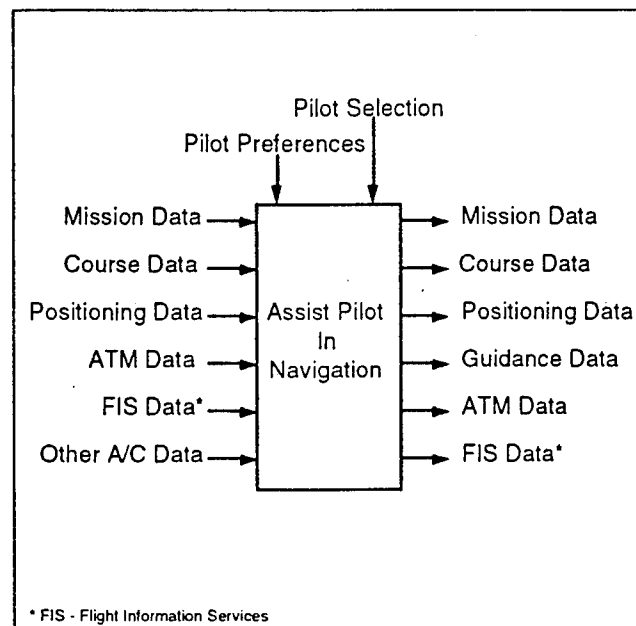


Figure 5. APAPS Top Level Activity Diagram.

The initial operation mode of the aircraft is also determined. The operation mode is either: taxi or airborne. When APAPS is turned on, it determines whether the aircraft is on the ground or in the air and places the APAPS into the appropriate mode. The information presented to the pilot is different for the two modes. For example, if there is a moving map display and the APAPS is in the taxi mode, a map of the airport surface will be displayed at a smaller scale, but in the airborne mode the course along with other navigation-related data will be displayed at a larger scale. Furthermore, the flight mode controls the way the navigation activities are performed. The technique used to provide the pilot with course guidance may be different, as an example.

The initial operation mode of the aircraft is also determined. The operation mode is either: taxi or airborne. When APAPS is turned on, it determines whether the aircraft is on the ground or in the air and places the APAPS into the appropriate mode. The information presented to the pilot is different for the two modes. For example, if there is a moving map display and the APAPS is in the taxi mode, a map of the airport surface will be displayed at a smaller scale, but in the

airborne mode the course along with other navigation-related data will be displayed at a larger scale. Furthermore, the flight mode controls the way the navigation activities are performed. The technique used to provide the pilot with course guidance may be different, as an example.

After APAPS has made the initial mode determination, the pilot makes all subsequent mode changes. When the pilot is ready for take-off, he selects the airborne mode. In addition to reconfiguring APAPS' mode of operation, the pilot's action may be used to notify others of his intent to depart, providing an accurate takeoff time for ATM planning and runway incursion detection systems. This procedure exemplifies how an action taken by the pilot for his benefit can be used to benefit others in the system conveniently. The pilot can also select the taxi mode while airborne to query the navigation database for information about the destination airport facilities. Finally, the pilot selects the taxi mode after clearing the runway after landing to get airport information, taxi guidance, and to possibly notify ATM that he is clear of the active runway.

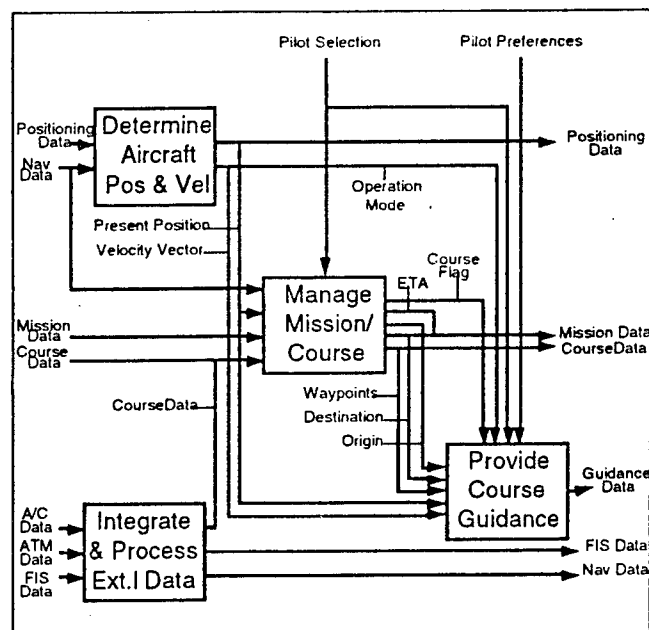


Figure 6. APAPS First Level Activity Diagram: Perform Positioning and Planning.

APAPS provides a convenient means for the pilot to enter mission parameters and define a course of flight. Through the pilot interface the pilot can enter and review mission data, as well as perform "what if" analysis. With communication links with ground facilities, weather data, notices to airmen, airport demand/capacity forecasts, and plethora of other information can be incorporated into the mission planning activity. In the background, APAPS registers the pilot's input with data from the navigation database, does rudimentary consistency checking, and polls ground facilities for relevant data. Without appropriate communication links, APAPS can still notify the pilot of known hazards, such as if the planned course will impinge special use airspaces, terrain, or fixed obstacles.

The Manage Mission and Course activity, shown in Figure 7, is optional to the pilot and its importance depends on the goals of the flight. Flights involving sight-seeing or aerobatics practice, for example, may not warrant much flight planning and thus, the role of APAPS mission planning and course guidance capabilities are needed less. However, the more information the pilot provides APAPS, the more benefit and utility the pilot will receive from doing so. It should also be noted that the amount of information we are talking about is small and is already known by the pilot as a result of his pre-flight planning activities. Immediate benefits to the pilot come from an increase in positional awareness and course guidance cues.

Figure 8 shows the two primary activities for providing the pilot with course guidance. Course guidance cues in the form of a TTS and a TVS are provided by APAPS to the pilot. Utilizing mission, course, position, and velocity vector information, APAPS provides horizontal and vertical course guidance. If there is insufficient information, such as no defined course, guidance is limited by the available information. APAPS assumes the information provided by the pilot corresponds to his stated intent and provides a TTS and TVS that are efficient with respect to the intent. Again, APAPS provides the pilot with supplement course guidance and flight optimization is not explicitly done. If the track of the aircraft deviates significantly from the defined course, the pilot is summoned to provide additional information to APAPS.

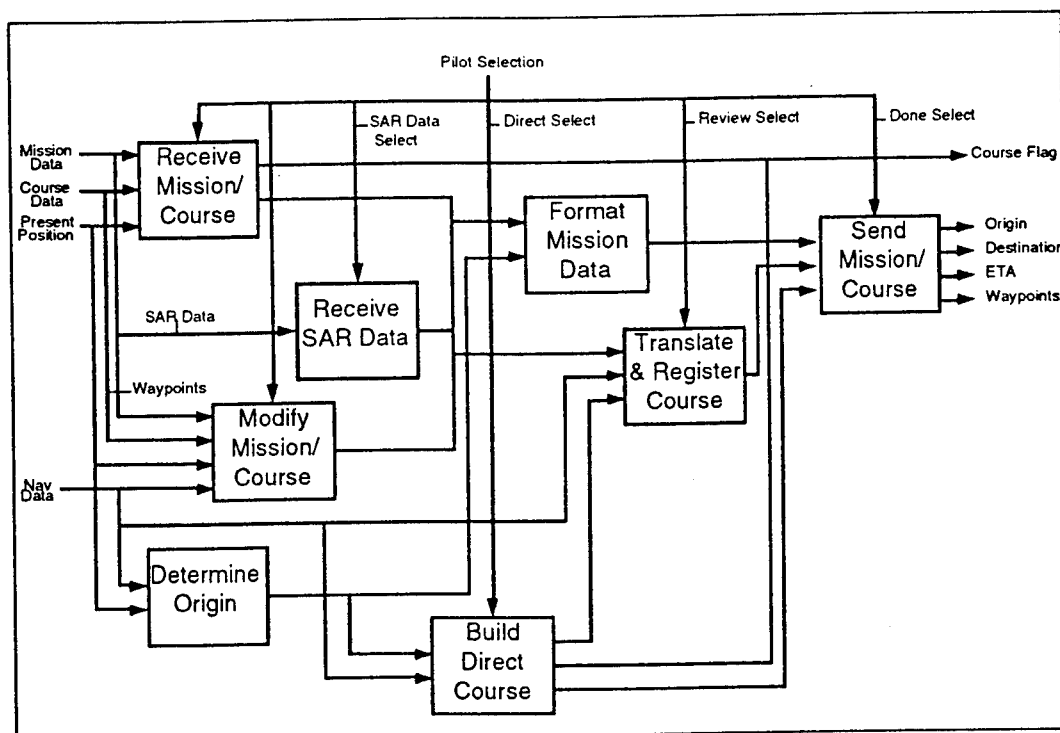


Figure 7. APAPS Third Level Activity Diagram: Manage Mission/Course.

The pilot can also constrain the guidance activity by either commanding a TTS, TVS, or by setting course deviation limits. This feature allows the pilot the flexibility to configure APAPS to be consistent with his mission or flying style.

The Integrate and Process External Data activity is synonymous with the external data integration function described in the pervious section. The role of this activity is to collect externally generated data, perform the necessary transformation required to integrate the data with the internally generated data. Some of the external data will go directly to the pilot interface, while other data will be incorporated with the navigation-related activities. For example, clearances and routing instructions from ATM can be combined with the course defined by the pilot. Definition of this activity is incomplete beyond the basic intent. Much of the work depends on the capabilities of a digital communication system and has, therefore, been deferred.

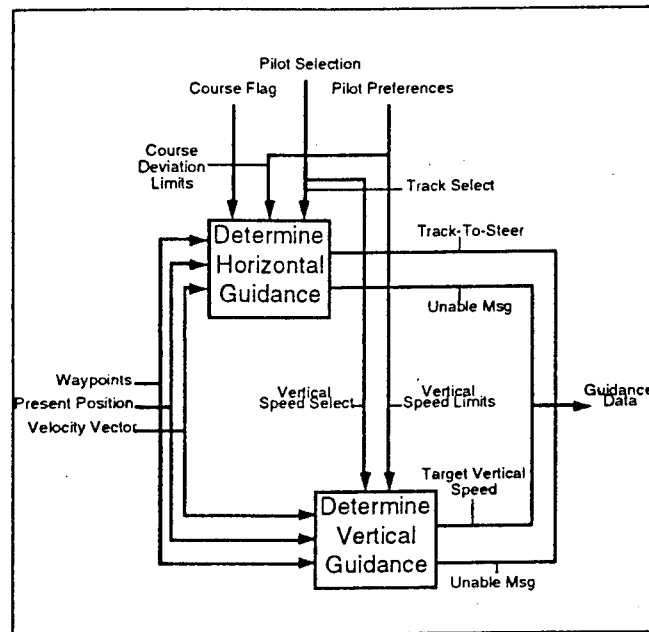


Figure 8. APAPS Third Level Activity Diagram: Provide Course Guidance.

SUMMARY

A general description of the Airborne Positioning and Planning System, or APAPS, has been presented. APAPS is a functional architecture for an airborne system that organizes a basic set of navigation functionality in a manner that is convenient and task compatible with normal piloting activities. The convenience is realized by APAPS' ability to package and communicate mission-related information with external system components. APAPS is task compatible in that information used by APAPS to support the mission are acquired at appropriate times and presented in an intuitive manner. Minimizing mental gymnastics and general work load are important design goals. The APAPS functionality was discussed from both a logical, organizational perspective and a process and information flow perspective. The following functions were described:

- Position Fixing
- Mission Definition

- Course Building
- Course Guidance
- External Data Integration

Coupled with a digital communication system, APAPS will facilitate the integration of airborne and ground-based systems, allowing the exchange of pertinent flight information to become common place. Together, APAPS and digital communication system provide the foundation for achieving the following goals:

- simplifying the process of providing ATM services
- improving the operational flexibility and efficiency of the air traffic system
- incorporating all classes of aero-mobile vehicles into a unified system
- evolving the airborne system into a new operational role

It is anticipated that using currently available technologies, such as GPS; digital displays; data compression techniques; and efficient, low-cost computers, APAPS will provide significant benefit and utility to the pilot that far outweigh the projected cost to equip. Furthermore, working toward the achievement of the above goals will manifest participation in the system by all classes of users and will provide both operational and economic benefits to the participants. At some point the process of change will begin to feed itself.

FUTURE WORK

Presently, a prototype of APAPS is being developed to illustrate the capabilities discussed in this paper. This prototype will be operational in three computing environments:

- on a personal computer for development and portable demonstration
- in MITRE's Advanced Reconfigurable Cockpit for Integration and Experimentation (ARCIE) Laboratory for procedural and human factors evaluations
- in an aircraft for flight testing and end-to-end evaluations

Initially, the guidance functions, the position fixing functions, and the pilot interface will be developed since these represent the core capabilities and provide the most immediate benefit to the pilot. Next, development of the course building and mission definition functions will commence. The data integration function will evolve over time as datalink applications and services are better defined.

In addition to developing the APAPS prototype, work continues to develop operational concepts that illustrate the integration of APAPS-equipped aircraft and ground systems. The motivation is to achieve the goals stated above.

REFERENCES

1. "United Airlines 737-300/500 Training & Reference Manual"

2. Wanke, C. R., G. W. Flathers, II, E. C. Hahn, R. C. Strain, " A Course Guidance Algorithm Using the Aircraft's Velocity Vector," 3rd Joint AIAA/FAA Symposium on General Aviation Systems, Mississippi State University, 24 May 1994.
3. SofTech, Inc., "IDEF0 Author's Guide to Creating Activity Diagrams," SofTech Deliverable no. 7500-13, September 1979.
4. Miller, J., *Living Systems*, McGraw Hill, New York, 1978.
5. Marca, D. A., C. L. McGowan, *SADT: Structured Analysis and Design Technique*, McGraw Hill, 1988.

PILOT AND CONTROLLER PERSPECTIVES ON TCAS II

by

**Prof. Robert F. Ripley and Dr. Margaret Klemm
Department of Aerospace Engineering
Auburn University, Alabama**

**3rd Joint Symposium on General Aviation Systems
May 24 - 25, 1994
Mississippi State University
Starkville, Mississippi**

PILOT AND CONTROLLER PERSPECTIVES ON TCAS II

Prof. Robert F. Ripley and Dr. Margaret Klemm
Auburn University

ABSTRACT

Public Law 100-223, amended by Public Law 101-236, required the installation and operation of TCAS II in commercial airplanes operating in the United States with a passenger capacity of more than 30 seats. Therefore, the operational experience of such equipment in air carriers is of prime significance. In this preliminary work, Professor Ripley and Dr. Klemm examine Aviation Safety Reporting System (ASRS) accounts involving air carrier TCAS II incidents.

Analysis of the data set revealed significant findings. Both pilots and controllers filed ASRS reports on TCAS II incidents. These reports involved a variety of circumstances from near midair collisions to altitude deviations. Most reported incidents occurred below 10,000 feet mean sea level (msl) and during the approach phase. Of particular note is that only 9.5% of the reported incidents occurred in instrument meteorological conditions.

The narratives revealed that TCAS II is an issue of consternation for controllers and an enabling device for pilots. Controllers overwhelmingly cited feelings of helplessness and frustration with actions taken by pilots in response to TCAS II advisories. Chaos and loss of separation, not to mention outright defiance of controller clearances, were often cited in the reports generated by air traffic controllers. Pilots, on the other hand, often saw TCAS II as "saving the day." It provided information on traffic that was not provided by ATC as well as information on how to resolve the conflict. In fact, some pilots appear to be using TCAS II as their own form of ATC.

Although this article provides preliminary information in support of TCAS II, further research over longer time periods is needed to assess the long-term impact of TCAS II implementation on the air traffic control system.

INTRODUCTION

The purpose of this paper is to present an historical perspective, technical information, and pilot/controller operational experiences with the Traffic Alert and Collision Avoidance System (TCAS II). As such, we have undertaken a study of TCAS II incident reports to NASA's Aviation Safety Reporting System for the period of June through August 1993. This study was designed to accomplish several objectives: (1) it would update previous analyses done by Mellone (1992, 1993a, 1993b) of TCAS II incidents, (2) it would provide a better understanding of reported TCAS II incidents—were the initial findings by Mellone just part of early implementation or are they common aspects of TCAS II utilization? and (3) it would provide a more detailed examination of the data to follow up on earlier problem areas identified by Mellone's work.

BACKGROUND

The airline industry has been working through the Air Transport Association since 1955 to find a workable collision avoidance system. It was not until the mid-1970s, however, that research centered upon the use of signals from the Air Traffic Control Radar Beacon System (ATCRBS) airborne transponders as the cooperative element of a collision avoidance system. This technical approach allows a collision avoidance capability on the flightdeck which is independent of the ground system. In 1981, the FAA announced its decision to proceed with the implementation of an aircraft collision avoidance concept called the Traffic Alert and Collision Avoidance System (TCAS). The concept was based upon agency and industry development efforts in the areas of beacon-based collision avoidance systems and air-to-air discrete address communications techniques utilizing Mode S airborne transponder message formats. With the passage of the Airport and Airway Safety and Capacity Expansion Act of 1987, the FAA received the impetus it needed for the rapid development of TCAS II.

HISTORICAL PERSPECTIVE

The Airport and Airway Safety and Capacity Expansion Act of 1987 directed the FAA to require the installation and operation of TCAS II in commercial airplanes operating in the United States that have a passenger capacity of more than 30 seats. Under a provision of the Act, 100% of this fleet was to be equipped with TCAS II by December 30, 1991. On February 10, 1989, the FAA promulgated the Traffic Alert and Collision Avoidance System rules [54 FR 940] requiring installation of TCAS II on civil airplanes, with more than 30 passenger seats, that were to be operated in the United States. Before the final rule was published, however, the Subcommittee on Aviation of the U.S. Senate Committee on Commerce, Science, and Transportation questioned whether the aviation community had the capability to comply with the statutory schedule for TCAS II equipage. The Subcommittee asked the Office of Technology Assessment (OTA) to investigate this question, to identify other important issues raised by the final rule, and to present its findings in a comprehensive report.

The OTA issued its report, "Safer Skies With TCAS," in February 1989. Subsequently, the House Subcommittee on Aviation held a hearing on the report where it received testimony supporting OTA's recommendations that the TCAS II implementation schedule be extended and that there be a relatively large-scale operational evaluation program to assess its impact on the safe and efficient operations of the Air Traffic Control (ATC) system. Based on the OTA report and testimony presented at the hearing and anticipating a statutory revision to extend the time for installing TCAS II, the FAA invited public comment on a modified TCAS II installation schedule and on the need for an operational evaluation. As a result of the OTA recommendation and public comments, the FAA extended the TCAS II installation deadline to December 30, 1993, for air carrier aircraft operated under 14 CFR Parts 121 (Certification and Operations: Domestic Flag, and Supplemental Air Carriers and Commercial Operators of Large Aircraft), 125 (Certification and Operations: Airplanes Having a Seating Capacity of 20 or More Passengers or a Maximum Payload Capacity of 6000 Pounds or More), and 129 (Operations: Foreign Air Carriers and Foreign Operators of U.S. Registered Aircraft Engaged in Common Carriage).

TCAS II TECHNICAL DESCRIPTION

As noted earlier in this paper, TCAS II is a system designed to provide airborne separation assurance or collision avoidance. The system does this by maintaining a surveillance area about the aircraft, through the use of replies received from the other aircraft transponders. The system maintains surveillance within a sphere determined by the transmit power and receiver sensitivity of the TCAS receiver-transmitter (rt). The area in which a threat is imminent depends on the speed and path of the aircraft and the threat aircraft. There is an area defined as TAU within the surveillance area which represents the minimum time the flight crew needs to discern a collision threat and take evasive action. The TCAS receiver-transmitter determines the possibility of collision using algorithms that define the speed and possible path of the aircraft. An algorithm is a set of rules or equations for solving a problem. In this case, the problem is whether the path and speed of two aircraft (or many aircraft) will result in the aircraft passing within a predefined spacing of each other. If the answer to this problem is yes, the TCAS receiver-transmitter issues an advisory to the flight crew.

The system is capable of providing resolution advisories to a pilot, allowing the pilot to avoid other aircraft equipped with an ATCRBS, or Mode S altitude reporting transponder and TCAS. The system will handle aircraft densities of 0.3 transponder-equipped aircraft per square nautical mile.

TCAS II consists of a TCAS receiver-transmitter, TCAS antennas, Mode S Transponder, L-band antennas, a control panel, and displays. The TCAS II system provides vertical corrective or preventive advisories. TCAS II provides bearing, range, and altitude information of aircraft within the surveillance area. Within the surveillance area, the system tracks and displays aircraft responding to the TCAS interrogations. The system will provide two different resolution advisories; corrective and preventive. The corrective advisory is a resolution advisory, advising the flight crew to alter the current flight path, in a vertical plane. A prevention advisory is a resolution advisory that advises the flight crew to avoid making certain maneuvers, in the vertical plane, to prevent conflict from occurring. A traffic display informs of an aircraft's presence within the surveillance area. The TCAS receiver-transmitter along with a Mode S transponder, appropriate displays, and control panel coordinates the collision avoidance and resolution advisory functions for the flight crew.

The function of the system is to interrogate ATCRBS/Mode S transponders on other aircraft and to determine from the replies, the range, altitude, approximate bearing to the aircraft. The system then computes the collision hazard each aircraft presents. The TCAS receiver-transmitter determines whether any of the ATCRBS/Mode S transponder-equipped aircraft constitute a collision threat, and coordinates its intentions with other TCAS-equipped aircraft through the Mode S transponder.

Collision avoidance resolution advisories may be displayed to the flight crew on one or more dedicated displays, or other flight instruments. All TCAS data is provided to the display via 2-wire digital data per ARINC specification 429. Altitude data is provided to the TCAS unit through the Mode S transponder.

HOW TCAS RESOLVES ENCOUNTERS

The TCAS receiver-transmitter transmits interrogations at a frequency of 1030 MHz (± 0.01 MHz) to the transponder equipped aircraft in the vicinity to generate transponder replies that the signal processing circuits of the TCAS will decode to identify the threat aircraft. Once each second the TCAS transmits an interrogation for all ATCRBS and Mode S transponder-equipped aircraft. This one-second period is referred to as the surveillance update period for all traffic within range of the TCAS equipped aircraft. The transmission interval is jittered to avoid chance synchronizations with ground-based transmitters or other Mode S equipped aircraft. The transmission time will be jittered between 0.95 and 1.05 seconds. It is not necessary to intentionally jitter Mode S interrogations because of the inherently random nature of the Mode S interrogation process.

ATCRBS interrogations from TCAS equipment employ the Mode C only All-Call three pulse format. Refer to Figure 1. Pulse S1 is of lower amplitude than pulse P1 and the two form a transponder suppression pair with a pulse separation of two micro seconds. Only transponders that receive P1 above a noise level of about S1 pulse amplitude will respond to the TCAS II interrogation. The P1-P3 pulse spacing is the normal 21 microseconds for a mode C altitude reporting interrogation. Pulse P4 is part of the format in order to suppress airborne Mode S transponders, which also would provide Mode S replies if not suppressed. The four pulse format group of Figure 1 are repeated at increasing power levels over an approximately 20-db range to generate a whisper-shout sequence. When an aircraft transponder is interrogated by the whisper-shout sequence, the transponder will reply if the amplitude of S1 is below the noise level and P1 is received at a greater level than the transponder minimum trigger level (MTL).

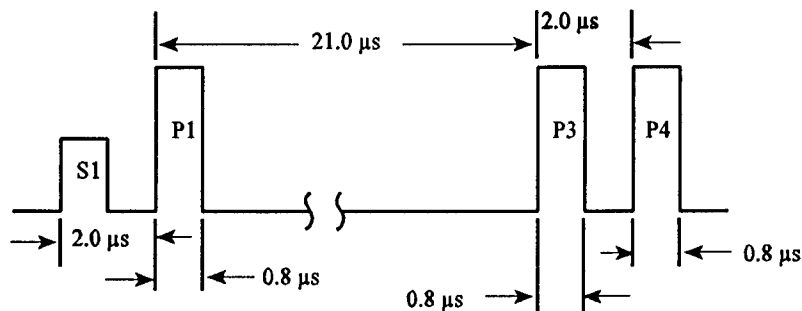


FIGURE 1. MODE C ONLY ALL-CALL.

Refer to the simplified block diagram of Figure 2. The block diagram shows the received signals entering the TCAS receiver-transmitter through a beam steering network and a diplexer. The received signal is then applied to the signal processing circuits that remove the altitude and aircraft identification information from the received signal. This information is then sent to the CPU for use in the threat algorithms stored in the program memory. The TCAS system uses the replies of transponder-equipped aircraft to determine the potential threat of the aircraft. The TCAS system is capable of determining range, bearing to the intruder and altitude of the intruder, if the intruder transponder is reporting altitude, from each reply.

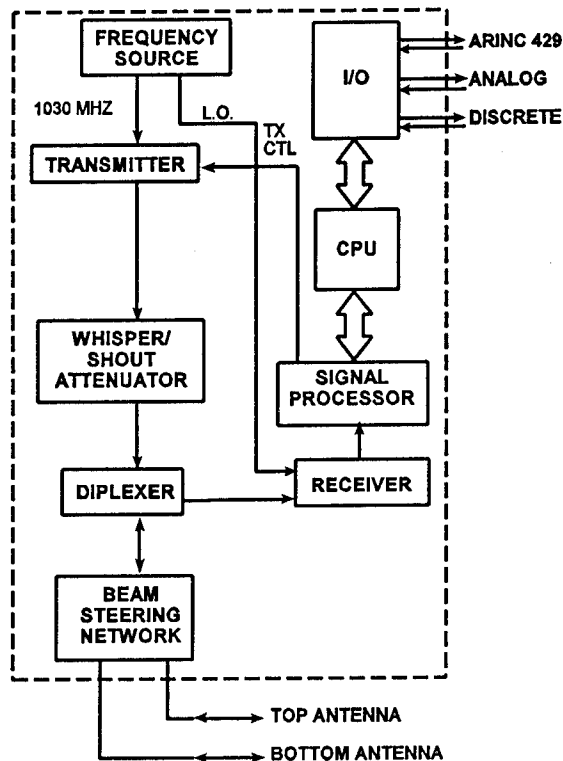


FIGURE 2. TCAS RECEIVER-TRANSMITTER BLOCK DIAGRAM.

The TCAS receiver-transmitter uses several replies from the intruder aircraft to determine the altitude rate and range rate of the intruder aircraft. In other words, the TCAS receiver-transmitter uses the reported altitudes to determine how fast the intruder aircraft is climbing or descending and uses the elapsed time between transmission and reply to determine whether the aircraft is approaching or leaving the surveillance area. The TCAS receiver-transmitter also uses the changing bearing positions to determine a probable flight path for the intruder.

The TCAS receiver-transmitter contains the algorithms for collision avoidance in TCAS II. These algorithms include tracking algorithms for intruder aircraft, threat detector algorithms, generating traffic advisory algorithms, and the algorithms for own aircraft altitude and sensitivity levels. The receiver-transmitter also handles the Mode S data link transmissions that are TCAS related. The Mode S data link capabilities are only required when two TCAS equipped aircraft approach each other, in order to coordinate the maneuvers of each aircraft.

From the transponder replies of intruder aircraft and, if available, the TCAS Mode S data link messages, the TCAS receiver-transmitter determines if the flight path and profile of the intruder aircraft will result in a conflict with its own aircraft's flight. Based on the TCAS own aircraft profile, the receiver transmitter determines the appropriate resolution advisory.

As part of the TCAS II development program the FAA and various airlines conducted in-flight evaluations, as recommended by the OTA and future industry users. This evaluation process will be discussed in the next section.

AIRLINE EVALUATION

In order to permit the aviation community to evaluate TCAS II prior to fleet-wide implementation, extensive in-service evaluations were conducted. The initial evaluation was conducted by Piedmont Airlines in 1982. Flying a TCAS II prototype unit manufactured by Dalmo Victor, approximately 900 hours of recorded data were obtained for analysis of the frequency and suitability of threat advisories (TAs) and resolution advisories (RAs). TCAS outputs were not displayed to the pilots.

In 1987 Piedmont flew an upgraded version of the Dalmo Victor equipment for 800 hours. During this period the TCAS II displays were operating in the cockpit of a B-727 aircraft, and trained flight crews utilized the system in normal revenue service. Pilot and guest observer comments on TCAS operation were obtained in addition to the TCAS recorder data.

In support of the FAA/Industry Limited Installation Program (LIP) Bendix-King and Honeywell Inc. built and tested TCAS II units in accordance with the TCAS II Minimum Operation Performance Standards (MOPS). Engineering flight tests using FAA aircraft as well as airline and corporate aircraft were conducted prior to FAA certification of the TCAS II installations on the airline aircraft used in the LIP. Bendix-King TCAS II units were evaluated on a B-737 and a DC-8 aircraft operated by United Airlines from January through July 1988. Northwest Airlines operated Honeywell TCAS II units on two MD-80 aircraft from September 1988 through March 1989. Over 2000 TCAS II operating hours were logged during the United flights with approximately 2500 hours from the Northwest evaluation.

The experience provided by the airline evaluations resulted in a number of enhancements to the TCAS II logic, improved test procedures and a more detailed understanding of TCAS certification and operational requirements. The most important information obtained, however, was the nearly unanimous conclusion by the participating pilots and airlines that the TCAS II concept was both safe and operationally effective.

RECENT DEVELOPMENTS

On January 5, 1994, an Airworthiness Directive (AD) was issued that requires all TCAS II manufacturers and users to upgrade TCAS II processors with logic version 6.04 A (v6.04A) by December 31, 1994. The v6.04A software contains changes that will increase the operational compatibility of TCAS and will reduce the frequency of Resolution Advisories (RAs) for specific encounters. The logic changes were developed as a direct result of input received from pilots and controllers during the TCAS Transition Program (TTP).

DATA ANALYSIS

In examining the data set, an overall picture of TCAS II incidents will be presented and then more specific areas will be examined. The first aspect of note in this data set is that almost as many reports came from controllers as from flight crews (see Figure 3). This is and is not surprising. Mellone (1993b) had reported that TCAS II incidents accounted for more controller reports on a single topic

than any other since the controller's strike of 1981. Even so, he found that most incident reports were made by flight crews for the period he examined. Given the large number of controllers filing incident reports in this data set, we may wonder if this is atypical or a new trend. It is also interesting to note that 46 percent of all controller reports came from O'Hare, one of the world's busiest airspaces.

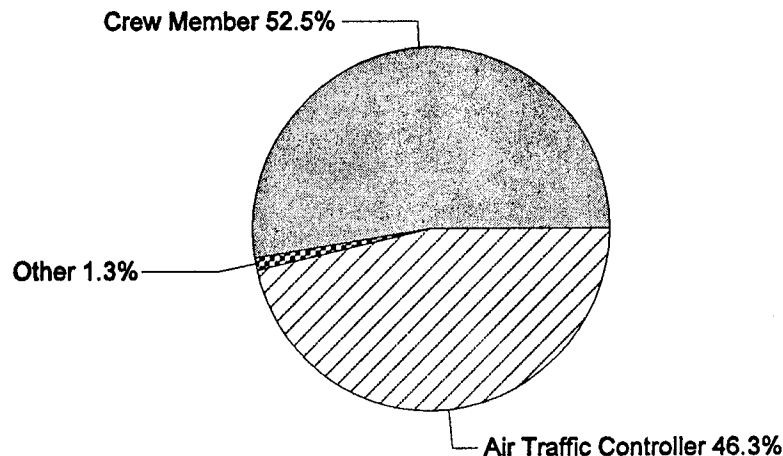


FIGURE 3. INCIDENT REPORTER

Figure 4 shows the specific function of each reporter, further highlighting who is making most of the incident reports. Captains, by far, make the most reports (35%) followed by their fellow crew members (first and second officers, respectively). Among controllers, TRACON controllers account for the majority of incident reports followed by ARTCC controllers. This is consistent with a later finding for this data set that a large percentage of incidents occur below 10,000 feet MSL (see Figures 6 and 7) and during the approach phase (see Figure 5).¹

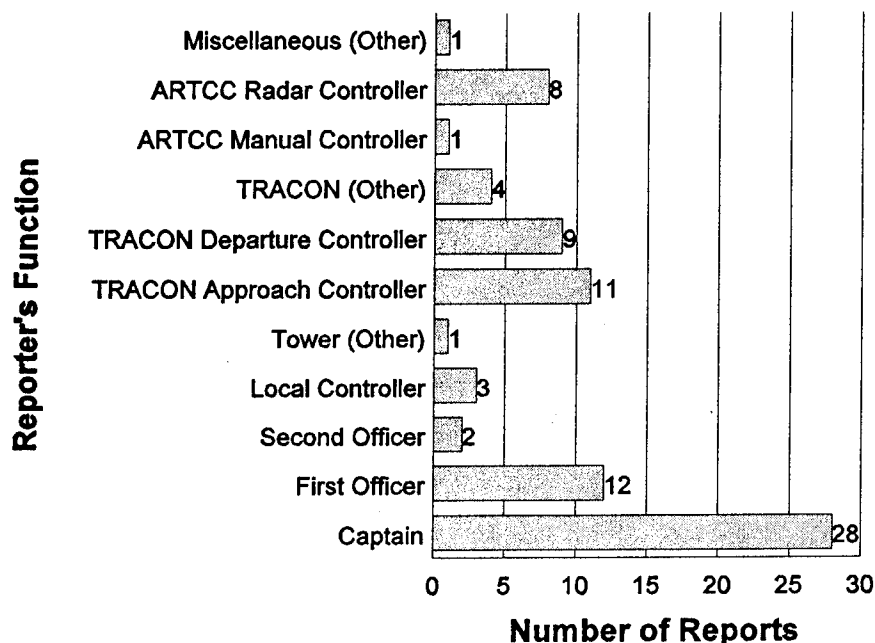


FIGURE 4. INCIDENT REPORTER'S FUNCTION

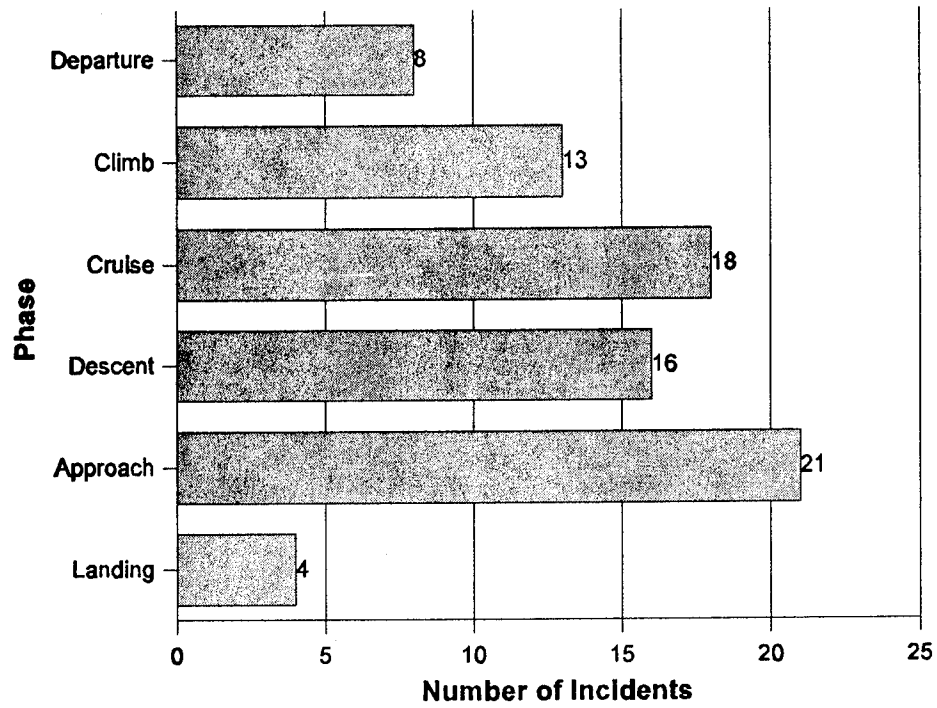


FIGURE 5. PHASE OF FLIGHT.

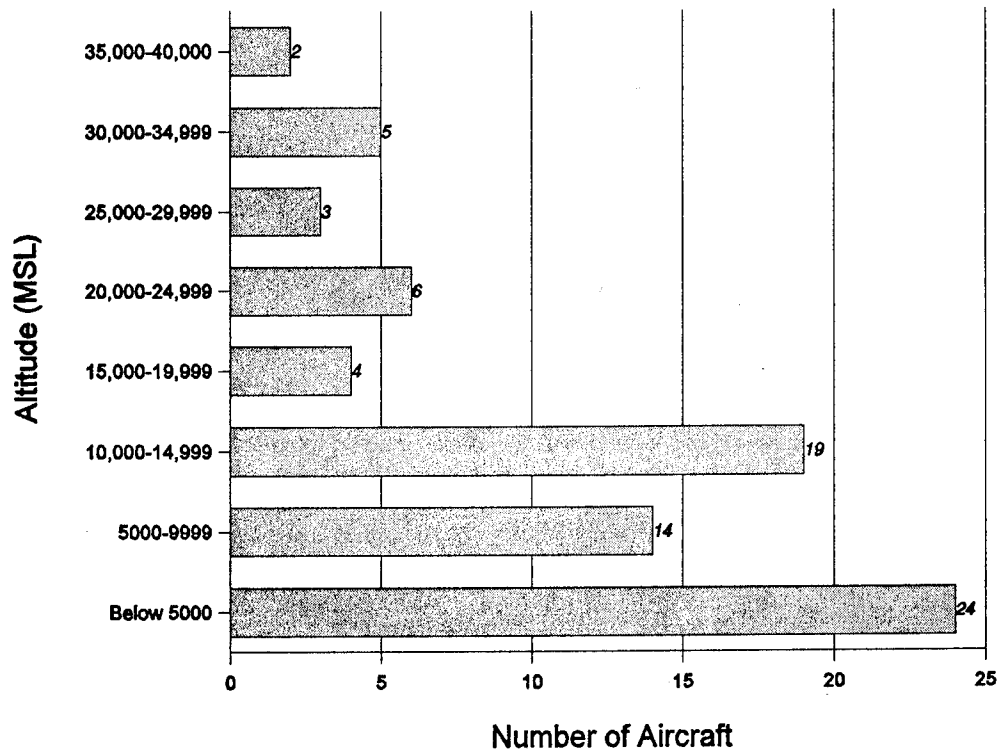


FIGURE 6. TCAS AIRCRAFT ALTITUDE.

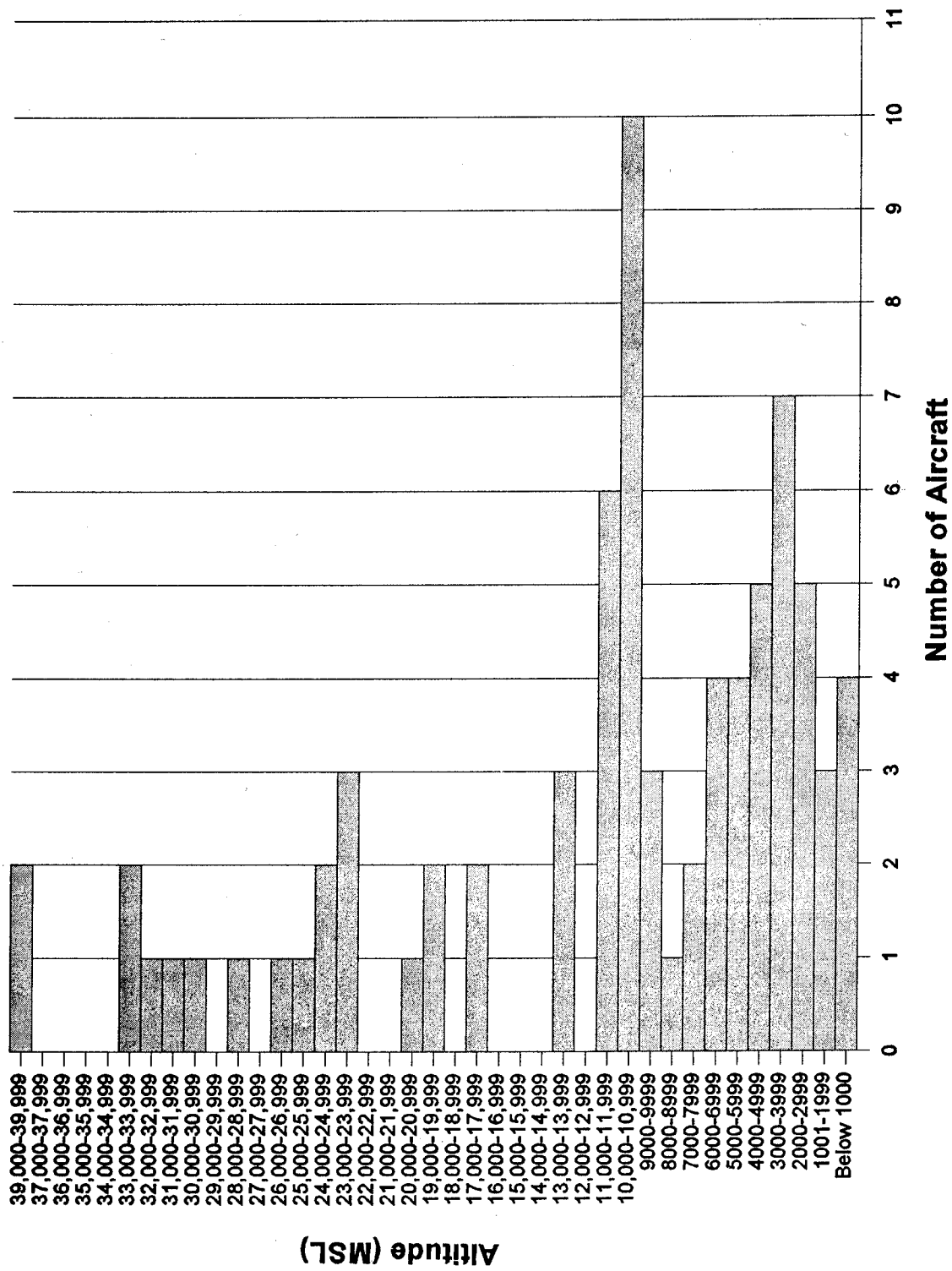


FIGURE 7. TCAS AIRCRAFT ALTITUDE.

The data set was examined with respect to TCAS II incidents reported during various phases of flight (see Figure 5). The categories here are mutually exclusive in order to emphasize the operational differences between phases (e.g., approach with its higher pilot workload and terminal environment with higher controller workload).² As noted above, the most TCAS II incidents were reported during the approach phase followed by cruise. Climb and descent were the next most prevalent phases. Landing and departure phases had the least frequent reports and from the narratives appeared to often be the result of improper spacing (e.g., fast aircraft cleared after slower aircraft) or aircraft mixing problem (e.g., helicopter patterns near short final of an air carrier).

As would be expected given the large number of incident reports occurring during the approach phase, aircraft altitudes during the incidents were primarily below 15,000 feet MSL (71%) with 30 percent occurring below 5,000 MSL and 48 percent occurring below 10,000 feet MSL (see Figure 6). Indeed, 13 percent of all incidents in the data set occurred at 10,000 feet MSL (see Figure 7).

Interestingly, three-fourths (73%) of all TCAS II incidents occurred during visual meteorological conditions (See Figure 8). This raises the question of whether flight crews are willing to follow TCAS II RAs only when visual sighting of the conflicting aircraft is possible or whether there are simply more possible conflicting targets during visual conditions (e.g., small aircraft).

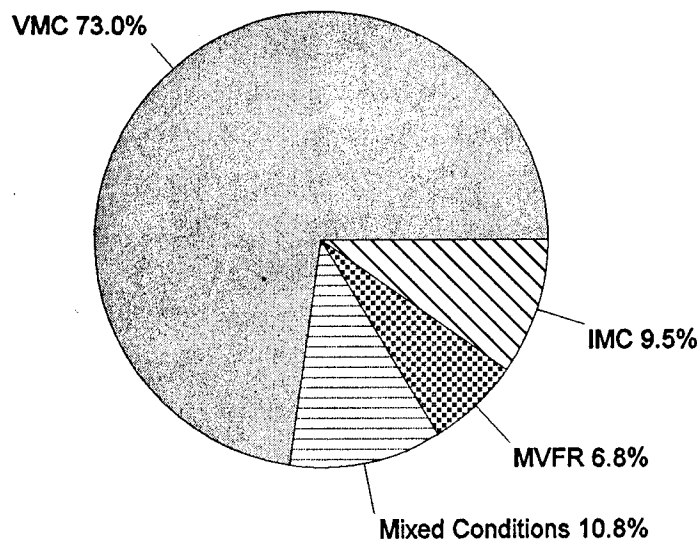


FIGURE 8. WEATHER CONDITIONS

TCAS II incidents in the sample occurred throughout the system. Figure 9 notes the eight states with the highest frequency of TCAS II incident reports. Over one-half of all states had no incidents reported while the others had 1 or 2 incidents reported.⁴ This should not be surprising, however, given the voluntary nature of ASRS.⁵ Further examination of the data found O'Hare with the most incident reports (17, all by controllers!). New York TRACON (N90) was second with 5 and Atlanta third with 4 reports. Washington (ZDC), New York (ZNY), and Jacksonville (ZJX) air route traffic control centers had the most incident reports. Other ATC facilities had 1 or 2 incidents reported in their airspace.⁶ This raises a question for future examination: are TCAS II incidents becoming more widespread or is the finding from this snapshot in time merely atypical?

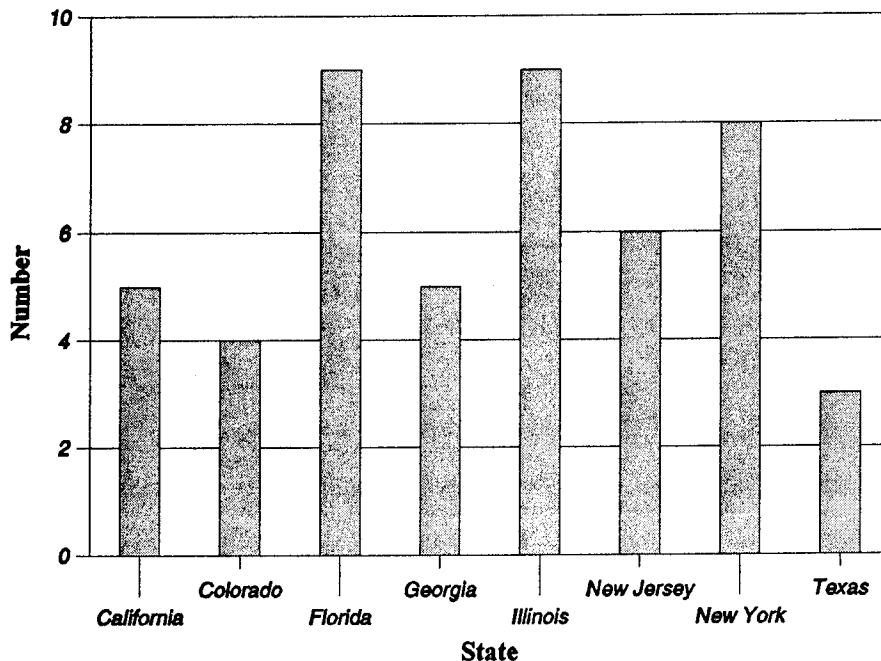


FIGURE 9. INCIDENTS BY STATE.

The above is basically descriptive information concerning the reporting of TCAS II incidents. And while it is important in and of itself, of even greater significance is the operational environment of TCAS II. A variety of information is available from the incident narratives which gives us valuable insight into the operation of TCAS II, pilot and controller attitudes on TCASII, and the ultimate, if subjective, question of whether TCAS II is of value.

It has been said that the objective of TCAS II is to aid the pilot in situational awareness and not to be used as an alternative to ATC. Pilots cannot use TCAS II as their own form of air traffic control. In spite of this, pilots are using TCAS II advisories and resolutions in ways not envisioned by TCAS II designers. Looking at the data, we see that the first report of traffic conflicts come from TCAS II 80 percent of the time; 19 percent of the time ATC alerts the flight crew of potential traffic conflict while the flight crew sees traffic (visually) only 1 percent of the time (see Figure 10). Flight crews are evidently relying heavily on both TCAS II and ATC for traffic advisories even though the majority of these incidents occur in visual meteorological conditions requiring see and avoid. Of further note is that in 43 percent of the incidents, the flight crew never acquires the traffic visually (see Figure 11).

Indeed, a common theme emerging from the narratives is the desire for more ATC information on traffic:

- Tower should have notified us of the traffic sooner. ACN #249076⁷
- His (the controller's) response was to issue a traffic advisory long after the fact with no explanation nor apparent concern for the situation. ACN #248869

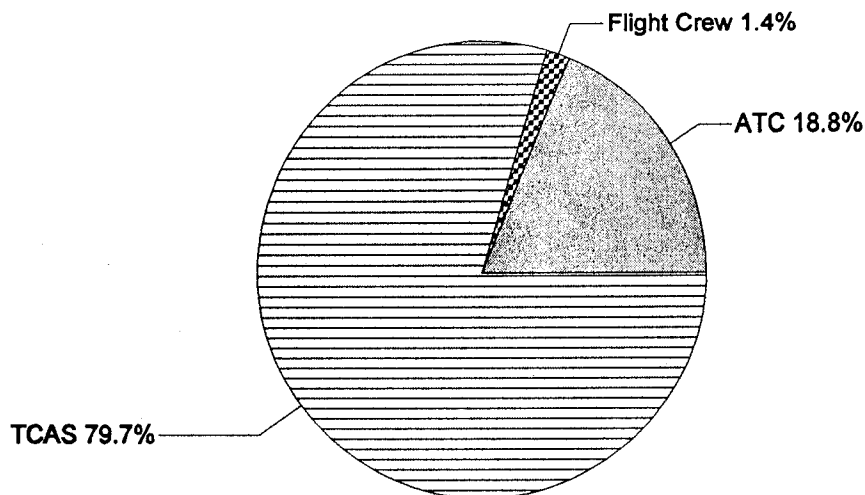


FIGURE 10. FIRST REPORT OF TRAFFIC CONFLICT.

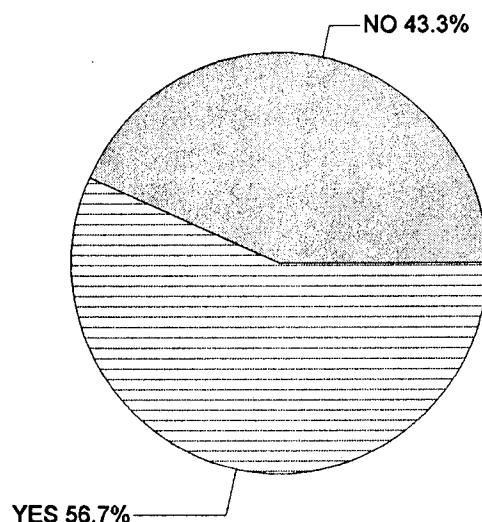


FIGURE 11. FLIGHT CREW SIGHTING OF TRAFFIC.

- No evasive action given by ATC or notification by ATC. ACN #249241
- The situation was well under control a great deal because of TCAS II since we had no traffic pointed out from the controllers. The controller should have advised us in regards to traffic. ACN #246956

In spite of the pilot's perceptions, ATC did advise the flight crews of traffic although the advisories were fairly evenly divided before and after the TCAS II advisory (see Figure 12). Forty percent of the time, ATC provided no traffic advisories to the flight crews.

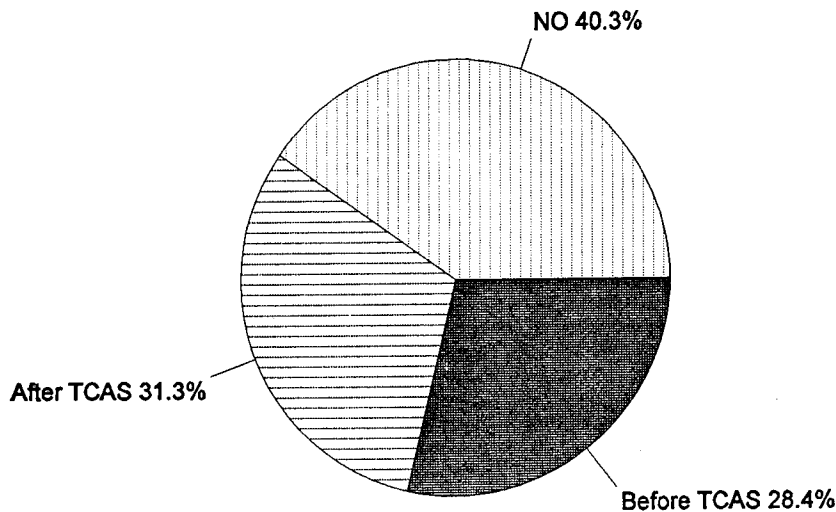


FIGURE 12. ATC ADVISORY ON TRAFFIC.

Further examination of the narratives might lead one to believe that some pilots are relying on TCAS II to provide information they expect but is not forthcoming from ATC:

- I was watching the TCAS II as the Captain got back in the loop. ACN #246651
- I know we're not supposed to use TCAS II for our own ATC, but what do you do when you feel you have information that points to a potential conflict? ACN #245675
- The pilot responded that left turn looked good on his TCAS II...The pilot came up with a plan based on an inadequate radar display. ACN #247727

It appears that some pilots are using TCAS II as a supplement, if not actual replacement, for ATC. Fortunately, this appears to be the exception at the moment. Most frequently, flight crews simply follow the RA and change altitude (see Figure 14). Less frequently, they acquire visual contact or query ATC about potential traffic conflict (see Figure 15). Other less common maneuvers include going around or changing heading. Sometimes, pilots will even ignore an ATC instruction and follow a contradictory RA (see Figure 16). One controller lamented on precisely this matter.

- I do not understand how pilots can just disregard ATC instructions, especially in a terminal environment. ACN #247315.

With regard to altitude deviations, original designers of TCAS II anticipated altitude changes of 200 to 300 feet. In this data set, however, the range of altitude deviation was from 300 to 2400 feet with an average deviation of 811 feet.⁸ As such, the flight crews were deviating 500 or more feet, creating a potential loss of separation and higher controller workload (see Figure 13).

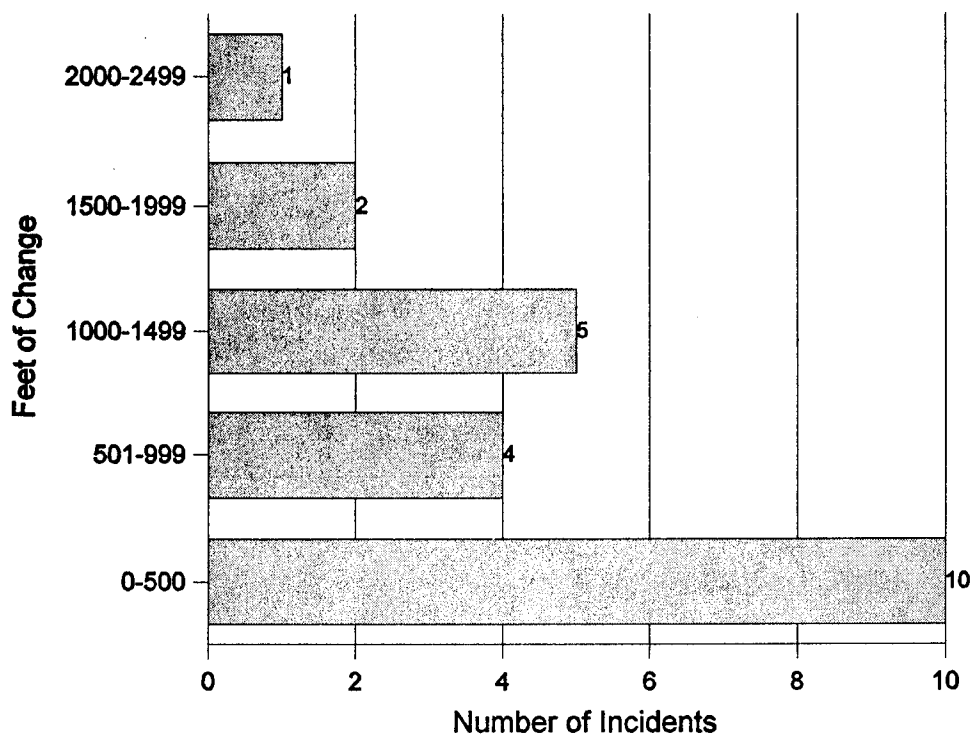


FIGURE 13. ALTITUDE DEVIATION.

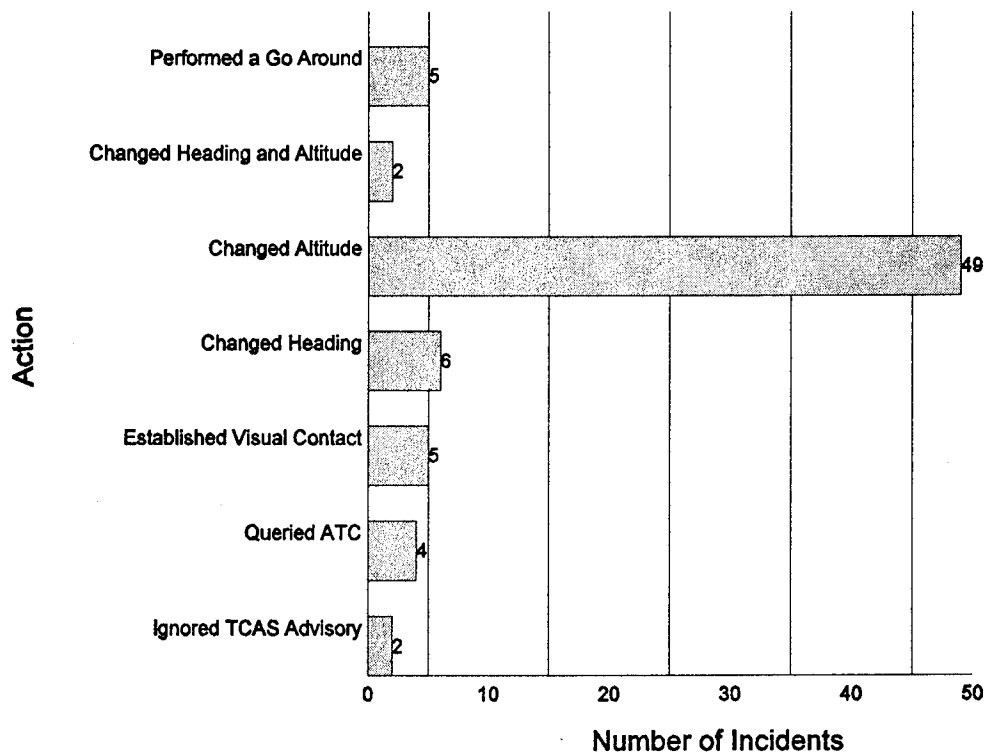


FIGURE 14. PILOT'S USE OF TCAS ADVISORY.

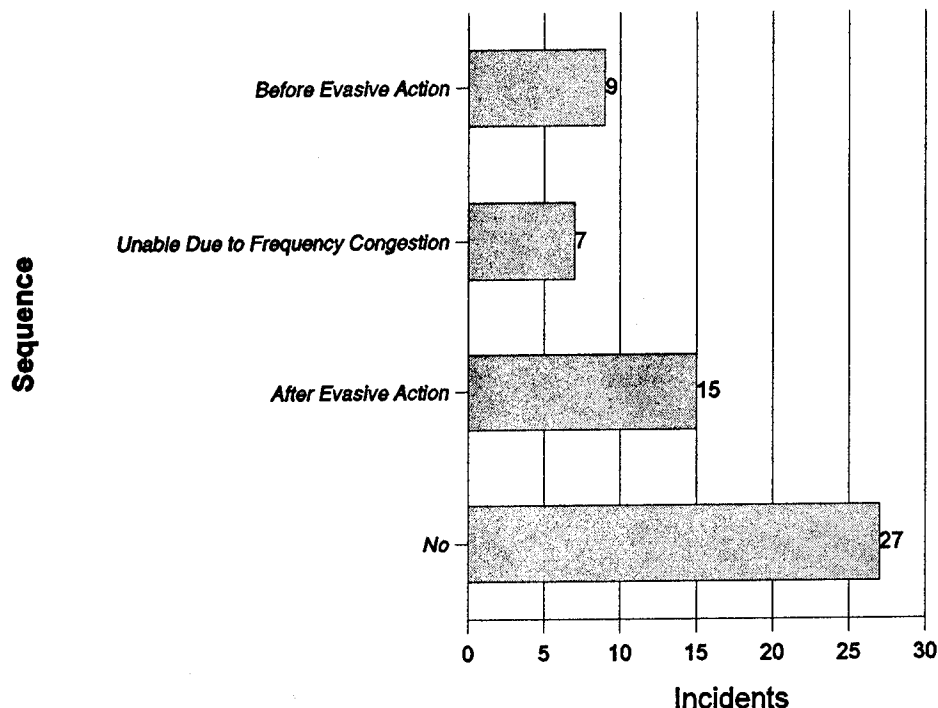


FIGURE 15. FLIGHT CREW QUERIES ATC ABOUT TRAFFIC.

- Aircraft X descended without a clearance to 9000 feet. This could have put Aircraft X head-on with opposite direction traffic. ACN #244912
- Aircraft X climbed to FL257 without advising ATC. The result was 15 minutes of a nearly unmanageable sector and the near loss of standard separation. ACN #245982.
- Aircraft X climbed to miss traffic. Just luck that standard separation was not lost. ACN #246538
- This particular controller states that with TCAS II equipped airplanes, he builds in an extra 1000 feet of separation when able, simply to avoid unnecessary RAs. ACN #247000

Of perhaps equal concern to controllers as the actual altitude deviation, is the lack of reporting by the flight crews. Figures 15 and 16 illustrate the communication process (or lack thereof) during TCAS II advisories and subsequent actions. In Figure 15 we can see that flight crews did not query ATC about traffic in 34 percent of the cases and were unable to do so in 9 percent of the cases. In only 11 percent of the cases did the flight crews ask ATC about the potential traffic conflict before taking evasive action. And in 19 percent of the cases, the flight crews notified ATC after the fact.

Figure 16 provides even greater detail about the communication process. Commonly, flight crews follow TCAS II RAs and deviate without communicating with ATC. No wonder controllers feel taken out of the loop. They are often "left helpless to get out of a jam that you didn't create" (ACN #248849).

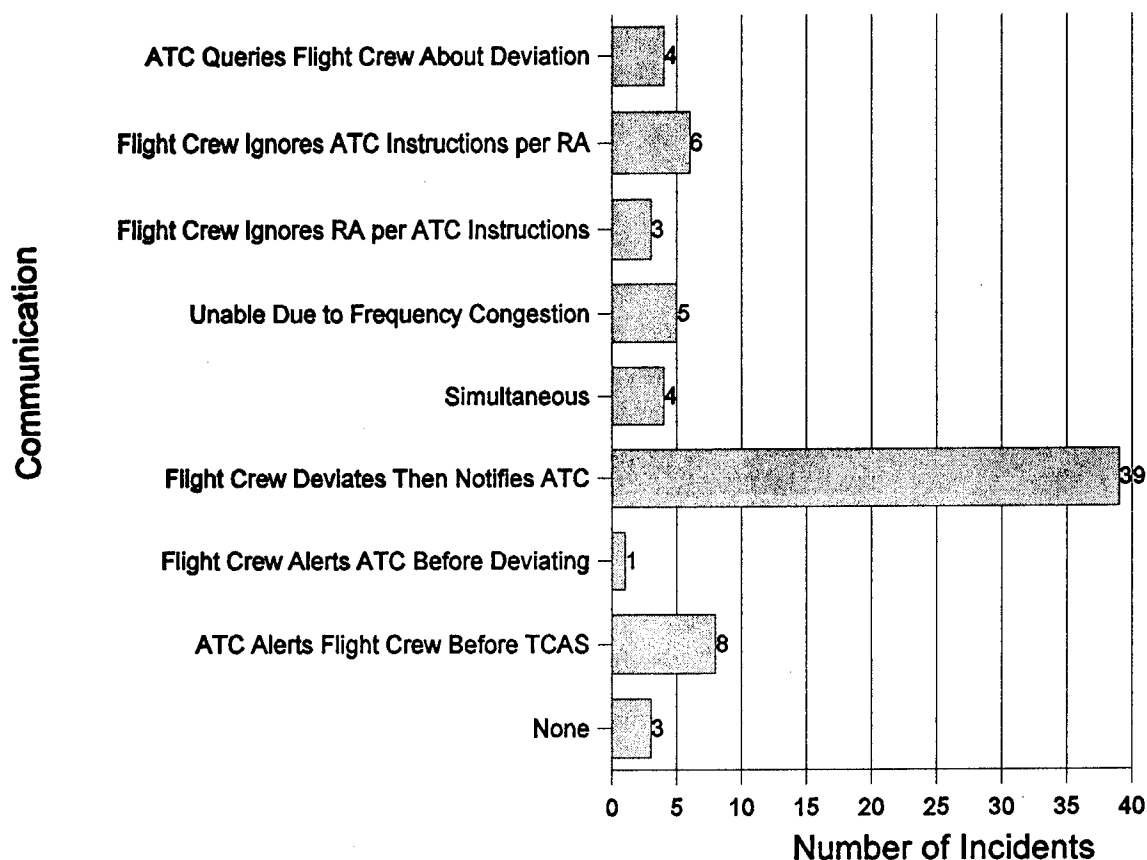


FIGURE 16. COMMUNICATION SEQUENCE REGARDING TCAS ADVISORIES.

ASRS data is coded into a variety of anomaly definitions as short cut descriptions of the events (see appendix). Using this coding scheme, Figure 17 shows the distribution of incidents. The most common anomaly is a conflict not qualifying as a near midair collision. This is followed by non-adherence to ATC clearance or published procedures, altitude deviations and near midair collisions.

Given the nature of anomalies present in the TCAS II incidents, it is not surprising that some sort of consequence should attach to the incidents. Figure 18 shows that of all reported incidents, 40 percent had some consequences (either flight crew or ATC review) and in 20 percent of all cases, a FAA follow-up investigation occurred. Of course, given the nature of ASRS reporting system and its availability as protection from violations (FAR 91.25), one can hardly be surprised at the seriousness of the consequences.

In this data set, 11 percent of the cases were "false" advisories where no traffic was present or TCAS II responded to a ghost target. From the controller's comments, it is evident that they feel TCAS II provides pilots with false TAs and RAs when they (controllers) have provided legally required separation. This further aggravates the controllers already poor opinion of TCAS II.

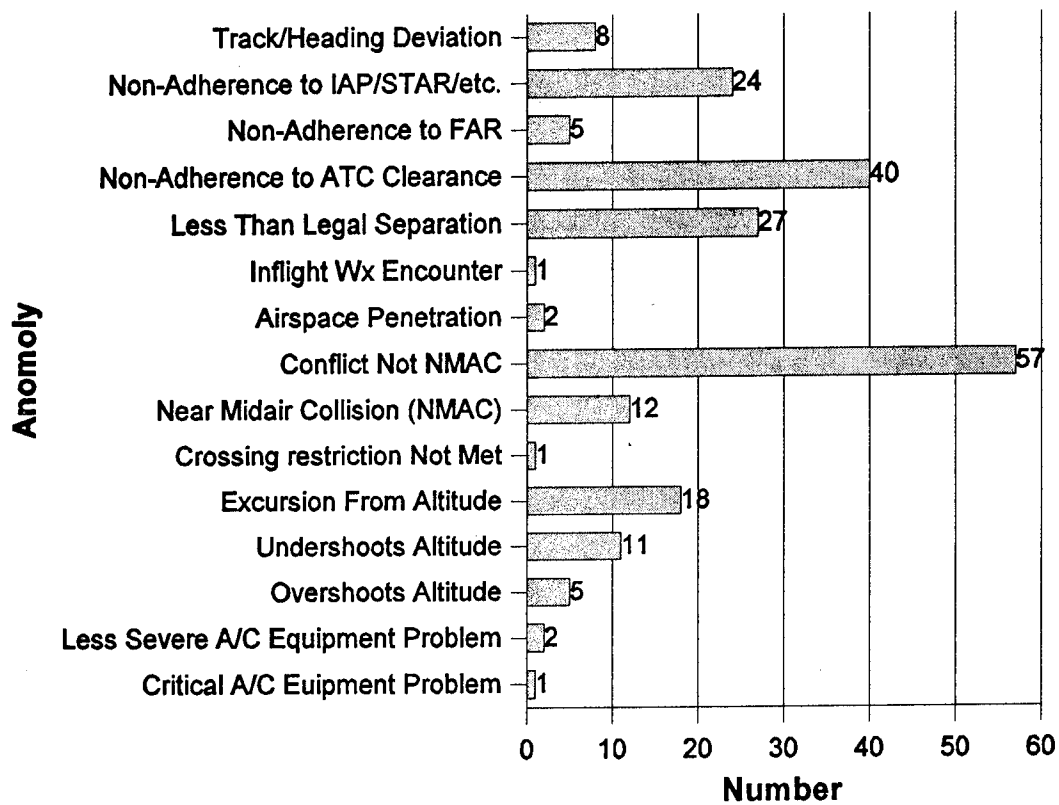


FIGURE 17. ANOMALY DISTRIBUTION.

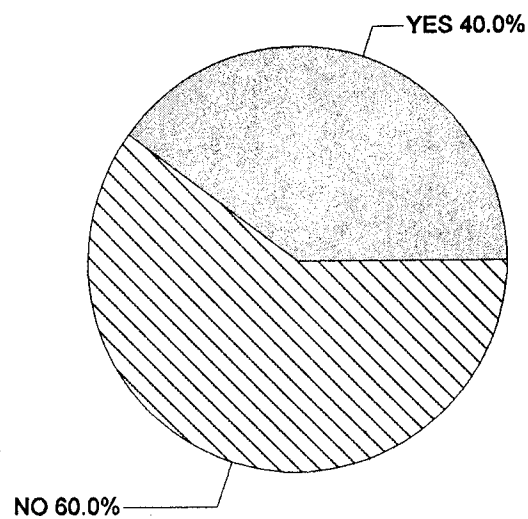


FIGURE 18. INCIDENT CONSEQUENCE.

- (Pilot) said that it must be his equipment because TA followed him up. The closest traffic was 6 miles in front and 7 miles behind. ACN #247002
- TCAS II alerts are generated by ships generally located in the naval base Little Creek Harbor. It's quite annoying. ACN #245134
- No traffic? No need for maneuver! ACN # 247011
- I advised him there wasn't any traffic. ACN #249813
- I already had desired spacing. ACN #246998
- There was no reason for the aircraft to climb. The traffic was at a verified altitude and in no way was a factor. ACN #247003
- There was no, repeat no, aircraft known or unknown within 4 miles in any direction. ACN #247008
- This appears to be a non valid RA because the VFR separation required by ATC is 500 feet vertical. ACN #247009
- Closest aircraft was VFR at 9 o'clock, 4 miles at 1600 feet. ACN #247006
- The only traffic in the area was the previous arrival 3 miles ahead and a departure 3 southeast of O'Hare climbing out of 3500 feet. No other targets in the area. This seems to be yet another example of TCAS II acting on a ghost target. ACN #247013
- There was no traffic. ACN #247004

Popular sentiment has controllers opposed to TCAS II and pilots in favor. This data confirms the popular view; controllers overwhelmingly have negative attitudes towards TCAS II (see Figure 19). Further, controllers are more likely to include comments in their incident reports than are flight crew members.

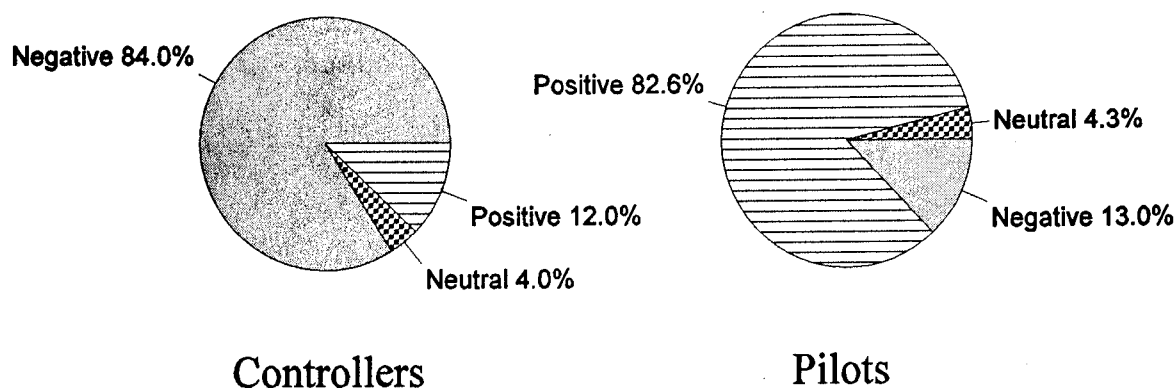


FIGURE 19. ATTITUDE ON TCAS—CONTROLLERS V. PILOTS.

- I believe TCAS II caused the conflict. There was no other traffic in the vicinity. TCAS II should be modified to include assigned altitude so aircraft will not take evasive action from other aircraft ATC has already provided separation from. ACN # 248328

- I hope that the visual acquisition of his traffic changed the way at least 2 pilots look at their TCAS II. ACN #247727

- Aircraft X advised he was receiving a TCAS II RA and was responding to it. The climb Aircraft X did was unnecessary and excessive. ACN #247005

- Just luck that standard separation was not lost. ACN #246538

- I feel this is very unsafe. ACN #245875

- TCAS II destroys pilot's confidence in ATC. ACN #245716

- I will not trust TCAS II until the bugs are worked out. ACN #244910

The flight crews were overwhelmingly positive in their comments on TCAS II:

- TCAS II worked as advertised, very effectively warning us of the conflict. ACN # 249076

- Throughout the event, TCAS II operated correctly, displaying in sequence, all of the alerts as well as commands. ACN #248769

- Thanks to TCAS II. It performed well. ACN #247191

- Without TCAS II, a midair collision would have been all but certain. ACN # 247036

- The situation was well under control a great deal because of TCAS II. ACN # 246956

- TCAS II prevented a near miss. It was nice to have TCAS II in this situation. ACN 246423

- TCAS II probably prevented the incident from developing into a NMAC. ACN #246229

- TCAS II clearly saved the day. ACN #245445

Very few negative comments were included in the flight crew's reports:

- I think the TCAS II needs to be modified so you don't get continuous RAs with no climb or descent indicated. ACN #248831

- TCAS II works, but can be a disaster. ACN #246004

From the narratives, it appears that TCAS II is seen by the flight crews as an enabling device, giving them more control over their environment. It provides them with time critical information often not

provided by ATC. In fact, pilots are more than willing to follow the instructions from TCAS II, without consulting ATC or even in some cases, in spite of ATC instructions. Controllers, on the other hand, see TCAS II as usurping their control authority and often as creating conflicts.

CONCLUSION

Finally, using a subjective evaluation of the narratives, we coded whether TCAS II helped or caused problems. Figure 20 shows that in 70 percent of the cases TCAS II actually helped resolve a conflict situation. In the other 30 percent of the cases, TCAS II caused such problems as increased controller workload, deviations from ATC clearances or at worst, actual loss of separation. To paraphrase one of the pilot's statements, an overall assessment of TCAS II could be that it works but without further modification of the system, it has the potential to be a "disaster."

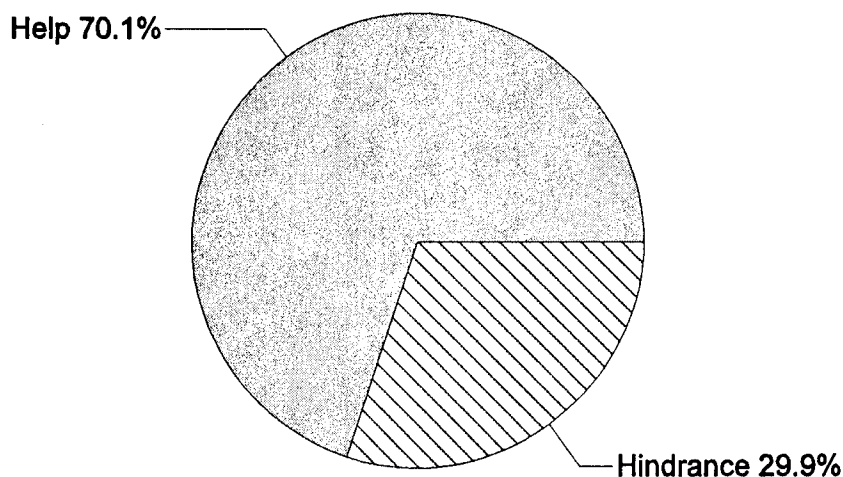


FIGURE 20. TCAS: HELP OR HINDRANCE?

NOTES

¹ Mellone (1992, 1993a, 1993b) found that most incidents in his data set occurred during cruise. The discrepancy between his finding and ours might be due to coding. Since he did not publish the specific criteria used to delineate cruise and other phases, we cannot positively address the discrepancy. See also Note 2.

² Mellone's (1992, 1993a, 1993b) categories were not mutually exclusive.

³ This question will be examined in a future study.

⁴ Alabama, Arkansas, Arizona, Alaska, Connecticut, Delaware, D.C., Idaho, Iowa, Kansas, Maine, Maryland, Montana, Nebraska, New Hampshire, North Dakota, Ohio, Oregon, South Dakota, Vermont, Virgin Islands, Washington, Wisconsin, and Wyoming had no reported incidents. Connecticut, Hawaii, Indiana, Louisiana, Minnesota, Mississippi, Nevada, Oklahoma, Puerto Rico, South Carolina, Utah, and West Virginia all had one reported incident. Kentucky, Michigan, Missouri, North Carolina, Pennsylvania, Rhode Island, and Virginia had two reported incidents each.

⁵ See Appendix A for caveat on the use of ASRS data.

⁶ The following ATC facilities had one reported incident: Augusta, GA (Bush Field) (AGS), Windsor Locks, CT (Bradley International Airport) (BDL), Baton Rouge, LA (Ryan Field) (BTR), Burbank, CA (Glendale-Pasadena Airport) (BUR), Dallas-Ft. Worth, TX (Dallas/Forth International Airport) (DFW), Detroit, MI (Metropolitan Wayne County Airport) (DTW), Greensboro, NC (Piedmont Triad International Airport) (GSO), Washington, DC (Dulles International Airport) (IAD), New York, NY (John F. Kennedy International Airport) (JFK), Los Angeles, CA (Los Angeles International Airport) (LAX), Midland, TX (Midland International Airport) (MAF), Orlando, FL (Orlando International Airport) (MCO), Memphis, TN (Memphis International Airport) (MEM), Oakland, CA (Metropolitan Oakland International Airport) (OAK), Kahului, HI (Kahului Airport) (OGG), Ontario, CA (Ontario International Airport) (ONT), Providence, RI (Theodore Francis Green State Airport) (PVD), Chicago/Wheeling, IL (Pal-Waukee Airport) (PWK), Reno, NV (Reno Cannon International Airport) (RNO), Louisville, KY (Standiford Field) (SDF), San Juan, PR (Luis Munoy Martin International Airport) (SJU), Santa Ana, CA (John Wayne/Orange County Airport) (SNA), St. Louis, MO (Lambert-St. Louis International Airport) (STL), Newburgh, NY (Stewart International Airport) (SWF), Syracuse, NY (Syracuse Hancock International Airport) (SYR), Tampa, FL (Tampa International Airport) (TPA), Tranaser City, MI (Cherry Capital Airport) (TVC), Tulsa, OK (Tulsa International Airport) (TUL), Chicago, IL (Chicago ARTCC) (ZAU), Miami, FL (Miami ARTCC) (ZMA), Memphis, TN (Memphis ARTCC) (ZME), Minneapolis, MN (Minneapolis ARTCC) (ZMP), Indianapolis, IN (Indianapolis ARTCC) (ZID), Kansas City, MO (Kansas City ARTCC) (ZKC), Nashua, NH (Boston ARTCC) (ZBW), Houston, TX (Houston ARTCC) (ZHU). Miami, FL (Miami International Airport) (MIA), Norfolk, VA (Norfolk International Airport) (ORF), and Atlanta, GA (Atlanta ARTCC) (ZTL) had two incidents reported in each facility's airspace.

⁷ Since ASRS reports are deidentified after preliminary processing, the only way to identify individual reports is through the accession number; a unique, sequential number assigned to each report.

⁸ The average of 811 feet is somewhat skewed to the high side by the one incident involving an altitude deviation of 2400 feet. The median of 600 feet and the mode of 500 feet are, in fact, more descriptive of the actual altitude deviation occurring in the data set.

REFERENCES

- Aarons, R. N., "TCAS Gets an Interim Report Card," Business and Commercial Aviation, 70:44, Mar. 1992.
- "Air Carrier Operational Approval and Use of TCAS II," U. S. Federal Aviation Administration, AC 120-55.
- Air Transport Association, "Operations Memorandum No. 90-35," April 6, 1990.
- "Can TCAS Help Expand ATC System Capacity?," *Business and Commercial Aviation*, 64:38, April 1989.
- George, Fred, "TCAS I," *Business and Commercial Aviation*, 72:60-4, Jan. 1993.
- Introduction to TCAS II*, U.S. Department of Transportation.
- Klass, Philip J., "Extensive Airline Use of TCAS PinPoints Desirable Software Changes," *Aviation Week & Space Technology*, 136:48-49, Jan. 1992.
- Lebron, John E. and Mulder, Steven J., "System Safety Study of Minimum TCAS II for Instrument Weather Conditions, FAA, Program Engineering & Maintenance Service, Washington, DC, 1985.
- Mellone, Vincent J. (1992) "TCAS Incident Reports Analysis," ASRS Quick Response No. 235, July 29, 1992.
- Mellone, Vincent J. (1993a) "TCAS II—Genie Out of the Bottle?" ASRS Directline, June 1993, Issue 4, pp. 2-9.
- Mellone, Vincent J. (1993b) "TCAS Incident Reports Analysis," Paper presented at Second International TCAS Conference FAA, September 9, 1993.
- Pryor, David, "TCAS Finally Moves Into the Cockpit," *Aerospace America*, 29:36-8, Feb. 1991.
- Rojas, Roberto G., "Simulation of the Enhanced Traffic Alert and Collision Avoidance System (TCAS II) Microform," Ohio State University, Columbus, OH, ElectroScience Laboratory; National Aeronautics and Space Administration, Langley Research Center, Hampton, VA, 1985.
- TCAS Transition Program (TTP) Newsletters*, Issues #1-22.
- U.S. Congress, "Safer Skies With TCAS: Traffic Alert and Collision Avoidance System: Special Report," Office of Technology Assessment, Washington, DC.
- U.S. Congress, "Schedule for Installation of the TCAS II Collision Avoidance System," House Committee on Public Works and Transportation.

U.S. Congress, "To Review the Status of the Airborne Traffic Alert and Collision Avoidance System (TCAS)," Hearing Before the Subcommittee on Investigations and Oversight of the Committee on Public Works and Transportation, House of Representatives, One Hundred Second Congress, First Session, October 8, 1991.

U.S. Department of Transportation, "System Safety Study of Minimum TCAS II," Federal Aviation Administration, Washington, DC, 1984.

What is TCAS? Collins Air Transport Division, Rockwell International, Aug. 1, 1989.

Williamson, T. and Spencer, N.A., "Development and Operation of the Traffic Alert and Collision Avoidance System (TCAS)," *Proceedings of the IEEE*, 77:1735-44, Nov. 1989.

APPENDIX A



Reply to Attn of: FL:262-1

MEMORANDUM FOR: Recipients of Aviation Safety Reporting System Data

SUBJECT: Data Derived from ASRS Reports


The attached material is furnished pursuant to a request for data from the NASA Aviation Safety Reporting System (ASRS). Recipients of this material are reminded of the following points which must be considered when evaluating these data.

~~ASRS reports are submitted voluntarily.~~ The existence in the ASRS database of reports concerning a specific topic cannot, therefore, be used to infer the prevalence of that problem within the national aviation system.

Reports submitted to ASRS may be amplified by further contact with the individual who submitted them, but the information provided by the reporter is not investigated further. ~~Such information may or may not be correct in any or all respects.~~ At best, ~~it~~ represents the perception of a specific individual who may or may not understand all of the factors involved in a given issue or event.

After preliminary processing, all ASRS reports are deidentified. There is no way to identify the individual who submitted a report. All ASRS records systems are designed to prevent any possibility of identifying individuals submitting, or other names, in ASRS reports. There is, therefore, ~~no way to verify information submitted in an ASRS report after it has been deidentified.~~

The National Aeronautics and Space Administration and its ASRS contractor, Battelle Memorial Institute, specifically disclaim any responsibility for any interpretation which may be made by others of any material or data furnished by NASA in response to queries of the ASRS database and related materials.


William Reynard, Director
Aviation Safety Reporting System

CAVEAT REGARDING STATISTICAL USE OF ASRS INFORMATION

Certain caveats apply to the use of ASRS statistical data. All ASRS reports are **voluntarily submitted**, and thus cannot be considered a measured random sample of the full population of like events. For example, we receive several thousand altitude deviation reports each year. This number may comprise over half of all the altitude deviations which occur, or it may be just a small fraction of total occurrences. We have no way of knowing which.

Moreover, not all pilots, controllers, air carriers, or other participants in the aviation system, are equally aware of the ASRS or equally willing to report to us. Thus, the data reflect **reporting biases**. These biases, which are not fully known or measurable, distort ASRS statistics. A safety problem such as near midair collisions (NMACs) may appear to be more highly concentrated in area "A" than area "B" simply because the airmen who operate in area "A" are more supportive of the ASRS program and more inclined to report to us should an NMAC occur.

Only one thing can be known for sure from ASRS statistics—they represent the **lower measure** of the true number of such events which are occurring. For example, if ASRS receives 300 reports of track deviations in 1993 (this number is purely hypothetical), then it can be known with certainty that at least 300 such events have occurred in 1993.

Because of these statistical limitations, we believe that the **real power** of ASRS lies in the **report narratives**. Here pilots, controllers, and others, tell us about aviation safety incidents and situations in detail. They explain what happened, and more importantly, **why** it happened. Using report narratives effectively requires an extra measure of study, the knowledge derived is well worth the added effort.

ANOMALY DEFINITIONS

ACFT EQUIPMENT PROBLEM/CRITICAL - Aircraft equipment problem that is vital to the safety of the flight.

ACFT EQUIPMENT PROBLEM/LESS SEVERE - Not qualifying as a critical aircraft equipment problem.

ALT DEVIATION - A departure from or failure to attain or failure to maintain an ATC assigned altitude. It does not include an injudicious or illegal altitude in VFR flight where no altitude has been assigned by ATC or specified in pertinent charts.

ALT DEV/OVERSHOOT - An aircraft climbs or descends through the assigned altitude.

ALT DEV/UNDERSHOOT ON CLB OR DES - An aircraft fails to reach an assigned altitude during climb or descent.

ALT DEV/EXCURSION FROM ASSIGNED - An aircraft departs from level flight at an assigned altitude.

ALT DEV/XING RESTRICTION NOT MET - Charted or assigned altitude crossing restriction is not met.

ALT-HDG RULE DEVIATION - Cruise flight contrary to the altitudes specified in FAR 91.159.

CONFLICT/NMAC (NEAR MIDAIR COLLISION) - A conflict is defined as the existence of a perceived separation anomaly such that the pilot(s) of one or both aircraft take evasive action; or are advised by ATC to take evasive action; or experience doubt about assurance of continuing separation from the viewpoint of one or more of the pilots or controllers involved. A near midair collision is when the flight crew reports, either directly or as quoted by the controller, that the reported miss distance is less than 500 feet.

CONFLICT/AIRBORNE LESS SEVERE - A conflict not qualifying as a NMAC.

CONFLICT/GROUND CRITICAL - A ground occurrence that involves (1) two or more aircraft, at least one of which is on the ground at the time of the occurrence, or (2) one or more aircraft conflicting with a ground vehicle. The flight crew reports, either directly or as quoted by a controller, that they took evasive action to avoid a collision (emergency action go-around, veering on runway or taxiway, takeoff abort, or emergency braking), and the balance of the report, including the narrative is judged consistent with a critical occurrence.

CONFLICT/GROUND LESS SEVERE - A ground conflict not qualifying as critical.

CONTROLLED FLT TOWARD TERRAIN - Flying at an altitude that would, if continued, result in contact with terrain.

ERRONEOUS PENETRATION OF OR EXIT FROM AIRSPACE - Self-explanatory.

IN-FLT ENCOUNTER/OTHER - In-flight encounter (e.g., bird strikes, weather balloons).

IN-FLT ENCOUNTER/WX - In-flight encounter with weather (e.g., wind shear, turbulence, clouds, high winds, storms).

LESS THAN LEGAL SEPARATION - Less than standard separation between two airborne aircraft (as standard separation is defined for the airspace involved).

LOSS OF ACFT CONTROL - Self-explanatory.

NON-ADHERENCE LEGAL RQMT/CLNC - Non-adherence to an ATC clearance.

NON-ADHERENCE LEGAL RQMT/FAR - Non-adherence to a Federal Aviation Regulation.

NON-ADHERENCE LEGAL RQMT/PUBLISHED PROC - Non-adherence to approach procedure, standard instrument departure, STAR, profile descent, or operational procedure as described in the AIM or ATC facility handbook.

NON-ADHERENCE LEGAL RQMT/OTHER - Non-adherence to SOPs for aircraft, company SOPs, etc.

RWY OR TXWY EXCURSION - An aircraft exits the runway or taxiway pavement.

RWY TRANSGRESS/OTHER - The erroneous or improper occupation of a runway or its immediate environs by an aircraft or other vehicle so as to pose a potential collision hazard to other aircraft using the runway, even if no such other aircraft were actually present.

RWY TRANSGRESS/UNAUTH LNDG - A runway transgression specifically involving landing without a landing clearance or landing on the wrong runway.

SPEED DEVIATION - Aircraft speed contrary to FARs or controller instruction.

TRACK OR HDG DEVIATION - Self-explanatory.

UNCTRL ARPT TRAFFIC PATTERN DEVIATION - Failure to fly the prescribed rectangular pattern or failure to enter on a 45 degree angle to the downwind leg.

VFR IN IMC - Flight conducted under Visual Flight Rules (VFR) into Instrument Meteorological Conditions (IMC) when not on an instrument flight plan and/or when not qualified to fly under Instrument Flight Rules (IFR).

INTEGRATING HELICOPTERS
INTO
THE NATIONAL AIRSPACE SYSTEM

Ralph D. Kimberlin, PhD.
The University of Tennessee
Space Institute
Tullahoma, TN 37388

ABSTRACT

Although the helicopter has been operational since the 1940's, civil use in instrument conditions today is almost non-existent. The primary reason for non-instrument flight by helicopters is that the current National Airspace System (NAS) was designed for fixed wing airplanes and contains many rules and regulations which nearly prohibit helicopters from flying on instruments. This problem has forced helicopter operators to attempt flights visually when weather conditions did not safely permit such flights. The result has been large numbers of accidents from flight into obstacles or the ground.

This paper describes some of the rules changes, research and testing necessary to integrate the helicopter into the NAS. It is the result of an eight month study conducted by the University of Tennessee Space Institute Flight Research Group under a Federal Aviation Administration (FAA) Grant.

INTRODUCTION

Since its invention the helicopter has been considered an aircraft for specialized purposes. As a result, the development of infrastructure specifically for helicopters has not received the attention paid that of fixed wing aircraft. Airways and terminal instrument procedures (TERPS) are designed around the operating characteristics of fixed wing aircraft and do not provide for the helicopters ability to fly very slowly, descend and depart steeply and to hover.¹

The growth of air transportation over the past several decades along with the rapid population expansion has begun to create

problems in the current system of air transportation.^{2,3} In addition, the current system in the United States does not connect well with other forms of transportation and, in many cases, makes the trip to and from the airport the most time consuming part of the journey. The helicopter, and other vertical flight capable air vehicles, offers the possibility of solving many of these air transportation problems. This is particularly true in areas of high population density where land for airfields is at a premium and travel distances are short.¹

In order for helicopters to respond to this need they must have the necessary infrastructure in the form of Helicopter Airways and TERPS that take advantage of their unique capabilities while minimizing their drawbacks such as noise. The Vertical Flight Program Office (ARD-30) of the Federal Aviation Administration (FAA) recognized this need and has funded a number of studies related to infrastructure as part of the Rotorcraft Master Plan (RMP). This paper presents a portion of the results of one of those studies conducted by the University of Tennessee Space Institute Flight Research Group under FAA Grant 93-G-007 begun in January 1993 and completed in November of that year.¹

PURPOSE

The purpose of the effort was to determine if additional testing or demonstrations were required to develop the Terminal Instrument Procedures (TERPS) for helicopters to be integrated into the National Airspace System (NAS) and, if so, to plan that testing.

METHODOLOGY

In order to determine if additional testing or flight demonstrations were required, an extensive literature search and review was conducted. During this phase of the effort some 185 relevant documents were reviewed and cataloged. In addition, two industry surveys and numerous face-to-face meetings were held with industry, the FAA, community leaders, helicopter operators, and other parties interested in all weather helicopter operations. Included was participation in the FAA sponsored Extremely Low Visibility IFR Rotorcraft Approach (ELVIRA) Workshop in Santa FE, NM. With this information in hand, concepts of rotorcraft operation were formulated, required testing was identified and planned including schedules and costs.

RESULTS

The background literature search and review revealed that considerable work had been done on many of the items related to helicopter TERPS. This work was categorized into seven topics which were:

1. Helicopter Terminal Area Procedures.
2. Helicopter Steep Instrument Approaches.

3. Helicopter Handling Qualities during Steep Instrument Approaches.
4. Navigational Methods and Required Avionics.
5. Visual Elements. (Cockpit Visibility, Helipad Marking and Lighting)
6. Community Impact Considerations. (Public Acceptance of Helicopter Operations)
7. Environmental Considerations. (Noise)

This paper will address the first three of these issues.

TERMINAL AREA PROCEDURES

A major problem identified in the literature is that of alternate airport weather minimums for helicopters during IFR operations.⁴ Currently the alternate airport weather minimums are the same as for airplanes even though the helicopter is capable of a much slower, safer instrument approach than an airplane. Since a helicopters cruise speed and range are much less than those of fixed wing airplanes, it may be difficult for a helicopter to find an alternate airport. This is particularly true in air mass weather situations where the weather is likely to be similar within the range of most helicopters. In our discussions with helicopter operators, the problem of alternate airport weather minimums was cited as one of the main reasons for not seeking IFR capability.

Another problem faced by the helicopter during IFR operations is that of communicating with Air Traffic Control (ATC). Since helicopters prefer to fly at lower altitudes than fixed wing aircraft, and Very High Frequency (VHF) communications are line-of-sight, it is possible for helicopters to be out of communications with ATC for extended periods of time. Although the Global Positioning System (GPS) will permit accurate navigation at altitudes below those currently used, it will only increase the communications problem.

Other terminal area considerations include separation from other traffic, particularly high speed traffic and wake turbulence concerns. Very little research has been accomplished regarding the effects of wake turbulence from helicopters on aircraft and vice versa. One method of reducing such concerns without extensive research is for the helicopter to have unique, steep approaches which are not aligned with airplane approaches.

STEEP APPROACHES

Due to its unique aerodynamics the helicopter prefers to fly steep approaches. However, the current instrument approach procedures are designed for airplanes which fly shallow 3⁰ approach angles. Therefore, for helicopters to fly steep approaches under instrument conditions a helicopter unique approach angle must be determined. Considerable research has been conducted to determine what that angle should be with references 5 through 10 being examples.^{5,6,7,8,9,10} A review of these references reveals that there are a number of limitations upon the approach angle a given helicopter can fly. These limitations can be classified into two general categories.

The first category is related to the performance of the helicopter while the second is related to its handling qualities. Since handling qualities will be discussed in the following section we will limit our discussion here to the performance limitations.

In a constant speed descent the maximum descent angle can be determined from:

$$(-\Gamma)_{\max} = \tan^{-1} (D/L)_{\max}$$

where: $-\Gamma$ = the descent angle

D = the drag of the helicopter

L = the lift of the helicopter

Figure 1, taken from reference 7, is a plot of descent angle for various lift to drag ratios and inflight winds. From this figure we can see that, in no wind conditions, the $(D/L)_{\max}$ must be at least 0.17 to achieve a 10° descent. For steep downwind approaches $(D/L)_{\max}$ must increase significantly. For most helicopters $(D/L)_{\max}$ is limited by flow around the main rotor. This limitation is caused by the helicopter entering vortex ring state and is primarily a problem for larger helicopters.

Small helicopters suffer another descent angle limitation which occurs when the torque on the rotor is zero and the helicopter enters autorotation. Figure 2, from reference 10, shows both the autorotation and vortex ring state boundaries as a function of airspeed. From this figure we can see that at a 90 knot approach speed a 10° approach is near the limit for autorotation. Most of the research conducted to date has shown that pilots are very reluctant to enter autorotation when in instrument conditions. Figure 2 also shows that if airspeed is reduced much steeper approaches can be flown without approaching autorotation limits. Table 1 shows the decision heights required as a function of approach speed based upon the current criteria for precision instrument approaches. This table also shows that the slower the approach speed the lower the decision height.

A lower approach speed may lead to flight in the AVOID region of the Height-Velocity (H-V) diagram for the helicopter. Since the H-V diagram is determined during Certification Flight Test of the helicopter under cruise or climb conditions^{11,12}, it appears reasonable that a steep approach where the collective was already near the autorotative position would not be critical. In other words, the H-V diagram for this condition is much smaller than for the most critical case which is published in the pilots handbook. However, the institution of steep approaches would make this an area of future investigation.

One other factor is significant in this discussion and that is the comfort level of the crew and passengers when making the steep approach. As mentioned previously, two industry surveys were conducted during this study to determine helicopter operators

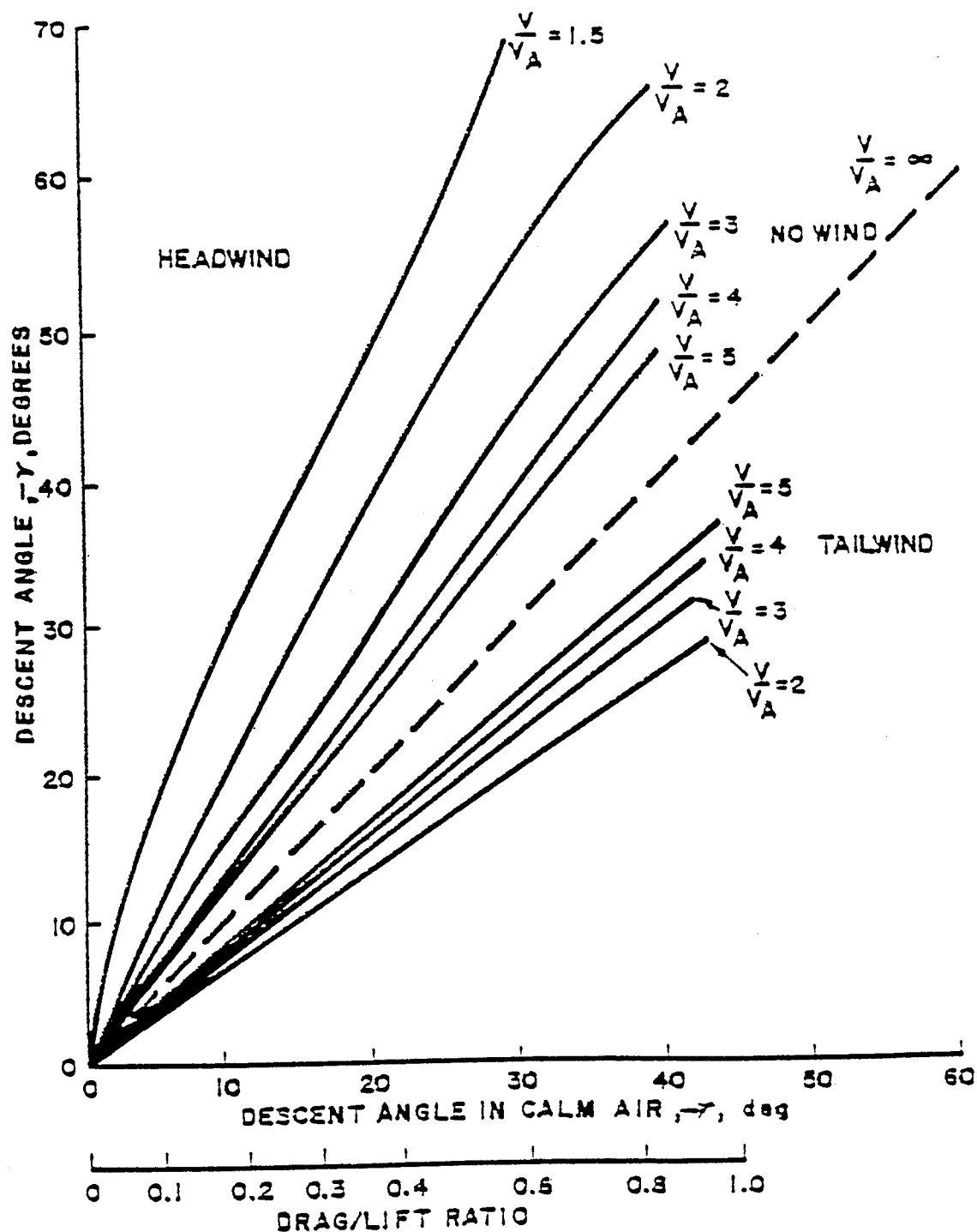
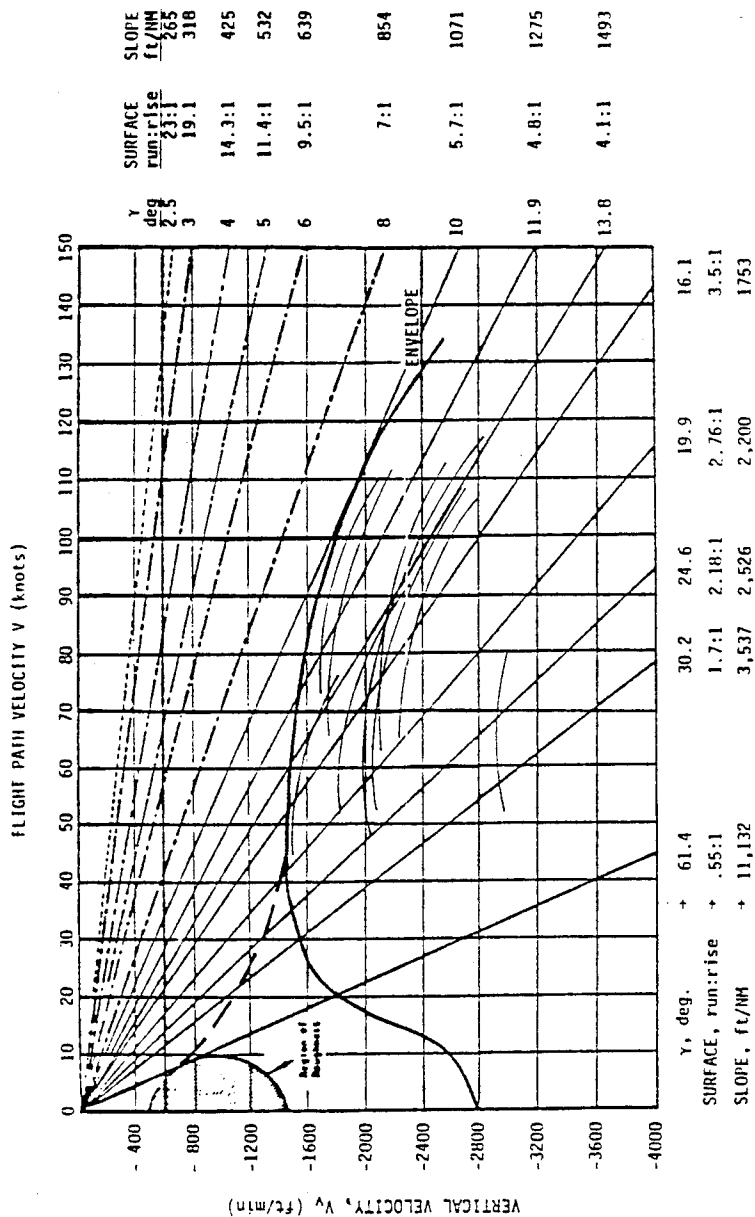


Figure 1. Effects of Headwinds, Tailwinds and Drag/Lift upon Descent Angle.

Source: Wolkovitch, Julian, and John A. Hoffman. "Stability and Control of Helicopters in Steep Approaches - Volume 1. Summary Report." USAAVLABS Technical Report 70-74A, AD 729847, May 1971.



Individual Helicopter Capability

Note: Helicopters cannot physically descend in controlled flight at a higher rate of descent than achieved in autorotation. This envelope curve, therefore, defines the regime of descending flight achievable by the family of IFR certified helicopters evaluated in this report.

Figure 2. Envelope of Autorotation Characteristics.

Source: DeLucien, A. G., et al. "Study of Helicopter Performance and Terminal Instrument Procedures." FAA-RD-80-58, June 1980.

TABLE 1

Decision Height (DH)
as a function of
Approach Angle and Airspeed

Approach Angle in Deg.	3	6	9	12
Airspeed in Knots	Decision Height (DH) in Feet			
90	79	159	238	316
60	53	106	159	211
45	40	79	143	158
30	26.5	53	79	105

Table is based on an assumption of a 10 second period from DH to ground impact if flight is continued at same airspeed and approach angle.

responses to questions such as the one just posed. Figure 3 shows the responses of the industry to the question of what the approach angle should be for a helicopter approach. From this figure we can see that the majority of the responses fall about a 9° approach. This approach angle would avoid most of the problems associated with the descent performance of the helicopter, however, would require quite high minimums if the current approach criteria shown in Table 1 were used. Approach minimums could be lowered to one hundred feet if speeds on the order of 35-40 knots were used. Using this low an approach speed or a decelerating approach leads to at least one other problem which is the handling qualities of the helicopter during a steep approach.

HANDLING QUALITIES

Much of the work done on steep approaches for helicopters under instrument meteorological conditions (IMC) is in the area of handling qualities. Some factors affecting the handling qualities of the helicopter during the steep approach include:

1. Trim changes with power change.
2. Longitudinal stability levels at low airspeeds.
3. Directional control problems at low airspeeds under IMC.
4. Wind effects, particularly cross-winds and tail-winds.

The helicopter is a very coupled machine. Any power change results in trim changes in several axes. For instance, at low airspeed a trim shift occurs in the unaugmented vertical degree of freedom due to the aircraft's power required curve⁶. In addition, heading control become particularly worrisome at low airspeed with changes in power.

The longitudinal stability of helicopters at low airspeed is nearly non-existent. As a result, the FAA has established a certified minimum IFR airspeed for helicopters called V_{MINI} . This speed which would limit the speed at which a helicopter could fly an IFR approach varies between 40 and 60 knots for most of today's IFR certified helicopters¹⁰. It should be noted, however, that military helicopters do not contain such limitations on minimum speed during IFR flight and there is discussion in the civil helicopter community as to its necessity¹⁰. Associated with this issue is the credit for Flight Directors and Heads-up Displays (HUD). Research conducted in Canada and reported in NAE-AN-44¹³ shows that the contributions of Flight Director displays to handling qualities improvements is readily apparent. However, Federal Aviation Regulations Parts 27 and 29^{11,12} which address the certification of helicopters do not address credit for these devices. The companion Advisory Circulars^{14,15} to these regulations do mention stability credit for Flight Directors but do not say how much it should be, leaving this up to the individual FAA Test Pilot. Therefore, most of the longitudinal stability issues related to helicopter steep approaches remain to be resolved.

Directional control during helicopter steep approaches is

What approach angle do you think would be acceptable for rotorcraft IFR flight?

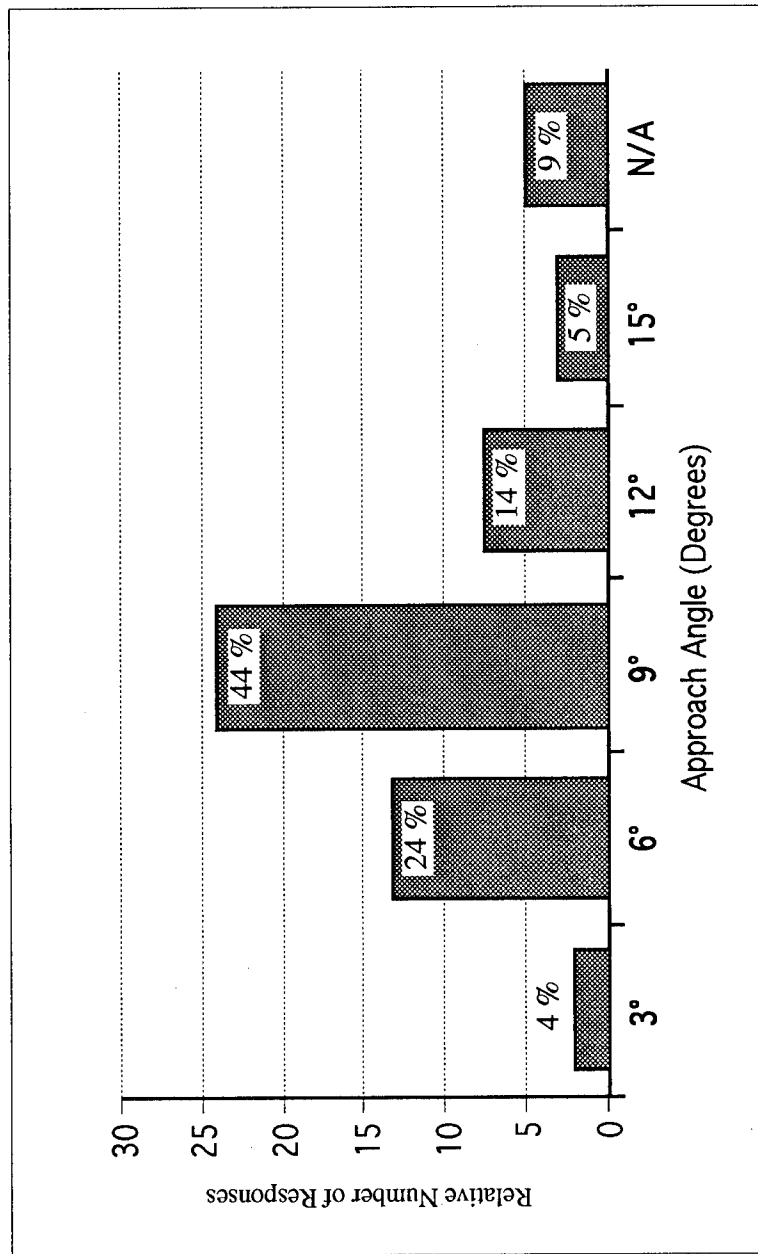


Figure 3. Favored Approach Angle from Industry Survey

significant due to the coupling between power and heading. The slightest power change will result in a directional trim change. This is particularly significant at low airspeeds where directional stability is non-existent. This control problem makes decelerating IMC approaches very difficult using raw data.

The directional control problems associated with helicopter steep approaches are also greatly improved by the addition of a Flight Director. This is particularly true when the steep approach is of the decelerating type. In fact, NAE-AN-44¹³ reports that the improvements in pilot workload and tracking error between a constant speed and a decelerating approach were not evident when a Flight Director was used. It appears then that either a Flight Director, HUD or Yaw Axis stabilization is required for helicopter steep approaches.

Adverse wind conditions also present the helicopter pilot with unique problems during a steep instrument approach. For instance, a strong tail-wind could force him into autorotation in order to maintain the glideslope, or cause him to be high on glideslope at the DH. Both present problems since, as discussed previously, the pilot is reluctant to enter autorotation while under IMC and being high on glideslope at DH makes it difficult to decelerate the helicopter to a hover over the pad. This latter problem has caused some to call for a Decision Range (DR) for helicopters rather than a DH. The effects of winds on steep helicopter approaches were studied in Canada and reported in NAE-AN-55¹⁶. This study evaluated using a "crab" and a "sideslip" technique for crosswind approaches. The "crab" technique was found to be superior from the standpoint of handling qualities, but presented a problem with acquiring the heli-pad visually after breaking out of the overcast.

As can be seen from this short discussion, a number of handling qualities issues need to be resolved prior to routine conduct of helicopter steep approaches.

CONCLUSIONS

The helicopter and other vertical flight capable vehicles offer the possibility of solving some of the nations transportation problems providing unique airspace infrastructure can be developed to accommodate them. Many of the problems associated with accomplishing this goal have already been solved, but others remain. As shown by this paper the remaining problems are a mix of regulatory and technical. It appears that most of the technology is in hand to solve the technical problems. However, the regulatory problems require political solutions. It is in this latter area that both fixed and rotary wing General Aviation interest need to work together.

REFERENCES

1. Kimberlin, Ralph D., Huneycutt, Roger, Green, David L., Bailey, Thomas and Sims, Paul, Program Plan for the Development of Helicopter Terminal Area Instrument Procedures (TERPS), Final Report, Federal Aviation Administration Grant Number 93-G-007, Tullahoma, TN, October 1993.
2. Anon., Civil Tiltrotor Missions and Applications Phase II: The Commercial Passenger Market, NASA/FAA Contractor Report NAS2-12393, January 1991.
3. Parke, Robert B., "Does Gridlock Threaten Europe's Airspace?" Business and Commercial Aviation, October 1991.
4. Freund, D. J. and Vickers, T. K., Preliminary Test Plans of ATC Concepts for Longer Term Improvement (Helicopter Operations Development Program), FAA-RD-80-87, May 1980.
5. Adams, Glen D., V/STOL APPROACH SYSTEM STEEP ANGLE FLIGHT TESTS, FAA-RD-66-68, September 1966.
6. Kelly, J. R., Niessen, F. R., Thibodeaux, J. J., et. al., Flight Investigation of Manual and Automatic VTOL Decelerating Instrument Approaches and Landings, NASA TN D-7524, July 1974.
7. Wolkovitch, Julian and Hoffman, John A., Stability and Control of Helicopters in Steep Approaches, Volume I, Summary Report, USAAVLABS Technical Report 70-74A, Fort Eustis, VA, May 1971.
8. Demko, Paul S. and Boschma, James H. Capt., Advances in Decelerating Steep Approach and Landing for Helicopter Instrument Approaches, Presented at the 35th Annual National Forum of the American Helicopter Society, Washington D. C., May 1979.
9. Peach, L. L., Jr., Hunting, A. W. et. al., NASA/FAA Flight Test Investigation of Helicopter Microwave Landing System Approaches, AHS Paper 80-55, AHS 36th Annual Proceedings, 1980.
10. DeLucien, A. G., Green, D. L., Price, H. R. and Smith, F. D. Study of Helicopter Performance and Terminal Instrument Procedures, FAA-RD-80-58, June 1980.
11. Anon., Certification of Normal Category Rotorcraft, Federal Aviation Regulation, Part 27.
12. Anon., Certification of Transport Category Rotorcraft, Federal Aviation Regulation, Part 29.
13. Kereliuk, S., and Sattler, D. E., Determination of Handling Qualities and Display Requirements for Helicopter Instrument Flight During Decelerating Approaches to Slow Speeds,

Aeronautical Note NAE-AN-44, NRC No. 27720, National Aeronautical Establishment, Ottawa, May 1987.

14. Anon., Certification of Normal Category Rotorcraft, Advisory Circular AC 27-1, Federal Aviation Administration, ASW-110, August 1985.
15. Anon., Certification of Transport Category Rotorcraft, Advisory Circular AC 29-2A, Federal Aviation Administration, ASW-110, Sep. 1987.
16. Baillie, S., Kereliuk, S. and Hoh, R., An Investigation of Lateral Tracking Techniques, Flight Directors and Automatic Control Coupling on Decelerating IFR Approaches for Rotorcraft, Aeronautical Note NAE-AN-55, NRC No. 29604, National Aeronautical Establishment, Ottawa, October 1988.

A TWO ELEMENT LAMINAR FLOW AIRFOIL OPTIMIZED FOR CRUISE

By

Mr. Gregory G. Steen

Dr. Kenneth D. Korkan

Mr. Oran W. Nicks

Department of Aerospace Engineering

Texas A&M University

Presented at the

3rd Joint Symposium on General Aviation Systems

Mississippi State University

Starkville, Mississippi

May 24 & 25, 1994

A TWO ELEMENT LAMINAR FLOW AIRFOIL OPTIMIZED FOR CRUISE

Mr. Gregory G. Steen, Graduate Student
Dr. Kenneth D. Korkan, Professor
Mr. Oran W. Nicks, Research Engineer
Department of Aerospace Engineering
Texas A&M University
College Station, Texas 77843

ABSTRACT

Numerical and experimental results are presented for a new two element, fixed geometry natural laminar flow airfoil optimized for cruise Reynolds numbers on the order of three million. The airfoil design consists of a primary element and an independent secondary element with a primary to secondary chord ratio of three to one. The airfoil was designed to improve the cruise lift-to-drag ratio while maintaining an appropriate landing capability when compared to conventional airfoils. The airfoil was numerically developed utilizing the NASA Langley Multi-Component Airfoil Analysis computer code running on a personal computer. Results show a nearly 12% decrease in overall wing drag at sailplane cruise conditions when compared to a wing based on an efficient single element airfoil with no increase in stall speed.

Section surface pressure, wake survey, transition location, and flow visualization results were obtained in the Texas A&M University Low Speed Wind Tunnel. Comparisons between the numerical and experimental data, the effects of the relative position and angle of the two elements, and Reynolds number variations from 1×10^6 to 3×10^6 for the optimum geometry case are presented.

INTRODUCTION

Since a wing is the primary source of lift and a major contributor to drag, it is of prime interest in any major attempt to increase aerodynamic performance. A good wing design will provide lift in the most efficient way possible. An important goal in the design of a wing is the selection of an airfoil with a high lift-to-drag ratio, as "the lift-to-drag ratio (L/D) is a measure of the aerodynamic efficiency..."¹

The use of flap systems on airfoils can greatly increase the maximum lift coefficient of the system. The primary use of flaps has been to increase the maximum lift for landing while maintaining a reasonably small wing for cruise conditions. Many low Reynolds number aircraft, including the new World Class glider², have been designed without moveable flap systems. Since they must cruise and land with the same wing, design trade-offs must be considered in the selection of an airfoil configuration.

PURPOSE

The current effort reports on the viability of a two element fixed geometry airfoil designed to provide low drag for cruise conditions and high lift for landing. The airfoil under study consists of two distinct elements arranged similar to wings having external airfoil flaps. Various combinations of profile shape, element location, and relative angle have been explored. The intent of this research was to develop a two element airfoil with an L/D greater than that for a comparable single element airfoil at cruise lift coefficients, while providing high lift coefficients for landing.

BACKGROUND

National Advisory Committee for Aeronautics (NACA) researchers embarked on a systematic study of various airfoil shapes in the early 1940's. The culmination of this work is the classic NACA Report No. 824 titled "Summary of Airfoil Data."^{3,4} Examination of some slotted flap data presented in the NACA report yields an interesting result. Small flap deflections often yield very little increase in drag coefficient but a significant increase in lift coefficient. For example, experimental data from a NACA 63,4-420 airfoil with a 25% slotted flap deflected 25° shows a nearly 40% increase in cruise L/D over the same airfoil with 0° flap deflection when adjusted for maximum lift coefficient.

Various airfoil configurations, from simple flaps to complex multi-component Fowler flaps have been extensively explored for use as high lift devices. It has even been mathematically proven that $n+1$ elements are better than n elements for providing maximum lift.⁵ However, very little research has been performed on using a multi-element airfoil for cruise conditions. The emphasis has always been on increasing lift and not L/D. Bauer did study the two element airfoil problem using hand launched gliders.⁶ His results, although not definitive, provide support to the basic concept of a two element cruise airfoil.

TEST APPARATUS

The current effort utilized both numerical and experimental tools to complete the study. All airfoil shapes were analyzed using the NASA Langley Multi-Component Airfoil Analysis (MCARFA) computer code. All single element airfoil shapes were also analyzed using the PROFIL computer code. Previously published or current experimental data from the Texas A&M University Low Speed Wind Tunnel (TAMU-LSWT) are presented for many configurations.

NUMERICAL TOOLS

MCARFA CODE. The primary numerical tool used in the study was the NASA Langley MCARFA computer code running on a personal computer.⁷⁻¹³ The MCARFA code computes the performance characteristics of multi-component airfoils in subsonic, compressible, viscous flow. The final converged viscous solution is obtained by successively combining an inviscid solution with a boundary layer displacement thickness. The surface of each airfoil element is approximated by a closed polygon with segments represented by distributed vortex singularities. The boundary layer solution is comprised of mathematical models representing the laminar, transition, turbulent, and confluent boundary layers.

Studies were performed to document the accuracy of the MCARFA results. Williams has developed an exact test case for the plane potential flow about two adjacent lifting airfoils.¹⁴ Case A is at an angle of attack (α) of 0° with the flap deflected 30° and Case B is at an α of 0° and a flap deflection of 10° . The calculated pressure distributions show excellent agreement with the theory. Aerodynamic load data from the exact test case and the MCARFA results are presented in Table 1. Close agreement is obtained for the lift values; the MCARFA results show some inaccuracy in the drag calculations.

NACA external airfoil flap data were used to test the viscous MCARFA results on airfoil designs similar to the current study.¹⁵⁻¹⁸ A NACA 23012 airfoil with a 20% chord 23012 external airfoil flap deflected 20° was tested at a Reynolds number of 1.05×10^6 . MCARFA results at Reynolds numbers of 1.05×10^6 and 3×10^6 are compared to the NACA experimental data in Figure 1. The lift coefficient (c_l) results show good agreement overall with the MCARFA program predicting a 12% higher maximum lift

coefficient (c_{lmax}). The c_{lmax} difference is due to the program not predicting the slope change in the lift curve at a c_l of about 1.2 as in the experimental data. The 3×10^6 Reynolds number case shows a higher lift curve slope and higher c_{lmax} than the 1.05×10^6 case as expected. The program predicts a slightly higher drag coefficient (c_d) at the lower c_l 's and a somewhat lower c_d at the higher c_l values than the experimental data show. The L/D results are similar to the c_d trends. The moment coefficient results are generally within 5%.

The MCARFA code does not predict a true maximum lift coefficient. It instead continues to predict increasing lift coefficients at increasing angles of attack. Comparison with numerous sets of experimental data and other numerical results has led to an empirical c_{lmax} criterion. The airfoil is said to have stalled when the code predicts separated flow over greater than 10% of the surface.

PROFIL CODE. The PROFIL computer code was also used in this study when possible. The PROFIL code, also known as the Eppler code, iterates a solution to the incompressible viscous airfoil problem by solving boundary layer equations near the surface and matching the results to potential flow solutions everywhere else.¹⁹⁻²² The code has options to either analyze an existing airfoil shape using panel method routines or solve the inverse airfoil design problem through a conformal mapping technique. Only the airfoil analysis option of the code was used in the present study. Previous experience utilizing the PROFIL code has shown it to be a very fast and accurate analysis tool.^{23,24} The primary drawback to the PROFIL code for the current study is the single airfoil element limitation.

Studies similar to those for the MCARFA code were performed to document the PROFIL code accuracy. Various single element airfoils were analyzed using both the PROFIL and MCARFA codes and compared to published experimental data.²⁵ Lift Coefficient results show the PROFIL code accurately predicts the slope and c_{lmax} , but misses the experimental zero lift angle of attack (α_0) by about 1° . The MCARFA code, as previously discovered, correctly predicts α_0 and the low c_l range, but does not show the slope change at higher lift coefficients. Both codes correctly predict the drag coefficient at lower c_l 's, but the MCARFA code underpredicts the c_d at higher lift coefficients. Both codes tend to underpredict the L/D. The MCARFA code tends to overpredict L/D, as the c_d , at the higher values of lift coefficient when compared to the experimental data. The PROFIL code overpredicts the moment coefficient by about 20%; the MCARFA moment results are quite accurate.

EXPERIMENTAL TOOLS

Experimental results of the final airfoil shape were obtained in the Texas A&M University Low Speed Wind Tunnel (Fig. 2). The wind tunnel is of the atmospheric closed circuit single return type capable of operating dynamic pressures of up to 4778 N/m² (100 psf).²⁶ The test section is 2.13 meters (7 feet) high and 3.05 meters (10 feet) wide. A contraction ratio of 10.4:1 in a distance of about 9.14 meters (30 feet) and three anti-turbulence screens provide excellent flow quality. Previous studies have shown the longitudinal turbulence intensity in the test section to be less than 0.2% for dynamic pressures less than 1676 N/m² (35 psf).²⁷ The power section is located downstream of the test section. A 3.81 meter (12.5 foot) diameter four blade Curtiss-Electric B-29 variable pitch propeller and a constant RPM 1250 kVA electric motor provide the airflow. Turning vanes on each corner complete the flow control devices.

AIRFOIL MODEL. A model was built of the final airfoil shape to be tested in the TAMU-LSWT. The model had a 609 mm (24 inch) overall chord with a 457 mm (18 inch) primary element chord and a 152 mm (6 inch) secondary element chord. The model span was 915 mm (36 inches) with 775 mm (30.5 inch) diameter circular endplates on each end. The model was mounted vertically in the test section and the facility's turntable was used to change angle of attack (Fig. 3). The model was constructed of a solid

Ren Shape lay-up consisting of 51 mm (2 inch) thick layers of material epoxied and pinned together. Center sections were hollow to allow the installation of the pressure ports. The secondary element was connected to the primary by the use of steel brackets at each end. Initial tests showed unacceptable secondary element defections under load; therefore, two additional brackets were made and installed 178 mm (7 inches) on either side of the pressure ports.

SURFACE PRESSURE MEASUREMENT. Surface pressure measurements were made of the final airfoil shape using a Scanivalve stepper system, Validyne pressure transducers, and a Preston 16-bit Analog-to-Digital (A/D) system. Sixty-three pressure port locations on the primary element and twenty-six pressure ports on the secondary element were distributed based on surface curvature. Port locations were staggered along the span to ensure any small disruption of the boundary layer due to a port did not affect the downstream ports.

Normal and chordwise force coefficient values were obtained by integrating the surface pressure readings. Lift and moment coefficient values were then obtained by equation from the normal, chordwise, and drag coefficient results.²⁸

WAKE SURVEY MEASUREMENT. Downstream wake surveys were performed to measure the airfoil drag coefficient. A wake rake with forty total pressure ports and five in-plane static pressure ports was located one chord length aft of the airfoil trailing edge. Total pressure ports were evenly spaced 6.35 mm (0.25 inches) apart. Rake pressures were measured using a Pressure System's Inc. PSI-8400 electronic pressure measurement system.

FLOW VISUALIZATION. A mixture of diesel fuel and white tempera paint was used to visualize the surface flow of the final airfoil shape. The mixture was brushed on the surface, then the wind tunnel was brought up to the desired operating speed and the diesel fuel was allowed to evaporate, leaving the tempera paint on the airfoil surface. Photographs were then taken for later analysis. Transition locations, as well as regions of laminar, turbulent, and separated flow were measured from the photographs.

RESULTS

Various combinations of profile shape, relative angle and relative position of the two elements of the new airfoil are presented. Numerical results of the systematic study are obtained at Reynolds numbers of 1×10^6 through 3×10^6 . Experimental results are presented for the optimum geometry cases.

NUMERICAL RESULTS

PROFILE SHAPE. The NASA NLF(1)-0416 airfoil was chosen as the primary airfoil shape for the initial study. The NLF(1)-0416 airfoil is a natural laminar flow, 16% thick airfoil designed for a cruise c_l of 0.4. It was developed primarily for light, single-engine, general aviation airplanes. A complete numerical and experimental database is published for the airfoil. The secondary airfoil choice should be a fairly benign section because of the high operating angle and the flow disruption from the primary airfoil. Four airfoil shapes were analyzed as the secondary airfoil: the NACA 0012, NACA 2412, NACA 4412, and the NACA 23012. Studies of external airfoil flap data show the optimum deflection of about 20° and the secondary leading edge should be located at 98% of the primary chord and 3% below the primary airfoil.²⁹ Figure 4 shows the MCARFA results of the variation of secondary airfoil shapes. The c_l results show the NACA 4412 secondary airfoil has the highest $c_{l_{max}}$, followed closely by the

NACA 2412. The NACA 23012 and NACA 0012 showed lower maximum lift coefficients. The NACA 4412 also had the lowest drag coefficient, again followed closely by the 2412 and the 23012 and 0012 with higher drag coefficients. The L/D results confirm the 4412 as the best choice, with the 2412 a close second. The drawback to the 4412 choice is the moment coefficient. The 4412 had the highest negative moment coefficient, followed by the 2412, the 23012, and the 0012 closest to zero. Based on these profile results, the NACA 4412 was chosen as the best secondary airfoil for further study with the 2412 also used for a more complete database.

RELATIVE ANGLE. The relative angle of the NACA 4412 secondary element with respect to the primary NLF(1)-0416 element was varied from 10° through 30° at a constant secondary leading edge position of 95% of the primary chord and 2% below the primary airfoil. The pivot point on the secondary airfoil was the leading edge. The angle of attack and relative angle values are referenced to the primary airfoil chord line. Figure 5 presents the results of this angle variation. The lift coefficient results show the highest c_{lmax} was calculated with a 30° deflection of the secondary airfoil. The drag coefficients were essentially the same for all relative deflections through the low c_l range, but the 30° deflection showed the lowest drag at the higher lift coefficients. The L/D results show a spike in the L/D for the 25° and 30° deflection angles. With or without this spike, the 30° results show the highest L/D through the low and high c_l ranges. The 30° case is not the best through the mid c_l range. The moment coefficient increases with larger relative deflections so the largest moment was calculated for the 30° case and the smallest moment was on the 10° case. Based on the desire for a high c_{lmax} and a high L/D at cruise conditions, the 30° deflection case was chosen for further study. The 20° case was a close second in most categories and has a smaller moment so it will also be used for a more complete database.

RELATIVE POSITION. The relative position of the NACA 4412 secondary element deflected 20° from the primary element was varied through a grid from 92% to 102% of the primary chord behind the primary leading edge and from 1% to 4% below the primary chord line. These studies showed the optimum position of the secondary element leading edge to be 95% behind and 1.5% below the primary leading edge. Lift-to-drag ratio results are presented for a grid from 93% to 98% behind and from 1% to 2% below the primary leading edge in Figure 6. The horizontal variation results show the highest L/D's at the 95% position with very little increase over the 94% and 96% cases. The 93% and 98% cases were significantly lower over the entire c_l range. The vertical variation results show the highest L/D values at 1.5% below the primary chord, but very little difference is observed at either the 1% or 2% cases.

A spike in the L/D cases and a drop in the drag coefficient at certain mid angles of attack is observed. A corresponding increase in the percentage of laminar flow on the lower surface is also calculated. The transition point has yet to start moving forward on the upper surface. The peak point occurs at the angle immediately before the upper surface primary element transition starts to move forward. At the maximum L/D point for the 95%, 1.5% case presented, the primary element has nearly 100% laminar flow on the upper surface and 34% laminar flow on the primary lower surface. This two element configuration has a total of 75% laminar flow on the upper surface and 50% laminar flow on the lower surface.

FINAL AIRFOIL SHAPE. The final task in the study was to modify the primary element in an attempt to further increase the performance. The new airfoil is named the AG9301 for the first (01) Texas A&M Aggie (AG) airfoil of 1993 (93). The final version of the two element airfoil consists of a primary element AG9301A airfoil with a local chord 75% of the total chord and a secondary element of NACA 4412 section with a local chord 25% of the total chord. The secondary airfoil is positioned with the leading edge 95% of the primary chord behind and 1.5% below the leading edge of the primary element. The secondary airfoil is deflected 20° with respect to the primary chord line. The angle of attack of the

AG9301 is defined relative to the primary chord line. The AG9301A section is a modification of the NLF(1)-0416 with the upper surface unchanged and the lower surface thicker from the leading edge to about 85% of the local chord and then faired to meet the upper surface trailing edge. This thickening was an attempt to increase the extent of laminar flow on the lower surface of the primary airfoil. The AG9301 airfoil shape, with both a 30° and 20° second element deflection, is presented in Figure 7.

Reynolds Number Effect. The effects of variation in Reynolds number from 1×10^6 through 3×10^6 on the performance characteristics are presented in Figure 8. The lift coefficient results show a slightly lower slope at lower Reynolds number, but no difference in the maximum lift coefficient. The drag coefficient shows lower drag with increasing Reynolds number, as expected. Consequently, the L/D is higher at higher Reynolds number. The moment coefficient results show very small changes with different Reynolds numbers.

EXPERIMENTAL RESULTS

Experimental results are presented for the AG9301 airfoil at various Reynolds numbers. Some differences exist between the designed and constructed airfoil shape, so MCARFA results for the measured coordinates are included. The endplates on the model were useful in increasing the effective span of the model, but the experimental data still shows some Aspect ratio effect. Therefore, the experimental angle of attack values were adjusted from an Aspect ratio of 7.3 to infinity. No adjustment was made to any of the force or moment data.

Figure 9 presents experimental results for the 30° deflection case at a Reynolds number of 1×10^6 . Higher drag coefficients were measured through the low c_l range than predicted. In addition, the c_{lmax} was measured to be 2.32 rather than the 2.83 predicted. The L/D values were measured to be somewhat lower at corresponding c_l values than predicted for this case.

Experimental results at a Reynolds number of 1×10^6 for the 20° deflection case are presented in Figure 10. The maximum lift coefficient was measured to be 2.58 and predicted to be 2.55. The drag coefficient was somewhat higher, but followed the shape of the curve well when compared with the numerically predicted data. Moment coefficient results show excellent agreement between the numerical and experimental values. The L/D experimental data are lower, due to the higher c_d , than predicted through most of the c_l range. The L/D values for the 20° deflection case at Reynolds numbers of 2×10^6 and 3×10^6 are presented in Figures 11 and 12 respectively. Good agreement between the numerical and experimental values is seen for both cases. Experimental data is limited at these higher Reynolds numbers to the cruise conditions due to model mounting structure loads and available pressure transducer ranges.

Experimentally measured and numerically predicted transition location values at a Reynolds number of 3×10^6 are presented in Figure 13. Numerical values are for the measured airfoil shape. Reasonable agreement between the predicted and measured values does exist. The lower surface experimental values show less laminar flow than the code predicts, but the upper surface measured transition location is further aft at higher angles of attack than predicted.

COMPARISON WITH OTHER AIRFOILS

The AG9301 airfoil is compared with other single element airfoils designed for similar conditions. Comparisons are made with the SM701 airfoil designed specifically for the World Class Glider³⁰ and the Wortmann FX 79-K-144/17 airfoil with a faired 17% chord simple flap deflected -9.3° for cruise. The

Wortmann airfoil is currently used on many state-of-the-art high performance sailplanes including the Ventus and Nimbus.³¹ Figure 14 presents the L/D comparison of the MCARFA and PROFIL results of the various airfoils. The single element airfoils have a higher L/D than the AG9301 at a given lift coefficient, but because of the significantly higher c_{lmax} , the AG9301 airfoil can cruise at a higher c_l value, and therefore, a higher L/D. Table 2 presents the cruise c_l and L/D values and the maximum lift coefficient for various airfoils. It can be seen that the AG9301 30° deflection configuration has a higher cruise L/D than the other airfoils with no increase in landing speed. A wing designed with the SM701 airfoil does offer a slower landing speed than the AG9301, but even if the cruise c_l is lowered to account for this speed difference the AG9301 still has a higher cruise L/D. The AG9301 20° deflection case offers an L/D ratio similar to the single element airfoils, but still a significantly higher c_{lmax} .

The benefits presented above did not include any aircraft weight savings which are expected with the smaller planform possible using the AG9301. This expected weight savings will lower the required amount of lift and thus the amount of drag produced and the same L/D. For example, the NASA NLF(1)-0416 airfoil has a 37.4% lower c_{lmax} than the AG9301 30° case. This c_{lmax} difference allows a wing with this AG9301 airfoil to have a 37.4% smaller planform area, and thus be 37.4% lighter, than a wing with the NLF(1)-0416 airfoil. Assuming the wing makes up 30% of the total original weight of a sailplane,³² then the wing weight reduction corresponds to a 13.8% reduction in total sailplane weight. The required lift is now 13.8% less and therefore, at the same L/D, the wing drag is also 13.8% less. Following the same logic for a wing based on the AG9301 20° deflection case the wing drag due to weight savings would be 11.5% less.

Combining the L/D values and the weight savings, a wing based on the AG9301 30° deflection case would have 27.75% less wing drag at cruise conditions than a wing based on the NLF(1)-0416. A wing based on the AG9301 20° deflection case would have 11.75% less total drag than the NLF based wing at the same flight conditions.

CONCLUSIONS

The concept of a two element airfoil designed for efficient cruise conditions has been verified. The two element airfoil at the 30° case produces a L/D value 3.5% higher than the Wortmann FX 79-K-144/17 airfoil at the cruise condition without taking any weight reduction benefit. When allowing for an expected weight reduction benefit, a wing based on the AG9301-30° airfoil will have nearly 28% less drag at cruise than a wing with a NLF(1)-0416 airfoil with the same stall speed. The 20° deflection case produces nearly 12% less wing drag than the NLF based wing at identical flight conditions. Numerical results show 75% laminar flow on the upper surface and 50% laminar flow on the lower surface at maximum L/D values.

While numerical results for the AG9301 30° deflection case show higher L/D values at cruise and a higher c_{lmax} than the 20° deflection case, the 30° case could not be experimentally verified while the 20° case shows good agreement between experiment and numerical results. Based on the experimental verification, the lower pitching moment, and the lower loads on the secondary element, the final AG9301 configuration recommended is the 20° deflection case.

A primary drawback to the AG9301 airfoil design is the high pitching moment. The moment coefficient is roughly twice that of most single element airfoils. This could lead to significant trim drag penalties if

the wing and aircraft are not properly matched. If the high pitching moment is accounted for in the wing placement on the airframe, no significant penalty should be necessary.

Future studies should be performed in an attempt to further tailor the primary element to the two element system. The primary element used in this experiment operated at an unusually low angle of attack and was not producing a proportionate amount of the total lift at low lift coefficients. An improved primary element design could remedy this situation and have larger percentages of laminar flow, particularly on the lower surface, at low lift values.

ACKNOWLEDGMENTS

This material is based upon work supported by the NASA-Langley Research Center under Grant No. NAG-1-1522. Any opinions, findings, and conclusions or recommendations expressed in this publication are those of the authors and do not necessarily reflect the views of the NASA-Langley Research Center. Sincere thanks are extended to Dr. Michael F. Card at the NASA Langley Research Center for supporting the effort. Acknowledgment is also due to Mr. Harry L. Morgan, Jr. of NASA Langley for providing a copy of the MCARFA computer code and Mr. Bill Cleary of Ciba-Geigy Corporation for donating the Ren Shape used in the wind tunnel model construction.

REFERENCES

1. Anderson, J.D., Jr., *Introduction to Flight*, Second Edition, McGraw-Hill Book Company, New York, 1985.
2. Schweizer, P.A., "An International One-Design Class and the Olympics," *Technical Soaring*, Vol XIII, No. 2, April 1989, pp. 42-44.
3. Abbott, I.A., von Doenhoff, A.E. and Stivers, L.S., "Summary of Airfoil Data," NACA Report No. 824, 1945.
4. Abbott, I.A. and von Doenhoff, A.E., *Theory of Wing Sections*, Dover Publications, New York, 1959.
5. Smith, A.M.O., "High-Lift Aerodynamics," *Journal of Aircraft*, Vol. 12, No. 6, 1975, pp. 501-530.
6. Bauer, A.B., "The Laminar Airfoil Problem," *Eighth Annual Symposium of the National Free-Flight Society*, 1975, pp. 40-45.
7. Brune, G.W. and Manke, J.W., "An Improved Version of the NASA-Lockheed Multielement Airfoil Analysis Computer Program," NASA CR-145323, 1978.
8. Brune, G.W. and Manke, J.W., "A Critical Evaluation of the Predictions of the NASA-Lockheed Multielement Airfoil Computer Program," NASA CR-145322, 1978.
9. Allison, D.O. and Waggoner, E.G., "Prediction of Effects of Wing Contour Modifications on Low-Speed Maximum Lift and Transonic Performance for the EA-6B Aircraft," NASA TP-3046, 1990.
10. Morgan, H.L., "A Computer Program for the Analysis of Multielement Airfoils in Two-Dimensional Subsonic, Viscous Flow," *Aerodynamic Analyses Requiring Advanced Computers*, NASA SP-347 Part II, 1975, pp. 713-747.
11. Smetana, F.O., Summey, D.C., Smith, N.S. and Carden, R.K., "Light Aircraft Lift, Drag, and Moment Prediction - A Review and Analysis," NASA CR-2523, May 1975.
12. Stevens, W.A., Goradia, S.H., and Braden, J.A., "Mathematical Model for Two-Dimensional Multi-Component Airfoils in Viscous Flow," NASA CR-1843, 1971.

13. Stevens, W.A., Goradia, S.H., Braden, J.A. and Morgan, H.L., "Mathematical Model for Two-Dimensional Multi-Component Airfoils in Viscous Flow," AIAA Paper 72-2, San Diego, CA, Jan. 1972.
14. Williams, B.R., "An Exact Test Case for the Plane Potential Flow About Two Adjacent Lifting Aerofoils," R&M No. 3717, Aeronautical Research Council, London, 1973.
15. Platt, R.C. and Abbott, I.H., "Aerodynamic Characteristics of NACA 23012 and 23021 Airfoils with 20-percent-chord External-airfoil Flaps of NACA 23012 Section," NACA Report No. 573, 1936.
16. Wenzinger, C.J. and Delano, J.B., "Pressure Distribution over an NACA 23012 Airfoil with a Slotted and a Plain Flap," NACA Report No. 633, 1938.
17. Wenzinger, C.J., "Pressure Distribution over an NACA 23012 Airfoil with an NACA 23012 External-airfoil Flap," NACA Report No. 614, 1938.
18. Wenzinger, C.J. and Harris, T.A., "Wind-tunnel Investigation of an NACA 23012 Airfoil with Various Arrangements of Slotted Flaps," NACA Report No. 664, 1939.
19. Eppler, R. and Somers, D.M., "A Computer Program for the Design and Analysis of Low-Speed Airfoils," NASA TM-80210, Washington, D.C., 1980.
20. Eppler, R. and Somers, D.M., "Supplement To: A Computer Program for the Design and Analysis of Low-Speed Airfoils," NASA TM-81862, Washington, D.C., 1980.
21. Eppler, R., *Airfoil Program System User's Guide*, Universität Stuttgart, March 27, 1991.
22. Eppler, R., *Airfoil Design and Data*, Springer-Verlag, Berlin, 1990.
23. Nicks, O.W., Steen, G.G., Heffner, M. and Bauer, D., "Wind Tunnel Investigation and Analysis of the SM701 Airfoil," *Technical Soaring*, Vol. XVI, No. 4, Presented at the XXII OSTIV Congress, Uvalde, Texas, 1991, pp. 109-115.
24. Reed, R.C., "Wortmann FX 79-K-144/17 Airfoil Low Speed Wind Tunnel Test," Report No. TR-9231, Aerospace Engineering Division, Texas Engineering Experiment Station, Texas A&M University System, November 1992.
25. Somers, D.M., "Design and Experimental Results for a Natural-Laminar-Flow Airfoil for General Aviation Applications," NASA TP-1861, 1981.
26. "Low Speed Wind Tunnel Facility Handbook," Aerospace Engineering Division, Texas Engineering Experiment Station, Texas A&M University System, 1985.
27. Haffermalz, D.S. and Steen, G.G., "Freestream Turbulence Intensity Measurements in the Texas A&M University Low Speed Wind Tunnel," Report No. TR-9211, Aerospace Engineering Division, Texas Engineering Experiment Station, Texas A&M University System, July 1992.
28. Anderson, J.D., Jr., *Fundamentals of Aerodynamics*, Second Edition, McGraw-Hill, Inc., New York, 1991, pp. 70-71.
29. Wentz, W.H. and Ostowari, C., "Additional Flow Field Studies of the GA(W)-1 Airfoil with 30-Percent Chord Fowler Flap Including Slot-Gap Variations and Cove Shape Modifications," NASA CR-3687, 1983.
30. Somers, D.M. and Maughmer, M.D., "The SM701 Airfoil: An Airfoil for World Class Sailplanes," Presented at the XXIII OSTIV Congress, Uvalde, Texas, August 1991.
31. Johnson, R.H., "Flight Testing/Performance Improvements Through Wing Profile Correction," *Technical Soaring*, Vol. XIII, No. 3, pp. 84-89.
32. Roskam, J., *Airplane Design Part V: Component Weight Estimation*, Roskam Aviation and Engineering Company, Ottawa, Kansas, 1985.

Table 1 - MCARFA and Williams' Exact Aerodynamic Load Results

Case A		
$\alpha = 0^\circ, \delta = 30^\circ$		
	c_l	c_d
Exact Main	2.9065	-.3839
MCARFA Main	2.8705	-.3686
Exact Flap	0.8302	0.3838
MCARFA Flap	0.8453	0.3836
Exact Total	3.7367	-0.0001
MCARFA Total	3.7158	0.0150

Case B		
$\alpha = 0^\circ, \delta = 10^\circ$		
	c_l	c_d
Exact Main	1.6915	-0.0898
MCARFA Main	1.6758	-0.0847
Exact Flap	0.3366	0.0897
MCARFA Flap	0.3435	0.0900
Exact Total	2.0281	-0.0001
MCARFA Total	2.0193	0.0054

NACA 23012 with 20% 23012 External Airfoil Flap
 $\delta = 20^\circ$

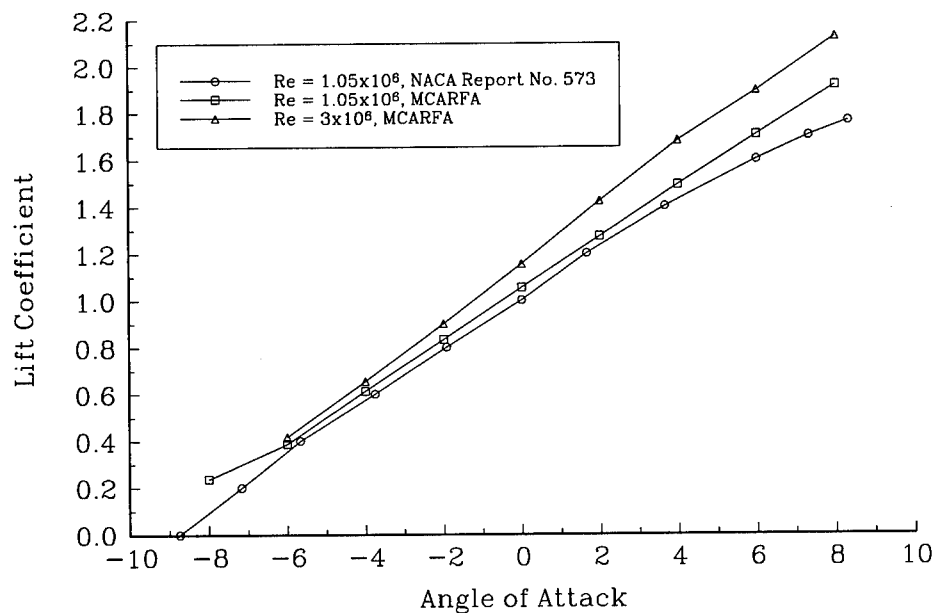


Figure 1A - NACA 23012 with 23012 Flap Lift Coefficient Results

NACA 23012 with 20% 23012 External Airfoil Flap
 $\delta = 20^\circ$

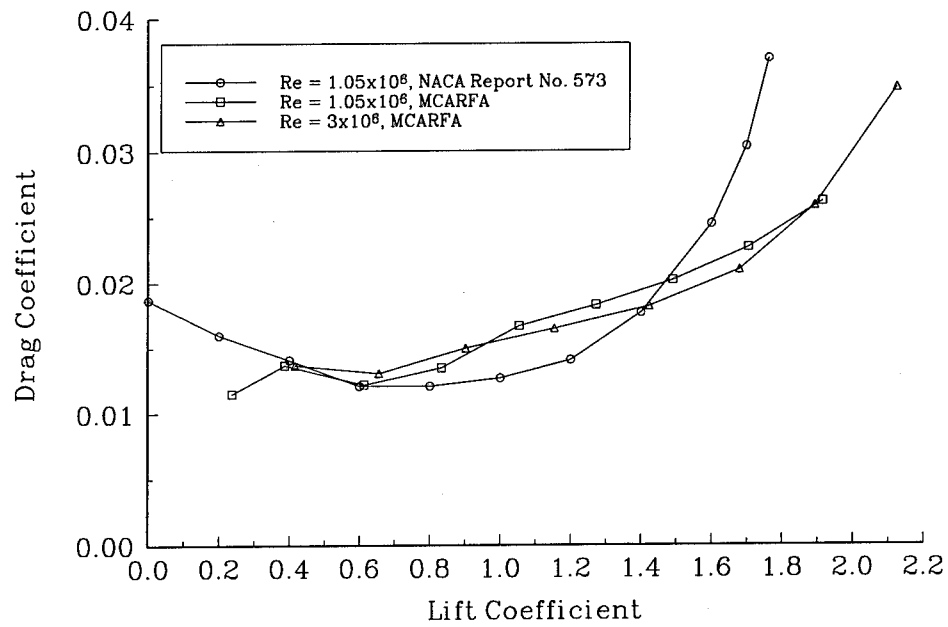


Figure 1B - NACA 23012 with 23012 Flap Drag Coefficient Results

NACA 23012 with 20% 23012 External Airfoil Flap
 $\delta = 20^\circ$

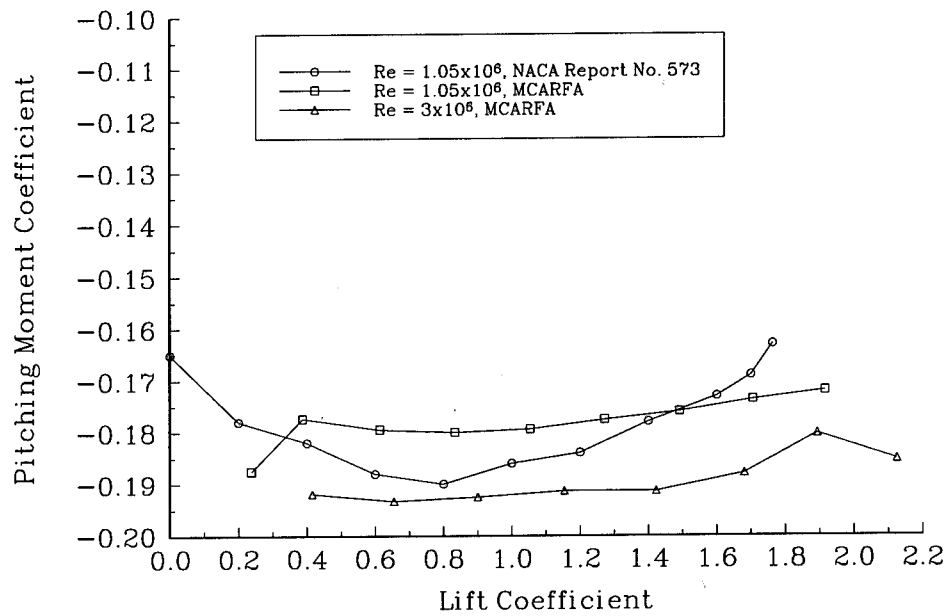


Figure 1C - NACA 23012 with 23012 Flap Moment Coefficient Results

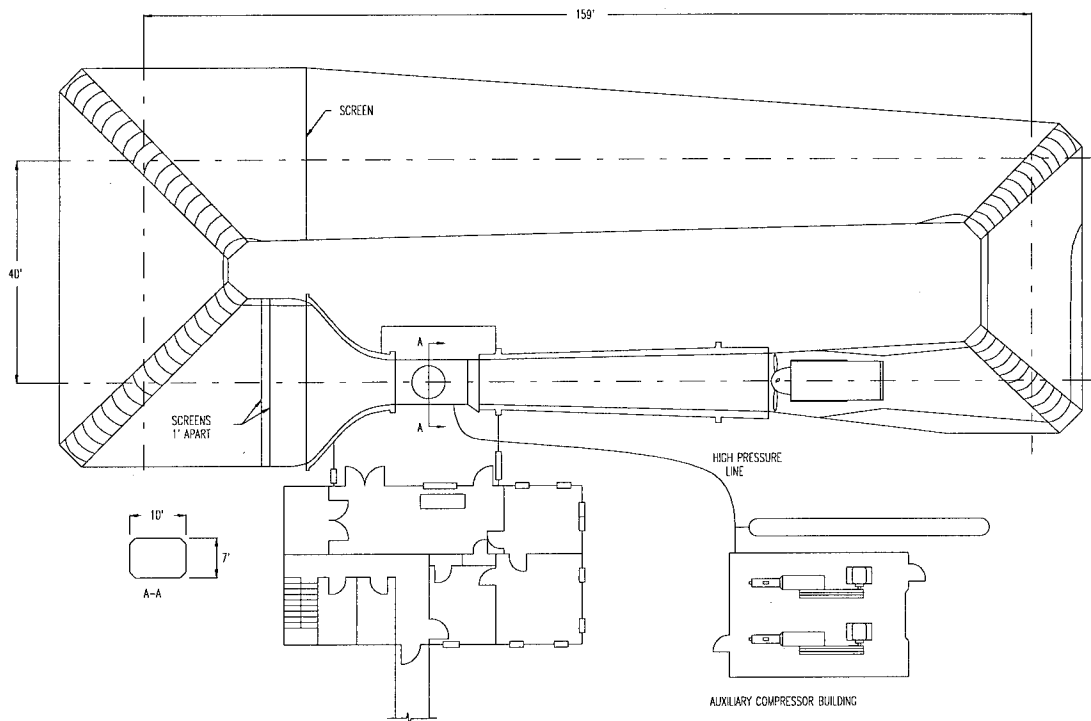


Figure 2 - Texas A&M University Low Speed Wind Tunnel Facility Diagram

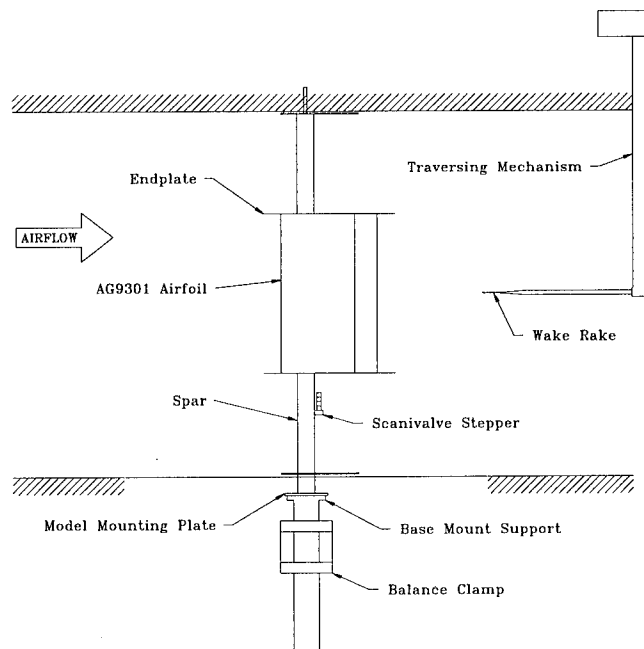


Figure 3 - AG9301 Installed in TAMU-LSWT

MCARFA Results of Two Element Airfoils $\delta_2 = 20^\circ$

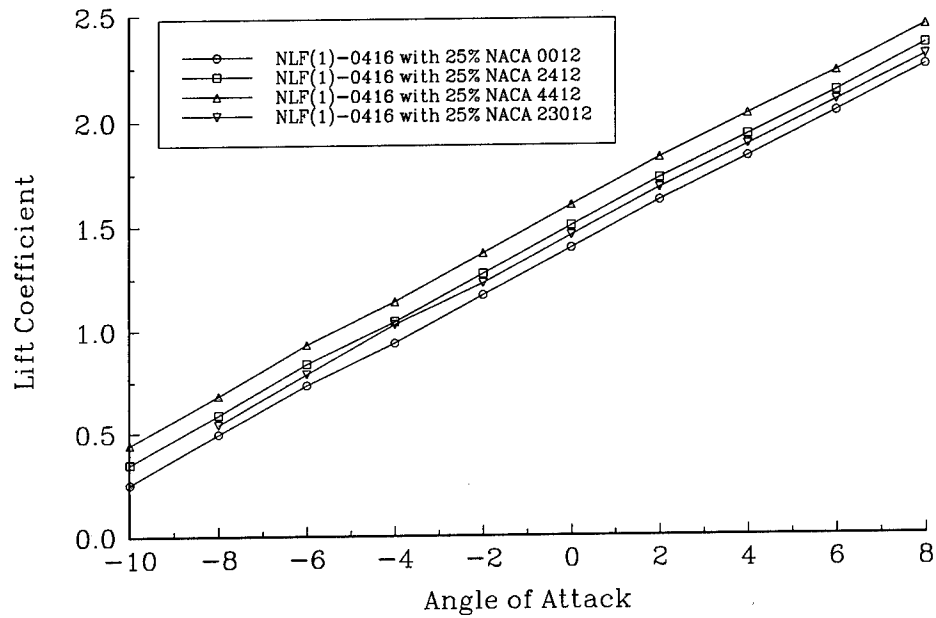


Figure 4A - Effect of Secondary Element Profile on Lift Coefficient

MCARFA Results of Two Element Airfoils $\delta_2 = 20^\circ$

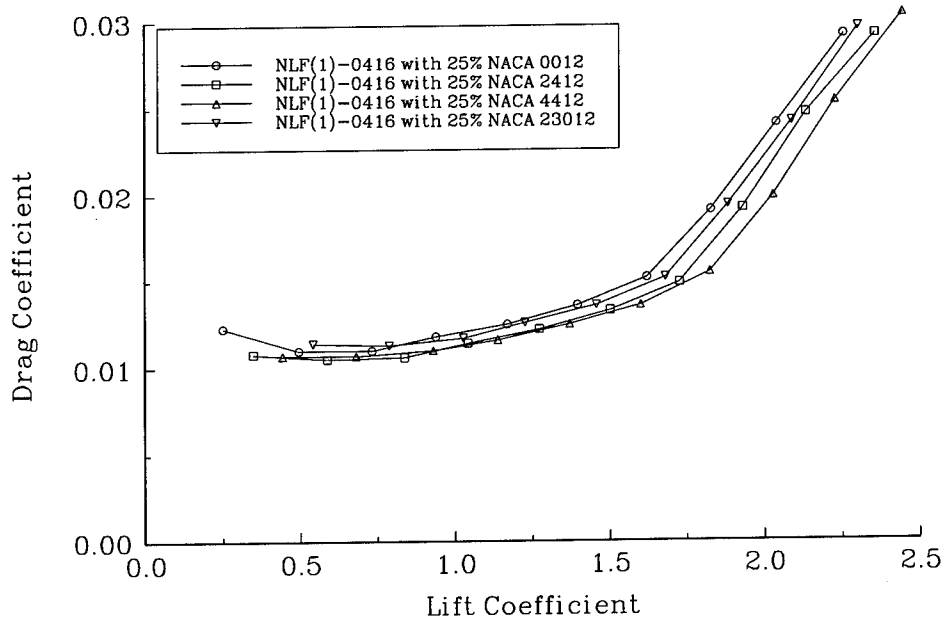


Figure 4B - Effect of Secondary Element Profile on Drag Coefficient

MCARFA Results of Two Element Airfoils
 $\delta_2 = 20^\circ$

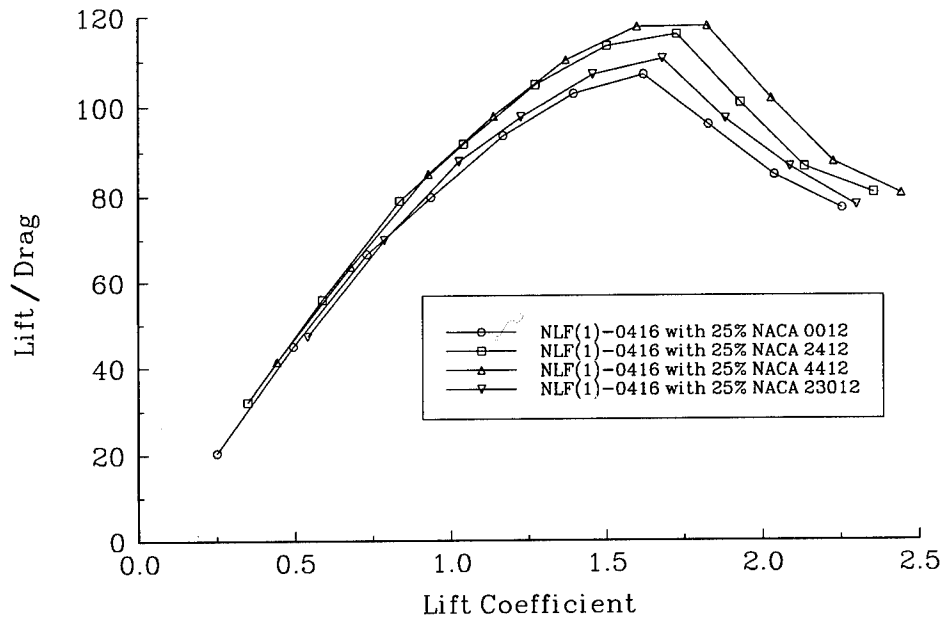


Figure 4C - Effect of Secondary Element Profile on L/D

MCARFA Results of Two Element Airfoils
 $\delta_2 = 20^\circ$

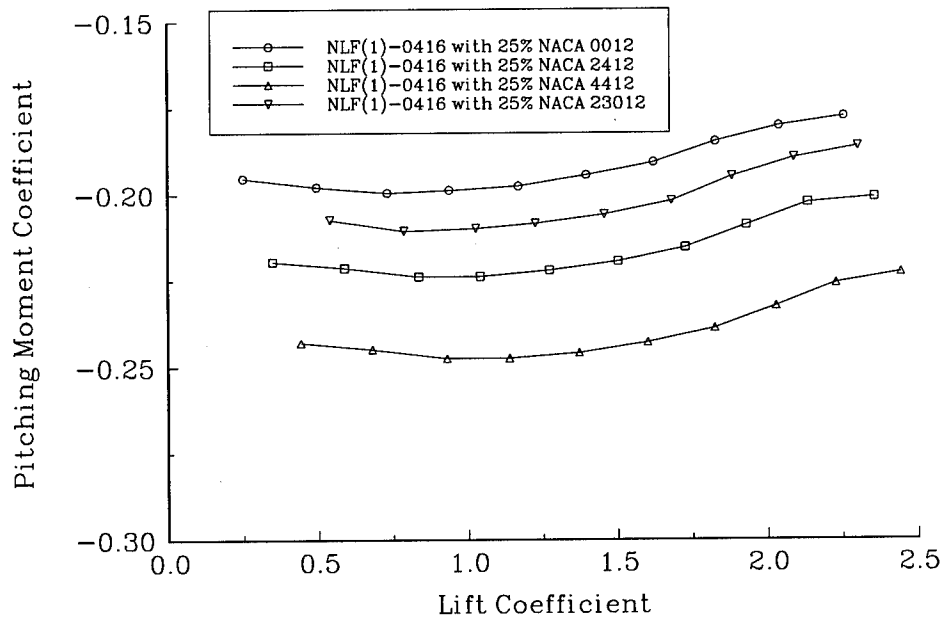


Figure 4D - Effect of Secondary Element Profile on Moment Coefficient

MCARFA Results of NLF(1)-0416 with 25% NACA 4412
 $XLE_2 = 95\% c_1$, $YLE_2 = -2\% c_1$

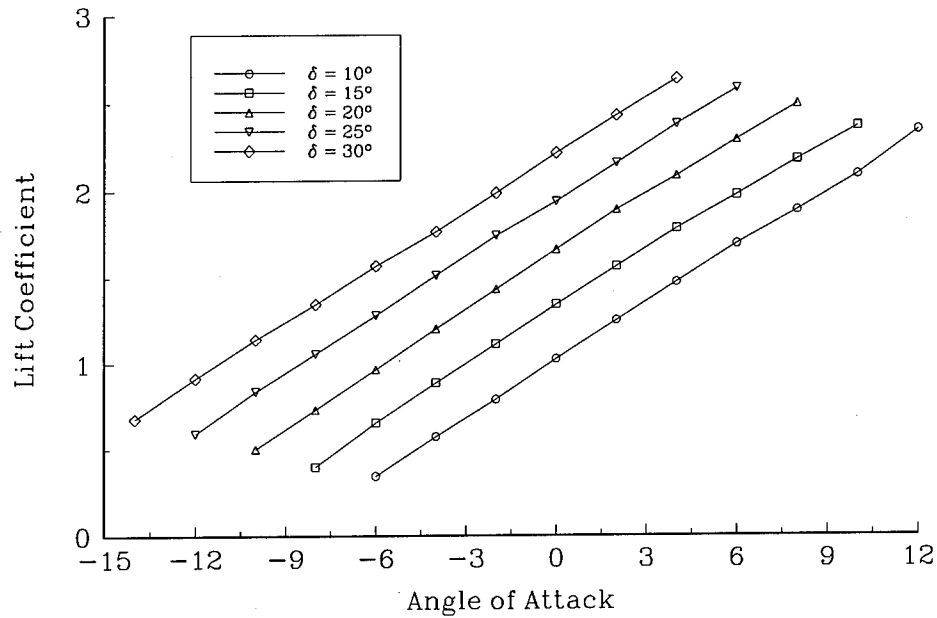


Figure 5A - Effect of Secondary Element Relative Angle on Lift Coefficient

MCARFA Results of NLF(1)-0416 with 25% NACA 4412
 $XLE_2 = 95\% c_1$, $YLE_2 = -2\% c_1$

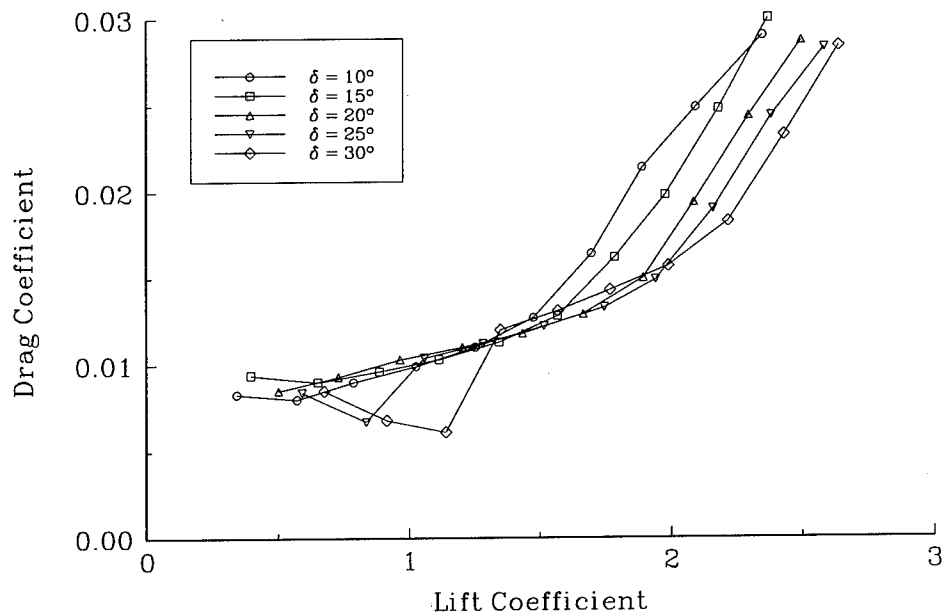


Figure 5B - Effect of Secondary Element Relative Angle on Drag Coefficient

MCARFA Results of NLF(1)-0416 with 25% NACA 4412
 $XLE_2 = 95\% c_1$, $YLE_2 = -2\% c_1$

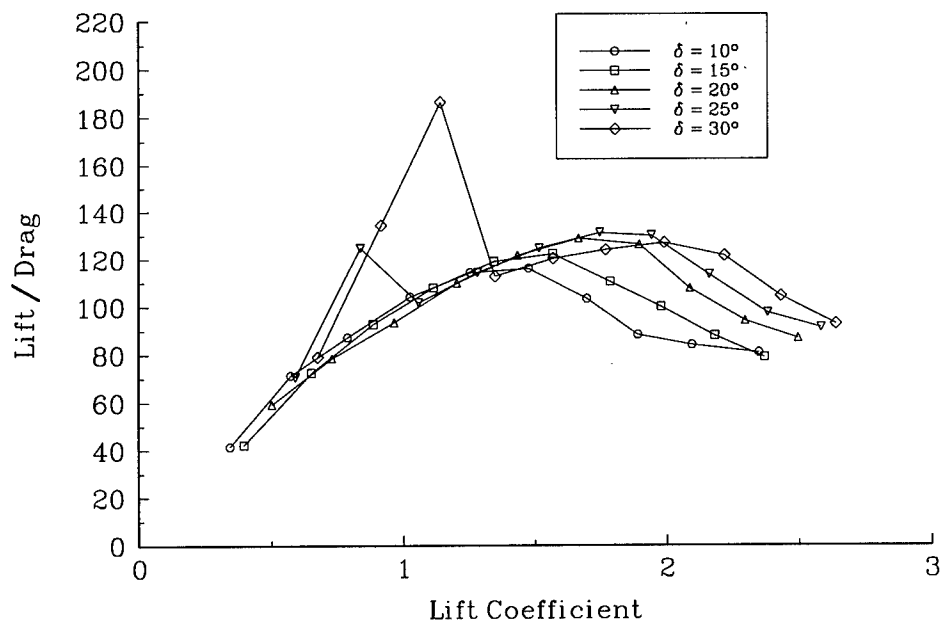


Figure 5C - Effect of Secondary Element Relative Angle on L/D

MCARFA Results of NLF(1)-0416 with 25% NACA 4412
 $XLE_2 = 95\% c_1$, $YLE_2 = -2\% c_1$

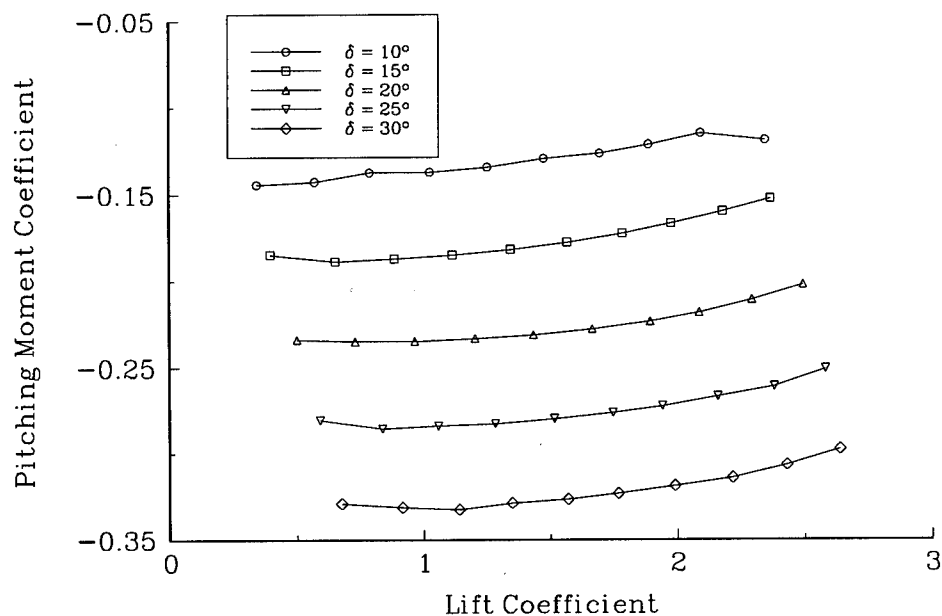


Figure 5D - Effect of Secondary Element Relative Angle on Moment Coefficient

MCARFA Results of NLF(1)-0416 with 25% NACA 4412
 $Y_{LE2} = -1.5\% c_1, \delta_2 = 30^\circ$

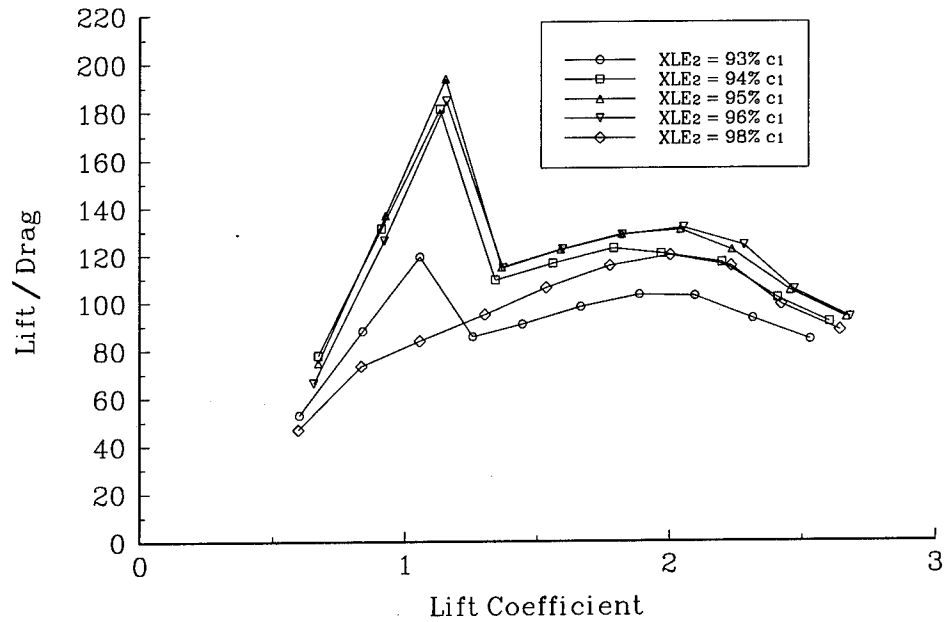


Figure 6A - Effect of Secondary Element Relative Horizontal Position on L/D

MCARFA Results of NLF(1)-0416 with 25% NACA 4412
 $X_{LE2} = 95\% c_1, \delta_2 = 30^\circ$

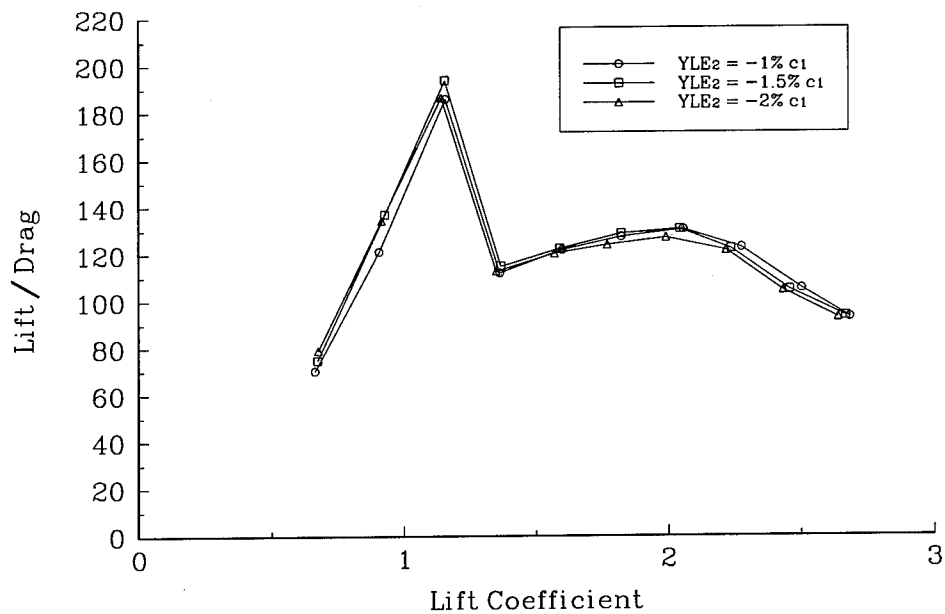


Figure 6B - Effect of Secondary Element Relative Vertical Position on L/D

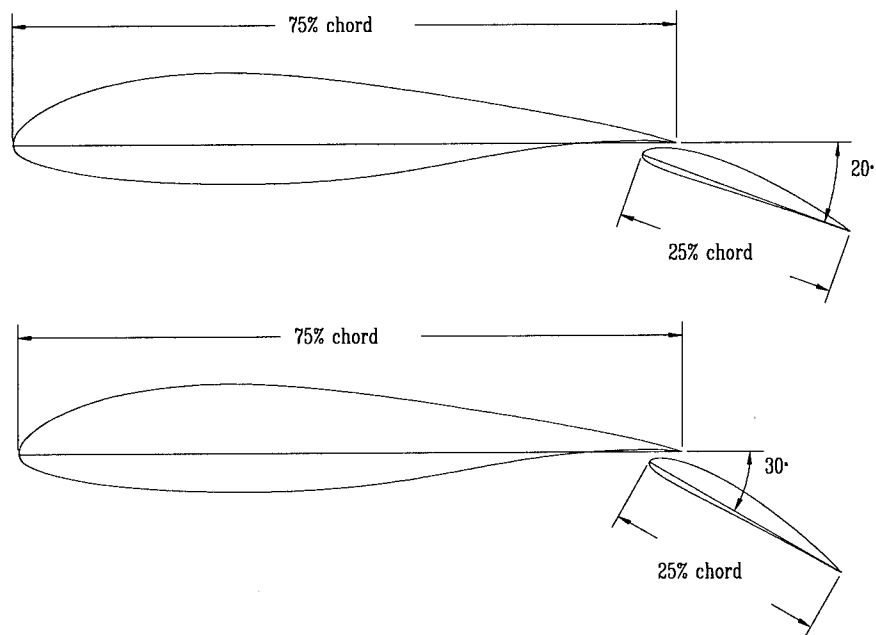


Figure 7 - AG9301 Airfoil Shape with 20° and 30° Secondary Element Deflections

MCARFA Results for AG9301 Airfoil
 $XLE_2 = 95\% c_1$, $YLE_2 = -1.5\% c_1$, $\delta = 20^\circ$

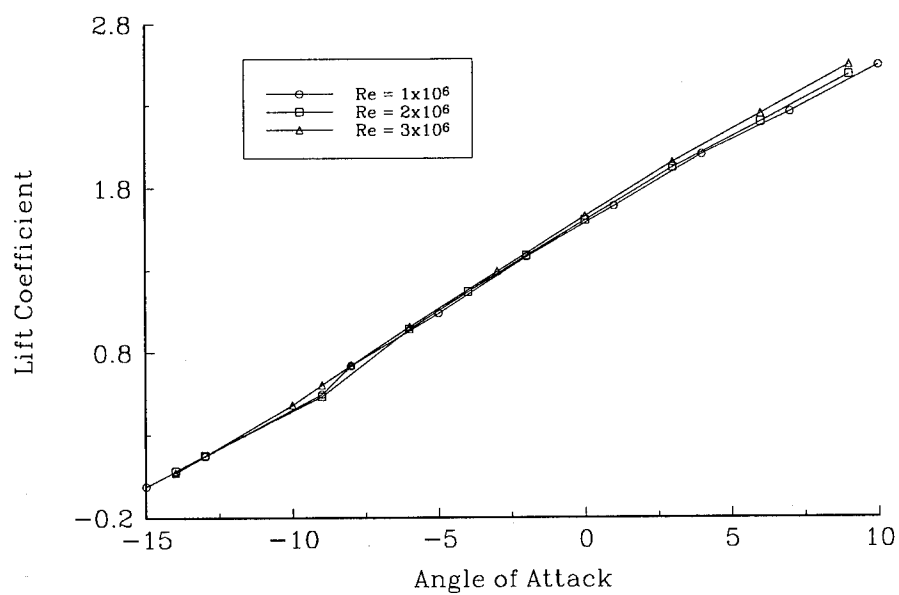


Figure 8A - Reynolds Number Effect on AG9301 Lift Coefficient

MCARFA Results for AG9301 Airfoil
 $XLE_2 = 95\% c_1$, $YLE_2 = -1.5\% c_1$, $\delta = 20^\circ$

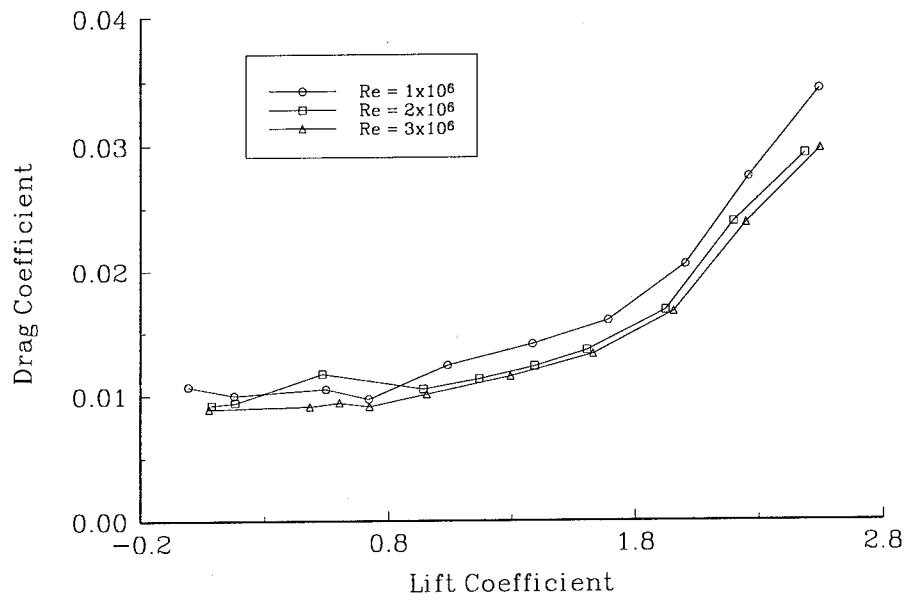


Figure 8B - Reynolds Number Effect on AG9301 Drag Coefficient

MCARFA Results for AG9301 Airfoil
 $XLE_2 = 95\% c_1$, $YLE_2 = -1.5\% c_1$, $\delta = 20^\circ$

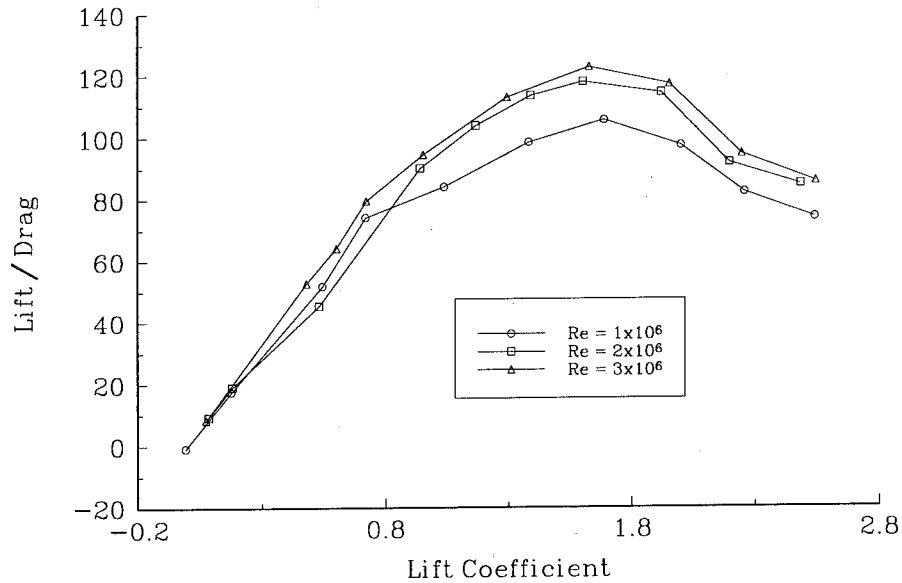


Figure 8C - Reynolds Number Effect on AG9301 L/D

MCARFA Results for AG9301 Airfoil
 $XLE_2 = 95\% c_1$, $YLE_2 = -1.5\% c_1$, $\delta = 20^\circ$

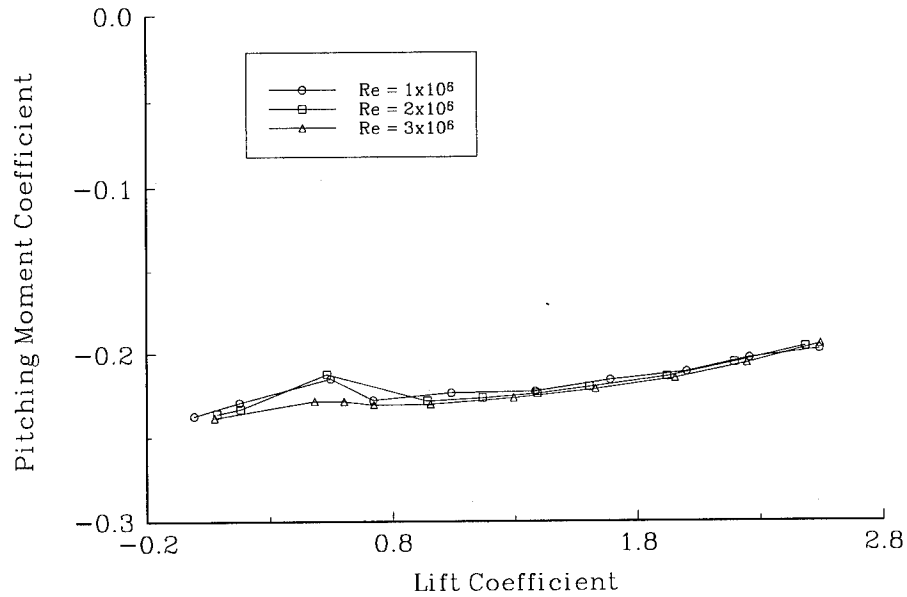


Figure 8D - Reynolds Number Effect on AG9301 Moment Coefficient

Numerical and Experimental AG9301 Airfoil Results
 $Re = 1 \times 10^6$, $XLE_2 = 95\% c_1$, $YLE_2 = -1.5\% c_1$, $\delta = 30^\circ$

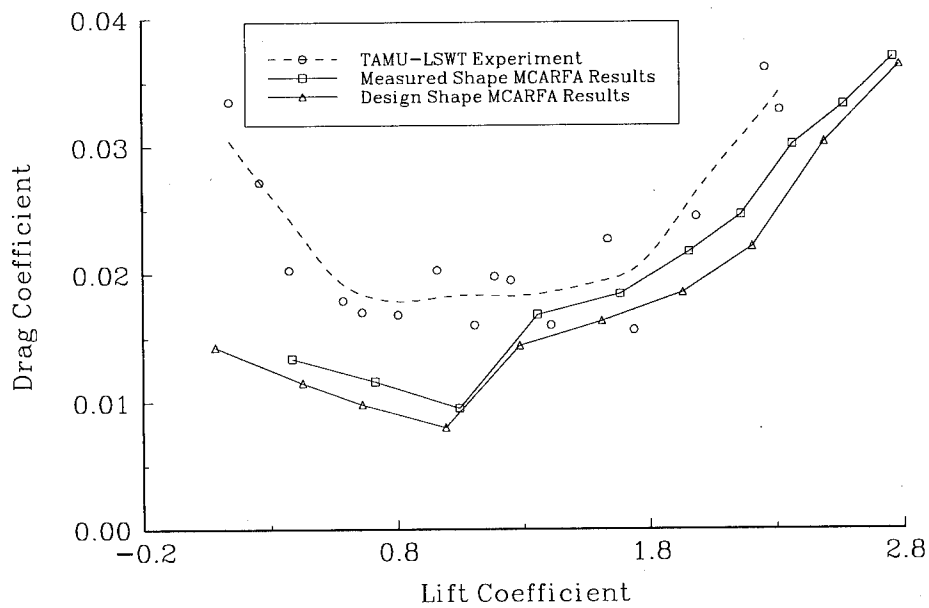


Figure 9A - AG9301-30° Airfoil Experimental Drag Coefficient at $Re = 1 \times 10^6$

Numerical and Experimental AG9301 Airfoil Results $Re = 1 \times 10^6$, $XLE2 = 95\% c_1$, $YLE2 = -1.5\% c_1$, $\delta = 30^\circ$

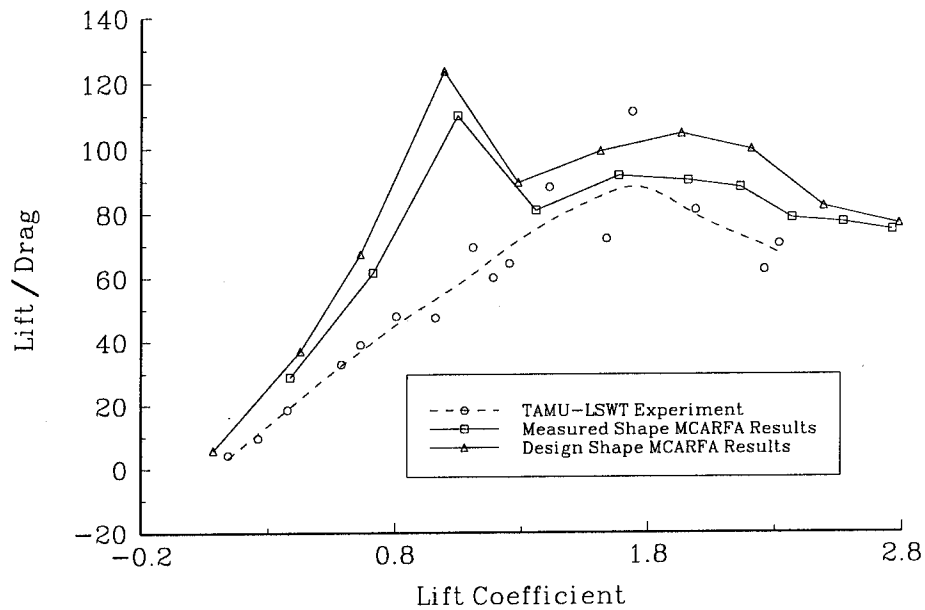


Figure 9B - AG9301-30° Airfoil Experimental L/D at $Re = 1 \times 10^6$

Numerical and Experimental AG9301 Airfoil Results $Re = 1 \times 10^6$, $XLE2 = 95\% c_1$, $YLE2 = -1.5\% c_1$, $\delta = 20^\circ$

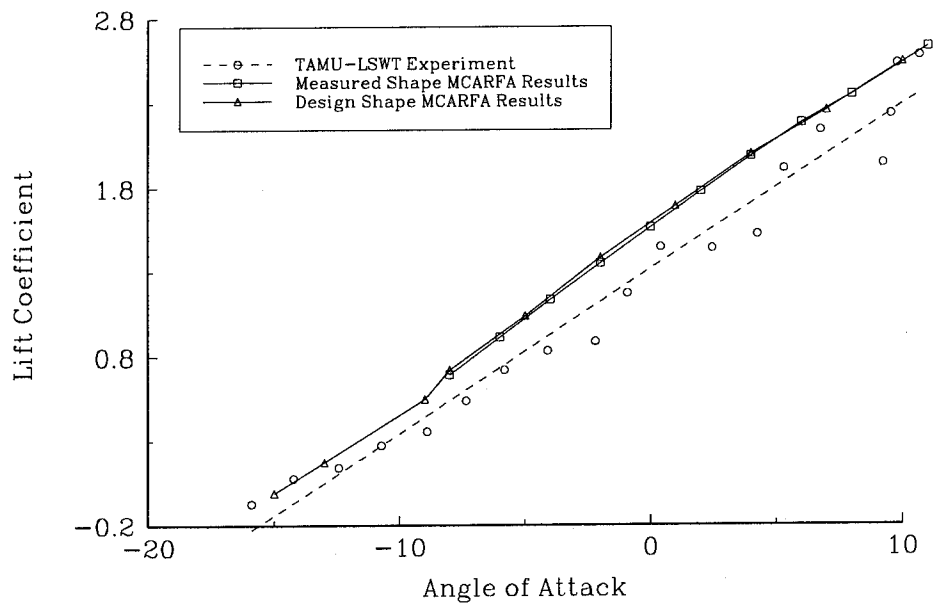


Figure 10A - AG9301 Airfoil Experimental Lift Coefficient at $Re = 1 \times 10^6$

Numerical and Experimental AG9301 Airfoil Results
 $Re = 1 \times 10^6$, $XLE2 = 95\% c_1$, $YLE2 = -1.5\% c_1$, $\delta = 20^\circ$

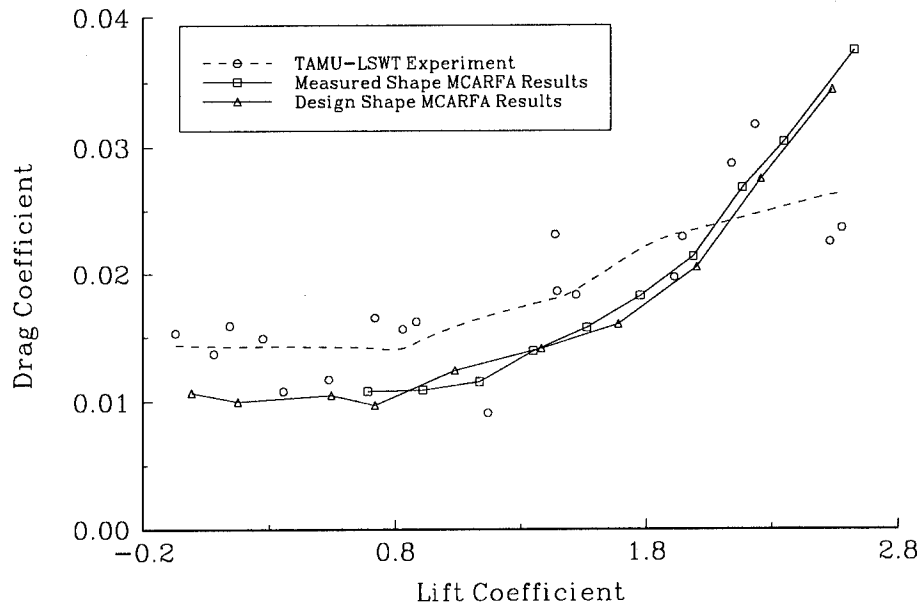


Figure 10B - AG9301 Airfoil Experimental Drag Coefficient at $Re = 1 \times 10^6$

Numerical and Experimental AG9301 Airfoil Results
 $Re = 1 \times 10^6$, $XLE2 = 95\% c_1$, $YLE2 = -1.5\% c_1$, $\delta = 20^\circ$

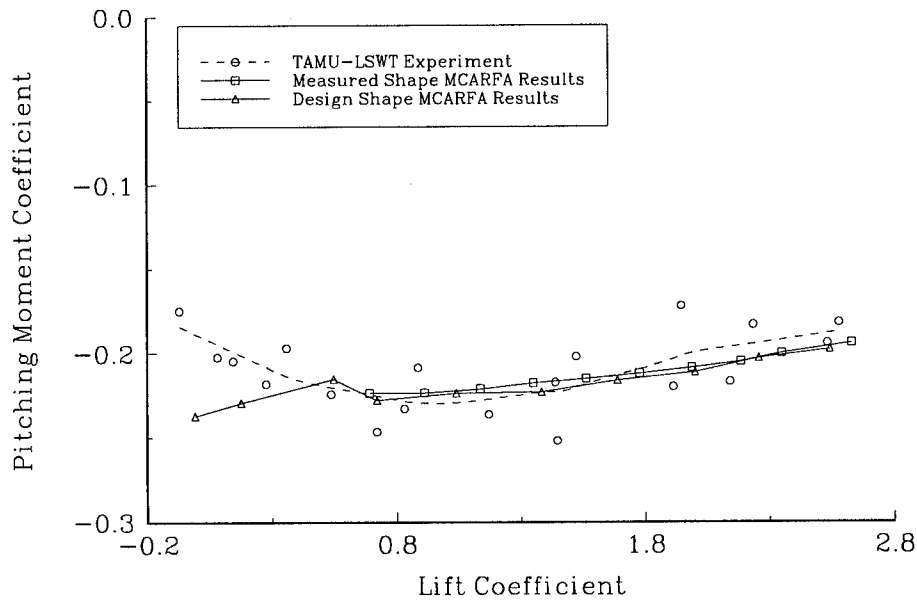


Figure 10C - AG9301 Airfoil Experimental Moment Coefficient at $Re = 1 \times 10^6$

Numerical and Experimental AG9301 Airfoil Results
 $Re = 1 \times 10^6$, $XLE_2 = 95\% c_1$, $YLE_2 = -1.5\% c_1$, $\delta = 20^\circ$

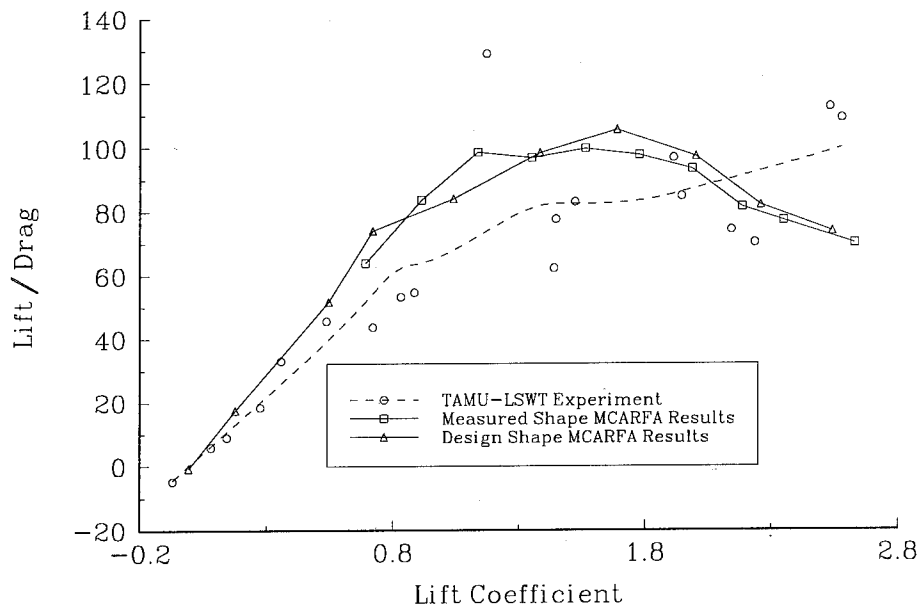


Figure 10D - AG9301 Airfoil Experimental L/D at $Re = 1 \times 10^6$

Numerical and Experimental AG9301 Airfoil Results
 $Re = 2 \times 10^6$, $XLE_2 = 95\% c_1$, $YLE_2 = -1.5\% c_1$, $\delta = 20^\circ$

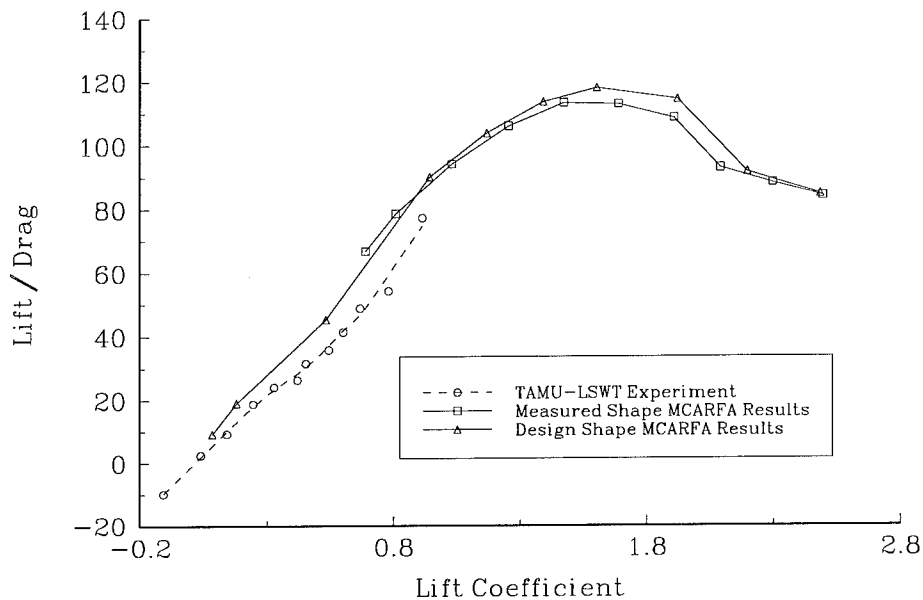


Figure 11 - AG9301 Airfoil Experimental L/D at $Re = 2 \times 10^6$

Numerical and Experimental AG9301 Airfoil Results
 $Re = 3 \times 10^6$, $XLE_2 = 95\% c_1$, $YLE_2 = -1.5\% c_1$, $\delta = 20^\circ$

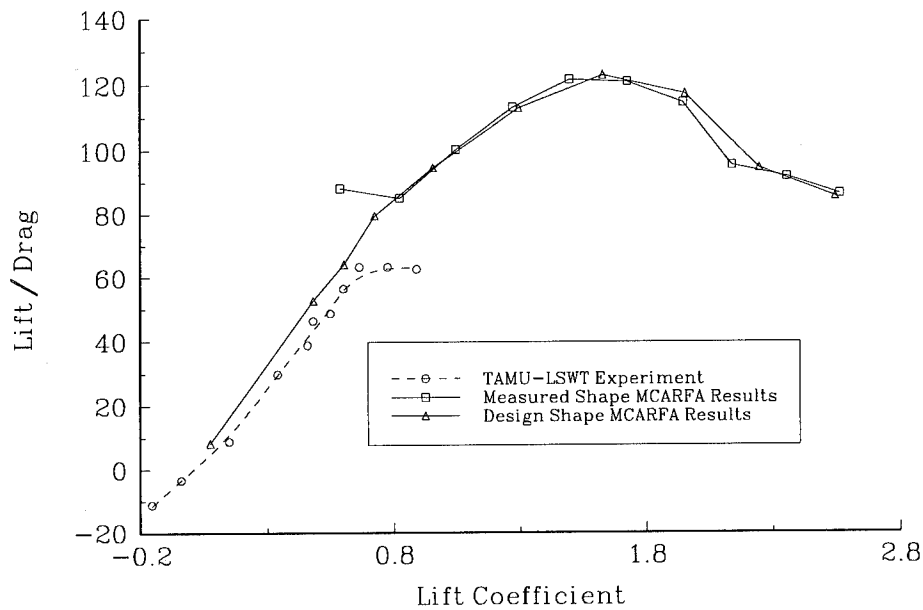


Figure 12 - AG9301 Airfoil Experimental L/D at $Re = 3 \times 10^6$

Numerical and Experimental AG9301 Airfoil Results
 $Re = 3 \times 10^6$, $XLE_2 = 95\% c_1$, $YLE_2 = -1.5\% c_1$

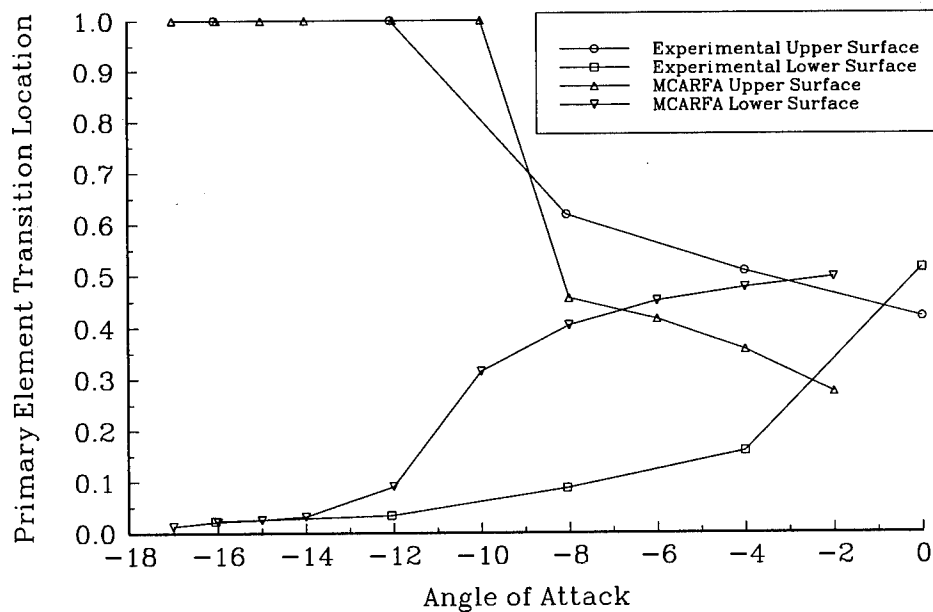


Figure 13 - AG9301-30° Primary Element Transition Location Results

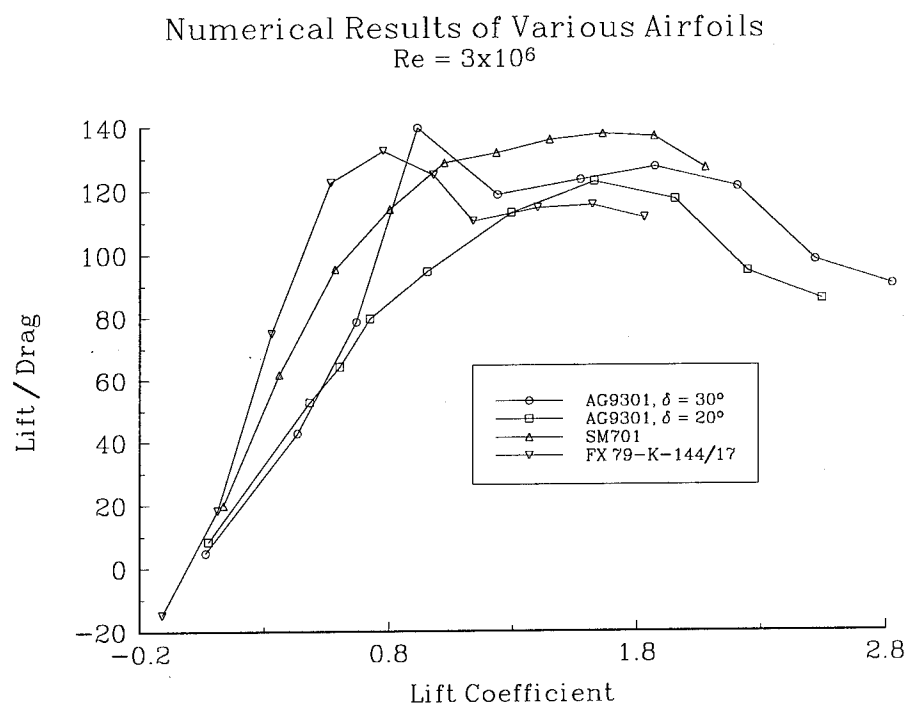


Figure 14 - Comparison of L/D for Various Airfoils

Table 2 - Airfoil Cruise Performance Comparison

$Re = 3 \times 10^6$				
Airfoil	Result Source	C_{lmax}	$C_{lcruise}$	L/D_{cruise}
AG9301 - 30°	MCARFA	2.827	.63	72.67
AG9301 - 20°	MCARFA	2.545	.57	61.06
NLF(1)-0416	NASA TP-1861	1.68	.4	65.57
	MCARFA	1.77	.4	60.92
	PROFIL	1.69	.4	60.02
SM701	MCARFA	1.87	.4	67.97
	PROFIL	1.82	.4	68.55
FX 79-K-144/17	MCARFA	1.40	.31	70.18
	PROFIL	1.51	.34	70.92

WINGLET PERFORMANCE FOR HIGH ASPECT RATIO WING PLANFORMS

David Colling
Texas A&M University
Aerospace Engineering
College Station, Texas

ABSTRACT

A wind tunnel test was conducted at the Texas A&M University 2.1 x 3.0 meter (7 x 10 ft) Low Speed Wind Tunnel to study the change in wing performance and other aerodynamic characteristics from the use of winglets on a sailplane wing. The winglet used in this study was designed by Mr. Peter Masak. It is the prototype winglet design used on a German sailplane called the Discus. A full-scale model of the outer 1.5 meters of a 15-meter sailplane wing was used for the test. Performance comparisons were made by measuring the amount of drag reduction from the use of the winglet as compared to the standard wing tip used on the Discus sailplane. A few test runs were also made using no wing tip. Other aerodynamic characteristics studied included the following. The change in pitching moment caused by the winglet. The amount of side force created by the winglet and how it relates to the lift generated by the wing. The change in the wing lift coefficient due to the winglets. The boundary layer transition on the winglet and how it relates to the amount of winglet side force, and the effect that the winglet has on boundary layer transition on the top surface of the wing.

INTRODUCTION

A series of winglets have been designed which are used on different production sailplanes. The winglet used in this study shares the same basic design as the Ventus winglet shown in Figure 1. Three days of wind tunnel testing were conducted. The first two days of testing were used to gather force and moment balance data. Flow visualization was conducted on the final day of testing. It was during flow visualization testing when it was discovered that laminar flow separation, in which the air flow did not reattach, was occurring on the outside surface of the winglet. A laminar separation bubble, in which the air flow reattaches as a turbulent boundary layer, was occurring on the inside winglet surface. Turbulator zig-zag tape was installed on the winglet before the laminar separation on the outside and the laminar bubble on the inside to trip the boundary layer to turbulent. A series of tests then followed to gather more force and moment balance data. The installation of the turbulator tape showed a significant improvement in the amount of drag reduced and thus an increase in the lift to drag ratio (L/D).

PURPOSE

The goal of this wind tunnel test was to determine the change in lift and drag of a high aspect ratio, laminar flow, wing using a winglet as compared to the same wing with a standard wing tip. Other points of interest were the amount of side force produced and its relation to the lift of the wing, and the changes in pitching moment of the wing caused by the winglet.

WINGLET THEORY

Winglets are designed to enhance the maximum L/D particularly at lower airspeeds for sailplane applications. This occurs because of a number of factors. A side force produced by the winglet creates a

"thrust" component. The lift vector generated by the winglet is directed toward the fuselage in the forward direction (Figure 2). The winglet surface is set at a slight negative angle of attack with respect to the wing tip to take advantage of the inflow caused by wing tip effects. The lift distribution of a wing can be changed by the winglet so that the total lift of the wing is greater at the same angle of attack. This should allow the wing to operate at a lower angle of attack (Figure 3). A reduction in stall speed has been measured in flight testing which allows for slower circling speeds in thermals. The winglets cause a reduction of pressure on the top surface of the wing at the wing tip which improves lateral control. Winglets can also move the point of boundary layer transition from laminar to turbulent further back on the wing which reduces skin friction drag. The added surface area of the winglet can add to the skin friction drag at high airspeeds causing the L/D of the sailplane with the winglets to be less than the L/D with the standard wing tips at higher airspeeds. For this reason, there has been a trade off between low speed and high speed performance. Past flight testing of winglets on 15-meter high performance sailplanes have shown performance gains from 2.1 to 3.8 L/D points above the usual L/D of around 42/1 at an airspeed of 120 Km/Hr. The cross over point where the L/D with the winglets is less than the L/D with the standard wing tips has been measured to be at a high airspeed which is typically not reached during a flight.

WIND TUNNEL MODEL CONSTRUCTION

A fiberglass composite structure using an extruded polystyrene foam core as a base was used for construction of the wind tunnel model. The wing planform used for the model was that of a new elliptic planform 15-meter class sailplane currently under construction. Since the wind tunnel model has an elliptic leading edge, Figure (4), the foam core was cut using five different sections to approximate this shape. A main spar was constructed by cutting a trough in the foam core with a router and placing pultruded S2-glass roving in the trough until the spar cap was level with the outside surface of the foam core. The skins of the model were made with two layers of uni-directional E-glass and one layer of bi-directional E-glass with the bi-directional running at a 45 degree angle and located between the two spanwise uni-directional layers. A micro balloon and epoxy filler was used to allow the model to be sanded to the exact airfoil profile. The model was then painted with an acrylic urethane and then wet sanded and polished to a smooth surface finish.

The winglet and the standard wing tip used for the test were from a Discus sailplane. This winglet was built in 1991 but was only used for a few flights since it did not provide the expected performance gain. The wind tunnel model was built to match this particular winglet and the standard wing tip used on the Discus sailplane. The wind tunnel model uses a Wortmann 79-K-144 airfoil for the first 1.2 meters (4 ft.) of the span. On the outer 0.3 meters (1 ft.) of the span, the airfoil transitions to the Discus airfoil to match the wing tips used.

TEST PROCEDURES

A total of 63 test cases were run in the wind tunnel. Each force and moment balance data test case included a fixed airspeed and aileron deflection during an angle of attack sweep. In this report, force and moment balance data is presented for only those cases where the aileron deflection is zero and for airspeed velocities of 80, 105, 145, and 175 Km/Hr (50, 65, 90, and 110 mph). Included in the 63 test cases were 12 boundary layer flow visualization tests. The flow visualization technique used was that of coating the wing surface with kerosene and black tempera paint. These tests were conducted using a fixed aileron deflection, wing angle of attack, and airspeed.

RESULTS

Points of interest for this study included boundary layer transition points, winglet side force, lift and moment coefficients, drag coefficients, and the lift to drag ratio. With this data, the change in performance of the full-scale aircraft can be estimated. The changes in aerodynamic characteristics between the different wing tip configurations can also be determined.

FLOW VISUALIZATION TESTS

Flow visualization testing was conducted at airspeeds of 80, 145, and 175 Km/Hr and aileron deflections of -6, 0, and +6 degrees. Flow visualization testing provided many clues as to the explanation of the test results. The location of the boundary layer transition on the wing affected the wing lift curve slope while the boundary layer transition point on the winglet affected the coefficient of drag of the wing, the L/D, and the amount of side force produced by the winglet. Boundary layer transition from laminar to turbulent moves forward with increased angle of attack. Sketches of the boundary transition regions for the wing with the standard wing tip at angles of attack of 2.5, 5, and 7.5 degrees at an airspeed of 80 Km/Hr are shown in Figures 5, 6, & 7, respectively. At 5 degrees, the boundary layer transitions to turbulent at a distance of 50 percent back from the leading of the wing. Where at 7.5 degrees, the boundary transitions to turbulent at the leading edge. In Figure 5, the streamlines at the wing tip show the angle of inflow at the wing surface caused by wing tip effects. The location of boundary layer transition for the wing with the winglet is located in similar positions to that of the standard wing tip (Figures 8-10). One point of interest is the location of the boundary layer transition on the winglet. A laminar separation bubble appears on the inside surface of the winglet at airspeeds less than 120 Km/Hr. The region of boundary layer transition moves forward on the inside surface of the winglet with increased angle of attack of the wing. This gives an indication of the relative angle of attack of the winglet since the laminar bubble is located at 50% chord at the root and 25% chord at the tip of the winglet.

A laminar separation bubble is a region of stagnate flow in the boundary layer where the boundary layer actually separates and then reattaches as a turbulent boundary layer further down stream. Streamlines outside of the boundary layer must go around or over this bubble as if it were a physical obstruction on the surface. This extra motion of the streamlines cause an additional loss of energy in the air flow which results in extra drag.

WINGLET SIDE FORCE

The amount of side force produced by the winglet shows a linear trend when plotted as a function of the wing lift coefficient (Figures 11-14). From these graphs, it can be seen that the amount of side force produce by the winglet is directly proportional to the amount of lift produced by the wing. At a wing lift coefficient of zero, the winglet also produces zero side force. With negative values of wing lift coefficient, the winglet will begin to produce a negative side force, i.e. the lift vector is directed away from the fuselage.

At an airspeed of 80 Km/Hr, the winglet with turbulator tape installed has an increased amount of side force at low values of wing lift coefficient (Figure 11). This trend begins to reverse at an airspeed above 105 Km/Hr. At the higher Reynolds number, the flow separation bubble on the winglet begins to reduce in strength. The addition of the turbulator above this airspeed affects the amount of side force produced by the winglet.

WING LIFT COEFFICIENT AND MOMENT COEFFICIENT

Winglets change the lift distribution of the wing. The side force produced by the winglet lowers the pressure in the region of the wing tip. Therefore, the boundary condition that the lift of the wing go to zero at the wing tip no longer applies as was shown in Figure 3. At higher wing lift coefficients, the winglet produces more side force. Therefore, the lift curve slope for the wing with the winglet is steeper than that of the wing with the standard wing tip (Figures 15-18).

A sudden change in the lift curve slope occurs at around a 7.5 degree angle of attack. This is where the boundary layer transitions from laminar to turbulent at the leading edge of the wing. The transition point makes a sudden jump from 50 percent of chord to the leading edge in this angle of attack region. Full stall occurs at an angle of attack of 18 degrees. The aileron is in a region of separated airflow at an angle of attack of 10 degrees. The angles listed in the data are reference angles and not the actual angle of attack of the wing. The actual angle of attack is about 5 degrees greater.

The pitching moment coefficient of the wing shows a trend similar to that of the wing lift coefficient in that it depends on the amount of winglet side force being produced. The pitching moment coefficient of the wing is more negative than that of the standard wing tip when the winglet is producing a positive side force at positive values of wing lift coefficient. At negative lift coefficients, the pitching moment is less negative than that of the standard wing tip. This small change in pitching moment is due to the amount of forward, or reverse, "thrust" produced by the winglet. The additional moment is approximately equal to the "thrust" force multiplied by the distance from the surface of the wing to the center of pressure of the winglet.

WING DRAG COEFFICIENT

Values of wing drag coefficient varied greatly depending of whether or not the winglet had turbulator tape installed and the Reynolds number of the model. At an airspeed of 80 Km/Hr, the winglet without the turbulator tape showed the highest values of drag coefficient on the wing (Figure 19). This was due to the laminar separation bubble on the inside surface of the winglet and the laminar flow separation on the outside surface of the winglet. Once turbulator tape was installed on the winglet to trip the boundary layer to turbulent before it could separate, the coefficient of drag matched that of the standard wing tip at low values of wing lift coefficient and were less than that of the standard wing tip at a wing lift coefficient of 0.40 and above. At an airspeed of 105 Km/Hr, the laminar separation bubble on the winglet was not as strong but still exists. The coefficient of drag values are the lowest for the winglet with the turbulator tape installed, while the standard wing tip configuration had the highest amount of drag (Figure 20). The values of the wing coefficient of drag at an airspeed of 145 Km/Hr are almost identical for the winglet with and without turbulator tape (Figure 21). At this airspeed, the laminar separation bubble is non-existent on the winglet. The turbulator tape therefore creates a small amount of extra drag as compared to the clean winglet. One interesting note is that the wing with no wing tip produces the least amount of drag at low values of wing lift coefficient. At an airspeed of 175 Km/Hr, the wing drag coefficient values of the standard wing tip and the clean winglet are almost identical for the lower values of wing lift coefficient (Figure 22). The coefficient of drag is less than that of the standard wing tip at higher lift coefficients. A test using the winglet with turbulator tape installed was not run at this airspeed for a zero aileron deflection.

WING LIFT TO DRAG RATIO

Winglets are designed to increase the L/D of the wing. As expected, the L/D was greater than that of the standard wing tip at wing lift coefficients expected to be produced in flight. At the lower airspeeds of 80 and 105 Km/Hr, the winglet with the turbulator tape installed provide the greatest gain in the L/D of the model (Figure 23, 24). At 145 Km/Hr, the L/D values are almost identical between the winglet with and without the turbulator tape installed (Figure 25). The values of L/D at this airspeed show a large gain in

L/D with the winglets as compared to the wing with the standard wing tip. The winglet with no wing tip is shown to have the worst of the L/D values. At 175 Km/Hr, the clean winglet shows a larger value of L/D as compared to the standard wing tip for the wind tunnel model (Figure 26). The percent increase in L/D is however not as great as it was for the 145 Km/Hr case. No test was run for the winglet with turbulator tape at this airspeed. As was mentioned before, the laminar separation disappears at airspeeds above 145 Km/Hr. Therefore, at higher airspeeds it would be expected that the addition of turbulator tape will show a value of drag greater than that of the clean winglet. Therefore, a lower value of L/D as compared to the clean winglet would be seen. The L/D however should still be greater than that of the standard wing tip. This was shown to be the case for a test run at a -6 degree aileron deflection.

The L/D values shown for the model can only be used for a comparison of the different wing tip configurations on the model. In order to estimate the change in L/D for the entire sailplane, the amount of drag reduced on the model from the use of the winglets must be multiplied by two and subtracted from total drag of the sailplane with standard wing tips. A new L/D value can then be calculated for the sailplane using this new value of drag. Since the amount drag reduced by winglet depends on the lift coefficient of the wing, knowledge of the sailplane mass, airspeed, wing area, and lift to drag polar must be obtained. With this information, the lift coefficient of the wing can be estimated for a range of airspeeds. An L/D increase of 1.8 points was calculated for a sailplane with an L/D of 42/1 at an airspeed of 105 Km/Hr, a mass of 425 Kg, and a wing area of 10.2 m². This increase in L/D tapers off to zero at an airspeed of 175 Km/Hr at which point the L/D of the sailplane decreases as a result of the winglets.

CLIMB CALCULATIONS

The rate of climb can be calculated as a function of $CL^{(3/2)}/CD$. For the wind tunnel model, it would appear that climb performance would be improved simply from this factor alone as shown in Figures 27-29. For the entire aircraft, the most important factor is the improvement in low speed performance provided by the winglet. Since the winglets provide a slower stall speed, the sailplane can circle in thermals at a slower airspeed and therefore can out climb sailplanes flying at a faster airspeed.

CONCLUSIONS

The use of winglets on sailplanes can provide improvements in both glide ratio and lateral control. Wind tunnel testing provides a good controlled environment in which to test and perfect a winglet design. A series of accurate flight tests will be necessary to determine the actual performance gain. The winglets used in this wind tunnel test have been flight tested with the installation of the turbulator tape. The pilot cannot notice any change in performance so he elected not to bother using them for any future flights. These winglets are small compared to the winglets used on other sailplanes because of the narrow wing tip chord of 265 mm (10.4 in.). It would therefore be expected that the calculated L/D gain of 1.8 may be accurate based on figures obtained from other sailplanes. This small gain in L/D will be hard to notice in sailplane racing competitions since the average speeds are usually around 145 Km/Hr which is much higher than the best L/D speed of the sailplane. Other sailplanes such as the HP-18 and the Ventus have shown a very noticeable improvement in both L/D and lateral control with the addition of properly designed winglets.

REFERENCES

1. Schlichting, Hermann, "Boundary-Layer Theory" Seventh edition, McGraw-Hill Publishers. 1976.
2. Masak, Peter C. "Design of Winglets for Sailplanes" , Soaring Magazine, June 1993.
3. Nicks, Oran W., "A Physical View of Wing Aerodynamics", Technical Soaring Journal of The Soaring Society of America, Inc. and Organization Scientifique et Technique Internationale du Vol a Voile., October, 1993.
4. Webber, G. W. and Dansby T., "Wing Tip Devices for Energy Conservation and Other Purposes - Experimental and Analytical Work in Progress at the Lockheed-Georgia Company" Canadian Aeronautics and Space Journal., Vol. 29, No. 2, June 1983.
5. Whitcomb, R. T., "A Design Approach and Selected Wind-tunnel Results at High Subsonic Speeds for Wing-tip Mounted Winglets", NASA TN D-8260, July 1976.
6. Canadair Challenger, "Pilots Information Sheet, Handling Characteristics of the CL-600 with Winglets", Service Bulletin No. 600-0401, January, 1985.
7. Montoya, L. C., "KC-135 Winglet Flight Results", NASA Dryden Flight Research Center, 1980

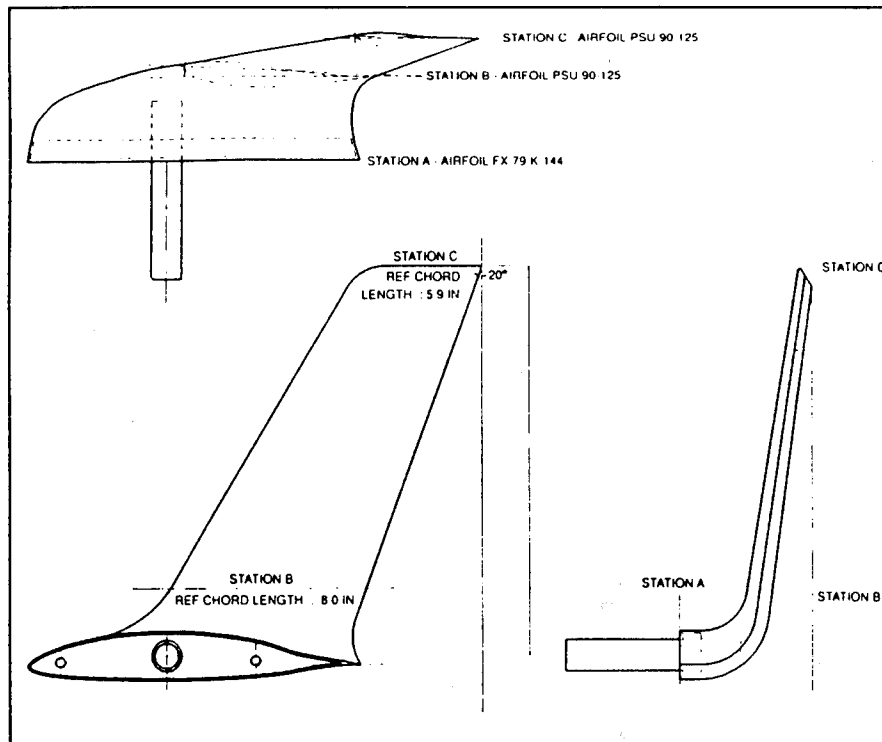


Figure 1. Three view of Ventus winglet. The prototype Discus winglets were used for this test. Both winglets share the same basic design except that the Discus winglets are smaller in size.

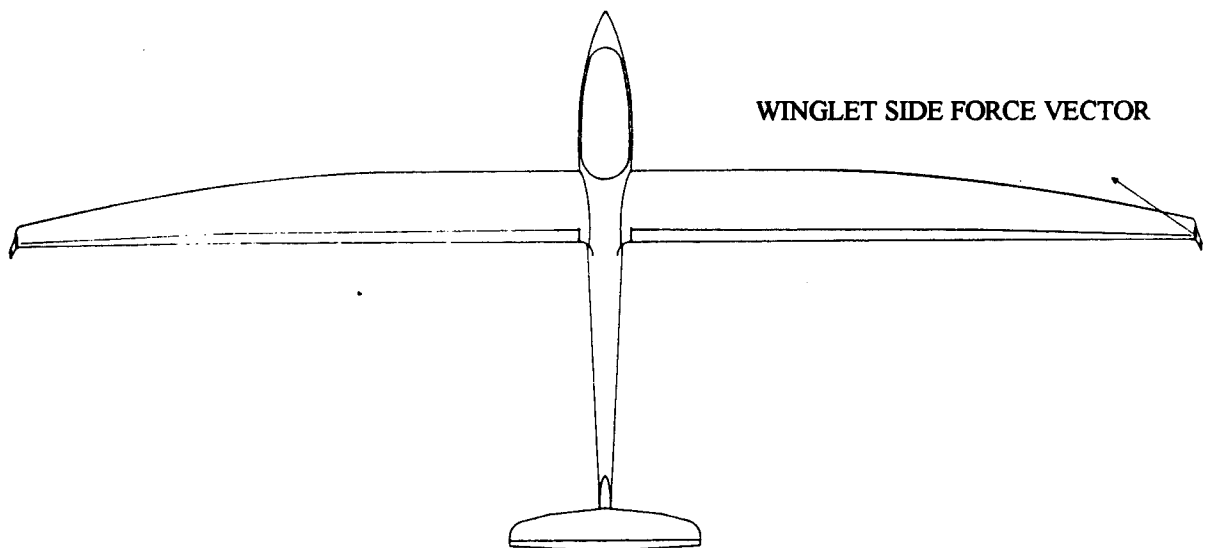


Figure 2. Forward "thrust" vector component created by the side force generated from the winglet.

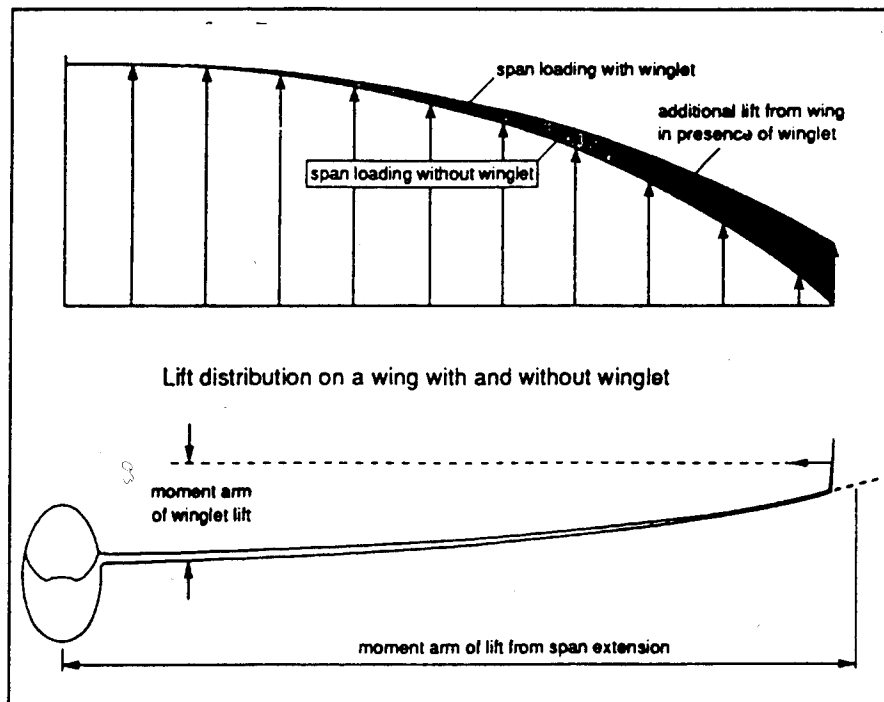


Figure 3. The wing lift distribution is changed by the winglets such that the lift does not taper off the zero at the wing tip.

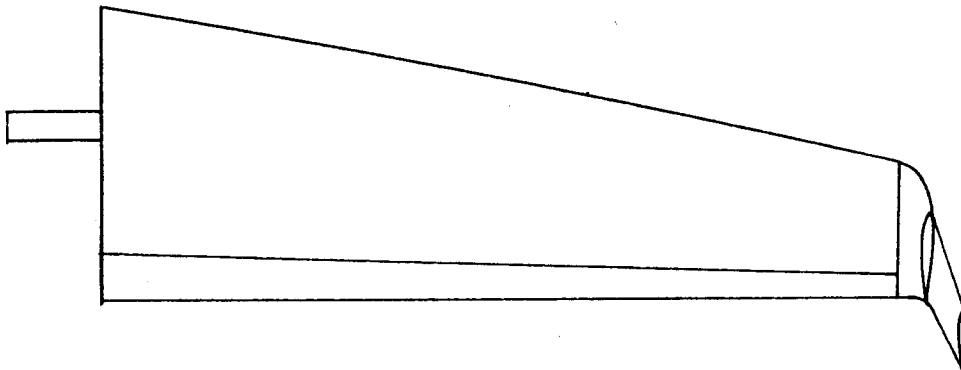


Figure 4. The wind tunnel model was built with an elliptic leading edge and a straight trailing edge.

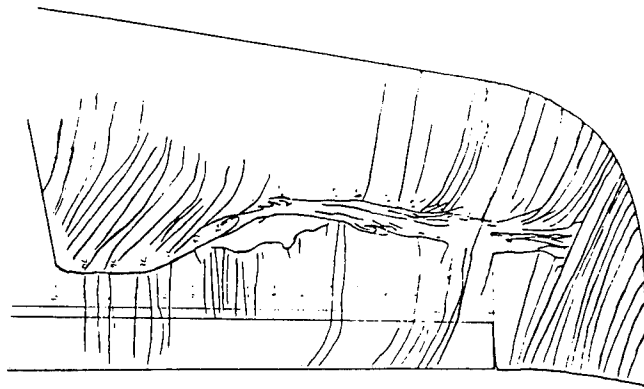


Figure 5. Streamlines and boundary layer transition areas for the standard wing tip at an angle of attack of 2.5 degrees and airspeed of 105 Km/Hr.

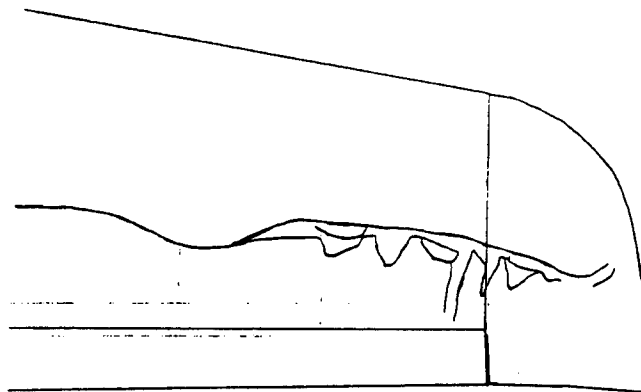


Figure 6. Boundary layer transition for the standard wing tip at an angle of attack of 5.0 degrees and an airspeed of 105 Km/Hr. At this angle of attack, the boundary layer transitions to turbulent at 50 percent of chord.

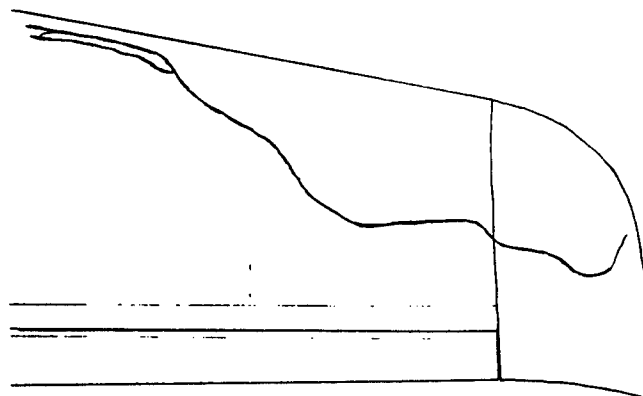


Figure 7. Boundary layer transition for the standard wing tip at an angle of attack of 7.5 degrees and an airspeed of 105 Km/Hr. At this angle of attack, the boundary layer transitions to turbulent at the leading edge.

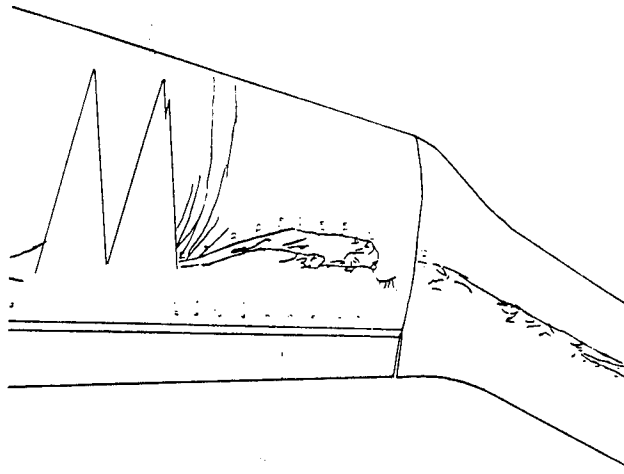


Figure 8. Streamlines and boundary layer transition areas for the winglet configuration at an angle of attack of 2.5 degrees and airspeed of 105 Km/Hr.

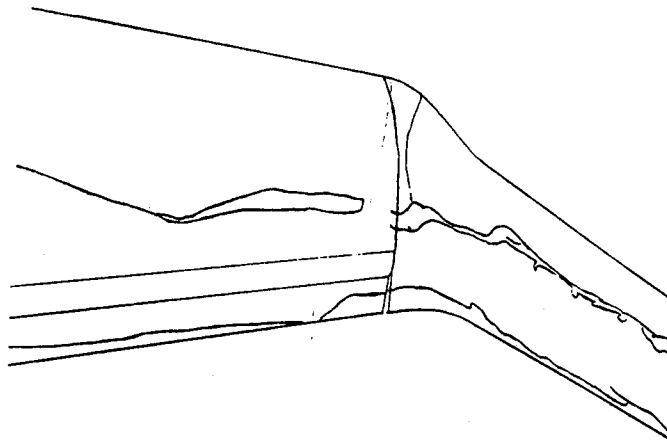


Figure 9. Boundary layer transition for the winglet configuration at an angle of attack of 5.0 degrees and an airspeed of 105 Km/Hr. At this angle of attack, the boundary layer transitions to turbulent at 50 percent of chord.

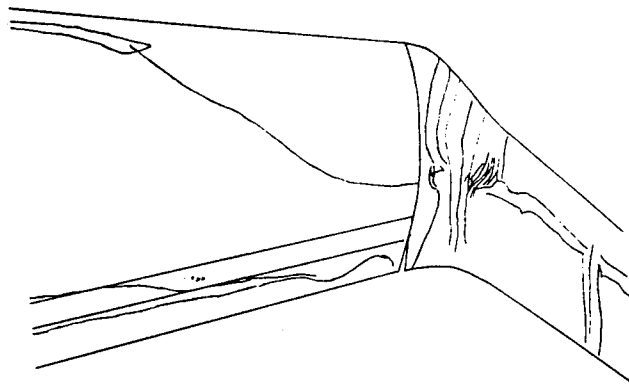


Figure 10. Boundary layer transition for the winglet configuration at an angle of attack of 7.5 degrees and an airspeed of 105 Km/Hr. At this angle of attack, the boundary layer transitions to turbulent at 50 percent of chord.

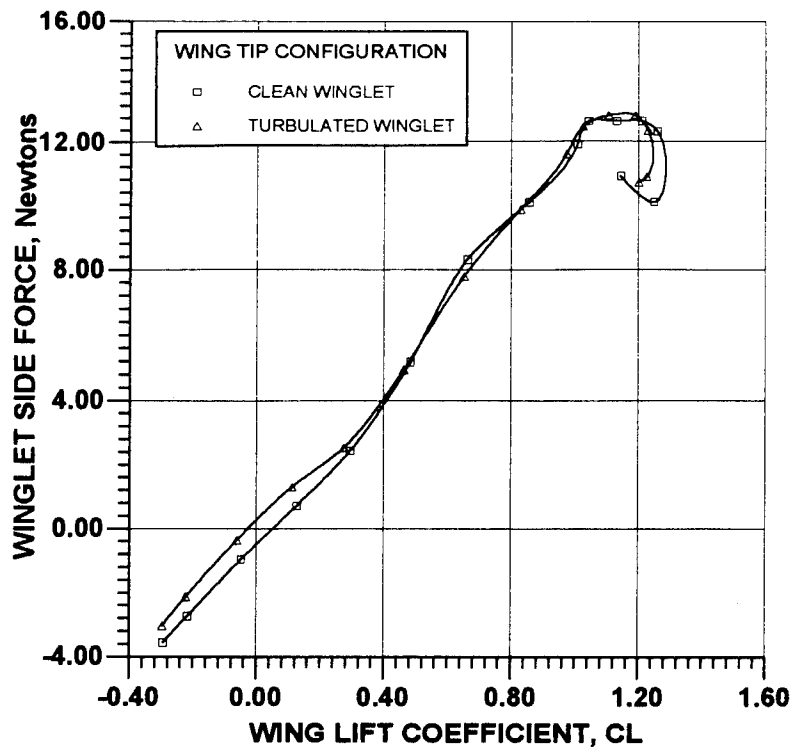


Figure 11. Winglet side force plotted as a function of wing lift coefficient at an airspeed of 80 Km/Hr.

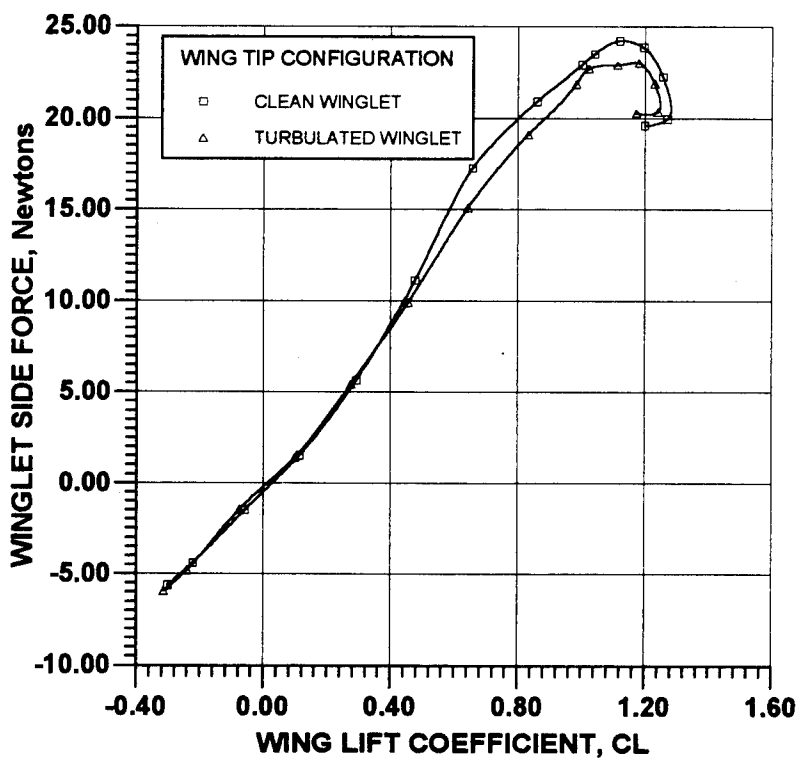


Figure 12. Winglet side force plotted as a function of wing lift coefficient at an airspeed of 105 Km/Hr.

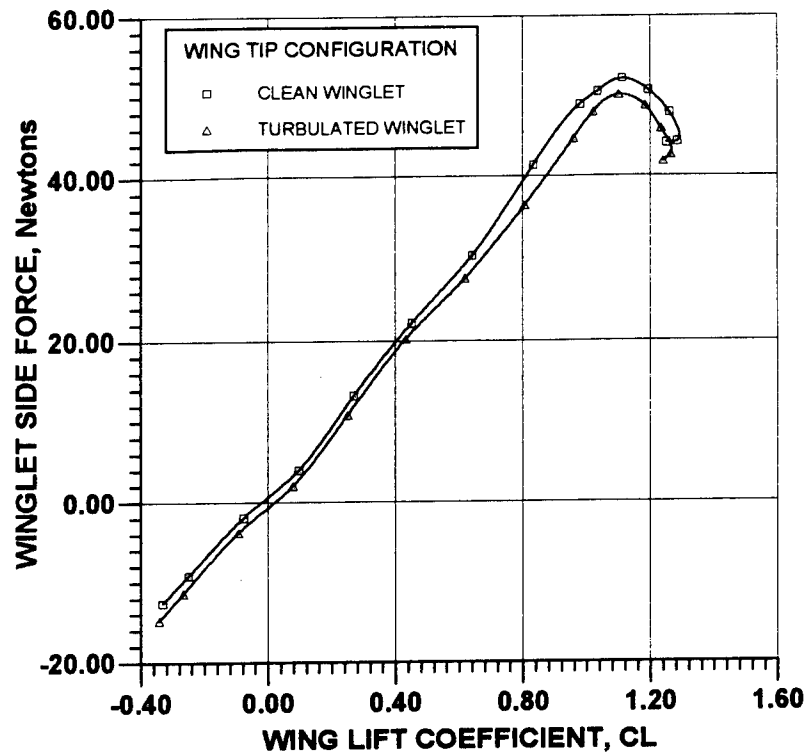


Figure 13. Winglet side force plotted as a function of wing lift coefficient at an airspeed of 145 Km/Hr.

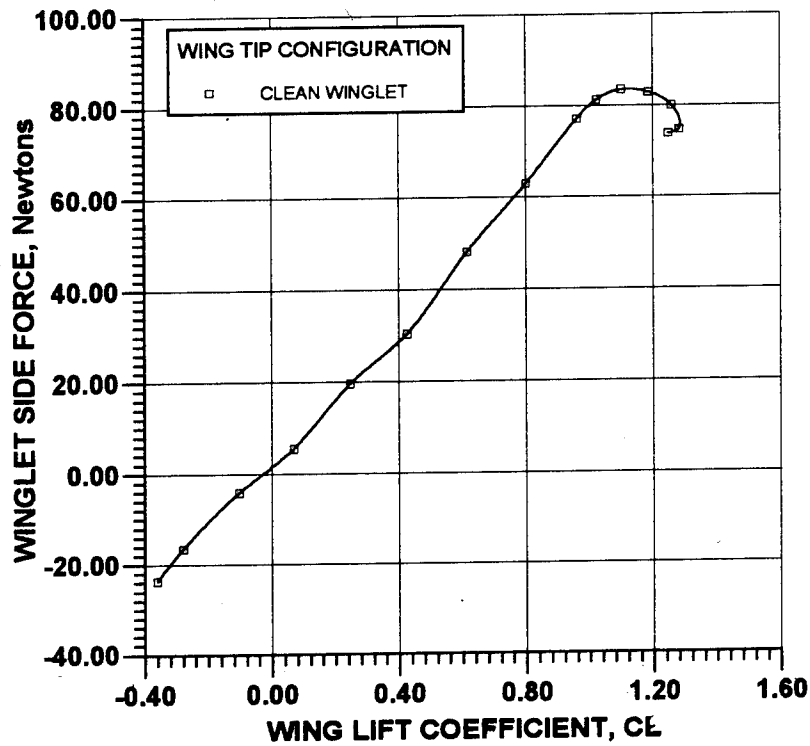


Figure 14. Winglet side force plotted as a function of wing lift coefficient at an airspeed of 175 Km/Hr.

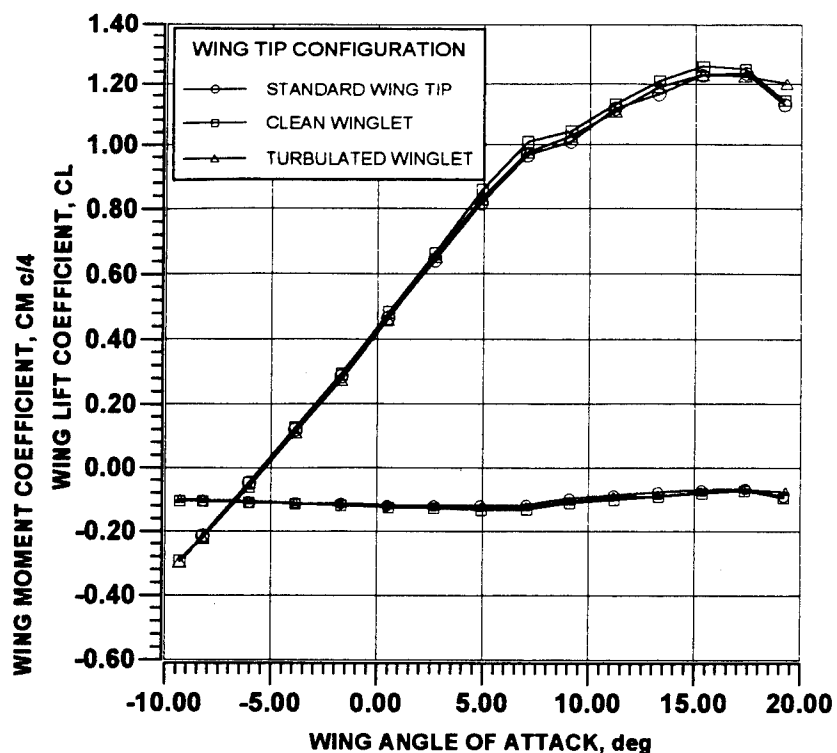


Figure 15. Lift coefficient and pitching moment coefficient of the wing at and airspeed of 80 Km/Hr.

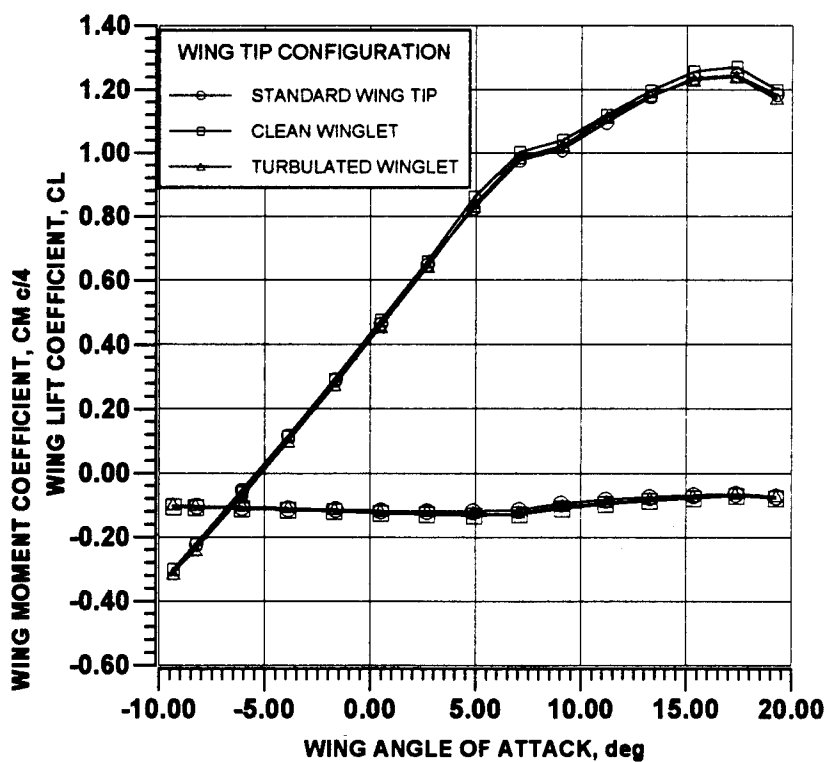


Figure 16. Lift coefficient and pitching moment coefficient of the wing at an airspeed of 105 Km/Hr.

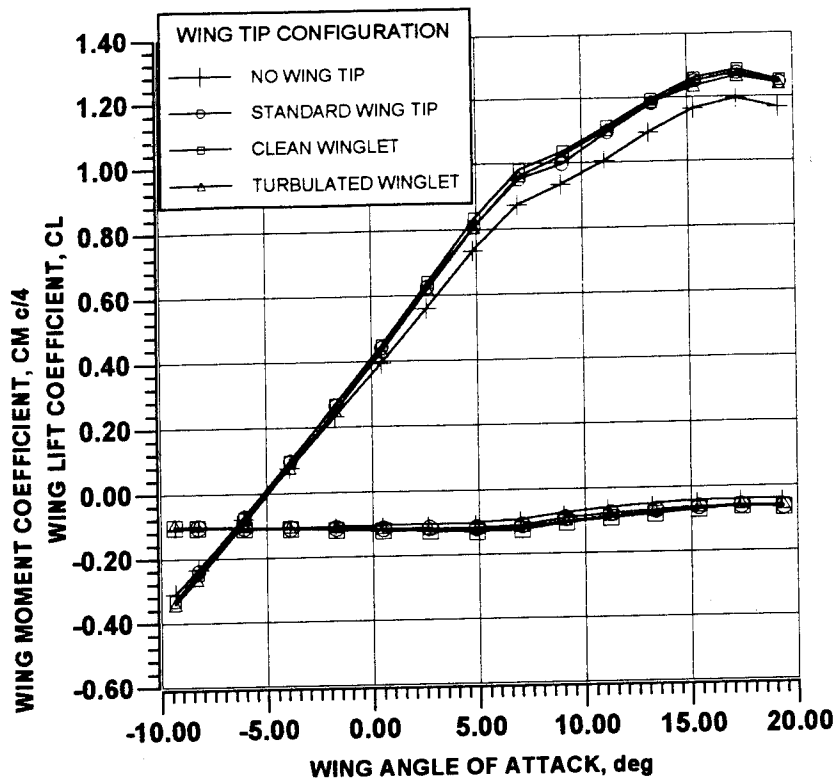


Figure 17. Lift coefficient and pitching moment coefficient of the wing at and airspeed of 145 Km/Hr.

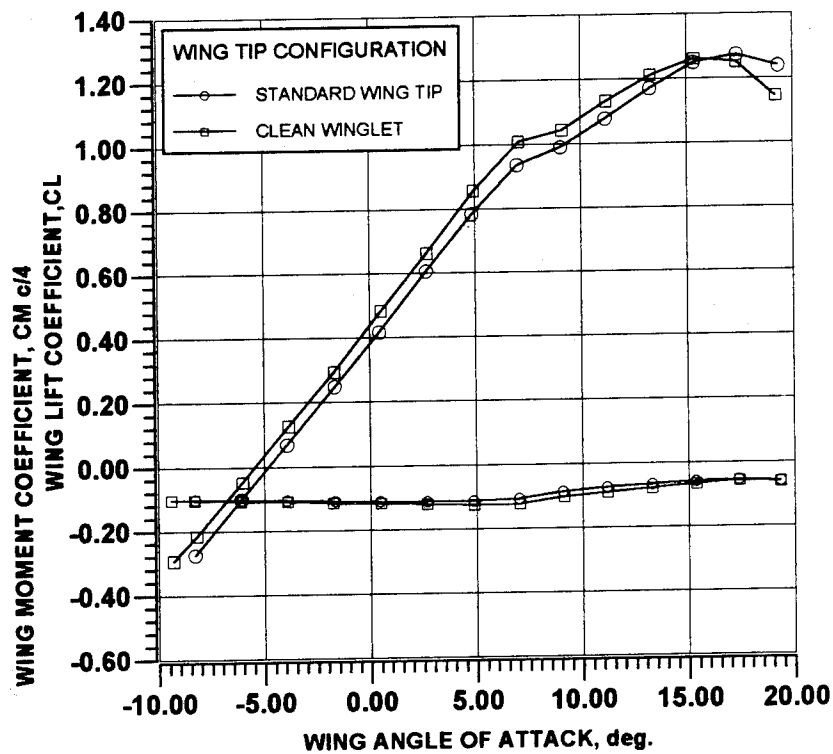


Figure 18. Lift coefficient and pitching moment coefficient of the wing at an airspeed of 175 Km/Hr.

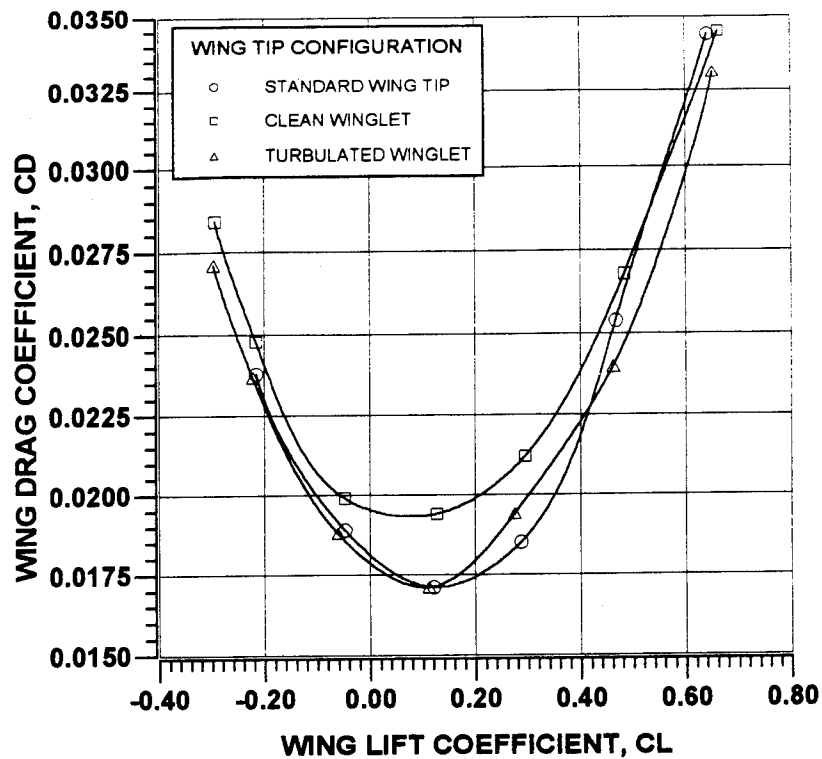


Figure 19. Wing drag coefficient plotted as a function of wing lift coefficient at an airspeed of 80 Km/Hr.

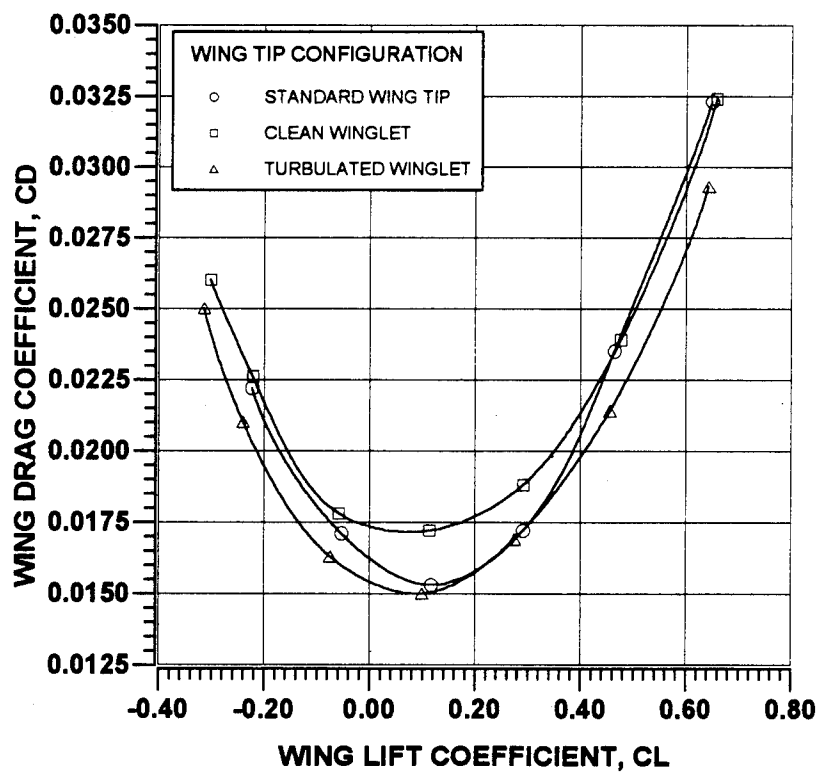


Figure 20. Wing drag coefficient plotted as a function of wing lift coefficient at an airspeed of 105 Km/Hr.

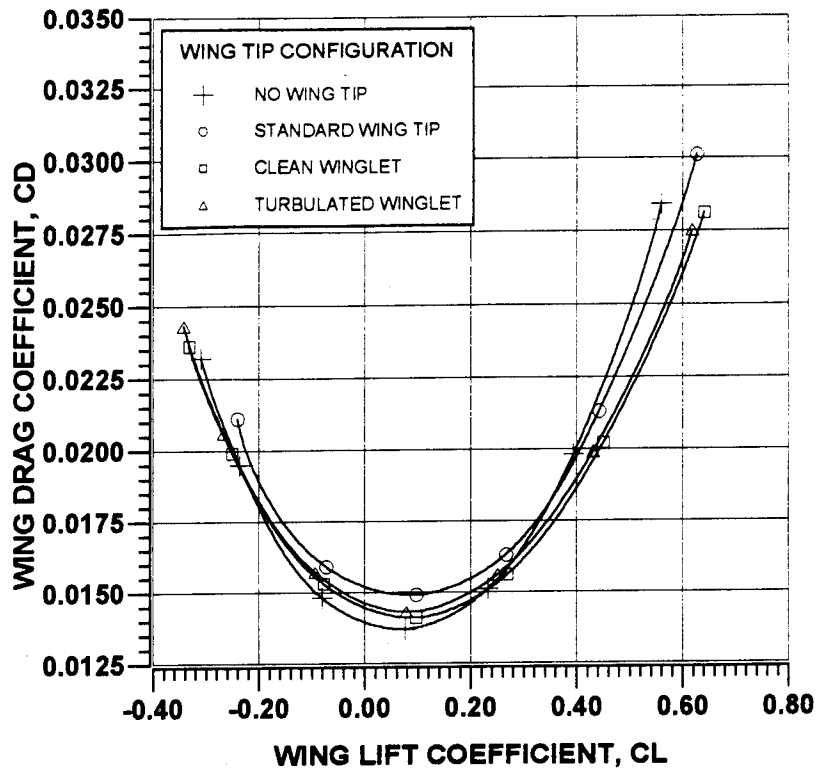


Figure 21. Wing drag coefficient plotted as a function of wing lift coefficient at an airspeed of 145 Km/Hr.

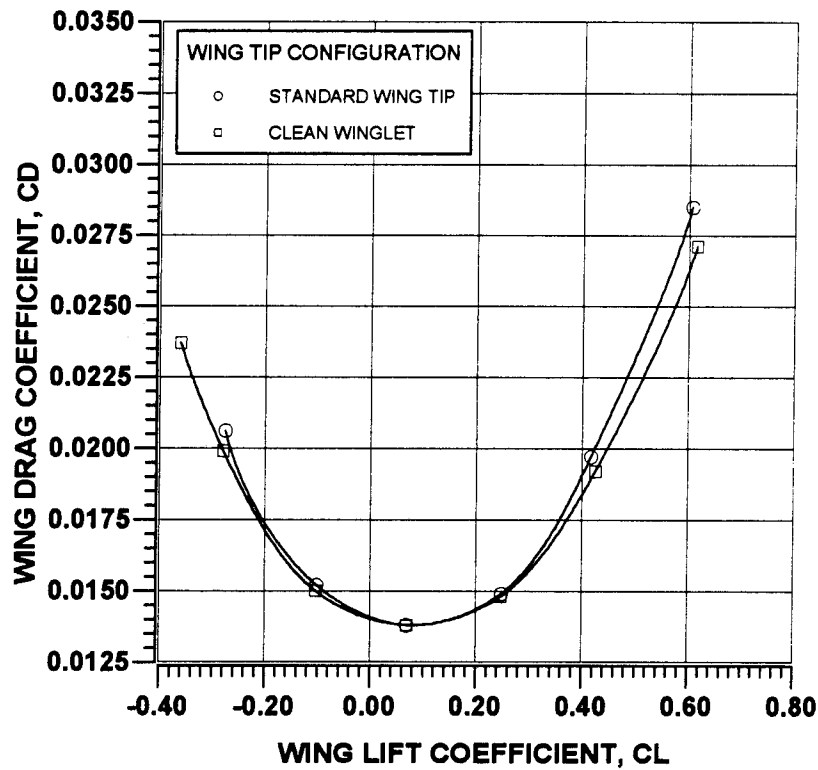


Figure 22. Wing drag coefficient plotted as a function of wing lift coefficient at an airspeed of 175 Km/Hr.

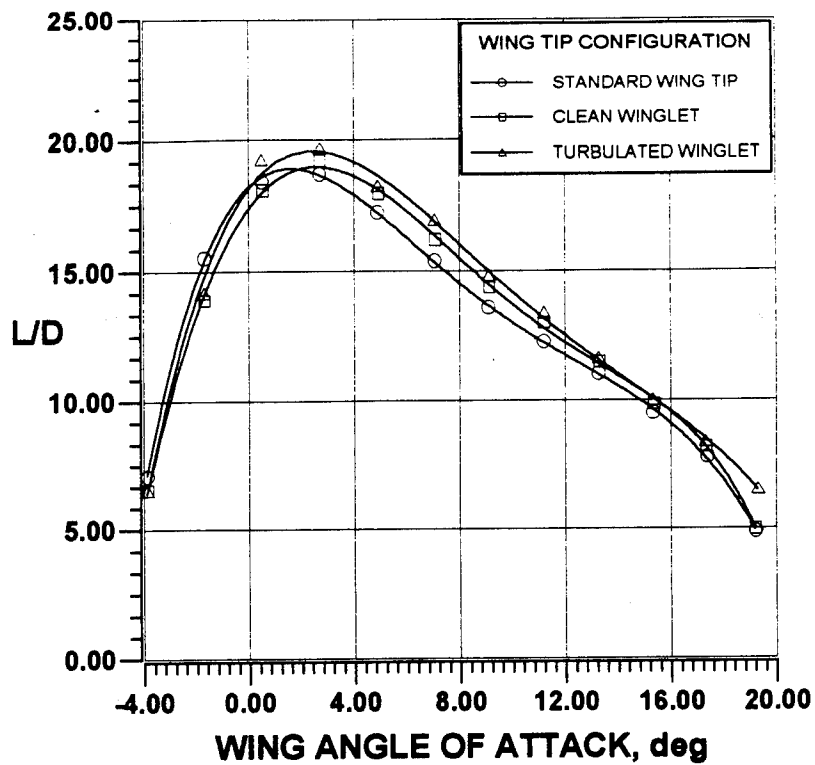


Figure 23. Lift to drag ratio of the model plotted as a function of wing angle of attack at an airspeed of 80 Km/Hr.

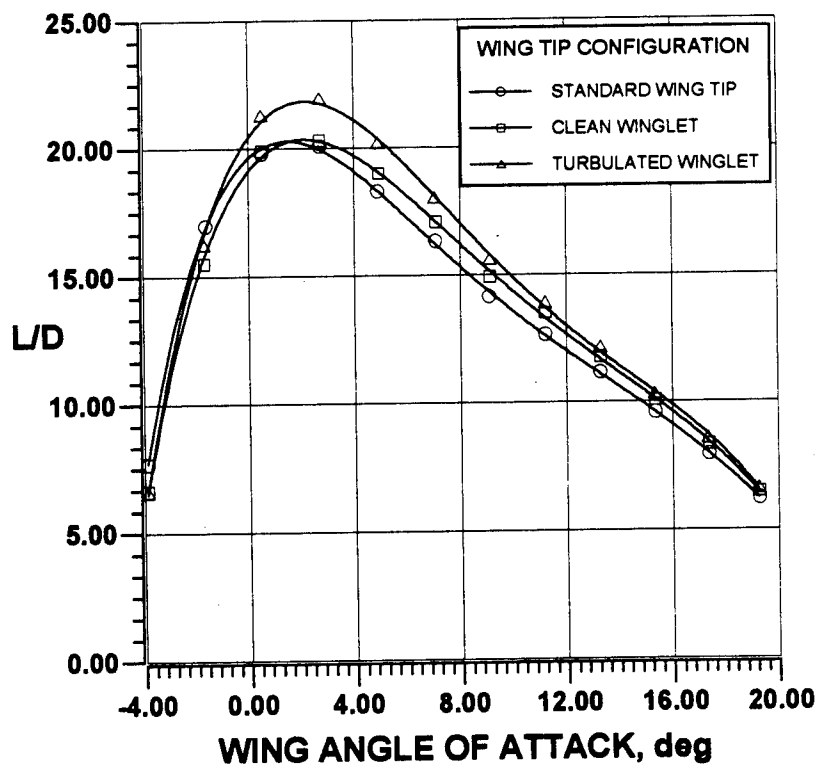


Figure 24. Lift to drag ratio of the model plotted as a function of wing angle of attack at an airspeed of 105 Km/Hr.

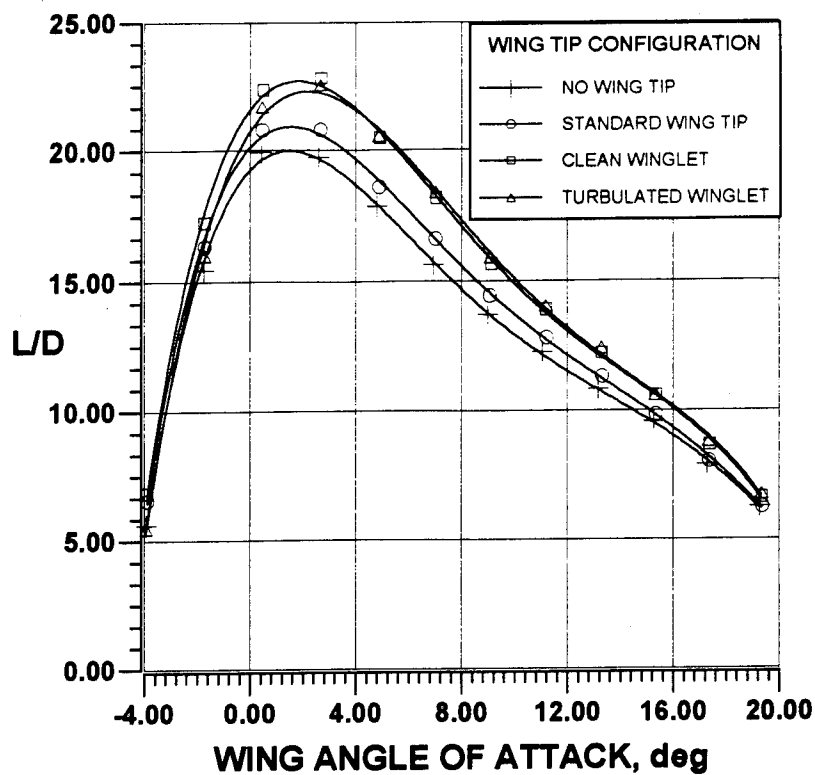


Figure 25. Lift to drag ratio of the model plotted as a function of wing angle of attack at an airspeed of 145 Km/Hr.

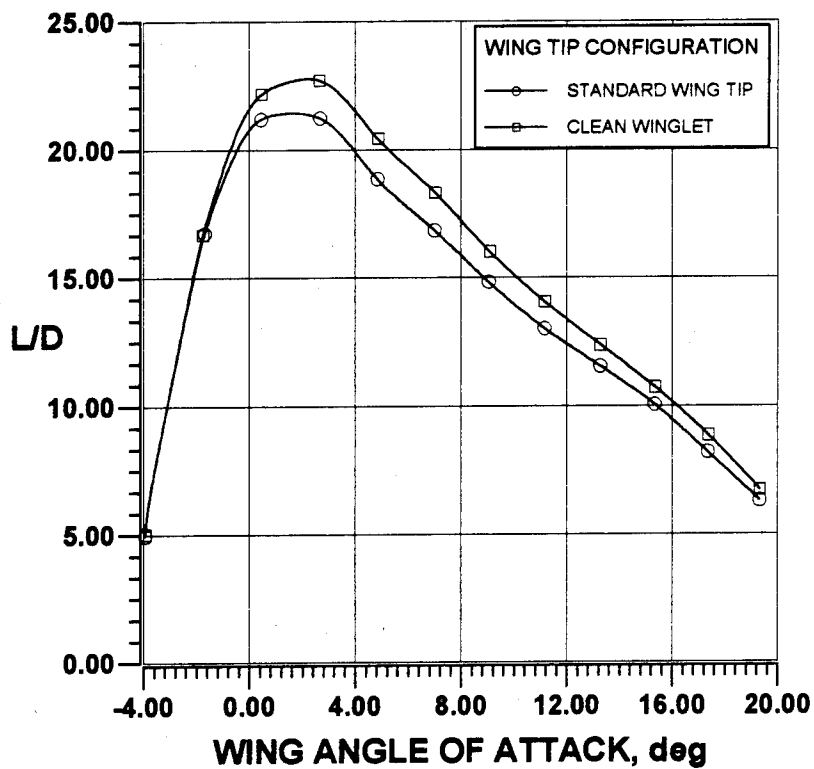


Figure 26. Lift to drag ratio of the model plotted as a function of wing angle of attack at an airspeed of 175 Km/Hr.

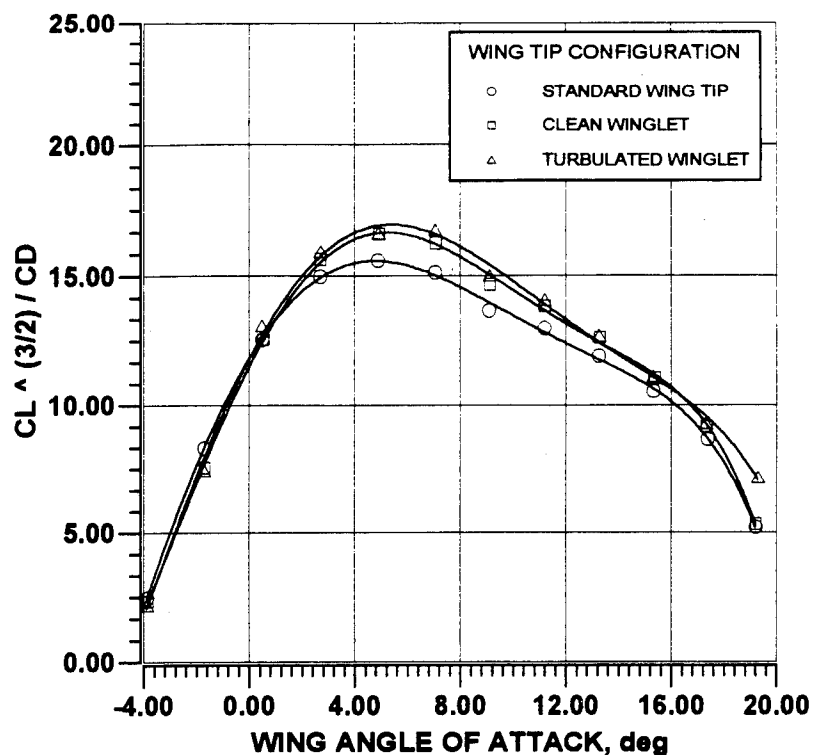


Figure 27. Climb calculation parameter, $CL^{3/2}/CD$, for the model plotted as a function of wing angle of attack at an airspeed of 80 Km/Hr.

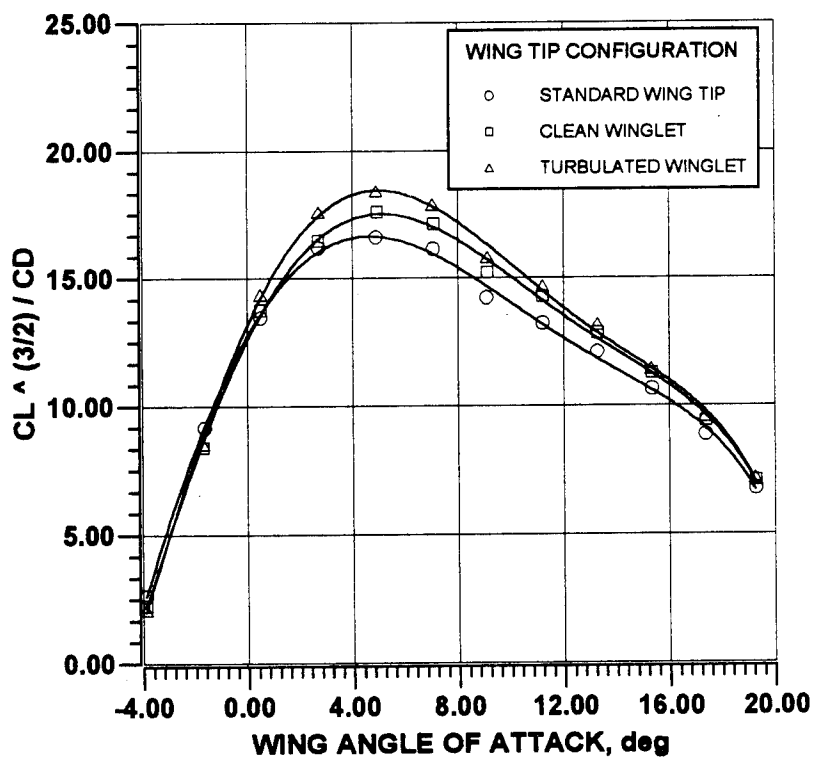


Figure 28. Climb calculation parameter, $CL^{3/2}/CD$, for the model plotted as a function of wing angle of attack at an airspeed of 105 Km/Hr.

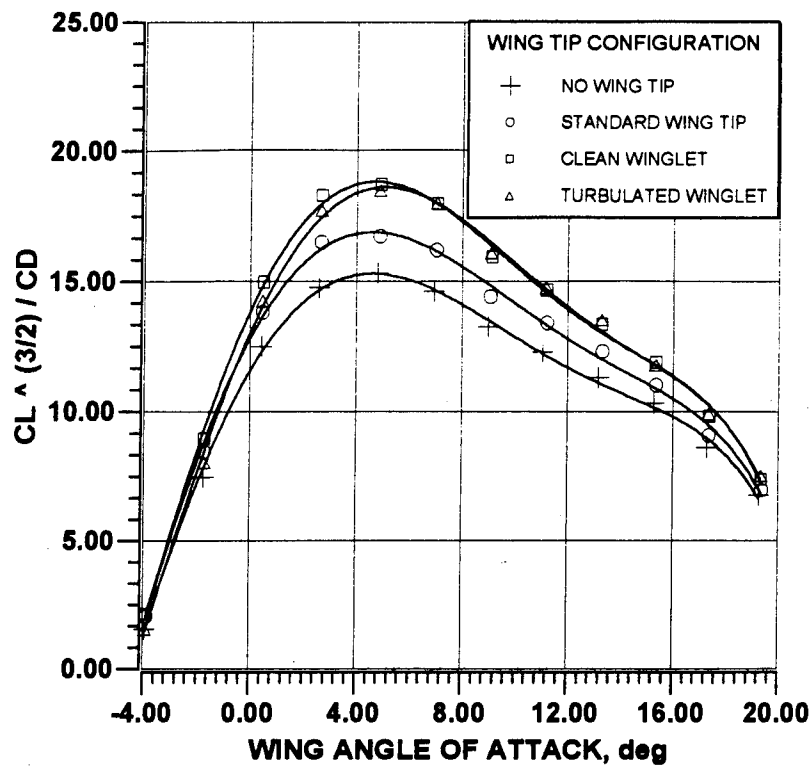


Figure 29. Climb calculation parameter, $CL^{3/2}/CD$, for the model plotted as a function of wing angle of attack at an airspeed of 145 Km/Hr.

AERODYNAMIC AND AEROELASTIC DESIGN
OF THE EXPERIMENTAL AIRCRAFT HONDA MH02

Michimasa Fujino
Honda R & D, Wako Research Center
1-4-1, Chuo, Wako-shi, Saitama, Japan

1.ABSTRACT

The purpose of this paper is to present the configuration design, aerodynamic design, stability and control analyses, and aeroelastic analyses of the HONDA experimental aircraft MH02, with particular reference to characteristics of the unconventional configuration. To achieve the prescribed design goals such as short runway performance, very low cabin floor height, etc., an unusual configuration -- the forward swept wing with an over-the-wing engine mount, a triple slotted flap, and a T-tail was explored. The forward swept wing was designed by aerodynamic and aeroelastic analysis. A divergence analysis showed that a wing designed by strength does not exhibit divergence characteristics and, therefore, wing sweep angle and other geometric characteristics were designed to achieve good stall characteristics and high span efficiency with minimum weight penalty. The over-the-wing engine mount design required many analyses and experiments. Inlet distortion characteristics were investigated using a powered model and showed no problems. However, the over-the-wing engine mount configuration showed relatively high interference drag. The high interference is due to the installation of large engines and thick pylons in the upper side of the wing. The effect of the high thrust line on the longitudinal flight characteristics was analyzed and the pitch changes caused by different thrust settings proved to be acceptable. The longitudinal flight characteristics satisfied MIL-8785C. By installing large engines, the lateral-directional characteristics were degraded and some modification of the fin was required to improve directional static stability. The T-tail configuration has several advantages but it has disadvantages as well, such as deep stall and T-tail flutter. The deep stall design was based on a statistical approach and wind tunnel tests. Flutter analyses, including T-Tail flutter analysis, were also performed to show that any aeroelastic problems do not occur below a speed which is 20% higher than the design dive speed V_D .

2.INTRODUCTION

The all composite research jet MH02 was designed, fabricated, and tested under a joint research project between Honda R&D and Mississippi State University. The objective of the research was not to develop a production airplane but, rather, to explore new technologies for general aviation aircraft. The MH02 is a lightweight (about 8000LB maximum take-off weight), small jet primarily designed for operations from short runways and over relatively short distances. The cruising speed is about 600km/h which falls near the high end for turboprops or the low end for fan jets. The airframe is most suitable for the installation of a 600kg-class thrust (maximum take-off thrust), high-bypass-ratio fan engine or an advanced turbo prop. This paper is to present the aerodynamic and aeroelastic design, analyses, and

experiments conducted in the development of the MH02.

In the next section, the process to freeze the unconventional configuration will be discussed and characteristics and advantages of this configuration will be presented. In the aerodynamic design section, design of the forward swept wing, the high lift systems, and the over-the-wing engine mount, including wind tunnel tests will be discussed. In the stability and control section, trim analyses, stability analyses, and deep stall analyses will be discussed. Because the MH02 has the forward swept wing and the T-tail configuration, it is very important to evaluate the aeroelastic characteristics from a safety standpoint. In the aeroelastic section, stiffness tests, ground vibration tests, divergence analyses, flutter analyses will be discussed.

3. GENERAL ARRANGEMENT

One of the most important requirements for the MH02 aircraft (Fig.1) is the capability of operating in regions with a 3500 feet runway. To achieve high maximum lift and make a FAR Pt135 required landing field length $[1.67 \times (\text{landing distance})]$ below 3500 feet without sacrificing cruise performance, a triple slotted flap was incorporated. In general, the high lift systems for general aviation airplanes are made simple to reduce mechanical complexity and cost. For small jets like the MH02, aerodynamic advantages of triple slotted flaps may not overcome the disadvantages of structural complexity and the weight penalty. However, the triple slotted flap configuration was finally selected as a research theme to investigate the efficiency of complex high lift systems including the structure and the mechanism. Leading edge slats were also installed to reduce the suction spike produced by the trailing edge high lift systems.

Another requirement of the MH02 is that the crew and passengers can easily get on and off the aircraft without any steps or other devices, just like automobiles. The MH02 was designed for the short range operations with a short cruising time, therefore, it was considered to be relatively important for the passengers to get on

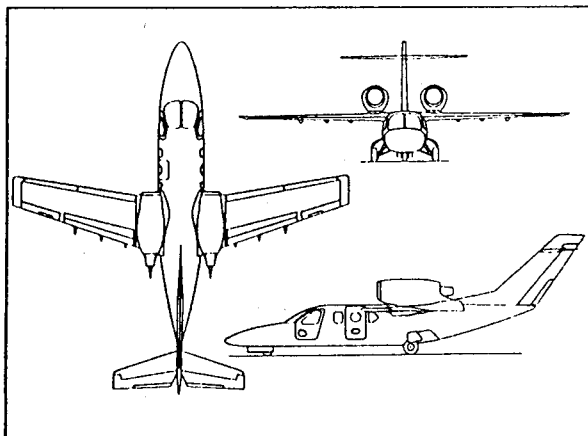


Fig.1 MH02 General Arrangement

and off the aircraft very easily. The short landing gear which places the aircraft very close to the ground [The distance from the ground to the cabin floor is only 444mm (17.5 in)] was installed to achieve this requirement. The short landing gear is also advantageous in that any space for storing the landing gears can be smaller and, of course, the landing gear itself is lighter.

Because of the high lift system and the short landing gear which characterize the MH02, it is necessary to locate the wing in a high position to prevent the wing

tips and flaps from contacting the runway during take off and landing with an angle of bank. A high wing configuration is also favorable with respect to maximum lift characteristic in general. However for a high wing configuration, the carry-through between the two wings passes through the cabin at a longitudinal position of the airframe which is determined by the relative relationship between the aerodynamic center and the center of gravity of the entire aircraft. If the carry-through structure passes through the cabin, the available volume of the cabin is reduced. If the carry-through structure passes above the cabin, drag is increased. Positioning the carry-through structure aft of the cabin may be one solution to these problems. By concentrating the heavily loaded structures such as the wing-fuselage joint and the landing gear attachment in the same reinforced load carrying structure, any increase in the weight of the structure is minimized. Although locating the carry-through structure in the rear fuselage gives the structural advantage described above, it is necessary from a stability point of view to position the aerodynamic center of the wing near the aircraft center of gravity by employing a forward swept wing or a canard (or three surface) configuration to shift the aerodynamic center of the aircraft forward. A canard configuration allows the aerodynamic center of the aircraft to be shifted without requiring a forward swept wing which may have structural disadvantages such as divergence. However, the canard configuration has disadvantages, for example, the structural members in the forward portion of the fuselage must be reinforced, and the space available for installing accessories or cargo is reduced. The advantages and disadvantages of three different configurations, a forward swept wing plus tail configuration, a canard configuration, and a three surface configuration were studied through extensive analyses and wind tunnel tests. Finally it was concluded that the forward swept wing plus tail configuration is best for this experimental aircraft for the following reasons.

① Configurations which employ canards sometimes exhibit undesirable flight characteristics. For instance, the canard must always stall first to prevent the main wing stall which would cause a dangerous pitch up. This means, however, that the main wing lift can not be used up to maximum lift as can be done with a conventional configuration. Because the main wing is in the flow field of the canard, the flow approaching the wing is very complex and wind tunnel tests showed a pitch-up characteristic at certain angles of attack. This characteristic might be cured by changing the canard decalage angle or by adding the leading edge droop to the outboard wing, but both of these cause additional drag. Even if the canard always stalls first, this canard stall sometimes causes an abrupt pitch down which, if it happens on takeoff or landing due to, for example, gusts, is very dangerous and may damage the nose gear. A relatively small allowable center of gravity range is also a disadvantage of the canard configuration. Such a configuration also does not allow high lift systems which produce a large nose down pitching moment. On the other hand, the forward swept wing-tail configuration does not exhibit aerodynamic interference between the canard and the main wing and the center of gravity range is large enough to allow a high lift system which can satisfy the short runway requirement.

② It is generally thought that because the canard produces an up-load at the trim condition and, therefore, contributes to the overall airplane lift, it is very efficient. Analysis and wind tunnel tests showed that those advantages are small and they can be achieved only at a particular trim condition. For the three surface

configuration potential flow theory shows that the mutual induced drag can be minimized by the appropriate design of the canard, the wing, and the tail. (Ref.1) However, for the high speed condition, the interference drag and the parasite drag of the additional surface (horizontal tail) outweigh the advantage in induced drag. Finally, the advantage in the drag for the canard and the three surface configuration is very small.

③ From an aeroelastic point of view, a divergence analysis showed that there is almost no disadvantage for the forward swept wing as long as the sweep angle is not extreme. Structurally, the weight penalty due to the structure to carry the kick load (twisting moment which is the component of the bending moment due to the wing sweep) at the root is also small as long as the sweep angle is not extreme. For the canard configuration, the airload on the main wing at the trim condition can be smaller than that for the wing-tail configuration but the gust loads on the main wing tend to become larger because the canard, which is located ahead of the main wing, penetrates the gust before the main wing and this will cause a pitch up response. This pitch up causes an increase in the angle of attack of the main wing, which increases gust load. For the three surface configuration, the weight penalty of the additional surface is not negligible.

④ Because of the short runway requirement, it is desirable to utilize a high lift wing. The wing high lift capability should not be limited by poor stall characteristics or roll control effectiveness. Thus, good stall characteristics and a sufficient roll control power at a low speed range are required. The forward swept wing is very favorable with respect to stall characteristics because the inboard portion of the wing stalls first. Analyses showed that by employing a forward swept wing, good aileron control effectiveness can be maintained up to a high angle of attack without twist, which would result in a reduction in the span efficiency except at the design point.

The engine and inlet location was the next major design decision. In general, there are three kinds of well known types of engine installations,

- buried engine at the wing root
- podded engine mounted below the wing
- podded engine mounted at aft fuselage side

Each location has advantages and disadvantages. For example, the buried engine can reduce the total wetted area, but it also reduces the fuel volume near the wing root which is the most suitable place for the storage of large fuel amounts. Also, the structural weight tends to be greater because the wing root is a highly loaded region. The skin may have to be removable at the root for access to the engine, which is disadvantageous because of the high stresses near the wing root. Inlet distortion is also a problem with this engine location.

The podded engine mounted below the wing has a very high inlet pressure recovery. Also, the pylons sometimes produce a favorable effect on the wing stall characteristics of a swept wing. Structurally, the mass of the engine can reduce the bending moment of the wing and an engine properly located with respect to the

elastic axis acts as a mass balance against wing flutter. On the other hand, this configuration has a larger wetted area than the buried engine. It also produces a large yawing moment under the One Engine Inoperative(OEI) condition. (As a result, a large fin is needed.) Occasionally, flaps need to be cut out to avoid damage from the hot exhaust.

The podded engine mounted at aft fuselage sides is very popular for small airplanes and very good for the wing because there is no interference between the wing and the pylon, i.e., the wing is very clean. The yawing moment produced in the OEI condition is so small that this condition does not drive the fin design in many cases. The center of gravity of the entire aircraft tends to move aft, however, and the tail moment arm becomes small so that the tail area must become larger. If this engine location is combined with a T-tail configuration, it sometimes causes deep stall problems.

By studying these factors, an unusual engine location, over-the-wing engine mount, is found to be optimum for this experimental aircraft for the reasons stated below:

①For the forward swept wing configuration, the heavy structures tend to be located aft and the center of gravity of the aircraft moves aft. If the engines are located on the aft fuselage, the center of gravity of the aircraft moves further aft because of the reinforcement of the fuselage for the attachment and the engine weight itself. This shortens the tail moment arm considerably so that the empennage must become much larger. Locating the engines near the wing root, like the current configuration, does not require additional structural reinforcement for the engine installation because the wing root is already sufficiently strong. Thus, the weight increase is minimized.

②Because of the low stall speed, the OEI condition is important for this aircraft design. With the engines mounted below the wing, it was found that the engines should be located outboard on the wing to prevent interference between the fuselage and the nacelle, which causes a large yawing moment for the OEI condition. For the over-the-wing engine mount configuration, it is possible to position the engines near the aircraft center line similar to the location for the aft fuselage side mounted engine configuration. The minimum control speed V_{MC} can be as low as that for the aft fuselage side mounted engine configuration.

③Positioning the engines below the wing places the engines very close to the ground because of the short landing gear and makes it easy to ingest foreign objects. Positioning the engines above the wing minimizes Foreign Object Damage(FOD) problems. This configuration allows the airplane to operate on a semi-prepared field.

④If the engines are mounted below the wing, it becomes necessary to cut out some of the flaps, or limit the flap deflection, to prevent impingement of the jet exhaust. To cut out or discontinue the flaps greatly reduces the efficiency of the flaps and decreases the short runway performance which is one of the most important performance goals of this experimental aircraft.

⑤ The wing is located below the engine for the over-the-wing engine mount

configuration so that the noise level on the ground is reduced. Safety on the ground is enhanced because the engine inlet and the exhaust are high in spite of the short landing gear and low aircraft position.

⑥Because the engines are located near the aircraft center of gravity and above the wing, it is possible to install many kinds of engines regardless of weight and size.

This configuration does, however, have some disadvantages as well. From an aerodynamic design standpoint, wing-nacelle interference and inlet flow distortion may become problems. From a stability and control standpoint, the high thrust line may cause an unacceptable pitch change with different thrust settings. These problems were analyzed in detail and will be discussed later.

The MH02 was designed based on the installation of a 600kg-class thrust high-bypass-ratio turbofan engine. However, during the airframe development, a 600kg-class thrust engine, which was supposed to be installed, was not available. By looking for new engines available for this aircraft, the Pratt&Whitney-JT15D was selected. This engine is less expensive and can be used as a substitute engine even though its thrust is 1043kgf(2300LB), and it is larger and heavier than planned for this aircraft. It was decided that this engine was to be used with derated thrust. Because of the over-the-wing engine mount configuration, these engines could be installed in spite of their larger diameter and heavier weight without any significant modification.

4.AERODYNAMIC DESIGN

(1)WING DESIGN.

For the aerodynamic design of the wing, the main goal is to maximize the span efficiency while maintaining good stall characteristics. In addition, for the MH02 wing design, the carry-through-structure should be positioned such that the cabin volume is not reduced as stated earlier. The structural weight penalty due to the forward swept wing also had to be studied with respect to divergence, which will be discussed in 6-(3).

A preliminary aerodynamic analysis using a Vortex Lattice Method(modified VLM program of Ref.2,3) was conducted to study the sweep angle and the planform. Because the local lift coefficient C_l for the outboard portion of the forward swept wing is lower than that for the aft swept wing and the local chord for the outboard portion is larger (i.e. higher local Reynolds numbers) when they have an elliptical load distribution, which corresponds to a span efficiency of one, it is possible for the forward swept wing to exhibit good stall characteristics without decreasing the span efficiency. An example of these studies is shown in Fig.2. The lift coefficient (C_l) distributions for three different sweep angles with the same taper ratio and no twist are presented. The local lift coefficient for the outboard portion of the forward swept wing is lower than those for the straight or the aft swept wing while maintaining nearly the same span efficiency "e". This means that the stall margin for the aileron of the forward swept wing is larger than that of the aft swept wing. This is considered to be the advantage of the forward swept wing, especially for an

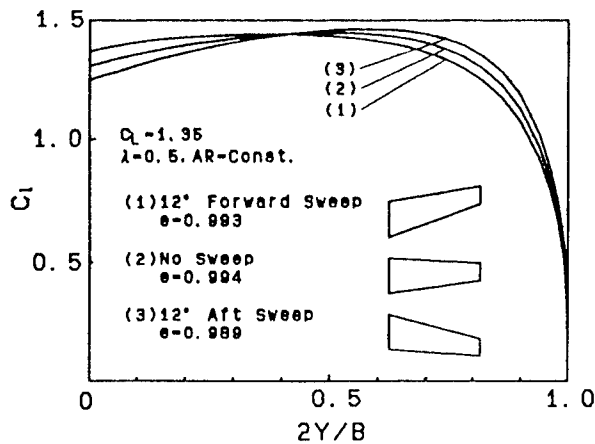


Fig.2 Variation of Lift Distribution with Sweep

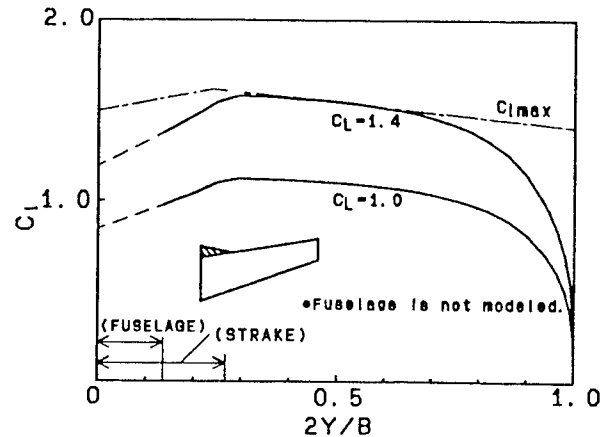


Fig.3 Lift Distributions without Nacelle (VLM)

airplane having a low stall speed.

An aeroelastic analysis showed that it is possible to have higher forward sweep without any significant weight penalty from a divergence point of view. However, an excessively high forward sweep angle exhibited undesirable stall characteristics near the wing root, so that a moderate forward sweep angle was desired. After considering the geometric constraint imposed by the cabin layout with aerodynamic and aeroelastic studies, it was finally determined that quarter chord sweep should be -12° (forward), the taper ratio 0.48, and the twist 0° . Zero twist has an advantage from the aerodynamic design standpoint. Washout is often used to reshape the lift distribution. However, if twist is employed to reduce the local lift coefficient over the outboard portion of the wing for stall characteristic improvement, it reduces the span efficiency at cruise. If twist is used to produce a lift distribution which is close to elliptical at one lift coefficient, the efficiency at other lift coefficients will be reduced. In other words, it is impossible to maximize the efficiency at all lift coefficients. In addition, from the structural design standpoint, it avoids the manufacturing problems produced by geometric twist. The lift distribution of the MH02 calculated by VLM is shown in Fig.3. The wing stalls first around 45 to 50% semispan and there is also an adequate stall margin over the outboard portion of the wing where the ailerons are located. The root portion of the wing is extended forward like a strake to reduce the local lift coefficient and to reduce the interference between the wing and the fuselage. The span efficiency without the fuselage and the nacelle-pylon calculated from VLM (far field method) is 0.987.

Because the engine nacelles are located on the upper surface of the wing, the aerodynamic design of the wing-nacelle-pylon integration is very important. The loss of lift, Oswald's span efficiency "e" and the interference drag caused by the engine installation should be minimized. For the pylon design, there were two geometric constraints. First, the pylons must provide sufficient thickness for the engine mount and the accessories because the JT15D engine has no attachment points under the engine for this type of installation. Second, to minimize thrust pitch coupling and the nose down pitching moment for the takeoff and go-around conditions, the engines should not be positioned too high above the aircraft center of gravity. In addition, from an aeroelastic standpoint, the engine-pylon vibration mode should be

decoupled from the wing vibration mode, because this coupling effect was important for wing flutter. To design optimum pylon geometry, an aerodynamic design was performed using the panel method VSAERO and wind tunnel tests, including flow visualization using tufts. Because the panel method is based on potential flow theory, it is not possible to evaluate the absolute value of the lift loss caused by separation or interference drag. However the panel method is useful to develop shapes which produce pressure distributions which are favorable with respect to separation and interference. The designed geometry was also checked by wind tunnel testing. The spanwise lift distribution calculated using the panel method with and without engine nacelles is shown in Fig.4. Flow visualization using tufts showed that the experimental stall pattern is very close to the predicted one. The flow over the aileron at the airplane stall angle is still attached (Fig.5). The lift curves obtained from the 1/6-scale wind tunnel test with and without nacelles are shown in Fig.6. The lift coefficients of the wing with nacelles are almost the same as without nacelles. The lift loss at low to moderate angles of attack and the loss in maximum lift coefficient are negligible. However, Oswald's span efficiency "e" of the nacelle-on configuration obtained from wind tunnel tests is found to be 5 to 10% less than that of the nacelle-off configuration. This is due to the load deviation of the nacelle-on configuration from an elliptical load distribution. Also, a small separation observed near the rear part of the pylon which increases with increasing angle of attack is thought to contribute to the reduction of "e". In flight, the separation tendency becomes less because of Reynolds number effects. The efficiency obtained from flight tests was indeed higher than wind tunnel tests. The efficiency obtained from flight tests is 0.85 to 0.89 depending on the test condition. The local pressure distributions were designed to remain below the sonic limit (critical C_p^*) at the cruise Mach number of 0.54, as shown in Fig.7 to try to minimize the interference between the wing and the nacelle-pylon. However, even the low speed wind tunnel tests showed an interference drag of about 0.002, which is higher than expected. The cause of this high interference drag is thought to be the relatively high negative pressure and the small separation. The installation of large engines and the relatively thick pylons for the engine mount and accessories may be the main cause of this drag. It should be possible to minimize the interference drag by installing the proper size engines on the airframe.

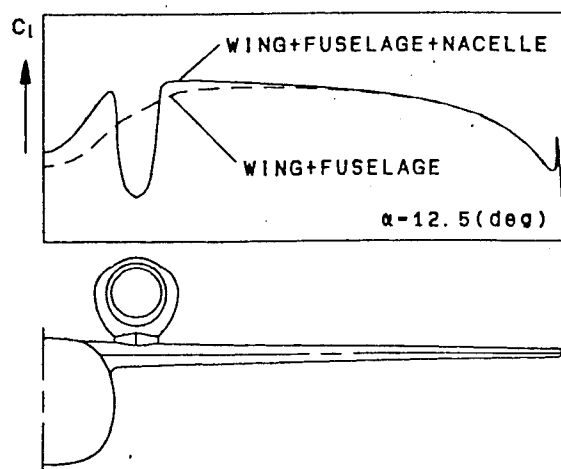


Fig.4 Lift Distribution with Fuselage and Nacelle (VSAERO)

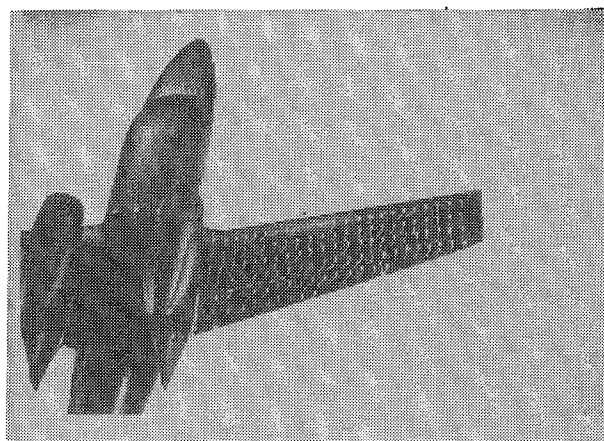


Fig.5 Wing Stall Pattern

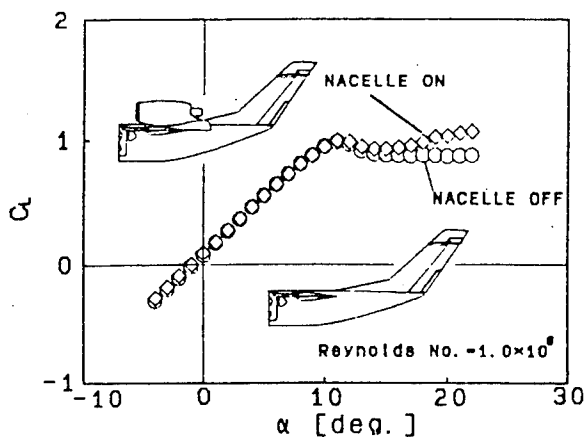


Fig.6 Comparison of Lift with and without Nacelles

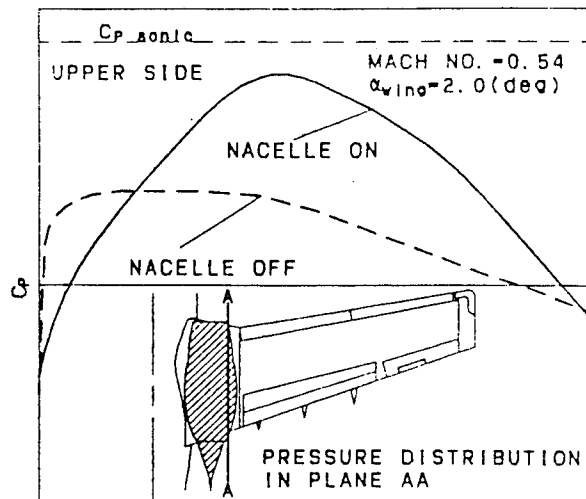


Fig.7 Pressure Distribution of Wing-Nacelle (VSAERO)

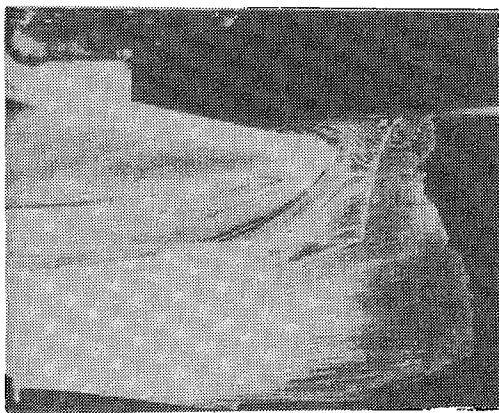


Fig.8 Oil Flow Photograph of Wing-Fuselage Intersection

The wing leading edge near the root was extended forward to reduce the relatively high local lift coefficient. This extension also contributes to reducing the interference around the wing-fuselage juncture and reduces the adverse pressure gradient over the rear portion of the wing which leads to the flow separation. However there is still a strong adverse pressure on the fuselage upstream of the wing leading edge which causes the separation such as a necklace vortex (Fig.8). A wing-body fairing was designed to minimize this vortex separation. Wind tunnel testing confirmed that the relatively large fairing extended forward could eliminate this separation, but such a large fairing could not be

incorporated on this aircraft because it would interfere with the passenger windows of the fuselage. The final fairing, although smaller than that stated above, does minimize the vortex and the interference drag between the wing and the fuselage.

(2) HIGH LIFT SYSTEM.

The goal of the flap design is to achieve very high lift coefficients with minimum weight increase and mechanical complexity. The flap design should be based on these trade studies. In this section, only aerodynamic design will be discussed.

The aerodynamic design of high lift systems is not an easy problem, even today. Because no highly accurate theoretical methods were available, the aerodynamic development of the high lift systems relied heavily on experiments and empirical methods. In the preliminary design stage, the lift coefficient increments ΔC_l in the linear range and the maximum lift coefficient increments ΔC_{lmax} which could be

achieved with flap deflection were estimated by DATCOM and Young's method(Ref.4). These methods must be modified in some cases because they cannot handle triple slotted flap configurations. The shape of vane, positions, gaps and overlaps were temporarily determined by referring to the existing experimental results(Ref.5). Then scale model tests were conducted to optimize the positions, gaps and overlaps. The model used was a rectangular wing with the large end plates to minimize three dimensional effects. Because of facility and equipment limitations, the test Reynolds number was approximately 0.5×10^6 which is 13% of the full scale Reynolds number. Thus, optimized gaps determined by using such a scale model are probably not optimal at the full scale Reynolds number. Special care was taken in the scale model test to avoid unusual flow phenomena, which would not occur in the full scale. By considering the Reynolds number effect on the boundary layer, the final gaps employed on the aircraft are slightly smaller than those optimized by the scale model test. The contours of the vanes were also slightly modified from the preliminary shapes to improve the pressure distribution (suction peak and pressure recovery region) by using the panel method combined with the confluent boundary layer method - Modified MCARF(Modified version of Ref.6). The MCARF analysis was also used to estimate the airloads which were needed for structural and mechanical design. As the MCARF cannot simulate separated flow, the computational results should be evaluated carefully. As long as the separation is not extreme, it seems possible to estimate the pressure distributions relatively accurately by using the MCARF after correlating the predicted results with experimental results and getting experiences.

The spanwise lift distribution for the flap down condition was analyzed using Vortex Lattice Method(VLM). Because the VLM is based on potential flow theory, some corrections are needed to simulate the flap effect more realistically. The geometric flap deflection angle was corrected by the section flap effectiveness η which is defined as the ratio of the actual flap effectiveness to the theoretical flap effectiveness. For this triple slotted flap configuration, the section flap effectiveness η was estimated from experimental data and the literature (for example, Ref.7). The spanwise lift distribution of the flap down configuration using this corrected flap deflection angle is shown in Fig.9. The three dimensional stall

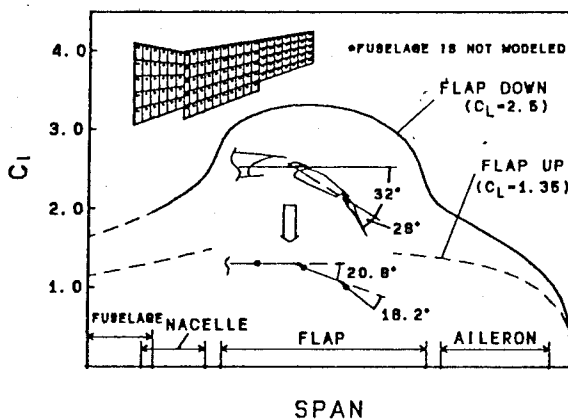
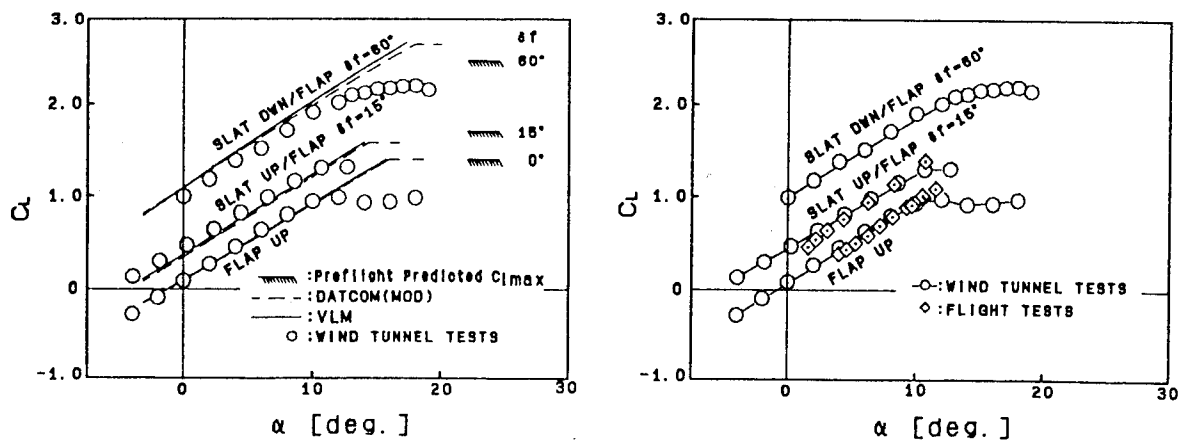


Fig.9 Spanwise Lift Distribution with Flap Deflected

patterns were estimated by comparing the computed spanwise lift coefficient distribution to the local maximum lift coefficient in the same way as the flap up case. The stall patterns were also checked in the wind tunnel.

The comparison of the lift curves from analyses and 1/6-scale wind tunnel tests is presented in Fig.10(a). The lift coefficients from the VLM with corrected flap deflections agree well with those from the other empirical method(DATCOM). Also, the predicted lift curves by the methods stated above are in reasonable agreement with those from the wind tunnel



(a) Analyses and Wind Tunnel Experiments (b) Wind Tunnel Test and Flight Test

Fig.10 Comparison of Lift Curves

tests except that the DATCOM and the VLM with corrected deflection angle slightly overpredict lift coefficient for landing flap configuration (flap deflection $\delta_f = 60^\circ$). Thus, section flap effectiveness used to correct the flap deflections is considered to be reasonable for flap deflection $\delta_f = 15^\circ$ configuration, but slightly higher for the landing flap configuration. The pre-flight predicted maximum lift coefficients are also shown in Fig.10(a) for the flap up and flap down ($\delta_f = 15^\circ, 60^\circ$) conditions. The comparison of lift curves from the 1/6-scale wind tunnel test and flight tests is shown in Fig.10(b). For the flap up configuration, the lift coefficients agree well at low to moderate angles of attack. This is due to the fact that the flow is predominantly attached for these conditions and, accordingly, the Reynolds number effect is small. For the flap deflection $\delta_f = 15^\circ$ configuration, the lift curve slope from flight tests is slightly higher than that from the wind tunnel test and the lift coefficients from flight tests at low angles of attack are slightly lower than those from the wind tunnel test. As for the lift coefficients for the landing flap configuration (flap deflection $\delta_f = 60^\circ$), flight tests have not been conducted yet. The maximum lift coefficients for all configurations from flight tests are not yet available for correlation.

Another important consideration in the flap design was the trim change characteristic due to flap deflection. When the flaps are extended, the downwash angle at the horizontal tail as well as the pitching moment of the wing changes. Both of these affect the pitch characteristics of the aircraft. A slight pitch down with flap extension was considered desirable. The horizontal tail size and position were studied and determined to produce a slight pitch down when the flaps are extended. This tendency was confirmed in the flight test.

(3) OVER-THE-WING ENGINE MOUNT.

Two turbofan engines are mounted on pylons near the wing root. Because of this unusual engine location, it was necessary to investigate the aerodynamic and the structural dynamics in detail. In this section, one of those investigations, the inlet distortion test is presented.

With an over-the-wing engine mount configuration, it is easy to get a disturbed flow

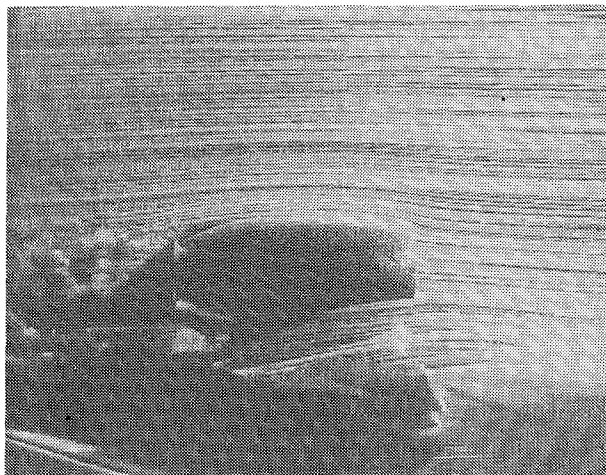


Fig.11 Smoke Wire Flow Visualization of Inlet at Cruise Condition

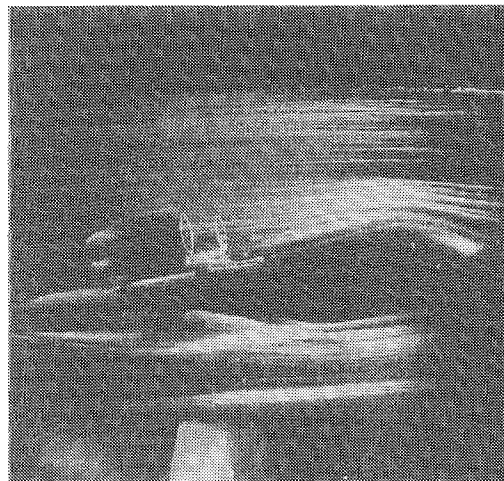
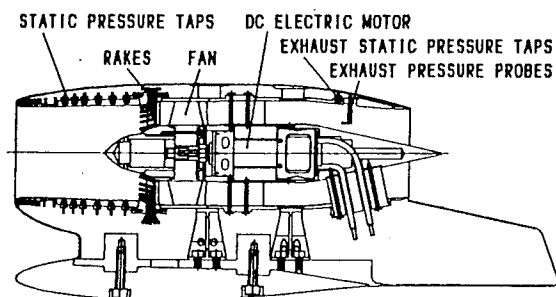


Fig.12 Vortices Into Inlet with Sideslip and High Angle of Attack

and a wake from the wing at high angles of attack. To gain insight into this problem, flow visualization tests using the smoke wire method were conducted. The smoke wire method is very useful tool because the flow around the wing and the nacelle-inlet can be evaluated qualitatively. However, the method cannot be applied at high speeds so the results must be evaluated carefully because of the relatively low Reynolds number. Based on the tests, it appears that the flow into the inlet does not have any problems below the wing stalling angle (Fig.11). However, a separated wake may cover the inlet at angles of attack above the stalling angle. Vortices from the fuselage with sideslip and high angle of attack were also observed to impinge on the inlet (Fig.12).

To evaluate the inlet flow distortion level quantitatively, a powered model test was conducted. Two DC motors which are electrically driven by 35 volts and 30 amperes up to 18000 rpm were installed in the 1/6-scale model. The inlet, duct shape, and fan spinner were scaled from the full scale nacelles. Forty total pressure probes were positioned at the fan face and mounted at the center of five rings of equal area,



SPEC.
 • SCALE: 16.7%
 • FAN DIAMETER: 95.8mm
 • MOTOR: PLATTENBERG HP355/40
 • MAXIMUM FAN RPM: 18000 (35V, 30A)

Fig.13 Engine Simulator Construction

and distributed circumferentially (Fig.17(a)) to allow a good determination of the pattern entering the engine as described in the JT15D engine installation manual (Ref.8). The rakes were aerodynamically faired and had a blockage of less than 6%. Fifty two static pressure orifices were located on the inlet duct wall to detect lip separation. Two total pressure probes and two static pressure orifices were also installed to measure the pressures at the exit. The inlet distortion was calculated from measured pressures. The aircraft pitch, yaw, air speed, engine fan speed, flap configuration, etc. were systematically

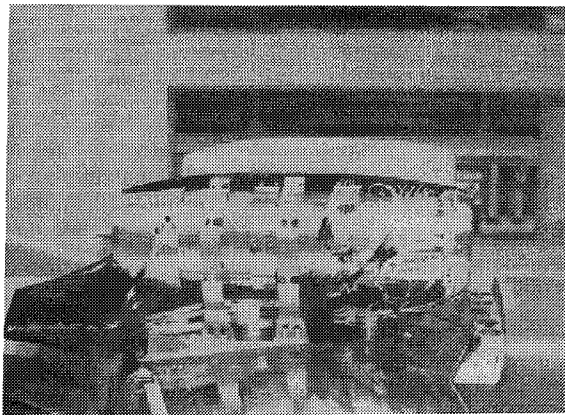


Fig.14 Engine Simulator Installed on 1/6 Scale Model

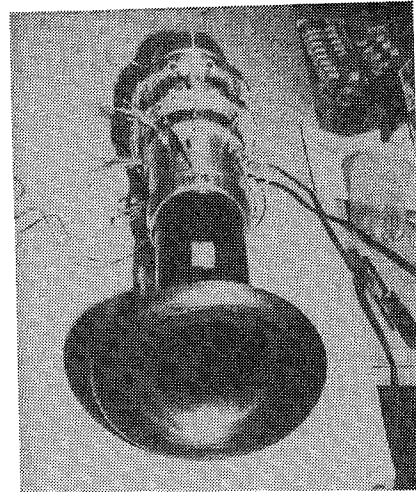


Fig.15 Mass Flow Calibration (with bell mouth)

varied to determine their combined effects on the inlet total pressure distribution. The engine simulator construction is shown in Fig.13, and the engine simulator installed on the 1/6-scale model is shown in Fig.14. Before installing the engines on the model, a bench test was conducted to calibrate the fan flow properties. A bell mouth was attached to the inlet duct (Fig.15) and the effective exhaust area was determined from pressure measurements at the fan face and the exhaust duct (static and total pressures). The mass flow ratio at each test condition was calculated from this effective area and the exhaust duct pressure measurement. According to the engine installation manual, the inlet pressure distortion is expressed in terms of the parameter,

$$\Delta P_0/P_{0\infty} = (P_{0\infty} - P_{AV.LOW})/P_{0\infty} \quad \text{in the segment of } \theta$$

$$(P_{0\infty} - P_{OMIN})/P_{0\infty} \quad \text{elsewhere}$$

where

$P_{0\infty}$ is the Maximum total pressure at any point in the plane of the fan,
 $P_{AV.LOW}$ is the segment average pressure at a given radius, which is the average local total pressure in the segment where the local total pressure is less than the ring average pressure, and
 P_{OMIN} is the minimum total pressure at any point.

An investigation was conducted to determine if the measured distortion exceeds the limits specified by the engine manufacturer (Fig.16). However these limits apply only to measurements made at a corrected fan speed of 100% and should vary as speed squared for other fan speeds. In addition, the model does not simulate the same inlet conditions at the same fan speed as the JT15D engine and, therefore, the allowable distortion limits for the model must be corrected to be consistent with those presented for the JT15D engine. It is noted, however, that these limit do not have to be less than $\Delta (P_0)/P_{0\infty}=0.020$. The distortion pressure patterns at three different angles of attack ($\alpha=0, 10, 16$ deg) with a mass flow ratio of about 0.86 are shown in Fig.17(b). From these test results, the distortion limits were estimated for the flight test (Fig.18). It should be noted that these limits were estimated from the scale model tests and Reynolds number effects have not been taken

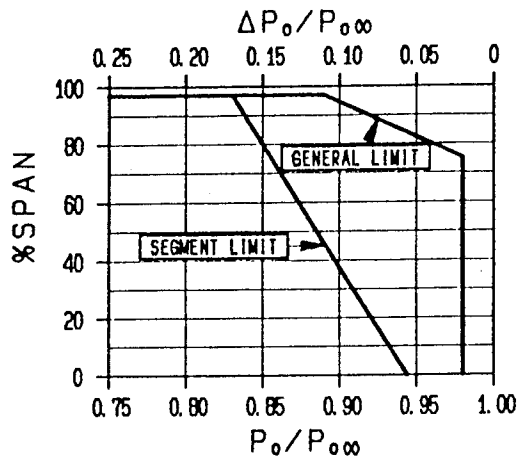


Fig. 16 Inlet Pressure Distortion Limits for JT15D Engine

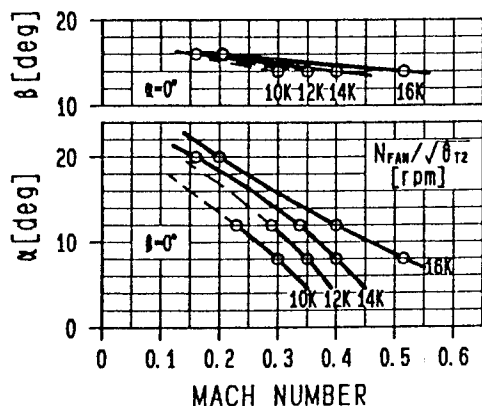


Fig. 18 Predicted Allowable Limits for Flight Test

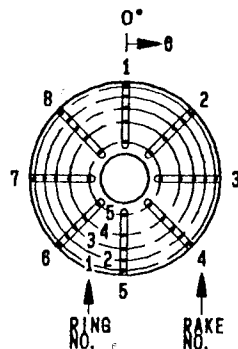


Fig. 17(a) Total Pressure Probes at Fan Face Atation

RH ENGINE
CRUISE CONDITION
V=200 km/h
N=17500 rpm
β=0 deg
MFR=0.86

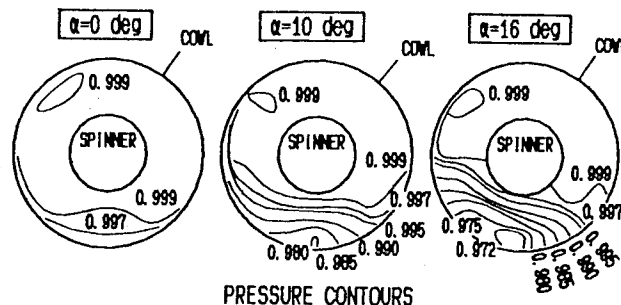
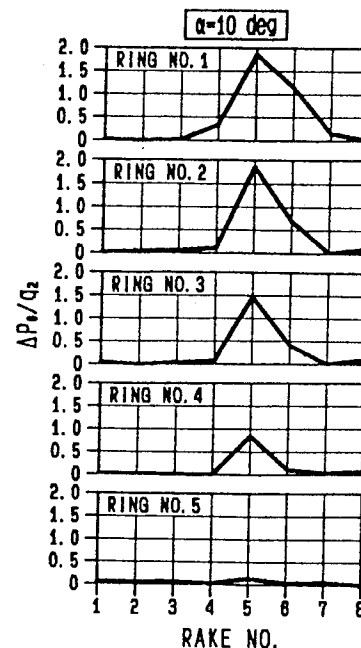


Fig. 17(b) Pressure Distribution Patterns Obtained from Powered Model Test

into account. By sweeping the wind speed and maintaining the same mass flow ratio, the Reynolds number effects on inlet distortion was investigated. However, because of the model size and the wind tunnel facility limitation, high Reynolds number simulation was not feasible and it is difficult to extrapolate these results to full scale. In general, the Reynolds number effect on the lower inner inlet lip is considered to be less sensitive to Reynolds number than that of outer lip and it was decided to use the scale model results without any correction to estimate the full scale characteristics even though it will be conservative.

5. STABILITY AND CONTROL

(1) WIND TUNNEL TESTING FOR STABILITY AND CONTROL.

During the development of the MH02, extensive six component force wind tunnel tests were conducted to obtain stability derivatives, to determine the stall characteristics, to validate the analytical estimations and to improve the stability characteristics. Three different wind tunnels - the Japan Automobile Research Institute Wind Tunnel (1/5-scale model test), the Honda Multi-Purpose Low Speed Wind

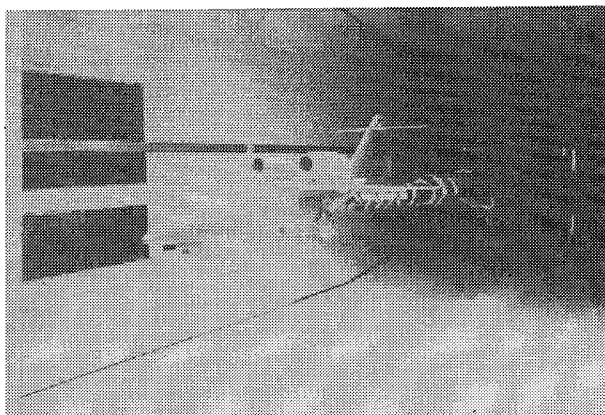


Fig.19 Honda R&D Wind Tunnel Test
(5X3.5m test section,
Maximum speed 350km/h)

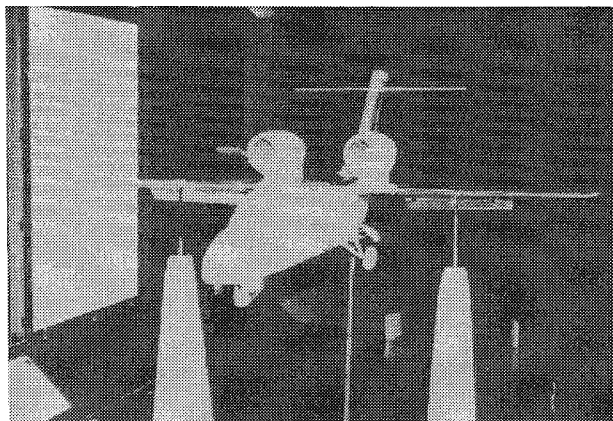


Fig.20 Texas A&M Wind Tunnel Test
(3X2.1m test section,
Maximum speed 320km/h)

Tunnel (1/6-scale model test - Fig.19), and the Texas A&M Wind Tunnel (1/6-Scale model test - Fig.20) were used. The model mount types in each wind tunnel were different but the correlation among them was generally good with the exception of pitching moment. The pitching moment measured using the sting mount (Honda) is more negative (pitch down tendencies) than that measured using one strut attached to the fuselage (JARI) or three struts attached to the wing and fuselage (Texas A&M). The cause of this difference is that the sting mount attached to the rear fuselage altered the fuselage pressure distribution. These results provide a correction factor for the pitching moment measured in the Honda Wind Tunnel. For each test, trip strips were installed on the wings, fuselage, tail, and nacelles to fix the location of the boundary layer transition. By knowing the exact laminar/turbulent portion length, the total airplane drag can be calculated and corrected.

After installing the JT15D engines which are larger than the original engines which had been planned to be installed, the directional stability $C_{n\beta}$ over a small range of sideslip angles became much worse than that of the configuration with the

original engines. The cause of this degradation was traced to the sidewash caused by the channel flow between the large engines. To improve the directional stability $C_{n\beta}$ in this region, both a ventral fin and a fin tip extension were studied. Wind tunnel investigations showed that the ventral fin was not very effective for the flap down condition because the flow coming up along the rear fuselage mixed with the flow from the flaps so that the ventral fin did not work very well. The fin tip extension was very effective (Fig.21) for both the flap up and the flap down conditions. Finally the fin tip was extended to increase $C_{n\beta}$.

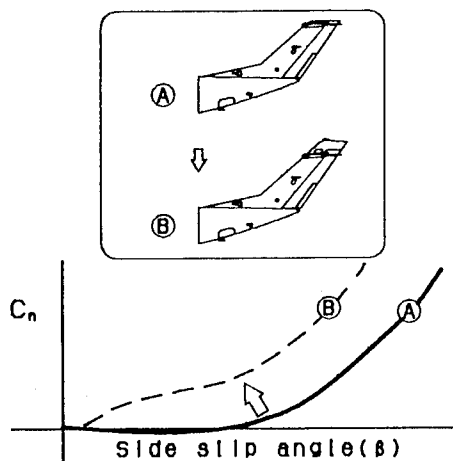


Fig.21 Directional Stability
Improvement by Fin Tip Extension

(2) TRIM ANALYSIS.

Because the engine thrust line is located higher than the aircraft center of gravity, it is important to take into account the thrust effect on the longitudinal trim characteristics. To size the elevator and determine the incidence of the horizontal stabilizer, a detailed trim analysis was performed. In the equilibrium equation for pitching moment, the pitching moment produced by the parasite drag and the induced drag of each lifting surface (the wing and the tail) as well as that produced by the thrust were included to simulate more accurately the trim condition. The thrust used for the pitching moment equilibrium calculation is determined from the required thrust which depends on the aircraft parasite drag (a function of angle of attack) and induced drag. An example of the power effect on the pitch characteristics for the flap up condition is shown in Fig.22. The elevator deflections required to maintain zero pitching moment $C_M=0$ are shown for the required thrust, maximum thrust, and thrust off (windmill) conditions. It should be noted that the aircraft maintains steady level flight for the required thrust condition whereas the aircraft climbs or descends steadily ($C_M=0$) for the maximum thrust or the thrust off condition, respectively. Analysis shows that the trim change caused by different thrust settings can be compensated for by an elevator deflection which is less than two degree (from the required thrust condition to the maximum thrust condition or from the required thrust condition to the thrust off condition); this is considered to be

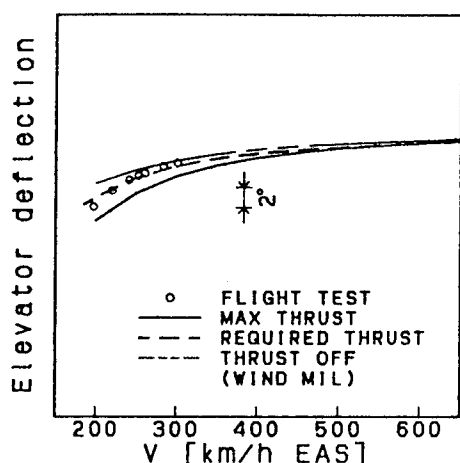


Fig.22 Effect of Power on Elevator Deflection

acceptable. The elevator deflections obtained from flight tests are also shown in Fig.22. The agreement between the predictions and the measurements from flight tests is very good. It was confirmed that the estimated stick fixed and stick free neutral points were in good agreement with those from flight tests. For the design of the elevator, it was also considered that the deflection should not exceed 75% of the total travel during takeoff rotation and the control should be sufficiently effective in landing up to the touchdown speeds as specified by MIL-8785C. Stick force per g and stick force in landing were also checked to determine if they satisfy the MIL-8785C requirements.

(3) DYNAMIC STABILITY ANALYSIS.

A dynamic stability analysis was performed using the longitudinal and lateral motion equations linearized by small perturbation theory. Stability derivatives were computed using DATCOM, ESDU and other methods. Some of them were corrected by referring to wind tunnel results. The dynamic stability characteristics, such as short period, phugoid, Dutch roll, spiral, and others, were studied by computing the undamped natural frequency, damping ratio, time to half (or double) and checked to determine if they comply with MIL-8785C requirements. The undamped natural frequency and damping ratio for short period in category B flight phase are shown in Fig.23 and Fig.24, respectively. Both satisfy Level 1 of the MIL-8785C requirement. The short period time response produced by an elevator pulse input computed using a 6-

Degree Of Freedom(DOF) nonlinear simulation is shown in Fig.25. The response shows good damping and the oscillation is heavily damped. The same analysis was performed for the lateral-directional flight characteristic evaluation. The Dutch roll undamped natural frequency and damping ratio at each flight speed are shown in Fig.26 and Fig.27, respectively. The airplane satisfies Level 1 of the MIL-8785C requirement for the category B flight phase at this altitude. Because the dihedral effect(Cl_β) and the static directional stability(Cn_β) vary with angle of attack, those should be considered in each analysis. According to the analysis, the flight characteristics of the MH02 aircraft generally satisfy Level 1 of the MIL-8785C requirement but the Dutch roll damping at high altitude is slightly lower than the Level 1 requirement and the spiral mode (time to double) in the landing flap configuration is in the Level 2 to 3 for category C flight phase at very low speed because the deployment of the flaps reduces the dihedral effect at high angles of attack.

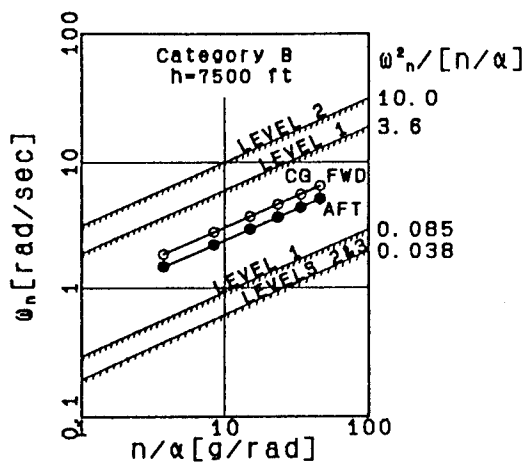


Fig.23 Short Period Natural Frequency

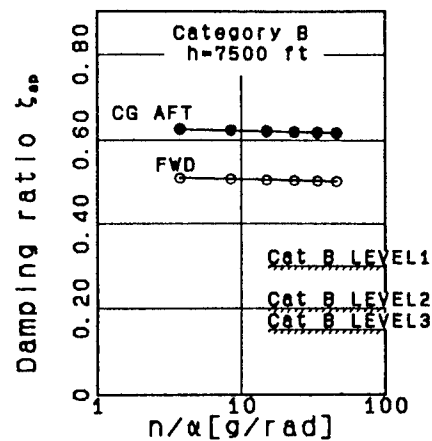


Fig.24 Short Period Damping Ratio

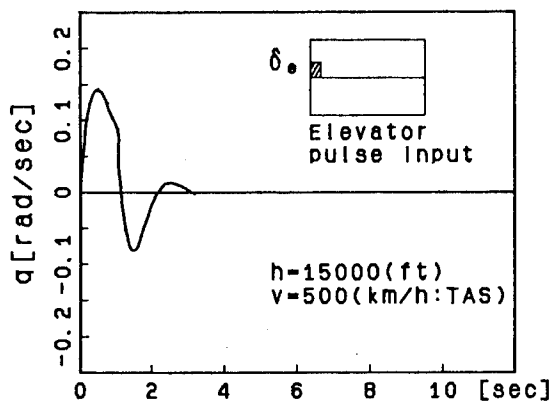


Fig.25 Short Period Time Response

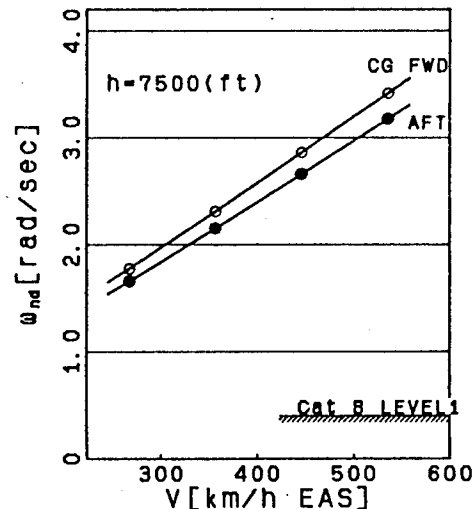


Fig.26 Dutch Roll Natural Frequency

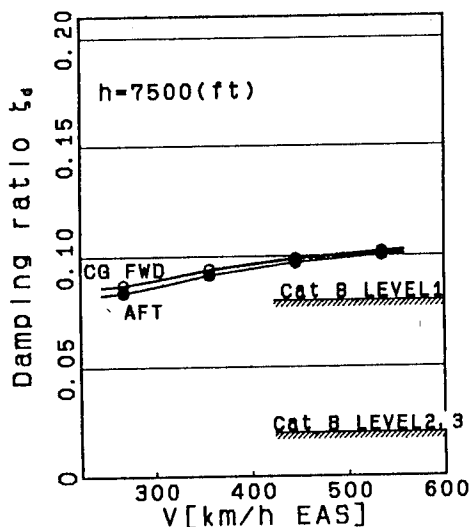


Fig.27 Dutch Roll Damping Ratio

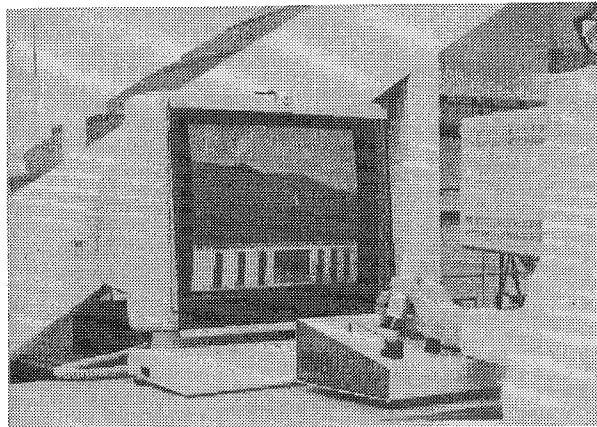


Fig.28 6DOF Real Time Simulator

To check the stability and control characteristics, a simple real time flight simulator which solves 6 DOF nonlinear equations was developed (Fig.28). The simulator consists of a stick, an A/D converter, and a Silicon Graphics IRIS workstation. The display shows the cockpit view which is computed from the solution of 6DOF nonlinear equations corresponding to the control surface and thrust inputs for each speed and altitude. Although no reaction force is simulated in the stick, it was valuable to evaluate the feeling of controllability of the aircraft in the design process.

(4) DEEP STALL CHARACTERISTICS.

By employing a T-tail configuration, the horizontal tail arm can be increased, also the rate of change of downwash with angle of attack ($\partial \epsilon / \partial \alpha$) decreases and the dynamic pressure ratio (q_t/q) at the horizontal tail becomes higher than that for a low tail configuration. As a result, it is possible to reduce the horizontal tail size so that the weight and the skin friction drag of a T-tail configuration can be reduced. The T-tail configuration has negative attributes as well, such as deep stall which is a locked-in stall condition at very high angles of attack where recovery is impossible because of the reduction in the elevator effectiveness. To avoid this dangerous characteristic, deep stall was carefully studied in the design stage using statistical approaches and wind tunnel tests. During the preliminary design phase, aspect ratio and wing sweep angle were set not to have a pitch up tendency based on NASA TN-1093. The characteristic was confirmed in wind tunnel testing (the tail off pitching moment characteristic). The horizontal tail location was also determined based on NASA TMX-26. The horizontal tail span sometimes plays an important role in avoiding deep stall (for example, Ref.10). The horizontal tail span was studied statistically by comparing T-tail airplanes which do not exhibit deep stall problems. However, because the configuration of the MH02 is unconventional, these studies can only be used as a rough guideline. To evaluate the deep stall characteristics more realistically, a 1/6-scale wind tunnel test was conducted. To evaluate this deep stall characteristic, a Deep Stall Margin (DSM) defined as the pitching moment margin $\Delta(C_M)$ between $C_M=0$ and the peak of the $C_M-\alpha$ curve beyond stall angle and the elevator effectiveness at very high angles of

DSM DATA (ΔC_M)			
	ΔC_M	CG [MAC%]	δ_e^1 [deg]
MU300	-0.16	35	FULL DOWN
DC-9	-0.03	40	FULL DOWN
C-141	-0.20	N.A. ²	N.A. ²
	-0.23	34	+15
			Reference
			Ref. 9
			Ref. 10
			Ref. 11
			Ref. 12

*1 δ_e : Elevator deflection
*2 N.A. : Not Available

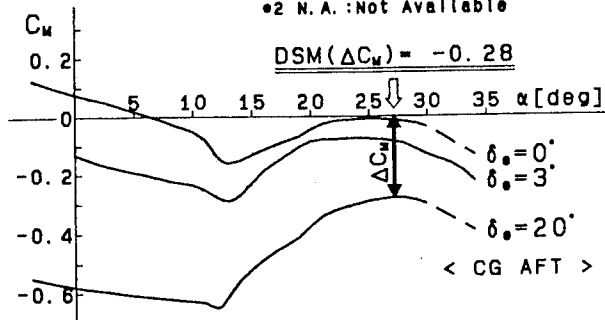


Fig.29 MH02 Deep Stall Characteristic

of attack. There is an disadvantage for this relatively large elevator power because the full up elevator produces a large nose up pitching moment and may put the airplane into high angles of attack. Many production airplanes incorporated a stick pusher to avoid unnecessary penetration of these high angle of attack region. However, because the MH02 is an experimental aircraft, it is concluded that the device to avoid the flight in the deep stall region does not have to be installed as long as the recovery from high angles of attack is possible.

attack were investigated. The C_M - α characteristics of the MH02 obtained from wind tunnel tests are shown in Fig.29. The deep stall margins for three other airplanes (MU-300, DC-9, C141) are also shown in this figure. Compared to the other airplanes, the MH02 aircraft exhibits an ample deep stall margin. (It may be of interest to note that Ref.13 states that it is possible to recover from high angles of attack as long as some deep stall margin is available ($C_M(\text{peak}) < 0$)). As for the control effectiveness, it was found that the effectiveness at high angles of attack (above 25deg) is still about 50% of the initial values. From these experimental results, it is thought that the MH02 has sufficient elevator power to recover from the stall at any angle

6. AEROELASTICITY

(1) STIFFNESS MEASUREMENT TEST.

Stiffness distributions are very important for the aeroelasticity analysis. To verify the design stiffness, stiffness tests were conducted for the wing, the horizontal tail, and the fin. Bending slopes were measured using techniques that employ mirrors and transits (Fig.30) and twist angles were measured using displacement gages. From the experiments, it was found that the measured bending

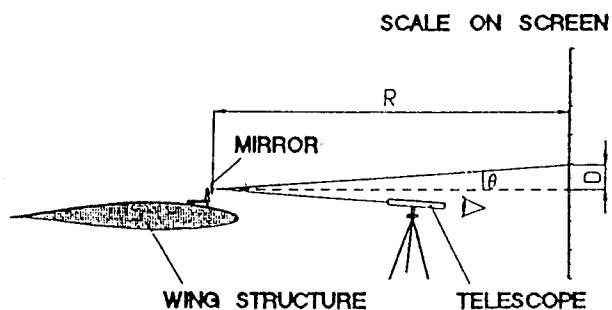


Fig.30 Stiffness Test Wing Optical Lever Method

stiffness (EI) was higher than estimated while the measured and estimated torsional stiffness (GJ) agreed very well. The reason for this discrepancy in bending stiffness was that the contribution of the honeycomb skin structure to the bending stiffness is larger than estimated. These measured stiffness values were then used for a vibration analysis and Ground Vibration Test (GVT) correlation analysis.

(2) GROUND VIBRATION TEST AND VIBRATION ANALYSIS.

To measure the coupled vibration modes of the entire aircraft and establish the correlation with those computed analytically, extensive Ground Vibration Tests (GVT) were conducted. Ground vibration test techniques employed were the traditional Tune Sine Dwell (TSD) method, which defines one mode at a time by tuned sinusoidal input, and the Frequency Response Function (FRF) method, which uses a Fast Fourier Transform (FFT) analyzer and a modal analysis program. The aircraft was excited by electrodynamic shakers which were attached to the aircraft by means of telescoping thrust rods having flexible hinges. The structural responses were measured by piezoelectric accelerometers attached to the aircraft. The aircraft was excited by two shakers with current feedback. The FRF excitation system used for these tests is shown in Fig.31. By using multiple shakers, it is not only possible to excite the

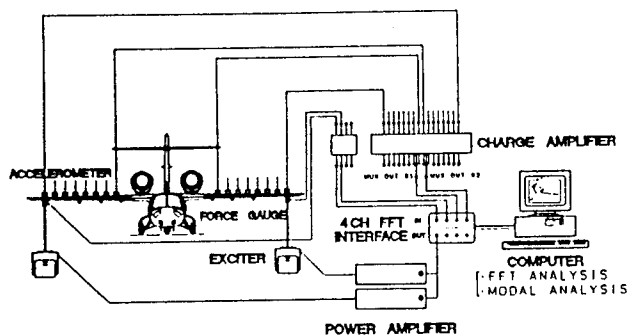


Fig.31 Ground Vibration Test System (FRF)

Table.1
Coupled Frequency Comparison

UNIT < CPS >

TUNED SINE DWELL HORIZONTAL TAIL EXC.	FRF METHOD WING EXC.	ANALYSIS
5. 50 (4.3)	5. 73 (2.06)	5. 69
8. 12 (6.1)	8. 17 (1.50)	8. 75
10. 08 (3.6) [WING MODE]	10. 08 (3.94) [WING MODE]	10. 20 [WING MODE]
13. 61 (7.4)	NOT OBTAINED	13. 47
16. 86 (9.7)	16. 80 (4.98)	17. 28

() ... STRUCTURAL DAMPING VALUE

airplane well and obtain a high quality frequency response function but also to reduce the modal density in half by exciting the airplane in phase or out of phase, respectively. For this dual input excitation with correlated signal method, the algorithm is identical to that for single point excitation and, therefore, the data processing is much simpler and faster than that for the general multi point random excitation procedure. Hanning windows were used to minimize leakage errors. The frequencies from the TSD and FRF methods are presented in Table.1. There are small differences in frequencies for some modes between the TSD and FRF methods but these are due to differences in the weight at each test condition. By considering these, the frequencies from the TSD method generally agreed well with those from the FRF method. However, the values of structural damping obtained from the FRF method tend to be lower than those from the TSD method. (see Table.1) The antisymmetric tail coupled modes obtained from the dual input excitation with correlated signal method are shown in Fig.32(a)-(d).

A normal mode vibration analysis was performed employing the superposition of the uncoupled mode method and a Finite Element Method (FEM). The finite element computer code, which was specially developed for aircraft vibration analysis, was mainly used for this vibration and correlation analysis. In this code, the aircraft is represented by beams which have stiffness (EI, GJ), mass, and moment of inertia. Because the torsional and bending stiffness distributions were measured

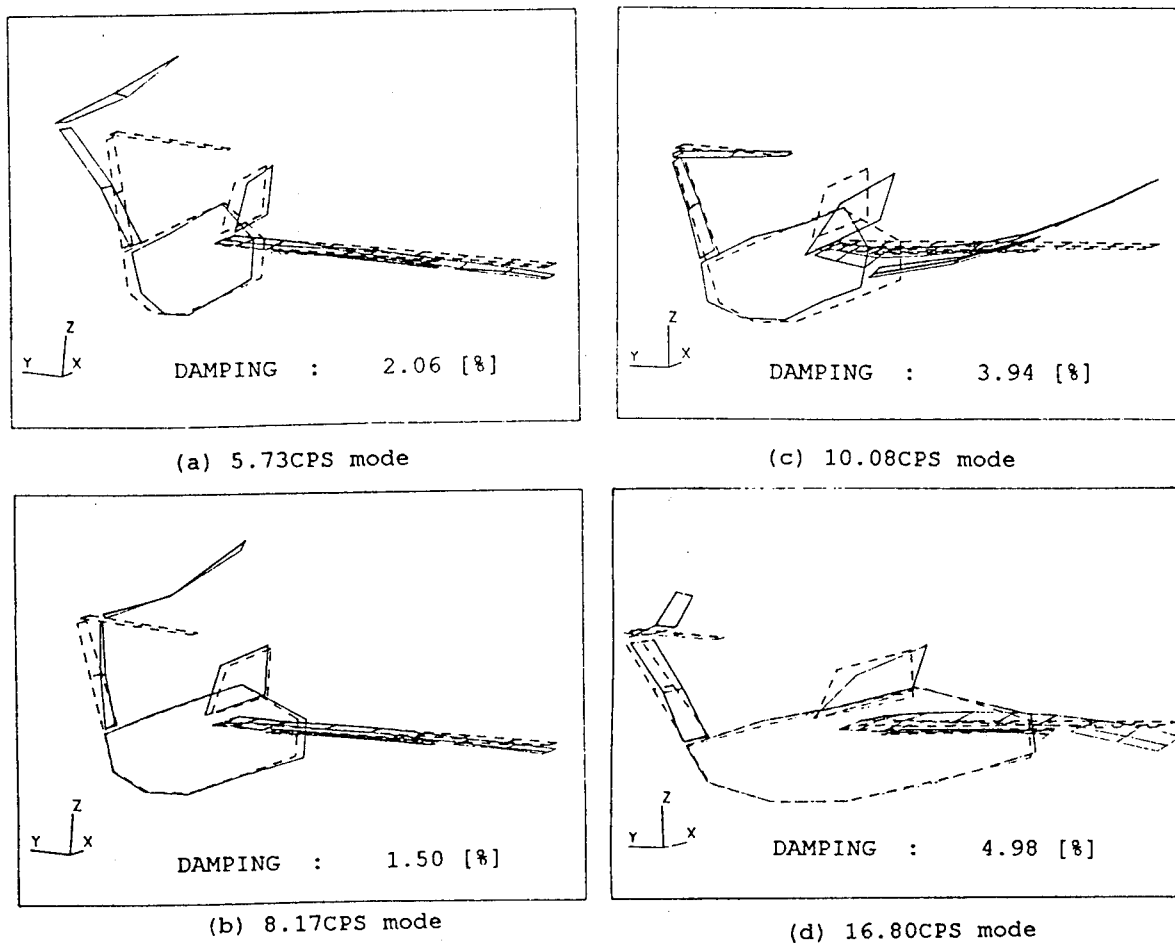


Fig.32 Tail Coupled Modes

experimentally, the correlation between the analysis and normal modes obtained from ground vibration tests agreed quite well after small modification of the mass distributions. The comparison between the antisymmetric tail normal modes from analysis and experiments (from TSD & FRF method) is shown in Table.1.

(3) DIVERGENCE ANALYSIS.

The forward swept wing has a well known divergence characteristic and, therefore, it was important to evaluate the divergence characteristics in the preliminary design phase. The divergence analysis was conducted by solving the integral divergence equation formulated using generalized coordinates. The effect of wing sweep on divergence speed is shown in Fig.33(a), (b). The bending and torsional stiffnesses used for this divergence analysis are based on the structure designed by strength. As seen in Fig.33, divergence speed decreases rapidly as the sweep angle varies from 0 to -20 deg but it remains still well above $1.2V_D$ (curve-A) at low to moderate sweep angles. One might think that the reason for this high divergence speed is the relatively conservative structural design philosophy for the MH02. However, as indicated in Fig.33(a) and Fig.33(b), divergence analyses of other wings having bending (EI) and torsional (GJ) stiffness distributions which are decreased to 75% and 50% of the original EI and GJ still show relatively high divergence speeds in this range of sweep angles. From these results, it can be inferred that divergence is not

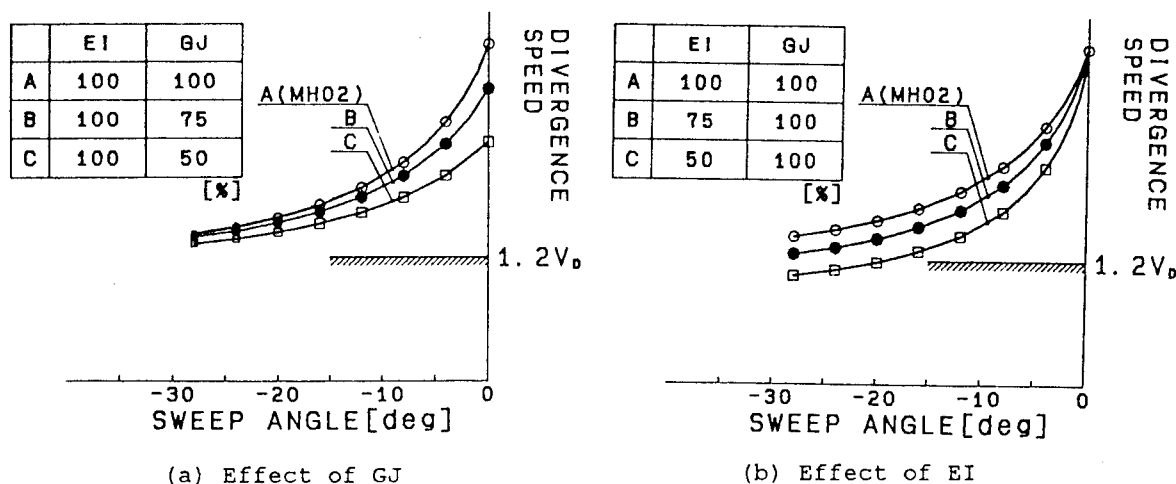


Fig.33 Variation of Divergence Speed with Forward Sweep Angle

critical for an aircraft having a cruise speed which is relatively low (say, $M < 0.60 - 0.65$) as long as the forward sweep angle is not extreme. (for example, sweep angle $> -15^\circ$) In other words, the forward swept wing which is designed by strength will generally not suffer from divergence problems except for high speed aircraft.

Because it is found that divergence is not critical, the sweep angle for the MH02 aircraft was determined by studying good stall characteristics (as stated in 4-(1)) with high span efficiency, cabin layout (carry-through structure should be located aft of the cabin as stated in 2.) and structural loads such as bending moment, kick load at the root produced by the sweep angle, etc.. Based on these studies, a sweep angle of -12° at quarter chord was selected.

It is of interest to note that, from Fig.33(a) and Fig.33(b), bending stiffness is more important at large forward sweep angles whereas torsional stiffness is important at small sweep angles for divergence. For the MH02 wing skin, the anisotropic laminate patterns were employed so that the wing has negative coupling stiffness as well as relatively high torsional stiffness without reducing bending stiffness. These result in a higher divergence speed.

(4) FLUTTER ANALYSIS.

A modal flutter analysis was performed to estimate the flutter speed of the MH02 aircraft. The flutter determinant was solved using k-method. The plots of speed vs. damping (V-g curve) present the flutter stability characteristics. For the generalized aerodynamic force, a two dimensional incompressible unsteady strip theory along the stream direction was mainly used. To take account of the aerodynamic loading due to the finite span effect, the local lift curve slope at each section is corrected based on the distributions of section lift curve slope computed from steady flow theory.

Symmetric and antisymmetric flutter mode of wing and tail (for example, horizontal tail-elevator rotation, T-tail flutter mode, and fuselage side bending with rudder rotation flutter mode, etc.) were carefully studied. Analyses of each flutter mode

were carried out with the control surface fixed and free condition respectively and the effects of control surfaces on the flutter modes were also investigated. In some cases, the aerodynamic moment about the hinge axis $T \beta \beta$ term (control surface rotation due to control surface rotation term) was corrected by multiplying by a factor to simulate more severe conditions.

Because T-tail flutter mode is violent in nature, it is important to check this flutter mode. After the first Ground Vibration Test (GVT) was conducted, the fin torsional frequency was found to be lower than the design value and the T-tail flutter speed became significantly lower. The cause of this low torsional frequency was that the horizontal tail and the elevator weight were heavier than the initial estimated values and, therefore, the moment of inertia of the horizontal tail increased. Especially the additional elevator mass balance required by the elevator weight increase in particular affected the moment of inertia, because mass balances are located at the tips of the horizontal tail. To increase the fin torsional frequency, the skin thickness had to be increased and reinforcement joints were added to increase the yawing stiffness between the horizontal stabilizer and the fin. After these modifications, the fin torsional frequency was increased and the T-tail flutter characteristics were much improved. The results of the antisymmetric tail flutter mode analysis with rudder fixed condition are shown in Fig.34(a). Curve-A shows the T-tail flutter mode and it can be seen that the flutter speed is above $1.2 V_D$. The antisymmetric flutter mode with rudder free condition is shown in Fig.34(b). For this analysis, the measured moment of inertia and static unbalance of the rudder were used. The humped flutter mode (curve-B) appears and presents the mode including rudder rotation. However, this mode is stable and the rudder is adequately mass balanced.

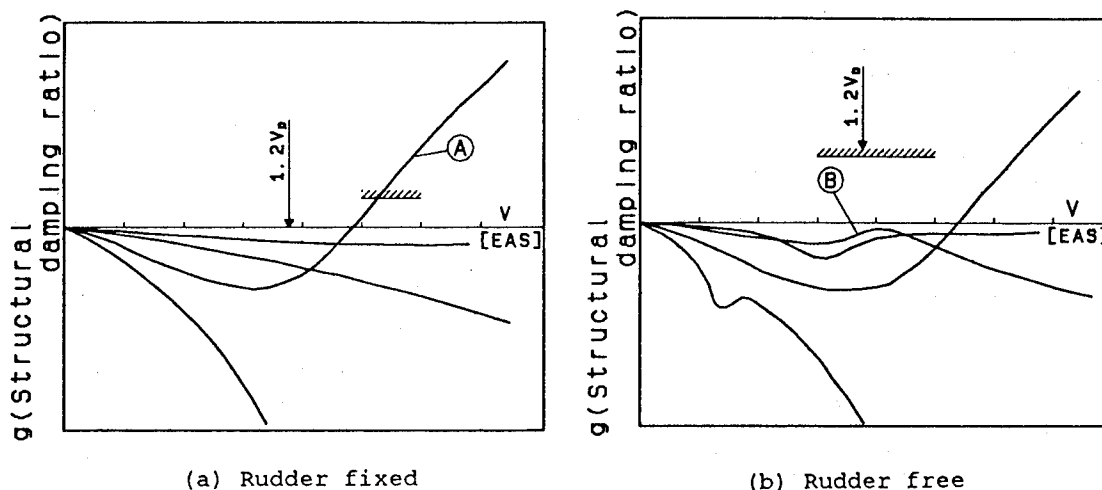


Fig.34 U-g Diagram for Antisymmetric Tail Flutter(h=16,000ft)

7.CONCLUSION

The forward swept wing is generally thought to be impractical because of the large weight penalty required to prevent divergence. However, for low to moderate speed aircraft such as the MH02, it is probable that a wing designed by strength will not suffer divergence problems as long as the sweep angle is not excessive. There is the

possibility of taking advantage of the good stall characteristics with a high efficiency offered by the forward swept wing configuration for low to moderate speed aircraft. The unusual engine location does not exhibit any problems with respect to inlet distortion, wing lift characteristics, and structural dynamic characteristics. However, interference drag between the wing and the nacelles is relatively high because the large nacelles and pylons are located in the upper side of the wing and near the wing surface. The pylon shapes were designed to minimize separation and interference, but wind tunnel experiments showed high interference drag. Further investigations will be needed to reduce this interference drag. The T-tail flutter characteristics depend primarily on the fin torsional frequency. An unexpected weight increase of the horizontal tail resulted in the reduction of the fin torsional frequency so that additional torsional stiffness was required to avoid T-tail flutter. Weight management of the horizontal tail is very important from a T-tail flutter standpoint.

8. REFERENCES

- (1) E. R. Kendall, The Theoretical Minimum Induced Drag of Three Surface Airplanes in Trim, *Journal of Aircraft* Vol. 22, No. 10, Oct. 1985.
- (2) R. J. Margason and J. E. Lamer, Vortex-Lattice FORTRAN Program for Estimating Subsonic Aerodynamic Characteristics of Complex Planforms, NASA TN D-6142
- (3) H. E. Herbert, Production Version of Extended NASA - Langley Vortex Lattice FORTRAN Computer Program, NASA TM83303
- (4) A. D. Young, The Aerodynamic Characteristics of Flaps, R&M No. 2622, 1947.
- (5) Bjorn L. G. Ljungstrom, 2-D Wind Tunnel Experiments with Double and Triple Slotted Flaps, FFA-AU993
- (6) W. A. Stevens, S. H. Goradia, Mathematical Model for Two Dimensional Multi Component Airfoils in Viscous Flow, NASA CR-1843
- (7) E. Torenbeek, Synthesis of Subsonic Airplane Design, Delft University Press
- (8) Pratt & Whitney Canada, Installation Manual JT15D-1, JT15D-1A and JT15D-1B Turbofan Engines, Section 3
- (9) T. Hanai, Deep Stall Characteristic of MU-300, *Journal of the Japan Society for Aeronautical and Space Science*, Vol. 33, No. 377, Jun. 1985.
- (10) R. S. Shevell and R. D. Schaufele, Aerodynamic Design Features of the DC-9, *Journal of Aircraft* Vol. 3, No. 6, Nov.- Dec. 1966.
- (11) A. L. Byrnes, W. E. Hensleigh, L. A. Tolve, Effect of Horizontal Stabilizer Vertical Location on the Design of Large Transport Aircraft, *Journal of Aircraft*, Vol. 3, No. 2, Mar.-Apr. 1966
- (12) F. A. Cleveland and R. D. Gilson, Development Highlights of the C-141 StarLifter, *Journal of Aircraft*, Vol. 2, No. 4, July.-Aug. 1965
- (13) M. D. White and G. E. Cooper, Simulator studies of the deep stall, NASA SP-83, pp101-111

9. ACKNOWLEDGMENTS

The author wishes to thank Honda R&D for permission to publish this paper and my colleagues - K. Morishita, K. Goto, Y. Wariishi, M. Aoki, J. Sawada, K. Mahiko, T.

Tabata, Y. Kawamura for their invaluable assistance. The author also thanks L. A. Tolve who shared the valuable experience with me, and D.Somers for valuable discussions, and duPont and Andersen for their cooperation. Finally the author would like to express the appreciation to the staff members of Raspet Flight Research Laboratory who gave us the opportunity to fabricate and test the MH02 aircraft.

FLIGHT AND FULL-SCALE WIND TUNNEL INVESTIGATIONS OF TRANSITION PHYSICS ON THE WING OF A PROPELLER-DRIVEN AIRCRAFT

S.J. Miley, K.-H. Horstmann and G. Redeker
Deutsche Forschungsanstalt für Luft- und Raumfahrt e.V. (DLR)
(German Aerospace Research Establishment)
Institut für Entwurfsaerodynamik
(Institute for Design Aerodynamics)
Braunschweig
Federal Republic of Germany

ABSTRACT

Detailed measurements of the wing laminar boundary layer, using traversing hot-wire probes, have been performed in-flight, and, with the same wing, in a full-scale, low-turbulence wind tunnel. The objective of the research program was to add to the calibration data base of a laminar flow design procedure utilizing instability amplification rates for laminar/turbulent transition criteria. For a given flight condition, the character of the laminar boundary layer at the probe location was controlled by the wing flap. Utilizing the infrared imaging method for locating the transition front, the wing flap was adjusted until the transition front was located at a desired position relative to the probe location. After the flight program, the wing was removed from the aircraft with all flight instrumentation, was installed and tested in a full-scale, low-turbulence wind tunnel. For both test regimes, simultaneous measurements of the mean and disturbance velocity distributions across the boundary layer, were obtained. Analyses of the data show, that the initial disturbances within the laminar boundary layer, which grow and ultimately lead to transition, are associated with acoustic radiation from the propeller. No differences in transition were found between flight and wind tunnel.

INTRODUCTION

Design for laminar flow requires mathematical tools which allow one to determine the viscous flow about, or through, a given geometric shape. The maintenance of laminar flow is realized if the laminar boundary layer is held within certain bounds related to the physics of viscous flow. These bounds are generally referred to as a *transition criterion*, in that, if they are exceeded, then transition to turbulent flow will occur. Until recently, transition criteria were totally empirical in nature. The respective curves were developed from careful experiments in high quality flow tunnels and formalized utilizing boundary layer parameters which stability theory identified as being important. Two of the most successful of these transition criteria were those of Granville [1] and of Michel [2]. While used over a wide range of different flow regimes in practice, one always had the concern of their validity, if the particular application was for a flow regime or circumstances relatively removed from those which generated the criterion. This would particularly be the case for attempting to predict transition for three-dimensional flows such as those for swept wings. These empirical transition criteria were developed from two-dimensional flows where the instabilities were of one type; Tollmien-Schlichting (TS) waves. In more recent times, a new

approach to predicting transition has been developed [3-6]. This new approach utilizes powerful computational procedures to model and analyze the actual instability physics within the laminar boundary layer, which ultimately lead to transition. With this approach, there is no concern about applications far removed from the flow conditions which generated the old empirical criteria. The different instability processes which can occur, particularly on swept wings, are modeled and accounted for. However, at the present time, the modeling does not extend beyond the growth of instabilities. It does not carry into and through the actual flow breakdown, that is transition. In effect, the modeling carries you to the doorway of transition, but not through it. The location of this doorway can not be determined by the modeling. At the present, these new transition prediction methods still require experimental input, or more specifically, require experimental calibration. The calibration of one of these methods was the overall objective of the research program discussed in this paper.

The two types of laminar boundary layer instabilities which lead ultimately to transition are Tollmien-Schlichting (TS) and cross-flow (CF). TS instability is the source of transition where the flow is primarily two-dimensional, as in the case of aircraft with little or no wing sweep. It also occurs on swept wings, well back from the leading edge. CF instability occurs near the leading edge of wings with moderate or high degrees of sweep. Both instability flows are strongly influenced by pressure gradient, although in opposite ways. CF instability occurs in strong favorable pressure gradients, which tend to reduce TS instability, and TS instability occurs in pressure gradients which range from adverse to weakly favorable, which tend to reduce CF instability. The practical result of this is that laminar flow design of swept wings requires transition models which include both TS and CF physical representations, whereas only TS instability need be considered for wings of little or no sweep. This paper concerns only the TS instability.

Figure 1 illustrates the model used for Tollmien-Schlichting (TS) instability. The sinusoidal wave depicted, is not the true physical appearance of the instability disturbance, but is a representation of the way the disturbance manifests itself in the form of a flow velocity fluctuation. As the disturbance grows in size, so does the associated velocity fluctuation grow in amplitude. The growth of the disturbance is dependent on the Reynolds number and on the pressure gradient of the flow. Initially, all disturbances are damped out. At some stage of the development of the boundary layer, some disturbances start to grow. This is defined as the point of neutral stability in the figure. Beyond this point, disturbances which lie within a particular frequency band will grow. As the boundary layer progresses, the frequency band in which disturbances are amplified changes. As this band shifts, some disturbances which grew initially will damp out and others, which had much smaller growth rates will accelerate in growth. The growth of the disturbances is related to a parameter called the amplification factor, or N-factor, as defined in the figure. The N-factor is used to determine transition as shown in figure 2. As the laminar boundary layer progresses, the frequency band in which disturbances are amplified, shifts. For favorable pressure gradients, disturbances at higher frequencies are amplified. As the pressure gradient shifts to adverse, the amplified disturbance frequency band shifts to lower values. According to the procedure, once the disturbances have reached a certain amplitude, the flow structure breaks down and transition to turbulence occurs. The critical disturbances may be in any frequency band, so all bandwidths have to be monitored. Figure 2 illustrates the growth

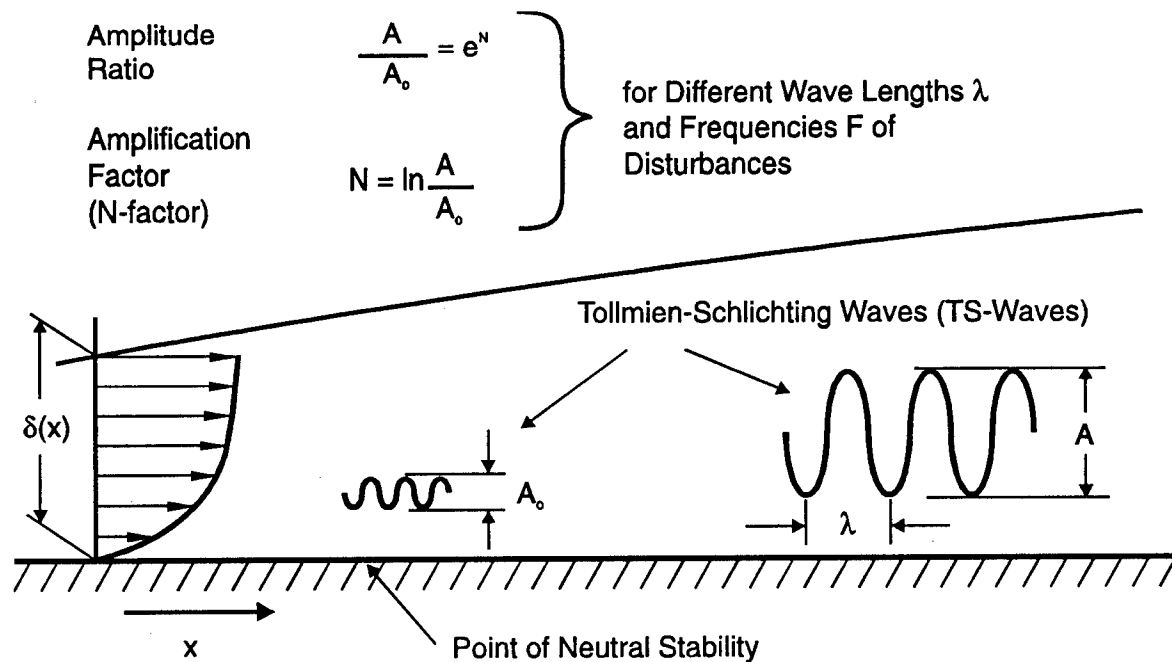


Figure 1. Growth of instability disturbances within the laminar boundary layer

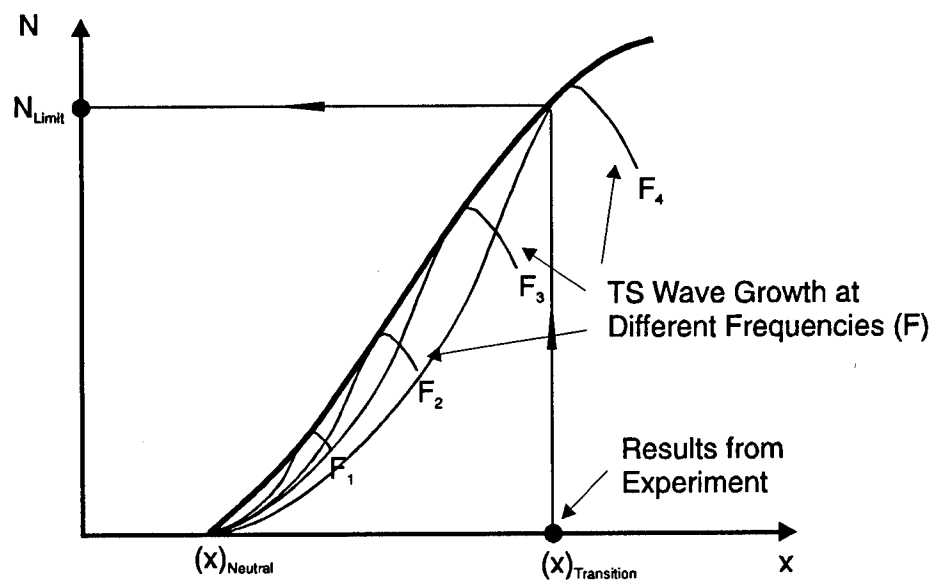


Figure 2. N-factor envelope and determination of transition N-factor

and decay of disturbances in specific bandwidths as the boundary layer progresses in the x -direction. An N-factor envelope is generated which gives the maximum growth of the respective disturbance bands. Since present models do not yet represent the subsequent breakdown process, the N-factor at which this occurs, must be determined from experiment. This is the calibration that is required to make the method practical. The calibration of these

methods has been a major object of laminar flow research in recent years. The critical N-factor range for TS disturbances is different than that for CF disturbances, so calibrations must be carried out for each of the models. The work presented in this paper is part of the calibration effort of the Deutsche Forschungsanstalt für Luft- und Raumfahrt (DLR) laminar flow research program. This effort is described in more detail in references [7] and [8].

TEST APPARATUS

The measurements were carried out on the DLR research aircraft LFU-205, shown in figure 3. It is a four-place single-engine aircraft of composite material construction. It is a laminar

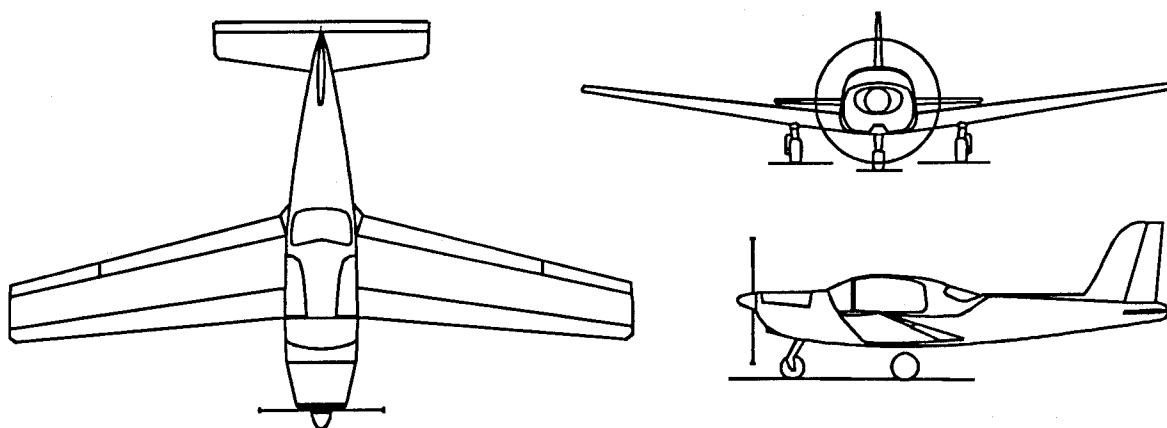


Figure 3. DLR flight research aircraft LFU-205

flow design, utilizing Eppler airfoils for the wing. The maximum level-flight speed of the aircraft is 330 km/hr, yielding a Reynolds number based upon aerodynamic mean chord of $Re = 10^7$. A special instrumented test glove was added to the wing on the right side of the aircraft. The basic wing geometry, test glove and test instrumentation are shown in figure 4. The glove contains 74 static pressure orifices arranged as shown in the figure. In addition to the pressure orifices, the glove is equipped with three hot-wire probe boundary layer traversing systems, located at chord stations of $x/l = 0.25, 0.43$, and 0.60 . The first two locations were constrained by the box spar of the wing. The first location is as far aft, and the second location as far forward as possible without penetrating the spar structure. The third location was based upon previously observed laminar flow extending to 70 percent chord. Each of the traversing systems contained three single-sensor hot-wire probes. Additionally, there was a fourth single-sensor probe mounted separately, adjacent to each of the traversing systems. The probe arrangement is shown in figure 5. Each of the probes carried a designation as is indicated in the figure. A cross-sectional view is given in figure 6. The geometric arrangement of the three traversing probes was designed to provide a means of determining TS disturbance wavelength and wavefront direction through time-correlation of the respective probe signals. The traversing systems had a vertical position accuracy of 10 microns. The height of the fourth (Reference) probe was manually

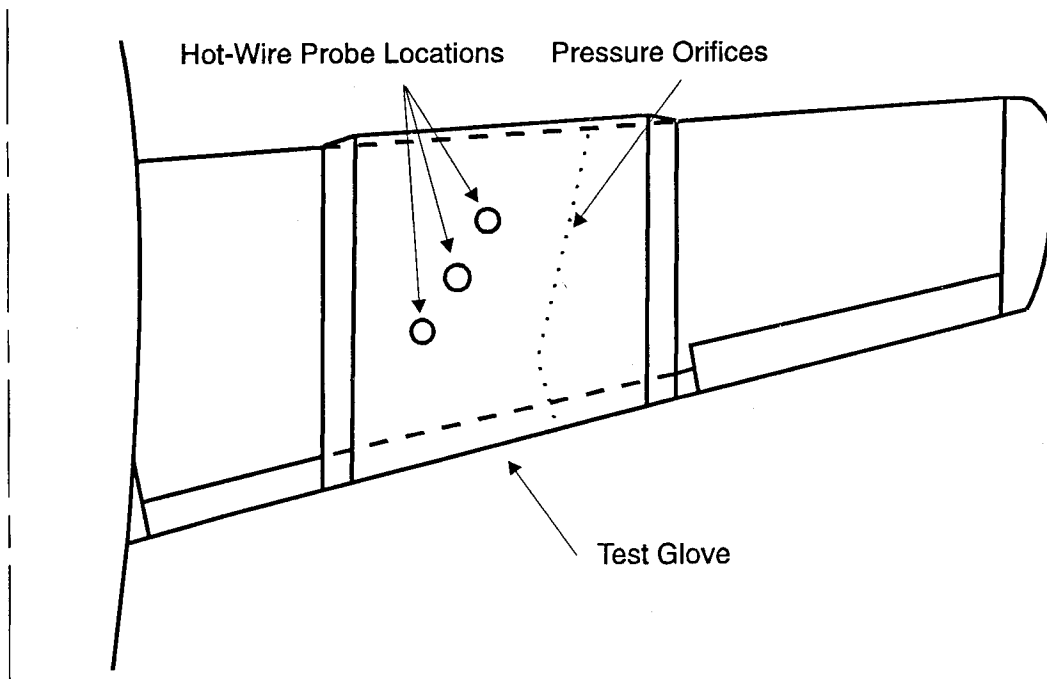


Figure 4. Test glove and flow instrumentation

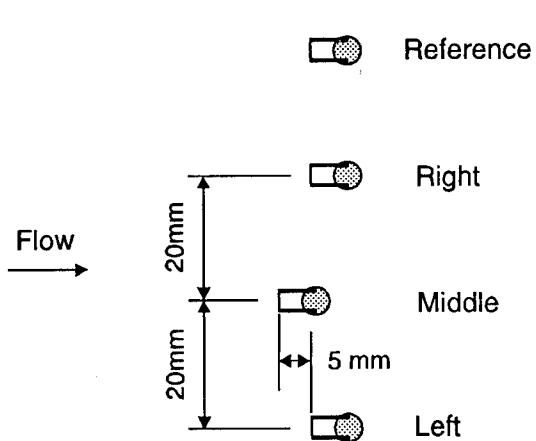


Figure 5. Hot-wire probe arrangement

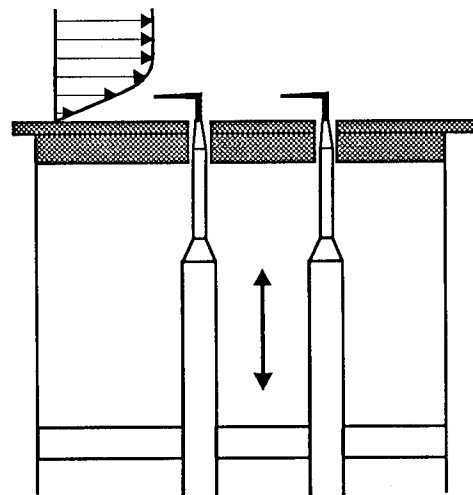


Figure 6. Cross-sectional view of traversing mechanism

adjustable on the ground. The purpose of the Reference probe was to provide a base signal of TS-wave amplitude with which to normalize the TS-wave amplitudes measured by the three traversing probes at different vertical points within the boundary layer. This normalization was necessary in order to reconstruct the TS-wave amplitude distribution across the boundary layer from data taken at different points in time during the traversing operation. The normalization was performed using root-mean-square values of the

measured amplitudes. All measurements, hot-wire probes and pressure; probe traversing; data acquisition, and data storage were carried out under computer software control. A series of programs were available to the flight investigator, to perform different measurement tasks. A detail description of the development and operation of the measurement system is given in reference [9].

TEST PROCEDURE

A set of 5 airspeeds were used to give a range of Reynolds numbers. For a given test airspeed, the chordwise location of transition could be moved over a range of approximately 30-percent chord through use of the wing flap. The location of the transition front was identified in real-time by use of the infrared imaging technique [10]. The location of the imager and the viewing area covered, is shown in figure 7. A typical test point was

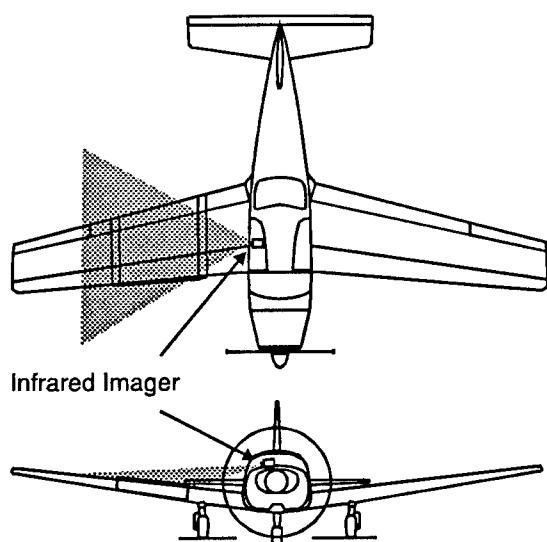


Figure 7. Location of infrared imager

established by selecting one of the test airspeeds, and then observing the location of the transition front, adjusting the flap setting until the front was at a desired position relative to the hot-wire probe location. If a more stable boundary layer was desired, the transition front was located will aft of the probes, and if a less stable boundary layer was desired, the transition front was located immediately aft of the probes. Once the test point was established, glove surface pressure and hot-wire probe data were taken. The flight investigator could select from four different measurement programs: Hot-Wire Calibration, in which the glove pressure distribution and the flow velocity outside of the boundary layer were measured; TS Profile, in which the glove pressure distribution and the flow velocity at up to 40 preselected points within the boundary layer were measured; TS Plot, which provided

a real-time plot of the TS-disturbance amplitude distribution across the boundary layer; and Manual Position, which enabled the flight investigator to select a particular probe position within the boundary layer. The time required for a 40-point traverse of the boundary layer was approximately 150 seconds. Much of this time was spent in the movement of the probes from one measurement point to the other. Given the constraints under which a flight research program must operate, such as weather, pilot availability, etc., it required a large number of flights to achieve test conditions in the atmosphere where the aircraft's speed could be held constant for the length of time necessary to perform a complete traverse of the boundary layer.

WIND TUNNEL TEST PROGRAM

After the flight program was completed, the wing and all instrumentation and data acquisition systems were removed from the aircraft and installed in the Deutsch-Niederländischen Windkanal (DNW) (German-Dutch Wind Tunnel). Test conditions covering the range of Reynolds numbers and transition locations experienced in flight were run. However, concerns with the loading of the wing structure in the wind tunnel, led to testing at lower wing angles of attack, than in flight. Consequently, the chordwise pressure distributions for the same Reynolds number and transition location were different between the flight test and the wind tunnel test. In so far as the calibration of the transition prediction procedure, this difference has no effect. The procedure correctly models the effect of the pressure distribution on the growth of the TS waves.

Another difference between the flight program and the wind tunnel program, was the use of wing angle of attack to move the transition front. Wing angle of attack was more readily adjustable in the wind tunnel, and therefore was used to place the transition front at the desired location for the test point. Again, as in flight, the infrared imaging technique was used to determine the transition front. To give some variation in test pressure distributions, some test conditions were repeated for different flap settings.

TEST RESULTS

A complete set of test results have been published in the form of a data report [11], which has a limited distribution. Analyses of the results is still in progress. Once completed, one or more detailed research reports will be published, with a wider distribution. Selected examples of the data are given in the following, and some initial conclusions are offered regarding the source of the initial disturbances in the boundary layer in flight.

Figure 8 shows representative boundary layer mean velocity profiles measured in flight. Two conditions are shown: Condition 1 (less stable), and Condition 2 (more stable). The probe location was at 43 percent chord. For the more stable condition (2), the transition front was located at 70 percent chord, and for the less stable condition (1), transition was located at 55 percent chord. The limiting bound for the less stable condition was the appearance of intermittent turbulent bursts. The transition front was moved as close as possible to the probe location, without the appearance of intermittency.

One sees in the figure that the mean velocity profile is somewhat fuller in shape for the more stable condition (2) than for the less stable condition (1). This is as classic boundary layer stability theory predicts. Also evident in the figure is the detail to which the wing laminar boundary layer was measured. It is noted here again, that these measurements were performed on a wing, in flight, rather than in a wind tunnel, where heretofore detail boundary layer investigations have been conducted. The measured chordwise pressure distributions corresponding to the mean velocity profiles are given in figure 9. We see, as

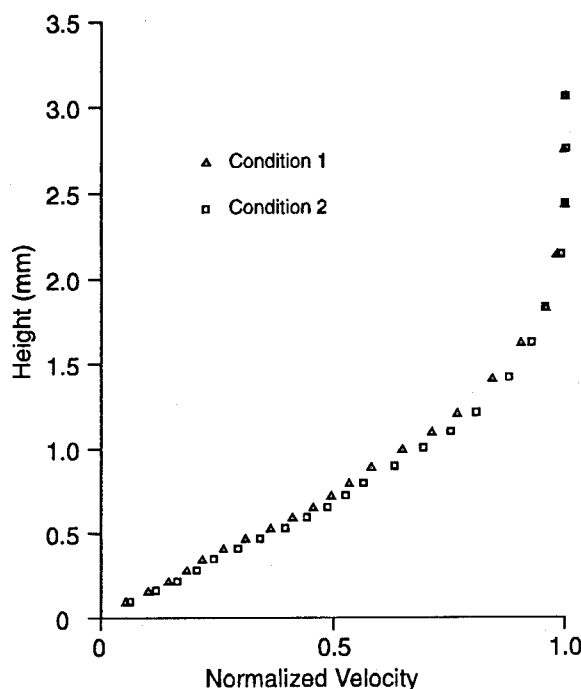


Figure 8. Boundary layer velocity profiles

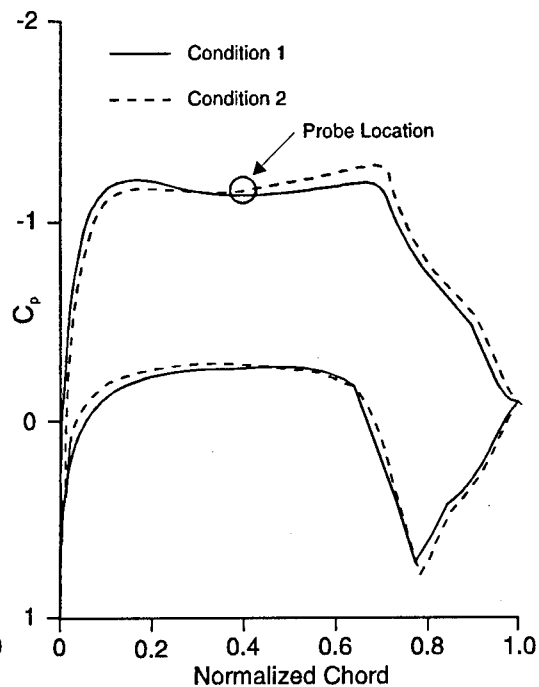


Figure 9 Chordwise pressure distributions

theory predicts, that the pressure gradient is relatively more adverse for the less stable boundary layer (1) than for the more stable boundary layer (2). Figure 10 shows longitudinal velocity fluctuations associated with the TS waves. The sinusoid wave pattern is typical of these disturbances. The data were recorded simultaneously from the three-probe array at the same height in the boundary layer. The probes are separated in the spanwise direction by 20 millimeters. There is some small degree of correlation between the three probe signals, indicating the extent of spanwise structure of the disturbances. At present, the instability models, which are used for transition prediction, would assume that there is no local spanwise variation. It has been observed experimentally, that beyond some point, the TS-wave disturbance structure becomes three-dimensional, with spanwise variation also. This is the final phase of instability leading to breakdown and the onset of turbulence. The amplitude variation seen in the traces is consistent with stability theory. A range of disturbance frequencies is amplified. If we superimpose a series of waves whose respective frequencies differ by a small amount, then we get the picture seen in figure 10.

Frequency spectra of the disturbance amplitudes are given in figures 11 and 12. Figure 13 shows a comparison between flight measurements and theory. According to theory, a range of frequencies will be amplified, with the most amplified being in the middle of this range. For this comparison, theory starts with the measured pressure distribution, proceeds with the calculation of the boundary layer development, and then performs the stability analysis. We see in the figure, that theory (the basis of the transition prediction method) and flight measurements agree quit well. Figures 11 and 12 show amplitude spectra for the Conditions 1 and 2. The more stable condition (2) is shown in figure 11, and the less stable

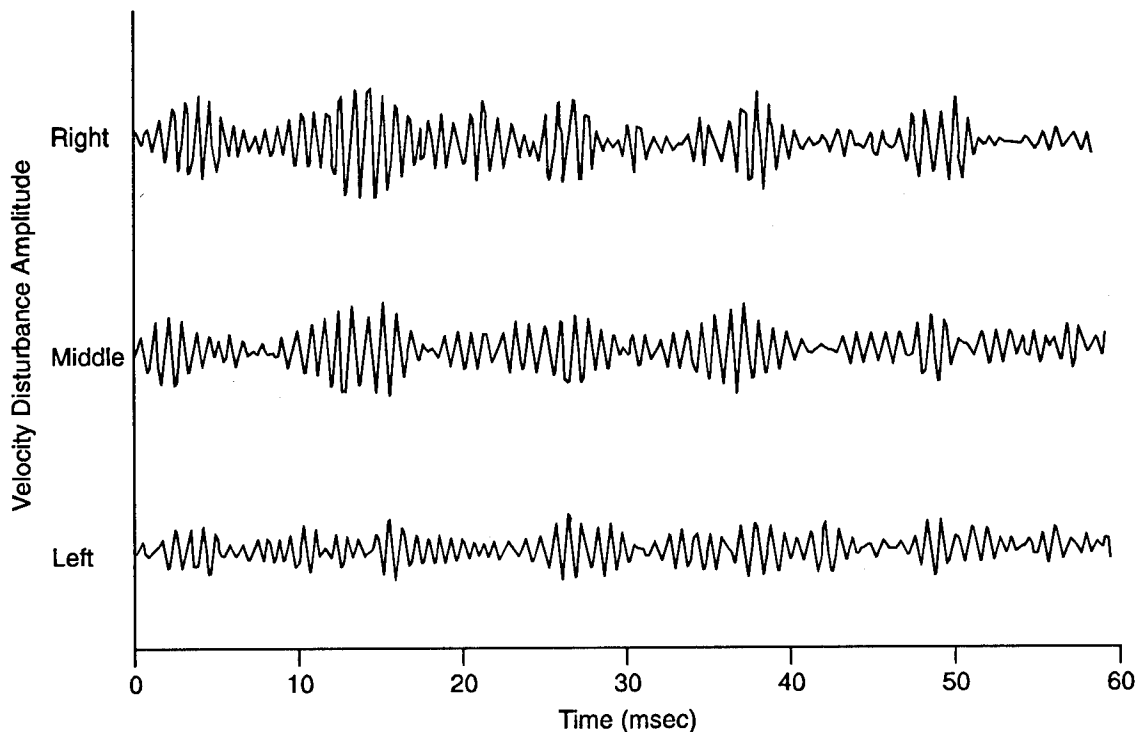


Figure 10. Time history of disturbance longitudinal velocity fluctuations

condition (1) is shown in figure 12. In figure 11, only disturbances at discrete frequencies are being amplified, whereas in figure 12, a much broader range of disturbances are being amplified. The amplitudes in figure 11 are an order of magnitude smaller than those in figure 12. This corresponds to an N-factor of 2.3. Calibration experiments show that the predicated N-factor for transition is in the neighborhood of 10. Consequently, the smallest disturbances we were able to measure with our instrumentation in flight, are at least three orders of magnitude larger than the theoretical limiting values which first appear in the boundary layer. Nevertheless, figure 11 suggests the origin of the disturbances which grow and ultimately lead to transition. We see that the dominant amplitudes are multiples of 80 Hz. We also note that there is a disturbance, at 80 Hz, although not as highly amplified as the higher frequency disturbances. The 80 Hz frequency corresponds to the blade passage rate of the propeller. The disturbances that are amplified are harmonics of a propeller blade passage disturbance that is propagated away from the propeller.

Figures 14 and 15 show how disturbances in different frequency bands are amplified across the boundary layer. Utilizing the same set of measured data, digital filtering is applied to show the behavior in different pass bands. In figure 14, the pass band includes the fundamental of the blade passage disturbance. In figure 15, the pass band is the most amplified for the particular state of the boundary layer. In both figures, the effect of local boundary layer stability is seen. In figure 15, the shape of the distribution is similar as to that predicted by theory. The difference here is that theory predicts only one maximum, and the experimental results show a second maximum. This second maximum is indicative of

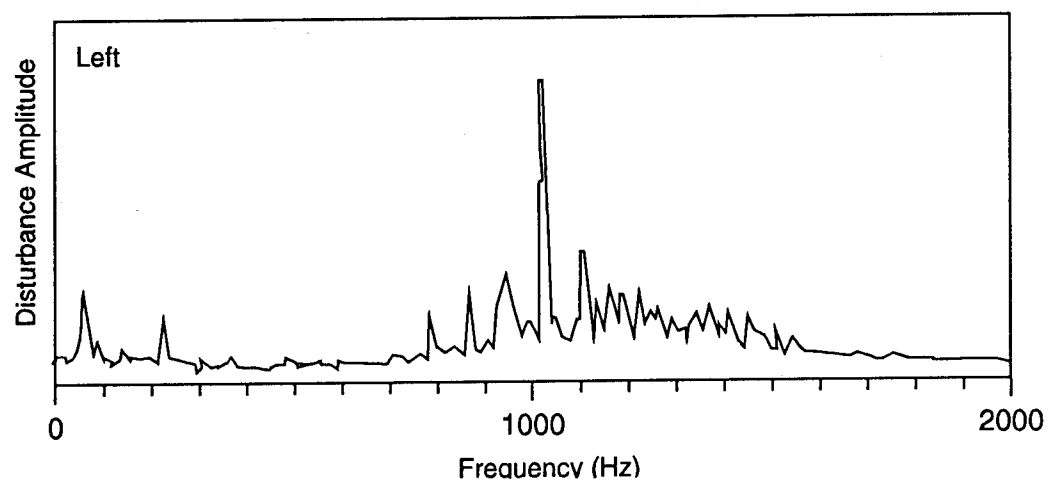
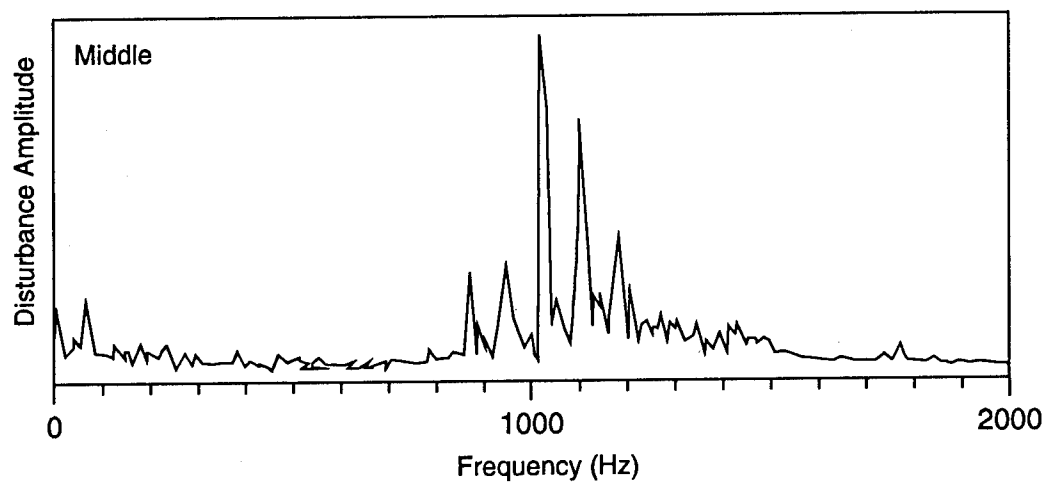
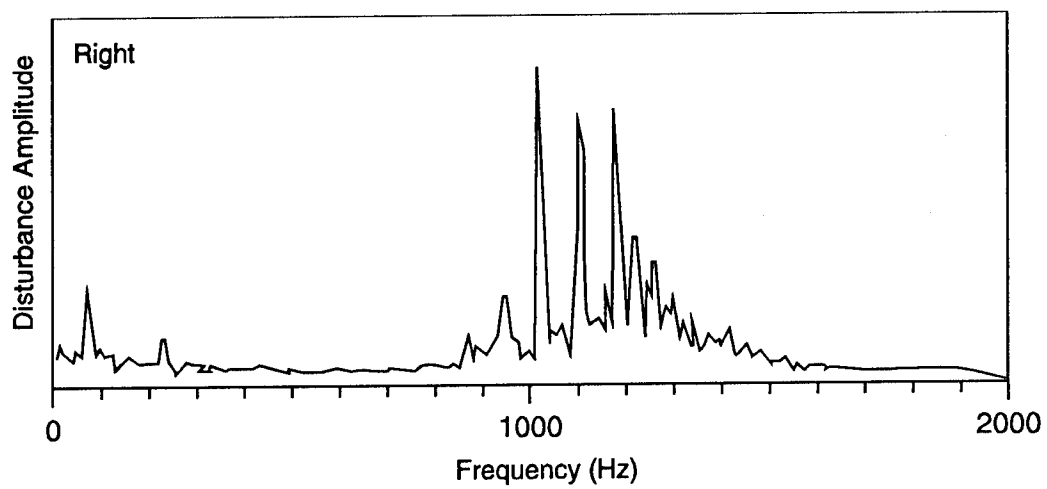


Figure 11. Disturbance amplitude spectra for Condition 2

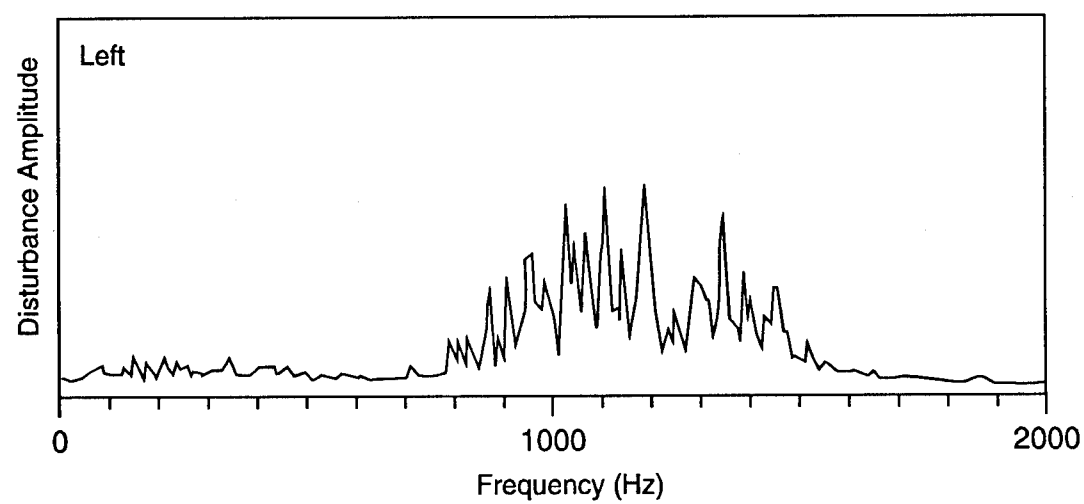
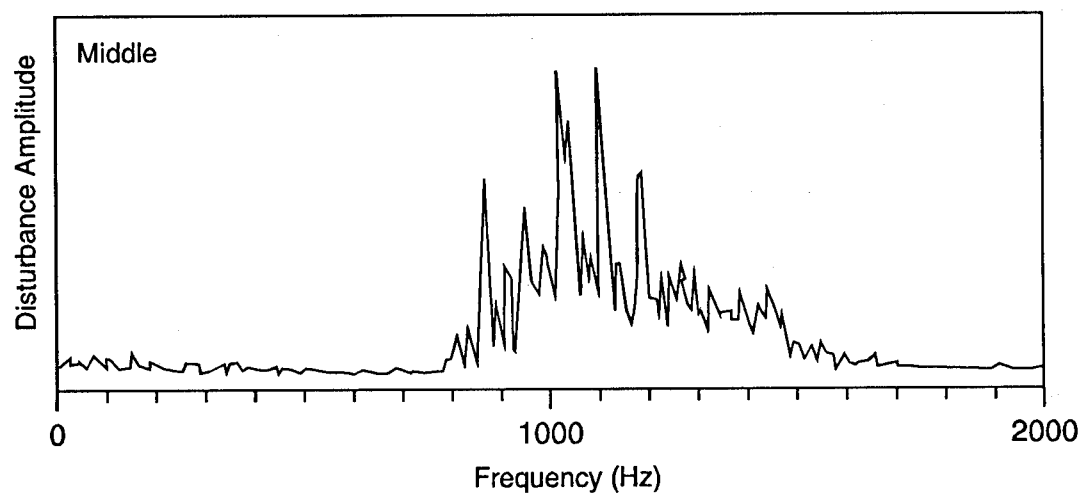
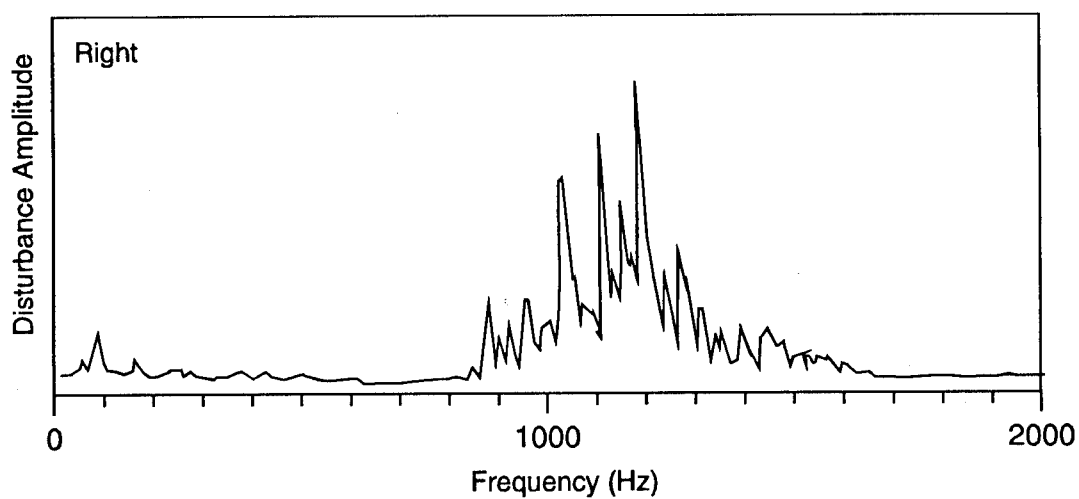


Figure 12. Disturbance amplitude spectra for Condition 1

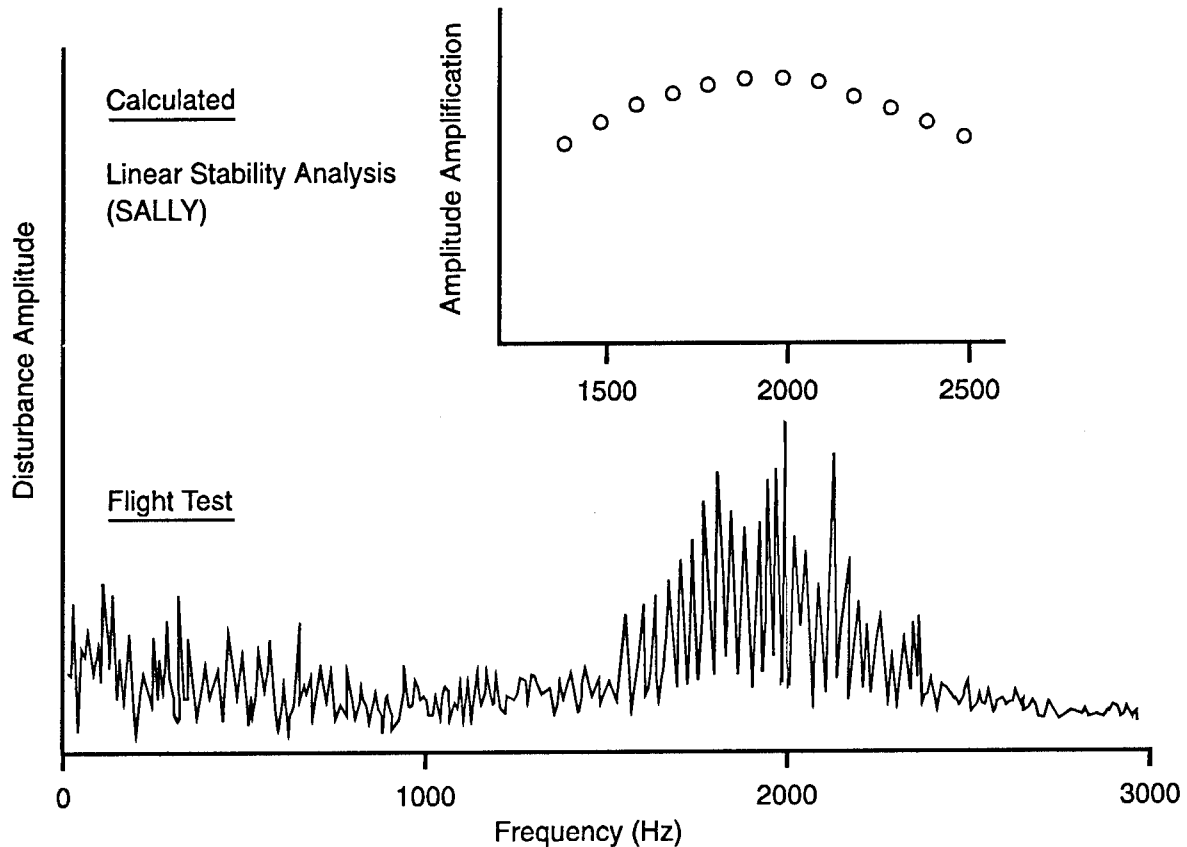


Figure 13. Comparison between the linear stability model and flight

the disturbances having become three-dimensional versus the two-dimensional model of the theory. It is concluded that the less stable conditions, which were measured in flight, exceed somewhat the true applicable range of present theory. Present theory is a linear model, and our data extends outside of the linear range.

CONCLUSIONS

Comparisons between current instability theory based transition prediction methods and measured flight data show good correlation. Differences that appear are due to experiment exceeding the limitations of the theoretical model. The flight measurements show that the initial disturbances which grow and ultimately lead to transition are associated with the aircraft propeller

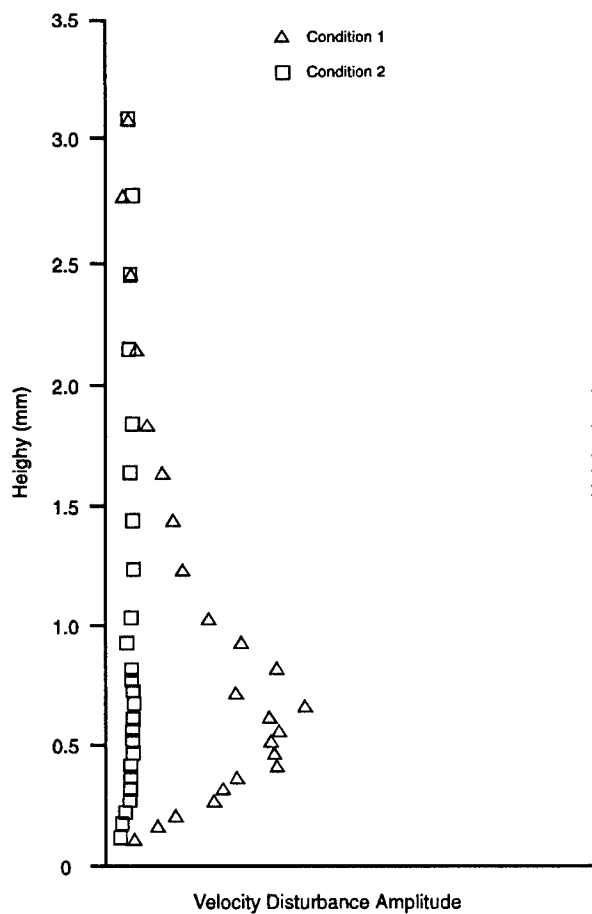


Figure 14. Disturbance amplitude distribution for the frequency range of 0 - 250 Hz

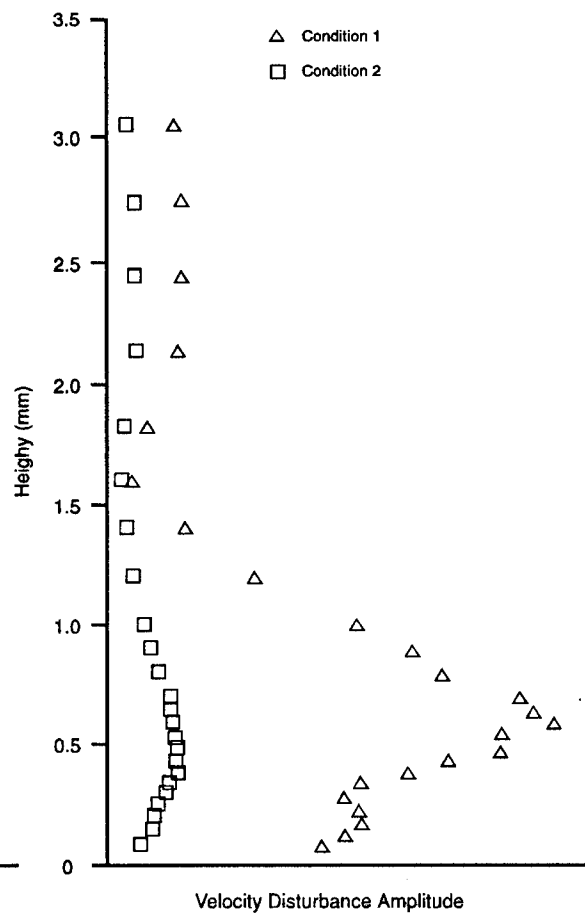


Figure 15. Disturbance amplitude distribution for the frequency range of 800 - 1600 Hz

REFERENCES

1. Granville, P.S., "The Calculation of the Viscous Drag of Bodies of Revolution", David Taylor Model Basin Report 849, 1953.
2. Michel, F., "Critère de Transition et Amplification des Ondes d'Instabilité Laminaire", La Recherche Aerosp. No. 70, 1959.
3. Jaffe, N.A., Okamura, T.T., and Smith, A.M.O., "Determination of Spatial Amplification Factors and their Application to Predicting Transition", AIAA Journal, Vol. 8, 1970, pp. 301-308.
4. Runyan, J., and George-Falvy, D., "Amplification Factors at Transition on an Unswept Wing in Free Flight and on a Swept Wing in Wind Tunnel", AIAA-Paper No. 79-0267, 1979.
5. Hefner, J.N., and Bushnell, D.M., "Status of the Linear Boundary Layer Stability Theory and the e^N -method with Emphasis on Swept-Wing Applications", NASA TP-1645, 1980.
6. Obara, C.J., and Holmes, B.J., "Flight-Measured Laminar Boundary Layer Transition Phenomena Including Stability Theory Analysis", NASA TP 3117, 1985.
7. Redeker, G., and Horstmann, K.-H., "Die Stabilitätsanalyse als Hilfsmittel beim Entwurf von Laminarprofilen", DGLR Bericht 86-03, 1986, pp. 317-348.
8. Horstmann, K.-H., Quast, A., and Redeker, G., "Flight and Wind-Tunnel Investigation on Boundary Layer Transition", Journal of Aircraft, Vol. 27, 1990, pp. 146-150.
9. Miley, S.J., Horstmann, K.-H., Ketthaus, B., Krückeberg, C.-P., and Wandert, H. "Direct Measurement of Laminar Instability Amplification Factors in Flight", DGLR Bericht 88-05, 1988, pp. 93-102.
10. Quast, A., "Detection of Transition by Infrared Image Technique", ICIASF'87 Record, 1987, pp. 125-133
11. Miley, S.J. and Horstmann, K.-H., "Data Report of Flight and Wind Tunnel Investigations of Tollmien-Schlichting Waves on a Aircraft Wing", Bericht IB 129-91/18, Institut für Entwurfsaerodynamik, DLR, December, 1991..

USING LEWICE TO PREDICT DEICING AND ANTI-ICING REQUIREMENTS FOR GENERAL AVIATION AIRCRAFT

Dr. Dudley E. Smith
School of Aerospace and Mechanical Engineering
865 Asp Ave., Rm. 212
Norman, Oklahoma 73019-0601

Dr. Baxter R. Mullins, Jr., P.E.
Mechanical and Aerospace Engineering Department
UTA Box 19018
University of Texas at Arlington
Arlington, Texas 76019

Dr. Kenneth D. Korkan, P.E.
Aerospace Engineering Department
701 H.R. Bright Building
Texas A&M University
College Station, Texas 77843-3141

ABSTRACT

Most of the icing related aircraft accidents involve general aviation and small commuter aircraft. These types of airplanes, which are usually single or twin-engine power producers, normally operate at altitudes below 25,000 feet where icing conditions are most likely to occur. With the increased awareness of icing related accidents, the study of aircraft performance in icing situations has also increased. The results of these studies have shown that aircraft icing can lead to significant changes in aircraft performance, such as increased stall speeds and phenomena such as horizontal tail-stall.

Recent studies have used NASA's LEWICE computer program to predict shapes for various icing conditions including liquid water content, temperature, airspeed, and droplet size. These predicted icing shapes were used to construct models that could be attached to various two and three-dimensional airfoils to determine the performance degradation in wind tunnel test. The wind tunnel models varied from twenty-four percent to full-scale and included an as manufactured empennage in the full-scale test. In addition, airfoil and wing aerodynamic performances were studied. Various levels of chordwise residual icing were examined.

The results of the wind tunnel test showed that LEWICE can be used to assist the designer of deicing systems for general aviation aircraft. However, the airfoil characteristic must be taken into account in order to provide the full chordwise protection required to minimize aerodynamic performance degradation.

INTRODUCTION

DESCRIPTION OF THE PROBLEM

The vast majority of aircraft icing accidents involve general aviation and small commuter aircraft. Generally, these types of aircraft are single or twin-engine reciprocating or turboprop aircraft. The fundamental operating limitation of these powerplants restricts the normal operating range of these vehicles to the lower portions of the troposphere. In most cases, the operations are below 25,000 feet where the probability of icing is significantly increased. These accidents usually involve flight into levels of icing that can cause significant reductions in the aerodynamic performance and possible loss of control of the vehicle. With the increased awareness of icing related accidents, the study of aircraft performance in icing situations has also increased. The results of these studies have shown that aircraft icing, and especially residual icing, can cause significant increases in the drag and stall speed of the vehicle and phenomena such as horizontal tail-stall.

The classic solution to these performance problems is the design and incorporation of either anti-icing or deicing systems, primarily applied to the aerodynamic surfaces of the vehicle. Due to the lower cost and inherent ability to apply in the "post design" period of the aircraft, the pneumatic deicing boot has become the dominate application. The design of these devices has been guided historically by semi-empirical methods such as ADS4. This methodology provided guidance to the design engineer as to the physical extent of the pneumatic boot required, given the level of icing present and an angle of attack operating range. When combined with extensive experimental results and substantial design experience, the results usually provide adequate protection for light to moderate rime icing and light clear icing. However, for greater levels of icing, the inability to accurately predict runback extent hampered the methodology in the prediction of residual icing effects, or ice contamination remaining after boot activation. Additionally, the inability to predict ice shapes greatly limited its accuracy in the prediction of changes in the aerodynamic performance. To overcome many of these limitations, significant research both in the analytical modeling and development of empirical data base information have been performed over the last twenty years. The primary analytical result of these efforts was the development of NASA's LEWICE ice prediction code. When combined with the extensive empirical data, the LEWICE modeling overcomes many of the prediction shortfalls of the previous methodologies. LEWICE has the ability to accurately predict both the extent and shape of the ice formation over a wider range of icing conditions. Because of this improved capability, LEWICE has become the industry standard for the prediction of aircraft icing. The ability to predict both the shape and extent of possible runback could now provide the necessary tool to evaluate the aerodynamic performance effects of residual icing.

OBJECTIVES OF THE PRESENT RESEARCH

The primary objectives of the research were: (1) to examine the levels of residual ice predicted by LEWICE for moderate to heavy icing conditions for deicing systems designed using the earlier methodology; (2) empirically evaluate the aerodynamic performance effects of the predicted residual icing; and (3) to evaluate the use of LEWICE as a guide to establish design criteria for the deicing systems. The thrust of the effort is to develop a systematic approach to the application of the ice prediction tool to develop design criteria of deicing systems, which would provide protection for the required design operating spectrum of the vehicle including residual icing.

OVERALL ANALYTICAL APPROACH

Standard NASA airfoils were selected for the evaluation due to the availability of existing test data on their performance both clean and in icing conditions. Additionally, selected airfoils and the horizontal tail of an existing twin-engine, general aviation, turboprop aircraft, whose deicing system was designed using the ADS4 methodology, was utilized due to its availability. Analytical studies of the ice formation for the series of airfoils were performed, using LEWICE, for moderate to heavy icing conditions. These conditions were selected to evaluate the shape and extent of possible runback and the size of residual ice given the existing deicing system. The resulting shapes were then evaluated via wind tunnel testing utilizing both two-dimensional airfoil models and three-dimensional, full-scale, as manufactured, aircraft components. The results were then evaluated in terms of the effects of the predicted residual ice on the aerodynamic performance. Additional levels and extents of the residual ice were then examined to establish a correlation between the amount of residual icing present and acceptable aerodynamic performance degradation.

LEWICE ANALYSIS

DESCRIPTION OF LEWICE PROGRAM

The NASA LEWICE ice prediction program is described in reference 1. The program embodies an analytical ice accretion model that evaluates the thermodynamics of the freezing process that occurs when supercooled droplets impinge on a body. The atmospheric parameters of temperature, pressure, and velocity and the meteorological parameters of liquid water content (LWC), mean droplet volume diameter (MVD), and relative humidity are specified to determine the shape of the ice accretion. The analysis uses a time stepping procedure to "grow" the ice accretion, with initial droplet impingement characteristics determined from the initial clean state. Knowledge of the flow field about the body, the droplet trajectory and impingement characteristics on the body, the thermodynamics of the freezing process, and the accumulation of ice on the body surface and relative change in body shape are utilized to determine the type and shape of ice that will form on the body under the given conditions. Modifications to the original program, described in reference 2, have been made to include multiple stagnation points and interactive boundary layer methods to improve accuracy. This version of the program, utilized in this research, is commonly described as the "robust" version that includes the ability to track multiple stagnation points and evaluate icing runback.

ATMOSPHERIC MODELING

The most recent standard modeling of the atmosphere for the probability distribution of mean droplet diameters with liquid water content is contained in reference 3. These data are based on a compilation of the information gathered by NACA, the U. S. Air Force, the University of Washington, and the University of Wyoming using modern data measuring equipment. One should note, see figure 1, the significant increase in the probability of the occurrence of larger droplet sizes relative to previous published data. Additional work now under way at the National Severe Storm Center in Oklahoma using the new NEXRAD radar system to measure droplet size variations from the aspect ratio of the returns, indicates even higher probabilities when vertical rotaries occur. Thus the probability of encountering moderate to heavy icing conditions is significantly greater than what was once predicted.

The atmospheric icing conditions modeled in this research, as noted, were for the moderate to heavy icing levels of icing. The icing conditions modeled included liquid water content from 0.2 to 1.0

gm/cm and droplet sizes of 10 to 40 microns at temperatures between 20 to 31 degrees F. The above range of conditions bracketed a series of icing levels reported in numerous accident reports.

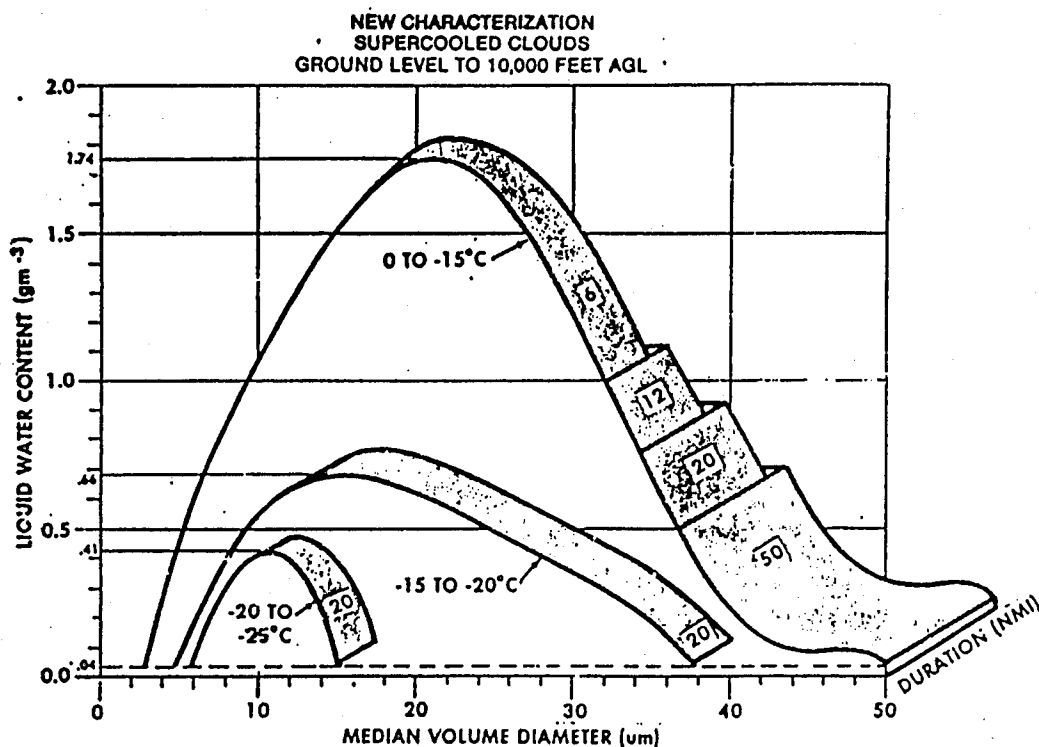


Figure 1 New Characterization of Supercooled Clouds, Ground level to 10,000 Feet

PREDICTED ICE SHAPES

The resultant ice shapes from the analysis for the series of airfoils evaluated are shown in figures 2 through 9. The extent of active ice protection on the subject horizontal tail is shown in figure 9 by the vertical lines on the upper and lower surface. The residual ice models were begun with a height specified at the chordwise location of the end of the active portion of the deicing system, which extended to approximately 5% of the chord. This was done to simulate the activation of the system and a partial rejection of the ice formation. Additional boot activations were simulated which allowed re-accumulation for a series of activation's. The simulated residual ice shapes used in the test are shown in figures 10 through 13. These shapes were used to define a range of test heights and icing extents. Additionally, heights and icing extents were systematically moved rearward and reduced to determine the relative changes in the aerodynamic performance degradation with the position of the residual ice and thus establish an acceptable extent of necessary active ice protection.

WIND TUNNEL TESTS

DESCRIPTION OF TWO-DIMENSIONAL TEST

DESCRIPTION OF WIND TUNNEL FACILITY. The wind tunnel used for the two-dimensional airfoil tests was the University of Texas at Arlington Low Speed Wind Tunnel, figure 14. This facility is a closed circuit, single return low speed wind tunnel. The rectangular test section is two by

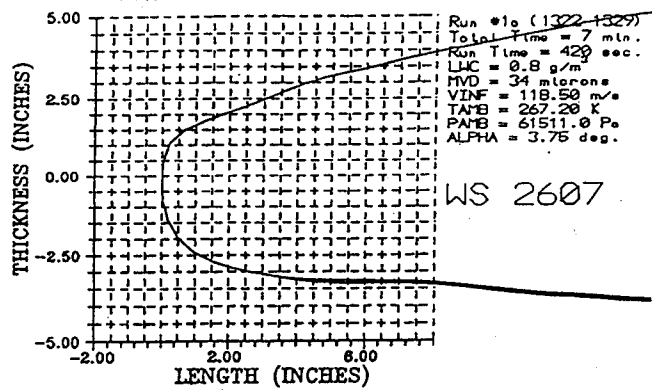


Figure 2 Wing Inboard Profile - Time 240 sec

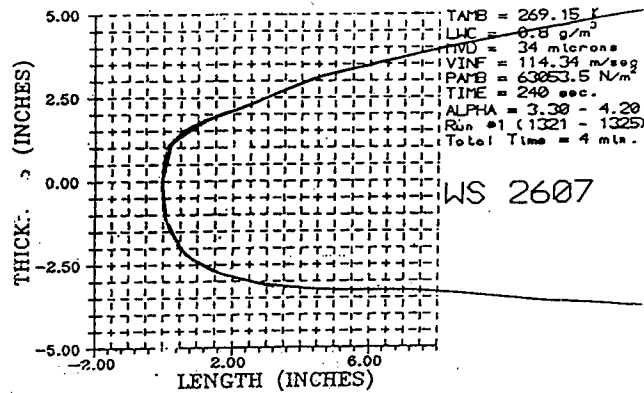


Figure 3 Wing Inboard Profile - Time 420 sec - boot triggered

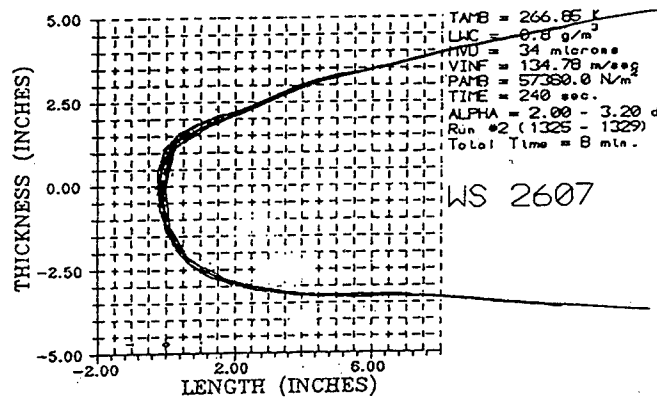


Figure 4 Wing Inboard Profile - Time 8 min

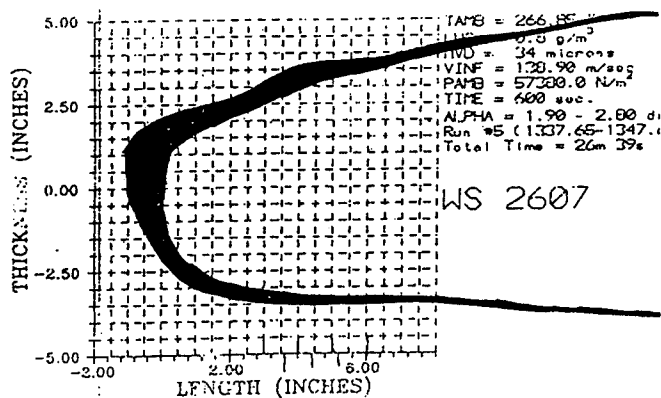


Figure 5 Wing Inboard Profile - Time 26 min

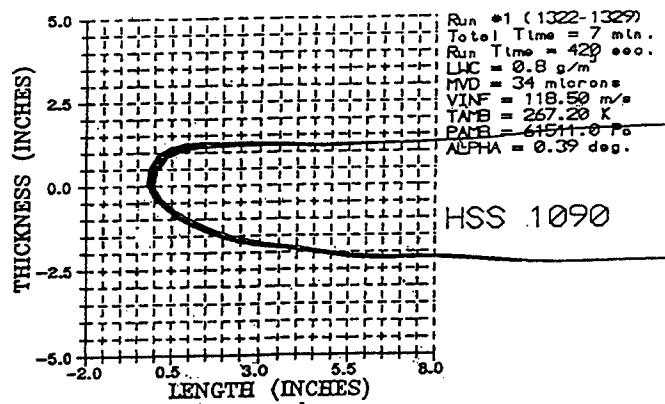


Figure 6 Horizontal Tail Profile - Time 420 sec

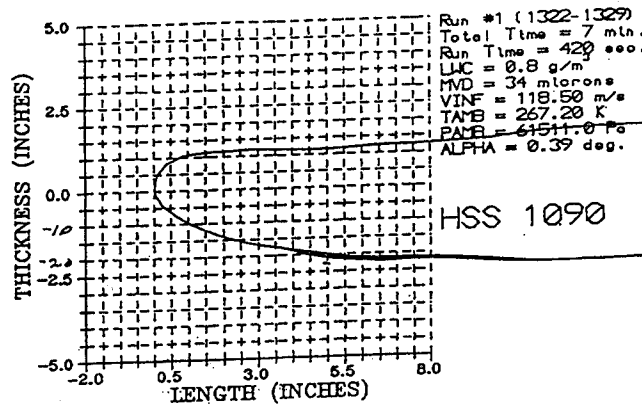


Figure 7 Horizontal Tail Profile - Time 420 sec - boot triggered

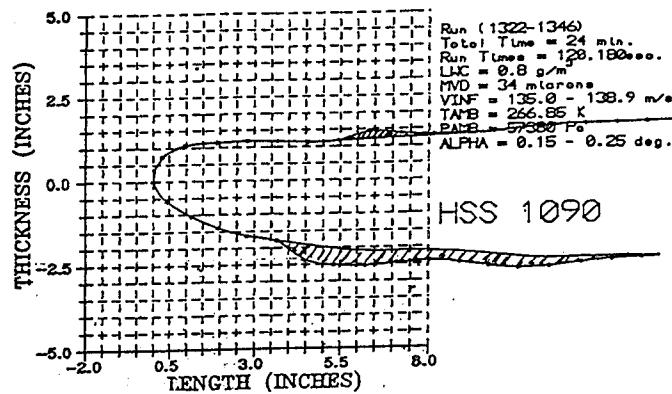


Figure 8 Horizontal Tail Profile - Time 24 min - residual

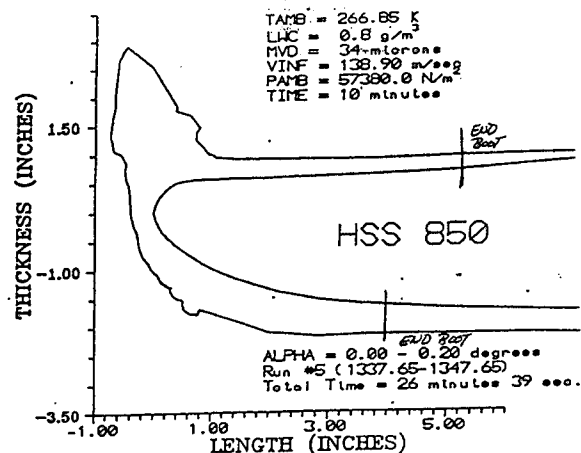


Figure 9 Horizontal Tail Profile 4 Time 24 min - no boot activations
 480

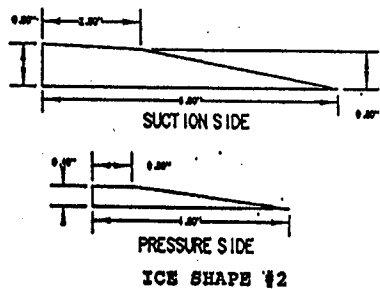


Figure 10 Test Ice Shape

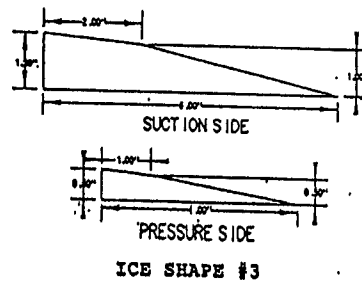


Figure 11 Test Ice Shape

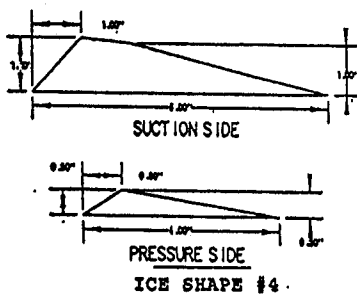


Figure 12 Test Ice Shape

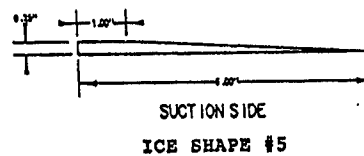


Figure 13 Test Ice Shape

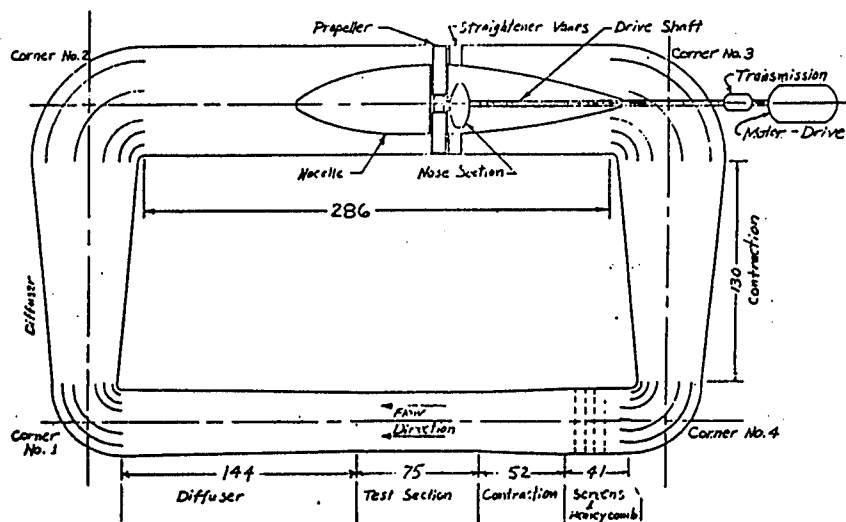


Figure 14 UTA Low Speed Wind Tunnel

three feet and five feet long. The tunnel provides a dynamic pressure capability corresponding to a Reynolds number of approximately 1.25 million per foot with a tunnel turbulence factor of approximately 1.04. A complete description of the wind tunnel and its capability can be found in reference 4.

DESCRIPTION OF MODELS. The wind tunnel models used in this initial test were single element, ten inch chord, full-span (test section), pressure instrumented airfoils. These models represented approximated 24% scale models of the mean geometric chord of the full-scale horizontal tail test article, reference 5. The airfoils tested, figure 15, included a NACA 23012, a NACA 64-010 modified, and a NACA 64-215 modified. The modifications include increased leading edge nose radius and leading edge camber or "droop." Additionally, a 24 inch chord two element airfoil consisting of a horizontal stabilizer and elevator was evaluated. This model represents a 57% scale model of the mean geometric chord of the full-scale test article. In this model the stabilizer, gap, and elevator are all pressure instrumented. This model provided significant insight into the effect of icing on the relative load sharing of the stabilizer and elevator. A complete description of the models with pressure port locations and details can be found in reference 6.

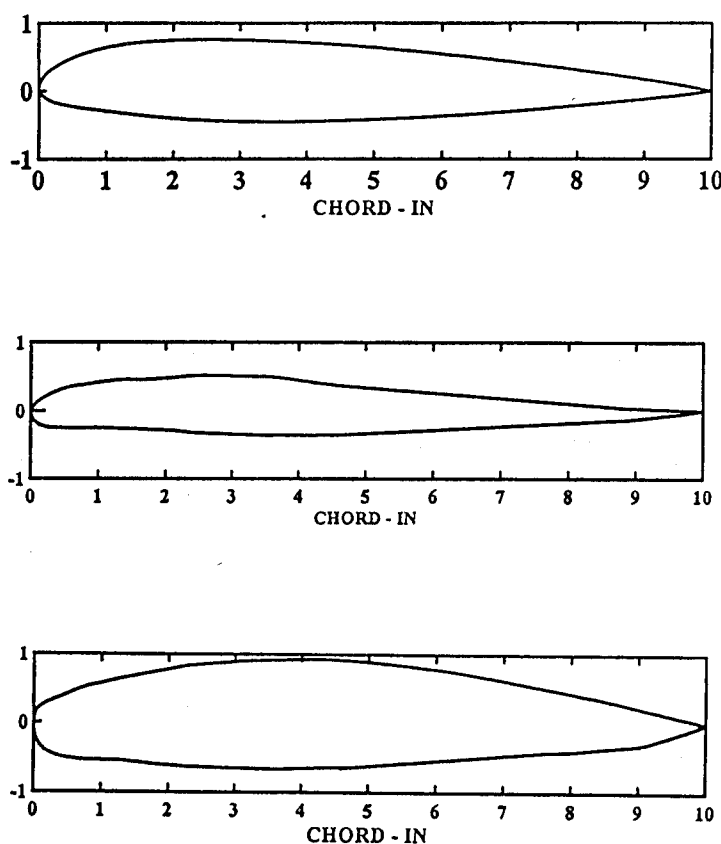


Figure 15 Test Airfoils Sections

DISCUSSION OF TEST PROCEDURE. The models were installed horizontally in the aft portion of the test section with a wake rake mounted vertically approximately 1.5 chord lengths aft of the trailing edge of the airfoils. All pressure measurements were taken with a scanivalve system and stored on a PC. A schematic of the data acquisition system is shown in reference 4. Data reduction procedures and applied wind tunnel wall correction utilized in the final results are from Pope, reference 7. For each defined configuration, a sweep of angles of attack was made and the relative pressure measurements performed. At each angle of attack, the data were reduced and the surface pressures and wake rake values integrated to establish the lift, drag, and pitching moment of the section. Beginning with the clean airfoils as the baseline, the relative levels of icing were then systematically increased to provide a complete map of the relative performance.

SUMMARY OF TWO-DIMENSIONAL RESULTS. Representative results of the two dimensional test are contained in figures 16 and 17. Figures 16 show the variation of the lift curve slope, variation of maximum lift coefficient, and angle of attack of maximum lift coefficient for ice configuration number 2, figure 10. Figures 17 shows the drag polar for the same configuration. Note the significant increase in the minimum drag coefficient and the early separation with ice.

DESCRIPTION OF THREE-DIMENSIONAL TEST

DESCRIPTION OF WIND TUNNEL FACILITY. The wind tunnel used in the three-dimensional airfoil test was the Low Speed Wind Tunnel at Texas A&M University, figure 18. This facility is a closed circuit, single return low speed wind tunnel. The rectangular test section is seven by ten feet and is approximately twenty feet long. The tunnel provides a dynamic pressure capability corresponding to Reynolds number of approximately 3.25 million per foot with a tunnel turbulence factor of approximately 1.06. A complete description of the wind tunnel and its capability can be found in reference 8.

DESCRIPTION OF MODEL. The wind tunnel model used in this series of test was an "as manufactured" horizontal tail from a service aircraft. The tail was sectioned at the root end to simulate the exposed surface as installed on the vehicle and produce a semi-span model. The model was mounted via an installed standpipe to the six component pyramidal balance system, figure 19. The elevator had the ability to be locked at different deflections over the complete operating range of the actual aircraft.

DISCUSSION OF TEST PROCEDURE. The model was installed vertically in the center of the test section. A pitot-static probe was mounted on the tunnel traversing mechanism at a level coincident with the level of the mean geometric chord approximately 1.5 chord lengths aft of the trailing edge of the airfoil. All pressure measurements were taken with a scanivalve system and stored on a minicomputer. A complete description of the data acquisition system can be found in reference 8. Data reduction procedures and wind tunnel wall corrections were utilized in the final results are found in reference 7. Again, for each defined configuration, a sweep of angles of attack were made and the balance readings as well as selected wake surveys measurements performed. At each angle of attack, the force data and pressure data were reduced and the wake rake values integrated to establish the lift, drag, and pitching moment of the semi-span model and the two-dimensional drag of the mean geometric chord. Beginning with the clean airfoils as the baseline, the relative levels of icing were then systematically increased to provide a complete map of the relative performance. A sample test configuration is shown in figure 20 with a simulated ice shape and the extent of the pneumatic boot system.

SECTION LIFT COEFFICIENT

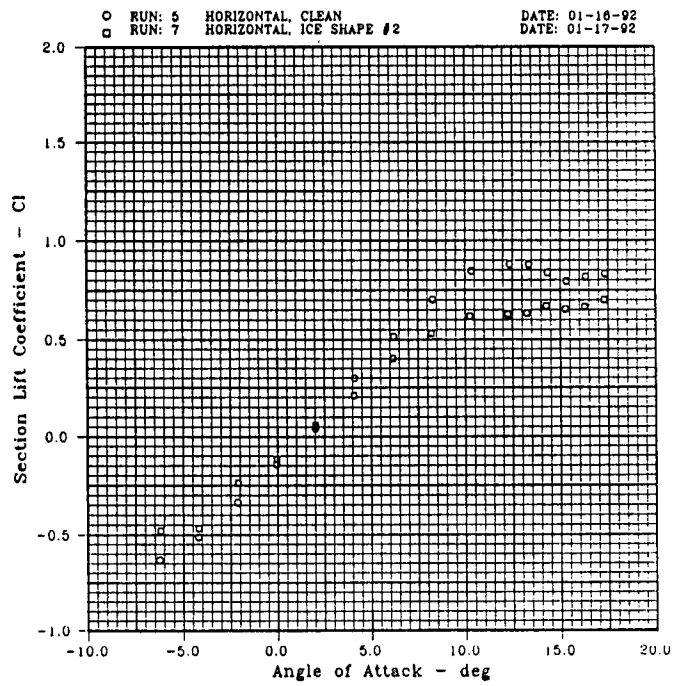


Figure 16 Lift Curve

SECTION LIFT AND DRAG PROPERTIES

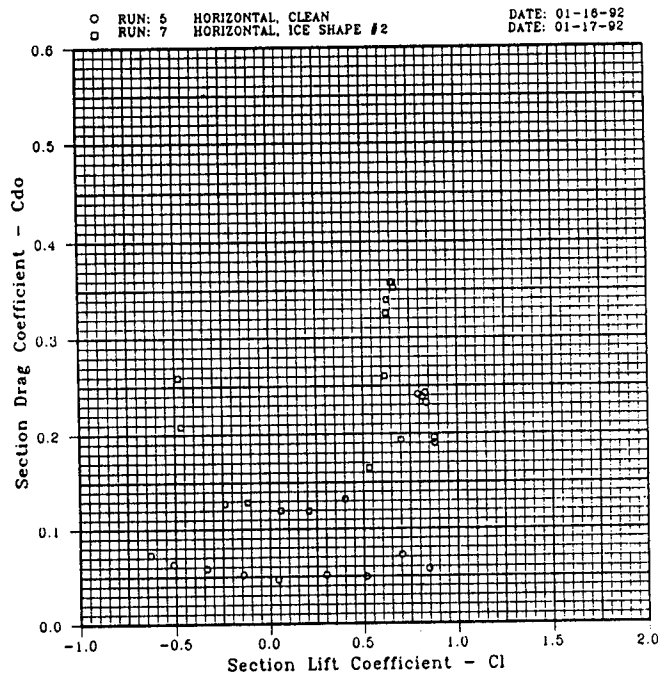


Figure 17 Drag Polar

SUMMARY OF THREE-DIMENSIONAL RESULTS. Summary results of the three dimensional test are contained in figures 21 through 24. Figures 21 demonstrates the variation of lift curve slope, maximum lift coefficient, and angle of attack of maximum lift coefficient with the various ice configurations. Figure 22 demonstrate the corresponding variations of drag coefficient with lift coefficient. Figure 23 is a typical wake rake survey at the empennage mean geometric chord position. Finally, figure 24 is an expanded look at the minimum drag coefficient, note the significant increase in the drag coefficient.

RESULTS

The principal results in this research indicate the following:

- 1) with very limited amounts of ice accumulation, the aerodynamic performance of lifting surfaces is significantly reduced lifting capability is reduced by as much as 60% and drag increased by 300-500%,
- 2) the particular type of airfoil involved effects the magnitude of the aerodynamic degradation, i.e., the laminar airfoils demonstrate larger changes than turbulent airfoils, between 60-100% greater,
- 3) the extent of active ice protection recommended by ADS4 is inadequate for moderate icing,
- 4) residual ice contaminants needs to be limited to aft of the 15% chordwise location or aft of the position of the peak pressure gradient to minimize aerodynamic performance degradation,
- 5) the ability of LEWICE to more accurately predict the extent and shape of the ice formation when combined with the empirical results provides the designer with the necessary tools to develop systems with improved safety.

REFERENCES

1. NASA CR-185129, Users Manual for the NASA Lewis Ice Accretion Predictor Code (LEWICE), Ruff, G. A., Berkowitz, B. M., Sverdrup Technology Inc., Lewis Research Center Group, Brook Park, Ohio, May 1990
2. Cebeci, T., Chen, H. H., Alemdarglut, N., Fortified LEWICE with Viscous Effects, Aerospace Engineering Department, California State University, Long Beach, AIAA A90-20009, 1990
3. Masters, C. D., A New Characterization of Supercooled Clouds Below 10,000 Feet AGL, DOT/FAA/CT-83/22, June, 1983.
4. Low Speed Wind Tunnel Facility Handbook, The University of Texas at a Arlington, Arlington, Texas, Revised 1987.
5. Mullins, Jr., B. R., Smith, D. E., Wind Tunnel Test of Three Airfoils with Simulated Ice Shapes, TCS 92-001, March 1992

6. Mullins, Jr., B. R., Smith, D. E., Wind Tunnel Test of a 57 Percent Scale Flapped Airfoil with Simulated Ice Shapes, TCS 92-002, March 1992

7. Pope, A., Harper, J. H., Low Speed Wind Tunnel Testing, John Wiley & Sons, New York, NY 1966

8. Low Speed Wind Tunnel Facility Handbook, Aerospace Engineering Division, Texas Experimental Station, The Texas A&M University System, College Station, Texas, January 1985.

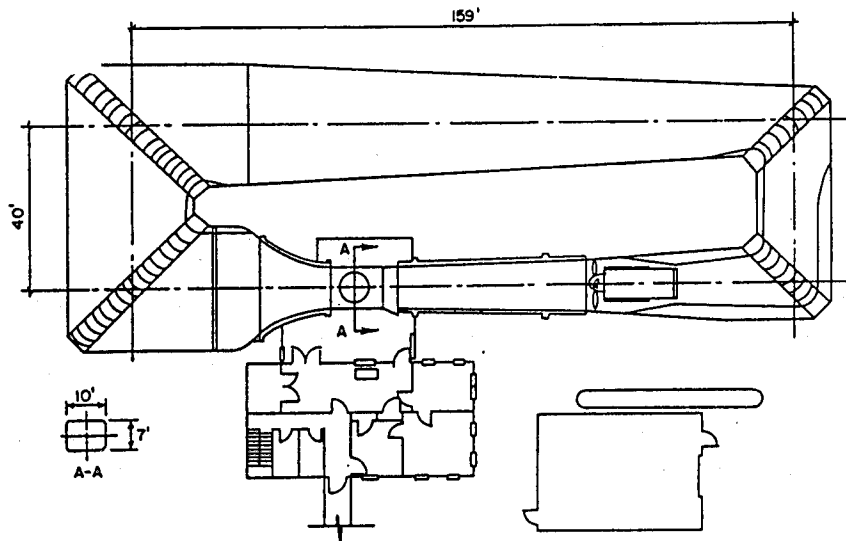


Figure 18 Texas A&M Low Speed Wind Tunnel

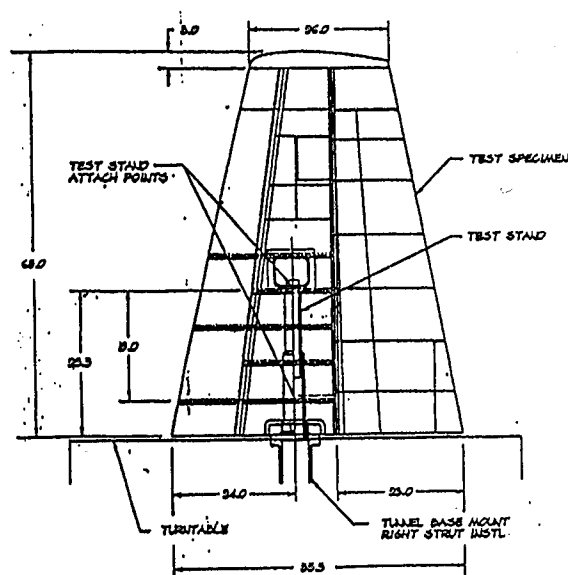


Figure 19 Full Scale Empennage Model

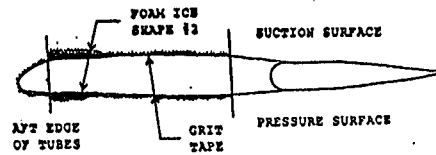
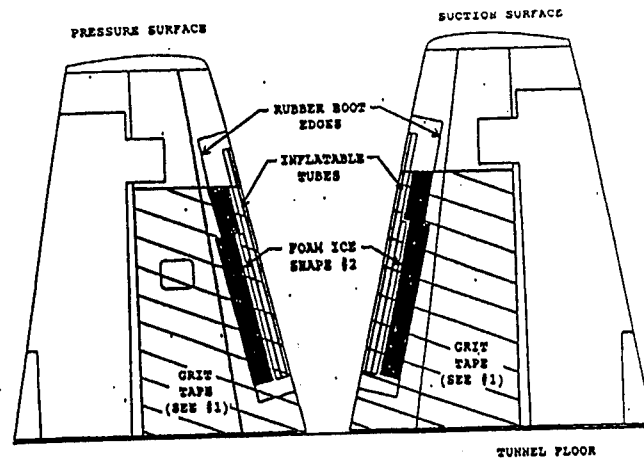


Figure 20 Example Test Configuration

Run	Test	Alpha	Configuration
1	2225	0	CLEAN AIRFOIL
2	2225	30	TAPE GRIT 10.00 BOTH SIDES
3	2225	30	ICE SHAPE #1
4	2225	30	ICE SHAPE #2
5	2225	30	ICE SHAPE #3
6	2225	30	ICE SHAPE #4

Run	Test	Alpha	Configuration
1	2225	0	CLEAN AIRFOIL
2	2225	30	TAPE GRIT 10.00 BOTH SIDES
3	2225	30	ICE SHAPE #1
4	2225	30	ICE SHAPE #2
5	2225	30	ICE SHAPE #3
6	2225	30	ICE SHAPE #4

Run	Test	Alpha	Configuration
1	2225	0	CLEAN AIRFOIL
2	2225	30	TAPE GRIT 10.00 BOTH SIDES
3	2225	30	ICE SHAPE #1
4	2225	30	ICE SHAPE #2
5	2225	30	ICE SHAPE #3
6	2225	30	ICE SHAPE #4

Run	Test	Alpha	Configuration
1	2225	0	CLEAN AIRFOIL
2	2225	30	TAPE GRIT 10.00 BOTH SIDES
3	2225	30	ICE SHAPE #1
4	2225	30	ICE SHAPE #2
5	2225	30	ICE SHAPE #3
6	2225	30	ICE SHAPE #4

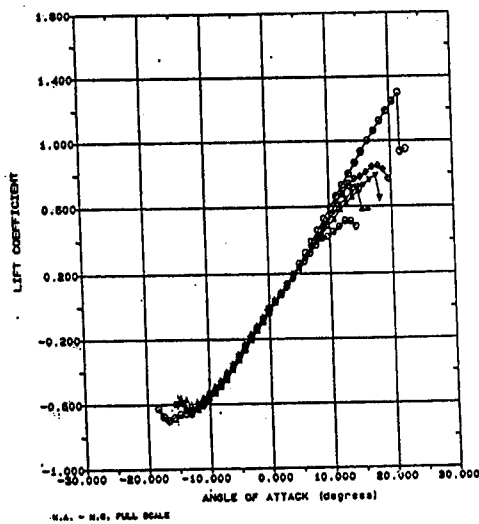


Figure 21 Lift Curve

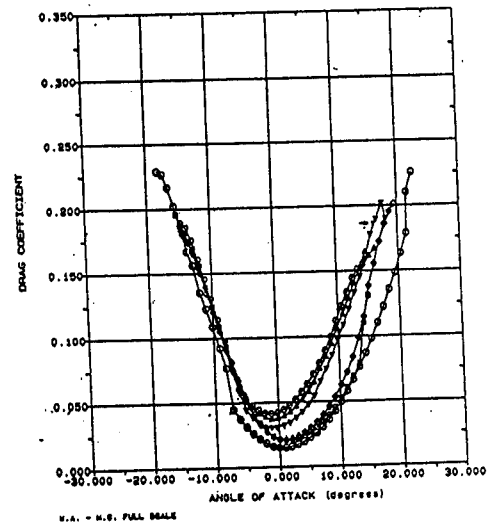
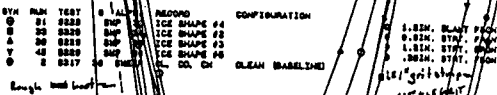


Figure 22 Drag Polars



DATE: 8/31/88



N.A. - N.C. FULL SCALE

A GENERAL OVERVIEW OF THE FABRICATION AND QUALITY CONTROL ACTIVITIES FOR THE HONDA MH-02

Rani W. Sullivan*, Keiichi Sato⁺, George Bennett*

* Miss. State University
Raspert Flight Research Lab.
Miss. State, MS 39762

⁺ Honda R & D Co., LTD
Wako Research Center
Japan

ABSTRACT

The establishment of standardized procedures for composite structures fabrication and quality control was a major objective of the development of the Honda MH-02 all-graphite, twin turbo-fan research aircraft. The structural architecture of the MH-02 and the fabrication methods for some of the parts are described. It was found that the establishment of standardized processes and detailed documentation must be developed as an evolutionary activity with careful inspection and testing of sub-assemblies and assemblies to verify the processes. After many hard lessons learned, the expected material properties and structural quality and integrity were achieved. The most important lesson for a process driven quality assurance of structural integrity is that the test activity must very closely duplicate the fabrication processes of the aircraft part and assembly.

INTRODUCTION

The objective of the project was to design, fabricate, and test an all-graphite aircraft to the highest possible standard. The activity originated with the MSU RFRL-Honda team, who had limited experience working with 350°F, 50-100 psi, autoclave cured prepreg and 250°F cure adhesive for all assemblies.

There had been the earlier development of the Beechcraft A-36 aircraft tail and wing modification (shown in Figure 1) by MSU RFRL personnel and a small Honda team from 1986-1989 (1). The main objective of this project was to learn and establish procedures by which fabrication and assembly of high quality composite structures could be accomplished. The tail and wing structures were converted to Kevlar and graphite construction. Autoclave cured prepreg of 250°F, 50 psi was used for the spars, 250°F vacuum-bag cure was used for the sandwich components, and a room temperature adhesive was used for the assembly. The weight of the composite components and the original aluminum structure was very close, with a ten percent reduction in power required. The objectives of the project were completed and the study concluded that an aggressive quality control program is required to produce high quality flight worthy composite structures. The fabrication of the MH-02 began with this knowledge and experience.

One of the major complications of the project was the structure of the work force. The project management, coordination, and quality were difficult due to the widespread efforts. The design

group was based in Japan, while parts were being fabricated mainly in the United States, and all the assembly was performed at the RFRL Annex. Communication of information was difficult not only because of the diverse geographical locations of the various groups, but also due to the language barrier between the American and Japanese work forces. Although the conveying of information was difficult, the quality and integrity of the composite structures was maintained as first priority.

The development process was done in steps of increasing complexity. Laboratory tests established the material properties which were used for design. Because fabrication of composite parts was the first step, quality control was initially established for this process. The fabrication phase began with the making of female molds from the male molds. The horizontal tail was the initial structure that was assembled. The assembly of the vertical tail proceeded more smoothly, and the experience from both was very helpful for the construction of the much larger and complex wing and fuselage. An overall project description and discussion can be found in Reference (2).

The "common thread" in this project was the quality control program, which was established through an iterative process. The QC program took time and effort to establish, because the process was proposed first, the procedures were then implemented, and finally, due to the results, the QC program was revised and refined. By establishing procedures for the various processes, inspection, and thorough record-keeping, the final QC program covered every facet of the project: from the assurance of material properties to the fabrication and assembly of the final structure.

TOTAL QUALITY CONTROL CONCEPT

Figure 2 shows the all composite main structure of the MH-02. Since the Honda research aircraft is an original design, there was special emphasis placed on the quality control activities. The underlying concept behind the MH-02 project is "Safety First". The quality for material, fabrication, assembly, and inspection was described to establish the basis of this concept.

The final mechanical properties of a cured composite structure are manufactured into the structure as part of the fabrication process. For this reason, the control of materials, the fabrication process, and final inspection are of primary importance. Inclusive in the quality control program, the physical appearance of a part and a method by which problems could be traced were included. This was incorporated so that poor quality parts would not be overlooked. The process was achieved by including a "standardization of process", a "conclusive inspection", and a "complete record". Table 1 summarizes these aspects of the QC program. By developing a method of thorough and methodical inspection, problems were not only difficult to overlook but also were quickly resolved. Meticulous book-keeping provided an avenue to trace and repeat a process.

MATERIAL PROPERTIES ASSURANCE

Laboratory testing in Japan established the target material properties that were used for design. The experimental results were compared with the manufacturer's data. A large margin of safety

was built in by designating a range of values which were lower than either the experimentally obtained values or the manufacturer's data. The laboratory testing not only established the material properties needed for design purposes, but also defined procedures which had to be transferred to the shop environment. The chosen materials had to be implemented in the real structure and the out-time or exposure time criteria was established by laboratory testing. Table 2 lists the selected composite materials for the fabrication of the MH-02 and their design values.

The first article to be dealt with was the handling and storage of the incoming composite materials. Storage of raw composite materials (prepregs) at very low temperatures was necessary for preventing and/or delaying the degradation of the resin properties. Factors such as out-time, expiration date, temperature, and humidity during the fabrication of a composite component influence the final and overall properties of the composite structure. To reduce condensation on the composite material, it was gradually brought up to room temperature by first placing the material in a cooler which maintained the temperature at about 40° F. After approximately eight hours in the refrigerated unit, the material was allowed to reach room temperature. The environmental control of the prepreg is listed in Table 3.

Additional efforts were made concerning the film adhesive used for the bonding of honeycomb to prepreg. A special control was established on film adhesion which was based on a visual check of fillet formation in a honeycomb panel. The fillet formation was found to be a good indicator of the wetability of the adhesive. Upon the arrival of the film adhesive, a panel was fabricated and fillets checked. Also, other honeycomb panels were fabricated for various exposure times of the film adhesive. Table 4 shows a schematic of a "good" and "bad" fillet, and also lists the steps by which good adhesion was assured.

A database was created for all materials which required storage in freezers. All pertinent information about each roll, such as shipping dates, expiration date, weight, total exposure times, etc., were input and updated weekly. Figure 3 is a sample form used for tracking individual rolls of composite materials. The individual histories of each roll were maintained on a daily basis by recording the exposure times in various environments and the part for which the particular roll of material was used. This was very important, for if any problems surfaced about a specific part, the roll of composite material could be traced and flagged for other parts which had been fabricated from the same roll of prepreg.

STANDARDIZATION OF PROCESS

Quality and integrity of the completed composite structure were achieved by standardizing the major processes: fabrication, assembly, and inspection.

FABRICATION OF PARTS. The fabrication process governs the quality of a composite part in terms of its external appearance, dimensions, and internal defects. Because correct procedure and operation are vital to obtaining a high quality part, many steps were taken to insure accuracy and quality. To reduce costly mistakes and avoid misunderstandings, meetings between the fabrication team, quality control, and the designer were held and all items pertinent to the fabrication of the part were discussed. Preparation of the tool, reference lines on the mold and drawings were verified; the lay-up sequence and any special bagging techniques were discussed.

A "Composite Fabrication Manual" was developed which covered every aspect of fabrication from the environmental conditions to the final cure procedure. Although quality control monitored the entire fabrication process, it was quickly determined that it would be a good idea to have the designer check the part at various and important stages during fabrication.

Shown in Figure 4 is a "Fabrication Log Sheet" which included every detail about a particular part during the fabrication phase. This part log was often referenced since it provided the entire fabrication history about a part. Reasons for poor quality and defects could easily be traced through this log. During the fabrication phase of the project, the Composite Fabrication Manual was constantly refined until the procedure was established.

Templates. From the original drawing of the part, the primary template was first completed. Any stable material, such as mylar film, acrylic sheet, aluminum plate, etc., was used for the template. For small, relatively flat parts, the mylar could be made by tracing the original drawing. It was found that the blueline copy of the original drawing was usually distorted, and this distortion was more marked for large parts. For parts and tools which had complex curves, the mylar was first secured to the tool, and the reference lines drawn. The dimensions from the original drawing were then projected onto the template. This was a very time consuming process, and an area where costly mistakes could easily be made. Eventually, computer generated mylar drawings were prepared, and these proved to be invaluable. By generating the mylar drawing via computer, the designer was able to circumvent another problem area, save time, and insure greater accuracy of the part.

Molds. Excellent male molds with high quality tooling were made by a numerically controlled direct cutting method, and were very valuable in establishing dimensional integrity. Majority of the female molds were made from the male molds from wet fiberglass lay-up utilizing a high temperature resin (CIBA -Geigy EPOCAST 88432). The epoxy resin proved useful in tooling and the molds were made quickly and inexpensively. Small shrinkage and high dimensional stability permitted the fabrication of parts to very tight tolerances (Table 5). After lay-up, the molds were vacuum bagged and cured, followed with a heat cycle for post-curing. Before lay-up could begin, the scribe lines on the molds were verified and each mold was leak checked.

Lay-up. After verification of drawings, templates, and molds, lay-up was performed. A ply sequence sheet was generated which listed the ply number, material, direction, and its location. As plies were placed on the tool, the backing sheets were removed, marked, and placed in a container. Traffic through the lay-up area was held to a minimum during the lay-up of parts. It was realized that an organized, clean environment was necessary to reduce careless errors and produce a high quality part. This was especially true for parts which had small and/or numerous plies such as the reinforced ribs. For parts which had exposed surfaces, structural adhesive film Nitrile Phenolic (AF-30) from 3M was used for the outermost ply. AF-30 was used not only for protection from corrosion, but also to provide a smooth surface for painting purposes. Since the dry film has very little tack, it was laid in short lengths on the tool, and then vacuum bagged.

Once the mold and master drawing were confirmed, the dimensional accuracy of the part was totally dependent on the master mylar drawing. The correctness of the mylar template was particularly important for parts in which the location of the honeycomb was critical. Sometimes,

the honeycomb's placement and dimensions posed interference with other parts during the assembly process. This was true for the reinforced ribs. As shown in Figure 5, the honeycomb was located exactly by the use of reference and code lines on the template and tool. By using the code lines and reference lines to position and place plies and honeycomb in the lay-up, the accuracy of the lay-up was insured as shown in Table 5. Upon completion of lay-up, parts were vacuum bagged and leak checked, with the criteria being that the bag experience no more than a 25.4 mm (1 in) Hg drop in five minutes.

Some problems with honeycomb core were experienced during the fabrication and assembly phase of the project. A process known as stabilization of the honeycomb was terminated when it became apparent that a good bond was not forming between the honeycomb and the carbon prepreg. In stabilization, the honeycomb was cut slightly larger than the actual needed shape; narrow strips of film adhesive were then cured on the outer edges of the honeycomb. This stabilized the honeycomb by producing a stiffer edge which when beveled or trimmed to final size produced a very clean and accurate piece. The problem occurred when the honeycomb panel went through moderate, but repeated heat cycles (for adhesive curing during assembly). It was found that the core separated from the graphite in all the stabilized areas. Although the adhesive manufacturer suggested that the stabilized edge can be sanded and then wiped with a cleaning agent, it was decided to terminate stabilization, and no more problems were experienced with the adhesion between the carbon and the core.

Another area which required attention was the bevel angle of the honeycomb core. Depending on the honeycomb density and thickness, an edge taper of less than 30 degrees was found to minimize the possibility of core crush. For the case of thick honeycomb (greater than 15 mm), which required an edge taper of greater than 30°, multi-layer honeycomb was used for sandwich panel fabrication (Figure 6). Kevlar prepreg and carbon prepreg were used for the binder layers. Depending on the requirement of the part specifications, the designer and fabrication team discussed and selected the mode of sandwich construction.

Due to the geometry of some parts, there were certain parameters that were difficult to control. This was true for the C-shaped spars. Depending on the thickness of the flanges, the C-spars exhibited a tendency to spring inward as shown in Figure 7. Many factors contribute to this phenomenon, such as different thermal expansion characteristics between the tool and part, laminate pattern, and other complex conditions. By offsetting the tool dimensions, this problem was alleviated.

An important step during fabrication was the lay-up of a flat panel which simulated the actual part. This particular laminate proved quite important during many phases of the project, because potential problems could be discovered by cutting and inspecting this panel. For instance, after honeycomb skins were cured, the test panel was cut so that the bond between the graphite and the honeycomb core could be confirmed. These panels also proved useful when attempting to test a completed structure nondestructively. In many instances, access from only one side was possible, and these panels provided a starting point in gaging thicknesses for bond testing. Whenever possible, the test panels were cured on the part mold for good representation of the actual part. Excess from final trimming was also saved for future NDE needs. The main

purpose of fabricating the test panels was to check the parameters of the cure cycle - temperature, pressure, and time.

Separate test panels from every material used in a part were also fabricated for tensile and compressive testing following the standards for composite materials (3,4). Figure 8 shows the result for some of the parts, and it can be seen that the established design values were surpassed. Figure 9 shows the results for tensile testing of parts and test parts fabricated at Raspet Flight Lab. This plot is representative of the entire fabrication process. As experience was gained, and procedures were established, the testing improved, and quality of the parts improved. After procedures for each portion of the fabrication process were established, high results were achieved. This plot clearly displays how the quality of parts was driven by quality control. Some of the highest quality parts which were produced were the flap skins. These included small radius leading edges, large plies, custom bagging, and silicone inserts for applying pressure in the tight radiuses.

ASSEMBLY. The first step in assembly was the cataloging and collecting of all components, drawings, and jigs needed to assemble a structure. For large structures, such as the horizontal and vertical tails, the skin molds were used as the jigs. Leveling of the molds was accomplished before every significant step, and it was found that assembly went smoothly if the mold was stable and handled minimally.

The main structure of the MH-02 is bonded with EC 3448, a 250°F structural paste adhesive. The design criteria of this adhesive is conservative. Figure 10 shows the results of the deterioration of the lap shear strength as a result of fatigue and environment. The design value of 35 kg/cm² was determined for the worst environment condition, whereas the shear strength value of 150 kg/cm² was the established design value for dry room temperature conditions. The proper cure cycle and thickness of the adhesion layer were established from pre-tested data (Figure 11 & Figure 12). Adhesive thickness in the range of 0.2 mm to 0.6 mm was determined to be acceptable. An Adhesion Specification Manual was assembled from this data.

A glue clearance check was accomplished on all bondlines with a room temperature adhesive. All areas on the skin and the spar caps were covered with teflon tape; the structure was positioned and assembled with clecoes. A room temperature adhesive was applied and allowed to cure. Upon complete cure of the adhesive, the thickness was measured with a micrometer every 38.1 mm (1.5 in) to an accuracy of 0.0254 mm (0.001 in). Due to this check, it was quickly determined where shimming was required and where scrim cloth was required. Since the wing, fuselage, and empennage structures were assembled in stages, several adhesive cure cycles were required which exposed the structure to 250°F. Every step in the adhesion process was recorded on the "Adhesion Process Sheet". Lap shear coupons were made simultaneously with every adhesion process, and the shear strength of the adhesive was determined (5). By performing single lap shear tests, the integrity of the cure cycle and any degradation were determined. Pressure on the adhesive joints was applied by lead bags and the accuracy of the final assembled structure was measured to be quite high (± 0.1 degree of wing twist of main wing).

INSPECTION. Once parts were cured, they were visually checked for defects, and tagged with the part name, number and cure date. The final quality control team with the designer checked the parts for dimensional accuracy and either passed or failed the part. After the part passed the QC inspection, it was trimmed to final specifications.

As shown in Table 6, each part was inspected in several different ways, and the records of inspection were managed by the quality control system. All parts were visually checked for external defects and geometric dimensions were verified. For verification of the material properties, coupons were prepared for the spars, keels, skins, and straps. Adhesive lap shear strength was determined for the spar-skin bonding cycles and fillets were checked for the honeycomb sandwich panels. For critical parts which carry large loads, such as a spar and keel, NDI techniques were implemented.

One of the most important areas which needs to be addressed is the area of Nondestructive testing. The current Nondestructive Evaluation techniques are not sufficient due to the difficulty in interpretation of results and the lack of established pass/fail criteria. For bonded structures to become common place, nondestructive inspection of bonded assemblies must not only be reliable, but should be accomplished with ease.

For final inspection, the main six components - main wing, empennage, slats, ailerons, flaps, and fuselage were inspected and the structure was certified for air safety. Many structural tests were done on assemblies and sub-assemblies and more information on structural testing of the MH-02 can be found in Reference (6).

Table 7 shows an example of a component inspection. A component's history of materials, parts, and assembly can easily and quickly be found at a glance. The component inspection file includes the inspection results of the individual parts. The visual and dimensional inspection along with any problems with the assembled component and its parts were recorded. Any repairs, improvements, or design changes were noted. Once the overall component inspection was completed, the results were summarized by listing the individual part inspection results (bottom of Table 7).

An outline of the complete quality control system is shown in Table 8. The establishment of a quality control system necessitated the creation of specifications and the compiling of data and procedures into manuals. In this project, four manuals were prepared which covered the entire fabrication process. For example, the Fabrication Manual included information on the standard tool and materials and their inspection procedures. Standard methods to fabricate a composite part were outlined in the Lay-up Manual. These two guides were used for the actual fabrication of a specific part. The Material Usage Log was used for tracking prepregs and adhesive lots and also for documenting their histories. The fabrication details of the part, such as ply pattern, fabrication environment, and cure cycle were recorded in the Fabrication Log and/or Part Inspection Sheet. The results of all inspections were compiled in the Quality Assurance Manual, and were also listed in the Part Inspection Sheet. The assembly process was controlled by the Adhesive Specification Guide. Results of the lap shear test and bond line thickness (during assembly) were compiled in the Adhesive Sheet.

CONCLUSION

To produce the high quality composite structure of the MH-02 required a team effort between the design team, fabrication team, and the quality control team. Accuracy and attention was necessary in all phases of the project. The final quality control system emerged due to the process, which took time and effort to establish. The QC procedure was first postulated, parts were fabricated, and the process was refined until the process was established. The data which was used for design purposes was determined in the laboratory and compared with the manufacturer's data. The chosen materials had to be implemented and the out-time of the materials was simulated. Figure 13 is a representation of the different facets required to create a high quality composite part. As shown by Figure 14, the standardization of the process was developed through the various interconnecting processes of the quality control system. The process records and the inspection records (accumulated through the local inspections of each procedure) formed the database, from which the specification manuals were developed. The quality control system developed for the MH-02 worked very well in developing a quality aircraft structure. The Honda MH-02 received FAA Experimental Type Certificate on March 3, 1993. The first flight was successfully completed on March 5, 1993.

REFERENCES:

1. Bennett, G., J. McWhorter, G. Bryant, H. Koelling, G. Bull. "Composite Prototype Aircraft Development - A Method For Design, Fabrication and Test Training". SAE Tech Paper; 1991 SAE General, Corporate, & Regional Aviation Meeting & Exposition Wichita, Kansas. April, 1991. 911015.
2. Nakayama, H. "Introduction of MH-02 Experimental Aircraft as a Result of Joint Research Effort of MSU and Honda". 3rd Joint AIAA/FAA Symposium on General Aviation Systems, 1994.
3. American Society for Testing and Materials. Tensile Properties of Fiber-Resin Composites. ASTM D 3039, 1976.
4. American Society for Testing and Materials. Compressive Properties of Rigid Plastics. ASTM D 695, 1985.
5. Federal Specification. Adhesives, Heat Resistant, Airframe Structural, Metal to Metal, MMM-A-132A, 1965.
6. Misumi, Etsumi. "Assurance of the Safety of Flight for the Honda MH-02". 3rd Joint AIAA/FAA Symposium on General Aviation Systems, 1994.



Figure 1. A-36 with Composite Wing & Tail

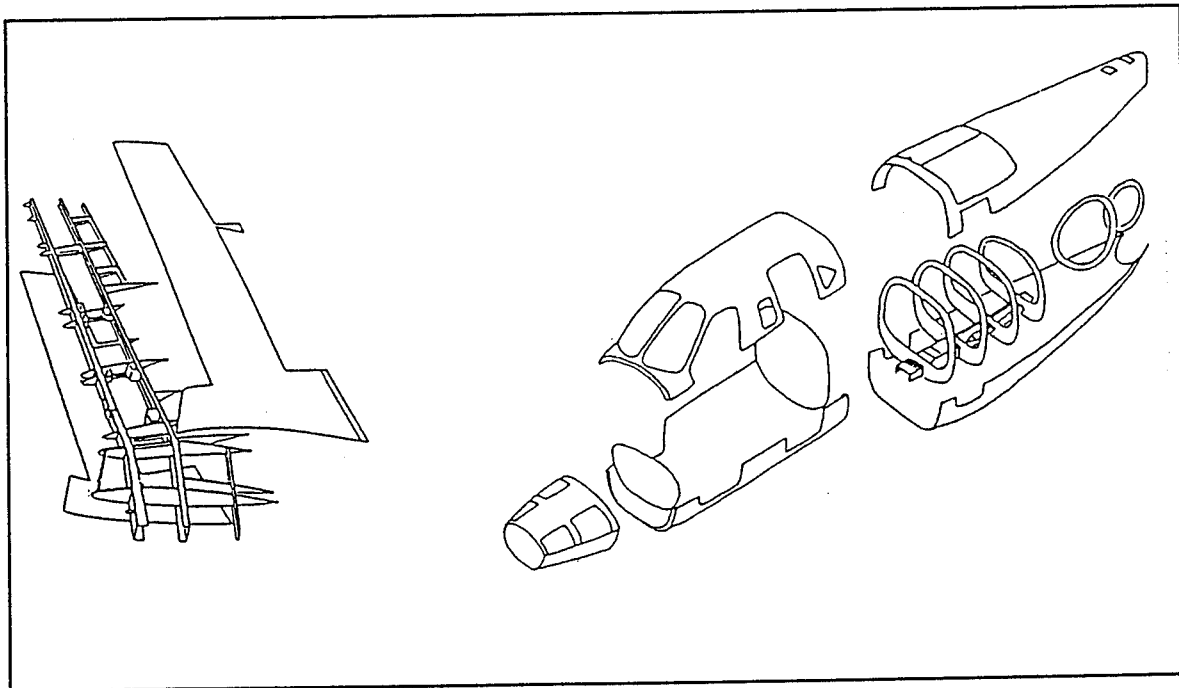


Figure 2. The All-Composite Structure of the MH-02

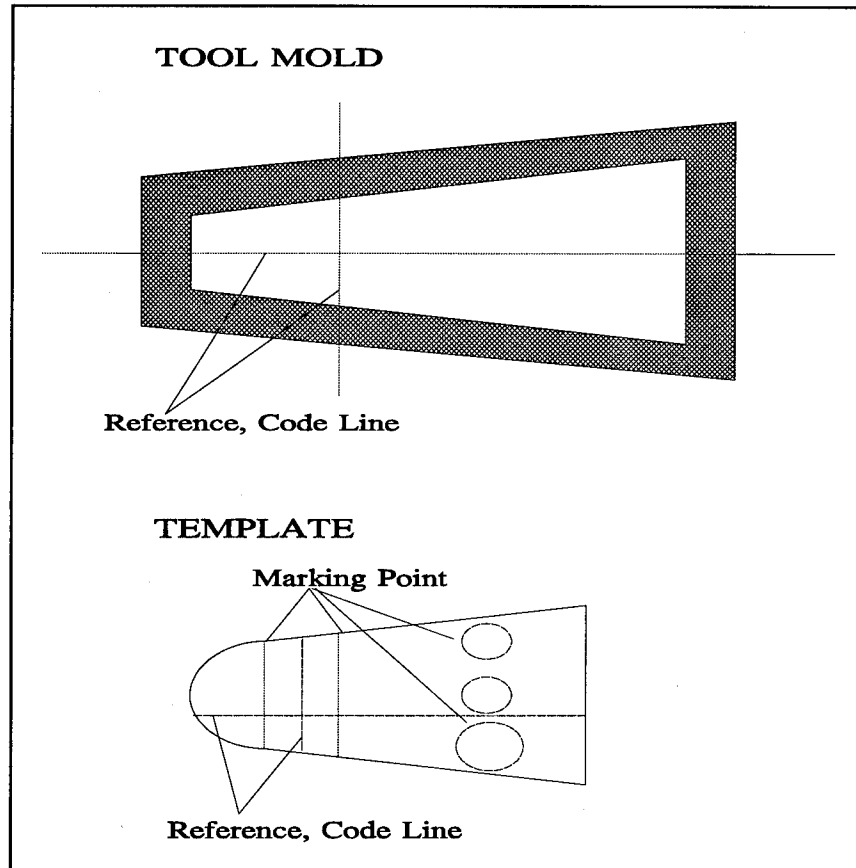


Figure 5. Positioning of H/C on Tool by Reference Lines

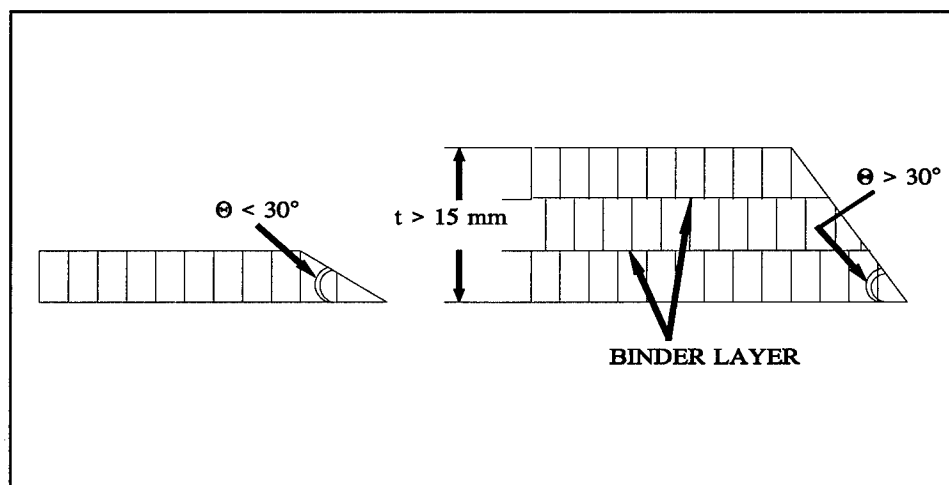


Figure 6. Honeycomb Taper & Construction

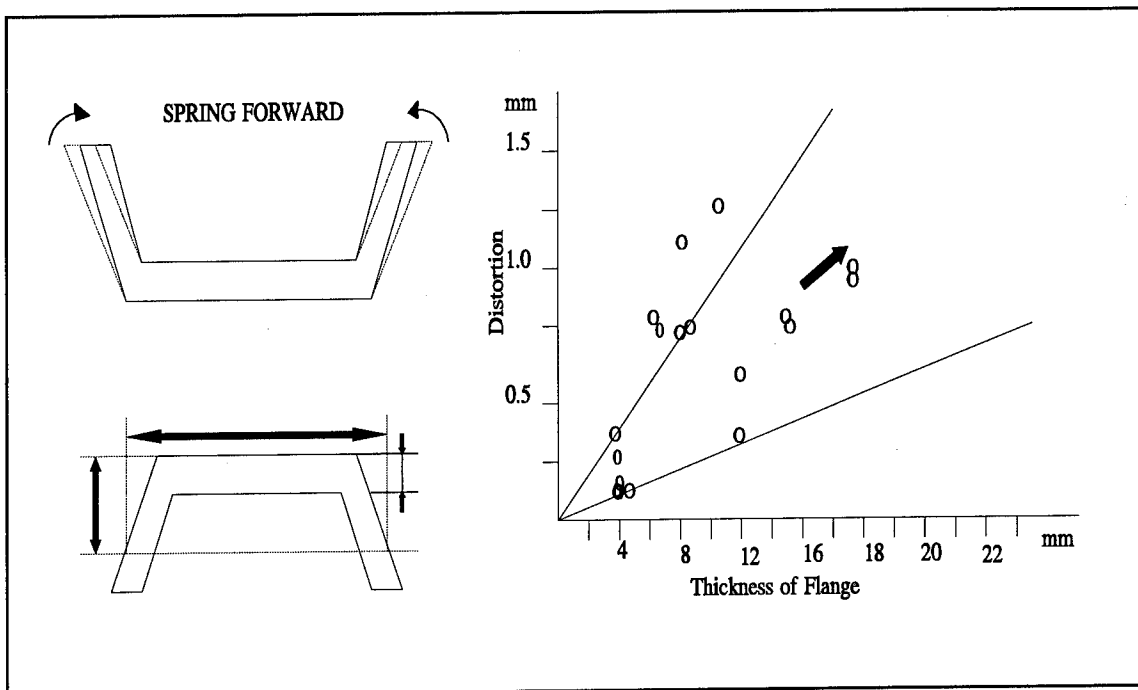


Figure 7. C-Spar Flange Distortion

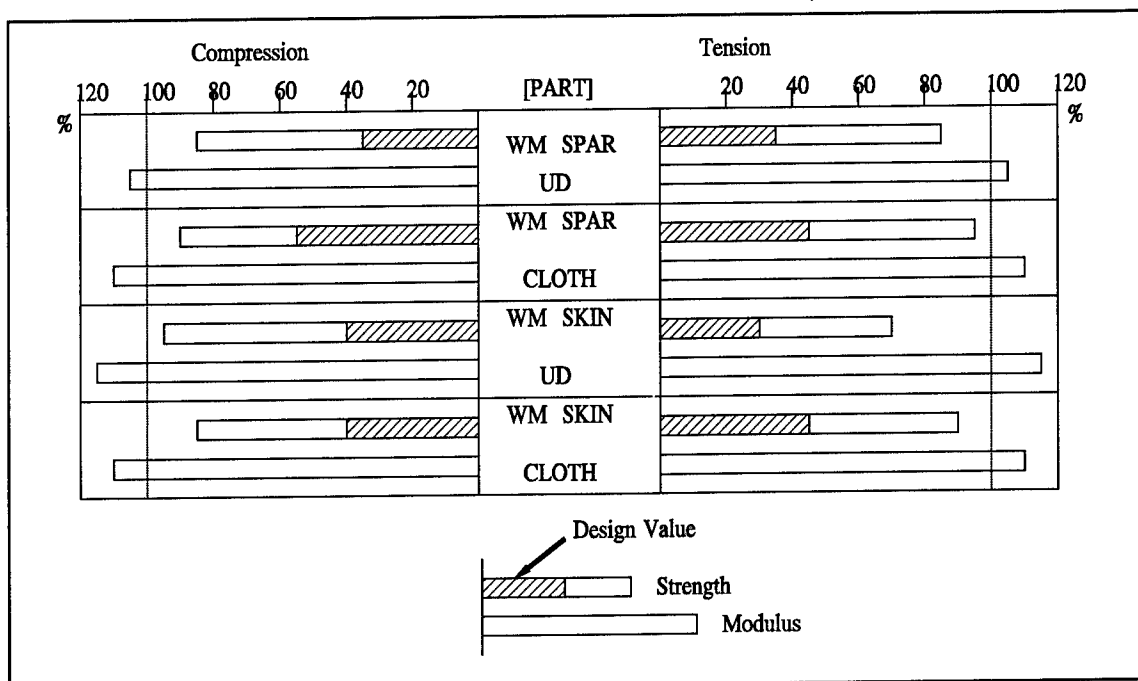


Figure 8. Tension & Compression Results for Some Parts

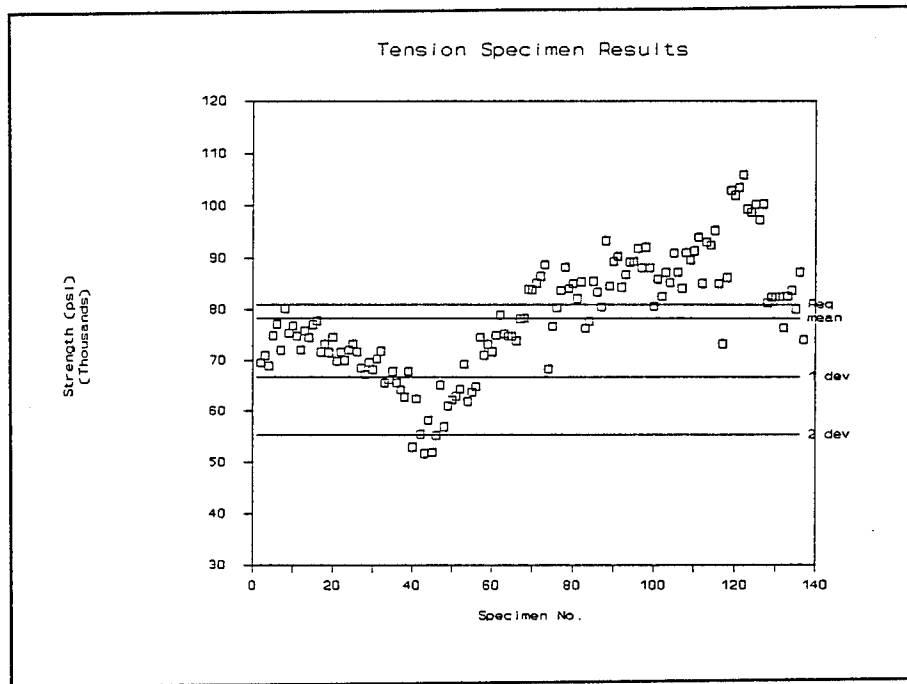


Figure 9. Tension Results of Test Parts Fabricated at RFRL

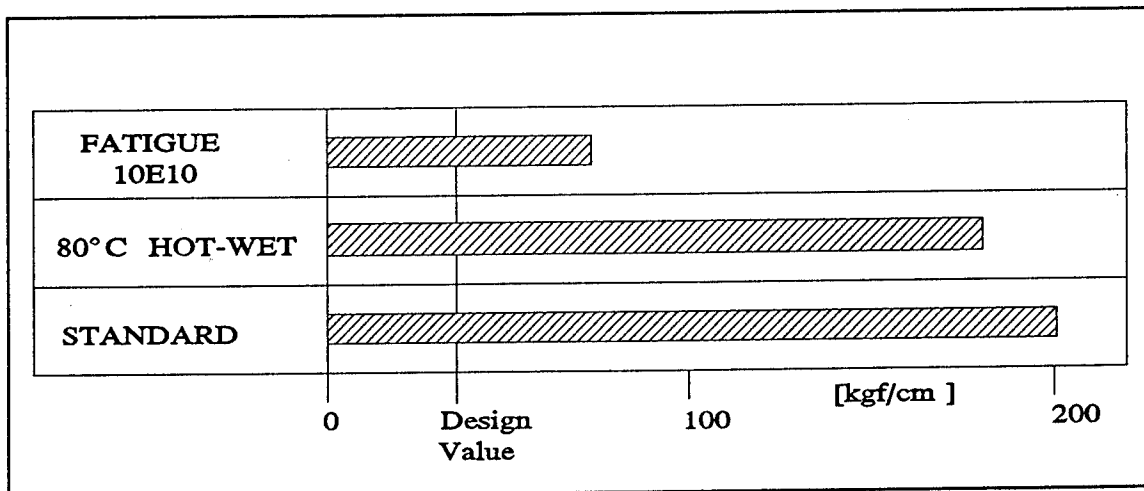


Figure 10. Lap Shear Strength of 250°F Adhesive

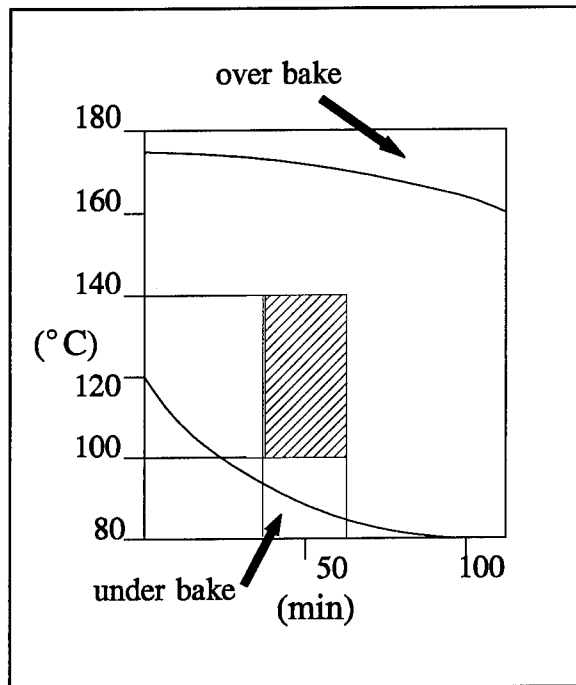


Figure 11. Determination of Cure Cycle for 250°F Adhesive

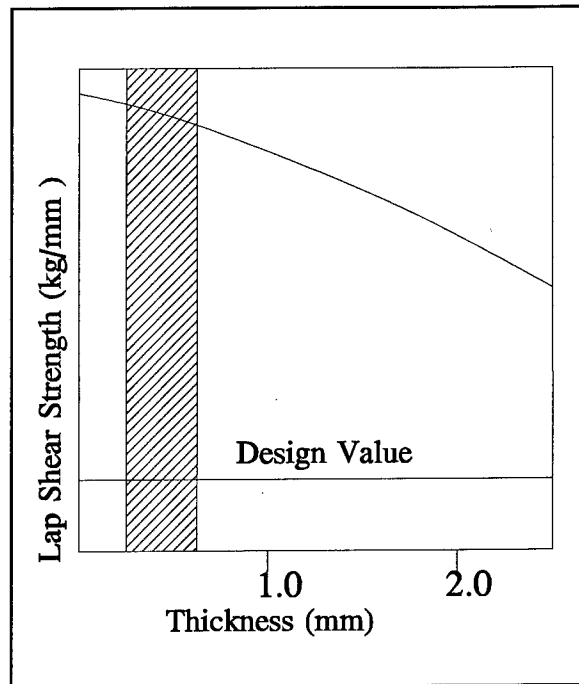


Figure 12. Determination of Adhesive Thickness

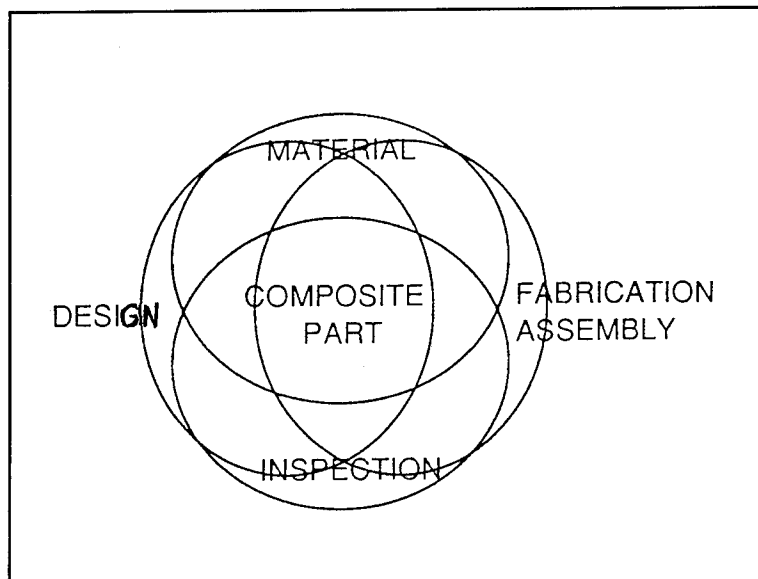


Figure 13. Major Parts in the Development of the MH-02

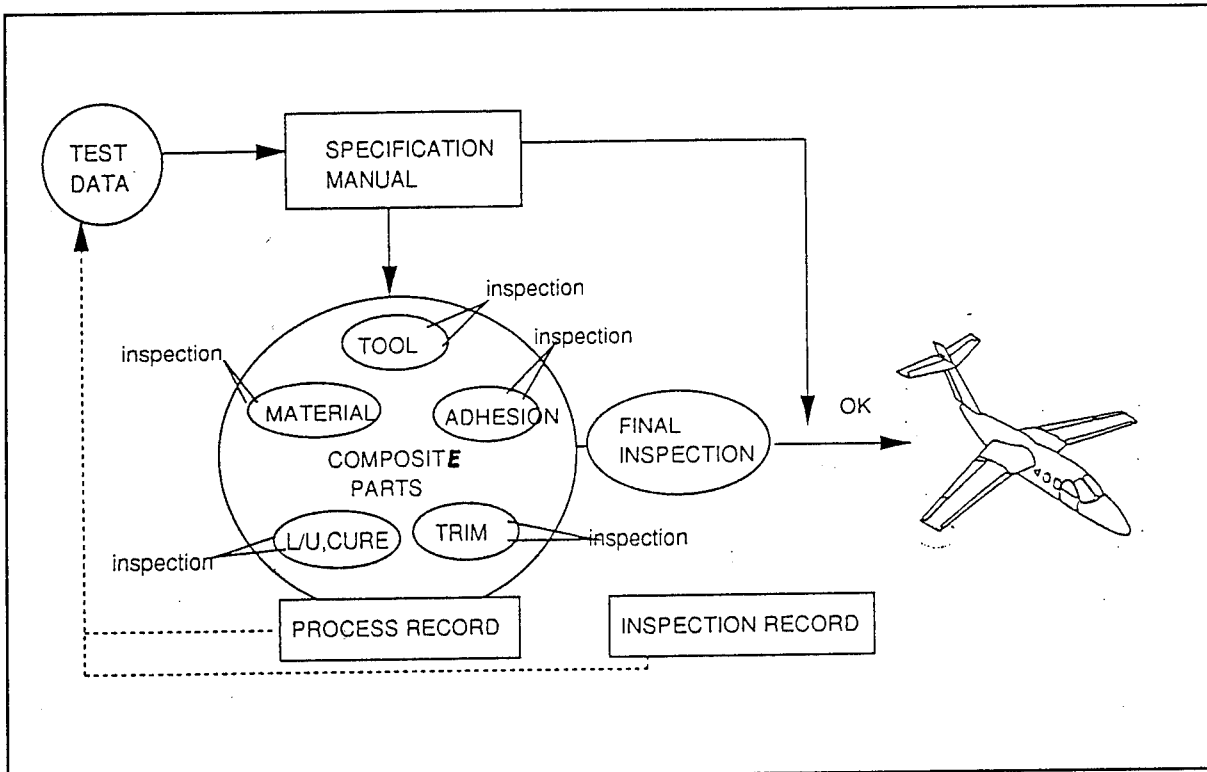


Figure 14. Standardization of Process

Table 1. Total QC Concept

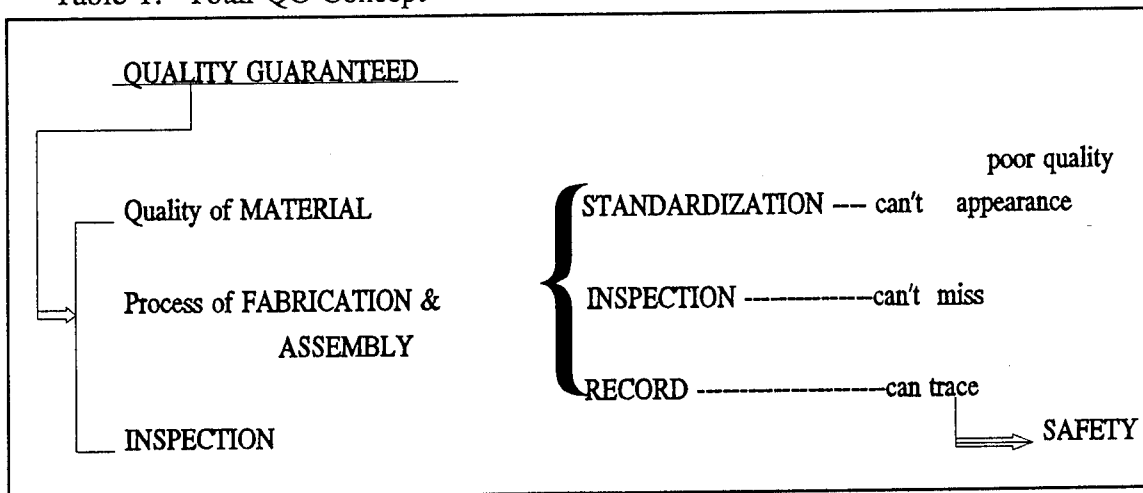


Table 2. MH-02 Construction Materials

Material	Manufacturer	Purpose/ Description	Design Values
HMF 322/34	Fiberite	Graphite Fabric Prepreg	Axial Modulus (kg/mm ²) = 6100
HYE 1034	Fiberite	Graphite Unidirectional Prepreg	Axial Modulus (kg/mm ²) = 13100
AF 191	3M	Film Adhesive for Sandwich Panels	
EC 3448	3M	Paste Adhesive for Airframe Assembly	Allowable Shear Stress (kg/cm ²) = 35
AF 30	3M	Film Adhesive for Outer Surface	
3 PCF & 8 PCF Honeycomb	Nomex	Core Materials	

Table 3. Environmental Control of Prepreg

Storage Temperature	Time Limit (Max)	Memo
below -18°C (Freezer)	6 Months	To avoid condensation formation, 8 hours in cooler required before material is brought to RT for lay-up.
0 - 5°C (Cooler)	2 Months	
22 ± 2°C Relative Humidity <54% (Lay-up room)	15 days (desired) 30 days (max)	

Table 4: Adhesion Control Parameters for Honeycomb Bonding



Good:  Bad: 	
Arrival	Fillet Check
Storage	-18°C - Freezer (6 months maximum)
Usage	0-5°C for 2 hours before removal to RT
RT limit	22 ± 2° C (14 days Maximum)

Table 5. Obtained Accuracy of Tools and Lay-up

Master Mold (resin)	1/1 NC Direct Cut
Tool Mold (Glass, wet-lay-up)	-12/10000 - -16/10000
Cured Part (CFRP)	-2/10000 - -3/10000

Table 6. Part Inspection

	TEST ITEMS	SPAR, KEEL	SKIN	STRAP	RIB	L-Angle
BASIC	External, Visible	O	O	O	O	O
	Dimension	O	O	O	O	O
Same Time Cured Test Panel	CFRP Tag Coupon	O	(O)	O		
	Adhesive Tag Coupon	(O)	(O)			
	S/w Fillet	(O)	O			
NDI	Coin Tapping	O	O		O	
	Ultrasonic	O				

Table 7. COMPONENT INSPECTION

OUTLINE OF INSPECTION

I. PART VISUAL INSPECTION

II. DIMENSION INSPECTION RESULT

III SUMMARY OF POINTS OF CONCERN

Problems & Solutions

IV. POST INSPECTION RECORD

COMPONENT INSPECTION CHECK SHEET

ACCEPT

MAR 26 193.

MSU PROJECT

APPR. Manager

APPR. _____ ↑

APPR. Fabricator

APPR. Designer

APR. Inspector

DAT

DAT

DAT

DAT

DAT

COMPONENT NAME: HT-COMPONENT

DRAWING No. : 12345 - MSU

ACKNOWLEDGMENTS

• PART INSPECTION RESULTS (OK)

• ADHESION PROCESS RESULTS (OK) [

COMPONENT APPEARANCE

OK / NG [

• COMPONENT DIMENSION

(OK) / NG | See attached sheet

COMPONENT WEIGHT 45.0 KG

ITEMIZE

COMPONENT PAST RECORD (REPAIR, IMPROVEMENT, DESIGN CHANGE etc.)

PARTS INSPECTION SUMMARY REPORT
COMPONENT: HT

[illegible]

Table 8. Total Quality Control System

PROCESS FLOW	INSPECTION PROCESS RECORD	CONTENT	SPECIFICATION MANUAL
DRAWING		Dimension	
MASTER TOOL	Tool Inspection	Leak	
INCOMING MATERIAL	Certification (Fillet Test)	Fillet	
TOOL			
STORAGE (RE-TEST)	Material Usage Log (Recertification)	Name, Lot, Storage Temperature, Time	FABRICATION MANUAL
HANDLING CUTTING	Material Usage Log	Amount, Purpose, Residual Qty.	
TOOL PREP			
LAY-UP	Lay-up Book	Lay-up Pattern Check	LAY-UP MANUAL
LEAK CHECK	Fabrication Log	Worker, Date, Environment, Substance	
CURE	Autoclave Cure Cycle	Temp., Pres., Time	
CURED PART	Part Inspection	Appearance, Dimension, NDT, Test, etc.	QUALITY ASSURANCE MANUAL
REPAIR			
TRIM	Working Book	Work	
PRE-ASSEMBLY			
ADHESIVE PREP.		Adhesive Lot, Amount, Temp., Time, Test, Treatment, NDT	
ADHESIVE APPL.	Adhesive Sheet		ADHESION SPECIFICATION
ADHESIVE CURE		Appearance, Dimension, Part Inspect., A/D-P, Summary Report	
COMPONENT	Component Inspection		

EVALUATION OF TACKIFIER AGENTS FOR RESIN TRANSFER MOLDING

Gail Brinkman, Carlos Cadenas-Montes, Robert Phillips, Adam Arnold
National Institute for Aviation Research
Wichita State University
Wichita, KS

ABSTRACT

The development of resin transfer molding (RTM) has been a major break-through in low cost manufacturing methods for composite materials. The RTM technique continues to develop and its applications have advanced beyond fiberglass reinforced non-structural to high performance fiber reinforced structure. The inherent cost savings and reduced equipment dependency of RTM make it an excellent composite fabrication candidate for general aviation hardware manufacturers.

Resin transfer molding relies upon the use of a preconsolidated dry fiber package, or preform. The preform is frequently held together by through-the-thickness stitching or adhesive binders in order to retain shape and structure during tool loading and injection. These adhesive binders or tackifiers are available in solvent based and dry formulations and applied with varying techniques. The majority of application techniques are manual and do not allow for a uniform tackifier application. Further, residual tackifier frequently remains in the laminate. The presence of residual tackifier has not been a concern in non-structural hardware but its impact on structural hardware had not been fully questioned until recently.

The National Institute for Aviation Research (NIAR) Composites Laboratory has evaluated the effect of several commonly used tackifiers on laminate mechanical performance. The project has been structured into two phases. Phase I was designed to quickly determine acceptable and unacceptable levels of tackifiers and binders. Phase II was an expansion of Phase I to more fully characterize what was believed to be acceptable levels of tackifiers and binders while also pursuing the evaluation of alternate process methods and new tackifiers and binders. The study has revealed there are acceptable tackifiers and tackifier levels with minimal structural effect and has also determined unacceptable levels. This paper discusses the ongoing project, its results, conclusions and recommendations.

INTRODUCTION AND PURPOSE

As RTM makes the transition from a prototype process to a production process, more material allowable type data must be generated in order for the RTM process to be a viable alternative to traditional composite processing with a well established database. In addition to the need for characterizing RTM resin systems, there is also a need to determine the effect of the addition of tackifiers or binders. Tackifiers are preform adhesives based on the same or similar resin systems as the RTM resin systems. Binders are preform adhesives that may be soluble or insoluble in the RTM resin system, but most typically are considered a contaminant to the matrix material. It is well known that excessive concentrations of these tackifiers and binders are detrimental to laminate properties. However, it is

necessary to quantify these material knockdowns and correlate binder and tackifier concentrations to the knockdown.

TACKIFIER SYSTEMS

Tackifiers for RTM most often take the form of either a solvated uncatalyzed liquid epoxy, a solvated uncatalyzed solid epoxy, or an uncatalyzed powdered epoxy. The logic behind using an epoxy based tackifier for an epoxy matrix lies in the theory that the epoxy tackifier will become part of the cured part matrix and present no foreign particle contamination. However, by using uncatalyzed epoxies as tackifiers, there is still potential for detrimentally affecting the matrix dominated mechanical properties due to the fact that the ratio of curing agent to resin has been changed in the matrix resin system.

Liquid epoxies are typically diluted with solvent (e.g., methyl-ethyl ketone, trichloroethane, or acetone) to render them sprayable and are used in preform layup applications where a tacky adhesive is required to hold fiber plies to the tool surface or to adjacent plies. After the solvent evaporates, the tacky epoxy resin is left to hold preform plies in position. Solid epoxies (e.g., Shell 1002 or Dow DER 662) are dissolved into a solvent to make the mixture sprayable, and are used in applications where only a short period of tack is required before the solvent evaporates, leaving a solid epoxy binder to hold the preform plies in position. These two spray tackifier systems are used most frequently where the preform is assembled in whole or in part in the RTM tool and the fiber package is not a true "preform".

Powdered epoxies (e.g., Shell 1002 or Dow DER 662) are applied to the individual preform plies before preform assembly, usually at 2-5% by weight. Another option is to powder coat or bath impregnate entire rolls of the woven broadgoods and heat set the powder or liquid coating to the fiber. Individual plies are cut and assembled into the preform and consolidated with heat and pressure. This consolidation operation can be performed using various heating and pressurizing techniques, but most often heat is supplied by an oven (approximately 110C (230°F) is required for melt temperature) and pressure is supplied by vacuum bag or clamped tools. Upon removal of the preform assembly from the oven, the preform must be cooled below the tackifier melting point before removing clamping pressure in order for the preform to retain the desired shape.

A powdered catalyzed epoxy tackifier based on a toughened RTM resin system has recently become available commercially (3M's PT-500) and should prove to have no material property knockdown when used with the parent resin system. It may prove to improve the mechanical properties of untoughened resin systems. Another formulated tackifier product has recently become available (Dexter Hysol LX 79303.1) in the form of a 5-7 g/m² tackifier film. This product is also derived from a toughened epoxy resin system and is formulated to be compatible with RTM resin systems that cure at 121C (250°F) and 177C (350°F).

It is highly desirable for tackifiers and binders to be in film or veil form in order to make application simpler and more uniform in coverage. Non-uniform coverage is a problem in manual spraying and dry powder application of tackifiers and binders.

BINDER SYSTEMS

Binders for RTM most often take the form of aerosol-based repositionable adhesives, nonwoven melt-fusible veil plies, sprayable polyester binder emulsion, or powder polyester binders. Both woven and

nonwoven glass and carbon materials can be purchased with binders pre-applied to the fiber surface or as woven fabrics with co-mingled thermoplastic fibers. Binders are most often used in applications where a slight reduction in mechanical properties due to foreign material contamination is acceptable.

Aerosol-based repositionable adhesives are used in preform layup applications where a tacky adhesive is required to hold fiber plies to the tool surface or to adjacent plies. They are commonly used as spray tackifiers where the preform is assembled in whole or in part in the RTM tool, and the fiber package is not a true "preform". Due to the aerosol propellant, this type of binder can be messy and inappropriate for clean room use.

Nonwoven melt-fusible veil plies, thermoplastic polyester binder emulsion, and fabrics with preapplied binder or co-mingled thermoplastic fibers are most often used in preform thermoforming operations where a rapid preforming cycle is necessary due to high volumes. Preform thermoforming operations may utilize vacuum bag pressure and oven heat for low volume applications, or forming operations may utilize oven heat and matched dies mounted in a pneumatic or hydraulic press for high rate production.

TACKIFIER AND BINDER SCREENING - PHASE I

A test matrix was designed to initiate a screening of four categories of commonly used tackifiers and binders and is shown in Table I. The primary focus of the screening was to establish a comparative ranking of the tackifiers and binders applied in concentrations ranging from the minimum quantity required for holding the preform plies together to two times the typical industry accepted concentration.

Table I. Initial Tackifier and Binder Screening

Tackifier or Binder	Concentration by Percent of Preform Weight			Test Method
	2%	4%	8%	
Powder epoxy, 575-885 EEW*	2%	4%	8%	Compression ASTM D695
Powder Epoxy, 675-750 EEW*	2%	4%	8%	Compression ASTM D695
Repositionable spray adhesive	0.3%	1%	1.8%	Compression ASTM D695
Melt fusible veil	-	-	10%	Compression ASTM D695

* = Epoxide Equivalent Weight

Tackifier concentration for the powdered epoxies was selected because 3-5% is an accepted industry standard, and it was desirable to test both a maximum (8%) and minimum (2%) concentration. Two grades of powder epoxy tackifier varying in epoxide equivalent weight were tested in order to determine the performance difference between the two grades. Repositionable spray adhesive concentration was determined by the minimum quantity required for holding tack (0.3%), increased to a typical concentration (1%), and a maximum concentration of 1.8%. Melt fusible veil concentration is normally dictated by the area weight of the veil (13 g/m²), but it was desirable to evaluate a 10% concentration that

would be representative of using a 13 g/m² melt fusible veil on a lightweight (130 g/m²) fabric. Additional veil material was unavailable for testing at low and normal concentration levels.

TEST PANEL AND SPECIMEN FABRICATION

Preforms for the test panels were fabricated using a Fiberite produced 374 g/m² eight harness satin fabric constructed of 3K AS-4 carbon fiber produced by Hercules. Individual plies were cut, weighed, treated with tackifier or binder, and weighed again to assure proper tackifier and binder concentration. Tackifiers requiring heated consolidation (powder epoxy and melt fusible) were consolidated with a household iron set at 132 - 166C (270-330° F).

It was found that powder based tackifiers were preferred over the aerosol spray adhesive binder in terms of ease of application for flat layup work. In preforming the flat panel test specimens, the aerosol spray adhesive binder produced an over spray mist that settled on work surfaces and tools, requiring more cleanup than the powder based tackifiers. This over spray may prohibit the aerosol spray adhesive binder from being used in a clean room environment. However, powder based tackifiers do not provide any holding tack until the preform is heat set, and the aerosol spray adhesive binder may work better for preforming on a vertical or highly contoured surface requiring hand layup. The melt fusible veil binder was the most convenient tackifier or binder tested because the material is supplied in a lightweight veil form which can be simply cut to size, placed between reinforcement plies, and heat set. No powder or messy over spray was required to be cleaned up, and an even binder distribution was assured by the uniform weight of the veil.

All tackifiers and binders tested performed adequately in holding the preform together during tool loading. No problems were experienced with fiber fraying, ply shifting, or ply distortion as is normally experienced when attempting to layup individual plies into the RTM tool without tackifier or binder. The use of a binder or tackifier to preconsolidate the fabric plies and stabilize these plies for tool loading greatly expedited the tool loading process as compared to not using a tackifier or binder.

Preforms were loaded into the RTM tool and injected with an untoughened low viscosity epoxy resin system (Shell DPL-862/Curing Agent W). A fixed volume of resin (400 g) was vented in each injection cycle to maintain consistent tackifier and binder concentration within each test panel. This precaution was taken because the tackifiers and binders have a tendency to flow in the direction of the injection, and can possibly flow out of the preform with the vented resin.

Once, the fabrication of the panel was completed, the specimens were trimmed and machined. In order to obtain a standardized and industry approved specimen, the ASTM D695 was followed exactly. The coupon cutting was accomplished by using a saw specifically modified for machining composite coupons to specified tolerances. The ends were machined on a mill to achieve the desired parallelness from end to end.

COMPRESSION TEST RESULTS

Compression testing was performed according to ASTM D695, and it was found necessary to bond fiberglass tab stock to the specimens in order to prevent brooming at the specimen ends. The coupon utilized was a straight sided coupon with a 4.8 mm (0.188 in.) gage section. When tabs were included, the specimens failed in the gage area between the tabs in a typical compression failure mode. A

theoretical analysis of the elastic stability of the specimens was performed previous to testing. Given the specimen's geometry and the boundary conditions, it was numerically proven that the buckling critical load was much higher than the compression critical load. This was corroborated experimentally since there was no evidence of buckling. Compression test results are shown in Table II and summarized in graphical form in Figure 1.

Table II. Phase I Compression Test Results

Tackifier/ Binder Type	Tackifier/ Binder Concentration	Average Compressive Strength, MPa (ksi)	Range, MPa (ksi)	Std. Dev., MPa (ksi)/ Coeff. Var.
none (control)	none (control)	675.8 (98.0)	672.4 - 713.6 (97.5 - 103.5)	24.6 (3.58)/3.6
Powder epoxy, 575-885 EEW	8%	552.8 (80.2)	502.0 - 619.1 (72.8 - 89.8)	36.2 (5.25)/6.5
Powder epoxy, 575-885 EEW	4%	663.1 (96.2)	606.4 - 697.0 (88.0 - 101.1)	24.6 (3.57)/3.7
Powder epoxy, 575-885 EEW	2%	659.8 (95.7)	559.7 - 752.9 (81.2 - 109.2)	48.6 (7.05)/7.4
Powder Epoxy, 675-750 EEW	8%	522.5 (75.8)	469.9 - 592.2 (68.2 - 85.9)	48.2 (7.00)/9.2
Powder Epoxy, 675-750 EEW	4%	667.2 (96.8)	586.0 - 730.1 (85.0 - 105.9)	49.3 (7.15)/7.4
Powder Epoxy, 675-750 EEW	2%	667.8 (96.9)	600.6 - 777.7 (87.1 - 112.8)	48.1 (6.98)/7.2
Repositionable spray adhesive binder	0.3%	543.5 (78.8)	498.7 - 602.9 (72.3 - 87.5)	35.8 (5.19)/6.6
Repositionable spray adhesive binder	1%	536.1 (77.8)	432.1 - 578.2 (62.7 - 83.9)	48.9 (7.10)/9.1
Repositionable spray adhesive binder	1.8%	445.6 (64.6)	328.8 - 573.0 (47.7 - 83.1)	75.1 (10.90)/ 16.8
Melt fusible veil	10%	525.5 (76.2)	492.0 - 572.3 (71.4 - 83.0)	28.9 (4.19)/5.5

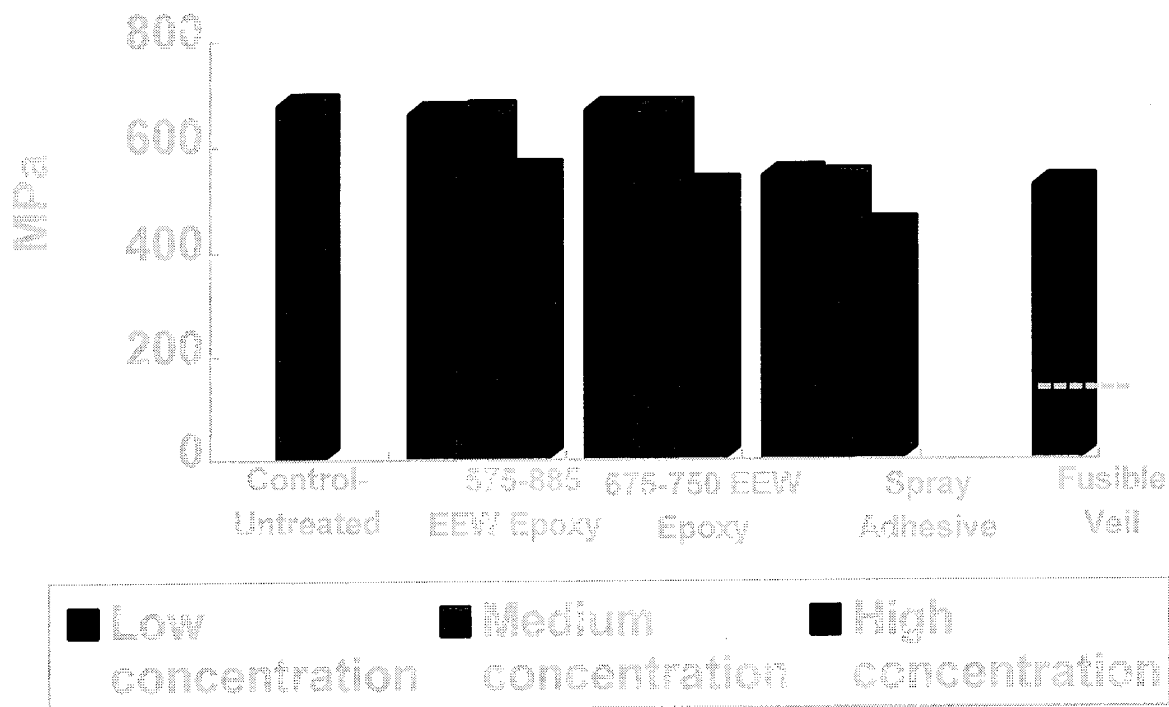


Figure 1. Graphical Summary of Compression Test Results

These test results confirmed that all tested tackifiers and binders detrimentally affected the compression strength of the laminates, and a trend was established showing a reduction in compressive strength with increasing concentration of tackifier or binder. Further, the data scatter increased as a function of increasing concentration. The tackifiers (powder epoxies) had less impact on compressive strength than the binders (repositionable adhesive and melt fusible veil), but showed a definite decrease in compressive strength at maximum concentrations. No significant difference in compressive strengths was observed in varying the epoxide equivalent weight of the powder epoxy tackifier.

TEST MATRIX DESIGN, PHASE II

Based on data generated from the Phase I tackifier and binder screening, it was deemed desirable to conduct an expanded evaluation. Further testing needed included an evaluation of tackifier effects on a higher performance toughened epoxy resin system, testing of tackifier flow or movement at varying mold preheat temperatures, testing at elevated temperature wet conditions, and binder effects in fiberglass preforms. It was also decided to expand the test matrix to include other test modes that would further characterize the effect of tackifiers and binders on mechanical performance. Included were shear (via a +/- 45° tension test) and compression after impact (CAI).

Toughened epoxy resin systems are typically used in demanding structural applications where any material property knockdown caused by processing characteristics is a major concern, and therefore warranted an evaluation of the effects of tackifiers. Varying mold preheat temperatures causes a change in the viscosity of the tackifier and, therefore, the flow characteristics of a tackifier in a preform.

Testing was required to substantiate theories that tackifiers and binders flow or migrate differentially with respect to different processing temperatures.

Testing was required to determine if the material property knockdowns caused by tackifiers and binders is further aggravated by elevated temperature wet test conditions. Testing was also required to evaluate the effects of a binder system on fiberglass panels representative of nonstructural laminates to determine if fiberglass/epoxy laminates experience the same degree of material property knockdown as is seen in carbon/epoxy laminates. A test matrix was designed to evaluate these parameters and is shown in Table III.

Table III. Phase II Test Matrix

	Specimen Group ₍₁₎	0° Compression	+/- 45° Tension (RTA) ₍₂₎	+/- 45° Tension (ETW) ₍₃₎	CAI
PR-500/control	1	8	5	5	5
PR-500/powder PR-500/2%	2	8	5	5	5
PR-500/powder epoxy, 575-885 EEW/2%	3	8	5	5	5
862/control	4	8	5	5	5
862/powder epoxy, 575-885 EEW/2%/177C (350° F) inject	5	8	5	5	5
862/powder epoxy, 575-885 EEW/2%/121C (250° F) inject	6	8	5	5	-
862/spray adhesive/1%/121C(250° F) inject.	7	8	5	5	5
Glass/862/control	8	8	5	-	-
Glass/862/spray adhesive/1%	9	8	5	-	-
Glass/862/polyester powder/2%	10	8	5	-	-
PR-500/powder PR-500 migration	11	8	-	-	-
862/powder epoxy, 575-885 EEW/2%/177C (350° F) inject	12	8	-	-	-
862/powder epoxy, 575-885 EEW/2%/121C (250° F) inject	13	8	-	-	-
862/spray adhesive/1%/121C (250° F) inject	14	8	-	-	-

Notes:

- (1) Specimen groups 1-3 were designed to evaluate the effects of tackifiers suitable for use in structural applications utilizing a toughened epoxy matrix resin system.
Specimen groups 4-7 were designed to evaluate tackifier and binder effects on an untoughened epoxy matrix resin system.
Specimen groups 8-10 were designed to evaluate the effect of binders suitable for nonstructural applications in an untoughened epoxy matrix resin system.
Specimen groups 11-14 were designed to evaluate the migration of tackifier and binder from treated areas of the preform to untreated areas of the preform.
- (2) RTA = Room Temperature Ambient
- (3) ETW = Elevated Temperature Wet

TEST PANEL FABRICATION

Preforms for the test specimen groups 1-8 and 12-15 were fabricated using 270 g/m² five harness satin fabric constructed of 3K AS-4 carbon fiber. Preforms for the test specimen groups 9-11 were fabricated using 302 g/m² eight harness satin fabric (style 1581 E-glass). Individual plies were cut, weighed, treated with tackifier or binder, and weighed again to assure proper tackifier and binder concentration. Tackifiers requiring heated consolidation (powder epoxy and film) were consolidated with a household iron.

Preforms were loaded into the RTM tools and injected with the required epoxy resin systems. A paint pressure pot was used to inject the Shell 862/W resin system, while a hot melt RTM resin dispensing unit was used to inject the PR-500 resin system. A fixed volume of resin (200-400 g, depending on panel size) was vented in each injection cycle to maintain consistent tackifier and binder concentration within each test panel. This precaution was taken due to the fact that the tackifiers and binders have a tendency to flow in the direction of the injection, and can possibly flow out of the preform with the vented resin.

Specimen groups 12-15 were designed to evaluate this tackifier and binder migration effect by treating only a two inch wide band of the preform along the edge of the preform adjacent to the injection port with tackifier or binder. The injected resin flowed through these treated bands of preform before reaching the untreated preform, allowing the binder or tackifier an opportunity to migrate into the untreated preform with the injected resin.

The test panels for the second phase of this project have been fabricated and specimen machining and testing is underway. The majority of the room temperature ambient testing is complete and the results are included and discussed below.

COMPRESSION TEST RESULTS - PHASE II

Compression testing was performed according to ASTM D695 with fiberglass tabs bonded to the specimens to prevent end brooming. The failures were all in the gage area between the tabs in a typical compression mode with no evidence of buckling.

Table IV. Compression Test Results for Phase II Test Program

Fiber/Resin	Specimen Group No. (Table III)	Tack./Binder Type	Conc.	Avg. Comp. Strength, MPa (ksi)	Range, MPa (ksi)	Standard Dev., MPa (ksi)
Carbon/PR-500	1	None	None	723.9 (105.0)	699.1 - 786.0 (101.4 - 114.0)	34.5 (5.0)
Carbon/PR-500	2	Powder PR-500	2%	767.4 (111.3)	695.7 - 848.7 (100.9 - 123.1)	64.5 (9.5)
Carbon/PR-500	3	575-885 EEW	2%	In Test		
Carbon/862	4	None	None	586.0 (85.0)	501.9 - 632.2 (82.2 - 91.7)	48.3 (7.0)
Carbon/862	5	575-885 EEW (177C)	2%	In Test		
Carbon/862	6	575-885 EEW (121C)	2%	512.7 (74.4)	439.8 - 618.0 (63.8 - 89.6)	72.4 (10.5)
Carbon/862	7	Spray adhesive	1%	471.5 (68.4)	340.0 - 551.0 (49.3 - 79.9)	76.0 (11.0)
Glass/862	8	None	None	487.4 (70.7)	453.0 - 537.7 (65.7 - 78.0)	37.9 (5.5)
Glass/862	9	Spray adhesive	1%	329.6 (47.8)	276.4 - 370.9 (40.1 - 53.8)	31.02 (4.5)
Glass/862	10	Polyester powder	2%	490.2 (71.1)	465.4 - 513 (67.5 - 74.4)	20.68 (3.0)
Carbon/PR-500	11	Powder PR-500 migration	2%	748.0 (108.5)	659.8 - 792.8 (95.7 - 115.0)	52.4 (7.6)
Carbon/862	12	575-885 EEW, 177C inject, migration	2%	632.9 (91.8)	510.8 - 683.3 (74.1 - 99.1)	71.01 (10.3)
Carbon/862	13	575-885 EEW, 121C inject, migration	2%	568.8 (82.5)	473.7 - 634.3 (68.7 - 92.0)	55.15 (8.0)
Carbon/862	14	Spray adhesive, migration	1%	488.1 (70.8)	414.4 - 603.3 (60.1 - 87.5)	68.2 (9.9)

SHEAR TEST RESULTS - PHASE II

The shear tests were conducted as $\pm 45^\circ$ tension coupons tested per ASTM D3518. The specimens were tested in a Material Test System (MTS) 55 kip servo-hydraulic test stand. The load rate was selected in accordance with ASTM D3518 to eliminate the danger of inducing dynamic or creep effects

in the specimens. Peak load values were extrapolated from the data sheets for calculation of shear strength. Both the carbon and fiberglass specimens responded linearly for axial stress levels below 70 MPa.

The test matrix in Table III indicates that testing is to be conducted in both the room temperature ambient conditions as well as the elevated temperature wet (tested at 82C (180° F) after conditioning at 95% relative humidity and 63C (145° F) to saturation) condition. The majority of room temperature ambient coupons have been completed while the elevated temperature wet tests will be conducted in late summer 94 after environmental conditioning is complete.

Table V. Shear Test Results for Phase II Test Program

Fiber/Resin	Specimen Group No. (Table III)	Tack./Binder Type	Conc.	Average Shear Strength, MPa (ksi)	Standard Dev., MPa (ksi)/Coeff. of Variation
Carbon/PR-500	1	None	None	123.0 (17.8)	11.7 (1.7)/9.5
Carbon/PR-500	2	Powder PR-500	2%	128.9 (18.7)	3.8 (0.5)/2.9
Carbon/PR-500	3	575-885 EEW	2%	in test	
Carbon/862	4	None	None	101.0 (14.7)	3.1 (0.4)/3.1
Carbon/862	5	575-885 EEW (177C)	2%	in test	
Carbon/862	6	575-885 EEW (121C)	2%	109.0 (15.8)	8.7 (1.3)/8.0
Carbon/862	7	Spray adhesive	1%	99.7 (14.5)	1.4 (0.2)/1.4
Glass/862	8	None	None	97.2 (14.1)	5.1 (0.7)/5.2
Glass/862	9	Spray adhesive	1%	78.6 (11.4)	2.6 (0.4)/3.3
Glass/862	10	Polyester powder	2%	99.4 (14.5)	4.8 (0.7)/4.8

CONCLUSIONS AND RECOMMENDATIONS

The test program to date has yielded several interesting conclusions. From Phase I it was learned that low concentration levels (2 to 4%) of epoxy based tackifiers are sufficient to hold dry fiber plies together and do not have a detrimental effect on compressive strength. High levels (8%) begin to significantly impact compressive strength. However, Phase II indicated that compressive strength is detrimentally affected even by low concentrations yet shear strength increased slightly. Therefore, if mechanical performance is critical, it is recommended that the minimum levels be used. The recommended low concentration level (2%) will be more fully characterized in Phase II.

Repositionable spray adhesive binders were found to significantly affect compressive strengths at any concentration. While this may not be a problem in nonstructural hardware, the use of this material should be carefully monitored in a shop environment to prevent its use on structural hardware. Testing completed to date in Phase II has revealed that the 1% concentration level for spray adhesive has had an even more detrimental effect on the compressive strength of fiberglass panels (33% reduction) than it did on carbon panels (20% reduction). While not planned for fiberglass testing, it is anticipated that

environmental conditioning will further aggravate mechanical performance. The spray adhesive is extremely popular with RTM shops and consequently will be more fully characterized in Phase II. A potential acceptable alternative to the spray adhesive was found during Phase II. The polyester powder appears to hold promise as a suitable binder when powder epoxy tackifiers are not available.

The new tackifier (3M's PT-500) designed for use with the higher performance toughened epoxy resin (3M's PR-500) increased both the shear and compression strength when compared to control panels. In the case of this product, one might be able to argue that for maximum performance the tackifier should always be included. Further testing (compression after impact and hot/wet shear) is planned for this system.

Testing performed to study the effects of placing all of the tackifier or binder in one location prior to injection yielded panels with slightly higher compressive strengths than uniform distribution of the tackifier or binder. It is believed that the tackifier or binder did not distribute itself uniformly during injection resulting in test coupons with less tackifier or binder than did the panels with uniform application. It was also observed that the higher temperature injection for the powder epoxy tackifier (177C versus 121C) resulted in higher compressive strengths. While the complete microscopic evaluation of the coupons has not been completed, it is theorized that the higher temperature placed the tackifier into solution and allowed it to move more effectively through the panel.

The National Institute for Aviation Research (NIAR) Composites Laboratory sponsored evaluation of tackifiers and binders has yielded some interesting results to date. In one case it has quantified the effects of a commonly used spray adhesive binder and in other cases piqued our interest further. For prudent manufacturing efforts, tackifiers or binders should not be used unless necessary. In those cases necessary, techniques should be developed to maintain the minimum concentrations recommended and structural performance monitored where appropriate. The NIAR Composites Lab will continue to study tackifiers and binders in order to provide non biased evaluations and recommendations.

CRASHWORTHINESS CONSIDERATIONS IN AIRCRAFT SEAT CUSHION DESIGN

Steven J. Hooper^{*}, Terence Lim^{**}, Manoj Rahematpura^{**}, Brian Goedken^{**}, and Elias Dakwar^{**}

National Institute for Aviation Research

Wichita State University

Wichita, KS 67260-0093

ABSTRACT

Aircraft seats are designed to provide occupant comfort and to satisfy safety requirements. This paper addresses the issue of occupant safety in regards to lumbar load. Static and dynamic tests were conducted to investigate the performance of a seat cushion fabricated from an open celled, rate-dependent polyurethane foam. It is shown that this particular foam material has potential to be employed as an effective energy absorbing mechanism. The effectiveness of this foam material when used as an energy absorbing device is sensitive to the test and design parameters. It was observed that the results of the lumbar load were strongly affected by the amount of preload exerted by an occupant on the cushion. The test results indicate that the lumbar load varies linearly with cushion thickness. At elevated temperatures the potential of the cushion to absorb impact energy is significantly reduced.

INTRODUCTION

The recently adopted dynamic seat test requirements by the Federal Aviation Administration [1,2] have motivated a number of recent research initiatives in the crashworthiness area. These efforts include aircraft drop tests conducted at NASA Langley Research Center and the FAA Technical Center as well as horizontal sled tests of aircraft seats conducted at the FAA's Civil AeroMedical Institute and the National Institute for Aviation Research. The objective of these, and similar efforts, is to improve aviation safety by developing an understanding of the mechanics governing aircraft seat/occupant dynamics. This understanding will ultimately lead to safer aircraft due to enhanced occupant protection.

Typical aircraft seats can be designed to absorb energy through the use of mechanisms involving the deformation of the seat cushion, seat pan, and seat legs. However, some popular aircraft configurations, such as low wing monoplanes, require the development of innovative seat designs since the wing spar location precludes the use of deformable seat legs. For these configurations, the energy absorption must be developed by deformations of either the seat cushion or seat pan.

^{*} Associate Professor, Department of Aerospace Engineering, Member AIAA

^{**} Graduate Student, Department of Aerospace Engineering, Student Member AIAA

This paper presents the results of a study demonstrating that the lumbar load injury criteria of 6.67 kN (1500 lb) can be satisfied for a 19 g crew seat deceleration with the seat cushion as the primary energy absorbing mechanism. The purpose of these tests was to investigate the effectiveness of rate-sensitive foam materials when used as energy absorbing devices. The results of these tests indicate that the lumbar load of the anthropomorphic test dummy (ATD) is sensitive to several design parameters including the thickness and temperature of the cushion. It was also observed that the results are strongly affected by the initial conditions such as the amount of cushion preload imposed when installing the ATD in the seat.

EXPERIMENTAL TESTS

In this investigation, an open celled, rate-dependent, slow recovery polyurethane foam called CONFOR™ foam was utilized¹. This particular foam is graded based upon its varying stiffness which is controlled by the size and the number of cells. CONFOR™ foam, hereon referred to as 'foam' in this paper, also offers the flexibility to tailor the shape of the cushion to conform to the shape of the seat pan.

The tests were conducted in two parts. First, hydrostatic compression tests were conducted on the foam material to characterize its constitutive properties and also to empirically verify its rate-sensitivity. The second part consisted of dynamic tests conducted on a seat cushion made of the same foam material. These cushions were tested using the horizontal deceleration sled facility at the National Institute for Aviation Research per the crew seat conditions specified in 14 CFR, Part 23, Section 562.(b).1 [1, 2].

STATIC TESTS.

Static hydrostatic compression tests were performed to measure the load-deflection properties and also to determine whether these properties were rate-sensitive. The tests were conducted with a hydrostatic compression test fixture, shown in Fig. 1, on a MTS servo-hydraulic test stand. The foam specimens were loaded in displacement control at five different compression rates : 2.54, 5.08, 25.4, 1524.0, and 3048.0 mm/min (0.1, 0.2, 1.0, 60.0, and 120.0 inches per minute, respectively). The tests were performed at room temperature, 22.5° C (72.5° F).

¹ Note that the results presented in this paper are based on the study of a specific foam material. This foam was utilized for research purposes and the use of this material does not constitute an endorsement of this product on behalf of NIAR.

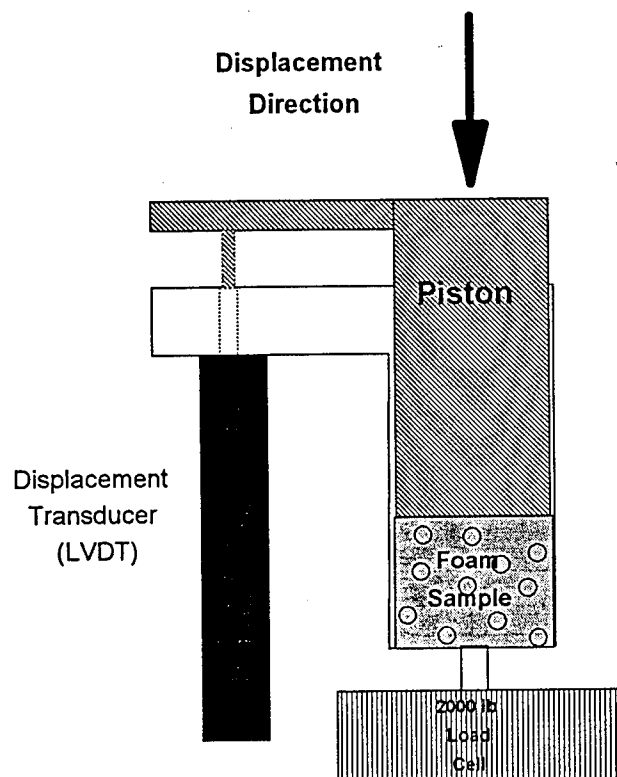


FIGURE 1. HYDROSTATIC TEST FIXTURE

DYNAMIC TESTS.

Dynamic tests were performed to investigate the effects of preloading, foam cushion thickness, and temperature variations on the performance of the foam to determine if the results obtained from the static tests were applicable in the dynamic environment. The tests would also provide necessary data for aircraft seat manufacturers to consider incorporating the foam material in their seat design as an alternative energy absorbing mechanism. The effects of these parameters on the lumbar load were studied individually through three different series of tests.

In performing crashworthiness tests, it is a common practice to place the dummy onto the seat in the final steps of preparation just prior to the launch of the sled. In order to accurately simulate an occupant that is already seated on the cushion when the test is conducted on a 60° inclination (FAR Test 1 [1,2]), a 1g preload on the cushion was applied by pushing the dummy into the seat. However, inconsistencies in the procedure for simulating a 1g preload can greatly affect the results. These inconsistencies result in variations of the preloads which directly affect the lumbar load readings. Thus to show the effects of variations in the preloads on the resultant lumbar load, a series of tests were conducted. For this test series, the degree of preloading was varied from 125 to 890 N (28 lb to 200 lb) and was monitored utilizing the ATD lumbar load cell. The tests

were conducted using five different cushions identified as 31151, 33201, 34201, 35201 and 3-layer foam.

The thickness of the seat cushion is a critical factor in seat design when it is the only energy absorbing mechanism available. The seat designer must maintain some degree of balance between comfort and safety when considering the thickness of the cushion to be employed. The question of practicality is also of concern when the designer has a limited amount of cockpit space to work with. A thick cushion may be the solution to achieve a safe lumbar load but may not be practical if it impedes the pilots' ability to operate the aircraft. Impact tests were conducted on seat cushions made from foam of varying thickness to determine the minimum thickness required to obtain a safe lumbar load. The thickness was varied from 10.16 cm to 15.24 cm in 1.27 cm (4 to 6 inches in half inch) increments. The nominal density of the material tested was 0.0913 g/cm^3 (5.7 lb/ft^3).

The material properties of open celled polyurethane foam are known to be sensitive to temperature changes. Therefore, the foam cushion was first tested at room temperature followed by tests where the cushion surface temperature was increased to 37.78°C (100°F). The seat cushion was placed in an oven and heated for 1 hr. A *J-type* thermocouple was used to measure the temperatures at the surface of the cushion, at 2.54 cm (1 inch) below the surface and at the center of the cushion. When the desired temperatures were recorded at the surface and at the center of the cushion, it was quickly placed on the seat. The temperature was maintained at 37.78°C (100°F) by placing a set of heating pads on the top and bottom surfaces of the cushion.

The dynamic impact tests were conducted in the Impact Dynamics Laboratory at the National Institute for Aviation Research facility located at Wichita State University. The specification for 14 CFR, Part 23, Section 562.(b).1 [1], requires the impact tests to be conducted at a 60° pitch inclination, a minimum velocity at impact of 9.45 m/sec (31 ft/sec), a minimum peak deceleration of 19 g, and a maximum rise time of 50 milliseconds. The regulation also requires that the maximum compressive loads measured between the pelvis and the lumbar column of the ATD do not exceed 6.67 kN (1500 lb) [4]. A plot of a typical 19 g deceleration pulse as well as an ideal pulse are shown in Fig. 2.

The layout of the Impact Dynamics test facilities is shown in Fig. 3. The impact system consists of four major components [3] : (1) a horizontal impact test sled that is used as a platform to mount test articles; (2) a compressed air propulsion system that is used to launch the test sled; (3) a deceleration system that uses a combination of steel straps to absorb the kinetic energy of the sled and shapes the deceleration pulse; (4) a data acquisition system that records and stores test information for post processing.

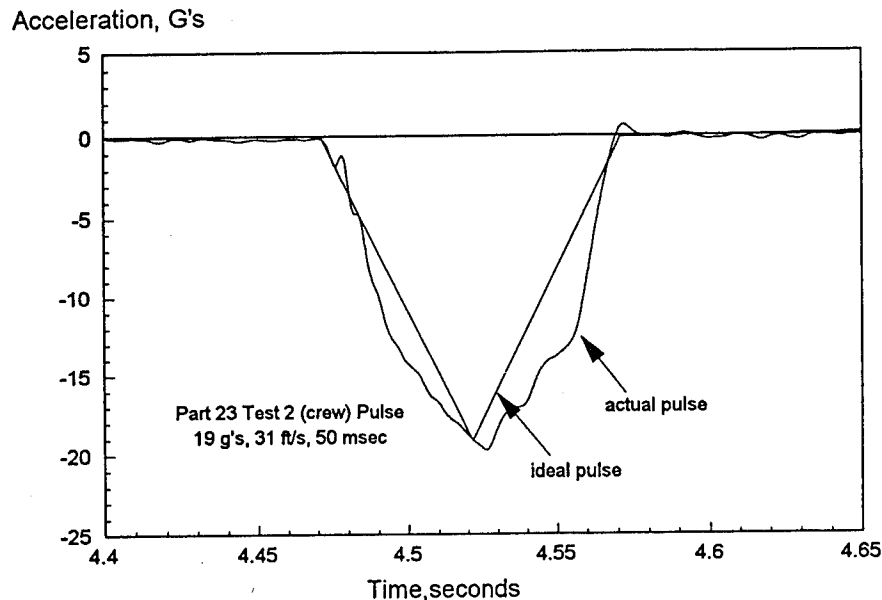


FIGURE 2. TARGET DECELERATION PULSE AND AN ACTUAL PULSE

A rigid seat was employed for this investigation using the test set-up shown in Fig. 4. A rigid seat was used to facilitate measurement of the dynamic response of the seat cushion. The rigid seat was mounted on a 60° pitch fixture and seat cushions were attached to the seat using Velcro™ to prevent the cushion from sliding during impact. A Hybrid II anthropomorphic test dummy (ATD) representing a 50th percentile (78.9 kg) male was used during these tests [4].

A Digital Signal Processor (DSP) Technology Transient Signal and Processing System (TRAQ P) was employed for data acquisition. The system consists of a system controller, memory module, digitizer and sixty transducer conditioning amplifiers as shown in Fig. 5. All the collected data were recorded and filtered per SAE J211 [4-6]. The sled acceleration was measured using a ENDEVCO model 7290-30, S/N AM21, 100 g accelerometer and the data was filtered at channel Class 60. To measure the axial compressive load transmitted by the lumbar spinal column to the pelvis, a 6-axis pelvic-lumbar spine load cell, R.A. DENTON model 2121, S/N 0148, capable of measuring compressive loads up to 15.6 kN (3500 lb) was inserted into the dummy pelvis just below the lumbar column. The lumbar load data was then processed at channel

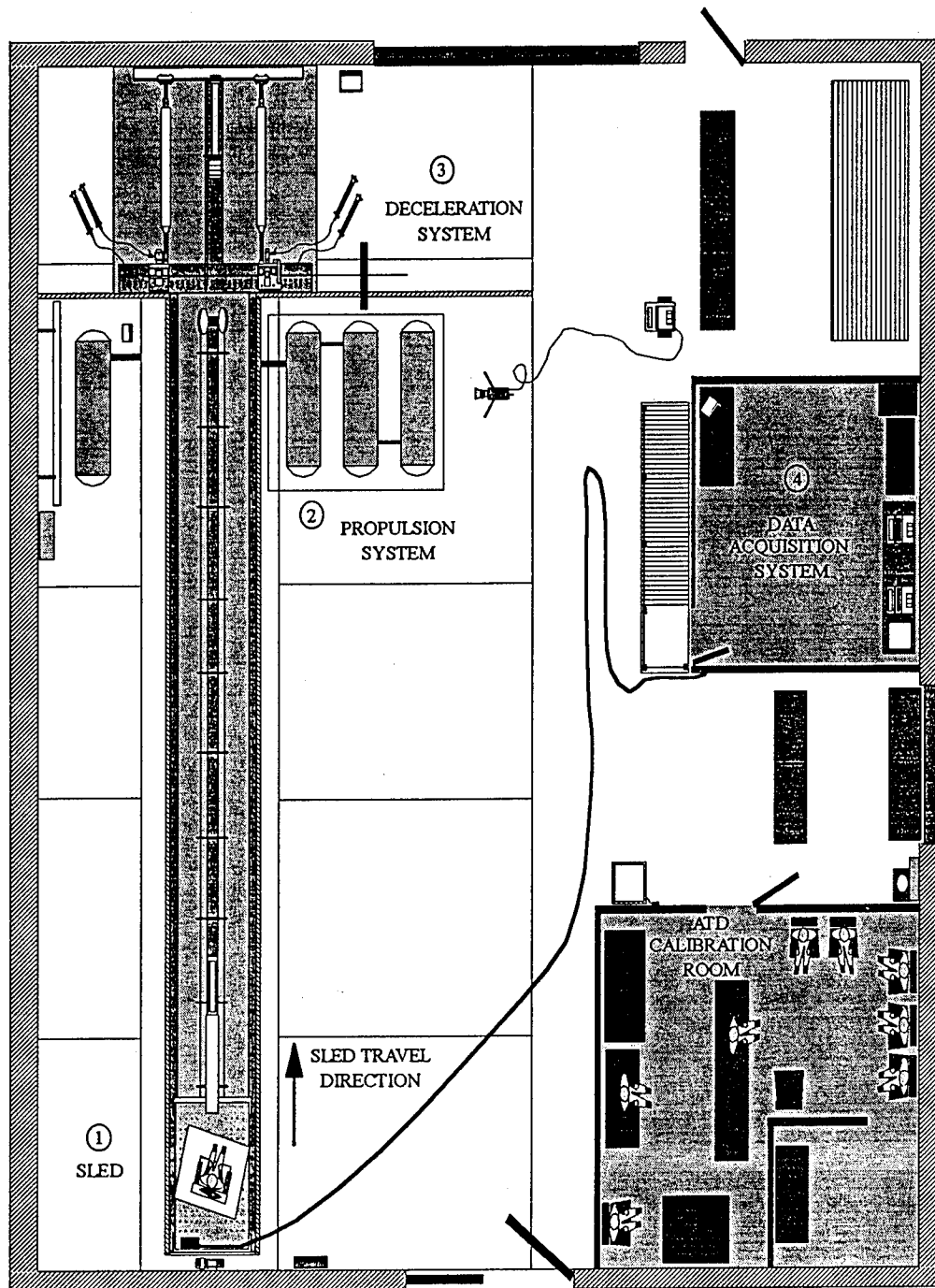


FIGURE 3. IMPACT DYNAMICS LABORATORY

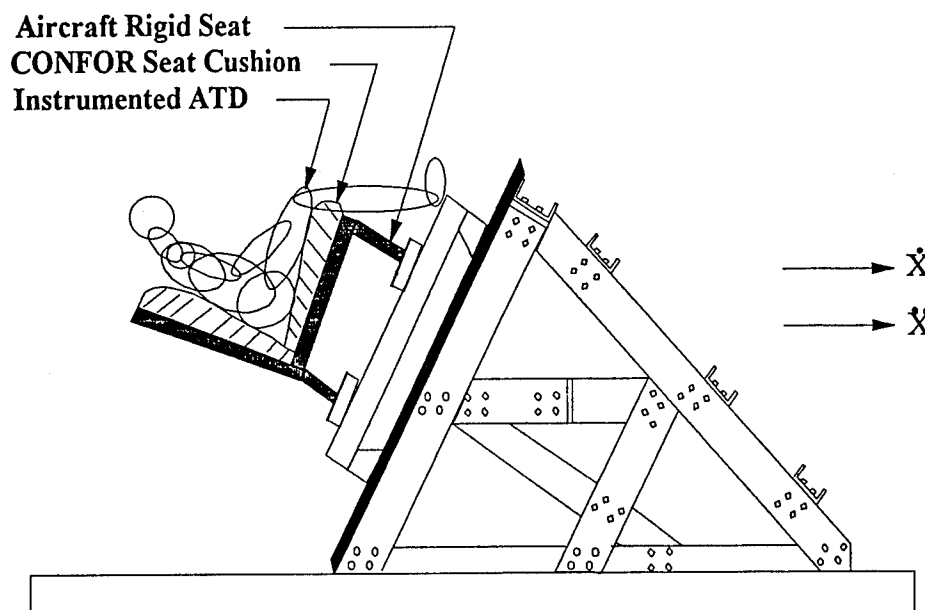


FIGURE 4. TEST ARTICLE MOUNTED ON THE 60⁰ FIXTURE FOR THE DYNAMIC TEST

Class 1000. A 2.54 cm (1 in) optical velocity trap was used to record the velocity of the sled at impact. The occupant restraint system consisted of a lap belt, shoulder harness, and a crotch belt. This five-point restraint belts are commonly employed in crew seating systems. A webbing load transducer, R.A. DENTON, S/N 0227, was installed on the lap belts to monitor the preload on the restraint system. The DSP IMPAX [7] software was used to evaluate the data that was collected and stored by the controller.

Preliminary tests were conducted to identify and isolate the secondary factors which directly affect the lumbar load. The objective was to eliminate or minimize the contribution of these effects and therefore maintaining a consistent test procedure. Thus a consistent set of results were obtained for every test which were then easier to interpret and compare.

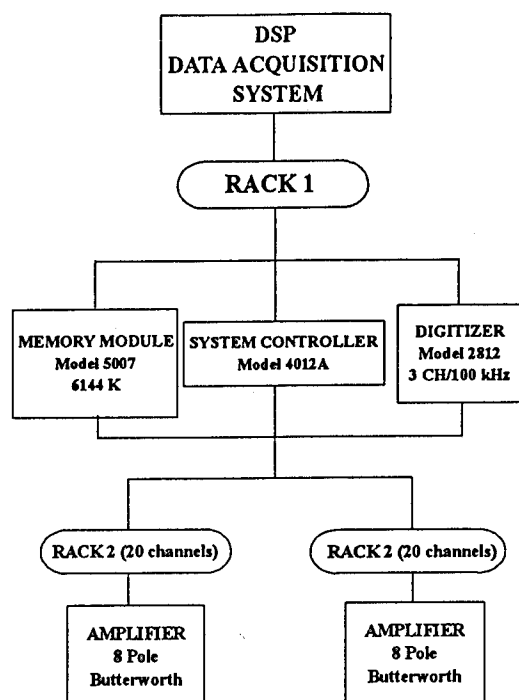


FIGURE 5. SCHEMATIC DIAGRAM OF THE DATA ACQUISITION SYSTEM

These tests had indicated that the lumbar load was sensitive to the variation of the seating position of the ATD. In order to minimize this secondary effect, the dummy was placed in the exact position in every test. Measurements were taken at three key locations on the ATD with respect to some fixed reference points as shown in Fig. 6. A height gage was used to measure the distance, h_1 , from the center of the knee bolt to the base of the 60° fixture. A second measurement, h_2 , was taken using the center of the hip bolt of the ATD to the base of the inclined fixture. The heels of the ATD were rested at a constant distance, x_1 , from the front legs of the seat. In addition, a fourth measurement was taken to determine the amount of deflection the ATD's weight asserts on the foam when it is seated on the rigid seat in a non-inclined position. The dummy was allowed to sink into the cushion for a duration of time until equilibrium was obtained. A probe was inserted from the bottom side of the seat pan to measure the thickness of the cushion with the ATD on the seat. The measurement was then subtracted from the thickness of the undeformed cushion. This procedure yields the amount of deflection the ATD asserts on the cushion prior to impact. Seat belt load cells were also used to monitor the tension in the harness. This assured that the same amount of force was employed in restraining the ATD to the seat, i.e. the seat cushion loads remained constant for every test.

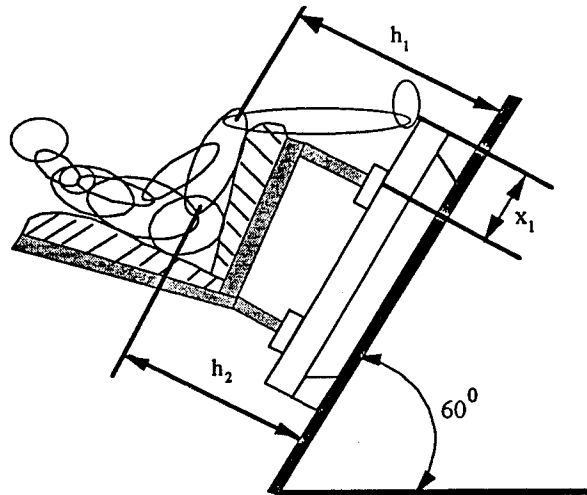


FIGURE 6. REFERENCE MEASUREMENTS FOR SEATING THE ATD

RESULTS AND DISCUSSIONS

The results of the hydrostatic static tests conducted on the foam material are presented in Fig. 7. This plot shows the force-deflection curves at various displacement rates. The work

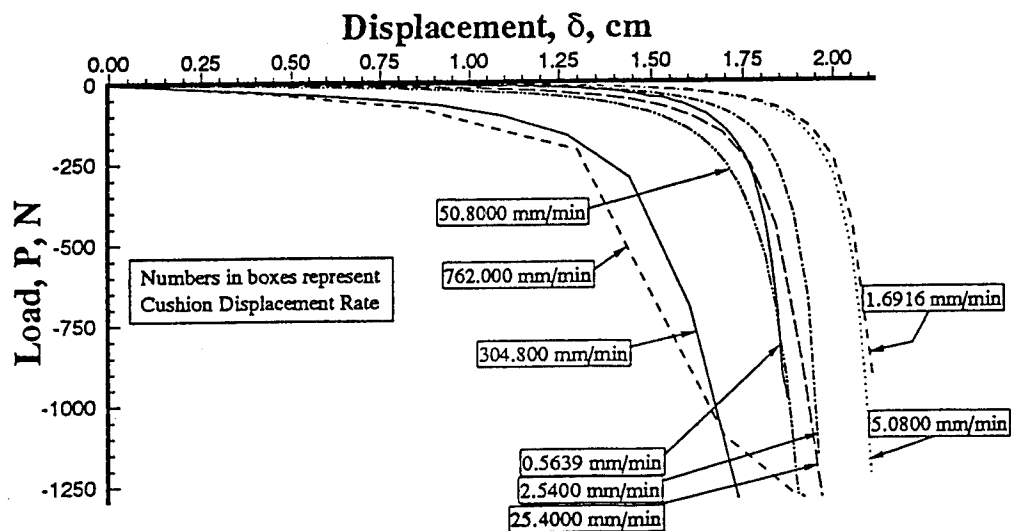


FIGURE 7. HYDROSTATIC TEST RESULTS

done, or equivalently the energy absorbed by the foam is the area underneath the force-deflection curve. Similarly, in thermodynamics the work is said to be done on a gas when it is compressed in a piston. The air trapped in the cells of the foam behave in an identical manner. As shown in the figure, at slow loading rates the work done is significantly low. This is due to the fact that air has ample time to escape slowly from the cells of the foam. This is analogous to thermodynamic system where the piston compresses the gas in a cylinder which has a leak(s) and therefore less work is done in compressing the gas (air). Whereas at high rate of loading, or impulsive loading, air from the cells is prevented from escaping at the same rate, hence the trapped air in the cells have an added resistance and stiffening effect.

Also, as shown in the figure, the slow rate of loading requires higher foam deflections to absorb the same amount of energy as for the higher rate of loading. For example, at displacement rate of 1.691 mm/min (0.0666 in/min) and a compressive load of 448.2 N (100 lb) the foam deflection is approximately 11.76 mm (0.44 in) whereas for the same compressive load but at a displacement rate of 762.0 mm/min (30.0 in/min) the foam deflection is 6.55 mm (0.258 in). This characteristic may be desirable in seat cushion applications

The foam cushion exhibits similar energy absorbing characteristics in the dynamic tests. The effectiveness of the foam cushion to absorb impact energy is indicated through the response of the lumbar load. A typical transient response of the lumbar load acquired during a dynamic test is shown in Fig. 8. The results obtained from the dynamics tests on the effects of preload, cushion thickness, and temperature variations on the lumbar load are presented next.

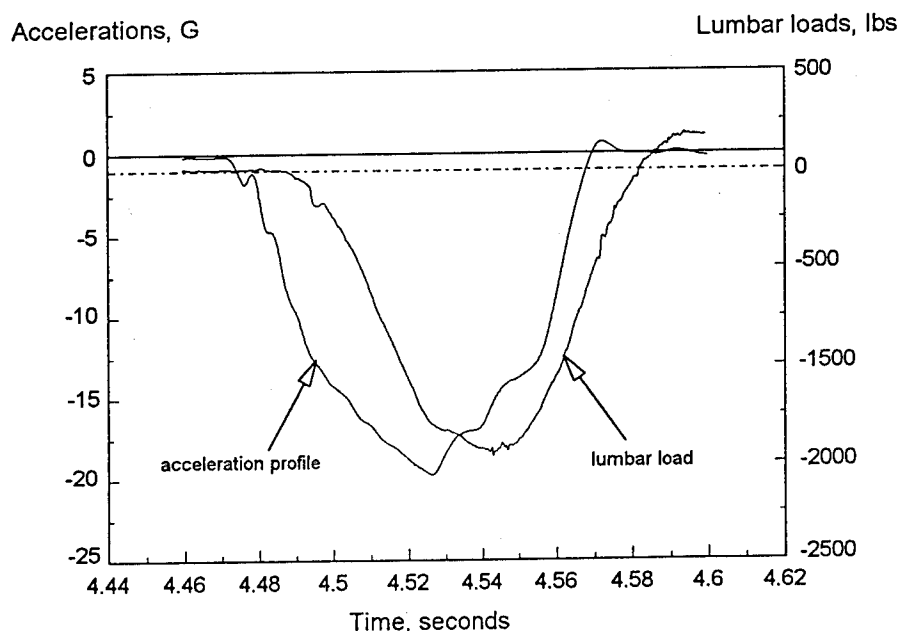


FIGURE 8. TYPICAL TRANSIENT RESPONSE OF A LUMBAR LOAD.

The variation of preloading versus the lumbar load is shown in Fig. 9. The lumbar loads obtained from the tests of five different cushions are plotted against the amount of applied

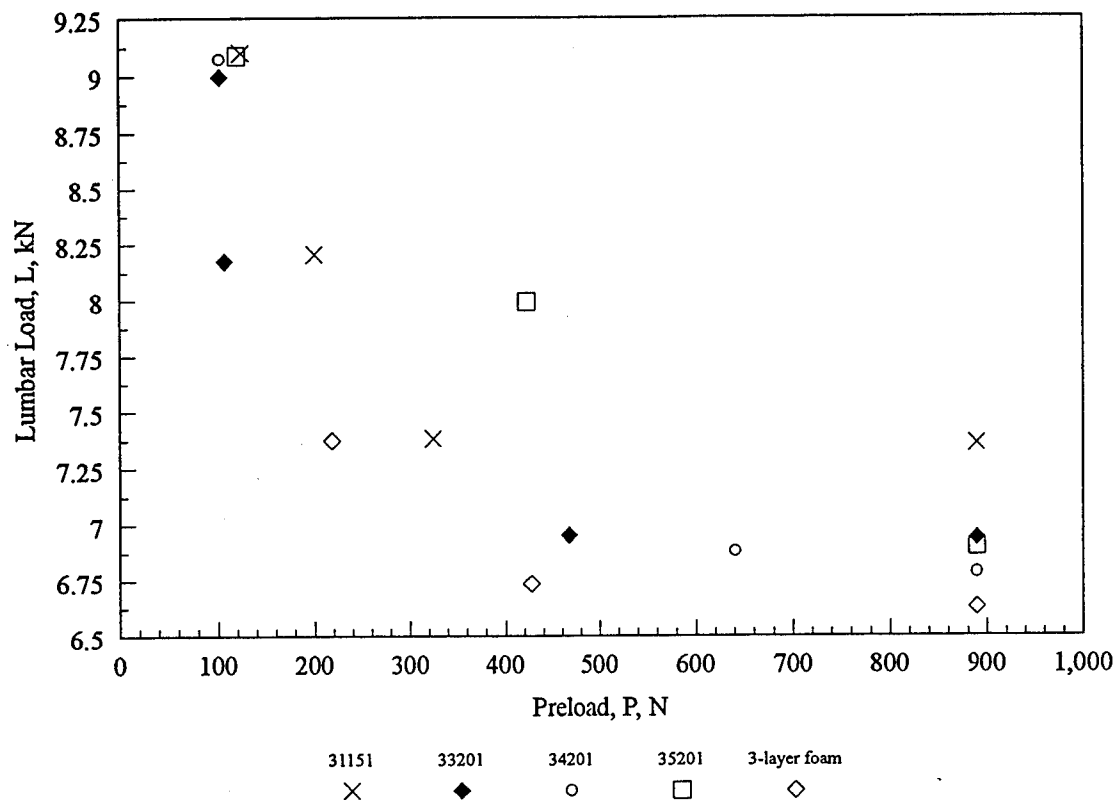


FIGURE 9. EFFECT OF PRELOADING ON THE LUMBAR LOAD

preload. The applied preload is equivalent to initial cushion deflection. At lower preload levels, approximately 100 N (22.5 lb), the results from all the cushions indicated lumbar loads higher than 9.00 kN (2024 lb). As the preload levels are increased, the lumbar load drops significantly. However, beyond 420 N (95 lb) of applied preload, there is no further reduction in the lumbar load. This amount of preload (420 N) is equivalent to a 1 g load exerted by the dummy onto the cushion at an inclined pitch angle of 60°.

The above results support the results obtained from the hydrostatic test. When the ATD is subjected to preloads, it is equivalent to a static test situation where at slower rate of loading the foam is displaced without absorbing significant amount of energy. In other words, the preload procedure is equivalent method of increasing the energy absorbing capabilities of the cushion at slower rate of loading.

The results obtained from the second series of test is presented in Fig. 10. The plot shows the variation of the lumbar load as a function of cushion thickness. Two data points representing the lumbar load were obtained for each cushion thickness. The results were then averaged and curve-fitted. As shown in the figure, a linear relationship exists between the cushion thickness and the lumbar load. With each centimeter increase in cushion thickness, the lumbar load decreases by

0.5 kN (280 lb/in). In order to obtain a safe lumbar load for a 19 g pulse, the minimum thickness of the cushion employed in the present study was 13 cm (5.12 in).

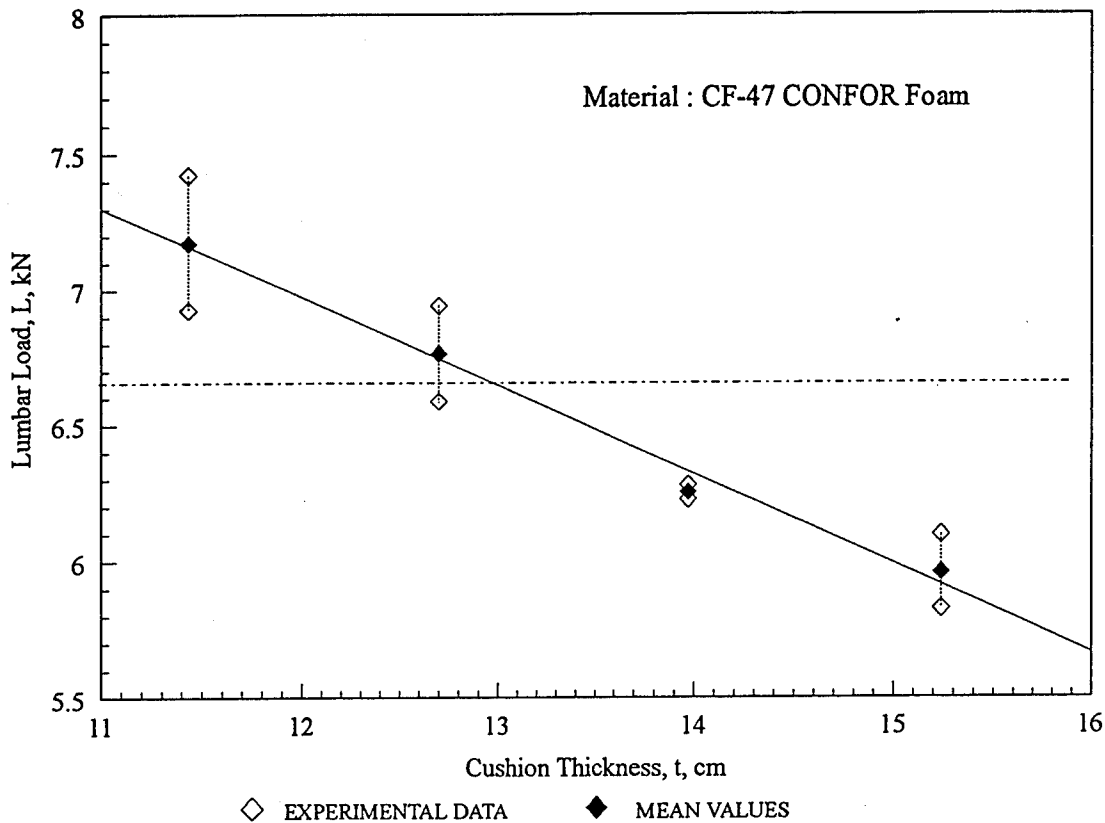


FIGURE 10. LUMBAR LOAD vs. CUSHION THICKNESS

The effects of temperature on the thermal response of the foam is presented in Fig. 11. Physical changes were observed when the foam was heated to 37.78° C (100°F). The material was much softer then at room temperature and possesses a "marshmallow-like" texture. The material recovered at a faster rate when compressed and thus was less stiffer. The test results indicated a significant increase in the lumbar load of the occupant for the elevated temperature tests. For example, the 15.24 cm (6 inch) cushion exhibited a 64 percent increase in lumbar load at 37.78° C (100° F) compared to 5.54 kN (1247 lb) at room temperature.

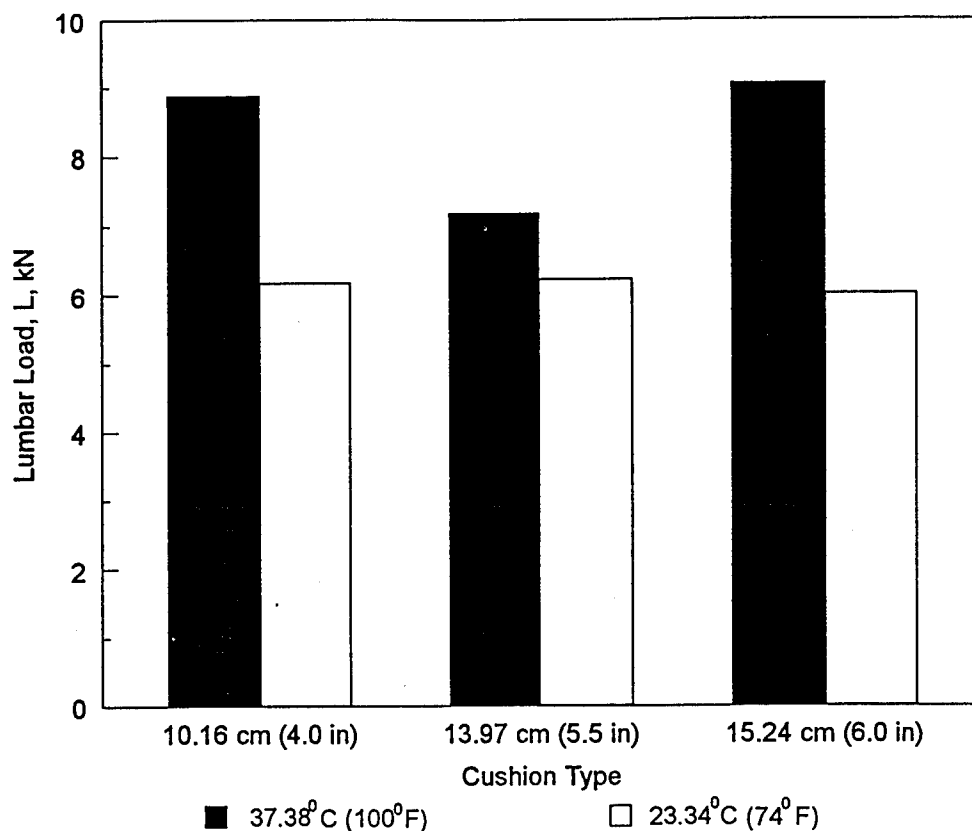


FIGURE 11. EFFECT OF TEMPERATURE VARIATIONS OF THE CUSHION ON THE LUMBAR LOAD

CONCLUSION

In the field of aircraft seat design, the goal is to work towards increasing the survivability of the occupant in a crash event. Today, all aircraft seat manufacturers must comply with rigorous legislation that focuses on many aspects of crashworthiness and safety. With higher safety standards being considered, the challenge is to better understand the dynamics of the impact mechanisms involved and to incorporate this knowledge into future aircraft seat design. The results presented in this paper establish that aircraft seat cushions play a significant role in establishing the lumbar load in dynamic seat tests.

The results further show that open celled, rate-dependent foam can be a significant energy absorbing mechanism. The data also indicate that the capability of the foam material to absorb energy is dependent on the amount of applied preload. Specifically, that the energy absorbing capacity of the foam increases with an increase in preload and this is accompanied by a reduction in occupant lumbar load. Finally, test results show that the lumbar load is linearly dependent on

the thickness of the cushion and that the potential to absorb kinetic energy is significantly reduced at elevated temperatures.

ACKNOWLEDGMENTS

This work was partially supported under FAA Contract DTFA03-90-C-00050 with Mr. Tony Wilson serving as Technical Monitor. The authors would like acknowledge the contributions of Mr. Paul Fiduccia, Executive Director of SAMA and Mr. Bill Nissley for identifying the importance of this topic. The authors would also like to thank Mike Dennis of Oregon Aero for supplying the seat cushions used in this study and the crew of the Impact Dynamics Laboratory at WSU.

REFERENCES

1. *Federal Aviation Regulations, Part 23, Airworthiness Standards: Normal, Utility, Aerobatic, and Commuter Category Airplanes*, "Small Airplane Airworthiness," U.S. Department of Transportation, adopted 1988.
2. *Federal Aviation Regulations, Part 25, Airworthiness Standards: Transport Category Airplanes*, "Improved Seat Safety Standards," U.S. Department of Transportation, adopted 1988.
3. Bernhart, W.D., *Crashworthiness Experiments: Horizontal Impact Sled Development*, DOT/FAA/CT-92/93, Federal Aviation Administration Technical Center, Atlantic City Airport, NJ, Jan 1993.
4. *SAE AS 8049, Performance Standard for Seats in Civil Rotorcraft and Transport Airplanes*, Warrendale, PA, 1990.
5. *AC 23.562-1, Dynamic Testing of Part 23 Airplane/Restraint Systems and Occupant Protection*, FAA 1989.
6. *SAE J211, Instrumentation for Impact Test*, Warrendale, PA, 1988.
7. *IMPAX ver 2.0 Reference Manual*, DSP Technology, Inc., Fremont, CA, May, 1992.

ASSURANCE OF FLIGHT SAFETY FOR THE HONDA MH-02

Etsumi Misumi
HONDA R&D CO., LTD
WAKO RESEARCH CENTER

ABSTRACT

The first flight of a research aircraft built by Mississippi State University (MSU) and HONDA was successfully performed on March 5, 1993. This paper describes mainly structural tests, from a single wing spar test up to ground vibration testing for the complete aircraft, that were conducted to assure the safety of flight. Because only one prototype was manufactured, the aircraft was never allowed to be damaged by the tests. Therefore the flight envelope was restricted to a smaller load factor than design limit load, and proof test loads were 115 percent of the operational limit load according to MIL-87221 § 3.10.6. Strength and destruction tests with test structures were also carried out for critical components such as a wing inboard torque box and a fuselage-vertical tail joint structure.

INTRODUCTION

The MH-02 is a twin turbo-fan aircraft that HONDA designed and fabricated under the guidance and cooperation of the Raspet Flight Research Laboratory of MSU. This aircraft has several marked features such as all composite airframe, forward-swept wing, large triple slotted flaps, T-tail, and engines installed over the wing. The assurance of flight safety was a very important concern during all stages of aircraft development. Very extensive work was carried out before the first flight according to a safety assurance program, the basic scenario of which is shown in Figure 1.

The safety assurance program consisted of the following four main components:

1. Verification of the design and fabrication process by experts.
2. Reliability analysis by FMEA (Failure Mode and Effects Analysis) and FTA (Fault Tree Analysis).
3. Quality control systems.
4. Ground tests.

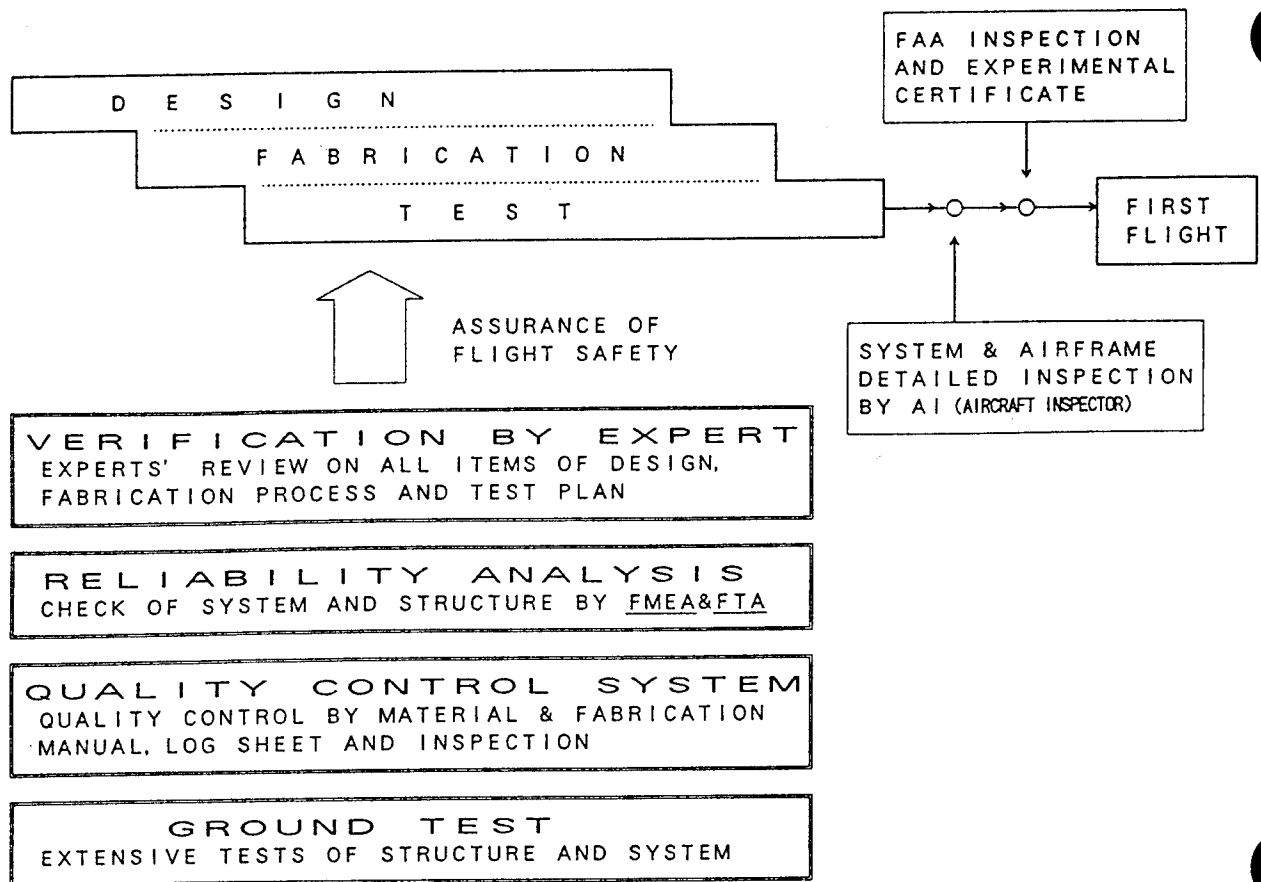


FIGURE 1 SAFETY ASSURANCE PROGRAM

VERIFICATION BY EXPERTS

The detailed and systematic review of the design and the fabrication process was conducted by MSU faculty and Designated Engineering Representatives. A verification matrix composed of all aircraft components and check points such as design loads, strength analysis and fabrication processes was prepared. All items of the matrix were checked one by one at meetings which were termed "Review Meetings". More than fifty review meetings were held until all items were confirmed as meeting the requirements of flight safety. This verification system was very effective in finding problems, mistakes, or oversights in the design and in the fabrication process. All unacceptable items were modified and fed back into the design and the fabrication process.

As a part of the review meetings, wind tunnel test data reviews were held, and the test results were evaluated to confirm the validity of the aerodynamic design.

FMEA AND FTA

These analyses were also very useful in determining problems in both the design and the assembly process of systems. FMEA was conducted first for every system part and component, and then FTA was conducted for serious failure modes. The analysis results were reflected in the design, and inspection required by the analyses was carried out after the system was installed in the airframe.

QUALITY CONTROL SYSTEM

Quality control is important in all processes of manufacturing composite structures. The following three main activities were done to produce composite structure of reliable quality:

1. Records such as material storage log sheets, autoclave cure charts, and fabrication log sheets were made. This made it possible to trace every part when a problem was found.
2. Manuals. Various kinds of work manuals were prepared. Fabrication and adhesive bonding assembly were made in accordance with the standard manuals.
3. Inspection. Visual checks, coin tapping inspections and/or NDI of composite structures were performed according to their importance level. Inspection by tag coupon testing was also conducted after autoclave cures and adhesive bonding assembly.

GROUND TESTS

Although testing takes considerable labor and cost, it is a direct and positive way to assure integrity of structure and system. For a developer with relatively little experience, testing is very effective in detecting problems that are overlooked by designers. Extensive tests of structures and systems were performed in each stage of the development.

Some structural tests are discussed below.

WING GROUP TESTS

The wing is one of the most important components of the airframe, and its fabrication started first in the MH-02 development program. Therefore a systematic test program of element, subassembly and assembly was planned and carried out to verify the validity of the composite structural design and the fabrication process. This test program is shown in Figure 2.

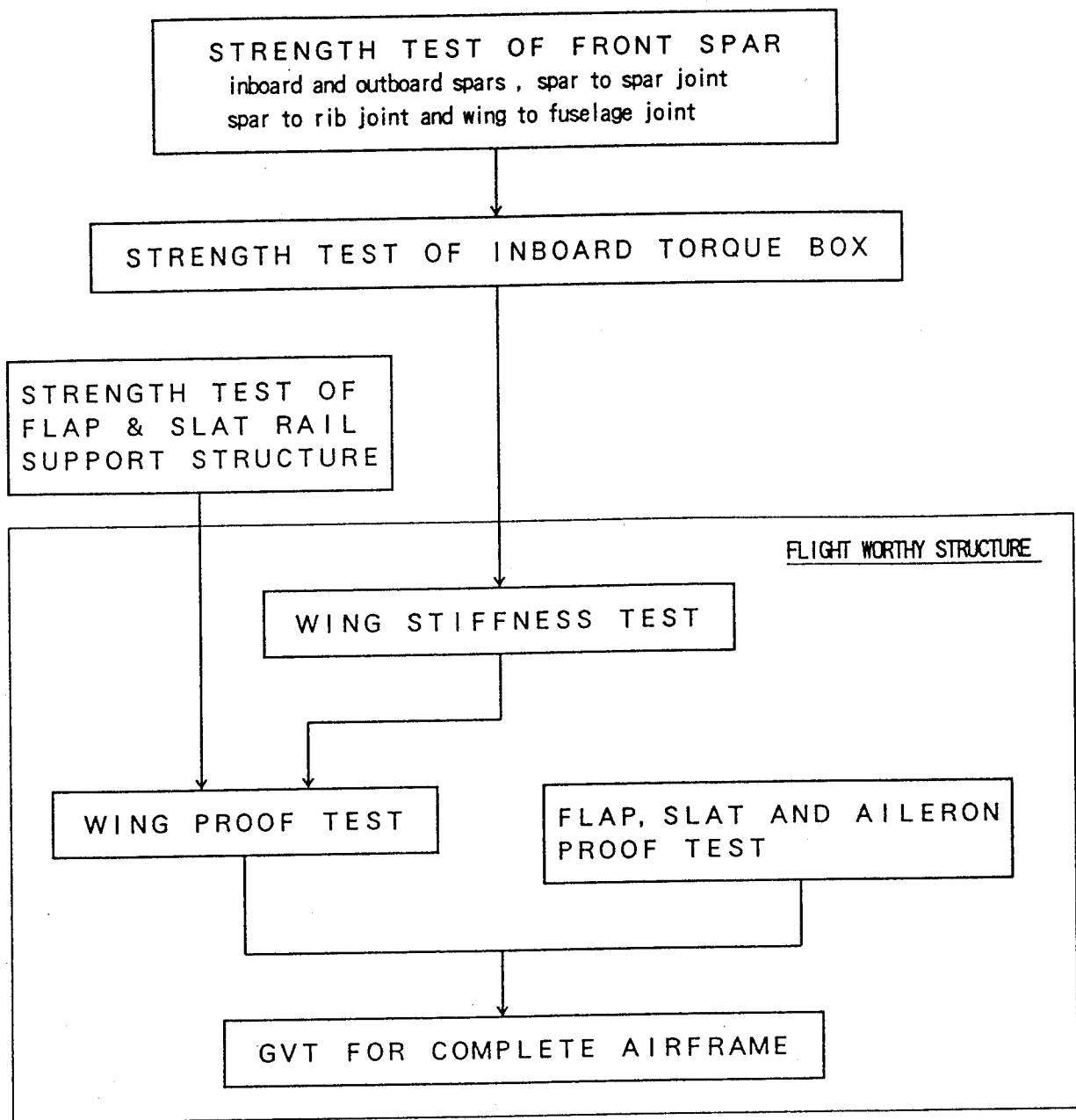


FIGURE 2 WING TEST PROGRAM

STRENGTH TESTS OF FRONT SPAR

The front spar was composed of four members, right and left outboard/inboard spars, and had several important details such as a spar-spar joint, wing-fuselage joint and inboard spar-kick rib joint as shown in Figure 3. Test spars were fabricated and tested to verify the validity of the design of these critical details before fabrication of flight worthy parts.

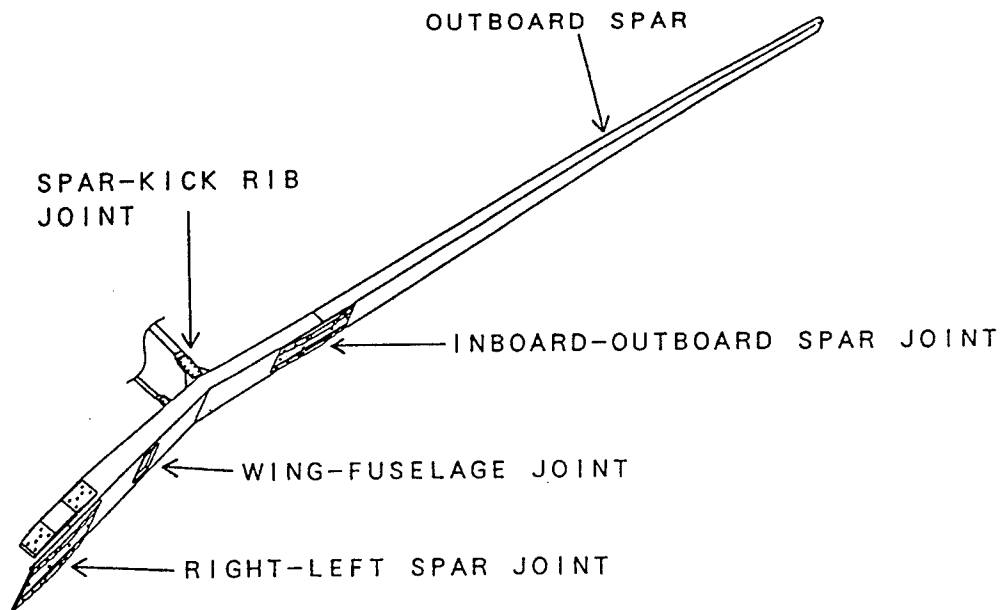


FIGURE 3 WING FRONT SPAR

The following series of tests were conducted:

1. Outboard spar strength test.
2. Inboard spar strength test.
3. Inboard spar-kick rib joint strength test.
4. Outboard spar-inboard spar joint strength test.
5. Right and left inboard spar joint strength test.
6. Wing-fuselage joint strength test.

Each test specimen was fixed in a test fixture and a concentrated load was applied to it by a hydraulic cylinder as seen in Figure 4. Deflections and strains on spar flange and web, rib, and joint metal fittings were measured.

The test results showed that each composite member and metal fitting satisfied design strength and stiffness requirements, and it was confirmed that the design and the fabrication process was appropriate.

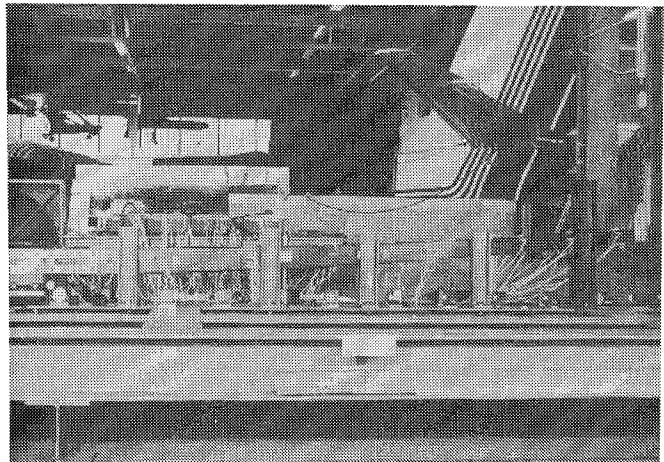


FIGURE 4 WING SPAR TEST

As examples of the test results, vertical deflection distributions and strain distributions on the outboard spar flange are shown in Figures 5 and 6 in comparison with calculation by finite element method. The measured value and the calculation show good agreement.

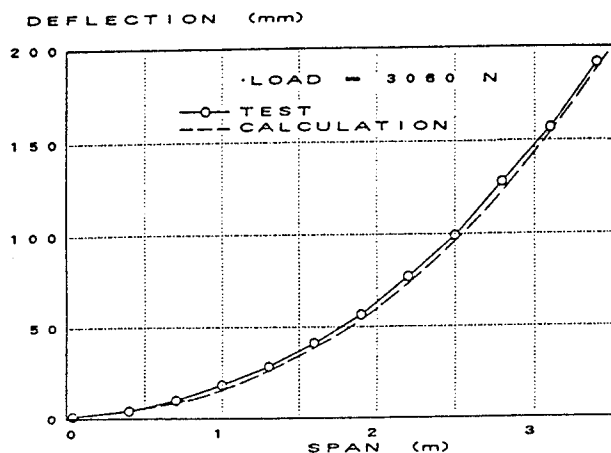


FIGURE 5 DEFLECTION OF OUTBOARD SPAR

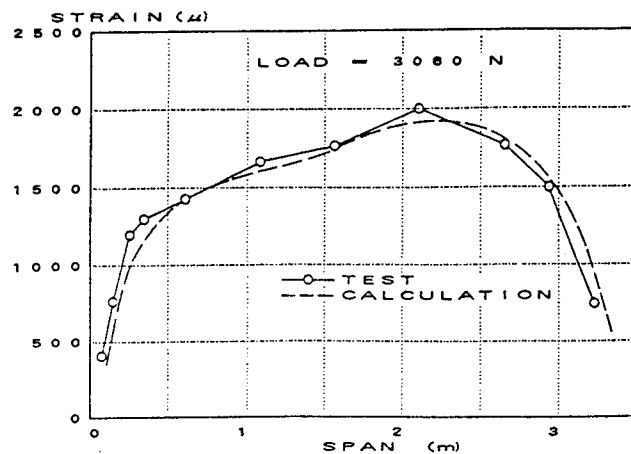


FIGURE 6 STRAIN OF OUTBOARD SPAR FLANGE

STRENGTH TEST OF INBOARD TORQUE BOX

The next step was to verify the design and fabrication process used to bond structural components. The wing inboard torque box was chosen as the test structure because it included adhesive bonding of spars, ribs, and skins, and also included critical design aspects such as spar-spar joint, spar-rib joint, wing-fuselage joint, and engine mount attachment as shown in Figure 7.

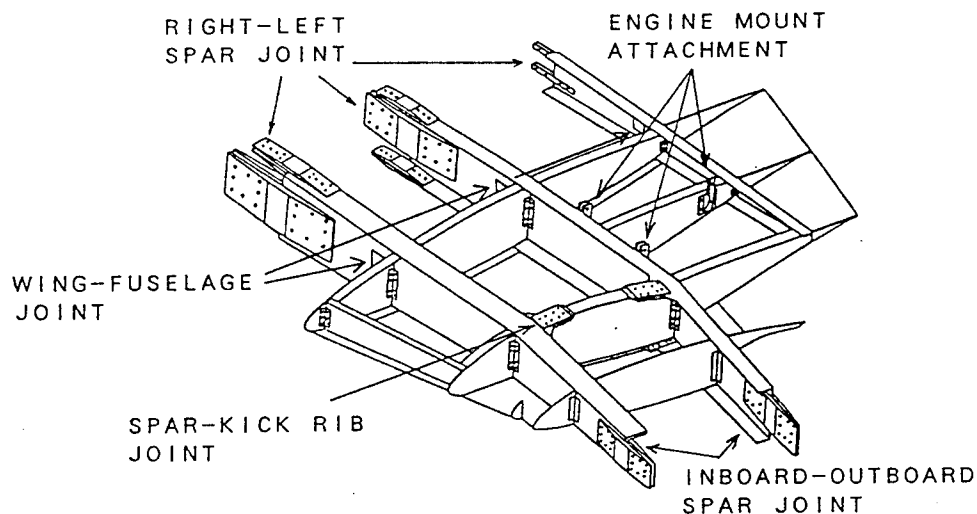


FIGURE 7 WING INBOARD TORQUE BOX

The left wing torque box was fabricated and connected to right wing dummy spars. This test structure was fixed on a test fixture through wing-fuselage joint metal fittings. Then left wing dummy outboard spars were connected to the torque box for application of a test load as seen in Figure 8. A concentrated load corresponding to aerodynamic lift was applied at the end of the outboard dummy spar. Engine thrust was also applied on the structure through the engine mount attachment metal fittings. The structure was tested under several load conditions in the V-n diagram.

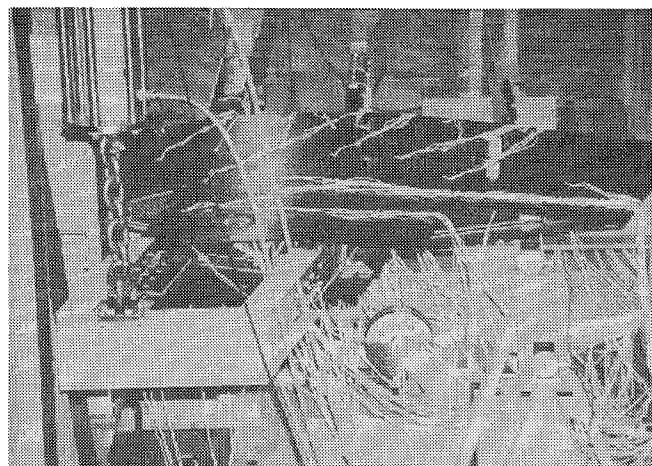


FIGURE 8 WING INBOARD TORQUE BOX TEST

Reaction forces at the wing-fuselage joint, deflections, and strains were measured. Because the strain was a major design criteria for the composite structure, about one hundred twenty rosettes and uniaxial strain gauges were bonded to each member of the structure to investigate the strain distribution in detail.

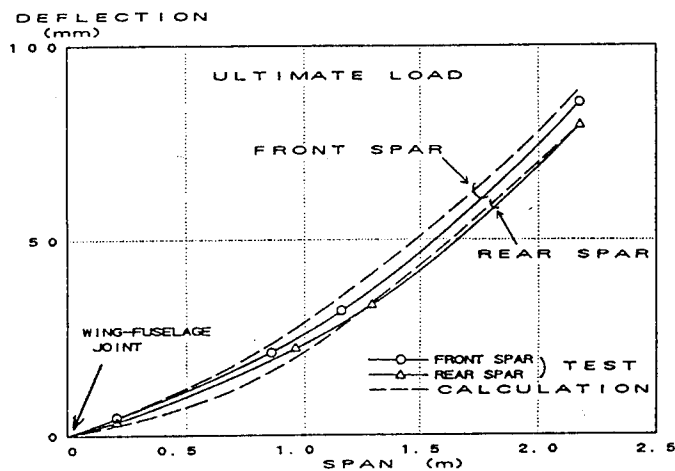


FIGURE 9 DEFLECTION DISTRIBUTION

The measured strains and deflections under limit load and ultimate load conditions were analyzed and confirmed to be within the design allowable value. An example of the measured data (vertical deflection distribution along the front and rear spars) is shown in Figure 9.

After the limit load and ultimate load tests, destructive tests were performed. The structure could withstand the load without any failures up to the ultimate load. The test load was increased gradually at a constant increment over the ultimate load. At 109% and 132% of the ultimate load, the upper skin came off locally from the front spar and rear spar caps respectively. This local failure didn't affect the strength and stiffness of the whole structure.

These delaminated sections were inspected after the test. It was observed that the delaminations occurred between the adhesive and the

inner face of the upper skin, and debonded regions were noticed at the sections where these delaminations occurred. It was assumed that the delamination was caused by the peeling stress concentration around the debonded region due to local buckling of the upper skin. This was very valuable lesson for the subsequent adhesive bonding work.

The test load was increased further after these local delaminations were observed. Almost no growth of delamination was observed until destruction of the structure. The rear spar broke first and then the front spar followed it instantaneously under 140% of the ultimate load. The starting point of the destruction was the edge of a bolt hole for the rear inboard spar-outboard spar joint. This hole was located at the most inboard and lower side, and therefore it was subjected to the largest tension load.

This test structure was fabricated in a relatively early stage of development. Many problems were encountered during the fabrication, and each of them was overcome one by one. Through the fabrication and the testing, many lessons were learned and much technical know-how and experience was obtained. This experience was very valuable in the subsequent design, fabrication, and composite quality control activities.

STRENGTH TEST OF FLAP AND SLAT RAIL SUPPORT STRUCTURE

The rail support brackets of the flap and the slat were attached to the wing spar webs. The webs were subjected to large out of plane loads due to aerodynamic forces acting on the flap and the slat. Even though these attachments were structurally analyzed and reinforced, tests had to be conducted before wing assembly to assure that the spar webs could withstand these large out of plane loads. Test spars, which had the same ply pattern as the flight worthy front and rear spars, were fabricated and ultimate load tests were performed as shown in Figures 10 and 11.

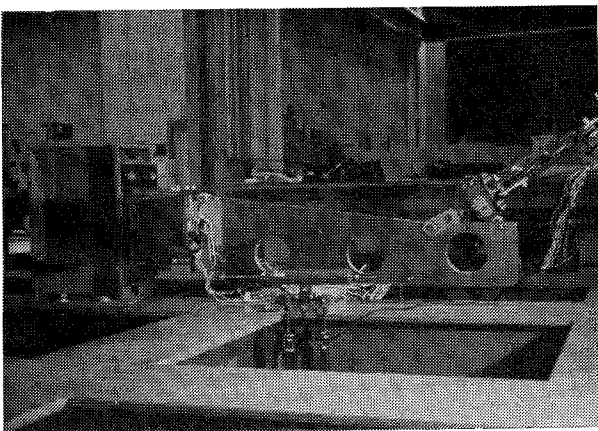


FIGURE 10 FLAP RAIL SUPPORT
STRUCTURE TEST

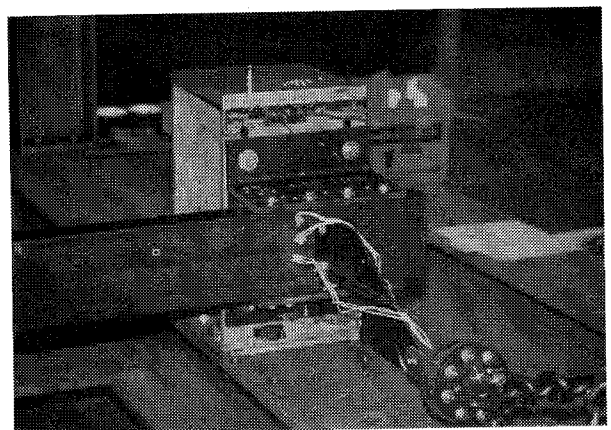


FIGURE 11 SLAT RAIL SUPPORT
STRUCTURE TEST

During the initial test very large stress concentration was found around the edge of a metal plate which was attached to the back side of the web. After the plate was modified, the test was conducted again. Integrity of the support structure was finally verified.

WING PROOF TEST

After fabrication of the flight worthy wing, a proof test was performed before its installation on the fuselage.

No full scale wing other than the flight worthy one was fabricated. Therefore it could not be damaged by the test. Because of this, the flight envelope was restricted to a smaller load factor than the design limit load factor. The proof load was 115% of the flight operational load according to MIL-87221 § 3.10.6, that is 'Any given air vehicle will be rated to have sufficient structural capability to operate up to 87 percent of the proof load strength demonstrated on that airframe'. All proof tests of other structures followed this rule.

The wing was fixed upside down on a test fixture through the wing-fuselage joints. The proof load was applied by putting cement bags on the skin as shown in Figure 12. The wing was tested for symmetrical and antisymmetrical load conditions. Measured items were vertical deflection distribution along the front and rear spars and strains on the spar webs. Rosettes and uniaxial strain gauges had been bonded to the spar webs at several sections

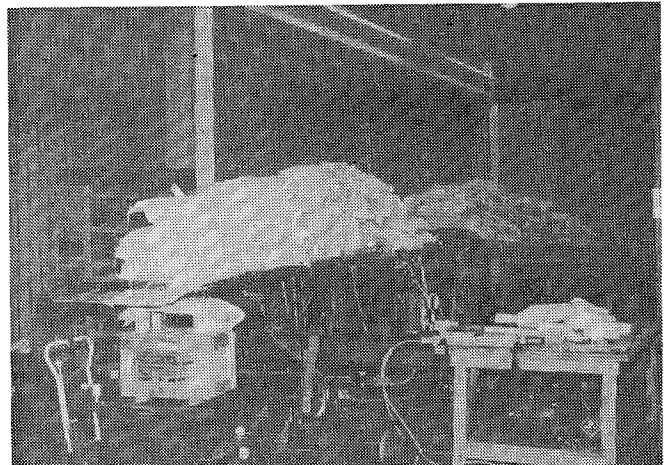


FIGURE 12 WING PROOF TEST

before the wing was covered with skins. These strain gauges were intended to be used not only in the proof test, but also in a future flight test to get the flight load distribution.

The test result showed that the wing structure was within the elastic deformation range, and it was demonstrated that the wing could carry the flight operation load.

WING STIFFNESS TEST

The following stiffness tests were conducted for the wing structure which was fixed horizontally on a test fixture through the wing-fuselage joints:

1. Shear center measurement.
2. Bending stiffness measurement.
3. Torsional stiffness measurement.

Shear Center Measurement An upward force was applied on the wing section and the torsional angle was measured. The force application point was moved chordwise and a point giving zero torsional angle was found. The measurement was conducted for eight sections to get a spanwise distribution.

Bending Stiffness Measurement The same upward forces were applied at the shear center of both the right and left wing tip sections, and the spanwise slope distribution was measured.

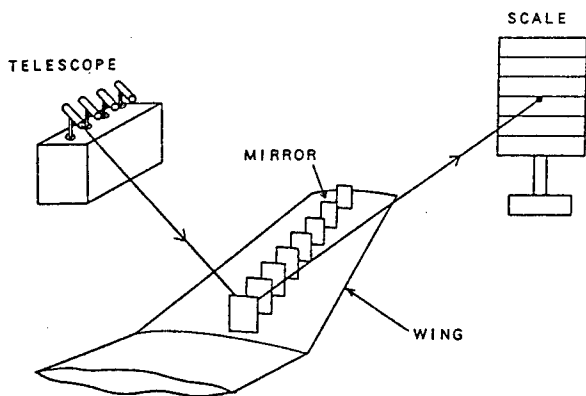


FIGURE 13 SLOPE MEASUREMENT

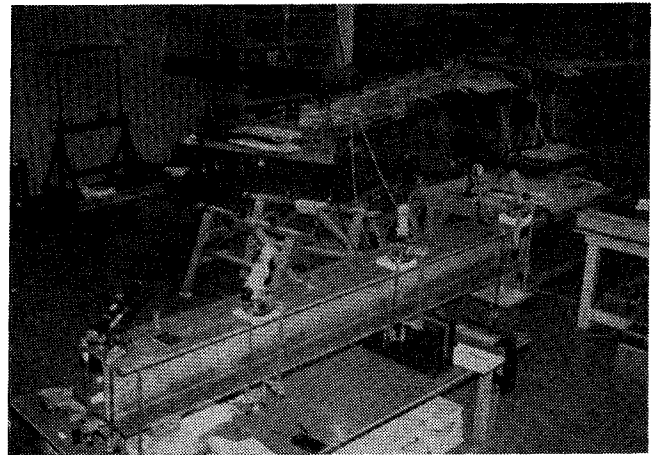


FIGURE 14 BENDING STIFFNESS TEST

The slopes were measured by using mirrors set on the upper skin as shown in Figure 13 and 14. That is, the scale reflected on the mirror was read with the telescope and the slope was calculated by the following equation:

$$\text{SLOPE } \theta = \tan^{-1} (\Delta h / 2 L)$$

Where, Δh : vertical increment of scale due to wing bending
 L : distance between the mirror and the scale along span direction

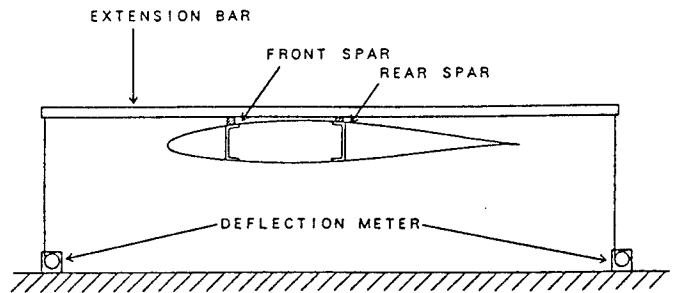
This method is primitive, but very reliable and accurate for the measurement of slopes.

Then the bending stiffness was calculated as follows:

$$E I = \frac{M t}{(\theta_{i+1} - \theta_i) / \Delta X}$$

Where, $E I$: average bending stiffness between i -th and $(i+1)$ -th section
 M_t : bending moment
 θ_i, θ_{i+1} : slope at i -th and $(i+1)$ -th section
 ΔX : span length between i -th and $(i+1)$ -th section

Torsional Stiffness Measurement A coupled torque was applied at both ends of the wing tip, and torsional angles were measured by using extension bars which amplified the angles. As shown in Figure 15, the bars were set on the upper skin through small wooden blocks on the front and rear spar to avoid the effects of local skin deformation. The torsional angle was calculated by the following equation:



$$\phi = \sin^{-1} (\Delta d / l)$$

Where, ϕ : torsional angle
 Δd : difference of vertical deflection at both ends of extension bar
 l : length of extension bar

FIGURE 15 TORSIONAL ANGLE MEASUREMENT

Then the torsional stiffness was calculated as follows :

$$G J = \frac{T q}{(\phi_{i+1} - \phi_i) / \Delta X}$$

Where, $G J$: average torsional stiffness between i -th and $(i+1)$ -th section
 $T q$: torque
 ϕ_i, ϕ_{i+1} : torsional angle at i -th and $(i+1)$ -th section
 ΔX : span length between i -th and $(i+1)$ -th section

The measured bending and torsional stiffnesses were both well over the design allowable value, so it was confirmed that the divergence requirement was satisfied. The measured stiffness data were also used in calculation of flutter speed, together with GVT data.

PROOF TESTS OF FLAP, SLAT AND AILERON

After these movable surfaces were installed on the wing, their structural proof tests and functional tests were performed.

Flap The wing was fixed upside down with a nineteen degree inclination

of the test fixture so that the vertical direction was in accordance with the aerodynamic force direction acting on the flap. The flap was fully extended, and cement bags were put on the skin as shown in Figure 16. Deflection of the flap relative to the wing and strains on the flap skin and the wing rear spar web were measured. It was confirmed that the flap structure and the flap rail support structure could withstand the proof load.

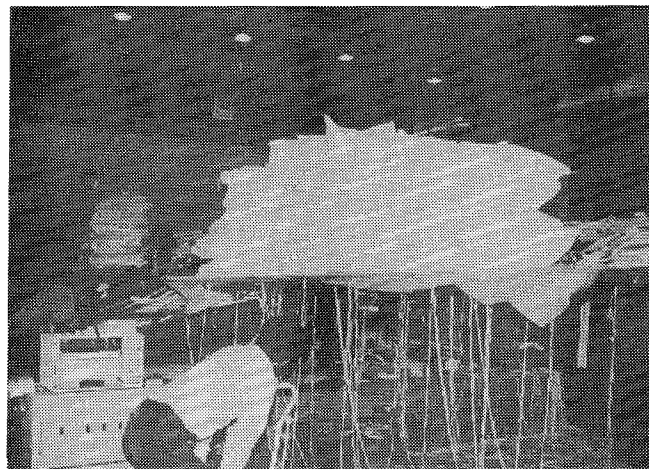


FIGURE 16 FLAP PROOF TEST

Under the loaded condition, the flap was operated by a flap motor within a short range of deflections where the cement bags did not fall. It was confirmed that the flap moved smoothly under load.

Slat The wing was fixed upside down and the slat was fully extended. The proof load was applied on the slat by using whiffle trees as seen in Figure 17. The slat structure and the slat rail support structure were substantiated to withstand the proof load.



FIGURE 17 SLAT PROOF TEST

Aileron After the wing was installed on the fuselage and the control linkage was connected to the aileron, the proof test was performed. The proof load corresponding to limit pilot force, the severest load condition, was applied to the aileron. The aileron and its support structure were confirmed to have a sufficient structural capability.

TAIL GROUP TESTS

The tail structure with its adhesive bonded assembly of spars, ribs and skins is basically identical to the wing structure, and the validity of the design and the fabrication process were already verified by the wing

spar test and the wing inboard torque box test in the early stages of the development program. Therefore detail and subassembly tests were eliminated, and only proof test and stiffness test were performed for the flight worthy structure.

The proof tests of the vertical and horizontal tails were performed separately. These structures were fixed horizontally and loaded with cement bags on the skin. An equivalent horizontal tail load was also applied on the vertical tail. A proof test of the vertical and horizontal tail connection was also performed by applying a couple horizontally at both tips of the horizontal stabilizer after its installation on the fuselage. Integrity of the structures was substantiated by these tests.

The bending and torsional stiffness measurements were also conducted in the same way as the wing. As an example, the torsional stiffness testing and its result are shown in Figures 18 and 19.

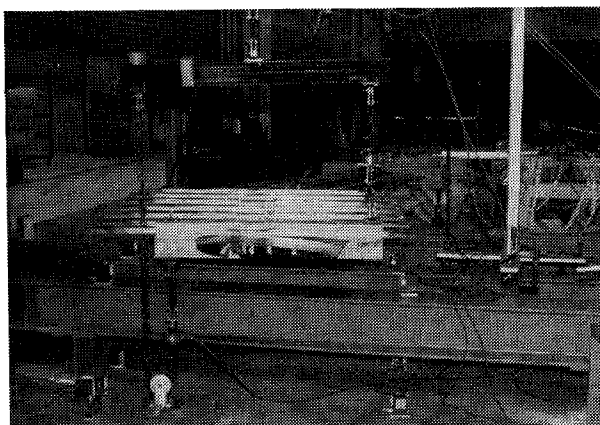


FIGURE 18 TORSIONAL STIFFNESS TEST

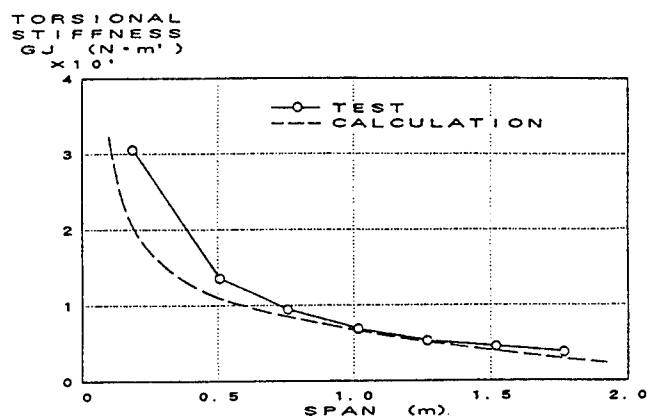


FIGURE 19 HORIZONTAL TAIL TORSIONAL STIFFNESS

FUSELAGE TESTS

In addition to extensive structural analysis with finite element models, the following tests were carried out to confirm integrity of the fuselage:

1. Strength tests of seat belt attachment structure.
2. Strength tests of vertical tail and fuselage joint structure.
3. Proof tests of landing gear attachment structure.

STRENGTH TEST OF SEAT BELT ATTACHMENT STRUCTURE

A panel insert was employed to attach the seat belt support brackets to the fuselage skin of a honeycomb sandwich panel. Destructive tests were conducted to assure that the attachment structure could withstand the seat belt tension load required by FAR part 23 (upward 3g, forward 9g, sideward 1.5g).

Test specimens of a $0.4\text{m} \times 0.4\text{m}$ (16" \times 16") honeycomb sandwich panel, with the same curvature as the flight worthy fuselage skin, were fabricated. The panel inserts were burried and fixed in the panel with adhesive, and then the bracket was attached to the panel with bolts. Three test specimens were tested by applying a seat belt tension load on the bracket as shown in Figure 20.

The bracket, together with the panel inserts, broke off from the outer laminate of the panel at a loading 4 ~ 5 times as large as the ultimate load as illustrated in Figure 21. Sufficient structural capability of the attachment structure was confirmed.

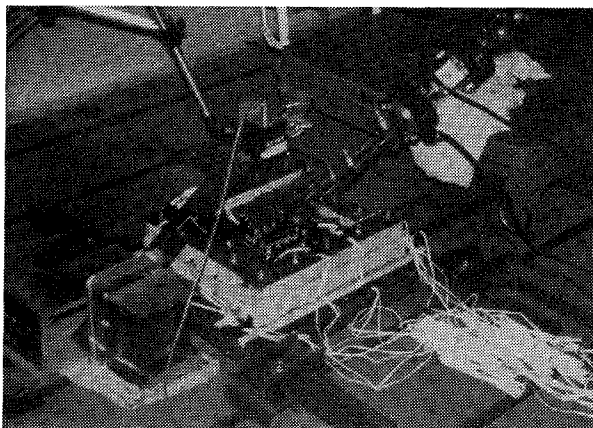


FIGURE 20 SEAT BELT ATTACHMENT
STRUCTURE TEST

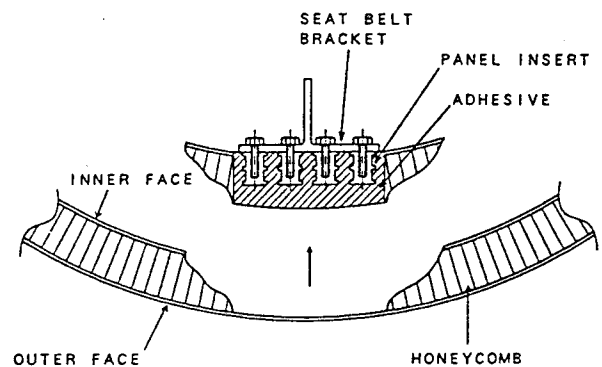


FIGURE 21 FAILURE MODE OF ATTACHMENT
STRUCTURE

STRENGTH TEST OF VERTICAL TAIL AND FUSELAGE JOINT STRUCTURE

The front and rear spars of the vertical stabilizer are joined to the front and rear fuselage frames with mechanical fasteners. The vertical tail has about a 45 degree sweep angle, and the horizontal tail is attached near the top. Any aerodynamic load acting on the vertical tail and the horizontal tail is transmitted to the frames and the skin of the fuselage through the mechanical joints. The path of the load transmission is very complicated, so it was determined that analytical calculation alone would not be sufficient to assure integrity of the joint structure.

About a 2 meter (6.6 feet) length of aft fuselage and a lower part of the vertical stabilizer were fabricated for the strength test. A steel beam was installed on the top of the stub vertical tail to apply a horizontal tail load. This test structure was turned by 90 degrees and fixed frontside down by joining a partially reinforced fuselage skin to a test base with bolts as shown in Figure 22.

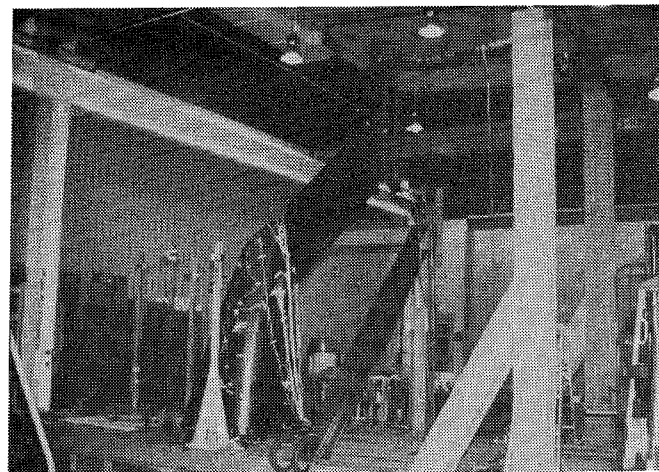


FIGURE 22 TEST OF FUSELAGE AND TAIL JOINT STRUCTURE

Various combinations of a vertical tail load and a symmetrical or antisymmetrical horizontal tail load were applied on the test structure by using hydraulic cylinders. Deflection and strain were measured during the test. After the limit and ultimate load tests, the destructive test was conducted under the severest load condition. The fuselage skin failed under 110% of the ultimate load.

The starting point of the break was located at a corner of the hole for the vertical tail rear spar. Measured principal strains around the hole are shown in Figure 23. The strain of the #2 gauge in the vicinity of the break line shows a large tension stress and a sudden increase just before the failure. After the test, the skin around the hole was reinforced on the flight worthy fuselage.

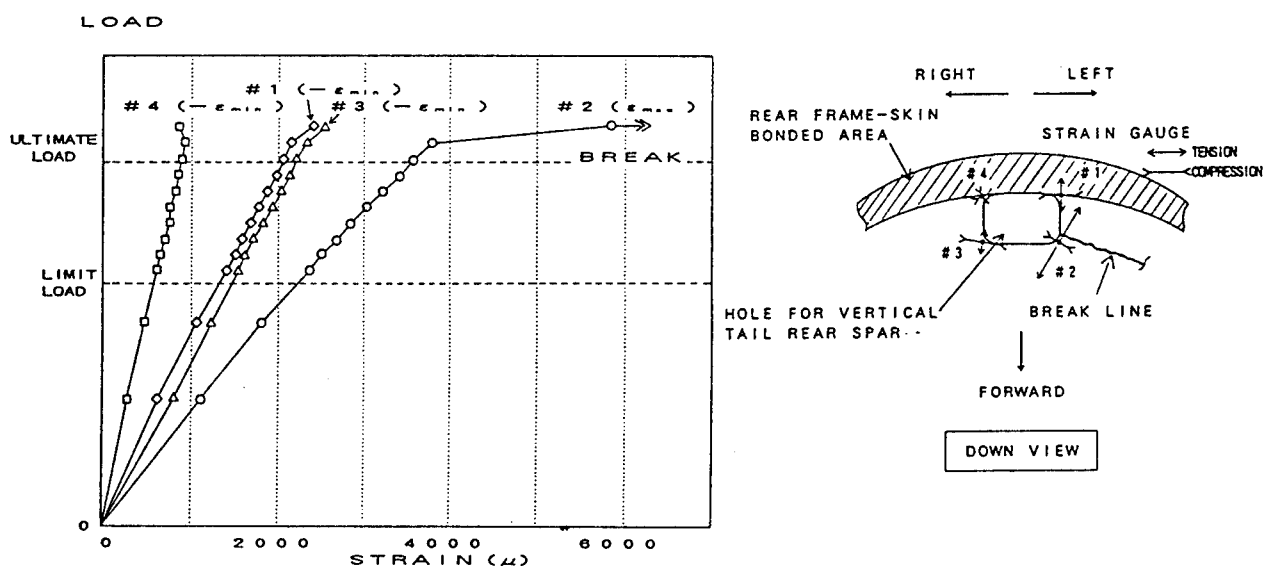


FIGURE 23 STRAINS OF FUSELAGE SKIN AROUND CORNER OF HOLE

PROOF TEST OF LANDING GEAR ATTACHMENT STRUCTURE

After installation of the landing gear on the fuselage, the static proof test was performed to demonstrate the integrity of the attachment structure. While the airframe was lifted up, three load meters were set under the gear wheels. The airframe was put down slowly on the load meters, and then the test started. As seen in Figure 24, a load was applied statically by putting cement bags on the wing and the fuselage skin and also in the cabin and baggage space. Strains were measured on the attachment structure and landing gear members. The load was applied up to 1.6 g.

The strains of the ultimate load were estimated by extrapolating the measured data. The strains on the primary structure were well below the allowable value. One of the gear members was found to have a small stress margin region, so a modification was made.

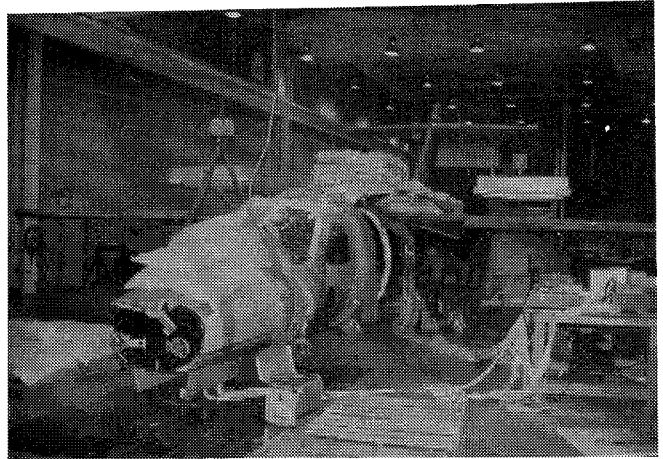


FIGURE 24 LANDING GEAR PROOF TEST

ENGINE MOUNT TEST

An engine mount must withstand several load conditions such as FAR part 23 loads (thrust, gyroscopic load,...), an impact load and an unbalance load induced by a bird strike. It also must meet requirements such as the vibration limits given in the engine installation manual. Static strength tests and extensive analytical calculations were conducted to assure integrity of the engine mount. In addition to the static tests, vibration tests were also conducted to examine validity of the bird strike dynamic load and stress calculations. After confirmation of the structural integrity, the engine mounts were installed on the wing. Vibration measurement was performed during engine run-up and it was confirmed that the vibration amplitude was smaller than the limit value.

GVT

After the completion of the aircraft, GVT (Ground Vibration Testing) was conducted to measure aircraft vibration modes and their frequencies. The airframe was excited by two shakers and the response of the structure was measured by accelerometers which were attached to the surface of the airframe. The location and direction of the shakers were changed to

get all vibration modes. The obtained data, together with the measured stiffness data, was used in the calculation of flutter speed.

By the flutter analysis based on the first GVT, it was found that T-tail flutter speed was unsatisfactorily low. The main cause was that the horizontal tail was over weight, and consequently its moment of inertia was larger than the design value. To solve this problem, an additional skin was bonded to the original skin of the vertical stabilizer, and the torsional stiffness was increased. After confirmation by stiffness measurement that the increased vertical tail stiffness met the requirement, the second GVT was performed, and then flutter analysis was conducted again. The results showed that the all mode flutter speed was above $1.2 \times V_D$.

SYSTEM TESTS

Extensive ground tests of the aircraft systems were conducted to assure their satisfactory operation in flight. The tests which were conducted before the first flight are presented below.

SYSTEM	T E S T
FLIGHT CONTROL SYSTEM	<ul style="list-style-type: none">• Elevator and rudder control linkage mock-up test.• Stiffness and functional test of control wheel and rudder pedal.• Pilot limit force proof test.
FLAP SYSTEM	<ul style="list-style-type: none">• Motor drive torque measurement.• Motor characteristics measurement.• Screw jack endurance test.• Universal joint endurance test.• Preliminary functional test.• Complete system functional test.
LANDING GEAR	<ul style="list-style-type: none">• Shock absorber drop test.• Preliminary functional test.• Gear doors operation test.• Actuator endurance test.• Landing gear proof test.
FUEL SYSTEM	<ul style="list-style-type: none">• Fuselage tank leakage and vibration test.• Mock-up functional test.• Complete system fuel flow test.
ELECTRIC SYSTEM	<ul style="list-style-type: none">• Starter generator functional test.• Wiring mock-up test.• Complete system functional test.

- | | |
|---------------|--|
| VENTILATION | • Plumbing leakage and pressure-resistance test. |
| SYSTEM & | • Pressure regulator functional test. |
| INSTRUMENT | • Sensor calibration test. |
| | |
| WHOLE SYSTEMS | • Engine run up. |
| | • Low speed taxi test. |
| | • High speed taxi test. |

CONCLUSION

To assure the flight safety of the HONDA MH-02, extensive work was conducted according to the safety assurance program throughout the aircraft development. The structural capability of each airframe component was assured by proof test. 115 percent of the flight operational limit load was used as the proof load. The stiffness measurement and GVT were also performed for the flutter analysis. The result of the analysis showed that the flutter speed was over $1.2 \times V_D$. The wing spar test and the inboard torque box test, which were conducted in the earlier stage of the development, were very useful not only in confirming the validity of the design but also in examining the fabrication process during the fabrication of the test structures. Many valuable lessons and much information were obtained and reflected in the subsequent design and fabrication of the flight worthy structure.

The verification by experts and the reliability analysis (FMEA&FTA) which were conducted as a part of the safety assurance program were very effective in finding problems, particularly in the design stage. The quality control activity was also very useful in insuring the fabrication of reliable composite structure.

ACKNOWLEDGEMENT

The author would like to express his appreciation to Dr. Albert G. Bennett, Director of the Raspet Flight Research Laboratory of Mississippi State University (MSU), Dr. John C. McWhorter, Head of Aerospace Engineering Department of MSU, Mr. Grady W. Wilson, Chief Test Pilot of the Raspet Flight Research Laboratory of MSU, and Mr. Leon A. Tolve for their advice and discussion in the design verification ("Review Meeting") and test planning & implementation.

REFERENCE

- 1) MIL-A-87221 ' General specification for aircraft structure "
 - 2) MIL-A-8867C ' Airplane strength and rigidity ground tests "
 - 3) E. Kottkamp et. al., ' Strain gauge measurements on aircraft "
- AGARDograph No.160 Vol.7, April 1976.

LIGHTNING PROTECTION TECHNOLOGY FOR SMALL GENERAL AVIATION COMPOSITE MATERIAL AIRCRAFT

J. A. Plumer
Lightning Technologies, Incorporated
10 Downing Parkway
Pittsfield, MA
Telephone (413) 499-2135
FAX (413) 499-2503

E. Rupke
Lightning Technologies, Incorporated
10 Downing Parkway
Pittsfield, MA USA
Telephone (413) 499-2135
FAX (413) 499-2503

S. Siddiqi
Analytical Services & Materials, Inc.
107 Research Drive,
Hampton, VA.
Telephone (804) 865-7093
FAX (804) 865-7309

T. E. Setzer
Stoddard-Hamilton Aircraft, Inc.
18701-58th Avenue, N.E.
Arlington, WA USA
Telephone (206) 435-8533
FAX (206) 435-9525

ABSTRACT

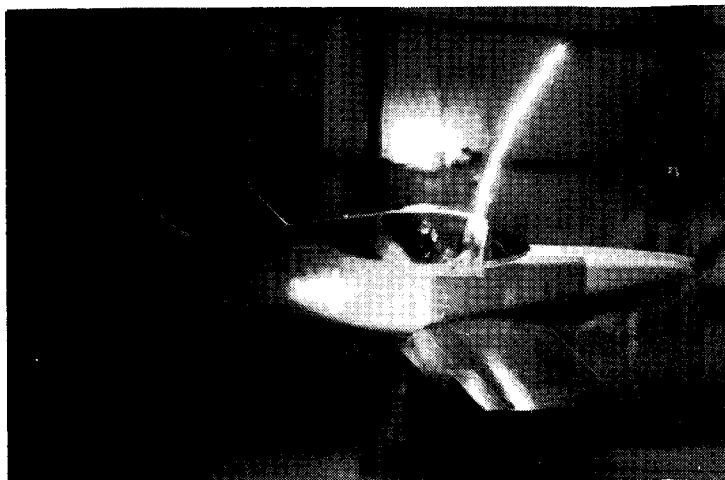
A NASA SBIR (Small Business Innovation Research) Program Phase I & Phase II design and development program produced the first lightning protected fiberglass, General Aviation aircraft that is available as a kit. The primary objective of the program was to develop a lightning protection design for the Glasair III airframe and verify its adequacy with full scale laboratory testing. The verification testing results demonstrated that the lightning protection design methodology and materials chosen provided protection for the composite material airframe from lightning puncture and structural damage associated with severe threat lightning strikes.

Another objective was to create a lightning protection design database for application to the General Aviation industry's composite material airplanes' and to enable these airplanes to meet lightning protection certification requirements.

The protection design goals achieved were to provide a Federal Aviation Administration (FAA) Federal Aviation Regulation (FAR) part 23 level of protection in the following four areas in event of a lightning strike:

1. Maintain structural integrity of the airframe.
2. Protect the occupants from hazardous electric shocks.
3. Prevent ignition of fuel vapors due to lightning strike effects.
4. Provide sufficient protection to flight critical items such as flight controls and avionics systems to allow the aircraft to fly safely and land following a lightning strike.

This paper describes the protection design approaches and development testing results, together with design methodology which was used to achieve the design goals listed above.



THE FLIGHT SAFETY NEED FOR LIGHTNING PROTECTION

Lightning is a serious flight hazard that can also occur in what was previously thought to be "lightning safe", non-thunderstorm conditions. Currently there are about 18,000 experimental category aircraft flying in the US. Approximately 5000 of these are cross-country capable composite material kit/amateur built aircraft that have no protection against lightning strikes or static electric charges that may accumulate on their surfaces during flight through precipitation or flight near a thunderstorm crossfield. There is a growing awareness of these hazards among General Aviation pilots that has come about as a result of several direct or nearby lightning strike reports or electric shocks and avionics malfunctions from static charges. Awareness has also resulted from the information disseminated by NASA and the FAA in publications as well as in aviation forums. However, the growing availability of higher performance aircraft and of sophisticated cockpit avionics enables pilots to fly longer trips often in Instrument Flight Rules (IFR) weather conditions thus increasing their hazard exposure. The most frequently practiced lightning hazard avoidance technique is the circumnavigation of active thunderstorm areas. This offers protection against well-defined storm areas, but the lightning hazard is also prevalent in what was previously thought to be "lightning safe" stratus clouds and other non-thunderstorm conditions.

Some of the better equipped IFR capable composite aircraft are equipped with Stormscopes and Strikefinder lightning strike detectors and their pilots use them to circumnavigate areas of strong electrical activity. However, the information currently available suggests that flight near or in stratiform clouds with temperatures near the freezing level, at any altitude, has a large lightning hazard potential, even though there may be little or no activity in such clouds before the aircraft enters these areas. General Aviation aircraft can routinely fly within 500 feet to 1000 feet of stratus cloud decks when operating under visual flight rules (VFR) conditions below an altitude of 18,000 feet.

FIBERGLASS AIRCRAFT SUSCEPTIBILITY TO LIGHTNING

The fiberglass skins of the Glasair and any other airplanes fabricated from this material have no electrical conductivity. Electric fields presented by approaching lightning leaders, or from the presence of the aircraft directly within the atmospheric electric field, will penetrate the fiberglass and appear around conductive parts inside, such as wiring harnesses, control rods or cables, and engine parts. The result is that the airplane still appears as a conductive object to the lightning flash, and is still "attractive" to the lightning flash. Use of non-conductive airframe materials therefore does not diminish the probability of the airplane being struck by lightning. There is a likelihood that fiberglass skins will be punctured and damaged by a lightning strike, and also by static charge that has accumulated on the exterior of the skins because fiberglass is not a perfect insulator.

This possibility was demonstrated during Phase I tests in which an unprotected Glasair fiberglass wing and a fuselage skin section were subjected to simulated lightning leaders (strike attachment tests) and punctures of both sections occurred resulting in severe damage to the structure.

LIGHTNING PROTECTION DESIGN CONCEPTS

Lightning protection design for airplanes is done on the basis of the following two principles.

1. A path with sufficient conductivity must be available on the airframe between all possible lightning entry and exit points.
2. No hazardous side effects should result due to the flow of lightning currents in the airframe.

Lightning protection must be built-in into the airframe preferably at the design stage. There is no black box that can provide airframe protection. However new hardware on the basis of new protection techniques can be retrofitted to an airframe for improving the protection for a particular component. Lightning protection design is not routine even for metal airplanes.

The airframe lightning protection method used for the Stoddard-Hamilton Glasair III airframe was expanded Aluminum foil bonded to the fiberglass surface to provide a conductive path and so prevent airframe punctures.

THE TEST PROGRAM

A layout of the simulated lightning threat test facility used by LTI is shown in Figure 1. The test voltage was applied to the airframe from an electrode positioned one meter away, an electric field was established which increased as the generator voltage rose and the air gap between the electrode and the specimen broke down. This impressed a rapidly increasing electric field between the conductive elements in the aircraft and the electrode. As the field increased, either due to the increase in generator voltage or the partial breakdown of the electrode-to-aircraft gap, corona sparks or streamers propagated from the metallic element within the aircraft. In an unprotected structure a steamer from an electrical field intensified source within the aircraft penetrated the aircraft skin to meet the oncoming streamers from the electrode. A conductive path was established allowing the high voltage discharge that caused skin punctures. For an unprotected airplane, this would happen almost everywhere on the airframe.

The purpose of the development tests done in the SBIR Phase-II project were to finalize protection design details. A complete, fully protected Glasair III airframe was then fabricated for full scale verification testing. The test airframe lightning protection verification testing was conducted in October of 1992.

The purpose of the verification tests carried out in the SBIR Phase II project was to evaluate the quality of the protection design in protecting the airplane from atmospheric lightning. This was accomplished by conducting a series of high voltage and high current tests on the full scale test airplane.

These tests were used to evaluate the response of present skin and structural materials to lightning effects, and to demonstrate the level of protection achieved in event of a severe lightning strike.

The direct effects verification test criteria were as described in SAE Committee AE4L Report, "Lightning Test Waveforms and Techniques for Aerospace Vehicles and Hardware," dated June 20, 1978, and US Mil Standard 1757. This criteria is also reproduced in the Users Manual for FAA AC 20-53A. Atmospheric measurements established a conservative design maximum current limit of 200,000 amperes. Indirect effects evaluations was based on criteria of FAA AC 20-136. These criteria relate to protection of electrical and avionics systems from the indirect effects of lightning.

1. Antenna Protection

Two methods of antenna protection were tested:

1. Dielectric film, adhesively bonded to the interior surface of the aircraft between the skin and antenna.
2. Segmented diverters which were installed on the exterior surface of the aircraft in close proximity to the antenna locations.

Segmented diverters are plastic strips on which a row of small metal segments are fastened and separated by a short distance, or gap. Typical gaps range from 0.005 - 0.010 in. Radio frequency (RF) waves to pass through the gaps unimpeded. During a lightning strike, the intense electric field causes sparks to form between the segments, thereby creating a continuous electrically conductive path which guides the lightning flash along these diverters that were on the non-conductive surface of the aircraft to an external conductive skin or other object.

Testing revealed that the segmented diverters proved more effective in preventing punctures of the aircraft skin than did additional layers of dielectric, although the latter approach was not fully developed.

2. Conductive Paint

Strike attachment tests conducted on the skin panel specimens finished with carbon loaded paints, presently being used to prevent ultraviolet radiation from degrading resin, revealed that insufficient conductivity exists in the carbon loaded paints to prevent punctures of the skin specimens.

3. High Current Testing

The lightning tests were conducted using aircraft industry standard lightning test criteria and methods, since the in-flight lightning environment is the same regardless of aircraft size. This criteria 200,000 amperes maximum design limit represents a severe, but not the most severe lightning strike. It should be noted here that the smaller the airplane, the higher the densities of lightning currents in conductive portions of the airplane. The task of protection design is, therefore, potentially more challenging for a small airplane such as the Glasair, than it is in a large transport airplane or in a typical twin or business jet airplane.

High current physical damage tests, were done to simulate the flow of severe currents through the airframe by lightning leaders or the high voltage attachment tests. In unprotected structure, this damage is mostly the result of intense blast pressures contained within the punctured skin or other airframe component.

In Phase I, high current physical damage tests were conducted on two unprotected fiberglass specimens which included a complete owner-built wing and a single skin panel. The skin panel tested were representative construction of the sides of the fuselage or of the wing skins. The two specimens suffered extensive physical damage as a result of the high current tests; which may have been catastrophic had the damage occurred in flight.

Intense over pressures associated with stroke currents inside composite structures were sufficient to fracture, debond or delaminate large areas, in some cases resulting in loss of air worthiness.

Evaluation of the test results conducted in the Phase I demonstrated that lightning strikes can extensively damage unprotected fiberglass skins and structures as well as internal metal hardware such as control rods, antennas and wiring harnesses. Since the pilot is frequently in contact with these elements, the possibility also exists for severe electric shock physiological hazards.

The lightning strike damage evaluations were conducted on typical fuselage and wing skin sections fabricated of fiberglass sandwich configurations with foam cores. Fiberglass and carbon fiber composite (CFC) empennage skins were tested, along with a full scale fiberglass wing, complete with internal metal components such as control rods and antennas.

Typical Glasair fiberglass structures protected with one exterior layer of expanded metal foil or mesh, typically 0.003 - 0.006 in. thick, were capable of sustaining full threat lightning currents with little or no damage. Several approaches for conducting lightning currents across manufactured and owner-built joints and splices were proven by verification testing to be successful. Candidate protection materials and devices that were examined in detail in the protection development testing of Phase II were as follows:

- Woven aluminum meshes
- Expanded aluminum and copper foils
- Thin, conformal shield foils based on printed circuit technology
- Metal bonded, electrically conductive paints
- Segmented-type diverter strips
- Dielectric films

SUMMARY OF PHASE I TEST RESULTS

The strike attachment tests demonstrated that lightning leaders may puncture non-protected fiberglass skins and attach to electrically conductive hardware inside the aircraft, such as antennas, electrical wiring harnesses, control rods, and avionics equipment. The high current tests demonstrated that lightning stroke currents may cause extensive damage to fiberglass skins due to the high pressures associated with lightning channels within the airframe. Punctures and delamination of fiberglass skins are possible, along with debonding of adhesive joints and rupture of seams due to excessive over pressures. The fact that much of the airplane may be fabricated of non conductive material, such as fiberglass, does not make it less likely to receive a lightning strike than an all-metal aircraft since, as noted earlier, as the lightning leader approaches, the rapidly increasing electric field induces sparks, called streamers, from the internal conductors, and these propagate outward to intercept the leader, puncturing the on conductive skins. The leader currents themselves are of low amplitude and will often leave only a pin-hole in a fiberglass skin, but if the lightning current intensifies, and the first return stroke uses the conductive path established, damaging pressures are reached.

The Phase I tests demonstrated that nearly all fiberglass surfaces of small composite airplanes can be punctured. These included the fuselage, wing, and empennage skins.

The high current tests demonstrated the extent of physical damage that severe lightning stroke currents may inflict on unprotected structural components. Some of this damage, at least, would cause severe structural damage, at least, would cause severe structural damage and destroy the air worthiness of the airframe.

THE PHASE II PROTECTION DESIGN VERIFICATION TEST PROGRAM

The purpose of the Phase II program was to explore in detail the promising approaches identified in the Phase I study. This involved a detailed design, fabrication, and verification program on a Glasair III airframe with all relevant systems and equipment installed. Thus, protection was provided not only for the airframe and skins, but also for flight safety related systems and components within. The airframe was completed in September of 1992 at Stoddard-Hamilton and shipped to Lightning technologies, Inc. where it underwent an extensive series of full and reduced scale lightning direct and indirect effects tests in October of 1992. The design of a lightning protected Glasair III kit (to be called the Glasair III LP) was finalized by, Stoddard-Hamilton and Lightning Technologies, Inc., the protection design guidelines database should be useful for protecting other small composite airplanes.

The lightning protection design solution adopted began with metallized exterior skins of the airplane with expanded aluminum foil. Nearly the entire exterior surface was metallized, to prevent skin punctures and to provide adequate electrical bonding among protection plies of foil. Considerable effort was expended to design electrical bonding methods that can be implemented reliably by the kit builder.

Protection of internal systems and components has been accomplished by a combination of the following approaches:

- Electrically **insulating** components which the pilot comes in contact with (i.e. control rods, cables) lightning current conductors, such as the exterior skin.
- Electrically bonding other components, such as pedals, control pedestal, instrument panel and pilot's armrest (which also encloses control system components) together so as to create an equipotential plane surrounding the pilots.
- Electrically insulating other systems, such as fuel tanks and fuel quantity sensing probes, from lightning current paths to prevent arcing or sparking from these currents.
- Use of traditional methods bonding, shielding and surge suppression for protection of flight critical electrical and avionics components.

- Careful attention to insulation of the pilot's upper body from contact with airplane exterior conductors, such as aluminum foil, by providing insulating barriers, covers, interior finish and upholster panels and replacing traditional metal fittings with non-conducting plastic parts. This latter approach required considerable attention to detail and completeness, as the pilots are in such close proximity to the airframe in such small airplanes.

Integration of flight control and landing gear hydraulics into the airframe requires a design approach that prevents hazardous current flowing from these items to the cockpit. Instead, lightning currents was transferred from the control surfaces to the airframe via the hinges. Insulating segments in the control rods and cables were designed to prevent currents from following these paths to the cockpit. This approach was also be followed for the landing gear installation. Here, lightning currents must follow the struts and trunions to fuselage frames or spar webs and not be allowed to flow in hydraulic lines or actuator cables that enter the cockpit.

ELECTRICAL AND AVIONICS

The first step in protection design for the Glasair III electrical and avionics systems was to provide an airframe which prevents direct strike effects from entering or damaging electrical components or interconnecting wiring harnesses. This is one of the objectives of the airframe protection design effort. Protection of the airframe from direct strike effects does not, however, eliminate indirect effects, which sometimes cause induced voltage transients of sufficient magnitude to damage or upset solid state electronic components. Protection of all of the electronic components from damage or upset may require that much of the interconnecting wires be enclosed within shields also and that some of the equipment itself be fitted with transient protection devices, a modification that may not be practical for some of the electronics. Instead, emphasis was placed on protection of the following systems/equipment which were considered essential for continued safe flight and landing of the Glasair. The items in this flight essential list are shown in Table 1.

Table 1 ELECTRICAL/AVIONICS SYSTEMS REQUIRING PROTECTION

Electrical power generation & distribution	Digital Engine Instruments & Display
Electric Gyroscopic Rate of Turn Indicator	Mode C Transponder
Gyroscopic Attitude Indicator	Vertical Speed Indicator
A typical Radio (or GPS + Nav & Comm)	Airspeed Indicator
Audio Panel/Intercomm	Altimeter
Autopilot Control Panel and Servo	Gyroscopic Heading Indicator

Solid state cockpit instruments have recently become available of this class of aircraft. The manufacturers of this equipment were contacted to ascertain the degree of hardness (if any) incorporated in its design, and the possibilities of modification to incorporate surge protection devices such as zener diodes, and Metal Oxide Varistors (MOVs) in the equipment. This, of course, was a longer range solution not likely to bear fruit within the time period of this program.

Other protection methods were employed to reduce the magnitudes of lightning-induced transients reaching the equipment. These methods include installation of equipotential planes to minimize potential differences throughout the aircraft, and shielding of electrical wiring harnesses associated with the equipment and systems listed in Table 1.

Evaluations of lightning current effects on internal components and digital avionics systems were done in the Phase II program. It was clear that currents of this magnitude, if allowed to flow unrestricted among internal conductors, would cause extensive damage to such items as flight controls, electrical/avionics, and fuel system components. The results of extensive development testing were applied in the design and manufacture of the full scale test airframe.

VERIFICATION TESTS

These tests were conducted to verify the protection goals listed in the Abstract. Since each of these is related or dependent to some extent on the others, protection verification depends on tests of a complete, fully equipped airframe, and integrated systems and components.

Testing a complete, protected full-scale aircraft is rarely possible due to test facility limitations and availability of an aircraft for such a test, even if one could be conducted. Aircraft return circuit lengths that are large present excessive impedance so that full levels cannot be applied. Smaller composite aircraft do, however, permit test facility programs with full threat test voltages and currents application. A complete lightning protected Glasair airframe with wiring harnesses, control systems, and representative equipment installed was used in these verification tests. Examples of the systems/equipment that were included on the verification test airframe are shown in Table 1. Figure 2 shows the verification testing entry and exit locations of the high currents.

Adequacy of human protection was tested on a buildup basis, beginning with measurements of voltage potentials between pairs of conducting objects that an occupant might be in contact with, such as rudder pedals and control column, or in the intercom and headphones. The same approach was utilized successfully during protection tests of the NASA F106B flight research aircraft prior to thunderstorm penetration flights. After the voltage differences were established with confidence and protection of the cabin against direct effects (i.e. skin or canopy puncture) were verified, a dummy was placed in the cockpit during further tests. This test also started at low levels and progressed upward on a step-by-step basis.

The specific objectives of the Phase II program did not include complete protection of all of the cockpit avionics components against damage (i.e., component burnout or malfunction) or upset (erroneous displays or commands.) Much of the avionics currently employed in small composite aircraft does not have inherent immunity to lightning induced transients. Integration of lightning protection at the equipment (box) level will be accelerated by the increased interest in lightning protected equipment from aircraft owners and operators, and the availability of airframes with sufficient protection to prevent massive burnout of electronic equipment.

The verification tests were successful, the test full scale Glasair IILP airframe withstood severe threat level lightning strike in the laboratory facility without damage to the structure or to the IFR flight capable avionics that were operating under electric power during the testing. The four SBIR project goals listed in the abstract were achieved. The final report will provide detailed test results along with details of the protection design technology.

ACKNOWLEDGMENTS

The authors wish to acknowledge the support of the NASA Langley Research Center of this program under the Small Business Innovation Research grant NAS1-19316 awarded to Stoddard-Hamilton Aircraft, Inc.

The authors will also like to credit the engineering design work contributed by the following SBIR project team members: Bob Gavinsky, Chief Engineer, Stoddard-Hamilton Aircraft and Norman Crabill, Aero Space Consultants. The authors are also grateful for the program guidance provided by NASA Langley Research Center personnel especially Mr. Joseph Stickle and Mr. Bruce Fisher.

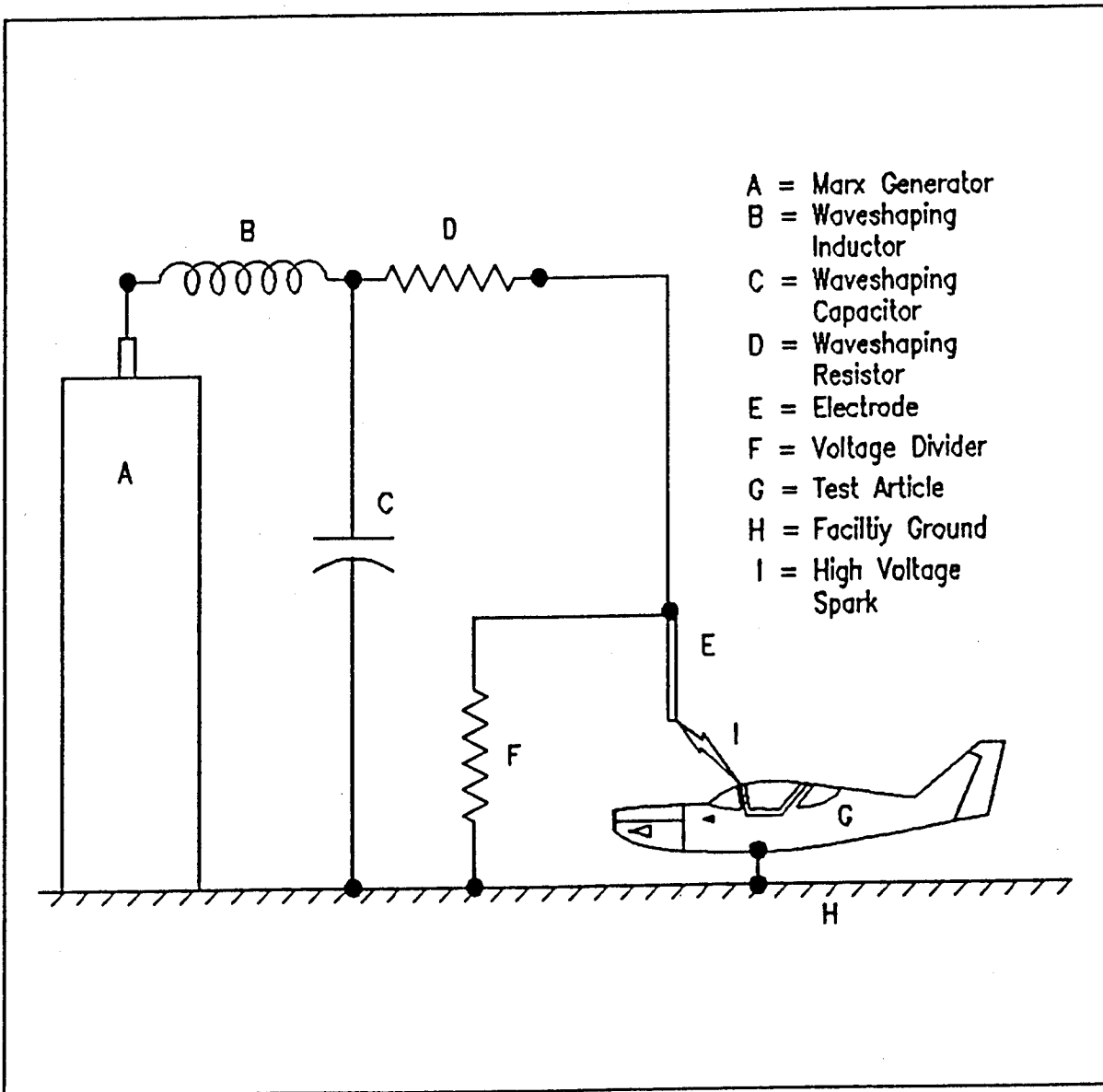


Figure 1. Lightning Technologies Inc. Test Facility Layout

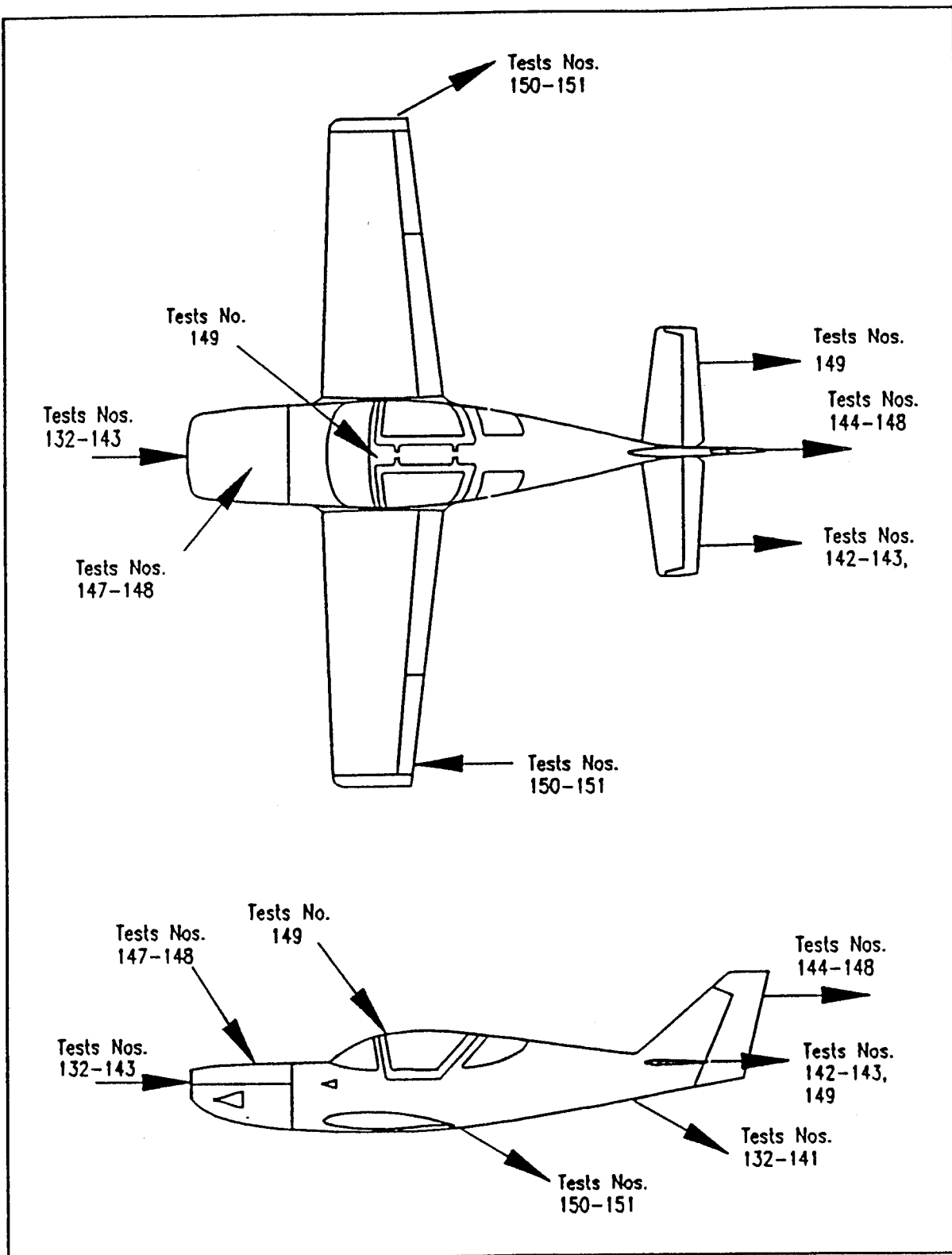


Figure 2. High Current Testing Entry and Exit Locations on the Glasair III

BOX-AND-BEAM CARRYTHROUGHS OF THE RP-SERIES COMPOSITE SAILPLANES

Brian E. Thompson, Sean Doyle, Volker Paedelt, and Olivier Bauchau

Department of Mechanical Engineering, Aeronautical Engineering and Mechanics
Rensselaer Polytechnic Institute, Troy, NY 12180-3590

ABSTRACT

The Rensselaer Composite Aircraft Studio has produced three composite aircraft over its seventeen year history and has given students invaluable practical experience, knowledge of aircraft, and skills for engineering aircraft with composite materials. An important objective has been the evolution of pedagogical schema to integrate large-scale aircraft projects into the Rensselaer Engineering curriculum. The program began with RP-1, an open cockpit, single seat glider, followed by RP-2 which was an enclosed cockpit, single seat medium performance sailplane. First flight of RP-1 and RP-2 were in 1980 and 1985, respectively. Engineering and fabrication of RP-3 which is a two seat medium performance sailplane nears completion and its first flight is expected in 1995. Increases in size of the RP-series aircraft have increased complexity of the aircraft structure, and the subject of this paper is the progression of design of RP-series carrythroughs. RP-series aircraft join wings and fuselage with box-and-beam carrythroughs. RP-1 has an interference-fit, box-and-beam configuration to transfer forces between wings and fuselage. RP-2 repeated this configuration but the carrythrough failed during static testing due to peeling of the capstrips of the box at ninety-five percent of design load. Because of this failure the RP-2 carrythrough was redesigned with clearance between box and beam and with two pins transferring loads, and this redesign was adopted for RP-3. The RP-1, RP-2 and RP-3 carrythroughs and associated flight-worthiness tests are presented here and their implications for design pedagogy and aircraft design are discussed.

1. INTRODUCTION

The Rensselaer Composite Design Studio has produced three composite aircraft and has developed from an independent project into an integrated studio course in the Rensselaer Engineering curriculum. These aircraft were designed and built by over 1000 undergraduate and graduate students from Mechanical Engineering, Aeronautical Engineering, Physics, Chemistry, Computer Science and Materials Engineering. A feature of the studio is its faculty-student team approach that encourages students to learn from experienced practitioners from a variety of disciplines each with their own expertise and approach. The program has focused on three main objectives: to attract engineering students into the study of composite materials and aircraft design; to explore the challenges of applying composite materials in aircraft; and to mentor student development in an industrial-like setting in preparation for careers in the aircraft industry. Students obtain practical, supervised, hands-on laboratory and design experiences, and are taught to perform in complex, multi-year, multi-phase projects in a manner which complements and motivates their academic coursework.

The design of carrythrough structures for RP-series aircraft has been a critical and challenging problem, and associated engineering practices have evolved as the RP-series program progressed from building light gliders to two-pilot sailplanes. This paper presents a history of RP-series carrythroughs and places emphasis on lessons-learned with RP-2 and the application of those lessons in the RP-3 aircraft. The following section presents a brief history of the RP-series aircraft and Section 3 outlines the design

motivations for the RP-1 carrythrough. Section 4 presents the initial and redesigned RP-2 carrythroughs with emphasis placed on the knowledge gained from RP-2 static and flight tests. Section 5 follows with a description of the functions and design of the RP-3 carrythrough structure and the combination of test results that support its flight worthiness. The paper closes with remarks on advantages and limitations of the box and beam approach used for RP-series carrythroughs.

2. HISTORY OF THE RP-SERIES AIRCRAFT

The first aircraft RP-1, was a single-pilot, open-cockpit, lightweight glider shown in Figure 1. Salient dimensions and weights are shown on Table 1. RP-1 was an all-composite aircraft and featured Kevlar and carbon fiber construction for an empty weight of 110 pounds. It first flew in 1980 and was donated after approximately 60 flight hours to the Empire State Aerosciences Museum for display as the first student-built, all-composite glider in the United States.

The RP-2 is a more ambitious single-pilot and all-composite sailplane which featured an enclosed cockpit and moderate aerodynamic performance. Flight tests demonstrated a minimum sink rate of 1.7 ft/s at 42 mph and a maximum 28:1 glide ratio at 38 mph for its empty weight of 270 lb. Figure 2 shows a photograph of RP-2 during one of its first flights in 1985 and Table 2 provides its dimensions, wing loading and weights.

Figure 3 shows the RP-3 aircraft layout which is in preparation for static and flight tests in 1995. The overall dimensions of RP-3 are on Table 3 and its empty weight is expected not to exceed 650 lb which is almost 6 times the weight of the RP-1 aircraft. RP-3 features side-by-side seating, expected glide ratio of 33:1 at 51 mph, and a significant increase in complexity from both RP-1 and RP-2.

3. THE RP-1 CARRYTHROUGH

RP-1 was designed as a lightweight foot-launch glider with an empty weight of 90 lb. Emphasis in its design had to be placed on minimal weight of all aircraft components to allow foot-launch. Because the carrythrough represents a significant fraction of its empty weight, the primary design priorities for the RP-1 carrythrough were lightweight, simplicity, separability so wings can be removed for storage and transport, as well as load transmission. The optimum carrythrough for this configuration was chosen to be the interference-fit box-and-beam design that is shown in Figure 4¹. This design features a carrythrough which has no bulkheads associated with its structure, and is called "free-floating." The design is based on strict separation of load paths where the carrythrough transmits only wing bending loads, while the torsional loads, forward yaw moment and fuselage-wing attachment are transmitted through four torsion pins, located at the leading edge and trailing edge of the wing-root rib. In addition, one pin holds the box in the beam and carries negligible load. The RP-1 was successfully static tested with a 4g static load prior to its approval as an experimental aircraft and subsequent successful flight tests.

4. RP-2 CARRYTHROUGH

After many successful flights of RP-1, the RP-2 carrythrough was designed by copying the RP-1 configuration although with the minor changes shown on Figure 5 that include the addition of swivel bearings for the torsion pins and the relocation of torsion pins closer to the carrythrough to accommodate the primary fuselage structure. This box-and-beam, interference-fit concept was again chosen for its lightweight, appropriateness for the low design loads in RP-2, and because of the experience gained in

design, analysis and fabrication of the similar RP-1 structure.

Two static tests were performed on the RP-2. First, pure bending was tested with the airplane loaded to 4g with 1680 pounds of dead weight that was distributed in 10 pound sand bags to simulate an elliptic lift distribution. This loading resulted in a slight permanent set, drooping the wing tips of about 0.28 inches after unloading. This test demonstrated structural integrity of the box and beam in pure bending.

The second test was a bending-twist test for 4g loading. This test again required a total load of 1680 pounds but weights were placed at the wing's aerodynamic center, resulting in both bending and twist in the structure. When the load reached about 840 pounds the rear torsion pins were observed to slip in the fuselage bushing that resulted in small forward rotation of the wings. Loading was continued and the carrythrough structure failed at ninety-five percent of the anticipated maximum test load. Figure 6 shows the damaged wing. Figure 7 details the top capstrip peeling off the box side. Initial failure analysis focused on the wing pin slippage, as this slippage would have stressed the sides of the box with torsion loads that were designed to be taken by the torsion pins. The actual loading of the test were not considered in the design of the box and failure may have been due to shear flow that exceeded design specifications and caused the secondary bond and graphite wraps to fail at the discontinuity at the box corners: this mechanism would have resulted in the observed peeling of the capstrips. However, further damage occurred when the wings collapsed after the carrythrough broke and it could not be established if this was either the root cause or the only failure mechanism. Failure could also have been due to damage during assembly, stress concentration at the tip of the beam, or a combination of these and the pull-out mechanism described above. Although the specific failure mechanism could not be isolated, failure analysis provided both insights into this carrythrough design and opportunities for improvement as discussed below.

After the static-test failure, the RP-2 carrythrough was redesigned with the clearance-fit, two-pin concept shown in Figure 8. This redesign was chosen for its size similarity to the interference-box-and-beam concept, and because it offered two structural advantages: first, there is clearance between box and beam so non-design, complex loading is not possible and, second, the loads carried in the shear web are transferred by the pins rather than having to travel from shear webs into capstrips and back into the shear web. A tie rod was also added to prevent deflection that allowed slippage of the wing-root torsion pins. Static tests for pure bending and bending-twist were repeated and maximum loads were successfully carried. RP-2 now has over 80 flight hours.

The failure of the RP-2 carrythrough was a significant event that affected construction of aircraft at Rensselaer. All involved in the project were stunned by the breakage, and a regular visit of sponsors was planned for three days after the failure which further focused concerns. However, these sponsors found the carrythrough failure to be worthwhile because it allowed students to understand the importance of testing and aircraft design philosophy, and because students could learn from the failure analysis of the carrythrough and its materials. It was the attitude of the sponsors that led to increased student involvement in future aircraft engineering at Rensselaer.

5. THE RP-3 CARRYTHROUGH

Design objectives for the RP-3 carrythrough structure were similar to those for the RP-1, RP-2 and redesigned RP-2 carrythroughs and include lightweight, separability and simplicity, although there are substantive differences both in the load carrying capacity for RP-3 and in the RP-3 design strategy which was improved based on experience with the previous three carrythroughs. This section presents the RP-3 carrythrough, its strategy for transmission of loads, and the design functions of the carrythrough including

box and beam components, tie rod, wing torsion pins, carrythrough-bulkhead bolts, and components associated with assembly. Emphasis is placed on design features that avoid the possible failure mechanisms found with RP-2.

Figure 9 shows the structure of the RP-3 wings². The aerodynamic loads on the wing are carried in the following manner: wing skins combine with three shear webs, front, main and rear, to create a torsion box for transmission of torsional loads to a structural root rib. Two torsion pins located at 10% and 80% chord on each root rib, transmit the torsional loads from the root rib to secondary bulkheads: these pins slipped during the RP-2 breakage. Capstrips bonded to the main shear web transmit bending to the carrythrough structure where the box and beam components of the carrythrough distribute these bending loads to the fuselage through main bulkheads. The beam component is an extension of the left wing main shear web and capstrip, and is attached to the box component and the two main bulkheads with two pins as shown in Figure 10. The box structure on the right wing is built up from the main shear web and tapered into the box cross-section as shown on Figure 10. Finally, a tie rod is located at about 85% of chord and carries the component of lift acting in the upstream direction during high angle of attack operation: it is designed to provide sufficient stiffness to avoid slippage of the wing-root torsion pins and is sized for dive pull-out. Design criteria and validation tests are presented below for the critical components of the RP-3 carrythrough.

Bending moment and shear-force diagrams are shown in Figure 11 for RP-3 which were calculated with the sailplane performance and loading analysis of Bahr³ which solved inviscid equations with boundary-layer corrections and provided estimates of the distribution of aerodynamic loads at critical flight conditions. The aircraft structure was designed to a 6g load factor and never-to-exceed speed of 237 feet per second. The wing root bending moment and maximum shear are 30,000 foot-pounds and 2450 pounds, respectively, which is more than about 5 and 3 times higher than for RP-1 and RP-2, respectively. For all of the carrythrough structure, a factor of safety of 3 was applied and is twice that required currently for FAR Part 23 Certification.

An important objective in the design of the RP-3 carrythrough was avoidance of possible mechanisms that resulted in the failure of the RP-2 carrythrough, and this was addressed with the following: sizing of the carrythrough to insure clearance between the box and beam throughout the flight envelope; addition of gussets at the discontinuous joint between capstrips and shear webs in box and beam to provide a better load path to carry shear flows and provide reinforcement for bonds that may be uncertain; a tension rod to carry forward moments at high angles of attack and provide sufficient stiffness to prevent slippage of wing-root torsion pins; and guide vanes to prevent prying by the beam on the box during assembly.

The dimensions of the carrythrough and the associated structure of box and beam components are shown on Figure 12a and 12b. Transmission of bending moment created by aerodynamic lifting forces was the main design constraint for the wing capstrips which were tapered uniformly from 52 to 3 layers of unidirectional graphite pre-impregnated fabric (Fiberite 1048) between the wing root and tip. The wing-to-bulkhead pins, herein called bolts to distinguish them from the wing-root torsion pins, connect the wings and main bulkheads and were located with the maximum separation possible which is 30 inches and limited by the fuselage diameter. The wing-root bending moments result in bolt forces of 12000 pounds and required 1-inch diameter ASI 4130 pins heat treated to a ultimate tensile strength of 140 ksi⁴. These fit through bushings made of identical material and were bonded with epoxy resin into the bulkhead, beam and box structures.

Deflections were estimated to quantify capstrip clearances due to aerodynamic loading by summing the contributions due to beam bending, box bending and deflection of the pin bushings in their epoxy seat. During normal loading the box and beam deflect in the same direction so clearance diminished only by

the difference in deflections which was calculated to be less than 0.008 inches: this calculation was validated by deflection and strain measurements obtained with a full-scale model of the beam carrythrough which compared within 10% of calculated values and was adequate for the safety factors applied here⁵. Bushing deflection in its epoxy seat was measured in test specimens to be 0.015 inches. These sum to a reduction in clearance of 0.023 inches due to 6g aerodynamic loading within an actual 0.375 inch gap as discussed below⁶.

The stress distribution around the bulkhead bolts was calculated and reinforcing plates were designed to diffuse loads into the shear web of the box. Test plates built to confirm stress distributions on the reinforcing plates, were loaded cyclically to 6000 pounds which is the pin force divided equally into the two bushings. Bushing damage was apparent at 21,000 cycles and failure occurred at 48,000 cycles. Strain-gauge measurements showed stresses diffuse adequately and no evidence of excessive stress concentration in the vicinity of the reinforcing plate and capstrip.

Shear flow was calculated and confirmed by the previously discussed beam test. Shear flows around the box and beam required gussets to reinforce the bond between capstrips and shear webs in the carrythrough. The bond between capstrip and shear webs is a secondary bond and alone would have been insufficient to transmit the shear flow. The carrythrough box is reinforced with additional layers as seen in Figure 12a and 12b and comprises 6 layers of 45 degree bidirectional graphite cloth wrapped around the box exterior and one partial wrap of 45 degree graphite cloth on the inside of the box at the corners. The beam has 3 graphite flanges within the beam structure, as well as two final wraps over the beam exterior.

A tie-rod was incorporated at the rear of the wing to stiffen the wing-fuselage junction and carry aerodynamic loads that pull the wing upstream at high angles of attack. Each end of the tie rod is attached to a steel plate bonded to a wooden blocks which disperse load into wing skins and webs through graphite flanges. The tie rod was designed for maximum lift in dive pullout which results in a 2400-pounds axial load on the tie rod. The stiffness of this rod, which prevents deflections that might result in pull out of the rear torsion pins as experienced by RP-2, is the critical constraint and a threaded rod of diameter 0.375 inches made from ASI 4130 aircraft-grade steel with a tensile strength of 140 ksi was selected⁷. Fatigue analysis estimated a life of 100,000 and 1,000,000 cycles under 6g and 3g oscillating loading, respectively, for the tie rod.

Tolerances within the carrythrough were 1/16 inches for composite parts which makes manufacturing difficult with the construction methods used for RP-3. All parts, with the exception of the capstrips are layed up by hand and room temperature cured under vacuum based on the procedures described by Friess⁸. Warping of vacuum tables, bonding of complex assemblies, and inaccuracies from construction by students, all contributed to the difficulties in maintaining design tolerances in the carrythrough. For example clearance between the capstrips of the box and beam reduced from the design value of 0.75 inches to about 0.375 inches which is however adequate as discussed above.

The box component is closed on five sides and there is not access inside the carrythrough after assembly. Inspecting and fitting the carrythrough are both difficult. After fitting, feeler gauges were used to maintain clearances inside the carrythrough while epoxy resin that bonds bushings into the bulkhead, the box and the beam cured with the wings and fuselage aligned at prescribed angles of fuselage-to-wing incidence and dihedral. Actual clearances cannot be measured. During field assembly, care must be taken to avoid internal damage as may have occurred during RP-2 assembly. The beam carrythrough is positioned using a wing-tip fixture and torsion pins for support. The box carrythrough slides into position on guide vanes that help prevent misalignment or excessive relative movement inside the carrythrough during insertion. Final adjustments are then made and the main wing pins installed. This procedure was designed to

prevent opportunities for prying damage inside the box.

6. CONCLUDING REMARKS

The box-and-beam concept was chosen for the RP-1 carrythrough and then used on RP-2 and RP-3 aircraft. Implementation of this design became progressively more difficult with increasing take-off gross weight. The failure of the RP-2 carrythrough, its successful redesign, and the resulting engineering required for the RP-3 carrythrough provided many Rensselaer undergraduates with a quick and efficient education in engineering practices, management, and interrelationships between complex design factors typical of the aircraft industry. The Rensselaer community looks forward to completion of RP-3 and to the design of RP-4 with all of the new challenges it will present for students and faculty.

7. ACKNOWLEDGMENTS

The authors are grateful for the efforts of the Sailplane Advisory Committee especially the technical contributions of Professors S.S. Sternstein, R. Loewy, and H. Hagerup and Dr. A. Lemnios. In addition the authors are pleased to thank the many students who contributed to the RP series aircraft and enriched the aircraft design community here at Rensselaer.

8. REFERENCES

1. Helwig, H.G., "CAPGLIDE and RP-1" *Soaring*, Hobbs, New Mexico, Feb. 1980.
2. Jaranson, J.W., "The RP-3 Sailplane, A Design and Manufacturing Guide", M.Sc. Thesis, Rensselaer Polytechnic Institute, NY, 1989.
3. Bahr, F.H. "Computer Aided Structural and Performance Analysis of a Composite Sailplane", M.Sc. Thesis, Rensselaer Polytechnic Institute, Troy, NY, 1987.
4. Hsu, P., Robinson, G., and Tom, E., "Wing Connection Group, Phase III Report", Composite Aircraft Studio Technical Report 94-374965-02, Rensselaer Polytechnic Institute, Troy, 1994.
5. Dec., J., Barrett, T., and Quortrup, C.O., "Carrythrough Deflection Test", Composite Aircraft Studio Technical Report 93-374961-04, Rensselaer Polytechnic Institute, Troy, NY, 1993.
6. Dave, S.V., "Report on Strain Testing", Composite Aircraft Studio Technical Report 93-374961-04, Rensselaer Polytechnic Institute, Troy, NY, 1993.
7. Maloney, J., Milliken, A., and Patricia, M., "Tension Rod Analysis, Phase III Report", Composite Aircraft Studio Technical Report 94-374965-07, Rensselaer Polytechnic Institute, Troy, NY, 1994.
8. Friess, W.A., "RP-3 Progress Report", Composite Aircraft Studio Technical Report 92-374940-11, Rensselaer Polytechnic Institute, Troy, NY, 1992.

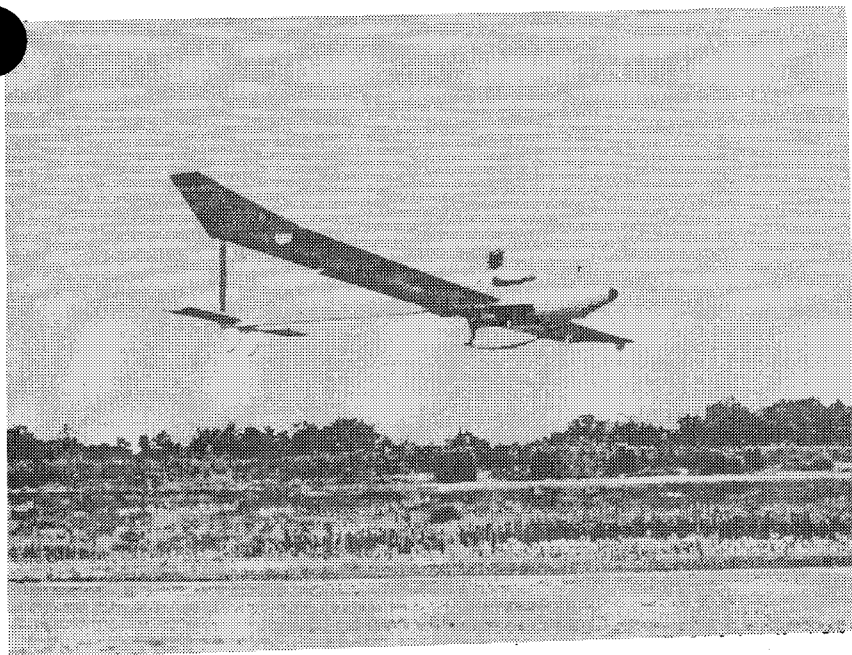


Figure 1
RP-1

Table 1

RP-1

Maximum Takeoff Weight.....	270 lbs
Empty Weight.....	115 lbs
Aspect Ratio.....	11
Length.....	18.9 ft
Height.....	4.2 ft
Wingspan.....	37.8 ft
Wing Area.....	129 ft ²
Maximum Glide Ratio.....	20:1 at 32 mph
Minimum Sink Rate.....	2.0 ft/s
Wing Loading.....	2. lb/ft
Stall speed.....	22 mph
Occupancy.....	1, open

Table 2

RP-2

Maximum Takeoff Weight.....	450 lbs
Empty Weight.....	270 lbs
Aspect Ratio.....	16
Length.....	21.6 ft
Height.....	4.1 ft
Wingspan.....	44.2 ft
Wing Area.....	120 ft ²
Maximum Glide Ratio.....	28:1 at 40 mph
Minimum Sink Rate.....	1.7 ft/s
Wing Loading.....	3.8 lb/ft
Stall speed.....	29 mph
Occupancy	1, enclosed

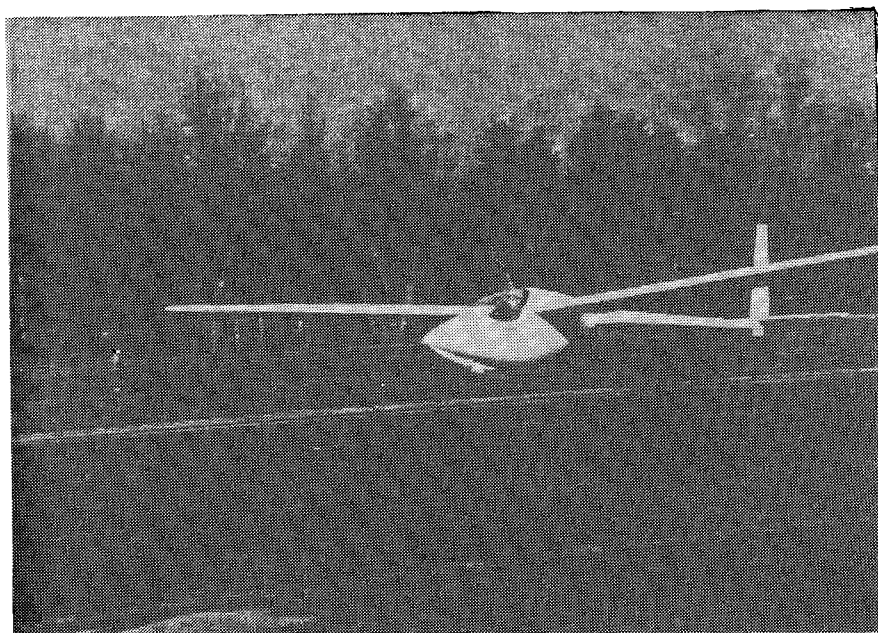


Figure 2
RP-2

Table 3

RP-3

Maximum Takeoff Weight.....	1000 lbs
Empty Weight.....	650 lbs
Aspect Ratio.....	17
Length.....	23.6 ft
Height.....	3.9 ft
Wingspan.....	54 ft
Wing Area.....	180 ft ²
Maximum Glide Ratio.....	33:1 at 51 mph
Minimum Sink Rate.....	2.1 ft/s
Wing Loading.....	5.5 lb/ft
Stall speed.....	42 mph
Occupancy.....	2, enclosed

Figure 3
RP-3

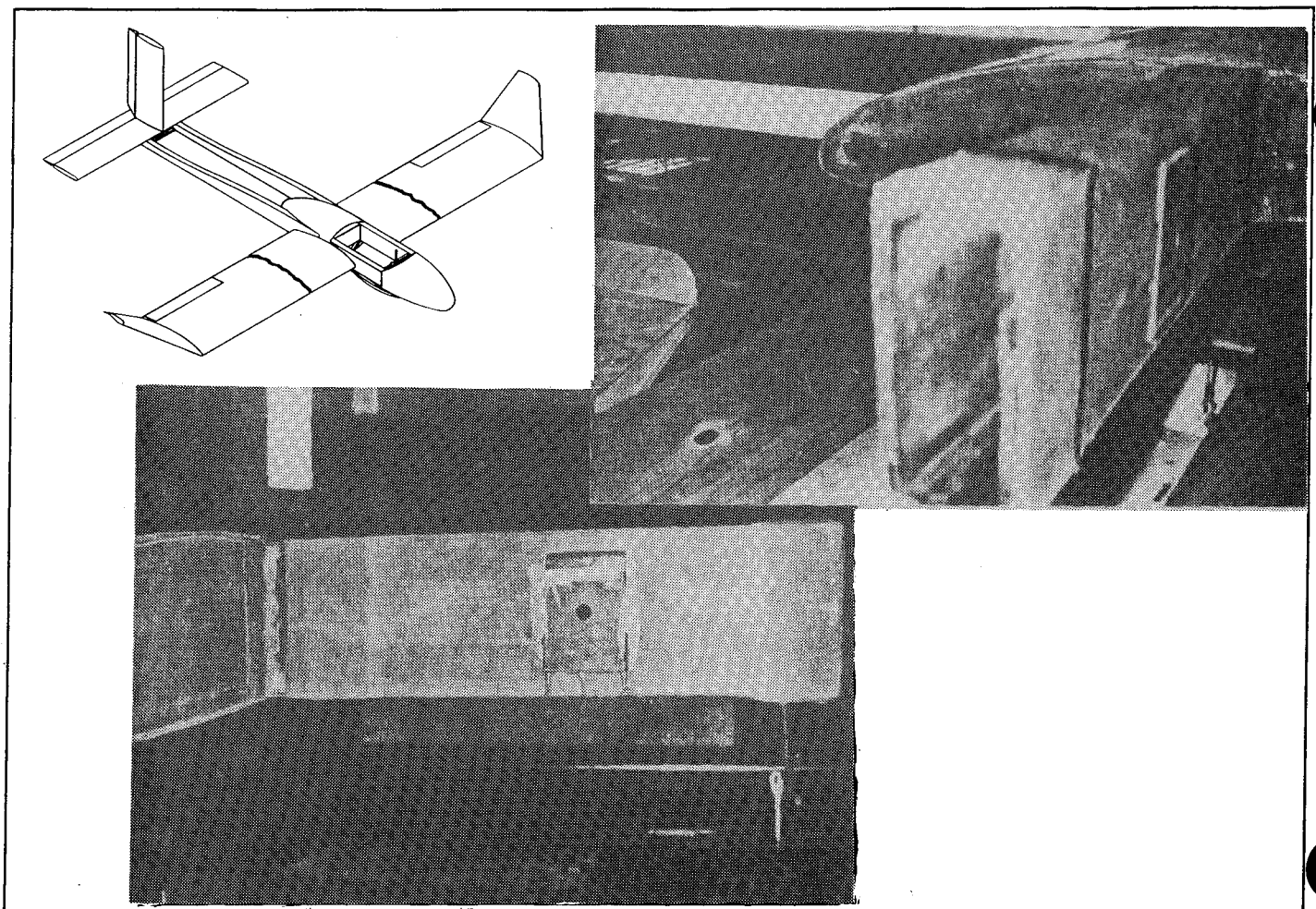


Figure 4
RP-1 Carrythrough Details

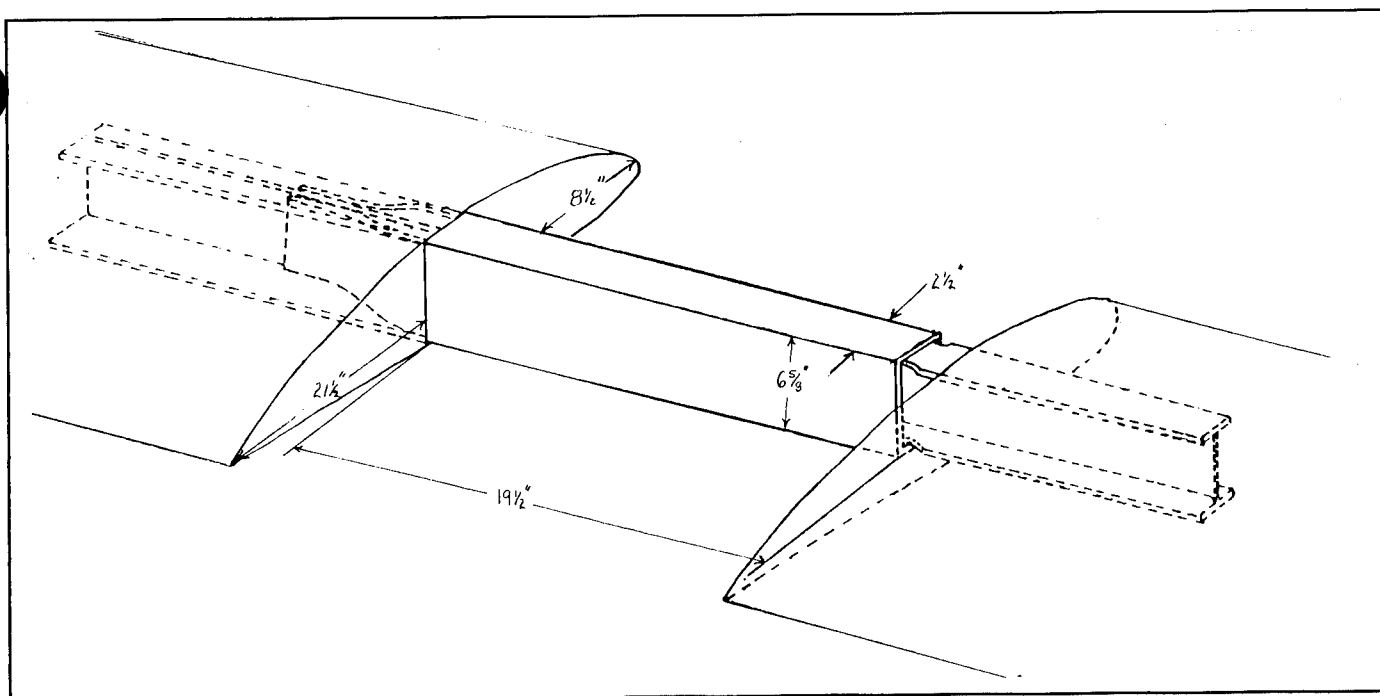


Figure 5
RP-2 Original Carrythrough

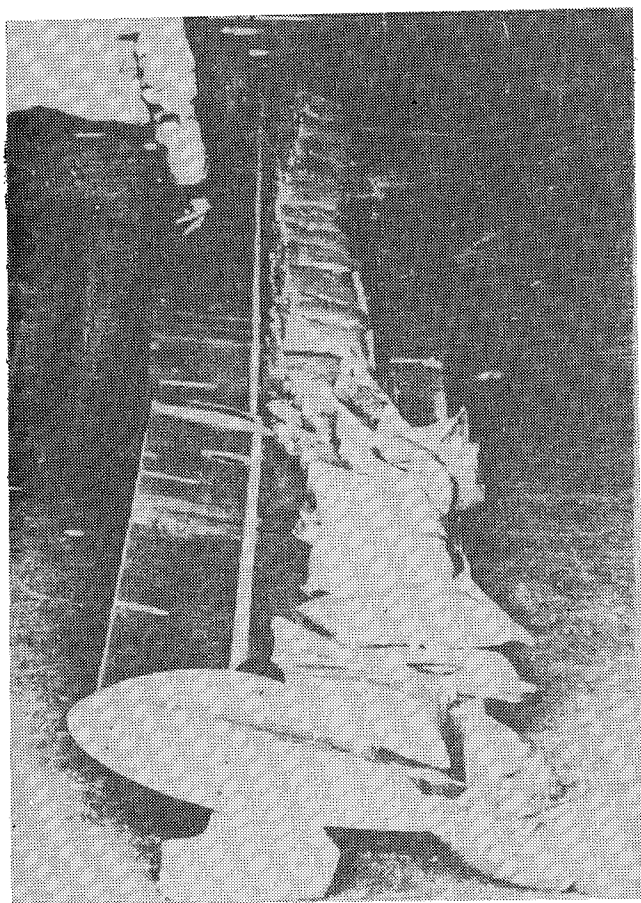


Figure 6
RP-2 Wing After Carrythrough Failure

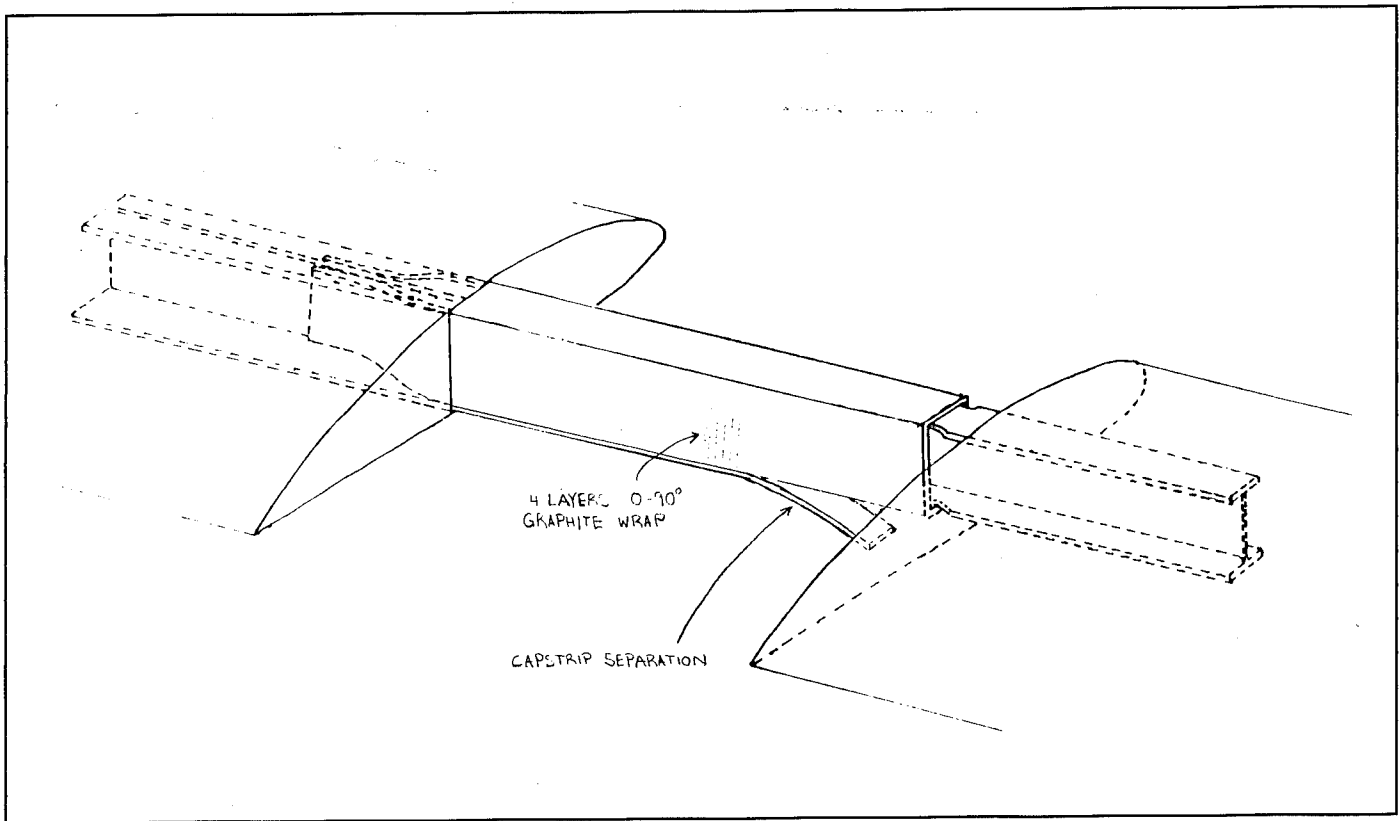


Figure 7
RP-2 Carrythrough Failure Details

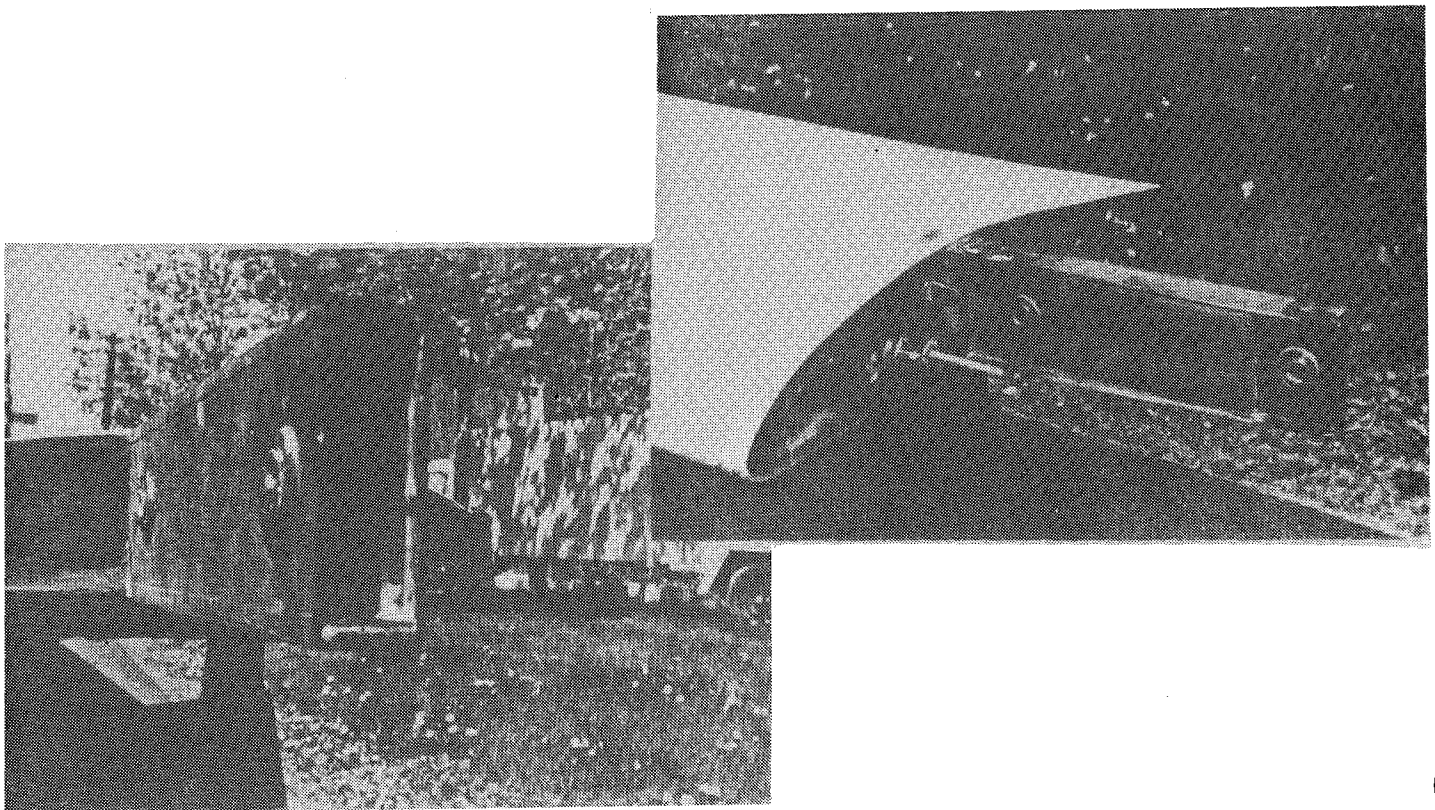


Figure 8
RP-2 Modified Carrythrough

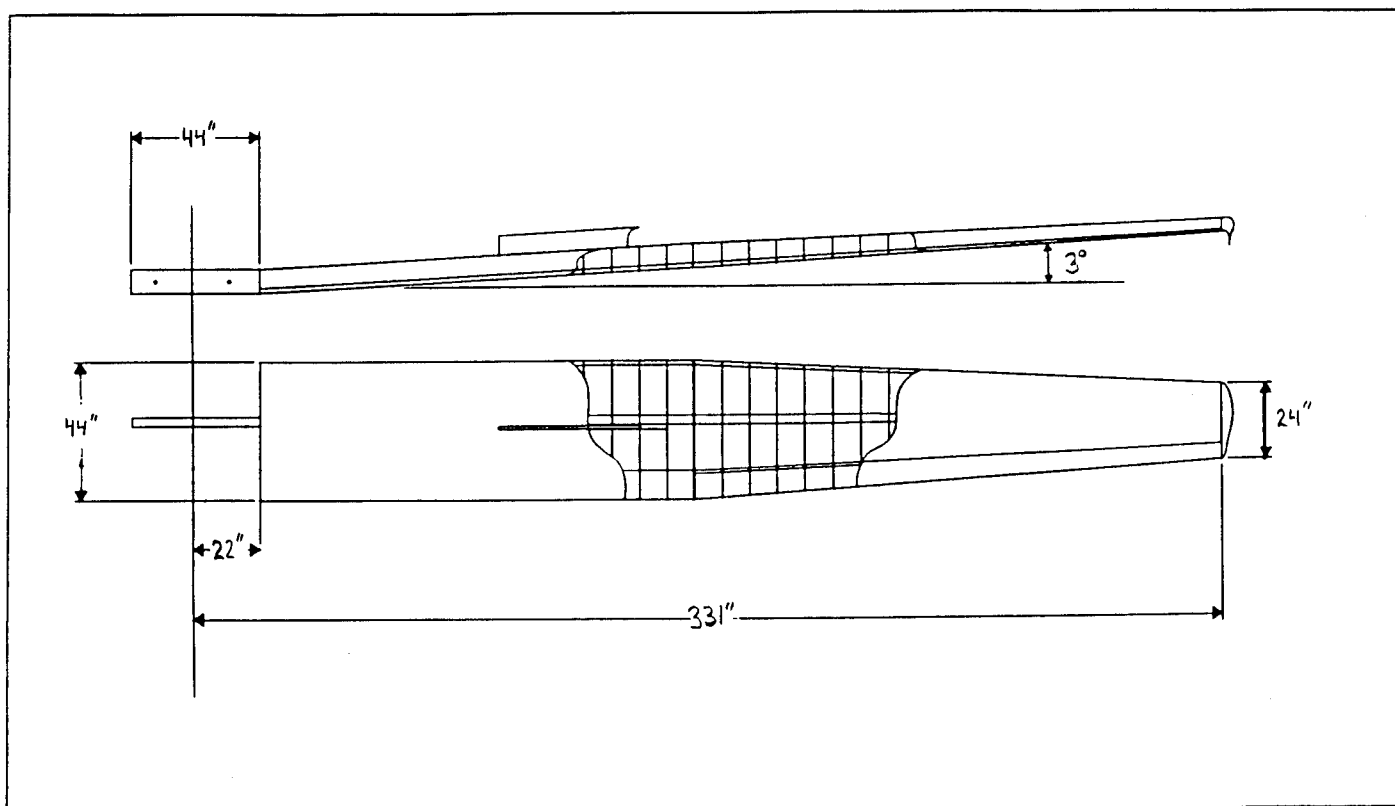


Figure 9
RP-3 Wing Structure

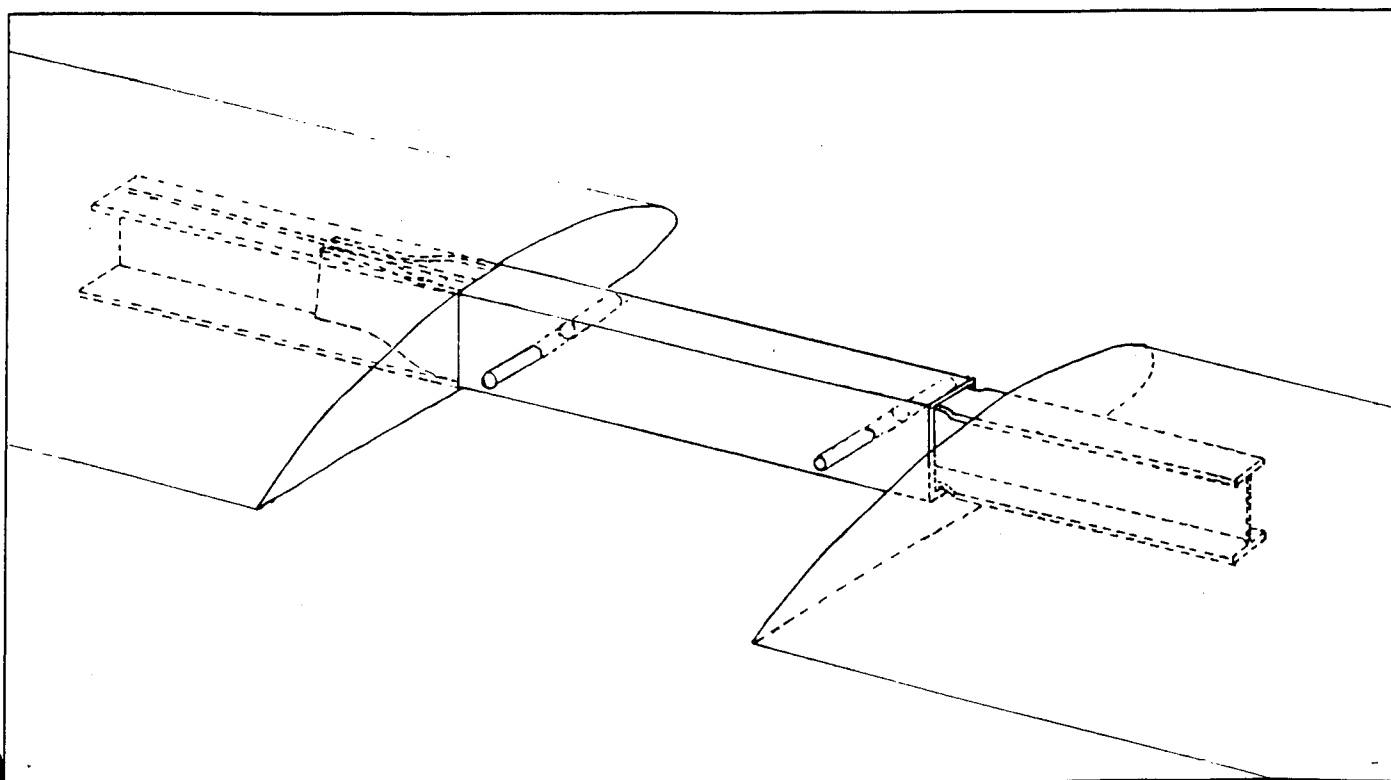


Figure 10
RP-3 Carrythrough Buildup

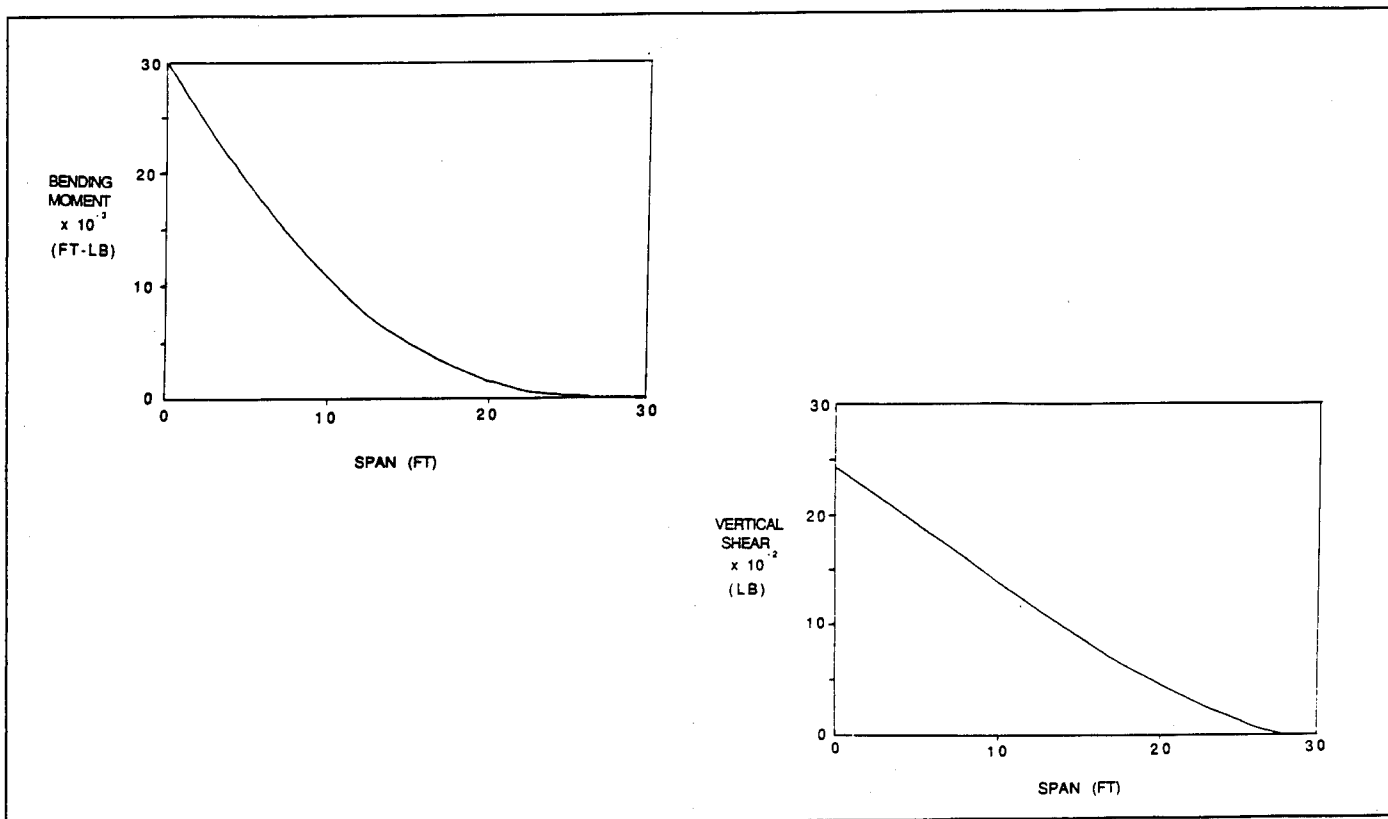


Figure 11
Bending Moment and Shear Force Diagrams

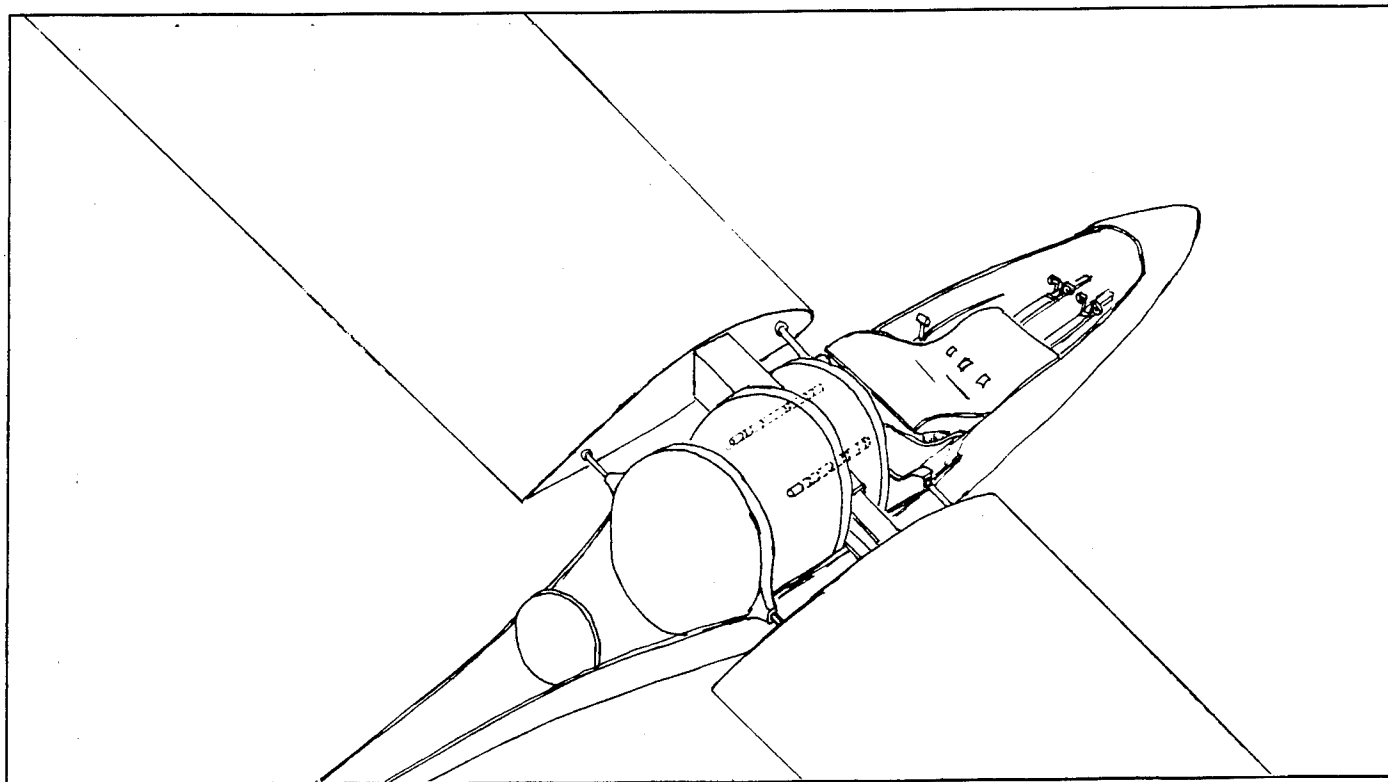


Figure 12a
RP-3 Carrythrough Specifications

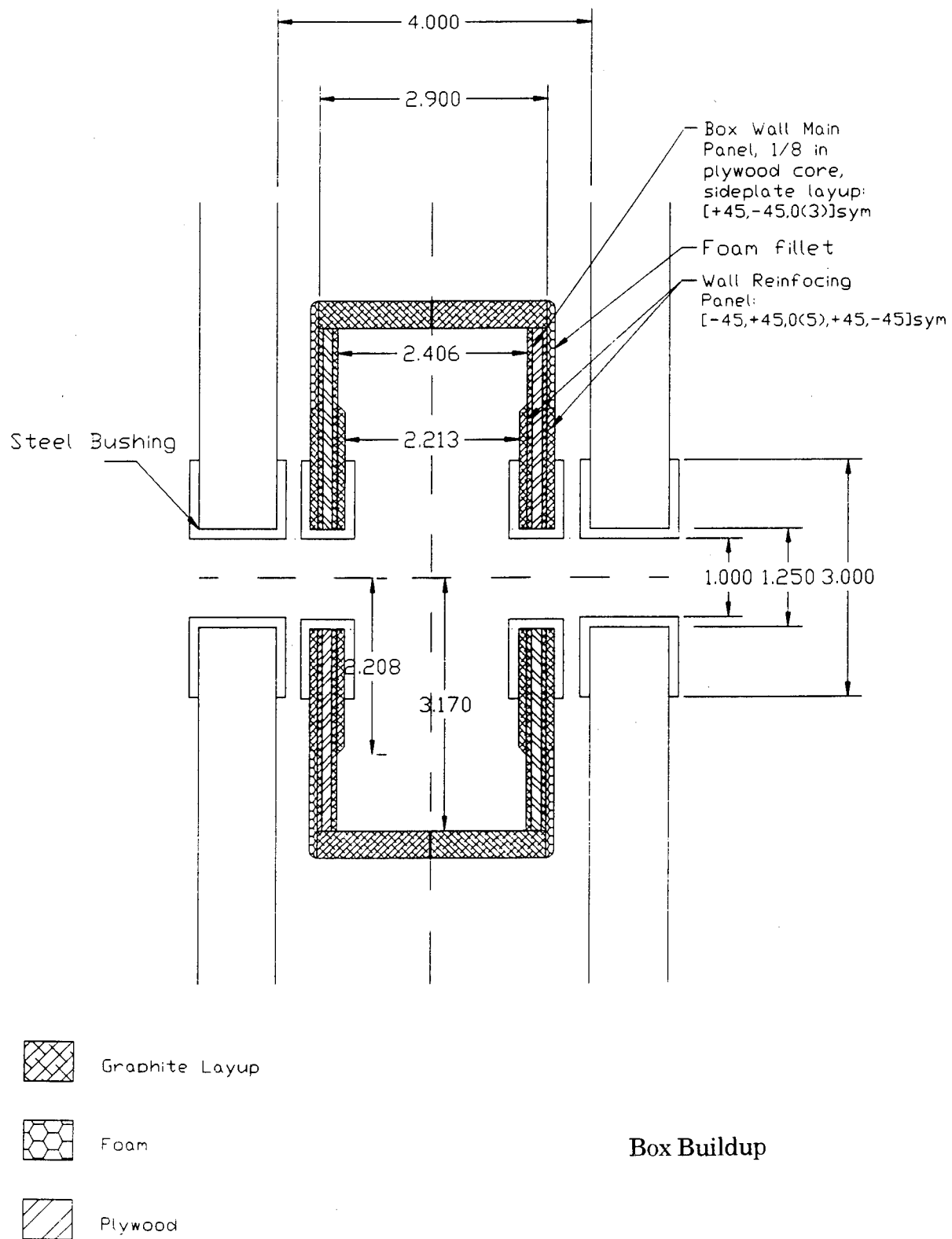


Figure 12b
RP-3 Carrythrough Specifications

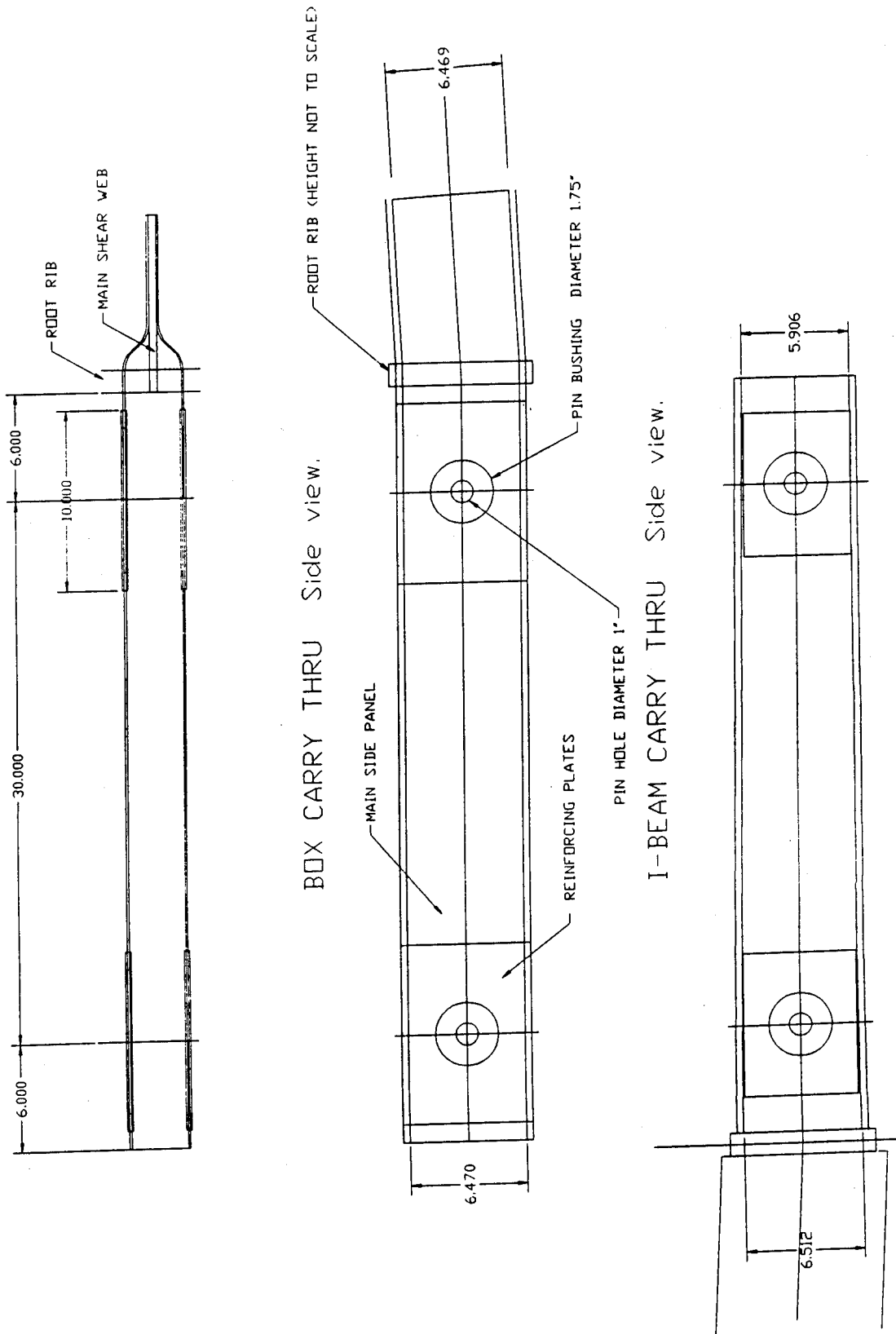


Figure 12b
 RP-3 Carrythrough Specifications

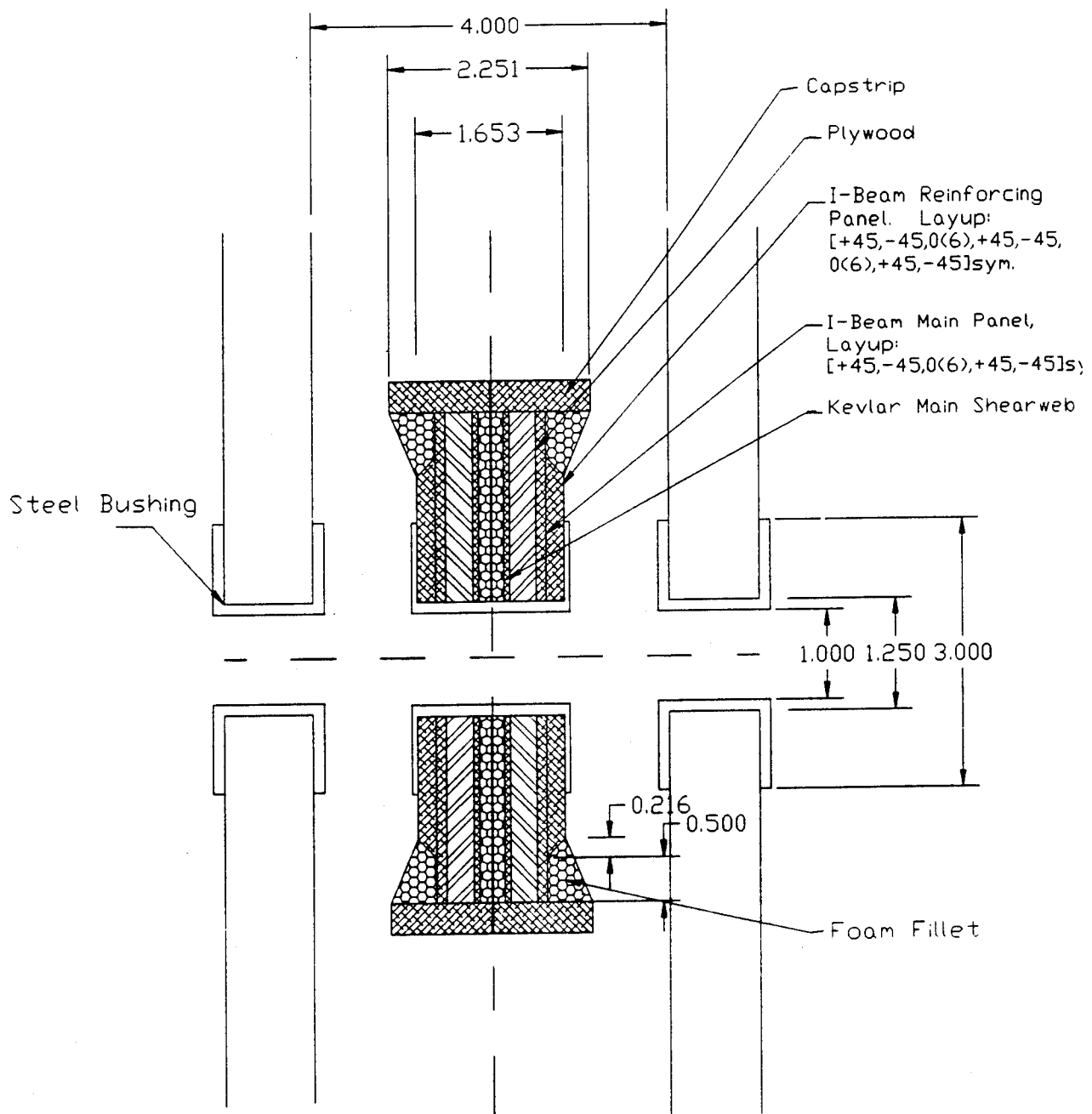


Figure 12b
RP-3 Carrythrough Specifications

DETERMINATION OF THE STABILITY AND CONTROL DERIVATIVES OF A TURBO-FAN RESEARCH AIRCRAFT USING A MAXIMUM LIKELIHOOD METHOD

Carl Lewis, Philip Bridges, Michael Cavanaugh

Raspert Flight Research Laboratory, Mississippi State University
Starkville, MS U.S.A.

ABSTRACT

Predicted and wind-tunnel lateral-directional stability and control derivatives of an all composite multi-engine turbo-fan research aircraft are compared with flight test results. A maximum likelihood parameter estimation procedure is used to extract the "most probable" control parameter of interest based upon *a priori* information and flight test data. A linear model based upon the wind-tunnel data is analyzed using the maximum likelihood method and compared with flight test results. The flight test data is obtained from data recorded over a series of flights with various flight conditions. Several types of control input sequences are used in the research aircraft to excite the appropriate lateral modes. The flight test matrix included aileron and rudder inputs at various deflection magnitudes and angles of attack. The Cramer-Rao bound of the estimates is used to provide an indication of the accuracy of the parameters obtained. The maximum likelihood method estimated the stability and control derivatives from flight test data with acceptable uncertainty levels.

INTRODUCTION

The determination of aircraft stability and control derivatives, known as parameter estimation, is an important result of flight testing aircraft. Wind tunnel testing can provide estimates of the stability and control derivatives, but the wind tunnel data is typically obtained from low Reynolds number testing. Aircraft operate at Reynolds numbers 5 to 10 times that of the wind tunnel. Since the Reynolds number and Mach number affect the stability and control derivatives, the ability to estimate stability and control derivatives from actual flight data provides an important tool to the control analyst and designer.

PURPOSE

This parameter estimation research started with the desire to identify the stability and control derivatives directly from flight test data. Better estimates of the stability and control derivatives are needed to facilitate the analysis and design of a displacement autopilot or a stability augmentation system, such as a yaw damper. In particular, the aerodynamic parameters associated with the Dutch roll mode needed reviewing and parameter estimation provided the opportunity to obtain a better understanding of these aerodynamics characteristics. By incorporating actual flight test estimates with wind tunnel and

DATCOM¹ data, it would be possible to increase confidence in the lateral stability derivatives used to design a planned yaw damper. Good correlation between tunnel data and that obtained from flight test would also increase confidence in the parameter estimation procedure.

Of course, any method used to estimate unknown parameters will have certain deficiencies. The shortcomings of wind tunnel testing are potential model differences, support system or sting effects, flight condition variations, and scaling errors. The largest errors arise from the effects of scale or Reynolds number differences between wind tunnel and flight tests, and flight condition variations.

The DATCOM method of predicting stability and control derivatives is a synthesis of theoretical and empirical data. The empirical data comes from testing of conventional aircraft, but the MH-02 is not of conventional aircraft design. Therefore, it is likely that some values estimated with DATCOM are suspect. For instance, the prediction of the directional stability derivative, $C_{n\beta}$, is dependent on the calculation of sidewash, the lateral-directional plane equivalent of downwash. The DATCOM method does not account for the unusual nacelle placement in the calculation of sidewash, and hence uncertainties exist the calculation of $C_{n\beta}$. As an example, predictions of $C_{n\beta}$ from DATCOM for the MH-02 are higher than wind tunnel estimates by a factor of two. Historically, wind tunnel tests are used to obtain static derivatives and not rotary derivatives. Hence, DATCOM methods were used to estimate the rotary derivatives, C_{lp} , C_{np} , C_{lr} , and C_{nr} .

BACKGROUND

The majority of physical systems are inherently nonlinear and time dependent. The coupled translational and rotational motions of an aircraft are modeled by an ordinary, nonlinear set of differential equations, but a linear model is more practical for the purposes of parameter estimation. Application of small disturbance theory allows us to represent an aircraft as a linear, time-invariant system. It is assumed that the motion of the aircraft, regardless of the input to the system, consists of small deviations from a reference condition of steady flight. The linear equations of motion neglect aerodynamic cross-coupling and rotor gyroscopic effects. The neglect of coupling between the longitudinal and lateral modes remains valid as long as perturbations away from the reference condition remain small. Maine and Iliff² state that the modified maximum likelihood estimator (MMLE) is suitable for the evaluation of parameters from data obtained in level flight, steep descents, and coordinated turning flight.

EXPERIMENTAL AIRCRAFT. The MH-02 is a composite, high wing, twin turbo-fan aircraft being developed by a joint research program between HONDA R&D, North America and Mississippi State University's Raspet Flight Research Laboratory. The MH-02 airframe is composed primarily of carbon fiber composite and has forward swept wings, slats, and triple slotted flaps with a maximum takeoff weight of 3609 kg (7957 lbs). In addition, the MH-02 has upper mounted turbo-fan engines on the high wings. Flight testing of the MH-02 began March 5, 1993 and to date the MH-02 has completed 38 flight tests. The MH-02 is certified by the FAA as an experimental R&D aircraft.

MAXIMUM LIKELIHOOD ESTIMATION. The maximum likelihood estimation method is used extensively at NASA's Dryden Flight Research Center in Edwards, California and other facilities to estimate the stability and control derivatives.³ The work started almost 28 years ago based on the theoretical work of Balakrishnan. The maximum likelihood estimation method was chosen because it was designed particularly for estimation of the stability and control derivatives and has the ability to handle state and measurement noise. MATLAB's State-Space Identification Toolbox⁴ (SSIT) developed by MathWorks Inc. is based on Maine and Iliff's extensive work on parameter identification. MATLAB's SSIT is used to evaluate a linear time-invariant MH-02 model and the flight test data.

MATLAB's State-Space Identification Toolbox uses the latest version of the modified maximum likelihood estimator, MMLE3. The estimates obtained from the modified maximum likelihood estimator are unbiased, consistent, and efficient.⁵ In addition, the MMLE3 formulation minimizes noise covariance estimation problems often encountered in the maximum likelihood estimation process.

The maximum likelihood estimation method considers a vector of unknown parameters, θ , and a set of observations or measurements, z , and maximizes the conditional probability $p(z/\theta)$. The maximum likelihood estimate of θ is that value of θ that maximizes the conditional probability. That is, we choose the parameter in the probability density function such that the occurrence of the observations, z , is "most likely." A pictorial representation of this process is shown in figure 1, reprinted with permission.

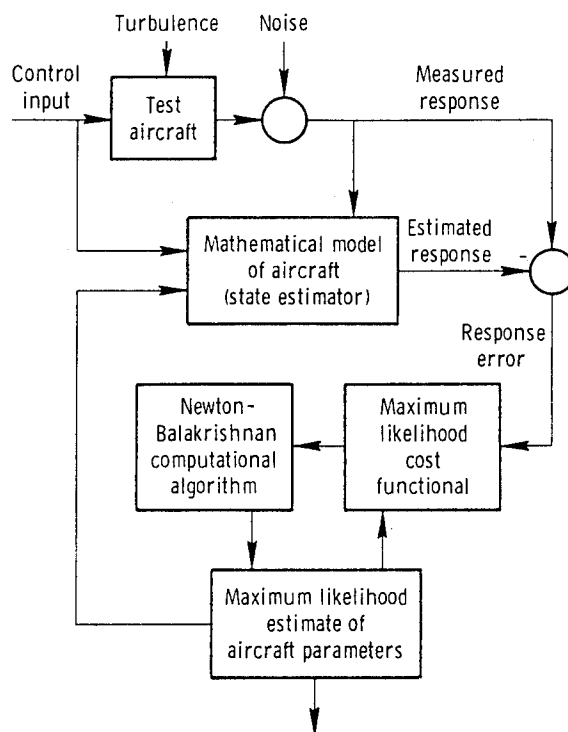


Figure 1. Maximum Likelihood Estimation Concept⁶

In using MMLE3, the system of interest is considered linear and time-invariant. MMLE3 assumes the actual aircraft system can be represented by the following equations

$$\dot{x} = Ax(t) + Bu(t) + Fn(t)$$

$$y(t) = Cx(t) + Du(t)$$

$$z(t) = y(t) + \eta(t)$$

where η is the measurement noise vector, n is the state noise vector, and F is the square root of the state noise spectral density. The noise is assumed to be zero mean, white, Gaussian, and stationary. The controls, $u(t)$, are presumed noiseless and known. The unknown stability and control derivatives appear in the A , B , C , D , and F matrices. In this analysis, the A , B , C , D , and F matrices are time independent. The maximum likelihood estimates of the unknown coefficients, θ , are obtained by minimizing the following

cost functional⁷ with respect to θ

$$J(\theta) = \frac{1}{T} \int_0^T [z(t) - \hat{y}(t)]^T G^{-1} [z(t) - \hat{y}(t)] dt$$

where the weighting matrix G is the measurement noise covariance matrix. Minimizing the above cost functional is equivalent to maximizing the negative logarithm of $p(z, \theta)$, the conditional probability density function. In addition, MMLE3 estimates the standard deviation of each unknown. This estimated value, known as the Cramer-Rao bound, gives the user an assessment of the accuracy of each unknown parameter.

TEST PROCEDURES

The majority of the control inputs analyzed were implemented during the descent phase of flight test maneuvers, and the remainder of the control inputs analyzed were executed during steady level flight at various angles of attack (AOA). All control inputs were pilot induced without the aid of an automatic control system or a mechanical device.

Both of the lateral-directional controls, aileron and rudder, were exercised in the flight tests. Two types of inputs were induced by the pilot to the controls, the doublet and the "3211." The "3211" input is an optimized multistep input⁸ (3 time units positive deflection, 2 time units negative, 1 time unit positive, and 1 time unit negative). The doublet input, applied to the aileron and rudder in succession, was used primarily during steady level flight; an example is illustrated in figure 2. The "3211" input, also applied to the aileron and rudder in succession, was executed predominately during descent.

The data recorded from these maneuvers included angle of attack, angle of sideslip, bank angle, pitch angle, roll rate, yaw rate, airspeed, dynamic pressure, rudder and aileron deflection. The flight test data generated by the control inputs was recorded by an onboard PC driven data acquisition system⁹ designed specifically for the MH-02 with a simple copilot controllable key pad. The data acquisition system recorded the data from aircraft sensors, performed corrections from indicated airspeed to calibrated airspeed and many other corrections, then output the data to files in U. S. Customary engineering units.

RESULTS

The results from a doublet input at an angle of attack of 7.97 degrees and a 3211 input at an angle of attack of 3.37 degrees are presented in Table 1. The table summarizes the comparison between DATCOM predicted derivatives, wind tunnel calculated derivatives, and the MMLE estimates. The DATCOM and wind tunnel derivatives are based on an AOA of approximately 8 degrees, listed in per radians and the rotary derivatives in per radians per second. The column listing of calculated values* are from DATCOM predictions and wind tunnel tests. The corresponding MMLE parameter estimates are shown with their Cramer-Rao bound. The MMLE estimates for $C_{y\beta}$, $C_{y\delta r}$, and $C_{l\delta r}$ compare well with tunnel data, and the aileron power, $C_{l\delta a}$, is only slightly lower than wind tunnel estimates. However, the directional stability derivative, $C_{n\beta}$, is significantly less than wind tunnel estimates at 8 degrees AOA, and its dependence on AOA can be seen. Also, the rolling stability derivative, $C_{l\beta}$, is less than wind tunnel estimates at 8 degrees AOA. One source of these differences could be the result of Reynolds number effects. A more likely source, however, may be the effect of the jet exhaust from the upper mounted engines affecting the flow near the vertical stabilizer during sideslip. The power effects were not

measured in the wind tunnel. The damping derivatives, C_{lp} and C_{nr} , agree reasonably well with DATCOM prediction. The cross derivatives, C_{lr} and C_{np} , have a large dependency on lift coefficient, and the differences between MMLE estimates and prediction conceivably occur due to the aircraft's unusual configuration. Rudder power, $C_{n\delta r}$, does not compare closely with tunnel data. The rudder power is considerably less than wind tunnel estimates. It is not clear at this time why the flight test estimate is less than 50% of the tunnel value. Further investigation and testing of this control derivative should be conducted.

The reason for the Cramer-Rao bound difference in the doublet inputs and the 3211 input is unknown. In practice, the 3211 input gives better excitation of the aircraft's modes and this generally yields more accurate estimates and lower Cramer-Rao bounds. It is possible that simultaneous inputs to the rudder and aileron during the 3211 maneuver degraded the quality of the estimates.

Figure 3 illustrates the output time history of the aircraft measured response and the estimated response of the bank angle to the doublet input.

CONCLUSIONS AND RECOMMENDATIONS

The flight tests yielded consistent estimates of the lateral stability and control derivatives. For most of the values, the Cramer-Rao bounds indicated that there is sufficient information to extract the coefficients. Differences between the flight test derived data and the wind tunnel/DATCOM coefficients may be due to Reynolds number and power effects. Further flight tests and analysis will be conducted to better understand and verify the differences. Also, flight tests need to be conducted to accurately determine those derivatives that are functions of the angle of attack, and to evaluate the obscure center of gravity effects. In the future this method will be expanded to analyze the longitudinal stability and control derivatives.

ACKNOWLEDGEMENTS

The authors would like to express their appreciation to HONDA R&D, North America for the opportunity to participate in the MH-02 project. Also, we would like to thank Dr. Albert G. Bennett, Director of Raspet Flight Research Laboratory, for his engaging presence and invaluable time. Last, but certainly not least, we would like to thank Grady Wilson, Chief Test Pilot, for applying the desired control inputs to the MH-02.

REFERENCES

1. Hoak, D., Ellison, D., et al., *USAF DATCOM*, Air Force Flight Dynamics Laboratory, Wright-Patterson AFB, OH.
2. Iliff, Kenneth W. and Maine, Richard E., *Practical Aspects of using a Maximum Likelihood Estimation Method to Extract Stability and Control Derivatives from Flight Data*, NASA TN D-8209, April 1976.
3. Maine, Richard E. and Iliff, Kenneth W., *User's Manual for MMLE3, a General FORTRAN Program for Maximum Likelihood Parameter Estimation*, NASA TP 1563, November 1980.
4. Milne, Garth, *State-Space Identification Toolbox: For Use with MATLAB*, The Mathworks, Inc., Natick, Mass., July 1993.

5. Maine, Richard E. and Iliff, Kenneth W., *The Theory and Practice of Estimating the Accuracy of Dynamic Flight-Determined Coefficients*, NASA RP 1077, July 1981.
6. Iliff, Kenneth W., Maine, Richard E., and Montgomery, T. D., *Important Factors in the Maximum Likelihood Analysis of Flight Test Maneuvers*, NASA TP 1459, April 1979.
7. Balakrishnan, A. V., *Communication Theory*, McGraw-Hill Book Co., Inc., 1968.
8. Klein, Vladislav, *Estimation of Aircraft Aerodynamic Parameters From Flight Data*, Progressive Aerospace Science, Vol. 26, pp. 1-77, 1989.
9. Chaney, V. G., et. al., *Design of a Fully Automated PC Driven Data Acquisition System for an Experimental Aircraft*, 3RD Joint Symposium on General Aviation Systems, May 1994.

TABLE 1. SUMMARY OF DATCOM, WIND TUNNEL, AND MMLE ESTIMATES

Derivative	Calculated Value* $\alpha = 8^\circ$	MMLE estimate $\alpha = 3.37^\circ$	MMLE estimate $\alpha = 7.97^\circ$
$C_{y\beta}$	-.6990	-.6638 \pm .0224	-.6944 \pm .0130
$C_{y\delta r}$.1261	.1542 \pm .0224	.1168 \pm .0130
$C_{l\beta}$	-.0510	-.0640 \pm .0094	-.0342 \pm .0054
C_{lp}	-.4792	-.5274 \pm .0221	-.5580 \pm .0129
C_{lr}	.2245	.1893 \pm .0224	.3465 \pm .0129
$C_{l\delta a}$.1107	.0770 \pm .0063	.0887 \pm .0058
$C_{l\delta r}$.0242	.0251 \pm .0065	.0261 \pm .0028
$C_{n\beta}$.0842	.0600 \pm .0127	.0442 \pm .0061
C_{np}	-.1190	-.1050 \pm .0223	-.1906 \pm .0130
C_{nr}	-.8797	-.8785 \pm .0224	-.8135 \pm .0129
$C_{n\delta a}$	0	-.0126 \pm .0128	-.0896 \pm .0104
$C_{n\delta r}$	-.0699	-.0334 \pm .0096	-.0270 \pm .0048

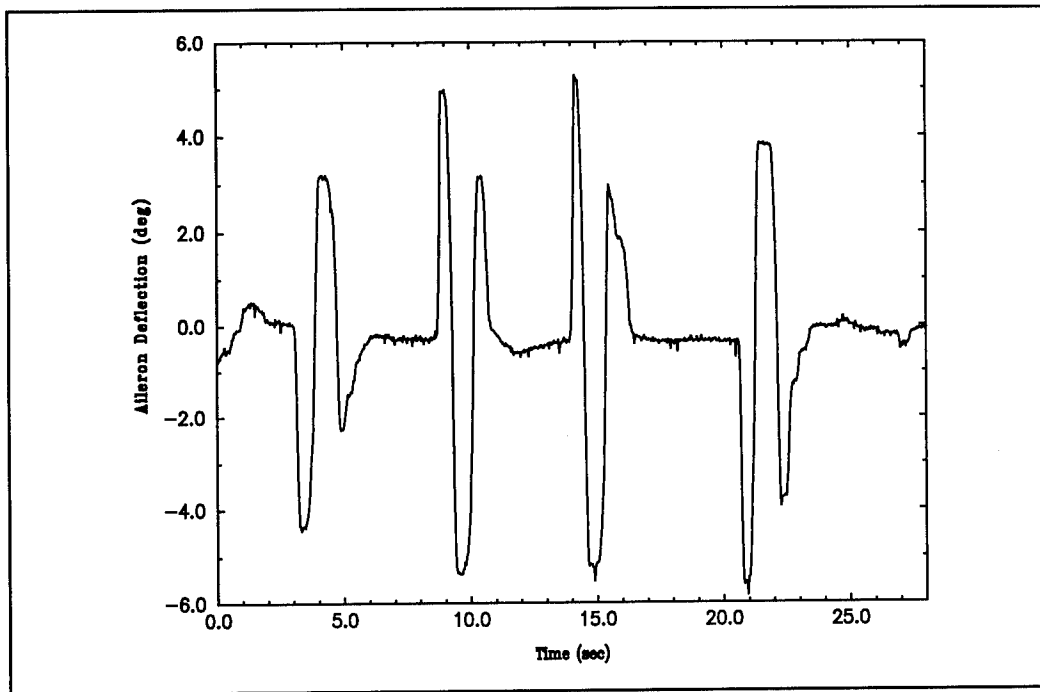


Figure 2. Aileron doublet input time history.

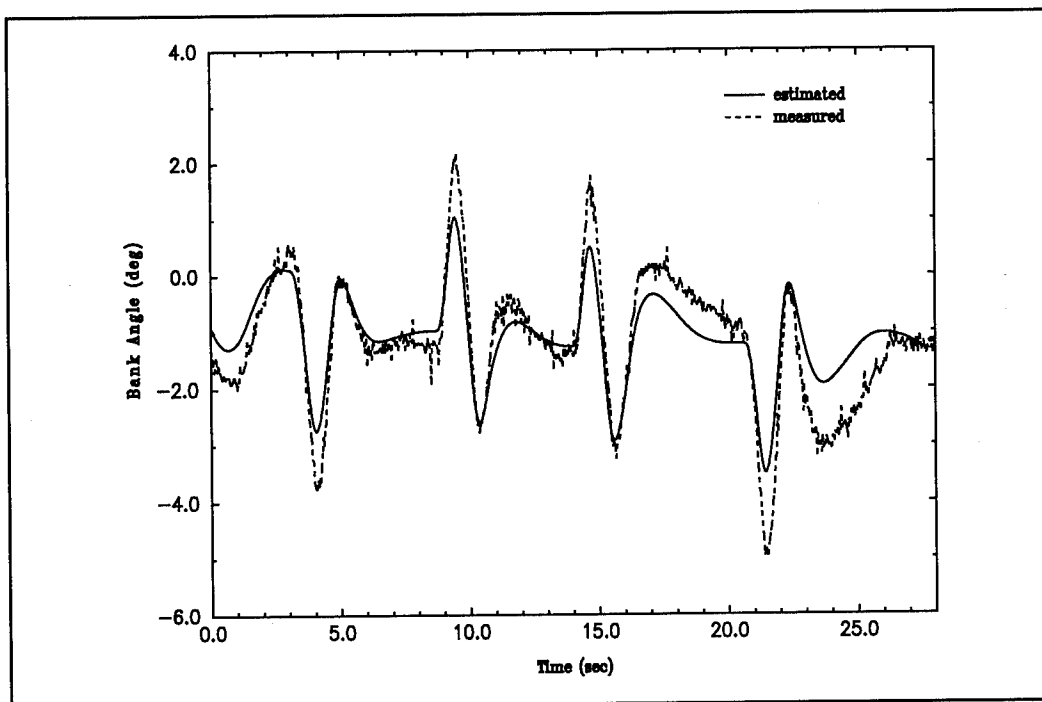


Figure 3. Estimated and measured bank angle aircraft response.

OVERVIEW OF CERTIFICATION AND FLIGHT TESTING
OF PRIMARY CATEGORY AIRCRAFT USING THE
TRANSPORT CANADA TP101-41E ULTRA-LIGHT DESIGN STANDARD

M. W. Anderson *
Federal Aviation Administration
Des Plaines, Illinois

ABSTRACT

This paper discusses certification standards, flight testing and eventual provisional type certification of a primary category aircraft using the Transport Canada TP101-41E Ultra-Light Design Standard as the certification basis. For many years manufacturers maintained that 14 CFR part 23 certification standards were overly restrictive with regard to small aircraft of simple design, and therefore restrict growth and innovation in the small airplane industry. The FAA, in conjunction with industry set forth to design a streamlined certification standard for these type aircraft. The FAA adopted the primary category rule for type certification of aircraft of simple design intended for pleasure or personal use. The purpose of this rule is to help reduce the time and expense of type certification. The primary category rule allows manufacturers to select a certification basis from a list of acceptable certification standards. Presented is an overview of certification and flight test of the Quicksilver GT 500 aircraft which was certified under the primary rule using the Transport Canada TP101-41E Ultra-Light Design Standard. Certification flight test plans and flight test techniques used to gather data are presented. Flight test data and compliance with TP101-41E are discussed. Noncompliant findings are discussed. The Quicksilver GT 500, the first aircraft certified in the primary category, was awarded a provisional type certificate on August 1, 1993.

NOMENCLATURE

ACO	Aircraft Certification Office	RPM	engine or propeller revolutions per minute
AFM	airplane flight manual	SLSD	sea level standard day conditions
cg	center of gravity	VFR	visual flight rules (14 CFR part 91)
FAA	Federal Aviation Administration	V_D	design dive speed, $1.1 V_{NE}$
FAR	Federal Air Regulation	V_F	design flap operating speed
F_S/G	longitudinal stick force per g	V_{NE}	never exceed speed
gw	gross weight in pounds	V_{SO}	stall speed in the landing configuration
g	longitudinal acceleration	V_{S1}	stall speed in a specified configuration
JAR-VLA	Joint Airworthiness Requirements for Very Light Aircraft	V_X	speed for best angle of climb
KIAS	knots indicated airspeed	V_Y	speed for best rate of climb
MIAS	miles per hour indicated airspeed		
NPRM	Notice of Proposed Rulemaking		
PA	pressure altitude		

INTRODUCTION

BACKGROUND

In September, 1992, the FAA established the primary category of aircraft.¹ This new category includes airplanes powered by a single, naturally aspirated engine, with a 61 knot maximum stall speed, weighing no more than 2700 pounds and seating four people in an unpressurized cabin. Unlike airplanes in the experimental category, these airplanes may be used for rental and flight instruction under certain

conditions, although the carriage of persons or property for hire is still prohibited. This category of aircraft was developed through a joint effort between the aviation industry, the Experimental Aircraft Association, the Small Aircraft Manufacturers Association and the FAA. The objective of creating the new category was to streamline the certification requirements and procedures for small aircraft of simple design without compromising the safety of the design.

Certification costs can be a large part of the total development cost of small aircraft, especially those used primarily for pleasure or flight training. The primary category rule, by effectively reducing certification costs, helps manufacturers fill a demand for smaller, low cost aircraft. The requirements for type certification of an aircraft in the primary category are somewhat varied and may be proposed by those applying for type certification.

PRIMARY CATEGORY CERTIFICATION STANDARDS. The FARs state that the Administrator may find other airworthiness criteria appropriate to the specific design, and the aircraft intended use, in lieu of the corresponding Federal Air Regulations.² The noise standards of FAR Part 36, however, are applicable to all primary category aircraft. Applicants seeking to type certify an aircraft in the primary category may propose a set of airworthiness standards to the servicing ACO when applying for a type certificate. The FAA reviews and comments on the proposed standards. An NPRM is then issued and comments gathered from the public. After all comments are addressed, if the proposed standards are found to be appropriate for the category, the FAA publishes a rule in the Federal Register. At this point, the certification standard becomes available to any applicant seeking a type certificate in the primary category. To date, the acceptable airworthiness standards for type certification under the primary category rule are FAR 23 and 27, JAR-VLA and TP101-41E.³ The first aircraft type certified in the primary category was certified using the TP101-41E Ultra-Light Design Standard.

THE SPORTPLANE DESIGN STANDARD. The Transport Canada Design Standards for Ultra-Light Aeroplanes, TP101-41E, was renamed the Sportplane Design Standard to avoid any confusion with the Ultralight category of vehicles. The Sportplane standard applies to propeller driven aircraft designed to carry a maximum of two persons. Additionally, the two place aircraft is limited to 1200 pounds maximum gross weight and a V_{SO} not exceeding 45 MIAS (39 KIAS).³ Aircraft are restricted to day VFR non-aerobatic operations such as stalls, spins, lazy eights, chandelles, steep turns and maneuvers incident to normal flying. The Sportplane Design Standard is a streamlined set of certification requirements that reduces the time and cost of other traditional design standards without compromising the safety of the design. In the area of required flight tests, some traditional flight test data are not required to be gathered or analyzed. For example, a pitot-static calibration is not explicitly required and no limits are set on the allowable magnitude of the total position error. Airspeeds, however, must be presented in the AFM in both indicated and calibrated airspeed. The airspeed calibration is therefore implied. Static directional and lateral stability is determined by examination of the spiral mode vice the conventional method of examining steady heading sideslips. Additionally, no requirement is stated for dynamic testing of modes other than the longitudinal short period mode. Other differences from classical standards are apparent when examining the test results presented below. Certain other areas such as spin testing, engine cooling and unusable fuel demonstrations are not addressed in the Sportplane standard. The applicability of these other areas was determined as the flight test plan was developed and were added to the test plan where appropriate.

THE CERTIFICATION FLIGHT TEST PLAN

The objectives of the flight test program were: 1) to substantiate contractor furnished data, 2) to determine specification compliance and 3) to ensure that the aircraft exhibited no unsafe flight characteristics.

The areas listed below and the flight test techniques selected for the evaluation were chosen to meet the objectives of the flight test plan. In some cases, additional tests not called out in the Sportplane Design Standard were performed to ensure the aircraft had no unsafe flight characteristics. These additional tests are authorized by FAR Part 21 and were deemed necessary by the flight test team.⁴ Instrumentation consisted of simple measuring devices and hand recorded readings. This simplistic approach was deemed appropriate given the amount and type of data to be recorded, and the subjective nature of the data required by the Sportplane standard.

TAKEOFF PERFORMANCE. Takeoff performance was evaluated by measuring ground roll using flour bag markers and estimating the takeoff distance over a fifty foot obstacle using a simple theodolite type apparatus.

PITOT-STATIC CALIBRATION. Pitot-static system calibration was accomplished using a flight test airspeed boom with known position error to calibrate the ship's pitot-static system. Though not specifically required by the Sportplane Design Standard, the calibration was used to verify published calibrated airspeeds and was necessary for later flight testing at V_D .

V_X AND BALKED CLIMB GRADIENTS. Best angle of climb and balked landing climb gradients were estimated by flying over a surveyed ground course laid out on the runway and recording altitude gained for a given horizontal distance. This technique is not exact, but was found acceptable if winds were calm and the observed gradients substantially exceeded the gradients required.

V_Y CLIMB. The speed for best rate of climb and climb rate were determined using the sawtooth climb technique.⁵

STALL PERFORMANCE AND CHARACTERISTICS. Stall speeds and characteristics were determined using procedures specified in the Sportplane Design Standard. Where no guidance was given, the techniques outlined in Advisory Circular 23-8A were used.⁶

SPINS. The Sportplane design standard does not state a requirement for spin characteristics or testing. The requirements of FAR paragraph 23.221(a)(1) were applied to evaluated aircraft spin and recovery characteristics.

LONGITUDINAL STATIC STABILITY AND CONTROL. The stabilized method was used to evaluate longitudinal static stability with stick forces measured using a hand held force gauge.⁷ Longitudinal control was evaluated using power on and off stick only accelerations. $F_{S/G}$ data was gathered using the wind up turn technique while estimating g loading.⁸ Accelerometer data were deemed unnecessary because only a subjective examination of gradient stability was required. This subjective evaluation was considered appropriate for this class of aircraft.

LATERAL DIRECTIONAL STABILITY. Lateral Directional stability was evaluated using steady heading sideslips and examination of the spiral mode. Steady heading sideslips were not required but deemed necessary in the interest of safety. Ground handling characteristics were also evaluated in crosswinds of 15 knots.

DYNAMICS. The short period and dutch roll modes were evaluated using excitation doublets with controls free and fixed.⁹ The Sportplane Design Standard required examination of only the short period mode. The dutch roll mode was evaluated to ensure no unsafe characteristics were present.

VIBRATION AND BUFFET. Vibration and buffet characteristics were evaluated at V_d using three axis control raps.

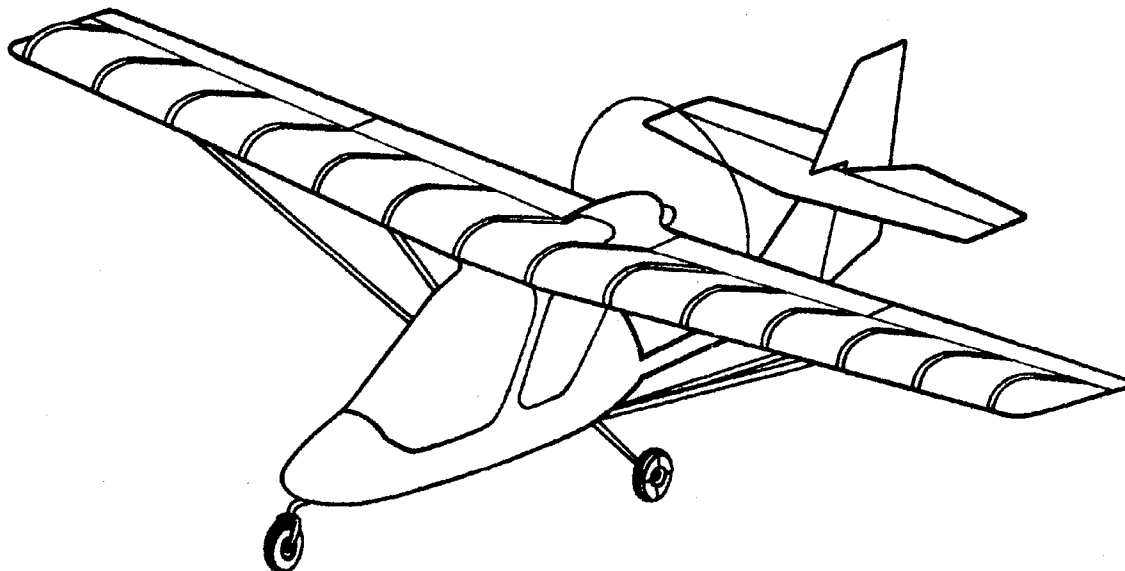
PROPELLER OVERSPEED. Propeller overspeed limits were evaluated at V_{NE} with power on and off.

LANDING PERFORMANCE. Landing performance data was gathered by measuring ground roll distances using flour bag markers and estimating the landing distance from 50 feet using a simple theodolite type setup.

FLIGHT TEST AIRCRAFT

The GT 500 aircraft, registration number N6573R and serial number 137, was equipped with a Rotax 582 uncowled, liquid cooled power plant and a Warp Drive ground adjustable, fixed pitch propeller. A complete description of the aircraft can be found in the AFM.¹⁰ An isometric view of the aircraft is shown in Figure 1. Weight and balance data for each flight is shown in Table 1.

Figure 1. GT 500 Aircraft



Flight	Takeoff GW (pounds)	Takeoff CG (inches)
#1	1039	71.86
#2	804	57.00
#3	1095	69.82

Table 1. Flight Test Weight and Balance

Flights #1 and #3 were primarily performance flight tests with flying qualities tests completed as time allowed. Flight #2 was dedicated entirely to flying qualities testing. The center of gravity envelope of the GT500 aircraft is very narrow at most aircraft weights, usually less than four inches of travel. The useful load with full fuel was 470 pounds. Ballasting for extreme forward and aft center of gravity for flight testing was impractical given the size of the aircraft, flight test crew requirements and lack of suitable

ballast locations. Considering the small center of gravity travel involved between fore and aft limits at all aircraft weights, extreme cg testing was not considered critical to the flight test program.

FLIGHT TEST RESULTS

Flight testing of the GT 500 aircraft was conducted from the Waukegan, Illinois airport from July 28 to July 30, 1993. Weather was clear throughout the flight test period. Performance testing was done during wind conditions of less than ten knots. Flight test data were gathered by hand recording readings from the standard flight instruments. Control forces were estimated using a hand held force gauge whenever possible.

All data were reduced to standard conditions. Data were reduced to SLSD where required unless data gathered at altitude exceeded requirements specified for sea level conditions. Specific flight test data are presented below along with a brief summary of the associated Sportplane compliance requirement.

PROPELLER SPEED

REQUIREMENT. No unsafe overspeeds are permitted under normal conditions to include max takeoff RPM during takeoff and 110% of maximum continuous RPM during power off V_{NE} dive.

RESULT. Propeller RPM did not exceed AFM limits during takeoff and power off and on V_{NE} dives.

STALLING SPEED

REQUIREMENT. V_{SO} must not exceed 45 mph and V_{S1} (flaps up) must not exceed 60 mph. Conditions are power off, 1 mph bleed rate, maximum GW, forward cg. Attitude and yaw control must be maintained to V_{SO} . The Sportplane standard is ambiguous in defining maximum stall speed as a calibrated or indicated speed. The intent of the requirement was interpreted to state the limits in calibrated airspeed.

RESULT. Demonstrated V_{SO} was 42 MIAS and V_{S1} was 47 MIAS. Stall was defined by an uncontrollable pitch down. Attitude and yaw control were satisfactory at V_{SO} . Data were gathered as indicated airspeed but were compared to calibrated values to insure that the aircraft did in fact stall at or below the stated airspeed requirement.

TAKEOFF DISTANCE

REQUIREMENT. Ground roll and takeoff distance over a 50 ft obstacle must be measured and published in AFM using specified procedures at SLSD conditions and maximum GW.

RESULT. Fifteen takeoffs were accomplished over the three day test period. Average ground roll was 220 feet and correlated with AFM data. Average takeoff distances to 50 feet were 700 feet and correlated with AFM data.

CLIMB

REQUIREMENT. At full throttle, the V_Y rate of climb must not be less than 300 fpm at SLSD conditions and V_X climb gradient must not be less than 1:12 at SLSD conditions.

RESULT. Data taken at 2000 feet PA, 6100 RPM and a V_Y of 54 MIAS yielded a rate of climb of 570 fpm and correlated with AFM data presented at 2000 feet PA. At a V_X of 45 MIAS and flaps 10°, a V_X

climb gradient of 1:6.25 at 500 feet PA exceeded the certification requirement. Reduction to SLSD to determine compliance was deemed unnecessary.

LANDING DISTANCE

REQUIREMENT. Ground roll and 50 ft landing distance must be measured and published in AFM using specified procedures at SLSD conditions and maximum GW.

RESULT. Fifteen landings were accomplished over the three day test period. Average ground roll was 240 ft and correlated with AFM data. Average landing distance from 50 feet was 600 feet and correlated with AFM data.

BALKED LANDING CLIMB

REQUIREMENT. At $1.3 V_{SO}$, full throttle and flaps extended, the climb gradient must not be less than 1:30. The rule was interpreted to allow 2 seconds of flap retraction to 20° Flap as is allowed in FAR Part 23.11

RESULT. Data taken at 500 feet PA and 6100 RPM yielded a gradient of 1:8.25. Data reduction to SLSD to show compliance was not necessary. The flap retraction to 20° flap could be safely accomplished without large angle of attack changes or exceptional pilot skill.

CONTROL & MANEUVERABILITY

REQUIREMENT. Pull up must yield nose up and push right must yield right wing down. Right rudder must yield nose right. Smooth transitions must be possible without excessive control forces. The Sportplane Standard lists maximum forces for temporary and prolonged application. The listed maximums are very generous for this class of aircraft. The aircraft must at least be trimmable for level cruise at an average weight and center of gravity.

RESULT. Controls were in proper sense during all phases of flight. Control forces were well below temporary and prolonged maximums allowed. Aircraft was trimmable at average weight and center of gravity at a variety of typical cruise speeds.

LONGITUDINAL CONTROL

REQUIREMENT. F_S/G gradient should increase steadily. Full longitudinal control must be available when extending and retracting flaps. Accelerations using longitudinal control only from $1.1V_{S1}$ to $1.5V_{S1}$ and $1.1V_{SO}$ to V_F must occur in less than 3 seconds with power on and off.

RESULT. F_S/G was stable at approximately 8 lb/g. Full control was available during flap extension and retraction. Longitudinal control only accelerations were acceptable but required very steep attitudes with power off.

DIRECTIONAL AND LATERAL CONTROL

REQUIREMENT. A 60 degree roll from 30 degrees of bank through level flight must be done in 4 seconds or less at $1.3 V_{SO}$ (full flaps with power off) and at $1.2 V_{S1}$ (flaps up, power off). The aircraft must be capable of performing traffic patterns with rudder only and aileron only. Rapid roll and yaw

inputs must not induce uncontrollable characteristics. Aileron and rudder forces must not reverse with increased control deflection.

RESULT. The time required to roll at $1.3 V_{SO}$ was 1.75 seconds and was 2.5 seconds at $1.2 V_{S1}$. Rudder only and aileron only traffic patterns require normal pilot skills. Rapid control use yielded a docile response in all cases. Aileron and rudder forces increased with increased deflection and gradients were stable throughout the flight envelope.

LONGITUDINAL STATIC STABILITY

REQUIREMENT. Longitudinal static stability must be positive from V_{S1} to V_{NE} at critical cg and power.

RESULT. Longitudinal static stability was positive throughout the flight envelope. Longitudinal stick force gradient was noticeably small but not objectionable.

DIRECTIONAL AND LATERAL STATIC STABILITY

REQUIREMENT. Stability is acceptable if the spiral mode stability is at least neutral from $1.2 V_{S1}$ to V_{NE} .

RESULT. Spiral mode was neutral to very slightly positive throughout the speed range. Steady heading sideslip tests showed directional stability only slightly positive with doors on. Stability was more positive with doors off. There is no requirement to do sideslip testing, but steady heading sideslip tests were added to ensure no undesirable characteristics were noted with the doors installed.

DYNAMIC STABILITY

REQUIREMENT. The longitudinal short period mode must be heavily damped with controls free and fixed.

RESULT. The short period mode was deadbeat from $1.1 V_{S1}$ to V_{NE} . The dutch roll mode was also evaluated and found to be heavily damped throughout the same envelope.

WINGS LEVEL STALL

REQUIREMENT. Bank and yaw excursions must not exceed 15 degrees with normal use of controls throughout the stall.

RESULT. The requirement was easily met if sideslip angle was normally managed. The aircraft was not equipped with a slip indicator, but did have a yaw string. Without the yaw string, sideslip management would have been more difficult.

TURNING FLIGHT AND ACCELERATED STALLS

REQUIREMENT. Power on, flaps up and down accelerated stalls shall cause no tendency to spin, cause excessive altitude loss or airspeed buildup. When started from a 30 degree bank turn, stall recovery shall cause no speed build up and return to level flight must be accomplished in less than 60 degrees of roll.

RESULT. Accelerated stalls were docile with no unusual departure or spin tendencies and no large altitude loss. Bank excursions required 30-45 degrees of roll to return to level flight. No excessive airspeed build up was noted throughout the recovery. Once again, use of the yaw string was required to manage the sideslip angle.

SPINS

REQUIREMENT. No requirement is specified in the Sportplane Design Standard. FAR paragraph 23.221 (a)(1) was applied to evaluate spin characteristics.

RESULT. Ten spins were attempted in all aircraft configurations and power settings. Pro-spin controls were held for one turn. Aircraft rotation was slow, smooth and without oscillations. Recoveries using the AFM procedure and hands free recoveries were accomplished in less than one half turn. During several entries, the aircraft transitioned into a spiral dive in less than one half turn and was easily recovered without excessive airspeed buildup.

DIRECTIONAL STABILITY AND CONTROL

REQUIREMENT. Use of right rudder must yield right turn. No special skill must be required for ground handling up to manufacturer's demonstrated crosswind limit.

RESULT. Rudder sense was proper throughout flight envelope. No unusual ground handling qualities were noticed during operations in crosswinds of 15 knots during taxi, takeoff and landing.

AIRPLANE FLIGHT MANUAL

REQUIREMENT. Specific data must include: Operating limitations, normal procedures and limited performance data.

RESULT. The original AFM was reviewed and found to be inadequate in airspeed and engine limitations, cg envelope description, usable fuel description and performance data. Many references were made to ultralight vehicles and the ultralight category of vehicles and had to be deleted. Manufacturer's update included correct speed limitations, updated placards and revised performance data. Engine cooling data provided by the applicant was accepted after observing the cooling characteristics of the uncowed, liquid cooled Rotax 582 engine during flight tests. Dedicated FAA conducted cooling climb tests were not deemed necessary.

PILOT COMPARTMENT

REQUIREMENT. Designed for 'good' visibility, accessibility, exit, reach and occupant protection.

RESULT. Cockpit layout and controls were found satisfactory except for the location of the fuel indicator sight gauges and the lack of a sideslip indicator.

FLUTTER

REQUIREMENT. No part of the aircraft shall exhibit heavy buffeting, flutter, control reversal or divergence up to V_D . Advisory Circular 23.629-1A lists several analytical methods used to determine susceptibility to flutter.¹²

RESULT. Report 45 analysis allowed by Advisory Circular 23.629-1A indicated the aircraft to be flutter free throughout the flight envelope.¹³ V_D dive was accomplished to 124 MIAS. Three axis control raps were accomplished at V_D . No undesirable vibration, buffet or control divergence was noted.

NONCOMPLIANT FINDINGS

Three areas were discovered during flight testing that were not in compliance with the Sportplane design standard. Before an unrestricted type certificate can be issued, the non compliant findings from the engineering review and flight test must be resolved.

SIDESLIP INDICATOR

The lack of a sideslip indicator combined with near neutral directional stability made sideslip control more difficult during low speed flight and stalls. A yaw string was successfully employed during flight test and was added to the type design to provide sideslip indications during all phases of flight.

FUEL INDICATING SYSTEM

The fuel indicating system consisted of sight lines painted on the plastic fuel tanks located in the wing root and visible in the crew compartment. The fuel level could not be read while flying from the front seat. Only total fuel was indicated by the fuel tank markings and hence no usable fuel indications were present nor was the usable fuel level placarded.

AIRPLANE FLIGHT MANUAL

As described in the flight test results presented earlier, the AFM was inadequate in several areas. The AFM was subsequently revised and found satisfactory.

CONCLUSION

The Quicksilver GT 500 design was awarded a provisional type certificate based on review of engineering data and results of flight tests. The limitations of the provisional type certificate will be removed when all discrepancies identified during data review and flight test are corrected. The Sportplane Design Standard was found to be a satisfactory certification tool for aircraft certified in the primary category. Each new aircraft design must, however, be individually evaluated to determine what additional testing should be done to ensure the type design exhibits no unsafe characteristics.

REFERENCES

1. The Federal Register, Vol. 57, No. 175, Wednesday, September 9, 1992. pp 41360-70.
2. 14 CFR part 21, paragraph 21.17(f) (1).
3. The Federal Register, Vol. 58, No. 114, Wednesday, June 16, 1993. pp. 33297.
4. 14 CFR part 21, paragraph 21.24(a)(3)(ii).
5. Flight Test Guide for Certification of Part 23 Airplanes, Advisory Circular 23-8A, February 2, 1989. pp. 40-45.
6. Flight Test Guide for Certification of Part 23 Airplanes, Advisory Circular 23-8A, February 2, 1989. pp. 74-79.
7. Flight Test Guide for Certification of Part 23 Airplanes, Advisory Circular 23-8A, February 2, 1989. pp. 67-68.
8. Flight Test Guide for Certification of Part 23 Airplanes, Advisory Circular 23-8A, February 2, 1989. pp. 64-66.

9. Flight Test Guide for Certification of Part 23 Airplanes, Advisory Circular 23-8A, February 2, 1989. pp. 70-74.
10. Quicksilver GT 500 Airplane Flight Manual, Quicksilver enterprises, Inc., March 9, 1994.
11. 14 CFR part 23, paragraph 23.77.
12. Means of Compliance with Section 23.629, Flutter, Advisory Circular 23.629-1A, October 23, 1985.
13. Robert Rosenbaum, Airframe and Equipment Engineering Report No. 45, Simplified Flutter Prevention Criteria for Personal Type Aircraft, ca. 1949.

PROCEDURES FOR AIRSPEED CALIBRATION BY USE OF GPS

Hubert C. Smith and Richard P. Anderson
Department of Aerospace Engineering
Penn State University
University Park, PA 16802

ABSTRACT

Highly accurate airspeed measurement is required to ascertain the difference between indicated and calibrated airspeed. The extreme accuracy associated with Global Positioning System (GPS) navigation would suggest that this system could be utilized for such purposes. This paper reports the results of a study at Penn State University using GPS to calibrate the airspeed system of a Piper Arrow. The GPS receiver is relied upon to measure both wind direction and groundspeed. This information is then utilized to determine true airspeed, and, ultimately, calibrated airspeed. Flight tests were conducted using a small portable receiver costing under \$1000. Results showed that this approach, involving simple procedures and minimal equipment, is an accurate and reliable method for calibrating airspeed systems in light aircraft.

INTRODUCTION

BACKGROUND

One of the first steps in flight testing is to obtain an accurate calibration of the airspeed indicating system. As basic and as old as this procedure may be, it still is rather difficult to perform accurately. Various methods are used, such as flying over a measured course (speed course method), flying by a photo-grid, pacing with a calibrated aircraft, etc. All of these involve procedures that are subject to a number of experimental errors. The often small difference between indicated and calibrated airspeed requires a procedure with minimal error, however.

In recent years, a revolutionary system of global navigation was developed, known as Global Positioning System, or GPS. This system depends on signals from 24 orbiting satellites, which are now in place for the full operation of the system. Numerous receivers have been developed to utilize these signals for highly accurate navigation by aircraft, ships, and almost any other mode of transportation. The system is also adaptable to such things as surveying, spotting fishing and mineral deposit locations, and measuring groundspeed of everything from aircraft to joggers.

PURPOSE

This study looks at the use of GPS as a possible means of improving the accuracy of airspeed calibration, and also as a method involving minimal equipment and expense. A small portable receiver costing less than \$1,000 was utilized. The procedures developed involved light aircraft at low speeds and altitudes.

TEST PROCEDURES

COMBINED METHODS

The method that was previously used at this institution was the speed course method, which is to fly over

a measured course, and time the passing of boundary markers. Passing is determined visually by an observer in the aircraft. The aircraft is headed perpendicular to the boundary markers so that the true airspeed vector is aligned with the course, as shown in Fig. 1. A repeat flight is then made in the opposite direction, and the true airspeed determined from the average of the two groundspeeds measured.

$$V_T = \frac{V_{G_1} + V_{G_2}}{2} = \frac{(V_T - V_w \cos\Theta) + (V_T + V_w \cos\Theta)}{2} \quad (1)$$

This value is then converted into calibrated airspeed through appropriate application of the density ratio, and compared to the indicated value. Strictly speaking, this airspeed is equivalent airspeed, but at low speed and altitude it is the same as calibrated, and is referred to as such in this report.

For the initial testing of the GPS airspeed measurement, the speed course method was again used, but the groundspeed was also measured by the GPS receiver. A Trimble Flightmate handheld GPS receiver was used for these tests. The aircraft was a Piper Arrow II. The aircraft had all standard factory instrumentation, except for a boom-mounted, swivel-head pitot-static probe connected to a sensitive airspeed indicator in the cockpit. The measured course consists of two parallel roads 3.65 statute miles apart.

In flying the speed course method, the aircraft is allowed to drift, as shown in Fig. 1, so that only the true airspeed plus or minus the component of the wind parallel to the heading is involved in the recorded speed. Hence, if any crosswind is present, the aircraft ends up, not at point b., but rather at point c. This is of no consequence in the speed course method. However, the GPS is calculating groundspeed along its ground track, the line a-c. Thus, if a crosswind is present, there will be an error between the value determined by the speed course method and that determined by the GPS.

In order to measure true airspeed from GPS groundspeed, it is necessary to know the wind direction. Figure 2 shows the velocity diagram for the aircraft flown with a headwind component. The groundspeed measured by the GPS along the track is labeled V_G , and ϕ is the drift angle. Thus,

$$V_G \cos\phi = V_T - V_w \cos\theta \quad (2)$$

and true airspeed can be determined as,

$$V_T = V_G \cos\phi + V_w \cos\theta \quad (3)$$

where ϕ is

$$\phi = \sin^{-1} \left[\frac{V_w \sin\theta}{V_G} \right] \quad (4)$$

True airspeed could also be calculated in the same fashion from groundspeed measured on the reverse course. If groundspeed were measured by the GPS in both direction, the true airspeed could be determined from an averaged value similar to the speed course method, but the drift angle in each

direction would be involved. The resulting equation would be,

$$V_T = \frac{V_{G_1} \cos \phi_1 + V_{G_2} \cos \phi_2}{2} \quad (5)$$

Note the analogy to Eq. 1. It would appear that if the drift angles were very small, the cosines would be approximately 1, and the two methods could be utilized simultaneously, and compared.

An examination was then made of the error involved in neglecting the wind in the GPS measurements, while heading the aircraft perpendicular to the course boundaries for the speed course measurements. An example was looked at for the case of an aircraft at 100 knots true airspeed with a 20 knot wind at an angle of 30 degrees to the heading. This situation gave a crosswind of 10 knots, and a headwind-tailwind component of 17.3 knots. Using the above relations, an accurate GPS was calculated to read 83.36 knots with the headwind component, and 117.79 in the reverse direction, averaging out to about 100.6 knots. Accurate measurement by the speed course method, of course, should give exactly 100 knots. Hence, the error here is small, as hypothesized. For relatively light winds, which normally is the case on days chosen for flight testing, this procedure should prove effective.

EXCLUSIVE GPS MEASUREMENT

Recognizing that the main purpose of utilizing the GPS was to improve the accuracy of the calibration procedure, a revised method was considered necessary. It was also desirable to devise a stand-alone procedure that could be performed anywhere, at any altitude. Such procedure would require accurate wind information. Winds aloft forecasts could be used to approximate the wind speed and direction at the appropriate altitude. However, such information is only a forecast, and has been proven to be in considerable error at times. Most navigational devices of the complexity of a GPS receiver have an inherent capability of determining the wind vector, given the proper inputs. This situation proved to be true of the instrument being used.

The device has a mode for solving wind triangle problems. With inputs of heading, airspeed, pressure altitude, and temperature, it will solve for the wind vector as the dependent variable. The airspeed input, however, should be calibrated airspeed, which, of course, is not yet known. The prompt actually asks for indicated airspeed, and this value seems to be close enough for purposes of determining wind. Given wind speed and direction, the true airspeed could be calculated from Eq. 3 or 5.

A simpler approach, however, would be just to take the wind direction determined by the GPS unit, and fly both into and away from that heading. This procedure eliminates any drift, and hence, the need to compute it. The true airspeed is then the average of the two groundspeeds recorded.

Tests run utilizing this method revealed that there is not a high degree of accuracy in the measurement of wind direction if the wind is relatively light. However, as noted above, a light wind also introduces minimal error in the resulting true airspeed, in the event the aircraft is not headed exactly into and away from the wind. Thus, some uncertainty here does not seem to be a problem.

Note that the GPS unit does directly compute a true airspeed reading, but this is based on the assumption that the indicated and calibrated airspeeds are the same. This is usually close enough for navigational purposes, but not for airspeed calibration. If the value of true airspeed read out by the GPS were converted to calibrated, it would be the same as the indicated input value, and the whole purpose of the calibration defeated. Hence, a computation of true airspeed from averaged groundspeeds is necessary.

RESULTS

The results of the combined tests are shown in Fig. 3. These flight tests were made on a day when the winds were light and variable, so that the GPS measurements should be reliable. In both methods, true airspeed was determined from an average of the groundspeeds in both directions, and converted to calibrated through the density ratio. Calibrated values are then plotted against the indicated values. Since the data for each case appeared to be in a straight-line relationship, curves were fitted by linear regression. The error between calibrated and indicated airspeed for the GPS measurement is about 3% at the low-speed end of the range, and about 2% at the high end. Comparable data measured by the speed course method indicates about 3% error in the low range, increasing to about 7% at the high end. These results seem to be reasonable. The boom-mounted pitot static system and sensitive airspeed indicator used was expected to give minimal position error. Hence, the relative error between the two methods seems to indicate the relative accuracy of each.

Figure 4 shows the results of high altitude tests made solely by use of the GPS. Flights for these tests were made at 6,250 ft. pressure altitude on a day when the winds were 45 knots at that altitude. Hence, there was not much problem in determining the wind direction. The groundspeed was averaged from flight directly upwind and downwind. A linear fit is again made of the data. Again, the calibrated airspeed varies from indicated by about 3% at the low end of the scale to about 1.5% at the high end. This result seems to be in good agreement with the results at low altitude on a calm day, obtained by neglecting the wind.

CONCLUSIONS

This study shows that use of a GPS receiver to measure true airspeed from averaged groundspeed readout is an accurate and simple method of calibrating the airspeed on light aircraft at relatively low speeds and altitudes. The device can also be used to determine wind direction, which is necessary for the procedure. If winds are very light, the aircraft heading relative to the wind appears not to be significant. Therefore, under such conditions, the GPS method can be used as a backup to other methods of airspeed calibration.

BIBLIOGRAPHY

1. George, Fred, "GPS Special Report," Flying, September 1992.
2. Hamlin, B., Flight Testing Conventional and Jet-Propelled Airplanes, The Macmillan Co., New York, NY, 1946.
3. Smith, H. C., Introduction to Aircraft Flight Test Engineering, IAP, Inc., Casper, WY, 1981.
4. Trimble Flightmate GPS Operating Manual, Trimble Navigation, Sunnyvale, CA, 1993.
5. Ward, D. T., Introduction to Flight Test Engineering, Elsevier Science Publishers B.V., Amsterdam, The Netherlands, 1993.

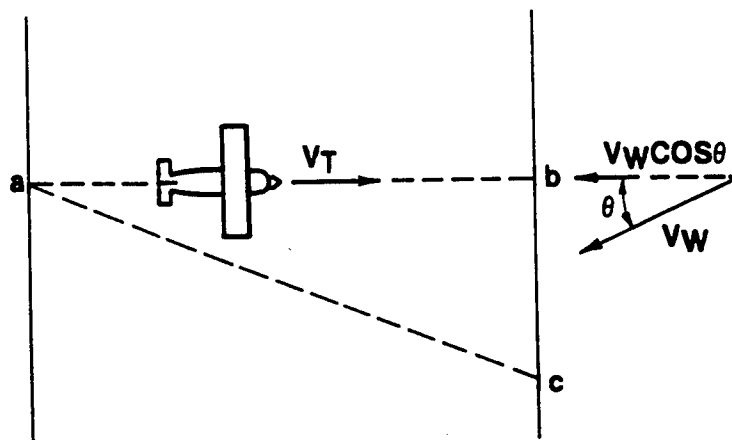


Figure 1. Traversing speed course with wind acting.

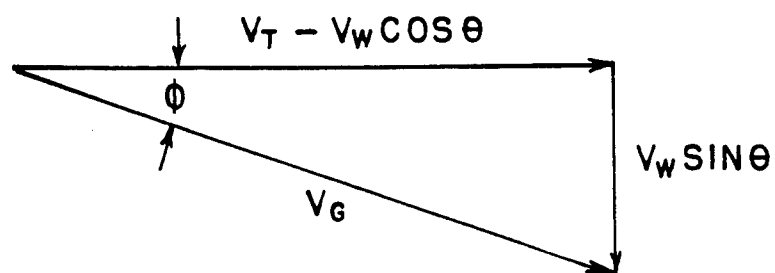


Figure 2. Velocity vectors resulting from wind on speed course.

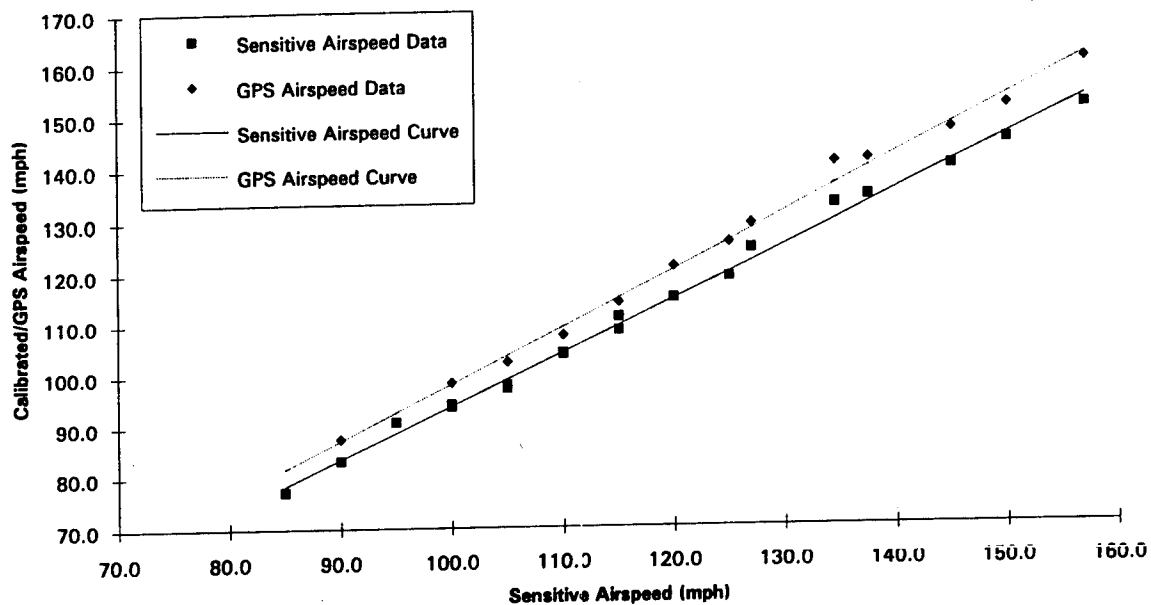


Figure 3. Airspeed calibration curves for combined speed course and GPS measurement.

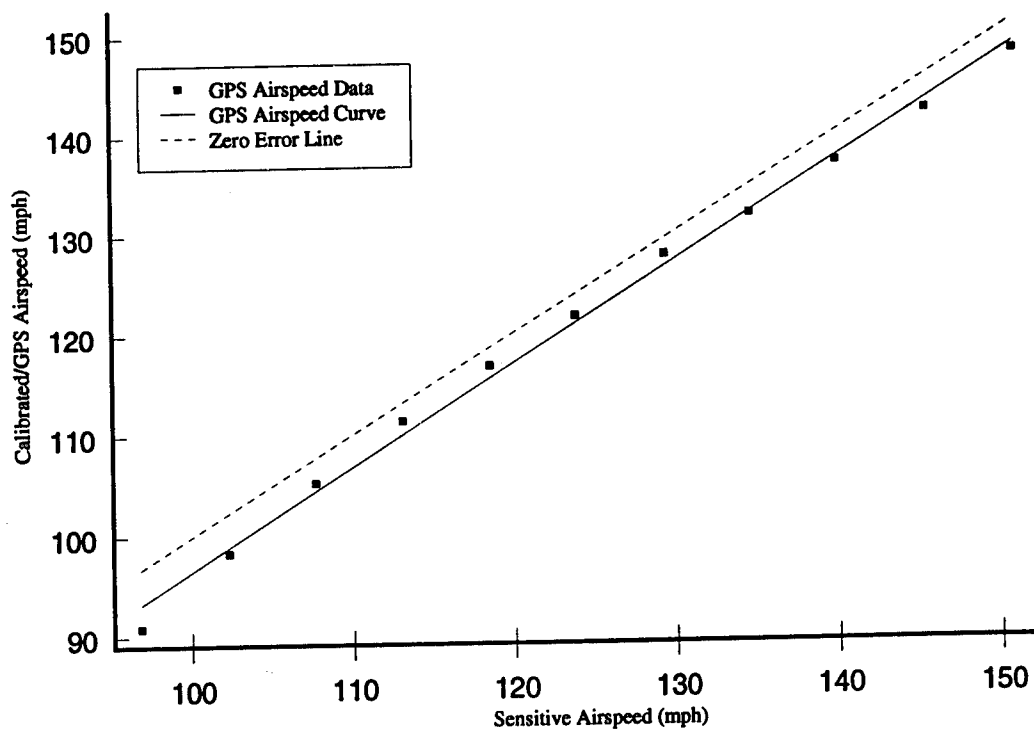


Figure 4. Airspeed calibration curve as measured by GPS alone at altitude.

DESIGN OF A FULLY AUTOMATED PC DRIVEN DATA ACQUISITION SYSTEM FOR AN EXPERIMENTAL AIRCRAFT

Mr. Van G. Chaney*, Dr. Keiichi Motoyama**, Mr. Rodney L. Lincoln*,
Mr. Kenneth L. Ledlow*, Mr. Yuya Otsuka**

* Raspet Flight Research Laboratory, Mississippi State University
Starkville, MS U.S.A.

** HONDA R&D North America
Starkville, MS U.S.A.

ABSTRACT

A personal computer (PC) driven data acquisition system was designed for the MH-02 experimental aircraft which was developed by a joint research program between HONDA R&D and Raspet Flight Research laboratory, Mississippi State University. The system consists of a PC, sensors, signal conditioners, Analog to Digital converter, etc. It uses flight data for warning systems and other displays to enhance flight safety. A simple operation by the pilot initiates the data system which measures aircraft performance parameters, structural vibration, landing gear loads, and control surface position. Special attention was paid to engine thrust estimation. An engine ground test was conducted to measure the static thrust. The test results were compared with calculations made by an engine deck program. After each mission, in-flight thrust is calculated by the engine deck program using measured fan speed (N1), pressure altitude, and other parameters. More than thirty flights were conducted, and the procedure to conduct flight test and data analysis was established. The ultimate goal of the flight test program is to determine the performance, handling quality, validate the design, and recommend improvements.

INTRODUCTION

The authors have been studying the instrumentation and data analysis methods needed to conduct flight tests for an experimental aircraft. In the previous study by Chaney et. al.,⁽¹⁾ a multi-computer in-flight data acquisition and analysis system was developed for general aviation aircraft. In that paper, the flight test of a 690 Turbo Commander was discussed. Since a 690 Turbo Commander has enough room, a multi-computer system was installed, and flight tests were conducted by two pilots and one flight engineer. However, the MH-02 has more stringent weight constraints which limit the flight test crew to two people. Therefore, a single computer system that can be operated by the pilot was designed and is discussed in this paper. The flight data mainly consists of: 1) data to insure in-flight safety and: 2) data to calculate performance, handling quality, structural vibration and landing gear loads. The system has some special features such as a warning system to indicate excessive tail vibration and cockpit displays of measured data for the pilot to observe while flying. The authors are especially interested in in-flight thrust determination.⁽²⁾⁻⁽⁴⁾ The method used to estimate thrust with fundamental research data, engine ground test data, and an engine deck program is discussed in this paper.

EXPERIMENTAL AIRCRAFT

The MH-02 experimental aircraft is being developed by a joint research program between HONDA R&D and Raspet Flight Research Laboratory, Mississippi State University. The MH-02 has a forward swept wing, slats, and triple slotted flaps. Two JT15D-1 engines are installed on the wings. Most of the airframe is made of carbon fiber composite. The external dimensions and the maximum take off weight are as follows;

Wing Span	:	11.24 m
Length	:	12.25 m (without nose boom)
Height	:	4.18 m
Maximum Take off Weight	:	3,629 Kgf

The MH-02 is certified by the FAA as an experimental R&D aircraft. Flight test began March 5, 1993. The instrumentation system discussed in this paper is installed mainly in the cabin. The general drawing of aircraft is shown in Figure 1.

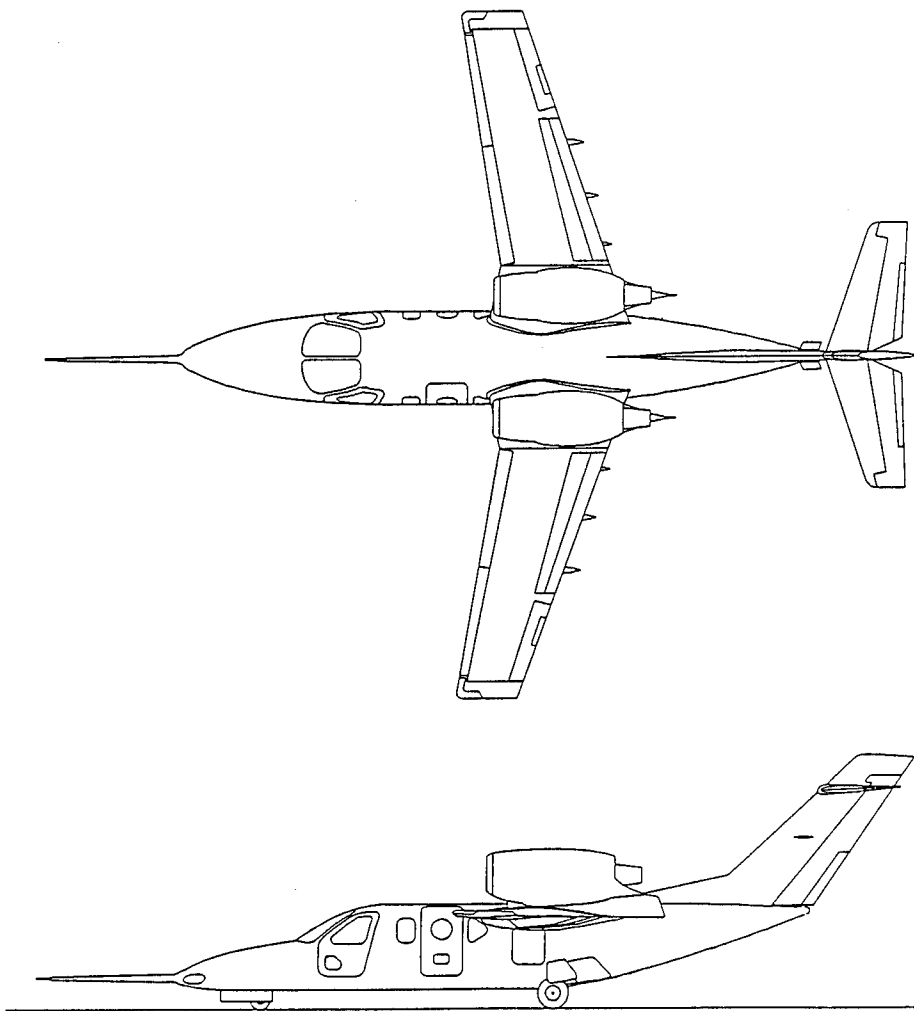


Fig. 1 Experimental Aircraft MH-02

INSTRUMENTATION SYSTEM (Data Acquisition Hardware, Software and Sensors)

The MH-02 data acquisition system consists of a 486-33DX PC, five Input/Output cards, and corresponding sensors. The PC is powered by a 1 KVA capacity static inverter which is connected to the 28 Vdc aircraft power system. The pilot activates the system with a pair of toggle switches, one for 28 Vdc and one for 120 Vac. The PC automatically boots and begins reading the sensors. The pilot stores data by depressing a thumb switch located on the yoke. If required, the co-pilot can also control the DAS with a miniature (5×7.5 mm) multiple button key pad. The key pad has many functions such as changing the sampling rate, starting new data files and controlling the graphics on a video monitor. After booting the PC drives a few of the cockpit's indicators such as an angle of attack meter, a side slip angle meter, an LED indicating data reading or saving, and a data event counter. Other cockpit instrumentation include aileron, rudder, elevator, and flap control surface position displays. These are current driven, 1 mA full scale deflection, horizontal analog meters. Displacement is measured at the push rod with a 1 K Ω potentiometer with built-in spring return. The wiper is used for the output signal.

Stick and rudder forces are measured by a Kohlman pilot force measurement unit⁽⁵⁾. The system uses strain gauges in a four-arm active Wheatstone bridge and beam bending theory of operation. Prior to installation a number of tests were performed on the force wheel to determine the extent of signal cross coupling between the yoke pitch and roll strain gauges. Also, tests to determine what effect changes in the location of the pilot's grip might have. The results showed that the force measurement system was amazingly accurate and in-sensitive to either problem.

A tail vibration warning light is located on the instrument panel. The light is connected to two Endevco accelerometers mounted in the tips of the horizontal tail. The accelerometer on the right side measures vibration along the longitudinal axis. The left sensor measures vertical acceleration. Hardware in the cabin integrates the signal to obtain displacement. The light is automatically illuminated if the measured vertical or horizontal displacement meets or exceeds 17 mm. Ground vibration tests of the aircraft were performed by Leon Tolve, FAA designated engineering representative, to calibrate the system. The amplitude of vibration selected to trip the light is considered as dangerous but below the limit strain of the tail structure.

A Rosemount flow angle sensor mounted on the nose of MH-02 sends pneumatic pressure to the lower angle of attack port pressure (P_{a1}), upper angle of attack port pressure (P_{a2}), right side slip angle port pressure ($P_{\beta 1}$), left side slip angle port pressure ($P_{\beta 2}$), local pitot, and static port which are located inside of the Rosemount Data package. Three 1/2 PSID Rosemount transducers, model #1221F1VL5A1A; one 2.5 PSID Rosemount transducer, model #1221F2AF7A1B; and one Rosemount, model #1241A4BCD are connected to these ports as shown in Figure 2. Signals from these transducers are used to extract airspeed, angle of attack, side slip angle, altitude, and rate of climb. The data air package inside temperature (PIT) is measured and recorded. It is used during post flight data reduction for temperature compensation of the Rosemount transducers. Other measured data include: nine channels of the fuel system, six channels for the flap monitor system, seven accelerometers, six engine signals, four forces, six gear door signals, eight horizontal tail strain gages, three positions (aileron, rudder, elevator), two temperatures, alternate Rosemount air speed, and aircraft 28 Vdc buss.

Analog to digital conversion is done by an 8 channel 16 bit Analog Devices RTI-850 card and two 16 channel 12 bit MetraByte cards. There are also four 12 bit expansion chassis, each of which adds an additional 16 channels to the systems capacity. If needed, the computer can be retro-fitted with up to 32 expansion boards for a total of 520 channels. Once all data has been saved on the PC, it is easily transferred to an external magneto optical disk with a capacity of 128 MB per diskette. This data is then transferred to a local PC in the Data Reduction Office.

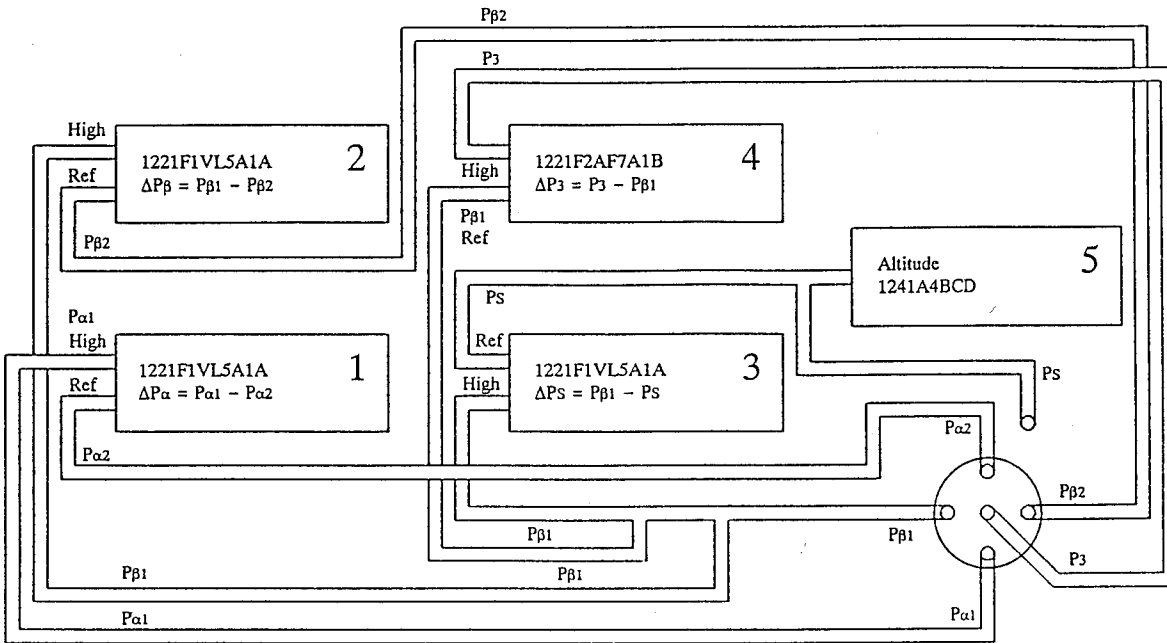


Fig. 2 Air data boom circuit

The "black box" philosophy of design was used to help make the system easy to maintain and to increase its reliability. Most of the hardware is mounted on a single removable rack in the aft cabin area. A defective component, including the PC, can be replaced in minutes. To date, the design has worked well beyond expectations. In 38 missions flown, none have been canceled or aborted due to problems with the DAS.

Software is written in Quick-Basic (QB45). It was chosen over Fortran and C because it is more user friendly and has adequate graphics. It turns out that the issue of simplicity was much more important than originally anticipated. Graduate assistants do a substantial amount of the data reduction work. Unfortunately, they are somewhat transitory, usually only working about 18 months. Their replacements typically have very little experience with higher level computer languages but are exposed to Basic as undergraduates and have no problem understanding the MH-02's data acquisition/reduction software. As a result, it was discovered that the time required for training is very short. Normally, new graduate students can become useful members of the flight test team in only a matter of days.

Quick-Basic graphics are used to display sensor data on a video monitor. The monitor and keyboard shown in Figure 3 can be attached to the aircraft externally with an electrical umbilical. This is used during ground tests of the hardware and for sensor calibration. The data is shown in engineering units and voltage. The co-pilot's keypad can also be used to scroll between different pages of sensor data. This was done in case future missions require a monitor in the cockpit.

The aircraft is equipped with three SONY miniature CCD color video camera modules. Their locations are changed depending on the mission requirements, but, in general one is focused on the instrument panel, the vertical tail tufts, and the upper wing tufts. The cameras activate automatically with 28 Vdc and record continuously throughout mission.

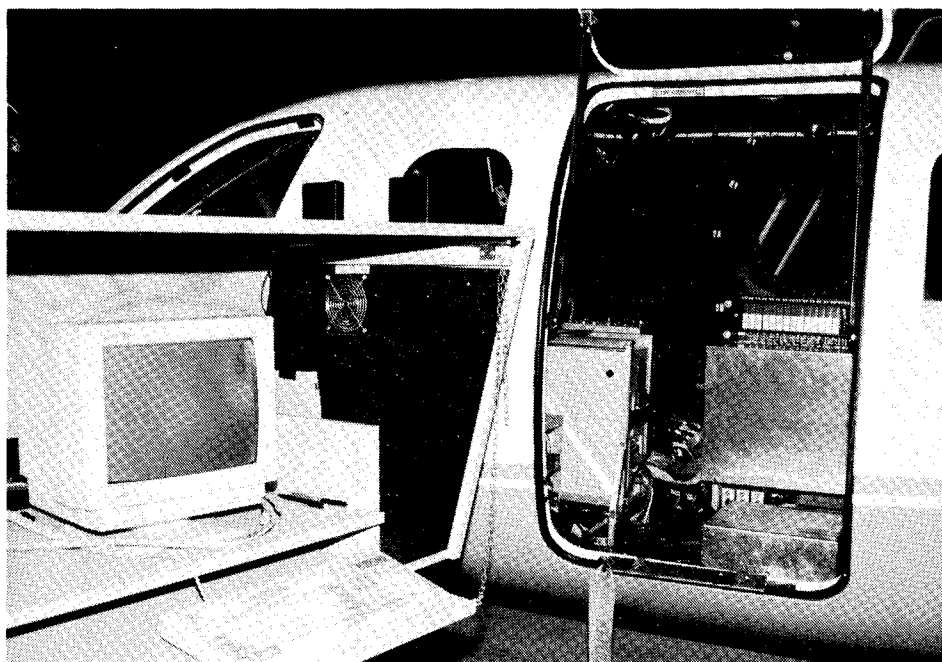


Fig. 3 External Video Monitor and Keyboard

Aboard the MH-02 is a MUP-ISS Type C Inertial Measurement System manufactured by Japan Aviation Electronics Industry, Limited. The system consists of the Global Positioning System (GPS), the Inertial Measurement Unit (IMU), the Control Unit (CU), the pressure sensor, and the laptop PC. The IMU contains the three-axes rate integrated gyros and the three accelerometers. The CU is the heart of the system. The barometer, IMU, PC, and GPS connect to the CU which contains all integrations and processor hardware. Power is distributed from the CU to all other devices except the GPS and PC. The system measures rates and accelerations in three axes and integrates them to derive angles, velocities, and positions. Because of the inherent errors associated with such a system, the MUP-ISS Type C utilizes the position from the GPS to reduce the error. The MUP-ISS Type C also utilizes the pressure transducer for altitude in the same way. The system may output up to fourteen analog channels continuously. Six of these channels are full time, direct output from the gyros and accelerometers. The other eight channels may be selected during initialization from the three angular rates, angles, accelerations, velocities, or positions.

GROUND ENGINE TEST

Accurate measurement of aircraft performance depends on a good estimation of the engine thrust. In steady level flight, thrust is used to determine the aircraft drag. Unfortunately, thrust is very difficult to measure in flight. As an alternative, the authors chose to use Pratt & Whitney's performance estimation program P1591. The program was developed for the JT15D engine which is used in the MH-02 aircraft. After each flight, thrust is calculated with the engine deck program. P1591 inputs include the atmospheric conditions of the test day, the throttle settings, the velocity, pressure altitude, and bleed air setting. It computes engine thrust and fuel flow as well as several other parameters.

Before the flight test program began, the performance estimation program was calibrated with a static ground test.

The setup of ground engine test is shown in Figure 4. The aircraft was restrained with 14000 lb capacity chain. Digital strain meter DRA-10A manufactured by Tokyo Sokki Kenkyujo Co., Ltd recorded the thrust measured by load cell. Handheld instruments were used to acquire the weather conditions. The other engine parameters, such as fan speed (N1), high pressure turbine speed (N2) and fuel flow, were sent to the ships computer. The test was conducted by controlling the N1 with the throttle and recording the engine measurements when stabilized.

After the tests had been completed some differences were found in the measured and computed thrust. As a result some parameters like the intake pressure loss were adjusted. Since the thrust of the fan jet engine is mainly affected by N1, the engine deck was tuned to estimate the thrust as a function of N1. Figure 5 (a) shows the measured data of " $N1\sqrt{\theta}$ vs. T/δ ", where θ is the ambient temperature ratio, T is thrust, and δ is the ambient pressure ratio. Also, " $N1\sqrt{\theta}$ vs. $W_f/(\delta\sqrt{\theta})$ " and " $N1\sqrt{\theta}$ vs. $N2\sqrt{\theta}$ " are shown in Figures 5 (b)-(c), where W_f is the fuel flow rate.

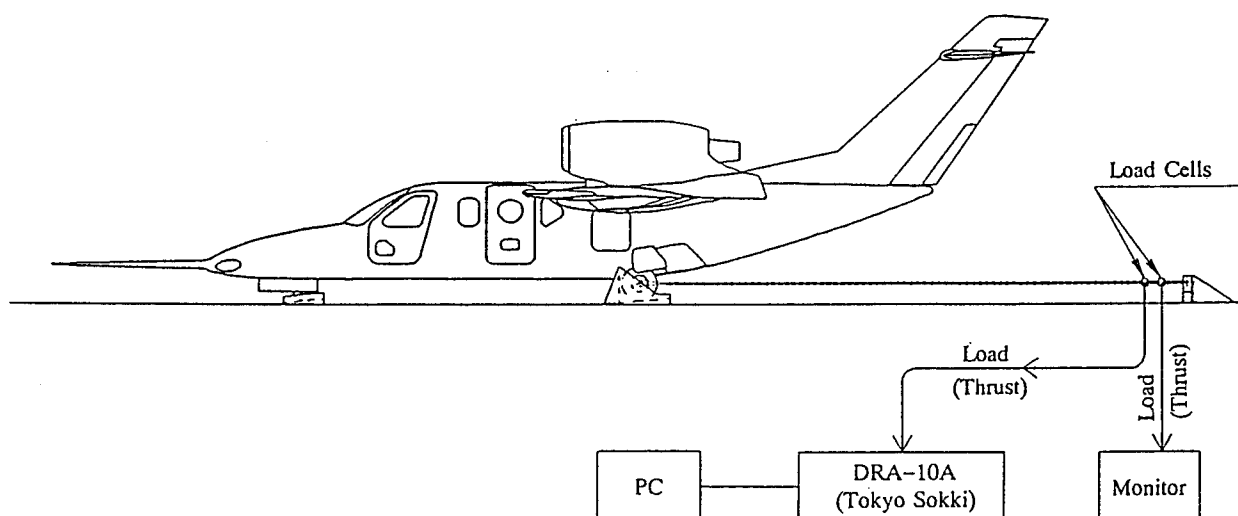


Fig. 4 Setup of ground engine test

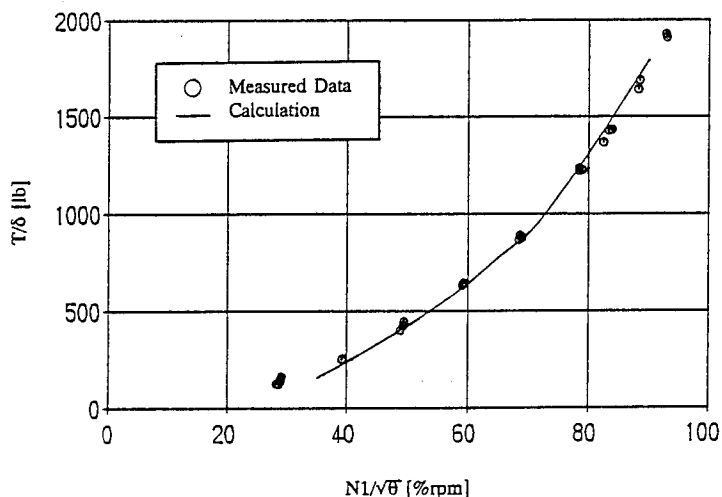


Fig. 5 (a) Comparison of measured data and estimated results ($N1\sqrt{\theta}$ vs. T/δ)

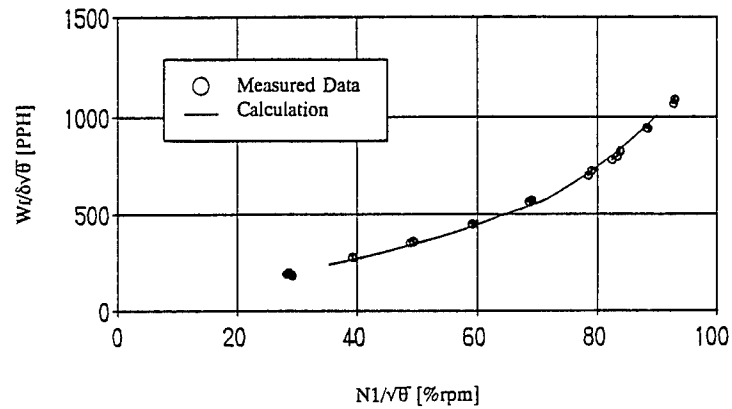


Fig. 5 (b) Comparison of measured data and estimated results ($N1/\sqrt{\theta}$ vs. $Wt/(\delta\sqrt{\theta})$)

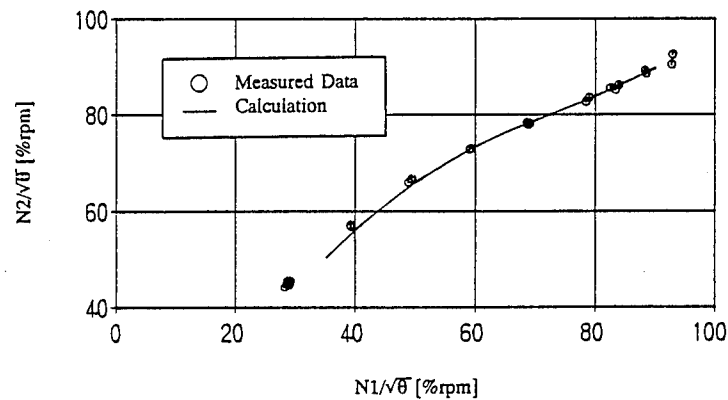


Fig. 5 (c) Comparison of measured data and estimated results ($N1/\sqrt{\theta}$ vs. $N2/\sqrt{\theta}$)

FLIGHT TEST AND DATA ANALYSIS

The flight test is discussed by the aircraft crew and engineers in a pre-flight briefing. The contents of the test program, test procedure, and job assignments for the flight crews are clarified. Information such as the fuel consumption is calculated before the briefing with the engine control deck and trim condition analysis. An example of a typical test sortie is shown in table 1.

Table 1 Flight test program

Seg#	Test Name	Config.	Alt[ft]	IAS[kt]	Fuel Burned	R/L N1[%]	Time
1	Cont.Surf.CHK	F-To,G-Dn	333.	0.0	0.0 / 0.0	0.0 / 0.0	1:00 / 1:00
2	E/G Start	F-To,G-Dn	333.	0.0	19.1 / 19.1	31.7 / 31.7	3:00 / 4:00
3	Pre FLT CHK	F-To,G-Dn	333.	0.0	12.8 / 31.9	31.7 / 31.7	2:00 / 6:00
4	Taxi	F-To,G-Dn	333.	0.0	31.9 / 63.8	31.7 / 31.7	5:00 / 11:00
5	T/O	F-To,G-Dn	333. - 433.	0.0 - 130.0	12.4 / 76.2	81.5 / 81.5	0:30 / 11:30
6	Climb	F-To,G-Dn	433. - 7500.	130.0	137.1 / 213.2	75.5 / 75.5	7:05 / 18:35
7	130[kt] Trim	F-Up,G-Up	7500.	130.0	12.2 / 225.4	68.6 / 68.6	1:00 / 19:35
:	:	:	:	:	:	:	:
56	T/D to Stop	F-To,G-Dn	333.	99.5 - 0.0	4.2 / 1019.2	31.5 / 31.5	0:40 / 77:45
57	Taxi	F-To,G-Dn	333.	0.0	31.9 / 1051.1	31.7 / 31.7	5:00 / 82:45
58	E/G Shut Down	F-To,G-Dn	333.	0.0	0.0 / 0.0	0.0 / 0.0	0:30 / 83:15

The flight test begins after the briefing. The measuring system is designed to be user friendly and robust. When the data system power is applied, the PC automatically boots, performs a self test, displays its operation status, and immediately begins monitoring all sensors. Once the pilot initiates data acquisition by depressing a yoke thumb switch, data storage of the first segment begins. Each successive operation of the pilot's data switch closes the current data file and opens the next data segment. The entire mission is stored. Continuous acquisition of data is necessary in order to calculate the weight of aircraft by integration of fuel flow rate. The following information is displayed in the cockpit when the PC is running.

- 1) Two blinking red lights inform the crew that data has been taken properly.
- 2) The measured angle of attack, side slip angle, control surface position, and flap position.
- 3) A red warning light which illuminates when the horizontal tail exceeds the predetermined calibrated amplitude of vibration.

The file name of each data segment consists of the date, time, and month. This prevents files from being overwritten in the event the PC is rebooted in flight.

The measuring system has the three sampling rates of 6, 20, and 80 Hz. Usually the 6 Hz sampling rate is used for level flight test, static stability test, etc; the 20 Hz rate is used for dynamic stability test; and finally, the 80 Hz is used for vibration test.

Data Analysis

After landing, data is transferred to the magneto optical disk. The data files are converted to engineering unit files and plotted as time histories by a 486DX-66 PC. The data is sent to EWS and analyzed by spread sheet. The review meeting is held with time histories and VCR record. To analyze the flight data in detail, some programs are developed such as an auto-scaling program, average program, maximum-minimum program, etc. The detail analysis of the flight data will be discussed in further report.

CONCLUSION

The purpose of this study was to conduct a safe flight test and to evaluate the aircraft. To accomplish this, an automated PC data acquisition system was designed. Concluding remarks are as follows;

- 1) The system is easy to operate and only needs one pilot to perform flight tests.
- 2) The system is relatively inexpensive and light, because there is no need for a data recorder or data logger.
- 3) The system displays flight status which is helpful to the pilot.
- 4) The system is designed so that the number of parameters measured can easily be expanded or changed.
- 5) After landing, thrust can be determined by using the engine deck program tuned by ground engine test.
- 6) Software written in Quick-Basic proved to be beneficial due to its inherent user friendliness.

ACKNOWLEDGEMENT

The authors would like to express their appreciation to Dr. Albert G. Bennett, Director of Raspet Flight Research Laboratory, Mississippi State University, and Mr. Grady W. Wilson, Chief Test Pilot of Raspet Flight Research Laboratory, Mississippi State University, for their valuable advice and discussion. The authors also would like to express the special thanks to Dr. Ralph D. Kimberlin, University of Tennessee Space Institute for his advice for the ground engine test and the first flight.

REFERENCE

- (1) V. G. Chaney et. al., "Development of a multi-computer in-flight data acquisition and analysis system for general aviation aircraft", Feb. 1992 AIAA Aerospace Design Conference
- (2) T. W. Sanders, "The development and testing of an in-flight thrust determination method for a Pratt & Whitney JT15D-1 turbofan engine", M.S. Thesis, Mississippi State University, May 1993
- (3) M. N. Ramsey, "Experimental study of a simple thrust model for a Pratt & Whitney JT15D-1 turbofan engine", M.S. Thesis, Mississippi State University, Dec. 1993
- (4) Pratt & Whitney Aircraft of Canada LTD., "JT15D Series Engines Performance Estimation Program P1591 User's Manual", May 1991
- (5) Kohlman Systems Research, Inc., "Pilot Force Measurement System Operation and Reference Manual", May 1993

THE UTILIZATION OF GENERAL AVIATION AIRCRAFT: RECENT DEVELOPMENTS

Dong W. Cho
Department of Economics
Wichita State University
Wichita, Kansas 67260

Gerald S. McDougall
Donald L. Harrison College of Business
Southeast Missouri State University
Cape Girardeau, Missouri 63701

ABSTRACT

General aviation jet utilization rates are investigated using regression models based on cross-correlation analyses incorporating 7-year leads and lags. Several interesting results emerge. While the utilization rate is theoretically linked to total fleet hours and fleet size, our results show that changes in fleet hours is the dominant factor. Changes in fleet size (or aircraft acquisitions) plays a secondary role. The jet utilization rate is affected by aircraft operating costs and corporate profitability. The impact of weak economic conditions, changes in corporate culture, and institutional changes in the general aviation industry on jet utilization begins to show up statistically after 1988. It is anticipated, however, that declining operating costs and increased corporate profitability will cause the reported jet utilization rate for 1993 to be higher than the value reported for 1992. This increase should show up in new production, shipments and fleet growth in 1995 and 1996.

INTRODUCTION

The study of general aviation (GA) aircraft utilization rates is warranted because the utilization rate is a key indicator of the economic health and vitality of the general aviation industry, and it is an important input into the planning processes used by all of the major participants in the industry, including the Federal Aviation Administration (FAA). Furthermore, there have been some recent innovations in general aviation institutions and these could affect aircraft utilization rates in future years. A better understanding of the factors affecting the aircraft utilization rate is necessary to anticipate the impact of these innovations and new institutional arrangements.

This paper summarizes the results from an investigation of the factors affecting general aviation jet utilization. Restricting the analysis to general aviation jet aircraft is appropriate given the dominant position of turbojet aircraft in today's general aviation industry. Following the thrust of Granger causality tests, cross-correlations based on 7-year leads and lags are used to sift out directions of influence among flight hours and fleet size. This statistical investigation of "cause and effect" leads to the specification of a statistical model explaining aircraft utilization. The estimated utilization model suggests that operating costs are more important than the level of economic activity in explaining business jet utilization. Furthermore, there have been structural changes affecting general aviation flying and these may be linked to changes in tastes for flying and to the introduction of new communication technologies, as well as to the emergence of new institutional arrangements for providing GA services.

BACKGROUND

The utilization rate, or average flight hours, for general aviation aircraft is calculated using reported figures for total flight hours produced during a year and the number of aircraft in the active fleet. The size of the active fleet, of course, is affected by shipments of new aircraft. Theoretically, the utilization rate reflects both the demand for general aviation flying (i.e., operations) and the demand for new and used aircraft (i.e., acquisitions). By definition, *ceteris paribus*, an increase in business flying raises measured aircraft utilization through total fleet hours, while an increase in fleet size through the delivery of new aircraft or the importation of existing aircraft lowers the observed utilization rate.¹

Because of changes both in the demand for flying and in the demand for new aircraft, general aviation utilization rates have changed significantly over the last thirty years. For example, the utilization rate for general aviation turbojet aircraft exceeded 500 hours in the mid-1970's but fell to less than 400 hours by the mid-1980's. Since 1988, the general aviation jet utilization rate has fallen more than 100 hours, bringing the 1992 jet utilization rate well below 300 hours per year.²

Because of the wide swings in the various general aviation utilization rates over time, it is necessary to develop a model which explains aircraft utilization before observed utilization rates can be employed in predicting general aviation economic activity. In the absence of knowledge about the factors affecting the utilization rate, for example, it may not be possible for the FAA to project total flight hours, which in turn affect FAA workload through the demand for air traffic facilities and flight services, even if the fleet size can be forecasted with required accuracy.

Perhaps more important applications of the utilization rate are in forecasting, market development, and production planning by airframe and engine manufacturers and avionics suppliers. It is not unreasonable to expect an increase in the utilization rate to stimulate the demand for aircraft, resulting in increased production and shipment of new aircraft. Furthermore, any change in utilization that affects unit sales should filter down the production chain and affect avionics suppliers, engine manufacturers, and other providers of component parts.

Today, the general aviation industry is defined by business flying; that is, through the sale and use of general aviation jet aircraft.³ For this reason it is important to understand the various factors affecting the jet utilization rate to fully comprehend the impact of recent developments in our economic/business environment on the general aviation industry and to map the future course for general aviation activity.

One important development that portends significant change in the conduct of business is the advance of

¹ Algebraically, (average) aircraft utilization (UR) is defined as: $UR = \text{Total flight hours} / \text{fleet size}$. Thus the demand for flight services (i.e., hours) affects the numerator, while investment in new aircraft affects the denominator. The latter effect may not be one-for-one, however, because of fleet leakages associated with aircraft depreciation, net exports, and accidents.

² See the Federal Aviation Administration, General Aviation Activity Survey (various years) for data, and McDougall (1993,194) for further discussion and analysis of general aviation activity.

³ In earlier years, the general aviation industry was defined by different segments. From the end of world War II until 1960, the industry was driven by the piston segment, especially the single-engine segment linked to personal flying. There was some business flying, of course, with both single-engine and multi-engine piston aircraft. Between 1960 and 1978, business flying became more important to the industry with the introduction of turboprop and turbojet aircraft. During this period the turboprop segment tended to be more active than the turbojet segment in terms of units produced and sold. Since 1980, however, economics and technology, have decimated the piston and turboprop segments. It appears the only viable GA segment at this time is the business jet segment.

digital telecommunication technologies (e.g., telefaximile and teleconferencing via compressed video). Greater interactivity and increased connectivity are expected over the next ten years as the nation develops a national high speed information highway. As transmission quality increases, high speed networks expand, and up-front and transmission costs decrease, digital communications applications may reduce business travel, including general aviation business flying.⁴

Another noteworthy development that seems to be affecting general aviation business flying is the downsizing and restructuring of corporate America. Corporate re-engineering has been going on for at least ten years and it is expected to continue into the next century. The new cost consciousness emerging from this structural change in corporate culture may reduce business traveling or shift corporate attention to identifying less costly methods of providing corporate business flying.⁵

Of course, in the long run, sharpened cost-sensitivities could increase the measured utilization rate calculated on a smaller corporate/business fleet of general aviation aircraft. Because of increased demands for accountability to shareholders for return on investment, some corporations already have restructured their flight departments to increase efficiency and reduce costs. If this trend continues it could very well increase the measured utilization rate for the U.S. corporate fleet, as fewer and smaller corporate fleets are used more intensely to provide on-demand, point-to-point executive flight services.

There have been some innovative institutional changes in response to the changing economic environment for the general aviation, also. Examples include: (1) the replacement of corporate flight departments with aircraft management firms; (2) the increased number of corporate owners who have changed their operations from Federal Aviation Regulations (FAR), Part 91 to Part 135 certification, which allows the owner/operator to use the corporate fleet for charter or for-hire business and thereby increase use while decreasing overhead costs, and (3) the introduction of time-share arrangements through joint-ownership arrangements. For example, Executive Jet Aviation has a program called NetJet which owns and manages a large fleet of identical business jets (Citation S/II's and most recently Hawker 1000's) and sells one-quarter time-shares to end-users. The end-user is guaranteed a certain number of flight hours on demand, but these hours may be provided by any one or more of NetJet's aircraft. At this point, these innovations are in an embryonic stage of development and widespread acceptance is still uncertain.

Each of these innovations could increase the average utilization rate for the business jet fleet since each of these innovations promotes a more intense and efficient use of an aircraft. As such, with these innovations, the current levels of flight services could be provided with smaller fleets; thus, increasing hours per aircraft. Furthermore, we can expect an increase in demand for business jet services over time as these innovations become accepted by the corporate community. This should put additional upward pressure on utilization.⁶

⁴ At this time, many general aviation participants believe digital technologies will have a greater effect on commercial business air travel. In part, the industry holds this belief because general aviation business flying is focused on face-to-face communications at the executive level. Some even believe that new digital technologies complement flying by increasing communication and interaction and, thereby, this will increase the demand for personal contacts, especially at the executive level.

⁵ It is difficult for the general aviation industry to compete with commercial airlines on the cost of a seat-mile; that is, the direct cost of providing a seat-mile. A benefit-cost analysis shifts toward GA flying when time costs and management effectiveness are factored into the equation. Of course, it is difficult to value accurately an executive's time and to measure managerial productivity or efficiency. Nonetheless, it seems clear that GA business travel can save an executive's time and increase productivity by providing a complete work environment and reducing the personal toil of long distance travel.

⁶ There is evidence that the practical maximum number of flight hours for general aviation business jet aircraft is approximately 900 hours per year. See McDougall and Cho (1989).

FLIGHT HOURS, FLEET SIZE, AND THE UTILIZATION RATE

The ex post utilization rate is expressed by the ratio of flight hours to fleet size; that is, it is an algebraic relationship that is devoid of any behavioral content. Explaining and predicting utilization rates in the future, however, requires a conceptual basis or theory explaining the choices made by buyers and operators. These choices determine fleet size and the use of aircraft to produce flight hours. Although ex post utilization is a definition, choice behavior driving the purchase and use of new and existing aircraft underlies ex ante utilization.

CAUSALITY

Theoretically fleet hours and fleet size determine aircraft utilization rates, but empirically one or the other could be a (the) dominating factor. The first step in modelling the utilization rate, therefore, is to determine if changes in flight hours cause the measured utilization rate to change or if changes in fleet size cause measured utilization to change.

Statistical methods can never establish the existence of a theoretical cause-effect relationship. Nonetheless, lead and lag relationships among variables are frequently employed to provide statistical evidence of cause-effect relationships. The Granger causality test is a commonly employed test to sift out "probable" cause-effect relationships.⁷ Unfortunately, the Granger test requires stricter stationarity and cointegration properties than displayed by the data available for this study. Nonetheless, we believe a Granger-type analysis provides a basis for making tentative judgements about the operations of the general aviation aircraft.

For our purpose cross-correlations involving up to 7 years of lead and lag for percent changes in flight hours, fleet size, and the utilization rate are employed to sift out evidence of the direction of causation. The results are presented in Table 1.

Examination of flight hours and fleet size for the GA jet segment reveals high correlations (i.e., those exceeding one standard error) among present changes in flight hours (flight hours at time "t") with present and future (time "t" and "t+") percentage changes in fleet size. These are presented in the second column in Table 1, where there is a pattern of significant correlations favoring future ("t+") values for fleet size. The contemporaneous cross correlation is 0.61, which is almost three times as large as the standard error. Other relatively large correlations occur in all of the out-years except t+4 and t+6. There is some evidence, however, that fleet changes occurring two and four years in the past (t-2 and t-4) affect current total flight hours. Nonetheless, the preponderance of evidence suggests that present changes in flight hours have stronger ties to future changes in fleet size, rather than the reverse. Increases in flight hours appear to be related to future increases in fleet size.

The contemporary correlation between percentage changes in flight hours and jet utilization is strong. The contemporaneous correlation coefficient is relatively large (0.68) and it is more than three times larger than the standard error (see the third column, Table 1). Much weaker relationships exist in the out years (the "t+" years). On the other hand, the contemporary co-movement between the percentage change in fleet size and the percentage change in the jet utilization rate is small (-0.18, see the fourth column) and insignificant. Taken together, these results indicate that changes in the jet utilization rate result from contemporaneous changes in flight hours rather than contemporaneous changes in fleet size.

⁷ See Granger (1969) for a discussion of the formal Granger test.

**Table 1: CROSS CORRELATIONS
1970-1992**

k	FLIGHT HOURS at t with	UTILIZATION RATE at t with	
	FLEET SIZE	FLIGHT HOURS	FLEET SIZE
(1)	at k (2)	at k (3)	at k (4)
t-7	.04	-.04	-.13
t-6	.08	.15	.20
t-5	.08	-.11	-.09
t-4	.37*	.20	.22*
t-3	.08	-.09	.07
t-2	.36*	.20	.00
t-1	.11	.02	-.01
t	.61**	.68***	-.18
t+1	.35*	.24*	.29*
t+2	.41*	.25*	.06
t+3	.41*	.21*	.48**
t+4	.17	.02	-.02
t+5	.38*	.17	.29*
t+6	.05	.11	.17
t+7	.28*	.19	.18
Standard Error	.21	.21	.21

Note: All variables are percentage changes calculated by first converting variables to logarithms and then taking differences.

*** Greater than 3 times of the standard error.

** Greater than 2 times of the standard error.

* Greater than 1 standard error.

There is some support for believing that changes in the utilization rate are linked to the future size of the jet fleet. Notice the correlation between current changes in utilization rate and changes in fleet size three years in the future; it is relative large (0.48) and more than two times the standard error. Smaller effects are seen one and five years out. Overall, the cross correlations between flight hours and fleet size and between the utilization rate and fleet size suggest that the utilization rate may be an important indicator of future production and sales of new aircraft.

THE UTILIZATION RATE AND THE DEMAND FOR FLYING

Results from the Granger-type tests suggest that it is appropriate to model changes in the utilization rate in terms of the factors determining the use of jet aircraft, rather than the acquisition of aircraft. For our purposes, therefore, we can ignore factors, e.g., aircraft price, that influence the demand for aircraft. Generally, it seems that demand factors hold only secondary importance in explaining jet utilization.

Assuming, initially, that preferences for flying and air travel, and that the availability of competing communication technologies are stable, the demand for flying as reflected in the utilization rate is

hypothesized to be affected by two independent economic variables: (1) the cost of flying and (2) the level of corporate business activity; that is,

$$\text{Utilization Rate} = f(\text{Operating Costs, Economic Activity})$$

The cost of flying is measured by the FAA's index of the operating costs for general aviation jet aircraft.⁸ This cost index includes changes both in fuel costs and aircraft maintenance expenses. This nominal index is adjusted for inflation using the Consumer Price Index, providing an index for real operating costs. This real operating costs index should be negatively related to the utilization rate.

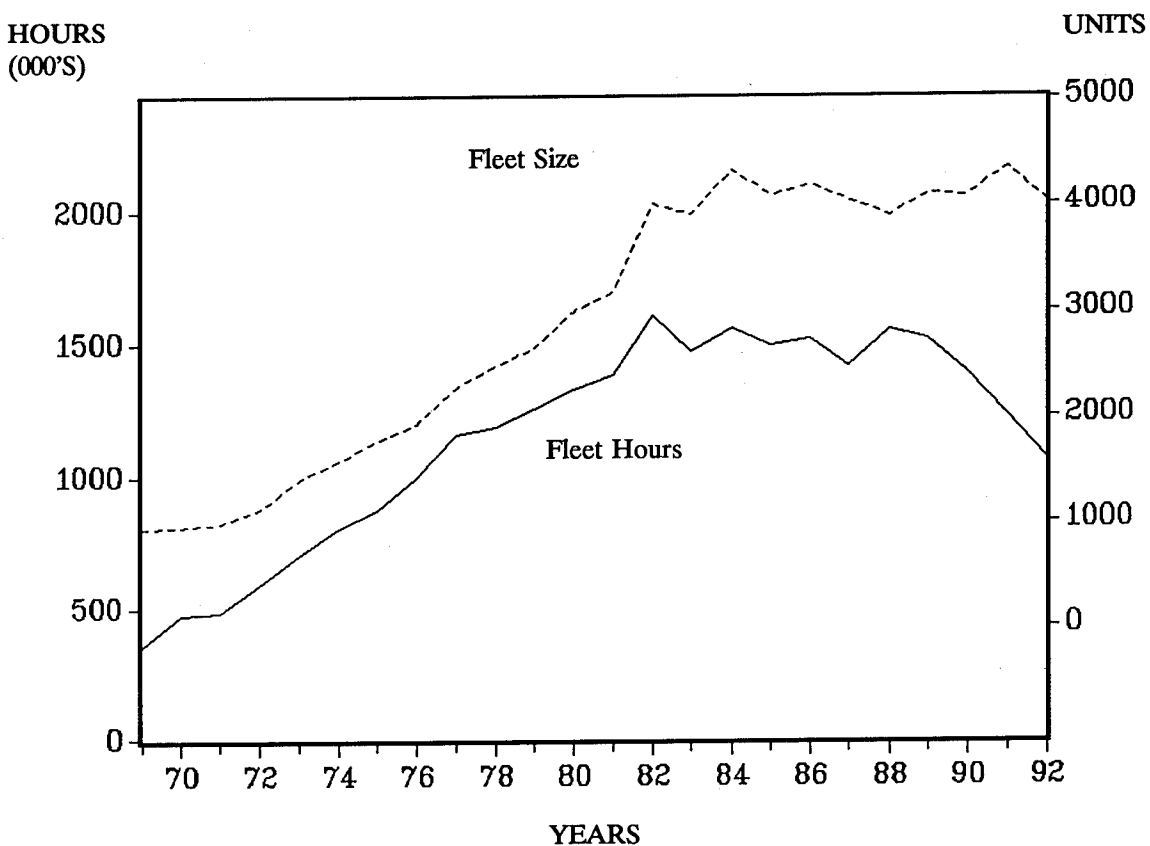


FIGURE 1. TOTAL FLIGHT HOURS AND FLEET SIZE

⁸ These data are taken from FAA Aviation Forecasts, (various years).

Corporate business activity is measured by real after-tax corporate profits. Real after-tax profit is based on nominal after-tax corporate profits deflated by the Consumer Price Index.⁹ It is expected that after-tax corporate profits will be positively related with the jet utilization rate.

The FAA's estimates for turbine jet flight hours and active fleet are shown in Figure 1 for the 24 year period running from 1969 through 1992. These series show significant changes since 1969. The change most relevant to the current analysis of the general aviation turbojet segment is the sharp drop in total flight hours, beginning in 1988. Since 1988, total flight hours for general aviation turbojets has declined approximately 33 percent, dropping from approximately 1.5 million hours per year in 1988 to approximately 1 million hours in 1992. Fleet size, however, has remained nearly constant over this period, fluctuating around 4,000 general aviation jet aircraft. Needless to say, this pattern of constant fleet size and declining total hours means utilization has fallen; in fact, it has fallen dramatically since 1988. Between 1988 and 1992 the jet utilization rate declined 33 percent, also, falling from approximately 400 hours per plane per year to approximately 267 hours per plane per year.

JET UTILIZATION MODELS

Given the significant structural changes since 1988, two statistical models explaining general aviation jet utilization are estimated: One for the period 1971 through 1988 and another for the longer period 1971 through 1992. The results for the truncated period are shown below. Here UR denotes the percentage change in the measured jet utilization rate, ROP is the percentage change in the index of real operating costs, and PRFT measures the percentage change in real after-tax corporate profits. The subscript denotes the time period. Calculated t-values are given in parentheses.

Jet Utilization. Truncated Period (1971-1988)

$$UR_t = -.008 -.422ROP_t + .181PRFT_{t-1}$$

(-2.03) (2.85)

Adjusted R² = .32

Standard error = .045

Durbin-Watson statistics = 2.43

Together, the independent or exogenous variables explain 32 percent of the total variation in the percentage change in jet utilization rates. Although the fit is not impressive and the standard error is relatively large at 4.5 percent, the independent variables have statistically significant explanatory power. It is not possible to confirm either the presence or absence of serial correlation in the residuals using the Durbin-Watson test. The calculated Durbin-Watson value is 2.43 and this is in the inconclusive range for this random variable.

A one percent increase in real operating cost (ROP) reduces the jet utilization rate 0.42 percent. That is the operating cost elasticity of jet utilization is 0.42. The t-statistic shown in the parenthesis indicates that the variable is significant at a 10 percent level.

⁹ These data are taken from DRI historical series. The index of industrial production was also used as a variable of business activity. However, this variable is not as closely related with utilization rate as real after tax corporate profits. It appears that the index of industrial production is too broad a measure to capture the fluctuations corporate business activity which would influence the demand for flying.

On the other hand, a one percent increase in real after-tax corporate profit (PRFT) increases the jet utilization rate by 0.18 percent with a one year lag.¹⁰ The profit elasticity is 0.18. The variable is statistically significant at the 1 percent level. If we accept these significance levels, it appears that operating costs are more important than corporate performance in explaining business jet utilization rates.

The regression for the period between 1971 and 1992 performed much worse.

Jet Utilization. Full Period (1971-1992)

$$UR_t = -.027 - .356ROP_t + .128PRFT_{t-1}$$

(-1.34) (1.58)

Adjusted R² = .16

Standard error = .062

Durbin-Watson statistics = 1.87

For the full sample period, the Adjusted R² is much smaller and both independent variables are statistically insignificant. As expected with these kinds of results, the regression standard error is larger in this model compared with the previous model. Again, it is not possible to confirm the presence or absence of serial correlation since the Durbin-Watson statistic falls in the inconclusive range.

The breakdown in the statistical model when the most recent years are included in the statistical analysis points to possible structural changes in the GA industry; perhaps related to changes in tastes for flying, the emerging role or place of new communications technologies as substitute modes of business interaction, or related to innovations in the delivery of corporate flying.

STRUCTURAL CHANGE AND FUTURE PROSPECTS

The recent declines in the jet utilization rate are analyzed with the help of the statistical results obtained for the 1971-88 period. Specifically, utilization rates for 1989 through 1992 are predicted using the 1971-1988 statistical model, incorporating actual values for the exogenous variables over this recent period. More specifically, this means the jet utilization rates for 1989 through 1992 are predicted assuming there have been no structural changes in the GA industry, including the behavior underlying corporate flying. We then compare these predicted results with what actually was observed.

The results from this comparative analysis are plotted in Figure 2. Notice that the predicted utilization rates are consistently higher than the actual utilization rates for the 1989-92 period.¹¹ Although jet utilization rates for 1989 through 1992 declined, in part, due to increases in real operating costs and weak real corporate profits, the consistent over-prediction is indicative of unaccounted for structural factors that reduced utilization rates more than expected from our historical experience.

¹⁰ Contemporaneous PRFT is not statistically significant. It is interpreted that business flying increases after corporate business activity picks up.

¹¹ Examination of Figure 2 shows that this is not true for the pre-1988 period. The model both under-predicts and over-predicts the actual jet utilization rate for years between 1971 and 1988.

The over-predictions of the statistical model since 1988 provide reason for returning to the major structural changes possibly affecting corporate jet utilization mentioned above. The results we have reported are consistent with the tentative hypotheses that corporate restructuring, new institutional arrangements, and advances in telecommunications technologies are reducing traditional business jet flying. And from among these, it seems reasonable to us to believe that corporate restructuring and cultural change is the dominant influence at this time.

To date, movements toward the certification of corporate jets for charter service, or any impacts from corporate reorganization and the development of institutional innovations on corporate flight departments have failed to increase the overall utilization rate. These, of course, are influences with longer term effects that must work through operating costs and fleet disinvestment decisions. Furthermore, they must overcome the natural reluctance to adopt new forms of business flying such as time-sharing arrangements or outside fleet management services. Privatization has not yet hit flight departments like it has hit corporate graphics departments, food service, security, and some corporate maintenance functions such as house cleaning.

HOURS/PLANE

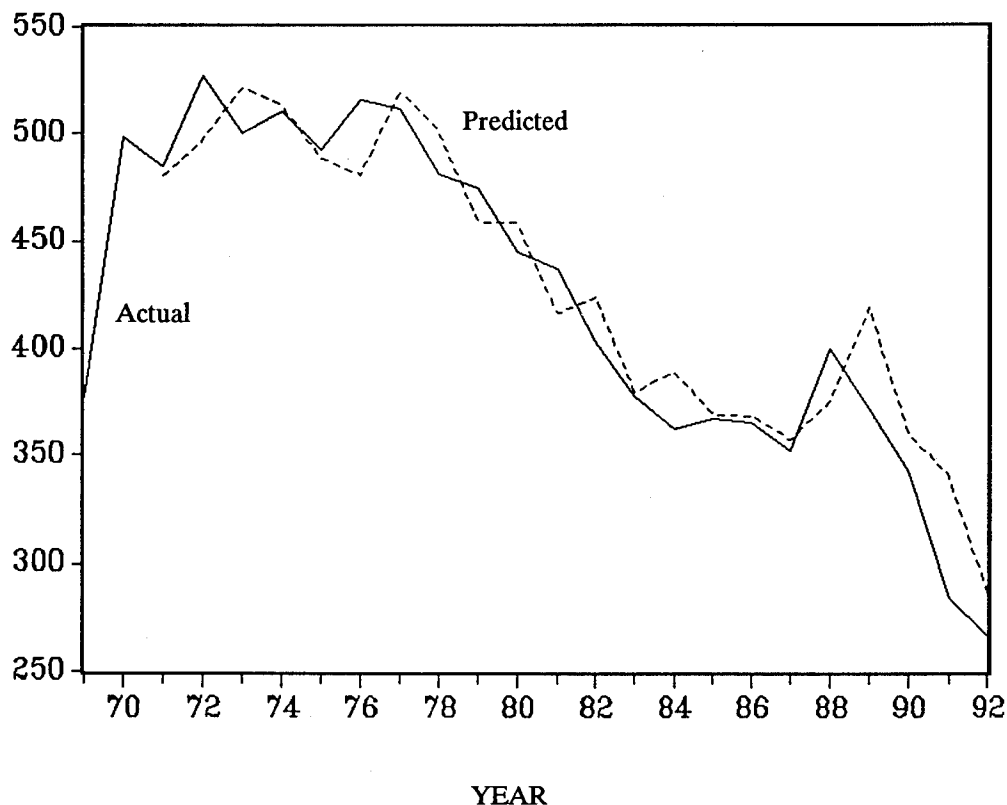


FIGURE 2. ACTUAL AND PREDICTED UTILIZATION RATES

Nonetheless, we may very well see jet utilization rates increase in 1993 and 1994. The economy has strengthened in 1993 (a revised fourth quarter growth rate of approximately 7.0 percent was recently reported for 1993) and continued moderate (3 percent) growth is expected through 1994.¹² Corporate after-tax profits increased 3.7 percent in 1992 and profits are expected to show even greater strength through 1994 as the impact of corporate restructuring reduces the cost structure of corporate America and, thereby, increases our competitiveness on world markets and spurs export growth.

According to the estimated models, the influence of higher 1992 corporate profits should show up in the 1993 jet utilization rate. Depending on the sample used for estimation purposes, the increase in real profits for 1992 is expected to cause 1993 jet utilization to increase between 0.49 percent (based on an elasticity of 0.12) and 0.67 percent (based on an elasticity of 0.18).

The index for aircraft operating costs declined 3.7 percent in 1992. We expect this decline in operating costs to continue through 1993 because of weakened conditions in world energy markets. For example, the price of oil has fallen approximately 20 percent since November 1993 and this should put additional downward pressure on jet fuel prices. If the 1993 FAA index of real operating costs comes in 5 percent below its 1992 level, the jet utilization rate should increase between 1.75 percent (based on an elasticity of -0.35) and 2.1 percent (based on an elasticity of -0.42).

Our cross-correlation analysis suggested that changes in utilization rates affect fleet size with a lag of three years. If we accept this lag structure, then the anticipated increases in utilization for 1993 will show up in a larger 1996 active fleet. In turn, this means that any effect on original equipment manufacturers will show up in 1995 orders. This assumes a 12-month lag between orders and shipments.

The connection between changes in the utilization rate and new aircraft shipments, however, is somewhat tenuous. First, the lag between the change in utilization and fleet additions or deletions is relatively long. Much can happen with our economic conditions over any 24 to 36 month period. Second, changes in fleet size (additions or deletions) can be achieved through net exports. While little is known about the international flow of existing aircraft, we do know that in recent years approximately 40 percent of new business jet production has gone to non-U.S. markets. Historical data series indicate that net imports are affected by international exchange rates. Furthermore, previous studies have shown that new jet shipments can be better predicted by the cost of new aircraft and other economic variables influencing aircraft investment demand.¹³ In summary, while the predicted increase in the jet utilization rate for 1993 should be considered positive news for manufacturers of general aviation jet aircraft and component parts, its precise impact on future unit sales is difficult to determine.¹⁴ For all of these reasons it remains prudent for the industry to focus on the development of non-U.S. markets, especially those in Asia, Central America, and South America, for growth in new business jet sales. The short term prognosis for Western Europe among industry participants points to continued softness as major European economies; e.g., Germany, continue their transition to a unified economic union.

¹² The Blue Chip Consensus Forecasting service recently announced a 3.6 percent real growth rate for 1994. And the Federal Reserve Board has expressed concern about the economy over-heating by increasing interest rate.

¹³ For example, see Cho and McDougall, "Demand Estimates for New General Aviation Aircraft," Applied Economics, March 1988, pp. 315-324 for an economic model for aircraft investment demand.

¹⁴ The connection between utilization and sales was discussed in McDougall and Cho, "Another Dimension to General Aviation--Is There a Link Between Sales and Utilization?" Business & Economic Report, March 1988.

CONCLUSIONS

This study of business jet utilization offers several interesting results. First, changes in fleet hours is the main factor influencing the turbojet utilization rate. Changes in fleet size, and, therefore, factors affecting the demand or acquisition of aircraft, play a secondary role. Second, the jet utilization rate is affected by changes in the cost of flying and in the level of economic activity, as reflected in corporate profitability. This is especially true for the 1971-1988 period. Since 1988, the statistical relationship has weakened. We speculate that this is related to structural and institutional changes occurring in the industry. Third, in the context of these fundamental changes which still must play out, we expect to see upward pressure on jet utilization rates over the next two years because of recent declines in operating costs and short term increases in corporate profitability. If realized, this increase in jet utilization could have a positive affect on production and shipments of new business jets in 1995 and 1996.

REFERENCES

Cho, D. W. and G. McDougall, "Demand Estimates for New General Aviation Aircraft," Applied Economics, Vol. 20, No. 3 (March 1988), pp. 315-324.

Federal Aviation Administration, General Aviation Survey (various years), Office of Aviation Policy, Plans and Management, Washington, D.C.

Federal Aviation Administration, FAA Aviation Forecasts, FAA-APO 93-1, Washington, D.C. (February 1993).

Granger, C. W. J., "Investigating Causal Relations by Econometric Models and Cross-Spectral Methods," Econometrica, 37 (1969), pp. 424-38.

McDougall, G. S. "Modeling The Turbine Aircraft Industry," FAA General Aviation Forecast Conference, Proceedings of the Third Annual Conference. FAA-APO (March 1993).

McDougall, G.S. "The Short Term Outlook for the General Aviation Industry - As Good as it Gets?" Annual Meeting of the Transportation Research Board, Washington, D.C. (January 1994).

McDougall, G. and D. W. Cho, "Explaining General Aviation Aircraft Utilization," The Logistics and transportation review, Vol 24, No. 1 (March 1988), pp. 69-79.

McDougall, G. and D. W. Cho, "Another Dimension to General Aviation--Is There a Link Between Sales and Utilization," Business & Economic Report, Vol. 18, No. 1, Center for Business and Economic Research, W. Frank Barton School of Business, Wichita State University, Wichita, Kansas (March 1988).

McDougall, G. and D. W. Cho, "Estimating Practical Maximum Flight Hours for General Aviation Turboprop and jet Aircraft," Transportation Research Board Record, #1214: Modeling and Analysis of Airport and Aircraft Operations, Transportation Research Board, Washington, D.C. (1989).

REVITALIZING GENERAL AVIATION

-- THE REST OF THE STORY --

THIRD JOINT SYMPOSIUM
ON GENERAL AVIATION SYSTEMS

May 25, 1994

Emmett F. Kraus

The Cessna Aircraft Company

BACKGROUND

Just over fifteen years have passed since domestic production of General Aviation aircraft reached its peak of 17,811 units. In those fifteen years, production has fallen to less than 5% of the 1978 level. Much has been said and written about General Aviation's predicament, and every imaginable suggestion has been offered for reestablishing growth. Many of those suggestions have been tried. Still, unit sales continue to fall.

Figure 1 traces the history of General Aviation deliveries by domestic manufacturers. There are two remarkable events depicted here - the sharp peak immediately after WW II, and the deep drop in the 1980s to levels lower than at any time since the Great Depression.

The post-war surge occurred as manufacturers converted from wartime to civilian production, anticipating a large market that didn't fully materialize. The dashed line shows the average of all deliveries from 1942 through 1954, which matches demand before and after this period quite well. This indicates that production in 1946 and 1947 simply outstripped the actual demand for those two years and satisfied most of the demand for the wartime and immediate post-war period, a case of temporary oversupply. Nothing like it has occurred since.

Then followed a long period of substantial growth as new models and features were introduced. There was a significant wartime trough during the Vietnam era, but growth resumed immediately afterward. In fact, general growth was sustained for 30 years, overcoming recessions, surtaxes, uncertainties associated with on-again/off-again investment tax credits, wage-and-price controls, the oil embargo, and high inflation. The industry showed great strength in overcoming all these downward pressures and looked forward to more growth in the 1980s and beyond.

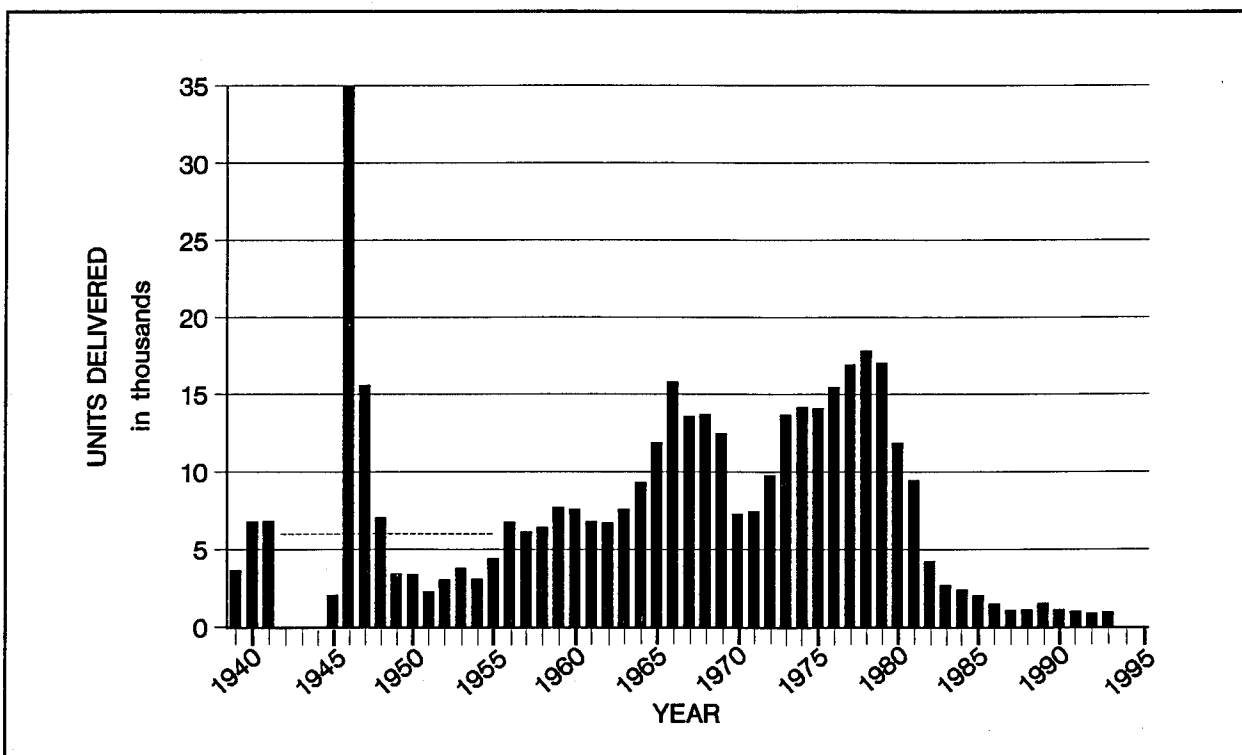


Figure 1. Domestic General Aviation Production

What followed, instead, was an unprecedented drop in sales to only 964 deliveries of piston, turboprop, and jet airplanes by domestic companies in 1993. There were heavy downward economic pressures during this time - periods of inflation, recessions, high oil prices, new tax rules, and more airline competition - but under normal circumstances, pressures like these are simply something to be managed, as was done successfully before the 1980s. Indeed, all of these problems together do not compare in difficulty to the Depression, the oversupply after WW II, or the economic turmoil associated with the Vietnam conflict. Yet, sales have dropped even lower than in those times.

TECHNOLOGY TO THE RESCUE?

With something so obviously wrong, the root problem ought to be obvious to everyone; but for a long time it was not. For example, exotic new technology was frequently mentioned in the 1980s as the certain solution for General Aviation's problems. A number of unusual new designs were announced, complete with optimistic promises that virtually predicted the inevitable outcome. Meanwhile, good, basic development work in the fundamental technical areas most useful for General Aviation was coming to a near standstill.

The question of how technology could be realistically focused to make a significant difference in General Aviation was first raised as a national issue in 1986 by Lou Williams, Director of NASA's General Aviation Office in Washington. It was natural for NASA to ask this question, since aviation technology is one of its chief products; but Lou wasn't getting any convincing answers.

People were recommending some interesting R & D in the usual technologies - aerodynamics, materials, propulsion, and avionics. Still, there was no evidence that the few available percentage points improvement that the latest technologies could provide in drag, weight, or propulsive efficiency would make any significant difference, especially in the size of the piston aircraft market. Likewise, there was no evidence that the precipitous drop in sales during the 1980s was caused by some sudden, collective rejection of General Aviation technology. In other words, it is unlikely that very many pilots stopped flying because airplanes didn't have the latest laminar flow wings or composite construction.

If exotic designs are not the answer, and if the usual technologies do not offer breakthrough improvements, what then is the appropriate role for technology in revitalizing General Aviation? Could it be used in different ways or with a different emphasis that might make a difference in the market? The answer is yes, definitely, under the right circumstances. These circumstances go beyond the traditional concerns of the technical community, so it is helpful to consider a broader picture of the marketplace in order to appreciate the conditions that will permit new technologies to have the greatest success.

THE GENERAL AVIATION MARKETPLACE

In General Aviation, as in any business, it takes two to make a market. There have to be both buyers *and* sellers (Figure 2). Customers typically choose those products with utility and features that provide the best perceived value. This is where technology and design have a role and this was the focus of Reference 1. The companies that build and sell products need a positive business environment that enables them to exist, otherwise there will be few products brought to the marketplace. The business environment is dominated by non-technical factors.

- **BUYERS**
 - LOOK FOR UTILITY, FEATURES, AND PRICE
 - TECHNOLOGY IS A KEY FACTOR
- **SELLERS**
 - REQUIRE AN ENABLING BUSINESS ENVIRONMENT
 - BUSINESS ENVIRONMENT IS DOMINATED BY NON-TECHNICAL FACTORS

Figure 2. Elements of a Marketplace

These fundamentals indicate the role of aircraft technology in the General Aviation marketplace. In practical terms, technology determines what design features or utility can be provided - where utility is generally comprised of speed, payload, range, field length, and cabin size (Figure 3). In the context of revitalizing General Aviation, the focus is on the low end of the market where people enter into aviation, get their training, and then gradually move up into larger, faster aircraft. It is in this market segment that revitalization has to begin, so the most appropriate technologies are those that benefit growth in the single-engine market.

It is unlikely, however, that advanced technology can be the primary solution for the industry's current condition. The test of this is whether technology can be developed to enable designers to provide features and utility at a cost that will completely overcome both the competing alternatives to General Aviation (the automobile and airlines) as well as all the external, downward pressures on the General Aviation marketplace. At the moment, no existing or near-term proposed design shows any realistic promise of achieving such an aggressive goal by itself. This fact, together with the failed high-technology aircraft programs of the past 15 years, makes it clear that technology is not, and under current circumstances cannot be, the dominant factor in the marketplace. It cannot be the primary stimulus for revitalizing the market because it addresses only half the marketplace.

- **THE ROLE OF TECHNOLOGY**
 - FOCUS ON THE NEEDS OF THE BUYER
 - PROVIDE THE OPPORTUNITY TO DESIGN FOR DESIRABLE FEATURES AND UTILITY AT AN ACCEPTABLE MANUFACTURING COST
- **OTHER KEY FACTORS FOR SUCCESS**
 - BUSINESS ENVIRONMENT
 - PRODUCT LIABILITY
 - ECONOMY
 - POLITICAL ENVIRONMENT
 - REGULATIONS
 - INTERNAL COMPANY OPERATIONS
 - MARKETING
 - FINANCE
 - MANUFACTURING
 - MATERIAL
 - PRODUCT SUPPORT

There are other key factors on the sellers' side of the market, and one of them has become dominant. First, there are external factors, such as the legal, economic, political, and regulatory conditions that shape and control the very opportunity for a successful business environment. Second, there are those internal factors that are within a manufacturer's control. These include marketing and sales, financial strategy, manufacturing and material management, and customer support.

Figure 3. Airplane Technology Is Only One Factor In General Aviation

PRODUCT LIABILITY

The external factor that dominates General Aviation - product liability - is the first part of *"the rest of the story"*. The two aspects of this problem that are of particular interest are its overwhelming effect on the General Aviation business environment and the relationship of product liability to new technology and design.

One of the most striking aspects of the liability problem is how rapidly it grew, even though General Aviation's safety record had been steadily improving. Figure 4 shows the steep, unexpected rise in liability costs that began about 1977 (Reference 2). Annual industry costs still exceed \$200M per year.

Of course, the 1980s were a singularly bad time for General Aviation, but in normal circumstances all the downward pressures - high interest rates, high fuel costs, recessions, the air traffic controller strike, and so on - would have a short or cyclic effect that could be counteracted with imaginative management and aggressive marketing. It was the sudden rise in the cost of product liability to excessive levels that overwhelmed all other factors. It was product liability that uncoupled General Aviation from the economy.

By 1986, when Cessna discontinued piston aircraft production, the manufacturers' average liability insurance cost had grown to \$70,000 per aircraft delivered that year from a little over \$2,000 per aircraft in the mid-70s. In addition, there are the substantial costs of defending against the hundreds of lawsuits that are filed against the industry each year. Worse, there are huge risks of losing, with some awards reaching into the tens of millions and one over \$100 million.

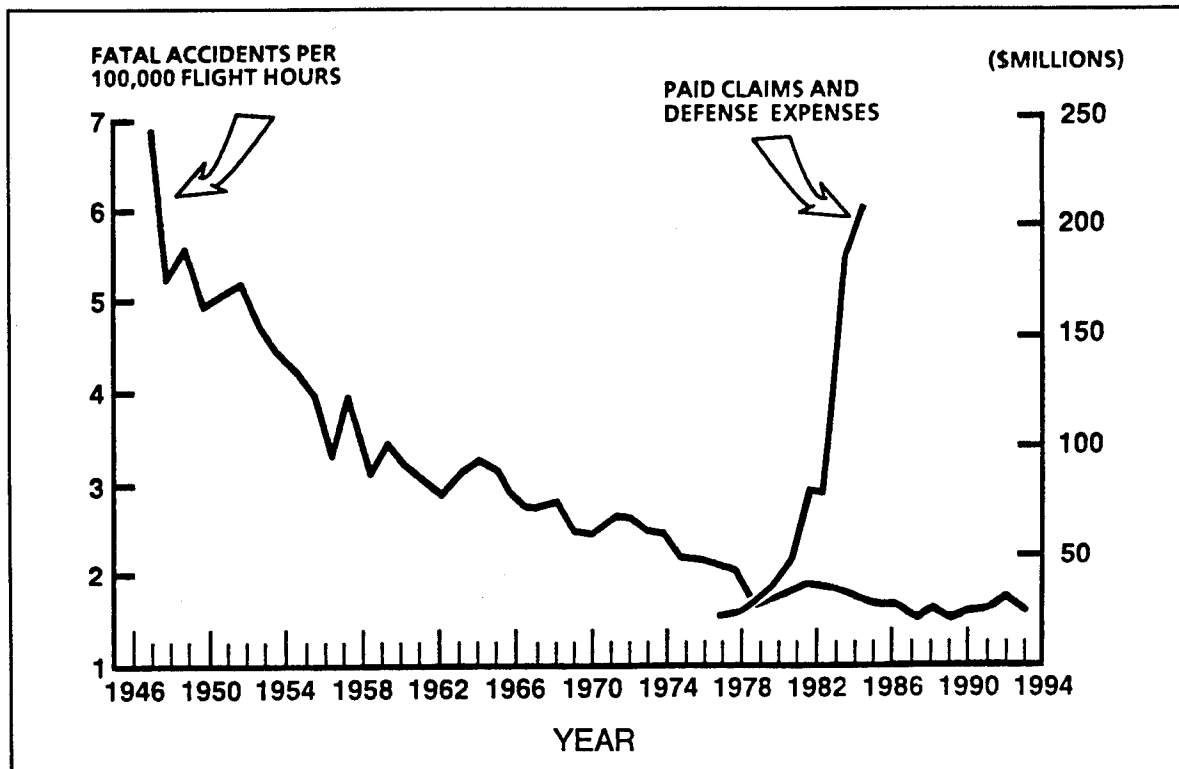


Figure 4. General Aviation Product Liability Costs

These are costs that a manufacturer's liability insurance typically does not pay; because that insurance, though extremely expensive, is only bearable with a very large deductible amount. Piper's experience is representative. In 1987, Piper paid \$30 million for liability insurance with a \$25 million deductible. This at a time when its annual sales were only \$75 million.

New production piston aircraft cannot absorb such extreme costs. Even when only part of these costs were allocated to new airplane prices in the late 1970s and early 1980s, sales fell, starting a sales downtrend that dropped in lockstep with the price-demand curve. Meanwhile, the enormous costs of liability lawsuits continue and there is still no limit.

Unlimited exposure to litigation is the sole reason Cessna closed its single-engine production lines in 1986 and the sole reason those lines are still closed. There is no other reason. This was a rational business response to irrational liability costs that are allowed to continue without limit, long after the airplane has become more a product of its operational and maintenance history than of its manufacturer.

The result of unlimited liability exposure is obvious. There are now only 5 GAMA (General Aviation Manufacturers Association) members delivering piston aircraft. These companies are American General, Beech, Commander, Mooney, and Piper. Two are foreign-owned, two are bankrupt, and the fifth needs income from other business to cover its piston airplane liability losses. *Because of unlimited liability, no domestic manufacturer with substantial assets has a light aircraft product line that stands on its own as a profitable enterprise.*

There are other manufacturers not in GAMA - small, established operations as well as new grass roots players. Some of the new companies are working to re-start production of discontinued models, others are evolving from their kit aircraft background into producers of certified airplanes. They are proceeding despite the liability environment, but they do so under the protection of two *temporary* advantages. First, their cash and other assets are small enough to avoid much attention from plaintiffs' lawyers, who prefer to pursue larger bait. Second, they have no long tail of liability from preceding decades of production. These companies certainly must understand that they exist, for the time being, only at the pleasure of the 16 law firms that prey on General Aviation. Should they begin to appear successful, their honeymoon will be over.

TECHNOLOGY AND LIABILITY

It is natural for a good engineer to wonder whether there might be some technical or design solution to this problem. Unfortunately, this is something about which technology can do very little (Figure 5).

In the first place, liability is not about safety. There is, in fact, a reverse correlation, as indicated in Figure 4 by the long term improvement in General Aviation safety that preceded the runup of liability costs; and the rate of improvement has actually decreased since the start of the liability runup.

- THE STEEP RISE IN LIABILITY COST DOES NOT CORRELATE WITH GENERAL AVIATION'S LONG TERM SAFETY IMPROVEMENTS
- SAFE DESIGNS ARE ATTACKED WITH CONJECTURE AND EMOTIONAL ASSERTIONS UNRELATED TO THE DESIGN OR THE APPROPRIATE DESIGN CRITERIA
- MOST ACCIDENTS INVOLVE MISUSE, ABUSE, INADEQUATE MAINTENANCE, AND IMPROPER SERVICING THAT ARE UNFORESEEABLE OR BEYOND A DESIGNER'S CONTROL
- DESIGN IMPROVEMENTS ARE USED AGAINST OLDER AIRPLANES

Figure 5. Technology and Design Cannot Significantly Reduce Liability

Second, even the best designs are subjected in court to emotionally seductive conjecture and theories about the cause of a crash, regardless of how illogical, improbable, or irrelevant. The courts usually give credence to these junk science arguments, leaving the designer in the position of having to "prove there was no needle in the haystack."

Third, most lawsuits lost by manufacturers involve cases where obvious misuse or abuse of the airplane, inadequate maintenance, or improper servicing go beyond anything foreseeable by a designer or resolvable by technology or design.

Fourth, new design features that affect safety become the benchmark against which older aircraft are tried in court. Even aircraft produced before the new feature was even conceived can be found to be "deficient," making a designer's best work a two-edged sword.

For all these reasons, there is no *final* technical solution to the liability problem.

All this was well-known in 1987 and the Reference 1 technical paper recognized liability as leading the list of General Aviation's problems. Product liability was the first basic cause listed in the first exhibit. Liability still holds that place, because of its effect on prices; but since it was a technical paper, presented to engineers at a technical meeting - and since there is no final technical solution to liability - the paper looked beyond to what might be accomplished in the eventual absence of unlimited liability.

The Association of Trial Lawyers of America (ATLA) misconstrued that work and began using it in Washington to support its arguments against tort reform. It is still misused this way, as recently as last May in hearings before the House Judiciary Subcommittee.

The result is that the people in this industry no longer feel free to discuss or resolve aviation systems or design issues in a public forum. Product liability also stifles the industry in other significant ways (Figure 6).

Because the cost exposure due to liability is unlimited, it is a major cost driver for current production aircraft, which carry the burden for all previous years' production. Today's dismal sales picture reflects the stifling effect of high liability costs.

- **RAISES COSTS**
- **ATTACKS INNOVATION**
- **TAKES RESOURCES FROM RESEARCH AND DEVELOPMENT**
- **DRIVES AWAY MANUFACTURERS AND SUPPLIERS**
- **SEVERELY INHIBITS THE CAPITAL FORMATION
ESSENTIAL FOR REVITALIZING THE INDUSTRY**

Figure 6. Product Liability Stifles General Aviation

Liability attacks innovation, directly and indirectly. In court, innovations are exposed to the natural predisposition of juries against anything new or unfamiliar, regardless of how badly the product was mistreated. As a result, designers now stop and ponder every possible misuse or abuse of a new product. Creativity is stifled by the need, even if futile, to second-guess the unlimited realm of the unreasonable.

Liability has already taken well over \$3 billion from the industry, money that could have been used to design, develop and re-tool for an entirely new generation of light airplanes.

The excessive risks of liability have driven manufacturers and numerous suppliers from the market. Beech has reported losing over 100 suppliers. Cessna has had the same experience. These risks also make the financial community wary of investments in general aviation, which prevents the capital formation necessary to rebuild the industry and to fully implement new technologies.

Manufacturers, pilots associations, labor unions, and others strongly support the "General Aviation Revitalization Act" (S. 1458), which was passed by the Senate last March. It will soon come to a vote in the House of Representatives, where it has a clear majority with more than 300 co-sponsors. Getting it out of the House Judiciary Committee and to the floor for a vote has become the issue, with powerful Congressmen sympathetic to ATLA blocking action.

It is important that you write your Representatives, urging them to sign a discharge petition on Senate bill S. 1458, so the issue can be voted in the House. Alternatively, if an acceptable bill is sent out of the House Judiciary Committee, urge your Representative to vote for it.

The livelihood, careers, and professions of those involved in General Aviation depend on passage of meaningful limits to product liability. Otherwise, production of light aircraft will continue as a cottage industry, where companies can hope to avoid being destroyed by liability only by staying small, bankrupt, and/or keeping their critical assets out of this country. This is hardly a normal business environment, and it will continue to keep airplanes from the market.

[Note: On June 27, under pressure from nearly 200 signatures on the discharge petition, the House Judiciary Committee referred its version of the bill to the House floor, where it passed easily on a voice vote. Minor differences in the Senate and House versions were resolved and the final measure passed the House on August 3. It now goes to the President for his signature.]

TECHNOLOGY'S POTENTIAL

Assuming that a satisfactory resolution of the liability problem will be achieved, then the key marketplace issue becomes the proper direction for aircraft design and technology. As a point of departure, it is worth remembering the presumption often voiced in the mid-1980s that exciting new configurations and massive infusions of technology were the key to revitalizing the industry. With the results now in on the new airplane programs that tried this approach, it is hard to find much support for that claim.

It was partly in response to this widespread misconception about technology that the General Aviation systems analysis study in Reference 1 was conducted. The intent was to show more appropriate uses for technology in light airplane design (Figure 7).

Interestingly, a key result was that if all the best available aerodynamic, materials, and propulsion technologies were applied to new models *in the usual way*, but to the maximum level, it

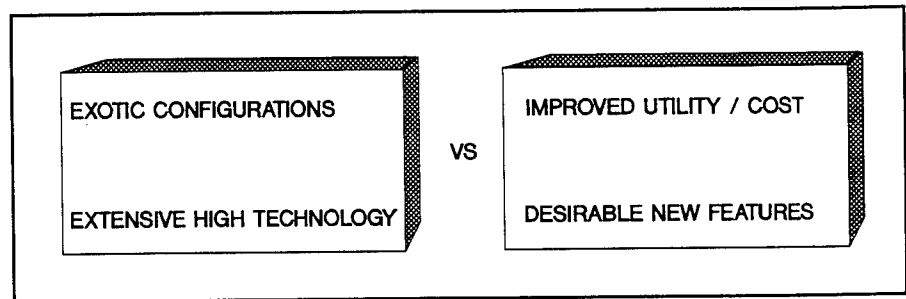


Figure 7. The Technology Issue

wouldn't make much difference in the market, even if those technologies were free; because the utility improvement resulting from the available new technologies would not be enough to draw people away from used airplanes to new ones. Nor would these technology applications provide the kinds of features that would make flying more attractive to substantially more people.

Two comments on these results are appropriate. First, the high technology applications do provide significant and exciting improvements in performance. There are parts of the market where some of these benefits are effective and practical today. Second, the rise in used airplane prices over the last seven years makes the cost of those technologies relatively more competitive today than in 1987. At the same time, some new technology applications are coming down in price. So cost trends have begun to move in technology's favor. A great deal more movement is needed.

Before leaving this point, it is well to emphasize that continued work in the basic technologies is still essential, because large and useful advances are possible and are being pursued by both NASA and the General Aviation manufacturers. Cessna has incorporated laminar flow technology on its most recent new jet model, the CitationJet; and Cessna will look for more uses for new technologies on light aircraft, if and when the liability issue is resolved. One critical focal point for research and development is to assure that new technologies can be implemented with little or no cost increase.

This important cost issue and the equally important need for the right kind of features are the remainder of "*the rest of the story.*"

A REASON FOR OPTIMISM

As a positive lead-in to the discussion of cost and features, Figure 8 shows the history of a significant measure of flight activity that demonstrates real strength in the marketplace and skewers the notion that people don't want to fly light airplanes any more.

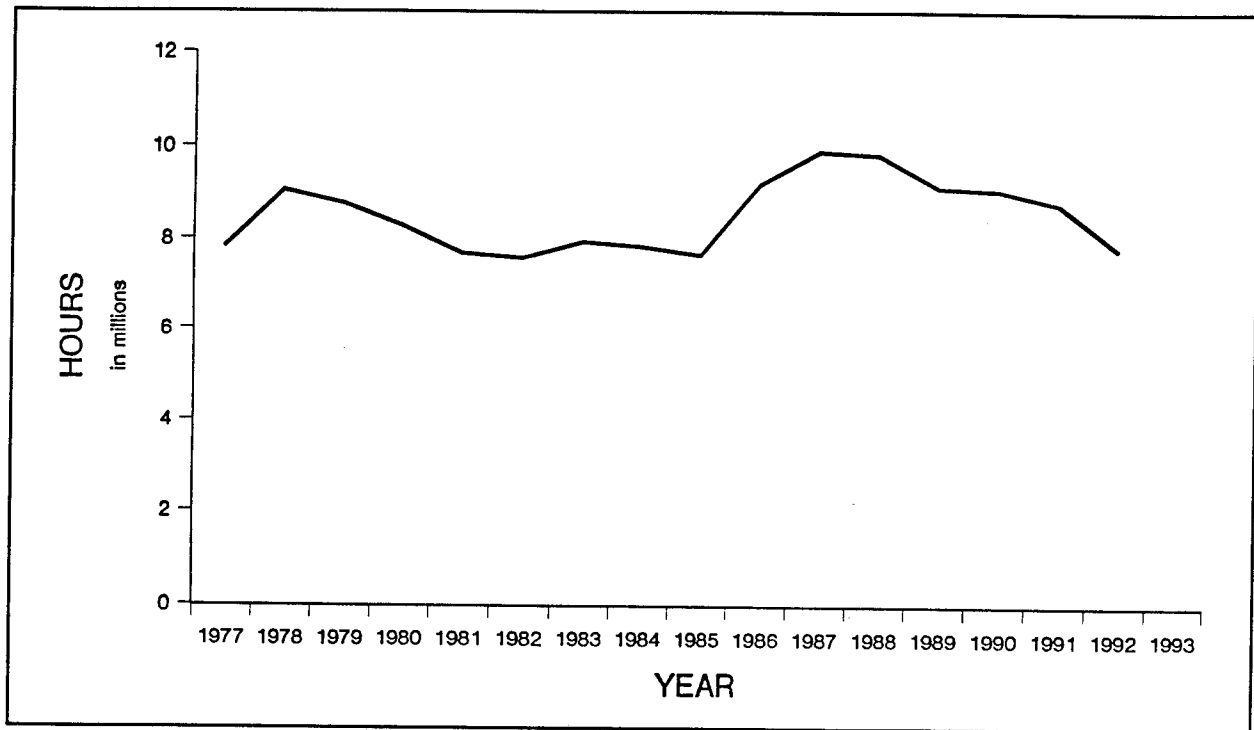


Figure 8. Single-Engine Personal Flight Hours

This chart of single-engine personal flight hours shows consistently strong activity over the last 15 years. No major drop, no hint of any rejection of the product as unsuitable, unsafe, or lacking in any way. The decline from 1978 to 1981 is an expected result of rising operating costs during that period. Those costs began to stabilize and flight hours held steady for the next four years. Then began a remarkable burst of activity that lasted six years. Finally, the age of the fleet and the lack of low-time aircraft brought this period of high activity to an end. Nevertheless, this key measure of consumer interest in light airplanes is as strong as it was 15 years ago. The product is still popular.

So the directions for new technologies that are suggested here and in Reference 1 for revitalizing General Aviation are not proposed for the purpose of overcoming any presumed negative perceptions about the industry or its airplanes; rather, they are suggested as a means for re-establishing growth with new airplanes, once the unreasonable burden of unlimited liability is removed.

IT'S THE COST!

A recent issue of *Flying* magazine includes the results of a pilot survey that highlights the importance of price (Reference 3). Airplane sales have always been highly price-sensitive, and competitive pressures on the manufacturers to minimize margins and maximize operating efficiencies are stronger than ever. In the end, however, prices are driven mostly by other costs; and these must be addressed if prices are to be more attractive.

While liability is clearly a cost driver, this short look at costs will approach the problem from just two perspectives - manufacturing cost and product value (Figure 9).

In the absence of the cost burden of liability, manufacturing cost becomes the main obstacle to lower prices. Of course, liability was the prime cause of the price spiral in the first place, but now that sales of single-piston-engine lightplanes by all domestic and foreign manufacturers are down to only about 600 units per year, they are far removed from any economies of scale. Prices will still be high without liability. This is one of the enduring legacies of product liability; and it will take some years to overcome, as the industry rebuilds the infrastructure and bootstraps itself up to economic production quantities.

Reducing manufacturing cost is largely a design issue. It requires considerable attention to design details to assure that each has a necessary function, that all details interrelate in the best way, and that the manufacturing processes are no more complex than necessary. In addition to the producibility of each individual part, there is an equally important technique, design-for-assembly. Designers working closely with toolmakers, machinists, and assemblers can reduce assembly costs substantially while improving quality.

- **LIMIT PRODUCT LIABILITY**
- **LOWER MANUFACTURING COST**
 - PRODUCIBILITY OF PARTS
 - DESIGN FOR ASSEMBLY
 - REDUCE VENDOR PARTS COSTS
- **IMPROVE VALUE (UTILITY / PRICE)**
 - INCREMENTAL IMPROVEMENTS IN UTILITY
 - INCREMENTAL ADDITION OF FEATURES

Figure 9. Reducing Costs

Even more important are the costs of items purchased by manufacturers - material, hardware, systems components, engines, instruments, and avionics. Most designers are surprised to hear that about 75% of their total product cost comes from vendors. This underscores the importance of working with suppliers to understand how airplane specifications drive their costs, and to explore alternate approaches that will save money. Vendors also need to rethink their designs and manufacturing processes in order to reduce costs.

In many cases, low production quantities of specialized airplane parts keep vendors' prices high; so whenever a mass-produced item can be appropriately used and certified, it is usually a worthwhile substitute for a standard aircraft part, even if it is a bit heavier. Designers should more often consider using or modifying mass-produced items.

Importantly, most of this has to be done up front; because with low production rates, once an airplane is certified and tooled the costs of re-designing, re-certifying, and re-tooling typically overwhelm most cost-saving ideas. The last chance to accomplish any significant cost savings is usually before the production drawings are started.

An alternative to cost/price reductions is to increase value by improving utility (speed, payload, range, field length, or cabin size) while holding the associated price increase to a minimum. Incremental improvements are a typical approach in General Aviation.

But reducing costs or incrementing utility to give somewhat better value are only part of the picture. There is a different side to this point that needs to be examined. While lightplanes are a hard sell at a price of roughly \$30,000 per seat, turbine aircraft sell almost as well for about \$500,000 per seat. Of course, the more expensive aircraft have considerably more to offer. They are larger, faster, and more comfortable; and they have more systems and features.

Still, it bears repeating that turbine airplanes, which cost as much as 17 times more per seat than single-engine lightplanes, sell about as well - roughly 600 units were sold in each category in 1993 by domestic and foreign manufacturers. This leads to some interesting questions. Is there some combination of performance and features that we might incorporate into piston aircraft in order to increase their desirability, even though their prices might be higher? Could demand for such airplanes be high enough to return the industry to economic production quantities, thereby eventually lowering the real prices?

This may seem backwards, yet it is exactly what made General Aviation airplanes more popular in the past. Examples are aluminum airframes (comfort, appearance, and durability), tricycle gear (easier to use), VOR nav aids (reliable navigation), and pressurization and turbochargers (comfort and utility).

GOALS FOR NEW TECHNOLOGY FEATURES

The success of those breakthrough developments in the past encourages designers to consider the kinds of features that will attract more people to General Aviation and keep their interest. These include both aircraft and airspace features that make General Aviation more accessible, reduce the entry requirements, improve comfort, and make it more user-friendly (Figure 10).

The intent here is to focus on appropriate goals for new features, rather than to describe those features in detail. The actual designs that will realize these goals are a matter of individual inventiveness and resources.

The goals for new-technology features amplify the need for greater attention to aircraft systems. This is where the features are - the perceived comfort and convenience - and most of the cost. Packaging systems is at the heart of successful aircraft design. The correct approach will take a fresh look at the hardware and software used to implement functions, both existing and new ones, with the goals of improving the product, reducing costs, or both.

- **APPLICATION**
 - AIRCRAFT
 - AVIATION ENVIRONMENT
- **GOALS**
 - MAKE GENERAL AVIATION MORE ACCESSIBLE
 - REDUCE ENTRY BARRIERS
 - IMPROVE COMFORT
 - PROVIDE A USER-FRIENDLY SYSTEM

Figure 10. Directions for New Technology

For example, light aircraft typically do not have air conditioners today because of the load on the engine. One solution would be to use a larger engine. Instead of this, could a small, lightweight, piston-driven auxiliary power unit be developed for light airplanes to provide power for some comfort and convenience items that don't need a certified propulsion system? Could this APU also be a backup electrical and vacuum source?

In some cases, the weight or drag of an additional feature might reduce utility or flexibility; yet it can still be successful. This comment isn't really as puzzling as it may seem at first. When designers began widely incorporating tricycle gear, for example, they dealt with exactly this problem. The nose gear added weight and drag - lots of both, as well as more cost - and the market loved it. Demand increased, which improved production efficiencies. The net result was no increase in real price.

The list of other possibilities includes reducing noise and vibration levels, simplifying the cockpit, and providing direct, context-sensitive information to the pilot with minimal coding.

Reducing noise and vibration can be done with changes or additions to soundproofing, the airframe, engine mounts, or the propulsion system. Simplifying the cockpit involves engine controls, flight and engine instrumentation, and communication and navigation equipment. The list of possibilities here may be endless.

In the last few years, NASA, the FAA, and others have started work on technologies that address the goals outlined in Figure 10. The \$63 million NASA program organized by Dr. Bruce Holmes is now underway, with work planned in cockpit systems, propulsion systems, icing protection, and integrated design and manufacturing (Reference 4). What remains is to continue building on these efforts and then to proceed with the design work, combining these technologies with advances in materials and aerodynamics to provide new, desirable features along with balanced utility and performance.

The ultimate vision for technology for some pilots might be a system that does the flight planning automatically, keeps track of all pertinent weather, flies the airplane, monitors the aircraft systems and the progress of the flight, and executes appropriate emergency procedures if required. This would certainly broaden the appeal of General Aviation, but seasoned pilots sometimes speak with disdain that such a thing might eventually come about. Visions of losing their independence in the air run about equal with fears of having green pilots in complex airplanes and marginal weather.

These concerns can be answered in time, as technology moves closer to providing such capabilities. For example, it is possible to configure an automated system to operate as a subset or overlay of the existing airspace system, so that it still allows independence and flexibility. And it is certain that the FAA will assure that pilots are qualified. The technical challenge will be to design reversion modes that take care of the pilot when there are problems, rather than increase workload and training requirements. Imaginative and realistic reversion modes will prove to be the key for certification and widespread acceptance of the automated cockpit.

It is important to not be constrained by the fears and disdain of insiders; but it won't do to ignore them either. The goal must be to retain or improve upon the independence and flexibility

provided today, while making General Aviation more accessible to those who remain on the outside - people who love the idea of flying, but find the effort and rigors a bit beyond their interest; people more interested in its transportation value than in the technicalities of flying as it is today.

This symposium is another example of the rising level of energy and enthusiasm in General Aviation technology. There is no reason to be hanging crepe over General Aviation because of all the negative, external pressures on the industry. All of them but one, product liability, can be overcome by a positive attitude and good design, marketing, and business skills.

REFERENCES

1. E. F. Kraus, *Technical Thresholds for Revitalizing General Aviation*, AIAA-87-2933, September 1987.
2. Max E. Bleck and Bruce E. Peterman, *The Impact of Product Liability Litigation on the Aviation Community - A General Aviation Manufacturer's View*, SAE-871329, June 1987.
3. Pilot Opinion Survey, *Flying*, June 1994, pp. 26-32.
4. B. Holmes, U.S. General Aviation: *The Ingredients for a Renaissance*, Proceedings of the 3rd Joint Symposium on General Aviation Systems, Mississippi State University, May 1994.